FATIGUE MECHANISMS

Jeffrey T. Fong, *editor*

ASTM STP 675

AMERICAN SOCIETY FOR TESTING AND MATERIALS

FATIGUE MECHANISMS

A symposium sponsored by
ASTM Committee E-9 on Fatigue
National Bureau of Standards
National Science Foundation
Kansas City, Mo., 22-24 May 1978

ASTM SPECIAL TECHNICAL PUBLICATION 675
Jeffrey T. Fong, National Bureau of Standards, editor

List price $65.00
04-675000-30

AMERICAN SOCIETY FOR TESTING AND MATERIALS
1916 Race Street, Philadelphia, Pa. 19103

Library of Congress Catalog Card Number: 78-74562

NOTE

The Society is not responsible, as a body,
for the statements and opinions
advanced in this publication.

Printed in Baltimore, Md.
October 1979

SHUJI TAIRA
1920–1978

Dedication

It was with great sorrow and disbelief that we all learned of the sudden and untimely death of Shuji Taira in October 1978. Professor Taira had long been active in fatigue research, had contributed to this symposium as a member of its international advisory board and the co-author of an invited paper, and had journeyed to Kansas City with Mrs. Taira in May 1978 to interact, for the last time, with an international group of fatigue researchers. It is with sincere appreciation for his life-long contribution in fatigue and his personal interest in ASTM Committee E-9 on Fatigue that we dedicate this symposium volume to his memory.

Professor Taira was born on 22 October 1920 in Nishinomiya, Hyogo Prefecture, Japan. He received a Bachelor of Engineering degree from Kyoto University in 1943 and the Doctorate of Engineering from the same University in 1952. From 1954 to 1956, he spent two years at the University of Illinois-Urbana, an association that furthered continuing interactions between scientists and engineers in the United States and in Japan. Professor Taira was well known for his excellence as a researcher and research leader in the field of high temperature studies and X-ray diffraction studies of the

mechanical behavior of materials. He wrote and edited fifteen books as well as numerous technical articles, and was a founder of the Japan Society of Materials Science as well as the International Conferences on the Mechanical Behavior of Materials. Among his many distinctions was the presentation by the Emperor of Japan of the Academy Award of the Japanese Academy of Sciences in 1971. The international materials research community has lost one of its most respected and capable members, and this dedication is but an indication of our high regard for this fine gentleman.

Foreword

Engineering and medicine are two professions that share several traits, one of which may be described as the responsibility to ensure the health of an object, animate or inanimate. To the extent that this analogy holds true, engineers who design for fatigue may be compared with some obstetricians who dare to predict how long babies might live. Clearly anyone who reads census data can predict that a newly born infant in the United States has a 90 percent chance of living to at least 50 years old, but it takes a medical scientist with the support of some sophisticated test data to even consider a request for stretching that prediction to a life span of 70 years. This is understandable, because the first prediction requires no understanding, while the second does. Similarly, a design engineer who is called upon to produce a product for a reasonably long life would know not only the codes and standards for fatigue testing but also the underlying mechanisms of fatigue. It is to the latter that this book is dedicated.

For three days during May 1978, more than 200 leading scientists and research engineers from 12 countries (see Appendix for a list of attendees) gathered at Kansas City, Missouri, to listen to the presentation and discussion of 28 papers on fatigue mechanisms. This book, which resulted from the three-day symposium sponsored jointly by the ASTM Committee E-9 on Fatigue, the National Bureau of Standards (NBS), and the National Science Foundation (NSF), contains the text of all those papers as well as the written and oral discussions transacted at this conference. Hence the total number of contributors to this book exceeds 100.

The book is divided into eight chapters. As expected, the emphasis of the conference was on direct observations of fatigue damage. Following the introductory essays in Chapter 1, four chapters deal almost exclusively with direct observations of different physical characteristics (Chapter 2 on dislocation level, Chapter 3 on slip bands up to microcracks, Chapter 4 on striations, voids, and microcracks, and Chapter 5 on time-dependent damage). The basic concepts of quantitative microscopy and microstructural modeling are dealt with in Chapter 6. Composites and environment-assisted fatigue are touched upon briefly in Chapter 7. The book ends with a chapter summarizing the consensus arrived at by the conference attendees in the form of a symposium summary and a collection of remarks (Chapter 8).

It has been 20 years since the last major meeting on the subject of fatigue mechanism was sponsored by ASTM (Boston, Mass., June 1958, *ASTM STP 237*). Opinions differ as to the extent the field has been influenced by major advances in electron microscopy, computer science,

mathematical modeling, and fracture mechanics. In order to update as thoroughly as possible direct observations of fatigue damage at all microscopic levels, the organizing committee assembled a 22-member international advisory board to invite and review contributions from leading laboratories around the world. To promote a sharper exchange of views at the conference, the organizers invited at least one official discusser for each paper, and distributed a symposium preview to all participants who preregistered. This symposium preview, which contains abstracts and official discussions of all 28 papers, proved most beneficial to the participants in reaching a better understanding of the technical issues presented at the conference.

On behalf of the symposium organizing committee, I wish to thank all the authors, invited discussers, session chairmen, session coordinators, members of the symposium advisory board, and numerous others who helped shape the contents of this conference. In addition, I wish to mention specifically the following individuals whose assistance and support were essential to the organizing effort of this meeting:

ASTM	*NBS*	*NBS* (continued)	*NSF*
Cavanaugh, W.	Aller, D.	Kopec, J.	Astill, C.
Gross, P.	Burrell, D.	Lorden, J.	
Hoersch, H.	Colvin, B.	Lucas, A.	
Kaufman, G.	Fields, R.	McCoubrey, A.	
(Alcoa)	Fong, E. N.	Martin, R.	
Palmer, J.	Greenfield, P.	Polyzos, T.	
Stremba, H.	Hoffman, J.	Serig, G.	
Wheeler, J.	Hope, M.	Uglik, B.	
	Horowitz, E.	Umberger, S.	
	Johnson, R.	Wright, C.	
	Kave, B.	Wright, J.	

Finally, I would like to thank two persons whose assistance was crucial in having this book published in time as scheduled. They are Bette Johnson of NBS who came to me after the conference to help me complete the job of editing an enormous amount of draft manuscripts, and Jane Wheeler of ASTM whose patience and efficiency have endeared her to so many of us who believe in ASTM.

Jeffrey T. Fong

Editor, and Chairman of Symposium Organizing Committee.

October 1978.

A Note of Appreciation to Reviewers

This publication is made possible by the authors and, also, the unheralded efforts of the reviewers. This body of technical experts whose dedication, sacrifice of time and effort, and collective wisdom in reviewing the papers must be acknowledged. The quality level of ASTM publications is a direct function of their respected opinions. On behalf of ASTM we acknowledge with appreciation their contribution.

ASTM Committee on Publications

Related ASTM Publications

Fatigue Testing of Weldments, STP 648 (1978), $28.50, 04-648000-30

Corrosion Fatigue Technology, STP 642 (1978), $32.00, 04-642000-27

Use of Computers in the Fatigue Laboratory, STP 613 (1976), $20.00, 04-613000-30

Manual on Statistical Planning and Analysis for Fatigue Experiments, STP 588 (1975), $15.00, 04-588000-30

Editorial Staff

Jane B. Wheeler, *Managing Editor*
Helen M. Hoersch, *Associate Editor*
Ellen J. McGlinchey, *Senior Assistant Editor*
Helen Mahy, *Assistant Editor*

Contents

Dedication iii
Foreword v

CHAPTER 1: INTRODUCTION

Fatigue Mechanism—Key to the Solution of the Engineer's Second Fundamental Problem—J. T. FONG 3
Fatigue Mechanism—An Historical Perspective—L. F. COFFIN, JR. 9

CHAPTER 2: QUANTITATIVE MICROSCOPY AND DIRECT OBSERVATIONS AT DISLOCATION LEVEL

Quantitative Microscopy and Fatigue Mechanisms—F. N. RHINES 23
Discussion and Closure—G. A. MOORE, E. E. UNDERWOOD, J. B. VANDER SANDE, D. T. PATTEN, AND F. N. RHINES 35
On the Process of Subsurface Fatigue Crack Initiation in Ti-6Al-4V—J. RUPPEN, P. BHOWAL, D. EYLON, AND A. J. MCEVILY 47
Discussion and Closure—T. MURA, P. NEUMANN, AND J. RUPPEN 65
Persistent Slipbands in Fatigued Face-Centered and Body-Centered Cubic Metals—H. MUGHRABI, F. ACKERMANN, AND K. HERZ 69
Discussion and Closure—R. DEWIT, W. PLUMBRIDGE, C. LAIRD, R. STEPHENS, A. WINTER, B. DITCHEK, AND H. MUGHRABI 97
Dislocation Structures Around the Crack Tips in the Early Stage in Fatigue of Iron—K. KATAGIRI, J. AWATANI, A. OMURA, K. KOYANAGI, AND T. SHIRAISHI 106
Discussion and Closure—A. PLUMTREE, J. SIMMONS, H. MUGHRABI, AND K. KATAGIRI 123
Closing Remarks by Session Chairman—L. F. COFFIN, JR. 129

CHAPTER 3: DIRECT OBSERVATIONS FROM SLIPBANDS TO NUCLEATION OF MICROCRACKS

Opening Remarks by Session Chairman—J. C. GROSSKREUTZ 133
Grain Size Effect on Crack Nucleation and Growth in Long-Life Fatigue of Low-Carbon Steel—S. TAIRA, K. TANAKA, AND M. HOSHINA 135
Discussion and Closure—A. MCEVILY, S. WEISSMEN, T. YOKOBORI, K. TANAKA, AND S. TAIRA 162
Mechanisms of Fatigue and Environmentally Assisted Fatigue—S. P. LYNCH 174

Discussion and Closure—C. LAIRD, K. TAKAO, P. NEUMANN, R. WEI, I. LEMAY, B. TOMKINS, W. PLUMBRIDGE, AND S. LYNCH 203
Factors Influencing Stage I Crack Propagation in Age-Hardened Alloys—M. WILHELM, M. NAGESWARARAO, AND R. MEYER 214
Discussion and Closure—E. STARKE, JR., S. BRETT, AND M. WILHELM 230
Direct Observation and Mechanism of Fatigue Crack Propagation—M. KIKUKAWA, M. JONO, AND M. ADACHI 234
Discussion and Closure—D. DAVIDSON, P. MAYR, J. SIMMONS, H. LIU, AND M. KIKUKAWA 248
The Study of Fatigue Mechanisms with Electron Channeling—D. L. DAVIDSON 254
Discussion and Closure—B. DITCHEK, A. RUFF, AND D. DAVIDSON 269
Closing Remarks by Session Chairman—J. C. GROSSKREUTZ 276
Dynamic, Real-Time Fatigue Crack Propagation at High Resolution as Observed in the Scanning Electron Microscope—D. L. DAVIDSON AND J. LANKFORD 277

CHAPTER 4: DIRECT OBSERVATIONS OF DUCTILE AND BRITTLE STRIATIONS, VOIDS, AND MICROCRACKS

Direct Observations—The Essential Ingredients for Discovering Fundamental Mechanisms of Fatigue—J. T. FONG 287
A Review of Fatigue Fracture Topology Effects on Threshold and Growth Mechanisms—W. W. GERBERICH AND N. R. MOODY 292
Discussion and Closure—C. WELLS, J. LANGFORD, R. HERTZBERG, K. DEVRIES, A. MILLER, H. MUGHRABI, P. NEUMANN, E. KREMPL, I. LEMAY, R. STEPHENS, J. FONG, C. ATKINSON, AND W. GERBERICH 334
Microstructural Aspects of the Threshold Condition for Nonpropagating Fatigue Cracks in Martensitic-Ferritic Structures—T. KUNIO AND K. YAMADA 342
Discussion and Closure—K. MILLER, R. RITCHIE, S. WEISSMAN, A. MCEVILY, H. LAMBA, K. DEVRIES, J. BEEVERS, T. KUNIO, AND K. YAMADA 361
Experiments Concerning Brittle, Ductile, and Environmentally Controlled Fatigue Crack Growth—P. NEUMANN, H. FUHLROTT, AND H. VEHOFF 371
Discussion and Closure—J. BEEVERS, J. DRIVER, A. MCEVILY, C. LAIRD, W. GERBERICH, AND P. NEUMANN 388
Some Effects of Microstructure and Environment on Fatigue Crack Propagation—R. B. SCARLIN 396

Discussion and Closure—L. COFFIN, T. CRUSE, J. BEEVERS, N. STOLOFF, B. TOMKINS, N. DOWLING, W. PLUMBRIDGE, AND R. SCARLIN 414
Quantitative Analysis of Fatigue Process—Microcracks and Slip Lines Under Cyclic Strains—H. KITAGAWA, S. TAKAHASHI, C. M. SUH, AND S. MIYASHITA 420
Discussion and Closure—G. SIH, K. MILLER, T. YOKOBORI, AND H. KITAGAWA 439

CHAPTER 5: DIRECT OBSERVATIONS OF MICROSTRUCTURAL DAMAGE DUE TO FATIGUE WITH TIME DEPENDENCY

Fatigue Behavior of Polymers—P. BEARDMORE 453
Discussion and Closure—A. PETERLIN AND P. BEARDMORE 465
Fatigue Fracture Micromechanisms in Engineering Plastics—R. W. HERTZBERG, M. D. SKIBO, AND J. A. MANSON 471
Discussion and Closure—K. DEVRIES, P. WORTHINGTON, AND R. HERTZBERG 491
Micromechanisms of Low-Cycle Fatigue in Nickel-Based Superalloys at Elevated Temperatures—J. C. RUNKLE AND R. M. PELLOUX 501
Discussion and Closure—B. TOMKINS, D. MICHEL, R. PELLOUX, AND J. RUNKLE 524
Low-Cycle Fatigue Damage Mechanisms at High Temperature—D. SIDEY AND L. F. COFFIN, JR. 528
Discussion and Closure—E. ELLISON, E. KREMPL, K. MILLER, W. PLUMBRIDGE, AND D. SIDEY 554
A Mechanism of Intergranular Fracture During High-Temperature Fatigue—B. K. MIN AND R. RAJ 569
Discussion and Closure—J. EARLY, D. MICHEL, B. MIN, AND R. RAJ 585
Cyclic Stress-Strain Response and Damage Mechanisms at High Temperature—S. P. BHAT AND C. LAIRD 592
Discussion and Closure—R. THOMSON, E. ESZTERGAR, H. MUGHRABI, S. WEISSMAN, A. PLUMTREE, S. BHAT, AND C. LAIRD 613
Concluding Remarks on Session—B. TOMKINS, S. MANSON, D. SIDNEY, AND B. MIN 624

CHAPTER 6: QUANTITATIVE MICROSCOPY AND MATHEMATICAL MODELING FOR BASIC MECHANISMS OF FATIGUE

Quantitative Stereological Methods for Analyzing Important Microstructural Features in Fatigue of Metals and Alloys—E. E. UNDERWOOD AND E. A. STARKE, JR. 633
Discussion and Closure—J. SMITH, A. WILSON, J. SIMMONS, G. MOORE, E. UNDERWOOD, AND E. STARKE, JR. 671

A Critical Evaluation of Mathematical Equations for Fatigue Crack Growth with Special Reference to Ferrite Grain Size and Monotonic Yield Strength Dependence—T. YOKOBORI 683
Discussion and Closure—V. IVANOVA, M. KANNINEN, AND T. YOKOBORI 701
Micromechanics Theory of Fatigue Crack Initiation Applied to Time-Dependent Fatigue—T. H. LIN AND S. R. LIN 707
Discussion and Closure—C. ATKINSON, J. MORROW, P. NEUMANN, T. MURA, D. HOEPPNER, T. LIN, AND S. LIN 722
Statistical Aspects of Fatigue at Microscopic, Specimen, and Component Levels—J. T. FONG 729
Discussion and Closure—K. HECKEL, P. PERZYNA, E. KRONER, H. REEMSNYDER, G. MOORE, AND J. FONG 747

CHAPTER 7: FATIGUE OF COMPOSITE MATERIALS AND ENVIRONMENT-ASSISTED FATIGUE

Opening Remarks by Session Chairman—J. T. FONG 761
Fatigue Damage Mechanisms in Composite Materials: A Review—W. W. STINCHCOMB AND K. L. REIFSNIDER 762
Discussion and Closure—G. DVORAK, G. SENDECKYJ, H. LAMBA, D. DAVIDSON, S. STINCHCOMB, AND K. REIFSNIDER 782
Fatigue Mechanisms in Nickel and Cobalt-Base Eutectic Composites—N. S. STOLOFF AND D. J. DUQUETTE 788
Discussion and Closure—R. STEPHENS, S. KULHARNI, R. SCARLIN, W. STINCHCOMB, D. HOEPPNER, C. BEEVERS, AND N. STOLOFF 810
On Understanding Environment-Enhanced Fatigue Crack Growth—A Fundamental Approach—R. P. WEI 816
Discussion and Closure—R. EBARA, J. KRUGER, P. NEUMANN, N. DOWLING, I. LEMAY, R. STEPHENS, AND R. WEI 831
Model for Prediction of Fatigue Lives Based Upon a Pitting Corrosion Fatigue Process—D. W. HOEPPNER 841
Discussion and Closure—R. PELLOUX, P. WORTHINGTON, R. EBARA, K. MILLER, H. KITAGAWA, AND D. HOEPPNER 863

CHAPTER 8: SUMMARY AND CONCLUDING REMARKS

Symposium Summary and an Assessment of Research Progress in Fatigue Mechanisms—I. LEMAY 873
General Discussion and Concluding Remarks—S. MANSON, R. STEPHENS, J. FONG, S. TAIRA, L. COFFIN, J. FONG, AND J. MORROW 889
Appendix: List of Symposium Participants and Correspondents 893
Subject/Keyword Index 903
Author/Discussor Index 907

Chapter 1: Introduction

Jeffrey T. Fong[1]

Fatigue Mechanism—Key to the Solution of the Engineer's Second Fundamental Problem

REFERENCE: Fong, J. T., **"Fatigue Mechanism—Key to the Solution of the Engineer's Second Fundamental Problem,"** *Fatigue Mechanisms.* Proceedings of an ASTM-NBS-NSF symposium, Kansas City, Mo., May 1978, J. T. Fong, ed., *ASTM STP 675,* American Society for Testing and Materials, 1979, pp. 3-8.

ABSTRACT: The rationale for studying fatigue and fatigue mechanism is examined by considering two fundamental problems in engineering, namely, the problem of feasibility, by asking whether a product works, and the problem of fatigue, by asking whether a product lasts. It is shown that the first problem (feasibility) is easier than the second (fatigue) because the solution to the second requires experimental information of a time scale incompatible with that available to the engineer or the material scientist. To resolve this dilemma, it is proposed that advances in computer-aided quantitative microscopy, fracture mechanics, and many other allied disciplines, be incorporated in measuring microstructural changes due to fatigue at a time scale workable in a laboratory. It is concluded that such study in discovering fundamental mechanisms of fatigue holds the key to the solution of the second fundamental problem in engineering.

KEY WORDS: cost-benefit, engineering, fatigue, fatigue mechanism, feasibility, fracture mechanics, mathematical modeling, quantitative microscopy, statistical analysis, stereology

On behalf of the symposium organizing committee, I would like to welcome you all to this international conference on fatigue mechanisms. On behalf of the American participants, I would like to bid a special welcome to those of you who are visiting the United States. We hope you will have a pleasant stay, and, if something does go wrong during this three-day period, please inform us so we can learn from our shortcomings.

[1] Physicist and project leader, Center for Applied Mathematics, National Engineering Laboratory, National Bureau of Standards, Washington, D. C. 20234.

As you know, the organizing committee prescribed two rules for the operation of this conference. There are no parallel sessions during this entire meeting, and we shall try to allocate equal time for the presentation of papers and their discussion. We hope you will all take advantage of the open forum to contribute and to learn from each other our latest understanding of the subject. To the best of our knowledge, the last major symposium on fatigue mechanisms was also sponsored by ASTM Committee E9, and was held at Boston in 1958. We hope that when our deliberations are over, the proceedings will reflect both the advances of the past two decades and our insights for guiding future research in the next decade or two.

A Message to our Sponsors

One of the unique features of this conference is its three-way sponsorship, namely, a technical committee of ASTM with an industry-wide representation, a Federal research laboratory (National Bureau of Standards) with the lead agency responsibility for technical measurement standards, and the National Science Foundation, which supports university research. In a few minutes, Dr. Coffin of ASTM Committee E-9 on Fatigue will speak on the activities of his committee and will review the 1958 symposium in order to place the present one in the proper perspective. But first I would like to speak briefly for the record as to why we are here and how the public at large may expect to benefit from this symposium. My talk therefore will not be as technical as you would expect from the rest of the conference, but I believe the subject matter to be equally relevant to a meeting of this kind.

Fundamental Problems of Science and Engineering

As a means of communicating with both the technical and the nontechnical audience, let me define what science and engineering are in terms of what I call their fundamental problems. In the minds of the public and occasionally even among technically informed circles, there exists a confusion of the fundamental goals of what we call separately "science" and "engineering." For example, the landing of a man on the moon is invariably acclaimed as an achievement in science, whereas the real credit should go to the engineers who designed the rockets, the instrumentation, and the very complicated system of guidance and control, all of which are engineering activities. The public image of an engineer is so poorly projected that a newspaper editor will generally label any success story as a scientific advance, and any failure story as an engineering blunder, even though the former may be an engineering achievement and the latter due to an error in the existing scientific principles. To shed some light on this

misrepresentation of science and engineering, I propose to use the following three questions to characterize the two subjects:

Question No. 1:	Is it (information) true?
Question No. 2:	Does it (product) work?
Question No. 3:	Does it (product) last?

By and large, science deals with the collection of human activities that consist of observing, experimenting, theorizing, and verifying some aspects of natural or man-made phenomena in order that Question No. 1 can be answered. On the other hand, society has pressing needs that cry for some solution before all the answers to the appropriate set of Question No. 1 are available. Engineering came into being when a bridge was built before we could predict its deformed shape under load. Most of our engineering activities aim to answer Question No. 2 in the affirmative. The distinction between "good" and "bad" engineering has to do with other considerations such as economics and taste, but the two key ingredients that distinguish engineering from science are:

1. An urge to apply the answers to Question No. 1.
2. In the absence of all the necessary information, an ability to extrapolate related experience into unknown areas in order that certain human needs can be met. This ability is sometimes called "engineering judgment," and has led to the development of numerous codes and standards, including the choice of safety factors.

In short, an urge to apply and an ability to extrapolate with judgment in order to solve a practical problem with either some information or a product at an acceptable cost characterize the human traits of an engineer. Once a product is demonstrated to work, a natural question to ask is, How long will the product last? This is what the study of fatigue is all about.

Let me summarize what I have just said. To a scientist, the fundamental question to ask is: "Is it true?" For an engineer, the two fundamental problems are:

1. Does it work? or, *Engineer's First Fundamental Problem.*
2. Does it last? or, *Engineer's Second Fundamental Problem.*

The broad purpose of this conference is to shed some light on the solution of the second fundamental problem.

Why is Fatigue More Difficult than Feasibility?

Relatively speaking, the first fundamental problem (feasibility) is much easier to solve than the second (fatigue). Anyone who has bought an automobile knows that a car that performs well at the dealer's lot is not nec-

essarily trouble-free during the expected lifetime of the vehicle. To predict when a major breakdown of the car will occur, we need to know a great deal about the car, the owner's driving habits, the maintenance data, etc., etc., and, even with all this detailed information, we are not sure whether we could make a reasonable prediction. What, then, is wrong with our "superb" scientific method, and how can we improve on our current approach in studying fatigue?

It turns out that there is nothing wrong with our scientific method, but it alone is inadequate for solving the second fundamental problem (fatigue). The main reason lies in the incompatibility of the time scale of the problem and that of the solution. For instance, in the case of the first fundamental problem (feasibility), the engineers need to gather only the so-called short-term behavior of the ingredients that go into a product, because the time scale for the demonstration of a product is relatively short. On the other hand, to show that a product will last 30 to 40 years, as many of our critical structures and components are designed to last, we need to know not only the long-term response of the product but also the operating conditions during these periods. Very few experiments are planned to either monitor the long-term response of a given system or to verify the simulation of the long-term response by a short-term test. Furthermore, no science can ever predict what the operating conditions of a system will be 10, 20, or 30 years from its initial date of service. This explains why the second fundamental problem (fatigue) is more difficult, by orders of magnitude, than the first (feasibility).

Fatigue Mechanism as the Key to Solving the Problem of Fatigue

I now wish to argue that the problem of fatigue is, fortunately, tractable. It is true that we cannot simulate exactly how a product will behave in a span of, say, 20 to 40 years. But we can study the microstructural changes of a system under some typical service conditions for a month or a year provided we can meaningfully measure the changes. During the past 20 years, the development of our powers of observation and analysis has matured to the point that the study of fatigue can now materially benefit from such allied fields as computer-aided quantitative microscopy, stereology, fracture mechanics, statistical and mathematical modeling of nonlinear phenomena, and surface physics and chemistry. Where this collection of knowledge and tools will lead us is the question our symposium participants will address during the next three days. By fatigue mechanism, we mean the underlying principle which explains the microstructural changes at a laboratory time scale due to simple and combined loadings of either a mechanical, thermal, or chemical origin, or some combination thereof. Every presentation at this conference is concerned with the discovery of that unknown principle, and it may take years before all the

hypotheses we make can be verified. On the other hand, the combined use of tools from allied disciplines may well lead to a major breakthrough within the next five years and this conference may act as the catalyst to accelerate that event. Most of us who work in fatigue design and research have felt for some time that the subject of fatigue mechanism has been neglected during the past two decades, to the detriment of all, and the objective of my talk is to remind the public as well as our colleagues that here is an opportunity to act and the time is ripe.

Economic Aspect of the Conference

I now wish to share with you a simpleminded calculation to demonstrate the economic aspect of this conference. Approximately 300 participants will spend on an average four working days to attend this three-day symposium, and about 180 individuals contributed an average of 10 working days to shape the content of this meeting as authors, discussers, reviewers, and administrators. My estimate, therefore, comes to a total of 3000 person-days as the direct labor cost of the conference. This means that, at $300 per person-day, including overhead, the labor cost for a conference of this size and duration would be close to $900 000, and the overall cost could well be close to one million dollars (U.S.).

A Naive Cost-Benefit Estimate

In chairing an organizing committee for a conference with a price tag of one million dollars, I felt all along that I owed the public an explanation as to the likelihood of the return to them of this sizeable investment. I would be less than candid if I assert that there is a reliable answer to that question. But if you will allow me some latitude in making an educated guess, I would like to think of the benefit in terms of dollars saved if all our structures and components can remain in service a little longer as a result of a better understanding of fatigue.

To guide my naive estimate, I wish to quote two numbers, one genuine and one suspect but nevertheless relevant for this exercise. The genuine one is from a recent report on corrosion cost to the United States, as prepared by Bennett et al,[2] which concludes that "in 1975, corrosion cost the United States an estimated $70 billion," and, interestingly enough, "of this total, about 15 percent of $10 billion was avoidable."[3] The suspect

[2]Bennett, L. H. et al, "Economic Effects of Metallic Corrosion in the United States—A Report to Congress by the National Bureau of Standards," National Bureau of Standards Special Publication NBS SP 511-1 (Stock No. 003-003-01926-7), U.S. Government Printing Office, Washington, D. C., May 1978.

[3]It was also noted in Bennett et al that "an uncertainty of about ±30 percent for the total corrosion cost figure results from inadequate data in some areas and unsure technical and economic judgments. The uncertainty in the avoidable costs is considerably greater."

figure appears in one of my other contributions to this conference[4] where I estimate that in the United States we probably spend about $0.5 billion on fatigue testing and research per year for all engineering purposes. Without any basis for my judgment, I venture to suggest that the benefit due to fatigue research is comparable to the avoidable cost ($10 billion) of corrosion or at least of the same order of magnitude as that quoted in Bennett et al. Two ratios can now be calculated: (1) a ratio of $1 million to $0.5 billion or 1 to 500 when we compare the cost of this conference with the annual expenditure on fatigue engineering, and (2) a ratio of $1 million to $10 billion of 1 to 10 000 when we compare the cost of this meeting with the possible savings per year on account of a better understanding of the problem. The second ratio would look even better if we were to count all the benefits for years following the first year used in this estimate.

Summary of Remarks

In summary, I would like to make three key points in opening this symposium:

1. Fatigue, or the Engineer's Second Fundamental Problem as I call it, is considerably more difficult to solve than what engineers have been trained for, namely, to show simply that a system works instead of how long it lasts.
2. Fatigue mechanism, the key to the solution of the problem of fatigue, can now benefit by a confluence of expertise in many allied fields, both experimental and analytical.
3. The cost of conducting basic research in fatigue is not small, as noted in a naive estimate of the cost of convening merely a symposium such as this, but the potential return on the investment is, again by a judgmental estimate, so high that any delay in supporting mechanism research may be a poor economic decision.

[4] Fong, J. T., this publication, pp. 729-758.

L. F. Coffin, Jr.[1]

Fatigue Mechanism—An Historical Perspective

REFERENCE: Coffin, L. F., Jr., **"Fatigue Mechanism—An Historical Perspective,"** *Fatigue Mechanisms,* Proceedings, of an ASTM-NBS-NSF symposium, Kansas City, Mo., May 1978, J. T. Fong, Ed., *ASTM STP 675.* American Society for Testing and Materials, 1979, pp. 9-20.

ABSTRACT: Following a note of welcome to the symposium participants, the activities of the ASTM Committee E9 on Fatigue are described. To place the 1978 symposium on fatigue mechanisms in perspective, some general comments on a symposium held in 1958 and some specific comments on each of the technical papers presented at that meeting are made. The conclusion one draws from a review of that symposium is that many investigators were seeking to understand fatigue by the use of special materials. Lithium fluoride, silver chloride, single crystals, and so forth, were the tools that could be used to increase our powers of observation on the basic behavior that was involved. Since then, the study of fatigue has advanced not so much from the aspect of mechanism, but more from phenomenology, including low-cycle fatigue, crack propagation, environment-enhanced fatigue, etc. It remains for this symposium to indicate whether we have gained more understanding of the basic mechanisms of fatigue during the past 20 years, and whether the proceedings will yield some new insight leading to a breakthrough in fatigue research.

KEY WORDS: acoustic fatigue, crack nucleation, crack propagation, dislocation motion, fatigue, fatigue mechanism, internal friction, low-cycle fatigue, plastic strain, slip mechanism, stress relaxation, ultrasonics

I would like to welcome you all here on behalf of the E-9 Committee on Fatigue of the American Society for Testing and Materials. It is a particular delight to me to have you all here, and to renew a lot of old acquaintances and to make some new contacts. We hope this is going to be a stimulating meeting, and well worth all the effort that many of us, and in particular Dr. Fong, have put into preparing it.

[1] Chairman, ASTM Committee E9 on Fatigue (1974-78), and mechanical engineer, General Electric Co., Corporate Research & Development, Schenectady, N.Y. 12301.

Brief Remarks on ASTM Committee E-9

I would like to say a few words about ASTM Committee E-9. Many of you are familiar with our activities, but perhaps some of you are not. We are a committee within ASTM devoted to the subject of fatigue. We have been active over quite a few years in many, many aspects of the field, as perhaps you may be aware of through our numerous STP's (Special Technical Publications) that have come out.

For example, in recent years have appeared such topics as "Thermal Fatigue," "Fatigue in Composites," "Computers in the Fatigue Laboratory," and "Fatigue at High Temperature." Soon to come out are "Fatigue in Welded Structures" and "Fatigue Service Load Monitoring Simulation and Analysis." These and many, many other topics represent the work of a great many people.

Our committee is broken down into subcommittees which are directed toward an exchange of information and development of standards, standardizing testing methods, and definitions in the various subcategories of fatigue.

Looking Back at the 1958 Symposium

In introducing this symposium, it might be appropriate to look back a bit. In the early planning it was brought out that Committee E-9 has not had a meeting of this type since 1958—just about 20 years ago. And although this topic has been dealt with by other societies over the years, it might be interesting to look back and see what the state of affairs was in 1958 as represented by the contents of the STP that appeared at that time.

One of the unusual features of that particular publication was that it represented only 121 pages. This is miniscule by comparison with many of the STP's that we put out these days on perhaps a topic nowhere near as worthy as this one was. It is very interesting to see the type of material that was covered at that point in time, and compare it with the things we talk about now regarding fatigue mechanisms. From this we can try to make a comparison as to whether we did, or did not, know very much in those days. Table 1 gives the table of contents of that STP. The first paper (by Keith and Gilman), you will note, had to do with the use of lithium fluoride crystals in cyclic loading. The second paper, by Forsyth, dealt with fatigue crack formation in silver chloride. The third paper was by Mason on acoustic fatigue, that is, fatigue at very high frequencies. Paper No. 4, by Hempel, considered slipband formation and fatigue cracks under alternating stress. The fifth paper, by Morrow and Sinclair, was on cyclic-dependent stress relaxation, and the final paper, by Wood, was a study of then recent observations on fatigue failure.

TABLE 1—*Contents of ASTM STP 237.*

	PAGE
Introduction—T. J. Dolan	1
Progress Report on Dislocation Behavior in Lithium Fluoride Crystals During Cyclic Loading—R. E. Keith and J. J. Gilman	3
Discussion	19
Fatigue Crack Formation in Silver Chloride—P. J. E. Forsyth	21
Internal Friction, Plastic Strain, and Fatigue in Metals and Semiconductors—Warren P. Mason	36
Discussion	51
Slipband Formation and Fatigue Cracks Under Alternating Stress—M. R. Hempel	52
Discussion	82
Cycle-Dependent Stress Relaxation—JoDean Morrow and G. M. Sinclair	83
Discussion	104
Recent Observations on Fatigue Failure in Metals—W. A. Wood	110
Discussion	120

Brief Remarks on Each Paper of the 1958 Symposium

I thought it might be worthwhile to say a brief word about each of these papers, just to give you some feeling for the types of things that people were worrying about in those days regarding the basic mechanisms of fatigue.

For example, Fig. 1, from the paper by Keith and Gilman, has to do with the use of lithium fluoride to study the movement of dislocations during cyclic stressing. From their work they observed that dislocation motion was involved, by looking at etch pits and how they moved under load, that the dislocation movement was irreversible under cyclic stress, and that the dislocation density tended to increase with increasing amount of applied cycles.

From their observations they concluded that coalescence of point defect clusters, which were found in the glide bands, tended to serve as the nucleating sites for cracking.

The paper by Forsyth considered the use of silver chloride subjected to cyclic loading. He observed evidence of extrusions and intrusions as seen from Fig. 2. Of course, this phenomenon was well known at that time. From these observations, he could get some insight about the nature of extrusions and intrusions. From this, he developed a model for describing the process of formation of these extrusions and intrusions.

Another paper, that of Hempel, traced the role of slip both in single crystals and in large polycrystalline structures of iron and aluminum, and contained some observations on the nature of the slip mechanisms and their interaction with the fatigue process (Fig. 3).

Wood reported on a technique whereby he could look at the surface irregularities on a highly magnified scale through taper sections. Thus, he

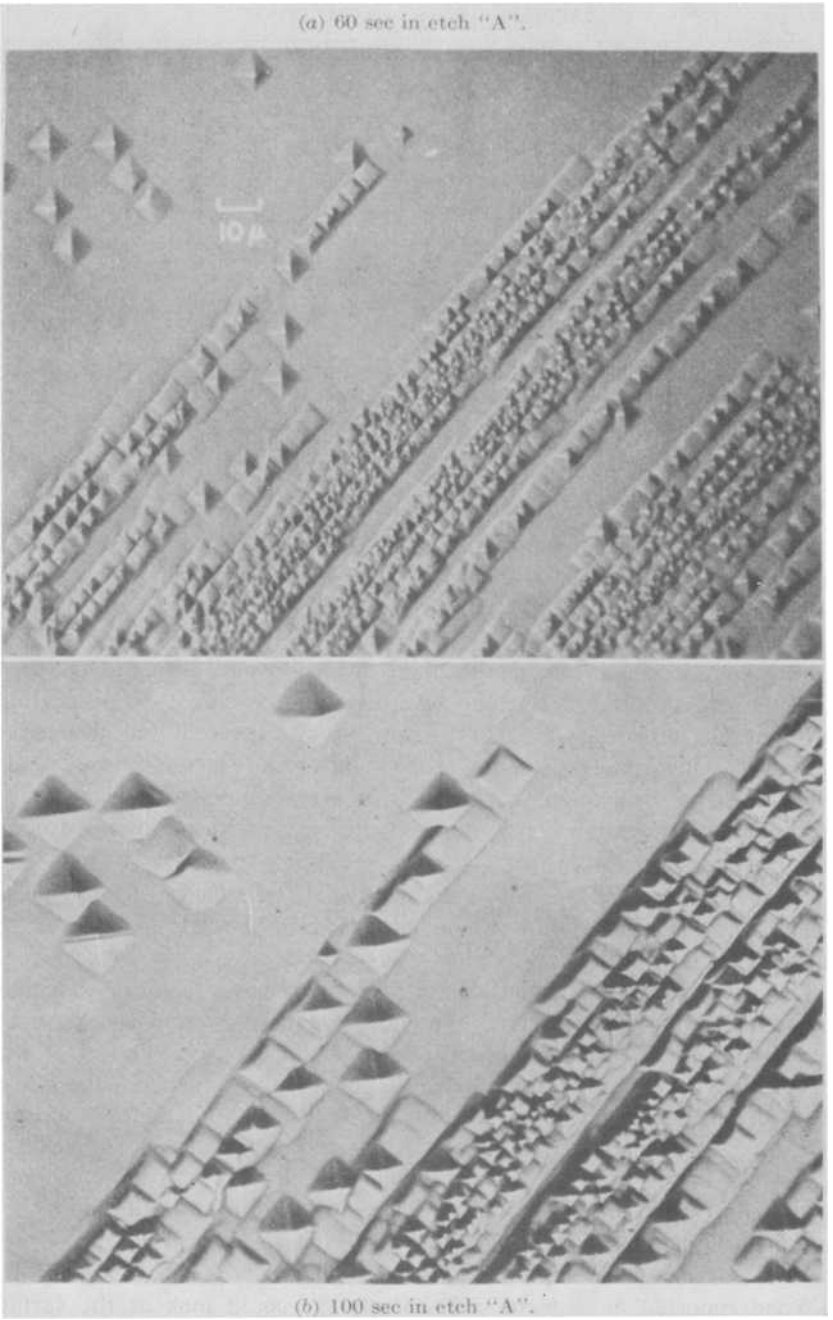

FIG. 1—*Flat-bottomed etch pits dispersed along glide planes of edge-dislocations in specimen given 5.2 × 10⁶ Hz of Stress [±1125 g/mm² (1600 lb/in.²)], as reproduced by permission from* ASTM STP 237, *p. 16.*

could introduce magnifications on the order of 20 000 to 30 000 and study the nature of the surface changes that developed. From this, he could learn something of the interaction between slip and surface roughening leading to nucleation of cracks. These observations are shown in Fig. 4.

Mason described an ultrasonic device which allowed the production of frequencies on the order of 17 000 Hz and permitted 10^7 Hz of loading in just a few minutes. From this he studied the fatigue processes occurring in a very short period of time, looked at such things as internal friction and the role of plastic strain at various stress levels, and reported on a theory for the behavior, based on a Frank-Reed source process. Figure 5 shows a picture of the ultrasonic horn that he used to drive his test specimen.

Morrow and Sinclair studied cyclic stress relaxation, and just to show you that some things have changed over the years, Fig. 6 is from their paper and presents one of our now more respected researchers in his earlier years. These investigators studied the effect of mean stress relaxation of an alloy steel under conditions of constant mean strain amplitude, and developed a model from their findings. They compared that model with the observed behavior as indicated in Fig. 7.

From an historical review of this sort, one can draw some general conclusions which I think probably can be drawn from almost any symposium of this general nature.

From this work, for example, one sought understanding and obtained information by the use of special materials. Lithium fluoride, silver chloride, single crystals, and so forth, were the tools that could be used to increase our powers of observation on the basic behavior that was involved. Special techniques were employed—techniques such as dislocation etch pits, metallography, and the use of taper sections. New equipment was introduced such as an ultrasonic horn and special testing machines. These were all coupled with the insights that could be derived from the experiments through the development of models and the application of known concepts such as dislocation mechanisms, vacancy clusters, and Frank-Reed sources.

Anything New Since 1958?

That was 20 years ago. One can ask what has happened in the meantime. I think you will get the feeling from this work that it was, indeed, of a fairly basic nature and might even be readily acceptable today in terms of the types of things we are now doing.

Actually, we have made a great deal of progress over the past 20 years, and I am not about to comment on that point other than to say that, during the period, we have been through the whole question of low-cycle fatigue phenomenology; we have learned how to relate this to crack initiation, and a great deal has been developed in terms of studying fatigue as a multistage type of process of initiation and propagation.

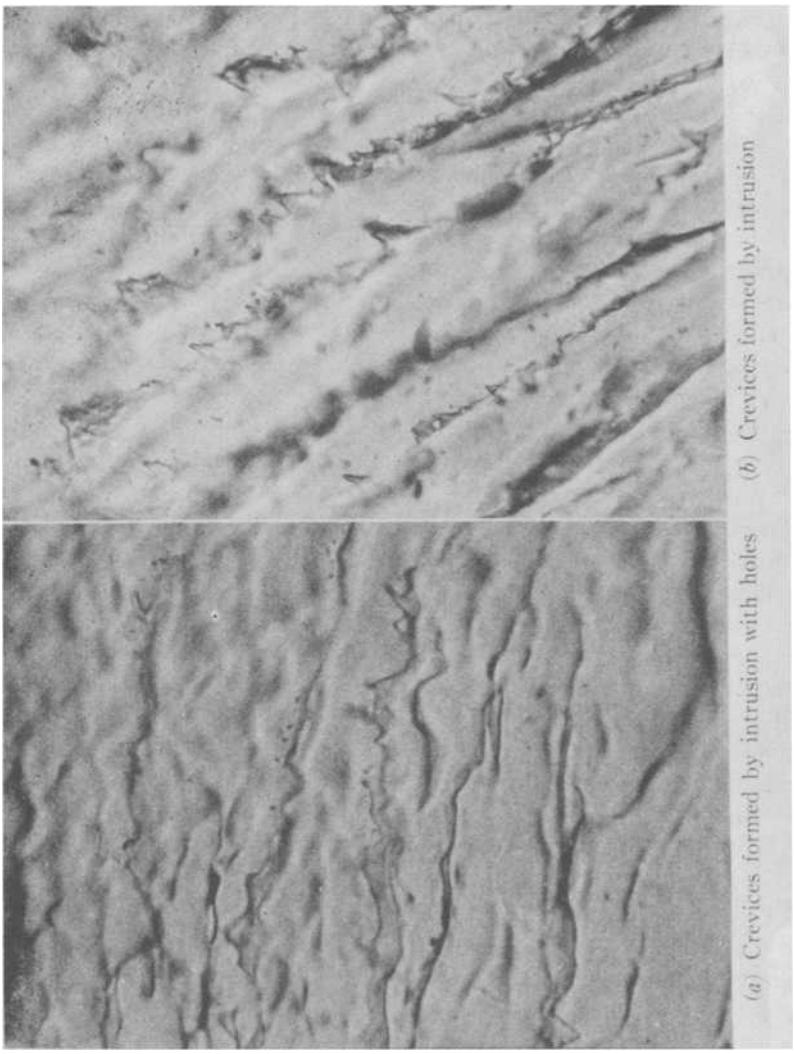

(*a*) Crevices formed by intrusion with holes (*b*) Crevices formed by intrusion

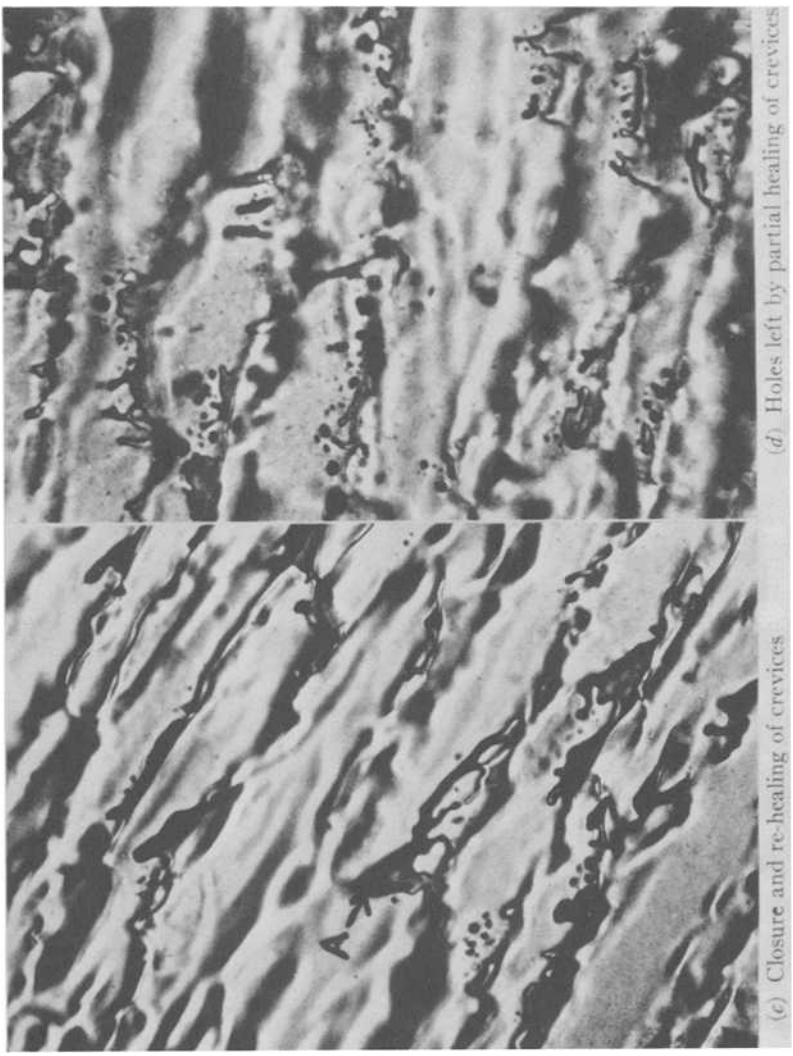

FIG. 2—*Fatigue cracks and slipband holes in silver chloride under transmitted light* (×850), *as reproduced by permission from* ASTM STP 237, *p. 26.*

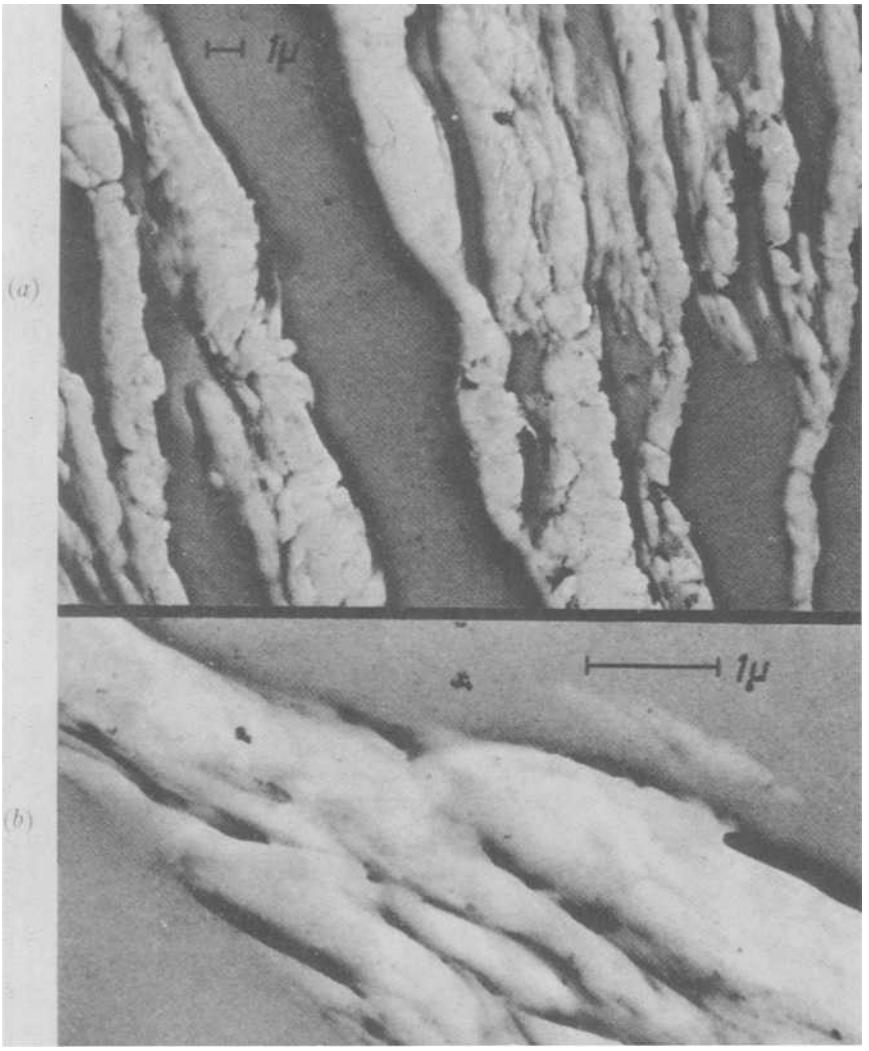

FIG. 3—*Plastic replica of slipbands under the electron microscope, as reproduced by permission from* ASTM STP 237, *pp. 52-81.*

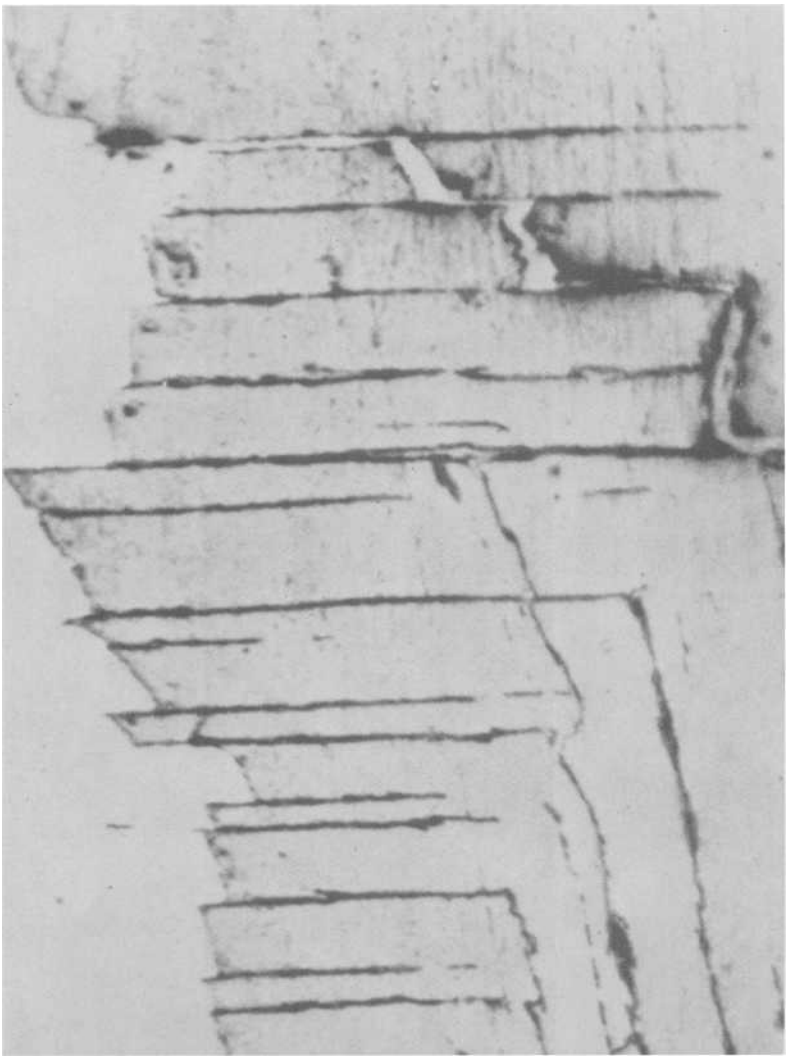

FIG. 4—*Crack jumping from fissure to fissure (×12 000), as reproduced by permission from* ASTM STP 237, *pp. 110–119.*

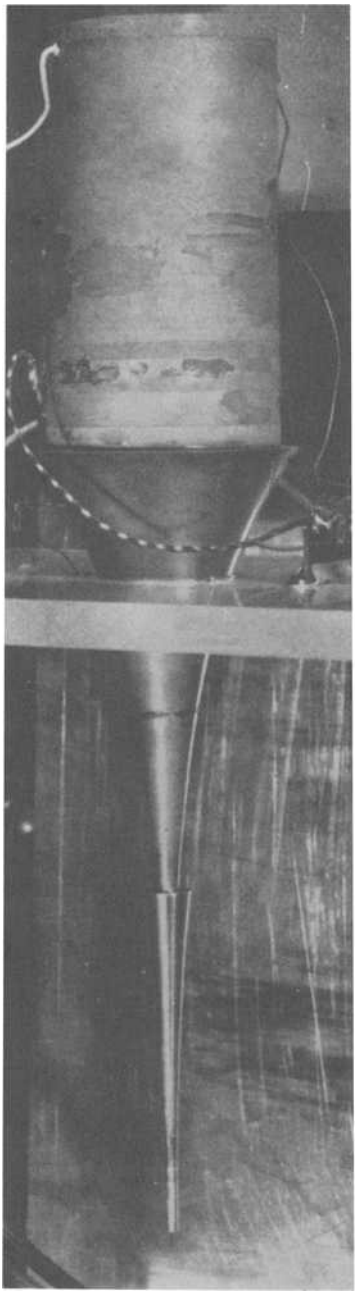

FIG. 5—*Barium titanate driver and two exponential brass horns with lead specimen in lowest horn, as reproduced by permission from* ASTM STP 237, *p. 37.*

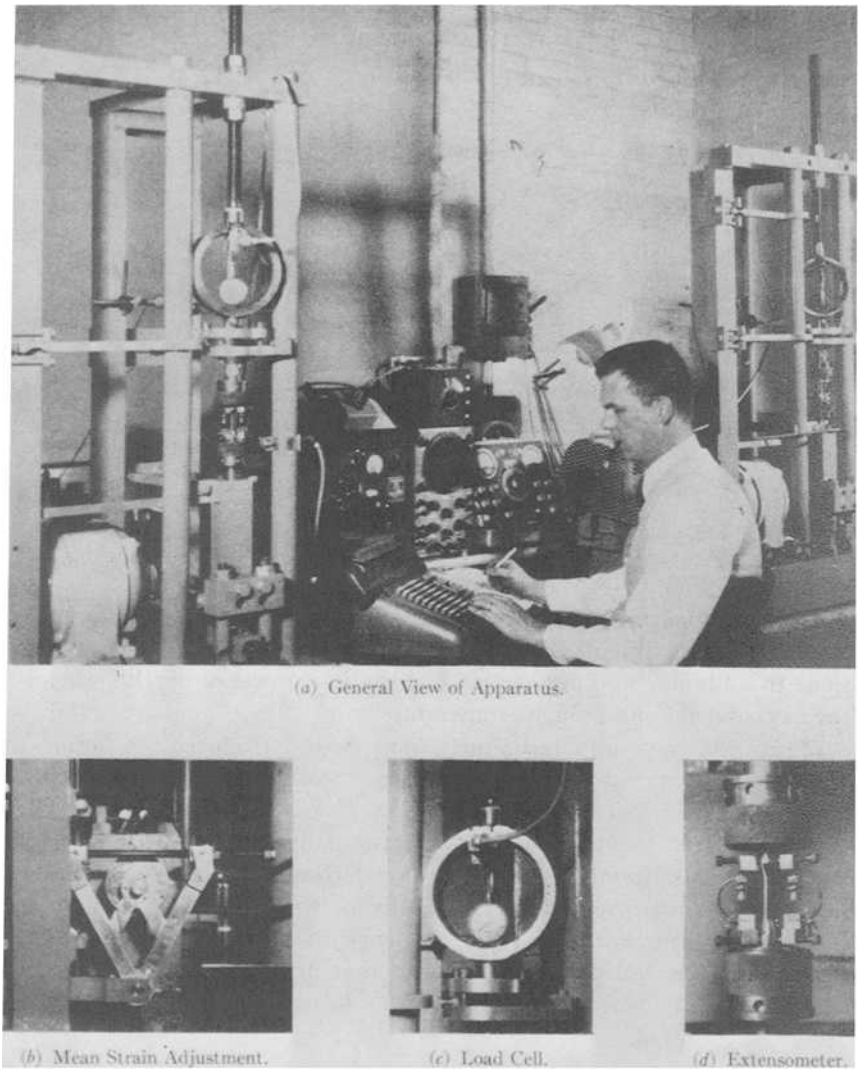

FIG. 6—*Test equipment for measuring relaxation of mean stress under conditions of constant mean strain amplitude, as reproduced by permission from* ASTM STP 237, *p. 87.*

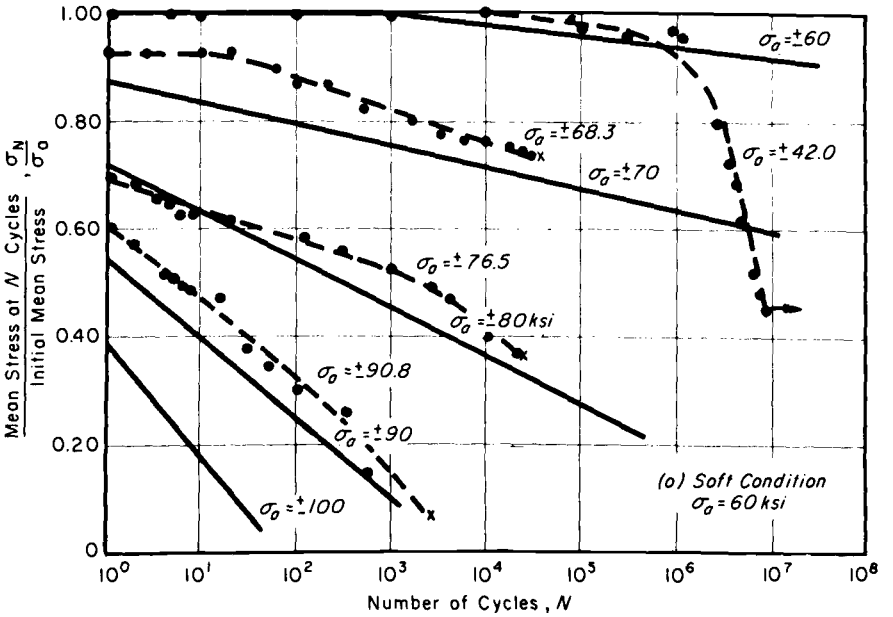

FIG. 7—*Comparison of computed and test relaxation of mean stress, as reproduced by permission from* ASTM STP 237, *pp. 83–103.*

A tremendous effort has been devoted to the study of crack propagation, both in a highly formalized sense by analysis and by experimental information. In addition, we have carried out studies to extend our knowledge of the environment and at high temperature.

Many new tools and techniques have been introduced, including the scanning electron microscope, Auger spectroscopy methods, and closed-loop testing.

One wonders, though, whether our basic understanding over this period has really made tremendous strides. My feeling is that it really has not, but perhaps these proceedings will prove me wrong. I certainly hope that over the next three days we will challenge this conclusion, and perhaps from all of this will come new insights that may lead to a breakthrough in the field and a new appreciation of what fatigue is all about.

A Word on the "Cost-Benefit" Aspect of the Symposium

In closing, perhaps we will be able to do justice to the cost analysis described by Dr. Fong. Bear in mind that a single good idea that might come out of this symposium can be worth more by a factor of 10 than the largest of the dollar figures he quoted.

Chapter 2: Quantitative Microscopy and Direct Observations at Dislocation Level

F. N. Rhines[1]

Quantitative Microscopy and Fatigue Mechanisms

REFERENCE: Rhines, F. N., **"Quantitative Microscopy and Fatigue Mechanisms,"** *Fatigue Mechanisms*, Proceedings of an ASTM-NBS-NSF symposium, Kansas City, Mo., May 1978, J. T. Fong, Ed., *ASTM STP 675*, American Society for Testing and Materials, 1979, pp. 23-46.

ABSTRACT: During the 135 years since Hood rightly associated fatigue failure with the internal structure of a metal by wrongly concluding that the metal had "crystallized," there have been many hundreds of metallographic studies of fatigue that have deluged us with observations from which we have not yet been able to extract a really satisfying understanding of the basic principles involved in fatigue. It seems that the time is ripe for the application of the recently developed methods of quantitative microscopy. In so doing, it is important to appreciate, however, that there exists a mathematically rigorous geometry of microstructure which directs and limits the kinds of observations that can yield exact relationships between microstructure and physical properties. *Additive* geometric properties, such as total volume or total area of surface, are shape-insensitive and, hence, are readily measured and related to additive physical properties like density or hardness. Conversely, the *average* geometric properties, such as grain size, or average curvature of surface, are shape-sensitive and are limited in their application to a situation in which a regularity of shape prevails. Of particular interest in the field of fatigue are the geometrical *extrema* that are associated with localized mechanical effects, such as fracture. These are observable after the fact, chiefly in the two-dimensional parameters of the fracture surface. The scope of the application of quantitative microscopy to the study of fatigue is broad and the prospect of obtaining useful results is excellent.

KEY WORDS: area fraction, average geometric properties, connectedness, curvature, dislocations, fatigue, fatigue mechanism, global parameters, grain size, microstructure, quantitative microscopy, structure-property relationship

During the 135 years since Hood [*1*][2] correctly related fatigue failure to metal structure, by incorrectly citing "crystallization of the metal" as a cause, there have been innumerable studies seeking to correlate fatigue

[1] Distinguished service professor, Department of Materials Science and Engineering, University of Florida, Gainesville, Fla. 32611.

[2] The italic numbers in brackets refer to the list of references appended to this paper.

behavior with microstructure. Some have tried to relate a general feature of microstructure, such as grain size, or the particle size and shape of micro-constituents, with the endurance limit. Others have attempted to trace the origin and growth of the fatigue crack in its relation to microstructural features. Trends have thus been noted, but no precise relationship that can be used to define the structural mechanism of fatigue failure has yet emerged. Today, little more can be said with certainty than that fatigue failure is structure-sensitive.

Purpose of this Paper

A primary reason for the lack of success just noted is probably to be found in the nature of the geometry of microstructure itself, rather than in any lack of perception on the part of the investigators. Only recently, through the development of the parameters of quantitative microscopy, has it become evident that microstructure has a special kind of geometry which is fundamental and precise, though by no means intuitive. By its use, several exact structure-property relationships have already been found in other areas of physical metallurgy and it is to be expected that it could similarly benefit the field of fatigue failure. It should be appreciated, however, that the undisciplined use of the parameters of quantitative microscopy (or of improvized parameters) can yield quite unsatisfactory results. An understanding of the geometry of microstructure is a prerequisite, therefore, to the development of any structure-property correlation. It is the purpose of this paper to describe this geometry.

Difficulties of Modeling a Microstructure

A most important fact about real microstructures is that they contain no exactly repeating patterns, such as those encountered in crystal structure. No two grains are ever of quite the same size and shape. No two particles of separate phases are ever exactly alike (Fig. 1). Yet the structure is space filling, as it must be for the metal to have the physical properties of a dense body. If one were to take apart the grains that compose a piece of metal and then attempt to reassemble them, every grain would have to be returned to its original position and orientation in the structure in order to achieve space filling. A corollary of this situation is that there can be no such thing as a typical unit of microstructure that can be multiplied to describe the mass of the material. An average shape is meaningless. In order to describe the structure in terms of the shapes and sizes of its parts, it would be necessary to describe each particle of the system individually and with its relation to other particles, an obviously impossible task! This limitation is by no means trivial, nor is it avoidable. It means that it is not reasonable to deal with microstructure in terms of models, as has so

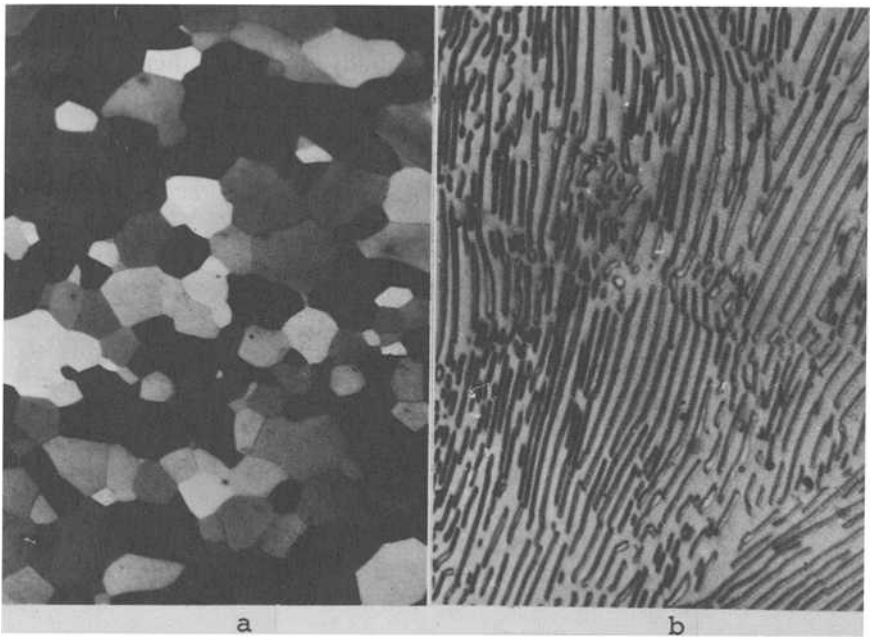

FIG. 1—*Illustrating the unlimited diversity of shape in metal microstructure.* (a) *Annealed pure aluminum, displaying equiaxed grains. From D. A. Rousse. Magnification* ×*44.* (b) *Iron-carbon eutectoid pearlite, isothermally transformed at about 690°C. Magnification* ×*1760, picral etch.*

often been attempted. One can represent microstructure precisely by employing parameters that are insensitive to the individual shapes and sizes of its particles, but see it as a whole. But, how is this possible?

Global Parameters

The answer, as we now see it, is to use only those measurements that are additive for the system as a whole, that is, the "global parameters," such as the total number of grains in the specimen, the total volume of each phase, or the total of grain boundary area. These quantities are insensitive to the individual particle shape and size. In applying this method it is tacitly assumed, of course, that the material observed is typical of the whole of the material to be characterized. Unexpectedly perhaps, this approach does not complicate the problem of defining microstructure usefully; indeed it simplifies it and with considerable gain in precision.

Just as the global parameters pertain to the body of material as a whole, so do the properties that correlate with the global parameters correspond to the material in bulk. Typical correlatable properties are density, hard-

ness, and electrical conductivity. At least some properties of this class are germane to fatigue behavior in the sense that the endurance limit increases in a general way with hardness. The probability of the initiation of a fatigue crack and the stress required to propagate it are both sensitive to bulk properties of the material, as well as to local properties.

The global parameters that are accessible through quantitative microscopy are listed in Table 1, together with the statistical relationships that are used for their experimental determination. The metallographic methods of quantitative metallography will not be detailed in this paper, since they are adequately dealt with elsewhere [2,3]. Those global parameters which apply to three-dimensional structure are all expressed in terms of totals in unit volume, a condition that is indicated by following the symbol of the parameter with a subscript v. Thus, v_v denotes volume in unit volume (or volume fraction) and A_v represents the total of surface area in unit volume of specimen. Each such parameter is independent of any of the others, which is to say that one can evaluate the structure of a specimen with respect to any one, or more, of the eight parameters listed in Table 1 without in any way limiting, or prejudicing, the value of any of the others. One way of describing this situation is to say that these parameters are shape-insensitive.

Description of the Dislocation Structure

In order to utilize the global geometry for the quantitative expression of microstructure, it is helpful to cultivate a "feeling" for its characteristics. As an example, consider the description of the dislocation structure of a piece of metal. Dislocation is a linear feature of the microstructure (Fig. 2). As such, it can have the property of existing in a number of pieces (N_v) and it can have total length (L_v) quite independent of its state of subdivision. As edge dislocation it can have curvature, which can be integrated for all of the dislocation line in unit volume of metal (C_v). As mixed edge and screw dislocation it can also have torsion, which likewise can be integrated in unit volume (R_v). It is possible for dislocation to branch, producing a multiply connected lineal system having a total connectedness (G_v) in unit volume. Some of these parameters can be measured with an optical microscope and the rest can be evaluated in the image of a transmission electron microscope (TEM) [4]. The result would be a precise description of the dislocation structure, with a wealth of detail surpassing anything that could be imagined with Euclidean parameters, and it would all be expressed by five numbers.

Thus far, the only one of these parameters that seems to have been used in evaluating dislocation structures is the total length of line (L_v), which has been shown to be proportional to the square of the stress required to continue plastic flow. Otherwise the geometric properties of dislocations

TABLE 1—*Global parameters of volume measurement.*

ASTM Designation	Geometric Property in Unit Volume	Symbol	Measuring Relationship	Nature of Sampling Device	Units
N_v	length of line	L_v	$L_v = 2\,N_A$	N_A = point intercepts in unit area	cm^{-2}
S_v	area of surface	A_v	$A_v = 2N_L$	N_L = line intercepts with unit length	cm^{-1}
V_v	volume fraction	V_v	$V_v = A_A = L_L = P_P$	A_A = area in unit area L_L = length in unit length P_P = points per point	cm^{0}
k'_v	curvature of line	C_v	$C_v = \pi\, T_v$	T_v = planar tangencies in unit volume	cm^{-3}
None	torsion of line	R_v	$R_v = \pi\, I_v$	I_v = inflections in unit volume	cm^{-3}
K_v	curvature of surface	M_v	$M_v = \pi\, T_A$	T_A = lineal tangencies in unit area	cm^{-2}
None	number	N_v	direct counting	serial sections	cm^{-3}
C_v	connectedness	G_v	$G_v = B_v - K_v + 1$	B_v = branches in unit volume K_v = nodes in unit volume	cm^{-3}

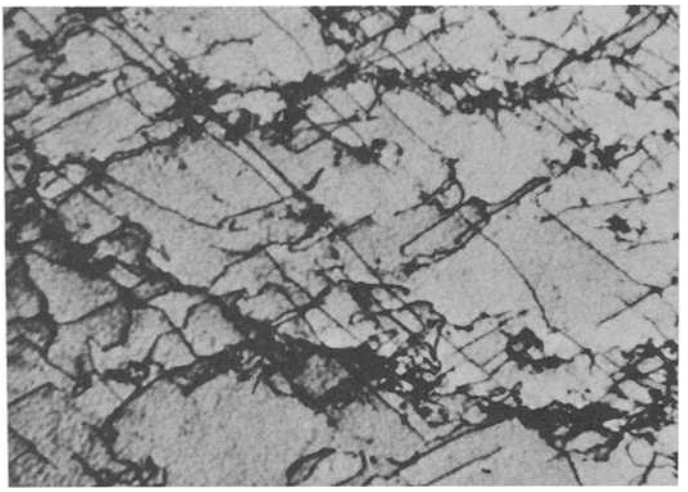

FIG. 2—*Dislocations in a TEM image of a thin foil single crystal of pure iron (Ferrovac E, decarburized), cold-rolled 70 percent. Magnification about ×275 000. Courtesy of B. B. Rath.*

that can be measured by quantitative microscopy remain to be connected with mechanical properties of the metal. It seems at least possible that some of the less familiar properties of the line, such as curvature, torsion, and connectedness, could be related to the probability of initiating a fatigue crack.

Other Examples of Microstructural Features

There are, of course, other kinds of unidimensional features that are found in metal microstructures. These include such lineaments as grain edge and lines of intersection where three phases meet. Two-dimensional features of microstructure include grain boundary surfaces, phase interface and, perhaps, internal cracks. Surface is partitionable and, hence, can have the property of number (N_v). It can have total area (A_v), total two-dimensional curvature (M_v), and two-dimensional connectedness (G_v). The total area of both grain boundary and phase interface has been found to relate to Brinell hardness number, which in turn could correlate with the endurance limit. Three-dimensional features of microstructure, such as grains, particles, and cavities, have the global properties of total number (N_v), total volume (V_v), and total three-dimensional connectedness (G_v).

Structure-Property Relationships

Where a relationship exists between a physical property and a global

parameter, its mathematical expression commonly takes the form of some function of the property equal to a constant multiplied by the global parameter [5,6]; thus

$$f(\text{property}) = k \times (\text{global parameter}) \tag{1}$$

This very simple form, which has now been found repeatedly [4,5], seems to denote an essential simplicity of the natural laws that govern structure-property relationships.

Average Geometric Properties

The global parameters can also be used to formulate ratios such as the average volume of the particles in a system, obtained by dividing the total volume of the particles by their number V_v/N_v, or as the average surface area of the particles A_v/N_v. The mean free path across the particles of a phase is four times the total volume of the phase divided by its surface area $4\ V_v/A_v$. The average curvature of surface is the total curvature divided by the total surface area M_v/A_v. Essentially every ratio that can be written represents some average geometry property of the system. In many cases these average geometric properties may seem to be just what we need for a correlation with a physical property, but look out! Although the global parameters are, themselves, insensitive to particle shape and size, their ratios are usually shape-sensitive in one way or another. This necessarily limits their use in property correlations.

Flow Through a Spongy Body—A Demonstration

Consider the case of a spongy body through which a fluid is passing. It might appear, at first thought, that the rate of flow would be simply related to the average mean free path across the channels within the sponge. A comparison among several sponges might well show, however, that no such relationship obtains. A cause is easy to find. If the channels that make up the average are of a variety of sizes, as is most likely to be the case, the flow will be restricted by the smaller channels. If the several sponges that are compared have different distributions of channel sizes, even though all average the same, then the flow rates will differ from one sponge to the next. Only if all of the channels are alike, or if they exist in the same distribution of sizes, can the average mean free path be simply related to the flow rate. The point of this demonstration is that the flow property is not controlled by the total volume of channels, which would be shape independent, but rather by the local openings throughout the system, each of which would have its individual influence upon the flow of the fluid. These effects are not additive, because they are associated in a

network where each affects what happens elsewhere. In other words, the average flow rate and the average mean free path are both shape-sensitive, but in different ways.

As it happens, nature is often kind in simplifying the problems of relating average properties to average structural parameters [5,6]. In the case of porous materials, just cited, sinter-bodies made from metal powders retain a constant mean free path across their pores throughout the second stage of sintering, making it possible to relate the permeability of the sponge directly to the connectedness of its porosity as the body densifies. Several cases [5,6] are now known in which the average geometric property is made specific by virtue of its individual parts occurring in a reproducible Gaussian distribution. This circumstance has given us very simple relationships for the kinetics of grain growth and of the solution of second-phase particles in a solid solvent, as well as for the sintering force. The problem of relating average properties with average geometric parameters is far from being a hopeless one.

Average Grain Size of Metals

An especially difficult case of an average geometric parameter, however, exists in the average grain size of metals. It has been customary to report as "grain size" the mean intercept, obtained by dividing the length of a test line by the number of grains that it crosses in a microsection of the metal, that is, $1/N_L$. This is, in fact, the reciprocal of half of the total grain boundary area, $2/A_v$ (see Table 1, "Area of surface"), and is not a property of the volumes of the grains. Nor can grain volume (nor number) be deduced from the mean intercept. Attempts to do so by assuming typical grain shapes inevitably lead to illusory results, owing to the almost infinite diversity of grain shapes in any piece of metal. This problem is easily overlooked, because there is little hint of the actual diversity of grain shape to be seen in the two-dimensional microsection. The associated misunderstanding of the realities of the mean intercept measurement has tended to becloud most of the attempts to relate grain size with various properties.

There is, of course, nothing wrong with the mean intercept measurement, except our interpretation of it, in calling it "grain size," plus the fact that it is shape-sensitive. On the whole, we should be better off to give up our insistence upon measuring grain size and use instead the grain boundary area, which comes from the same measurement and which is independent of grain shape and size. After all, the properties that we have been accustomed to regarding as being related to grain size have, in reality, been functions of the total grain boundary area all along.

Where we must have a measure of grain size, in terms of the volumes of the grains, however, this can be had quite simply by dividing the volume of the metal by the number of grains of which it is composed, that is, $1/N_v$.

Unfortunately, the counting of grains is a laborious undertaking, whether done by serial sectioning, or by the separation and counting of the grains. But it can be done. The resulting average grain volume is insensitive to grain shape, because volume is independent of shape. But, in this case the average may contain an assortment of different grain volumes. It is here that nature, in its pity on bewildered metallurgists, bestows its largess. Every grain volume distribution that has been reported in the literature, as well as every one analyzed by the present author, whether of cast grains, recrystallized grains, or grains that have sustained extensive growth, has been found to be of log-normal form. The average grain volume occurs at a cumulative frequency of 0.5 on the log-normal plot. Because nature has provided that the log-normal slope should remain constant during grain growth, the average grain volume $1/N_V$ is related simply to the time of growth at fixed temperature.

Initiation and Growth of Fatigue Cracks

Thus far I have considered only the bearing that the total, or average, properties of the bulk of the metal may have upon its susceptibility to fatigue failure. Another group of vitally important questions relates to the where and the when of the initiation of the fatigue crack and how it grows. These are questions that reach beyond the predictive capacities of the bulk properties, because failure must be initiated at a weakest, or otherwise most susceptible, site, the local properties of which lie at the extreme of the range covered by the average of the bulk properties. The chances that any metallographic sampling of the metal would encounter such a site, or if encountered that it could be recognized, are essentially nil. Such localities are recognizable only after fracture has occurred, when the two-dimensional fracture surface lays before us the whole story of the initiation and growth of the fatigue failure. In order to obtain quantitative information relating to these matters, we must of necessity learn to read the fracture. Fortunately, the principles of quantitative microscopy are applicable to two-dimensional subjects, although the relations by which the two-dimensional global parameters are measured are different in some cases.

Among the two-dimensional global parameters that may be of use in the characterization of fatigue fractures are length per unit area (L_A), area fraction (A_A), curvature of line in unit area (C_A), number in unit area (N_A), and connectedness in unit area (G_A). These, together with the relations by which they can be evaluated, are compiled in Table 2. Their use depends upon the basic requirements that the area in which the measurement is made is known and that the features to be measured are subject to an unbiased statistical evaluation. Thanks to the circumstance that the surfaces of fatigue fractures are often nearly flat, in part or in whole, the first of these requirements, that the area should be known,

TABLE 2—*Global parameters of areal measurement.*

ASTM Designation	Geometric Property in Unit Area	Symbol	Measuring Relationship	Nature of Sampling Device	Units
None	length of line	L_A	$L_A = \frac{1}{2}\pi N_L$	N_L = line intercepts with unit length	cm^{-1}
None	area fraction	A_A	$A_A = L_L = P_P$	L_L = length in unit length P_P = points per point	cm^0
k_A	curvature of line	C_A	$C_A = \pi T_A$	T_A = lineal tangencies in unit area	cm^{-2}
None	number	N_A	direct count	N_A = number in unit area	cm^{-2}
C_A	connectedness	G_A	$G_A = B_A - K_A + 1$	B_A = branches in unit area K_A = nodes in unit area	cm^{-2}

seems to be attainable. Where the structure of the fracture is such as to create a bias in some measurement, this may sometimes be overcome by combining readings made in several directions. As surfaces of increased ruggedness are encountered, it becomes a matter of judgment whether the measurements are significant. So little experience has accumulated thus far in the quantitative evaluation of fracture surfaces that little more than intuitive advice can be offered to those about to undertake such studies. Upon the basis of my limited experience, however, I venture to offer some suggestions.

Two Promising Parameters for Characterizing Fracture

The scanning electron microscope (SEM) is an excellent tool for the observation of fractures, because of its almost unlimited depth of focus. The image which it furnishes is an orthographic projection of a tilted specimen surface. The angle of tilt can be measured on the original specimen and can be used to obtain a corrected measure of specimen surface area in the SEM image. This is done by multiplying the area of the image by the cosine of the angle of tilt. The corrected area is, of course, reliable only to the extent that the specimen surface is planar.

The area fraction parameter (A_A) promises to be one of the most useful in characterizing fracture. With it one can, for example, detect any tendency for the fracture to run preferentially through a particular phase. The author has used it to measure the area fraction of torn metal, as distinguished from pore, in the fracture of a sintered metal. The area of torn metal was found to be accurately proportional to the measured tensile strength of the material. Since the area fraction is a ratio of areas, it is unnecessary to correct for the tilt of the specimen in the SEM in order to evaluate this parameter. All that is required is to make a point count of the subject phase in the photographic image.

Also of probable usefulness is the measure of total linear feature in the fracture (L_A). The total length of outline of the ruptured phase in glass-like materials has been found to correlate with tensile strength. Fatigue fractures sometimes display "rivers," lines that seem to indicate a step-like progress of the fracture (Fig. 3). The total length of these might be significant in describing the nature of the propagation of the fatigue crack. In reading the length of lineal feature, it is necessary to correct the SEM image for its tilt. Where a family of lines that are in other than random directions is to be evaluated, it is important, of course, to average the readings taken by random directions of sampling.

Additional Parameters for Studying Fracture

Curvature of line is to be seen in the boundaries of ruptured particles of

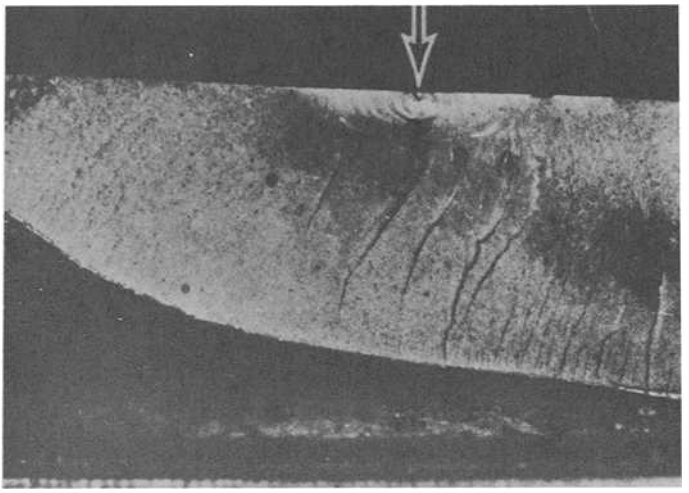

FIG. 3—*Illustrating rivers in a fatigue fracture in a 1050 steel gear. Arrow indicates a forging defect at the origin of the crack. Magnification about* ×2. *From* Metals Handbook, *Vol. 9, pp. 405, #4890.*

microconstituents, as well in such features as the rivers cited in the foregoing. This can be measured as C_A and could very well turn out to be significant in the fracture mechanisms. Number in unit area (N_A) is obviously applicable to many features of the surface structure. Connectedness (G_A) may sometimes be useful, where, for example, the ruptured phase exists as a network. In measuring any of these parameters, the area correction for tilt is necessary. These parameters are also probably more sensitive to irregularity of surface than are the area fraction and length of line.

Concluding Remarks

So, these are the tools by which we may hope to gather the data that will tell us something new about the mechanism of fatigue fracture. How, then, shall we proceed to make them work for us? I find the only answer that I can offer rather embarrassing. I wish that I could honestly say that one should now dream up a hypothesis and proceed to test it through the metallographic measurements. My own score in following this procedure has been very close to zero and I have had no better success in pursuing the postulates of others. My considered advice, therefore, is to go fishing for answers with a net. Measure every global parameter that is reasonably accessible, plot each one against any physical property that can be measured, and look for simple relationships. This method has worked for

me. Rarely have I come up empty-handed and the result has on several occasions pointed the way to a new and previously unsuspected advance in the understanding of the subject under examination. I hope that these suggestions may be of service to some of you in your quest for a better understanding of the mechanism of fatigue failure.

References

[1] Hood, C. in *Proceedings Institution of Civil Engineering*, Vol. 2, 1842-1843, p. 180.
[2] DeHoff, R. T. and Rhines, F. N., *Quantitative Microscopy*, McGraw-Hill, New York, 1965.
[3] Underwood, E. E., *Quantitative Stereology*, Addison-Wesley, Reading, Mass., 1970.
[4] Dehoff, R. T. and Gehl, R. M. in *Proceedings* 4th International Congress for Stereology, Gaithersburg. Md. 1975.
[5] Rhines, F. N., *Metallurgical Transactions*, Vol. 8A, 1977, pp. 127-133.
[6] Rhines, F. N., *Metal Progress*, Aug. 1977, pp. 60-65; Sept. 1977, pp. 47-50.

DISCUSSION

G. A. Moore[1] *(discussion)*—As one of the founding fathers of stereology—the deduction of real three-dimensional structure—Dr. Rhines was presenting this subject in a well-organized manner before I had heard of its existence. Thus, I cannot question any of the points he has presented nor suggest that any of his clear presentation could be further clarified. I, therefore, will confine my remarks to a few thoughts which may extend his presentation, and a bit of data to supplement his views.

Dr. Rhines designates the additive and average geometric properties of an aggregate as "global properties," emphasizing that these are properties of the aggregate as a whole. I must compliment him for so clearly demonstrating the impossibility of properly describing a material by describing its individual particles. Eight basic global properties are normally considered independent, but combinations of these can also be global properties. It is important to note that only three of the basic properties can be determined exactly by practical measurements on a single plane surface. Tangencies can be reasonably counted only with substantial "machine intelligence," or by laborious manual methods.

It is instructive to additionally designate a small selection of global properties as "gestalt properties," meaning those specific expressions of

[1] Metallurgist (ret.), National Bureau of Standards, Washington, D. C. 20234.

global geometry which may be found to be *most directly* and *significantly* related to some specific mechanical or service behavior of the material. The proper selection of the gestalt properties must depend on the behavior which we desire to control. Volume concentration (V_v) will almost always be expected to have gestalt significance. The best representation of size, or of directional size, depends on the application. To control ductility, we probably would select mean free path in the matrix ($\overline{l_\alpha}$). To control brittle fracture either in fatigue or shock loading, we probably would do better to use surface-to-volume ratio (S_V), or its directional projections ($S_{V'}$) in three principal directions. All size measurements normally derive from intercept counts and, of course, are completely redundent. A great convenience is provided in the ASTM Specification for Estimation of Average Grain Size (122-77), where the dimensionless logarithmic grain size number used as a quality control is the same regardless of how measured and of the system of units used. Tables and equations are provided by which "size" can be re-expressed in whichever form is most significant to the practical problem. Shape-sensitive size parameters *are* appropriate when the material behaves anisotropically! There are, of course, many causes where the true gestalt parameter remains unknown and we must try the fishnet method in order to find a firm and, it is hoped, linear relationship.

Dr. Rhines has emphasized the importance of extrema of geometric properties in the actual fracture mechanism. I believe that it is most improbable that any good commercial steel contains *individual* imperfections large enough to constitute the critical flaw which must exist just before fracture. I visualize the critical flaw as developing by cooperative actions between numerous nearby small inclusion particles (or other imperfections) until it finally reaches critical conditions (Fig. 4).

For such a mechanism we should be interested in knowing the extreme values of gestalt global properties as measured for many individual small volumes of the order of 1 to 0.01 mm^3, as opposed to the values of these properties averaged over volumes of many cubic centimetres. Can such extrema be determined in advance by quality-control inspection? A 1-cm^3 microspecimen, if serially sectioned, could yield at least two million *different* fields of the standard 0.5-mm^2 area; hence it should be obvious that description of the "worst" field found in examining 300 fields has no real possibility of being a description of the extreme field in even this small volume. The presumption that such inspection would find the extreme field may have resulted from a false assumption that the distribution of inclusion should be Gaussian normal and that nothing higher than the 3σ limit really occurs!

The distribution of observations of inclusion concentration ($A_A = V_v$) for a sample of 12 000 standard fields on a steel manufactured for automotive tire wire is shown in Fig. 5. Histogram bars and the ogive, "greater than," curve are shown at constant magnification up to $\overline{A} + 11\sigma$ in the

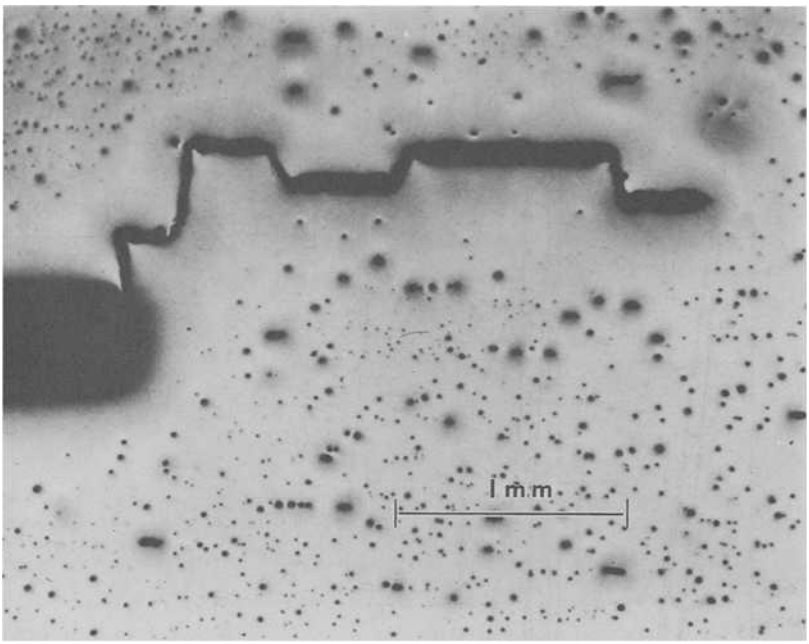

FIG. 4-*Cooperative inclusion interaction in the formation of a subcritical crack (Hy-100 steel in an interrupted notch bend test.) [Photo by Dr. Anne Fields—University of Cambridge, engineering Department.]*

main section, and the high tail is repeated with $\times 100$ magnification of the vertical frequency scale in the insert. This distribution bears no resemblance to a "normal" curve, but is highly skewed and has a ridiculously high kurtosis. More than 0.2 percent of the fields are seen to have concentrations above $\overline{A} + 9\sigma$, while more than 1 percent of all fields lie above $\overline{A} + 4\sigma$, where a normal distribution predicts less than one field in the 12 000 field sample! Dashed-line curves according to the normal frequency versus Z distribution are overlaid using assumptions of normality for three kinds of averages; namely, $\overline{A} + Z\sigma$, $Z\tilde{A}$ [root-mean-square (RMS) average], and ZA_4 (the 4th root of the 4th moment or "root-mean 4th power"). It may be seen that the RMS average fits the lower 99.5 percent of the observations better than the mean plus standard deviation while the root-mean 4th power weighting apparently represents the 0.2 percent extrema well, but is no fit at all in the lower portions.

Figure 6 shows the transverse projected surface-to-volume ratio (S_V') for the same 12 000 fields. The results are similar except that the standard deviation is somewhat larger and only 0.35 percent of the fields lie above the $\overline{S_V'} + 4\sigma$ limit. The RMS average assumption now reasonably fits the

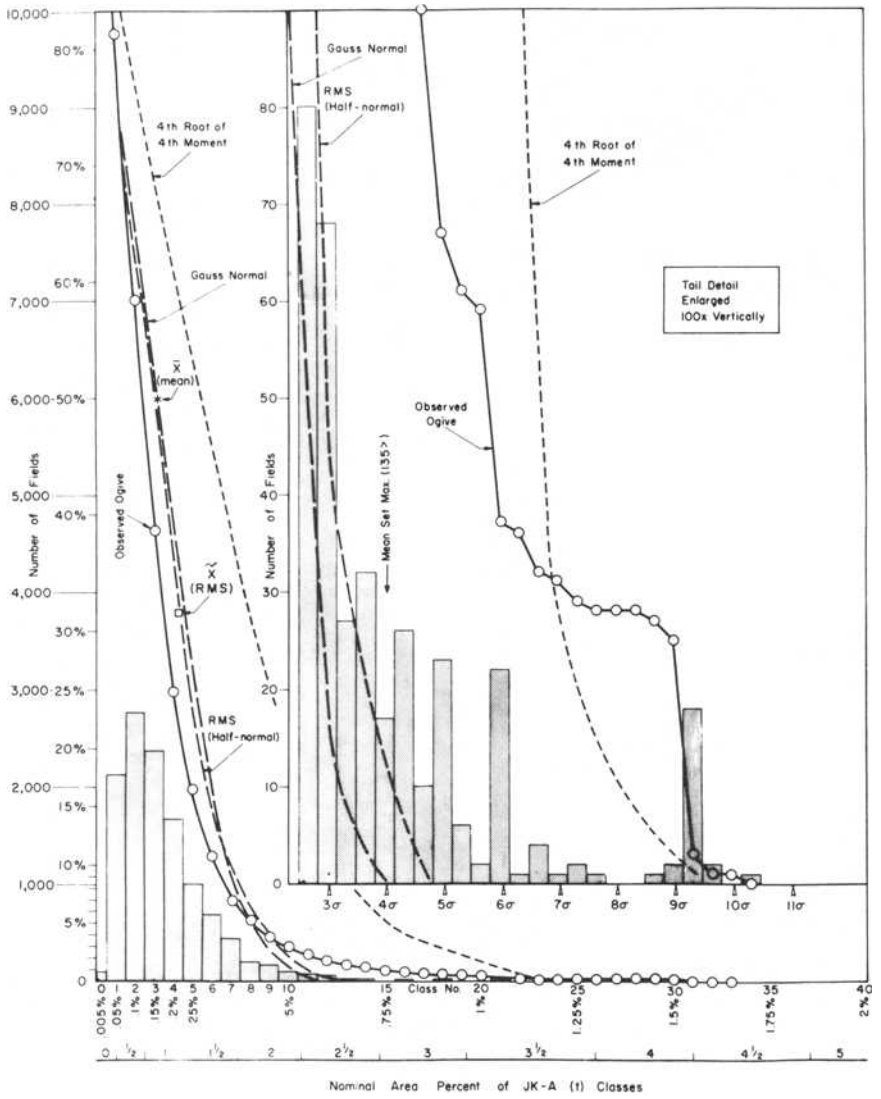

Legend: *Bars* = *field frequency in 40 histogram classes*
— o — = *observed ogive, number greater than class limit*
— — = *Gauss assumption,* $\bar{x} + z\sigma$
- - - = *assumption that RMS is "normal"*
------ = *assumption that root-mean 4th power is "normally distributed"*

FIG. 5—*Distribution of inclusion concentration* (A_A) *measurements for 12 000 fields of 0.50-mm² area each from 10 specimens of one heat of wire steel (preliminary measurements made toward developing an ASTM quantitative method, Task E4.14.04). Note: Insert graph, upper right, shows frequencies magnified* ×*100.*

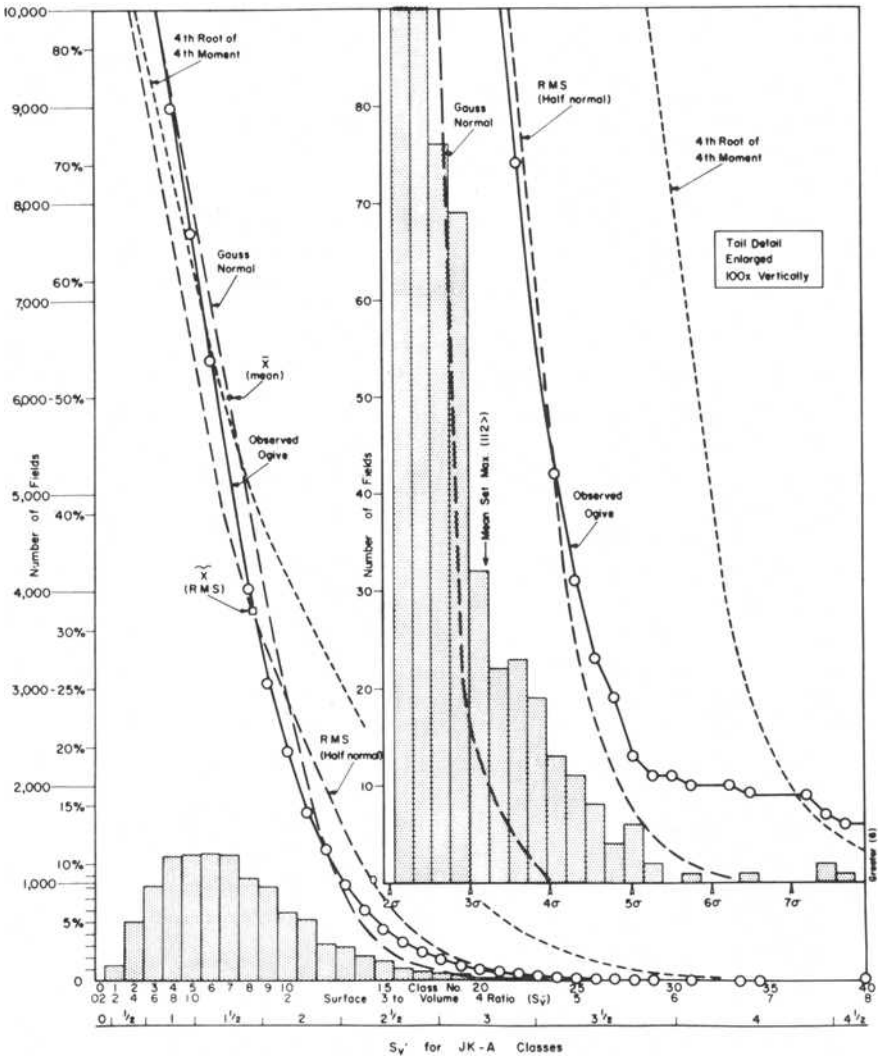

Legend: *Bars* = *field frequency in 40 histogram classes*
— o — = *observed ogive, number greater than class limit.*
— — = *Gauss assumption,* $\bar{x} + z\sigma$
- - - = *assumption that RMS is "normal"*
------ = *assumption that root-mean 4th power is "normally distributed"*

FIG. 6—*Distribution of transverse projected surface-to-volume ratio* (S_V') *measurements for 12 000 fields of 0.50 mm*^{2} *area each from 10 specimens of one heat of wire steel (preliminary measurements made toward developing an ASTM quantitative method. Task E4.14.04). Note: Insert graph, upper right, shows frequencies magnified* ×*100.*

lower 99.7 percent of observations and the root-mean 4th power assumption again reasonably fits the nine extreme observations. The "*J-K* chart" scale shown on the S_V' curve is exact according to the chart definitions in the ASTM Recommended Practice for Determining the Inclusion Content of Steel (E 45-76), but the chart scale on the area curve is approximated by using an assumed average width.

We do not at this time have either a formal explanation of the observed distribution nor an equation to fit the observations. Thus there is no assurance that the 4th-power weighting would predict even less frequent extrema. However, it appears reasonable to estimate the highest field as $Z\tilde{X}$ when the location of the significant flaw is restricted by geometry (as near a notch) and ZX_4 where a flaw might develop anywhere in a large volume. For standard 0.5-mm[2] fields, Z may reasonably be chosen for a probability factor of 2 million times the volume (in cubic centimetres) in which the flaw might develop. Thus Z multipliers between 4 and 7 would be appropriate for a range from very small to very large test volumes. Such a calculation can make no pretense of being exact, but should provide a realistic view of the maximum local inclusion content expected at a position where an actual failure mechanism is initiated.

E. E. Underwood[2] *(written)*—It is difficult to discuss this paper objectively because of the personal regard in which I hold the author, and because of the debt that all stereologists owe to his pioneer work in quantitative microscopy. However, I do not agree that the situation is as dismal as painted. Furthermore, some of his basic postulates are questionable and appear to be more an expression of opinion than of fact.

Central to these issues is his stated belief that only the "global" parameters (the *additive* ones) can be used to represent microstructures precisely, and, conversely, that the *average* values are "meaningless." Actually, to dismiss this entire class of microstructurally important quantities (the average values) is neither justified nor convincing.

And to do this because the average values are "shape sensitive" seems to avoid one of the most important areas in quantitative microscopy. The pervasive nature of "shape" in microstructures, and its influence on properties, is too well known to even question. A more positive approach, therefore, is not to ignore shape effects, but to work toward means for quantifying them.

For those who have not been following this difficult stereological problem of relating shape to properties, references to one systematic approach are appended herewith as footnotes 3-12. Admittedly such

[2] School of Chemical Engineering (Met.), Georgia Institute of Technology, Atlanta, Ga. 30328.

[3] Underwood, E. E., *Quantitative Stereology*, Addison-Wesley, Reading, Mass., 1970, Chapter 7, pp. 195-252.

[4] Underwood, E. E., *The Microscope*, Vol 22, 1974 pp. 69-80.

efforts represent only a small portion of the work going on in this area, and have far to go to reach the level of theoretical justification desired. From a practical point of view, however, simple or even complex microstructural parameters that derive from quantitative measurements, that yield unique values for a particular alloy specimen, that correlate well with specific material properties, and that do not involve *a priori* assumptions of any kind, have already proved useful in scientific research,[6-8] quality control,[9-11] property predictions,[5,10,11] and even patent claims.[10] These parameters involve all types of microstructural measurements and do not arbitrarily reject one class of quantities in favor of another.

In fact, drawing an analogy to the author's *additive* and *average* classification, we see the same general categorization in thermodynamics, in the *extensive* and *intensive* properties. All of these thermodynamic properties are completely interrelated through the four Maxwell equations, thus providing a complete and satisfying description of all facets of the system.

We can draw a similar parallel for the microstructural case. For example, the mean tangent diameter of convex grains or particles (which is rejected as "shape-sensitive" by the author) is given by $\overline{D} = N_A/N_V$, in which both N_A and N_V are "global" quantities. Also, the mean average curvature of surfaces $\overline{K_s}$ is equal to $(\pi/2)\, N_A/N_L$ for convex particles. Again, both N_A and N_L are global properties.

Another point of contention is that the volume of a grain or cell or particle is the *only* suitable parameter for expressing its "size" because a volume is shape-insensitive. But from the very general relationships for convex bodies, we see that

$$V = \overline{A}\,\overline{D} \quad \text{or} \quad V = S\,\overline{L_3}/4$$

which relates the volume V to the mean intercept area $\overline{A}$, the mean tangent diameter $\overline{D}$, the surface area S, and the mean (3-D) intercept length $\overline{L_3}$.

[5]Underwood, E. E. in *Practical Metallography*, Special Vol. No. 5. Dr. Riederer-Verlag GMBH, Stuttgart, Germany 1975 pp. 223-241.

[6]Underwood, E. E. in *Proceedings*, Fourth International Congress for Stereology, National Bureau of Standards Special Publication 431, E. E. Underwood, R. deWit, and G. A. Moore, Eds., 1976 pp. 91-92.

[7]Underwood, E. E. in *Proceedings*, Microscopical Society of Canada, Vol. 3, G. H. Haggis et al. Eds., 1976, p. 69.

[8]Underwood, E. E., *The Microscope*, Vol. 24, 1976, pp. 49-64.

[9]Underwood, E. E., in *Proceedings*, International Conference on Powder and Bulk Solids Handling and Processing, Rosemont, Ill., May 1977, pp. 380-390, published by Industial and Scientific Conference Meetings, Inc., Chicago, Ill. 60606.

[10]Underwood, E. E. in *Proceedings*, Beryllium 1977, London, U. K., 1977.

[11]Underwood, E. S. and Underwood, E. E. in *Practical Metallography*, Special Vol. No. 8, Dr. Riederer-Verlag, Stuttgart, Germany, 1978.

[12]Underwood, E. E. and Starke, E. Jr., this publication, pp. 633-682.

Thus, a mean "grain size" in terms of $\overline{A}$ or $\overline{L_3}$ seems perfectly reasonable, especially since $\overline{A} = 1/N_A$ and $\overline{L_3} = 1/N_L$, where N_A and N_L are both global quantities.

To conclude this brief discussion let me say that I agree wholeheartedly with Professor Rhines about the role of geometrical extrema in the fatigue process. I believe some progress is being made in this difficult area, however, as can be seen in the Underwood and Starke paper[12] elswhere in this publication.

J. B. Vander Sande[13] (*discussion*)—"Quantitative microscopy" involves a two-step process. First, the "microscopy" must be accomplished, followed by a "quantitative" analysis of the microstructure observed. The level of the microscopic observation may span the spectrum from the unaided eye, with a resolution of approximately 0.1 mm, through high-resolution electron microscopy, with a resolution of approximately 3 Å point-to-point.

Along with light microscopy, scanning electron microscopy (SEM) and transmission electron microscopy (TEM) have a significant role to play in analyzing fatigue microstructures in materials, as pointed out by Professor Rhines. Prior to discussing "quantitative microscopy," it is important to ask two questions:

1. What is a sensible expectation from microscopy exercise alone?
2. How can the microscopy information be quantitatively analyzed?

Professor Rhines has discussed each of these topics, concentrating, as I expect my fellow official discussers will, on the quantitative analysis aspect. Therefore, this discusser will concentrate on a few of the critical issues associated with the observation of microstructure.

The scanning electron microscope, perhaps the most widely used instrument for studying fatigue fracture surfaces, enjoys great popularity because of its good resolution ($\sim$ 100 to 200 Å), ease of specimen preparation, and excellent depth of field. However, it is expected that an operating resolution improvement of perhaps five to ten times, that is, 20 Å point-to-point resolution, would result in better statistics associated with the quantitative analysis of microstructures and, undoubtedly, knowledge of details of fatigue fracture mechanisms that could not be appreciated with poorer resolution observations. State-of-the-art SEM's equipped with field emission guns, which have a high enough brightness to provide a small-diameter electron beam with a large current, will operate with a resolution below 100 Å. The next step, which will provide for surface observations from bulk samples with a 20 to 25 Å resolution, will occur when secondary electron detectors are attached to high-resolution scanning

[13]Department of Materials Science and Engineering, Massachusetts Institute of Technology, Cambridge, Mass. 02139.

transmission electron microscopes (STEM). This is expected within the next few months.

Our ability to use transmission electron microscopy to study the microstructure of most cyclically deformed specimens is directly related to our ability to resolve the microstructural features observed. This raises the issue of the *practical* resolution of a TEM when observing a defect microstructure. If the practical resolution of the observed microstructure is defined as the ability to resolve the separation between two defect images, then the problem becomes quite clear. The bright-field image of a dislocation observed in the TEM is about 100 to 200 Å in width. These broad images of such defects have long been considered a natural consequence of TEM, but their disadvantages are many. As examples, dislocations that are closely spaced, such that their images overlap, cannot be individually resolved. Similarly, small second-phase particles in close proximity to a dislocation line as a result of a particle-dislocation interaction cannot be individually resolved because of the large image width of the dislocation. Clearly, this wide-image problem is acutely felt in fatigue microstructures characterized by high-dislocation-density cell walls, dense dislocation tangles, or dislocation/second-phase interactions.

The weak-beam technique in TEM, which uses a weakly diffracted beam to form an image of the dislocation, reduces the defect image width to about 10 to 15 Å, therefore providing a *practical resolution improvement* of approximately one order of magnitude. In brief, the weak-beam "samples" only a very small fraction of the displacement field of the dislocation with a parallel narrowing of the image from that defect. Although the experimental requirements for successful weak-beam microscopy are a bit more stringent than bright-field microscopy, the technique is well within the grasp of any qualified electron microscopist.

The weak-beam technique should play an important role in the detailed investigation of the defect microstructure of cyclically deformed materials. This is an important "first step" if the quantitative analysis of Dr. Rhines is to be profitably applied.

D. T. Patten[14] (*discussion*)—I would like to comment on the development of structure property relationships with regard to average structural properties. Dr. Rhines's paper mentions the limited applicability of such relationships. One reason for this may be the almost universal use of the algebraic average of the independent structural parameter. It is accepted that the structural parameter in such a relationship has a distribution of values and it is frequently found that the relationship between the dependent mechanical property and the independent structural property is nonlinear. Is it therefore reasonable to use a linear average to characterize the distributed structural parameter, or would an averaging technique more closely related

[14] Bendix Research Laboratory, Southfield, Mich. 48076.

to the observed functional relationship increase the applicability of the structure property relationship? For example, a material with a duplex grain size would not be expected to have the same yield strength as a material with a narrow grain size distribution of the same mean. Is this difference necessarily due to differing yield mechanisms or simply due to the use of the wrong type of averaging of the grain size in the Hall-Petch relationship?

F. N. Rhines (author's closure)—The author wishes to express his appreciation to the discussers for their interesting and important additions to the coverage of the field.

George Moore's discussion of the nature and distribution of conditions that initiate fatigue cracks is, indeed, appropriate and his contention that the active site is likely to consist of a clustering of weak points, rather than a single flaw, is most interesting. It gives us something more to look for, which may be helpful in the understanding of fatigue. I should like to clarify a point, however, concerning the distinction between global properties and average properties. I have distinguished these two, because the global parameters are capable of direct correlation with physical properties, whereas the averages are not. This is because the global parameters are shape-insensitive, so that in using them it is not necessary to establish, or even to know, anything about any other geometric property of the system. For example, the Brinell hardness of an annealed metal varies linearly with the grain boundary area, regardless of grain size, or shape, or curvature of boundary. But the averages, or ratios, of the global parameters are shape-sensitive, in the sense that it is necessary to establish something about shape in order to establish a correlation with a physical property. Thus, the engineering yield point correlates with the mean intercept grain size only where the structures being compared have equivalent grain shape, or shape and size distribution. This is auxiliary information that is usually difficult to obtain and, thus, it limits the utility of averages and ratios in quantitative correlations.

Most of Dr. Underwood's discussion bears upon this last point, which is, I think, a crucial issue in the field of property correlation. Perhaps the repetition here of a two-dimensional analog, which I have used in Ref 5, will help to clarify the role of shape in property correlations. Consider a highway, as represented on a map, or for that matter, as it exists on the surface of the earth. This road has total length, which may be measured and expressed to a fairly high degree of precision. Total length is an additive property, that is, a global property. It can be used for direct correlation with physical processes. For example, we can show that the length of time for an automobile, traveling at a fixed speed of a mile a minute, to traverse the highway from one end to the other is directly proportional to the length. The road also has a total area, which can be measured and expressed more or less precisely, and the area can be shown to be proportional to the quantity of paving material needed to

cover it. Neither length nor area depends in any way upon the curvature of the road, its number of intersections, its hilliness, or on any other geometric property. Now consider the average width of the road as defined by the ratio of the two additive parameters, namely, area divided by length (A_A/L_A). That this is shape-sensitive can be appreciated when we attempt to correlate it with a physical factor. Suppose that we are interested in how many cars this road can accommodate, all traveling at a constant speed and four car lengths apart. Clearly, the answer must depend not only upon the width of the road, that is, on how many traffic lanes exist, but on whether there are narrow stretches of the road. Unless the road is of uniform width, that is, having the same number of lanes throughout its length, the conditions set make the problem unsolvable. If variable car speed is allowed, then the problem becomes solvable in principle, but is very complex. All of this trouble has arisen because the average breadth of the highway is a shape-sensitive parameter which requires auxiliary shape information in order to become useful in a property correlation. In those cases in which we are lucky enough to find the shape simple and knowable, we can hope to achieve a simple correlation; otherwise the likelihood of correlation is small, even though it seems as though there ought to be a correlation.

This problem pervades the entire literature of shape measurement in materials. In every case in which a scheme is put forward as a means of determining three-dimensional shape from two dimensions, or in which an average property is applied without full specification of the content of the average, it turns out that there exists an assumption, often well hidden, but an assumption nevertheless. This is true because some kind of auxiliary information is required to connect a ratio with a process, or to connect a two-dimensional measurement to a three-dimensional parameter. In some cases, experimentally verifiable auxiliary information is available, as was illustrated by the case of grain growth described in the paper. Here the knowledge that the grain size distribution is log-normal and that the slope of the log-normal is constant during grain growth means that the shapes of the grains are topologically equivalent in the metal throughout grain growth. That is, there is at all times the same fraction of grains having any specific number of faces and edges. This is pretty much equivalent to finding that the highway is of uniform width. Under these conditions a simple relationship prevails between the average grain volume and the time of grain growth.

The thermodynamic analogy which Dr. Underwood has suggested is fairly apt. It will be recalled that the *intensive properties* can be derived from the *extensive properties*, but *not the reverse*. Indeed, it has been pointed out in Ref 5 that the existence of special conditions of shape that can be used in applying a ratio in a property correlation is rather like the existence of the equilibrium states at which thermodynamic quantities can be defined.

The new and forthcoming advances in the resolution of microscopy

equipment described by Dr. Vander Sande will certainly add greatly to the reach of quantitative microscopy. Each advance in resolution that has been attained in the past has brought with it unanticipated advances in the understanding of microstructure and structure-related processes. It will be stimulating to see what new structural knowledge will come within our reach. In looking toward these new methods, there are two factors that should be kept in mind. First, the parameters of quantitative microscopy must be based upon good statistics. Where the field of view becomes very limited, it may become necessary to introduce some special methodology in order to ensure reliability of the statistics of the measurements. Second, it should be kept in mind that the relationships of quantitative microscopy are not all accessible by all types of observation. Those that are derived from surface observations are not always adaptable to thin-section microscopy, while some of the tangent type of measurements are particularly fitted for thin-section measurement. In thin-section quantitative microscopy, one of the more difficult problems is that of determining the thickness of the section with sufficient precision.

Dr. Patten has again raised the question of why the average of a geometric parameter should not correlate with mechanical properties and has I think suggested that the problem lies in the average being algebraic, while the property arises from the summation of a group of responses that are not linearly averageable. This seems to be another way of looking at the situation that I have just been trying to describe. He is quite correct in postulating that a structure composed of a range of grain sizes differs in its yield point with different mixtures of sizes in the structure. Recent work has shown that during the first 25 percent of deformation, only the largest grains, amounting to less than 15 percent of the total grains in the system, account for most of the plastic deformation. Not until reductions approaching 50 percent are reached are the majority of the grains active in plastic flow. Accordingly, the tensile elongation is highly sensitive to the grain size distribution.

J. Ruppen,[1] *P. Bhowal,*[1] *D. Eylon,*[2] *and A. J. McEvily*[1]

On the Process of Subsurface Fatigue Crack Initiation in Ti-6Al-4V

REFERENCE: Ruppen, J., Bhowal, P., Eylon, D., and McEvily, A. J., **"On the Process of Subsurface Fatigue Crack Initiation in Ti-6Al-4V,"** *Fatigue Mechanisms,* Proceedings of an ASTM-NBS-NSF symposium, Kansas City, Mo., May 1978, J. T. Fong, Ed., *ASTM-STP 675,* American Society for Testing and Materials, 1979, pp. 47-68.

ABSTRACT: The process of subsurface crack initiation in Ti-6Al-4V has been investigated in some detail. At low stress amplitudes, slip occurs primarily on prism planes and is blocked at α-β interfaces. The piled-up dislocations induce slip in the β-phase under cyclic loading which can lead to the formation of a Cottrell cleavage knife and thereby provide a site for subsurface crack initiation. At high stress amplitudes, pyramidal slip becomes operative and as a consequence a more compatible type of plastic deformation between the two phases can develop. Under these circumstances the tendency for subsurface crack initiation may be reduced.

KEY WORDS: fatigue, electron microscopy, dislocations, titanium alloys

In recent years a number of investigators [*1-4*][3] have found that when titanium alloys are subjected to cyclic axial loading the fatigue origins are often located at subsurface sites. In some instances it is apparent that the presence of a silicide particle or a microvoid [*3*] is associated with this type of fatigue origin, but in other cases no apparent "defect" of such a nature is present. It appears therefore that crack initiation at a subsurface site can arise solely as a result of dislocation-microstructural interactions, a consideration initially raised by Neal and Blenkinsop [*2*]. Since fatigue crack initiation is generally considered to be a surface-related phenomenon, a subsurface cracking mode is of fundamental as well as practical interest,

[1] Graduate assistant, post doctoral research fellow, and professor, respectively, Metallurgy Department, Institute of Materials Science, University of Connecticut, Storrs, Conn. 06268.

[2] Department of Materials Science and Metallurgical Engineering, University of Cincinnati, Cincinnati, Ohio 45221.

[3] The italic numbers in brackets refer to the list of references appended to this paper.

and the purpose of the present paper is to investigate further the nature of such a cracking mode in the alloy Ti-6Al-4V.

Materials, Specimens, and Tests

Ti-6Al-4V is a two-phase alloy, 90 percent of which is the hexagonal close-packed α-phase and 10 percent of which is the body-centered-cubic (bcc) β-phase. A typical chemical analysis is as follows: aluminum:6.4 weight percent, vanadium:4.1, iron:0.07, carbon:03, oxygen:0.15, nitrogen:0.016, hydrogen:0.008, silicon: <0.05, titanium:remainder.

The specimens utilized in this study were obtained from the extensive program of axial load fatigue tests carried out by Steele and McEvily [*1,5,6*]. In that program hourglass-shaped fatigue specimens having a 0.635-cm-diameter waist were prepared from Ti-6Al-4V annealed hot-rolled bar and also from open die forgings, both of which had been processed in the α/β range. Prior to machining the forging material into test specimens, blanks were given either one of two treatments: (1) structure coarsening by slow cooling from just above the β transus (1020°C) through the α/β region, and (2) structure refinement of coarsened forging material by quenching into brine after β solution in neutral salt. Both treatments were followed by a one-hour air anneal at 700°C. The hot-rolled bar stock was tested in (1) the mill-annealed (MA) condition and (2) the coarsened condition as just described above.

The microstructural variations involved in the tests are shown in Fig. 1 (the coarsened bar stock structure is similar to Fig. 1*b*). For both coarsened bar and coarsened forging the microstructure was α/β Widmanstätten type with the α-platelet thickness ranging from 6 to 10 μ. The structure of the β-quenched and annealed forging was acicular in character with an average "needle" thickness of 1 μ. In the MA condition the α-phase had a non-planar interface with the beta (swirled structure), with an average α-phase thickness of 1.5 μ. Where planar α/β interfaces existed in the foregoing microstructures, the Burgers orientation relationship was found to hold between the two phases, that is [*7*]

$$\{110\}_\beta \| (0001)_\alpha$$
$$\langle 111\rangle_\beta \| \langle 11\bar{2}0\rangle_\alpha$$

The *S-N* curves for the three microstructures for $R = -1$ ($R = \sigma_{min}/\sigma_{max}$) axial loading are shown in Fig. 2 [*6*]. For both $R = -1$ as well as $R = 0$, subsurface fatigue crack nucleation was observed, particularly when N_f (cycles to failure) was greater than 10^6. The subsurface mode of crack initiation was most often observed in the Widmanstätten and acicular structures.

Foils for transmission electron microscopy (TEM) were obtained by

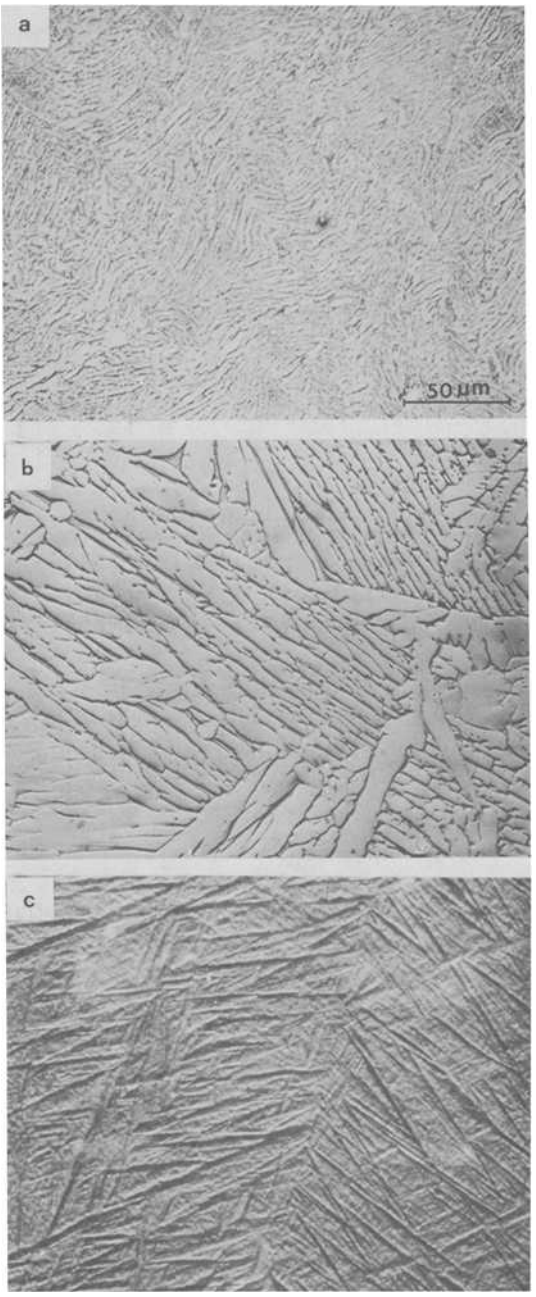

FIG. 1—*Ti-6Al-4V microstructures.* (a) *As received mill-annealed bar;* (b) *coarsened forging;* (c) *β-quenched and annealed.*

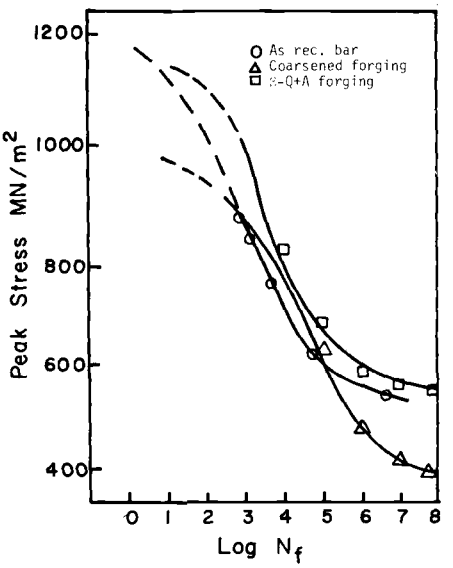

FIG. 2—*A comparison of* S-N *curves at* R = −1 *for three microstructural variations* [6].

electrodischarge machining 250-μ-thick slices from the test specimens. These slices were thinned by a twin-jet electropolisher in a 13 percent sulfuric-methanol solution. The foils were observed in a Philips 300 TEM equipped with a tilt-rotation stage.

Observations

Figure 3 provides a clear example of a subsurface fatigue initiation site in β quenched and annealed material. The facet at the crack origin is inclined at approximately 45 deg to the tensile axis, and no defect at this site is observed even at much higher (for example, ×3000) magnifications. Facet orientations of approximately 15 and 75 deg were also observed. The facet shown in Fig. 3 is of the order of 100 μ in size, but in other instances the facet size may be only of the order of 10 μ. As will be subsequently discussed, these facets exist within a prior β grain and can cross individual colonies. No cracking initially along an α-β interface or a prior β boundary was observed.

At low stress amplitude, dislocation arrays were found to be heterogeneous in their distribution. For example, Fig. 4 shows the appearance of dislocations developed in the hexagonal close-packed α-phase after cycling at ±413 MPa (±60 ksi), a comparatively low stress amplitude. At low stresses, slip occurs predominately along prism planes, and the Burgers vector of the dislocation is $\langle a \rangle$, where a is $1/3\langle 11\bar{2}0 \rangle$. At these stress

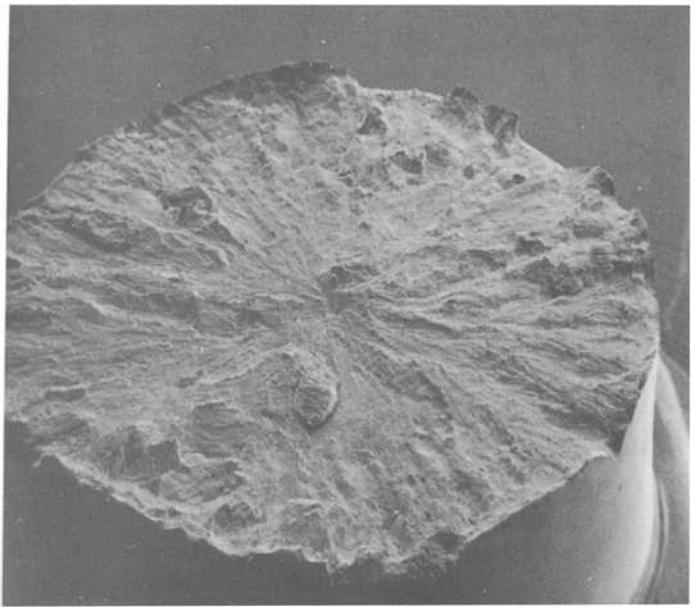

FIG. 3—*An example of fatigue crack nucleation at a subsurface site in β-quenched and annealed material* (×15).

amplitudes, slip is also seen to be operative within the β-phase, Fig. 5, which also shows the presence of interface phase [*8, 9*]. In this two-phase system it is important to understand how slip propagates from the α-phase through the β-phase and into the next α-region. Figure 6 provides evidence that slip in one α-region on prism planes is able to penetrate through a β-platelet and continue into the next α-region. In Fig. 6 the dislocations within the β-phase are not in contrast. It is also noted that Fig. 6 provides evidence for pyramidal slip although this slip mode was rare at low stress amplitudes.

At higher stress levels, for example, ±710 MPa (±103 ksi), dislocation arrays were more homogeneously distributed as shown in Fig. 7. As at lower stress amplitudes, the dominant slip plane was the prism plane. Foils were also obtained from the same specimen as in Fig. 7, but from regions of larger cross-sectional area and hence of lower stress amplitude, and in such regions dislocation pileups on prism planes were observed. Some isolated pileups on pyramidal planes were also noted as in Fig. 8. At the highest stress amplitude investigated, ±965 MPa (±140 ksi), both prism and pyramidal systems were operative, leading to dislocation tangles as in Fig. 9. These tangles consisted of both $\langle a \rangle$ and $\langle c + a \rangle$ dislocations.

A region close to a fatigue fracture surface is shown in Fig. 10, and is

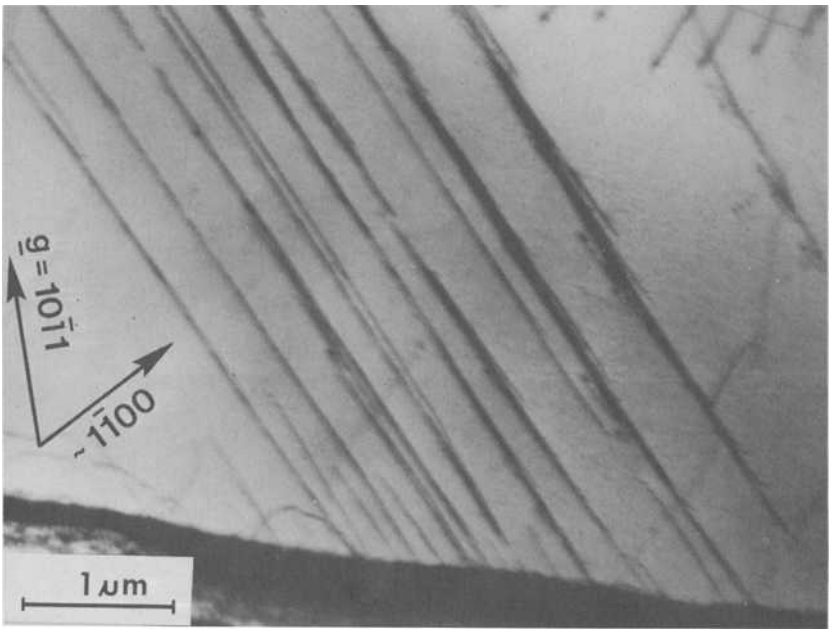

FIG. 4—*Dislocations with Burgers vector* ⟨a⟩ *on parallel prism planes at a* β*-interface. Prism planes are nearly perpendicular to the image plane. Coarsened forging:* ±*413 MPa* (±*60 ksi*); $N_f = 2.2 \times 10^6$ *cycles.*

of interest in that it shows that a specific pyramidal slip system is compatible with a slip system in the β-phase, enabling plastic deformation to propagate from one phase to the other with comparative ease. In contrast, note that the slip bands on the operative prism planes in this instance are not able to penetrate the β-phase as readily. From our observations it was clear that at low stress amplitudes prism slip was dominant, but as the stress amplitude increased, pyramidal slip also became active and general plastic deformation was promoted by the ease of slip propagation from one phase to the other as certain pyramidal slip systems became operative. Some basal slip was detected in the present analysis, but it was restricted to thin foils taken very near the fracture surface. Thus from our observations basal slip was found not to be an important slip mode in the fatigue deformation of these specimens.

A cross section through one of the fracture origins is shown in Fig. 11 [*10*]. The fracture is at 55 deg to the tensile axis and is entirely within a prior β grain. From the orientation of the colonies with respect to the facet it was suggested that the facet lies along a prism plane [*10*]. In additional studies of this nature there are indications that the facet plane may also be a basal plane [*3,11*]. The orientation of the facet indicates

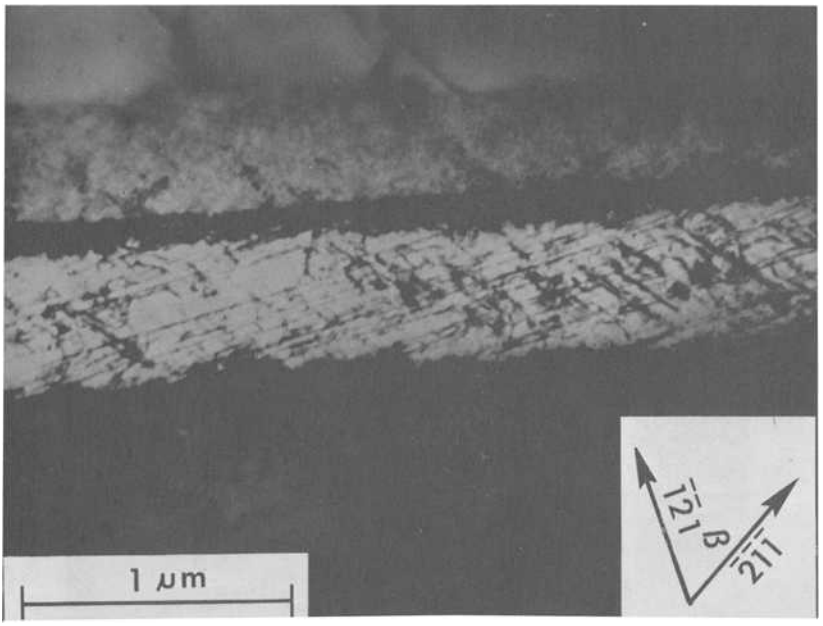

FIG. 5—*An example of multiple {112} slip in the β-phase of the coarsened forging. Dislocation debris (tangles) along intersections of slip bands. Note presence of interphase phase adjacent to β-phase.* [± 413 *MPa* (± 60 *ksi*), $N_f = 2.2 \times 10^6$ *cycles*].

that crack propagation occurred by a crystallographic or Stage I type of growth mechanism. As the initial crack grows into an adjacent β-grain or sometimes into a differently oriented colony, the mode of growth changes to a Stage II type. The size of the facet apparently depends upon the crystallographic relationship of adjacent colonies. If the relationship is unfavorable, the facet size may be limited by the colony size; on the other hand, if favorable, the facet may extend over several colonies. Further, when adjacent colonies belong to certain specific variants of the Burgers relation, it is possible for a crack on a prism plane in one colony to propagate without planar deviation on the basal plane of an adjacent colony.

Discussion

Based upon the foregoing observations it seems clear that subsurface fatigue crack initiation can indeed occur in the Ti-6Al-4V alloy in the absence of any local defect such as a microvoid or inclusion. It is of interest therefore to consider the mechanism by which such a fatigue crack can be initiated. In this regard Neal and Blenkinsop [*2*] at one time suggested that ⟨*a*⟩-type dislocations piled up on prism planes at boundaries

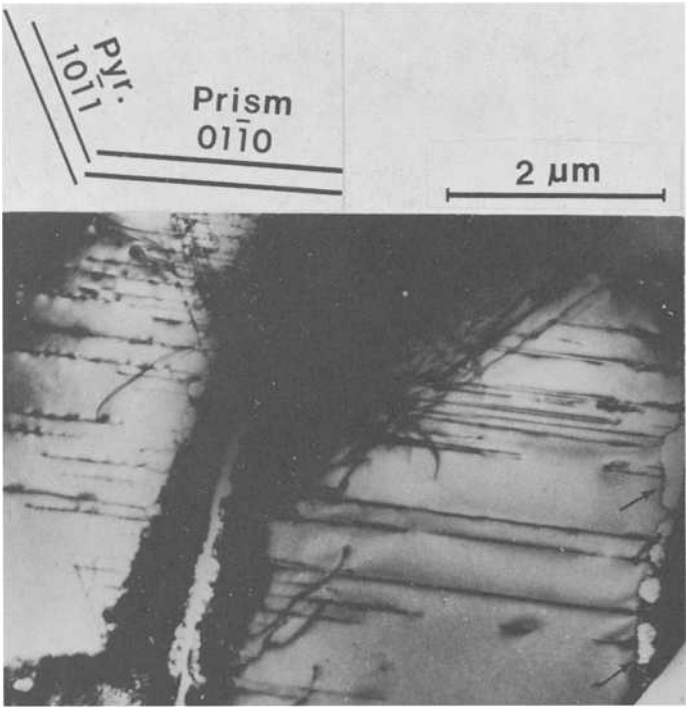

FIG. 6—*Prism slip* $\{1\bar{1}00\}$, *Burgers vector* ⟨a⟩, *propagating through* β*-phase in coarsened forging. Note absence of interphase cracking. An unidentified phase along* β*-interface is marked by arrows. Pyramidal slip* $\{1\bar{1}01\}$, *Burgers vector* ⟨c + a⟩, *also indicated* [±413 *MPa* (±60 *ksi*), $N_f = 2.2 \times 10^6$ *cycles*].

might trigger fracture by the Stroh mechanism [*12*] along a near-basal plane, that is, $\{10\bar{1}7\}$. However, this does not appear to be a geometrically correct model, and in fact Neal and Blenkinsop no longer hold to this view [*13*]. We look therefore for an alternative explanation.

In considering the boundary conditions for crack initiation under cyclic conditions, we note that principal pileups are on prism planes at α-β interfaces involving dislocations of ⟨*a*⟩ Burgers vector, and therefore we suspect that cracking is initiated in the vicinity of this interface. More specifically, since slip is suppressed at colony boundaries [*3*], we believe that the initiating site is located at an α/β interface within a colony. Further, we suspect that hydrogen, sometimes a cause of subsurface fracture, is not involved in this case. We have not observed any hydrides in this alloy, and Konieczny [*14*] found no effect on the fatigue life of this material after reducing the hydrogen content from 80 to 40 ppm. We also note that monotonic shear of the two-phase region does not lead to cracking; for example, large slip offsets along prism planes without crack

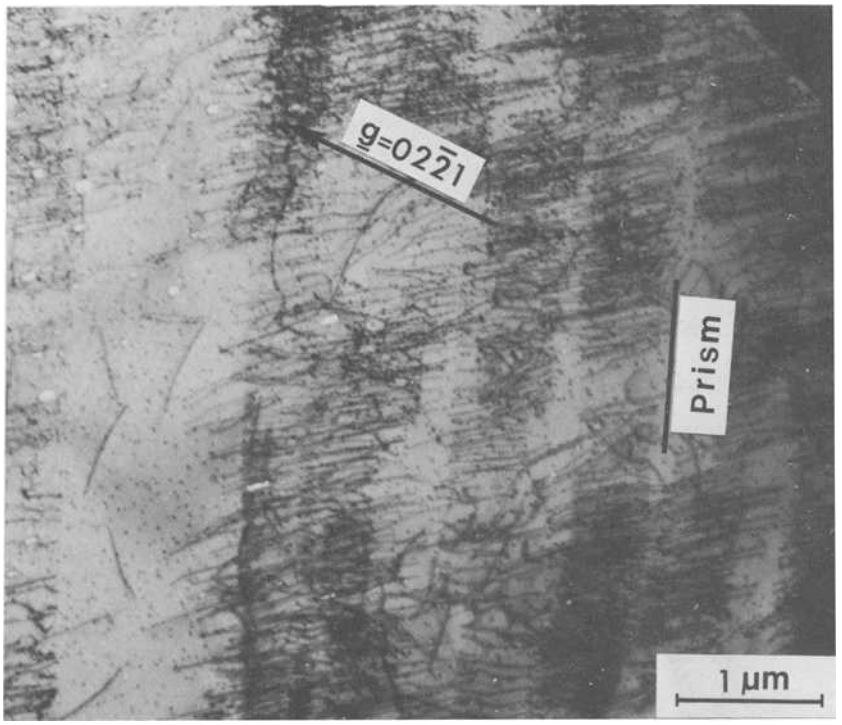

FIG. 7—*An example of arrays of dislocations of the same sign on a prism plane, Burgers vector* ⟨a⟩, *in coarsened forging at* ±*710 MPa* (±*103 ksi*), N_f = *7090 cycles. At this stress amplitude this type of array is continuously distributed.*

formation have been noted by Eylon and Hall [*3*]. Therefore something of a cyclic nature is probably involved, although the possibility of cracking of the β-phase as a result of a dislocation pileup exists. Figure 5 indicates that this phase is ductile, however, and we would expect it to deform plastically rather than crack. That pileups in some way are involved in the fracture process is supported by the large Bauschinger effect observed in this alloy as well as the fact that the alloy cyclically softens so that the number of dislocations in a pileup might increase with cycling under constant loading range testing [*1,5,6*].

Taking these various factors into consideration, a model of the following type is proposed to explain the occurrence of subsurface crack initiation. In Fig. 12, ⟨*a*⟩-type dislocations in the α-phase are piled up on a prism plane at an α-β interface. To accommodate this attendant plastic deformation, it is necessary that at least two slip systems operate in the β-phase. We assume that the two slip systems whose ⟨111⟩ are coplanar with the Burgers vector of the α-phase are the operative systems. On loading, the

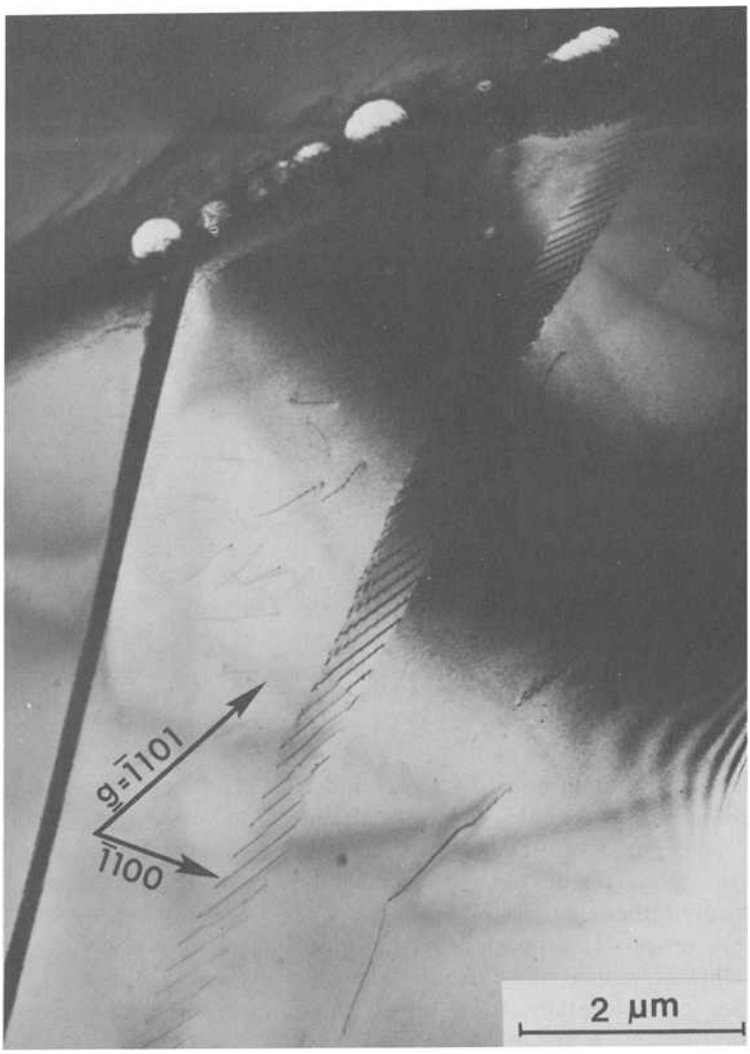

FIG. 8—*An example of an isolated dislocation pileup on a pyramidal plane. Burgers vector* ⟨c + a⟩. *Foil from same specimen as in Fig. 7, but from a region of lower stress.*

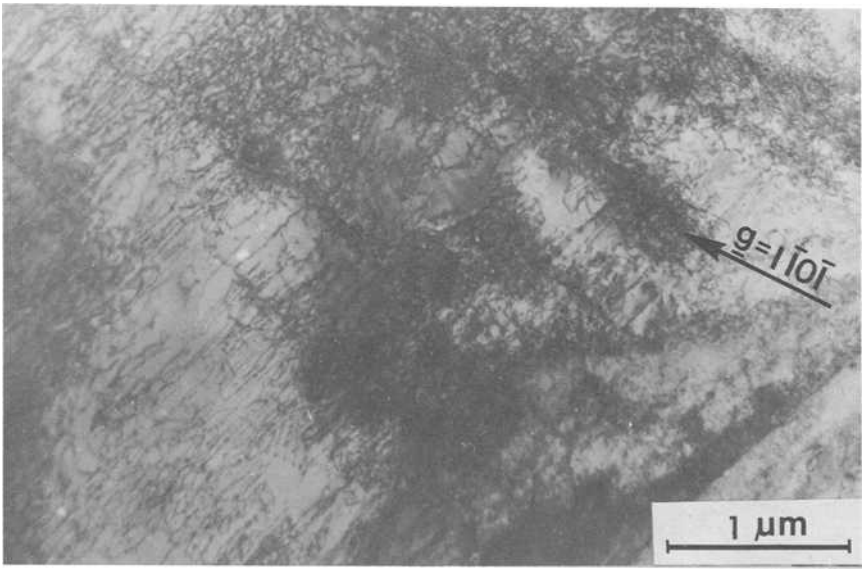

FIG. 9—*An example of dislocation tangles on both prism and pyramidal planes at a high stress amplitude* [± 965 *MPa* (± 140 *ksi*), $N_f = 100$ *cycles*].

dislocations in the β-phase of these two systems move away from each other, Fig. 12*a*. On reversal of the load the same dislocations in the β-phase now move toward each other and are assumed to coalesce to give a resultant displacement perpendicular to the {001} cleavage plane in the β-phase. This results in a situation similar to Cottrell's cleavage knife mechanism for initiation of a {100} cleavage in bcc metals [*15*]. In the present case the β-phase will cleave along a (001) cleavage plane as shown in Fig. 12*b*. The very planar nature of the slip in α will serve to localize the slip in β and promote this process of coalescense. Cracking in the {100} plane in the β would also be facilitated by the tensile stresses generated by the pileup in the α-phase at the interface. Once the crack is formed, it is then assumed to propagate across the β-platelet as indicated in Fig. 12*c*. It is possible that this crack is propagated either by cyclic loading or by fast cleavage.

In the proposed mechanism, certain simplifying assumptions have been made. For example, any contribution of the interphase phase to the fracture process has not been included. We note also that the mechanism would be expected to operate selectively in those colonies wherein the operative prism plane is close to the direction of maximum shear stress.

In support of the proposed model, the following additional evidence is provided. Figure 13 is a view of an internal fracture facet in a β quenched and annealed specimen. The main point of interest is that the fracture

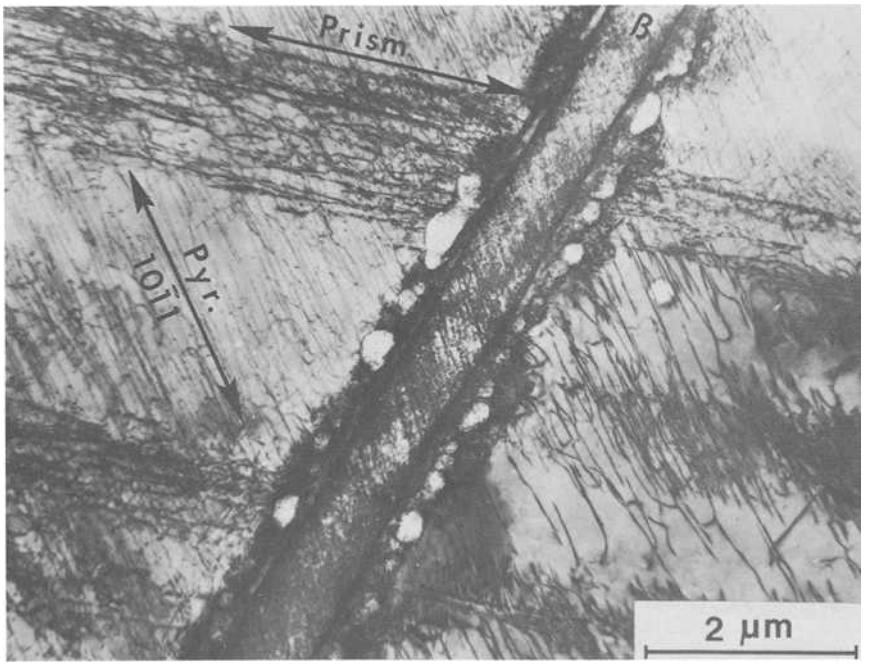

FIG. 10—*An example of dislocations in region close to fracture surface showing continuity of pyramidal slip through β on {110}. Note that prism slip has greater difficulty in penetrating β [±413 MPa (±60 ksi), $N_f = 5.1 \times 10^6$ cycles].*

origin in this case is linear in nature, and, to indicate this in better detail than the micrograph shows, a sketch of the origin and associated tear lines is shown in Fig. 13*b*. Somewhat similar regions are also observable close to and parallel to the line identified as the origin, and may be secondary fractures. We assume that the line in Fig. 13 is a β-platelet which has been fractured by cyclic loading by the aforementioned mechanism.

Once the crack has been formed in the β-phase, its manner of propagation through the colony is next of interest. As noted in the foregoing, the facet angles with respect to load axis were close to either 15, 45, or 75 deg, and we suggest two possible mechanisms which could account for these facet inclinations. Figure 14 provides one mechanism whereby propagation in α takes place utilizing two of the prism slip systems such that the resultant cracking plane is apparently along a prism plane. Since we expect that the pileup plane is the plane of maximum shear stress, the resultant crack plane in this case could be at angles close to 75 or 15 deg to the load axis.

The second proposed mechanism results in crack propagation along the primary slip plane and is illustrated in Fig. 15. The crack front is

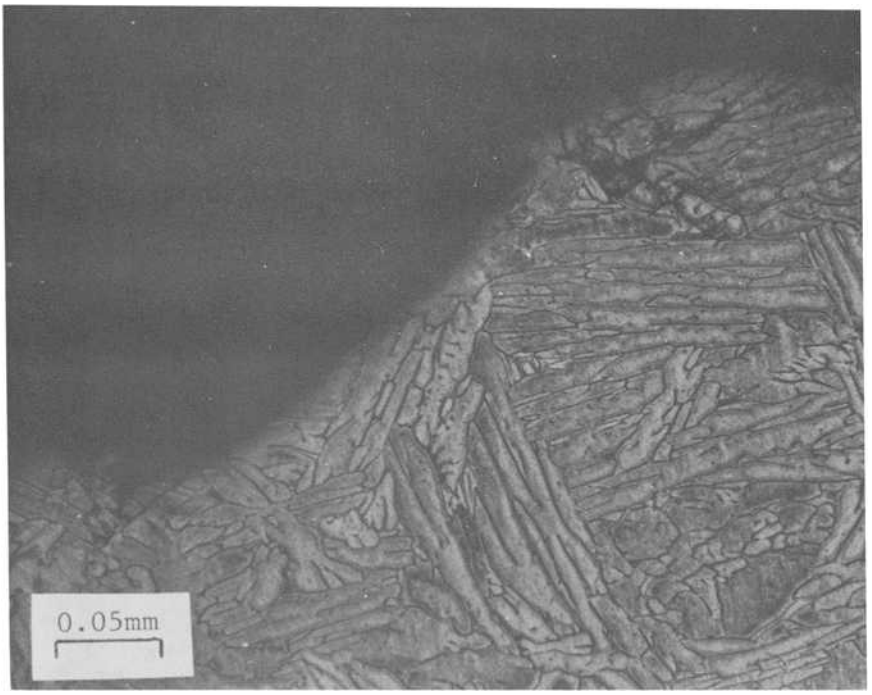

FIG. 11—*Cross section through fatigue fracture origin in coarsened forging. The angle between the fracture facet plane and the tensile direction is 55 deg. Orientation of the β-phase with respect to the fracture facets suggests that the facet is a prism plane.*

along the intersection of a prism plane and the interface plane, Fig. 15*a*. On the forward cycle, a displacement b is introduced by the forward motion of a dislocation on a prism plane, Fig. 15*b*. Figure 15*b* also shows that part of the dislocation segment AB′ has moved to a different but parallel prism plane via cross slip through a basal plane, leaving segment BB′ on the basal plane. Next, on the backward cycle, the segment AB′ moves back on its slip plane and eventually cross slips to a basal plane, Fig. 15*c*. In doing so, it intersects segment BC and creates a loop as shown in the inset of Fig. 15*c*. Note that the segment BC can also move back, but it is assumed that its motion is not fully reversible. Thus, each cycle will tend to leave a dislocation loop in front of the crack tip while the crack advances by b. This process can be repeated by the segment AC in subsequent cycles, resulting in crack advance along a prism plane. The loops generated in front of the crack tip may move out of the crack path through utilization of other intersecting slip systems as shown in Fig. 16. For example, Slips S_I and S_{II} in the forward and reverse cycles, respectively (Fig. 16*b* and *c*), can displace the material containing the dislocation loop.

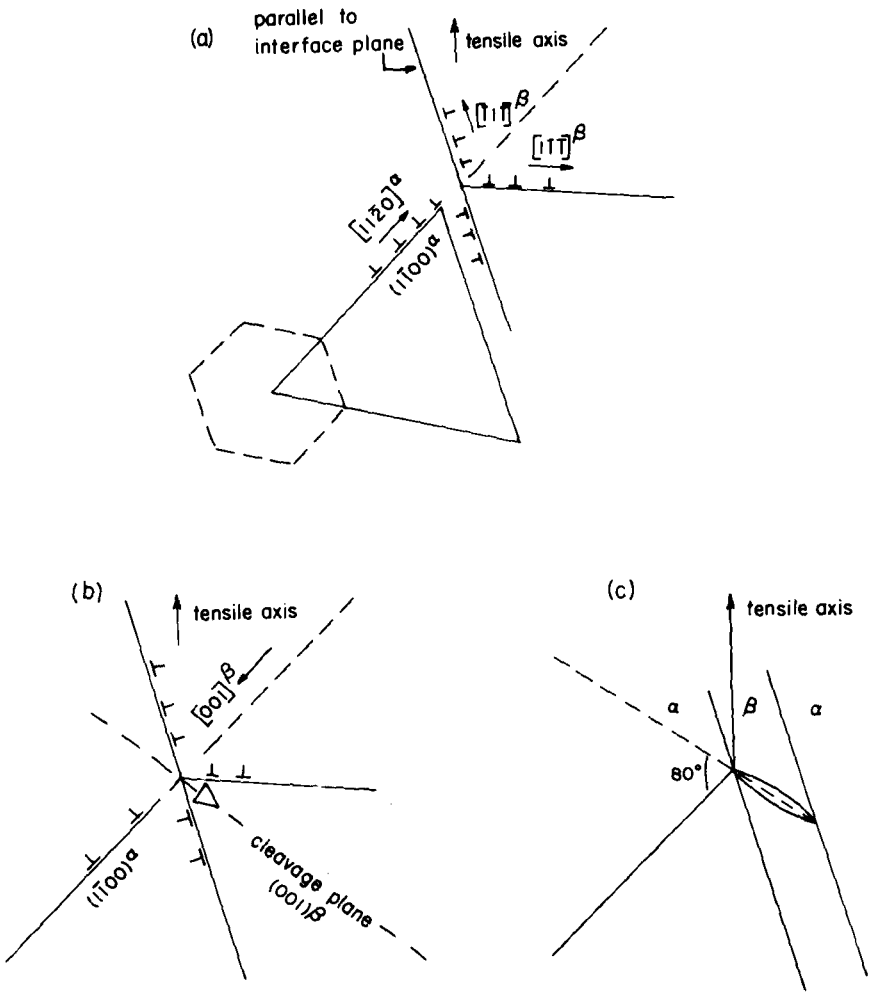

FIG. 12—*Proposed model for crack initiation in β due to cyclic loading.* (a) *On loading, slip in α is accommodated by slip on two planes of different Burgers vectors in β.* (b) *On reversal of loading, dislocations in β coalesce to give a [001] displacement and initiate a crack on a (001) of β.* (c) *Crack grows across β. Projection of (001) β plane into α-phase is at 80 deg to initial prism slip plane in α.*

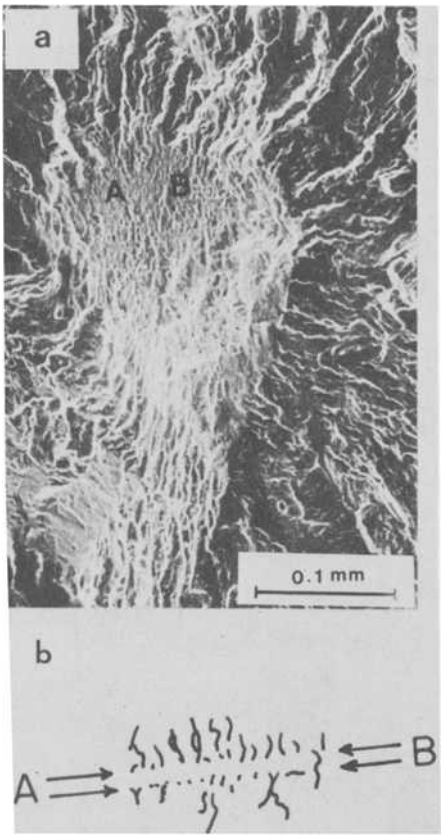

FIG. 13—*An example of fatigue crack initiating at the β-phase in a β-quenched and annealed specimen [at ±379 MPa (±55 ksi) after 10^7 cycles].* (a) *SEM micrograph* [16]; (b) *sketch of fracture origin characteristics.*

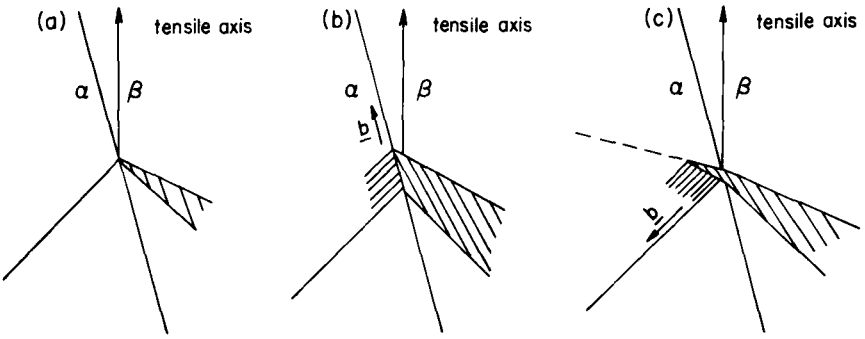

FIG. 14—*Schematic model for fatigue crack growth in α-phase following crack initiation in β-phase. Slip in α occurs on two prism planes, giving rise to propagation along a third prism plane.*

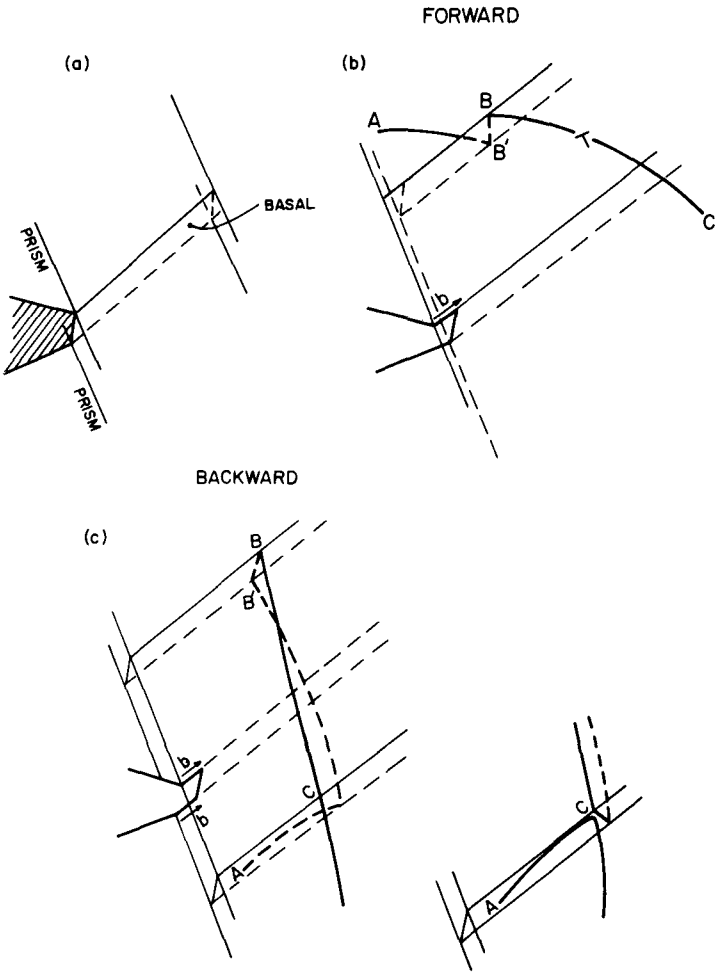

FIG. 15—*Proposed mechanism by which the subsurface fatigue crack can propagate along a primary prism slip plane through the formation of dislocation loops ahead of crack tip. See text for details.*

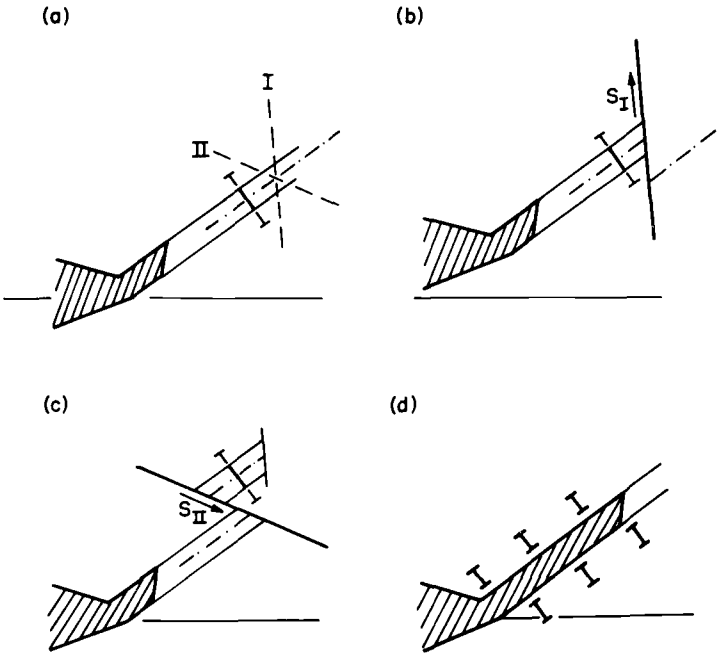

FIG. 16—*Proposed mechanism by which dislocation loops are removed and distributed on either side of the crack path. See text for details.*

Thus the loops will be distributed on either side of the crack front. Intensive plastic deformation occurs during this initial growth process and microbeam X-ray diffraction patterns are so blurred that attempts at orientation determination have thus far been unsuccessful.

Just when in the lifetime of a fatigue specimen this subsurface cracking initiates is not clear. Certainly Chait and DeSisto [*4*] have observed by acoustic emission that detectable cracking occurs late in life. However, it is possible that Stage I cracking occurs early in life soon after the intensifying pileup in the α is able to force slip into the β. Stage I cracking may be a process not as readily detected by acoustic emission as is the Stage II type of growth, which occurs late in life.

Concluding Remarks

In the previous section we have proposed a novel mechanism to account for subsurface fatigue crack initiation in α-β alloys wherein the two phases are closely interrelated as in Widmanstätten structures. In alloys heat-treated such that large volume fractions of primary α are present, perhaps the more usual surface type of crack initiation process may be operative,

but confined to the α-phase. It should be noted however that Savage and Avery [*17*] have observed that the surface layers of titanium 100A are apparently more resistant to plastic deformation than are the interior regions and this may favor subsurface nucleation. Perhaps oxygen pickup in the surface layers either during specimen preparation or during testing is responsible for such behavior. Surface fatigue crack initiation may also be important at high stress amplitudes if compatible slip between α- and β-phases can occur along pyramidal planes as noted in Fig. 10. In fact, Koss and Chan [*18*] have observed instances of compatible slip taking place during monotonic plastic deformation. However, where prism slip is the dominant mode and the two phases are closely intermixed, crack initiation during axial fatigue cycling will be expected at subsurface sites since there will be a higher probability of finding a suitably oriented colony at other than surface locations.

Acknowledgment

The authors express their appreciation to Professor S. Taira and Dr. K. Tanaka of Kyoto University and to Dr. M. Blackburn of United Technology Corp. for helpful discussions and assistance during the course of this work. The financial support for the research provided by the Air Force Office of Scientific Research, Grant 74-2703, is also gratefully acknowledged.

References

[*1*] Steele, R. K. and McEvily, A. J., *Engineering Fracture Mechanics*, Vol. 8, 1976, pp. 31-37.
[*2*] Neal, D. F. and Blenkinsop, P. A., *Acta Metallurgica*, Vol. 24, 1976, pp. 59-63.
[*3*] Eylon, D. and Hall, J. A., *Metallurgical Transactions*, A, Vol. 8, 1977, pp. 981-990.
[*4*] Chait, R. and DeSisto, T. S., *Metallurgical Transactions*, A, Vol. 8, 1977, pp. 1017-1020.
[*5*] Steele, R. K. and McEvily, A. J. in *Proceedings*, Third International Conference on Titanium, Moscow, U.S.S.R., 1976.
[*6*] Steele, R. K. and McEvily, A. J. in *Fracture Mechanics and Technology*, G. C. Sih and C. L. Chow, Eds., Sijthoff and Noordhoff, Netherlands, 1977, p. 33.
[*7*] Williams, J. C. in *Titanium Science and Technology*, R. I. Jaffee and H. M. Burte, Eds., Vol. 3, Plenum Press, New York, 1973, pp. 1433-1494.
[*8*] Williams, J. C. and Rhodes, C. G., *Metallurgical Transactions*, A, Vol. 6, 1975, pp. 1670-1671.
[*9*] Margolin, H., Levine, E., and Young, M., *Metallurgical Transactions*, A, Vol. 8, 1977, pp. 373-377.
[*10*] Eylon, D. et. al, "HCF Crack Initiation Analysis at Ti-6Al-4V by Precision Sectioning," to be published.
[*11*] Shechtman, D. and Eylon, D., *Metallurgical Transactions*, Vol. 9A, 1978, pp. 1018-1020.
[*12*] Stroh, A. N., *Advances in Physics*, Vol. 6, 1957, pp. 418-465.
[*13*] Blenkinsop, P. A., private communication, 1978.
[*14*] Konieczny, P. P., "The Effects of Hydrogen Content and Grain Coarsening on the Fatigue Strength of Ti-6Al-4V," M.S. thesis, Rensselaer Polytechnic Institute, Hartford, Conn., 1973.

[15] Cottrell, A. H., *Transactions* American Institute of Mining, Metallurgical, and Petroleum Engineers, Vol. 212, 1958, p. 192.
[16] Taira, S. and Tanaka, K., private communication, 1978.
[17] Savage, E. I. and Avery, D. H., "The Effect of the Surface on the Plastic Behavior of Titanium," The Metallurgical Society-American Institute of Mining, Metallurgical, and Petroleum Engineers, Fall Meeting (Chicago) Abstracts, 1977, p. 76.
[18] Koss, D. A. and Chan, K., "On Slip and Yielding of Alloys with Lamellar Microstructures," submitted for publication, 1978.

DISCUSSION

T. Mura[1] *(discussion)*—Most of you realize, after looking at the program of this session, that the chairman, Jeffrey Fong, intentionally put theorists as discussers for experimental papers. So I have no criticism of the present paper's experiments, but I have some opinions from the viewpoint of a theorist, particularly looking from a micromechanics viewpoint.

I would like to discuss here the stress concentrations of the piled-up dislocations in terms of the elastic moduli of the two phases, and also to discuss the instability of plastic flow in ellipsoidal inclusions by which weak zones in the material are simulated.

Let us consider first the piled-up dislocations in Phase "1" at an interface between two phases, "1" and "2," which can be considered as α and β phases, respectively. The stress components near the interface in Region "2" are obtained as for small $|x|$

$$\sigma_{12}(x) = -\frac{G_2 G_2}{G_1}\frac{b}{\sin \pi k}$$

$$\left[\frac{2k+1}{1+(3-4\nu_1)G_2/G_1} - \frac{2k-1}{(3-4\nu_2)G_2/G_1}\right]\frac{1}{|x|^{1-k}} \qquad (1)$$

where, according to Barnett[2]

$$0 < (1-k) \leq 1/2 \quad \text{if} \quad G_2/G_1 \geq (3-4\nu_2)/(3-4\nu_1)$$

$$1/2 \leq (1-k) < 1 \quad \text{if} \quad G_2/G_1 \leq (3-4\nu_2)/(3-4\nu_1)$$

G_1 and ν_1 are, respectively, the shear modulus and Poisson's ratio in Phase "1." Due to this large stress concentration at the interface, crack initiation

[1]Department of Civil Engineering, Northwestern University, Evanston, Ill. 60201.
[2]Barnett, D. M., *Scripta Metallurgica*, Vol. 3, 1969, pp. 543-546.

can be expected on a crystalline plane where the maximum tensile stress exerts.

The consideration just mentioned is rather limited to local phenomena at the interfaces. If the two-phase material is observed from a more overall structure, the material can be considered as a mixture of ellipsoidal inclusions and the matrix, which can be assumed to be α-phase and β-phase, respectively (see Fig. 17). For simplicity it is assumed that the ellipsoids are arranged in the x_1- and x_2-directions. Then the stress $\sigma_{12}{}'$ and strain $\epsilon_{12}{}'$ inside Inclusion "1" have the relation

$$\sigma_{12}{}' = -2G_2\left(\frac{1}{2S_{1212}} - 1\right)(1-f)\,\epsilon_{12}{}' + \sigma_{12}{}^A\left\{\frac{1}{2S_{1212}} - f\left(\frac{1}{2S_{1212}} - 1\right)\right\} \quad (2)$$

where

f = volume fraction of the ellipsoids,
$\sigma_{12}{}^A$ = applied stress, and
S_{1212} = Eshelby's constant,
= 7/30 for spherical ellipsoids, and
= 15/30 for penny-shaped ellipsoids.

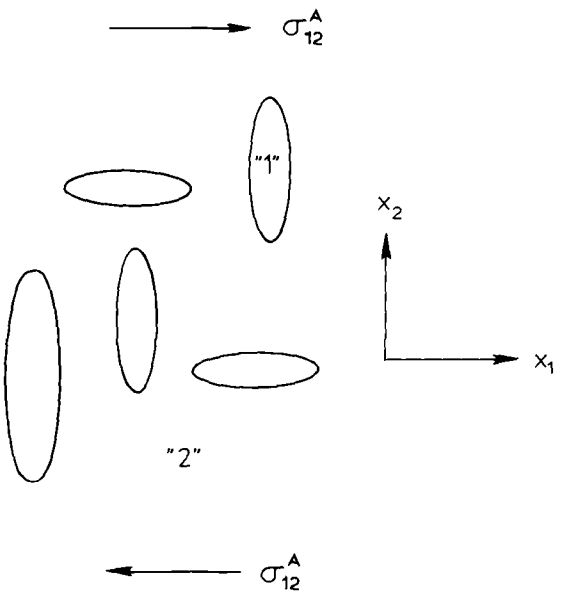

FIG. 17

Equation 2 was first obtained by Rudnieki[3] for an isolated inclusion where $f = 0$. In Fig. 18, Eq 2 is shown as the straight line ACDB for a given $\sigma_{12}{}^{A}$. If the constitutive equation of the inclusion is expressed by curve OCP, Point C is uniquely determined for a given $\sigma_{12}{}^{A}$ as the intersection of the straight line and the curve. On the other hand, if the constitutive equation is expressed by the curve ODQ, for instance, the plastic flow inside the inclusion becomes unstable, and perhaps cracks will be initiated to accommodate deformation.

J. Ruppen (authors' closure)—Professor Mura in his discussion indicates that a large stress concentration could occur in a second phase from a dislocation pileup in the first phase. This stress concentration might be an aid, in our model, in cleaving the β on the (001) plane. The β cleavage plane is at 80 deg to the α pileup plane. For a single-phase material, Stroh's calculation showed that the maximum tensile stress occurs on a plane at 75 deg to the pileup plane. Thus, we expect a higher tensile stress across the β cleavage plane.

Mura—Did you observe the crack at 45 deg, too?

Ruppen—Yes, we have observed facets at angles close to 45 deg.

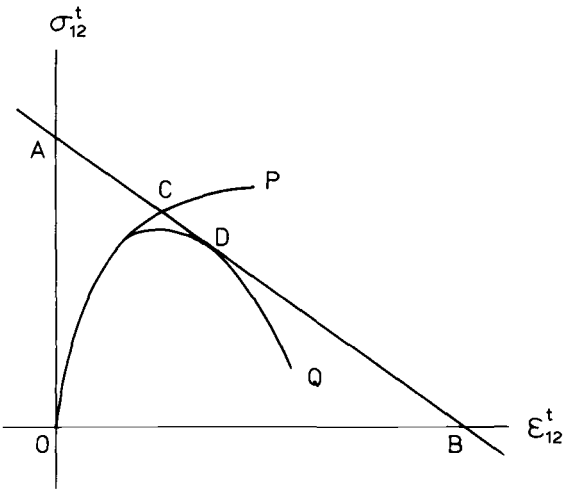

FIG. 18

[3] Rudnicki, J. W., *Journal of Geophysical Research*, Vol. 82, 1977, pp. 844-854.

P. Neumann[4] (*discussion*)—The proposition was made that the backrunning dislocations form a Lomer-Cottrell lock, and then the other dislocations, coming from the other grain, are piled up against this lock, and they therefore form a crack due to the stress concentrations.

If such a proposal is made, it should be checked whether it is really energetically more favorable to form a crack by the pileup instead of disintegrating the Lomer-Cottrell lock with the help of the pileup stress. Was such a comparison made?

J. Ruppen (*authors' closure*)—Our model is not one of forming a pileup against a Lomer-Cottrell lock. What we suggest is that the backrunning dislocations on the two slip planes within the β-phase can react to give a displacement perpendicular to a $\{100\}\beta$ cleavage plane. This creates a situation where the cleavage knife mechanism proposed by Cottrell for $\{100\}$ cleavage in bcc metals could be applied. The β-plate is thin and there was no pileup in β. Pileups, whose role in our model is to initiate localized slip in β, form only in α.

[4]Max-Planck-Institut fur Eisenforschung Gmbh, Dusseldorf, Germany.

H. Mughrabi,[1] *F. Ackermann,*[1] *and K. Herz*[1]

Persistent Slipbands in Fatigued Face-Centered and Body-Centered Cubic Metals

REFERENCE: Mughrabi, H., Ackermann, F., and Herz, K., **"Persistent Slipbands in Fatigued Face-Centered and Body-Centered Cubic Metals,"** *Fatigue Mechanisms.* Proceedings of an ASTM-NBS-NSF symposium, Kansas City, Mo., May 1978, J. T. Fong, Ed., *ASTM-STP 675,* American Society for Testing and Materials, 1979, pp. 69-105.

ABSTRACT: The cyclic stress-strain response, the development of persistent slipbands (PSB's), and the related dislocation microstructures have been investigated on single crystals of face-centered-cubic (fcc) copper, nickel, and silver and of body-centered-cubic (bcc) α-iron and niobium at room temperature. The formation of PSB's as a bulk phenomenon appears to be a general feature in fcc metal single crystals and can be described remarkably well in a simple model based largely on Winter's work. The present work clarifies and emphasizes the special roles of cross slip and of long-range internal stresses in the formation of the matrix structure, in the nucleation of PSB's, and in the steady-state deformation occurring in the PSB's. In pure bcc metals, on the other hand, PSB's are not found to be a feature of comparable generality. Under typical testing conditions, cyclic deformation of bcc metals occurs by the low-temperature deformation mode, characterized by the low mobility of the screw dislocations and impeded dislocation multiplication. However, a deformation mode similar to that in fcc metals, accompanied in some cases by the formation of PSB's as a bulk feature, is found under special conditions: low strain rate, elevated temperature (below the regime of self-diffusion), and the presence of interstitial impurity atoms. In conclusion, some general requirements that appear essential to the development of PSB's in fatigued metals are formulated.

KEY WORDS: cyclic stress-strain response, fatigue, persistent slipbands, copper, nickel, silver, α-iron, niobium, single crystals, dislocation microstructure, long-range internal stresses, cross slip, nucleation (of persistent slipbands), strain rate, interstitial impurities, dynamic strain aging, fatigue failure

A widespread feature of metal fatigue at low to intermediate amplitudes is the appearance on the surface of so-called persistent slipbands (PSB's)

[1] Research associate, doctorate student, and former doctorate student, respectively, Max-Planck-Institut für Metallforschung, Institut für Physik, 7000 Stuttgart 80, Federal Republic of Germany; coauthor Herz is now with Staatliche Materialprüfungsanstalt, Universität Stuttgart, 7000 Stuttgart 80, Federal Republic of Germany.

[1][2] which act as preferential sites for the nucleation of cracks [*1,2*]. In polycrystals the PSB's are largely a surface phenomenon and their investigation is confined to near-surface regions [*1-3*]. The recognition that in single crystals PSB's can traverse the whole cross section [*4-7*] has opened the possibility of studying their behavior as a bulk phenomenon. Recent work, in particular on copper single crystals [*4-13*], has led to an improved understanding of the evolution and the properties of PSB's in metals of the face-centered-cubic (fcc) structure. Similar observations on metals of other crystal structures are required in order to assess whether the development of PSB's is a general feature of metal fatigue, as has been suggested by some authors [*7,9,14,15*].

In this paper we present and contrast some recent observations on the cyclic deformation of single crystals of copper, nickel, and silver, and of α-iron and niobium as typical fcc and body-centered-cubic (bcc) metals, respectively. The interest in the cyclic deformation of bcc metals has its origin in well-documented similarities and differences of their mechanical properties with respect to those of fcc metals [*16-19*].

The Idealized Model

A simple model of the behavior of PSB's in single crystals as a bulk feature has emerged out of research on copper single crystals [*6-13*]. Figure 1 shows an idealized plot of the resolved shear stress τ_s in saturation as a function of the plastic resolved shear strain amplitude γ_{pl}. Such a cyclic stress-strain curve had been predicted by Winter on the basis of his studies of PSB's as a function of γ_{pl} [*9*] and had also been described by Grosskreutz and Mughrabi [*13*] in more qualitative terms.

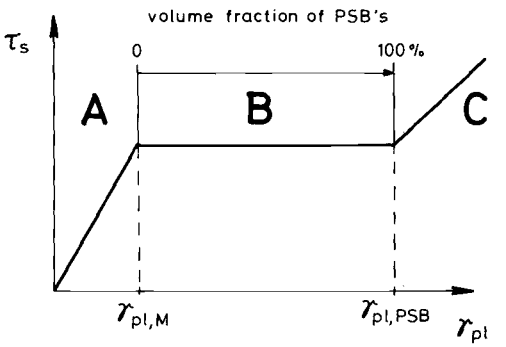

FIG. 1—*Idealized cyclic stress-strain curve of single crystal specimens exhibiting the formation of PSB's.*

[2]The italic numbers in brackets refer to the list of references appended to this paper.

According to Fig. 1 the cyclic stress-strain response falls into three regimes. In Range A, cyclic strain hardening occurs more or less homogeneously and τ_s increases with increasing γ_{pl}. The onset of Range B is marked by the first development of PSB's in thin lamellae parallel to the primary slip plane [*4-7*]. The PSB's possess a dislocation pattern that is characteristically different from that of the "matrix" between them [*3,6,7*] and that renders them softer [*4*]. As a consequence, deformation now becomes inhomogeneous and strongly localized in the PSB's [*4,5,10*]. As γ_{pl} is increased in Range B, the volume fraction of the PSB's increases accordingly [*9-13*]. The saturation stress τ_s, representing essentially the stress required for the localized deformation of the soft PSB's, remains virtually unaffected until the end of the "plateau" Range B, when the entire crystal is filled with PSB's. Deformation at higher γ_{pl} in Range C leads once again to a new structure and an increase of τ_s. In Winter's model [*9*] the values $\gamma_{pl,M}$ and $\gamma_{pl,PSB}$ at the extremes of Range B (see Fig. 1) are identified with the plastic shear strain amplitudes that can be accommodated by the matrix and the PSB's, respectively. The underlying assumption is that the properties of the matrix and the PSB's do not depend on γ_{pl} throughout Range B.

This simple model will be used as a guideline in the present study. We shall first deal with the simpler and more thoroughly investigated behavior of fcc metal crystals before discussing the more complicated case of the cyclic deformation of bcc metal crystals.

Experimental Details

The single crystals used in this work were orientated for single slip and had the following purities (in weight percent): copper (99.999), nickel (99.99), silver (99.99), iron (99.98), and niobium (99.998). The interstitial impurity contents (carbon, oxygen, nitrogen) of the α-iron and niobium single crystals were <5 atomic ppm and <2.5 atomic ppm, respectively. Studies were also performed on α-iron single crystals that were doped with 30 wt. ppm (~ 140 atomic ppm) carbon in solid solution in the as-quenched state after annealing at 700°C.

Typically, the gage lengths of the round specimens ranged from 12 to 20 mm; in some cases gage lengths up to 6 cm were used (see Ref *12*). The specimens had the following diameters: 3 mm (nickel, α-iron, and niobium), 4 mm (copper), and 5 mm (silver), and were mounted by soldering or clamping in cylindrical grips of 6 mm diameter. Special care was taken to ensure precise alignment of specimens, grips, and gripping fixtures of the testing equipment (see Ref *12*).

Cyclic deformation was performed at room temperature using plastic strain control and frequencies between 10^{-3} and 5 Hz. Some of the copper and α-iron single crystals were deformed in a modified Schenck "Pulser"

as described in more detail elsewhere [*12*]. In all other tests a servo-hydraulic MTS equipment was used. High accuracy of strain control and measurement ($\sim 10^{-6}$) was achieved with an extensometer that was calibrated to yield a signal of 10 V for an elongation of 0.1 mm.

The results are presented for the fcc crystals in terms of the resolved shear stresses τ and τ_s (in saturation) and the resolved plastic shear strain amplitude γ_{pl}. Since single slip is not always well-defined in the case of the bcc metals [*16–19*], the results for the α-iron and niobium crystals are expressed in terms of the axial stresses σ and σ_s (in saturation) and the axial plastic strain range $\Delta\epsilon_{pl}$ (twice the amplitude). For the orientations used, $\sigma \sim 2\tau$ and $\Delta\epsilon_{pl} \sim \gamma_{pl}$. The cumulative (shear) strains are $\gamma_{pl,cum} = 4N\gamma_{pl}$ and $\epsilon_{pl,cum} = 2N\Delta\epsilon_{pl}$, where N is the number of cycles. σ_s and τ_s always denote averages of the saturation peak stresses in tension and compression. The saturation stresses were determined both by cycling individual specimens at given plastic strain amplitudes into saturation and also by attainment of saturation after stepwise increases of the amplitude [*12*] for other specimens. Typically, cumulative shear strains in excess of $\gtrsim 20$ were required to reach saturation. In the case of the bcc specimens special efforts were made to ascertain well-defined cyclic plastic strain rates $\dot{\epsilon}_{pl} = 2\Delta\epsilon_{pl}\nu$, where ν is the frequency.

The metallographic studies included surface observations by optical microscopy, using also Nomarski interference contrast, and by scanning electron microscopy (SEM) and transmission electron microscopy (TEM) of orientated foils. The TEM-micrographs of fatigued copper single crystals presented in this paper pertain to specimens in which the dislocations had been pinned by fast-neutron irradiation in the stress-applied state (Fig. 8) or after unloading (all other figures). The crystallographic notations refer to the primary Burgers vectors $\mathbf{b}_p = \frac{1}{2}[\bar{1}01]$ and $\mathbf{b}_p = \frac{1}{2}[111]$ and to the primary slip planes (111) and ($\bar{1}$01) for the fcc and bcc crystals, respectively.

Cyclic Deformation of FCC Metal Crystals

Cyclic Stress-Strain Curves

The cyclic stress-strain curves of copper and nickel single crystals are shown in Fig. 2. For the purpose of comparison, the τ_s-values were divided by the respective shear moduli $G = [c_{44}(c_{11} - c_{12})/2]^{1/2}$ (c_{11}, c_{12}, and c_{44} are the elastic moduli). The normalized saturation stresses for both metals are found to be almost identical above $\gamma_{pl} \sim 10^{-4}$. Cyclic hardening is pronounced down to amplitudes smaller than 10^{-4}, leading to τ_s-values comparable to flow stresses in Stages II and III of tensile work-hardening. The fact that this remarkable hardenability extends down to even lower γ_{pl} in

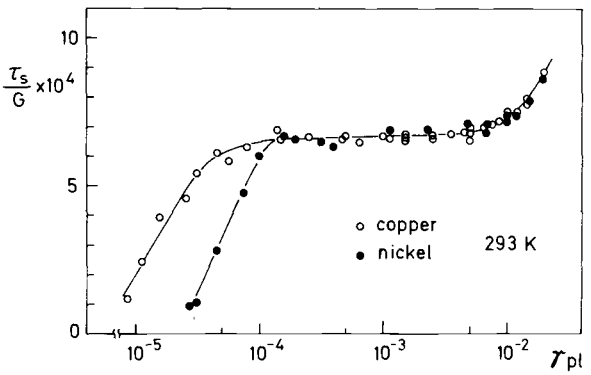

FIG. 2—*Cyclic stress-strain curves of copper and nickel single crystals. The logarithmic scale on the abscissa has only been chosen for convenient presentation.*

the case of copper as compared with nickel is suggested to be due to the higher purity of the copper single crystals.

Both cyclic stress-strain curves exhibit the basic features of the idealized curve introduced in Fig. 1 and represent, to our knowledge, the only direct evidence available of the existence of such a curve.[3] Moreover, PSB's were observed only after the onset of the pronounced plateau regimes B [*11,12,20*], which can be characterized by the set of values given in the upper half of Table 1. It should be noted that τ_s increases very weakly in Range B and that the stated τ_s-values (τ_{PSB}) refer to $\gamma_{pl} \sim 10^{-4}$. In the case of copper the values for $\gamma_{pl,M}$ and $\gamma_{pl,PSB}$ were obtained by determination of the volume fraction f of the PSB's from surface observations as a function

TABLE 1—*Characteristic parameters describing the properties of persistent slipbands and matrix in the specimens investigated.*

Metal	$\gamma_{pl,M}$	$\gamma_{pl,PSB}$	τ_{PSB}, MPa	$\frac{\tau_{PSB}}{G} \times 10^4$
Nickel	$\sim 10^{-4}$	$\sim 7.5 \times 10^{-3}$	52	6.6
Copper	6×10^{-5}	7.5×10^{-3}	27.5	6.5
Silver[a]	6×10^{-5}	7.5×10^{-3}	17.5	6.6
α-Iron + 30 wt. ppm C[a]	$\sim 4 \times 10^{-4}$ ($\Delta\epsilon_{pl}$)	$> 6 \times 10^{-3}$ ($\Delta\epsilon_{pl}$)	~ 49 ($\sigma/2$)	6.5

Values of $\gamma_{pl,M}$ and τ_{PSB} refer to the beginning and those of $\gamma_{pl,PSB}$ to the end of Range B, respectively.

[a] The behavior deviates from the idealized model.

[3] In the experiments of Hancock and Grosskreutz [*21*] on copper crystals, proper saturation had not been attained at the lowest values of γ_{pl} (which fall into Range B). Hence the apparent similarity of their published cyclic stress-strain curve with the idealized curve (Fig. 1) is misleading and not representative of the behavior discussed in this paper.

of γ_{pl} (see Refs *9,10,12*) and extrapolation to $f = 0$ and $f = 1$ [*12*]. The observations on the nickel single crystals were less detailed [*20*], but it may be noted that PSB's were first observed on the surface at $\gamma_{pl} = 1.6 \times 10^{-4}$ and that, according to Fig. 2, the ends of the plateau regimes coincide for copper and nickel, suggesting that $\gamma_{pl,PSB}$ is similar in both cases.

In the case of the silver crystals, PSB's were first observed at $\gamma_{pl} \sim 6 \times 10^{-5}$ and filled the entire gage length at $\gamma_{pl} \sim 7.5 \times 10^{-3}$ (as in the case of copper and nickel). The cyclic stress-strain curve, however, followed the idealized curve only up to $\gamma_{pl} \sim 2 \times 10^{-4}$. At higher γ_{pl}, the saturation stress increased in a complex manner with increasing γ_{pl}. These deviations from the ideal behavior will be presented elsewhere [*20*]. Here, it may suffice to state the conclusion that, in silver, impeded cross slip (low stacking fault energy) prevents an ideal adaptation of the dislocation behavior to the imposed plastic strain amplitude as in the typical wavy slip materials, copper and nickel. While TEM evidence is still lacking, the available observations indicate that the properties of the matrix and the PSB's are not independent of γ_{pl} (as required by the idealized model).

The low-amplitude cyclic stress-strain data for the three fcc metals investigated are plotted in Fig. 3. From this figure and from the observations of the PSB's, we conclude that characteristic thresholds of the stress and plastic shear strain amplitudes required for the formation of the first PSB's, expressed as τ_{PSB}/G and $\gamma_{pl,M}$, respectively, exist and have very similar values for the three metals (see Fig. 3 and Table 1).

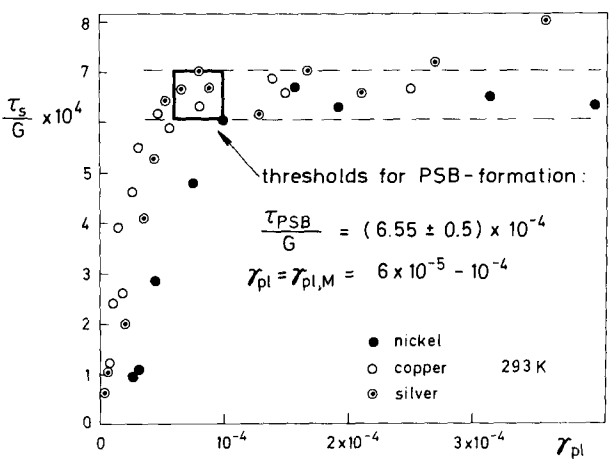

FIG. 3—*Cyclic stress-strain data for nickel, copper, and silver single crystals in the regime of very low* γ_{pl}. *The data pertaining to the formation of the first PSB's fall into the indicated rectangle.*

The mechanical tests provided two further observations of interest:

1. Saturation in Range A was always the result of gradually diminishing hardening. In Range B, on the other hand, saturation was inevitably preceded by slight cyclic softening. Such softening has been observed before [*7,9,22,23*]. As shown by Mecke [*23*], this softening is indicative of the transformation of the dislocation arrangement of the matrix into that of the softer PSB's (see also Ref *12*).

2. In Range A the hysteresis loops became slim and pointed in saturation, whereas in Range B they became more pointed during cyclic hardening and then, as saturation was approached, developed flat peaks at the beginning of Range B (see Fig. 4*a*) and became more rectangular later in Range B (see Fig. 4*b*). These latter changes were shown to be clearly related to the beginning slip activity (*plastic macroyielding*) in the PSB's [*9,12,24*], whereas the pointed hysteresis loops reflect the *plastic microyielding* of the matrix in the absence of PSB's [*12*].

Dislocation Arrangements in the Matrix and in the PSB's

The dominant features of the dislocation arrangements built up during cyclic hardening at low γ_{pl} are primary edge dislocations in dense multipole

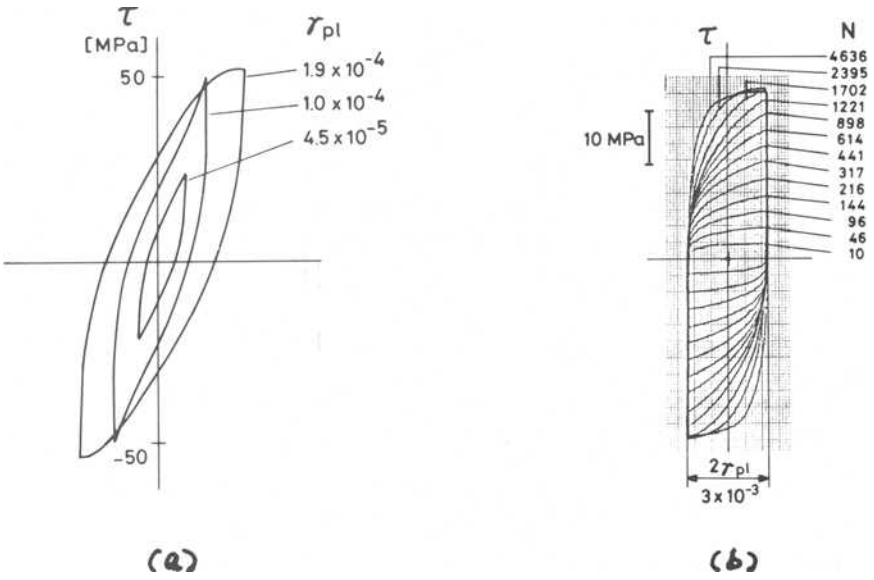

FIG. 4—*Shapes of hysteresis loops:* (a) *Saturation hysteresis loops of nickel single crystals in Range A and beginning of Range B.* (b) *Development of the shapes of the hysteresis loop during cyclic hardening of a copper single crystal at* $\gamma_{pl} = 1.5 \times 10^{-3}$. *In these plots, only the plastic component of the strain is recorded.*

configurations, called veins, separated by dislocation-poor regions [*5–13, 15,23,25*].[4] The screw dislocations are annihilated to a large extent by stress-induced cross slip as in tensile deformation [*26*]. At higher γ_{pl}, additional features develop, namely, a larger secondary dislocation content and long-range internal stresses [*13,21,28,29*]. Thus the matrix structures that evolve and out of which the PSB's develop in the approach to saturation are not strictly independent of γ_{pl} [*12,29*], as was assumed in the idealized model [*9*].

Figure 5 shows a three-dimensional TEM-construction of the dislocation arrangement of a copper single crystal in cyclic saturation at $\gamma_{pl} = 1.5 \times 10^{-3}$. The view on the $(1\bar{2}1)$-plane shows clearly the PSB's as ladder-like arrangements of walls perpendicular to $\mathbf{b}_p$ embedded in the more voluminous edge multipole veins of the matrix. The typical wall spacings in the PSB's of both copper and nickel are 1.5 μm. Apart from the mentioned dependence of the matrix structure on γ_{pl} and the fact that the volume fraction occupied by the PSB's increases with increasing γ_{pl}, Fig. 5 is representative of the dislocation arrangements in nickel and copper in Range B.

Further details follow from Figs. 6 and 7. Figure 6 is a micrograph of a foil whose plane is slightly inclined with respect to the primary glide plane (111), showing the transition from the vein to the wall structure. The observation of many short curved edge dislocation segments bowing out of the walls of the PSB-structure (in the unloaded state) indicates the existence of *long-range internal stresses* at these sites [*13,28,29*]. There is no such evidence of internal stresses in the matrix. In the dislocation-poor regions, in particular of the wall structure, primary screw dislocations can be seen bowing out weakly between the walls or veins. These screw dislocations are frequently arranged in groups [*13,28*]. Their density is much higher between the walls ($\sim 10^{13}$ m^{-2}) than between the veins ($\sim 10^{12}$ m^{-2}). The screw dislocations, which often occur as dipoles, are also visible in the $(1\bar{2}1)$-section along the direction parallel to $\mathbf{b}_p$ (Fig. 7). The observation that the narrowest screw dipoles observed have widths of $h \sim 500$ Å [*29*] suggests that this is a critical value and that narrower screw dipoles are unstable and are annihilated.

Together with other observations [*7,13,28,29*], the dislocation arrangement in the PSB's can be characterized by the following differences with respect to that of the matrix: (1) The dense dislocation arrays occupy a smaller volume fraction; (2) the secondary dislocation content is larger; (3) the density of free (mobile) screw dislocations is higher; and (4) long-range internal stresses whose amplitude corresponds to the peak stress

[4]These veins differ from the multipole bundles or braids observed after tensile deformation (see Refs *26,27*). They are more voluminous, have a higher dislocation density, and contain almost no secondary dislocations.

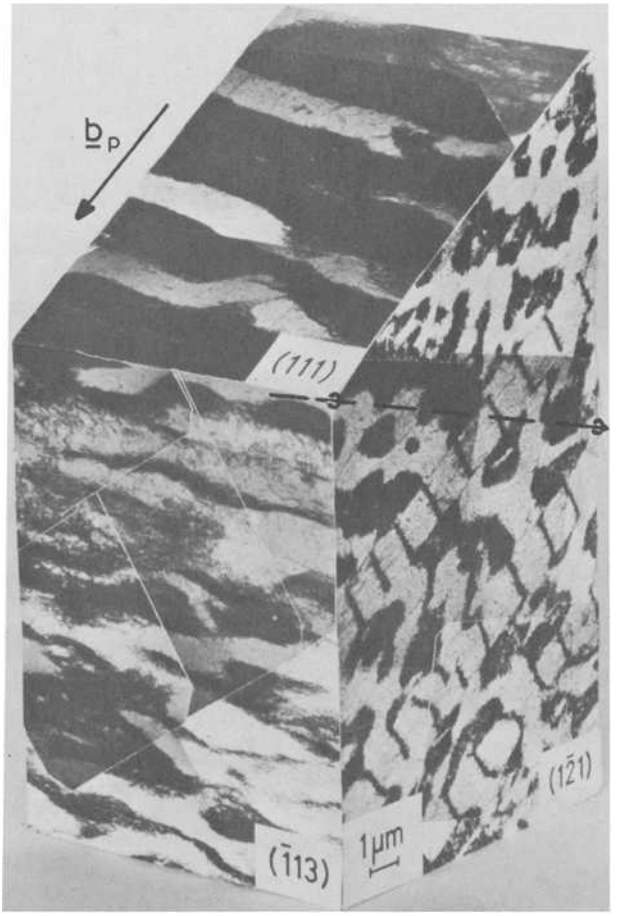

FIG. 5—*Three-dimensional construction of dislocation arrangement of a cyclically saturated copper single crystal in Range B.* $\gamma_{pl} = 1.5 \times 10^{-3}$. *The specimen axis, which is indicated by a dashed line, lies almost in the* $(1\bar{2}1)$*-plane and makes an angle of 47 deg with* $\mathbf{b}_p$.

are present. These features are considered to reflect the much larger strain localized in the PSB's with respect to the strain in the matrix [*5,9,10,12*]. This is also evident from Table 1, according to which $\gamma_{pl,PSB} \sim 10^2 \gamma_{pl,M}$.

Metastability of the Matrix; Nucleation of Persistent Slipbands

Both the matrix and the PSB's can be visualized as composites consisting of hard dislocation-rich and soft dislocation-poor components. In this picture the matrix is expected to be harder than the PSB's because of the larger volume fraction occupied by the hard component, namely, the

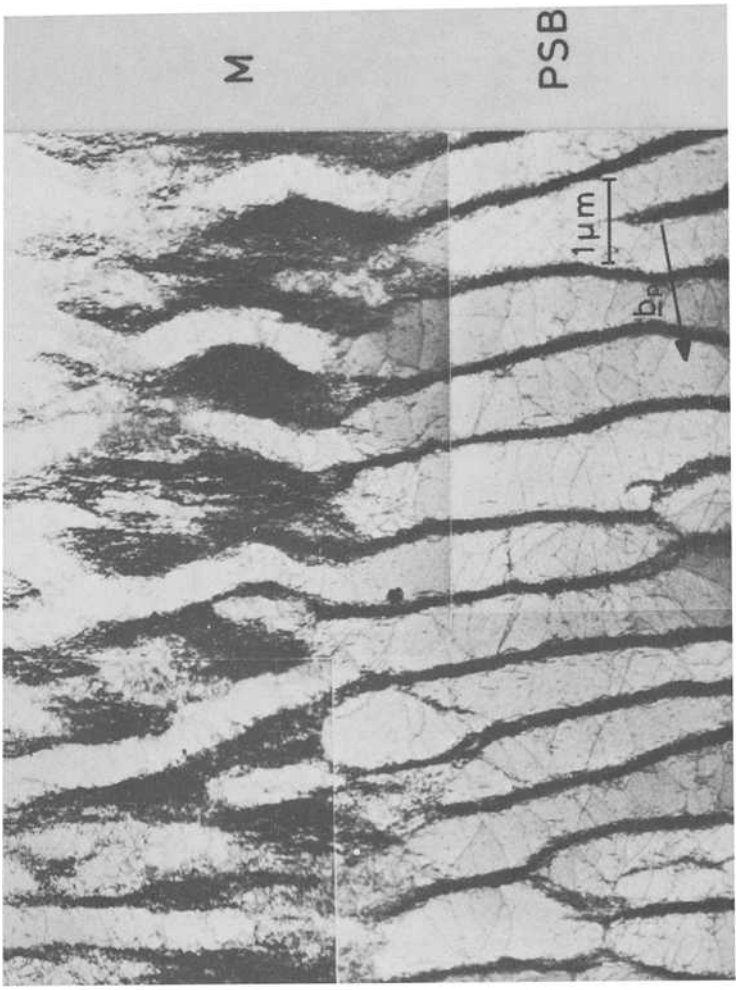

FIG. 6—*TEM-micrograph of a section that is very slightly inclined to the primary glide plane (111) of a copper single crystal in cyclic saturation at* $\gamma_{pl} \approx 10^{-3}$. *M = matrix; PSB = persistent slipband.*

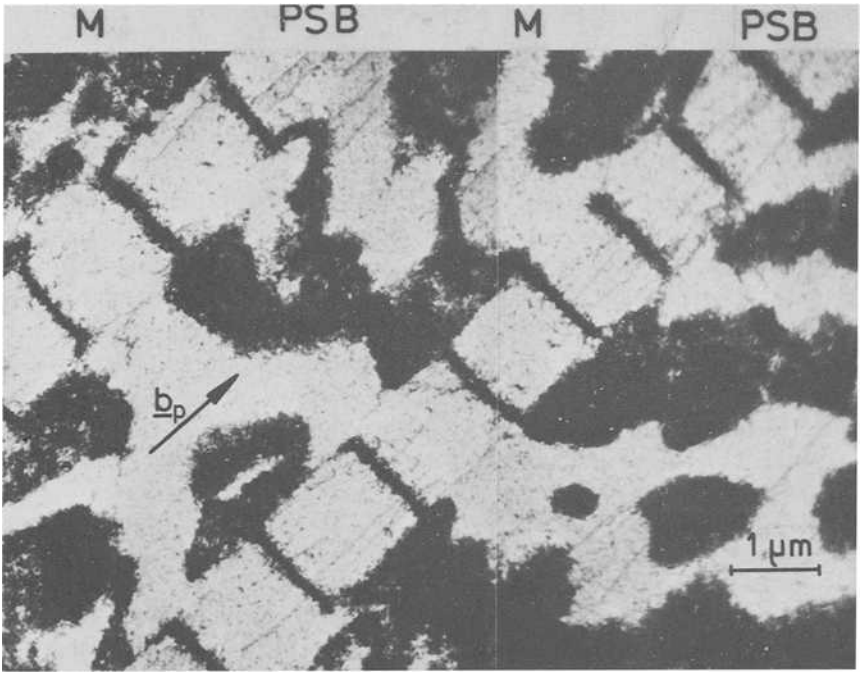

FIG. 7—*TEM-micrograph of (121)-section of same copper single crystal as in Fig. 5. Note screw dislocations in the channels between the walls of the PSB's.*

veins. The only dislocation mechanism that is considered to be capable of producing some non-hardening *plastic* strain in the veins is Feltner's [*30*] flip-flop motion of edge dipoles [*13*]. A crude estimate shows that the veins cannot accommodate plastic strains in excess of $\sim 10^{-4}$ [*13*], a value that is compatible with the values of $\gamma_{pl,M}$ in Table 1. Hence, it is reasonable to assume that the matrix cannot be strained plastically beyond this critical value unless structural changes occur at the same time. Neumann's strain burst experiments [*31*] have demonstrated that the simple multipolar veins are metastable and capable of undergoing rearrangements in an avalanche-like fashion. Provided the stress level is high enough, similar dynamic rearrangements, accompanied by fluctuating internal stresses and some secondary slip, should be able to trigger the nucleation of PSB's, if γ_{pl} is larger than $\gamma_{pl,M}$.

The stresses at which first signs of slip activity in the softer PSB's can be inferred from an analysis of the shapes of the hysteresis loops during cyclic hardening (see Fig. 4) are very nearly equal to the saturation stress at the beginning of Range B but significantly lower toward the end of Range B [*12*]. If these stresses are identified with the stresses necessary to nucleate PSB's in the matrix, it is found, for example, that in copper

single crystals the nucleation stresses τ_n are ~28 MPa at $\gamma_{pl} = 1.5 \times 10^{-4}$ and only about half as much at $\gamma_{pl} = 5 \times 10^{-3}$ [*12*]. This finds its explanation in the observation that for $\gamma_{pl} \gtrsim 10^{-3}$ the dislocation arrangement of the matrix becomes increasingly similar to that of the PSB's (see the previous section) and that the available internal stresses [*12,13,28*] can facilitate the nucleation of PSB's.

The finding that τ_n depends so strongly on γ_{pl} is difficult to reconcile with earlier suggestions that PSB's develop at a stress comparable to the stress level τ_{III} at which Stage III, characterized by profuse cross slip [*32*], begins in tensile work-hardening (see Refs *4,33–37*). Furthermore, since at the beginning of Range B, that is, in the absence of long-range internal stresses, $\tau_n \sim \tau_{PSB}$, Figs. 2 and 3 imply that τ_n/G is almost identical for nickel, copper, and silver single crystals. The consistancy of τ_n/G suggests that the nucleation process is largely athermal. If the τ_{III}-hypothesis were correct, this result, unless purely fortuitous, would be difficult to understand in view of the rather different stacking-fault energies of the three metals.

Nevertheless, we emphasize that we do assign a special significance to the ease of *cross slip* (that is, high stacking-fault energy) as a factor facilitating the development of PSB's. The elimination of the screw dislocations by cross slip is a major prerequisite for providing the simple edge multipole dislocation arrangement that appears predestined for undergoing the structural changes leading to the formation of the PSB's. The kind of stress-induced cross slip that is responsible for the mutual annihilation of screw dislocations of opposite sign, however, occurs also in tensile Stage I work-hardening [*26*] and should be distinguished [*13,38*] from the long-range cooperative cross-slip processes observed in Stage III [*32*].

Mechanisms of Steady-State Cyclic Deformation—the Roles of Internal Stresses and Cross Slip

The basic requirement of (cyclic) steady-state deformation, namely, that the dislocation density does not change, can be fulfilled by two mechanisms (see Refs *10,13*): (1) The same dislocations glide forward and backward in the absence of dislocation multiplication and annihilation and (2) There exists a dynamic equilibrium between dislocation multiplication and annihilation. We shall show in the following that Mechanism 1 applies to the matrix and Mechanism 2 to the PSB's.

The dislocation-poor regions shall be considered first. Our TEM-observations suggest that the strain in these regions is accommodated to a large extent by the glide of the primary screw dislocations [*13,28*]. Denoting the density of the screw dislocations by ρ and their mean slip distances within a quarter-cycle by L, we can write

$$\gamma_{pl} = \rho b L, \tag{1}$$

where b is the modulus of the Burgers vector. Taking into account that encountering screw dislocations of opposite sign on glide planes less than a critical distance h apart can annihilate mutually by cross slip and that screw dislocations in the PSB's can be arranged in groups [*13,28*], we obtain

$$\rho < \frac{n}{2 L h} \tag{2}$$

where n is the number of screw dislocations of one sign in a group. Combining Eqs 1 and 2 we find that annihilation will occur only if

$$\beta = \frac{2 \gamma_{pl} h}{b n} = 1 \tag{3}$$

whereas for $\beta < 1$ annihilation cannot occur. This simple criterion is applicable to any local dislocation arrangement, provided h and the local value of γ_{pl} are known. Inserting the experimental values for h ($\sim$500 Å), $\gamma_{pl,M}$ and $\gamma_{pl,PSB}$ (from Table 1), we find for the matrix and the PSB's, respectively

$$\beta_M \sim 0.024 \; (n = 1)$$

and

$$\beta_{PSB} = 1 \qquad \text{for } n = 3$$

We conclude that annihilation of screw dislocations is not important in the matrix. The result for the PSB's implies that the screw dislocations *must* be arranged in groups (of about three dislocations of the same sign). This conclusion is supported by the observation of groups of screw dislocations by TEM in the stress-applied state [*13,28*]; see also Fig. 8. In order to maintain the steady-state dislocation flux in the PSB's, some dislocation multiplication mechanism must operate continuously. We regard the bowing of edge dislocation segments out of the walls beyond the critical Frank-Read radius as the most probable mechanism. It has been pointed out earlier that, although these segments are in general too short to be activated as dislocation sources by the peak stress alone, source activation is possible with the aid of the available long-range internal stresses [*13,28*]. Figure 6 provides some indication of this process. An example of the much more direct evidence which has been obtained by TEM of copper single crystals, in which the dislocations were pinned under load by neutron-irradiation [*13,28*], is shown in Fig. 8.

In spite of recent interesting studies of the structure of the veins in the

matrix by weak-beam TEM [*39,40*], there is as yet no direct evidence for the responsible dislocation mechanisms in the veins. However, the conclusion that was derived earlier, namely, that the small plastic strain ($\gamma_{pl,M}$) in the veins must be accommodated essentially by the flip-flop motion of dislocation dipoles, suggests that in saturation neither multiplication nor annihilation of dislocations occurs in the veins.

On the other hand, the following observations indicate that the dislocation arrangement of the wall structure in the PSB's undergoes continuous changes: (1) Edge dislocations bow out of the walls and become entangled in neighboring walls; (2) edge dislocations that are newly formed in the wake of moving screw dislocations are incorporated into the walls, and (3) a larger density of point defect clusters has been observed in the walls than between them [*39,41*]. This suggests that, because of the high local dislocation density in the walls of 10^{15}–10^{16} m^{-2} [*13,39*], annihilation of edge dislocations [*42*] is a probable process. In spite of these persisting changes, it appears improbable that the walls are continuously destroyed totally and rebuilt, since the walls, as opposed to the veins, are stabilized by the entangled secondary dislocations. The main conclusion is that the localized dislocation activity in the PSB's is the result of a dynamic equilib-

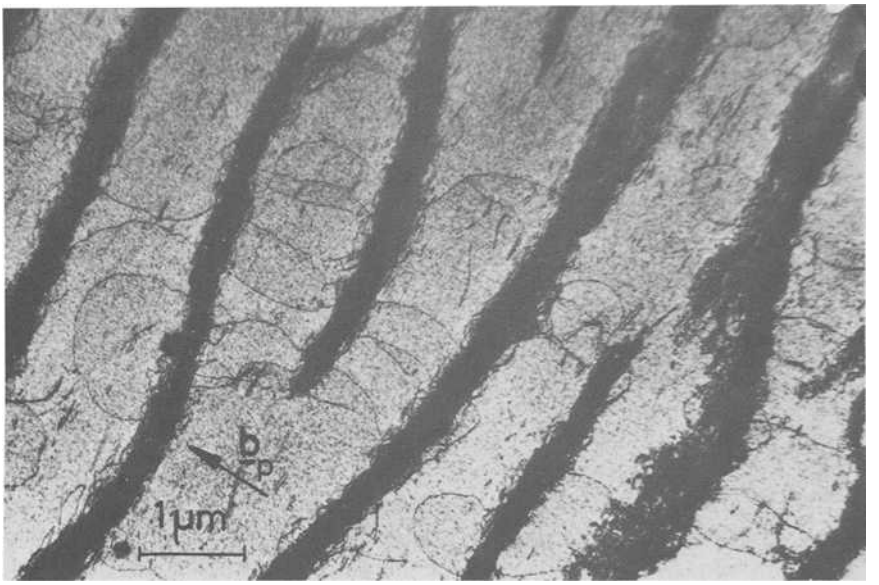

FIG. 8—*TEM-micrograph of a section parallel to the primary glide plane of a copper single crystal cycled into saturation at* $\gamma_{pl} \sim 5 \times 10^{-3}$. *Dislocations pinned by fast-neutron irradiation in the stress-applied state (tensile peak stress). Note primary edge dislocations bowing out of the walls and curved primary screw dislocations between the walls. Dislocations of the same sign exhibit the same sense of curvature* [28].

rium between different processes and not at all as reversible as some observations could suggest [*4,5,10,13,28*]. This could provide a hint that the statistical nature of the discussed processes plays a role in the development of the notch-peak geometry found in the PSB's at the surface [see Refs *2,3*], as is suggested also by the work of Finney and Laird [*10*].

Within the scope of this presentation, there is no room for a detailed comparison of these findings with existing ideas on dislocation mechanisms in cyclic deformation. We wish to point out only that the described specific roles of cross slip and of long-range internal stresses, both prior to and in the saturation regime [see also *12,13,28,29*], have so far not been considered by other authors [*7,10,15,40,43*].

Cyclic Deformation of BCC Metal Crystals

It is well known from studies of the unidirectional deformation that the mechanical behavior of bcc metals depends strongly on temperature, strain rate, and on small amounts of (interstitial) impurities [*16–19*]. In the following we shall show that these factors, which do not play a comparable role in the case of fcc metals, are also important in cyclic deformation of bcc metals and must hence be specified and taken into account appropriately.

Pure BCC Metals

"High" Strain Rates—At room temperature and typical cyclic strain rates $\dot{\epsilon}_{pl} \sim 10^{-4}$-$10^{-2}$ s^{-1}, the cyclic stress-strain curves of pure α-iron single [*11,44–46*] and polycrystals [*47*] generally follow the course shown in Fig. 9. Under comparable conditions the cyclic stress-strain response of pure niobium single crystals is very similar [*48*]. Some fundamental features of this behavior are:

1. There is an appreciable contribution to σ_s by the effective stress component σ_s*, characteristic of thermally activated dislocation glide. For example, in α-iron at $\dot{\epsilon}_{pl} = 10^{-2}$ s^{-1}, σ_s* in fact exceeds appreciably the athermal component $\sigma_{s,G}$ that is due to the elastic interaction of dislocations [*11,46,49*].

2. For $\Delta\epsilon_{pl} \lesssim 5 \times 10^{-4}$, cyclic hardening and microstructural changes are almost negligible. The dislocation arrangement in cyclic saturation consists mainly of screw dislocations in low density ($\sim 5 \times 10^{11}$ m^{-2}) and can be explained by assuming that only non-screw dislocations move to-and-fro in a non-hardening quasi-reversible manner [*11,44–49*].

3. Above $\Delta\epsilon_{pl} \sim 5 \times 10^{-4}$, cyclic hardening becomes more pronounced and increasing cell formation is observed [*11,45,46,49*]; see Fig. 10. The cell walls consist mainly of primary and secondary screw dislocations and

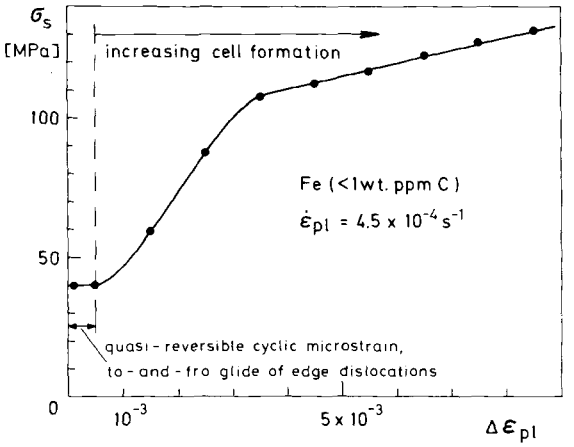

FIG. 9—*Cyclic stress-strain curve of pure α-iron single crystals* [11,44,45].

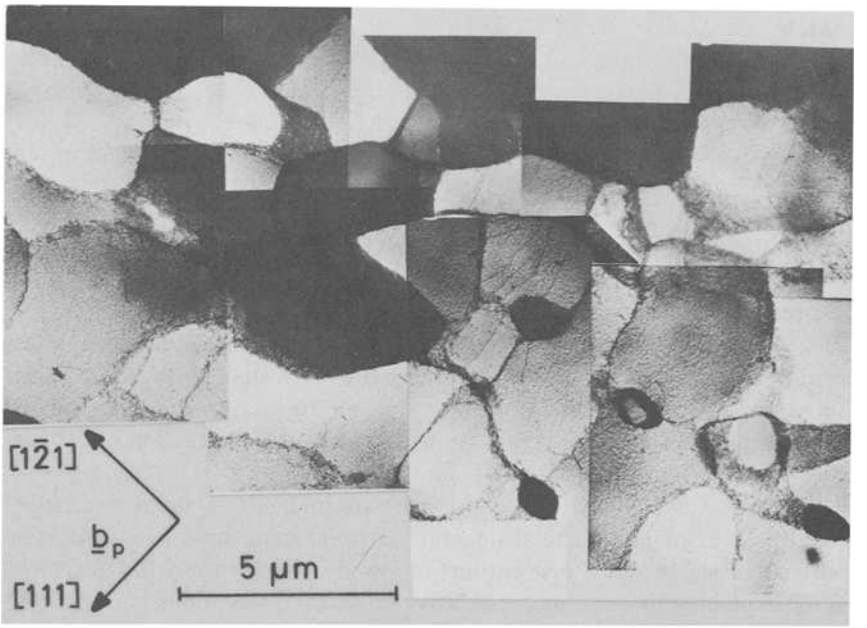

FIG. 10—*Cell structure in cyclically deformed α-iron single crystal after cyclic deformation into saturation at* $\dot{\epsilon}_{pl} = 4.5 \times 10^{-4} s^{-1}$ *and* $\Delta\epsilon_{pl} = 5 \times 10^{-3}$. *Section parallel to* ($\bar{1}01$); *TEM.*

frequently resemble low-angle twist boundaries. They do not exhibit any preferential crystallographic orientation.

4. The surface pattern exhibits some resemblance to that observed after tensile deformation (see Refs *16–19*). On the side face ($1\bar{2}1$), slip traces parallel to $\mathbf{b}_p$ and a band structure (reminiscent of kink bands) perpendicular to $\mathbf{b}_p$ are visible [*46,48-50*]; see Fig. 11. The features on the top face are diffuse and much less developed. SEM reveals bands of slip that do not follow the trace of the primary slip plane, as shown in Fig. 12.

5. Neither the surface nor the bulk observations provide indications of PSB's [*11,46,49*] similar to those observed in fcc single crystals.

6. After cyclic deformation, in particular for $\Delta\epsilon_{pl} \gtrsim 5 \times 10^{-4}$, the originally round cross sections of the crystals become strongly elliptical [*44,48,51*]. These shape changes are related to the so-called slip plane asymmetry [*44,51,52*], that is, to slip of screw dislocations on different slip planes in tension and compression, respectively [*16,18,19*].

The described dislocation behavior (and the observed slip plane asym-

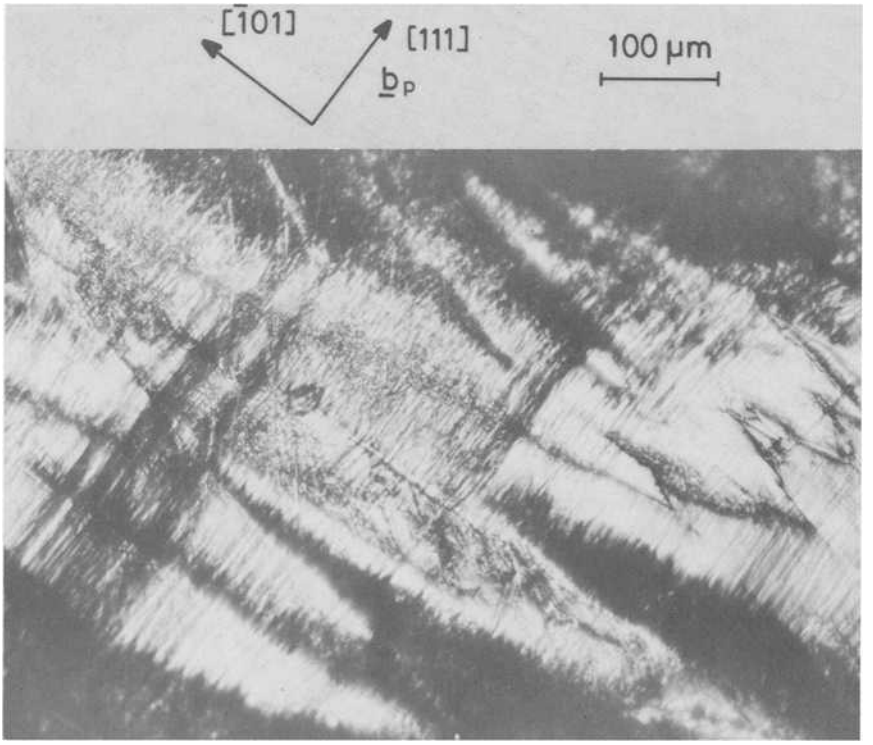

FIG. 11—*Side face* ($1\bar{2}1$) *of niobium single crystal after cyclic deformation into saturation at* $\dot{\epsilon}_{pl} = 10^{-3}\ s^{-1}$ *and* $\Delta\epsilon_{pl} = 5 \times 10^{-3}$ *(Nomarski interference contrast). Axis horizontal.*

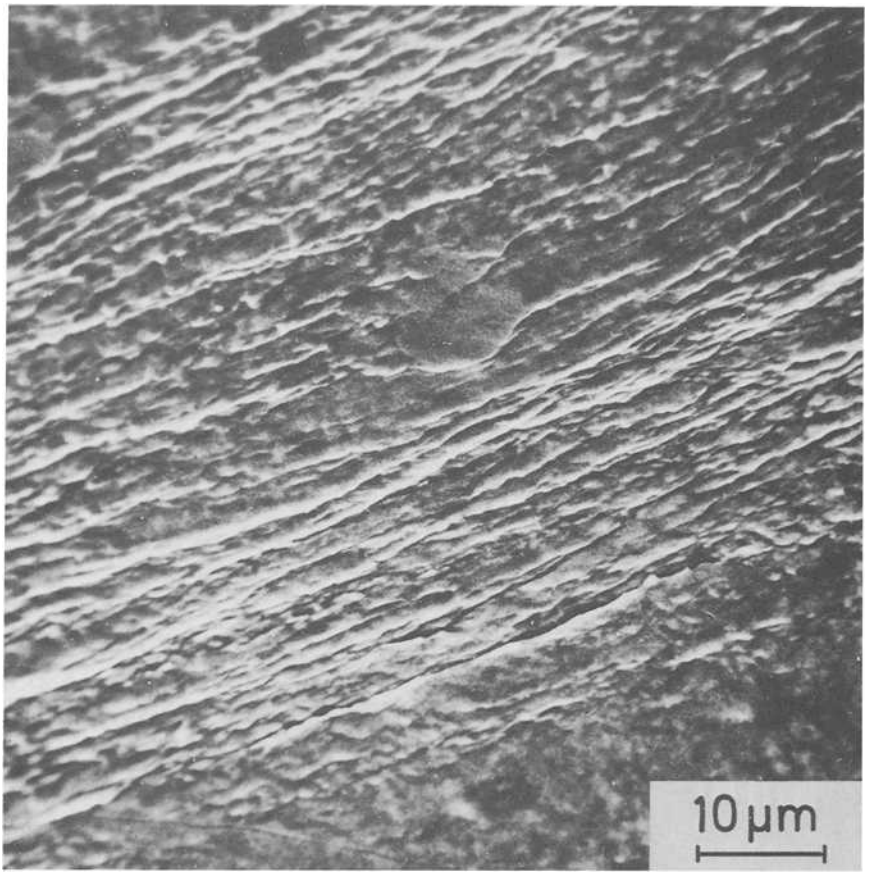

FIG. 12—*SEM-micrograph of top face of same niobium single crystal as in Fig. 11 after further cyclic deformation (to fracture) at* $\Delta\epsilon_{pl} = 7 \times 10^{-3}$. *Axis vertical. Trace of primary glide plane horizontal.*

metry) is typical of the low-temperature mode of deformation of bcc metals. Below a certain temperature T_0, the glide of the screw dislocations in bcc metals is governed by the thermally activated overcoming of an intrinsic lattice friction stress [*16–19*] that limits their mobility. As a consequence, dislocation multiplication is impeded and multiple glide of the more mobile non-screw dislocations leads to the formation of dislocation arrangements consisting predominantly of screw dislocations.

Our findings suggest that the rather "high" cyclic strain rates ($\gtrsim 10^{-3}\ s^{-1}$) promote the observed low-temperature behavior [*44–47*] by raising the transition temperature T_0 above room temperature. (At moderate strain rates [$\sim 10^{-5}\ s^{-1}$] the room-temperature mechanical behavior of α-iron

and niobium is not characteristic of the low-temperature mode of deformation but is rather similar to that of the fcc metals [*16–19*].)

Governing Factors of the Deformation Mode—The foregoing considerations indicate that the produced dislocation arrangements depend on the *relative* mobility of the screw dislocations with respect to that of the non-screw dislocations. We hence expect that the following measures would favor a (cyclic) deformation behavior that is more similar to that of fcc metals:

1. Higher temperatures ($\gtrsim T_0$).
2. Lower strain rate ($\sim 10^{-5}\ s^{-1}$)
3. Doping with solute interstitial impurity atoms (carbon, oxygen, nitrogen).

The effects of measures 1 and 2 would be primarily to enhance the mobility of the screw dislocations by facilitating thermal activation, whereas obstructing the glide of dislocations by measure 3 would mainly affect a reduced mobility of the non-screw dislocations relative to that of the screw dislocations.

"Low" Strain Rates—In accordance with these ideas, the following observations were made on pure α-iron single crystals that were deformed cyclically at $\dot{\epsilon}_{pl} = 2.5 \times 10^{-5}\ s^{-1}$ [*11,46,49*]:

1. The cyclic hardenability was enhanced considerably down to $\Delta\epsilon_{pl} = 10^{-4}$.
2. Dense arrays of primary edge dislocation multipoles were observed at low $\Delta\epsilon_{pl}$, and dislocation walls perpendicular to $\mathbf{b}_p$, in addition to cell structures, at higher $\Delta\epsilon_{pl}$.
3. The contribution of $\sigma_{s,G}$ was dominant over σ_s^* at all $\Delta\epsilon_{pl}$.
4. The shape changes were much less pronounced.
5. The surface observations revealed, besides kink-band-like structures, slip lines running parallel to the trace of the primary slip plane. In some cases these slip lines developed into rough slip bands (Fig. 13).

Thus, although the overall behavior becomes similar in many respects to that of cyclically deformed fcc crystals, convincing evidence of localized deformation in PSB's was not obtained.

Cyclic Deformation of Single Crystals of α-Iron + 30 wt. ppm Carbon at "Low" Strain Rates

We now describe the results of studies on α-iron single crystals containing 30 wt. ppm carbon that were deformed cyclically at $\dot{\epsilon}_{pl} = 2.5 \times 10^{-5}\ s^{-1}$ (simultaneous application of measures 2 and 3). Figure 14 shows the cyclic hardening behavior observed upon deformation at successively increasing values of $\Delta\epsilon_{pl}$. Cyclic hardening was found to be appreciable already at the lowest plastic strain amplitude ($\Delta\epsilon_{pl} = 2 \times 10^{-4}$). The resulting cyclic stress-strain curve, shown in Fig. 15, exhibits a sharp bend

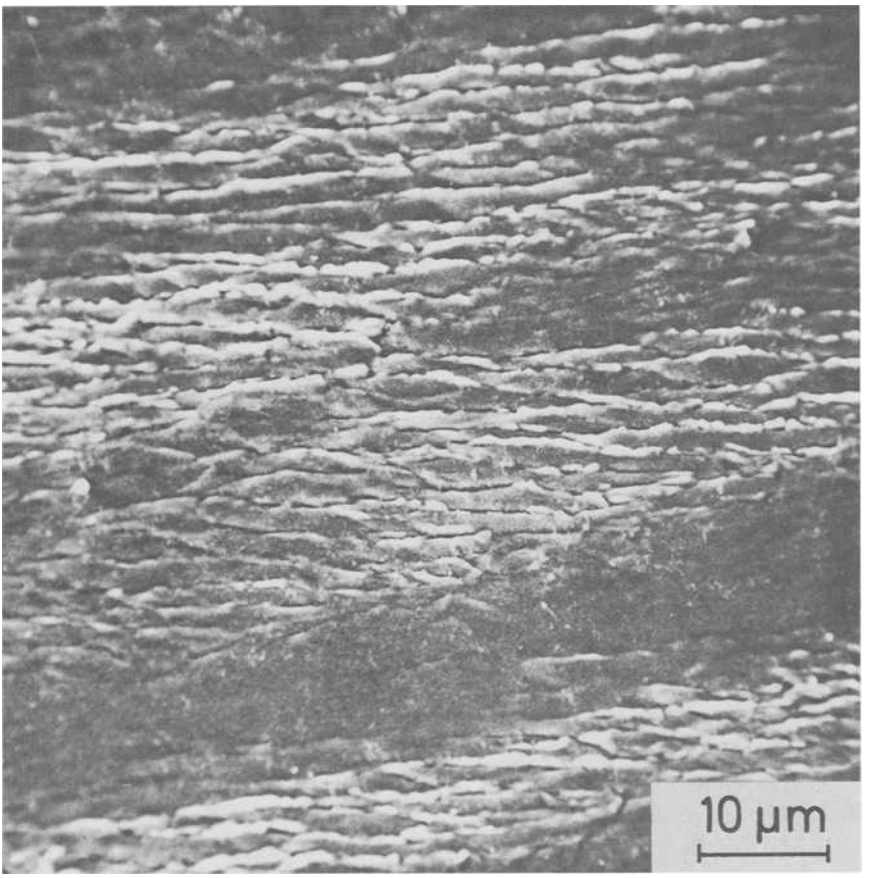

FIG. 13—*SEM-micrograph of top face of pure α-iron single crystal after cyclic deformation into saturation at* $\dot{\epsilon}_{pl} = 2.5 \times 10^{-5}\ s^{-1}$ *and* $\Delta\epsilon_{pl} = 8.5 \times 10^{-3}$. *Axis vertical. Trace of primary glide plane horizontal.*

at $\Delta\epsilon_{pl} \sim 4 \times 10^{-4}$, and σ_s is then found to increase much more weakly with increasing $\Delta\epsilon_{pl}$ than below $\Delta\epsilon_{pl} \sim 4 \times 10^{-4}$. The findings for $\Delta\epsilon_{pl} > 4 \times 10^{-4}$ can be characterized as follows:

1. Cyclic softening always preceded saturation (see Fig. 14).
2. In the approach to saturation the hysteresis loops became more rectangular.
3. Slip traces developed around the whole circumference of the crystals parallel to the primary glide plane $(\bar{1}01)$.
4. The slip traces became denser as $\Delta\epsilon_{pl}$ was increased (see Fig. 16*a*,*b*).
5. At higher magnification the slip traces were observed as wavy bands out of which material had been extruded (see Fig. 16*c*).

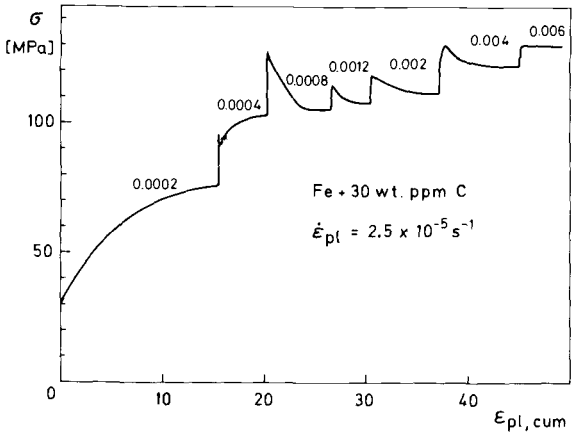

FIG. 14—*Cyclic hardening behavior of single crystal of α-iron + 30 wt. ppm carbon deformed cyclically at* $\dot{\epsilon}_{pl} = 2.5 \times 10^{-5}\ s^{-1}$ *and at successively increasing values of* $\Delta\epsilon_{pl}$. *Numbers refer to* $\Delta\epsilon_{pl}$.

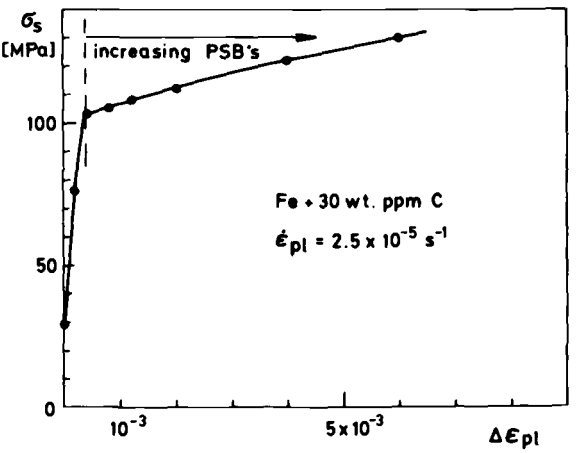

FIG. 15—*Cyclic stress-strain curve of specimens deformed as shown in Fig. 14.*

6. In sections parallel to the primary slip plane, mainly dense arrays of predominantly primary edge dislocations in multipole configuration were observed (see Fig. 17). The study of sections cut perpendicular to the primary slip plane showed that the dense dislocation arrays consisted of veins and walls, interrupted by dislocation-poor channels of about a micron in width, running more or less parallel to the trace of the primary slip plane (see Fig. 18).

The analogy of these features to those characteristic of the behavior of

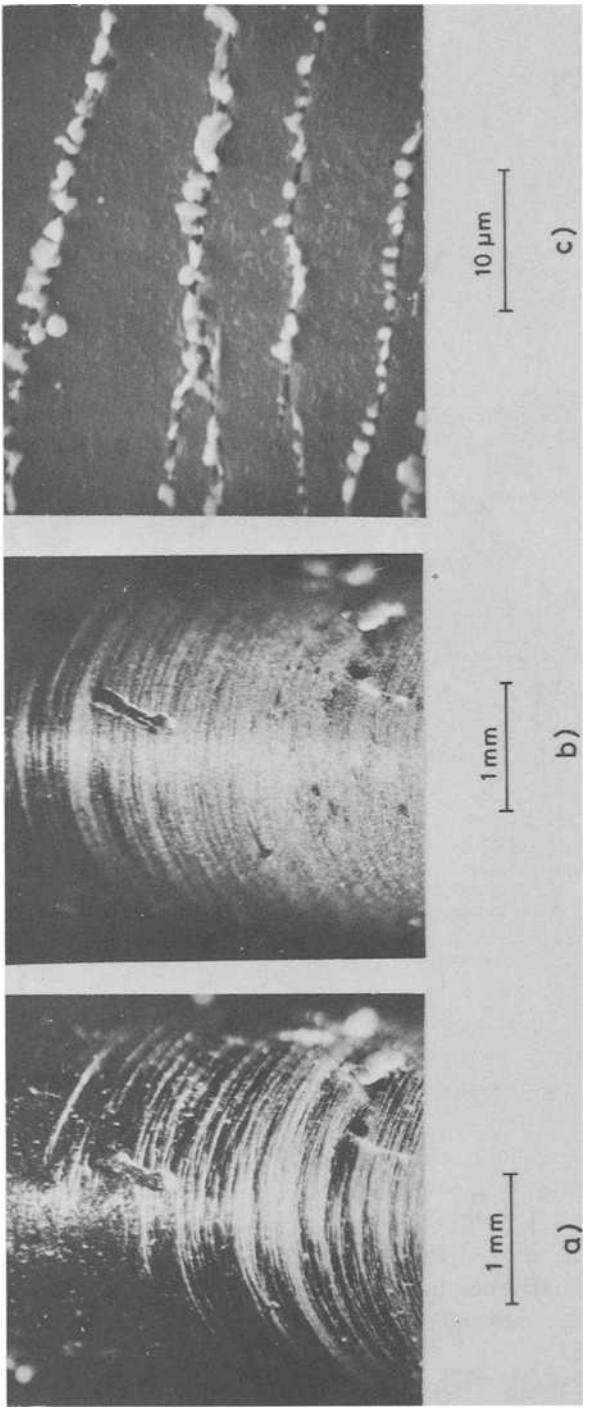

FIG. 16—*Surface patterns of specimen deformed as shown in Fig. 14. top face:* (a) $\Delta\epsilon_{pl} = 2 \times 10^{-4}$; (b) $\Delta\epsilon_{pl} = 6 \times 10^{-4}$, (c) $\Delta\epsilon_{pl} = 6 \times 10^{-3}$ *(SEM).*

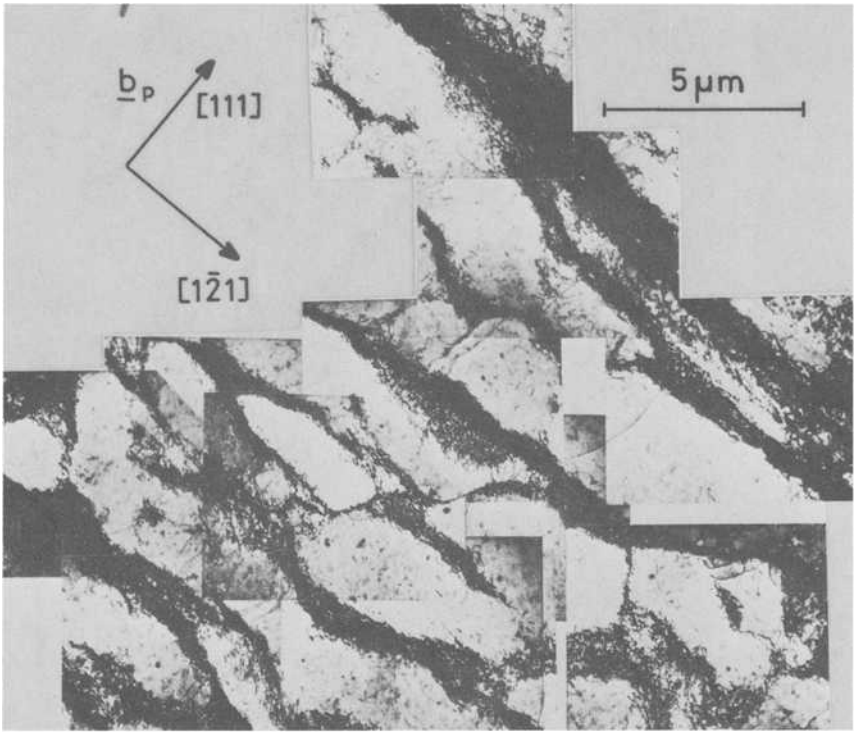

FIG. 17—*Section parallel to primary glide plane* ($\bar{1}01$) *of specimen deformed until* $\Delta\epsilon_{pl} = 6 \times 10^{-3}$ *as shown in Fig. 14 (TEM).*

PSB's in fcc metal crystals as a bulk phenomenon is obvious. We conclude that the dislocation-poor channels play the role of the ladder-like wall structure of the PSB's in fcc metals.[5] In addition to the differences in the dislocation arrangements of the PSB's in the two classes of metals, the following should be noted. In α-iron + 30 wt. ppm carbon the PSB's are more wavy than in fcc metals and not strictly confined to the crystallographic slip planes. PSB's ending within the field of view at walls are not rare events. Although the cyclic stress-strain curve shows a sharp bend at the onset of the development of the PSB's, the fact that σ_s continues to increase non-negligibly along the "plateau" indicates that the simple idealized model (Fig. 1) applies only very approximately. Hence, the set of values listed in the lower half of Table 1 should serve only as a guideline.

The most closely related work reported in the literature appears to be a study by Wilson and Tromans [*53*] on PSB's formed in surface grains of low-

[5]It appears probable that the dislocation-poor channels form because the low-temperature mode of dislocation glide operates locally in the PSB's as a result of the rather high local strain rate which arises from the localization of strain.

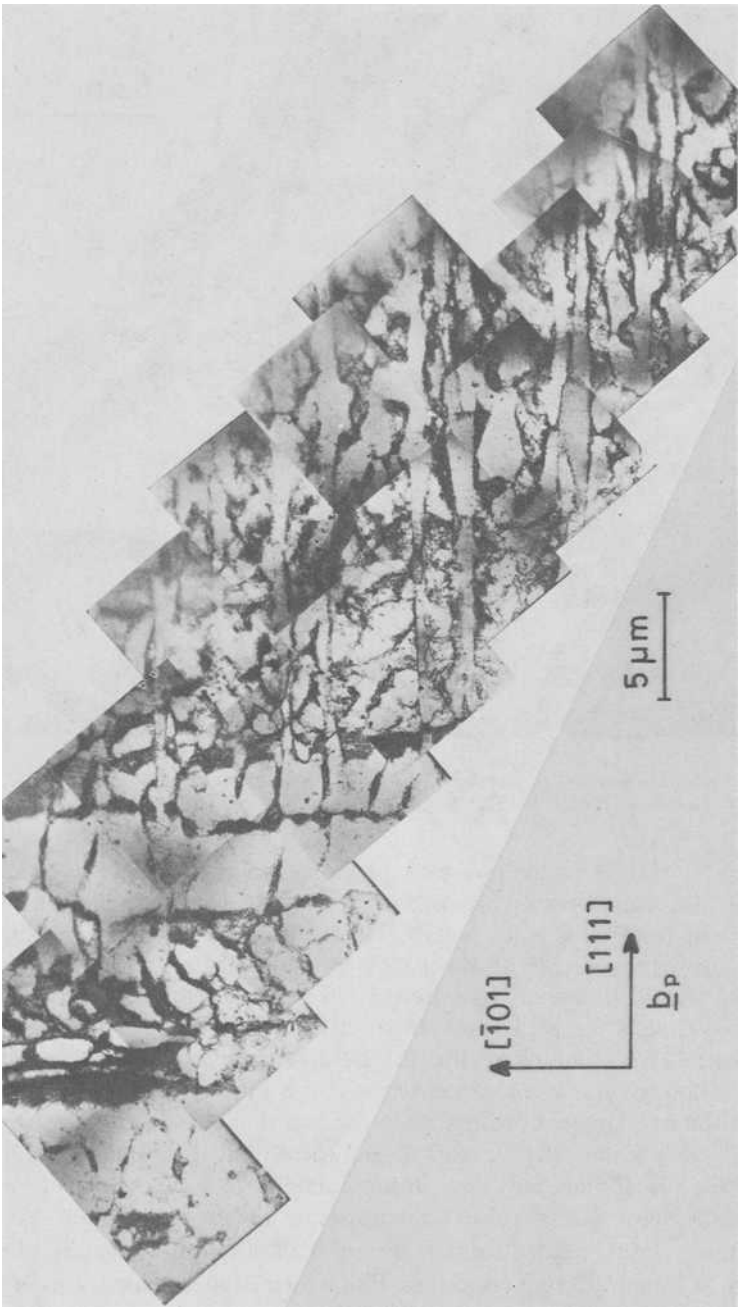

FIG. 18—*Section parallel to* $(\bar{1}21)$, *same specimen as in Fig. 17 (TEM).*

carbon steel that was fatigued in the as-quenched state at temperatures between 60 and 130°C. These authors found both PSB's, forming very similar extrusions at the surface as in our case (Fig. 16*c*), and dislocation-poor channels in a matrix of dense veins. In their experiments (at $\dot{\epsilon}_{pl} \sim 10^{-2}$ s^{-1}) the elevated temperature was an important prerequisite just as the low strain rate was in our study at room temperature (at high $\dot{\epsilon}_{pl}$ our specimens behaved very much more like pure α-iron [*45*]). Wilson and Tromans describe their observations in terms of dynamic strain aging,[6] a concept that appears to be equally applicable in our case. Specifically, we attribute our observations to the combined effects of the solute carbon atoms and the low strain rate that render the mobilities of screw and non-screw dislocations very nearly equal, permitting the formation of very dense primary edge multipole structures, accompanied by pronounced cyclic hardening, in a fashion similar to that of the fcc metals.

Resumé of the Observations on BCC Metals

The reported absence of PSB's in pure α-iron and niobium single crystals appears to be in contradiction to published work (see Refs *56–58*). These studies are frequently confined to surface observations on polycrystals of unspecified purity, low carbon steel, or α-iron containing substantial amounts of interstitial impurities. To the best of our knowledge, convincing evidence of PSB's having the properties described at the outset has so far not been obtained on *pure* bcc metals. In a typical cyclic deformation test ($\dot{\epsilon}_{pl} \gtrsim 10^{-3}$ s^{-1}) at or below room temperature, we expect that the pure bcc transition metals will deform by the low-temperature mode of deformation and that the dislocation arrangement will be an open cell structure (see Refs *11,49*) with no obvious need to give way to PSB's except perhaps at very high amplitudes.

On the basis of the experiments performed so far, the possibility still exists that, in limited regimes of temperature (below the range of self-diffusion) and strain rate in which pure bcc metals subjected to fatigue behave similarly to fcc metals, they will exhibit the formation of PSB's in an analogous manner. Further experiments, preferably above room temperature, would be desirable.

This discussion clearly raises the question what kind of failure mechanism is operative in the absence of PSB's and slipband cracking. In addition to grain boundary cracking in the case of polycrystals (see Refs *2,47*), we point out two possibilities:

1. Experiments on bcc single crystals have shown that the severe shape changes, related to the asymmetry of slip [*44,51,52*], perhaps in conjunction with the surface rumpling due to the king-bank-like surface markings (see

[6]Other authors [*54,55*] have also presented evidence showing that dynamic strain aging promotes inhomogeneous plastic deformation.

Fig. 9), can lead to "premature" failure by the development of regions of localized strain. The detailed mechanism is not yet fully understood [*44,52*].

2. In the near-surface regions, a mode of deformation, differing significantly from that in the bulk, could be operative and lead to fatigue crack initiation (see Figs. 12 and 13).

Some General Conclusions

In our opinion, the present work demonstrates that studies on single crystals are a useful and necessary tool in order to characterize the formation and the properties of PSB's quantitatively in terms of dislocation microstructure and mechanical data (see Table 1). With this knowledge, further progress can be expected in polycrystal fatigue.

In all cases in which PSB's were observed, well-defined thresholds of plastic strain (or stress) amplitude exist below which PSB's do not develop. These thresholds should correspond to fatigue limits [*4,9,11,12,14,15*] in the case of single- and polycrystals under the condition that cracks initiate exclusively at PSB's. The situation is less clear in the case of pure bcc metals, where convincing evidence of PSB's is lacking at present.

The conclusion that PSB's are a much more general feature in fcc than in bcc metals is in broad agreement with recent convincing TEM observations of the dislocation arrangements at crack tips in fatigued copper and α-iron. Katagiri and co-workers (see Refs *59,60*, and also the contribution of the same group to this publication, Ref *61*) have observed (in the early stage of fatigue) PSB's adjacent to the crack tip in copper but not in α-iron, where a cell structure was found.

The following basic requirements are considered to be essential to the formation of PSB's in single-phase metals: (1) The dislocation arrangement formed during cyclic hardening must contain a hard component that is so densely packed with dislocations hindering each other's motion that the plastic strain can no longer be accommodated in these parts of the specimen; (2) the volume fraction of this hard component must be appreciable, say 50 percent or greater; and (3) this hard component must be metastable in the sense that it can dissociate and rearrange under the conditions of the experiment into a more open structure that permits plastic flow at a reduced stress level.

The presented observations suggest that the dense veins, built up of edge dislocation dipoles, fulfill these requirements of the hard component in an ideal manner in fcc metals and, under special circumstances, also in bcc metals. In the special case of the multipole vein structure, single slip, comparable mobilities of edge and screw dislocations, and effective elimination of the screw dislocations by cross slip have been shown to be three factors that favor the formation process. It is not known whether there exist other, perhaps radically different, dislocation distributions that are

equally "suitable". We do not consider this very probable. For example, it is difficult to see how a dislocation arrangement consisting predominantly of screw dislocations as the other extreme, as is typical of low-temperature deformation of bcc metals, could acquire the necessary dislocation density, since annihilation by stress-induced cross slip would always set a natural limit.

Acknowledgments

The kind interest and support of Prof. Dr. A. Seeger and Dr. M. Wilkens and the helpful criticism of Dr. U. Essmann are deeply appreciated. Sincere thanks are extended to Prof. Dr. H. Mecking, who kindly supplied the silver single crystals, and to Dipl. Phys. S. Zwiesele for performing the carburizing treatment.

References

[1] Thompson, N., Wadsworth, N. J., and Louat, N., *Philosophical Magazine,* Vol. 1, 1956, pp. 113-126.
[2] Laird, C. and Duquette, D. J. in *Corrosion Fatigue,* A. J. McEvily and R. W. Staehle, Eds., National Association of Corrosion Engineers, Houston, Tex., 1972, pp. 88-117.
[3] Lukáš, P., Klesnil, M., Krejči, J., and Ryš, P., *Physica Status Solidi,* Vol. 15, 1966, pp. 71-82.
[4] Helgeland, O., *Journal of the Institute of Metals,* Vol. 93, 1964/1965, pp. 570-575.
[5] Watt, D. F., Embury, J. D., and Ham, R. K., *Philosophical Magazine,* Vol. 17, 1968, pp. 199-203.
[6] Roberts, W. N., *Philosophical Magazine,* Vol. 20, 1969, pp. 675-686.
[7] Woods, P. J., *Philosophical Magazine,* Vol. 28, 1973, pp. 155-191.
[8] Atkinson, J. D., Brown, L. M., Kwadjo, R., Stobbs, W. M., Winter, A. T ., and Woods, P. J. in *Proceedings,* 3rd International Conference on the Strength of Metals and Alloys, Cambridge, U.K., 1973, pp. 402-406.
[9] Winter, A. T., *Philosophical Magazine,* Vol. 30, 1974, pp. 719-738.
[10] Finney, J. M. and Laird, C., *Philosophical Magazine,* Vol. 31, 1975, pp. 339-366.
[11] Mughrabi, H., Herz, K., and Ackermann, F. in *Proceedings,* 4th International Conference on the Strength of Metals and Alloys, Nancy, France, 1976, Vol. 3, pp. 1244-1248.
[12] Mughrabi, H., *Materials Science and Engineering,* Vol. 33, 1978, pp. 207-223.
[13] Grosskreutz, J. C. and Mughrabi, H. in *Constitutive Equations in Plasticity,* A. S. Argon, Ed., Massachusetts Institute of Technology Press, Cambridge, Mass., 1975, pp. 251-326.
[14] Laird, C., *Materials Science and Engineering,* Vol. 22, 1976, pp. 231-236.
[15] Brown, L. M. in *Proceedings,* "Fatigue 1977" Conference, Cambridge, U.K., *Metal Science,* Vol. 11, 1977, pp. 315-320.
[16] Hirsch, P. B. in *Proceedings,* International Conference on the Strength of Metals and Alloys, Supplement to *Transactions,* Japanese Institute of Metals, Vol. 9, 1968, pp. XXX-XXXIX.
[17] Šesták, B. and Seeger, A., *Physica Status Solidi* (b), Vol. 43, 1971, pp. 433-444.
[18] Šesták, B. in *Proceedings,* 3rd Internationales Symposium über Reinststoffe in Wissenschaft und Technik, Dresden, 1970, Akademie-Verlag, Berlin, German Democratic Republic, 1972, pp. 221-262.
[19] Christian, J. W. in *Proceedings,* 2nd International Conference on the Strength of Metals and Alloys, Asilomar, Calif., American Society for Metals, 1970, pp. 31-70.
[20] Mughrabi, H., to be published.

[21] Hancock, J. R. and Grosskreutz, J. C., *Acta Metallurgica,* Vol. 17, 1969, pp. 77-97.
[22] Kettunen, P. O. and Kocks, U. F., *Acta Metallurgica,* Vol. 20, 1972, pp. 95-103.
[23] Mecke, K., *Physica Status Solidi* (a), Vol. 25; 1974, pp. K93-K96.
[24] Basinski, S. J., Basinski, Z. S., and Polák, J. in *Corrosion Fatigue,* A. J. McEvily and R. W. Staehle, Eds., National Association of Corrosion Engineers, Houston, Tex., 1972, pp. 143-145.
[25] Basinski, S. J., Basinski, Z. S., and Howie, A., *Philosophical Magazine,* Vol. 19, 1969, pp. 889-924.
[26] Essmann, U., *Acta Metallurgica,* Vol. 12, 1964, pp. 1468-1470.
[27] Mader, S., Seeger, A., and Leitz, Ch., *Journal of Applied Physics,* Vol. 34, 1963, pp. 3368-3375.
[28] Mughrabi, H. in *Proceedings,* 3rd International Conference on the Strength of Metals and Alloys, Cambridge, U.K., 1973, pp. 407-409, and unpublished work.
[29] Ackermann, F. and Mughrabi, H., in preparation.
[30] Feltner, C. E., *Philosophical Magazine,* Vol. 12, 1965, pp. 1229-1248.
[31] Neumann, P., *Zeitschrift für Metallkunde,* Vol. 59, 1968, pp. 927-934.
[32] Seeger, A., Diehl, J., Mader, S., and Rebstock, H., *Philosophical Magazine,* Vol. 2, 1957, pp. 323-350.
[33] Feltham, P., *Philosophical Magazine,* Vol. 6, 1961, pp. 1479-1486.
[34] Ham, R. K. and Broom, T., *Philosophical Magazine,* Vol. 7, 1962, pp. 95-103.
[35] Rudolph, G., Haasen, P., Mordike, B. L., and Neumann, P. in *Proceedings,* 1st International Conference on Fracture, Sendai, Japan, 1965, Vol. 2, pp. 501-514.
[36] Nine, H. D. and Kuhlmann-Wilsdorf, D., *Canadian Journal of Physics,* Vol. 45, 1967, pp. 865-880.
[37] Kettunen, P. O. and Kocks, U. F., *Czechoslovak Journal of Physics,* Vol. B19, 1969, pp. 299-314.
[38] Seeger, A. in *Work Hardening,* J. P. Hirth and J. Weertman, Eds., Gordon and Breach, New York, 1968, pp. 27-60.
[39] Antonopoulos, J. G. and Winter, A. T., *Philosophical Magazine,* Vol. 33, 1976, pp. 87-95.
[40] Antonopoulos, J. G., Brown, L. M., and Winter, A. T., *Philosophical Magazine,* Vol. 34, 1976, pp. 549-563.
[41] Picqueras, J., Grosskreutz, J. C., and Frank, W., *Physica Status Solidi* (a), Vol. 11, 1972, pp. 567-580.
[42] Essmann, U. and Rapp, M., *Acta Metallurgica,* Vol. 21, 1973, pp. 1305-1317.
[43] Kuhlmann-Wilsdorf, D. and Laird, C., *Materials Science and Engineering,* Vol. 27, 1977, pp. 137-156.
[44] Mughrabi, H. and Wüthrich, Ch., *Philosophical Magazine,* Vol. 33, 1976, pp. 963-984.
[45] Mughrabi, H., Herz, K., and Stark, X., *Acta Metallurgica,* Vol. 24, 1976, pp. 659-668.
[46] Herz, K., Doctorate Thesis, Stuttgart University, Stuttgart, Federal Republic of Germany, 1976.
[47] Mughrabi, H., *Zeitschrift für Metallkunde,* Vol. 66, 1975, pp. 719-724.
[48] Ackermann, F., unpublished.
[49] Herz, K., Mughrabi, H., and Wilkens, M., Arbeitsbericht MPI 77/P3 (in English) des Max-Planck-Institut für Metallforschung, Institut für Physik, Stuttgart, Federal Republic of Germany.
[50] Doner, M., Diprimio, J. C., and Salkovitz, E. I., *Acta Metallurgica,* Vol. 21, 1973, pp. 1547-1559.
[51] Neumann, R., *Zeitschrift für Metallkunde,* Vol. 66, 1975, pp. 26-32.
[52] Nine, H. D., *Journal of Applied Physics,* Vol. 44, 1973, pp. 4875-4881.
[53] Wilson, D. V. and Tromans, J. K., *Acta Metallurgica,* Vol. 18, 1970, pp. 1197-1208.
[54] McGrath, J. T. and Bratina, W. J., *Czechoslovak Journal of Physics,* Vol. B19, 1969, pp. 284-293.
[55] Abdel Raouf, H., Topper, T. H., and Plumtree, A. in *Fatigue at Elevated Temperatures, ASTM STP 520,* American Society for Testing and Materials, 1973, pp. 300-310.
[56] Hempel, M. R. in *Fracture,* B. L. Averbach, D. K. Felbeck, G. T. Hahn, and D. A. Thomas, Eds., Technology Press, Massachusetts Institute of Technology, Cambridge, Mass., and Wiley, New York, 1959, pp. 376-411.

[57] Kettunen, P. O., *Journal of the Iron and Steel Institute,* Vol. 202, 1964, pp. 209-215.
[58] Klesnil, M. and Lukáš, P., *Journal of the Iron and Steel Institute,* Vol. 203, 1965, pp. 1043-1048.
[59] Awatani, J., Katagiri, K., and Nakai, H., *Metallurgical Transactions,* Vol. 9A, 1978, pp. 111-116.
[60] Katagiri, K., Omura, A., Koyanagi, K., Awatani, J., Shiraishi, T., and Kaneshiro, H., *Metallurgical Transactions,* Vol. 8A, 1977, pp. 1769-1773.
[61] Katagiri, K., Awatani, J., Omura, A., Koyanagi, K., and Shiraishi, T., this publication, pp. 106-128.

DISCUSSION

R. deWit[1] *(discussion)*—I think Dr. Mughrabi and his coauthors have given an excellent paper. I think they have given a coherent picture of persistent slipbands to make me understand much better what they are, and I have no criticism of this paper. This may well be because the management has cleverly chosen theoreticians to discuss experimental papers, as Dr. Mura said.

It is interesting that the authors are most interested in the nucleation of the slipbands. I think what interests people in fatigue is the nucleation of cracks, which is a point that they did not at all emphasize; the surface irregularities of the slipbands may be considered as being the incipient cracks. I think the importance of this paper is that it may throw light onto the nucleation of cracks, and so this work should go a long way toward helping to elucidate the initiation of cracks, which, in turn, is what we want to know in order to avoid failure by fatigue.

W. J. Plumbridge[2] *(discussion)*—The paper reports an extensive examination into the conditions for the formation of persistent slipbands, and also their structure, in single crystals of copper and nickel (fcc), and iron and niobium (bcc). For the former, which have received much previous attention, the model of Winter,[3] relating the cyclic stress-strain curve and the appearance of persistent slipbands, is experimentally verified. Here, a plateau in the cyclic stress-strain curve is equated with the formation of persistent slipbands, and the saturation shear stress increases again, only when the volume fraction of persistent slipbands reaches 100 percent.

Dislocations in the matrix are arranged in a vein structure (consisting of primary edge dislocations in multipole configuration), while in the persistent slipbands a ladder-like arrangement of walls exists. The latter, due to their smaller volume fraction of high dislocation density bands, are softer

[1]Center for Materials Science, National Bureau of Standards, Washington, D.C. 20234.
[2]Department of Mechanical Engineering, University of Bristol, Bristol, U.K.
[3]Winter, A. T., *Philosophical Magazine,* Vol. 30, 1974, p. 719.

than the matrix, which is first strained to saturation ($\gamma_{pl} \sim 10^{-4}$), prior to the nucleation of persistent slipbands. Following previous work,[4,5] it is suggested that subsequent strain is then localized in the bands.

Mechanistic differences between the behavior of the matrix and the persistent slipbands in the cyclic steady state are put forward. The requirement for a constancy of dislocation density is satisfied in the matrix by a dislocation flip-flop process, while in the bands a balance between annihilation and multiplication provides this. Generation occurs by bowing segments from the walls, and the necessary stress arises from the applied stress and long-range internal stresses.

The cyclic stress-strain response in pure single crystals having a bcc structure differs from that previously described for fcc materials. For $\Delta\epsilon_{pl} < 5 \times 10^{-4}$ little change is induced, but, at greater strain amplitudes, hardening and an associated cell structure, the walls of which contain primary and secondary screw dislocations, occur. Increase in temperature or reduction in strain rate tends to produce dislocation arrangements similar to those observed in fcc crystals (primary edge dislocation multipole arrays), but no persistent slipbands are formed. These appear only on the addition of impurities, when the cyclic stress-strain curve exhibits immediate rapid hardening until a quasi-plateau is reached, and at this point bands begin to be created. Dynamic strain aging and its effect on dislocation mobility are tentatively suggested as explanations for this observation. Contrary to earlier work reported in the literature,[6] it is argued that persistent slipbands have not been observed in *pure* body cubic materials, although it is admitted that conditions of temperature and strain rate appropriate for their formation may exist.

This paper provides a sound contribution to our increased understanding of the basic mechanisms of fatigue, and so satisfies the first objective of this symposium. I would like to mention a few specific points here, before considering more general issues associated with the symposium's second stated objective.

First, greater detail of, or reference to, the experimental aspects of the work would have been helpful, both for interest to those not involved in single crystal testing, and also to facilitate comparison with other work. Winter,[3] for example, considers in some depth the effect of specimen gripping. Perhaps the authors could elaborate on specimen geometry, method of strain measurement, grips, etc?

Secondly, the small plastic strains in the matrix veins are said to be accommodated by flip-flop motion of dislocation dipoles. This appears at variance with Finney and Laird,[5] who suggest that loop flipping contributes

[4]Helgeland, O., *Journal of the Institute of Metals*, Vol. 93, 1964/1965, p. 570.
[5]Finney, J. M. and Laird, C., *Philosophical Magazine*, Vol. 31, 1975, p. 339.
[6]Kettunen, P. O., *Journal of the Iron and Steel Institute*, Vol. 202, 1964, p. 209.

very little to the saturation state. Regarding the changes in the shape of the hysteresis loop associated with PSB formation, and in particular Fig. 4*a* ($\gamma_{pl} = 1 \times 10^{-4}$), is there a convex-concave transition in curvature near the peak stress levels, and if so, is it significant? A change from general micro to local macroplasticity may be inferred from the text at the onset of PSB formation. In some two-phase alloys,[7] noticeable 'kinks' (substantial curvature transitions) in the hysteresis loops have been observed. Is it possible that these may be considered in similar terms?

The present work falls into a category at one extreme of the expertise spectrum at this symposium, that is, that of the physicist physical metallurgist who studies fatigue on the 'micron' scale (Fig. 19). At the opposite end of the spectrum is the engineer on whom the onus of specifying a safe working life for a structure is placed. In order that the potential benefits from symposia such as this may be fully realized, it is vitally important to cross the knowledge and expertise channels as well as to push forward the individual routes. The role of the reviewer, particularly of papers in the extreme categories, should be that of linkman and interpreter. Unless bridges are created and utilized, then the symposium will become simply a more sophisticated version of the one 20 years ago, and little advance in the 'art' or 'science' of fatigue life prediction of engineering materials will be made.

The foregoing discussion of the paper by Mughrabi et al is thus aimed primarily at the mechanical metallurgists and the materials engineers rather than the solid-state physicists. Thoughts in the minds of the former groups might be along the lines that "most engineering materials are polycrystalline solid solutions or two-phase mixtures, so what contribution can this general type of work make to the solution of the fatigue problem, or indeed, how does it contribute to the understanding of the fatigue process in real materials?" The ability to accurately predict fatigue life under both laboratory and service conditions would be regarded as an adequate solution. A thorough discussion of this question, considering both the 'thermodynamics' and the 'kinetics' of a contribution to the fatigue problem being provided by this type of work, should be undertaken at this symposium. More specifically, typical queries might be:

1. What is the effect of polycrystallinity?
2. What happens in a solid solution alloy containing substantial solute?
3. What changes are caused by the presence of a second phase?
4. What is the role, if any, of persistent slipbands when geometrical stress concentrating features exist?
5. How long will it take to provide the answers to the foregoing questions?

An open appraisal of questions such as these should do much to enable

[7] Stoltz, R. E. and Pelloux, R. M., *Scripta Metallurgica*, Vol. 8, 1974, p. 269.

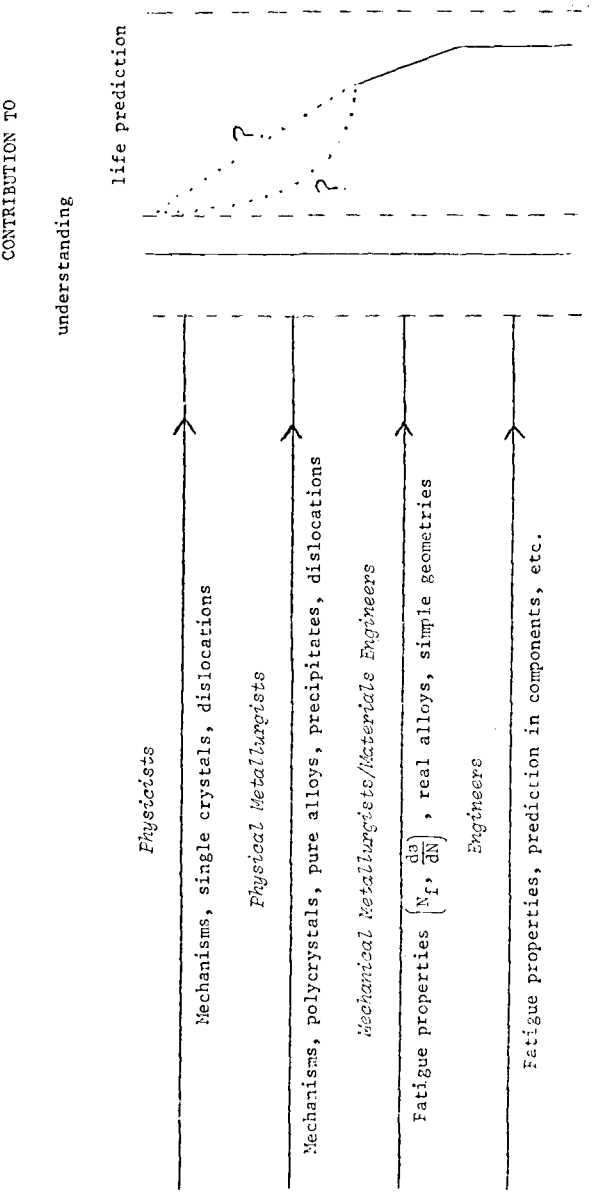

FIG. 19—*Participants, and their areas of interest, in the study of fatigue.*

the second objective of this symposium to be achieved. Finally, to be utterly contentious, one might ask where, in these times of limited budgets and increased accountability, should our resources be placed to most effectively solve the 'fatigue problem'?

C. Laird[8] *(discussion)*—I was very interested in your demonstration regarding the plateau in the cyclic stress-strain curve, namely, that the normalized PSB stress is the same for several different metals. While this will be very useful, I would like to address some of the more mechanistic aspects of your presentation.

The model that you have proposed for the formation of the PSB from the matrix structure is closely akin to the one that Doris Kuhlmann-Wilsdorf and I published about a year ago. However, we have since moved a little away from that position, because of having to face up to two problems.

One problem is: How do you see the strain occurring in the matrix? Especially, how do you see flip-flop going on in the veins, in relation to what is going on in the channels of the matrix?

The second problem is that we have had to come to grips with a micrograph by Winter which shows the PSB forming on the inside of the vein and not on the outside. Now, as you suggested, a group of dislocations that breaks free from the surface of the vein and sets up an avalanche, à la Peter Neumann, could cause the PSB to be formed by a "crash" from outside. But the crash actually seems to start from the inside; and I wonder if you have thought about that, and what guidance you could give us?

R. Stephens[9] *(discussion)*—I fall into the lower category that Bill Plumbridge pointed out, and I have always felt that persistent slipbands do occur in bcc materials, yet the paper seems to imply that they do not. Now, maybe it is because of the single crystal purity, but let us consider mild steel for engineers. And do I get the impression, then, that you are saying that persistent slipbands would not occur in these low-carbon steels?

A. Winter[10] *(discussion)*—What strain amplitude do you estimate is available from the mechanism of dipole flipping?

B. Ditchek[11] *(discussion)*—I have a few questions. First, I would like to ask you to elaborate on you mechanical testing apparatus. You have controlled plastic strains at lower levels, I would say, than most people

[8]Department of Metallurgical Engineering, University of Pennsylvania, Philadelphia, Pa. 19104.

[9]Materials Engineering Division, University of Iowa, Iowa City, Iowa 52242.

[10]Brookhaven National Laboratory, Upton, N.Y. 11973.

[11]Metallurgy Division, National Bureau of Standards, Washington, D.C. 20234; current address: Martin Marietta Laboratory, Baltimore, Md. 21227.

have before. Investigators most commonly make measurements down in the 10^{-3} to 10^{-4} range. You have lowered this by a factor of 10.

Secondly, I have observed that persistent slipbands become more fragmented, in addition to just increasing in their degree of coverage of the specimen's gage length. Have you observed a similar effect?

Finally, in the wall structure, TEM indicates a rapid generation of dipoles every cycle, formed by the motion of gliding screw dislocations. As no one observes a significant increase in the dipole concentration between the walls with the number of cycles, doesn't this mean that a steady-state behavior has been reached where dipoles are also being annihilated? Does this imply the motion of dipoles, possibly by a flip-flop mechanism?

H. Mughrabi (author's closure)—Well, one point has come up twice, namely, the question of equipment and testing procedure. Some details are given in the paper. The experiments have been performed in closed-loop control, partly on servohydraulic equipment (MTS), partly on a modified electromechanic excenter-type Schenck Pulser. The extensometer was calibrated to yield a signal of 10 V for an elongation of 0.1 mm. In the range of very low strain amplitudes we resorted to rather long specimens (up to 6 cm) in some cases in order to increase the strain resolution, since we were not able to measure (and control) the specimen length to a higher accuracy than ~ 0.2-$0.5\ \mu$m. The achieved accuracy of strain control and measurement was better than $\sim 5 \times 10^{-6}$. Special care was necessary in order to ensure precise axial alignment of the specimens. A final remark to this point: cyclic deformation at plastic strain amplitudes of $\sim 10^{-5}$ and less not only requires adequate equipment but affords considerably more patience and attention during the tests than in the more common low-cycle fatigue experiments.

In further response to Dr. Plumbridge, I do not share his opinion that our conclusion that the dipole flip-flop mechanism operates in the veins of the matrix is at variance with Finney and Laird. While we all agree that the dipole flip-flop mechanism does not contribute much to the strain, our contention is that it can accommodate the *small* plastic strain required in the veins of the matrix, namely, $\lesssim 10^{-4}$. In Ref *13* of our paper, Grosskreutz and I estimated that the flip-flop mechanism could only contribute $\sim 10^{-4}$ to the plastic strain and concluded that this was not enough to accommodate the plastic strain in the matrix, which at that time was considered to be $\sim 10^{-3}$. The present results show that the plastic strain amplitude in the matrix is only $\sim 10^{-4}$ or less. Such a value appears compatible with the dipole flip-flop mechanism.

In the same context I should like to respond to Dr. Winter as follows. Only a very small fraction of the available dipoles fulfill the requirements necessary for the flip-flop mechanism. As stated in the original paper by Feltner, the dipoles must not only be wide enough but at the same time

their length must be short enough so that, after flipping has occurred, the restoring stress due to the line tension will prevent the flipped segments from bowing out overcritically and breaking up the dipole altogether. For those (few) dipoles meeting these requirements, no obvious reason exists why they should not undergo flip-flop. I am aware of the (negative) results of the weak-beam TEM study by Antonopoulos, Brown, and Winter (Ref *40* of our paper). Still, it appears doubtful whether this observation is statistically significant, since the number of dipoles investigated (not stated in the paper) was probably not large enough. I should also point out that the dipole flip-flop mechanism has recently been observed directly by *in situ* high-voltage electron microscopy by Imura and co-workers.

In reply to Dr. Plumbridge's question concerning the shapes of the hysteresis loops at very low γ_{pl}, the answer is yes—there is a convex-concave transition in curvature. This behavior is believed to reflect the spectrum of obstacles encountered by the gliding dislocations and is discussed in more detail in Ref *12* of our paper. In that general sense a resemblance may exist with respect to the observations by Stoltz and Pelloux which Dr. Plumbridge refers to. Otherwise there is little similarity. The hysteresis loops observed by Stoltz and Pelloux mainly in the first few cycles relate to an enhanced Bauschinger strain and internal stresses caused by second-phase particles, whereas our observation refers to cyclic saturation of pure single-phase crystals containing only the dislocation arrangements of the matrix or of the matrix and PSB's.

Dr. Plumbridge finally asks what contribution can be expected from our more fundamental studies to the real problem. To our knowledge, the kind of work on single crystals presented in this paper provides the only means to assess quantitatively the properties of persistent slipbands. In principle, similar quantitative data can also be obtained on single crystals of more complex (structural) materials. This kind of knowledge is applicable to polycrystals in the sense that PSB's will form in a similar fashion (as in single crystals) in favorably oriented grains at the surface and will serve as preferential sites for fatigue crack initiation. In those materials that are susceptible to PSB formation, stress raisers such as scratches and notches will be preferential nucleation sites (see also the paper by Dr. Katagiri and co-workers in this publication [*61*]).

The answer to Dr. Stephens's question is that in *pure* bcc metal crystals fatigued under typical circumstances (strain rate $> 10^{-3}$ s^{-1}) at room temperature, we do find ill-defined bands of slip. While these bands do not follow the trace of the primary slip plane and do not exhibit the typical properties of *persistent* slipbands as shown for the fcc metals, they may lead to crack initiation. In our paper we have shown that at low cyclic strain rates ($\sim 10^{-5}$ s^{-1}), α-iron single crystals containing some carbon develop PSB's in a fashion very similar to that described for the fcc metal crystals. Instead of the low strain rate, a somewhat higher temperature

can serve the same purpose. In both cases the effect of dynamic strain aging promotes conditions similar to those prevailing in fcc metals. Hence, in less-pure bcc metals (mild steel) some sort of persistent slipbands may be found. To what extent they deserve the name "persistent slipbands" depends on their detailed properties in terms of surface appearance, slip plane, dislocation microstructure, and localization of strain. This will require further investigation, preferably on single crystal material.

Next, I shall try to answer Dr. Laird's question on whether PSB-formation is triggered by breaking-up of the veins in their interior or at their edges. In our paper there is a picture (Fig. 6) that is very similar to the one by Dr. Winter[12] that Dr. Laird is referring to. Such pictures taken from sections that are very weakly inclined to the primary slip plane *can* suggest in some cases that the walls of the PSB's merge into the edges of the veins of the matrix, as concluded by Winter. Still, caution should be exercised as to the generality of this observation. Also, for this particular section, complications can arise from projection effects. In our opinion, the $(1\bar{2}1)$ section perpendicular to the primary glide plane (which was not investigated by Winter) is more easily interpreted; see our Fig. 7. This picture shows unambiguously that walls merge (with comparable probability) into the centers or into the edges of the veins and some even end in the channels between the veins! While it may be possible that continued cycling in saturation will readjust veins and walls in such a way as to link them up in order to reduce the elastic strain energy associated with the free ends, the available observations do not favor a special mode of vein disintegration at the onset of PSB-formation.

I now come to the questions of Drs. Laird and Ditchek relating to the mechanisms of dislocation glide which are described in more detail in the paper. We consider the plastic deformability of the *matrix* to be limited by the strongly impeded dislocation glide *in* the veins and propose that flip-flop motion of dipoles is the only significant glide mechanism that can operate in the veins without destroying them. The capacity of "safe" dislocation motion is, however, fully exploited in the veins, which cannot be overstrained without dissociating. We see little relation between the dipole flip-flop in the veins and the glide activity of the screw dislocations in the channels between the veins. The density of these screw dislocations is low (10^{11}–10^{12} m^{-2}) and one can estimate that they will glide to-and-fro distances of only a micron or less with little or no correlation. Two screw dislocations of opposite sign will rarely approach close enough to annihilate mutually. It follows that if the deformation in the channels were not linked to that in the veins for reasons of compatibility, much larger plastic strains could be accommodated in the channels.

The situation in the wall structure of the PSB's is different. The glide

[12]Winter, A. T., *Philosophical Magazine A*. Vol. 37, 1978, p. 457.

of screw dislocations, whose density is about 10^{13} m^{-2}, occurs over distances of some microns and serves to produce new edge dislocations which are deposited in the walls. Newly formed dislocation dipoles are swept into the walls. Both the edge dislocations in the walls and the screw dislocations between the walls are suggested to be produced and annihilated continuously. Our evaluation, as outlined in the paper, shows that in the PSB's, as opposed to the matrix, screw dislocations are annihilated extensively as a natural consequence of their high glide activity. We have evidence that two screw dislocations of opposite sign that approach each other a distance smaller than about 500 Å annihilate.

C. Laird—What did you measure on the distribution of screw dislocation dipole widths?

H. Mughrabi—We have measured the distribution of screw dislocation dipole widths and found a sharp cutoff at about 500 Å.

C. Laird—Were the specimens neutron-irradiated?

H. Mughrabi—Yes, we pinned the dislocations in the case of copper by neutron irradiation. Otherwise these screw dislocation dipoles would annihilate or glide out of the thin foil and one would not be able to see them.

I agree with Dr. Ditchek's remark on the fragmentation of PSB's in the sense that, at a given strain amplitude, PSB's, once formed, become more fragmented subsequently. However, in relation to the coverage of the specimen's gage length, I hesitate to say that the few PSB's at low amplitudes are less fragmented than the many PSB's at higher amplitudes. This aspect was not studied conclusively.

In my final remarks *after* the symposium, I wish to express concern about critical comments made at this conference which reveal a tendency to base the value of research in the field of fatigue primarily on whether immediate progress has been made in solving the fatigue *failure* problem. While this attitude is valid from the engineering point of view in real life, it does not, at a symposium on *fatigue mechanisms*, do justice to all those involved in the overall interdisciplinary effort in a complicated field having more than one facet. If our main objective is a better understanding, then this effort must comprise the entire range of basic and applied studies on a microscopic and a macroscopic level from the beginning of cyclic loading to fracture under a variety of conditions. The responsibility of evaluating and interrelating the important aspects of the individual contributions goes beyond sound criticism, which is necessary but not adequate.

K. Katagiri,[1] *J. Awatani,*[1] *A. Omura,*[1] *K. Koyanagi,*[1] *and T. Shiraishi*[2]

Dislocation Structures Around the Crack Tips in the Early Stage in Fatigue of Iron

REFERENCE: Katagiri, K., Awatani, J., Omura, A., Koyanagi, K., and Shiraishi, T., **"Dislocation Structures Around the Crack Tips in the Early Stage in Fatigue of Iron,"** *Fatigue Mechanisms*, Proceedings of an ASTM-NBS-NSF symposium, Kansas City, Mo., May 1978, J. T. Fong, Ed., *ASTM STP 675*, American Society for Testing and Materials, 1979, pp. 106-128.

ABSTRACT: Dislocation structures around the early stage fatigue cracks up to 170 μm in length formed in polycrystalline iron specimens were directly observed through an ultrahigh-voltage electron microscope operating at 2 MV. For this purpose, thin foils perpendicular to the surface were prepared from bulk specimens cycled up to 60 percent of the fatigue life of 2.5×10^5 cycles, by means of electroplating and jet electropolishing technique.

There were found some small straight cracks penetrating the cells (size: 2 to 5 μm), formed beneath the specimen surface as well as in the interior. Some straight screw dislocation lines parallel to the direction of the crack growth, one of the projections of the ⟨111⟩ directions, were observed in the cells just ahead of the crack. No marked entanglement of dislocations was observed within these cells.

On the other hand, some tangled dislocations were observed in the cells formed just around the cracks growing along grain boundaries.

The results just described are compared with those of the early stage fatigue crack formed in two kinds of face-centered-cubic (fcc) metals with different stacking fault energy (copper and α-brass) obtained previously, and the mechanisms of fatigue crack initiation and growth in the early stages are discussed.

KEY WORDS: iron (polycrystalline), fatigue (material), dislocation arrangements, crack propagation

It is well known that fatigue cracks begin at a surface in most metals.

[1]Assistant professor, professor, technical official, and research fellow, respectively, Institute of Scientific and Industrial Research, Osaka University, Yamadakami, Suita, Osaka 565, Japan.

[2]Formerly, graduate student, Faculty of Engineering, Osaka University; now, assistant professor, Faculty of Engineering, Fukui University, Japan.

Also, there is much evidence that crack initiation and propagation in the early stage of fatigue show a crystallographic aspect, and, therefore, they are thought to be closely related to motions of dislocations associated with dislocation structures beneath the surface as well as those around the crack. Dislocation arrangements beneath the specimen surface formed by cyclic stressing have been studied by many workers, with special emphasis on the structures in the persistent slip bands (PSB's) [*1-15*],[3] but direct information on the dislocation structure just around the crack tips in the early stages of fatigue has been absent until recent years. The present authors have reported dislocation arrangements around the short cracks in copper and α-brass specimens fatigued at relatively low stresses corresponding to fatigue lives of about 10^6 cycles [*16,17*]. However, our knowledge about these materials seems to be insufficient to understand the phenomenon in the early stage of fatigue.

This paper describes dislocation structures beneath the specimen surface and around the cracks in the early stage of fatigue. The results are based upon observations of thin foils prepared from bulk iron specimens with the use of a 2-MV electron microscope.

Experimental Procedure

Rods (15 mm in diameter) of polycrystalline iron, the chemical composition of which was C0.01-Si0.01-Mn0.28-Cu0.02-P0.01-S0.01 and iron the remainder in weight percent, were annealed at 950°C (1742°F) for 1 h, and were then rolled down to 3-mm-thick strips. After machining into specimens having a cross section of 3 by 8 mm, they were annealed again at 700°C (1292°F) for 2 h in vacuum, and finally electropolished to remove the surface layer by about 50 μm before testing. The grain size was about 60 μm in diameter.

The test specimens were fatigued under completely reversed plane bending of a constant moment with a Shimadzu UF-15 fatigue testing machine operating at 33 Hz. Observations of the dislocation structure around the crack were made of the specimens stressed at 20 kg/mm^2 (196 MN/m^2) until 60 percent of the expected life $N_f = 2.5 \times 10^5$ cycles.

Immediately after stressing, surfaces of the fatigued specimens were protected by an electrodeposited iron layer of approximately 2 mm in thickness. They were then cut longitudinally into slices (1.8 mm thick) perpendicular to the specimen surface by means of a milling cutter. The slices were thinned first mechanically with emery paper to the thickness of 600 μm and then electrolytically in order to remove the damaged layer. The area including cracks immediately next to the interface between the specimen and electrodeposit was thinned using jet electropolishing until per-

[3] The italic numbers in brackets refer to the list of references appended to this paper.

foration was witnessed by an optical microscope. (For the other details of the technique for thinning, see Ref *18*.)

Another observation was made of thin foils parallel to the specimen surface prepared by covering one side of specimen surface with a protective layer of paint and electropolishing from the rear. Thus, correlation between surface slip bands and underlying substructures was studied. In this case, specimens cycled until 0.6 N_f at a low stress amplitude [16 kg/mm^2 (157 MN/m^2), $N_i \cong 10^6$ cycles] were included besides the specimens fatigued at 20 kg/mm^2 (196 MN/m^2).

The foils were examined in an ultrahigh-voltage electron microscope operating at 2 MV.

Results

Surface Topographs and Substructures Beneath the Surface (Foils Parallel to the Specimen Surface)

On the surface of specimens fatigued at stress amplitude of 16 kg/mm^2 (157 MN/m^2), coarse slip bands were observed in some grains, but almost no markings in other grains. Band structures consisting of clusters of debris and some dislocation lines observed beneath the coarse slip bands are shown in Fig. 1*a*, together with the corresponding surface appearance observed by an optical microscope. Many long-dispersed dislocation lines of two kinds of direction were observed in the grains showing no surface markings (Fig. 1*b*). Screw dislocations straddling band structures and the formation of cell walls are seen especially in the neighborhood of grain boundaries.

The specimens fatigued at the stress of 20 kg/mm^2 (196 MN/m^2) revealed many more slip lines on their surface. The dislocation arrangement in most grains beneath the surface consisted of well-developed cell structure (Fig. 2). No direct relationship between the cell structure and surface irregularity was found. As can be seen at the top of Fig. 3, grains appearing black are covered with dense fine slip lines (the spacing between the slip lines being 0.1 μm); one end of each dislocation line terminates at these slip lines in these grains. This photograph shows that the size of the cells near the grain boundary is somewhat smaller than in the interior of the grains.

Dislocation Structures Around the Crack Tips (Foils Perpendicular to the Specimen Surface)

Cracks in the Early Stage (Straight Shear Mode Crack)—A well-developed cell structure was observed in the layer beneath the specimen surface remote from cracks, though the size of the cells was more or less smaller

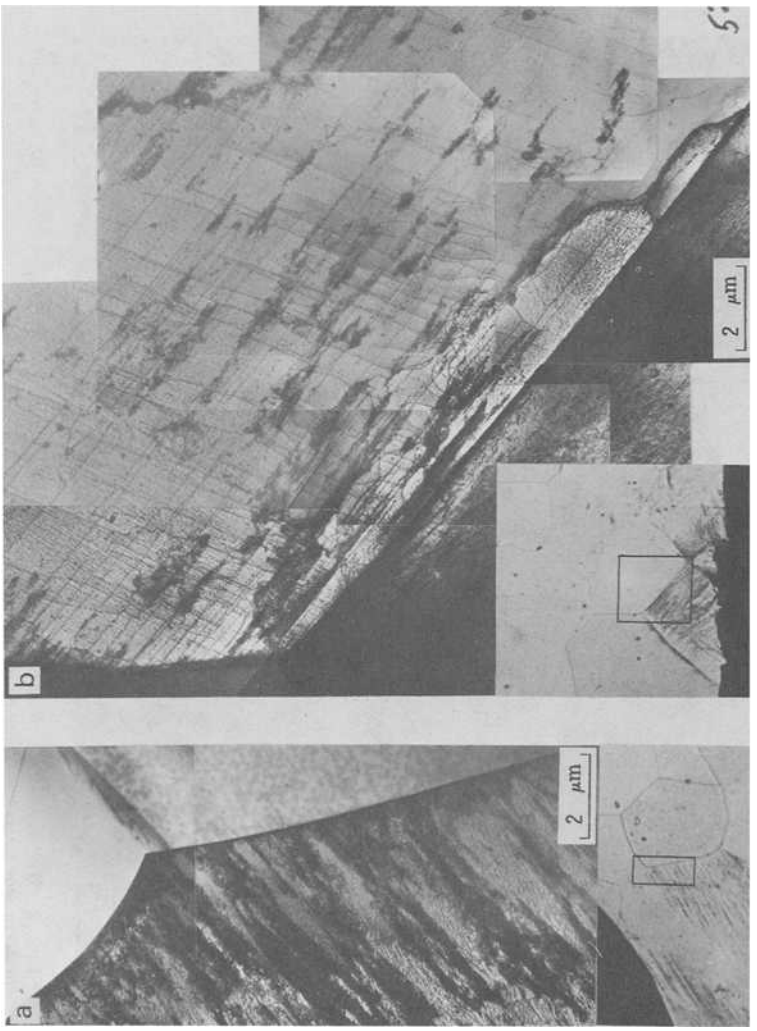

FIG. 1—*Dislocation structures beneath the surface of the specimens fatigued at a stress amplitude of 16 kg/mm² (157 MN/m²). Inserts show the areas from which the electron micrographs were taken, the thin foils being parallel to the surface* (a) *Grain with slipbands.* (b) *Grain without appreciable markings.*

FIG. 2—*Well-developed cell structure beneath the surface of the specimen covered with many slip bands; fatigue stress amplitude of 20 kg/mm² (196 MN/m²).*

FIG. 3—*Dislocation structures around a short straight crack growing about 45 deg to the stress axis [7 μm in length; stress amplitude of 20 kg/mm^2 (196 MN/m^2)]. The insert shows the optical micrograph of the foil taken perpendicular to the specimen surface, indicating the crack and the interface between specimen and electrodeposit.*

than that in the interior. No evident correlation between the profile of the surface and the cell structure was found. Considerable numbers of screw dislocation lines which were untangled were also seen in the cells.

Dislocation structures representative of the vicinity of the crack are shown in Figs. 3 and 4, in which straight cracks growing at approximately 45 deg to the specimen surface and well-developed cell structures around them can be seen. Although the size of the cells there is somewhat smaller, these are almost the same as that in the matrix. No specific dislocation arrangement was found ahead of their tips. These results suggest that the cracks grow penetrating the cells ahead of them, because (1) some crack tips are impinging into cells and (2) both the walls and contrast of the cells observed in mating sides across the cracks are sometimes continued.

The dislocation density within the cells around the crack is not necessarily high, and arrays of long straight dislocation lines in the direction of the crack are usually seen together with dislocations intersecting them. Electron diffraction analysis showed that, in Figs. 3 and 4, the direction of the crack coincides with the trace of one of {110} planes, and the dislocation lines in almost the same direction to the crack are parallel to the projection of ⟨111⟩. We can safely presume these to be screw dislocations.

Figure 5 shows the dislocation arrangement in the vicinity of the straight shear mode crack, the length of which reaches approximately 90 μm. The tip of the crack is growing inside the cell, near the wall. As in the case of the shorter cracks, straight dislocation lines parallel to the direction of crack growth are also seen in the cells ahead of its tip. The cell size apparently increases from approximately 1 to 5 μm with increasing distance from the tip; the shape of cells is somewhat elongated in the direction of crack growth. These features are similar to those of the dislocation structure around cracks growing at relatively high rates, which will be mentioned later.

The site of the crack initiation seems to be associated with grain boundary in many cases, presumably as a consequence of concentrated strain. The crack shown in Fig. 3 nucleates where the grain boundary intersects the specimen surface. Figure 6 shows an initial crack growing along a grain boundary; strictly speaking, it deviates slightly to the grain at the right of the grain boundary. Together with cells formed in this grain, there can be seen many straight dislocation lines in the direction of the grain boundary, that is, in the direction of crack growth. A marked step in the surface profile across the grain boundary is also seen. This crack appears to proceed eventually in the grain at the right of the grain boundary.

Although it is not always the case, many dislocation loops of approximately 0.05 μm in size and patches consisting of debris are found in the grain near the surface (Fig. 6). These loops seem to result from the pinching off of dislocations, it being more evident in another photograph taken by tilting the foil.

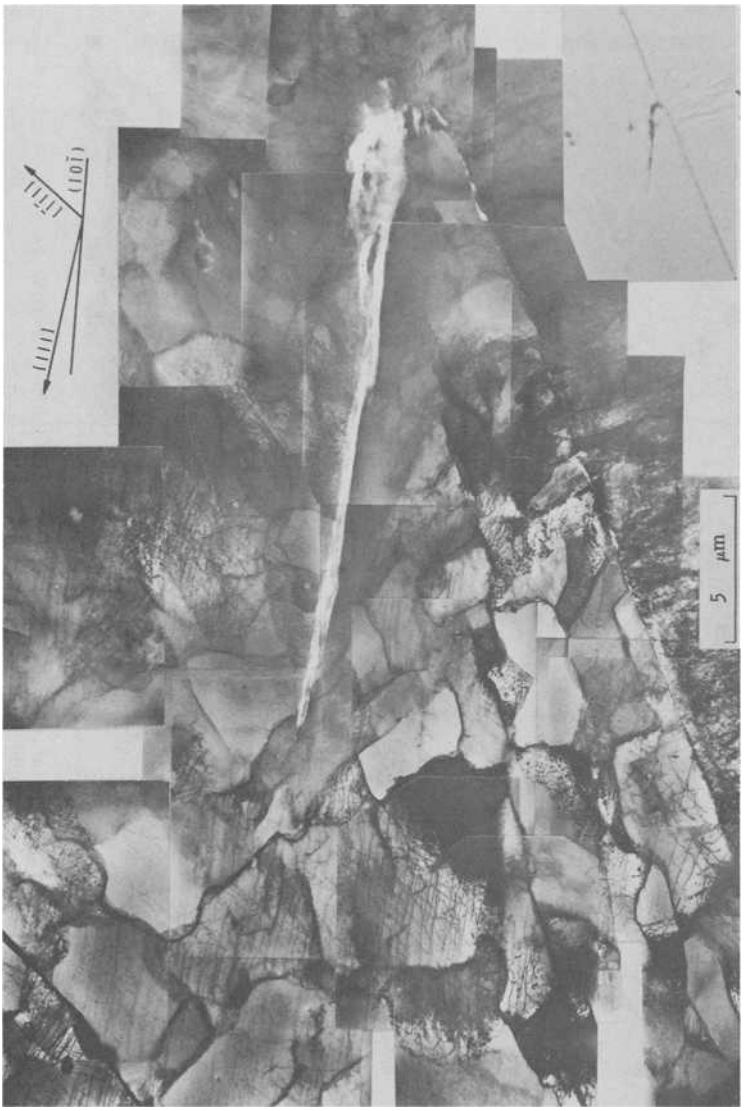

FIG. 4—*Dislocation structures around a straight crack growing about 45 deg to the stress axis [22 μm in length: stress amplitude of 20 kg/mm² (196 MN/m²)].*

FIG. 5—*Dislocation structure around a long straight crack growing about 45 deg to the stress axis [approximately 90 μm in length; stress amplitude of 20 kg/mm² (196 MN/m²)].*

FIG. 6—*Dislocation structures around a crack growing along a grain boundary which lies about 45 deg to the stress axis [13 μm in length; stress amplitude of 20 kg/mm^2 (196 MN/m^2)].*

Cracks in the Subsequent Stage (zigzag-Shaped Tensile Mode Crack)—Dislocation configurations around a crack which has grown to a length of approximately 35 μm are shown in Fig. 7. Although the overall direction is perpendicular to the stress axis, it takes a zigzag route, penetrating cells. The size of cells changes from 2 μm immediately next to the crack tip to about 5 μm only a few micrometres away. Neither arrays of dislocations parallel to the crack growth nor marked entanglements of dislocations were observed around the crack tip.

Figure 8 shows dislocation structures ahead of the tip of a crack which has grown up to 170 μm in the direction perpendicular to the stress axis. Although the dislocation arrangement just ahead of the crack is not so clear on account of bending of the foil, fine cells not larger than 1 μm are seen at both sides of the crack near the tip. The increase of cell size with distance from the crack tip is seen in the range of 10 μm ahead of it, and the average cell size is relatively small compared with that mentioned in the foregoing.

Dislocation structures around the crack which initially grows across a grain and then along a grain boundary are shown in Fig. 9. Although the micrograph is not so clear, there are found cells of significantly smaller size at the sides of the crack, and tangled dislocations of relatively high density around the crack.

Discussion

Stage I Crack Growth

Klesnil and Lukas [*15*] have reported in their investigations on fatigued α-iron that a group of zones with a very high dislocation density separated by zones with a very low dislocation density (structure of PSB) develops in the matrix consisting of indefinite cells. In the present studies, however, the dislocation structures observed beneath the specimen surface of fatigued iron are somewhat different from their results. In the copper specimens, Lukas and Klesnil also showed the difference in dislocation structure beneath the surface depending on the stress level—ladder-like structure and the matrix vein structure in the low stress, but only cell structure in the high stress [*4*]. The present results and those of Klesnil and Lukas on iron are analogous, but some discrepancy in structure remains, notwithstanding that these two experiments were carried out at the stress levels corresponding to a lifetime of 10^5 to 10^6 cycles. The ratio to the applied number of cycles to fracture (N/N_f) is 0.6 in the present experiment, which is larger than that by Klesnil and Lukas (0.3 to 0.4). This fact, however, cannot explain the discrepancy, because the structure is known to be unchanged after saturation hardening ($N/N_f \cong 0.01$) [*4*]. In either event, there is a possibility of redistribution of dislocation arrangements during

FIG. 7—*Dislocation structures around a crack taking a zigzag route in an overall direction perpendicular to the stress axis [35 μm in length; stress amplitude of 20 kg/mm² (196 MN/m²)].*

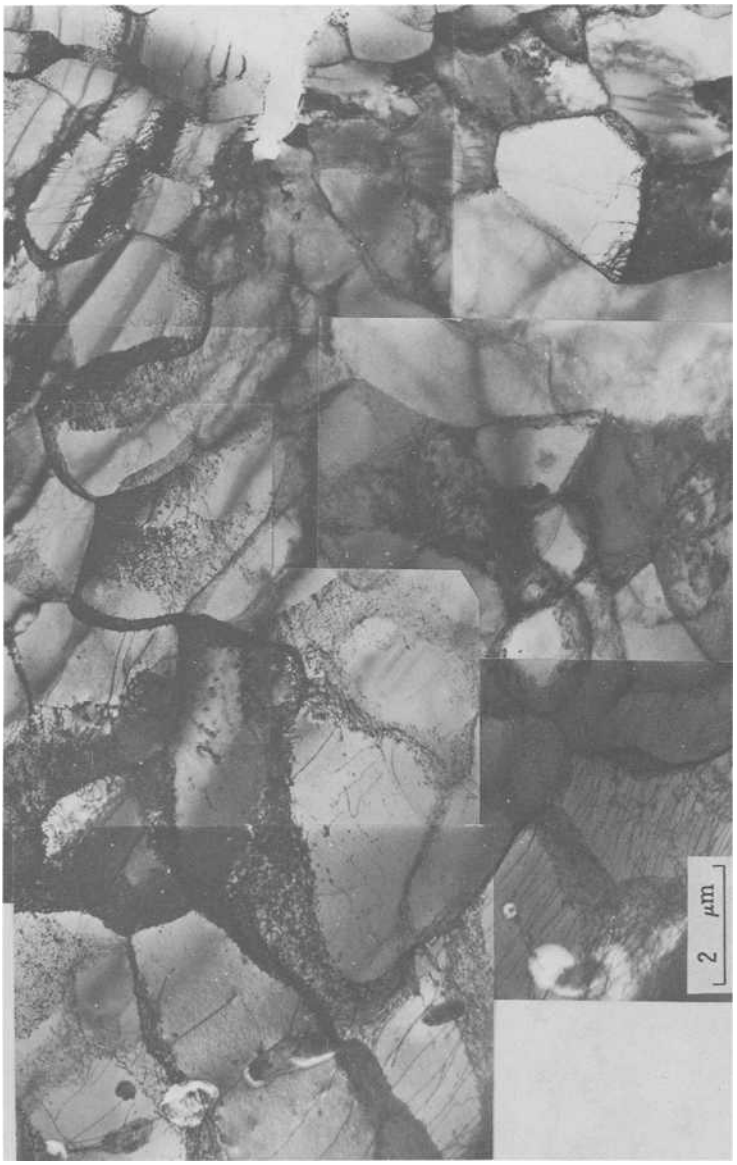

FIG. 8—*Dislocation structures around a crack growing in the direction perpendicular to the stress axis* [170 *μm in length; stress amplitude of 20 kg/mm*^{2} *(196 MN/m*^{2}*)*].

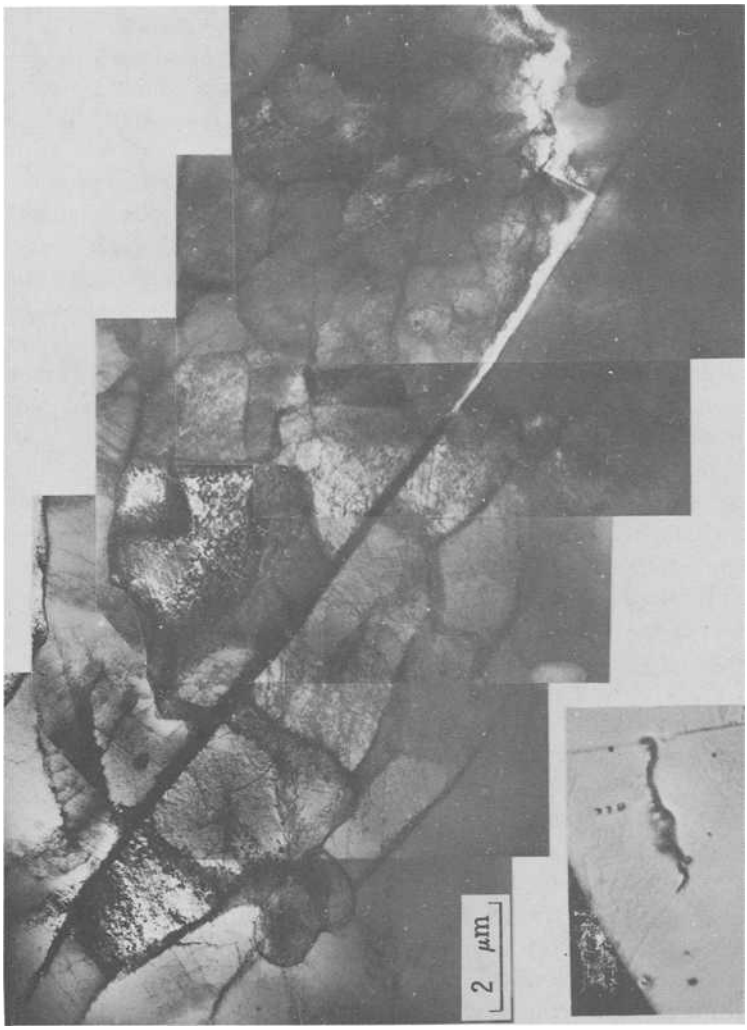

FIG. 9—*Dislocation structures around a crack growing along a grain boundary (40 μm in length; stress amplitude of 20 kg/mm² (196 MN/m²)).*

an initial stage of fatigue. The experimental results mentioned in the preceding section cannot necessarily give correct information for initiation of cracks. However, if there is no essential distinction between initiation and growth of crack, the present results might be applicable to the clarification of the mechanism of crack initiation as they are so in the case of crack propagation.

The present authors reported on the dislocation structures around cracks in the early stage of fatigue in copper and α-brass specimens fatigued at the stresses corresponding to the fatigue life of approximately 10^6 cycles. It was clarified that in copper the crack initiated and grew along the ladder-like structure (PBS structure), which penetrated across the vein structure (matrix) [*16*], whereas the crack in α-brass grew along the primary slip plane in which dislocation lines and loops were densely distributed [*17*]. The present experiment on iron specimens fatigued at the high stress level showed that the crack was growing across the well-developed cell structure which was not different from that in the matrix. As has been mentioned in the foregoing, the dislocation arrangements in the region where movements of the dislocation contribute to the formation and growth of the crack are different according to the stress level applied and the stacking fault energy. Nevertheless, the crack in the early stage grows along the slip plane of maximum resolved shear stress, and its fracture surface reveals a flat facet accompanied by parallel lines along the slip direction [*19,20*]. So, the crack is thought to grow through the same mechanism in these metals. Although decohesion of crystal along the slip planes due to increased density of dislocation and debris on them might contribute to Stage I crack growth for α-brass, it is not applicable to that for iron, in which the crack is growing across cells. It is reasonable, therefore, to imagine the model for Stage I crack growth involving a process like unslipping of crystal by the primary dislocations [*21*], though the details are not specified.

Slip on one slip system alone cannot produce a steadily growing crack, because the motion of dislocations in one direction produces slip steps, but annihilates them on the way back. Recently, through a fractographic study on copper single crystals, Neumann [*22*] has given evidence showing that surface reactions with the environment deteriorate the new surface of each slip step such that the surface is not annihilated during back slip. However, there is no reason why slip other than primary slip is excluded. It is possible to show from a model similar to that proposed by Neumann [*23*] that a crack grows along a primary slip plane, without atmospheric attack, by the motion of dislocations on a primary slip plane in cooperation with slip on secondary slip planes. This model is consistent with the present result; numerous straight dislocations parallel to the crack lying on the primary slip plane together with ones intersecting them were found within cells ahead of the crack.

Neumann reported in the same paper that a Stage I crack can grow

without a preexisting soft zone; that is, it is possible for a Stage I crack growth to occur subsequently to a Stage II crack if the loading condition is preferable. An experimental result of this kind has also been reported for polycrystalline iron by Otsuka et al [*24*]. This is in agreement with the present result on dislocation arrangements around a Stage I crack formed at high stress. The specific dislocation arrangement beneath the surface is not a prerequisite for shear mode cracking to occur.

It seems useful to notice in the foregoing discussion that motion of screw dislocations through the cell walls seems to occur readily as has been evidenced by direct observations of aluminum foil in unidirectional deformation by Fujita [*25*].

Stage II Crack Growth

There were found no considerably tangled dislocations within the cells ahead of the cracks propagating perpendicular to the stress axis. Although we cannot explain from these micrographs what the mechanism of Stage II crack growth is, it is inferred that the crack in early Stage II grows without an extremely hardened region just ahead of its tip. It seems interesting that the dislocation morphology around the crack subsequent to Stage I is analogous to those in the preceding stage, notwithstanding the difference in the route of crack growth. The main difference is that the dislocations parallel to the Stage I crack are not found in Stage II. From these circumstances, it is supposed that the possible mechanism of the crack growth in Stage II is not significantly different from that in Stage I. In Stage I, dislocation motion on the primary planes plays an important role with the aid of the auxiliary motion of dislocations on the secondary slip planes, and, in the subsequent stage, two cooperative slip systems crossing each other at the front of the crack are operative [*23,26,27*]. If it is the case, changeover from Stage I to Stage II crack growth would depend how much the primary slip exceeds the secondary one at the crack tip. Therefore the transition appears to be controlled by crystallographic orientation and constraint from surrounding grains. These factors are expected to explain why a crack of length 35 μm shown in Fig. 7 has changed to Stage II crack growth, whereas the crack of length 90 μm shown in Fig. 5 is growing in the Stage I mode.

In the present observations, as compared with the case of the cracks of high growth rate in fatigued iron specimens [*28–30*], (1) neither tangled dislocations nor piles of elongated cells were found in front of the crack tips, and (2) the cell sizes around the tips as well as the sides of the cracks were not so small (about 2 and 1 μm, respectively). Therefore, the early Stage II crack growth studied here seems to be somewhat different from that of higher growth rate, though the mechanism itself is thought to be essentially identical. The fact that the size of cells decrease the closer they

are to the crack tip, within a small region ahead of the tip, suggests that the strain concentration region is localized in a very small area.

Dislocation entanglement observed around the grain boundary crack growing in this stage is not so different from that in the case of the crack of high growth rate [*28*]. It is suggested that crack growth occurs through marked dislocation motion at both sides of the grain boundary.

Conclusions

Dislocation structures around the short cracks (the length of which being 7 to 170 μm) formed in fatigued polycrystalline iron specimens were observed through an electron microscope operating at 2 MV. The main conclusions are:

1. Small straight cracks seem to grow along the primary slip plane penetrating the cells. Within the cells, straight screw dislocations parallel to the direction of the crack growth are observed.
2. There was found no difference between the structure around these cracks and that away from them. Therefore, it is inferred that some specific dislocation structure corresponding to the persistent slip band is not a prerequisite for shear mode crack propagation.
3. Dislocation morphololgy around the cracks growing in the zigzag route in the overall direction perpendicular to the stress axis was revealed to be well-defined cells. This is not significantly different from that around the small straight crack.
4. Some tangled dislocations were observed together with small cells around the crack growing along a grain boundary.

Acknowledgments

The authors would like to thank Prof. H. Fujita and the members of HVEM center in Osaka University for giving them facilities to use the ultrahigh voltage electron microscope.

References

[*1*] Laufer, E. E. and Roberts, W. N., *Philosophical Magazine*, Vol. 10, 1964, pp. 883-885 and Vol. 14, 1966, pp. 65-78.
[*2*] Lukas, P., Klesnil, M., Krejci, J., and Rys, P., *Physica Status Solidi*, Vol. 15, 1966, pp. 71-82.
[*3*] Lukas, P., Klesnil, M., and Krejci, J., *Physica Status Solidi*, Vol. 27, 1968, pp. 545-558.
[*4*] Lukas, P. and Klesnil, M., *Physica Status Solidi* (a), Vol. 5, 1971, pp. 247-258.
[*5*] Woods, P. J., *Philosophical Magazine*, Vol. 28, 1973, pp. 155-191.
[*6*] Finney, J. M. and Laird, C., *Philosophical Magazine*, Vol. 31, 1975, pp. 339-366.
[*7*] Grosskreutz, J. C., Reimann, W. H., and Wood, W. A., *Acta Metallurgica*, Vol. 14, 1966, pp. 1549-1557.

[8] Lukas, P. and Klesnil, M., *Physica Status Solidi*, Vol. 37, 1970, pp. 833-842.
[9] Levine, E. and Weissmann, S., *Transaction*, American Society for Metals, Vol. 61, 1968, pp. 128-138.
[10] Mitchell, A. B. and Teer, D. G., *Philosophical Magazine*, Vol. 19, 1969, pp. 609-612.
[11] Krejci, J. and Lukas, P., *Physica Status Solidi* (a), Vol. 8, 1971, pp. 299-307.
[12] McGrath, J. T. and Waldon, G. W. J., *Philosophical Magazine*, Vol. 9, 1964, pp. 249-259.
[13] Forsyth, P. J. E., *Acta Metallurgica*, Vol. 11, 1963, pp. 703-715.
[14] Clark, J. B. and McEvily, A. J., *Acta Metallurgica*, Vol. 12, 1964, pp. 1359-1372.
[15] Klesnil, M. and Lukas, P., *Journal of the Iron and Steel Institute*, Oct. 1965, pp. 1043-1048.
[16] Katagiri, K., Omura, A., Koyanagi, K., Awatani, J., Shiraishi, T., and Kaneshiro, H., *Metallurgical Transactions* A, Vol. 8A, 1977, pp. 1769-1773.
[17] Katagiri, K., Omura, A., Koyanagi, K., Awatani, J., Shiraishi, T., and Kaneshiro, H. in *Fracture 1977, Proceedings*, 4th International Conference on Fracture, Waterloo, Ont., Canada, University of Waterloo Press, Vol. 2, pp. 695-702.
[18] Awatani, J., Katagiri, K., and Shiraishi, T., *Journal of the Society of Material Science*, Japan, Vol. 25, 1976, pp. 145-150 (in Japanese).
[19] Kobayashi, H., Nakazawa, H., and Komine, A., *Transactions*, Japan Society of Mechanical Engineers, Vol. 41, No. 341, 1975, pp. 9-21 (in Japanese).
[20] Katagiri, K., Omura, A., Koyanagi, K., Awatani, J., and Kaneshiro, H., *Journal of the Society of Material Science*, Japan, Vol. 25, no. 275, 1976, pp. 724-730. (in Japanese).
[21] Kaplan, H. I., and Laird, C., *Transactions of the Metallurgical Society of The American Institute of Mining, Metallurgical, and Petroleum Engineers*, pp. 1017-1025.
[22] Neumann, P., Vehoff, H., and Fuhlrott, H. in *Fracture 1977, Proceedings*, 4th International Conference on Fracture, Waterloo, Ont., Canada, University of Waterloo Press., Vol. 2, pp. 1313-1324.
[23] Neumann, P., *Acta Metallurgica*, Vol. 17, Sept. 1969, pp. 1219-1225.
[24] Otsuka, A., Mori, K., and Miyata, T., *Engineering Fracture Mechanics*, Vol. 7, 1975, pp. 429-439.
[25] Fujita, H., *Journal of the Physical Society of Japan*, Vol. 23, No. 6, 1967, pp. 1349-1361.
[26] Pelloux, R. M. N. in *Proceedings*, 2nd International Conference on Fracture, Brighton, Chapman and Hall, 1969, pp. 731-744.
[27] Bowles, C. Q. and Broek, D., *International Journal of Fracture Mechanics*, Vol. 8, 1972, pp. 75-85.
[28] Awatani, J., Katagiri, K., and Nakai, J., *Metallurgical Transactions* A, Vol. 9A, 1978, pp. 111-116.
[29] Ogura, T., Masumoto, T. and Imai, Y., *Transactions*, the Japan Institute for Metals, Vol. 17, 1976, pp. 733-742.
[30] Bathias, C., *Memoires Scientifiques De La Revue De Metallurgie*, Vol. 57, No. 3, 1970, pp. 165-171.

DISCUSSION

A. Plumtree[1] *(discussion)*—This work, together with that of Awatani et al[2] on larger fatigue cracks in iron, shows that the dislocation morphology around the tips of large and small cracks is very similar. Dislocation cells

[1]Department of Mechanical Engineering, University of Waterloo, Waterloo, Ont., Canada.
[2]Awatani, J., Katagiri, K., and Nakai, H., *Metallurgical Transactions*, Vol. 9A, 1978, p. 111.

have been observed at the tips of these cracks—even small cracks growing in a straight shear mode (Stage I). The cellular dislocation structure becomes more refined as the crack tip is approached, which is characteristic of an increasingly higher cyclic strain amplitude.

The work of Abdel-Raouf et al[3] on strain-cycled pure iron showed that the saturation cell size (l) may be related to the plastic strain amplitude ($\Delta\epsilon_p/2$) as follows

$$l = 0.675\,(\Delta\epsilon_p/2)^{-0.19} \tag{1}$$

Using Eq 1 for the present work, the approximate cell size at various distances ahead of the crack has been converted to an equivalent plastic strain range and plotted in Fig. 10 for three cracks. It is immediately apparent that there is an extremely large plastic strain gradient ahead of both Stage I (90-μm crack length) and Stage II (35- and 170-μm crack lengths) cracks. The highly strained region extends farther ahead of the

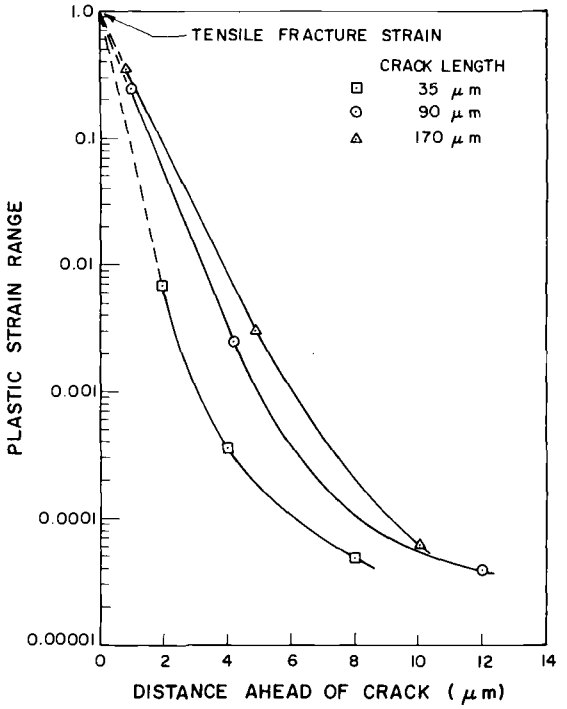

FIG. 10—*Plastic strain as a function of distance ahead of fatigue crack.*

[3]Abdel-Raouf, H., Benham, P. P., and Plumtree, A., *Canadian Metallurgical Quarterly*, Vol. 10, No. 2, 1971.

crack tip with increasing crack size. One can speculate at this point regarding the role of stacking fault energy and suggest that a lower stacking fault energy material with a higher cyclic work-hardening exponent would possess lower strain gradient for a given crack size, resulting in a slower crack growth rate. A lower stacking fault energy would also affect the dislocation motion on secondary and cross slip planes.[4-6]

The refined cell structure ahead of the crack indicates that crack extension will be a consequence of the high plastic strains. Such evidence supports the plastic-blunting model of Laird.[7] Two other important points which illuminate proposed fatigue crack growth mechanisms should be mentioned. First, void mechanism and crack nucleation ahead of the main crack was not observed by the authors; and second, no evidence was seen of crack propagation along cell boundaries.

J. Simmons[8] (*discussion*)—The need to obtain an understanding of what happens in front of a propagating crack, particularly in iron, is of central importance for the study of fatigue failure. This paper represents a careful, but preliminary study of the microstructure around small-scale fatigue cracks using the 2-MeV electron microscope at Osaka University.

Katagiri and co-workers have learned that dislocation arrangements in the vicinity of cracks formed in polycrystalline bcc iron of low purity ($C = 0.01$ percent) are quite different than those produced in 99.99 percent purity fcc polycrystalline copper. There, microcracks seemed to be associated with dramatic-appearing "ladder-like structures" usually associated with persistent slip bands. In this study, however, these ladder structures did not form and slip appeared to be relatively homogeneous.

At the stress amplitudes over which most of the results of this paper are based (196 MN/m^2) a reasonably well-defined cell structure was observed, but the correlation of a crack initiation or crack growth with the cell structure was not established. A major conclusion of the paper concerns features not observed; fatigue cracks in this material at this stress range do not appear correlated with either voids or persistent slip bands.

Ahead of most growing cracks could be seen an increase in dislocation density which often resolved itself after the crack had passed into a finer cell network than the remainder of the matrix. Several observations also show cracks associated with grain boundaries. Typical Stage I and Stage II cracks were both studied.

[4]Neumann, P., *Acta Metallurgica*, Vol. 17, 1969, p. 1219.

[5]Pelloux, R. M. N. in *Proceedings*, 2nd International Conference on Fracture, Brighton, U. K., Chapman and Hall, 1969, pp. 731-744.

[6]Bowles, C. Q. and Broek, D., *International Journal of Fracture Mechanics*, Vol. 8, 1972, p. 75.

[7]Laird, C. in *Fatigue Crack Propagation, ASTM STP 415*, American Society for Testing and Materials, 1967, p. 131.

[8]Center for Materials Science, National Bureau of Standards, Washington, D. C. 20234.

From the point of view of this discusser, which is that of a bystander in this field, the difficulty of making correlations between the dislocation cell structure and the near atomic criteria appearing to govern crack nucleation and motion in this material is not altogether surprising. The dislocation cell structure can be correlated reasonably well with that component of the internal stress state of the material whose wavelength is of the same order of magnitude as the cell size. Indeed, as the wavelength of the internal stress field and the corresponding cell size appear to become smaller, the material is generally more work-hardened; whether the amplitude of internal stress oscillations is correlated with cell size is not clear. However, the wavelength of that component of the internal stress field associated with the cell structure is of the order of micrometres, whereas the competition between dislocation generation near the crack tip and decohesion-like phenomena which appear to govern crack nucleation and migration in this material is probably of the order of tens of nanometres and, therefore, virtually independent of the internal stress field associated to the cell structure. Of course, internal stresses associated with the cell structure occur within the cell walls with much shorter wavelength and may influence crack motion while the crack is propagating through the cell wall. However, such effects cannot be detected by the techniques reported in this paper, and it is clear that any more macroscopic surface stresses that could be associated with cell walls have not affected the crack paths (see Fig. 8 of Ref. *28*). Indeed, the overall crack motion observed in this paper does not seem correlated with the cell structure to any appreciable degree, but is more related to the macroscopic loading conditions. Thus, one might infer that the internal stress variation within cells and the surface stresses on cell walls are not large enough to appreciably modify the crack path on the micrometre scale.

H. Mughrabi[9] (*discussion*)—First of all, I should like to express satisfaction that the observations of Dr. Katagiri and co-workers show convincingly that the dislocation microstructure prevailing at the crack tip is that of persistent slip bands in copper but not in α-iron, where a cell structure is found. This result corresponds clearly with our studies of the bulk dislocation microstructure. Both sets of observations supplement each other beautifully.

In the cell structures in iron that were presented by Dr. Katagiri, screw dislocations were dominant, showing that the low-temperature deformation mode was operating at room temperature as in our case (at the higher strain rate). The fact that the iron used by Dr. Katagiri contained more carbon than ours is not so important. Our results show that, at high strain

[9]Max-Planck-Institut für Metallforschung, Institut für Physik, Stuttgart, Germany.

rates, the dislocation arrangements in pure iron and in iron containing some carbon are very similar.

I have a comment on Prof. Plumtree's suggestion on how to correlate the cell sizes. While I agree basically, I wish to remark that we have found for a variety of tests at different plastic strain amplitudes and strain rates that the only quantity that will relate uniquely with the cell size is the athermal component of the (saturation) stress. This is the macroscopic stress parameter that should be related to any dimension of the dislocation microstructure.

Regarding the remark made by Dr. Simmons about differentiating between (local) stresses, I think this can be met in some materials, namely, by measuring by transmission electron microscope the radii of curvature of free dislocations, provided you succeed in retaining them in the specimen by pinning. These radii of curvature give a direct measure of the *locally* acting internal stress, if pinned in the unloaded state, or of the combination of external plus internal stress, if pinned in the loaded state.

K. Katagiri, J. Awatani, A. Omura, K. Koyanagi, and T. Shiraishi (authors' closure)—We appreciate Prof. Plumtree showing the curves (Fig. 10) which quantitatively elucidate the strain distributions ahead of the tips of both Stage I and Stage II cracks. The conversion from the cell size to an equivalent plastic strain range appears to be applicable if the crack growth rate is not so high. The number of stress cycles before the crack tip is approached should be large enough to lead the cells to saturation size; the conversion seems to hold in the present case. We also fully agree with the remarks made by Prof. Plumtree except for the following point.

Regarding the speculation made by Prof. Plumtree, we would like to know in detail why a lower strain gradient for a given crack size results in a slower crack growth rate. Anyhow, we have little information on the strain distribution in the vicinity of cracks which have grown into the interior of bulk specimens of lower stacking fault energy metals. Our recent study on α-brass showed that no cell formation is found ahead of a crack propagating at a growth rate of 0.05 μm/cycle.[10] Therefore, we have to find other measures which show the local strain distribution around the cracks in such materials. The proposed speculation may be estimated at that time.

We quite agree with the comments made by Dr. Simmons. It seems to be one of the important resuts that the crack extension does not seem correlated directly with the observed dislocation structures (cells) which have already been formed before the crack is approached.

[10]Awatani, J., Katagiri, K., and Koyanagi, K., *Metallurgical Transactions A*, Vol. 10A, 1979, pp. 503-507.

Dr. Mughrabi's works on the PSB's of fcc and bcc metals[11,12] clearly indicate the possibility that the dislocation structure corresponding to the PSB is absent in iron, and also that the dislocation structures around initial cracks (therefore, motion of the dislocations contributing them) are different for copper and iron, which is the case in the present study. Now the question is whether the mechanisms for crack nucleation and also propagation are essentially different for both metals or not. Although we have not presented direct evidence, it does not seem inconsistent with the experimental results to think of the mechanisms as being virtually identical for both as described in the text. On this most important problem, further work is, of course, expected.

[11] Mughrabi, H., Ackermann, F., and Herz, K., this publication, pp. 69-105.

[12] Mughrabi, H., Herz, K., and Ackermann, F. in *Proceedings*, 4th International Conference on the Strength of Metals and Alloys, Nancy, France, Vol. 3, 1976, pp. 1244-1248.

L. F. Coffin, Jr.[1]

Closing Remarks by Session Chairman

I think a number of the discussers have commented on the fact that this is a session which has attempted to merge the interests and the discipline of quantitative microscopy with those of direct observations at dislocation level.

Not knowing a great deal about either one of these subjects, I have come away from this with the feeling that we have not quite connected these subjects as closely as we might, and that we have got quite a bit of work ahead of us if these two fields are to interact in any constructive way.

[1]General Electric Co., Corporate Research & Development, Schenectady, N.Y. 12301.

Chapter 3: Direct Observations from Slipbands to Nucleation of Microcracks

J. C. Grosskreutz[1]

Opening Remarks by Session Chairman

I am substituting for Bill Ruff who was unavoidably detained by another engagement at the National Bureau of Standards. That affords a happy occasion for me to be chairman of this session, and to participate in a symposium which is very close to my heart because I worked in this field for many years. Also, I have not seen many of you for at least five or six years, so that makes it a doubly happy occasion.

I was asked to say a few remarks, but all the remarks I can make about fatigue are at least five or six years old and you are here to hear the latest remarks about fatigue. So, I am not going to bore you with that kind of conversation.

I would like to say for those of you who have not talked to me recently that I am no longer working in this field but am now at the Solar Energy Research Institute in Golden, Colo., where I am director of the Research Division. We will be doing some fatigue research there because thermal fatigue occurs in all solar energy devices. Over a 30-year solar system lifetime, at least 10 000 cycles occur as the sun goes up and down every day, and if operation is at high temperatures there are thermal fatigue problems. So I cannot get away from this subject even though I left it and went into solar energy.

I continue to have a great and abiding interest in fatigue mechanisms, and it is appropriate to make a few remarks in response to some questions that were asked this morning about the importance of basic mechanisms research.

I do believe it is important. I hope that everyone continues to recognize that there are many mechanisms of fatigue, depending upon the material and on the environment, both stress and atmospheric. I do think that people involved in basic mechanisms research must look for the extrapolations or generalizations that can come out of their research and apply these extrapolations to engineering materials.

[1] Solar Energy Research Institute, Golden, Colo. 80401.

This extrapolation is a difficult job, and it is a job that has to be managed. It does not just occur spontaneously. I think E-9 and the Subcommittee on Research has a unique opportunity here—has always had a unique opportunity—to help manage and make that sort of thing happen—by symposia such as this, or by your own committee-week meetings which you have several times a year.

Engineers make the mistake sometimes of extrapolating things from fundamental research that should not be extrapolated, so you have an obligation to the engineering profession, to help them make the proper extrapolations or projections or else they will misuse fundamental data. And that is to their detriment and to ours as well.

It is true that most engineering materials contain stress risers or defects, inclusions, or just plain dirt that usually are the nuclei of fatigue cracks. On the other hand, many engineering materials are being made more pure to obtain better environmental protection or better strength properties, as the case may be. I think it is vitally important that we understand the fundamental mechanistic processes in simple materials as well as in complicated materials, because the ultimate question we are trying to answer is: Are materials basically unstable under cyclic stressing?

And I think we all agree that they are, and that finding the mechanisms by which that instability occurs in one material certainly leads us to understand more complex materials. So with that sort of "commercial" for basic mechanisms research, we will get on with the program here.

I want to congratulate Committee E-9 and the Committee on Research—Joe Morrow, Dave Hoeppner, and Jeffrey Fong—for planning this symposium. It is very timely and I, for one, am enjoying it.

The things I have heard this morning say that there certainly has been progress in the past five years since I left this field. One of the things that is vital to advancement is the development of new experimental techniques. You can continue to use the old ones and you can continue to use the old mathematics and the old statistics. But in understanding a mechanism, the thing that is vital to progress (in my experience anyway) is the development of new experimental techniques or the refining of old experimental techniques that allow you to go back and reevaluate what you saw five or even ten years ago to get a new insight into what is happening.

S. Taira,[1] *K. Tanaka,*[1] *and M. Hoshina*[1]

Grain Size Effect on Crack Nucleation and Growth in Long-Life Fatigue of Low-Carbon Steel

REFERENCE: Taira, S., Tanaka, K., and Hoshina, M., **"Grain Size Effect on Crack Nucleation and Growth in Long-Life Fatigue of Low-Carbon Steel,"** *Fatigue Mechanisms,* Proceedings of an ASTM-NBS-NSF symposium, Kansas City, Mo., May 1978, J. T. Fong, Ed., *ASTM STP 675,* American Society for Testing and Materials, 1979, pp. 135–173.

ABSTRACT: The ratios of the number of cycles to slipband formation and to crack nucleation to the total life were determined experimentally in fatigue tests of smooth specimens of low-carbon steel with several grain sizes. The number of cycles spent in propagating a nucleated fatigue crack was predicted by an analysis based upon the results of a through-crack growth study. The change of crystal deformation with number of cycles was studied by the X-ray microbeam diffraction technique, and the characteristics of cyclically induced substructure were discussed in comparison with substructure due to monotonic deformation. A micromechanistic model for the fatigue limit was proposed to interpret the Petch-type relation between fatigue limit and grain size under the assumption of the critical value of microscopic stress intensity factor at the tip of cracks blocked by the grain boundary. From through-crack growth experiments at several values of the stress ratio R, it was found that the threshold stress intensity factor ΔK_{th} increased linearly with the square root of the grain size l for each R-value, and the relation between the effective value of ΔK_{th} and $\sqrt{l}$ was independent of R-value. In order to interpret these findings, a model for the threshold of crack growth was proposed under the assumption that the threshold condition was determined by whether the slipband near the crack tip propagated into an adjacent grain or not.

KEY WORDS: crack growth, crack nucleation, fatigue (materials), fracture mechanics, grain size, low-carbon steel, micromechanics, microstructure, threshold condition

The fatigue fracture of structural materials containing large flaws or cracks is caused by the growth of these defects under cyclic loading. The growth behavior of cracks due to fatigue has been successfully predicted by fracture mechanics parameters, such as the stress intensity factor (SIF).

[1] Professor, research associate, and graduate student, respectively, Department of Engineering Science, Kyoto University, Kyoto, Japan.

The sigmoidal variation of growth rate with SIF range has been reported by many investigators [*1,2*].[2] The grain size of metals has a predominant influence on the rate of crack growth in the low-rate region near the threshold conditions [*3*], although its effect is minimal in the high-rate region [*4*]. In this work, the quantitative nature of the grain size effect on near-threshold crack growth and the micromechanisms of crack growth at very low rates were explored.

For metallic materials which are initially free of large flaws or cracks, slip motion leads to the formation of fatigue cracks which eventually propagate to the critical length for final fracture [*5*]. The grain size of the metal can play a different role in the slip motion, crack nucleation, and growth stages of the fatigue process. Most previous studies which used smooth specimens to determine the grain size effect on the fatigue strength have dealt exclusively with the total life or the fatigue limit [*6–8*] and little attention has been paid to the role of the grain size in each stage composing the total process of fatigue fracture. The growth behavior of very small cracks nucleated on smooth specimens may be affected by microstructure [*4,6*]. It is still uncertain whether a crack growth law established for longer cracks can be applied to the cases of those very small cracks [*9,10*]. To assess the influence of microstructural constituents such as the grain size on the fatigue strength, a quantitative understanding of the nature of the basic mechanism working in each stage of the fatigue process is essential.

In the present paper, the grain-size-sensitive nature of the mechanical characteristics of crystal deformation, crack nucleation, and crack growth in long-life fatigue of a low-carbon steel with several grain sizes was investigated based on the results of microscopic observation. The microstructural change due to cyclic stress was measured quantitatively by using the X-ray microbeam diffraction technique, and optical and scanning electron microscopies. The nucleation of fatigue cracks and the threshold condition for fatigue crack growth are discussed based on microstructure mechanics combined with crack mechanics.

Experimental Procedure

Material and Specimen

The low-carbon steel used (0.20C-0.92Mn-0.26Si-0.11P-0.15S-0.009N) was supplied in hot-rolled strip of 8-mm thickness. Three different kinds of microstructure were obtained by heat treatment. The microstructure is a mixed structure of ferrite and pearlite grains. The ferrite grain size

[2] The italic numbers in brackets refer to the list of references appended to this paper.

measured by the linear intercept method is 7.8, 20.5, and 55 μm and the material with each grain size is designated as A, B, and C, respectively. The heat-treatment condition and the mechanical properties derived from simple tension tests are summarized in Table 1. Simple tension tests were conducted in a Shimadzu AUTOGRAPH IS-5000 by using strip specimens whose thickness and width were 4 and 10 mm and whose gage length was 50 mm. The crosshead speed of the machine in tension testing was 1.0 mm/min.

Prior to machining the specimens, the plates of experimental material with 5-mm thickness were first quenched in water from 900°C and then tempered at 450°C for 20 min. The specimens were re-heat treated after machining according to the condition given in Table 1. The decarburized layer of the specimen surface due to heat treatment was taken off by electropolishing. Before fatigue tests, all the specimens were etched by 3 percent nital solution for microscopic examinations. The final shape and the dimensions of the specimen are shown in Fig. 1, where (*a*) is for smooth specimen fatigue tests and (*b*) for fatigue crack propagation tests. The former specimen has a weak stress concentration with the elastic stress concentration factor of 1.04 [*11*]. The applied stress amplitude used in the following sections is the nominal value multiplied by 1.04.

Mechanical Tests

The fatigue tests for smooth specimens were performed in a resonance-type bending test machine operated at a test speed of 33.3 Hz. The specimens were subjected to a fully reversed plane bending moment; that is, the ratio of the maximum to minimum stress, R, was -1.

Fatigue crack propagation experiments were conducted in a servohydraulic fatigue testing machine, Shimadzu SERVO-PET, at three R-values: -1, 0, and 0.5. The frequency of stress cycling was 30 Hz. The length of a fatigue crack was monitored with a traveling microscope at $\times 400$ magnification and the minimum increment of crack length to be resolved with this

TABLE 1—*Heat-treatment condition and mechanical properties of material.*

Material	Post-Machining Heat-Treatment	Grain size, l (μm)	Yield Strength, σ_Y (MPa)	Tensile Strength, σ_B (MPa)
A	annealed at 900°C for 10 min followed by air cooling	7.8	366	528
B	annealed at 1000°C for 1 h followed by furnace cooling	20.5	275	466
C	annealed at 1200°C for 5 h followed by furnace cooling	55	194	433

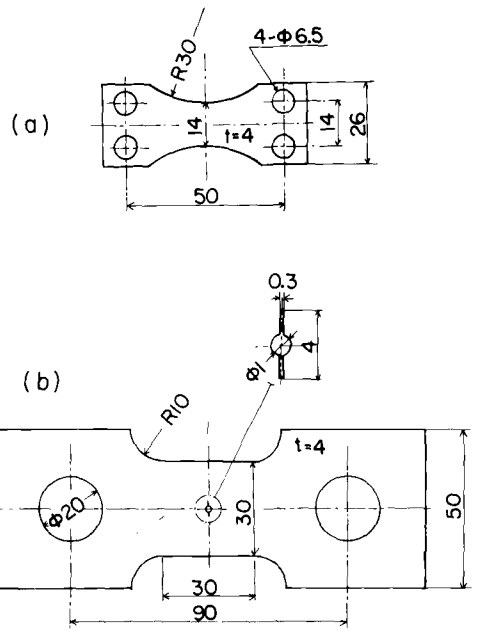

FIG. 1—*Test specimens (dimensions are in mm)*: (a) *smooth specimen for fatigue experiment and* (b) *notched specimen for fatigue crack propagation experiment.*

method was 0.5 μm. The SIF value, K, was calculated by the secant formula [*12*]

$$K = \sigma\sqrt{\pi a}\,\sqrt{\sec(\pi a/2W)} \tag{1}$$

where σ is the applied gross stress, and a and W are the half crack length and the half specimen width, respectively. The rate-versus-ΔK relation in the high-rate region was obtained in fatigue with constant stress cycling. In the region near the threshold condition, the stress value was decreased so as to lower the SIF from ΔK_1 to ΔK_2 by less than 10 percent of ΔK_1, keeping the R-value constant. The preliminary experiment indicated that the growth rate was unaffected by the SIF decrease from ΔK_1 to ΔK_2 after the crack had propagated three times the plastic zone size ω_F*, calculated by substituting ΔK_1 for ΔK in the following equation

$$\omega_F^* = \frac{1}{2\pi}\left(\frac{\Delta K}{2\sigma_y^*}\right)^2 \tag{2}$$

where the monotonic yield stress σ_Y is used for σ_Y*. The data on the rate unaffected by stress decrease were taken as valid to generate a *da/dN*-

versus-ΔK relation. The threshold SIF, ΔK_{th}, was defined as the value under which the crack increment was less than 10 μm after the stress cycling of 10^6.

Microscopic Observation Techniques

During fatigue tests of smooth specimens, the machine was stopped and the specimen removed. The microstructure and small cracks on the specimen surface were examined by optical microscopy, scanning electron microscopy (SEM), and the back-reflection X-ray microbeam technique. In the fatigue crack propagation experiment, the specimens were removed from the machine only for observation of microstructural change near the crack tip. The observation of crack length and the determination of the opening point of the crack faces were conducted *in situ*. For observation of substructure by means of the X-ray microbeam technique, the diffraction images reflected from the ferrite {211} plane by irradiating with the characteristic X-ray Cr-Kα were examined in the experiment. The details of the X-ray observation conditions are the same as those used in the previous experiment of the authors [*13–16*]. Among the microstructural parameters supplied by the technique, the following two quantities were measured:

1. Excess dislocation density, which was calculated from the tangential width of a diffraction arc on a Debye ring.
2. Microlattice strain, which was calculated from the radial width of the arc.

The excess dislocation density means a difference in density of dislocations with positive and negative signs.

Fatigue Process and Crack Nucleation in Smooth Specimen

S-N *Curves*

The microstructural changes on the specimen surface during the fatigue process were observed with optical microscopes and SEM's. Figure 2 presents examples of micrographs which were taken from the fatigued specimens. Figure 2*a* corresponds to the time when the slipband was first observed. The arrow in Figs. 2*b* and 2*c* indicates the growth of fatigue cracks along directions not parallel to the slip plane, which is a characteristic feature of the Stage II crack propagation defined by Forsyth [5]. The crack is nucleated along the grain boundary in the former case and along slipbands in the latter case. An SEM of another crack nucleated along the grain boundary is shown in Fig. 2*d*. Figures 2*e* and 2*f* were taken from specimens fatigued to 10^7 and the former picture corresponds to the microstructure of the specimen fatigued just below the fatigue limit and the latter one to that just above the limit of slipband formation.

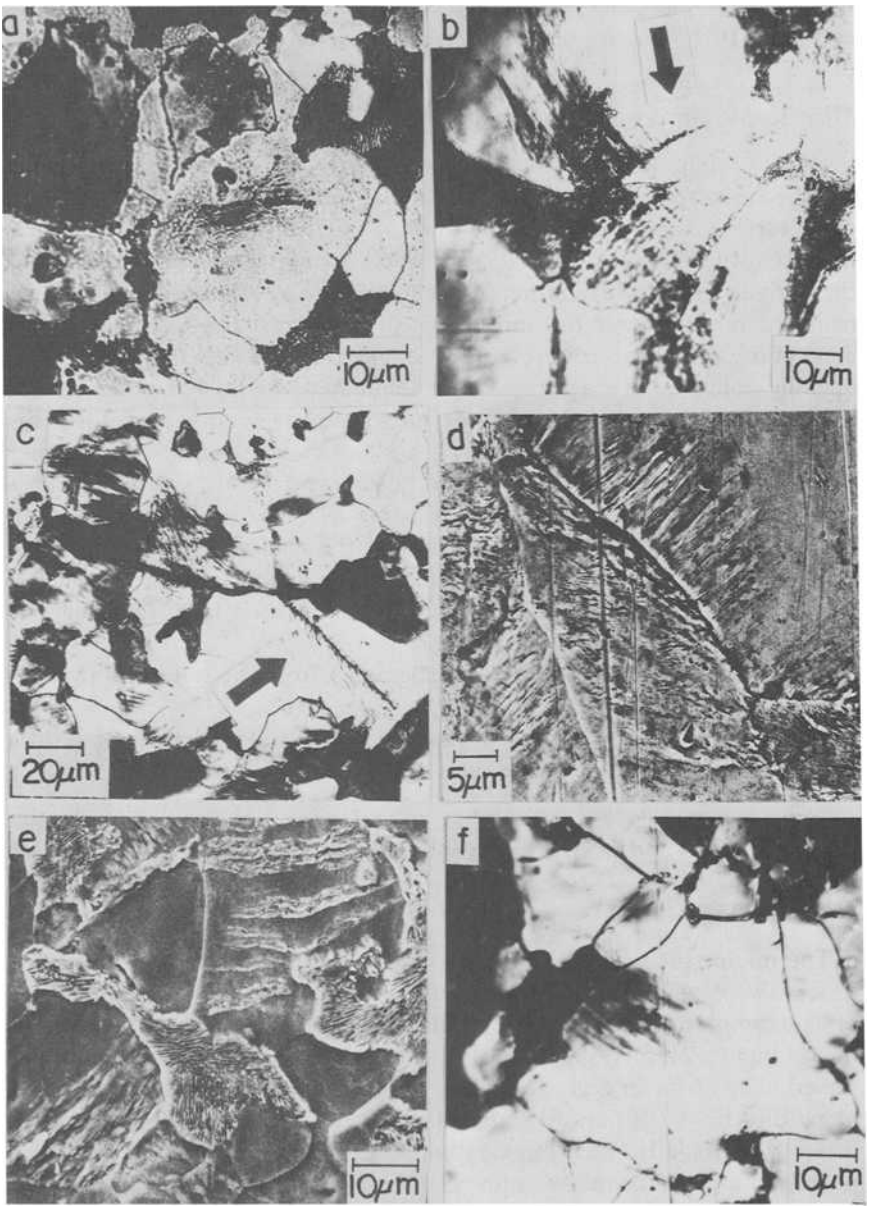

FIG. 2—*Optical micrographs (OPM) and scanning electron micrographs (SEM) taken from fatigued specimens of Material B (stress axis is vertical)*: (a) *OPM, at slipband formation* $\sigma_a = 245$ *MPa,* $N = 1.0 \times 10^4$; (b) *OPM,* $\sigma_a = 245$ *MPa,* $N = 2.5 \times 10^5$; (c) *OPM,* $\sigma_a = 245$ *MPa,* $N = 2.7 \times 10^5$; (d) *SEM,* $\sigma_a = 245$ *MPa,* $N = 3.0 \times 10^5$; (e) *SEM,* $\sigma_a = 178$ *MPa,* $N = 1.4 \times 10^7$; (f) *OPM,* $\sigma_a = 122$ *MPa,* $N = 1.1 \times 10^7$.

The fractions of the number of cycles at slipband formation, N_s, and at crack nucleation, N_c, to the total life, N_f, were determined. The results are presented in Figs. 3*a*, 3*b*, and 3*c*, corresponding to Materials A, B, and C, respectively. The relation between N_s and the stress amplitude σ_a is independent of the grain size, and the limit of stress amplitude σ_{wos} for slipband formation is 107 MPa. The number of cycles to initiate a crack, N_c, is smaller in larger grain size material and the amount of its difference in N_c with different sizes diminishes for the cases of higher stress amplitude fatigue. The number of cycles, N_p, spent for propagating a nucleated crack to final fracture is larger in smaller grain size material, when compared at the same stress amplitude.

The fatigue limit, σ_{wo}, is plotted against the inverse of the square root of grain size, l, in Fig. 4. In the figure, the data on the lower yield stress and the flow stress at each plastic strain ϵ_p are also presented. The value of σ_{wo} (MPa) is correlated to l(metres) in the form of the Petch equation [7] as

$$\sigma_{wo} = 114 + 3.29 \times 10^{-1}/\sqrt{l} \tag{3}$$

The inclination of the line is about the same as that in the flow stress versus $l^{-1/2}$ relation for 2-5 percent plastic strains, but smaller than that in the yield stress σ_Y (MPa) versus $l^{-1/2}$ ($m^{-1/2}$) relation

$$\sigma_Y = 103 + 7.19 \times 10^{-1}/\sqrt{l} \tag{4}$$

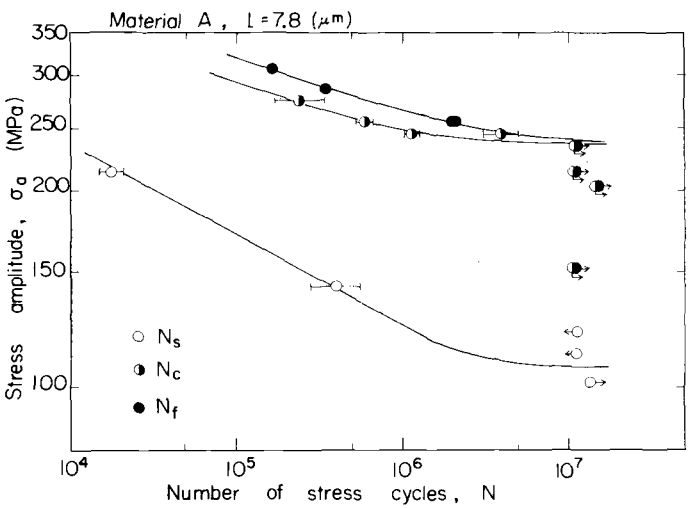

FIG. 3*a*—S-N *curve for Material A.*

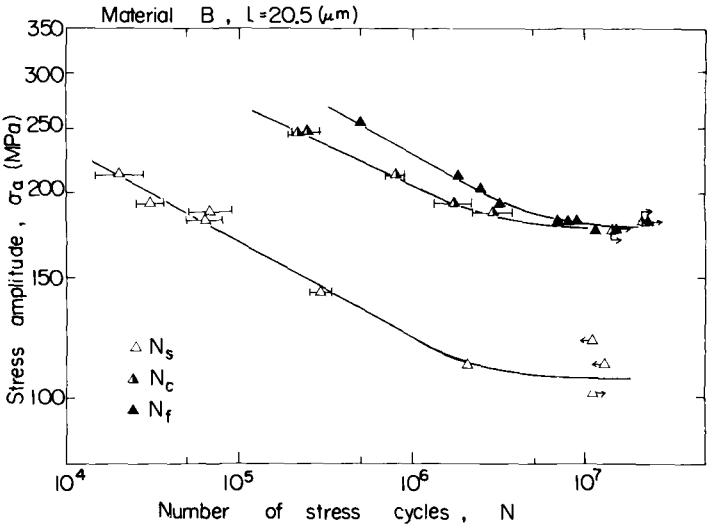

FIG. 3*b*—S-N *curve for Material B.*

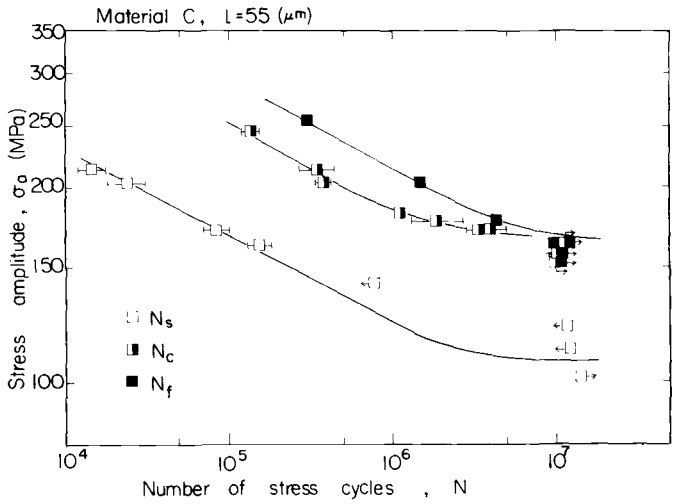

FIG. 3*c*—S-N *curve for Material C.*

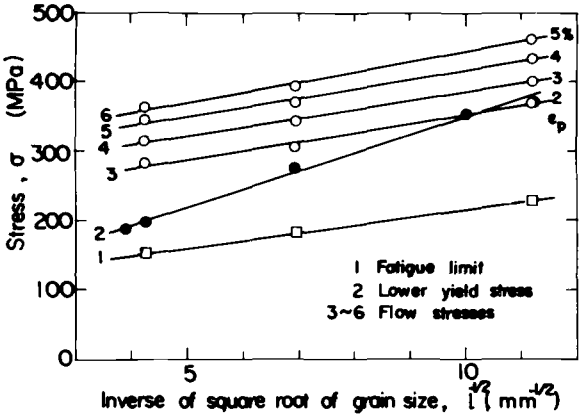

FIG. 4—*Relation between stress and inverse square root of grain size.*

X-Ray Microbeam Observation of Substructure

According to X-ray microbeam observation of the substructure during the fatigue process, the excess dislocation density, D, and the microlattice strain, $\Delta d/d$, increase in the early stage of the fatigue process and do not change markedly in the middle stage, that is, in the range of cycle ratio $N/N_f = 0.2$-0.7 [*14*]. The values of D and $\Delta d/d$ were measured from several diffraction arcs which indicated a greater change in diffraction patterns taken in the middle stage. The mean values of the measurements of D and $\Delta d/d$ are presented with open marks in Figs. 5 and 6 as a function of the stress amplitude. As a comparison, the figures include also the results obtained for monotonic deformation. The excess dislocation density,

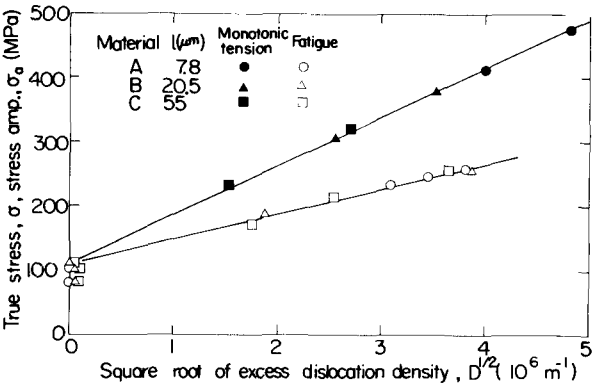

FIG. 5—*Relation between stress and square root of excess dislocation density.*

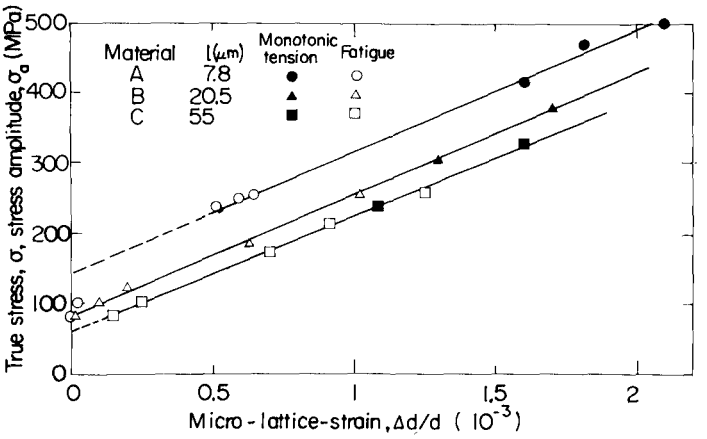

FIG. 6—*Relation between stress and microlattice strain.*

D (m^{-2}), is correlated to stress amplitude, σ_a (MPa), or to true stress, σ (MPa), by the following relations [*13,14*]

$$\sigma_a = 111 + 3.81 \times 10^{-5}\sqrt{D} \tag{5}$$

$$\sigma = 110 + 7.55 \times 10^{-5}\sqrt{D} \tag{6}$$

The relation between $\Delta d/d$ and σ_a is the same as that between $\Delta d/d$ and σ, which is expressed by

$$\sigma_a \text{ or } \sigma = C_1 + C_2\,(\Delta d/d) \tag{7}$$

where C_1 is related to l as $C_1 = 3.92 \times 10^{-1}/\sqrt{l}$ and C_2 is 1.72×10^5 for all grain sizes.

Characteristics of Cyclic Deformation

The grain size of low-carbon steel has no influence either on the limit of slipband formation σ_{wos} or on the relation between stress amplitude and number of cycles to slipband formation. The σ_{wos} value of 107 MPa is nearly equal to the friction stress derived from Eqs 4 or 6. This agreement was observed in other low-carbon steels with different carbon contents [*14*]. A large number of repetitions of cyclic stress above the friction stress can generate dislocations in local areas in particular grains in each material and eventually cause slipbands to appear in several grains on the specimen surface. The initial stage of slipband formation due to cyclic stress is insensitive to the grain size, in contrast to the monotonic yielding behavior,

and the place where slipbands first appeared was in the vicinity of the grain boundary as shown in Figs. 2*a* and 2*f*. From these findings, it can be concluded that the slipband formation in the very early stage of the fatigue process is a phenomenon which takes place over a local area close to the grain boundary whose dimension is smaller than the minimum grain size tested.

The following process is the continuation of dislocation generation and the lengthening of the slipbands. The saturated substructure built up in the thin layer of the specimen surface, attained at about 20 percent of the total life, was compared with the substructure in monotonic deformation whose micromechanics are relatively well established. For all grain sizes examined, the stress value was a linear function of the square root of the excess dislocation density, D, both in cyclic and monotonic deformation, as guessed from a work-hardening theory which expresses the flow stress as a linear function of the square root of the total dislocation density [*17*]. The difference of the coefficient of the second term in Eqs 5 and 6 comes from the difference in dislocation configuration as implied in the X-ray diffraction patterns, which consisted of sharp small spots in cyclic deformation, indicating the substructure more clearly developed [*13.14*]. The microlattice strain $\Delta d/d$ is the total range of the lattice strain variation in one grain and is related to the long-range internal stress. Therefore, $\Delta d/d$ is expected to be larger in larger grain size material even when D has the same value as found in the experiment. Relations such as Eqs 5 and 6 can be used to estimate the stress value in the local area from the measurement of D or $\Delta d/d$.

Crack Nucleation and Fatigue Limit

According to microscopic observation, no crack propagating in a manner characteristic of Stage II propagation was observed at stress levels below the fatigue limit, and most slipbands were blocked by the grain boundary as seen in Fig. 2*e* [*18*]. On the other hand, under stress amplitude above the fatigue limit, cracks were nucleated either along the slipband or grain boundaries and propagated in a Stage II fashion. The fatigue limit is determined by whether a Stage II type of crack is formed or not. Substructural parameters which correspond to the fatigue limit are summarized in Table 2, where the values of D and $\Delta d/d$ are obtained by substituting σ_{wo} into Eqs 5 and 7. The value of $\Delta d/d$ is 5-6 $\times$ 10^{-4} independent of the grain size. The value of D increases with decreasing grain size, while the value of D multiplied by the grain size l is nearly constant. Substituting this constant value of $\Delta d/d$ or Dl into Eqs 5 or 7, we obtain the equation which is almost equivalent to Eq 3. The value of $\Delta d/d$ was found to be a parameter correlated uniquely to the number of stress cycles at crack nucleation for all the grain sizes tested as shown in Fig. 7. Under the same

TABLE 2—*Substructural parameters corresponding to fatigue limit.*

Material	Grain Size, l (μm)	Fatigue Limit, σ_{wo} (MPa)	Excess Dislocation Density, D, 10^{12} m^{-2}	Microlattice Strain, $\Delta d/d$ (10^{-3})	Square Root of Dl, $\sqrt{Dl}$ (10^3 m$^{-1/2}$)
A	7.8	235	10.8	0.52	9.17
B	20.5	178	3.19	0.55	8.09
C	55	163	1.94	0.62	10.3

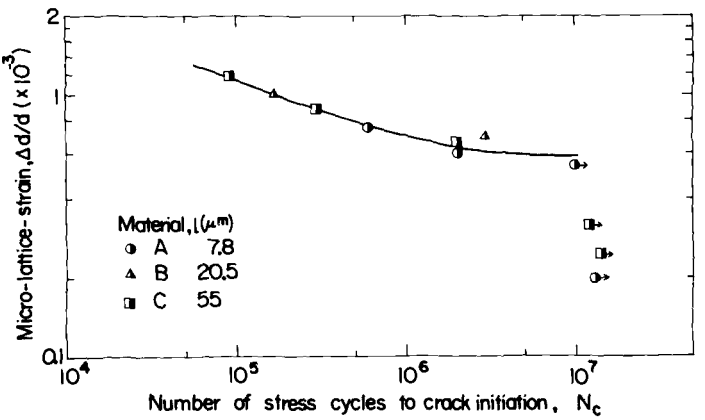

FIG. 7—*Relation between microlattice strain and crack nucleation life.*

stress amplitude, the increase in grain size yields larger microlattice strain and thus corresponds to shorter nucleation life. The value Dl multiplied by the Burgers vector is the total misorientation in one grain and so can be interpreted to be correlated with the long-range internal stress like $\Delta d/d$. The foregoing correlations are very suggestive on the role of the long-range internal stress played in the process up to the formation of the Stage II type of crack.

Crack Growth in Smooth Specimen Fatigue

Small Crack Growth Behavior

The nucleation site of fatigue cracks is either within grains or along the boundary of grains. The number of cracks formed on the specimen surface increases with increasing the stress amplitude and the grain size. At lower values of the ratio of the stress amplitude to the yield stress, the number of nucleated cracks decreases and the nucleation site is predominantly within a grain [*18*]. The minimum size of a crack to be resolved by optical

microscopy is on the order of the grain size. The growth of these very small cracks was observed.

Figure 8 indicates the growth behavior of several small cracks with number of stress cycles, where the length is the half length for surface cracks and the total length for corner cracks. A few cracks such as those numbered 6 and 8 continue to grow, while others stop growing. The deceleration or stopping of crack growth was caused by either blocking by grain boundaries or interaction of cracks [*19*]. The rate *da/dN* was calculated by averaging several experimental points, until the point when cracks decelerate with cycle number. The variation of *da/dN* with the length *a* is shown in Fig. 9; the cracks numbered 1 and 2 correspond to micrographs (*c*) and (*b*) in Fig. 2. The total number of cracks measured for the present case was 18 and the data marks in Fig. 9 correspond to those in the growth

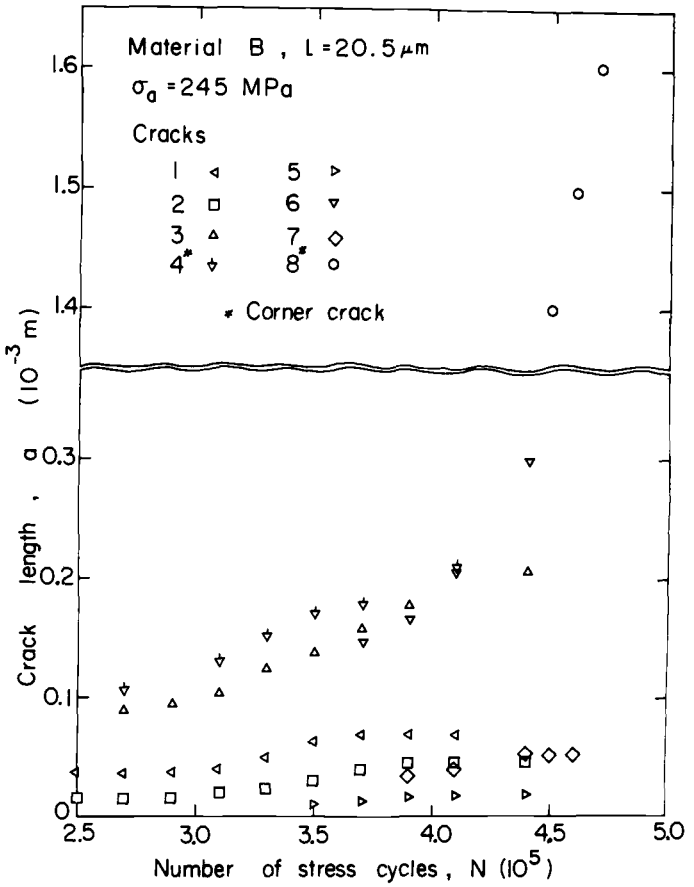

FIG. 8—*Growth of surface cracks in Material B fatigued under* $\sigma_a = 245$ *MPa.*

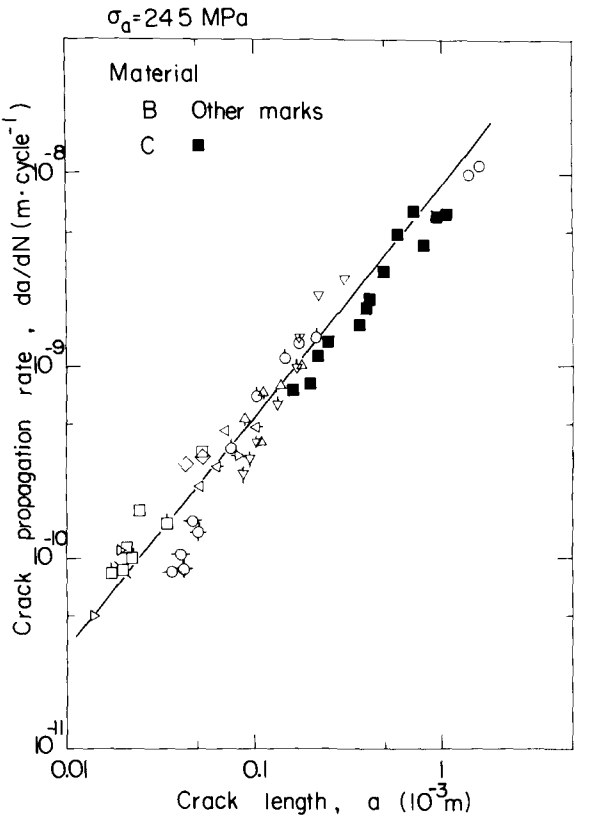

FIG. 9—*Relation between crack propagation rate and crack length for* $\sigma_a = 245$ *MPa.*

curves in Fig. 8. Figure 9 also includes the data for Material C obtained in a similar manner for the case of the same stress amplitude. The variation of da/dN (m/cycle) with a (m) for all cracks measured can be approximated by a single straight line, whose equation is

$$da/dN = 3.5 \times 10^{-5}\, a^{1.20} \tag{8}$$

In Fig. 10, the propagation rate is plotted against $\sigma_a\sqrt{\pi a}$ for several cases denoted. The dashed line in the figure indicates the relation given by Eq 8. The propagation rate of cracks in Material A is lower than that in Materials B and C for the case of the stress amplitude $\sigma_a = 245$ MPa. For the experimental points presented in Fig. 10, the following equation is established between da/dN (m/cycle) and $\sigma_a\sqrt{\pi a}$ (MPa $\sqrt{\text{m}}$)

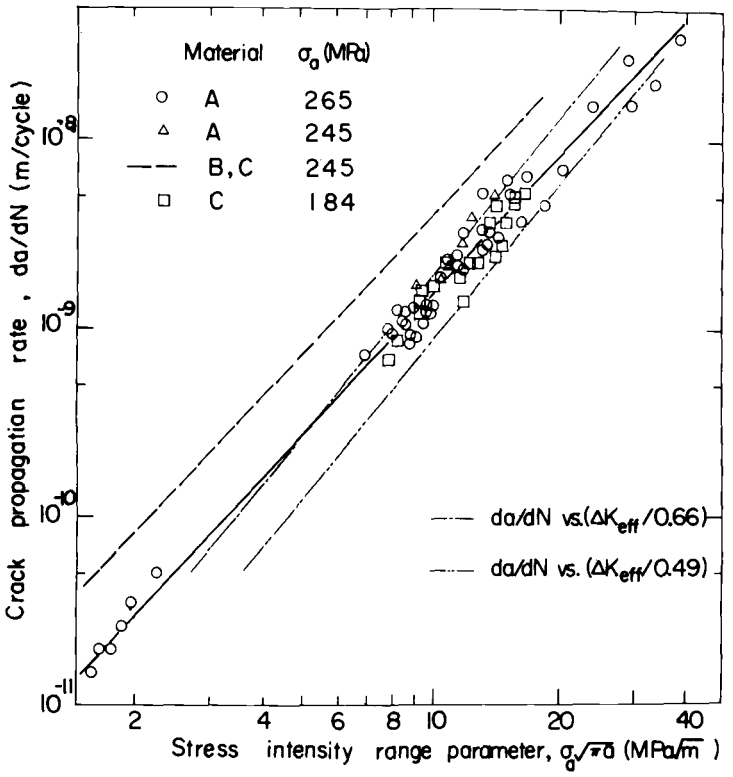

FIG. 10—*Relation between crack propagation rate and* $\sigma_a\sqrt{\pi a}$.

$$da/dN = C_s(\sigma_a \sqrt{\pi a})^{m_s} \tag{9}$$

where $C_s = 5.5 \times 10^{-12}$ and $m_s = 2.44$.

Calculation of Crack Propagation Life

Even when the length of a fatigue crack is on the order of the grain size, the rate of its growth follows the same law as established for large macrocracks before cracks are decelerated due to interaction with the grain boundary or with other cracks. Very small cracks which join together to form a main crack are called *submacrocracks* in the present paper in the sense that they have the same propagation characteristics as long cracks, even though the length is on the order of the grain size. The number of cycles spent for propagating a submacrocrack or macrocrack is predictable by integrating Eq 8 or Eq 9. If only one macrocrack is nucleated and

grown to critical length for fracture, the propagation life, N_p, can be calculated as

$$N_p = \int_{a_i}^{a_c} \frac{1}{C_s(\sigma_a\sqrt{\pi a})^{m_s}}\, da \tag{10}$$

where a_c is the critical crack length and a_i the nucleation crack length. Table 3 presents the value of a_i calculated from Eq 10 for several cases, where a_c is taken as 4 mm. In the case of the stress amplitude $\sigma_a = 245$ MPa in Material A, $2a_i$ is nearly equal to the grain size l. For other cases, the ratio of $2a_i/l$ is larger than unity. This comes from the joining of several submacrocracks to form a main crack. Therefore, the total propagation life should be given by

$$N_p = N_{p1} + N_{p2} \tag{11}$$

where N_{p1} is the number of cycles from crack nucleation to main macrocrack formation and N_{p2} is that for propagating a macrocrack to the critical length for final fracture. If the number of nucleation facets is counted on the fracture surfaces, the estimation of N_{p1} may be possible by assuming that each submacrocrack grows independently until several join together to form a microcrack.

Propagation of Through-Crack near Threshold Condition

Near-Threshold Propagation Behavior

Figure 11 shows the relation between the crack growth rate and SIF range for the cases of stress ratio $R = \sigma_{min}/\sigma_{max} = -1$. In the region of growth rate higher than about 3×10^{-9} m/cycle, the rate da/dN (m/cycle) is correlated to the SIF range ΔK (MPa $\sqrt{m}$) by the following unique power relation

$$da/dN = C(\Delta K)^m \tag{12}$$

TABLE 3—*Nucleation crack length calculated from Eq 10.*

Material	Grain Size, l (μm)	Stress Amplitude, σ_a (MPa)	Total Life, N_f	Propagation Life, N_p	a_i, μm	$2a_i/l$
A	7.8	265	1.4×10^6	1.1×10^6	90	23
		245	5.0×10^6	3.9×10^6	3.1	0.79
B	20.5	245	6.6×10^5	4.4×10^5	118	12
C	55	245	3.9×10^5	2.6×10^5	377	14
		184	3.5×10^6	2.6×10^6	104	3.8

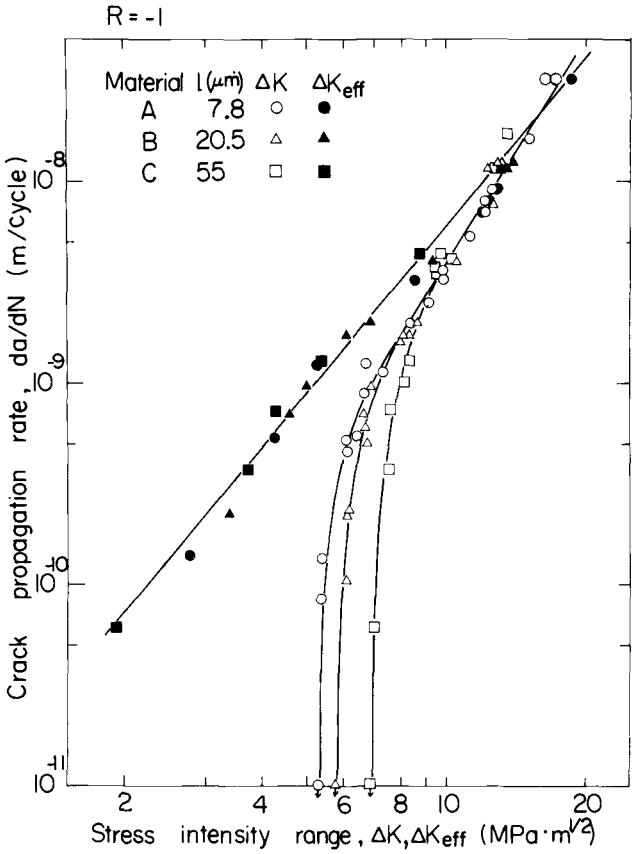

FIG. 11—*Relation between crack propagation rate and stress intensity range for* R = −1.

where

$C = 8.9 \times 10^{-13}$,
$m = 3.68$, and
ΔK = taken to be that for the tension part of the cycle only, that is, K_{max} for $R = -1$.

In the lower-rate region near the threshold, the rate and SIF relation deviates from Eq 12 and the rate is lower in material with larger grain size than that in smaller grain-size material when compared at the same SIF range. The relation of da/dN against ΔK was obtained for the cases of $R = 0$ and $R = 0.5$, and a similar tendency concerning the grain-size effect on near-threshold crack growth was found [*21*]. The variation of the threshold values, ΔK_{th}, of SIF range with grain size is shown in Fig. 12.

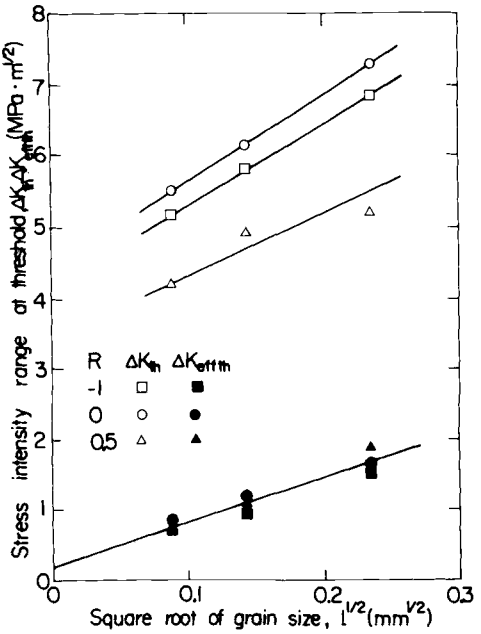

FIG. 12—*Relation between threshold stress intensity range and grain size.*

The value of ΔK_{th} increases linearly with $\sqrt{l}$ as reported by Masounava et al [*3*].

The effective SIF range ΔK_{eff}, which is defined as the difference between the maximum SIF and SIF value at the crack opening point [*20*], was measured by either the electrical potential method or the compliance technique. Both methods yield almost the identical opening point [*21*]. The opening point was in the compression portion of the cycle at high ΔK-values and was in the tension portion of the cycle near threshold. The relation between da/dN (m/cycle) and ΔK_{eff} (MPa $\sqrt{m}$) is shown in Fig. 11 for the case of $R = -1$ and is approximated by the equation

$$da/dN = C' (\Delta K_{eff})^{m'} \tag{13}$$

where $C' = 1.2 \times 10^{-11}$ and $m' = 2.71$. The power equation, Eq 13, is applicable to the growth rate down to 5×10^{-11} m/cycle for all grain sizes and there is no downward curvature as seen in the relation between da/dN and ΔK. For the threshold value of ΔK_{eff}, the following equation approximates the experimental relation

$$\Delta K_{effth} = 0.19 + 1.96 \times 10^2 \sqrt{l} \tag{14}$$

for the cases of $R = -1$, 0, and 0.5 as shown in Fig. 12.

Structure Sensitive Nature of Fatigue Crack Growth

The spread of the slipband zone (SBZ) near the crack tip was observed by optical microscopy. Examples of the optical micrographs taken from the tips of fatigue cracks are presented in Fig. 13. The spread of the SBZ in the forward direction ξ_F and in the sideward direction ξ_s was measured. The relation between ΔK and ξ_s or ξ_F is shown in Fig. 14. The SBZ size was found to be approximately proportional to the square of the SIF range except in the vicinity of the threshold. The ratio of ξ_s to ξ_F is 2.5 for Materials A and B. The size of the SBZ, ξ_F, was from 0.5 to 0.6 times the size ω_F* calculated from Eq 2. The SBZ size is much smaller at the threshold than that predicted from the foregoing relation. The point of structure sensitive-insensitive transition found in the growth curve occurred when the SBZ size ξ_F or cyclic plastic zone size ω_F* became comparable to the grain size l [*21*]. At the transition point, the ratio of ω_F* to l is 1.5–2 for all cases of R-value examined [*21*], and so the ratio of ξ_F to l is 0.7–1.2 for $R = 0$. This sort of structure sensitive-insensitive transition has been observed in other metals [*22*]. The blocking of crack-tip slipband may be responsible for a smaller fraction of the effective component of ΔK near the threshold.

Threshold Condition

As seen in the optical and scanning electron micrographs taken from the tip of the nonpropagating fatigue crack presented in Fig. 13*c* and *d*, the SBZ size is smaller than the grain size. Figure 15 shows the variation of the SBZ size in the sideward direction ξ_s with the grain size l. The relation between ξ_s (m) and l (m) is

$$\xi_s = 0.51\, l \tag{15}$$

The SBZ size in the forward direction ξ_F is calculated to be 0.20 l from the mean value of the ratio of ξ_s to ξ_F, 2.5, established for the cases of cracks with higher growth rates. Based on these findings, the critical value of the slipband zone is a potential criterion for the threshold condition of each material, although the value of K_{th} is dependent on R-value. The mechanical parameter which controls the slipband formation at the crack tip is expected to be the effective component of the SIF.

Discussion

In the growth of fatigue cracks, the transition from grain-size sensitive to insensitive nature takes place when the SBZ size is nearly equal to the grain size. A downward curvature in the da/dN-versus-ΔK relation at low rates has been observed in most materials [*1,2*], while no such transition was observed in da/dN versus ΔK_{eff}. Near the threshold condition, the

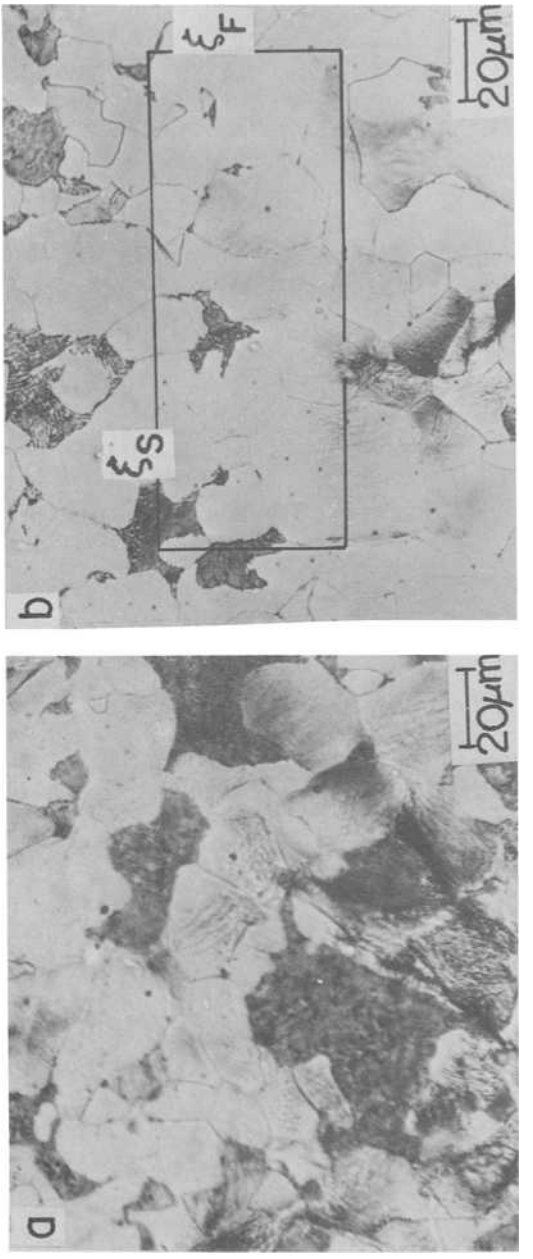
b
ε_S
ε_F
20μm
a
20μm

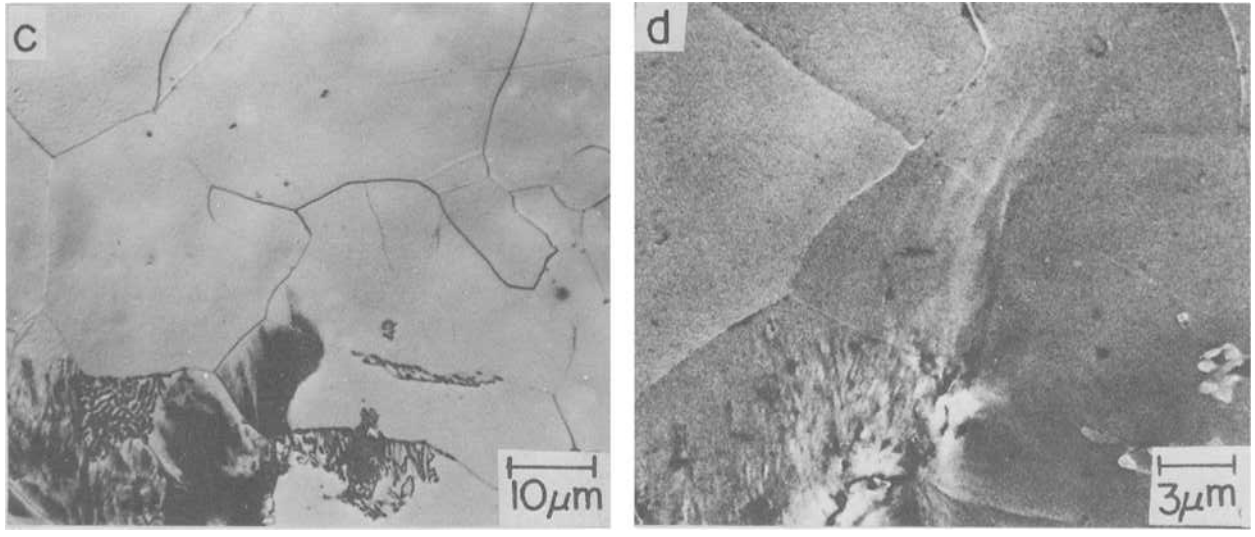

FIG. 13—*Optical micrographs (OPM) and scanning electron micrograph (SEM) taken from near crack tips of Material B for* $R = -1$ *(stress axis is horizontal)*: (a) *OPM*, $\Delta K = 12.2\ MPa\sqrt{m}$, $da/dN = 1.1 \times 10^{-8}\ m/cycle$; (b) *OPM*, $\Delta K = 8.5\ MPa\sqrt{m}$, $da/dN = 2.0 \times 10^{-9}\ m/cycle$; (c) *OPM*, $\Delta K = 5.8\ MPa\sqrt{m}$, $da/dN < 10^{-11}\ m/cycle$; (d) *SEM*, $\Delta K = 5.8\ MPa\sqrt{m}$, $da/dN < 10^{-11}\ m/cycle$.

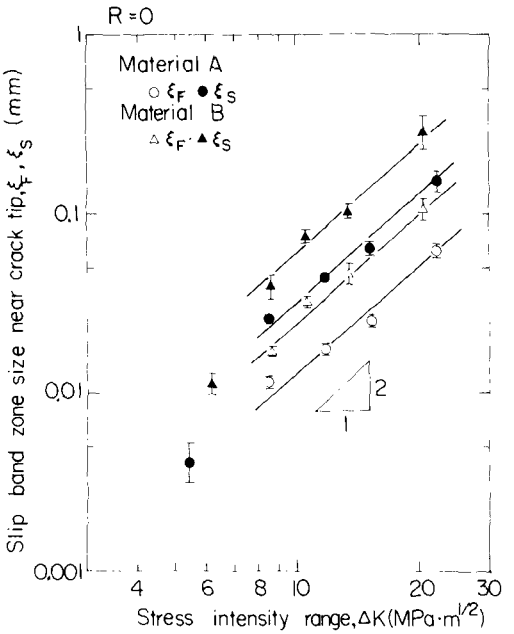

FIG. 14—*Relation between slipband zone size and stress intensity range for* R = 0.

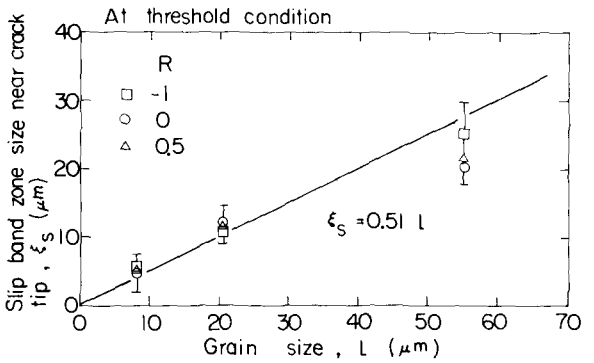

FIG. 15—*Variation of slipband zone size with grain size at threshold condition.*

length of slipband emanating from the crack tip will be influenced by the grain boundary, and the SBZ size is much smaller than that predicted from the relation between ξ_F and ΔK established for the high-rate region as seen in Fig. 14. This may be explained by the fact that the opening stress is increased when SBZ formation near the crack tip is affected by the grain boundary. A model will be proposed for the threshold condition of crack growth under the assumption that the threshold condition is deter-

mined whether the slipband near the crack tip propagates into an adjacent grain or not. The situation is schematically illustrated in Fig. 16*a*. The criterion for slipband propagation is here assumed to be determined by the SIF at the slipband tip in a microstructural sense. This criterion has been used to interpret the Petch relation between yield stress and grain size in low-carbon steel based on the dislocation pileup model [*23*]. The value of the microscopic SIF, K^m, can be approximately evaluated by the simpler situation shown in Fig. 16*b*. The SIF at slipband tip is

$$K^m = K - K_{fr}^* \tag{16}$$

where K_{fr}^* is given from the flow stress in SBZ, σ_{fr}^*, and SBZ size, ξ_F, as [*24*]

$$K_{fr}^* = 2\sqrt{2}\,\sigma_{fr}^*\sqrt{\xi_F/\pi} \tag{17}$$

In the Bilby-Cottrell-Swinden model for plastic flow, the equilibrium situation of slipband zone is assumed, that is, $K^m = 0$ [*24*]. On the other hand, at the tip of a slipband near the threshold, the stress is unbounded and the intensity of stress singularity is given by K^m. From Eq 16, the applied K-value is

$$K = K^m + 2\sqrt{2}\,\sigma_{fr}^*\sqrt{\xi_F/\pi} \tag{18}$$

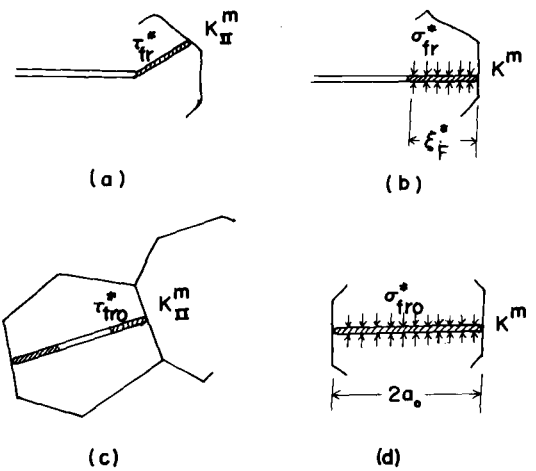

FIG. 16—*Micromechanistic models for threshold condition and fatigue limit:* (a) *threshold condition,* (b) *simplified model for threshold condition,* (c) *micro- or macrocrack formed at fatigue limit, and* (d) *simplified model for fatigue limit.*

At the threshold condition

$$K_{th} = K^{m}_{critical} + 2\sqrt{2}\ \sigma_{fr}^{*}\sqrt{0.20l/\pi} \tag{19}$$

The equation has the same form as Eq 14. The value of $K^{m}_{critical}$ is 0.19 MPa $\sqrt{m}$ and σ_{fr}^{*} is 275 MPa. The value of σ_{fr}^{*} is nearly equal to the stress value, 230 MPa, in SBZ near the threshold condition evaluated from the excess dislocation density measured on the fracture surface by the X-ray microbeam method [*21*].

The propagation behavior of very small cracks in smooth specimen fatigue should be correlated to the propagation law of through-cracks. The rate of surface crack growth is a power function of $\sigma\sqrt{\pi a}$. The SIF value on the free surface for small surface cracks under bending conditions was evaluated approximately by Grandt and Sinclair [*26*] and is given by

$$K = M_B\ \sigma\sqrt{\pi b}/\Phi \tag{20}$$

where $2a$ is major axis parallel to the surface and $2b$ is the minor axis of a semi-elliptical crack. The coefficients M_B and Φ are the function of the aspect ratio $\lambda = b/a$ of a crack. Equation 20 can be rewritten as

$$K = F(\lambda)\ \sigma\sqrt{\pi a} \tag{21}$$

where

$$F(\lambda) = M_B\sqrt{\lambda}/\Phi \tag{22}$$

The value of $F(\lambda)$ is calculated to be 0.49 from the Grandt and Sinclair result as far as $\lambda = 1.0 \sim 0.2$ and the ratio of a to specimen thickness is 0.1 to 0.5. From the results of experimental observation of the aspect ratio, λ changes from 1 to 0.3 as the crack length a changes from 0.1 to 4 mm [*19*]. Pearson used 0.66 as $F(\lambda)$ of Eq 21 in his analysis of growth data of surface cracks with semicircular shape [*10*]. In Fig. 11, the rate da/dN-versus-$\sigma_a\sqrt{\pi a}$ relation is fairly linear down to the rate of 10^{-11} m/cycle and any downward curvature corresponding to the threshold condition is not observed in this range. Yokobori [*9*] and Pearson [*10*] reported a similar tendency in the relation of da/dN versus $\sigma_a\sqrt{\pi a}$, but they did not explain the discrepancy in growth law observed between long through-cracks and small surface cracks. This fact is explained as follows. In generating the data shown in Fig. 11, only accelerating cracks were observed. From the consideration just described, only the rate of surface cracks which were not blocked heavily by the grain boundaries was measured. For these cracks, the crack opening level should be very low and the most tensile part of the SIF is expected to be effective. Therefore, the da/dN-versus-$\sigma_a\sqrt{\pi a}$ relation

may be correlated to the da/dN-versus-ΔK_{eff} relation for through-cracks. In Fig. 10, the dot-dash line is for the relation of da/dN against $\Delta K_{eff}/0.66$ and the two-dot-dash line against $\Delta K_{eff}/0.49$, where both lines are drawn based on Eq 13. Agreement between the lines and the experimental points is fairly good. In Eq 9, correlating da/dN with $\sigma_a\sqrt{\pi a}$ for surface cracks, the coefficient C_s increases for high values in larger grain-size material. This may come from the nonlinear effect of material properties at high stresses in larger grain-size material, and the growth behavior of surface cracks in this situation is expected to be predictable by the cyclic J-integral [*19,27*].

A similar model based on the critical value of microscopic SIF will be applied to interpret the grain size effect on the fatigue limit. The crack which exists at the fatigue limit is named here the *endurance crack* with the length $2a_o$. Since the microscopic structure of the endurance crack is still unclear, it is assumed to be slipbands containing several microcracks. This situation is illustrated simply in Fig. 16*c* and the model is further simplified in Fig. 16*d* for the sake of mathematical simplicity. The microscopic SIF, at the tip of the endurance crack, is given by

$$K^m_{critical} = K_{wo} - K_{fro}^* \tag{23}$$

where K_{wo} is the macroscopic SIF for the endurance crack of $2a_o$ long. The value of K_{wo} is given by the following equation similar to Eq 21

$$K_{wo} = F(\lambda)\,\sigma_{wo}\sqrt{\pi a_o} \tag{24}$$

If the friction stress σ_{fro}^* is distributed over the $2a_o$ region uniformly, it is

$$K_{fro}^* = F(\lambda)\,\sigma_{fro}^*\sqrt{\pi a_o} \tag{25}$$

The fatigue limit σ_{wo} is given from Eqs 23–25 as

$$\sigma_{wo} = \sigma_{fro}^* + \frac{K^m_{critical}}{F(\lambda)\sqrt{\pi}}\,\frac{1}{\sqrt{a_o}} \tag{26}$$

Assuming the endurance crack length $2a_o$ is proportional to the grain size l with the proportional constant α, we obtain

$$\sigma_{wo} = \sigma_{fro}^* + \frac{K^m_{critical}}{F(\lambda)\sqrt{\pi\alpha/2}}\,\frac{1}{\sqrt{l}} \tag{27}$$

By comparing Eq 27 with Eq 3 and substituting $K^m_{critical}$ of 0.19 MPa $\sqrt{\text{m}}$, α is calculated to be 0.84. The length of the endurance crack is about the

grain size. The value of σ_{fro}* is 114 MPa and is a little larger than the frictional stress, σ_{fr} 103 MPa, obtained from Eq 4. In the results of 0.11 percent carbon steel reported by Klesnil et al [7], the σ_{fro}* value is also larger than the friction stress in the Petch equation and smaller than the friction stress at 2 percent plastic strain. From X-ray microbeam observation, the values of the excess dislocation density multiplied by grain size and microlattice strain were constant at the fatigue limit. These values correspond to substructure formed by cyclic loading and might reflect the microscopic structure of endurance cracks. The micromechanical characteristics of endurance cracks should be studied further both theoretically and experimentally. The unique relation established between microlattice strain and crack nucleation life may be useful for micromechanical analysis of nucleation and growth of microcracks.

Conclusions

The grain-size sensitive or insensitive nature of mechanical characteristics of crystal deformation, crack nucleation, and growth in long-life fatigue of low-carbon steel with several grain sizes was clarified based on the results of quantitative microscopic observations done with the X-ray microbeam diffraction technique and optical and scanning electron microscopes. The grain size of low-carbon steel does not affect either the limit of slipband formation or the relation between stress amplitude and number of cycles to slipband formation. The grain size has a significant influence on nucleation and propagation lives of cracks, and on the fatigue limit. The growth law of very small cracks formed on the specimen surface was established and correlated with the growth law of through-cracks. A micromechanistic model for the fatigue limit was proposed to interpret the Petch-type relation of the fatigue limit against the grain size under the assumption of the critical value of microscopic stress intensity factor at the tip of endurance cracks blocked by the grain boundary. A similar model was used to explain the empirical relation found between the threshold stress intensity factor and the grain size. The effect of the grain size on the nucleation and the early growth of fatigue cracks at the notch root will be analyzed with the methodology, which is basically the same as that used in the analysis of the fatigue strength of smooth specimens. The present approach will be further extended to a general assessment of the effect of microstructural constituents on the fatigue strength of engineering material with more complex structure, if a further refinement of crack nucleation and endurance crack models is attained.

Acknowledgments

The authors wish to thank Mr. Toshinobu Nakanishi, Kawasaki Steel

Corp., Ltd., formerly a graduate student in the Department of Mechanical Engineering, Kyoto University, for his assistance in carrying out a part of the experiments. They extend their gratitude to Central Research Laboratories, Kobe Steel, Ltd., for providing the material used in the present study.

References

[1] Donahue, R. J., Clark, H. M., Atanmo, P., Kumble, R., and McEvily, A. J., *International Journal of Fracture Mechanics*, Vol. 8, 1972, pp. 209-219.
[2] Ritchie, R. O., *Journal of Engineering Materials and Technology*, American Society of Mechanical Engineers, Vol. 99, 1977, pp. 195-204.
[3] Masounava, J. and Bailon, J-P., *Scripta Metallurgica*, Vol. 10, 1976, pp. 165-170.
[4] Hoeppner, D. W. in *Fatigue Crack Propagation, ASTM STP 415*, American Society for Testing and Materials, 1967, pp. 486-504.
[5] Forsyth, P. J. E., *Physical Basis of Metal Fatigue*, Blackie and Son, London, U.K., 1969.
[6] Forrest, P. G. and Tate, A. E. L., *Journal of the Institute of Metals*, Vol. 93, 1964-65, pp. 438-444.
[7] Klesnil, M., Holtzmann, M., Lukáš, P., and Ryš, P., *Journal of the Iron and Steel Institute*, Vol. 203, 1965, pp. 47-53.
[8] Thompson, A. W. and Backofen, W. A., *Acta Metallurgica*, Vol. 19, 1971. pp. 597-606.
[9] Yokobori, T., Nanbu, M., and Takeuchi, N., *Report of the Research Institute on the Strength and Fracture of Materials*, Tohoku University, Sendai, Japan, Vol. 5, 1969, pp. 1-17.
[10] Pearson, S., *Engineering Fracture Mechanics*, Vol. 7, 1975, pp. 235-247.
[11] Neuber, H., *Kerbspannungslehre*, 2nd ed., Springer-Verlag, Berlin, Germany, 1958, p. 73.
[12] Feddersen, C. E. in *Plane Strain Crack Toughness Testing of High Strength Metallic Materials, ASTM STP 410*, American Society for Testing and Materials, 1967, p. 77.
[13] Taira, S., Tanaka, K., and Tanabe, T. in *Proceedings*, 13th Japan Congress on Materials Research, 1970, pp. 14-19.
[14] Taira, S., Tanaka, K., and Kawanami, Y., *Journal of the Society of Materials Science* (Japan), Vol. 21, 1972, pp. 791-799.
[15] Taira, S. and Tanaka, K., *Engineering Fracture Mechanics*, Vol. 4, 1972, pp. 925-938.
[16] Taira, S. and Tanaka, K. in *Proceedings*, Symposium on Mechanical Behavior of Materials, Kyoto, Japan, Vol. 1, 1974, pp. 237-253.
[17] Hirsch, P. B. in *The Physics of Metals, Defects*, P. B. Hirsch, Ed., Cambridge University Press, London, U.K., 1973, Chapter 5.
[18] Taira, S., Tanaka, K., and Hoshina, M., "X-Ray Microbeam Study of Grain-Size Effect on Fatigue Damage in Smooth Specimen of Low-Carbon Steel," to be published in *Transactions*, Japan Institute for Metals.
[19] Taira, S., Tanaka, K., and Hoshina, M., "Small Crack Growth in Fatigue of Smooth Specimen of Low-Carbon Steel," to be published in *Transactions*, Japan Institute for Metals.
[20] Elber, W. in *Damage Tolerance in Aircraft Structures, ASTM STP 486*, American Society for Testing and Materials, 1971, pp. 203-242.
[21] Taira, S., Tanaka, K., Nakanishi, T., and Hoshina, M., "Micromechanistic Study of Near-Threshold Fatigue Crack Growth in Low-Carbon Steel with Several Grain Sizes," to be published in *Transactions*, Japan Institute for Metals.
[22] Yoder, G. R., Cooley, L. A., and Crooker, T. W., "A Micromechanistic Interpretation of Cyclic Crack-Growth Behavior in a Beta-Annealed Ti-6Al-4V Alloy," NRL Report 8048, Naval Research Laboratory, Washington, D.C., Nov. 1976.
[23] Tetelman, A. S. and McEvily, A. J., *Fracture of Structural Materials*, Wiley, New York, 1967, p. 186.

[24] Taira, S., Tanaka, K. and Yokomaku, T., *Journal of the Society of Materials Science* (Japan), Vol. 24, 1975, pp. 733–740.
[25] Bilby, B. A., Cottrell, A. H., and Swinden, K. H. in *Proceedings of the Royal Society*, London, Vol. A272, 1963, pp. 304–314.
[26] Grandt, A. F. and Sinclair, G. M. in *Stress Analysis and Growth of Cracks, ASTM STP 513*, American Society for Testing and Materials, 1972, pp. 37–58.
[27] Mowbray, D. F. in *Cracks and Fracture, ASTM STP 601*, American Society for Testing and Materials, 1976, pp. 33–46.

DISCUSSION

A. McEvily[1] *(discussion)*—The authors are to be complimented for their comprehensive, multifaceted, and detailed study of the effects of grain size on fatigue crack initiation and growth processes, a subject of considerable interest.[2,3] One most interesting aspect is what appears to be the application of the continuum mechanics approach to the analysis of the growth of cracks on the microscale, that is, to cracks less than the grain size in length. As a point for discussion, the use of such a model in the prediction of the threshold level as well as the fatigue limit is somewhat surprising in view of the prevalent notion that these quantities, although perhaps interrelated, are structure-sensitive properties, and that only above the transition in the crack rate versus ΔK plot would the continuum approach be applicable. Even at the threshold, the empirical fracture mechanics approach to the condition for nonpropagation breaks down as the crack size decreases as indicated in Fig. 17, after Kitagawa and Takahashi.[4] This type of transition from continuum to microstructural control can be expressed in the form

$$\sigma_{th} = \frac{\text{Fatigue limit}}{1 + \sqrt{a/\rho_e}} \tag{28}$$

where

σ_{th} = stress for propagation,
a = crack length, and
ρ_e = a Neuber material constant.

[1] Metallurgy Department, Institute of Materials Science, University of Connecticut, Storrs, Conn. 06268.
[2] Armstrong, R. W., *Canadian Metallurgical Quarterly*, Vol. 13, No. 1, 1974, p. 187.
[3] Phillips, W. L. and Armstrong, R. W., *Journal of the Mechanics and Physics of Solids*, Vol. 17, 1969, p. 265.
[4] Kitagawa, H. and Takahashi, S. in *Proceedings*, 2nd International Conference on the Mechanical Behavior of Materials, American Society for Metals, Cleveland, Ohio, 1976, p. 627.

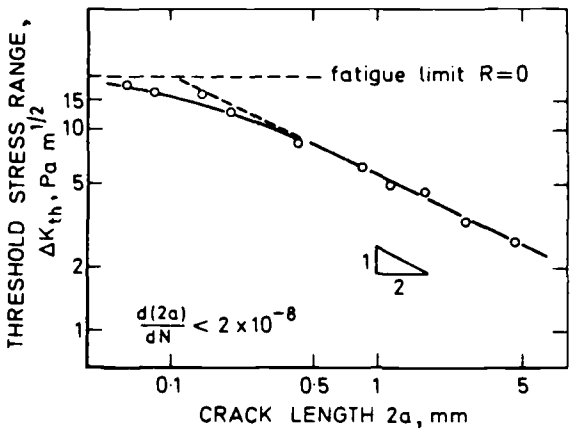

FIG. 17—*Effect of crack length on threshold stress range for fatigue-crack growth in HT80 steel (Kitagawa and Takahashi).*

Pearson's data, which the authors discuss, would fall in the region of Fig. 17 between the two curves.

Equations 16 and 17 appear to be central to the analysis developed by the authors, and further comment on the concepts underlying these equations would be welcome. In particular, clarification as to why K^m is zero in the Bilby-Cottrell-Swinden case but is finite at the threshold in the present case would be helpful. In addition, it appears from the work of Otsuka et al,[5] Fig. 18, that Mode II (Stage I) crack growth is important in the threshold region. However, the fatigue limit in the present case involves Mode I (Stage II) cracks, and on this basis one might expect they would not be directly correlatable unless the model took these mode shifts into account. The authors' view of this point would be of interest.

Finally, the authors make use of the ΔK_{eff} approach in establishing certain correlations, and by this means the continuum region is extended to lower ΔK levels. However, the physical basis underlying this modification is not clear since in the near-threshold, structure-sensitive region the mode of crack growth changes significantly, as shown in the authors' Ref *22*, and is dominantly Mode II.[5] It would be appreciated if the authors would comment on these various points.

S. Weissmann,[6] *R. Pangborn,*[6] *and I. Kramer*[7] *(discussion)*—In their report on fatigue studies of low carbon steel, Taira et al present a model of

[5]Otsuka, A., Mori, K., and Miyata, T., *Engineering Fracture Mechanics*, Vol. 7, 1975, p. 429.

[6]Department of Mechanics and Materials Sciences, Rutgers University, Piscataway, N.J. 08854.

[7]David W. Taylor Naval Ship Research and Development Center, Annapolis, Md.

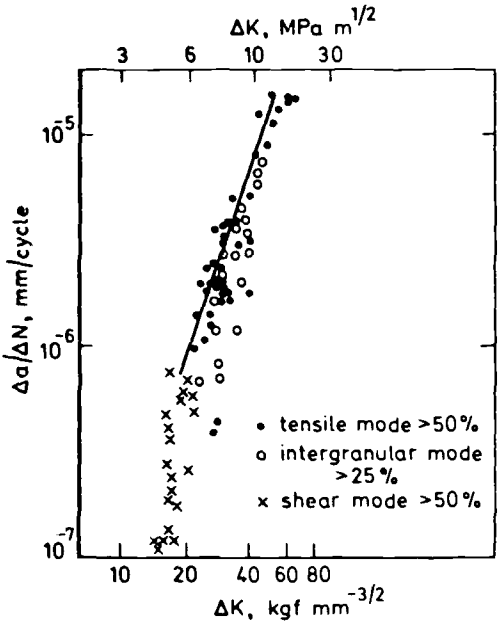

FIG. 18—*Fatigue fracture mode in relation to rate of fatigue-crack growth (Otsuka et al).*

micromechanistic fatigue deformation on which we would like to comment on the basis of our own investigations. Using an X-ray double-crystal diffractometer method in combination with X-ray topography,[8,9] we have studied the defect structure of Al 2024-T3 and aluminum single crystals induced by monotonic loading as well as cyclic tension-compression loading.[10] The general areas of common interest are (1) characterization of fatigue damage by measurement of excess dislocation density as a function of fraction of fatigue life, and (2) elucidation of cyclically induced substructure in comparison with microstructural mechanisms contributing to monotonic deformation.

The double-crystal diffractometry method we employed allows for quantitative determination of excess dislocation density in single crystals or in the individual grains of polycrystalline metals, and for a visualization of the defect structure by reflection topography. In good agreement with the authors, who used an X-ray microbeam method, we can also describe, as shown in Fig. 19, the substructural response as a function of progressive fatigue cycling, by a three-stage sequence: an initial stage manifested by a

[8] Weissmann, S. and Evans, D. L., *Acta Crystallographica*, Vol. 7, 1954, p. 733.
[9] Weissmann, S., *Journal of Applied Physics*, Vol. 27, 1956, p. 389.
[10] Pangborn, R. N., Weissmann, S., and Kramer, I. R., *Scripta Metallurgica*, Vol. 12, 1978, p. 129.

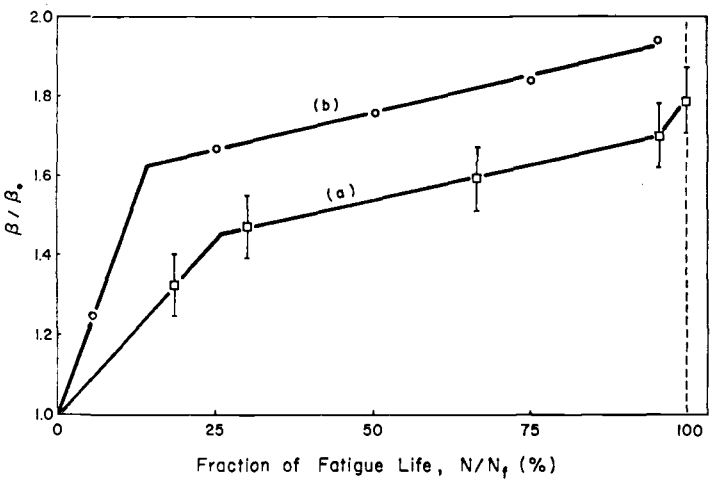

FIG. 19—*Dependence of rocking curve width on fatigue cycling for Al2024-T3: copper radiation; stress = ±200.6 MPa (29.1 ksi);* (a) *50-μm grain size;* (b) *40-μm grain size.*

rapid increase in excess dislocations in the near-surface regions, an intermediate stage in the range of $N/N_f = 0.2 - 0.9$, characterized by a more gradual rise in the excess dislocation density, and finally a period of rapid increase prior to failure. There is also good agreement with regard to the effect of grain size on the substructural deformation characteristics resulting from fatigue cycling. While the overall shape and slope of the curves are similar for the different grain sizes, the material with smaller grain size exhibited an excess dislocation density increase of greater magnitude. If the β/β_o values, expressing the increase of excess dislocations with respect to the undeformed specimen, are multiplied by the square root of the ratio of the grain diameters, then all our experimental points can be represented by a single curve. Application of our results to the Petch-type relationship given by the authors provides a linear correspondence analogous to theirs.

Also in confirmation of the authors' observations, we find that cracks are nucleated along slipbands or grain boundaries. Our studies, however, give evidence that the formation of through-cracks is related to the action of the near-surface defect structure as a blocking agent for dislocations generated in the bulk. Depth profiles of the defect structure show that uniaxial tension deformation produces a preferentially deformed surface layer with a decreasing excess dislocation density to a constant level at about 100 μm in depth. As may be seen from Fig. 20*a*, the profiles of cyclically deformed specimens also display a high excess dislocation density at near-surface regions which declines to a minimum at about 100 μm in depth, but subsequently increases again to a plateau level at about 250 μm into the bulk. The substructural changes in the bulk occur principally

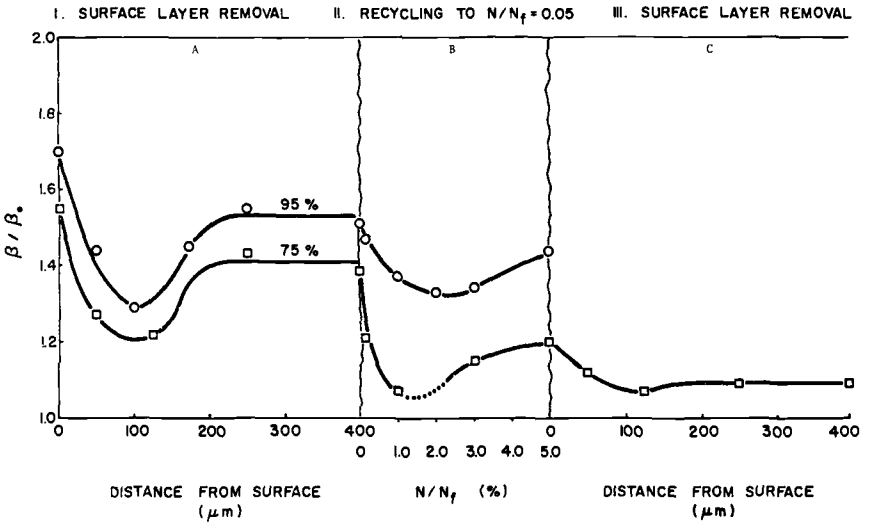

FIG. 20—*Composite diagram for specimens given prior fatigue cycling to 95 and 75 percent of their fatigue life, followed by surface layer removal, recycling to* $N/N_f = 0.05$, *and surface layer removal again.*

during the second stage of the fatigue life sequence (Fig. 19), and the bulk dislocation density never exceeds that near the surface. We propose that the long-range stresses set up by cumulative effect of excess dislocations at the regions near the surface influence the microplastic response of the bulk. As the magnitude of the surface and bulk excess dislocation densities increases with progressive cycling, the dynamic interplay of these long range-stresses induces crack nucleation and eventual failure when the local accumulation of excess dislocations exceeds the barrier strength at the surface.

The long-range stress effect emanating from near-surface sites into the bulk is disclosed by electropolishing a surface layer of 400-μm thickness, thereby removing the blocking defect structure of the near-surface region. As may be seen from Fig. 20*b*, the excess dislocations decrease during the initial stage of recycling in the absence of the surface layer. Further cycling increases the excess dislocation density because a new, blocking defect structure in the vicinity of the new surface is being formed. Figure 20*c* shows a second depth profile of the recycled specimen (previously cycled to 75 percent of its life followed by removal of a 400-μm surface layer). This profile reveals the striking effect that the excess dislocation density in the bulk approaches that of a virgin specimen. The phenomenon of dislocation egression and concomitant strain relief explains why the fatigue life of a material can be extended almost indefinitely if the surface layers are

judiciously removed, as previously found by Kramer.[11] These results are in very good agreement with those obtained by Hahn and Duquette in their recent investigation of fatigue deformation and crack nucleation in copper and copper-8 percent aluminum single crystals.[12] These authors show that under conditions of applied anodic current, the normal generation of near-surface dislocation entanglements characteristic of fatigue cycling in air is disrupted, leading instead to a loose array of dislocations clear up to the specimen surface and giving rise to a significant improvement in fatigue resistance. They also showed that there exists directly at the surface a layer of about 1 μm in depth which is free of dislocations and that the strained defect structure is formed beyond this dislocation-free zone at near-surface sites. We would like to suggest that structural investigations employing methods which do not take this dislocation-free layer effect into account may arrive at erroneous results. Our X-ray depth profile studies established the existence of long-range stresses set up by the defect structures at near-surface sites and in the bulk, and disclose their dynamic interplay on cycling. Therefore, these studies may be regarded as forming a bridge between the microscopic aspect of fatigue and the macroscopic aspect of continuum mechanics.

T. Yokobori[13] *(discussion)*—In relation to a ΔK_{th} model by the authors, may I make a comment.

Concerning the threshold stress intensity model, we have recently derived the ΔK_{th} from a model of unstable emission of dislocation from the crack tip under applied stress in the case of fatigue crack growth.[14-17] It was shown that there is a critical or threshold stress intensity factor below which dislocation emission cannot occur. Both of the following two requisites should be satisfied under applied stress in order that a dislocation can be emitted spontaneously from the crack tip.

1. The critical distance ξ_c at which straight dislocation is unstable under the influence of three forces—that is, the applied load, the image force, and the ledge force—is given by the solution for ξ of the following equation

$$f_{tot} = \mu b \left(\frac{K_1}{4\mu\sqrt{\pi b \xi}} - \frac{1}{4\pi\xi(1-\nu)} - \frac{2\gamma\alpha}{\pi\mu b(\xi^2 + \alpha^2)} \right) = 0 \qquad (29)$$

[11] Kramer, I. R., *Metallurgical Transactions*, Vol. 5, 1974, p. 1735.

[12] Hahn, H. N. and Duquette, D. J., *Acta Metallurgica*, Vol. 26, 1978, p. 279.

[13] Department of Mechanical Engineering II, Tohoku University, Sendai, Japan.

[14] Yokobori, T., Konosu, S., and Yokobori, A. T., Jr. in *Proceedings*, International Conference on Fracture, University of Waterloo, Waterloo, Ont., Canada, Vol. 1, 1976, pp. 665-682.

[15] Yokobori, T., Yokobori, A. T., Jr., and Kamei, A., *International Journal of Fracture*, Vol. 11, 1975, pp. 781-788.

[16] Yokobori, T., Yokobori, A. T., Jr., and Kamei, A., *International Journal of Fracture*, Vol. 12, 1976, pp. 519-520.

[17] Yokobori, A. T., Jr., *International Journal of Fracture*, Vol. 14, 1978.

where

$\xi = \rho/b$,
ρ = distance from crack front on slip plane,
b = Burgers vector,
μ = shear modulus,
ν = Poisson's ratio,
γ = true surface energy of crack plane, and
$\alpha = e^{3/2}\,\xi/2$.

The stress requisite for spontaneous emission of dislocation from the crack tip is given by

$$\xi_c < \xi_o \tag{30}$$

where ξ_o = core cut off of dislocation.

From Eqs 29 and 30, the stress requisite becomes

$$K_1 > \frac{\mu}{1-\nu}\sqrt{\frac{b}{\pi\xi_o}} \equiv K_{1cr.\ stress} \tag{31}$$

That is, $K_{1cr.\ stress}$ is the critical stress intensity factor below which dislocation emission cannot occur.[17] Numerically, for iron, $K_{1cr.\ stress} = 3.38$ kg mm$^{-3/2}$, and for aluminum, $K_{1cr.\ stress} = 0.82$ kg mm$^{-3/2}$.

2. On the other hand, the total energy change U_{act} for a crack which has emitted a dislocation loop is

$$U_{act} = \mu b^2\left[rU_o \ln\frac{r}{\xi_o} + U_l(r-\xi_o) - \frac{2}{3}U_s(r^{3/2} - \xi_o{}^{3/2})\right] \tag{32}$$

where

$$U_0 = (2-\nu)/8(1-\nu), \qquad U_l = 2\gamma/\mu b \qquad U_s = \frac{2.092K_1}{2\sqrt{2}\mu\sqrt{b}}$$

and r is the ratio of the distance between the dislocation and the crack tip to the Burgers vector b. If $dU_{act}/dr = 0$, then U_{act} will have a maximum, and, therefore, the energy barrier will exist against the dislocation emission and movement from the crack tip. Now dU_{act}/dr can be seen to have a maximum in the range of $0 \leq r < +\infty$. Therefore

$$\left(\frac{dU_{act}}{dr}\right)_{\max} < 0 \tag{33}$$

and then

$$\frac{dU_{act}}{dr} < 0 \qquad \text{for all values of } r \tag{34}$$

That is, U_{act} will decrease with increase in r, without attaining a maximum value. Thus Eq 33 is the energy requisite for spontaneous emission of dislocation from the crack tip.

From Eq 32, Eq 33 becomes

$$K_I > \left(\frac{2-\nu}{1-\nu}\right)\mu\left(\frac{eb}{8\xi_o}\right)^{1/2}\exp\left[-1+\frac{8\gamma(1-\nu)}{\mu b(2-\nu)}\right] \equiv K_{Icr.\ energy} \tag{35}$$

That is, $K_{Icr.\ energy}$ is also a critical stress intensity factor[17] below which dislocation emission cannot occur. Numerically, for iron, $K_{Icr.\ energy} = 3.119$ kg mm$^{-3/2}$, and for aluminum, $K_{Icr.\ energy} = 0.7257$ kg mm$^{-3/2}$.

The criterion for spontaneous emission of dislocation from the crack tip will now be given by the larger one of the two critical stress intensity factors, $K_{Icr.\ stress}$ and $K_{Icr.\ energy}$, according to Eqs 31 and 35, respectively. That is, the larger one of the two corresponds to the threshold stress intensity factor ΔK_{th}. The numerical value of $\Delta K_{th}/E$ thus obtained is of the order of $10^{-4}\ \sqrt{\text{mm}}$ for iron and aluminum, which is of reasonable value as reported by Speidel.[18] The symbol E in the previous expression denotes Young's modulus.

K. Tanaka[19] (*separate closure by coauthor*)—First, regarding Professor McEvily's discussion, I would like to clarify one point. We tried to treat the structure-sensitive properties of a material subject to fatigue crack growth, so we used crack mechanics and dislocation mechanics, but we did not use Neuber's block size concept. I think the concept is quite useful from an engineering application viewpoint, and we intend to explore further along that line.

Second, I agree that the fracture surface topography changes near the threshold condition. In the beginning of our study, we wanted to quantify that situation. But, once we measured the effective component of the stress intensity factor, the functional form correlating the rate and the effective stress intensity factor was found to be valid down to the threshold condition. Moreover, it could be used for predicting very small crack growth. I

[18] Speidel, M. O. in *Proceedings*, International Conference on Stress Corrosion Cracking and Hydrogen Embrittlement Cracking of Iron Base Alloys, National Association of Corrosion Engineers, 1974.

[19] Second author of paper under discussion and speaker who presented the paper at the symposium.

still do not know the physical meaning of our finding; that is, the relationship holds even though the fracture mode is different.

I thank Professor McEvily for his other comments, which are constructive for a refinement of our model.

I appreciate the comment by Professor Weissmann and his co-discussers. I personally am very glad to know that they are very keen on X-ray work on fatigue. Similarly, we did quite a bit of fatigue-related work using the X-ray microbeam diffraction technique. Professor Weissmann presented some interesting results on the measurement of the structural change progressing inward from the surface without destructing the bulk sample by using several X-rays with different penetration depths.

At the present, we are carrying out similar X-ray work on fatigue, especially on crack nucleation and early crack growth phases, that is, up to about 20 percent of the total life. Once a macrocrack is found, the fatigue life is predictable from crack growth mechanics as described in our presentation. As you may know, we proposed the method of damage detection based on the measurement of the half-value breadth change of diffraction profiles due to fatigue cycling. X-ray observations may be very significant especially for the mechanical modeling of the formation of persistent slipbands and microcracks. Your idea of surface layer stress is suggestive in formulating persistent slipbands formation criterion.

Finally, I am very glad to have our paper discussed by Professor Yokobori. His ideas and calculations have been helpful to us in the progress of our present research. Our approach to fatigue problems is basically experimental, and a simple and, we hope, an elegant model is our contribution to interpretation of the experimental data.

S. Taira, K. Tanaka, and M. Hoshina (main closure)—We appreciate the comments and the questions on our work by Discussers McEvily, Weissmann et al, and Yokobori. Their discussions are concerned with three topics, namely, (1) the near-threshold and the threshold of through-crack growth, (2) the growth behavior of very small cracks and the fatigue limit, and (3) the fatigue-induced substructure and crack nucleation. Our closure answers the comments and the questions in that order.

Professor McEvily cited the fractographic observation done by Otsuka and insisted on the importance of Mode II growth mechanism near the threshold. Although his observation of Mode II growth near the threshold does not seem conclusive, we agree with Prof. McEvily on the point that the micromechanisms of fatigue crack growth near the threshold are different from the striation mode mechanism working above the transition. In the near threshold region, the slipband formation and the direction of crack growth will be crystallographic, and so Mode II growth can be involved. The mechanistic aspect of the growth mechanism for this region,

described in the previous paper of the authors,[20] is that a fatigue crack grows intermittently along a certain plane after a critical amount of substructural damage is accumulated ahead of the crack tip. It certainly was a great surprise, as Prof. McEvily perhaps felt, to find that the relation between the rate and ΔK_{eff} for faster rates was valid near the threshold down to the rate 5×10^{-11} m/cycle. Later, we found a similar tendency in the results reported by Kikukawa and Jono.[21] Although the generality of our results and the physical basis underlying this correlation should be studied in the next step, we cannot deny the possibility that different mechanisms can yield approximately the same law. This speculation comes from our finding[22] that the rate above the transition region was proportional to the square of the range of the crack face opening 250 μm behind the tip, which corresponded to the damage accumulation model proposed by Weertman[23] although the rate was determined by an instantaneous value of the crack-opening displacement range.

When the crack segments near the tip are on certain crystallographic planes, the crack front runs zigzag across the specimen thickness in polycrystalline materials. The most simple two-dimensional model for this three-dimensional situation will be a straight crack, which was adopted in the paper. The crystalline structure was modeled in terms of the crack-tip slipband blocked by the grain boundary, and the continuously distributed dislocation theory was combined with crack mechanics in mathematical analysis. The increase of K_{op} near the threshold can be predictable based on this model.[24] The term "continuum mechanics" used by Prof. McEvily seems to mean macroscopic continuum mechanics. Theories of dislocations or other defects are still classified as continuum mechanics. Some confusion arises among researchers about the interpretation of the Bilby-Cottrell-Swinden model, because they used the continuously distributed dislocation theory to solve the macroscopic strip yield model, that is, the Dugdale mode.[25] In their model, the dislocation density or the microscopic stress intensity factor are assumed to vanish at the tips of yield strips, so that the stress is bounded everywhere in the material. The dislocation density and the stress are infinite at the tip of the blocked slipband in the

[20] Taira, S. and Tanaka, K. in *Proceedings*. 3rd International Congress on Fracture, Munich, Germany, Vol. 61, 1972.

[21] Kikukawa, M., Jono, M., and Tanaka, K. in *Proceedings*. 2nd International Conference on the Mechanical Behavior of Materials, Boston, Mass., special volume, 1978, pp. 254-277.

[22] Taira, S., Tanaka, K., and Ogawa, S., *Journal of the Society of Materials Science*, Kyoto, Japan, Vol. 26, 1977, pp. 93-98.

[23] Weertman, J., *International Journal of Fracture Mechanics*, Vol. 2, 1966, pp. 460-467.

[24] Taira, S., Tanaka, K., and Nakai, Y., "A Model of Crack-tip Slip Band Blocked by Grain Boundary," to be published in *Mechanics Research Communications*.

[25] Dugdale, D. S., *Journal of the Mechanics and Physics of Solids*, Vol. 8, 1960, pp. 100-104.

continuously distributed dislocation theory because of the pileup of dislocations under applied stress.

The threshold model proposed by Yokobori is based on the assumption that the threshold value is such a value below which a dislocation cannot emit from the tip. This criterion seems to give the lower bound of the threshold value in the sense that at least the criterion has to be satisfied. Experimental observations of the present paper, as well as Wilkins and Smith,[26] indicated the existence of the dislocation substructure ahead of the crack tip of nonpropagating fatigue cracks.

Professor McEvily used the concept of the Neuber block size in order to explain the decrease of K_{th} for very small cracks and derived a certain correlation between the threshold stress σ_{th} and the crack length $2a$. The size ρ_e in his equation seems to be larger than the crack length $2a$ when it is evaluated from the data reported by Kitagawa and Takahashi. If so, it might be difficult to use only the singular term in the series expansion of elastic stress distribution, upon which Prof. McEvily's equation may be based. The relation between σ_{th} and a can be derived by solving the model shown in Fig. 16*b* for an isolated $2a$-long crack. The critical condition is expressed by[24]

$$\sigma_{th}\sqrt{\pi b} = K^{m}_{critical} + 2\sigma_{fr}{}^{*}\sqrt{b/\pi}\cos^{-1}(a/b)$$
$$b \equiv a + \omega \tag{36}$$

where the notations mean the same as in the paper. Assuming $\omega = 0.5l$ and $a = 0$, we have the equation for the fatigue limit identical to Eq 27 in the paper. The fatigue limit and the threshold condition are now derived from a single model, and Eq 36 yields the relation between σ_{th} and a, which has a tendency similar to that seen in Kitagawa's data.

Professor Weissmann et al presented an important result of X-ray measurement of the depth profile of the excess dislocation density at near-surface regions. The progress of defect structure inward from the surface was also detected by one of the present authors in the study of damage detection in terms of the half-value breadth (HVB) change of diffraction profiles.[27] The surface zone with high HVB in low-carbon steel was about 30 μm from the surface at 90 percent of the total life. His model is that the crack nucleation takes place "when the local accumulation of excess dislocations exceeds the barrier strength at the surface." We suspect that this model may be applicable to the formation of the slipband or the persistent

[26] Wilkins, A. W. and Smith, G. C., *Journal of Materials Science*, Vol. 5, 1970, pp. 418-424.

[27] Taira, S. and Hayashi, K. in *Proceedings*, 9th Japanese Congress on Testing Materials, 1966, pp. 1-6.

slipband, and that the Stage I crack growth stage might be treated by crack mechanics combined with accumulated internal stress and surface layer considerations. The initial stage of the fatigue process from the persistent slipband formation to the Stage II type of crack nucleation in polycrystalline materials may be the most formidable problem to treat quantitatively both from theoretical and experimental points of view. The dynamic interaction of the applied and internal stress fields should be considered simultaneously. X-ray observation yields some insight into the internal stress field related to a specific configuration of dislocations and other lattice defects. Our model for the endurance crack should be refined in the next step of the study by considering a specific configuration of lattice defects and microcracks.

S. P. Lynch[1]

Mechanisms of Fatigue and Environmentally Assisted Fatigue

REFERENCE: Lynch, S. P., **"Mechanisms of Fatigue and Environmentally Assisted Fatigue,"** *Fatigue Mechanisms*, Proceedings of an ASTM-NBS-NSF symposium, Kansas City, Mo., May 1978, J. T. Fong, Ed.; *ASTM STP 675* American Society for Testing and Materials, 1979, pp. 174-213.

ABSTRACT: Fatigue cracks often initiate either by formation and development of coarse slip steps or by extensive deformation in localized soft bands producing intrusions and extrusions. Microstructural changes induced by fatigue, for example, formation of fine subgrain structures within soft bands, are probably necessary for intrusion, extrusion, and for subsequent Stage I crack growth. Stage II crack growth involves plastic-blunting/alternate-slip processes at crack tips. Increments of crack growth per cycle, for a given effective crack-opening displacement, depend mainly on the distribution of slip around crack tips during loading; this distribution is determined by both the microstructure and the environment. The effects of aggressive environments on crack growth can be explained, in many cases, on the basis that chemisorption of environmental species influences interatomic bonds and thereby facilitates nucleation of dislocations at crack tips. Striations ('ductile' and 'brittle' types) on fracture surfaces are produced because unloading deforms part of the fracture surface produced during loading.

KEY WORDS: fatigue (materials), mechanisms, dislocations (materials), aluminium alloys, environmental effects, liquid-metal environments, chemisorption, microstructure, crack initiation, crack propagation, metallography, fractography

This paper, based mainly on metallographic and fractographic studies of fatigue in aluminum alloys, discusses fundamental mechanisms of fatigue with particular emphasis on recent studies concerning the influence of environment on Stage II crack growth. Some earlier work on crack initiation and Stage I crack growth is briefly reviewed in the first section.

The figures in this paper contain two types of arrowheads. Single arrowheads on fractographs indicate local directions of crack growth. Double arrowheads on micrographs indicate stress axis.

[1] Research scientist, Aeronautical Research Laboratories, Department of Defense, Box 4331 GPO Melbourne, 3001, Australia.

Initiation of Fatigue Cracks [*1-3*][2]

Crack initiation during cyclic deformation generally occurs in regions where strain has become *localized*; overall hardening/softening may occur prior to strain localization but is generally not critical to the initiation of cracks. Strain localization may occur at (1) preexisting stress concentrations such as notches or corrosion pits, (2) steps/notches produced during fatigue by fretting or by coarse slip offsets at surfaces, and (3) localized soft regions such as precipitate-free zones (PFZ). In engineering components, the most severe strain localization, and subsequent crack initiation, often occurs where notches or fretting damage coincide with large inclusions or PFZ. Studies of the fundamental slip processes involved in crack initiation, however, are facilitated by using plane specimens with polished surfaces. Optical microscopy of such specimens after fatigue (for a variety of materials and conditions) suggests that there are several types of behavior. For example, initiation may involve the development of coarse slip steps adjacent to the grain boundaries (Fig. 1). In other cases, crack initiation is associated with either the formation of well-defined extrusions and intrusions (Fig. 2), or the development of a coarse notch-peak topography [*4*], along slip bands. Typical surface profiles produced by fatigue in these cases are illustrated in Fig. 3 and proposed explanations are outlined in the following.

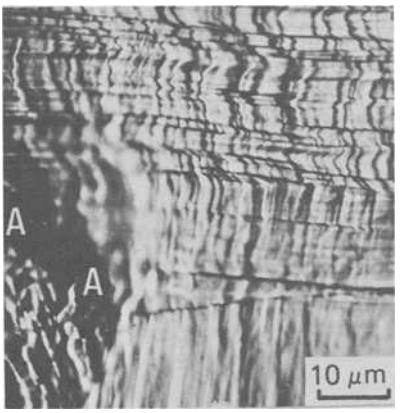

FIG. 1—*Optical micrograph showing notch-peak surface topography produced by coarse slip in aluminium polycrystal tested in high-strain torsional fatigue; crack initiation has occurred along grain boundary* A-A.

[2] The italic numbers in brackets refer to the list of references appended to this paper.

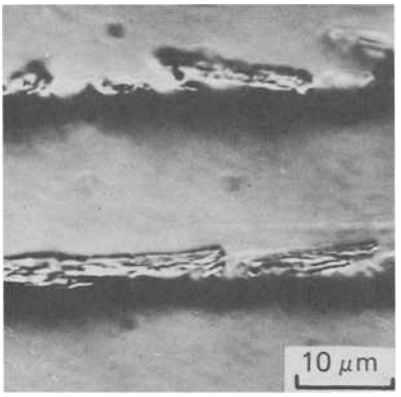

FIG. 2—*Optical micrograph showing slipband extrusions developed on surface of age-hardened aluminum-zinc-magnesium during high-strain torsional fatigue; note striations on surface of extrusions.*

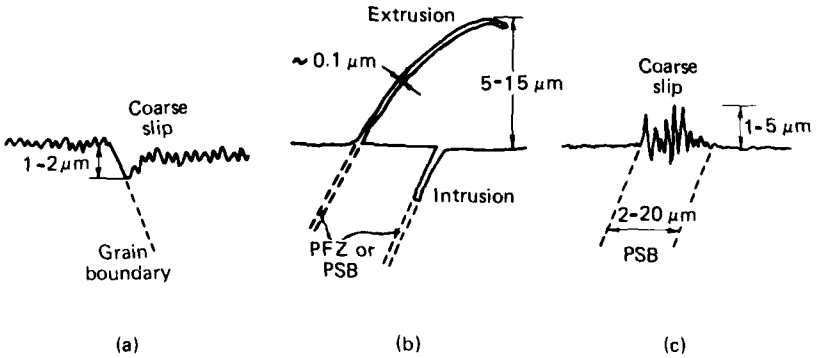

FIG. 3—*Schematic diagrams showing common surface profiles produced during fatigue:* (a) *coarse slip and crack initiation adjacent to grain boundaries,* (b) *extrusions and intrusions, and* (c) *coarse slip within PSB.*

Initiation Involving Coarse Slip

In low-strength ductile materials, fatigued at large strain amplitudes, the first half-cycle produces slip which is easily detected using optical microscopy. Reverse slip in the following half-cycle often occurs on different planes, subsequent cycles produce further slip, and a notch-peak topography progressively develops (Figs. 1 and 3*a*). The most severe notches, and subsequent crack growth, generally occur adjacent to grain boundaries or inclusions since, on either side of an interface, the strain often differs markedly. Crack initiation in these circumstances can be considered to have occurred, in effect, after the first cycle since significant nucleation

or egress of dislocations at the base of notches produced on the first cycle is likely on each subsequent cycle; such dislocation activity will generally extend the notch (crack). Details are discussed in sections on Stage II crack growth.

Initiation Involving Intrusion and Extrusion

In a wide variety of materials, particularly fatigued at low strain amplitudes, a considerable number of cycles may elapse with either no detectable slip or only very fine slip being observed (using optical microscopy); then, often within relatively few cycles, coarse slipbands develop and thin slivers and whiskers of material (extrusions), projecting up to about 10 μm from specimen surfaces along short lengths of slipbands, are observed (Figs. 2 and 3*b*). In addition, narrow slits and tubular pores (intrusions), which are the precursors of Stage I fatigue cracks, extend into specimens along slipbands. Intrusions and extrusions also develop at grain boundaries in some materials.

In precipitation-hardened aluminium-zinc-magnesium alloys, transmission electron microscopy (TEM) has shown that the formation of intrusions and extrusions along slipbands corresponded to resolution of precipitates and the formation of subgrains within slipbands (Fig. 4) [*5,6*]. Prior to fatigue, slipbands ('quench' bands) were generally not precipitate-free but often had a lower-than-average density of precipitates since deformation

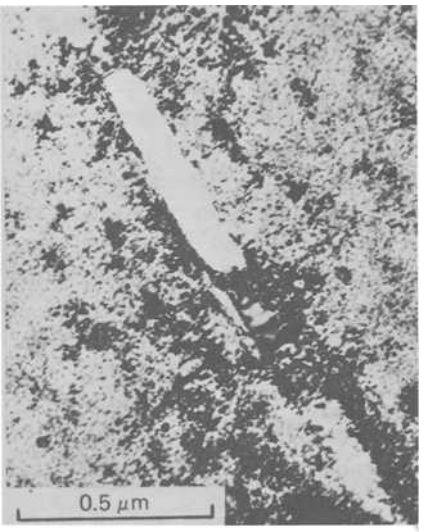

FIG. 4—*Transmission electron micrograph showing precipitate-free slipband and subgrains produced in age-hardened aluminum-zinc-magnesium during high-strain torsional fatigue.*

during quenching decreased the density of precipitate nuclei within 'quench' bands. Deformation during fatigue concentrates within 'quench' bands and produces re-solution of precipitates, possibly by a dislocation-enhanced diffusion process [6]. In steels, extrusion/intrusion is also associated with precipitate-free slipbands [7]. Extrusion/intrusion at grain boundaries in aluminium-zinc-magnesium corresponded to the formation of subgrains within *preexisting* PFZ [6]. In single-phase materials, extrusion/intrusion is probably associated with soft persistent slipbands (PSB), namely, bands of small cells or subgrains [1-3].

Mechanisms of Intrusion and Extrusion

Many mechanisms, based on the movement and interaction of individual dislocations in particular sequences, have been proposed to account for intrusions and extrusions [3]. However, such mechanisms generally do not consider the microstructural changes which often produce softening in slipbands nor account for all the experimental observations. Cottrell [8], on the other hand, suggested that extrusions result when soft material in slipbands is squeezed out plastically during the compression phase of the stress cycle and is not sucked back in again during the tension phase. Comparison of the behavior of soft PFZ and slipbands (~ 0.1 μm thick) in aluminium-zinc-magnesium during fatigue with the deformation behavior of 'model' specimens (soft layers ~ 100 μm thick sandwiched between and bonded to harder regions) strongly supported Cottrell's suggestion and provided additional insight into the processes involved [6].

Deformation of 'model' specimens in compression resulted in extrusions of thin ribbons of soft material (Fig. 5); under cyclic compressive loads, striations corresponding to each extrusion increment per cycle were observed on extrusion surfaces (Fig. 5, inset). Striations were also detected on extrusions from slipbands in aluminium-zinc-magnesium (Fig. 2). Tension tests on model specimens resulted in soft zones being sucked in, thereby producing intrusions (Fig. 6). Extrusions and intrusions from PFZ in aluminum-zinc-magnesium were also produced by single compressive and tensile loads, respectively. Other characteristics of extrusions in aluminum-zinc-magnesium and 'model' extrusions were similar and it was concluded that the deformation process occurring during intrusion/extrusion in the 'model' specimens and in aluminum-zinc-magnesium was also similar. Direct observations of 'model' specimens showed that intrusion/extrusion involved preferential plastic deformation within soft layers with relative displacement of hard and soft zones occurring by intense shear adjacent to their interfaces.

Some apparent discrepancies were noted between the behavior of 'model' specimens (which was consistent with the predictions of slip-line-field theory) and the behavior of PFZ in aluminum-zinc-magnesium. In the

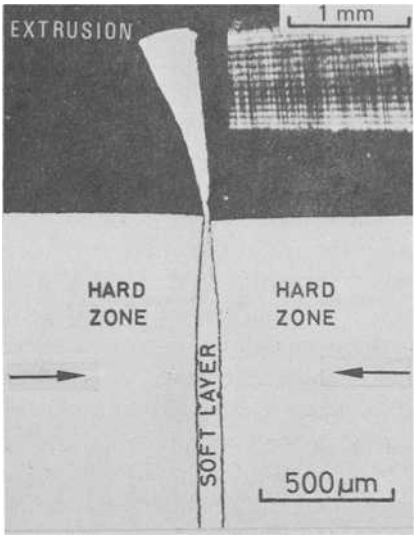

FIG. 5—*Optical micrograph showing section through a 'model' specimen (brass blocks soldered together with tin) after compressive loading; soft layer has been extruded. Inset shows striations on extrusion surface after cyclic loading of 'model' specimens.*

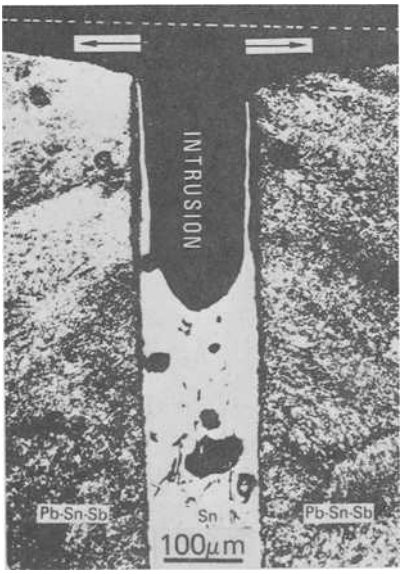

FIG. 6—*Optical micrograph showing section through a 'model' specimen (lead sandwiched between lead-tin-antimony) after tensile deformation; dotted line shows position of surface prior to deformation.*

'model' specimens, extensive deformation in the soft zones did not occur until the hard material yielded since, when interfacial friction is high, deformation of thin soft layers is constrained by the surrounding hard zones. In aluminum-zinc-magnesium, however, intrusion/extrusion during fatigue occurs at stresses well below general yield, and then occurs only after a number of stress cycles (even when soft PFZ are present prior to fatigue); in this case, intrusion/extrusion corresponded to the formation of subgrains in PFZ. These observations could be explained on the basis that subgrain boundaries formed at the interfaces between PFZ and matrix facilitate interfacial shear; the precise mechanisms, however, are not clear.

The characteristics of intrusion/extrusion in single-phase materials are often very similar to those in aluminum-zinc-magnesium and the mechanisms are probably also similar. However, it is not understood why PSB should be softer than adjacent regions. It is known that very small grains are one of the prerequisites for superplasticity and there could possibly be some similarities between the mechanisms of superplasticity and the deformation of very small subgrains in slipbands during fatigue.

The development of a coarse notch-peak topography along certain slipbands (Fig. 3*c*) in some instances possibly occurs when PSB are wider and when there is less difference in strength between PSB and matrix, compared with PSB associated with distinct extrusions/intrusions. Initiation involving coarse slip within PSB may be simply a geometrical consequence of the irreversibility of slip-step formation at the surface of PSB [*4*].

Stage-I Crack Growth [*1,2,6*]

Stage I crack growth often occurs by the progressive development and linking-up of intrusions along slipbands or grain boundaries at about 45 deg to the tensile-stress axis. Subgrain formation and intrusion often initially occur along short lengths of slipbands; subsequent subgrain formation between and ahead of intrusions probably enables their linking up and extension by further intrusion. After an increment of crack growth by intrusion during a tensile half-cycle, compressive deformation apparently does not reverse the process, (that is, soft zones are not squeezed back out again). Striations observed on Stage I fracture surfaces (Fig. 7) suggest (by analogy with striations on Stage II fractures—discussed later) that compression closes cracks by slip behind crack tips so that intrusion surfaces produced during loading are partially deformed. The proposed mechanism of intrusion/Stage I crack growth is illustrated schematically in Fig. 8. Preferential deformation within soft slipbands during Stage I crack growth may sometimes produce microvoids ahead of crack tips and dimples may be observed on fracture surfaces (Fig. 7).

The effects of environment on crack initiation and Stage I crack growth could be explained in some cases by the mechanism proposed for the influence of environment on Stage II crack growth discussed next.

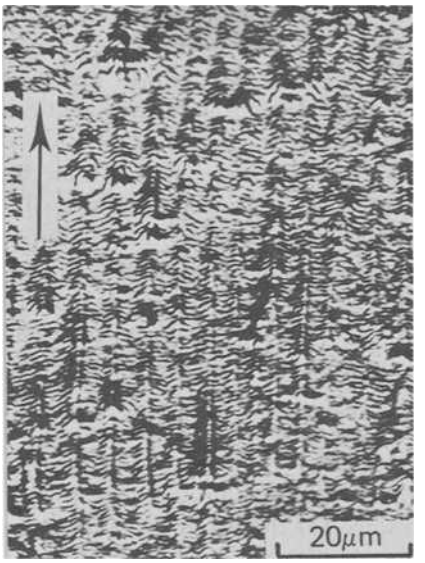

FIG. 7—*Optical micrograph showing striations on Stage I fatigue fracture ({111} facet) in PH aluminum-zinc-magnesium produced by high-strain torsion fatigue in air.*

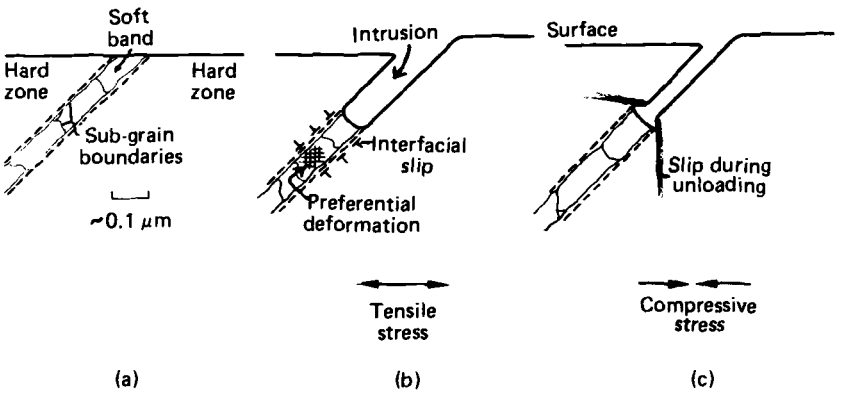

FIG. 8—*Schematic diagram illustrating proposed mechanism of intrusion (Stage I crack growth)*: (a) *subgrains are formed within fatigue-induced or preexisting soft bands,* (b) *intrusion of weakly constrained soft bands occurs under low tensile stresses, and* (c) *deformation during unloading is concentrated behind the crack tip.*

Stage II Crack Growth [*1,2,9*]

Transitions from Stage I to Stage II crack growth probably occur when increasing stress intensity or increasing constraint on plastic flow (or both) result in extensive slip activity on more than one slip plane around crack tips. Microstructural changes (for example, softening along slipbands) probably necessary for Stage I crack growth are generally not required for Stage II crack growth [*10,11*]. Proposed explanations for Stage II crack growth (and the formation of striations observed on fracture surfaces) include fracture-deformation sequences [*12*], plastic blunting followed by resharpening of the crack tip [*13*], and alternate-slip processes [*11,14*]. The effects of environment on crack growth have been attributed [*15*] to (1) adsorption of environmental species, (2) dissolution, (3) formation of oxide films, and (4) diffusion of 'embrittling' species ahead of crack tips. In aqueous environments, all the aforementioned processes may occur and it is difficult to establish which process is primarily responsible for facilitating crack growth.

In the present work, crack growth in aluminium and aluminum-zinc-magnesium single crystals has been studied in several environments, including liquid metals. Crack growth in liquid-metal environments has been studied in particular since (1) there has been little previous work in this area, and (2) the material-environment interaction generally involves only chemisorption at crack tips [*16*]. Some indication of the role of chemisorption during cracking in other (for example, aqueous) media may therefore be obtained by comparing the characteristics of cracking in liquid-metal with cracking in other environments.

Experimental Procedure

The influence of environments on Stage II crack growth was studied in aluminium (99.99 percent pure) and a high-purity Al-6.2Zn-2.9Mg alloy. Specimens (Fig. 9) were cut from sheet, which had been given a 'strain-anneal' treatment to produce a grain diameter of about 10 mm, then notched such that crack growth occurred within a single grain. Crack growth occurred along {100} planes in ⟨110⟩ directions under certain conditions. Crystals were generally orientated so that a {100} plane was approximately normal to the specimen sides; {100} planes were either normal to or inclined to the specimen axis, with ⟨110⟩ directions either parallel to or inclined to the bending axis. Crystal orientations were determined from analyses of slip traces on surfaces. Specimens were tested in cantilever bending at cyclic frequencies of 1 and 24 Hz. Aluminum-zinc-magnesium specimens were tested in three conditions of heat treatment:

1. Solution-treated at 450°C (842°F) for 60 min, then boiling water-

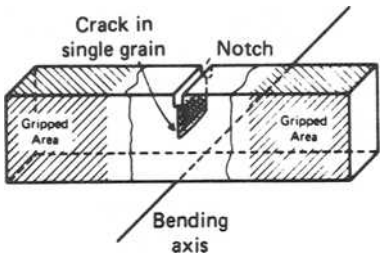

FIG. 9—*Specimen (40 by 10 by 3 mm) used for studies of Stage II crack growth.*

quenched (VHN 80). Most tests were carried out in this condition (subsequently designated ST).

2. As for Condition 1 plus aging at 100°C (212°F) for 60 min, then aging to peak hardness at 180°C (356°F) for 100 min (VHN 165) (subsequently designated PH).

3. As for Condition 1 plus aging at 330°C (626°F) for 15 h (VHN 60) (subsequently designated OA).

The environments used were as follows:

1. Liquid metal environments: a quinary eutectic of bismuth, lead, indium, tin, and cadmium (44.7, 22.6, 19.1, 8.3, and 5.3 percent by weight, respectively), which melts at 47°C (117°F), was generally used. Specimens were notched, using a fine saw, in the presence of the liquid alloy to ensure 'wetting.' The liquid alloy was removed from cracks and fracture surfaces by immersing specimens in concentrated nitric acid for 2 min. Tests established that fracture surfaces were not attacked by the liquid alloy after fracture or during its removal. Tests in liquid mercury and liquid gallium produced similar results as tests in the liquid alloy, but mercury and gallium were difficult to remove from cracks and fracture surfaces.

2. Saturated aqueous potassium iodide (KI) solution.

3. Laboratory air (~50 percent relative humidity).

4. Dodecanol (an inert liquid); some specimens were cathodically charged to produce hydrogen (in hydrochloric acid, pH 1, at a potential of −1.5 V versus the standard calomel electrode for 20 h) prior to testing in dodecanol.

Tests were carried out at ~70°C (~158°F) in the liquid alloy and at 25°C (77°F) in the other environments.

Experimental Observations

Crack Growth in Liquid-Metal Environments

Crack growth in aluminium and aluminum-zinc-magnesium specimens in the liquid-alloy environment produced fracture surfaces which were

approximately parallel to {100} planes for all conditions, namely, all orientations of crystals, all heat-treatment conditions, and for cyclic (1 and 24 Hz) and monotonic tensile loading. 'Brittle' striations and river lines were observed on {100} facets produced by fatigue (Figs. 10,11). As is usual, each striation was produced by a single stress cycle and defined the position of the advancing crack front. Crack growth generally occurred in ⟨110⟩ directions and, for specimens orientated so that ⟨110⟩ directions formed angles of 45 deg with the bending axis, crack growth in adjacent regions occurred in different ⟨110⟩ directions so that crack fronts had a zigzag form (Figs. 10,11). (The sharp transition to the black area in Figs. 10 and 11 is associated with a sharp change in fracture plane produced by changing to an inert environment—discussed later). For specimens orientated so that a ⟨110⟩ direction was parallel to the bending axis, crack fronts (striations) across the width of the specimen were fairly straight. Striations had a very shallow 'sawtooth' profile with peak matching peak on opposite fracture surfaces.

Crack fronts were generally not unduly perturbed by the presence of the side surface and there was only a very small amount of lateral contraction around crack tips at the specimen sides during crack growth. ST specimens, partially cracked by fatigue, then aged (to 'decorate' dislocations), sectioned, polished, and etched, showed that the slip distribution in the interior was similar to that on the side surfaces (Fig. 12). Thus, observations of slip on the specimen sides during fatigue give an indication of the slip process actually associated with crack growth. Repolishing the sides of specimens partially cracked in liquid alloy and then *increasing* the crack-opening displacement (COD) to produce an increment of crack growth in

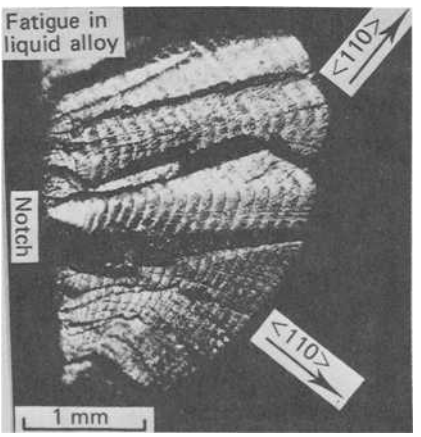

FIG. 10—*Optical micrograph showing striations on Stage II fracture surface in ST aluminum-zinc-magnesium produced by fatigue in the liquid-alloy environment at 1 Hz.*

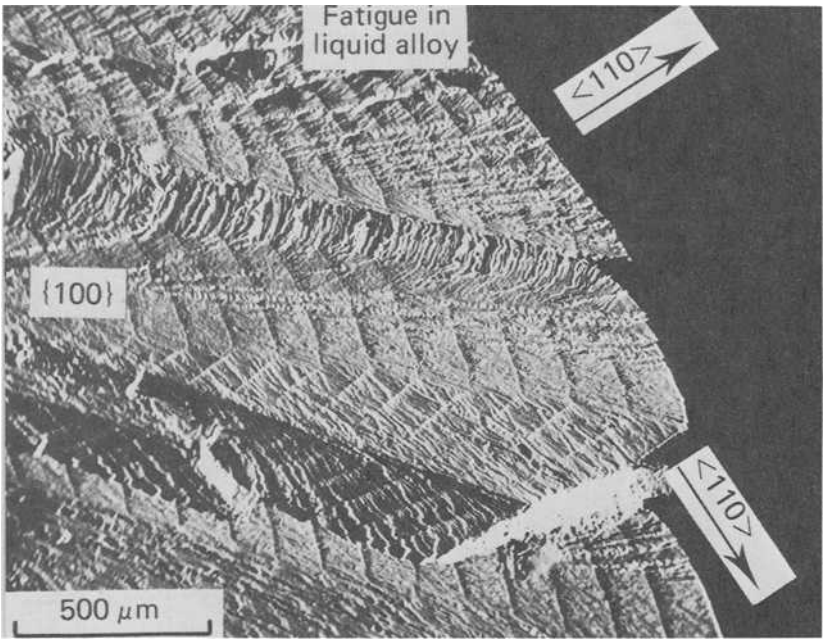

FIG. 11—*Scanning-electron micrograph of same specimen as in Fig. 10.*

liquid alloy showed that slip mostly emanated from the (advancing) crack-tip region with little slip activity directly ahead of this region (Fig. 13*a*). Repolishing specimens to remove previous slip markings and then *decreasing* the COD produced slip mostly *behind* the (stationary) crack tip so that the fracture surfaces were deformed (Fig. 13*b*). For specimens polished prior to fatigue, fine slip lines produced during loading were *partially* covered by coarse slip lines produced during unloading and, hence, regular slipbands were observed on the side surfaces (Fig. 12). These slipbands corresponded with striations on fracture surfaces.

The *detailed* appearance of fracture surfaces produced by crack growth in the liquid-alloy environment depended on the heat-treatment condition. (Fractures produced by monotonic tensile loading were examined in particular since they were similar to fatigue fractures but had not been subjected to deformation produced by unloading.) Fracture surfaces of ST specimens showed slip lines normal to, and river lines parallel to, the direction of crack growth; extremely small, shallow dimples were probably also present (Fig. 14*a*). Fracture surfaces of PH specimens were fairly similar to those of ST specimens except that slip lines were not observed and dimples were slightly larger. For OA specimens, fracture surfaces were entirely covered by well-defined, shallow dimples which were elongated in the direction of

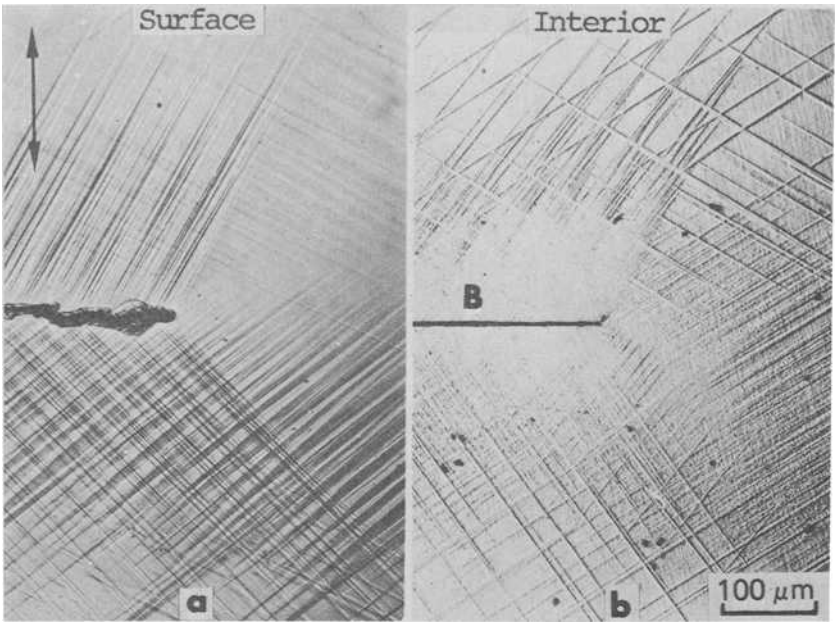

FIG. 12—*Optical micrographs showing slip distributions associated with fatigue-crack growth in the liquid-alloy environment at 1 Hz in ST specimen,* (a) *on the side of the specimen and* (b) *in the interior of the same specimen; slip markings are less clear in the more highly strained regions,* B, *close to the crack.*

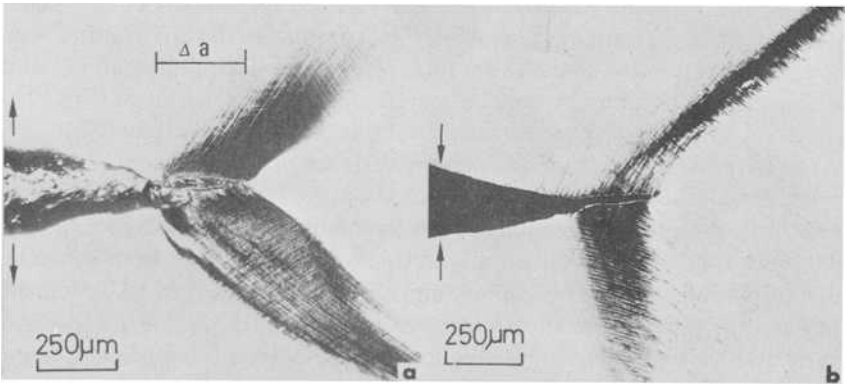

FIG. 13—*Optical micrographs showing slip on side surfaces of pure aluminium specimens tested in the liquid-alloy environment, associated with* (a) *a COD producing a crack-growth increment,* Δa, *and* (b) *a crack-closing displacement producing deformation of the fracture surface behind the stationary crack tip.*

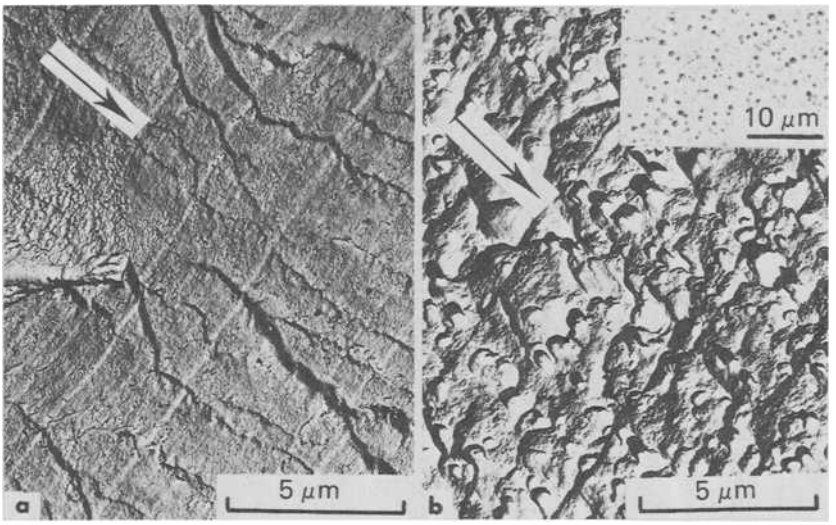

FIG. 14—*Electron micrographs showing fracture surfaces produced by crack growth in the liquid-alloy environment under monotonic tensile loading for* (a) *ST specimens and* (b) OA *specimens; inset (optical micrograph) shows precipitate distribution.*

crack growth on both fracture surfaces (Fig. 14*b*). (Much deeper dimples were produced by monotonic fracture of OA specimens in air.)

Preliminary studies on the influence of heat treatment, cyclic frequency, and wave shape on crack growth in the liquid-alloy environment showed that, for a given COD, crack-growth increments were (1) about an order of magnitude larger for PH specimens than for ST specimens, (2) about four times larger at 1 Hz than at 24 Hz for the ST specimens (Fig. 15), and (3) unaffected by hold times at peak load for ST specimens (Fig. 16).

Crack Growth in Aqueous Environments, Moist Air, and Inert Environments

For specimens tested in the solution-treated condition, aqueous and moist-air environments produced similar effects as the inert (dodecanol) environment; for specimens tested in the peak-hardness condition, however, aqueous and moist-air environments generally substantially increased rates of crack growth (and changed fracture-surface appearance) compared with specimens tested in the inert (dodecanol) environment.

Crack growth in *ST specimens* in aqueous, moist-air, and dodecanol environments usually occurred roughly normal to the specimen axis and produced 'ductile' striations on fracture surfaces. Figure 17 shows the change in the fracture-surface appearance associated with a change from

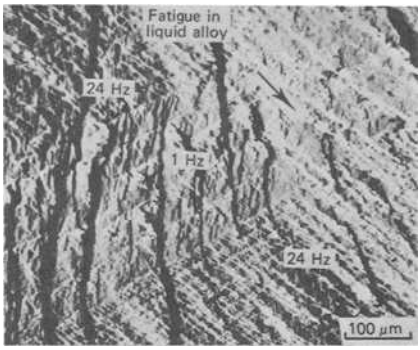

FIG. 15—*Scanning electron micrograph showing striations on fracture surface for ST aluminum-zinc-magnesium fatigued in the liquid-alloy environment at 24 Hz, then at 1 Hz for 5 cycles, and then again at 24 Hz.*

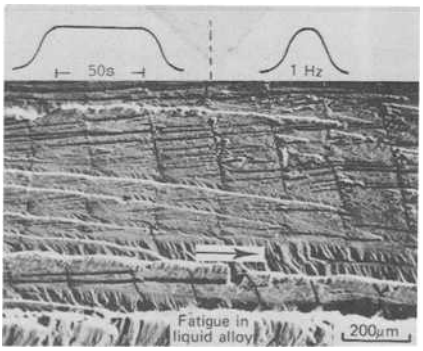

FIG. 16—*Scanning electron micrograph showing striations on fracture surface for ST aluminum-zinc-magnesium fatigued (for the wave shapes shown) in the liquid-alloy environment.*

fatigue in liquid alloy to fatigue in air at the same stress. There was (1) an abrupt change from 'brittle' to 'ductile' striations, (2) approximately an order of magnitude reduction in rate of crack growth, (3) a change in fracture plane from a {100} inclined to the specimen axis to a plane normal to the specimen axis, (4) a reduction in the number of river lines (cliffs) on the fracture surface, and (5) (not shown in Fig. 17) a gradual change in direction of crack growth from ⟨110⟩ directions inclined to the bending axis to a direction normal to the bending axis. These changes are illustrated in Fig. 18. Observations on the sides of specimens and in the interior showed that, in air, considerably more slip occurred around and ahead of crack tips, and that more blunting occurred at crack tips during crack growth, than in the liquid-alloy environment (Figs. 19, 20, and 21*a,b*).

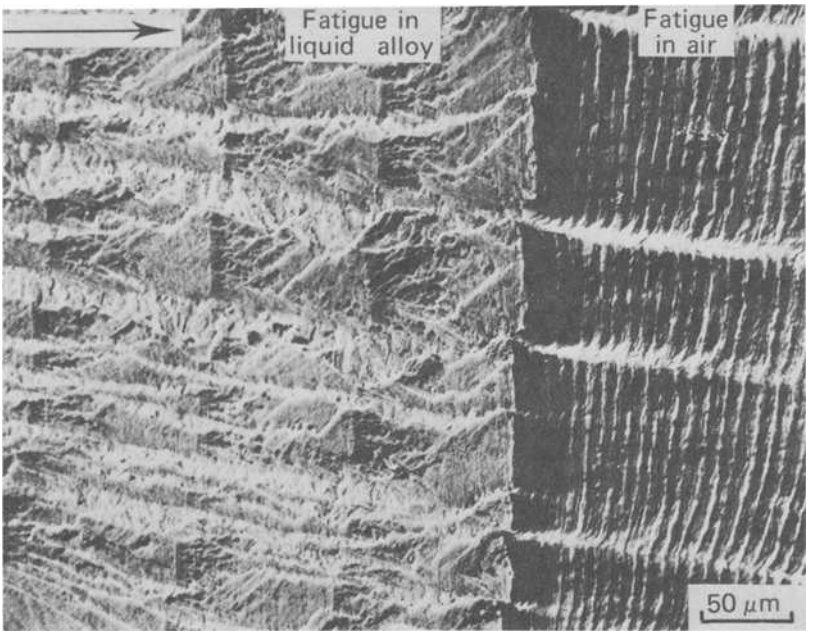

FIG. 17—*Scanning electron micrograph showing fracture surface of ST specimen produced by fatigue in the liquid-alloy environment at 1 Hz, forming 'brittle' striations, then by fatigue in air at the same stress and frequency, producing 'ductile' striations.*

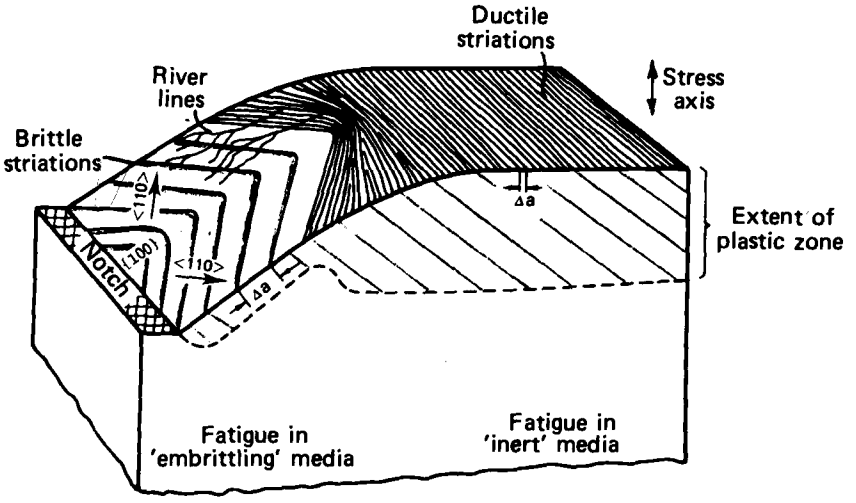

FIG. 18—*Schematic illustration of the influence of environment on fatigue-crack growth in aluminum-zinc-magnesium single crystals.*

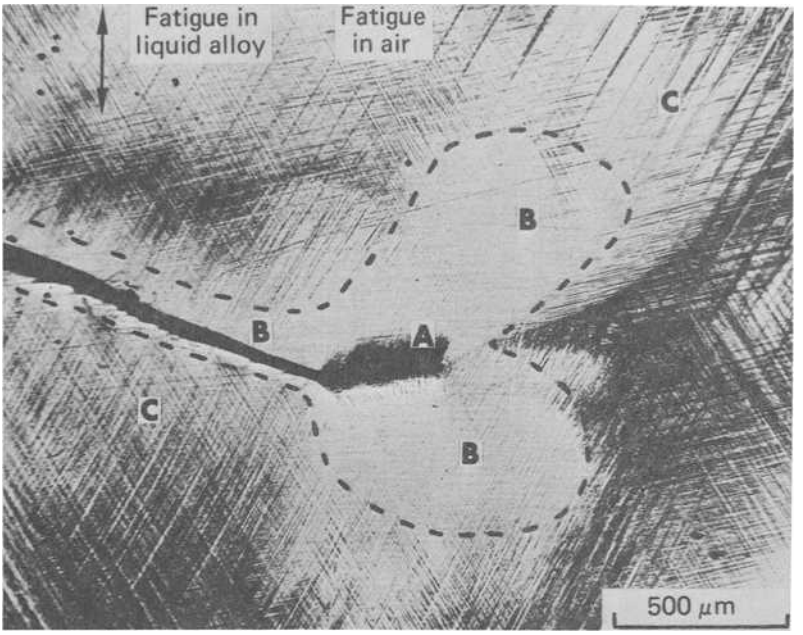

FIG. 19—*Optical micrograph showing slip distribution, in the interior of an ST specimen, around a fatigue crack produced first in the liquid-alloy environment at 1 Hz, then in air at the same stress and frequency. (Specimen was aged after fatigue, sectioned, polished, and etched.) Region* A *is a very highly strained region, Region* B *is moderately strained, and Region* C *is lightly strained.*

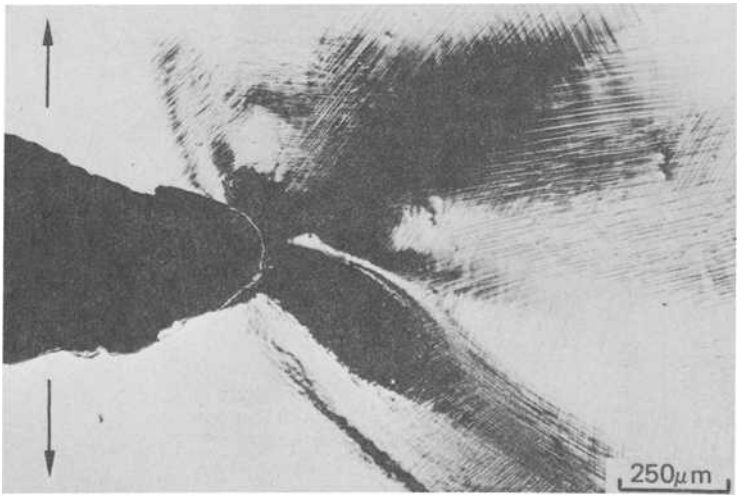

FIG. 20—*Optical micrograph showing same specimen as in Fig. 13*a *after removing the liquid-alloy environment, repolishing, and then increasing the COD in air.*

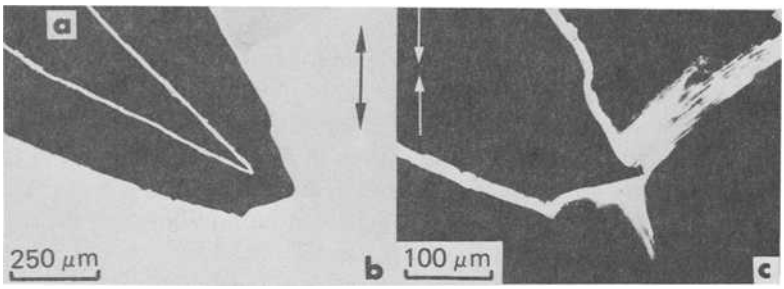

FIG. 21—*Optical micrographs showing crack tip profiles in ST aluminum-zinc-magnesium:* (a) *in the specimen interior after crack growth in the liquid-alloy environment,* (b) *as for* (a) *plus a crack-growth increment in air [specimen resectioned:* (a) *and* (b) *superimposed], and* (c) *as for* (b) *plus decreasing the COD (dark-field illumination).*

During unloading in air, slip occurred behind crack tips so that fracture surfaces produced during loading were partially deformed and crack tips were 'resharpened' (Fig. 21*c*).

For specimens in the *peak-hardness condition*, crack growth in the aqueous KI environment generally occurred parallel to {100} planes and in ⟨110⟩ directions, and 'brittle' striations and river lines were observed on fracture surfaces (Fig. 22). This behavior is remarkably similar to that of specimens tested in the liquid-alloy environment, although crack-growth increments, for a given COD (for PH specimens), were much smaller in the KI environment than in the liquid-alloy environment. In some cases, 'brittle' behavior was observed only in the center (plane strain) regions of specimens after fatigue in KI solutions. The effects of cyclic wave shape and frequency on fatigue in KI solution were also similar to those produced in the liquid-alloy environment; namely, there was no effect of hold time at

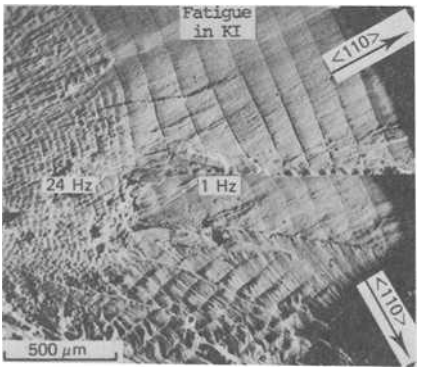

FIG. 22—*Scanning electron micrograph showing 'brittle' striations on {100} fracture surface produced by fatigue of PH aluminum-zinc-magnesium in the aqueous KI environment, first at 24 Hz, then at 1 Hz.*

peak load, and decreasing frequency increased rates of crack growth (Fig. 22). Slip distributions associated with crack growth in KI solution in the interior of specimens and on the specimen sides (when crack fronts were not greatly influenced by the specimen sides) (Fig. 23) were similar to those observed after crack growth in the liquid-alloy environment. Specimens partially fatigued in KI solution and then in an inert (dodecanol) environment at the same stress (Fig. 24) showed the same changes from 'brittle' to 'ductile' behavior as specimens fatigued in liquid alloy and then in air (see previous paragraph and Fig. 18). 'Ductile' behavior was also observed

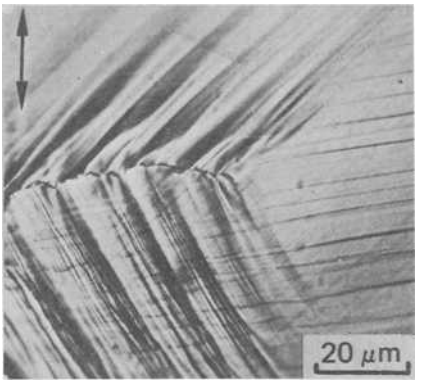

FIG. 23—*Optical micrograph showing slip distribution on the side surface of a PH specimen associated with fatigue crack growth in KI solution at 1 Hz.*

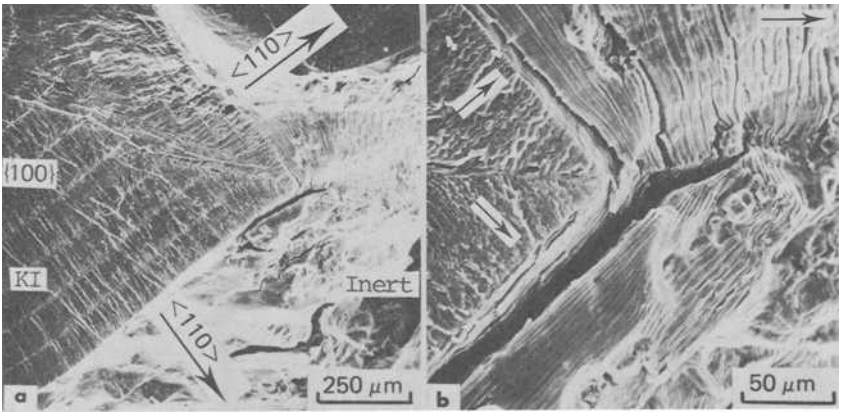

FIG. 24—*Scanning electron micrographs showing fracture surface in PH specimen produced first by fatigue in KI solution at 1 Hz, then by fatigue in an inert (dodecanol) environment at the same stress and frequency. Transition region in* (a) *is shown at a higher magnification in* (b).

for specimens which had been cathodically charged and then fatigued in dodecanol.

Specimens, in the peak-hardness condition, fatigued in moist air at *1 Hz* often produced 'brittle' striations on {100} fracture surfaces; however, rates of crack growth, for a given COD, were smaller than those produced by fatigue in KI solution. Crack growth in moist-air environments at *24 Hz* generally produced 'ductile' striations on fracture surfaces macroscopically normal to the specimen axis.

Comparison of the crack-growth characteristics of ST specimens with PH specimens in the *inert (dodecanol) environment* showed that, for a given COD, crack-growth increments were larger (about double) for ST specimens than for PH specimens (Fig. 25). Changes in cyclic frequency had only a very minor influence on crack growth in inert environments.

Discussion: Influence of Environment on Stage II Crack Growth

Liquid-Metal/Solid-Metal Interaction

For most cases of liquid-metal embrittlement (LME), including the liquid-alloy/aluminum-zinc-magnesium single crystals used in the present work, the mutual solubilities of solid and liquid metals are very small and, if suitably stressed specimens are 'wetted' with an embrittling liquid metal,

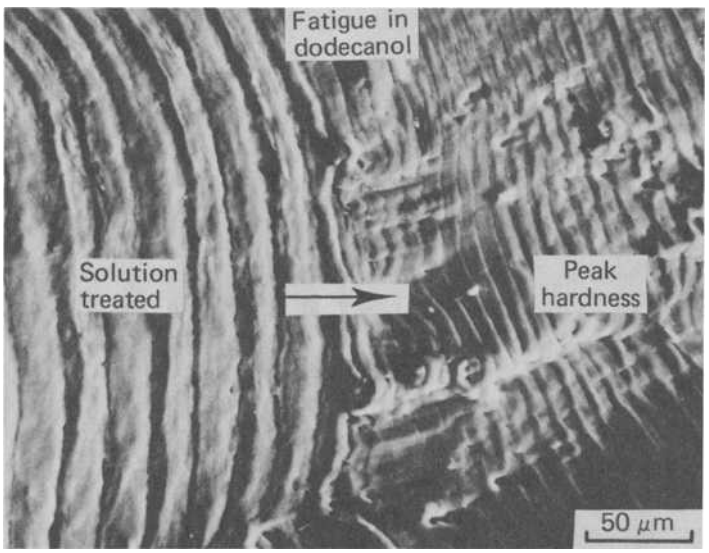

FIG. 25—*Scanning electron micrograph showing striations on fracture surface produced by fatigue in aluminum-zinc-magnesium specimens in the inert (dodecanol) environment at 1 Hz, first in the ST condition, then in the PH condition.*

rates of crack growth are extremely rapid ($\sim$100 mm/s). Thus, LME can generally be attributed to chemisorption at crack tips since other reactions, such as dissolution of the solid or diffusion of metal atoms into the solid, do not have time to occur [*16*]. (Oxide-film formation or generation of hydrogen obviously cannot occur.) During fatigue of aluminum-zinc-magnesium in liquid alloy, slight diffusion of alloy atoms into the solid could occur since cracks do not advance during unloading. However, maintaining the liquid alloy in contact with stationary cracks, even for much longer times than would occur during fatigue, then removing the liquid alloy and subsequently cracking in inert environments, results in 'ductile' behavior (Fig. 17). In addition, varying hold times at peak load during fatigue in the liquid-alloy environment had no effect on rates of crack growth (Fig. 16). Thus, it is considered that the effects of the liquid-alloy environment on fatigue were the result of the synergistic interaction between increasing COD and *chemisorption* at crack tips. Chemisorption involves an interaction of the electrons of the surface atoms of the solid with those of the adsorbed species and affects only the surface lattice of the solid metal since the high concentration of mobile electrons in metals screens out any influence of adsorbed species beyond the first few atomic layers.

Crack Growth in Liquid-Metal Environments: Slip Versus 'Decohesion'

In the past, many workers (for example, Ref *16*) have assumed that chemisorption of liquid-metal atoms substantially lowered the tensile strength of interatomic bonds at crack tips (but did not affect the shear stress required to move dislocations) so that, even in 'normally' ductile materials, crack growth occurred by repeated adsorption and tensile separation ('decohesion') of bonds at crack tips. Fracture surfaces produced by 'decohesion' would generally be flat and there would generally be little slip activity around cracks; *areas* of local plasticity could occur, however, by plastic tearing of material unaffected by the environment between advancing lobes of the main crack. However, recently published work [*17-19*] and the present results show that considerable slip activity is observed in *all* areas along crack fronts and that fracture surfaces are *entirely* dimpled in many cases. Moreover, dimples produced by LME were much shallower, and more elongated than dimples produced by fracture in air or inert environments. An important observation in the present studies was the very strong tendency for crack growth in the liquid-alloy environment to occur in $\langle 110 \rangle$ slip directions (on $\{100\}$ planes), even when the external conditions did not favor it (Figs. 10,11).

These metallographic and fractographic observations are not consistent with crack growth by 'decohesion' (nor with combinations of 'decohesion' and slip), but can be explained on the basis that crack growth occurs

primarily by *alternate slip* on {111} planes intersecting crack tips. In addition, the general dislocation activity around crack tips accompanying this alternate-slip process, and the number of void nuclei ahead of cracks, is sufficient for crack tips to blunt to some extent and for voids to form ahead of cracks; cracks and voids coalesce and, hence, fracture surfaces are microscopically dimpled (Fig. 26). Voids may be extremely small and, hence, fracture-surface dimples may be difficult to detect in some cases. Voids are usually initiated by second-phase particles although other sites such as dislocation cell walls have also been suggested [*20*]. The formation of voids ahead of cracks and blunting at crack tips enable crack growth to occur primarily by alternate slip without general yielding; if crack growth occurred solely by nucleation and movement of dislocations from crack

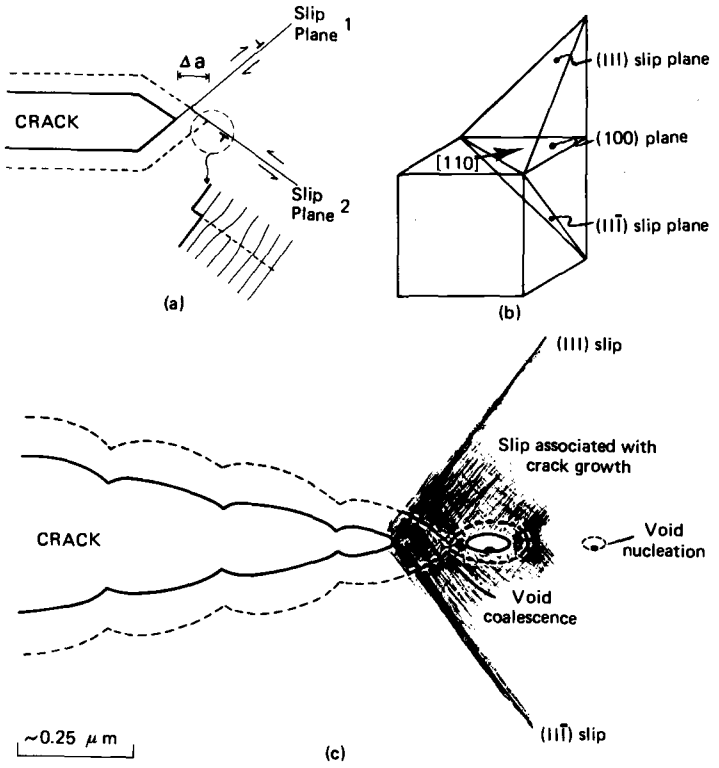

FIG. 26—*Schematic diagram illustrating* (a) *crack growth by alternate shear* [*crack-growth increment,* Δa, *is produced by slip on Plane 1 followed by slip on Plane 2*]; (b) *orientations of crystallographic planes and directions in face-centered-cubic material, showing that alternate slip on* {*111*} *planes produces crack growth in* ⟨*110*⟩ *directions; and* (c) *general slip, in addition to alternate slip, producing nucleation and growth of voids ahead of crack (full line). Dotted line shows position of crack after an increment of crack growth.*

tips, then, under monotonic tensile loading,[3] repulsion between those dislocations would eventually lead to general yielding and fracture by macroscopic shear [*21*]. Thus, the alternate-slip/microvoid-coalescence process described in the foregoing accounts for crack growth (under monotonic and cyclic loading) in ⟨110⟩ directions with the formation of dimpled fracture surfaces macroscopically parallel to {100} planes.

Influence of Chemisorption on Slip

In liquid-metal environments, crack growth produced {100} fracture surfaces for all testing conditions (for example, all crystal orientations). In inert environments, {100} fracture surfaces have been observed [*11,22*] but only after fatigue under certain conditions (for example, specific crystal orientations); an alternate-slip mechanism was proposed to explain these cases. Usually, crack growth in inert environments occurs by a more general plastic-flow process than alternate slip such that fracture surfaces are approximately normal to the tensile-stress axis and crack-growth directions are determined by the distribution of stress rather than by crystallography. Thus, it appears that liquid-metal environments (chemisorption) promote the alternate-slip process at the expense of general slip. Such an effect can be explained on the basis that *chemisorption facilitates the nucleation of dislocations from crack tips.*

An effect of chemisorption on dislocation nucleation at surfaces would be expected on theoretical grounds. Atoms at clean surfaces have fewer neighbors than atoms in the interior and hence the lattice spacings in the first few atomic layers often differ, probably by about ± 5 percent [*23*], from those in the interior. Such 'surface-lattice distortion' could hinder the nucleation and egress of dislocations at surfaces (and movement of screw dislocations intersecting surfaces), since dislocations moving in the first few atomic layers would be associated with larger-than-normal lattice distortions. Chemisorption effectively increases the number of neighbors around surface atoms and could reduce the 'surface-lattice distortion' (or shear strength of surface bonds) and facilitate dislocation activity at surfaces. Crack growth should mainly occur by nucleation (and subsequent movement) of dislocations from surface sources at crack tips since near-surface sources would probably not generally be present on slip planes intersecting crack tips.

'Ductile' Versus 'Brittle' Behavior

Easier nucleation of dislocations at crack tips would enable crack growth

[3]Under cyclic loading, crack growth could occur by alternate slip alone and produce {100} fracture surfaces since unloading resharpens the crack tip on each cycle [*11*].

to occur at lower stresses and with less blunting at crack tips. Extensive blunting at tips of cracks, in specimens below general yield, requires a general strain in the plastic zone ahead of cracks and, hence, generally necessitates extensive slip on at least five independent systems which freely interpenetrate and cross-slip; crack growth by alternate slip requires only the operation of two slip systems which intersect crack tips. The balance between crack growth and crack-tip blunting (both relax elastic strain energy around cracks) should therefore be determined by the relative proportion of slip on planes intersecting crack tips compared with 'general' slip around cracks. Chemisorption facilitates slip only on planes intersecting crack tips[4] and, hence, promotes crack growth. Thus, for a given COD, crack-growth increments in liquid-metal environments are larger, strains ahead of crack tips and plastic zones are smaller, and blunting at crack tips is less, than in inert environments. Since crack growth in liquid-metal environments probably predominantly occurs by nucleation (and subsequent movement) of dislocations from crack tips, any tendency for slip planes on one side of the crack tip to become more active than those on the other side (for example, when cracks are inclined to the tensile-stress axis and slip planes are unequally stressed) will be counteracted by a larger back stress from dislocations already present on the more active planes. Thus, slip generally alternates from one slip plane to the other so that fracture occurs macroscopically parallel to {100} planes in ⟨110⟩ directions.

In inert environments, the 'surface-lattice distortion' hinders nucleation and egress of dislocations at crack tips and favors the development of large strains ahead of cracks; nevertheless, crack growth still occurs by nucleation and egress of dislocations at crack tips, though probably in rather a chaotic fashion. Many more near-surface dislocation sources on slip planes intersecting crack tips are probably activated (since 'general' strains are larger and crack tips blunter) in inert environments than in liquid-metal environments. Thus, crack growth in inert environments probably occurs to a large extent by *egress* of dislocations at crack tips, while in liquid-metal environments cracks probably grow predominantly by *nucleation* (and movement) of dislocations from crack tips. Crack growth in inert environments, therefore, is not influenced by interactions between dislocations to the same degree as fracture in liquid-metal environments, and occurs normal to the tensile-stress axis to achieve maximum reduction in elastic strain energy for a given COD.

The more 'brittle' behavior of higher-strength materials can probably be explained by considerations of the balance between slip on planes inter-

[4] Chemisorption influences only the surface atoms and hence the stress required to move dislocations on slip planes not intersecting crack tips is unaffected; thus, the *bulk* flow characteristics of metals are the same in the liquid-metal environments as in inert environments.

secting crack tips and 'general' slip around crack tips. Obstacles to dislocation motion, for example, precipitates, are likely to restrict the extent of 'general' slip to a greater extent than slip intersecting crack tips since only the former require slip 'flexibility' (for example cross-slip) in order to produce a general strain in a small volume of material around crack tips. Such an effect would be consistent with observations that, in liquid-metal environments, increments of crack growth for a given COD were larger for PH specimens than for ST specimens.

Mechanisms of Crack Growth in Aqueous and Moist-Air Environments

Observations that aqueous, moist-air, and liquid-metal environments all promote 'brittle' crack growth along {100} planes in ⟨110⟩ directions, and other common effects of aqueous and liquid-metal environments on crack growth (see experimental section) suggest that the action of the environment could be the same in all these environments. On theoretical grounds, there is no reason why chemisorption of species other than liquid-metal atoms (for example, water molecules, iodide ions, or hydrogen atoms[5]) could not reduce the 'surface-lattice distortion' and facilitate nucleation of dislocations at crack tips. Such an effect would explain the experimental observations whereas theories based on other material-environment interactions are unsatisfactory. Oxide-film formation, dissolution, and generation of hydrogen at crack tips in aqueous media are not likely to promote 'brittle' crack growth in ⟨110⟩ directions along {100} planes. Oxide films form at crack tips in dry air but 'embrittlement' is not observed. The 'embrittlement' observed in moist air (which produces similar effects to aqueous media) cannot be explained by dissolution since, in moist air, there is not a liquid electrolyte at crack tips. Moreover, fracture surfaces did not show any signs that significant dissolution had occurred in aqueous media. Explanations for the present results based on 'hydrogen-embrittlement' seem unlikely because (1) hydrogen gas does not enhance fatigue-crack growth in aluminium alloys [*25*] (hydrogen probably does not chemisorb on aluminium [*26*]); (2) rates of hydrogen diffusion in aluminium alloys [*27*] are many orders of magnitude slower than would be necessary for hydrogen to accumulate ahead of cracks growing rapidly ($\sim$ mm/s) (rapid hydrogen transport by dislocations could possibly occur but would probably not concentrate hydrogen along {100} planes ahead of cracks); and (3) in any case, specimens cathodically charged with hydrogen prior to testing (in dodecanol) were not 'embrittled.' On the other hand, chemisorption of water molecules, which occurs prior to hydrogen generation, could explain the present results simply on the basis that chemisorption

[5] Observations of iron-alloy surfaces in the presence of hydrogen, using field-ion microscopy, do suggest that chemisorption of hydrogen activates nucleation of dislocations [*24*].

facilitates nucleation of dislocations at crack tips. Similarities between LME and environmentally induced crack growth in other cases, for example, intercrystalline stress-corrosion cracking and LME in aluminum-zinc-magnesium polycrystals [*17*] and cracking in high-strength steels in liquid-metal and hydrogen environments [*18*], suggest that a mechanism of environmentally assisted crack growth based on chemisorption at crack tips may be widely applicable, although dissolution, oxide-film formation, and effects of hydrogen diffusion ahead of cracks are obviously important in some circumstances.

Chemisorbed species which produce the largest reductions in 'surface-lattice distortion' and, hence, most facilitate the nucleation of dislocations at crack tips, should have the greatest effects on crack growth. The factors determining such effects are not well understood, although it is not surprising that liquid-metal environments (where both substrate and adsorbed atoms are metals) generally produce greater 'embrittlement' than aqueous environments. The difference in 'potency' between liquid-metal and aqueous environments would explain why low-strength materials (for example, ST aluminum-zinc-magnesium) are unaffected by aqueous environments but are embrittled by liquid-metal environments. For soft materials, 'general' slip around crack tips (and crack-tip blunting) predominates unless the stress required for dislocation nucleation at crack tips is reduced substantially; generally only liquid-metal environments are sufficiently 'potent' to produce a substantial reduction. For high-strength materials (for example, PH aluminum-zinc-magnesium), blunting at crack tips is already limited by microstructural factors, and aqueous as well as liquid-metal environments can produce embrittlement. Environmental effects tend to be greater at lower stresses, and also under plane-strain conditions, since the proportion of 'general' slip to alternate-slip at crack tips is probably decreased in these circumstances.

Effects of Cyclic Frequency

The effect of cyclic frequency and wave form on fatigue crack growth can be explained on the basis that the effectiveness of the environment in promoting crack growth depends on the surface (crack tip) coverage by adsorbed species during crack growth. Slower rates of loading should generally allow increased surface coverage by adsorbed species and should promote crack growth by alternate slip since longer dislocation sources, which probably require lower activation stresses, should then be nucleated at crack tips. The life of adsorbates on surfaces before reactions (such as dissolution, oxide-film formation, and desorption) should influence surface coverage at a particular instant and, hence, determine the effect of environment on crack growth. In aqueous environments, once oxide films have formed at crack tips, chemisorption on the metal surface cannot

occur and fracture of the oxide may be necessary before crack growth promoted by chemisorption recurs. Such considerations could explain the influence of temperature, applied potential [*14,28*], and the presence of inhibitors or halide ions [*28*] on crack growth since these factors will affect repassivation rates.

Formation of Fatigue Striations

In liquid-metal environments, the mechanism of formation of 'brittle' striations on fracture surfaces is readily deduced since crack fronts were not generally perturbed by the specimen sides and slip markings on the specimen sides correlated with striations on the fracture surface. In addition, the slip distribution on the specimen sides was fairly representative of the slip distribution in the interior (Fig. 12). It is clear from these observations that striations occur because unloading deforms *part* of the fracture surface produced during the previous loading excursion. Slip during unloading generally concentrates just behind the crack tip with less deformation farther from the crack tip (Fig. 27*a*). Thus, the 'second side' of striations shows a high density of slip markings or a rumpled appearance.

In inert environments, observations of crack-tip profiles at different stages of the stress cycle (Fig. 21) showed that 'ductile' striations were produced in a similar manner to 'brittle' striations. The difference in spacing and profile of the two types of striation arises because extents of blunting during loading differ (as already discussed); the blunter crack tip-profile produced in inert environments concentrates slip just behind the crack tip to greater extents during unloading (Fig. 27*b*). The detailed appearance of striations will depend on a variety of other factors, for example, ratio of loading to unloading amplitudes, orientation of the fracture surfaces to the stress axis (striation appearance often differs on opposing fracture surfaces since deformation during unloading occurs preferentially on one side of the crack), orientation of slip planes with respect to the crack, and ease of dislocation egress at fracture surfaces. The last factor will depend on the environment and could explain why well-defined striations are sometimes not observed after fatigue in vacuum; here, crack-growth increments are smaller than in other environments, and dislocation egress as fracture surfaces during unloading will not be impeded by oxide films, so that *all* the fracture surface produced during loading could be deformed on unloading.

Relationship between Crack Growth and Crack-Opening Displacement

The results of the present work suggest that increments of crack growth per cycle, Δa, depend primarily on crack-tip-opening displacements (in

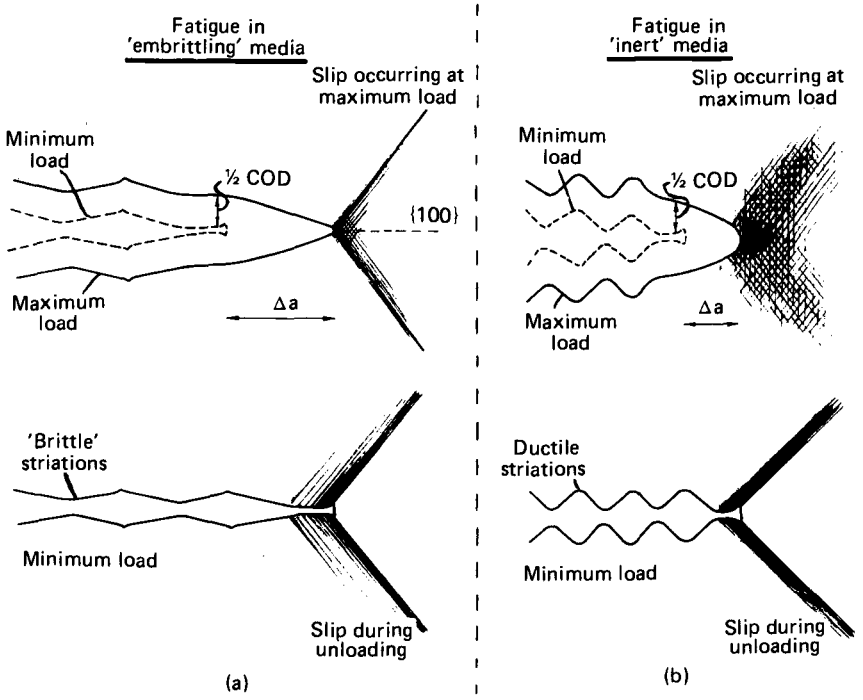

FIG. 27—*Schematic diagrams illustrating mechanisms of Stage II fatigue-crack growth and formation of striations for* (a) *'embrittling' environments and* (b) *inert environments. Nucleation and growth of microvoids (not shown) in the highly strained (shaded) areas occur during loading in many cases.*

the plastic range), Δ COD_{eff}, and the extent of blunting at crack tips, B. Thus, $\Delta a \propto COD_{eff}/B$. Easier nucleation of dislocations at crack tips (for example, produced by greater effects of chemisorption) should decrease B and increase ΔCOD_{eff}; thus, Δa is increased on both counts. Increasing strength should decrease B and decrease ΔCOD_{eff}; thus, these factors now have a conflicting effect on Δa. In inert environments, increasing strength (from ST to PH conditions in aluminum-zinc-magnesium) decreased Δa (Fig. 25), suggesting that the effect of increasing strength on decreasing ΔCOD_{eff} was dominant. In 'aggressive' environments, however, increasing strength greatly increased Δa, suggesting that the effect of increasing strength on decreasing B was now dominant, possibly because there is a synergistic interaction between 'aggressive' environments and high strength in decreasing B. Tests on single crystals under a wider range of conditions and with more emphasis on quantitative data than in the present work should lead to further understanding of environmentally assisted fatigue. Additional information on surface chemistry is also required.

Summary

The model proposed for Stage II crack growth in the present paper basically involves (1) crack growth by plastic-blunting/alternate-shear processes at crack tips during loading, and (2) 'resharpening' of the crack tip during unloading by slip behind crack tips (Fig. 27). The present model agrees to a large extent with plastic-blunting/alternate-slip mechanisms proposed previously by others [*11,13,14*] (but disagrees with models based on 'fracture-deformation' sequences [*12*]) and, additionally, proposes that the effect of environment on crack growth can be explained in many cases on the basis that chemisorption facilitates nucleation of dislocations at crack tips.

References

[*1*] Grosskreutz, J. C., *Physica Status Solidi (b)*, Vol. 47, 1971, pp. 11-31 and pp. 359-396.
[*2*] Plumbridge, W. J. and Ryder, D. A., *Metallurgical Reviews*, No. 136, 1969, pp. 119-142.
[*3*] Laird, C. and Duquette, D. J. in *Corrosion Fatigue: Chemistry, Mechanics, and Microstructure*, O. F. Devereux, A. J. McEvily, and R. W. Staehle, Eds., National Association of Corrosion Engineers, 1971, pp. 88-115.
[*4*] Finney, J. M., and Laird, C., *Philosophical Magazine*, Vol. 31, 1975, pp. 339-365.
[*5*] Forsyth, P. J. E., *Acta Metallurgica*, Vol. 11, 1963, pp. 703-715.
[*6*] Lynch, S. P., *Metal Science Journal*, Vol. 9, 1975, pp. 401-410.
[*7*] Wilson, D. V. and Tromans, J. K., *Acta Metallurgica*, Vol. 18, 1970, pp. 1197-1208.
[*8*] Cottrell, A. H., *Mechanical Properties of Matter*, Wiley, New York, 1964, p. 373.
[*9*] Plumbridge, W. J., *Journal of Materials Science*, Vol. 7, 1972, pp. 939-962.
[*10*] Garrett, G. G. and Knott, J. F., *Metallurgical Transactions*, Vol. 7a, 1976, pp. 884-887.
[*11*] Neumann, P., *Acta Metallurgica*, Vol. 22, 174, pp. 1155-1165.
[*12*] Wanhill, R. J. H., *Metallurgical Transactions*, Vol. 6a, 1975, pp. 1587-1596.
[*13*] Laird, C. in *Fatigue Crack Propagation, ASTM STP 415*, American Society for Testing and Materials, 1967, pp. 131-168.
[*14*] Pelloux, R. M. N., in *Fracture 1969, Proceedings*, Second International Conference on Fracture, Brighton, U. K., 1969, Chapman and Hall, New York, pp. 731-744.
[*15*] *Corrosion Fatigue: Chemistry, Mechanics, and Microstructure*, O. F. Devereux, A. J. McEvily, and R. W. Staehle, Eds., National Association of Corrosion Engineers, 1971.
[*16*] Kamdar, M. H., *Progress in Materials Science*, Vol. 15, 1973, pp. 289-374.
[*17*] Lynch, S. P. in *Mechanisms of Environment Sensitive Cracking of Materials*, P. R. Swann, F. P. Ford, and A. R. C. Westwood, Eds., The Metals Society, 1977, pp. 201-212.
[*18*] Lynch, S. P. and Ryan, N. E. in *Proceedings*, Second International Congress on Hydrogen in Metals, Paris, France, 1977, Pergamon Press, New York, Vol. 5, 3D12.
[*19*] Lynch, S. P. in *Fracture 1977, Proceedings*, Fourth International Congress on Fracture, Waterloo, Ont., Canada, D. M. R. Taplin, Ed., University of Waterloo Press, Vol. 2, 1977, pp. 859-866.
[*20*] Gardner, R. N., Pollock, T. C., and Wilsdorf, H. G. F., *Materials Science and Engineering*, Vol. 29, 1977, pp. 169-174.
[*21*] Cottrell, A. H. in *Proceedings*, First Tewksbury Symposium on Fracture, C. J. Osborn, Ed., University of Melbourne, Melbourne, Australia, 1965, pp. 1-27.
[*22*] Garrett, G. G. and Knott, J. F., *Acta Metallurgica*, Vol. 23, 1975, pp. 841-848.
[*23*] Latanision, R. M. in *Surface Effects in Crystal Plasticity*, R. M. Latanision and J. T. Fourie, Eds., North Atlantic Treaty Organization Advanced Study Institutes Series, Series E: Applied Science No. 17, Noordhoff International Publishing, Leyden, The Netherlands, 1977, pp. 3-47.
[*24*] Clum, J. A., *Scripta Metallurgica*, Vol. 9, 1975, pp. 51-58.

[25] Speidel, M. O. in *Hydrogen in Metals*, I. M. Bernstein and A. W. Thompson, Eds., American Society for Metals, 1974, pp. 249-273.
[26] Hayward, D. O. and Trapnell, B. M. W., *Chemisorption*, Butterworths, London, U. K., 1964.
[27] Tuck, C. D. S. and Scamans, G. M. in *Proceedings*, Second International Congress on Hydrogen in Metals, Paris, France, 1977, Pergamon Press, New York, Vol. 6, 4A11.
[28] Stoltz, R. E. and Pelloux, R. M., *Metallurgical Transactions*, Vol. 3, 1972, pp. 2433-2441.

DISCUSSION

C. Laird[1] (*discussion*)—Looking, then, at what Dr. Lynch has considered with respect to Stage II crack propagation, I find his views orthodox. He interprets the role of the environment as affecting the nature of the slip at the crack tip. Both environment and microstructure can act to control the fineness of the slip at the tip, rather in the sense suggested by Peter Neumann in his very carefully oriented single crystals cycled in bending, which produced sharp slipbands at the tip, thereby defining, through the geometry of the slip, the particular plane on which the cracks propagate and the particular directions in which they propagated.

And I am sympathetic with Dr. Lynch's position on chemisorption, which is similar to that adopted, say, by T. L. Johnston in his investigation of monotonic-type fracture under liquid metal environments, in planar slip materials. It is reasonable to expect that chemisorption acts to stimulate dislocation emission and to control the mode of slip in such environments and probably in aqueous environments as well. When the environment is less aggressive, then the slip, through work-hardening operations, ahead of the tip will tend to be more spread, and one will then observe ductile striations in Stage II propagation rather than the so-called brittle striations.

For the particular alloy of interest to Dr. Lynch, an interpretation of the morphological differences between ductile and brittle striations is more realistic in terms of slip differences than in terms of fracture *mechanism* differences, of the kinds once advanced, for example, by Ryder and Forsyth.

Dr. Lynch's paper contains a brief review of fatigue crack initiation, with special reference to one of his publications [6], and a report of a study of fatigue crack growth in aluminum alloys, as affected by a variety of inert and aggressive environments. The latter experiments are most

[1]Department of Metallurgical Engineering, University of Pennsylvania, Philadelphia, Pa. 19104.

interesting but the initiation review contains a number of points with which the discusser takes issue, as follows:

Initiation by Coarse Slip—Dr. Lynch believes that heavy reverse slip induces a notch-peak topography which progresses with cycles, and tends to be intensified at grain boundaries through slip inhomogeneity. He considers nucleation to have occurred after the first cycle on the grounds that the notches first established would act as stress concentrators. This view is at variance with the latest research on crack nucleation at high cyclic strains[2-4] Kim and Laird have shown that the slip bands within the grains act essentially reversibly within the available life and do not form cracks. At vulnerable grain boundaries, a step, which initially tends to be cancelled with reverse strain, is slowly established and serves as the crack nucleation site. The slip in the grain as a whole is shown to be important in this process. Limitations of space prevent more elaborate discussion here, but the details can be found in the references footnoted.

It would be extremely interesting to investigate crack nucleation mechanisms at high strains in single crystals.

Initiation Involving Intrusion and Extrusion—Dr. Lynch asserts that, in precipitation-hardened alloys, the formation of intrusions and extrusions corresponds to the resolution of precipitates and the formation of subgrains within slipbands. Of course there are many factors, such as precipitate disordering without resolution,[5,6] which can cause slip localization and hence intrusions and extrusions. Resolution and subgrains are not necessary; neither of these is observed in Al-4Cu alloy, nor indeed in many other systems.[7] The evidence for resolution is not unequivocal. In the papers used by Lynch to support this claim [*4,5*], there are TEM photographs of brightly contrasting regions in the slipbands. Calabrese and Laird also observed such effects (footnote 5), but when the specimens were tilted in the electron microscope it was found that the regions showing bright contrast did in fact contain precipitates, and the reason for the difference in contrast came about from the crystal of the slipband being slightly misoriented from the remainder of the grain. There is no evidence shown in the papers cited by the author on aluminum-zinc-magnesium that such

[2] Kim, W. H. and Laird, C., "Crack Nucleation and Stage I Propagation in High Strain Fatigue—I Microscopic and Interferometric Observations," *Acta Metallurgica,* in press.

[3] Kim, W. H. and Laird, C., "Crack Nucleation and Stage I Propagation in High Strain Fatigue—II Mechanism," *Acta Metallurgica,* in press.

[4] Kim, W. H. and Laird, C., "The Role of Cyclic Hardening in Crack Nucleation at High Strain Amplitude," *Materials Science and Engineering,* in press.

[5] Calabrese, C. and Laird, C., *Materials Science and Engineering,* Vol. 13, 1974, pp. 141-157.

[6] Fine, M. E. and Santner, J. S., *Scripta Metallurgica,* Vol. 9, 1975, pp. 1239-1241.

[7] Laird, C. in *Cyclic Stress-Strain and Plastic Deformation Aspects of Fatigue Crack Growth, ASTM STP 637,* American Society for Testing and Materials, 1977, pp. 3-35.

experiments were carried out. Hopefully he can reassure us on these matters. It is possible, of course, that the mode of stressing can give rise to different kinds of results because different accumulations of deformation occur before failure. Dr. Lynch, as well as Forsyth previously, used cyclic torsion, whereas Calabrese and Laird used tension-compression testing. Starke and his co-workers, who also used tension-compression testing (but in aluminum-zinc-magnesium based ternary alloys), observed tilted slipbands but no resolution (private communication, 1977).

In this connection, it would be valuable to carry out weak beam observations on the dislocation structures of slipbands in complex alloys. These structures are too dense and complex to be elucidated by conventional bright-and dark-field techniques.

Mechanisms of Intrusion and Extrusion—Dr. Lynch suggests that the characteristics of intrusion/extrusion in single-phase materials are similar to those in aluminum-zinc-magnesium and that the mechanisms are probably also similar. First, the literature is filled with many differences for these two types of material. Second, although the mechanisms of intrusion/extrusion behavior for model materials, such as eutectics (previously carried out by James[8]) or brass-tin composites [*6*], *may* apply to aluminum-zinc-magnesium, there seems no reason why the mechanism should apply to single-phase materials. We now know a considerable amount about persistent slipband behavior in copper single crystals (see Ref *4* of paper and Winter[9]); although extrusions are formed in this material, it is extremely difficult to reconcile the slip behavior with the "squeezed toothpaste" model supported by Lynch.

Dr. Lynch remarks that it is not understood why bands of small subgrains should be softer than adjacent regions where cells are large. Since this statement is made in the context of single-phase materials, he is presumably referring to persistent slipbands (PSB). His schematic Fig. 8, which shows the "ladder-like" dislocation structure of PSB's, also supports this assumption. One point to be clarified is that the dislocation walls in pure-metal PSB's are usually not subgrain walls, which imply crystalline misorientations, but are dipolar walls without misorientation. An attempt to answer Dr. Lynch's question (and a number of related questions) has recently been made,[10,11] but no details can be supplied in the space provided here.

Further, Dr. Lynch speculates on a connection between the mechanisms

[8] James, P., Ph.D. Thesis, University of Cambridge, Cambridge, U. K., 1961.

[9] Winter, A. T., *Philosophical Magazine,* Vol. 30, 1974, pp. 719-734.

[10] Kuhlmann-Wilsdorf, D. and Laird, C., *Materials Science and Engineering,* Vol. 27, 1977, pp. 137-156.

[11] Kuhlmann-Wilsdorf, D. and Laird, C., "Dislocation Behavior in Fatigue—II," submitted to *Materials Science and Engineering.*

of superplasticity and those of fatigue slipbands. The slip behavior of PSB's is now well established [see Ref *4* of paper and Winter (footnote 9 of this discussion)] and dislocation mechanisms which meet the observations quite well have been suggested (see footnote 10 of this discussion). There is no evidence supporting a connection with the mechanisms of superplasticity.

Stage I Crack Growth—Dr. Lynch cites striations observed on Stage I fracture surfaces and suggests, by analogy with Stage II striations, that compressive parts of the cycles close Stage I cracks by slip and thus deform their fracture faces. Since he does not reference these statements, it is not entirely clear which evidence he is citing. Presumably the statements relate to Fig. 7 of Ref *6*. In that figure, it is unfortunate that some Stage II striations are clearly evident adjacent to the Stage I face and with a size roughly equal to that of the striations claimed for Stage I. Since these striations are nearly 1 μm wide, they can hardly apply to the slow crack propagation rates normally associated with Stage I. Their regularity makes it unlikely that they could be formed by the mechanism for Stage I propagation described in Fig. 8, especially if the increments of crack growth associated with the striations occupied many cycles.

Quite aside from these considerations, there is another objection to the mechanism described in Fig. 8 . Figure 8*c* shows a Stage II type of striation mechanism; this clearly requires slip on systems other than that occupied by the PSB. However, the elegant TEM observations by Katagiri et al[12] clearly show large Stage I cracks present in PSB's without significant modification of their dislocation structures. If the model of Fig. 8*c* were to apply, the vein structures adjacent to the PSB would be seriously perturbed. But nothing of the sort was observed. Instead, cell structures were observed only when the crack was in transition from Stage I to Stage II.

Stage II Crack Growth—The discusser is broadly in sympathy with this part of the paper. He agrees with most statements regarding mechanisms of crack growth and striation formation, and also with the chemisorption interpretation of the environmental effect. In this connection, it might be interesting to explore the generation of dislocations at the crack tip in terms of environment-assisted reconstruction of the surface. For example, Rode[13] has suggested that expitaxial film growth occurs in association with surface dislocations nucleated at reconstructed steps. Reconstruction might occur at fracture surface steps, hence increasing the number of dislocations to advance the crack.

K. Takao[14] *(discussion)*—I have three questions or discussion points concerning this paper.

[12] Katagiri, K., Omura, A., Koyamagi, K., Awatani, J., Shiraishi, T., and Kaneshior, H., *Metallurgical Transactions,* Vol. 8A, 1977, pp. 1769-1773.

[13] Rode, D. L., *Physica Status Solidi,* Vol. A32, 1975, pp. 425-431.

[14] Saga University, Honjo-machi, Saga-shi, Saga-Ken, Japan.

1. On the proposed mechanism of intrusion/Stage I crack growth as illustrated in Fig. 8, I would like to ask the author's opinion on (1) the signs of arrayed edge dislocations described near the boundaries between the hard zone and the soft zone, and the driving force for making the array of dislocations; and (2) where the material, at first located in the soft zone near the surface, has gone after the intrusion has occurred, that is, whether the condition that the volume of the soft layer is constant is satisfied at the occurrence of intrusions.

2. As seen in Fig. 17, crack growth increments per cycle during fatigue are much smaller in air than in the liquid-metal environments (LME) even under the same stress amplitude. You explain the effect of LME on crack growth on the basis that chemisorption facilitates the nucleation of dislocations from crack tips. To add to this explanation, I think there is a difference in crack closure behavior under the two environments; that is, the effective COD (COD_{eff}) in LME is also larger than that in air under the same stress. Figure 17 shows that the spacing of a ductile striation just after the change in environment is larger than the subsequent normal spacings. This seems to indicate that the difference in crack closure behavior under the two environments may also be a factor controlling the growth of fatigue cracks, if chemisorption affects the surface lattice distortion in the first few atomic layers alone. Did you have any information concerning the difference in COD_{eff} between each environment?

3. Do you know the equations of fatigue crack growth in terms of the stress intensity range of the materials used in each environment?

P. Neumann[15] (*discussion*)—I have one question concerning the environmental control of crack propagation. Do you think that the nucleation of dislocations at the crack tip, as the only process which goes on there, is able to explain a crack tip angle which is smaller than the angle of the slip planes being activated?

Or do you think that in addition to this nucleation of dislocations, an additional kind of fracture process at the crack tip is necessary to explain the sharp crack tip?

R. Wei[16] (*discussion*)—Dr. Lynch has presented a very interesting paper. I would like to offer one comment and ask two related questions. My comment is that fractography is only one of the available tools for studying fatigue; and one must exercise caution in drawing conclusions based soley on fractographic data. My questions concern the mechanism for environment enhancement of fatigue crack growth. You draw the conclusion that, because liquid metal embrittlement may be attributed to a stress sorption

[15] Max-Planck-Institut fur Eisenforschung Gmbh, Dusseldorf, Germany.
[16] Department of Mechanical Engineering, Lehigh University, Bethlehem, Pa. 18015

type of mechanism, such an adsorption mechanism is also responsible for fatigue crack growth in aqueous environments. Do you have additional support for this conclusion? If "adsorption" is indeed the responsible mechanism (which would suggest the absence of time effects), can you explain the observed effect of frequency on fatigue crack growth?

I. LeMay[17] (*discussion*)—You have shown that changing from a liquid-metal environment into air produces a change from crack growth on a {100} plane inclined to the tensile axis to crack growth on a plane approximately normal to the tensile axis. Does this effect reverse? In other words, in changing from air back into liquid metal, does the crack revert to a {100} plane inclined to the tensile axis?

B. Tomkins[18] (*discussion*)—The paper seems to present a confused picture with regard to flow patterns observed during propagation in liquid metal and air (Fig. 19. As there is a clear change of growth direction from a predominantly shear direction (30 to 40 deg to the loading axis) to a direction normal to the load, one would not expect a similar extent of flow from mechanics considerations alone. In the shear case, flow would be concentrated ahead of the crack rather than to the sides for plane strain growth, when plastic zone extent is less than specimen thickness. There is some indication in Fig. 19 that such flow patterns have been present. So, the observed flow pattern variations may be more a result of crack orientation than environment.

W. Plumbridge[19] (*discussion*)—You have elegantly demonstrated the effects of liquid environments on crack growth and fracture surface topography. There is some evidence to suggest that entrapped liquids may exert a purely mechanical influence on fatigue crack growth and that the size of this effect is a function of liquid viscosity. Have you considered in your work the possibility of liquid wedging in the cracks?

S. P. Lynch (*author's closure*)—I appreciate Prof. Laird's interest in this work and am pleased that he agrees with the main part of the paper regarding the influence of environment on Stage II crack growth. However, I am puzzled by his comment that the proposed explanation for environmentally assisted fatigue (based on an effect of chemisorption on dislocation nucleation) is an orthodox one; there has not been general agreement with respect to such mechanisms in the past and the explanation proposed in this paper is considered to be a relatively new one. There is an important

[17] Department of Mechanical Engineering, University of Saskatchewan, Saskatoon, Canada.
[18] Reactor Fuel Element Laboratories, UKAEA (Northern Division), Springfields, Salwick, Preston, Lancs, U. K.
[19] Department of Mechanical Engineering, University of Bristol, Bristol, U. K.

difference between previous theories of LME (which were based on tensile separation of interatomic bonds) and the present theory. A common mechanism for LME and other cases of environmentally assisted cracking (for example, SCC) has been suggested previously[20] but has been discounted in the past because it was thought (incorrectly) that crack growth in liquid-metal environments was an absolutely brittle process;[21] the present results suggest that a common mechanism is quite probable in many cases.

It should be emphasized that environment and microstructure can affect crack growth via an influence on the *distribution* of slip (that is, on the extent of slip on planes intersecting crack tips versus 'general' slip ahead of cracks) rather than the 'fineness' of slip mentioned by Prof. Laird. In the work of Johnston et al[22,23] (presumably), also mentioned by Prof. Laird, the importance of slip character on fracture behavior is discussed in terms of its effect on the stress concentrations, developed at dislocation pileups, necessary to initiate a brittle crack; the considerations in the present paper are quite different.

Prof. Laird raises several issues, discussed in the following, in connection with fatigue-crack initiation and Stage I crack growth.

Initiation by Coarse Slip—The references cited by Prof. Laird are "in press" and, hence, it is not clear whether the disagreement is real or a question of semantics regarding the definition of a crack. Certainly steps (cracks?) formed at grain boundaries on the first half-cycle are unlikely to be exactly reversed during the second half of the cycle, particularly if oxide films form on slip steps.

Initiation Involving Intrusion and Extrusion—I agree that there are other factors beside re-solution of precipitates which can produce softening along slipbands and lead to intrusions and extrusions. In age-hardened aluminum-zinc-magnesium, TEM observations, before and after high-strain torsion fatigue, clearly show that re-solution of precipitates can occur during fatigue. Precipitates in aluminum-zinc-magnesium aged to around peak hardness, *unlike* those in the early stages of aging in aluminum-copper studied by Calabrese and Laird (footnote 5 of Dr. Laird's discussion), are visible under most viewing conditions so that re-solution in

[20] Nichols, H. and Rostoker, W., *Transactions*, American Society for Metals Vol. 56, 1963, pp. 494-507.

[21] *The Theory of Stress-Corrosion Cracking in Alloys*, J. C. Scully, Ed., NATO, published by the North Atlantic Treaty Organization, Brussels, 1971.

[22] Johnston, T. L., Davies, R. G., and Stoloff, N. S., *Philosophical Magazine*, Vol. 12, 1965, pp. 305-317.

[23] Stoloff, N. S., Davies, R. G., and Johnston, T. L. in *Environment-Sensitive Mechanical Behavior*, A. R. C. Westwood and N. S. Stoloff, Eds., Metallurgical Society Conferences, Vol. 35, 1965, pp. 613-655.

aluminum-zinc-magnesium is readily observed. Notwithstanding, foils were tilted during examination by both the present author and previous workers.[24] Mode of stressing and heat-treatment conditions do influence the re-solution phenomenon. In aluminum-zinc-magnesium alloys, re-solution of precipitates within slipbands occurs particularly when specimens are (1) tested in high-strain torsion fatigue (here the low normal-stress to shear-stress ratio promotes extensive dislocation activity within slipbands prior to crack initiation); and (2) heat-treated, prior to fatigue, to give, first, coherent or semicoherent precipitates, second, narrow PFZ at grain boundaries (if PFZ are wide, strain localization occurs mainly at grain boundaries rather than in slipbands), and third, 'quench' bands which contain a slightly lower density of precipitates than adjacent regions (if quench deformation is severe, slip bands may be free of precipitates prior to fatigue).

Mechanisms of Intrusion and Extrusion—In connection with intrusions and extrusions, Prof. Laird comments that the literature is filled with many differences in behavior between age-hardened and single-phase materials. Laird and Duquette [*3*] have stated previously that "Initially it was felt that extrusions were confined to age-hardened materials. Subsequently, however, extrusions were found to occur in almost every material examined. . . . " Both statements are probably true although there is a problem in that there is not a general consensus regarding what constitutes an extrusion. I have classified only the topography in Fig. 3*b* as an extrusion; others have sometimes included the topography shown in Fig. 3*c* as well. (Figure 3 was included in the revised paper in response to Prof. Laird's comments.) Extrusions similar to those in age-hardened materials *have* been observed in some cases in single-phase materials, for example, cold-rolled aluminium,[25] copper,[26] and magnesium;[27] it seems reasonable to suggest that a similar phenomenon occurs by a similar mechanism. It would be interesting to examine PSB beneath well-defined extrusions in single-phase materials in this connection. In single-phase materials where crack initiation is *not* associated with well-defined extrusions and intrusions, I agree that slip processes (and PSB structures) are probably different than in age-hardened materials.

Stage I Crack Growth—Striations on Stage I fracture surfaces have been observed for several materials (reported in reviews [*1,2*] cited at the start of this section of the paper). A micrograph showing striations on a Stage I fracture surface in aluminum-zinc-magnesium has been included in the

[24] Stubbington, C. A., Royal Aircraft Establishment Report CPM 9, Jan. 1964.
[25] Forsyth, P. J. E. and Stubbington, C. A., *Nature*, Vol. 175, 1955, pp. 767-768.
[26] Dover, W. D. and Jones, W. J. D., *British Journal of Applied Physics*, Vol. 18, 1967, pp. 1257-1260.
[27] Partridge, P. G., *Acta Metallurgica*, Vol. 13, 1965, pp. 517-525.

revised paper (Fig. 7). In this case, crack-growth increments per cycle (striation spacings) are quite large because specimens were tested in high-strain torsion fatigue. Microstructural softening occurs along slipbands ahead of such cracks, and a mechanism of crack growth involving preferential plastic deformation within the slipbands (Fig. 8) seems quite probable. Further work is, of course, required to determine the applicability of this model to other cases of Stage I crack growth.

K. Takao—Responding to Dr. Takao's questions in order:

1. Figure 8 is meant only to be schematic and to indicate that the process of shear at the interfaces between hard and soft zones during intrusion is important; the precise dislocation movements at the interfaces are probably quite complex. As to the second part of this question, the volume of the soft zone should be the same after extrusion or intrusion; thus, the width of the soft zone should increase during intrusion and decrease during extrusion, as was observed in the model specimens.

2. The spacings of 'ductile' striations, after a change from an 'embrittling' to an 'inert' environment, were generally fairly constant although, when crack fronts in the 'embrittling' environment had a zigzag shape, there was then a tendency for parts of the crack front 'lagging behind' to advance preferentially in the inert environment so that crack fronts became straighter. (The first few ductile striations in Fig. 17 are difficult to distinguish when the micrograph is printed to give good overall contrast.) Crack closure is probably not an important factor for the present results since damage to fracture surfaces, which would occur on closure, was generally not observed. However, I agree that, since the environment can influence the extent of plasticity associated with crack growth, crack-closure behavior could be affected by environment in some cases.

3. Equations relating rates of crack growth to the stress-intensity range were not determined.

P. Neumann—Some general slip, producing nucleation and growth of voids, ahead of crack tips usually occurs in addition to alternate slip (nucleation of dislocations) at crack tips (Fig. 26*c*). Crack growth can then occur well below general yield and crack-tip angles can be quite small on a macroscopic scale; on a microscopic scale crack tips are usually fairly blunt. I do not think that an absolutely brittle fracture process (decohesion) occurs in conjunction with alternate slip.

R. Wei—Fractographic and metallographic studies show how environment influences rates of crack growth, the extent and nature of slip processes associated with crack growth, as well as fracture-surface characteristics. I think these factors are probably the most important ones to consider in explaining environmentally assisted fatigue although I agree that infor-

mation regarding surface chemistry is also required. The conclusion that an effect of chemisorption was responsible for facilitating crack growth in aqueous environments was based on the many similarities between fatigue in liquid-metal environments (only chemisorption can occur) and fatigue in aqueous media; for example, both environments promote 'brittle' crack growth in ⟨110⟩ directions on {100} planes (a very specific effect). Decreasing frequency *does* increase rates of crack growth in both environments. Moreover, other possible mechanisms for the effect of aqueous environments cannot explain the experimental observations, as discussed in the paper.

I. LeMay—Yes, the effect reverses; changing from 'inert' to 'embrittling' environments produces a change from ductile to brittle behavior. Of course, when {100} planes are normal to the stress axis, there is not a marked change in fracture *plane* on changing from a liquid-metal environment to air.

B. Tomkins—Dr. Tomkins raises an important point regarding a possible effect of crack orientation on slip patterns. Deformation associated with crack growth was studied in crystals of several orientations; for cracks growing along {100} planes in liquid-metal environments, there was little difference (perhaps surprisingly) in slip patterns at crack tips between cracks which were normal to the stress axis and cracks which were inclined (up to 45 deg) to the stress axis (Fig. 12*a* and Fig. 28 of this closure, re-

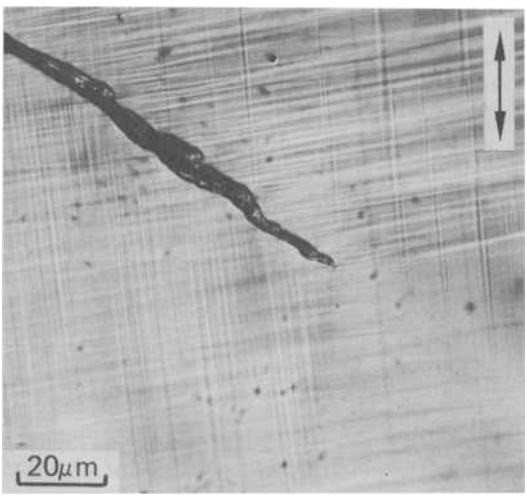

FIG. 28—*Optical micrograph showing slip distribution associated with fatigue-crack growth in the liquid-alloy environment at 1 Hz in ST specimen, when crack is inclined to the stress-axis. The slip pattern is similar to that around cracks normal to the stress axis (Fig. 12a).*

spectively). In both cases, slip occurred mainly on {111} planes intersecting crack tips with little slip directly ahead of cracks. Regardless of crack orientations, the extent of slip ahead of crack tips and plastic-zone sizes are much greater in 'inert' environments than in 'embrittling' environments (Figs. 13*a*, 19, and 20). (In Fig. 19, the flow *pattern* associated with fatigue in the liquid-alloy environment has been obscured by the deformation subsequently occurring in air.) Thus, for the present results, it is the environment (chemisorption), *not* crack orientation, which influences the distribution of slip around crack tips.

W. Plumbridge—In the present work, rates of crack growth are *increased* in liquid-metal and aqueous environments compared with gaseous environments. 'Liquid wedging' of cracks, which can apparently lead to small *decreases* in rates of crack growth in liquids compared with gases in some cases,[28] is therefore not applicable to explanations of environmentally assisted fatigue discussed in the present paper.

[28] Plumbridge, W. J., *Materials Science and Engineering,* Vol. 27, 1977, pp. 197-208.

M. Wilhelm,[1] *M. Nageswararao,*[1,2] *and R. Meyer*[3,4]

Factors Influencing Stage I Crack Propagation in Age-Hardened Alloys

REFERENCE: Wilhelm, M., Nageswararao, M., and Meyer, R., **"Factors Influencing Stage I Fatigue Crack Propagation in Age-Hardened Alloys,"** *Fatigue Mechanisms,* Proceedings of an ASTM-NBS-NSF symposium, Kansas City, Mo., May 1978, J. T. Fong, Ed. *ASTM STP 675.* American Society for Testing and Materials, 1979, pp. 214-233.

ABSTRACT: This paper reviews some recent experimental results on age-hardened Al-5Zn-1Mg, Al-4Cu, and Cu-2Co alloy single crystals. Experiments were performed with unnotched specimens to study their cyclic deformation behavior and with notched specimens to investigate the crack propagation in Stage I. Since at present no quantitative statement of the formation of persistent slipbands in age-hardened alloys is available, we choose to represent this important microscopic activity indirectly in terms of the amount of cyclic hardening. It is shown that lowering the test temperature and, in the aluminum alloys, changing the type of alloy additions from zinc plus magnesium to copper have qualitatively the same influence of impeding the formation of persistent slipbands and of homogenizing their distribution. The crack propagation experiments show that the same factors decrease the velocity of and the tendency to crack propagation in Stage I. In the Al-5Zn-1Mg alloy the presence of water vapor in the environmental atmosphere, which increases the Stage I crack propagation velocity at 50 Hz, was found to prevent crack propagation in Stage I if the frequency is lowered to 5 Hz, whereas in dry nitrogen gas Stage I crack propagation is not affected by a frequency change. The experiments show that easy formation of persistent slipbands and deformation highly localized in these bands are a prerequisite for the occurrence of extended slipband (Stage I) cracking. The influence on State I crack propagation exerted by the parameters considered is attributed to their effect on the formation of the persistent slipband ahead of the crack tip in which the crack propagates.

KEY WORDS: age-hardening, aluminum alloys, copper alloys, crack propagation, cyclic deformation, fatigue, hardening, hydrogen embrittlement, influence of frequency, influence of water vapor, persistent slipbands, single crystals, softening

[1] Research scientist and [3] former doctorate student at Max-Planck-Institut für Metallforschung, Institut für Werkstoffwissenschaften, Seestrasse 92, 7000 Stuttgart, Germany.

[2] Now deputy manager, Superalloys Project (Government of India enterprise), Hydeabad, India.

[4] Now division manager, Dornier GmbH, Werke München, 8000 München 66, Germany.

In crack propagation (CP) during fatigue, two different stages are usually discerned [*1,2*].[5] The earlier stage is characterized by very smooth crack propagation in crystallographic slip planes which experience the maximum shear stress. In this Stage I the crack surface is inclined about 45 deg to the applied stress direction, whereas in the later Stage II the crack propagates normal to the applied stress direction. The CP mechanism in Stage II is described fairly well by several models [*2–7*]. However, the fraction of fatigue life spent in Stage II CP is small, especially in high-cycle fatigue [*1,2*]. On the other hand, Stage I CP can comprise 80 to 90 percent of the fatigue life [*2,8*], whereby its importance is underlined. This CP mode is observed mainly at low levels of the stress amplitude and is particularly distinct in age-hardened alloys [*9–12*]. However, the mechanism of Stage I CP is not known at present and models are controversial [*1,2,13*]. Indications as to the mechanism involved could possibly be obtained by studying the influence of different parameters on CP in Stage I. Recently the influence of test temperature and alloy composition on cyclic deformation and CP behavior as well as the influence of the environmental atmosphere on CP in age-hardened alloys have been studied [*14–16*]. The present paper reviews these studies and shows that the influence on Stage I CP of the parameters considered can be understood in terms of their effect on the localization of plastic strain during cyclic deformation.

Experimental Procedure

To study the interrelation between cyclic deformation behavior and CP, experiments have been performed using single crystals of the following high-purity alloys:

1. Al-5Zn-1Mg. The alloy was homogenized 2 h at 450°C, water-quenched and aged 6.5 days at 60°C. After this heat-treatment the alloy contains large Guinier-Preston (GP) zones of 1.5-nm radius [*17*].
2. Al-4Cu, homogenized 2 h at 550°C, water-quenched, and aged 5 h at 160°C. After this heat-treatment the alloy contains θ'' precipitates of 40-nm diameter and a thickness of 2 to 3 nm [*18*].
3. Cu-2Co. The alloy was peak-aged by homogenizing 5 h at 1030°C, water-quenching, and aging 24 h at 600°C. In this condition the alloy contains coherent spherical precipitates of 8 to 9 nm radius [*19*].

The aluminum alloy single crystals were grown by the strain-anneal technique, whereas the Cu-2Co single crystals were produced by the Bridgman method. All specimens were oriented for single slip, the specimen axis lying in the center of standard orientation triangle.

[5] The italic numbers in brackets refer to the list of references appended to this paper.

Two kinds of experiments have been carried out:

1. Unnotched cylindrical specimens with a gage length of 10 mm and a diameter of 4 mm have been deformed in constant plastic strain controlled tension-compression tests ($\epsilon_{pl} = 0.001$) at a frequency of 0.33 Hz. Tests at room temperature (RT) were performed in laboratory air. For tests at 77 K the specimens were immersed in liquid nitrogen. The aim was to investigate the nature of damage introduced by cyclic loading and to understand it in terms of the observed cyclic work-hardening and work-softening behavior.
2. Flat single-edge-notched single crystals with a cross-sectional area of about 6 by 1.5 mm and a 0.6-mm-deep spark-cut notch were fatigued at 50 Hz in tension-compression under constant stress amplitude conditions at temperatures ranging from RT to 77 K. Besides 77 K, at which temperature the experiments were carried out in liquid nitrogen, the test environment was dry nitrogen gas with a dew point of about 90 K. The aim of the experiments was to investigate the CP modes and velocities.

The influence of test environment on fracture behavior was studied using Al-5Zn-1Mg single crystals of the same geometry as in the experiments of Type 2 just given. Heat treatment in this case was homogenizing 2 h at 450°C, water-quenching and aging 4 days at RT followed by 4 days at 135°C. In this approximately peak-aged condition the alloy contains small η'-particles of about 2.5-nm radius.

CP experiments were carried out at RT at two test frequencies (50 and 5 Hz), the test environment being either dry nitrogen gas or laboratory air with 40 to 60 percent relative humidity. After the fatigue loading history according to experiments of Type 1, metallographic observations were carried out on the originally electropolished specimen surfaces. In order to characterize the bulk deformation in the aluminum alloy specimens, $(\bar{1}01)$ surfaces were produced by spark-cutting perpendicular to the primary slip direction. The Al-4Cu specimens were artificially aged 16 h at 160°C to cause preferential precipitation at the deformation bands, and then the $(\bar{1}01)$ surfaces were electropolished and etched to make the deformation visible. No prior artificial aging was necessary to make deformation visible in Al-5Zn-1Mg.

Fatigue CP was monitored by microscopic observation at the electropolished side surfaces of the specimens using stroboscopic illumination and $\times 200$ magnification.

Results

Material Response to Cyclic Deformation

The results of the experiments of Type 1 are presented in the form of cyclic hardening/softening curves in Fig. 1. In these diagrams the stress amplitude recorded is plotted as a function of the number of cycles, which

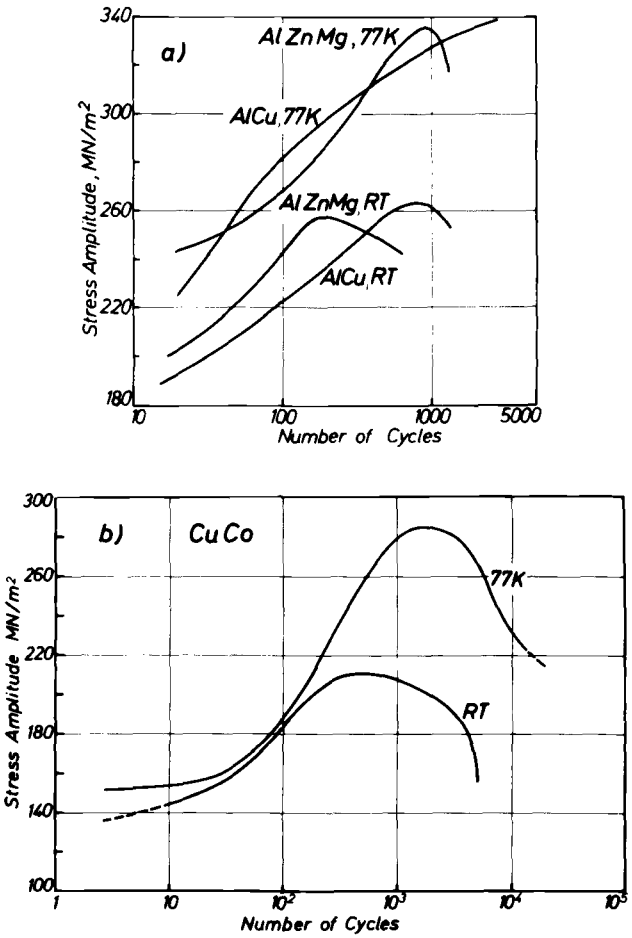

FIG. 1—*Cyclic strain hardening/softening curves at RT and 77 K;* (a) *Al-5Zn-1Mg and Al-4Cu, after Ref* 15; (b) *Cu-2Co.*

in the present case is proportional to the cumulative plastic strain. All curves display an initial hardening stage, but with different hardening rates. The experiment with Al-4Cu at 77 K (Fig. 1*a*) was interrupted after 4000 cycles while the hardening was still going on. In all other cases after reaching a maximum, the stress amplitudes decreased, indicating material softening. No extended range of constant stress amplitude, which could be attributed to a saturation stage, was observed.

Although, apart from Al-4Cu at 77 K, a softening stage was observed in all experiments, the individual curves can be distinguished by the amount of hardening which precedes the onset of softening (that is, the difference

between maximum stress amplitude, σ_{max}, and that at the 20th cycle, σ_{20})[6] and by the number of cycles (and thereby the amount of cumulative plastic strain) to reach the maximum stress amplitude, N_{max}. The corresponding values as taken from the diagrams in Fig. 1 are compiled in Table 1.

Figure 2 shows the deformation marking observed on the specimen surfaces of Cu-2Co. As can be seen, the persistent slipbands (PSB's) which are characterized by fine dark lines are less numerous after RT deformation (Fig. 2*a*) compared with deformation at 77 K (Fig. 2*b*). In the latter case, deformation appears to be more homogeneously distributed over the whole specimen, but the individual PSB's are often shorter and seem to be less well developed. Comparable differences have been found on the surfaces of the Al-5Zn-1Mg single-crystal specimens.

The deformation in the bulk of those aluminum alloy specimens which had displayed a softening stage (Fig. 1*a*) is characterized by PSB's parallel to (111) planes as shown on $(\bar{1}01)$ surfaces in Fig. 3. A comparison between Fig. 3*a* and 3*b* shows that in Al-5Zn-1Mg at 77 K the PSB's are more homogeneously distributed and appear shorter and not well developed, whereas at RT they are found to be fewer, more discrete, and well developed. This result compares well with the findings on the surfaces of the Cu-2Co specimens (Fig. 2). In comparing Al-5Zn-1Mg and Al-4Cu, both surface and bulk (Fig. 3*b* and *c*) deformation studies show that deformation at RT is concentrated in the former in a few distinct bands, whereas in the latter more bands of fainter appearance are observed. In Al-4Cu deformed at 77 K no indication for PSB's could be observed either on the surface or in the bulk material even though fatigue was continued to much higher cumulative plastic strains (see Table 1).

Fatigue Crack Propagation Characteristics

The CP modes in the aluminum alloys as observed as a function of test temperature are shown schematically in Fig. 4. The values of stress amplitudes σ_a required to produce a steadily propagating crack, about 0.2 mm long, in about 10^5 cycles, corresponding to an average CP velocity of about 2×10^{-6} mm/cycle are indicated as a fraction of the yield stress, σ_0, of the material at the test temperature.

At room temperature, crack nucleation and propagation in Stage I were obtained in both alloys. Especially in Al-5Zn-1Mg the resistance to Stage I cracking was very low; the crack propagated from the nucleation stage until the final unstable fracture occurred parallel to the primary slip plane. In aluminum-copper, under comparable loading conditions, the CP velocity

[6]The stress amplitude at the 20th cycle was used instead of that at the first cycle, since for experimental reasons the final plastic strain amplitude had to be built up gradually in the first 10 to 15 cycles.

TABLE 1—*Characteristics of the cyclic strain hardening/softening curves in Fig. 1 (for Al-4Cu at 77 K, values at test interruption are given;* σ_o = *flow stress).*

Alloy	Test Temperature	σ_o, MN/m^2	$\sigma_{max} - \sigma_{20}$, MN/m^2	N_{max}
Al-5Zn-1Mg	RT	196	57	185
	77 K	226	92	900
Al-4Cu	RT	186	74	825
	77 K	216	(>115)	(>4000)
Cu-2Co	RT	124	60	460
	77 K	116	128	1750

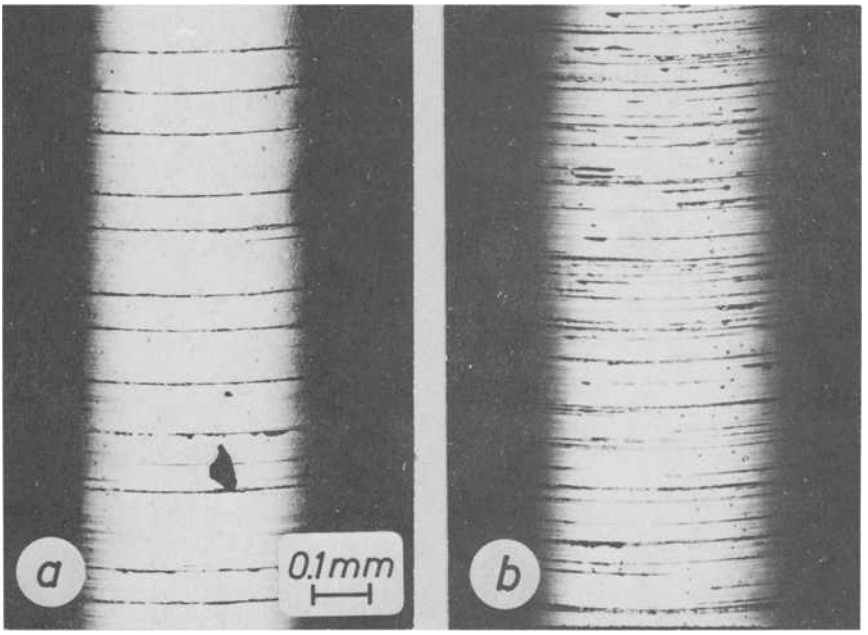

FIG. 2—*Optical micrographs of Cu-2Co specimen surfaces:* (a) *tested at RT;* (b) *tested at 77 K.*

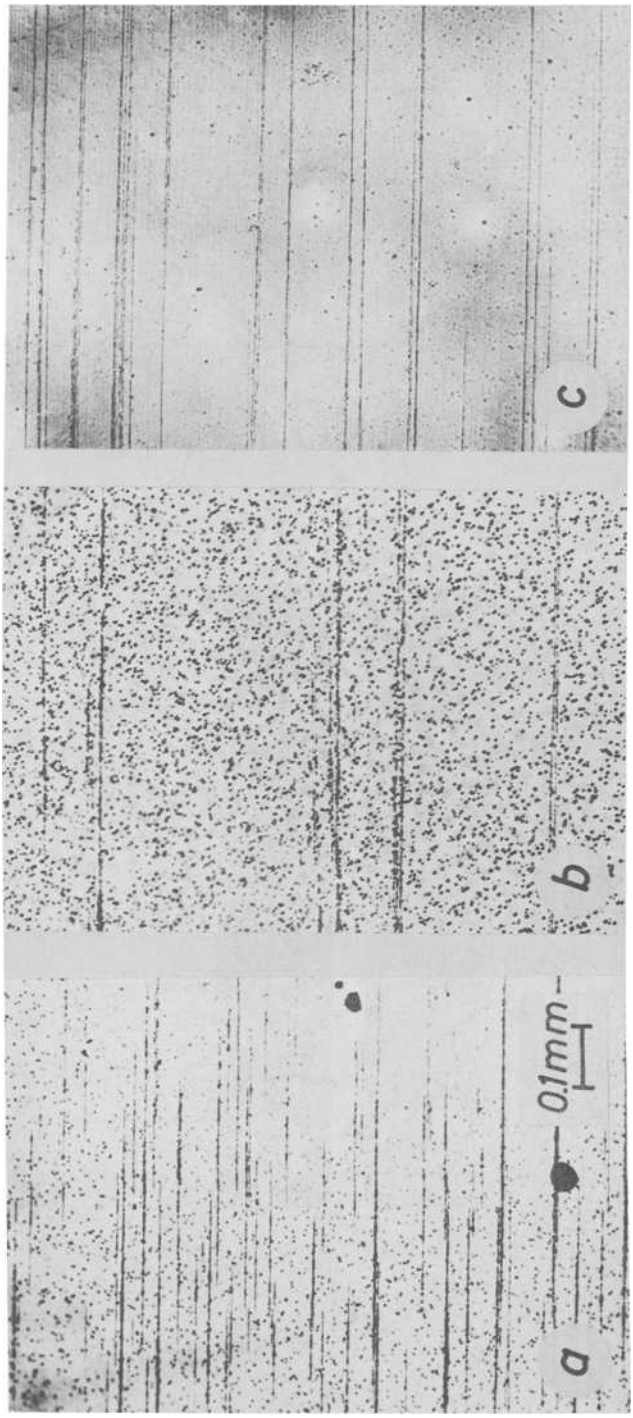

FIG. 3—*Optical micrographs of (101)-surfaces:* (a) *Al-5Zn-1Mg, tested at 77 K;* (b) *Al-5Zn-1Mg, tested at RT; and* (c) *Al-4Cu, tested at RT; all after Ref* 15.

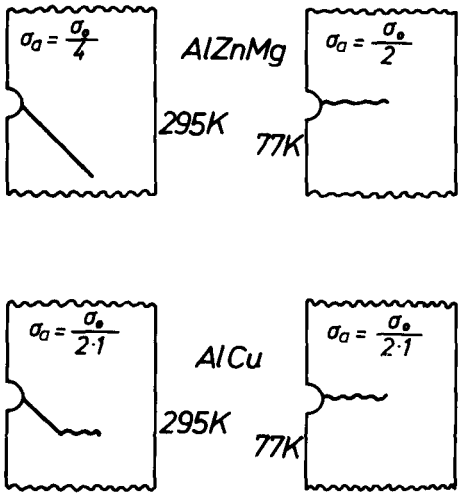

FIG. 4—*Schematic illustration of crack propagation in Al-5Zn-1Mg and Al-4Cu at RT and 77 K, after Ref* 15.

was markedly lower. When the CP velocity was increased by raising the stress amplitude, an early macroscopic deviation of the crack path from Stage I into Stage II occurred.

At 77 K Stage I crack nucleation was found to be difficult, and in both alloy systems crack propagation in Stage II was observed (Fig. 4). In order to study the influence of temperature on crack propagation in Stage I, a Stage I crack was produced at RT in Al-5Zn-1Mg, and the test was continued at 77 K at the same value of stress amplitude. Propagation at 77 K continued to occur in what can still be characterized as Stage I, but the propagation velocities were roughly four times smaller than those at RT. The fracture surface produced at 77 K, even though broadly lying in the crack plane produced at RT, is considerably rougher. It exhibits a larger number of steps and at places appears quite rugged.

With Cu-2Co the influence of temperature on the CP velocity has been studied in more detail. As a result, in Fig. 5 the CP velocity is plotted for two different crack lengths as a function of $1/T$, T being the absolute test temperature. For temperatures between RT and 90 K the tests were carried out in a dry nitrogen gas atmosphere. In this temperature range, the crack was found to propagate in Stage I, and the CP velocity decreased continuously with falling temperature. At 77 K, however, no Stage I CP was observed, but the crack nucleated and propagated from the beginning in a Stage II mode. It should be mentioned here that during the test at 77 K the specimen was directly immersed in liquid nitrogen.

The influence of temperature on the CP in Cu-2Co is clearly demonstrated

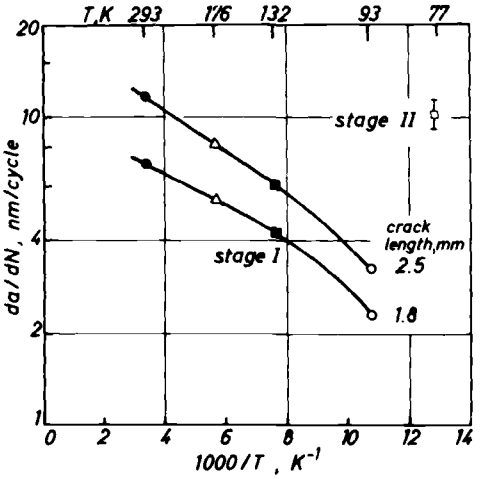

FIG. 5—*Crack propagation velocity as a function of test temperature in Cu-2Co, after Refs* 14 *and* 16.

in Fig. 6. In this experiment a Stage I crack was nucleated at RT. After CP until A at RT, the test was continued at 77 K at the same stress amplitude. The crack immediately ceased to propagate in Stage I. Instead, after a fairly long incubation time of about 5 h, a Stage II crack nucleated and propagated until B. After reheating the specimen to RT, at first the crack propagated in Stage II until C. Simultaneously at the crack tip the formation of strong, distinct PSB's could be observed which caused the crack to change its path again into a Stage I mode.

Influence of Test Environment

The test environment in combination with the test frequency was found to exert a strong influence on the tendency to Stage I cracking at RT, and Fig. 7 illustrates this effect for the case of Al-5Zn-1Mg. When the frequency was changed from 50 to 5 Hz during the crack propagation test, (Fig. 7, top) the Stage I propagation mode remained uninfluenced if the test environment was dry nitrogen gas. Furthermore, CP velocity and the fracture surface appearance at the two frequencies were identical. In a laboratory air environment, however, soon after changing over to 5 Hz, Stage II cracks nucleated which then grew preferentially at the expense of the Stage I crack. When the test was started already at a frequency of 5 Hz (Fig. 7, bottom) a smooth Stage I crack nucleated and propagated in dry nitrogen gas atmosphere, whereas Stage II CP was observed from the beginning in laboratory air.

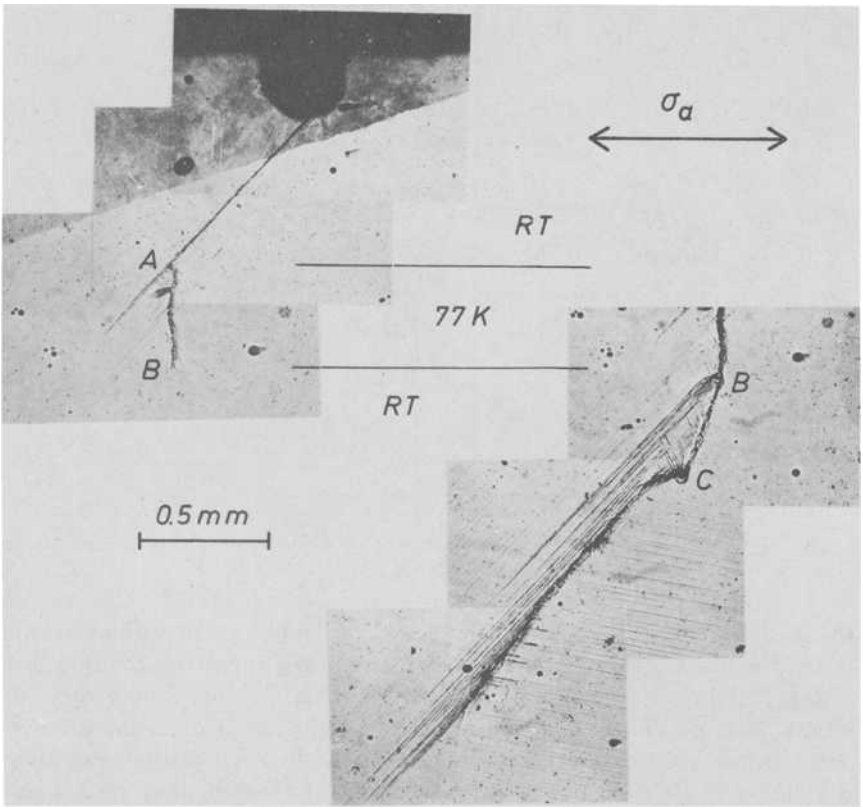

FIG. 6—*Optical micrograph of the side surface observations during testing Cu-2Co at changing temperatures, after Ref* 16.

Discussion

Cyclic Hardening/Softening Behavior and Strain Localization

Persistent slipbands in pure copper single crystals have been shown to be sites in which during fatigue loading cyclic deformation is concentrated [*20-23*]. Experimental observations indicate that the same is valid for PSB's in age-hardened materials [*24-26*]. This is plausible, at least for a great number of age-hardened alloys, because it is accepted that the material can be softened by cyclic deformation [*24-30*]. Therefore, once PSB's have nucleated, the material in them should be softened very rapidly, causing further localization of strain in them.

All mechanisms proposed to explain the material softening depend on the degradation of the originally hardening microstructure due to the dislocation movement [*24-31*]. Cutting by dislocations and resolution

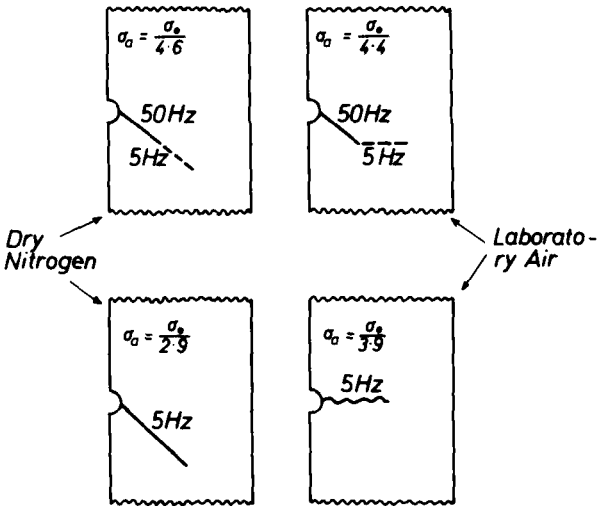

FIG. 7—*Schematic illustration of the influence of frequency and environmental atmosphere on Stage I crack propagation in Al-5Zn-1Mg, after Refs* 14 *and* 15.

[*24,25,28-30*] or overaging [*24,25*] of the hardening precipitations are the favored explanations for softening. After critically reviewing these mechanisms, Calabrese and Laird [*26,32*] attribute softening, which they observed during cyclically deforming polycrystalline Al-4Cu, to the decay of order in the precipitate particles by repeated dislocation cutting. For alloys containing single-element precipitates like copper-cobalt, they predict that no material softening should occur. Earlier observations in our laboratory [*14,29*] and the experiments presented here, which exhibit a distinct softening stage in Cu-2Co (Fig. 1*b*), are in contrast with the findings of Feltner and Laird [*34*]. Thus it is shown that destruction of order in the precipitate particles cannot be the only mechanism responsible for softening in age-hardened alloys. Moreover, electron microscopy studies on PSB's in Al-5Zn-1Mg containing η'-particles [*35*] clearly indicate a strong reduction of particle size in the bands.

In fatigue experiments with copper single crystals at constant plastic strain amplitude, it has been observed that PSB's form near the maximum of stress amplitude [*22*]. Light-optical observations at a ×25 magnification on the specimen surfaces during the present experiments, as well as earlier observations in our laboratory, show that this holds also for the age-hardening alloys studied here. Therefore, and since at present no other quantitative statement of the formation of PSB's in age-hardened alloys is available, the amount of hardening to reach the maximum stress amplitude, that is, the difference $\sigma_{max} - \sigma_{20}$ (Fig. 1, Table 1), can be taken as a measure to characterize differences in the susceptibility to PSB forma-

tion of different materials. The larger this stress difference, the more the matrix must harden before PSB nucleation sets in and the more the material is able to resist PSB formation. The number of cycles or the cumulative strain to reach the maximum depends on both the amount and the rate of hardening.

In this sense the present experiments (Fig. 1, Table 1) show that a temperature decrease obviously increases the resistance to PSB formation. Similarly, at RT the larger stress difference for Al-4Cu compared with Al-5Zn-1Mg indicates stronger resistance to PSB formation if the precipitates containing zinc plus magnesium are replaced by those rich in copper. The larger cyclic hardening rate of the Al-5Zn-1Mg alloy is in accordance with the results of unidirectional tension tests [*36*] and transmission electron microscopical (TEM) observations [*33*] which revealed a particularly strong particle-dislocation interaction in this alloy.

The light microscopy appearance of the PSB's does not say much about the actual number and width of individual bands and the plastic shear strain borne by them. TEM on $(1\bar{2}1)$-foils reveals a thickness of individual PSB's in age-hardened aluminum alloys and Cu-2Co in the order of 0.05 to 0.2 μm [*14,16,33,35*]. (In Fig. 3 of Ref *16* the scale factor is incorrect and should read 0.8 μm.) Moreover, the TEM observations show that with increasing particle-dislocation interaction the PSB's tend to group together in a few stacks with a distance between individual bands of about 1 μm [*33*]. This fact and the light-optical observations at the specimens' outer surface (Fig. 2) and at $(\bar{1}01)$-surfaces (Fig. 3) indicate that the lower the resistance to PSB formation is, the more the deformation is localized in a few narrow planar zones of the crystal.

Tendency to Stage I Crack Propagation

PSB's in which the plastic deformation is localized due to the material softening, are favored sites for crack nucleation at the specimen surface. The easier the PSB formation and, as a result, the stronger the strain localization in narrow zones, the earlier and easier crack nucleation in slip-bands will occur.

When a single-edge-notched single crystal is loaded by a low stress amplitude, due to the stress concentration, a PSB will form in the notch root parallel to the primary slip system and propagate into the material (Fig. 8*a*). When this PSB is sufficiently developed, or damaged, a Stage I crack will nucleate in the notch root and propagate into this PSB. As a result, the stress state in the specimen is changed in such a way that the PSB further propagates in front of the crack tip and so on (Fig. 8*b*).

Recent TEM observations of the dislocation structure in front of the tip of a Stage I crack in Al-5Zn-1Mg [*35*] are in agreement with this model conception. They show that after a CP test with low constant stress ampli-

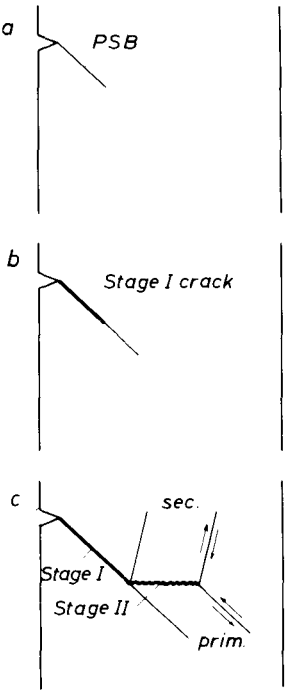

FIG. 8—*Model conception of crack propagation in age-hardened single crystals.*

tude at RT, a PSB expands in the material in a direction that is an exact extension of the Stage I crack. The length of the PSB measured from the crack tip increases with increasing Stage I crack length, that is, with increasing stress intensity at the crack tip [*35*].

Therefore, it is concluded that a Stage I crack is able to propagate only in a preformed and sufficiently developed, that is, sufficiently damaged, PSB. Thus, it is to be expected that all factors which influence the nucleation and development of a PSB should also exert an influence in the same direction on the CP in Stage I. The results of the CP experiments confirm this expectation.

Based on our observation that the maximum in σ-versus-N curves is associated with PSB formation, the cyclic work hardening curves in Fig. 1*a* can be interpreted to mean that PSB formation occurs most easily (and readily) in Al-5Zn-1Mg at RT compared with Al-4Cu and 77 K. Thus, according to the consideration made in the foregoing, the tendency to CP in Stage I should be greatest under these conditions (Al-5Zn-1Mg, RT). The experiment shows that this is the case (Fig. 4). Even at low stress amplitudes a smooth Stage I crack propagates rapidly in Al-5Zn-1Mg at RT until the final unstable failure occurs. The greater restraint to PSB

formation and the less-pronounced localization of slip in Al-4Cu at RT and in Al-5Zn-1Mg at 77 K are manifested in slower CP in Stage I and in an earlier transition from Stage I to Stage II. Obviously under these conditions nucleation and development of PSB's in front of the crack tip are so much hindered that the stress needed to maintain a certain CP velocity induces slip processes on secondary slip systems on a bigger scale before softening occurs in the primary slip systems which would localize deformation and CP in a PSB. But slip on two intersecting slip systems gives rise to crack propagation in Stage II according to the alternating slip model [*6,7*] (Fig. 8*c*). The exclusive Stage II CP in Al-4Cu at 77 K was expected anyway due to the cyclic hardening curve in Fig. 1*a*.

The restraint to Stage I CP at 77 K in Cu-2Co is very clearly shown in Fig. 6. Obviously at the low temperature the PSB formation in front of the Stage I crack tip is so strongly hindered that the Stage I crack is not able to propagate. Instead, at first a Stage II crack has to nucleate before CP can continue. After reheating to RT, easy PSB formation is rendered possible again and the micrograph (Fig. 6) documents the renewed increased tendency to Stage I CP.

Environmental Influence

From a series of experiments it is known that water vapor in the environmental atmosphere strongly influences fatigue CP in aluminum alloys [*11,40*] (for reviews, see for example Refs *38* and *39*). Recently, hydrogen embrittlement [*41,42*] is the preferential explanation for the results of the water vapor-metal reaction. An influence of humidity on the CP in Stage I has also been found in these alloys [*10,43*]; in the presence of water vapor the CP velocity is increased [*10*], whereas the tendency to Stage I cracking seems to be reduced [*43*]. The present experiments agree with the findings of Hockenhull and Monks [*43*], proving that the influence of humidity on Stage I CP is dependent on the test frequency. A frequency change in an inert atmosphere exhibits no influence, thus showing that at least in the frequency range considered there is no intrinsic frequency effect.

On the basis of considerations made before, and the experimental observation of decreased tendency to Stage I CP in the presence of water vapor, it is supposed that the formation of the PSB in front of the crack tip is restrained by the reaction of the water vapor with the fresh aluminum surfaces produced at the crack tip. The decrease of this influence at higher frequencies indicates that time-dependent steps are involved. A decreasing influence with increasing CP velocity points in the same direction. One can think of several time-dependent processes, such as the following.

1. Arrival of the reactive species in the environment to the crack tip.
2. Adsorption of these species on the freshly generated aluminum surface at the crack tip.

3. Diffusion of hydrogen into the plastic zone at the crack tip.

The exact mechanism by which the material-environment interaction influences the crack propagation is not known from the present experiments. However, in this case also, hydrogen embrittlement is considered to be an attractive hypothesis.

Recently, Donovan [*44*] has shown that during plastic deformation of a 5086 aluminum alloy, moving dislocations are able to transport hydrogen. Let us make the reasonable assumption that atomic hydrogen is produced by the reaction at the crack tip. Due to the slip process strongly localized in PSB's, the hydrogen will preferentially be transported into that band which starts from the crack tip. Thus, this PSB will be embrittled and cracked at an earlier state of development than without hydrogen. The result is the higher CP velocity observed [*10*] and, because of the increasing stress intensity, a more rapid penetration of the PSB in front of the crack tip into the material. However, this band will be less well developed since due to the embrittlement a fewer number of cycles will pass in the interval from its nucleation to its cracking. The lower the frequency, the more time per cycle is available for reaction and diffusion of hydrogen and the deeper the hydrogen will penetrate into the PSB, thus cracking it at a still earlier state of development. However, according to our considerations stated previously in connection with Fig. 8*c*, the poorer the development of the PSB in front of the crack tip, the greater is the probability that secondary slip becomes essential, resulting in a decreased tendency to Stage I cracking and a transition to the Stage II CP mode. The results of the present experiments are in excellent accordance with this hypothesis.

Conclusions

To extend a Stage I crack in a notched specimen, it is necessary that ahead of the propagating crack tip a persistent slipband continually reform. It has been shown that the influence of different parameters on crack propagation in Stage I can be attributed to their effect on the formation of persistent slipbands and the localization of cyclic strain in these bands. Factors which restrain nucleation and development of persistent slipbands, like a reduction of temperature from room temperature to 77 K or a change of alloying elements from zinc plus magnesium to copper in the aluminum alloys, also hinder crack propagation in Stage I by giving rise to a smaller crack propagation velocity or to an early transition to the Stage II mode. The increased crack propagation velocity and the decreased tendency to Stage I crack propagation in the presence of water vapor in the environmental atmosphere, especially at low test frequencies, can be understood if it is assumed that the persistent slipbands ahead of the crack tip are embrittled by hydrogen.

In age-hardened alloys a large fraction of the fatigue life of a cyclically loaded specimen can be occupied by crack propagation in Stage I. Therefore, it would be interesting to investigate if, from a simple experiment to determine the persistent slipband formation and strain localization, the relative fatigue life of an age-hardened alloy could be predicted.

Acknowledgments

We wish to thank Professor V. Gerold for his continued interest in this work and many helpful discussions. We also acknowledge alloy supply and financial support by Vereinigte Aluminium-Werke AG, Bonn, and Deutsche Forschungsgemeinschaft, Bonn-Bad Godesberg.

References

[1] Grosskreutz, J. C. in *Metal Fatigue Damage—Mechanism, Detection, Avoidance, and Repair, ASTM STP 495,* American Society for Testing and Materials, 1971, pp. 5-60.
[2] Laird, C. in *Fatigue Crack Propagation, ASTM STP 415,* American Society for Testing and Materials, 1967, pp. 131-180.
[3] Pelloux, R. M. N. in *Fracture 1969,* P. L. Pratt, Ed., Chapman and Hall, London, 1969, pp. 731-744.
[4] Bowles, C. Q. and Broek, D., *International Journal of Fracture Mechanics,* Vol. 8, 1972, pp. 75-85.
[5] Tomkins, B. and Biggs, W. D., *Journal of Materials Science,* Vol. 4, 1969, pp. 544-553.
[6] Neumann, P., *Acta Metallurgica,* Vol. 22, 1974, pp. 1155-1165.
[7] Neumann, P., *Acta Metallurgica,* Vol. 22, 1974, pp. 1167-1178.
[8] Grosskreutz, J. C., *Metallurgical Transactions,* Vol. 3, 1972, pp. 1255-1262.
[9] Nageswararao, M., Kralik, G., and Gerold, V., *Zeitschrift für Metallkunde,* Vol. 66, 1975, pp. 479-486.
[10] Nageswararao, M. and Gerold, V., *Metallurgical Transactions,* Vol. 7A, 1976, pp. 1847-1855.
[11] Nageswararao, M. and Wilhelm, M., *Aluminium,* Vol. 52, 1976, pp. 306-311.
[12] Gell, M. and Leverant, G. R., *Acta Metallurgica,* Vol. 16, 1968, pp. 553-561.
[13] Schijve, J. in *Fatigue Crack Propagation, ASTM STP 415,* American Society for Testing and Materials, 1967, pp. 415-459.
[14] Gerold, V., Nageswararao, M., and Wilhelm, M., *Zeitschrift für Metallkunde,* Vol. 67, 1976, pp. 800-806.
[15] Nageswararao, M. and Wilhelm, M. in *Fracture 1977, Proceedings,* Fourth International Conference on Fracture, Waterloo, Ont., Canada, Vol. 2, 1977, pp. 703-709.
[16] Meyer, R., Gerold, V., and Wilhelm, M., *Acta Metallurgica,* Vol. 25, 1977, pp. 1187-1190.
[17] Dünkeloh, K.-H., Kralik, G., and Gerold, V., *Zeitschrift für Metallkunde,* Vol. 65, 1974, pp. 291-296.
[18] Nicholson, R. B. and Nutting, J., *Philosophical Magazine,* Vol. 3, 1958, p. 531.
[19] Witt, M. and Gerold, V., *Zeitschrift für Metallkunde,* Vol. 60, 1969, pp. 482-487.
[20] Watt, D. F., Embury, J. D., and Ham, R. K., *Philosophical Magazine,* Vol. 17, 1968, pp. 199-203.
[21] Mughrabi, H., *Materials Science and Engineering,* Vol. 33, 1978, pp. 207-233.
[22] Winter, A. T., *Philosophical Magazine,* Vol. 30, 1974, pp. 719-738.
[23] Finney, J. M. and Laird, C., *Philosophical Magazine,* Vol. 31, 1975, pp. 339-366.
[24] Clark, J. B. and McEvily, A. J., *Acta Metallurgica,* Vol. 12, 1964, pp. 1359-1372.
[25] Stubbington, C. A. and Forsyth, P. J. E., *Acta Metallurgica,* Vol. 14, 1966, pp. 5-12.
[26] Calabrese, C. and Laird, C., *Materials Science and Engineering,* Vol. 13, 1974, pp. 141-157.

[27] McGrawth, J. T. and Bratina, W. J., *Czechoslovak Journal of Physics*, Vol. B19, 1969, p. 284.
[28] Kralik, G. and Schneiderhan, H., *Scripta Metallurgica*, Vol. 6, 1972, pp. 843-849.
[29] Schützner, P., "Computer-unterstützte Untersuchungen des Verhaltens kubisch-flächenzentrierter Metalle und Legie-rungen bei Wechselverformung," Ph.D. Thesis, Stuttgart University, Stuttgart, Germany, 1974.
[30] Abel, A. and Ham, R. K., *Acta Metallurgica*, Vol. 14, 1966, pp. 1495-1503.
[31] Wells, C. H. and Sullivan, C. P., *Transactions*, American Society for Metals, Vol. 57, 1964, pp. 841-855.
[32] Calabrese, C. and Laird, C., *Metallurgical Transactions*, Vol. 5, 1974, pp. 1785-1793.
[33] Maier, D., "Die Versetzungsstruktur in wechselverformten Cu-Co-, Al-Zn- und Al-Zn-Mg-Einkristallen mit kohärenten Ausscheidungen," Ph.D. Thesis, Stuttgart University, Stuttgart, Germany, 1976, to be published.
[34] Feltner, C. E. and Laird, C., *Transactions*, American Institute of Mining Engineers, Vol. 245, 1969, pp. 1372-1373.
[35] Vogel, W., Wilhelm, M., and Gerold, V., to be published.
[36] Dünkeloh, K.-H., Kralik, G., and Gerold, V., *Zeitschrift für Metallkunde*, Vol. 65, 1974, pp. 773-777.
[37] Ogura, T., Karashima, S., and Tsurukame, K., *Transactions*, Japanese Institute of Metals, Vol. 16, 1975, p. 43.
[38] Wei, R. P., *Engineering Fracture Mechanics*, Vol. 1, 1970, p. 633.
[39] Böhmer, M. and Munz, D., Part I, *Metall*, Vol. 24, No. 5, 1970, pp. 446-455, and Part II, *Metall*, Vol. 24, No. 8, 1970, pp. 857-863.
[40] Nageswararao, M., Gerold, V., and Kralik, G., *Journal of Materials Science*, Vol. 10, 1975, pp. 515-524.
[41] Gest, R. J. and Troiano, A. R., *Corrosion*, National Association of Corrosion Engineers, Vol. 30. No. 8, 1974, pp. 274-279.
[42] Speidel, M. O. in *Hydrogen in Metals*, J. M. Bernstein and W. Thompson, Eds., American Society for Metals, 1974, pp. 249-276.
[43] Hockenhull, B. S. and Monks, H. A., *Metal Science Journal*, Vol. 5, 1971, pp. 125-130.
[44] Donovan, J. A., *Metallurgical Transactions*, Vol. 7A, 1976, pp. 1677-1683.

DISCUSSION

E. A. Starke, Jr.[1] (*discussion*)—In keeping with the theme of the conference, Dr. Wilhelm and his coauthors use the cyclic response curve, where the applied stress is plotted versus number of cycles for a fixed plastic strain amplitude, to determine an alloy's resistance to persistent slipband formation and subsequent crack nucleation. The resistance is related to the difference between the maximum stress and the stress obtained after 20 cycles. I would like to compliment Dr. Wilhelm on attempting to quantify fatigue resistance and would offer the following points for his consideration.

The cyclic response curve of an age-hardened material depends on microstructural features such as the volume fraction of precipitates, the spacing of precipitates, the size and coherency of the precipitates, the initial

[1] Professor of metallurgy, Georgia Institute of Technology, Atanta, Ga. 30332.

orientation of the single crystals, and the point at which secondary slip is activated. These have not been described. Depending on these parameters, many changes can occur during the first 20 cycles of the cyclic response curve. The number of cycles to maximum hardening may be a constant with respect to plastic strain or may decrease with increasing strain.[2] In any event, the changes that occur in the first 20 cycles should not be ignored when quantitatively describing a material's resistance to persistent slipband formation.

The second point has to do with the effect of temperature on persistent slipband formation. Room temperature tests were made in laboratory air, which is an aggressive environment for these aluminum alloys, and low-temperature tests were made in liquid nitrogen, which is a nonaggressive environment. The environment may be an important parameter, and its effect should not be ignored. The observed temperature effect may be due, at least in part, to the presence of hydrogen or oxygen or both.

The final point I would like to make is that the cyclic response curves of age-hardened alloys are more complex than those for pure metals. The measured curves might represent a combination of two different mechanisms: a hardening mechanism, which begins on the first cycle and operates to a point of saturation, and a softening mechanism, which may or may not begin on the first cycle. The experimental curve represents the sum of the two effects. Consequently, the maximum in the cyclic response curve is not necessarily associated with the formation of persistent slipbands. It might be, but it also might not be.

S. J. Brett[3] *(discussion)*—The authors' conclusion that a period of development is required for a PSB to become a suitable crack path is an interesting one. The following points may be worth considering:

1. It has been pointed out by Sargent and Purdy[4] that, given a shearable precipitate of the type we are concerned with here, a single cutting event will result in resolution. In the case of a PSB we could expect undamaged precipitates in the matrix to grow at the expense of damaged precipitates in the band by a process of Ostwald ripening. This would be equally true, of course, of disordered precipitates. As a result therefore of localized damage within PSB, whether it be cutting or disordering, we could expect a net migration of solute atoms into the matrix. In a recent study of slip plane facets in two aluminum alloys at Sussex University, such solute migration has been detected.[5] It appears quite likely that the period of

[2] Stoltz, R. E. and Pineau, A. G., *Materials Science and Engineering*, Vol. 34, 1978, pp. 275–284.

[3] Metallurgy Department, The British Aluminium Company Ltd., Chalfont Technological Centre, Chalfont Park, Gerrards Cross, Buckinghamshire, SL9 0QB, U.K.

[4] Sargent, C. M. and Purdy, G. R., *Scripta Metallurgica*, Vol. 8, 1974, p. 569.

[5] Brett, S. J. and Doherty, R. D., *Materials Science and Engineering*, in press.

PSB development discussed in the present work is associated with this diffusion process.

2. It is not clear as yet whether solute diffusion from a PSB is a necessary preliminary to slip plane cracking, but clearly a decreased solid solution strengthening in the band will make it a highly favorable crack path. The reluctance of the fatigue crack to propagate in a slipband mode at 77 K may be attributable to the absence of solute migration at this temperature. In the case of the crack nucleated at room temperature and then propagated at 77 K, the relative roughness of the fracture surface could be the result of restricted solute loss. The more depleted a PSB is, the more highly defined the crack path and the cleaner the resulting facet.

3. Finally, if within a volume ahead of the fatigue crack significant solute depletion from PSB has occurred, it seems unlikely that environmental effects will alter the mode of cracking. Slipband cracking may, however, be suppressed if the environment shortens the total life of the specimen to the extent that solute diffusion cannot occur in the time available. Polycrystalline single-edge-notched specimens of Al-4Cu broken under constant stress range conditions at Sussex did not display slip plane facets when the life time was less than 3×10^4 cycles (17 min at 30 Hz). The maximum stress for these specimens varied from 70 to 120 MPa.

The authors may wish to comment on the presence or absence of such a threshold in their present study.

M. Wilhelm, M. Nageswararao, and R. Meyer (authors' closure)—In the discussion to our paper by Dr. Starke it has become clear that some details of our experiments and observations need more explanation:

1. For the tests, only single crystals were used, the tensile axis of which lay in the center of the standard orientation triangle. To what extent secondary slip is activated during cyclic straining in the unnotched specimens and to what extent this is necessary to form PSB's are not known from the present experiments. In the CP specimens, of course, due to the multiaxial stress state at a crack tip, secondary slip will increasingly be activated with increasing stress intensity.

All materials tested contain coherent or at least semicoherent precipitates in a size and distribution which allow particle shearing as a prerequisite for the observed material softening.

2. In copper single crystals it has been shown that the formation of PSB's is a result of the bulk deformation and hardening [*21*]. Our experiments with age-hardened alloys indicate that the same seems to hold for this class of materials. For instance, cyclic plastic strain controlled experiments by Kralik et al [*28*] with Al-9.2Zn as well as recent experiments with underaged Cu-2Co single crystals (to be published) have shown that in a wide range, irrespective of the plastic strain amplitude, the cyclic hardening curves exhibit a maximum after the same amount of hardening, whereas

the number of cycles and the cumulative plastic strain to reach the maximum differ essentially. Moreover, light-optical observations at $\times 25$ magnification show that in all alloys studied PSB's suddenly appear at the specimen surfaces at a stress amplitude close to the maximum. Therefore, the decrease of the stress amplitude is attributed to the strong softening of the material in the PSB's. A slight additional softening, homogeneous in the matrix, during the hardening stage cannot be excluded. But this will not give rise to the strong localization of deformation in PSB's which causes the macroscopic softening and which is fatal to the fatigue life.

These findings strongly indicate that the bulk deformation rather than surface effects is responsible for the PSB formation. Nevertheless, tests in vacuum or inert atmospheres should give information about additional influences of the environment.

3. Since, at present, no quantitative statement of the formation of PSB's is available at all, the difference $\sigma_{max} - \sigma_{20}$ is thought to be a semiquantitative measure for the tendency to PSB formation: Because of its simplicity its application is restricted. An improved version allowing a more general application is in preparation. In cases where the amount of hardening in the first 20 cycles is appreciable compared with total hardening (for example, in tests with large plastic strain amplitude), the difference $\sigma_{max} - \sigma_{20}$ will be less useful for semiquantitative considerations. However, experiments using improved testing equipment which allows application of the intended plastic strain amplitude from the first cycle on (see footnote 6 of our paper on page 218) have shown that the amount of hardening in the first 20 cycles at plastic strain amplitudes as small as 0.001 does not change the validity of the statement at all.

Although it is probable that the interrelation between PSB formation and Stage I crack propagation stated by us is valid also for other age-hardened alloys containing shearable precipitates, until now the experimental evidence, as shown in our paper, is restricted to the aluminum alloys and the copper-cobalt alloy. Additional experiments are planned to confirm and substantiate the conclusions of our paper.

Although solute depletion in the PSB's is not a necessary condition to explain our experimental results, Dr. Brett's contribution provides an interesting interpretation. Unfortunately our present experiments give no indication of whether solute depletion in the PSB's occurs or not. Future experiments must prove how far strain localization and slipband cracking are influenced by a possible solute depletion.

We would like to thank both discussers for their stimulating comments on our paper.

(Reference numbers relate to reference list appended to our paper.)

M. Kikukawa,[1] *M. Jono,*[1] *and M. Adachi*[1]

Direct Observation and Mechanism of Fatigue Crack Propagation

REFERENCE: Kikukawa, M., Jono, M., and Adachi, M., **"Direct Observation and Mechanism of Fatigue Crack Propagation,"** *Fatigue Mechanisms,* Proceedings of an ASTM-NBS-NSF symposium, Kansas City, Mo., May 1978, J. T. Fong, Ed., *ASTM STP 675,* American Society for Testing and Materials, 1979, pp. 234–253.

ABSTRACT: Fatigue crack propagation tests were carried out by using a specially designed testing apparatus in a scanning electron microscope. A grain-oriented silicon iron was used as a testing material and it was found that a nearly plane-strain state could be realized up to the specimen surface by selection of the loading axis to the specific orientation of the material. From the sequential observations of crack opening and closure behavior the mechanism of fatigue crack propagation by Mode I opening was confirmed to be an alternating slipping-off process at the crack-tip apex.

Quantitative evaluation of a relationship between crack-tip opening displacement and crack growth length is given by considering the slip direction, crack tip angle, and the amount of rewelding. Also, a relation between crack growth length and slipped length in Mode II fatigue cracks is discussed.

KEY WORDS: crack propagation mechanism, crack tip angle, crack-tip opening displacement (CTOD), direct observation, fatigue

Since the fatigue phenomenon is considered to be intrinsically localized in a very small portion of material, direct observation by an electron microscope can become a powerful means to understand the fatigue mechanism. However, it is feared that the observation on a thin foil specimen with a transmission electron microscope (TEM) does not indicate the true behavior of the bulky materials. On the other hand, a scanning electron microscope (SEM) can give information on the behavior of bulky materials, although its observation is limited to only the specimen surface. For this case, it becomes a problem that the fatigue crack propagation behavior observed at the specimen surface may be different from that of the specimen interior, because of the difference of constraint, that is, a plane-

[1] Professor, associate professor, and assistant, respectively, Deparatment of Mechanical Engineering, Osaka University, Suita, Japan.

stress condition at the specimen surface and plane strain in the interior. Furthermore, the crack propagation rate is thought to be controlled by the behavior of the latter condition.

In this work, therefore, an attempt was made to affect plane strain through the specimen thickness by selection of a grain-oriented test material. Direct observations and quantitative measurements of the fatigue crack propagation behavior for Modes I and II deformation were carried out by using a fatigue testing apparatus which was specially designed to operate in an SEM.

Fatigue Testing Apparatus

Figure 1 shows the mechanical portion of the fatigue testing apparatus which can conduct a fatigue test in the specimen chamber of an SEM (Japan Electron Optics Laboratory Co., Ltd., JSM U-3). The testing rig has a load capacity of 6000 N and has two types of driving systems. One is of the electro-servo-hydraulic type and can perform a test with a cyclic rate of 0 to 30 Hz. The other driving system is composed of a variable speed a-c motor, a reduction gear, and a worm gear which can give a very slow testing speeds of from 3.2 to 0.02 mm/min. Using the latter type of driving system, direct observation of the crack propagation behavior with high magnification during the fatigue test was found to be possible at any phase of loading cycles. The load was detected by a load cell connected to the specimen and the strain by a cantilever-type extensometer. Output from

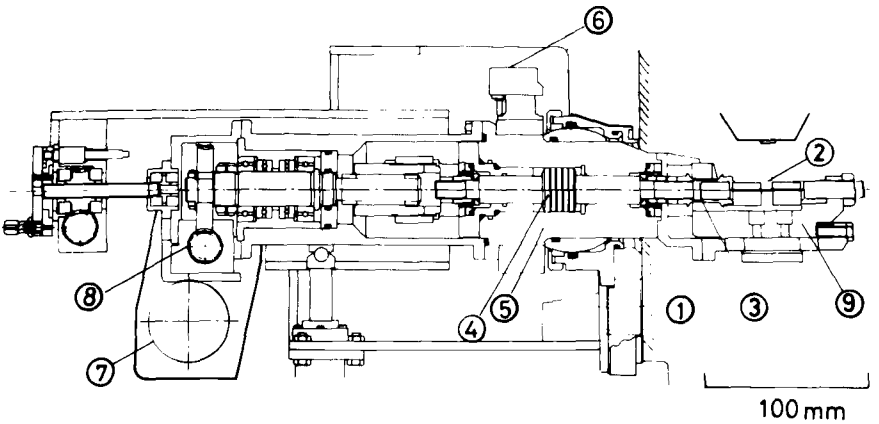

1. Specimen chamber of SEM, 2. Specimen, 3. Load cell,
4. Piston, 5. Cylinder, 6. Servo-valve, 7. AC-motor,
8. Worm gear, 9. Specimen grip

FIG. 1—*Fatigue testing apparatus.*

these transducers was fed to the measuring devices and also to a servo-amplifier to compose a closed-loop system. The details of the testing rig are described in an earlier paper by the authors [*1*].[2]

Material and Test Procedure

The material used was a grain-oriented silicon iron plate of 0.3-mm thickness which had a rolling surface and rolling direction of (011) and [100], respectively. The chemical composition of the material used is shown in Table 1. In order to realize the near state of plane strain through the specimen thickness, the loading axis was selected to be perpendicular to the rolling direction, that is, the $[01\bar{1}]$ direction. The dimensions of the test specimen are shown in Fig. 2 along with the crystallographic orientations of the material. The yield stress and the tensile strength of the material of this direction were about 302 and 411 MN/m^2, respectively. For this selection of loading axis, two of four feasible slip directions, that is, $[11\bar{1}]$ and $[1\bar{1}1]$, are made to be about ± 55 deg to the direction perpendicular to the loading axis in the (011) plane of the specimen surface, whereas the other slip systems, that is, [111] and $[\bar{1}11]$, are in the plane perpendicular to the loading axis. When loaded, therefore, it may be concluded that only the former two slip directions which are near to the maximum shear direction become active and there occurs little deformation along the thickness direction.

A fatigue crack was propagated from the central slit of 2.2-mm length and 0.3-mm width under pulsating tensile loading at the frequency of 10 Hz. When the crack propagated some distance from the slit and showed Mode I or Mode II crack opening behavior, the testing speed was reduced to 0.1 Hz and then the load was sometimes held at arbitrary levels during the loading or unloading cycle for the taking of photographs. Duration of a hold for photographing was about 50 s.

The deformation of the microscopically local region was measured by using the small markers (magnesium oxide crystals) which were uniformly distributed on the specimen surface. These markers were distributed on the specimen surface by holding the specimen for a short time over a gas of burning magnesium.

TABLE 1—*Chemical composition of the material used (weight percent).*

C	Si	Mn	S	O
0.006	3.03	0.09	0.009	0.0194

[2]The italic numbers in brackets refer to the list of references appended to this paper.

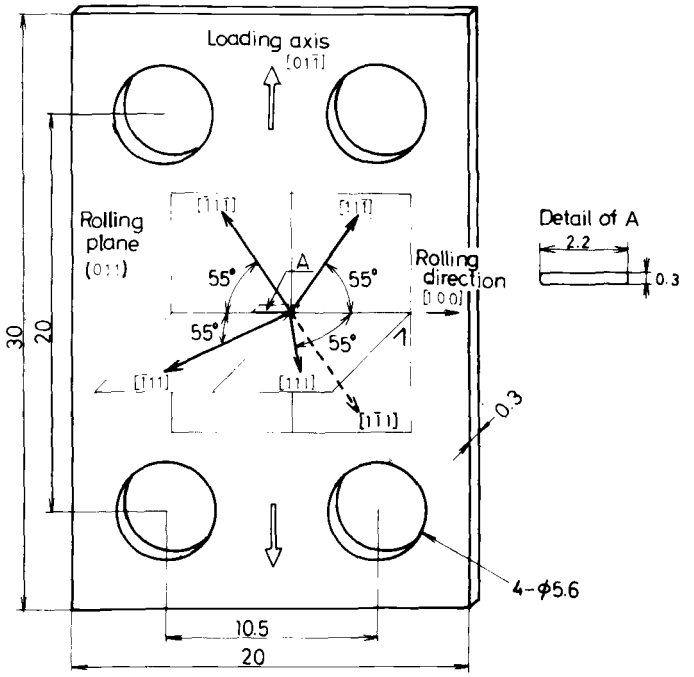

FIG. 2—*Dimensions of the test specimen and crystallographic orientations of the material.*

Experimental Results and Discussion

Crack Propagation by Mode I Opening

Figure 3*a* to *h* is an example of sequential photographs of fatigue crack propagation during one loading cycle of $K_{max} = 32.6$ MN/m$^{3/2}$ observed by the SEM. In this case, striations could be observed even near the specimen surface, as can be seen in Fig. 3*h*, and this spacing was confirmed to approximately coincide with the crack growth rate. The crack tip was found to be V-shaped and the tip angle, which was equal to 130 deg in this case, remained unchanged during both the unloading and loading cycles. And it was also found that the geometry of the crack surface behind the tip remained plastically undeformed. This means that slip occurred only at the apex of the crack tip, and thus successive slip of both upper and lower slip planes formed new surfaces at the crack tip during the loading cycle, which resulted in an increase of the crack-tip opening displacement (CTOD) and the crack length. Also, the crack closed backward from the tip by means of reverse slip at the apex during the unloading cycle. This behavior is similar to that reported by Neumann for a copper single crystal [*2*] and for a silicon iron single crystal [*3*].

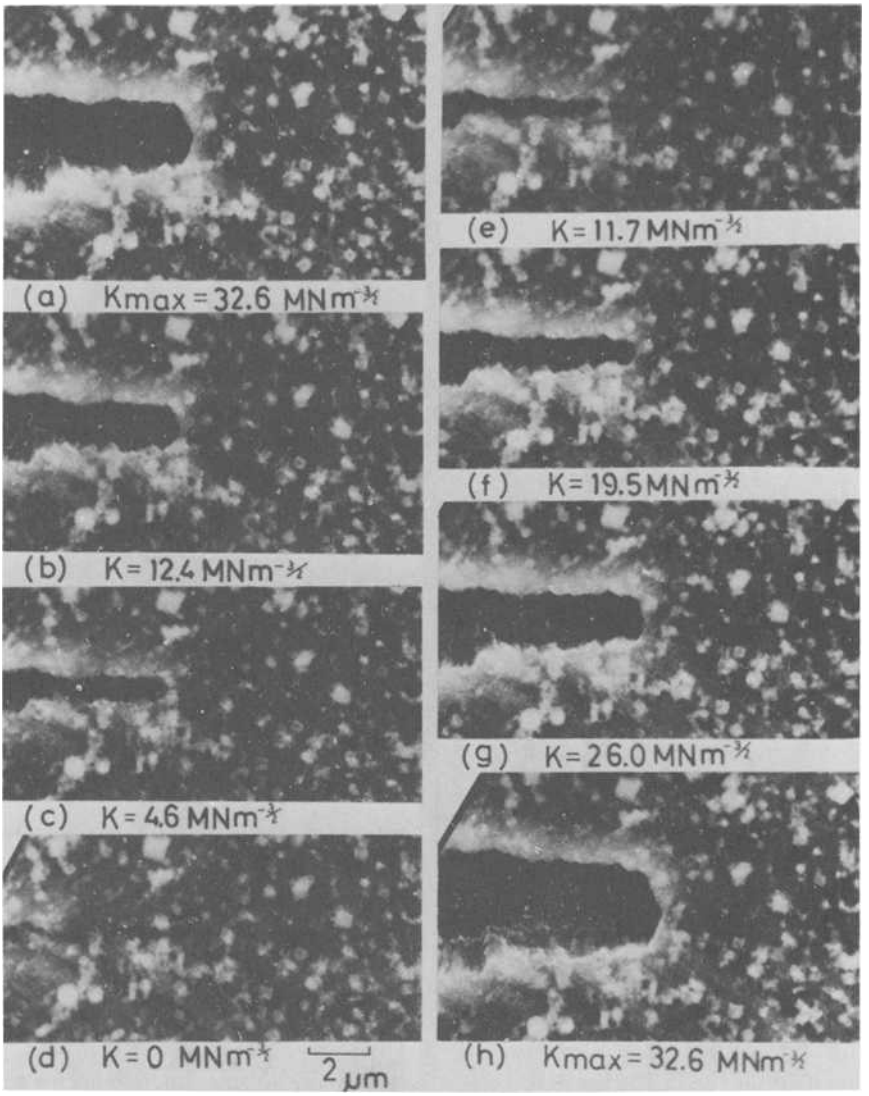

FIG. 3—*Sequential photographs of fatigue crack closure and opening during one loading cycle (in vacuum). Small white cubes distributed on the surface are magnesium oxide crystals used as a reference to measure deformation.*

Figure 4 shows the deformation near the crack tip from the state of zero load (Fig. 3*d*, shown by solid circles) to that of maximum tensile load (Fig. 3*h*, open circles). It was found that there occurred little deformation within the triangular region designated $A_2C_2B_2$. Deformation began to occur at the $A_2C_2B_2$ line, which passed through the apex of the crack tip, and almost uniform displacement was found in the region behind the $A_1C_1B_1$ line, passing through the crack tip of the last cycle. The deformation direction was found to be approximately ± 55 deg, which coincides with the slip directions of the material, and deformation in the reverse direction was found during the unloading cycle.

It may be concluded from the aforementioned observation results that the mechanism of fatigue crack propagation which will leave striation traces is explained by the alternating slipping-off process suggested by Pelloux [*4*]. However, the crack tip angle did not coincide with the included angle of the slip directions of the material. This discrepancy can be understood by considering the cross-slip mechanism suggested by Neumann [*5*]. According to his model, the crack-tip angle is usually larger than the included angle of the slip planes, and is determined mainly by the "coarseness of slip steps on the slip system," although this value seemed to be fixed by the experiments. In the experiments performed in this study, an angle of about 130 to 140 deg was observed for the V-shaped crack tips against 110 deg for the included angle of the slip directions. Also, a gradual increase of the tip angle with increase of CTOD was often observed, which formed a dull blunted round-shaped crack tip, although, even in this case, slip was found to occur only at the apex.

The yielded zone near the crack tip was a very narrow region bounded by lines of $A_1C_1B_1$ and $A_2C_2B_2$, as shown in Fig. 4, but it seemed to broaden

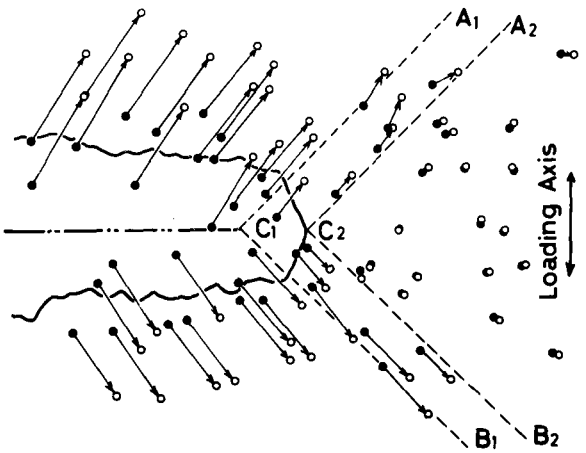

FIG. 4—*Schematic illustration of deformation near crack tip.*

between 55 and 83 deg with the increase in distance from the crack tip as shown in Fig. 5.

It was found that the crack began to open at the point a small distance back from the tip observed at the maximum tensile load of the last cycle in the vacuum environment (3×10^{-5} torr) as seen in Fig. 3*e* (see also Figs. 8 and 9). This fact suggested that rewelding occurred at the tip during the unloading cycle. On the other hand, Fig. 6*a* to *f* shows the behavior of a fatigue crack which was propagated in air to the stage of Fig. 6*a* and then brought into the vacuum chamber of the SEM and cycled for observation. In this case, the crack was found to open at the tip of the last cycle, and no rewelding was observed. It may be concluded that the oxidization of newly formed surface in an air environment prevents rewelding when load is released. But the deformation behavior of the following loading cycle is found to be almost the same between the air and vacuum environments, so rewelding can be considered to affect only the amount of crack length but not the following slipping-off process.

Figure 7 shows the relation between the current value of the stress intensity factor, K, and the corresponding CTOD during the loading cycle. The opening point was found to be about 6 MN/m$^{3/2}$ for both cracks, irrespective of the amount of rewelding, and the CTOD was found to be proportional to the square of the K-value for magnitudes greater than the opening value. The relations between CTOD and crack length during the loading cycle are shown in Fig. 8 for the case of $K_{max} = 26.4$ MN/m$^{3/2}$ and in Fig. 9 for $K_{max} = 28.2$ and 32.6 MN/m$^{3/2}$. Solid lines show the relations of the cracks with V-shaped crack tips and broken lines represent those with dull blunted round-shaped cracks. The crack length was measured as the distance from the crack tip at the maximum tensile load of the last cycle.

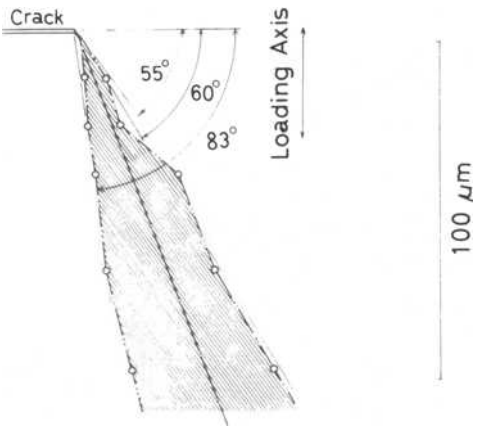

FIG. 5—*Yielded zone around fatigue crack tip.*

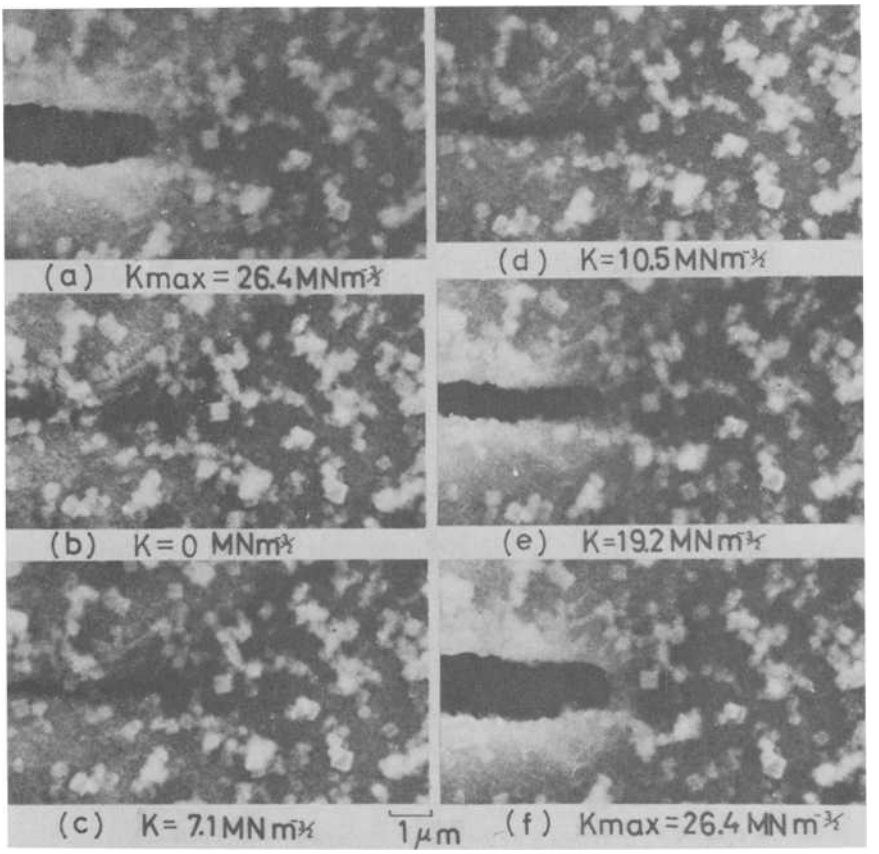

FIG. 6—*Sequential photographs of fatigue crack closure and opening during one loading cycle (propagated in air up to* (a) *and subsequently observed in vacuum).*

So the negative value represents the amount of rewelding. It should be noted that the crack growth length per cycle can be calculated from the model shown in Fig. 10, which was derived from the aforementioned observation results, when there is no rewelding, that is

$$\Delta a = \frac{1}{2}\left\{\tan\left(90 \text{ deg} - \frac{\alpha}{2}\right) + \tan\left(90 \text{ deg} - \frac{\beta}{2}\right)\right\} \text{CTOD}$$

where α is the included angle between the activated slip planes, and is equal to 110 deg in this material, and β is the crack tip angle. If the observed values of β are substituted in this equation, that is, 130 deg for the AV5 crack in Fig. 8 and 137 deg for the V8 crack in Fig. 9, we obtain the following relations: $\Delta a = 0.58 \cdot \text{CTOD}$ and $\Delta a = 0.55 \cdot \text{CTOD}$ for the AV5

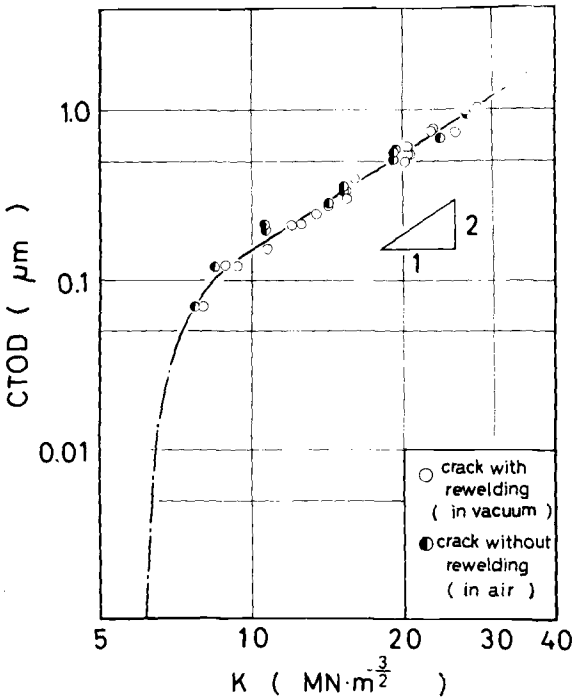

FIG. 7—*Increase of CTOD during loading cycle as a function of* K.

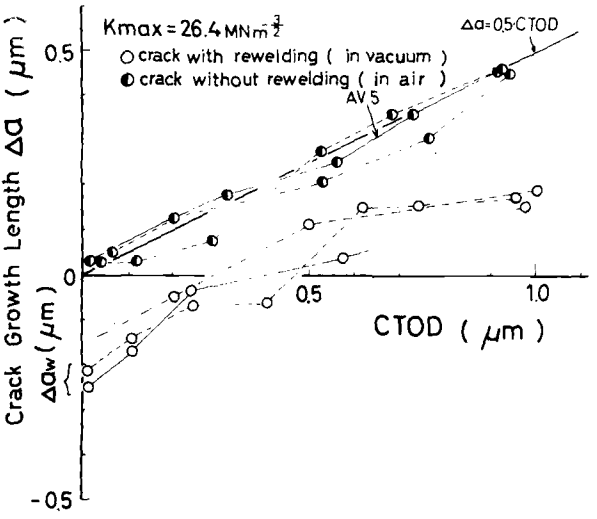

FIG. 8—*Relation between CTOD and crack growth length during loading cycle for* K_{max} *= 26.4 MN/m*$^{3/2}$.

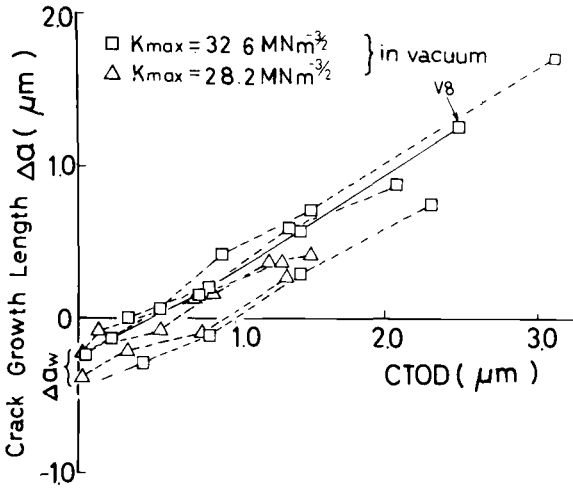

FIG. 9—*Relation between CTOD and crack growth length during loading cycle for* K_{max} = *28.2 and 32.6 MN/m*$^{3/2}$.

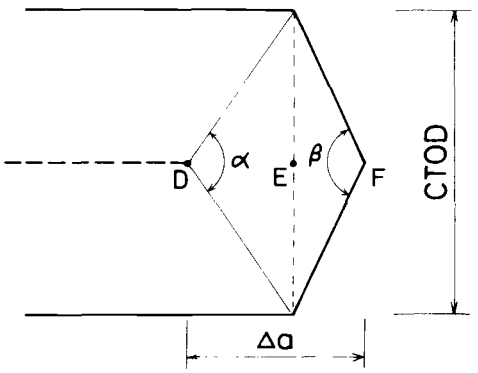

FIG. 10—*Schematic illustration of the relation between CTOD and crack growth length.*

and V8 cracks, respectively. In Fig. 8 this relation for the cracks without rewelding is found to be approximately expressed by the equation $\Delta a = 0.5 \cdot CTOD$. Moreover, it can be seen that the slope of this relation for the cracks which show rewelding exists within the range 0.5 and 0.6 and that the crack growth length is reduced by the amount of rewelding.

Thus the crack propagation length can be related with CTOD by considering the slip direction, crack tip angle, and the amount of rewelding.

This relation may be represented by the following equation for the material used in this study

$$\Delta a = (0.5\text{-}0.6) \times \text{CTOD} - \Delta a_w$$

where Δa_w is the length of rewelding. This equation does not seem to be strongly affected by the load level or the amount of CTOD for the range of experimental values determined in this study.

Based on the experimental results just given, a model for fatigue crack propagation by Mode I opening is proposed in Fig. 11.

Crack Propagation by Mode II Sliding

During fatigue tests conducted by the procedure outlined in the foregoing, cracks sometimes propagated in a zigzag manner and showed Mode II

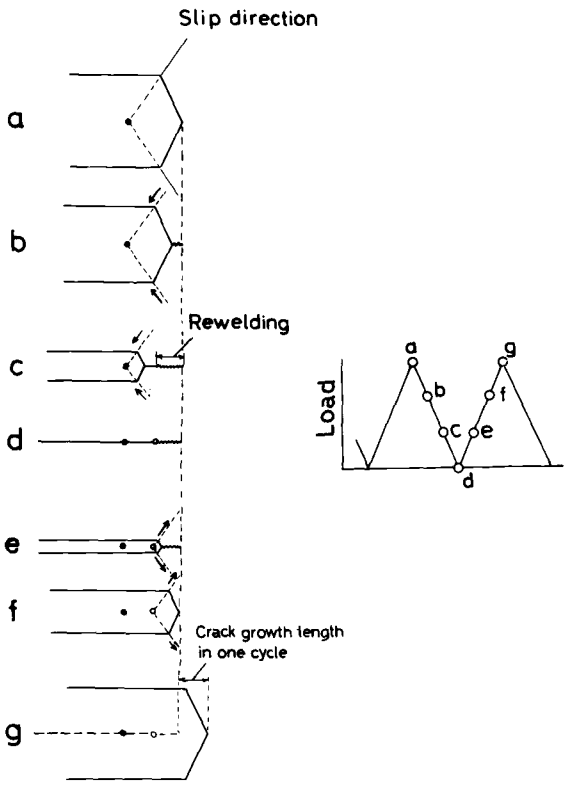

FIG. 11—*Suggested fatigue crack propagation model for Mode I opening (in vacuum, where rewelding occurs).*

deformation behavior (actually, there still exists a tensile stress component, so the deformation is of mixed mode of I and II). Figure 12*a* to *g* shows an example of sequential photographs of fatigue crack propagation by Mode II sliding, and Fig. 13 shows a schematic illustration of deformation near the crack tip sliding in this mode. Various symbols represent the deformed points corresponding to the load level shown in the upper right-hand side of Fig. 13. It was found that the shearing displacement occurred by means of slip along the crack propagation direction, although some tensile component was observed behind the crack, so that this crack may be considered as sliding in Mode II at the crack tip. It was found also that the shearing displacement was nearly constant in the region near the crack tip, so the shearing component of the displacement in the crack direction between the maximum and the minimum load in the neighborhood of the crack tip was employed as a crack-tip shearing displacement (CTSD) for Mode II sliding, which is shown by the symbol ΔS in the figure. The length designated by the single arrow represents the slipped length after crack closure. Crack growth length, Δa, was also measured and the correlation to the crack tip shearing displacement was examined. Although some scatter was observed, it was found that the ratio of $\Delta a/\Delta S$ was nearly equal to 0.16. This corresponds to a loading condition where the K_{II} component in the crack direction was about 8 to 12 $MN/m^{3/2}$. This value of $\Delta a/\Delta S$ is fairly small in comparison with the ratio of Δa/CTOD (~ 0.55) for Mode I opening. Moreover, it was found that this value did not discernibly differ between the air and vacuum environmental tests. One reason for understanding the aforementioned behavior may be that the ratio of shearing displacement after crack closure to the total slipped length is fairly large for Mode II sliding so that rewelding at the tip occurs easier for Mode II sliding than in the case of Mode I opening for both environments.

Conclusions

1. Direct observation of fatigue crack propagation under Mode I and Mode II deformation was successfully performed on a grain-oriented silicon iron with a specially designed fatigue testing apparatus which could operate in an SEM.

2. In the case of crack propagation by Mode I opening, successive slip of both upper and lower slip directions passing through the apex of the crack formed a new surface at the tip and increased CTOD under increasing loading. The crack closed from the tip by means of reverse slip during decreasing loading. Thus, the fatigue crack propagation mechanism was confirmed to be an alternating slipping-off process at the apex.

3. The crack propagation length could be quantitatively correlated with

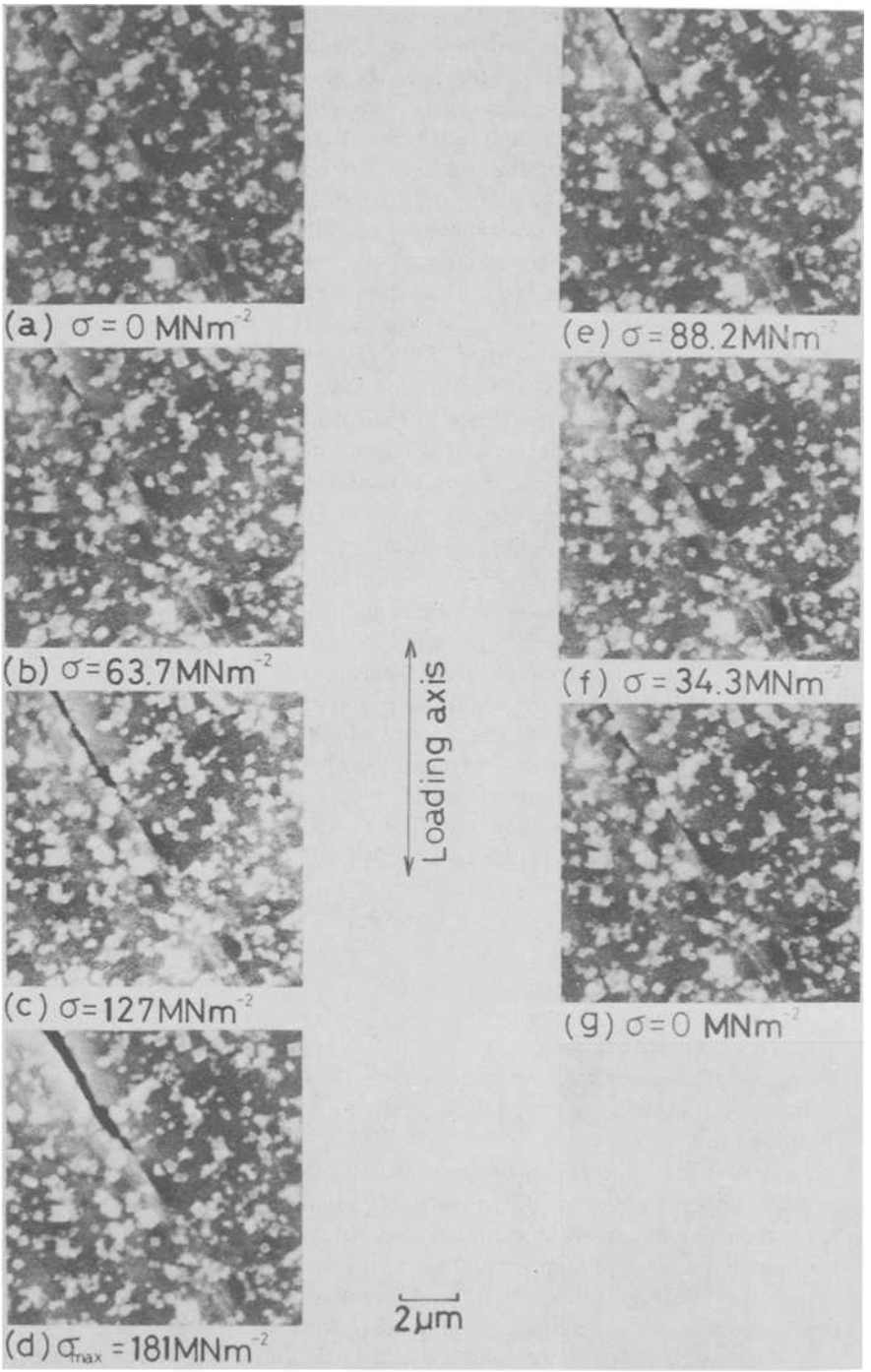

FIG. 12—*Sequential photographs of fatigue crack propagation by Mode II sliding.*

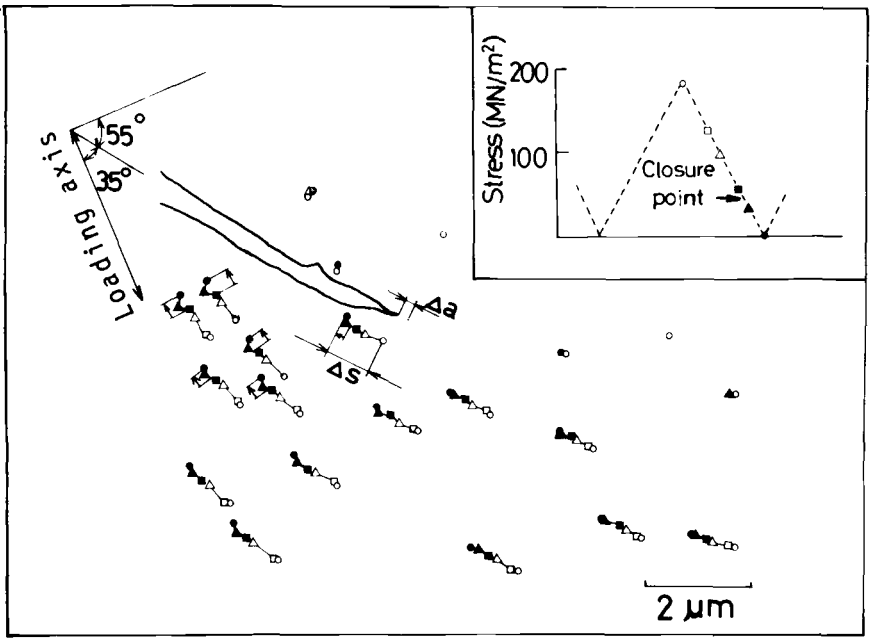

FIG. 13—*Schematic illustration of deformation near the fatigue crack tip for Mode II sliding.*

the CTOD by considering the activated slip directions of the material and crack tip angle, and a crack propagation model was suggested.

4. Rewelding at the crack tip, however, could occur during unloading in the vacuum environment, and the crack propagation length was reduced by that amount from the aforementioned relation.

5. The ratio of the crack growth length to the crack tip shearing displacement for Mode II sliding was found to be fairly small compared with the ratio of the crack propagation length to CTOD for Mode I opening, and not to be seriously affected by the difference in environments between air and vacuum.

References

[1] Kikukawa, M., Jono, M., and Adachi, M. in *Proceedings*, Symposium on Mechanical Behavior of Materials, Kyoto, Japan, 1974, p. 307.
[2] Neumann, P., *Acta Metallurgica*, Vol. 22, 1974, p. 1155.
[3] Neumann, P., Vehoff, H., and Fuhlrott, H. in *Proceedings*, Fourth International Conference on Fracture, Waterloo, Ont., Canada, Vol. 2, 1977, p. 1313.
[4] Pelloux, R. M. N., *Transactions*, American Society for Metals, Vol. 62, 1969, p. 281.
[5] Neumann, P., *Acta Metallurgica*, Vol. 22, 1974, p. 1167.

DISCUSSION

D. Davidson[1] *(discussion)*—The paper reports very interesting work and affords one of the few high-resolution, direct observations of the tip of a propagating fatigue crack published to date. The interesting findings are that the crack tip opens by a double slip-off mechanism (Figs. 3 and 4), as has been observed by Neumann more macroscopically for both copper and Fe-3Si single crystals, and that the crack advance per cycle is $\Delta a = (\sim 0.6)$ CTOD-Δa_w where Δa_w is a term said to relate to the rewelding of the crack upon unloading; $\Delta a_w \cong 0.25$ to 0.4 μm for vacuum, and zero for an air environment as shown in Figs. 8 and 9. The relation between stress intensity and CTOD is shown in Fig. 7 to be CTOD $= 0.0015\ K^2$ between $K = 10$ and 30 MN/m$^{3/2}$ both for air and vacuum. The reader will find other interestng observations as well.

The work reported, however, while useful and interesting, does bring up questions regarding the way it is to be interpreted. The main points of discussion, as I see them, are as follows.

1. One of the experiments used a grain of Fe-3Si oriented so that the slip systems were at ± 45 deg to the loading axis. This configuration was deemed to give plane strain, because slip perpendicular to the specimen surface is suppressed, and this is considered to be the condition deep within a thick specimen of a nontextured polycrystalline metal. The sequential photographs of Fig. 3 and sketch of Fig. 4 show predominantly Mode I opening, as opposed to the mixed-mode behavior illustrated in Fig. 13 for an unoriented slip geometry. An estimate of the plastic zone size

$$r_p = \alpha \left(\frac{\Delta K}{\sigma_y} \right)^2$$

where $\alpha = 0.1$ gives $r_p = 1.16$ mm. With a specimen thickness of 0.3 mm, this gives $t/r_p = 0.25$. For most cases, plane-strain conditions are not considered to be met until this ratio is 25, that is, until the specimen is 100 times too thin for plane-strain conditions to pertain for the K-levels used in the experiment. On this basis, then, does the special slip geometry represent a typical deep-section condition for an untextured material?

2. The mechanical properties of Fe-3Si depend strongly on the thermomechanical treatment used, and critically on the temperature of testing. At 20°C this material can exhibit nearly planar slip characteristics and can have a relatively low plane-strain fracture toughness. Is the combination of

[1] Division of Engineering Sciences, Southwest Research Institute, San Antonio, Tex. 78284.

special slip geometry and special material properties responsible for the results shown in Figs. 3 and 4?

3. The observed opening of the crack some distance behind the tip position of the previous cycle during cyclic loading in a vacuum may be due to compressive stresses which exist in the plastic zone near the crack tip. These stresses arise due to the material in the plastic zone being deformed during the tensile mode of loading, with subsequent partial reversal of that slip occurring on unloading due to the constraints of the material surrounding the plastic zone. The magnitude of these compressive stresses are not known, having never been directly measured.

The effect of environment on crack tip plasticity has been demonstrated in numerous instances. For low-carbon steel, both the extent of subcell formation near the crack and the mode of crack-tip deformation are altered by normally humid air. There is adequate reason to believe that the magnitude of the compressive stresses would be environmentally altered; therefore, the magnitude of the opening load would also be altered.

The authors make two observations which may refute the foregoing argument. The first is that for both environments the opening stress intensity was found to be 6 $MN/m^{3/2}$; it seems likely that a change in compressive stresses would change this value. The other finding is that the slope of the crack opening (Δa) versus CTOD relation is nearly unaltered by the environment.

4. The mixed-mode I and II crack-tip opening shown schematically in Fig. 13 may be more typical of the situation found in randomly oriented polycrystalline metals. The Mode II seems to be causing the formation of one shear band ahead of the crack tip instead of two, as seen in the oriented slip case. There is insufficient information given to further evaluate this experimental observation.

Summary—One of the main questions raised by this paper is that of the slip geometry of a "typical" crack tip in a nontextured polycrystalline specimen. Perhaps the most interesting observation is that of crack opening alteration due to a water vapor environment; several explanations for this phenomenon are possible. The displacement diagrams shown for the Mode I and the mixed-mode cases are interesting, but represent only a portion of the total plastic zone; larger-area, lower-magnification photographs would allow a more complete interpretation of crack-tip plasticity for the cases observed.

P. Mayr[2] (*discussion*)—In the introduction to their paper the authors point to the fact that investigations with sheet specimens are not representative of the behavior of the bulk material in the plastic zone of an

[2]Institut fur Werkstoffkunde I, Universitat Karlsruhe (TH), Karlsruhe, Federal Republic of Germany.

advancing crack because of the lack of plane-strain conditions. Therefore they try to overcome this difficulty by using specimens in which the grains are oriented in such a way that deformation through the thickness of the specimens is impeded. In addition to this condition, it must be assured that through the thickness of the sheet specimen there are at least 10 grains so that one could assume polycrystalline deformation behavior or correspondingly bulk material behavior. In spite of all these difficulties the results of the direct observation of an advancing crack in the scanning microscope could yield some insight into the mechanisms which are responsible for stable fatigue crack propagation.

The photographs taken at different times during a loading cycle show two typical shapes of the crack tip. In one case a V-shaped crack tip is observed whereas in another case a dull blunted round shape is revealed. As the differences in the shape of the crack tip could be due to different crack propagation mechanisms, there is the question if any criteria can be given for their occurrence. In this connection it is of interest to know if the V-shape could be observed only if the crack tip is in the interior of a surface grain and changes to the round form when the crack reaches the grain boundary. On the other hand, it seems possible that small differences in the orientation of the surface grains are due to the shape changes which could be proved using random oriented specimens. In order to throw some light on the question of whether different mechanisms are active, it would be of interest to know if there are any changes in the fracture surface when the crack tip changes its shape, and, additionally, if the changes of frequency during the experiments could influence the results.

A second part of the investigation deals with the influence of environment, and it is concluded from photographs (Fig. 3) that partial rewelding of the crack occurs in specimens fatigued in the vacuum chamber of the SEM whereas specimens fatigued in air showed no rewelding, looking on the surface of the specimen. The very good idea to stick magnesium oxide particles to the surface of the specimens to determine plastic deformation at the surface could also be used, to check possible rewelding of the crack. Applying this to Fig. 3*e*, it seems questionable if rewelding actually occurs. Is there any further evidence for rewelding processes of the crack? It is pointed out that the slipping-off process at the crack tip is not influenced by environmental conditions. If one looks to the quantitative relations given in the paper, it holds for air $\Delta a = 0.55$ CTOD and $\Delta a = 0.58$ CTOD, respectively, whereas for the vacuum condition $\Delta a = 0.50$ is observed. Is this difference in the proportionality factors not a consequence of an influence of environment if you mention a similar relation given by Neumann [5] which shows that the proportionality factor is strongly influenced by homogeneity of slip in the neighborhood of the crack tip? An interesting detail of the observations is the result that the amount of rewelding Δa_w is not strongly affected either by the imposed load or by the amount of CTOD.

Is it correct to conclude that Δa_w is a function only of the environmental conditions?

The paper shows cracks which propagate under an angle of about 60 deg to the tensile axis of the specimen. This inclined crack advance is assigned with Mode II crack propagation. From Fig. 13 it could not be seen whether the crack direction is coincident with the slip direction in the observed grain. If this is true, then it seems reasonable to designate this crack propagation behavior as slipband cracking or Stage I advance, and it would also explain the small $\Delta a/S$ values. In opposition to this assumption, however, is the reported independence of $\Delta a/S$ from the environment.

J. Simmons[3] (*discussion*)—I was fascinated to see the kind of work that Dr. Jono just showed. I am surprised that Professor Mura of Northwestern University didn't jump up here, because in fact what Dr. Jono showed relates to a well-known result in dislocation theory.

From the point of view that one can sum up the displacement associated with a material point during the crack motion, and if one knows the loading, one can calculate theoretically the elastic displacement due to that loading. Therefore, one can actually calculate the net microscopic dislocation flow, or plastic flow, around the crack tip.

I wonder if this has been done by investigators in the fatigue area?

H. Liu[4] (*discussion*)—I have two questions. First, what kind of vacuum did you use? Second, how do the measured crack-tip opening displacements compare with the calculated values?

M. Kikukawa, M. Jono, and M. Adachi (*authors' closure*)—We appreciate the comments and questions on our paper by Dr. Davidson, Dr. Mayr, Dr. Simmons, and Prof. Liu.

Concerning the comments by Dr. Davidson, we would like to say that the main purpose of this paper is to see the dynamical behavior of crack propagation at the specimen surface by the SEM similar to that of the plane-strain condition, which is the situation for the specimen interior. From this point of view, we could succeed in doing so by selection of the special orientation of the material regardless of the specimen thickness. Strictly speaking, however, we also have a question whether the crack propagation behavior shown here is the same as that of a nontextured polycrystalline material or not, although we think that the crack propagation mechanism of Mode I suggested in the paper, that is, the alternating slipping-off process at the crack tip apex, may be applicable to that of polycrystalline material, if the CTOD is fairly small compared with the

[3]Center for Materials Science, National Bureau of Standards, Washington, D.C. 20234.
[4]Department of Chemical Engineering and Material Science, Syracuse University, Syracuse, N.Y. 13210.

grain size and if the plane-strain condition is satisfied. This problem should be investigated.

For the second and third points of Dr. Davidson's question, the effects of environment are very important for crack propagation, as suggested in the paper, and should be the object of more sophisticated study. However, the "in air" condition we referred to is the situation that the crack was propagated in air to the maximum load of the last cycle, and subsequent behavior during the unloading and loading cycle was observed in the vacuum of the specimen chamber of the SEM. So what we can say here about the environmental effect is the change of behavior during the subsequent unloading cycle, and in this case we obtained the result that it affected the amount of rewelding of the crack tip but not the slipping-off process of the next loading cycle. Therefore, it is not surprising that the opening load and the slope of the Δa-CTOD relation are unaltered for these environments.

Finally, we agree with you that more information about the deformation behavior of a larger area for both Mode I and II cracks is needed in order to understand the crack-tip plasticity. At present, however, we have a small number of photographs which cover the larger area around the crack tip, because we have concentrated attenton on behavior near the tip. For the next step of our study we are preparing to observe the behavior of the larger area around the tip.

Concerning the questions by Dr. Mayr, we must explain first the specimen condition. The grain size of the material is about 2 to 4 mm, which means that there exists only one grain through the thickness, so that the crack opening behavior observed here is rather similar to that of a single crystal, although, in this case, general yielding, where slip runs through the specimen width, is suppressed by the grain boundary of the distant place.

As to the question concerned with the crack-tip shapes, it was found that both V-shaped and dull-blunted cracks propagated by the alternating slipping-off process at the apex. The difference of crack-tip geometry can be caused by the difference of the current amount of cross-slip at the crack tip apex. Also, the ratio of crack growth length to CTOD did not differ between the two types of cracks. Therefore, we consider that the mechanism of crack opening is basically the same for both cracks.

For the third point of the question, if you look carefully at the original photograph of Fig. 3, you may recognize the crack opening location. However, we determined the rewelding amount from the sequential measurement of the relation between CTOD and $\Delta\alpha$, as shown in Figs. 8 and 9.

Concerning the effect of environments, please see the second answer to Dr. Davidson. We think that the difference of proportionality factor between 0.5 and 0.6 would be meaningless considering the scatter of measured points.

Although rewelding length Δa_w was not affected by the load level for the range of this experiment where the range ΔK was from 26.4 to 32.6 $MN/m^{3/2}$, it would be affected by many factors such as materials and environments and also by load level if it was changed widely. The effects of such factors on rewelding is a problem to be studied.

As to the last question by Dr. Mayr, Mode II crack propagation shown in this experiment is considered to be similar to Stage I crack advance as he suggested. Therefore, we also consider that the propagation mechanism of this crack can be employed as a model for a Stage I crack. However, the magnitude of CTSD and Δa is largely different from those of the Stage I crack found at the crack initiation stage of the usual materials. So the effect of environments might be different between them.

Finally, we wish to answer the questions and comments of Prof. Liu and Dr. Simmons. The vacuum condition we used was 3×10^{-5} torr. and, concerning the calculation, we tried to calculate the CTOD by using some homogeneous isotropic models to compare with the experimental results. However, calculated results were not satisfied, probably because of the anisotropy of the material as well as the uncertainty of the material constants. So now we are looking for a suitable model for calculation.

D. L. Davidson[1]

The Study of Fatigue Mechanisms with Electron Channeling

REFERENCE: Davidson, D. L., "**The Study of Fatigue Mechanisms with Electron Channeling**," *Fatigue Mechanisms*, Proceedings of an ASTM-NBS-NSF symposium, Kansas City Mo., May 1978, J. T. Fong, Ed., *ASTM STP 675*, American Society for Testing and Materials, 1979, pp. 254-275.

ABSTRACT: The application of electron channeling techniques to the study of material response under cyclic loading conditions is providing some useful information on mechanisms from bulk specimens. Most of the effort thus far has been on examining the plastic zone parameters (size, shape, and strain distribution) but other useful information may be obtained as well (such as crystallographic interactions). Subcells may be observed directly in bulk specimens, and environmental effects may be studied. This paper reviews many of the details of the application of electron channeling to fatigue mechanism study, references results, and illustrates some of the concepts. A few of the possible future uses are also discussed.

KEY WORDS: aluminum alloys, crack propagation, electron channeling, electron diffraction contrast, fatigue fracture (materials), plastic properties, strain

Electron channeling is the term given the phenomenon of crystallographic selective electron absorption in crystals. Since it was discovered by Coates [*1*][2] in 1967, the phenomenon has been extensively utilized in the scanning electron microscope (SEM), although it can be, and has been, used in other systems having suitable scanning and detector capabilities (for example, scanning transmission and scanning Auger systems). One of the principal advantages of utilizing the electron channeling phenomenon is that it allows an interrogation of the crystal structure of a bulk solid (organic or inorganic) specimen of relatively large size over an adjustable surface area and to an adjustable depth of penetration. The technique is thus unique and versatile, although many aspect of this versatility have not yet been explored. As with any technique, electron channeling also has some disadvantages, which are discussed in the course of this paper. An extensive body of information exists

[1]Staff scientist, Department of Materials Sciences, Southwest Research Institute, San Antonio, Tex. 78284.

[2]The italic numbers in brackets refer to the list of references appended to this paper.

on electron channeling: the physics of the phenomenon, the theory, and its applications. For more information on aspects of electron channeling not covered in this paper, the reader is referred to the bibliography by Joy and Newbury [2].

Both the initiation and crack propagation phases of fatigue damage may be studied using the electron channeling phenomenon, although at present little use has been made of it in the study of initiation; thus, this paper will concentrate on crack propagation and what has been and may be learned by the use of channeling.

Electron channeling may be usefully exploited in the SEM in two ways:

1. Channeling, or grain, contrast.
2. Channeling patterns.

A description and discussion of the uses of each of these techniques are given in the following sections.

Channeling Contrast and Its Use

Channeling contrast is useful for the study of plasticity in general, but it is particularly useful in the study of creep and fatigue deformation [3].

Obtaining Channeling Contrast in the SEM

Channeling contrast may be obtained in any SEM equipped with specimen current or backscattered electron imaging systems, and is best done with the specimen perpendicular to the incident electron beam. Reversed biased Everhart-Thornley detectors (normally used for secondary electron collection) are not likely to give very satisfactory results because of their physical location relative to the backscattered electrons, the intensity of which falls as the cosine of the angle away from the incoming beam direction. Many of the best results reported have been made by using solid-state backscattered electron collectors positioned around the electron beam either as an annular collector or as a number of chips, but subtending a large solid angle relative to the focal point of the beam on the specimen surface. Such a system has a high collection efficiency and can provide very good high-resolution information up to TV scan speeds (system performance depends very much on the details of collector and amplifier design, electron optical conditions in the microscope, and on the specimen metallurgy and its preparation). An example of channeling contrast is shown in Figure 1. The contrast mechanism originates in the different crystallographic orientation between adjacent grains; each grain channels, and backscatters, a different fraction of the electrons impinging on it, thereby giving rise to a different gray level. The angular relation between impinging beam and crystal orientation sets the gray level, which may be altered by changing this relation, as by specimen translation or rotation. Very large grains viewed at low magnification may

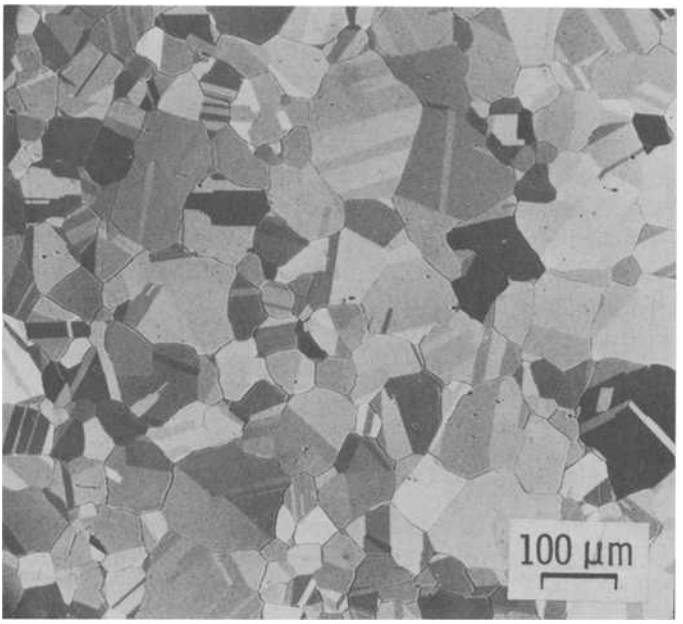

FIG. 1—*Channeling contrast from the grain structure of 304 stainless steel, 20 keV.*

be seen to change gray level across the grain, the manifestation, in fact, of a channeling pattern as it was first discovered on a single crystal [*1*], and is a factor which must be considered when using this technique [*3*].

The Use of Channeling Contrast

Cyclic deformation causes the regular grain structure of many metals to develop a substructure which may be observed by channeling contrast. A number of metallurgical and experimental factors determine the propensity for a metal to form dislocation cells, subgrains, or subcells, which are characterized by rotations of the material within each subcell relative to its neighbors. It is this misorientation (as small as 0.2 deg)[3] which may be detected by channeling contrast. An example of the subcell formation around a fatigue crack in Fe-0.05 weight percent carbon steel is shown in Fig. 2. From micrographs such as this, it has been possible to (1) determine the effects of cyclic stress intensity (ΔK) on plastic zone size [*4*], (2) determine the effect of environment on plastic zone size [*5*], (3) measure the energy dissipated in the lattice as the crack propagates [*6*], and (4) measure the

[3]This was determined from creep-formed subcells in platinum using selected-area electron channeling patterns from adjacent regions.

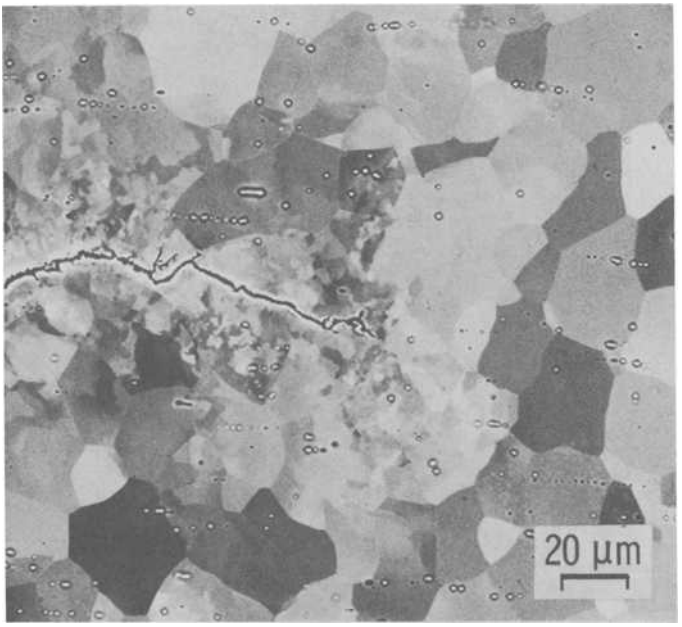

FIG. 2—*Subcell formation due to fatigue crack propagation in dry nitrogen as observed by channeling contrast: Fe-0.05 weight percent carbon steel,* $\Delta K = 10\ MN/m^{3/2}$, *30 keV.*

energy equivalent of a wet air environment on the crack propagation energy [*6*]. The energy determination requires a knowledge of the relation between equilibrium average subcell size and the cyclic energy dissipation required to obtain it, which can also be determined by using channeling contrast [*6*]. Future work utilizing this bulk subcell observational technique will include dynamic observation of subcell formation during cyclic loading experiments in the SEM and investigation of time-dependent cyclic loading (creep-fatigue interaction) and environmentally influenced cyclic loading, particularly where stress corrosion is an important factor.

The formation of subcells, as clearly definable and measurable regions, does not occur equally in all materials. Subcell formation due to cyclic loading has been studied by channeling contrast in 304 and 316 stainless steels [*7*, *8*], in Fe-3Si, in Fe-0.05 weight percent carbon, and to a limited extent in several aluminum alloys. An example of channeling contrast in 7075-T6 is shown as Fig. 3. Although no systematic study has been made to date, the extent of subcell formation in aluminum alloys appears to be more dependent on the orientation of specific crystallites relative to the crack than in the other materials which have been examined. Compared with the stainless steels and iron alloys investigated, the aluminum alloys do not form subcells extensively. Those cells that do form in aluminum alloys are comparably

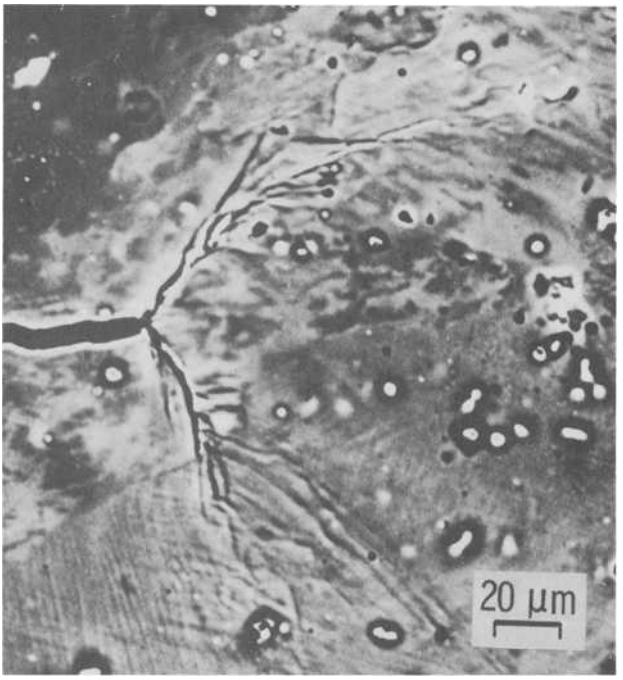

FIG. 3—*Subcell formation in the vicinity of a fatigue crack tip subjected to a one-cycle overload of* $K = 26\ MN/n^{3/2}$ *as observed by channeling contrast: 7075-T6 aluminum alloy, 20 keV.*

small and close to the crack plane, occupying only a small portion of the total plastic zone. Thus, the technique of energy dissipation measurement developed for the low-carbon steel does not seem as applicable for these alloys.

Selected-Area Electron Channeling Patterns and Their Use

Obtaining Channeling Patterns in the SEM

Selected-area electron channeling patterns (SACPs or SAECPs) are patterns produced in a small surface area by rocking the beam about a focal point at the specimen surface (as opposed to the patterns seen on large single crystals at low magnification due to the large angular change in scanning beam incidence). The SEM electron-optical column is configured so that the beam is made to cross over the column axis at the specimen surface. For double-deflection scan systems with electromagnetic lens systems, two methods of producing SACPs have been worked out: the deflection-focus method and the after-lens deflection method. Both methods have some

advantages and disadvantages [*9*], and must be used with an understanding of the instrumental parameters involved. Each method suffers from problems with lens aberrations, although some SEM manufacturers have dealt with these problems more than others. These aberrations limit the minimum size of the surface area being interrogated by the beam. To date, the smallest spot size reported [*10*] has been approximately 1 μm in diameter, which was obtained using special equipment, although there is no theoretical limitation to obtaining smaller spot sizes. For most of the currently available SEM equipment, a minimum spot size of 5 μm is possible. One of the ways of minimizing spot size is by minimizing rocking angle, but that also minimizes the information available in the pattern; thus, the parameters chosen for most channeling investigations of cyclic deformation will probably involve a compromise between minimum spot size and maximum information retrieval. Conversely, spot sizes of up to several hundred micrometres may be readily obtained, and there may be instances where it is useful to average the information collected from a larger area.

Orientation Dependence

As determined by Coates soon after discovery of the electron channeling pattern, Fig. 4, the patterns are uniquely orientation dependent, in the sense of a Laue X-ray pattern or a transmission electron microscope (TEM) Kikuchi pattern.[4]

The most frequent use of SACPs has been for crystal orientation (for example, see Ayers and Joy [*12*]). For orientation purposes, the largest portion of the stereographic triangle obtainable is desired; thus, the largest rocking angle of the beam is required, and again a compromise must be made between spot size and information retrievable. The use of the orientation capability of the SACP is illustrated later.

Strain Measurement

The other use of SACPs is derived from the fact that changes occur in a channeling pattern when the material interrogated has been deformed plastically.[5] The patterns contain pairs of dark/bright lines, called channeling bands. Each line represents a Bragg reflection angle [*11*], and as the dislocation density increases, the lattice structure is disrupted to an in-

[4]Electron channeling patterns were first called Coates patterns, then pseudo-Kikuchi patterns because of their resemblance to Kikuchi patterns. As the mechanism of the origin of channeling patterns became better understood, the name was changed to prevent confusion between the physics of the electron channeling phenomenon and that of the formation of Kikuchi patterns. See Ref *11*.

[5]There may also be changes in the patterns due to elastic deformation, but this point has not been thoroughly investigated.

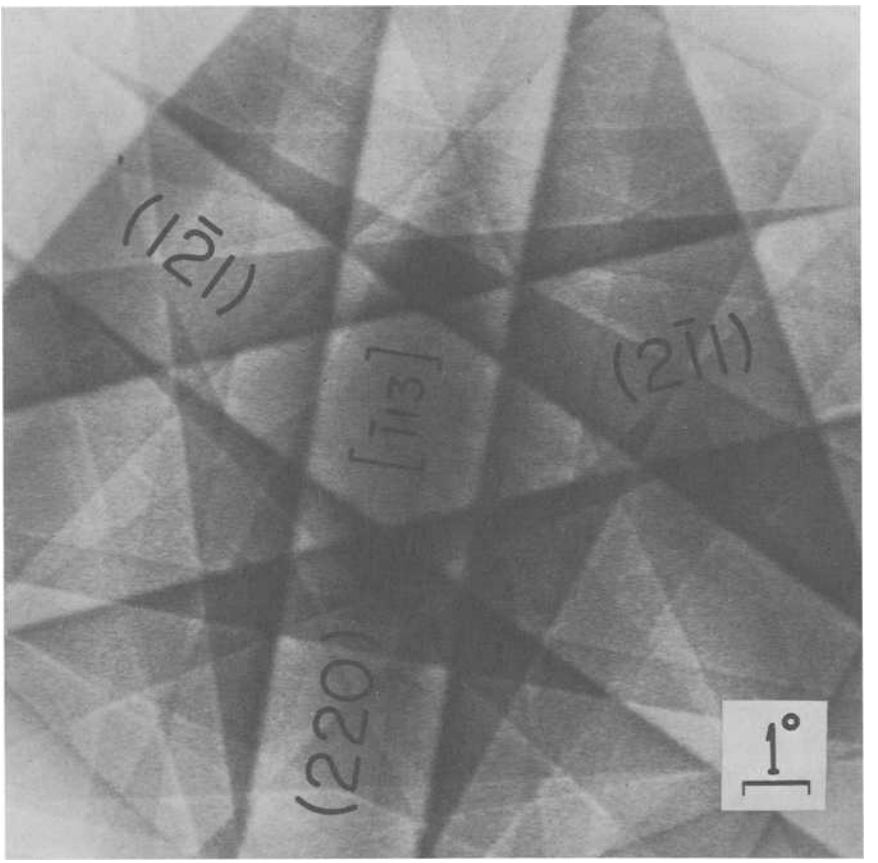

FIG. 4—*Selected-area electron channeling pattern from 2024-T4 aluminum alloy showing the crystallography of the area observed.*

creasing extent with a corresponding increase in width of the bright/dark line. Next, second and higher-order lines disappear, as do bands of subtle contrast from higher indice atomic planes. Finally, the dislocation density becomes sufficient to render the patterns unrecognizable. Quantification of this process is difficult because of the large amount of information in the patterns. For single crystals, or specific orientations of grains in a polycrystalline metal, contrast change measured across a channeling band may be related to the magnitude of strain. Ruff [*13*] has taken this approach in his study of wear tracks in iron. Stickler, Hughes, and Booker [*14*], who were among the first to investigate channeling pattern changes due to deformation, measured the angular width of the highest-order lines they could find on a pattern, and related this to dislocation density, as measured by TEM.

When working with fatigue cracks in commercial polycrystalline metals, another approach is necessary. Tapered strain-calibration specimens have been utilized [*15*] to obtain, for each value of tensile strain, SACPs from a number of grains so that orientation effects might be judged visually. The procedure is then to compare the channeling pattern changes in this calibration specimen with patterns from a specimen of unknown deformation magnitude, thereby assigning an "equivalent tensile strain" to the spot from which that pattern was made. The comparison is made by eye, which coupled with the brain, is capable of integrating together changes in the whole pattern. Attempts at finding a more quantitative method for specifying pattern changes have been frustrated by the large amount of data available in the patterns and by an inability to account for changes due to different crystallographic orientations.

Several methods have been attempted. Optical Fourier transformation of data in the entire pattern would allow assignment of a value to the resulting spatial frequency content of the pattern. This method failed because of the low spatial frequencies found in the patterns. Another attempt was made to deal with the spatial frequencies found in the patterns by measurement of their power spectral densities, and by use of the first moment of the magnitude versus frequency content of a spectrum to assign a number to the pattern [*15*]. This method will work satisfactorily for the same orientation, or for large crystals, but fails because it is too time consuming to allow for a large data sample from any specific pattern. For randomly oriented patterns, it appears as though an instrument suitable for assessment of channeling pattern changes due to deformation is still to be found which is superior to the eye-brain combination of an experienced observer, and is certainly an opportunity for further research.

Uses of Selected-Area Electron Channeling Patterns

The principal use to date of SACPs in studying fatigue has been in the delineation of plastic zone size and shape, and in assessing the magnitude of strain intensity within the zone. This work has been done in a variety of materials: by Stickler, Hughes, and Booker [*14*] on Diskalloy (weight percent 26Ni-13.5Cr-54Fe), and later on Fe-3Si, 6061-T6 aluminum alloy, and 304 stainless steel by Davidson and Lankford [*16*], who have also obtained results (as yet unpublished) on 2024-T4 and 7075-T6 aluminum alloys. Plastic zone size may be correlated with measurements by other techniques and in other materials through the relation

$$r_p = \alpha\left(\frac{\mathrm{K}}{\sigma_y}\right)^2 \tag{1}$$

where

r_p = maximum dimension of the plastic zone,
K = maximum stress intensity factor,
σ_y = yield stress, and
α = a constant, which has been found [*17*] to be material dependent.

Reference *17* is a detailed explanation of the numerous factors affecting plastic zone size and shape, including the relevant theory, and summarizes the technique used for the electron channeling measurements of the plastic zone parameters. For the aluminum alloys, the values of α in Eq 1 have been found to be $\alpha = 0.11$ for 6061-T6, $\alpha = 0.48$ for 2024-T4, and $\alpha = 0.78$ for 7075-T6.

Three questions arise concerning this material-sensitive variation in α with alloying:

1. Since all measurements are on the surface of the specimen, are not all these values plane-stress measurements?
2. Since the measurements were made from cracks grown in laboratory (humid) air, could not the differences seen be environmental effects?
3. Is not the plastic zone "boundary" sufficiently difficult to define so that the variations in α could be explained by a combination of statistical scatter in the plastic zone from measurement to measurement, together with difficulties in defining the zone boundary?

Electron channeling studies can answer some of these questions. Since channeling pattern changes result from dislocation density changes, the specimen can be sectioned, allowing the plastic zone parameters within the interior to be correlated with those on the surface. No comprehensive investigation of this point has yet been made, but the one section thus far investigated [*18*] indicates that the interior plastic zone is much like that on the surface. Fracture surface examination by SEM shows no difference in features across the specimen thickness for the cases investigated. Thus, all indications are that for the stress intensity range investigated and for the specimen thickness used, sufficiently small-scale yielding is occurring that plane strain conditions prevail through the specimen thickness. The maximum plastic zone dimension (approximately 500 μm) to thickness (2.5 mm) ratio is 0.2.

Environmental effects may contribute substantially to the observed differences in α, and this has yet to be investigated. A goal of this research would ultimately be to measure the environmental component of the energy input required to create a unit area of new fatigue crack, much as has been done for the Fe-0.5C steel [*6*].

Definition of the plastic zone boundary by electron channeling has been compared with the etching technique developed by Hahn, Hoagland, and Rosenfield [*19*] for Fe-3Si. The result [*17*] was that plastic zone size and shape are well defined in general, but that particular anomalies along the

boundary may not be delineated; thus, the technique tends to smooth out, or average, some of the variations which occur in polycrystalline materials. Plots of equivalent tensile strain (ϵ) versus normalized distance away from the crack tip ($\bar{r}$) indicate that for a variety of materials [*16*]

$$\epsilon = E - F \ln \bar{r} \tag{2}$$

where $E = 10$ and $F = 1.6$ (these values are considered approximate) and $\bar{r} = r/(\Delta K/\sigma)^2$. Near the plastic zone boundary, ϵ is a very strong function of $\bar{r}$, making delineation of the boundary especially clear. Variations between individual measurements of zone size and strain distribution occur because of such variables as interaction of the crack with the local crystallography of the grains being traversed, and local variation in crack front geometry.

To arrive at the values of plastic zone size, no less than three determinations are made, and usually a larger number is used. The values of α found for the aluminum alloys are sufficiently different so that no overlap between plastic zone size distributions occur. Plastic zone shapes vary according to material, even within an alloy system, and no two plastic zones are exactly alike, but, even considering these variables, there are clear differences in maximum zone size.

Perhaps one of the most successful uses of SACP's to define plastic zones has been in the study of overloads. Lankford and Davidson [*20*] studied 50 and 100 percent overloads in 6061-T6 and were able to explain crack retardation periods and subsequent crack paths from a knowledge of specific overload plastic zone shapes and sizes. Similar work (as yet incomplete) has shown that this correlation also holds for 2024-T4 and 7075-T6.

Another method of determining plastic zone size is to look at channeling patterns made from the actual fracture surface, and after successive material removal through electropolishing. Work in progress on Ti-11 [*21*] and IMI-685 [*22*] titanium alloy specimens is illustrated in Fig. 5. In addition to the plastic zone boundary, determined to lie about 20 μm below the fracture surface for the facet shown, the orientation of the crack path is found to be the basal plane of this hexagonal crystal structure. This application of SACPs is one in which large rocking angle, with attendant large spot size, was used; the spot size was approximately 50 μm, and the rocking angle 12 deg. Measurement of material removal by electropolishing and setup of the electron optic axis perpendicular to the facet plane were achieved using the methods described by Boyde and Howell [*23*].

Specimen Preparation Considerations

Since electron channeling is strongly influenced by crystalline perfection, it

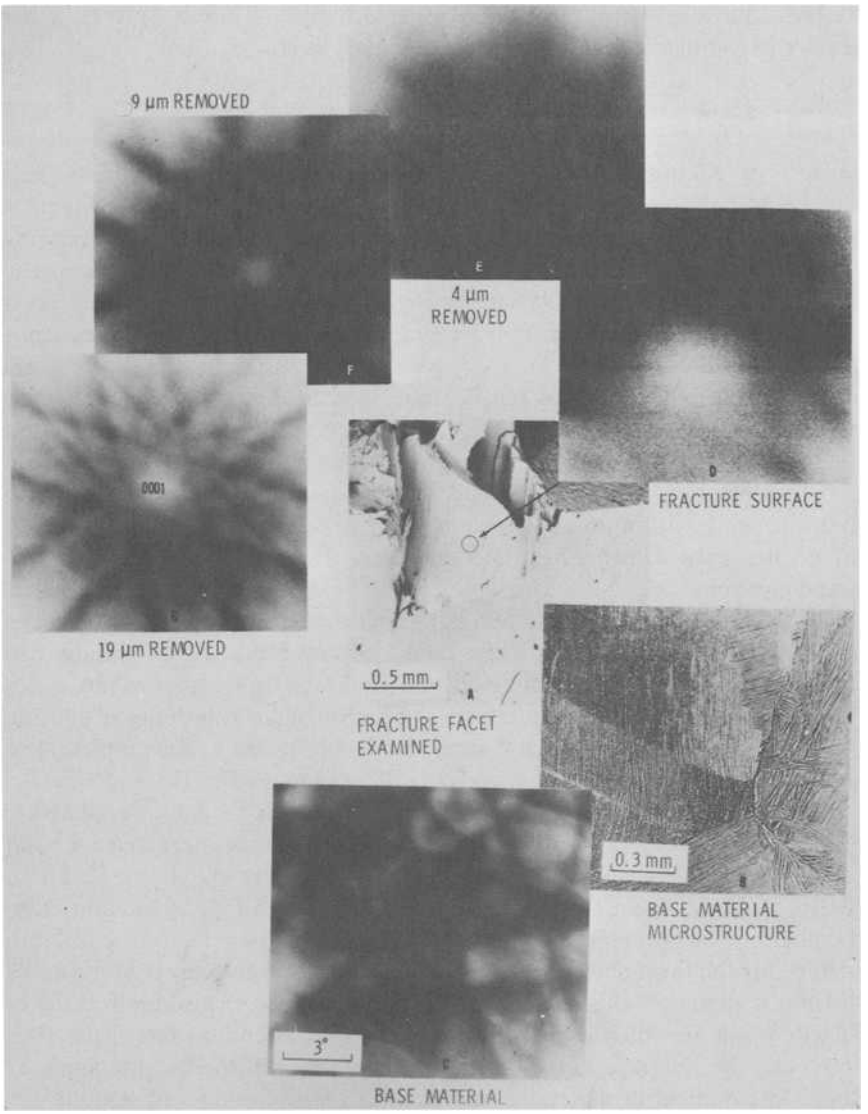

FIG. 5—*Orientation of a region of planar fatigue crack propagation* (A) *in Ti-11 titanium alloy. The microstructure of the base alloy* (B) *and quality of the SACP* (C) *are also shown, as well as the change in pattern quality as material is selectively removed from the fracture surface* (D, E, F, G), *which allows an estimate of the plastic zone dimension* (*20 μm*) *can be made.*

is usually desirable to begin with material of a fairly low dislocation density (less than 10^8 dislocations/cm^2). In many materials, thermomechanical processing is required to produce suitable starting material. For the aluminum alloys thus far examined, no change in channeling pattern line acuity has been found upon going from the quenched condition to that of precipitation hardening for maximum strength. For the stainless steels, quenching from annealing temperatures, instead of furnace cooling, induces a dislocation structure which noticeably affects the channeling patterns. Metals with allotropic transformations—notably iron and titanium—also have a dislocation density induced by the transformation. This dislocation density does not affect the channeling contrast nearly as much as it does the channeling patterns; thus, experiments utilizing channeling contrast may more easily be performed on some materials than experiments utilizing channeling patterns.

Surface preparation of all specimens is very important. The surface damage of most common mechanical metallurgical preparation processes is very great and may in some cases extend to large depths in the material. Considerable care is required in this phase of specimen preparation. Electropolishing is almost always required as the final step in preparation, where sufficient metal must be removed to get below damaged layers caused by prior preparation steps. Electropolishing develops a viscous film on the specimen which must be thoroughly removed by washing and ultrasonic cleaning. Thick oxide or contamination layers can cause changes in channeling patterns very similar to those due to an increased dislocation density [*15*]. Proper electropolishing procedures usually produce a very thin, uniform oxide layer, but on some metals, this oxide layer may grow in thickness quite rapidly with time. Considerable care must be exercised to recognize and cope with these possible problems, or erroneous data can be produced.

Future Uses

The general directions for studying the effects of cyclic loading with respect to crack propagation seem fairly well established, although further innovations in the technique will undoubtedly come about. But the opportunities for the use of electron channeling as a surface analysis tool, which would be useful in the study of fatigue crack initiation, are just being realized. In fact, electron channeling can be viewed as a nondestructive near-surface method of assessing the defect state of a metal, either through the use of channeling patterns or channeling contrast [*24*]. The contrast information carried in micrographs originates within the volume of material interrogated by the electron beam, and that volume is dependent both on the energy of the impinging beam and on the material. Table 1 relates total penetration depths to beam energy for two materials.

TABLE 1—*Beam energy and penetration depth for aluminum and iron.*

Eo, keV	Total Penetration Depth, μm	
	Al	Fe
5	0.18	0.03
10	0.58	0.11
20	1.85	0.35
30	3.63	0.70

The theories available [*25,26*] to describe the physics of electron channeling contrast development are insufficiently detailed to determine the relation between depth of the backscattering event and the contrast developed, so it is not yet possible to accurately determine the origin of information found in micrographs. It is clear, however, that subcells formed near the surface of a metal being cyclicly loaded should be observable, and that it should be possible to limit the region of observation to fractions of a micrometre (perhaps 100 to 1000 Å). Figure 6 is an illustration of the effect of incident energy change on the observation of subcells. Subcells visible at 30 keV, but not visible at 12 keV are presumed to lie within approximately 0.15 and 0.7 μm of the surface. Future correlations of near-surface material damage with surface chemistry could prove useful in the study of crack initiation.

Conclusion

The objective of this paper has been to review the ways thus far found for the phenomenon of electron channeling to be exploited in the study of the response of metals to cyclic loading. Electron channeling is but one tool which may be useful in this study, and by not having included a discussion of other techniques, there has been no intent to minimize their importance. But use of the electron channeling techniques offers some unique opportunities to study bulk specimens, and these should be exploited. A major limitation in the use of selected-area electron channeling patterns is their spatial resolution, and in their inability to yield information at strains above 10 to 20 percent (equivalent tensile values). To study the important region closer to the crack tip, the channeling contrast technique gives higher resolution. The construction and operation of cyclic loading facilities to study the propagation of cracks dynamically [*27,28*] is a recent complementary development which is expected to add important information to the mechanisms of fatigue crack initiation and propagation.

The study of crack tips by interferometry is also a valuable technique because it can be used on very complex, highly dislocated microstructures where channeling cannot be used. Other techniques using X-rays, micro-

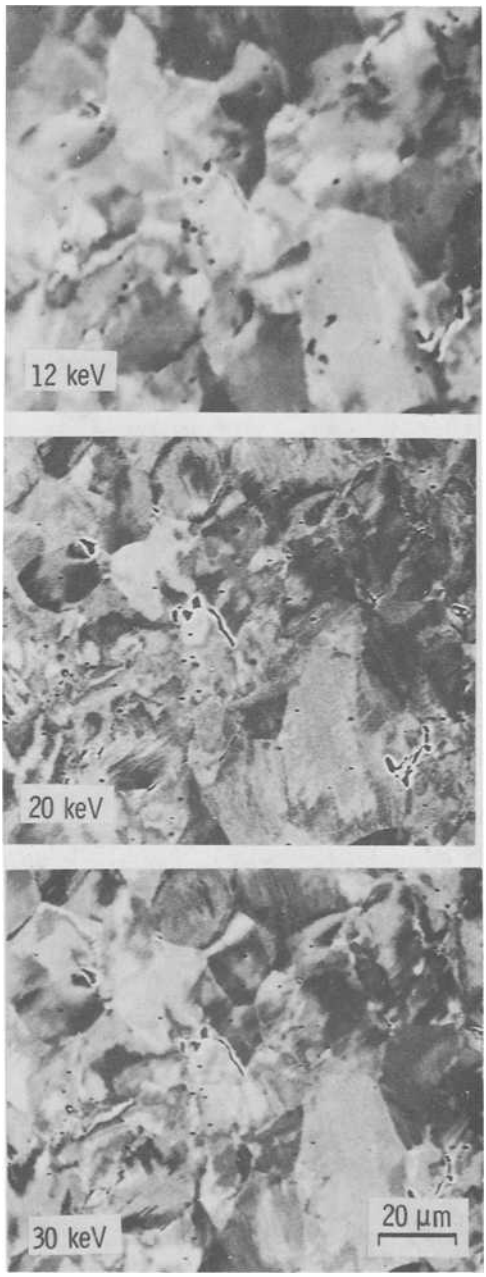

FIG. 6—*Effect of changing electron beam potential on the observation of dislocation subcells by channeling contrast: Fe-0.05 weight percent carbon steel deformed by reversed stress loading.*

hardness intentions, etching, carburizing, and recrystallization have also added useful information on fatigue mechanisms.

Finally, with the wider availability of SEMs, on which electron channeling can be routinely performed, and with a greater knowledge of what the techniques can do in the study of cyclic loading, it is hoped that wider applications will be found.

Acknowledgments

My colleague Dr. James Lankford and I have worked together on the study of fatigue mechanisms for the past seven years, and he is equally responsible for many of the results summarized in this paper. Much of the work reported here was sponsored by the Air Force Office of Scientific Research under Contract No. F44620-75-C-0050.

References

[1] Coates, D. G., *Philosophical Magazine*, Vol. 16, 1967, pp. 1179-1184.
[2] Joy, D. C. and Newbury, D. E., *Scanning Electron Microscopy/1977*, Vol. 1, IIT Research Institute, Chicago, Ill., 1977, pp. 445-461.
[3] Davidson, D. L., *Scanning Electron Microscopy/1977*, Vol. 1, IIT Research Institute, Chicago, Ill., 1977, pp. 431-438.
[4] Davidson, D. L., Lankford, J., Yokobori, T., and Sato, K., *International Journal of Fracture*, Vol. 12, Aug. 1976, pp. 579-585.
[5] Davidson, D. L. and Lankford, J., *Fracture 1977*, Vol. 2, University of Waterloo Press, Waterloo, Ont., Canada, pp. 897-904.
[6] Davidson, D. L. and Lankford, J. in *Environment Sensitive Fracture of Engineering Materials*, Z. A. Foroulis, Ed., American Institute of Mining Engineers, New York, 1979, (in press).
[7] Davidson, D. L. and Lankford, J., unpublished subcell observations on 304 and 316 stainless steels, 1972.
[8] de Vries, M. I., and Mastenbroek, A., *Metallurgical Transactions*, Vol. 8A, Sept. 1977, pp. 1497-1499.
[9] Davidson, D. L., *Journal of Physics E: Scientific Instruments*, Vol. 9, 1976, pp. 341-343.
[10] Joy, D. C. and Newbury, D. E., *Journal of Materials Science*, Vol. 7, 1972, pp. 714-716.
[11] Booker, G. R., *Modern Diffraction and Imagery Techniques in Materials Science*, North Holland Publishing Co., Amsterdam, The Netherlands, 1970, pp. 614-653.
[12] Ayers, J. D. and Joy, D. C., *Acta Metallurgica*, Vol. 20, 1972, pp. 1371-1379.
[13] Ruff, A. W., *Wear*, Vol. 40, 1976, pp. 59-74.
[14] Stickler, R., Hughes, C. W., and Booker, G. R., *Scanning Electron Microscopy/1971*, IIT Research Institute, Chicago., Ill., 1971, pp. 473-480.
[15] Davidson, D. L., *Scanning Electron Microscopy/1974*, IIT Research Institute, Chicago, Ill., 1974, pp. 927-934.
[16] Davidson, D. L. and Lankford, J., *Journal of Engineering Materials and Technology*, Vol. 98, Jan. 1976, pp. 24-29.
[17] Lankford, J., Davidson, D., L., and Cook, T. S. in *Cyclic Stress-Strain and Plastic Deformation Aspects of Fatigue Crack Growth*, *ASTM STP 637*, American Society for Testing and Materials, 1977, pp. 36-55.
[18] Davidson, D. L., *International Journal of Fracture*, Vol. 11, 1975, pp. 1047-1048.
[19] Hahn, G. T., Hoagland, R. G., and Rosenfield, A. R., *Metallurgical Transactions*, Vol. 3, May 1972, pp. 1189-1202.

[20] Lankford, J., and Davidson, D. L., *Journal of Engineering Materials and Technology*, Vol. 98, Jan. 1976, pp. 24-29.
[21] Eylon, D., Hall, J. A., Pierce, C. M., and Ruckle, D. L., *Metallurgical Transactions*, Vol. 7A, 1976, pp. 1817-1826.
[22] Eylon, D. and Hall, J. A., *Metallurgical Transactions*, Vol. 8A, June 1977, pp. 981-990.
[23] Boyde, A. and Howell, P. G. T., *Scanning Electron Microscopy/1977*, Vol. I, IIT Research Institute, Chicago, Ill., 1977, pp. 571-579.
[24] Davidson, D. L. in *Surface Effects in Crystal Plasticity*, R. M. Latanision and J. F. Fourie, Eds., Noordhoff Publishing Co., Leyden, The Netherlands 1977, pp. 80-809.
[25] Spencer, J. P., Humphreys, C. J., and Hirsch, P. B., *Philosophical Magazine*, Vol. 26, 1972, pp. 193-213.
[26] Spencer, J. P., "Diffraction Contrast in the Scanning Electron Microscope," Ph.D. dissertation, University of Oxford, Oxford, U.K., May 1974.
[27] Davidson, D. L. and Nagy, A., *Journal of Physics E: Scientific Instruments*, 1978 Vol. 11, pp. 207-210.
[28] Kikukawa, M., Jono, M., and Adachi, M., this publication, pp. 234-253.

DISCUSSION

B. Ditchek[1] *and A. W. Ruff*[2] *(discussion)*—The author has reviewed the application of electron channeling to the study of fatigue-induced plastic deformation in alloys. Further, he has noted the application of electron channeling to other studies of plasticity such as tensile deformation[3] and wear deformation.[4] Dr. Davidson has provided much of the original work on the application of electron channeling to fatigue and is to be commended for this excellent paper. We would like to raise a few issues in connection with the work reported here in order to further broaden the discussion on the channeling technique and its application. Further, it seems appropriate to place the electron channeling method in the proper perspective relative to other established methods of studying plasticity on a microscopic level.

As summarized by the author, the selected-area channeling pattern (SACP) method can be used (1) to measure the amount of plastic strain and (2) to reveal deformation substructure in the specimen. There are two principal advantages associated with the channeling method in the first type of application. First, the strain measurements can be made on a bulk specimen so long as its size is sufficient to fit within an SEM specimen chamber and so long as it can tolerate the microscope vacuum. Second, the

[1]National Bureau of Standards, Washington, D.C. 20234; current address: Martin Marietta Laboratory, 1450 South Rolling Road, Baltimore, Md. 21227.
[2]Center for Materials Science, National Bureau of Standards, Washington, D.C. 20234.
[3]Booker, G. R. in *Modern Diffraction and Imagery Techniques in Materials Science*, North Holland Publishing Co., Amsterdam, The Netherlands, 1970, p. 614-653.
[4]Ruff, A. W., *Wear*, Vol. 40, 1976, pp. 59-74; also Vol. 46, 1978, pp. 251-261.

strains can be measured locally in a very small volume, about 1 to 10 μm.[3] However, certain disadvantages must also be noted with this technique. It is not possible to directly calculate the plastic strains from measured values on SACP's since an adequate theory relating the necessary quantities has not been developed. Instead, it is usual to calibrate the SACP with reference to specimens deformed to known levels of plastic strain. Dr. Davidson has used specimens deformed in tension for calibrating the strain measured in front of a fatigue crack. As materials deformed in tension and fatigue generally differ in such microstructural parameters as total or excess dislocation density, dislocation cell size and geometry, and cell misorientations, and, further, since the sensitivity of SACP strain measurements to these parameters is unknown, the tensile calibration used here is not strictly appropriate. As a general rule, strain calibration should be performed in as similar a deformation mode as possible. In this case, it might be more appropriate for Dr. Davidson to calibrate the strain at the fatigue crack tip in terms of an "equivalent fatigue strain" formed in, for example, a copper single crystal cycled between constant plastic strain limits. This should be particularly valuable in light of the recent work of Katagiri[5] and co-workers, whose observations showed that dislocation substructures are similar in bulk fatigued copper to that in front of a fatigue crack in the same material.

It is worth noting that SACPs can be obtained in rapid succession from different areas of a specimen. It is possible to obtain a pattern (photograph) in a period of about 2 min. That pattern contains information on the average state of strain over a volume of about 1 μm deep (depending on electron beam voltage and material) and about 5 to 10 μm in lateral dimensions. Thus a rapid assessment of strain can be carried out in the space of an hour for 20 to 30 different areas of a specimen. Other techniques generally require a considerably greater investment of time.

Dr. Davidson discusses in his paper the difficulty of measuring the strain effect in a randomly oriented SACP. The method he employs involves an interpretation of line broadening (sharpness) by an experienced observer. A measurement method of that type involving personal judgment can produce different results on the part of different observers, so one is cautioned over the accuracy of particular strain values obtained. In our experience, an adequately reproducible technique (see footnote 4) involves measurements of channeling line contrast using one of a set of specific lines. In this method, the reduction of channeling line contrast that occurs for increasing plastic strain level can be measured using the SEM to a reproducibility of about 10 to 20 percent. A calibration specimen is also used in this method to determine strain. Application to specimens con-

[5]Katagiri, K., Omura, A., Koyanagi, K., Awatani, J., Shiraishi, T., and Kaneshiro, H., *Metallurgical Transactions*, Vol. 8A, 1977, p. 1769.

sisting of randomly oriented grains is possible since one usually can obtain one of the four or five low index lines from a given grain for which strain calibration can be carried out. For any chosen method, it is also important to use consistent specimen preparation and mounting methods within the SEM, and whenever possible to use a reference specimen of known strain level to periodically validate the measurement process.

The second application of electron channeling, imaging the microstructure in materials, is a promising technique. Relatively few studies of detailed structure have been reported. Careful attention must be paid to the problem of electron signal detection as noted by Dr. Davidson. The advantage of the technique again lies in the use of bulk specimens with little specimen preparation required. As an example, it might be valuable to use this technique in single crystal work where the three-dimensional nature of subcells can be more easily deduced than by TEM thin-section techniques. Of course, the widespread use of this technique will be affected by its present resolution limit of about 0.3 μm.

With regard to the statement that electron channeling contrast studies suggest that aluminum alloys do not form extensive subcells, we would like to ask Dr. Davidson if the depth of penetration of electrons might affect the observation. Figure 3 was formed using 20-keV electrons, which according to Table I yields an electron penetration in pure aluminum of 1.85 μm. This is several times larger than typical subcell diameters. Thus, overlap of several cells within the image occurs and this may cause difficulty in observing individual cells due to compensating contrast effects. Possibly a lower voltage of between 5 to 10 keV should be used when trying to observe subcells in aluminum alloys.

Finally, we believe that SACPs and channeling contrast are potentially useful tools in the study of fatigue and deformation in general. The major advantage offered is the ease of specimen preparation. A major disadvantage is the resolution limit of the standard SEM. It might be useful if Dr. Davidson could comment on the possibility of the new field emission STEM units in improving the resolution.

D. L. Davidson (author's closure)—The discussers for this paper, Drs. Ditchek and Ruff of the National Bureau of Standards have helped to bring out some of the additional advantages and disadvantages of using the electron channeling technique, and I am grateful for their comments. The other points discussed are (1) calibration techniques, (2) interpretation of deformation magnitude as related to electron channeling patterns, (3) the observation of subcells in fatigued aluminum alloys, and (4) the value of increasing the spatial resolution of the SEM through higher-brightness electron guns. I shall respond to these points in the order made.

1. Calibration techniques: The discussors question the use of a tensile calibration specimen for relating changes in channeling pattern line acuity

to strain, where the deformation being studied is caused by cyclic loading. In a logical sense, they are certainly correct to question this procedure, as I have also, but there are two considerations by which this methodology can be justified. First, the fatigue crack-tip plastic zone is widely believed to consist of an outer portion where the loading, although cyclic, is purely tensile, and an inner portion, where the loading is both tensile and compressive. This was the interpretation of experimental results by several investigators using widely different techniques[6-8] and was predicted theoretically by Rice.[9] Because of the small size of the inner zone and the limited resolution of the selected-area electron channeling technique, it is only the outer zone which can be studied. Since in this zone tensile loading is the predominant mode, the use of a tensile calibration specimen is not unreasonable. The second reason why this calibration method is used is because of the uncertainty in how to measure or calculate cumulative strain when using a variable-amplitude load which is partially tensile and partially compressive. Finally, the tensile calibration idea was derived directly from Hahn, Hoagland, and Rosenfield's[6] work on Fe-3Si; they too used a tensile calibration scheme for roughly the same reasons given in the foregoing.

In summary, I believe that the tensile calibration method is a reasonably accurate way of measuring plastic strain and the plastic strain boundary in the outer plastic zone of a fatigue crack in metals where the technique can be applied. Other methods having higher spatial resolution must be used for strain measurements within the inner plastic zone. These might include the channeling contrast technique (Fig. 2 of the paper), the replication technique,[10] or a new technique, the stereographic imaging of displacements[11] from which strains may be calculated.

2. Relating changes in electron channeling patterns to deformation is a particularly difficult problem, and provides a real limitation on the quantification of deformation using the selected-area electron channeling technique. Deformation of the interrogated material is manifested in the channeling pattern by a change in the acuity of the lines which make up the pattern (see Fig. 4). For material with a starting dislocation density of about $10^4/cm^2$, channeling patterns will indicate primary channeling bands such as from the (220) shown, as well as second-order and perhaps third-order lines, which may also be seen on the figure. As deformation

[6]Hahn, G. T., Hoagland, R. G. and Rosenfield, A. R., *Metallurgical Transactions*, Vol. 3, May 1972, pp. 1189-1202.

[7]Bathias, C. and Pelloux, R. M., *Metallurgical Transactions*, Vol. 4, 1973, pp. 1265-1273.

[8]Davidson, D. L. and Lankford, J., *Journal of Engineering Materials and Technology*, Vol. 98, Jan. 1976, pp. 24-29.

[9]Rice, J. R. in *Fatigue Crack Propagation, ASTM STP 415*, American Society Testing Materials, 1967, pp. 247-309.

[10]Lankford, J. and Barbee, J. G., *Journal of Materials Science*, Vol. 9, 1974, pp. 1906-1908.

[11]Davidson, D. L., *Journal of Materials Science*, Vol. 11, 1978 (in press).

proceeds and the dislocation density increases, the acuity of these lines will decrease, and then the lines will disappear entirely. Both the apparent width of the lines and the contrast which makes the line visible are affected. At sufficiently high dislocation density, about $10^9/cm^2$, the channeling pattern dissolves into a uniform gray level. From an instrumental viewpoint, there are two factors to be measured as a function of deformities: (1) spatial frequency, a measure of line acuity, and (2) contrast. Several attempts have been made to measure these factors across one or several line scans of a channeling pattern. The discussers have performed one of these studies,[12] and it is my opinion that the technique they used, while well thought out and carefully applied to their particular study, is still not a generally applicable or adequate technique for channeling pattern assessment. I also have tried several line scan techniques which are inadequate, and the general reason for this is because (1) the line scan samples only a small portion of the total pattern, thereby wasting 90 percent or more of the useful information available, and (2) the results of a line scan analysis are highly dependent upon orientation between the channeling band and the line scanned. In the general case, it will not be possible to find the same orientations exactly, on both the specimen and the calibration sample, and this difficulty increases as crystal systems other than cubic are used, for example, the hexagonal close-packed system.

I made an attempt in 1973 to use the optical transform msethod to assess spatial frequency in the entire channeling pattern, but discovered that the frequencies were too low for this method to be of use, at least with the instrumentation then available. The only alternative to the optical transform method I can currently imagine for using all the information available in the channeling patterns is to digitize the entire pattern and then operate mathematically on the resulting data to extract the desired spatial frequency and contrast information. This process, although entirely feasible with current technology, is expensive and would require considerable computer program and data handling development.

A study of the human eye and how it is able to gather and process information[13,14] indicates that this instrument fulfills many of the requirements for assessing channeling pattern changes with deformation. Furthermore, the eye-brain combination is capable of learning and bringing experience into the information processing sequence. Thus, it is my opinion that until such time as adequate instrumental techniques are developed for the processing of channeling patterns, the eye-brain combination is still the best instrument generally available.[15]

[12] Ruff, A. W., *Wear*, Vol. 40, 1976, pp. 59-74.
[13] Rose, A., *Advances in Electronics*, Vol. 1, 1948, pp. 131-166.
[14] Ross, J., *Scientific American*, Vol. 234, 1976, pp. 80-86.
[15] LePoole, J. B. in *Developments in Electron Microscopy and Analysis*, J. A. Venables, Ed., Academic Press, New York, 1976, pp. 79-81.

3. The problems of observing subcells in aluminum alloys with the channeling contrast technique are probably due to a combination of factors somewhat unique to aluminum alloys and to standard SEM construction. The interaction between the specimen and the impinging electron beam is another factor to be considered, as the discussers have suggested. At 20 keV the total penetration of electrons into aluminum ought to be about the 1.85 μm shown in Table 1 of the paper, but it is not well understood from what portion of that penetration range the backscattering events which build the image contrast are being derived. Certainly they are not occurring at a depth of more than half that range, 0.92 μm, and probably it is considerably less. Theoretical studies at Oxford indicate that channeling may be occurring as shallow as the 0 to 500 Å range. The most probable maximum information depth lies somewhere between these estimates.

In addition to the information depth, three other important considerations should be noted. (1) To obtain sufficient backscattering for image formation with aluminum in the SEM, it is necessary to use relatively high beam currents, with the associated larger probe diameters and lower resolution; the magnitude of the beam current required for the aluminum specimen is dictated by the detector and amplifier characteristics and by the scan rate. (2) Most of the subcells are forming close to the crack plane in aluminum alloys, as determined by TEM (see footnote 12). This fact, coupled with the "edge effect"—which causes an edge to appear bright in the SEM—causes what subcells there are to be difficult to observe.[3] Subcells in aluminum alloys are small, in the range of 0.25 to 1 μm, as compared with larger subcell sizes in ferritic alloys of 1 to 10 μm. These smaller sizes coupled with the relatively high beam currents cause them to be unresolvable with most currently available instrumentation. Some of these problems could be solved by going to lower accelerating voltages, for example, 5 keV, but for the lens system designs used in most instruments this would lead to a large decrease in performance of the electron-optical system, which probably would offset any gain made from changing the specimen-electron interaction.

4. Spatial resolution increases can indeed be achieved, as the discussers suggest, through the use of higher-brightness electron sources. The use of LaB_6 directly heated (filament) or indirectly heated (gun) would give a factor of 5 to 50 increase in source brightness (or current density), which would cause a 2.2- to 7-fold decrease in probe size. Use of a field emission source with a nominally 100 increase in brightness would cause a tenfold decrease in probe size. Translating these probe size changes into increased resolution is complicated by lens aberrations, which will likely be the limiting factor, but it is clear that brighter sources should allow higher-resolution channeling contrast studies to be performed.

Finally, I completely concur with the discussers that the electron channeling techniques will continue to be of great value in the study of deformation in general and fatigue mechanisms in particular. I also appreciate the opportunity afforded by the discussers' remarks and questions to expand on some of the issues they have raised.

J. C. Grosskreutz[1]

Closing Remarks by Session Chairman

First of all, I would like to congratulate all of the authors on papers well presented, research well done, and experiments well conducted. Second, if you will permit me, I would like to pass on some guiding philosophy for fatigue mechanisms research.

The reasons why we do this work to understand the mechanisms of fatigue are so that we can do a better job of predicting fatigue life, of finding ways of nondestructive testing for fatigue damage, and of developing new materials which will be fatigue-resistant. In the final analysis, that is why we do the work; or why you do the work now.

Sometimes there is a strong temptation to do an experiment, explain what you have seen, and draw "Q.E.D." at the end of a paper and publish it. If we are to make headway toward the ends that I just mentioned, we dare not fall into that trap. It is necessary to keep in mind always what the ultimate goal that you are seeking is; namely, better materials, better ways of detecting fatigue damage, better ways of defining what fatigue damage really is, and better ways of predicting fatigue life.

Of course, fatigue is a terribly complex problem as we have seen today—with many, many parameters that control its progress and the events toward failure. But I think, as I have said before, that it is one of the missions of Committee E-9, of Lou Coffin and the rest of his officers and subcommittee chairmen, to try and bring things together and make some progress toward the goal of better engineering structures, fewer fatigue failures, and better standards for measuring the fatigue life of materials.

[1] Solar Energy Research Institute, Golden, Colo. 80401.

D. L. Davidson[1] *and J. Lankford*[1]

Dynamic, Real-Time Fatigue Crack Propagation at High Resolution as Observed in the Scanning Electron Microscope[2]

REFERENCE: Davidson, D. L. and Lankford, J., **"Dynamic, Real-Time Fatigue Crack Propagation at High Resolution as Observed in the Scanning Electron Microscope,"** *Fatigue Mechanisms,* Proceedings of an ASTM-NBS-NSF symposium, Kansas City, Mo., May 1978, J. T. Fong, Ed., *ASTM STP 675,* American Society for Testing and Materials, 1979, pp. 277-284.

ABSTRACT: A videotape of dynamic, high-resolution, real-time fatigue crack propagation, made from experiments with a special cyclic loading stage in the scanning electron microscope, was shown to the conference attendees. This paper briefly summarizes the video presentation and illustrates a few of the main points made by it.

KEY WORDS: aluminum alloys, crack propagation, fatigue fracture, nickel-base alloys, scanning electron microscopy

This paper describes a television video presentation of dynamic fatigue crack propagation which was shown to the conference attendees. The television picture was projected onto a 1.8-m (diagonal) screen in order to accommodate the large audience. Total length of the presentation was 13 min.

The fatigue crack propagation sequences were taped from experiments conducted inside a scanning electron microscope (SEM) which was fitted with a cyclic loading stage. A description of this facility[3] provided an introduction to the subject. Next was shown the specimen design used for the experiments—a maximum gage section of 19-mm width and 6-mm thick-

[1] Staff scientist and senior metallurgist, respectively, Department of Materials Sciences, Southwest Research Institute, San Antonio, Tex. 78284.

[2] Presented as invited commentary on a videotape show at the conclusion of the session on direct observations from slipbands to nucleation of microcracks.

[3] Davidson, D. L. and Nagy, Andrew, *Journal of Physics E: Scientific Instruments.* Vol. 11, 1978, pp. 207-210.

ness. For high-strength materials, this gage section must be reduced for cyclic stress intensities to be reached for reasonable crack lengths with the available working loads of the stage, 4450 N (1000 lb).

Videotape Sequences

The first of the crack propagation sequences showed a crack propagating in 2024-T4 wrought ingot alloy at $\Delta K = 7.6$ MN/m$^{3/2}$ in a 3-mm-thick specimen. This material had a pancake grain structure with a grain size of approximately 300 μm. For the screen size used, this sequence, and most of the others shown subsequently, had a magnification of about $\times 35\,000$, making 1 μm appear as 3.5 cm. The sequence showed that the crack was opening by a mixture of Mode I (tensile) and Mode II (shear), and that crack propagation was discontinuous with the following sequence of events: from a sharp crack, gradual blunting occurred after a few cycles, together with the development of one or more shear bands. Subsequent crack formation was seen to occur along one of these shear bands. A typical observation as seen in this sequence is shown in Fig. 1.

The next sequence shown was for a crack propagating at $\Delta K = 8$ MN/m$^{3/2}$ in the experimental powder metallurgy aluminum alloy MA 87,

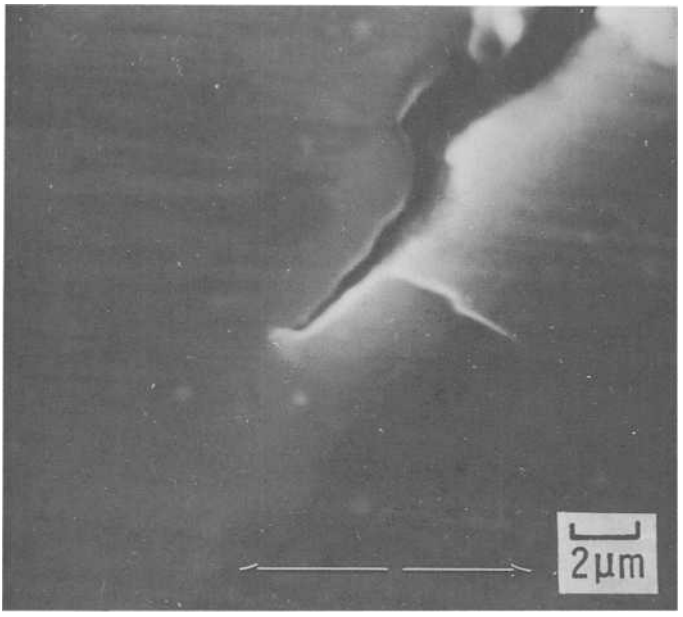

FIG. 1—*2024-T4 Ingot aluminum alloy,* K = *7.6 MN/m$^{3/2}$. Crack propagation is following the shear bands which form at the crack tip. Loading axis for all photographs is as shown by the arrows on this figure.*

having a grain size of about 20 μm. The microstructure of this alloy was much more homogeneous than that of the ingot alloy, yet the sequence showed nearly the same mixture of Mode I and Mode II crack opening as the ingot alloy. Figure 2 shows a crack tip typical of this material.

As a comparison to the powder metallurgy aluminum alloy, the third sequence showed crack propagation at $\Delta K = 18$ MN/m$^{3/2}$ in the isostatically pressed nickel-base superalloy IN-100 in a 1.25-mm-thick specimen. This material contains large blocky gamma-prime (0.5 to 1 μm), in addition to the smaller, strengthening gamma-prime cuboids, and has a grain size of approximately 3 μm. The sequence showed that crack propagation in this material is essentially the same as seen for the ingot and powder metallurgy aluminum alloys, except that there is some apparent interaction with the grain boundaries and blocky gamma-prime. It also requires a higher ΔK to obtain the same values of crack-tip opening displacement (CTOD) as found for the aluminum alloys. Figure 3 is typical of the crack-tip region for this material.

We believe that these three sequences showed a remarkable similarity in crack-tip mode response to load for alloys with widely differing metallurgical structures. For the cyclic stress intensities used in these sequences, the crack-tip plastic zone was calculated to be a small fraction of the specimen thickness. Thus, the mixed-mode crack opening observed is be-

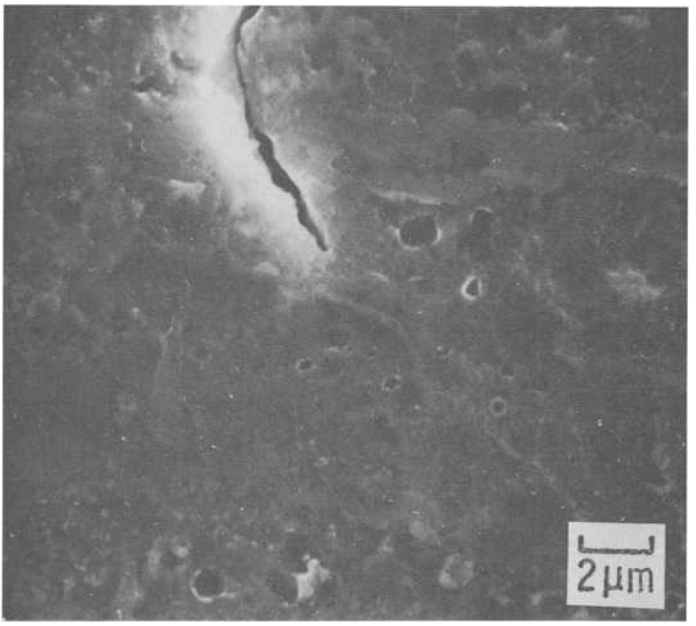

FIG. 2—*Powder metallurgy aluminum alloy MA-87.* K = *10.8 MN/m*$^{3/2}$.

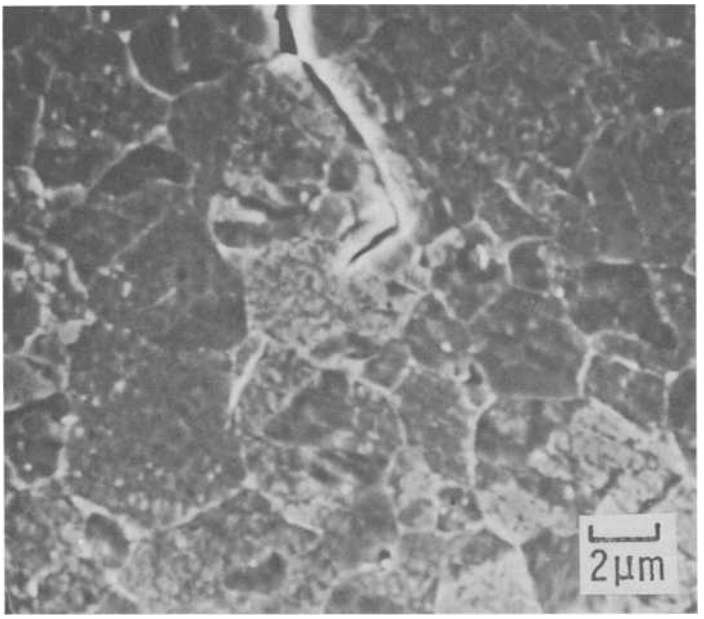

FIG. 3—*Powder metallurgy nickel-base alloy IN-100,* K = *18 MN/m*$^{3/2}$.

lieved to be typical of the entire thickness. Other experiments with this specimen geometry have indicated plastic zone sizes of about the magnitude expected for the plane-strain condition.[4] Another observation which may be made from these sequences is that microscopically, the crack plane is not perpendicular to the load axis, rather it is almost never perpendicular; thus, the mixed-mode crack-tip opening is at least partly attributable to nonsymmetric loading.

Another factor common to all the sequences presented is that crack opening occurs at a load above minimum load, and crack closure occurs at a load below opening load, indicating a hysteresis effect. Accurate numerical values of these loads have not yet been determined.

To contrast the behavior in metals described in the foregoing, the fourth sequence showed fatigue crack propagation in polymethylmethacrylate, an amorphous polymer, at $\Delta K = 0.5$ MN/m$^{3/2}$. The narrative used for this sequence describes in some detail the events which cause crack propagation:

> Crack growth consists of a combination of events. First, the initially sharp crack gradually blunts, while the crack tip craze lengthens. This is followed

[4]Lankford, James, Davidson, D. L., and Cook, T. S. in *Cyclic Stress-Strain and Plastic Deformation Aspects of Fatigue Crack Growth, ASTM STP 637,* American Society for Testing and Materials, 1977, pp. 36-55.

by void nucleation within the craze. Finally, link-up of the now microcracked craze produces an increment of growth. The entire process is repeated during subsequent cycles.

This material exhibited the only purely Mode I crack opening thus far observed in experiments with the SEM cyclic loading stage. A typical crack tip is shown in Figure 4. For the screen used, magnifications of approximately $\times 60\ 000$ were produced, the highest of those used in the presentation.

The next sequences showed a few of the complex events associated with crack propagation in the powder metallurgy aluminum and nickel-based alloys which had been observed. The first two sequences of this series showed cracking in the aluminum alloy which occurred ahead of the main crack during a number of loading cycles in which the main crack tip was becoming increasingly blunt. The first sequence could be interpreted as the main crack joining with a section of subsurface crack which had tunneled ahead of the main crack and finally broken through to the surface. The other sequence showed a small surface microcrack, approximately 2 μm long, which appeared to be associated with a large second-phase particle, linking up with the main crack, Fig. 5. During the 15 or 20 cycles required for linkup, both cracks are seen to grow, with the main crack growing

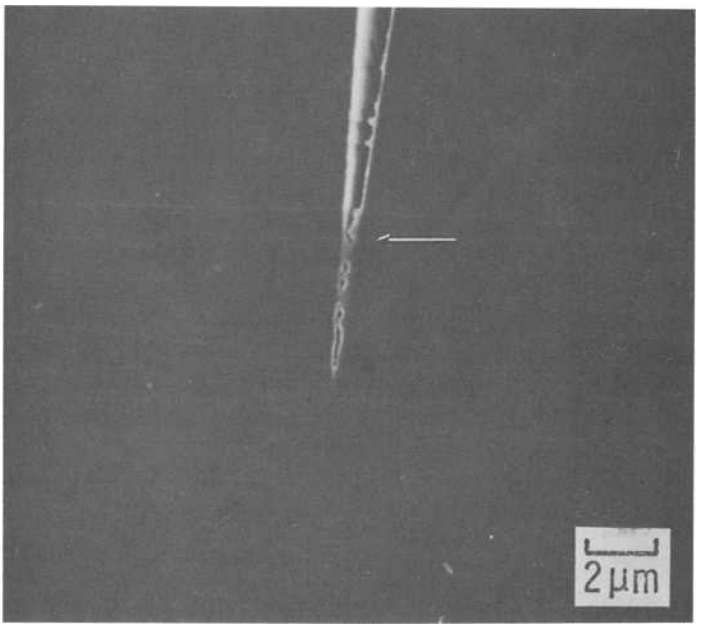

FIG. 4—*Polymethylmethacrylate,* $K = 0.5\ MN/m^{3/2}$. *The arrow indicates the crack tip.*

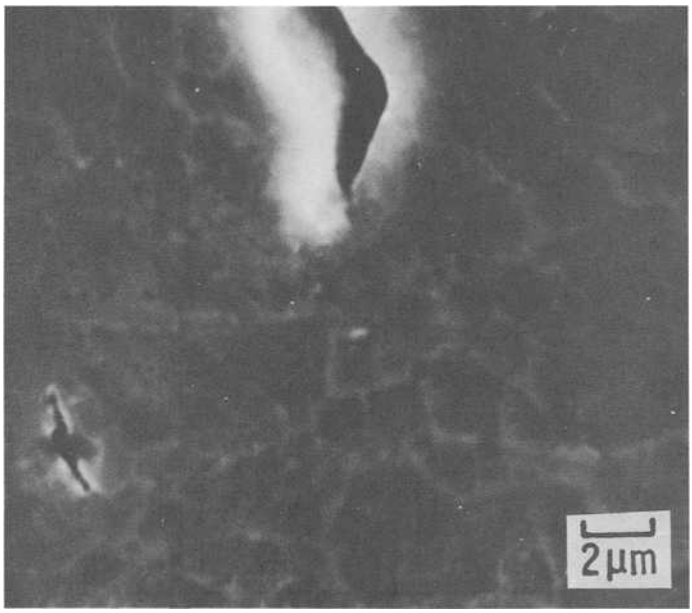

FIG. 5—*Powder metallurgy aluminum alloy MA-87.* K = *10.8 MN/m*$^{3/2}$, *showing small surface crack near the main crack tip.*

the most. This sequence showed events clearly different from those seen in the prior sequence, where tunneling was a plausible explanation.

The final sequence of this series showed the interaction of the crack in the nickel-base alloy with a grain boundary. In this complex interaction, the main crack was seen to be redirected after reaching the grain boundary.

The last sequences of the presentation showed the results of an experiment with the powder metallurgy aluminum alloy in which the ratio $R = K_{min}/K_{max}$ was varied from 0.36 to 0.62 at $\Delta K = 8$ MN/m$^{3/2}$. The changes in K_{min} and K_{max} used when going from one value of R to the next are shown schematically in Fig. 6. This sequence was used to avoid overload effects, and the powder metallurgy alloy was used because of its microscopic isotropy.

The largest effect due to changing R was seen to be in the K needed for crack-tip opening. With increasing R, the crack was seen to open at loads ever closer to the lower K-value, although K_{min} allowed the crack to close for each R-value used; however, at $R = 0.62$ the crack appeared to be barely closed at K_{min}. In contrast, the CTOD remained constant, or very nearly so, for each of the values of R. After the loading sequence for increasing R was complete (Fig. 6), the portion of the crack formed at lower R failed to close completely at K_{min}, whereas the portion of the crack which had been formed at higher R did close.

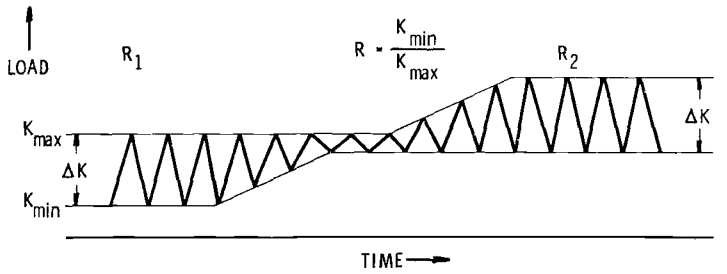

FIG. 6—*Schematic of the loading sequence used in changing load ratio.*

After cycling at $R = 0.62$, $K_{max} = 21$ MN/m$^{3/2}$, the crack was "underloaded" to $K = 2$ MN/m$^{3/2}$ and then reloaded to $K = 21$ MN/m$^{3/2}$ and subsequently cycled at the same $\Delta K = 8$ MN/m$^{3/2}$ as was used prior to the underload. At K_{min}, the crack tip was seen to be permanently open at the location of the underload, as shown in Fig. 7. For the portion of crack formed at $\Delta K = 8$ MN/m$^{3/2}$ after underload, CTOD and crack propagation rate appeared to be nearly the same as prior to the underload, although detailed measurements were not made. The R-change and underload sequences concluded the presentation.

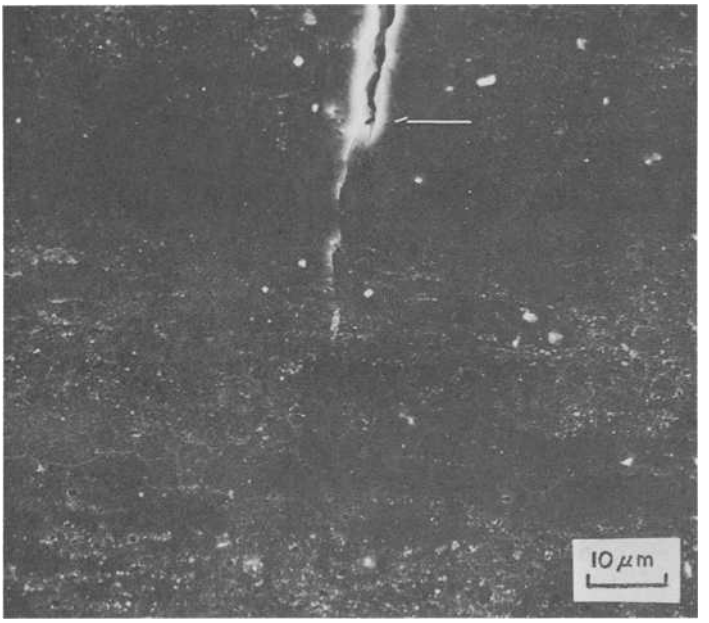

FIG. 7—*Powder metallurgy aluminum alloy MA-87.* K = *13 MN/m*$^{3/2}$. *Position of the underload to 2 MN/m*$^{3/2}$ *is shown by the arrow.*

Concluding Remarks

Because this videotape presentation represented the first real-time, truly high-resolution observations of actual fatigue crack propagation, we decided to present what we thought were typical events as "data," with only enough interpretive commentary and visuals as necessary to assist viewers in understanding how the experiments being shown were performed. We wanted each person to see and interpret personally what was shown. Since the presentation was limited to around 15 min, there was insufficient time to make it an instructional tool, with all the development of visuals and detailed explanation which such a presentation entails. The commentary which was made was interspersed with music[5] carefully chosen to quicken the observational senses required for interpreting the material being presented. This paper (footnote 2) offers more detail as to our interpretation of the sequences shown. We have had the benefit of 10 to 15 repeated viewings of the data; even so, there are still numerous observations which have not been described.

Experiments with the SEM cyclic loading facility are continuing, and the videotaped information, together with still photographs, such as shown in Figs. 1 through 5, should provide data for other presentations by film or videotape similar to that described in this paper.

[5] *El Curro + Guitar = Flamengo*, A Master Lab Production, San Antonio, Tex., 1965.

Chapter 4: Direct Observations of Ductile and Brittle Striations, Voids, and Microcracks

Jeffrey T. Fong[1]

Direct Observations—The Essential Ingredients for Discovering Fundamental Mechanisms of Fatigue

REFERENCE: Fong, J. T., **"Direct Observations—The Essential Ingredients for Discovering Fundamental Mechanisms of Fatigue,"** *Fatigue Mechanisms,* Proceedings of an ASTM-NBS-NSF symposium, Kansas City, Mo., May 1978, J. T. Fong, Ed., *ASTM STP 675,* American Society for Testing and Materials, 1979, pp. 287-291.

ABSTRACT: Through two stories from the history of medical science, both related to the theory of bloodletting as a treatment for inflammatory diseases, the importance of direct observations and the use of a numerical scheme in all scientific work, including fatigue mechanism research, are illustrated. Brief remarks on two specific questions arising from two earlier sessions on direct observations are inserted. The two questions are: (1) What is the connection between direct observations and quantitative microscopy? (2) What could fatigue design and testing engineers learn from the direct observations of fatigue damage at microscopic levels? A cautionary note on the temptation to extrapolate from insufficient direct evidence of fatigue damage is also included.

KEY WORDS: Benjamin Rush, bloodletting, direct observations, fatigue, fatigue mechanism, Pierre Louis, quantitative medicine, quantitative microscopy, statistical aspects of fatigue

As your session chairman for the third session of this symposium, I would like to make some brief remarks on the importance of direct observations of fatigue damage in response to two questions addressed to me yesterday following the first two sessions. The two questions are:

Question No. 1 (by Dr. Lou Coffin, General Electric Co.)—What is the

[1]Physicist and project leader, Center for Applied Mathematics, National Engineering Laboratory, National Bureau of Standards, Washington, D.C. 20234.

connection between quantitative microscopy on the one hand and the direct observations of microscopic fatigue damage on the other?

Question No. 2 (by Prof. Ralph Stephens, University of Iowa)—How can engineers who do fatigue testing and fatigue design benefit from viewing a large number of micrographs which supposedly show evidence of fatigue damage at dislocation and persistent slip levels?

As you all know very well, these two questions are "loaded" ones which cannot possibly be answered to their satisfaction during the brief period I have in opening this session. Nevertheless, as chairman of the organizing committee of this symposium, I cannot resist an opportunity to insert them in the record with a few remarks which, I hope, will satisfy both Dr. Coffin and Prof. Stephens in a partial sense.

The Medical Practice of Bloodletting, 1793

My remarks have to do with a classic story in the history of medicine as recently retold by Leon Eisenberg [*1*][2]. The story has to do with a famous medical doctor and university professor by the name of Benjamin Rush, who is also known to the American public as a signer of the Declaration of Independence. Trained at Edinburgh with a degree in medicine, Dr. Rush practiced in Philadelphia and taught at the College of Philadelphia, the predecessor of the first medical school in America. During a severe epidemic of yellow fever in Philadelphia in 1793, Dr. Rush was one of three physicians who remained behind to treat more than 6000 patients when a third of the city population fled to avoid the disease. In those days, the best medical theory, known as the Brunonian system, considered bloodletting as the appropriate treatment for yellow fever, with the following rationale:

> The action of bloodletting is to divert the force of the fever to [the bowels] and thereby save the liver and brains from a fatal and dangerous congestion. [*1*, p. 1106]

Dr. Rush went from patient to patient, letting blood copiously and purging with vigor. When he himself became ill, he instructed his assistants to bleed him plentifully and give him a dose of the mercurial medicine. From illness and treatment combined, he almost died. After a prolonged convalescence, he became well enough to write:

> Never before did I experience such sublime joy as I now felt on contemplating the success of my remedies. ... The conquest of a formidable disease was through the triumph of a principle in medicine. [*2*, p. 442]

Today, medicine has advanced so much that no one in his or her right

[2]The italic numbers in brackets refer to the list of references appended to this paper.

mind would accept Dr. Rush's theory and practice of bloodletting as an appropriate treatment for any disease. Even in those days, Dr. Rush's critics contended that his desperate remedies were more dangerous than the disease, but nothing was available to prevent Dr. Rush from committing grievous harm in the name of doing good.

A Study of Bloodletting by Direct Observations, 1835

Bloodletting continued to be a widely used medical remedy until the middle of the 19th century in both Europe and America. Since leeches were a particularly popular form of bleeding in France, Bollet [*3*, p. 94] noted that in 1827 Paris imported 33 million leeches a year, chiefly from Bohemia and Hungary. Fortunately, a French physician named Pierre Louis was not convinced that the theory of treating with bloodletting the class of diseases called "inflammatory" was correct. As a clinical clerk without pay, Louis worked in a hospital in Paris for almost seven years (1821-27). In 1835, Louis published ([*4*]; American translation, 1836) the first systematic study of the effect of bloodletting in pneumonia with a statistical table of the length of the disease, period of first bleeding, and the number of its repetitions, for a total of 78 cases. From this table of direct observations and the introduction of the numerical method, Dr. Pierre Louis concluded that

> bloodletting has had very little influence on the progress of pneumonitis ...; that its influence has not been more evident in the cases bled copiously and repeatedly, than in those bled only once and to a small amount; that we do not at once arrest inflammations, as is too often finally imagined; that, in cases where it appears to be otherwise, it is undoubtedly owing, either to an error in diagnosis, or to the fact that the bloodletting was practiced at an advanced period of the disease, when it had nearly run its course. [*4*]

Bollet [*3*] noted that Louis's paper marked the beginning of quantitative medicine, and his data were so convincing that bleeding quickly disappeared from medical practice shortly after his paper appeared.[3]

Direct Observations and Scientific Research

The stories of Benjamin Rush and Pierre Louis on the theory of bloodletting illustrate the fundamental approach that characterizes advances in all branches of science, namely, biological, physical, medical, material-related, and even the behavioral or social sciences. We need direct observations to motivate the choice of parameters, and we need a numerical scheme to quantify the observations such that a predictive theory can be formulated

[3] According to Bollet [*3*, p. 94], a few years after Louis's paper, only a few thousand leeches a year were being imported into Paris.

and tested with additional observations. In the case of fatigue mechanism research, the connection between direct observations and the numerical scheme known as quantitative microscopy is yet to be made, and that is why Dr. Coffin was unable to see the connection during the first two sessions of this symposium. On the other hand, I hope Dr. Coffin will agree with me that without a forum for discussing both the direct observations and the numerical scheme, the "marriage" of the two will perhaps never be realized, to the detriment of the fatigue research and design community. This concludes my remark on Question No. 1.

Direct Observations and Phenomenological Research

To answer Question No. 2 as posed by Prof. Stephens, I would like to refer once again to the stories of Benjamin Rush and Pierre Louis by observing that Louis's contribution was to disprove a theory by a careful documentation and analysis of a series of direct observations at the phenomenological level. If it were possible for Dr. Louis to have access to the means of making direct observations at various microscopic levels as we do today, his contribution most likely would not be limited to a negative finding; that is, he would first disprove the theory of bloodletting and then propose a new cure based on direct observations and scientific analysis. If the search for a better cure for an illness may be compared with the search for a better phenomenological theory of fatigue life prediction, the "patient" in the latter case being a specimen or a finished component, a fatigue design or testing engineer can profit a great deal by viewing a series of micrographs on various mechanisms of fatigue. This concludes my remark on Question No. 2.

Direct Observations and Fatigue Mechanism Research

Having said that direct observations are the essential ingredients for all scientific advances, including fatigue mechanism research, I wish to add one cautionary note on the difficulty we all face when we have to decide whether the observations we have already amassed are "enough." Since direct observations are invariably time-consuming and costly, it is not unusual for many research workers to propose "new" or "modified" fatigue mechanisms based on a limited amount of direct evidence. In a paper I prepared for this symposium for discussion in tomorrow's session [*5*], I intend to go into greater detail on the rationale for pooling our observations at different levels of characteristic lengths. In other words, I am of the opinion that a breakthrough in fatigue mechanism research is achievable through a concerted effort of collaboration among fatigue research workers and specialists in allied disciplines. The chance for a single

individual to achieve that breakthrough is relatively slim by virtue of the sheer magnitude of the demand for direct observations.

A Concluding Quote

To conclude, I wish to quote a passage, again written by Pierre Louis as documented by Osler [*6*], on the care in interpreting direct observations:

> Think for a moment, sir, of the situation in which we physicians are placed. We have no legislative chambers to enact laws for us. We are our own law-givers; or rather we must discover the laws on which our profession rests. We must *discover* them and not invent them; for the laws of nature are not to be invented. ... [*6*]

We who design machines and structures and dedicate ourselves to the safe performance of those objects are not unlike the physicians Dr. Louis was referring to. We must discover the fatigue mechanisms on which our profession rests. We must *discover* them and not invent them, as Dr. Louis said, and in the process of our discovery, direct observations with proper documentation and discussion are the guidebooks to the microscopic world of atoms, dislocations, slips, and cracks.

Acknowledgment

I wish to thank Dr. Thomas Chen of the Veterans Administration Hospital in South Orange, New Jersey, for providing me with a copy of Dr. Bollet's paper [*3*] and for discussions on the value of the quantitative method in medicine.

References

[*1*] Eisenberg, L., *Science,* Vol. 198, 16 Dec. 1977, pp. 1105–1110.
[*2*] Middleton, W. S., *Annals of Medical History,* Vol. 10, 1928, p. 434.
[*3*] Bollet, A. J., *The American Journal of the Medical Sciences,* Aug. 1973, Vol. 266, No. 2, pp. 92–101.
[*4*] Louis, P., *The American Journal of the Medical Sciences,* Vol. 18, 1836, p. 102.
[*5*] Fong, J. T., this publication, pp. 729–758.
[*6*] Osler, W., *Bulletin of Johns Hopkins Hospital,* Vol. 8, 1897, p. 161.

W. W. Gerberich[1] *and N. R. Moody*[1]

A Review of Fatigue Fracture Topology Effects on Threshold and Growth Mechanisms

REFERENCE: Gerberich, W. W., and Moody, N. R., **"A Review of Fatigue Fracture Topology Effects on Threshold and Growth Mechanisms,"** *Fatigue Mechanisms,* Proceedings of an ASTM-NBS-NSF symposium, Kansas City, Mo., May 1978, J. T. Fong, Ed., *ASTM STP 675,* American Society for Testing and Materials, 1979, pp. 292-341.

ABSTRACT: A review of fatigue crack propagation and near-threshold surfaces in α/β titanium and iron-base alloys reveals at least 10 types of alternate fracture processes, compared with the more common striation process. Microstructural influence was found in all materials with interactive effects of temperature, frequency, and environment. At low temperatures, alternate cleavage modes produce crack growth exponents that increase in a consistent way with either a decrease in test temperature or a decrease in fracture toughness. Such phenomena may be understood in terms of void-induced fracture strain concepts or, alternatively, with strain-rate sensitivity concepts applied to ductile ligaments. Factors of two to three increase in threshold are shown to exist through microstructural modification of either Widmanstätten colony or grain size. A semicohesive ligament zone based upon a modified Dugdale-Barenblatt model is shown to predict both of these microstructural effects. It is emphasized that such models are in their formative stages and require additional modification to include overload, *R*-ratio, and strain-hardening concepts.

KEY WORDS: analytical models, fatigue, fatigue crack propagation, fatigue threshold, fractography, iron alloys, low temperature, mechanical properties, microstructure, titanium alloys

As little as six years ago, the main approach to fatigue crack propagation involved plastic strain, crack-tip displacement, or shear band decohesion models. Although effects of crack branching, crack-tip blunting, and precavitation were becoming recognized [*1,2*][2] virtually all models emphasized the striation growth process. This review was prompted by the rapidly expanding view that microstructure plays a far more important role in governing fatigue crack propagation than was previously recognized. A

[1]Professor and graduate student, respectively, Department of Chemical Engineering and Materials Science, University of Minnesota, Minneapolis, Minn. 55455.

[2]The italic numbers in brackets refer to the list of references appended to this paper.

large number of the papers in a recent fatigue conference [*3-6*] emphasized the microscopic effects that may predominate in one region or another of the growth process. Even with these, there has been no recent attempt at pulling together microscopic and macroscopic views where alternate fracture modes are concerned. In particular there are either few or no reviews on

1. alternate microscopic fracture modes
2. how the grain size affects the threshold stress intensity
3. the influence of low temperature on fatigue crack surface morphology and growth rate, or
4. possible models of alternate microscopic fracture modes for either threshold or kinetics.

Major exceptions have been recent papers by McEvily [*3*] and Beevers [*5*], who reviewed the effects of load ratio, microstructure, environment, and crack closure on crack growth at low stress-intensity values. Beevers [*5*] emphasized that an increase in the grain size generally produces an increase in the threshold stress intensity. Although several threshold models were offered, there was no suggestion as to how grain size could be incorporated into such models.

An equally interesting microstructural effect concerns the shape and size of the second phase in α/β titanium alloys. There is mounting evidence that the controlling fracture process near threshold may be environmental and that crack growth rates may be changed by at least a factor of three by changing the character of the microstructure.

The underlying theme of this paper is to review fatigue crack growth with regard to such microstructural effects. Although such a review is too ambitious for a single paper, we will attempt to cover (1) and (2) of the foregoing but only touch on (3) and (4). As a further restriction, only two material classes will be evaluated and ductile striation mechanisms by themselves will be omitted. In the course of this investigation, some original contributions pertaining to iron-base and α/β titanium alloys are included.

Materials and Procedures

This paper will consider two classes of materials, the iron-base body-centered-cubic (bcc) systems and the titanium-base α [hexagonal-close-packed (hcp)] or α/β (hcp/bcc) alloys. Of primary emphasis in the iron-base systems will be ferrite or ferrite/pearlite steels although some mention of ultra-high-strength steels will be made. These systems were chosen since they both exhibit mixed modes of fatigue crack propagation which change as a function of ΔK. They also can be heat-treated to produce similar microstructures ranging from large- to fine-grain, two-phase duplex, partially martensitic or partially Widmänstatten-like structures. Several of these morphologies are depicted in Fig. 1. Besides generally reviewing

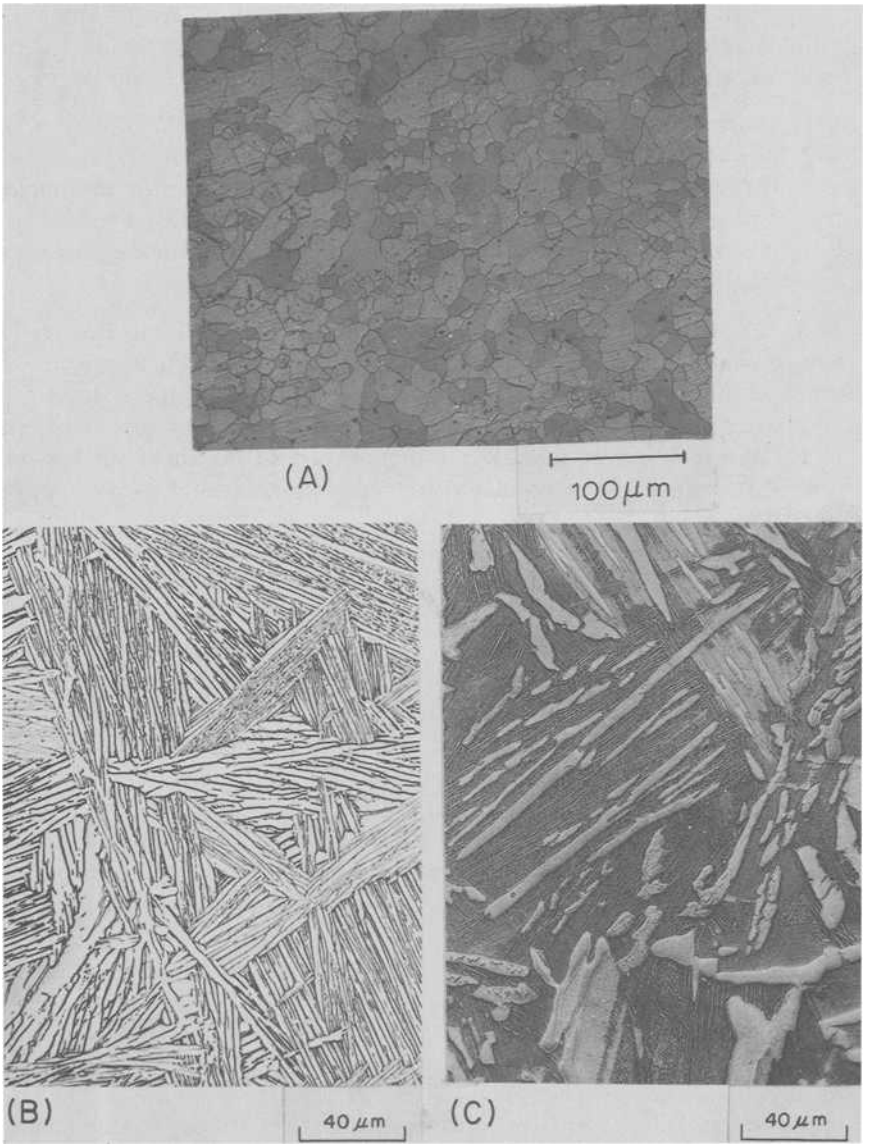

FIG. 1—*Typical microstructures for* (a) *medium grain size Fe-1Si;* (b) *Widmanstätten colonies in Ti-6Al-4V;* (c) α *grains in an* α/β *matrix of Ti-6Al-4V. Figure 1*b *courtesy of Chesnutt et al* [17].

microstructural effects, we have generated two new sets of data with regard to frequency effects in Ti-6Al-6V-2Sn and low-temperature fatigue crack propagation in iron, iron-nickel, and iron-silicon alloys, the details of the materials being given in Table 1. In the experimental portion, both compliance and fatigue-crack-propagation gage techniques were utilized to detect growth rates in compact tension specimens (5 by 4.5 by 1 cm) with a/w values ranging from 0.4 to 0.7. A hydraulic feedback control test machine was utilized at 20 Hz for most of the tests except for one low-frequency group tested at 0.2 Hz. Ambient tests were run in laboratory air while low-temperature tests were run in a controlled temperature chamber to ± 1 K with a dry nitrogen gas being used as the coolant.

No threshold data were measured in these materials. Where threshold data are reported from the literature, a growth rate of 10^{-8} mm/cycle was considered as threshold. It is quite true that a growth rate of 0.1 Å still might not represent threshold in some materials, indeed if there is any. However, for both low- and high-strength steels [*6*], there are few if any changes in ΔK for growth rates less than 10^{-8} mm/cycles.

Microstructural Overview

General Morphology

The premise of this paper is that microstructural effects must be carefully documented in all regions of fatigue crack propagation if realistic micromechanical or continuum mechanical models are to be forthcoming. The guiding principle is that, when alternate fracture modes are present, microstructure is fundamental to the rate limiting step. The generality of this principle is *not established* but there is sufficient evidence to suggest it [*3-18*]. If such a principle is valid, how common are such alternate modes and what form do they take?

Recognizing that only a limited number of materials have been reviewed, the schematic in Fig. 2 suggests at least 10 different fatigue crack propagation modes. The first four suggest transgranular "cleavage," the next four are intergranular types and the last one may be either. In Fig. 2*a*, the grain at the tip of a striated region has cleaved on a plane tilted at an angle ϕ to the crack plane. The cleaved grain could also be twisted at an angle, Ψ, as is discussed later. Such features are common in low-strength iron and steel alloys fatigued at low temperatures [*7-10*]. An example of this in Fig. 3 for Fe-4Ni tested at 123 K with a ΔK of 21.8 MPa-m$^{1/2}$ demonstrates that most grains have cleaved nearly normal to the applied stress although there are some obvious tilts and twists. In Fig. 2*b*, cyclic cleavage[3] is suggested on the crystal planes as identified by Neuman et al

[3]Cyclic cleavage will be defined as any brittle-appearing transgranular growth mechanism that is discontinuous whether it is truly cleavage [*11*] or glide-band decohesion [*12, 13*].

TABLE 1—*Composition (weight percent) and grain size of iron-binary alloys.*

Alloys	C	Ni	Si	Ti	Others	Fe	Grain size, μ	ASTM Grain Size No.
Fe	0.01	...	...	0.077	<0.05	balance	41	7
Fe-1Ni	0.02	1.11	...	0.099	<0.05	balance	36	7
Fe-2.5Ni	0.02	2.58	...	0.09	<0.05	balance	42	7
Fe-4Ni	0.02	4.11	...	0.09	<0.05	balance	48	6
Fe-1Si	0.01	...	0.49	0.088	<0.05	balance	24	8
Fe-2.5Si	0.01	...	1.22	0.096	<0.05	balance	31.8	8
Fe-4Si	0.02	...	1.92	0.123	<0.05	balance	50.3	6

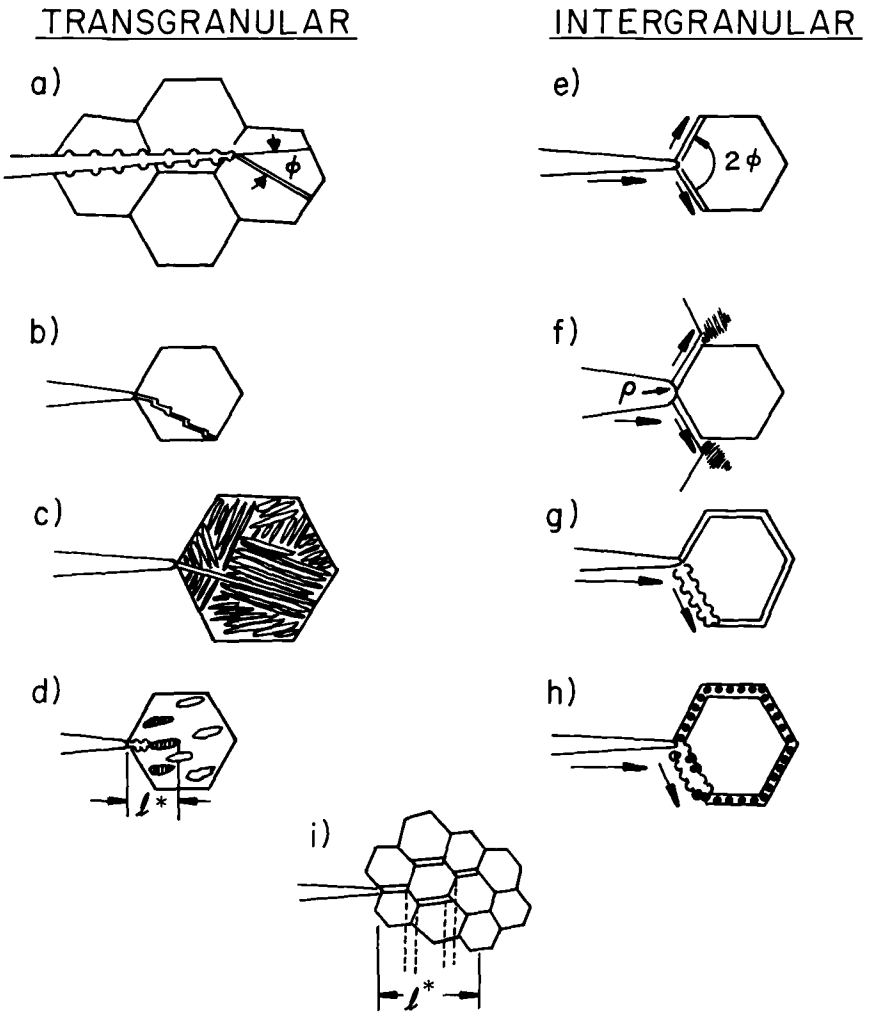

FIG. 2—*Types of alternate microscopic fracture modes:* (a) *tilted cleavage;* (b) *cyclic cleavage;* (c) α/β *interface fracture;* (d) *cleavage of* α *in an* α/β *phase field;* (e) *forked intergranular cracks in a hard matrix;* (f) *forked intergranular cracks in a soft matrix;* (g) *ductile intergranular striations;* (h) *particle nucleated ductile intergranular voids; and* (i) *discontinuous intergranular facets.*

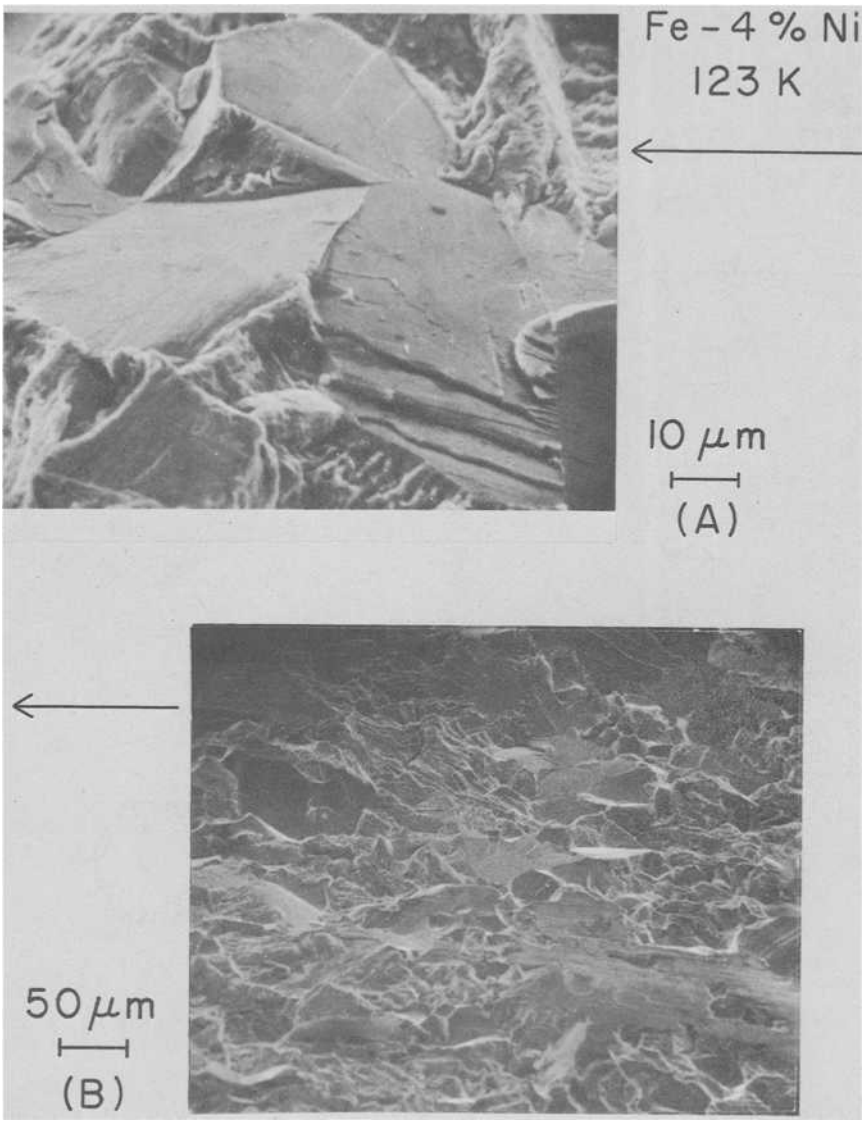

FIG. 3—*Fracture surface topography of Fe-4Ni fatigue cracked at 123 K with* $\Delta K = 21.8$ *MPa-m*$^{1/2}$.

[*11*] in Fe-3Si. Similar features have been observed in polycrystalline iron-silicon alloys in the present investigation and in Ti-6Al-4V at low ΔK values [*13,14*]. An example in this α/β titanium alloy is shown in Fig. 4, where the finest parallel lines indicate a minimum detectable growth rate of 1.43×10^{-7} m/cycle whereas the macroscopic average was 2.5×10^{-10} m/cycle. Such a fracture process may actually be closer to those suggested

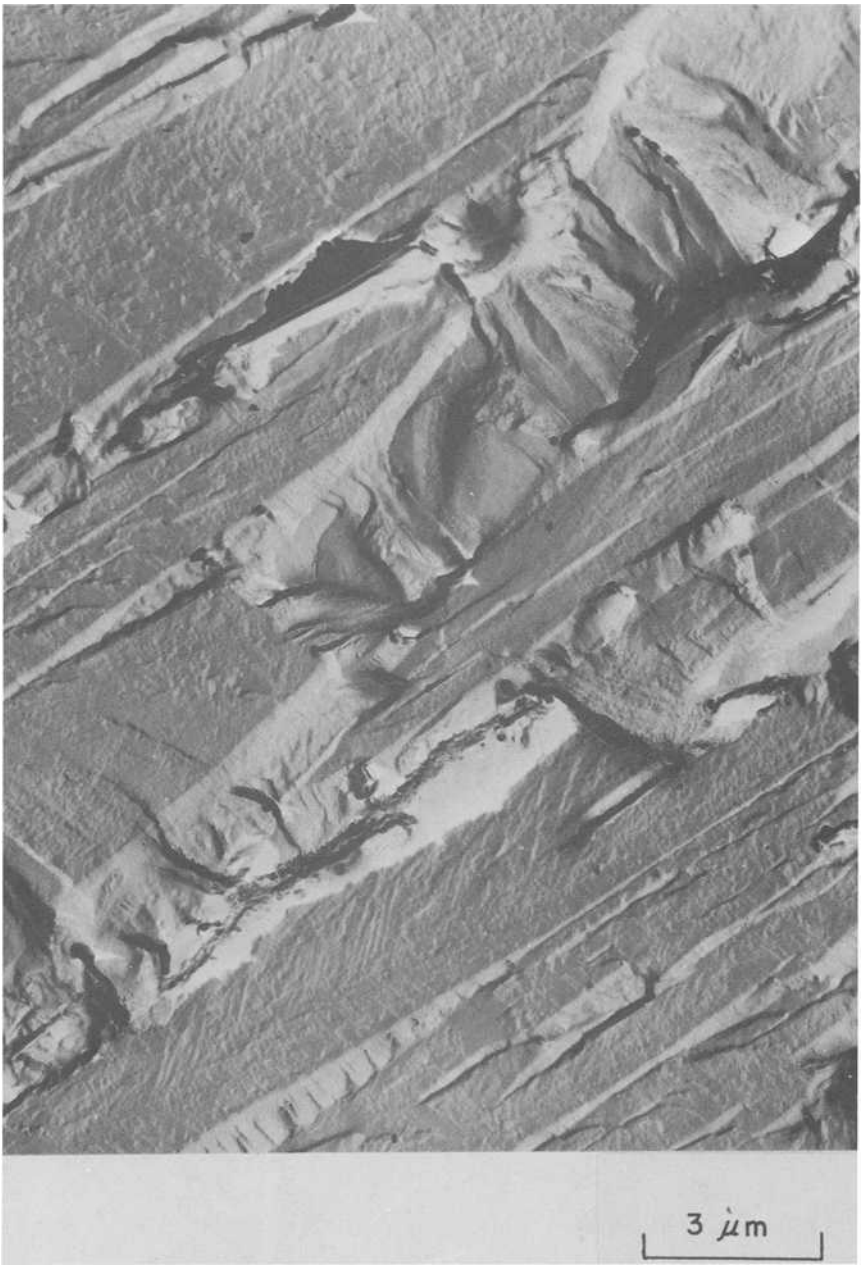

FIG. 4—*Typical Ti-6Al-4V fracture topography for* da/dN $< 2.5 \times 10^{-10}$ *m/cycle. Courtesy of Bucci et al* [14].

in Fig. 2*c* and *d*. For example, fatigue crack propagation can occur along either α/β interfaces [*15–17*] or across the alpha platelets [*17,18*] in the Widmanstätten microstructure of Fig. 2*c*. In either case, the intercolony spacing is considered to be the controlling microstructural feature. For larger α-platelets surrounded by a finer Widmanstätten α/β-matrix, there is a greater tendency for the primary α to "cleave" ahead of the main crack front [*16,19*] and leave ligaments behind which undergo a typical ductile striation mechanism. Such a transgranular mechanism, as depicted in Fig. 2*d*, would consist of a mixed-mode process where the controlling microstructural unit would be the interalpha spacing l^*. An excellent example of such a mixed-mode process in Ti-6Al-4V comes from Chesnutt et al [*17*] where it is obvious in Fig. 5 that the primary α is fracturing along a specific set of "cleavage" planes compared with the matrix.

At low ΔK values, the intergranular forked cracks (or tilts and twists) depicted in Fig. 2*e* are common to high-strength steels [*7,8*]. Although no example could be found, it is also possible to have an intergranular forked crack in a brittle boundary surrounding a soft matrix. If the grain size were sufficiently large, this could lead to localized crack-tip blunting as indicated in Fig. 2*f*. What appears to be a rare occurrence, as indicated by its absence in the literature, is intergranular ductile fatigue striations, as depicted in Fig. 2*g*. This was found to be a fairly common feature in the iron-nickel alloys of the present study at ΔK values less than 10 MPa-m$^{1/2}$. In the micrograph shown in Fig. 6, the resolvable striation spacing was a factor of six greater than the macroscopic value of 2×10^{-8} m/cycle. At least two studies have found microvoid coalescence along intergranular facets as indicated in Fig. 2*h*. One involved interface decohesion of incoherent grain boundary precipitates in an overaged iron-nickel-aluminum alloy [*20*] while the other resulted from a similar mechanism with silicide particles nucleating voids in a Ti-4Al-4Sn-4Mo-0.47Si alloy [*21*]. Finally, either a series of properly oriented intergranular cracks, as indicated in Fig. 2*i*, or fully cleaved grains could open up, leaving the remaining grains or ledges in between as ductile ligaments. This whole region could represent the critical microstructural unit, l^*, as the controlling event during fatigue crack propagation. Such a two-stage fracture process has been observed and interpreted by Robinson and Beevers [*22*] to explain both grain size and R-ratio (K_{min}/K_{max}) effects during fatigue growth in three α-titanium alloys.

Mixed-Mode Observations

Changing fracture modes are observed in virtually every material of this study. In fact, there are usually two major fracture mode changes [*3,5,23–25*] for both titanium and steel alloys. Ritchie [*24*] summarizes these transitions by describing the low ΔK Regime "A" as being microstructurally and

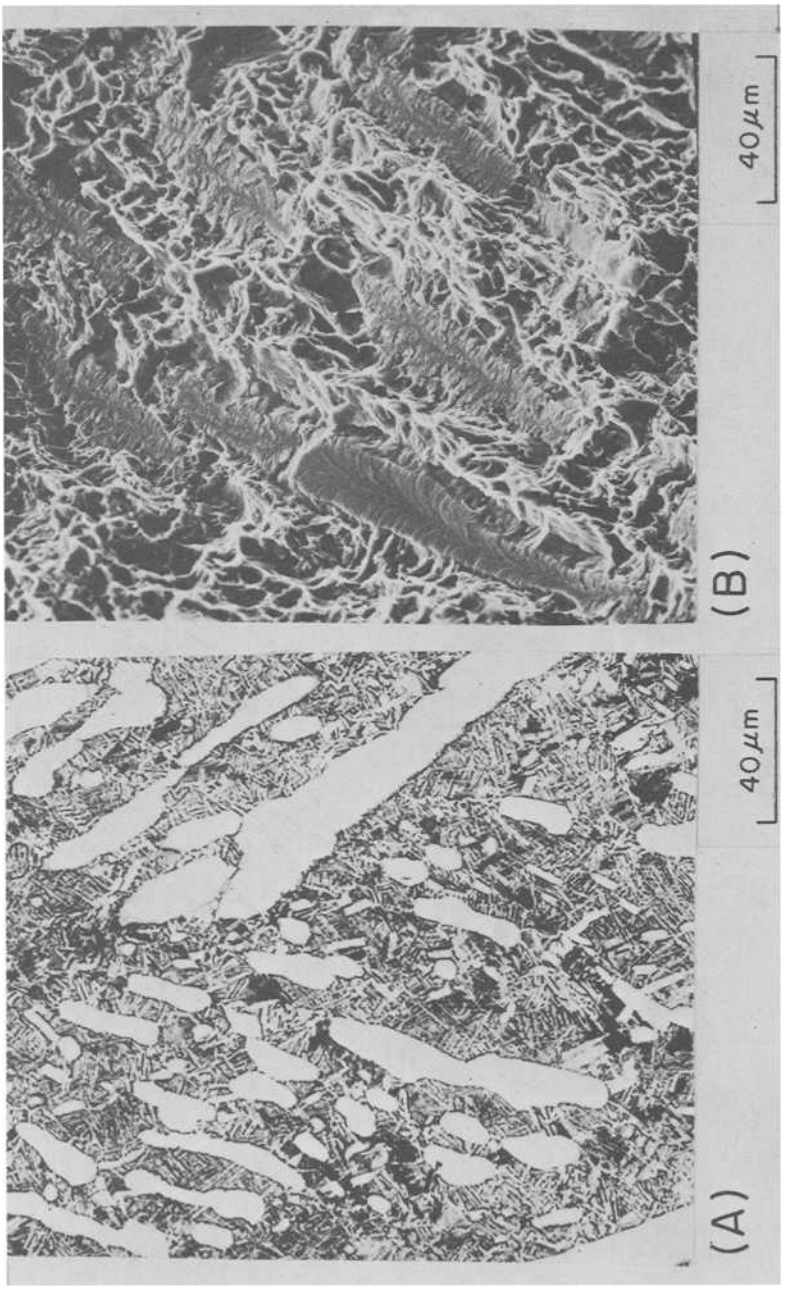

FIG. 5—*Second-phase cleavage fracture in Ti-6Al-4V: (a) light micrograph of polished and etched surface;* (b) *scanning electron micrograph of fracture surface. Courtesy of Chesnutt et al* [17].

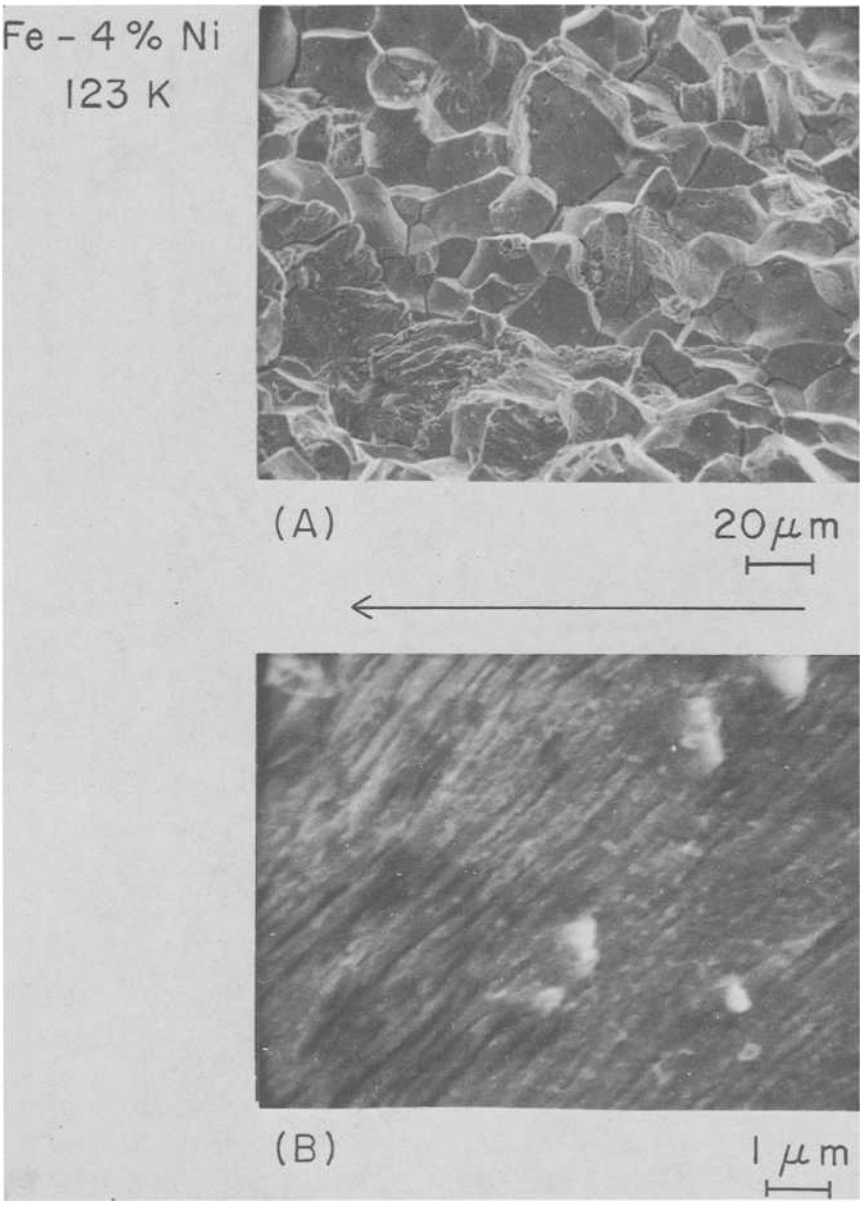

FIG. 6—*Fracture surface topography showing ductile intergranular fatigue striations in Fe-4Ni fatigue cracked at 123 K with* $\Delta K < 10$ *MPa-m*$^{1/2}$.

environmentally dependent, Regime "B" as being the microstructure-insensitive continuum regime characterized by striations, and Regime "C" as being static mode-dependent. The latter involves K_{max}-induced cleavage, intergranular or fibrous fracture modes which, again, give a microstructural dependence.

A classic example of the transition from Regime "A" to Regime "B" is given by Yoder et al [*26*], where they show fracture of Widmanstätten colonies in Ti-6Al-4V to predominate below the transition and ductile striations above. In this case, as well as in the correlations of Birbeck et al [*27*] and Beevers et al [*5,16,22*], the transition occurs when the reversed plastic zone size equals the controlling microstructural unit, that is, the Widmanstätten packet size or the grain size. The transition from Regime "B" to Regime "C" has been interpreted by Rosenfield [*28*] in terms of the fracture toughness and is discussed later. In addition to these transition observations, there have been several quantitative fractographic observations [*5,23-25*] of how much of each fracture mode is present as seen in Fig. 7. There are some decided similarities here. In each case there is a static fracture mode that signals the onset to Regime "C" near a ΔK of 30 MPa-m$^{1/2}$ for $R \approx 0$. For Ti-6Al-4V and 17-4 pH stainless steel, the static mode is ductile rupture while in the EN-24 high-strength steel it is intergranular. Below this regime, ductile striations are the dominant microscopic fatigue mode, representing from 80 to 100 percent of the growth process. Further lowering of ΔK produces a second microstructural-sensitive regime which may be faceted, intergranular, or cleavage in character and constitute as much as 100 percent of the microscopic process. To summarize mixed-mode observations, Fig. 7 makes it clear that at least three regimes of fatigue crack propagation exist, at least two of which are sensitive to microstructure and hence require incorporation into either micromechanical or continuum modeling.

With this overview, the next sections deal with how microstructure affects crack propagation first near threshold and then at higher growth rates.

Near Threshold

Grain Size

The effect of grain size on threshold and near-threshold behavior has been discussed by many investigators [*5,16,22,29-31*] with the consensus that there is a strong effect in several material classes. This is particularly pertinent to the present discussion since near-threshold behavior is often represented by alternate fracture modes and hence one might expect a strong grain-size effect. In contrast to this, a recent dislocation model [*32*] suggested that the ratio of threshold to shear modulus is nearly constant

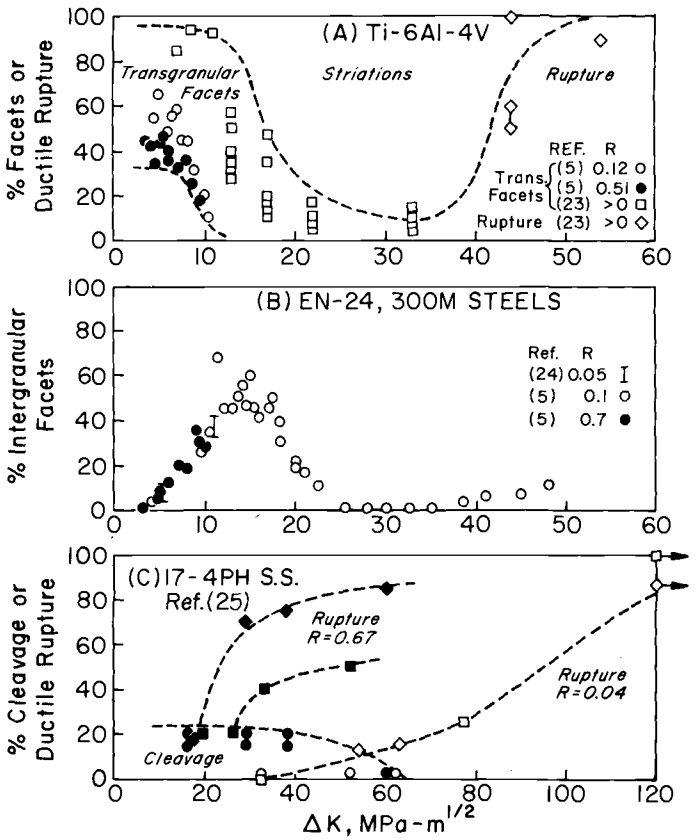

FIG. 7—*Effect of* ΔK *on mixed fracture modes in:* (a) *an* α/β *titanium alloy:* (b) *high-strength steels;* (c) *a precipitation-hardened stainless steel.*

for many materials, independent of any microstructural characteristics. However, at least two of the materials cited in that investigation [*32*] do show a strong grain-size effect. To illustrate this, threshold data[4] for three classes of materials [*5,9,16,22,29-35*] were normalized on modulus and plotted as a function of the square root of the grain size in Fig. 8. There is a reasonably strong positive correlation ($r = 0.69, 0.79$) between $\Delta K_{TH}/E$ and $d^{1/2}$ for the low-strength steels and titanium alloys while there is a slight negative correlation for the high-strength steels. The latter effect may be environmentally influenced as suggested by Ritchie and Carlson [*31,36*]. The fact is that grain size may affect the threshold value by at least 100 percent in two material classes. It is interesting that the low-strength steel

[4]It should be pointed out that where ΔK_{TH} was not obvious, extrapolation of log da/dN versus log ΔK to 10^{-8} mm/cycle was considered as the threshold.

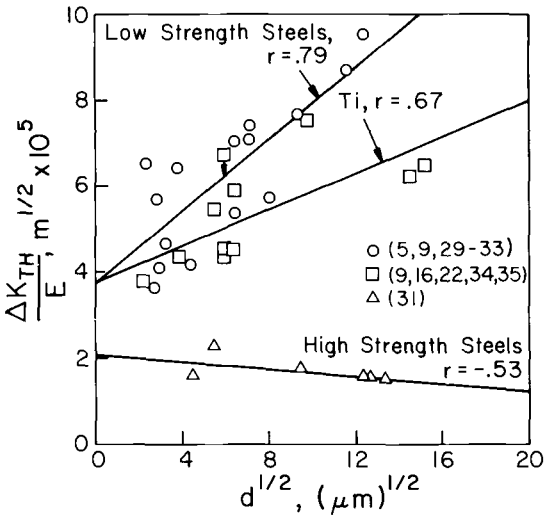

FIG. 8—*Influence of grain size on normalized fatigue thresholds in three classes of materials.*

and titanium linear regression curves do extrapolate back to the same normalized threshold value where, in the absence of microstructural or environmental effects, dislocation mechanisms may prove to be sufficient.

Microstructure

To further illustrate the strong microstructural effect near threshold, data [*16*] on Ti-6Al-4V heat-treated to four different microstructures are given in Table 2. It is seen that the ΔK value to produce one Burgers vector of growth per cycle varies by a factor of two. Furthermore, although the reversed plastic zone size might be fundamental to the transition between Regimes "A" and "B," near threshold this zone is about an order of magnitude smaller than the controlling microstructural parameter. In addition, the reversed plastic zone varies by a factor of seven at the same crack growth rate, which obviates any simple cyclic plasticity or emissary dislocation model. From Table 2, one might conclude that the yield strength is controlling since $\Delta K_{lb/cycle}$ is inversely proportional to σ_{ys}. This would be in accordance with a view recently postulated by Ritchie [*36*] for high-strength steels where the yield strength dependence was rationalized in terms of an environmental dependence. Nevertheless, there is reason to believe that this is not the case in this material because of the strong variation of fracture surface topology. Irving and Beevers [*16*] demonstrated that the structure-sensitive growth region involved large deviations out of

TABLE 2—*Effect of microstructure on near-threshold fatigue* [16].

Microstructure	α-grain, μm	β-grain, μm	σ_{ys} MPa	Reversed Plastic Zone Size, μm	ΔK^a at lb/cycle MPa/m$^{1/2}$
Martensitic	3.5	2.1	1,000	0.21	2.8
Mill-annealed	3.2	0.8	863	0.41	3.4
Transformed β	3.1	1.4	850	0.53	3.8
β-Annealed	8.0	93[b]	752	1.58	5.8

[a] $R = 0.35$.
[b] Widmanstätten colony size.

plane, with the scale of irregularities being commensurate with the scale of the microstructure. Furthermore, the fatigue cracks were shown to be stopped by β or transformed β material, which appeared as ligaments along the crack path. Alternatively, the crack path followed the α/β interface in the β-annealed material. These two processes would correspond to Fig. 2*d* and *c*, respectively. Based upon fractographic evidence, Irving and Beevers propose a two-stage model for structure-sensitive growth in which facets are first formed ahead of the crack and then the interfacet ligaments are parted. We concur in this mechanism and will later demonstrate how such a process may quantitatively explain both grain and microstructural size effects on ΔK_{TH}.

Temperature, Frequency, Environment

As several of the foregoing effects might involve external variables, an attempt to review temperature, frequency, and environment was made but few well-documented effects were found.

There are few frequency studies, although Hopkins, et al [*35*] did find that ΔK_{TH} increased by about 10 percent with an increase in test frequency. However, consider the following tabulation for Ti-6Al-4V aged at 977 K for 2 h

Reference:	[*35*]	[*16*]	[*14*]	[*35*]
Frequency, Hz	30	130	145 to 170	1000
[5] $\Delta K_{TH(R=0)}$, MPa-m$^{1/2}$	4.8	4.2	6.1	5.4

It appears that there is relatively little influence of frequency between 30 and 1000 Hz for this α/β titanium alloy. This does not mean that environment has no effect on ΔK_{TH}. In fact, both Beevers [*5*] and Ebara et al [*37*]

[5] These values of threshold were normalized to $R = 0$ using a formulation suggested by McEvily [*3*]: $\Delta K_{TH(0)} = \Delta K_{TH(R)} \sqrt{(1-R)/(1-R)}$

have demonstrated that ΔK_{TH} for mill-annealed Ti-6Al-4V in vacuum is about 2.5 times that tested in laboratory air, while Cooke et al [*38*] showed a similar trend for EN-24 steel. This suggests that some of the effects in Fig. 7 might be environmental. For example, consider the steel data from Fig. 7*b*; the data at $R = 0.1$ might be qualitatively explained as follows. At low ΔK values, striations predominate because the K_{max} is not sufficient to produce environmentally induced growth along grain boundaries. As K_{max} increases, the percentage of intergranular fracture increases to a peak where the transition from Regime "A" to Regime "B" takes place near a ΔK of 20 MPa-m$^{1/2}$. Unfortunately, the calculated reversed plastic zone size is only 10 μm whereas the prior austenite grain size is 88 μm. An even greater discrepancy results taking the $R = 0.7$ data at a K_{max} of 30 MPa-m$^{1/2}$, which represents a reversed plastic zone of 2 μm. Thus, the transition from faceted fracture to striation growth does not seem to follow the correlation of reversed plastic zone size to the grain size as it did for titanium [*5, 16, 22*]. An alternative explanation might be that, as the crack is growing faster, there is less time for the environmental effect and hence the striation growth takes over once again. Such a process may be envisioned by arbitrarily placing the shape of the *da/dt* versus *K* curve for internal hydrogen embrittlement [*39*] or aqueous stress-corrosion on the curve of $(da/dN)f$ versus K_{max}. As is noted in Fig. 9, a crossover in fracture mode might

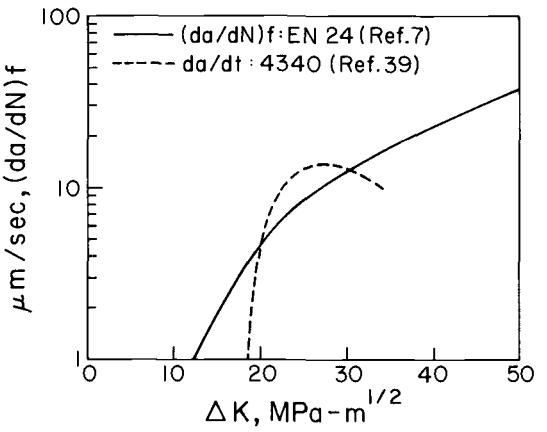

FIG. 9—*Possible environmental influence in producing an alternate microscopic fracture mode; intersection of cyclic-dominated and hydrogen-dominated crack velocity curves.*

occur. Above and below the crossover, striations might predominate, but, in the intermediate region, intergranular facets would be the microscopic mode.

Growth

Power-Law Limit

As the microstructure-sensitive Regime "A" is exceeded, fatigue crack growth is characterized by striations and the Paris [*40*] power law giving

$$\left.\frac{da}{dN}\right|_{\text{power law}} = C\,\Delta K^n \tag{1}$$

where

da/dN = crack growth rate,
C,n = constants, and
ΔK = stress intensity range.

Beyond Regime "B", the second microstructural-sensitive regime is entered as ΔK approaches instability at the fracture toughness limit. The transition to this static mode growth Regime "C" has been quantified by Rosenfield [*28*] for Ti-6Al-4V. He suggested that the Forman [*41*] equation be used in Regime "C" since it accounts for both the R-effect and the fracture toughness limit, giving

$$\left.\frac{da}{dN}\right|_{\Delta K \to K_c} = \frac{C\Delta K^n}{(1 - R)\,(K_c/\Delta K) - 1} \tag{2}$$

Rosenfield [*28*] reasoned that equating Eq 1 to Eq 2 should provide an upper bound on ΔK for power-law behavior, with the transition at

$$\left.\Delta K\right|_{\text{power-law limit}} = K_c\left(\frac{1 - R}{2}\right) \tag{3}$$

This relationship was tested with the data collected by Rosenfield [*28*] and others [*15,42*] on α/β titanium alloys and data on low-alloy [*7,24,43-46*] or martensitic stainless steels [*25*]. As shown in Fig. 10, the correlation is excellent for titanium and steel alloys. The microstructural significance is that an increasing amount of microvoid coalescence is most often found coexisting with striations once this limit has been exceeded. This has been observed in weld metal, EN30B steel [*7*] Ti-6Al-4V [*15,23*], 17-4 pH stainless steel [*25*], and was qualitatively indicated in Fig. 7.

Grain Size, Frequency, and Environment

There is no question that grain size has a large effect on growth rate near threshold in the low-strength steels and titanium alloys of Fig. 8. It is

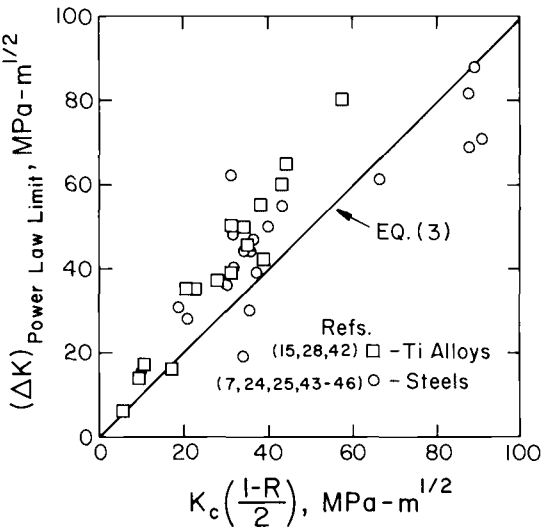

FIG. 10—*Fracture toughness prediction of the transition from power-law behavior in regime "B" to microstructural sensitive Regime "C."*

not clear at higher growth rates since grain size, frequency, and environmental effects are difficult to separate with available information. Sufficient data were found in α and α/β titanium alloys to indicate a strong grain-size effect on both nonenvironmental and environmentally enhanced growth rates. Data [*47-51*] were collected in Table 3 at relatively constant ΔK values with R near zero. The rationale was that either vacuum tests or tests at frequencies greater than 20 Hz would minimize the environmental effect. Alternatively, aqueous corrosion, external gaseous hydrogen, and internal hydrogen were all considered as possible environmental agents at low cyclic frequencies. Examination of these data show that there is a strong grain-size effect, with the large-grain-size materials generally providing an order of magnitude slower growth rates than the fine-grained ones regardless of whether hydrogen is involved or not. In addition, there is a strong environmental effect, with crack velocities being about two to twenty times faster regardless of how hydrogen is provided. To demonstrate the extent of this effect, five decades of da/dN results at 0.2 and 20 Hz are shown in Fig. 11. As the test conditions were otherwise identical, the separation in the curves is considered to be due to the 48-ppm internal hydrogen. It is of further interest that the perturbation in the curves near a ΔK of 30 MPa-$m^{1/2}$ represents a cyclic plastic zone size of 30 μm which is nearly equal to the average platelet size of 35 μm.

There is a microstructural effect here, but it is not clear how pervasive it is. As was shown in Fig. 5, the fatigue crack propagation process in mill-annealed titanium involves whole alpha grains "cleaving." Recent evidence

TABLE 3—*Grain size-frequency-environment interaction in α/β titanium alloys.*

Reference	Material	Grain Size, μm	Frequency,[a] f, Hz	Environment	ΔK, MPa-m$^{1/2}$	da/dN, m/cycle, ×10^8		Ratio
						High f or vacuum	H_2 Effect	
47	Ti-5Al-2.5Sn	105	0.5	1-atm external	40	5.5	210	38.2
47	Ti-5Al-2.5Sn	600	0.5	1-atm external	40	4.8	5.6	1.2
51	Ti-6Al-4V	~130	8.3	241 kPa external	20	33	81	2.5
50	Ti-6Al-4V	~50	0.1	215-ppm internal	30	40	500	12.5
This study	Ti-6Al-6V-2Sn	35	0.2	48-ppm internal	40	200	440	2.2
48	Ti-6Al-6V-2Sn	~35	0.5	? internal	40	230	460	2.0
48	Ti-6Al-6V-2Sn	~35	0.5	0.6 M NaCl	40	230	1780	7.7
49	Ti-8Al-1Mo-1V	~30	0.5	3½% NaCl	40	100	2500	25.0
49	Ti-8Al-1Mo-1V	~1600[b]	0.5	3½% NaCl	40	18	100	5.6

[a]Frequency for environmental tests.
[b]This represents the α grain size from β annealing for 4 h at 1340 K. The Widmanstätten colony size would have been smaller.

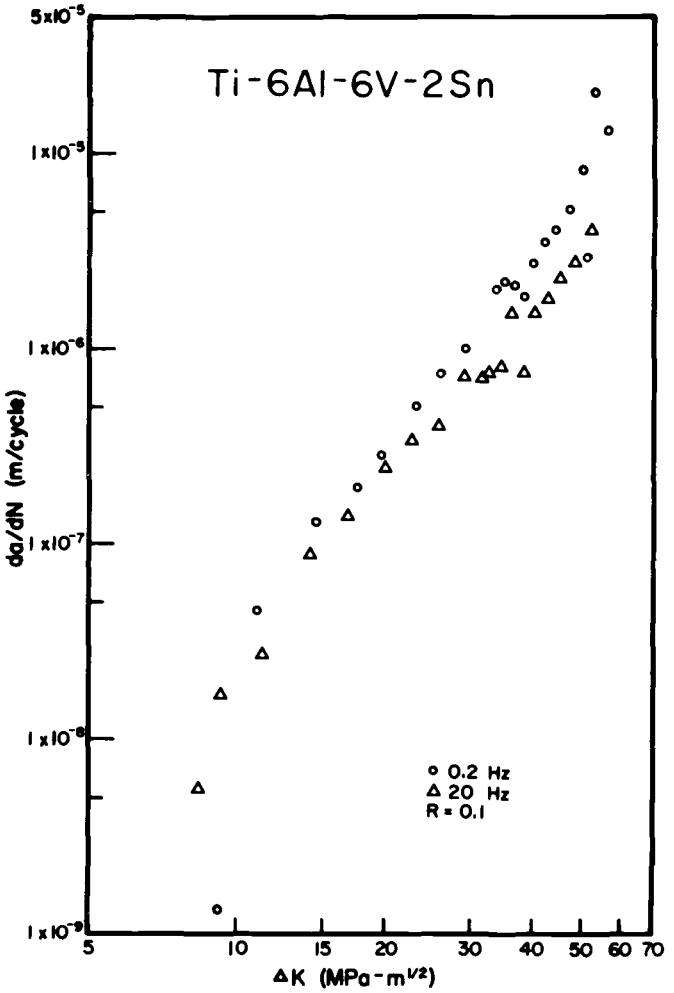

FIG. 11—*Frequency effect in Ti-6Al-6V-2Sn mill-annealed α/β microstructure.*

strongly indicates this to be a hydrogen effect. For example, the fatigue surface from the Ti-6Al-6V-2Sn specimen tested at 0.2 Hz exhibits striations at low ΔK in Fig. 12*a* but mixed modes or regions completely dominated by facets in Fig. 12*b* and *c*. During slow crack growth under *static load,* the same types of facets have been observed, Fig. 12*d*, and identified with an internal hydrogen effect [*52*]. In addition, the hydrogen effect could be involved with either cyclic-induced cleavage or a hydride effect, since Paton and Spurling [*53*] have recently identified hydride habit planes commensurate with "cleavage" surface observations [*5,52*].

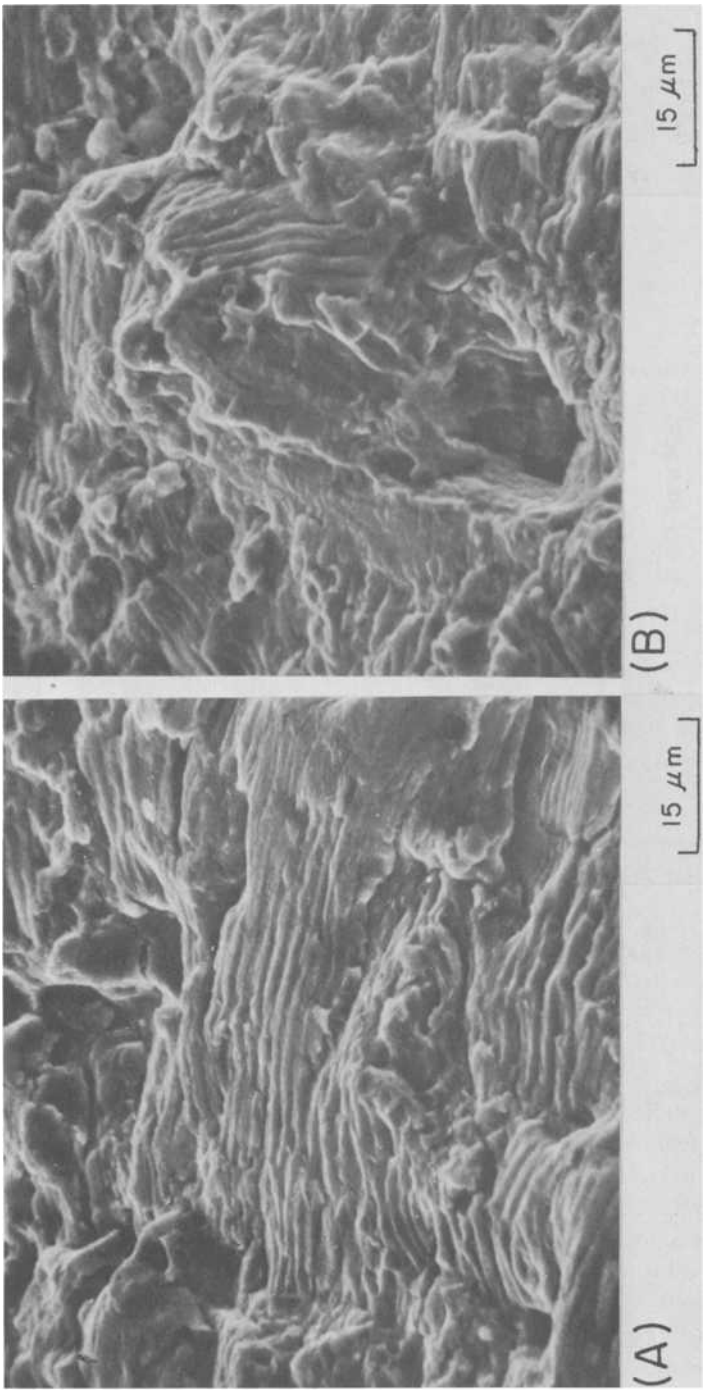
(A)
15 μm
(B)
15 μm

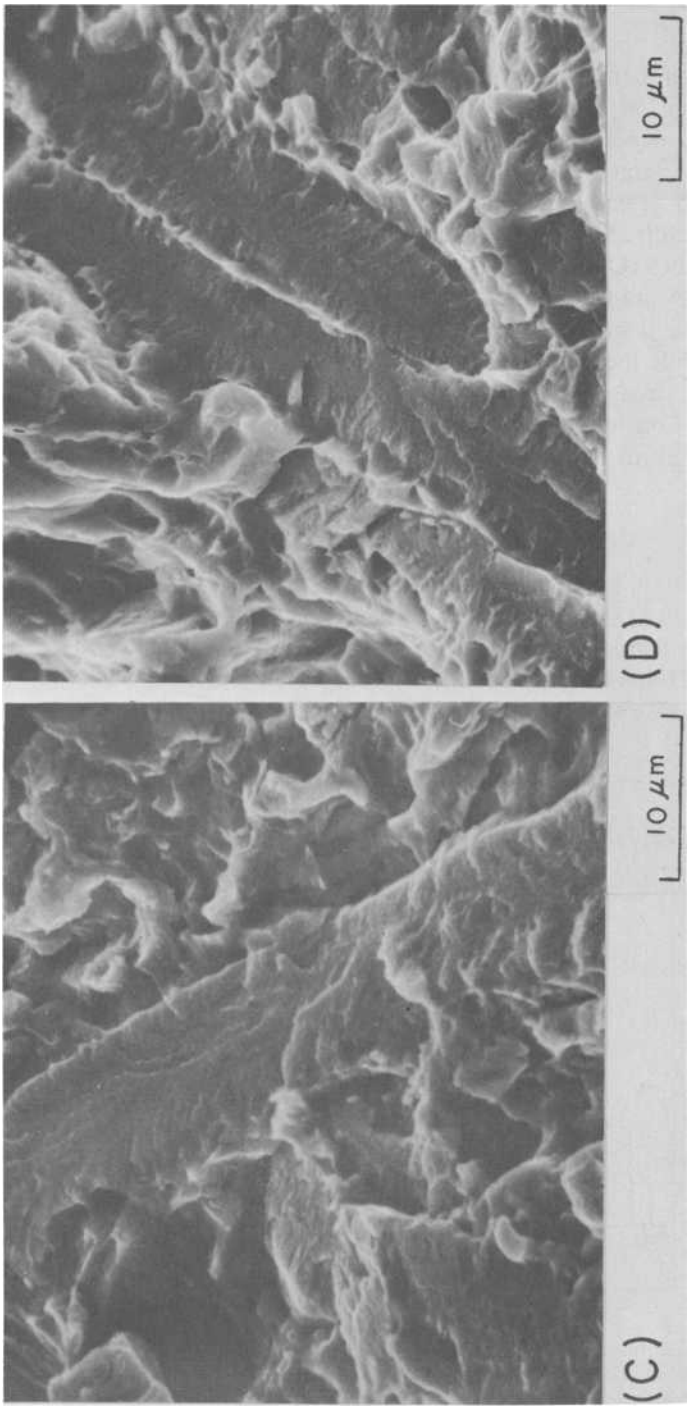

FIG. 12—*Cleavage facets observed in α-phase of Ti-6Al-6V-2Sn:* (a) *0.2 = Hz fatigue at* $\Delta K = 30$ *MPa-m*$^{1/2}$; (b) *0.2-Hz fatigue around an α-platelet at* $\Delta K = 40$ *MPa-m*$^{1/2}$; (c) *0.2-Hz fatigue in an α-platelet at* $\Delta K = 40$ *MPa-m*$^{1/2}$; (d) *slow crack growth in vacuum.*

Microstructure

Clear evidence of a microstructural effect in α/β titanium alloys was gathered from five separate sources [*14,15,17,18,42*]. Just as crack growth behavior was dependent on microstructure near threshold [*16*], it is also dependent at larger ΔK levels. This was documented by comparing the crack growth velocity at a constant ΔK of 25 MPa-m$^{1/2}$ for β-annealed (BA), recrystallized annealed (RA), mill-annealed (MA), and solution heat and overaged (STOA) conditions. Details of the heat-treatment procedures differ but they are generally in accord with those outlined by Chesnutt et al [*17*]. As is seen in Fig. 13, the β-anneal is superior to all other microstructures while the RA condition may be second best. This is not thought to be a yield strength effect, as the variation in σ_{ys} was generally less than 10 percent. Considering Fig. 7,8, and 13, microstructure emerges as a major effect at all applied stress-intensity levels in this class of materials.

Temperature

Information on low-temperature aspects of growth in titanium alloys was sparse. Pittinato [*51*] did find the exponent on ΔK to vary slightly from 3.6 to 4.2 as the temperature decreased from 297 to 144 K. As this was only one heat of Ti-6Al-4V in the solution heat-treated and aged condition, it is

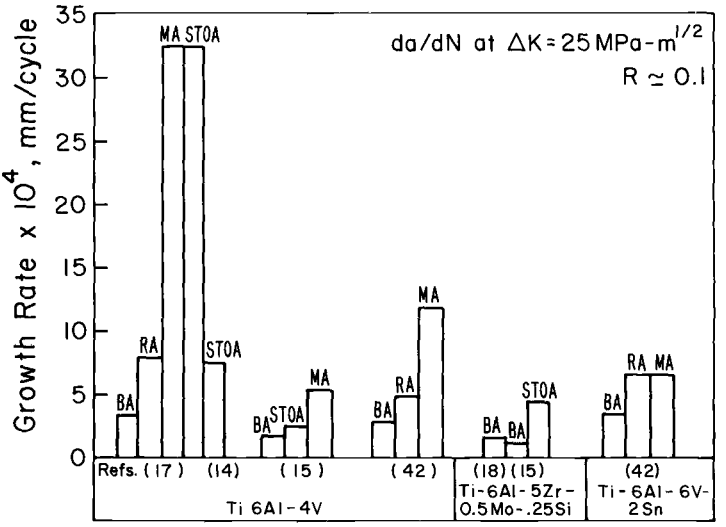

FIG. 13—*Microstructural influence on crack velocity in α/β titanium alloys tested at* ΔK = *25 MPa-m$^{1/2}$. BA = β annealed; RA = recrystallized annealed; MA = mill annealed; STOA = solution treat and overage.*

not clear how much of an effect low temperatures might have on other microstructures or α/β systems.

A similar state of affairs is the scarcity of low-temperature information on iron alloys, except for Burck and Weertman's data on iron-molybdenum [*10*]. Additional information was provided by evaluating seven additional materials from 123 to 296 K, the results being summarized in Table 4. In these iron-base systems, the effect of temperature is at least twofold. First, the yield strength is generally increased at lower temperatures, which should decrease crack growth rates as most models give σ_{ys}^{-1} to σ_{ys}^{-3} dependencies [*4,54-60*]. However, there is a competing effect here. As the test temperature drops below the ductile-brittle transition temperature (DBTT), static cleavage modes or cyclic cleavage become possible and growth rates may become enhanced. This is the prevailing view of investigators who have emphasized the fractographic nature of the process [*5, 7, 8, 10*]. The point is well illustrated in Fig. 14, where da/dN versus ΔK is presented for Fe-2.4Si at four test temperatures. As the temperature is lowered from room temperature to 233 K, the growth rates decrease by at least a factor

TABLE 4—*Strain-hardening, dislocation dynamic, and fatigue crack propagation parameters for iron-base systems at low temperatures.*

Alloy	Test Temperature, K	Strain-Hardening Exponent, β	Strain-Rate Sensitivity, m^*	Observed Power-Law Exponent, n
Fe	296	0.24	4	4.02
Fe	233	0.20	11.5	5.43
Fe	173	0.105	18	12.0
Fe	123	0.065	28.5	13.6
Fe-1Si	296	0.231	3.6	4.96
Fe-1Si	233	0.257	8	5.24
Fe-1Si	173	0.16	11.5	4.97
Fe-2.5Si	296	0.261	7	4.82
Fe-2.5Si	233	0.246	8.5	7.19
Fe-2.5Si	173	0.207	14	15.6
Fe-2.5Si	123	0.176	17.5	20.9
Fe-4Si	296	0.22	7.5	4.20
Fe-4Si	233	0.231	10.5	18.5
Fe-4Si	173	0.221	15	13.0
Fe-1Ni	296	0.332	3.8	3.53
Fe-1Ni	233	0.245	4.5	4.29
Fe-1Ni	173	0.187	10	5.84
Fe-1Ni	123	0.12	17	10.9
Fe-2.5Ni	296	0.332	5	4.38
Fe-2.5Ni	233	0.274	6.5	5.39
Fe-2.5Ni	173	0.236	8.5	6.75
Fe-2.5Ni	123	0.168	14.5	11.1
Fe-4Ni	296	0.252	6	3.11
Fe-4Ni	233	0.253	11	4.14
Fe-4Ni	173	0.242	13.5	7.50
Fe-4Ni	123	0.21	18	13.4

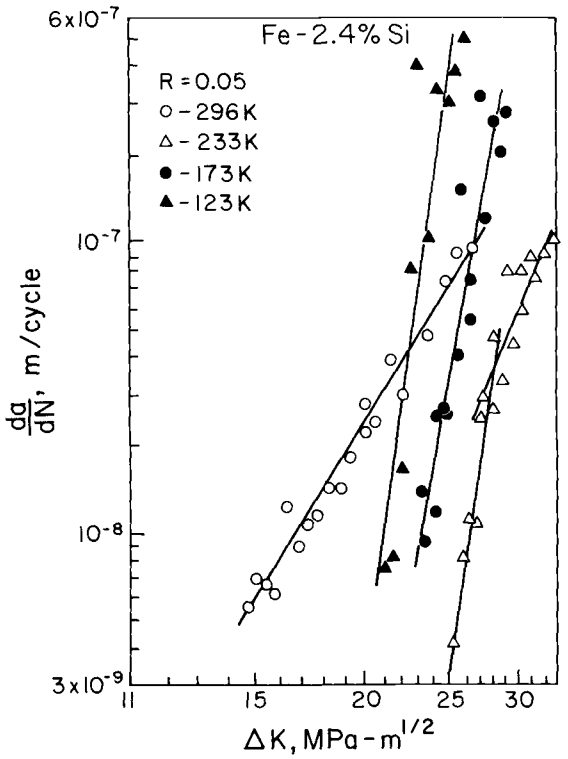

FIG. 14—*Temperature effect on crack growth rates in Fe-2.4Si. Materials as in Tables 1 and 4.*

of five. The yield strength does increase from 199 to 222 MPa, but it seems improbable that such a small increase can affect growth rate that much. At even lower temperatures, a further increase in yield strength from 222 to 370 MPa does not decrease growth rates as might be expected. Rather, the cleavage mode becomes predominant and the trend in growth rates is reversed. Similar behavior is noted in Fig. 15 for Fe-2.5Ni, where growth rates decrease by almost a factor of 30 as the temperature drops to 173 K. Corresponding to this was an increase in yield strength from 160 to 240 MPa. Comparing this with the Fe-2.4Si data, the extent of the reduction in growth rates and the temperature at which it occurs are greater because of the lower DBTT of the iron-nickel system. Once again, as the cleavage mode becomes the predominant influence, the trend in growth rates reverses at the lowest temperature. An example of this cleavage mode was illustrated in Fig. 3.

Consistent with the cleavage argument is that similar trends are observed at a *constant temperature* by varying the *alloy content.* That is, at 173 K a

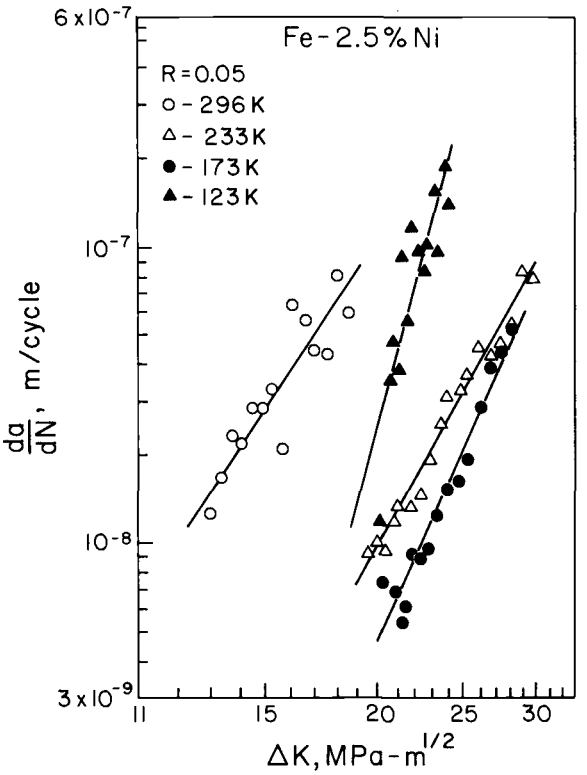

FIG. 15—*Temperature effect on crack growth rates in Fe-2.5Ni.*

crossover occurs in the iron-silicon system at high ΔK values in Fig. 16. Since it has been shown that 1 percent silicon actually decreases the DBTT slightly but a greater amount of silicon increases it [*61*], this could be strictly a static-mode argument. The reason for the Fe-1Si data having greater growth rates at lower ΔK values is that small silicon additions produce solute softening and hence the yield strength is actually lower than pure iron at 173 K [*61*].

To demonstrate that the effect of low test temperatures is qualitatively similar in many iron-base systems, data [*7,10,43,45,62,63*] on 15 alloy heats were collected in Fig. 17. Here, the exponent on ΔK is seen to increase sharply as temperature is reduced except for the iron-nickel steels. This one divergence is not surprising as the DBTT of such fine-grained steels is very low and their fracture toughness values are on the order of 100 to 200 MPa-$m^{1/2}$ at low temperature. Because of this fracture toughness (propensity toward cleavage) effect, and the expectation that static modes predominate, such data should produce a correlation between n and

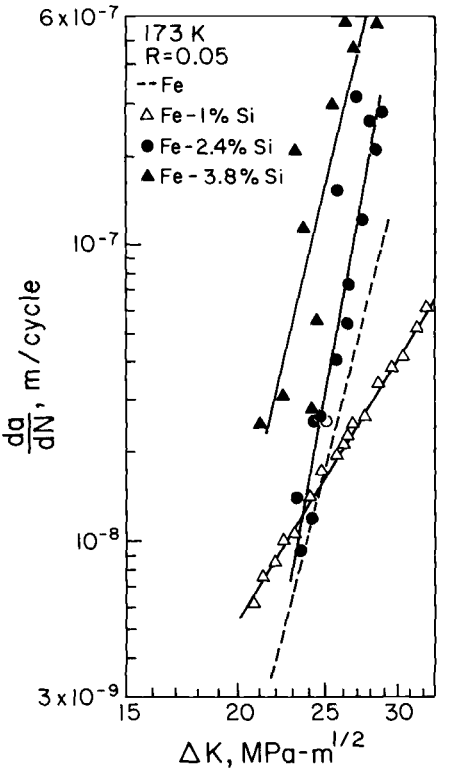

FIG. 16—*Alloy effect on crack growth rates in iron-silicon at 173 K. Materials as in Tables 1 and 4.*

K_{Ic} similar to what was found by Ritchie and Knott [*8*] at room temperature. Available data in the range of 77 to 173 K were used where both n and fracture toughness at the temperature of interest had been determined. Where a valid K_{Ic} was not obtained, the maximum value, K_m, at cleavage instability was used in the correlation. As is shown in Fig. 18, the trend is nearly identical to Ritchie and Knott's [*8*]. The difference is that n-values are higher, possibly representing the greater effect of cleavage on fatigue crack growth kinetics. Alternatively, this separation may be due to some temperature-dependent dislocation phenomenon, as will be discussed later.

Mechanisms

Threshold Concepts

Considering the microstructural dependence of the threshold regime, it is not surprising that the attempts at quantifying ΔK_{TH} have met with

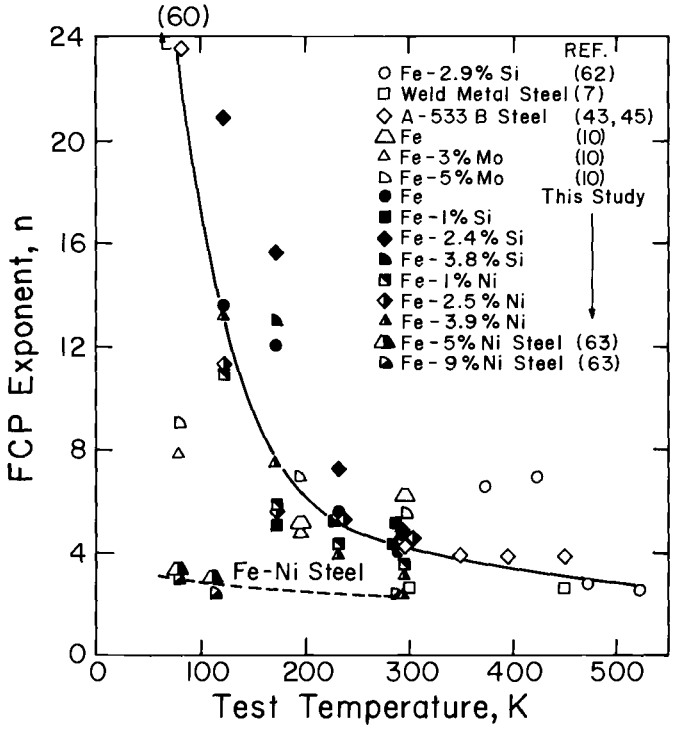

FIG. 17—*Test temperature influence on fatigue-crack propagation exponent in iron-base systems.*

difficulties. For example, Hopkins et al [*31*] concluded that crack-tip blunting, bifurcation, closure, and residual stresses may all contribute to a single-cycle overload effect which drastically increases thresholds in Ti-6Al-4V. There is no question that crack closure [*64-68*], residual stress [*69,70*], or crack-tip blunting [*71*] models can predict the effects of stress redistribution on fatigue growth retardation and probably many threshold effects as well. However, there have been few attempts to translate such continuum concepts to the microstructural level. Outside of some semi-empirical approaches [*5,29,30*], there have been few analytical treatments of microscopic quantities at threshold except Weiss and Lal's plastic particle [*72*], and the dislocation dynamics approach mentioned previously [*32*]. None of the analytical approaches deal with the grain-size effect documented in Fig. 8.

Both Beevers et al [*5,9,16*] and McEvily [*3*] have recognized that the crack front is moving in a discontinuous manner near threshold with the front being held up at various points by microstructural obstacles. In some cases, these might be second-phase ligaments as suggested in Fig. 2*d* or

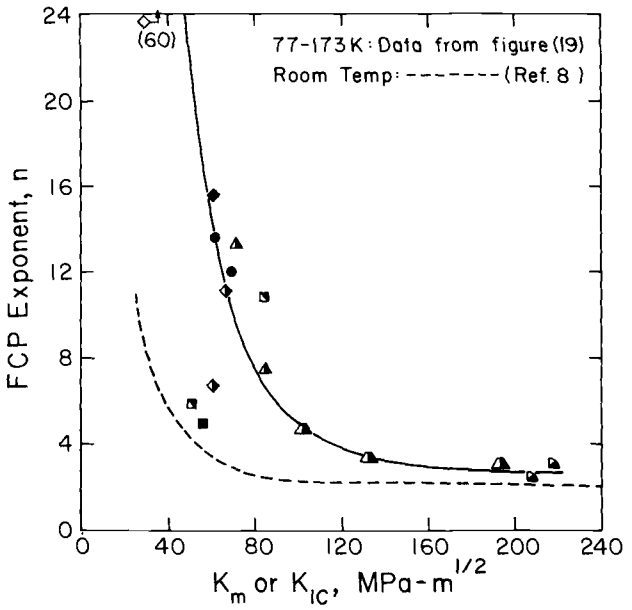

FIG. 18—*Fracture toughness influence on fatigue-crack propagation exponent in iron-base systems.*

improperly oriented colonies or grains as suggested by Fig. 2*c* and *i*. In any case, a semicohesive zone with different flow properties than a typical plastic zone may result because of its work-hardening, state of stress, and void content differences. It would be best to incorporate both closure or residual stress effects or both with the semicohesive nature of this microstructural zone, but this is beyond the scope of the paper. What can be done is to develop a microstructural concept realizing that it does not adequately take into account overload or R-value effects. The concept is depicted in Fig. 19. First, consider a mixed-mode fracture near threshold where cleavage[6] occurs in large grains but not in some small ones as indicated in Fig. 19*a*. The result is a ligament that acts as a traction on the crack opening, reducing the expected stress intensity at the tip of farthest advance. In a slightly different vein, the side and top view of a semicohesive zone in Fig. 19*b* is represented by uniform grains, some of which fracture because their cleavage planes are most favorably oriented. If the individual ligaments left behind are designated dl_i and dS_j in size, then an effective ligament behaving as a surface traction is

[6]Note that similar arguments could consider intergrannular facets.

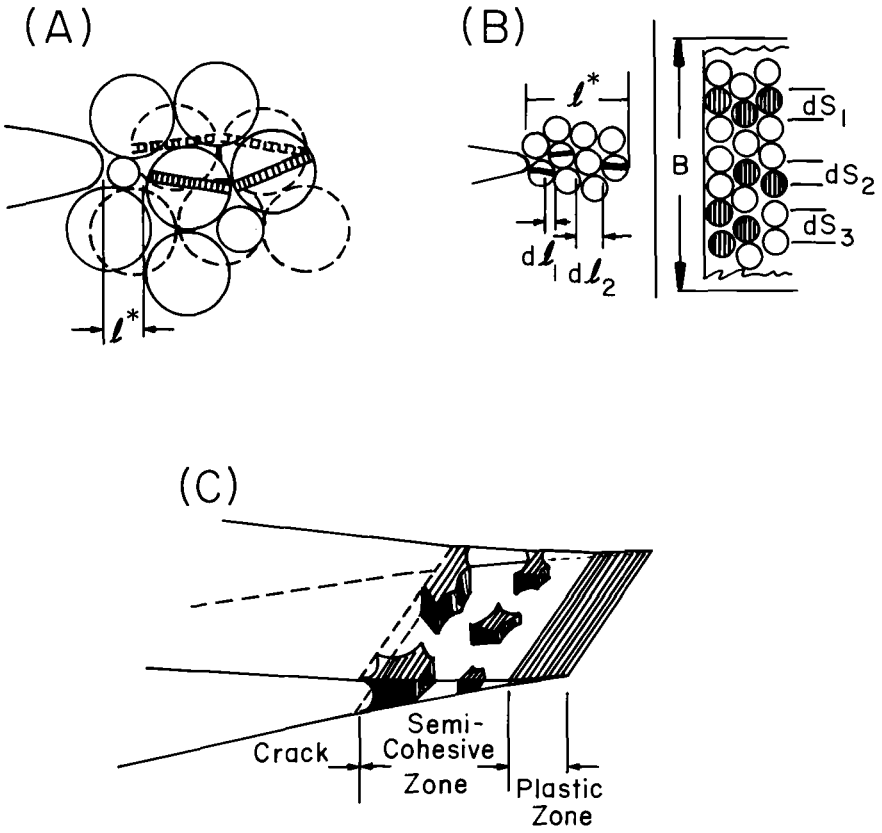

FIG. 19—*Semicohesive zone associated with selective cleavage in a microstructure:* (a) *two layers of selective grains;* (b) *two views of an equiaxed structure with B the thickness;* (c) *threee-dimensional depiction with shaded ligaments.*

$$l^*_{\text{eff}} = \sum_{i=1}^{n} \sum_{j=1}^{m} dl_i dS_j / l^* B = (1 - f)l^* \tag{4}$$

where f is the area fraction of the voids. This is only one way of treating this microstructural traction unit, and at least three ways are suggested:

1. Treating an effective l^*_{eff} as in the foregoing with the ligament material having work-hardened matrix properties.
2. Utilizing the full l^* with a reduced strength depending on the area fraction of voids.
3. Utilizing the full l^* with a reduced ductility depending upon the void content.

Since some experience has been gained by applying the No. 1 way to predict equilibrium growth of a craze (a semicohesive zone) in glassy polymers, this will be used for microstructural effects on thresholds. The model is depicted in Fig. 19*c*. It is seen that there is a cohesive plastic zone which is plane strain and undergoing reversed plastic straining. The stresses there are not sufficient to trigger cleavage or intergranular fracture as the local stress intensity is modified by the dark regions in the semicohesive zone. These are not oriented for an alternate microscopic fracture mode but must fail by a ductile striation mechanism. At threshold, the stress distributions associated with the crack, the semicohesive zone, and the plastic zone must be in equilibrium. The analysis is derived in the Appendix for a central crack of $2c$ in an infinite plate, the final result being

$$\pi\sigma - 2\sigma_{sc}\cos^{-1}\left(\frac{c}{a}\right) - 2(\sigma_{ys} - \sigma_{sc})\cos^{-1}\left(\frac{b}{a}\right) = 0 \tag{5}$$

here

σ = applied stress,
σ_{sc} = stress in semicohesive zone,
σ_{ys} = yield stress in plastic zone,
$2c$ = real crack,
$2b$ = real crack plus semicohesive zone, and
$2a$ = ficticious crack containing all three zones.

Note that the semicohesive zone, l^*, is given by b-c.

It is clear that l^* could be one or several grains or an intercolony spacing in a Widmanstätten α/β titanium alloy. For convenience, we have picked l^* to be associated with a single grain diameter or a Widmanstätten colony size in the case of titanium where pertinent. We have also assumed that work-hardening and state of stress effects[7] approximately cancel so that

$$\sigma_{sc} \approx [1 - f]\,(\sigma_{ys})_{R_p\pm} \tag{6}$$

where $R_{p\pm}$ indicates the yield strength in the reversed plastic zone. Upon selecting a ΔK_{TH} below which the microstructural effect becomes small, one can back calculate an R_p from the Dugdale [*79*] analysis. For the steels, a value of 1120 MPa was used for the work-hardened constrained yield stress in the reversed zone and f was taken as 0.5. Assuming the lowest ΔK to be 6 MPa-m$^{1/2}$, this gave a value of about 11 μm for $R_{p\pm}$,

[7]One would expect the yield stress in the highly strained ligaments of a semicohesive zone to be greater than that in the plastic zone due to work-hardening. At the same time, it would be less, since the ligaments are in a state of nearly plane stress or uniaxial tension while the cohesive zone is nearly plane strain.

which was slightly greater than the smallest grain size. This then allowed a new applied stress, σ, to be calculated for any grain size, b-c, realizing that $R_{p\pm}$, $(\sigma_{ys})_{R_{p\pm}}$, and σ_{sc} would be constant at threshold, that is, at equilibrium. As shown in Fig. 20, the agreement is reasonable, with the factor of three increase in ΔK_{TH} with grain size being approximately predicted. As one might expect, different values for $(\sigma_{ys})_{Rp\pm}$, f, and l^* could be arranged to allow a best fit to the data average. The main point is not how well the model fits the data but that it represents a microstructural approach that predicts the right trend in threshold with grain size. Furthermore, it is a microstructural approach with a continuum mechanics basis that should allow appropriate modification with regard to residual stress, R-value effect, and work-hardening.

Further encouraging results came from treating the available titanium data from Fig. 8. There were essentially two classes here, a near alpha group with a yield strength average of 380 MPa and a heat-treated α/β group with a value near 850 MPa. The assumption here was slightly different in that no work-hardening was assumed and the reversed plastic zone yield strengths were taken to be 760 and 1700 MPa, respectively. Furthermore, in keeping with the differences in faceted fracture between steel and titanium indicated in Fig. 7, a full 75 percent of the area was taken as

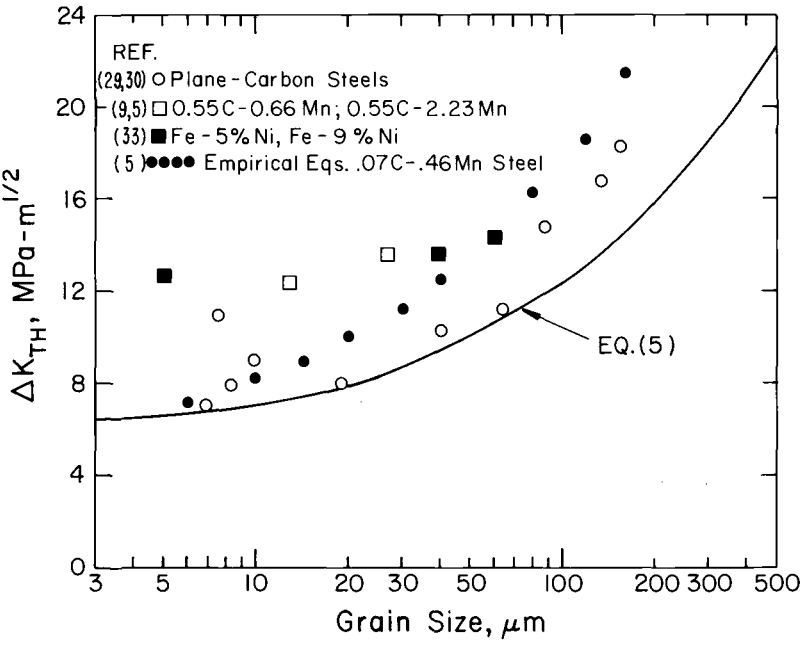

FIG. 20—*Prediction of grain size effect on threshold for low-strength steels using the semi-cohesive zone concept.*

faceted fracture or void content. The fit in Fig. 21 is excellent, with the separation of the data being closely predicted. That is, the higher-strength ligaments, for a given grain size, give higher thresholds, all other parameters being equal.

There are certainly other models to explain such data on a microstructural basis, one of which is briefly discussed. In the α/β titanium systems, it was suggested that a hydride mechanism is responsible for frequency effects. Even at moderately high frequencies, there is adequate time near threshold for hydrogen to diffuse to the crack tip from either the environment or the bulk. It is proposed that branched cracks form because a hydride cracks on a particular habit plane. The simplest model assumes that a hydride can form entirely across a grain in an all-α alloy, at an α/β interface or between Widmanstätten colonies in α/β alloys, or in whole α grains in α/β microstructures as suggested by Fig. 2*a*, *c* and *d*. A sufficient number of branched microcracks will be formed so as to make fracture of a new hydride in the next grain or colony more difficult. That is, at the branched crack indicated in Fig. 2*a*, the stress intensity at the tip of the angle-crack is less than if the crack had continued straight. The larger the grain or colony, the farther out along ϕ the hydride may fracture before it is stopped at a boundary. The further out on ϕ, the more the effective stress intensity is reduced.

Stress intensity factors for kinked and forked cracks have recently been reviewed by Bilby et al [*73*], with one of the most useful results due to

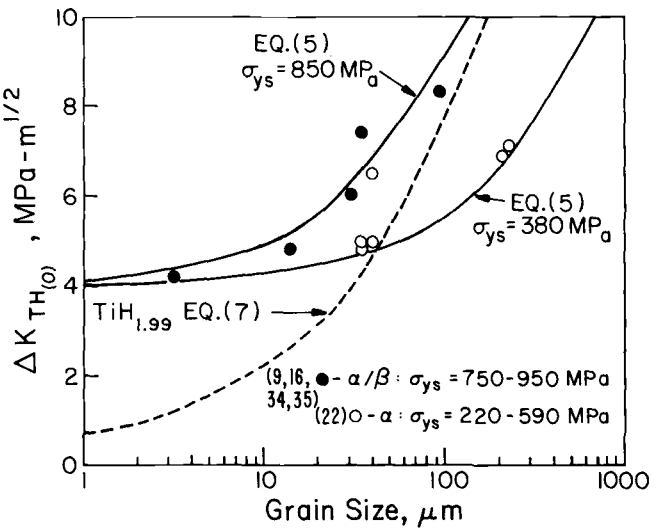

FIG. 21—*Predictions of grain size effect on thresholds of titanium alloys: (Solid curves) using the semi-cohesive zone; (dotted curve) using the branched-crack model for hydride fracture.*

Chatterjee [*74*]. In the latter, the stress intensity is given for both Mode I and Mode II as a function of angle and length, r^*, of the branch. In using this result, the assumption was that 50 percent of the cracks branched between 45 and 90 deg to crack prolongation. As a first-order approximation, a branched crack of $K_{I\phi=60\ deg}$ was compared at the farthest distance the hydride could fracture at $r^* = l^*$. If the stress intensity at the tip of the branched crack is not sufficient to exceed the hydride fracture stress in the next grain, the crack tip stops at that local position. Furthermore, if hydride fracture ceases in 50 percent of the grains, the ligaments provided are sufficient to arrest the crack as previously outlined. With the fracture stress for $TiH_{1.99}$ taken from Irving and Beevers [*75*] to be 170 MPa, it was possible to calculate a threshold stress intensity from

$$\Delta K_{TH} = \sigma^*_{TiH_{1.99}} \sqrt{2\pi l^*} f^{-1} (K_{I\phi=60\ deg}/K_{I\phi=0\ deg}) \tag{7}$$

where $f\{K(r^*,\phi)\}$ is taken from Chaterjee [*74*]. With virtually no adjustable constants and the single assumption[8] of $\phi = 60$ deg, the stress intensity at the branch of a 1-cm-long crack was plotted in Fig. 21 and is seen to give the correct trend with grain size. As the solution for the interaction of the local stress fields around an array of branched cracks having different values of ϕ is not known, one can only speculate that this is the controlling event. Qualitatively, however, this is one clear reason why some crack tips may be arrested in microstructural units of sufficient size.

Growth Concepts

Alternate microscopic fracture modes may control crack growth rate by

1. blunting,
2. branching,
3. void formation,
4. static discontinuous fracture modes, or
5. dynamics of ligament fracture,

all or in combination with each other. We will consider only two of these, one where a large number of grains cleave, producing a void content which controls fracture ductility, and by inference, crack growth kinetics. The other considers the dislocation dynamics associated with the ligaments left behind. In this case, the power-law portion of the kinetic relationship [*76*] would be given by

$$\frac{da}{dN} \propto \Delta K^{\left\{\frac{2\beta(m^*+1)+1}{\beta+1}\right\}} \tag{8}$$

[8]There is an inherent assumption here that the hydride forms over the whole grain or colony so that the stress at $1/\sqrt{r}$ for fracture is at $r^* = l^*$.

where the strain-hardening exponent, β, and strain-rate sensitivity exponent, m^*, are defined by

$$\beta = \frac{\partial \ln \sigma}{\partial \ln \epsilon_p}\bigg|_{\text{cyclic}}; \qquad m^* = \frac{\partial \ln \dot{\epsilon}_p}{\partial \ln \sigma^*} \tag{9}$$

Here, ϵ_p and $\dot{\epsilon}_p$ are plastic strain and strain rate and σ^* is the thermal component of the flow stress. Only the low-temperature results for iron, iron-nickel, and iron-silicon alloys will be considered since extensive information has been gathered on the parameters in Eq 9.

For these materials, cleavage is the alternate fracture mode at reasonably high ΔK values although it is not clear whether this involves cyclic cleavage. For example, Fig. 3*a* indicates some fracture arrest lines which may be associated with discontinuous growth across the cleaved grains rather than a complete discontinuous jump. In either case, the "holes" form as indicated in Fig. 22*a* and modify the subsequent crack growth velocity. The fraction of holes depends on the magnitude of the stress intensity since the higher the K, the higher the fraction, f, of improperly oriented grains which will cleave. As discussed elsewhere [*77*], this fraction may be given by

$$f = \frac{4}{\pi} \sec^{-1}(K_{\max}/K_{\text{nucl}})^{1/2} \tag{10}$$

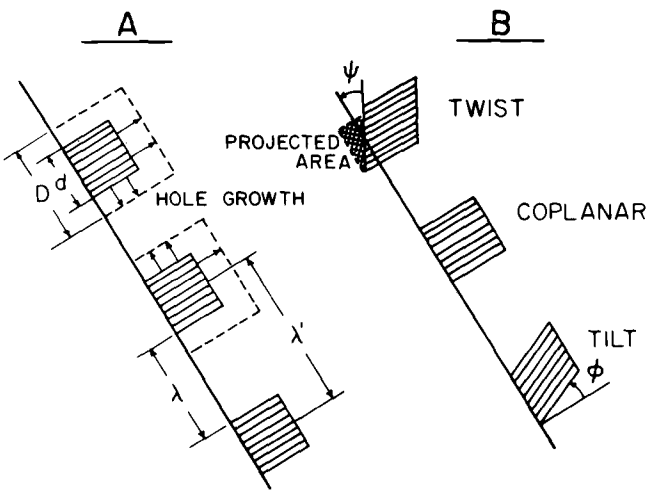

FIG. 22—*Fracture strain model for* (A) *coplanar cleavage holes and* (B) *tilt and twist cleavage holes.*

where K_{max} is the maximum stress intensity in the fatigue cycle and K_{nucl} is the stress intensity which is required to cleave the most favorably oriented planes. This result involves cleavage planes within ± 45 deg to the macroscopic growth plane as indicated in Fig. 22*b*. A similar argument can be invoked which demonstrates that ± 45 deg is also reasonable for a random network of varying-size grains involving intergranular fracture. Application of Eq 10 to the intergranular fracture results for EN-24 steel in Fig. 7*b* may be shown to give reasonable representation for small R-values but not for large R-values. Residual stresses, cyclic stresses, or environmental effects must play a factor in making ΔK important in a yet unknown manner. Applying this approach to the fraction of "holes" forming in front of a crack, the resulting effect on ductility was shown to enhance growth rates according to two fracture strain models [*77*], giving

$$\left(\frac{da}{dN}\right)_1 = \frac{\Delta K^4}{c_1 \sigma_{ys}^2 \left\{ \frac{1}{1 + \frac{8}{\pi} \sec^{-1} (K_{max}/K_{nucl})^{1/2}} - \frac{1}{3} \right\}}$$

$$\left(\frac{da}{dN}\right)_2 = \frac{\Delta K^4}{c_2 \sigma_{ys}^3 \left\{ \frac{1}{1 + \frac{8}{\pi} \sec^{-1} (K_{max}/K_{nucl})^{1/2}} - \frac{1}{3} \right\}} \tag{11}$$

Here, c_1 or c_2 are constants and may be calculated from the first data point at K_{nucl} which signals the onset of the static fracture mode. As indicated in Fig. 23, the models do predict reduced ductility and enhanced striation formation in the remaining ligaments, which produce increased slopes of da/dN versus ΔK. The slope at the left is four and holds up to the onset of static fracture modes.

The possibility of large exponents on ΔK resulting from dislocation dynamic effects was also explored. In a recent paper [*77*], Yokobori's model [*76*] was rejected primarily because the iron-silicon data produced neither the correct magnitude nor the correct trend in the exponent of Eq 1. Subsequently, the iron-nickel fatigue crack propagation data behaved in a different manner. Moreover, it was observed that the strain-rate sensitivity and fatigue crack propagation exponents did behave in a similar fashion at low temperature. Therefore, a reconsideration of the dislocation dynamics approach produced the correlation in Fig. 24, where values for n and m^* are taken from Table 4. A linear regression line through the iron and iron-nickel data produced a correlation coefficient of 0.94. Because of this strong correlation, it was decided to calculate the values of the exponent from Eq 8 and compare these to the observed ones. In Fig. 25, the resulting correlation is not so strong but the absolute magnitudes are

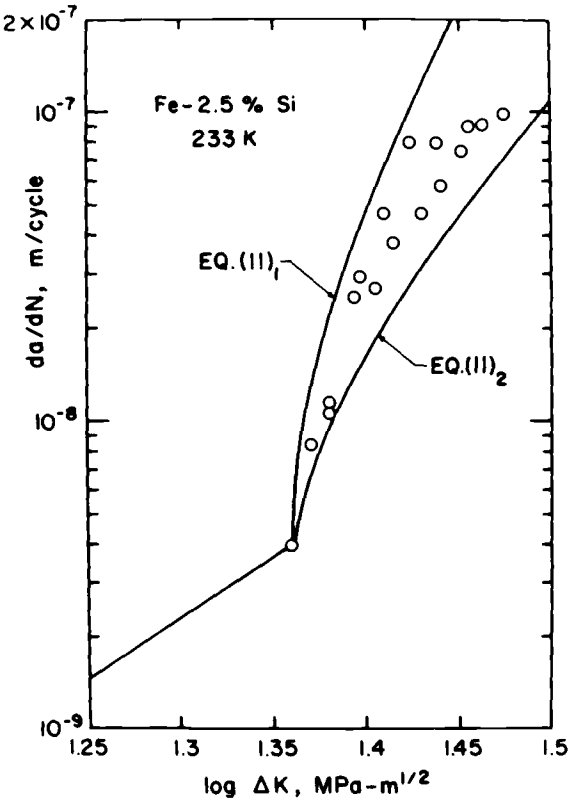

FIG. 23—*Comparison of cleavage-enhanced striation model with data for Fe-2.5Si at 233 K.*

predicted very well. Furthermore, the fact that static strain-hardening exponents rather than dynamic ones were used could have affected the strength of the correlation. Therefore, for iron and iron-nickel alloys at low temperatures, one must consider that the dislocation dynamics associated with a fatigue striation mechanism in ligaments may be controlling even though alternate microscopic fracture modes are prevalent.

Conclusions

1. Compared with ductile fatigue striations, at least 10 alternate microscopic fracture modes are identified for fatigue crack propagation in iron- and titanium-base systems.

2. The fraction of cleavage or intergranular facets varies as a function of stress intensity, temperature, environment, and frequency in different ways for the systems examined—in ways not totally understood.

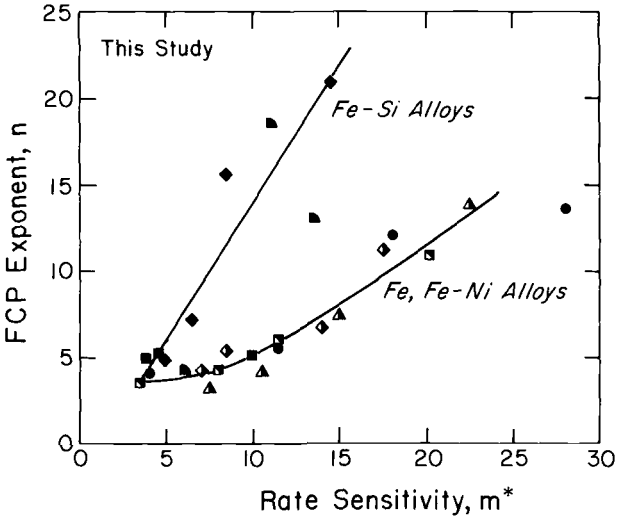

FIG. 24—*Correlation of fatigue crack propagation exponent to strain-rate sensitivity.* $\partial \ln \dot{\epsilon}_p / \partial \ln \sigma^*$.

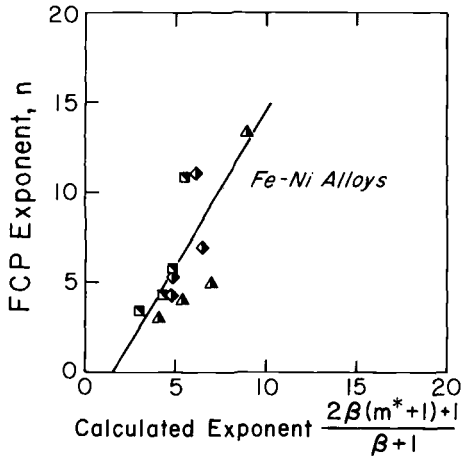

FIG. 25—*Comparison of observed exponents to those predicted by Yokobori's dislocation dynamics model.*

3. Two distinct microstructure-sensitive regimes exist in low- and high-strength iron alloys as well as in titanium-base systems:

(*a*) In high strength α/β titanium alloys, hydrogen is a causative factor in α-"cleavage" or hydride-induced static modes.

(*b*) The transition from a microstructure mode to a striation mode may be dependent upon the reversed plastic zone size in titanium alloys but not in high-strength steels at low cyclic stress intensities.

(*c*) At high stress intensities, the transition from a striation-dominant mode in the power-law regime to a microscopic-dependent mode most often involves microvoids and depends on fracture toughness.

4. A strong microstructure-size dependence exists in most of the materials examined:

(*a*) Increases in threshold or resistance to crack growth occur with increasing grain size in low-strength, single-phase steel or titanium alloys or with increasing Widmanstätten colony sizes in α/β titanium alloys.

(*b*) Threshold concepts in terms of either ligament models or crack branching have the ability of predicting microstructural size effects.

5. The effects of low temperature on fatigue crack propagation in iron-base systems are reviewed:

(*a*) Subtle interactions of temperature on yield strength, solid solution softening, and cleavage produce the best crack propagation resistance near 173 K for Fe-2.5Ni but near 233 K for Fe-2.4Si. The difference may be explained by the opposite effect of nickel and silicon on the propensity toward cleavage.

(*b*) The fatigue crack propagation exponent increases drastically with a decrease in temperature or fracture toughness.

(*c*) The increase in crack growth rate at low temperatures can be explained in terms of static fracture modes affecting the fracture strain and subsequent striation formation. Alternatively, for iron and iron-nickel, the strong correlation between strain-rate sensitivities and fatigue exponents implies that a dislocation dynamics model may control ligament fracture.

Acknowledgments

The authors express their indebtedness to Mr. Ken Peterson and Dr. Y. T. Chen for release of data prior to publication, to Dr. Chesnutt of Rockwell Science Center and Professor Hertzberg of Lehigh University for providing fractographs, and to the Air Force Office of Scientific Research for support under Grant AFOSR-77-3133A.

APPENDIX

A Dugdale-Barenblatt Equilibrium Model for Threshold

A simple model has been proposed [*78*] to modify the Dugdale [*79*] approach to account for the arrest of a crack growing in a material with two distinctly different nonlinear zones at the crack tip. The zone immediately next to the crack opening is only partially cohesive in that it is filled with microcracks or voids while the farthest cohesive zone is the standard plastic zone. By describing the traction forces in terms of a dual region, the allowance for microstructural influence on microfracture events

is possible. The equilibrium crack/semicohesive/cohesive zone concept can be written as a modified Barenblatt [*80*] criterion, giving

$$K_{(2a)} + \underset{\text{cohesive}}{K_{2(b\to a)}} + \underset{\text{semicohesive}}{K_{2(c\to b)}} = 0 \tag{12}$$

where the elastic stress-intensity term corresponds to the fictitious crack length, the cohesive term to the plastic zone contribution, and the semicohesive term to the microfracture region. This model has been successfully applied to static cracks in glassy polymers where an initially growing craze (a fibril-hole, semicohesive zone) will come to arrest under deadweight load conditions. In the present context, the physical picture is that there is a threshold applied stress intensity and hence, plastic zone, below which a semicohesive zone will not form. For example, this could represent a stress which triggers cleavage on the most favorably oriented grain, or cyclic cleavage, or environmentally induced intergranular fracture. Above this threshold, the semicohesive zone will start growing with an initial cohesive zone at its tip which is larger than what it is at threshold. As the semicohesive zone becomes longer, the remaining ligaments within it pull back on the opening surfaces, gradually reducing the effective stress intensity. Finally, at equilibrium, the plastic zone at the tip of the semicohesive zone has returned to the threshold value. One can see that large-scale microstructural discontinuities can produce large ligaments and thus be more effective in raising threshold. This concept was treated in the way that Eshelby [*81*] has done for the Dugdale/Barenblatt model, giving

$$\sigma\left(\frac{a}{\pi}\right)^{1/2}\int_{-a}^{a}\frac{dx}{(a^2-x^2)^{1/2}} - 2\sigma_{sc}\left(\frac{a}{\pi}\right)^{1/2}\int_{c}^{b}\frac{dx}{(a^2-x^2)^{1/2}} - 2\sigma_{ys}\left(\frac{a}{\pi}\right)^{1/2}\int_{b}^{a}\frac{dx}{(a^2-x^2)^{1/2}} = 0 \tag{13}$$

where

σ = applied stress,
σ_{sc} = stress within semicohesive zone, and
σ_{ys} = yield strength within plastic zone.

The solution of this leads to Eq 5 in the text.

References

[*1*] McClintock, F. A. in *Corrosion Fatigue*, NACE-2, National Association of Corrosion Engineers, Houston, Tex., 1972, p. 289.
[*2*] Tomkins, B. in *Corrosion Fatigue*, NACE-2, National Association of Corrosion Engineers, Houston, Tex., 1972, p. 303.
[*3*] McEvily, A. J., *Metal Science*, Vol. 11, 1977, p. 274.
[*4*] Irving, P. E. and McCartney, L. N., *Metal Science*, Vol. 11, 1977, p. 351.
[*5*] Beevers, C. J., *Metal Science*, Vol. 11, 1977, p. 362.
[*6*] Ritchie, R. O., *Metal Science*, Vol. 11, 1977, p. 368.
[*7*] Richards, C. E. and Lindley, T. C., *Engineering Fracture Mechanics*, Vol. 4, 1972, p. 951.
[*8*] Ritchie, R. O. and Knott, J. F., *Acta Metallurgica*, Vol. 21, 1973, p. 639.
[*9*] Cooke, R. J. and Beevers, C. J., *Materials Science and Engineering*, Vol. 13, 1974, p. 201.

[10] Burck, L. H. and Weertman, J., *Metallurgical Transactions*, Vol. 7A, 1976, p. 257.
[11] Neumann, P. Vehoff, H., and Fuhlrott, H. in *Fracture 1977, Proceedings*, Fourth International Conference on Fracture, Waterloo, Ont., Canada, Vol. 2, 1977, p. 1313.
[12] Duquette, D. J. and Gell, M., *Metallurgical Transactions*, Vol. 2, 1971, p. 1325.
[13] Hertzberg, R. W. and Mills, W. J. in *Fractography-Microscopic Cracking Processes, ASTM STP 600*, American Society for Testing and Materials, 1976, p. 220.
[14] Bucci, R. J., Paris, P. C., Hertzberg, R. W., Schmidt, R. A., and Anderson, A. F. in *Stress Analysis and Growth of Cracks, I, ASTM STP 513*, American Society for Testing and Materials, 1972, p. 125.
[15] Evans, W. J. in *The Practical Implications of Fracture Mechanisms*, Institution of Metallurgists, London, U.K. 1973, p. 153.
[16] Irving, P. E. and Beevers, C. J., *Materials Science and Engineering*, Vol. 14, 1974, p. 229.
[17] Chesnutt, J. C., Rhodes, C. G., and Williams, J. C. in *Fractography-Microscopic Cracking Processes, ASTM STP 600*, American Society for Testing and Materials, 1976, p. 99.
[18] Eylon, D. and Hall, J. A., *Metallurgical Transactions*, Vol. 8A, 1977, p. 981.
[19] Neal, D. F. and Blenkinsop, P. A., *Acta Metallurgica*, Vol. 24, 1976, p. 59.
[20] Hornbogen, E. and Zum Gahr, K. H., *Acta Metallurgica*, Vol. 24, 1976, p. 581.
[21] Hall, I. W. and Hammond, C. in *Science, Technology and Application of Titanium*, R. I. Jaffe and N. Promisel, Eds. Plenum Press, New York, 1973, p. 1365.
[22] Robinson, F. L. and Beevers, C. J., *Metal Science Journal*, Vol. 7, 1973, p. 153.
[23] Yuen, A., Hopkins, S. W., Leverant, G. R., and Rau, C. A., *Metallurgical Transactions*, Vol. 5, 1974, p. 1833.
[24] Ritchie, R. O., *Journal Engineering Materials and Technology*, Vol. 99. Transactions, American Society of Mechanical Engineers, 1977, p. 195.
[25] Crooker, T. W., Hasson, D. F., and Yoder, G. R. in *Fractography-Microscopic Cracking Processes*, ASTM STP 600, American Society for Testing and Materials, 1976, p. 220.
[26] Yoder, G. R., Cooley, L. A., and Crooker, T. W. in *Proceedings*, 2nd International Conference on the Mechanical Behavior of Materials, American Society for Metals, Cleveland, Ohio, 1976, p. 1010.
[27] Birbeck, G., Inkle, A. W., and Waldron, G. W. J., *Journal of Material Science*, Vol. 6, 1971, p. 319.
[28] Rosenfield, A. R., *Engineering Fracture Mechanics*, Vol. 9. 1977, p. 509.
[29] Masounave, J. and Bailon, J.-P. *Scripta Metallurgica*, Vol. 10, 1976, p. 165.
[30] Masounave, J. and Bailon, J.-P. in Proceedings, 2nd International Conference of the Mechanical Behavior of Materials, American Society for Metals, Cleveland, Ohio, 1976, p. 636.
[31] Carlson, M. F. and Ritchie, R. O., *Scripta Metallurgica*, Vol. 11, 1977, p. 1113.
[32] Sadananda, K. and Shahinian, P., *International Journal of Fracture*, 1977, p. 585.
[33] Stratmann, P. in *Fracture 1977, Proceedings*, Fourth International Conference on Fracture, Waterloo, Ont., Canada, Vol. 2, 1977, p. 79.
[34] Meyn, D. A., *Metallurgical Transactions*, Vol. 2, 1971, p. 853.
[35] Hopkins, S. W., Rau, C. A., Leverant, G. R., and Yuen, A. in *Fatigue Crack Growth Under Spectrum Loads, ASTM STP 595*, American Society for Testing and Materials, 1976, p. 125.
[36] Ritchie, R. O., *Metallurgical Transactions*, Vol. 8A, 1977, p. 1131.
[37] Ebara, R., Inoue, K., Crosby, S., Groeger, J., and McEvily, A. J. in *Proceedings*. 2nd International Conference on the Mechanical Behavior of Materials, American Society for Metals, Cleveland, Ohio, 1976, p. 685.
[38] Cooke, R. J., Irving, P. E., Booth, G. S., and Beevers, C. J., *Engineering Fracture Mechanics*, Vol. 7, 1975, p. 69.
[39] Gerberich, W. W., Chen, Y. T., and St. John, C., *Metallurgical Transactions*, Vol. 6A, 1975, p. 1485.
[40] Paris, P. C. and Erdogan, F. J., *Journal of Basic Engineering, Transactions*, American Society of Mechanical Engineers, Series D, Vol. 85, 1963, p. 528.
[41] Forman, R. G., Kearney, V. E., and Engle, R. M., *Transactions*, American Society of Mechanical Engineers, Vol. 89, 1967, p. 459.

[42] Yoder, G. R., Cooley, L. A., and Crooker, T. W., *Journal of Engineering Materials and Technology, Transactions*, American Society of Mechanical Engineers, 1977, p. 313.
[43] Stonesifer, F. R., "Effects of Grain Size and Temperature on Sub-Critical Crack Growth in A533 Steel," NRL Memo 3400, Naval Research Laboratory, Washington, D.C., Nov. 1976.
[44] Tetelman, A. S., Robinson, J. N., and Romain, I. in *Prospects of Fracture Mechanics*, Nordhoff International Publishers, Alphen Aan Den Rijn, The Netherlands, 1974, p. 563.
[45] Paris, P. C., Bucci, R. J., Wessel, E. T., Clark, W. G., Jr., and Mager, T. R. in *Stress Analysis and Growth of Cracks, ASTM STP 513*, American Society for Testing and Materials, 1976, p. 141.
[46] Riccardella, P. C. and Mager, T. R., in *Stress Analysis and Growth of Cracks. ASTM STP 513*, American Society for Testing and Materials, 1976, p. 260.
[47] Nelson, H. G., Tetelman, A. S. and Williams, D. P. in *Corrosion Fatigue*, A. J. McEvily and R. W. Staehle, Eds., National Association of Corrosion Engineers, Houston, Tex., 1972, p. 359.
[48] Dawson, D. B. and Pelloux, R. M., *Metallurgical Transactions*, Vol. 5, 1974, p. 723.
[49] Meyn, D. A., *Metallurgical Transactions*, Vol. 2, 1971, p. 853.
[50] Meyn, D. A. in *Fractography-Microscopic Cracking Processes, ASTM STP 600*. American Society for Testing and Materials, 1976, p. 853.
[51] Pittinato, G. F., *Metallurgical Transactions*, Vol. 3, 1972, p. 235.
[52] Peterson, K., Schwanebeck, J. C., and Gerberich, W. W., *Metallurgical Transactions*, Vol. 9A, 1978, pp. 1169-1172.
[53] Paton, N. E. and Spurling, R. A., *Metallurgical Transactions*, Vol. 7A, 1976, p. 1769.
[54] McClintock, F. A. in *Fracture of Solids*, Wiley, New York, 1963, p. 65.
[55] Rice, J. R. in *Fatigue Crack Propagation, ASTM STP 415*, American Society for Testing and Materials, 1967, p. 247.
[56] Weertman, J. in *Proceedings*, First International Conference on Fracture, Sendai, Japan, Vol. 1, 1966, p. 153.
[57] McEvily, A. J. and Johnston, T. L. in *Proceedings*, First International Conference on Fracture, Sendai, Japan, Vol. 2, 1966, p. 515.
[58] Tomkins, B., Wareing, J., and Sumner, G. in *Proceedings*, Third International Conference on Fracture, Munich, Germany, Vol. 6, 1973, p. v-422.
[59] Lardner, R. W., *Philosophical Magazine*, Vol. 17, 1967, p. 71.
[60] Schwalbe, K., *International Journal of Fracture*, Vol. 9, 1973, p. 381.
[61] Gerberich, W. W. and Chen, Y. T., *Metal Science*, Vol. 12, 1978, p. 151.
[62] Wright, R. N. and Argon, A. S., *Metallurgical Transactions*, Vol. 1, 1970, p. 3065.
[63] Bucci, R. J., Greene, B. N., and Paris, P. C. in *Progress in Flaw Growth and Fracture Toughness Testing. ASTM STP 563*, American Society for Testing and Materials, 1973, p. 206.
[64] Elber, W., *Engineering Fracture Mechanics*, Vol. 2, 1970, p. 37.
[65] Schmidt, R. A. and Paris, P. C. in *Flaw Growth and Fracture Toughness Testing, ASTM STP 536*, American Society for Testing and Materials, 1973, p. 79.
[66] Paris, P. C. and Hermann, L. in *Proceedings*, International Congress of Applied Mechanics, Delft, The Netherlands 1963.
[67] Bell, P. D. and Wolfman, A. in *Fatigue Crack Growth Under Spectrum Loads. ASTM STP 595*, American Society for Testing and Materials, 1975, p. 157.
[68] Alzos, W. X., Skat, A. C., Jr., and Hillberry, B. M., in *Fatigue Crack Growth Under Spectrum Loads. ASTM STP 595*. American Society for Testing and Materials, 1975, p. 41.
[69] Ho, C. L., Buck, O., and Marcus, H. L. in *Flaw Growth and Fracture Toughness Testing, ASTM STP 536*. American Society for Testing and Materials, 1973. p. 5.
[70] Klensil, M. and Lukas, P., *Materials Science and Engineering*, Vol. 9, 1972, p. 231.
[71] McEvily, A. J. in *Microstructure and Design of Alloys*. Metals Society, London, U.K., 1974, p. 204.
[72] Weiss, V. and Lal, D., *Metallurgical Transactions*. Vol. 5, 1974, p. 1946.
[73] Bilby, B. A., Cardew, G. E., and Howard, I. C. in *Fracture 1977. Proceedings*. Fourth International Conference on Fracture, Waterloo, Ont., Canada, Vol. 3, 1977, p. 197.

[74] Chaterjee, S. N., *International Journal of Solids and Structures*, Vol. 11, 1975, p. 521.
[75] Irving, P. E. and Beevers, C. J., *Journal of Materials Science*, Vol. 7, 1972, p. 23.
[76] Yokobori, T., Konosu, S., and Yokobri, A. T., Jr. in *Fracture 1977. Proceedings*, Fourth International Conference on Fracture, Waterloo, Ont., Canada, Vol. 1, 1977, p. 665.
[77] Gerberich, W. W. and Moody, N. in *Fracture 1977, Proceedings*, Fourth International Conference on Fracture, Waterloo, Ont., Canada, Vol. 3, 1977, p. 829.
[78] Gerberich, W. W., *International Journal of Fracture*, Vol. 13, 1977, p. 535.
[79] Dugdale, D. S., *Journal of the Mechanics and Physics of Solids*, Vol. 8, 1960, p. 100.
[80] Barenblatt, G. I. in *Advances in Applied Mechanics*, Vol. 7, Academic Press, New York, 1962, p. 30.
[81] Eshelby, J. D. in *Fracture Toughness*, The Iron and Steel Institute, ISI Publication 121, London, U.K., 1968, p. 55.

DISCUSSION

C. Wells[1] *and J. Lankford*[1] *(discussion)*

Dr. Wells[2]—This ambitious paper is impressive in its scope and clarity and succeeds in codifying a large number of complex effects of microstructure on fatigue crack mode, mechanisms, and kinetics. Its practical implications for alloy fabrications and structural design are that these microstructural variations known to increase the resistance to crack initiation appear to be detrimental to fatigue crack growth resistance, and this generality extends to austenitic alloys as well as composite materials. These contradictory effects of microstructure provide incentive to evaluate the applicability of fracture mechanics methods to cracks on the order of the size of the controlling microstructural unit.

While not a criticism of the paper, it may help to put the work in perspective to comment on two additional factors that govern mixed-mode fatigue fracture, namely, slip character and grain boundary composition. In discussing fracture at low ΔK levels, the authors do not distinguish between low-energy cleavage facets and cyclic-slip-induced crystallographic cracking. The latter is common in both α and Widmanstätten titanium microstructure, as well as austenitic alloys, and is a consequence of heterogeneous, planar slip. Such crystallographic slip is continuous across pockets of α-platelets and results in a striation-free fracture. Homogeneous slip, whether the result of dense intersecting multiple slipbands or of dislocation climb or cross-slip, produces striations. The relative amounts may be influenced by the spacing and strength of microstructural barriers to slip, but may be more significantly governed by external variables such as

[1]Division of Mechanical Sciences, Southwest Research Institute, San Antonio, Tex. 78284.
[2]Delivered at the symposium by Dr. Lankford at the request of Dr. Wells.

crack-tip opening displacement (CTOD), strain range, R-ratio, temperature, and frequency. Models that incorporate the strength of barriers such as grain boundaries and particle-matrix interfaces may shed additional light on the transition from faceted fracture to striation growth, and possibly on the effect of such microstructural features on initiation vis-a-vis propagation.

The authors discuss some of the effects of grain boundary precipitate morphology on mixed trans- and intergranular fatigue fracture. Cracking along a brittle grain boundary particle in an otherwise ductile matrix is observed in cases where planar slipbands intersect the boundary. Precipitate-free zones in low-alloy steels are believed to enhance intergranular fracture by a cyclic shear mechanism. However, it should be mentioned that the extent of grain boundary fracture may be more a function of the local concentration of trace elements, both at low temperature and in the creep range. Incidentally, several of the authors' concepts appear to apply to creep-fatigue interaction, in which case it is also found that certain microstructural variables that improve the resistance to crack initiation in stress rupture diminish the resistance to creep crack growth and conversely.

The microstructural models that predict an increase in ΔK_{TH} with increasing grain size have considerable conceptual appeal. However, in the case of the semicohesive zone model a question arises as to the fatigue endurance of the ligaments, which presumably must undergo cyclic plasticity, although the ligaments would be expected to be able to arrest cracks in static loading. Crack branching by brittle fracture of an interface is, of course, well understood by designers of composite materials. Additional microstructural features of importance to this mechanism are aspect ratio and orientation.

Despite the large numbers of combinations of fatigue crack propagation modes, it appears possible to reduce them to a relatively small number of micromechanical mechanisms.

J. T. Fong (session chairman)—Thank you, Dr. Lankford, for your presentation of Dr. Wells's discussion. Before we open the floor to questions, I wonder if you would like to add a personal note on Dr. Gerberich's work. Do you think his model is new?

Dr. Lankford—I think the thing that's new about the model is that Gerberich has taken observations made by people like Knott and Beevers, who have noticed these little holes, and then he has extrapolated from what people like Argon in the polymer world have done in their effort to characterize crack growth rates in those materials. So in the sense that he's using those notions, I think it is new. It is a kind of a bold step, but it's reasonable.

W. W. Gerberich (author's closure)—I think all of your comments are in

accord with what we stated in the paper. What we tried to do in the threshold model was to be quite quantitative about it, realizing that there are certain superimposed environmental effects that would control the rate at which a void-filled region or at which nonpropagating cleavage cracks would form.

That is why we only stretch the concept with respect to fatigue crack propagation models in some very specific senses, where we know exactly what the microstructural effects are. Every time you go to a new microstructural morphology, or to a new alloy system, you would have to take an extremely hard look at what the predominant cyclic or cleavage modes or both are to apply any such model. Conceivably, that model would change for almost each new system.

R. Hertzberg[3] (*discussion*)—When examining the fatigue behavior of an unnotched component, the classical approach had been to look at the endurance limit. The endurance limit we know is generally related to the strength of the material, which is in turn related to the inverse square root of the grain size. So in that context, a large grain is bad because the endurance limit will tend to go down. In the context of fracture mechanics where you have preexistent flaws, these new results that Dr. Gerberich discussed seem to indicate that big grains are good.

In the last few years, it has been suggested that ΔK_{TH} may really be related to the endurance limit with the addition of some characteristic defect in the structure. But if that relationship exists, we have a dichotomy in that the two sides of the equation are affected in an opposite way by the grain size.

Could you comment on this?

W. W. Gerberich (*author's closure*)—That's exactly right, Dick. As a matter of fact, in a recent *Metallurgical Transactions* paper, Eylon and Hall made similar observations on some α/β Widmanstätten microstructures. They demonstrated clearly that the large colony sizes, that is, the large grain materials, had lower fatigue crack initiation lives, with respect to smooth bar endurance, and larger ΔK_{TH} values for fatigue crack propagation, and they do have this dichotomy.

Dr. Hertzberg—So now, if I may interject a second question, how do you design a mechanical component against fatigue?

Dr. Gerberich—I don't have an answer for that one.

Dr. Hertzberg—If you assume it doesn't have a defect, then you make the grains as small as possible, but if you have a defect, you have now really a dilemma. It's a real problem, isn't it?

[3]Materials Research Center, Lehigh University, Bethlehem, Pa. 18105.

K. DeVries[4] *(discussion)*—My question has to do with the visual model you displayed on the Vugraph. That model was plastic, and I am a little concerned about trying to make too many analogies between plastics and metals.

In plastics such as the one you had that crazed, you are orienting part of the material in the craze at the crack tip. The result is a very small amount of material with very, very high strength, in the form of microfibrils, so that you can get substantial strength in these crazes.

What do you see as analogous features in the metals you are studying? I do not see how you can have much more than phenomenological similarities between the different types of materials. I have some concerns in making too many analogies between the behavior of different materials unless we can relate them to the mechanisms involved.

W. W. Gerberich (authors' closure)—Very specifically, the model that I displayed had a craze where the fibrils were actually soft, because as the methanol diffuses into the crack tip you get a plasticization. In the presence of the methanol the fibrils are actually much softer than the matrix. But you can apply this same model to the polymer where one has a strain-hardened, if you like, or a hardened microfibril, in a dry craze, and we have had success in doing both of those things.

Now the analogy in metals would be, for example, in a two-phase α/β microstructure. One can certainly see with two α-grains propagating that in between there are ductile β-ligaments that have torn, and if one envisions this ligament as a strain-hardened plastic region, all one has to do is to describe that ligament in terms of its strain-hardening properties and one should be able to model that.

A. Miller[5] *(discussion)*—I was intrigued by your model involving the semicohesive zone, because it turns out that we are trying to apply a similar model to zirconium alloys with respect to stress corrosion cracking resistance, and one of the questions that we always puzzle over, and I would like to ask your comment on this, is for how small a crack do you think this model is appropriate, as you reduce crack sizes down toward zero?

W. W. Gerberich (authors' closure)—Well, I think the limit would be dependent upon the flow characteristics of the material, and certainly then, as you approach general yield, I don't think this model would be applicable.

[4]Department of Mechanical and Industrial Engineering, University of Utah, Salt Lake City, Utah 84112.

[5]Department of Materials Science, Stanford University, Stanford, Calif. 94305.

H. Mughrabi[6] (*discussion*)—You showed us a picture of the increase of the fatigue propagation exponent with decrease in temperature. These were largely iron-based alloys. My question is, does it correlate with the temperature dependence of the yield strength of these materials and, if so, is it peculiar to these metals or does one find the same effect in other structures?

W. W. Gerberich (*authors' closure*)—It correlates partly with the temperature dependence of the flow stress, keeping in mind that you also have to describe the strain rate and strain-hardening dependence of flow and how this elevates the local stress to the cleavage fracture stress. It is further complicated in both iron-silicon and iron-nickel because you have a regime of solid solution softening, and in the paper we described that quite accurately. With those three effects—the temperature and strain-rate effect on the flow stress, the solid solution softening, and the cleavage fracture stress—we can model the crack propagation exponent. It would apply to other materials as well, but in a somewhat different way. It would depend on whether you had a superimposed cleavage fracture mode or not.

P. Neumann[7] (*discussion*)—I would like to get an idea of the predictive value of your model as far as you judge it. In order to get this, I would like to ask the following question. If I have a different material which you don't know, and I want to apply your model, how many parameters of the material, which characterize microstructure and all kinds of things, do I have to measure to be able to predict something?

W. W. Gerberich (*authors' closure*)—That's a very difficult question to answer.

You would certainly have to know the crystal plasticity laws associated with any ductile ligament. You would have to know the effects of either temperature or environment or both on a cleavage fracture process if cleavage were involved. These may require some detailed knowledge of the crystallographic texture. You would have to be able to describe the flow stress in this semicohesive zone by putting these two things together.

You would have to know the effective flow stress in the plastic zone in the cohesive material that is just in front of the crack-tip zone. That is basically it. Finally, you would have to know the controlling microstructural unit, such as a grain size or Widmanstätten colony size, so that the extent of the semicohesive zone could be described.

E. Krempl[8] (*discussion*)—This is actually a follow-up on the previous

[6]Max-Planck-Institut fur Metallforschung, Stuttgart, Germany.
[7]Max-Planck-Institut fur Eisenforschung Gmbh, Dusseldorf, Germany.
[8]Department of Mechanical Engineering, Aeronautical Engineering and Mechanics, Rensselaer Polytechnic Institute, Troy, N.Y. 12181.

question about predictive capabilities. Suppose I give you a material and you make a micrograph to identify the microstructure. Can you tell me in what mode the crack will propagate if, in addition, I specify the test temperature?

W. W. Gerberich—Did you say given a fractograph?

E. Krempl—No, not a fractograph. You make only a micrograph of the material so that you know its microstructure. Can you tell me what the predominant mode of crack propagation is going to be?

W. W. Gerberich—No.

E. Krempl—So you have to run the test to see in which mode the crack will propagate?

W. W. Gerberich—That's exactly right.

I. LeMay[9] (*discussion*)—Any physical modeling has to be based on observation, and I am little disturbed about the use of the Dugdale-Barenblatt model for other than polymers or perhaps for specialized conditions, particularly on the basis of what we saw yesterday in terms of plastic zone shape.

We have seen evidence for the shape of the plastic zone at the tip of a crack from Davidson's work and others, and then the alternate and complementary model, involving environmental effects, which Lynch showed and which follows on to the work of Peter Neumann.

I just do not see the physical basis for applying a plastic zone shape of the Dugdale-Barenblatt type. Would you like to comment?

W. W. Gerberich (*authors' closure*)—Well, I don't think that we should give up just because it's a very difficult thing to do.

In the semicohesive zone, where the remaining bridges are less constrained, the observed shape would be closer to the Dugdale-Barenblatt solution. Of course, the plane-strain zone at the tip of this semicohesive region would still be more of a lobed affair and would not conform. Nevertheless, what we are trying to do is to give some semblance of order to a very complicated process, where we have a number of microstructural factors involved, and to see how we can model them in the simplest possible way. Where we have two phases fracturing simultaneously in a different way, now we can actually model threshold and growth. I would be the last one to say that it's an easy task, but I think if you can show success in a

[9]Department of Mechanical Engineering, University of Saskatchewan, Saskatoon, Canada.

few simple model materials, then you go on from there and see what kind of modifications one has to come up with in order to model more complex behavior.

R. Stephens.[10] (*discussion*)—We're getting very interested in cold temperatures, and I was very interested in the figure that shows low temperatures giving better fatigue growth properties under constant amplitude testing.

Do you think you could extend this to variable-amplitude loading where all types of interaction influences could be involved?

W. W. Gerberich (*author's closure*)—There is a very good likelihood that one would get different behavior near the threshold regime at low temperatures than what we have observed at the higher ΔK. The reason I say this is that as one goes to very low stress-intensity values, one finds the propensity toward cleavage certainly much less. At very low ΔK values one may observe intergranular fracture—we did observe intergranular rather than transgranular cleavage—and obtain some very unusual crossover effects. In several instances we had ductile fatigue striations down grain boundaries, which is the first observation that I've made. So by no means can you extend these findings to the threshold regime at low temperatures. Variable-amplitude loading makes such extrapolations even more uncertain.

J. T. Fong[11] (*discussion*)—My question has to do with the way you present your data. I noticed in one of your slides, on the relationship between the nondimensionalized ΔK_{TH} versus the inverse of the grain size, points scattered all over the map, and then I saw you draw a straight line through the cloud of points.

Are you comfortable with that straight line?

W. W. Gerberich (*authors' closure*)—Well, the only reason I drew a straight line is because it's a least-square line and I wanted to show what the correlation coefficient was.

Considering the number of materials it involved, all that straight line was to show was that there is a trend, a very definite effect of grain size on threshold. One would have to do very controlled studies with controlled environments on a class of materials in order to generate that kind of curve with much greater confidence.

C. Atkinson[12] (*discussion*)—A model similar to the modified Dugdale-

[10]Materials Engineering Division, University of Iowa, Iowa Cita, Iowa 52242.
[11]National Bureau of Standards, Washington, D.C. 20234.
[12]Department of Mathematics, Imperial College, London, U.K.

Barenblatt model suggested by the authors has appeared recently.[13] In this paper the zone at the crack tip is represented as a two-stage zone, the stress in each zone being assumed to be a different fixed constant; one stage represented the craze zone and the other a collinear-plastic zone. It might be useful for the authors to compare the two models.

Although each of these models might at any given instant represent reasonably, say, the crack-tip displacement, there does not seem to be any mechanism in either of them by which the crack can advance.

W. W. Gerberich (authors' closure)—With regard to Professor Atkinson's comment, equilibrium models by their very nature do not provide for a crack advance. This applies to both ours and Williams' models. Thus, just as the Dugdale model cannot predict ductile fracture instability, this modified Dugdale-Barenblatt model cannot predict how fast a crack will grow when ΔK is increased beyond threshold. Crack growth models will necessarily have a failure mechanism such as a critical stress, strain, or strain energy density associated with them and an equation of state governing such parameters as crystal plasticity, strain-hardening, and strain-rate sensitivity.

From the discussion, it is apparent that many have been concerned with microstructural effects and how (or how difficult it is) to employ them in describing fatigue crack phenomena. There has been a sufficient history of predominantly microstructural investigations or purely continuum mechanical modeling. The time is propitious for, if not consummation, at least a closer union of the two disciplines. Specifically, there should be an infusion of microplasticity and microfracture concepts into more complete mathematical descriptions of fatigue phenomena, just as hole growth models have been developed for ductile fracture. This should not be done *carte blanche* but as a cooperative approach where well-defined microstructure and microfracture statistics have been developed. For example, combined continuum modeling based upon microstuctural observations of the statistics of secondary cleavage might be accomplished using electron channelling and quantitative electron fractography to define the local grain orientation and crack path.

[13]Williams, J. G., *Journal of Materials Science*, Vol. 12, 1977, pp. 2525-2533.

T. Kunio[1] *and K. Yamada*[1]

Microstructural Aspects of the Threshold Condition for Nonpropagating Fatigue Cracks in Martensitic-Ferritic Structures

REFERENCE: Kunio, T. and Yamada, K., **"Microstructural Aspects of the Threshold Condition for Nonpropagating Fatigue Cracks in Martensitic-Ferritic Structures,"** *Fatigue Mechanisms,* Proceedings of an ASTM-NBS-NSF symposium, Kansas City, Mo., May 1978, J. T. Fong, Ed., *ASTM STP 675,* American Society for Testing and Materials, 1979, pp. 342-370.

ABSTRACT: A study has been made of the critical condition for the growth of microscopic fatigue cracks at the endurance limit from metallurgical considerations. The specimens employed have a microstructure with a matrix of ferrite and the second phase of martensite, the volume fraction of which is about 50 percent. All the nonpropagating cracks nucleated in the ferrite matrix are stopped by the second-phase martensite at the endurance limit stress. The threshold condition for microscopic nonpropagating cracks in the ferrite matrix was investigated by restressing to slightly above the endurance limit. Subsequently it was found that the critical condition for the fatal growth of microscopic cracks into the second-phase martensite from the ferrite matrix can be evaluated by the linear theory of fracture mechanics. It is also recognized from the experiments that all the microscopic cracks in the ferrite matrix remain as nonpropagating unless the stress intensity factor at the crack tip exceeds the magnitude of the crack growth resistance of the second phase martensite, K_{thm}. Furthermore, experimental results show that the K_{thm} of the second-phase martensite is about 7.7 MPa$\sqrt{m}$. In addition, quantitative metallographic observations show that the critical length of the nonpropagating cracks at the endurance limits does not depend on the mean spacing of the second phase.

KEY WORDS: crack growth resistance, endurance limit, fatigue mechanism, linear fracture mechanics, martensite-ferrite microstructure, microscopic fatigue crack, nonpropagating crack, second phase spacing, threshold condition

Although there have been various reports [*1-8*][2] that the endurance limit of smooth specimens is not associated with the stress to initiate cracks

[1]Professor and assistant professor, respectively, Department of Mechanical Engineering, Keio University, 3-14-1 Hiyoshi, Kohoku-ku, Yokohama 223, Japan.

[2]The italic numbers in brackets refer to the list of references appended to this paper.

but with the stress to propagate a microscopic crack of the order of the grain size,[3] the influences of the microstructure on the threshold condition for a nonpropagating fatigue crack at the endurance limit of an engineering material are not well understood.

In previous reports, authors have concluded that the endurance limit of specimens of two-phase microstructures of martensite and ferrite can be described as the critical stress required for nucleated cracks in the ferrite to propagate into the second-phase martensite. This conclusion is based on microscopic observations that nonpropagating fatigue cracks existed in the ferrite matrix and their further growth was impeded at the endurance limit by the second-phase martensite [5]. However, the relationship between the threshold condition of the nonpropagating crack and the crack growth resistance of the second-phase martensite has not been discussed. In this paper, a study has been made of the threshold condition for microscopic cracks nucleated in the ferrite matrix and the role of the crack growth resistance of the second-phase martensite.

Materials and Heat Treatment

Plain carbon steel of 0.25 percent carbon was machined after annealing at 1150°C for 3 h into thin-walled cylindrical specimens with dimensions shown in Fig. 1. Figure 2 shows a typical example of the microstructure consisting of ferrite matrix and second-phase martensite, which was obtained from induction hardening at 840°C for 22 s. Specimens were treated by electropolishing and light nital etching so that both cracks and microstructures could be observed. Characteristic metallurgical parameters such as the volume fraction of second phase, hardnesses of matrix and second phase, and mean second phase spacing of microstructures are given Table 1. Fatigue tests were conducted with a rotating bending machine.

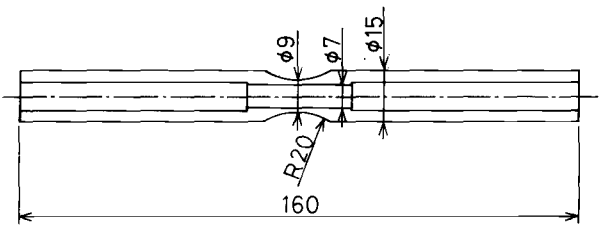

FIG. 1—*Dimension and shape of specimen (mm).*

[3]Forrest and Tate [4] reported that for large-grain-size materials such as 70/30 brass, nonpropagating cracks were not observed at the endurance limit. This could imply an opposite interpretation, valid for large-grain-size materials, that the endurance limit is not associated with the stress to propagate a crack but with a critical stress for crack initiation.

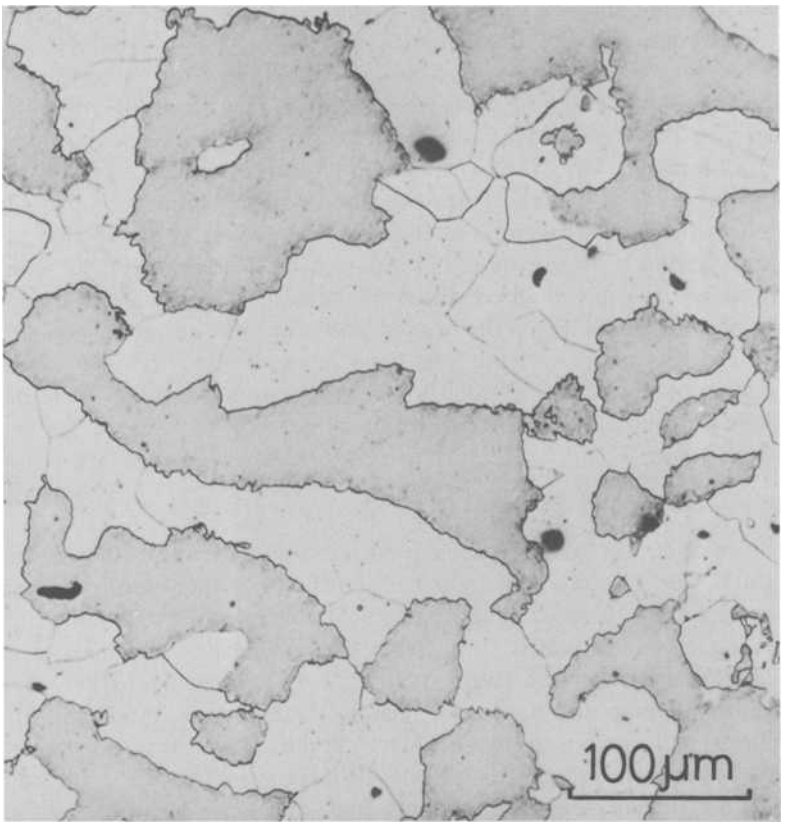

FIG. 2—*Typical microstructural features of the low-carbon steel, partially hardened by induction-hardening. Dark etched area is the second-phase martensite; white area is the ferrite matrix.*

TABLE 1—*Microstructural characteristics for the present material.*

Mean size of ferrite grains, μm	40	line counting method
Volume fraction of second-phase martensite, %	54	line counting method
Mean second-phase spacing, μm	84	line counting method
Mean hardness in micro-VHN	333	100 points by 100-g indentor
Mean hardness of matrix ferrite in micro-VHN	195	100 points by 20-g indentor
Mean hardness of second phase martensite in micro-VHN	734	100 points by 20-g indentor

Metallurgical observations of the specimens were made by optical microscope (×400) during fatigue to observe nucleation and propagation of microcracks in the surface microstructure. The projected lengths of cracks in the direction making a right angle to the axis of rotation were measured. Specimens having fatigue cracks still nonpropagating after 10^7 cycles in a rotating bending test (47 Hz) were restressed at appropriate stress levels in a reverse-bending fatigue test (33 Hz) and observed for possible growth of the aforementioned nonpropagating cracks. Special attention was given to the onset of growth of the largest crack into the martensite.

Results and Discussion

Crack Growth Resistance of Second-Phase Martensite

From microscopic observations on the surface of the specimens, it was found that for all the nonpropagating cracks nucleated in the ferrite matrix, their propagation was impeded by the second-phase martensite at the tip of the crack as shown in Fig. 3, and this was true for all the fatigued specimens having the aforementioned two-phase microstructure.

A study of the threshold condition for growth of microscopic cracks into martensite might be expected to elucidate the effects of metallurgical factors upon the endurance limit. Thus the following experiments were carried out. At first, measurements of the projected lengths of nonpropagating cracks were made on specimens which were fatigue-cycled to 10^7 at the stress level of the endurance limit (σ = 279 MPa) for rotating bending. Since various lengths of nonpropagating cracks were observed in the surface microstructure of specimens, a histogram was constructed of the length of nonpropagating cracks in a typical specimen; see Fig. 4. With the idea that the nonpropagating crack having the maximum length would be closely related to the magnitude of the endurance limit, a histogram of the maximum nonpropagating crack length from 38 specimens was also drawn; see Fig. 5. This figure shows that the maximum crack length which appeared in each specimen differed in spite of being fatigued at the same stress levels of endurance limit (σ = 279 MPa). The difference between sizes of the largest and smallest nonpropagating cracks in Fig. 5 is given by a factor of about five. Here a question arises as to whether the maximum length of crack in each specimen is simply related to the endurance limit.

Next, specimens having nonpropagating cracks due to rotating bending were restressed at stress levels slightly above the endurance limit (295 to 300 MPa) in a reversed bending fatigue test. Observations of surface microstructure during the process of fatigue stressing revealed fatal crack growth originating from the nonpropagating crack with the maximum length and also fatal crack growth originating from cracks of less than

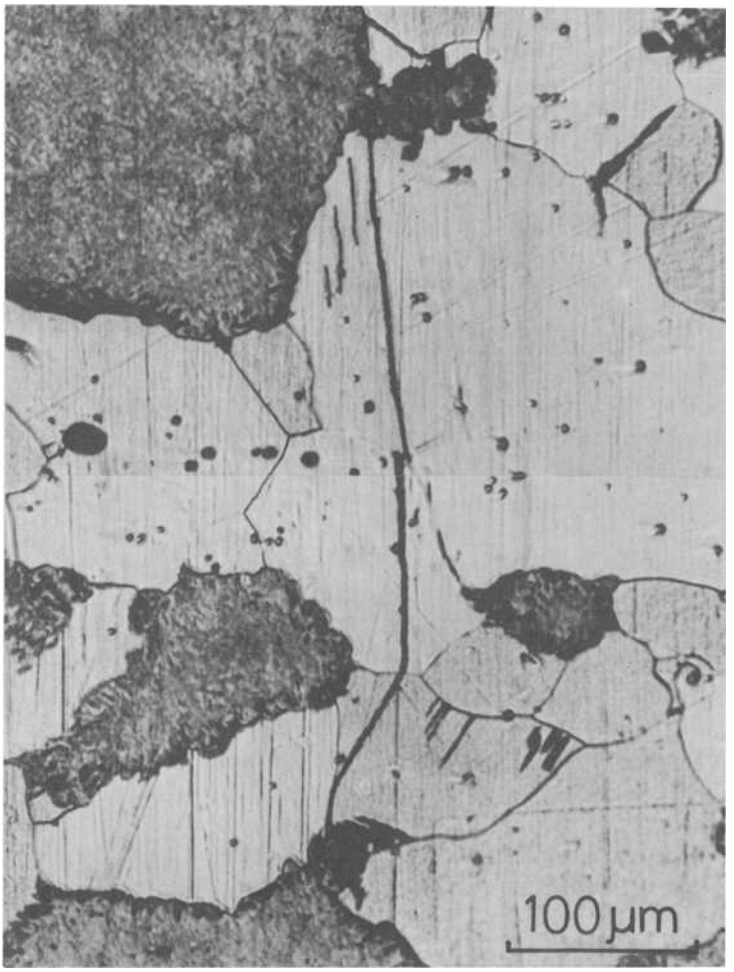

FIG. 3—*Typical features of a nonpropagating crack in the martensite-ferrite two-phase microstructure. The crack in the ferrite matrix is impeded in its further growth by the martensite ahead of the crack tip* (σ = *282 MPa*, $N = 10^7$ *cycles in rotating bending*, l = *186 µm*).

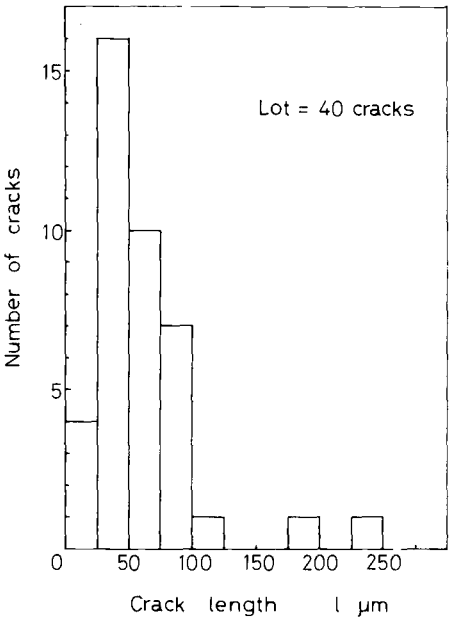

FIG. 4—*Histogram of length of nonpropagating cracks in a single specimen fatigued at the endurance limit* (σ = *279 MPa*).

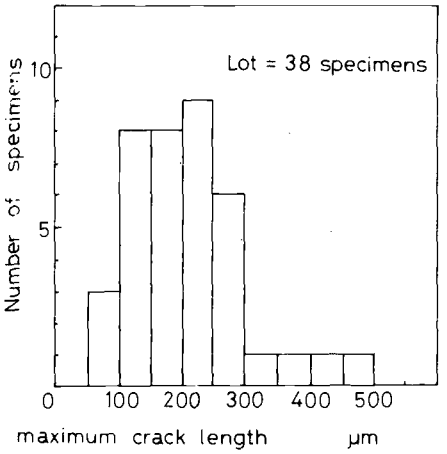

FIG. 5—*Histogram of the maximum lengths of nonpropagating cracks in 38 specimens fatigued at the endurance limit* (σ = *279 MPa*).

the maximum crack length. It was also found that, in either case, for cracks less than 400 to 500 μm, most cracks were still impeded by the second-phase martensite but a fatal crack propagated in the ferrite matrix, by-passing the second-phase martensite. On the other hand, for cracks larger than 400 to 500 μm, propagation into the second-phase martensite took place in a relatively easy manner.

In a further experiment, some of these specimens having crack lengths less than and larger than 500 μm were fatigued again at the endurance limit of 279 MPa. In this case, the short cracks would not propagate into the martensite—in other words, they became nonpropagating cracks at cyclic stressing of 10^7—while the long cracks propagated directly into the martensite, leading to a final fracture. This evidence implies that the second-phase martensite plays a role of impediment for crack propagation, and the crack length of about 500 μm corresponds to the critical length for crack propagation into the martensite at the endurance limit stress of 279 MPa. Now an estimation of the crack growth resistance of the second-phase martensite will be made from the foregoing critical crack length conditions at the endurance limit. Using the conventional linear theory of fracture mechanics, this may be represented by the following equation

$$K = K_{\text{thm}} \tag{1}$$

where K_{thm} is the crack growth resistance of the second-phase martensite and K the stress intensity factor calculated from[4]

$$K = \sigma \sqrt{\pi l/2} \tag{2}$$

where σ and l are applied stress amplitude and crack length in the ferrite matrix between martensite zones, respectively.

It is understood that the stress intensity factor (SIF), K, the left-hand side of Eq 1, is based on a mechanics approach given by the applied stress, crack length, and geometry, while K_{thm}, the right-hand side of the equation, could be regarded as a material characteristic related to the strength of the martensite. An evaluation of the magnitude of crack growth resistance of the second-phase martensite is possible by substitution of the endurance limit stress of 279 MPa and the corresponding critical crack length l = 500 μm into Eq 2, that is

$$K_{\text{thm}} = 279\sqrt{\pi \times 500 \times 10^{-6}/2} = 7.82 \text{ MPa}\sqrt{\text{m}}$$

[4]The simplest solution of the stress intensity factor was used in this calculation, because the appropriate solution for the present case has not yet been obtained. A solution of K for an arbitrary crack geometry can be given in the form of $K = \alpha \sigma\sqrt{\pi a}$, where α is a coefficient obtained from the geometry of the crack and specimen.

Since the value of K_{thm} represents the material characteristic, this should be independent of crack length. Therefore the following experiments were carried out in order to examine whether the value of K_{thm} is independent of crack length. The specimens used were prepared such that the tip of a crack larger than 500 μm in length impinged on a martensite boundary after rotating bending stressing at $\sigma = 295$ MPa, which was slightly above the endurance limit of 279 MPa. Then, the largest crack in these specimens was subjected to reversed bending fatigue. Thus was obtained the maximum applied stress by which the crack did not propagate into the second-phase martensite after 10^7 cycles. A substitution of this critical stress value and the corresponding crack length into the Eq 2 gives the crack growth resistance of the martensite. These results are presented in Table 2. This table shows that K_{thm} is about 7.7 MPa$\sqrt{m}$ irrespective of crack length, which ranged from 500 to 1000 μm. Furthermore, from the observation that previous nonpropagating cracks would not start to propagate into the second-phase martensite under any circumstance without an increase in the SIF, it was found that the surface behavior of crack propagation in the range of crack length from 500 to 1000 μm is closely related to the onset of fracture of the specimen.

TABLE 2—*Crack growth resistance of second-phase martensite* K_{thm}.

Specimen No.	Cyclic Stress, MPa	Crack Length, μm	Stress Intensity, K MPa$\sqrt{m}$	Remarks
106	255	580	7.70	S[a]
118	224	762	7.75	B[b]
	217	827	7.82	S
125	218	788	7.67	S
	228	788	8.02	B
129	232	693	7.65	S
226	201	943	7.74	B
229	191	1010	7.61	S
232	282	508	7.97	S
310	207	895	7.77	B
	204	918	7.75	B
325	221	782	7.75	S
331	206	904	7.76	B
	180	1132	7.59	B
333	178	1097	7.39	B
334	225	744	7.69	B
	186	1108	7.76	B
417	249	615	7.74	S
432	265	538	7.70	S
	277	538	8.05	B
434	279	489	7.73	S

[a] S: The cracks did not propagate into the second-phase martensite after the 10^7 stress cycles.

[b] B: The cracks propagated into the second-phase martensite.

Figure 6 shows a typical photograph of a crack of length 580 μm which does not propagate into the second-phase martensite after 10^7 cycles at the stress level of 255 MPa ($K = 7.7$ MPa$\sqrt{\text{m}}$). Consequently, it might be concluded that the crack growth resistance of the second-phase martensite is independent of crack length in the present experiments.

The foregoing calculation of the K-value was performed simply by substitution of the stress and crack length into the linear fracture mechanics equation without paying attention to the validity of its application to this problem. To discuss the validity, it is most essential that the plastic zone size ahead of the crack tip be taken into consideration. The plane-stress plastic zone size can be calculated from [9]

$$r_p = \frac{1}{2\pi}\left(\frac{K}{\sigma_y}\right)^2 \tag{3}$$

Since the value of the yield stress σy of the microstructure ahead of the microscopic crack tip is not generally measurable, it is usually estimated from the micro-Vickers hardness number (VHN).[5] Therefore, a reasonable yield stress of the martensite used in this calculation was 1500 MPa, which is smaller than the estimated corresponding value from the micro-VHN = 730 for the martensite. The size of plastic zone ahead of the crack tip was thus determined as approximately 4 μm. This plastic zone size is very small in comparison with the specimen thickness of 1 mm and the length of crack ranging from 500 to 1000 μm. Accordingly, it is considered that the basic assumption of small-scale yielding for linear fracture mechanics is satisfied. The foregoing discussion led to the conclusion that, if the SIF, K, of the surface crack having a length 500 to 1000 μm is less than 7.7 MPa$\sqrt{\text{m}}$, the crack will not start to propagate into the martensite for the present material.

Hitherto, discussions were limited to the surface crack of the specimen. However, the question arises as to how the crack propagates into the thickness of the specimen. Observations of the crack front were made on fractured surfaces which were produced artificially in a brittle manner at liquid air temperature, starting from the nonpropagating crack of the length 508 μm after 10^7 cycles at a stress level of 282 MPa. Figure 7*a* is a photograph of a nonpropagating crack in the surface microstructure before brittle fracture, while Fig. 7*b* is a scanning electron microscope (SEM) photograph of the fractured surface of the crack shown in Fig. 7*a*. The solid line in Fig. 7*b* indicates the borderline between the fatigued and brittle-fractured surfaces; that is, the region inside the line corresponds to the fatigued area. It is observed from this photograph that the front of the nonpropagating

[5] See, for instance, McClintock and Argon [10], p. 453.

FIG. 6—*A typical example of a nonpropagating crack impeded in its propagation by the second-phase martensite after 10^7 cycles. Dark shadowed patches in the photograph are second-phase martensite,* ($\sigma = 255$ *MPa*, $1 = 580$ μm, $K = 7.70$ *MPa*$\sqrt{m}$).

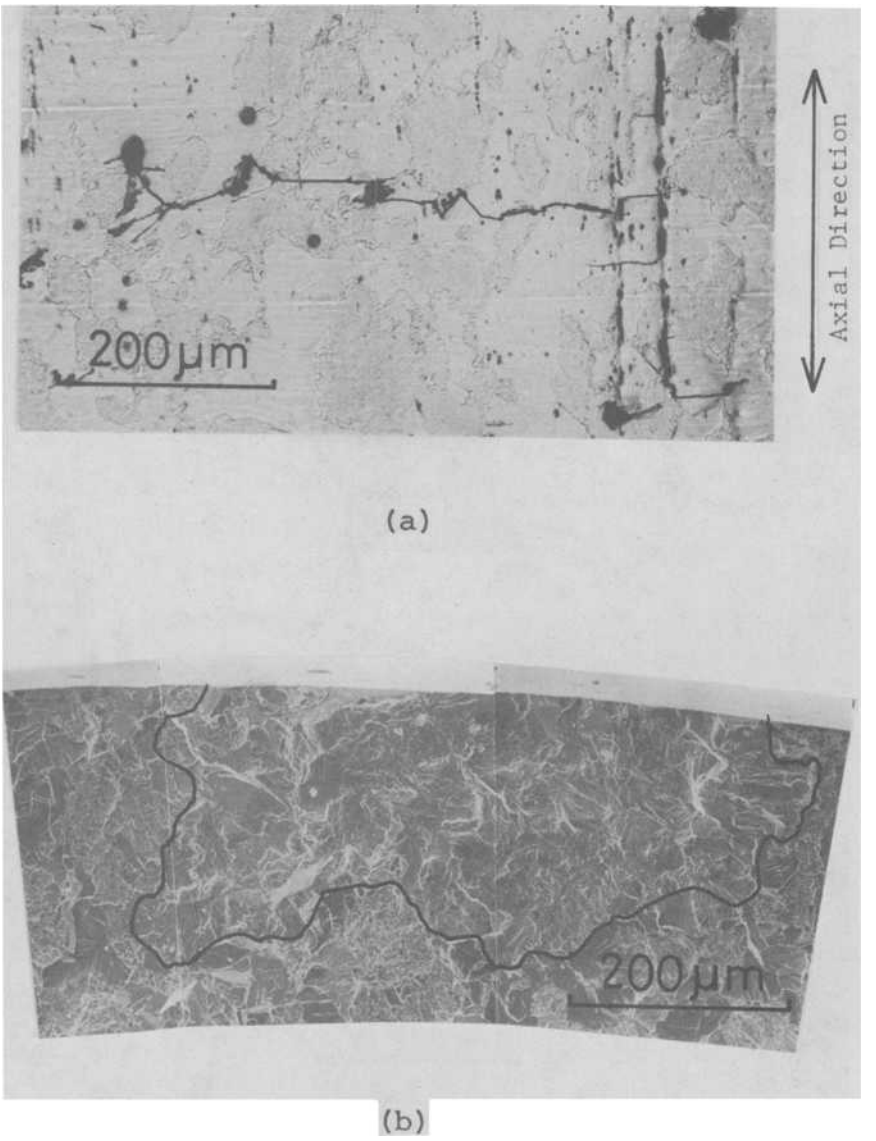

FIG. 7—*Two views of the same nonpropagating crack:* (a) *as viewed on the surface microstructure;* (b) *as viewed in the specimen cross section after fracture at liquid air temperature. The solid line in the photograph indicates the boundary between brittle and fatigue fracture surfaces* ($\sigma = 282$ *MPa*, $l \simeq 508$ μm, $K \simeq 7.97$ $MPa\sqrt{m}$, $N = 10^7$ *cycles*).

crack stops at the martensite while bowing out into the matrix ferrite. Figure 8 shows another example of a nonpropagating crack after the repetition of $K = 7.7$ MPa$\sqrt{\text{m}}$ for 10^7 cycles in reversed bending. In order to reveal how the crack extends in the depth direction, this specimen was successively sliced normal to the surface. Figures 9*a*-9*e* show photographs taken on the cross sections marked A-E in Fig. 8, respectively.

It can be concluded from these photographs that the cracks propagate in the matrix ferrite, bypassing the second-phase martensite in a manner similar to that observed in the surface microstructures.

Length of Nonpropagating Cracks and Mean Second-Phase Spacing

From the experiments mentioned previously, the crack growth resistance of martensite K_{thm} was obtained approximately as 7.7 MPa$\sqrt{\text{m}}$. Thus, the value of K of all nonpropagating cracks at the endurance limit must satisfy the following condition

$$K \leq K_{\text{thm}} \tag{4}$$

where the value of K can be calculated by substituting the crack length into the following equation

$$K = 279\sqrt{\frac{\pi l}{2}} \text{ MPa}\sqrt{\text{m}} \tag{5}$$

Figure 10 shows the curve of Eq 5 together with the plots of experimental data of the crack growth resistance of the martensite K_{thm}. This figure also shows that the K-value of the largest nonpropagating crack in each specimen must be either in a position given by the curve of Eq 5 or equal to the mean experimental value of K_{thm} ($= 7.7$ MPa$\sqrt{\text{m}}$), whichever is smaller. This means that the maximum length of a nonpropagating crack in a single specimen does not always reach the critical length at the endurance limit stress. A question therefore is, how can the length of a nonpropagating crack be determined at the endurance limit? It can be considered that the endurance limit for the specimen having two-phase microstructure is closely related to the mean second-phase spacing.

Since the mean second-phase spacing is not large, that is, 84 μm (Table 1), most cracks nucleated in the matrix ferrite cannot attain a stress intensity to propagate into the martensite when they reach the martensite boundary. This would explain the existence of nonpropagating cracks, the sizes of which are distributed near the mean second-phase spacing. On the other hand, particular cracks that were nucleated at sites preferable for propagation, or that propagated preferentially—in other words, bypassing the second-phase martensite in the matrix ferrite—would possibly reach a

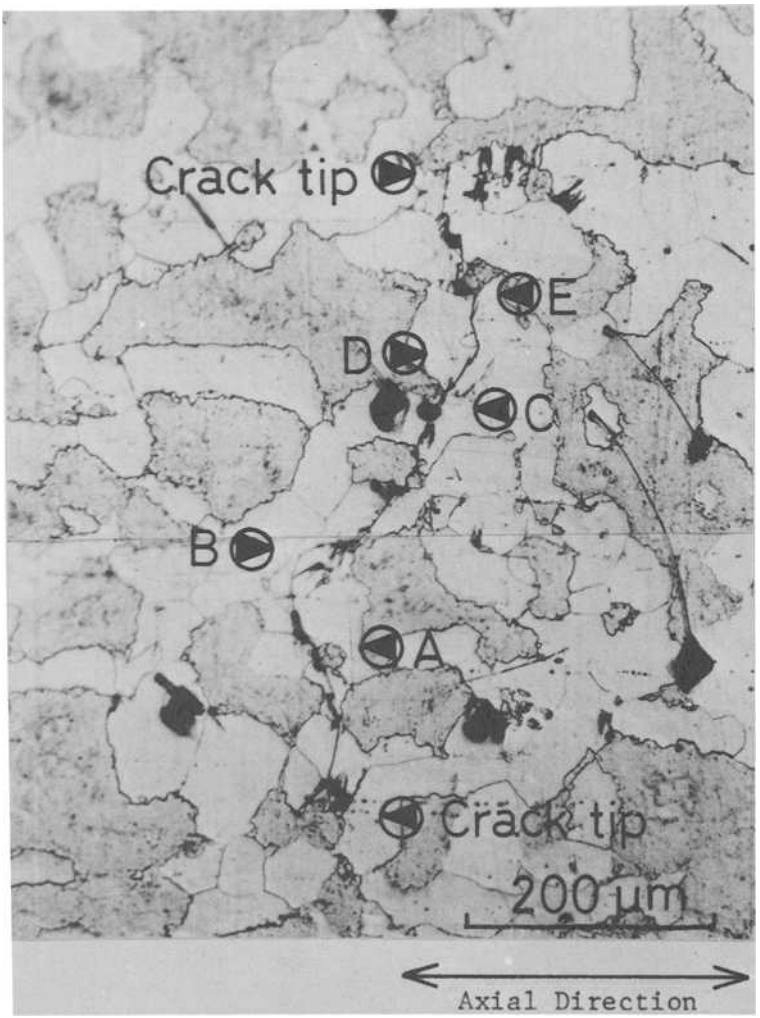

FIG. 8—*Features of a nonpropagating crack in the surface microstructure. Letters* A–E *indicate the points where the cross sections were examined by metallurgical treatments as shown in greater detail in Figs.* 9a–9e (σ = *279 MPa,* l = *489 μm,* K = *7.73 MPa*$\sqrt{m}$, N = 10^7 *cycles*).

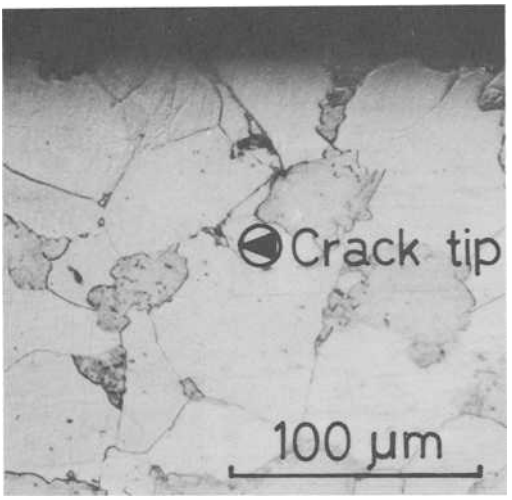

FIG. 9*a*—*Cross-section at Point A (Fig. 8) showing the crack path.*

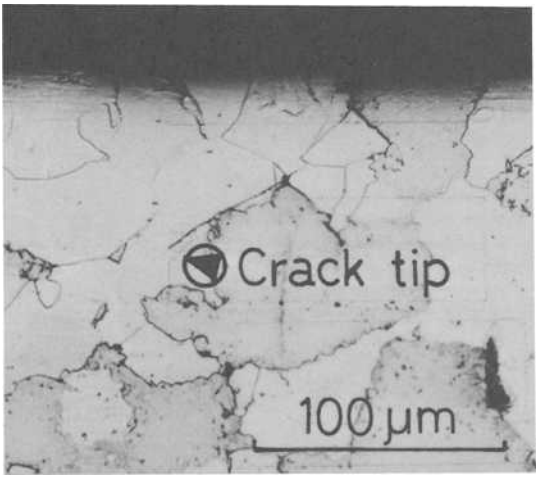

FIG. 9*b*—*Cross-section at Point B (Fig. 8) showing the crack path.*

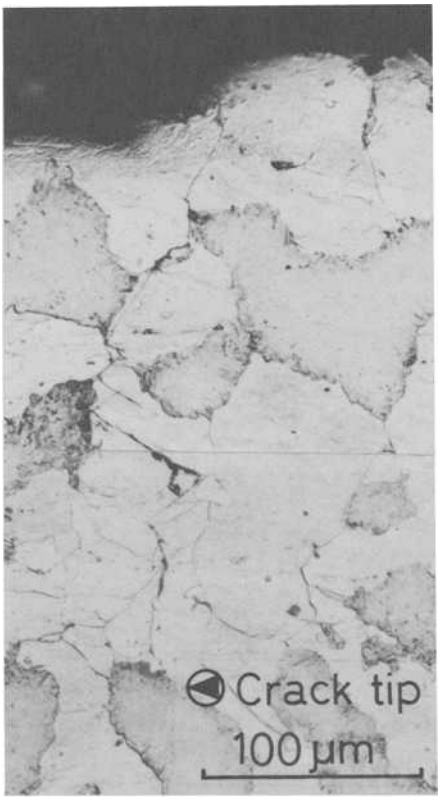

FIG. 9c—*Cross-section at Point C (Fig 8) showing the crack path.*

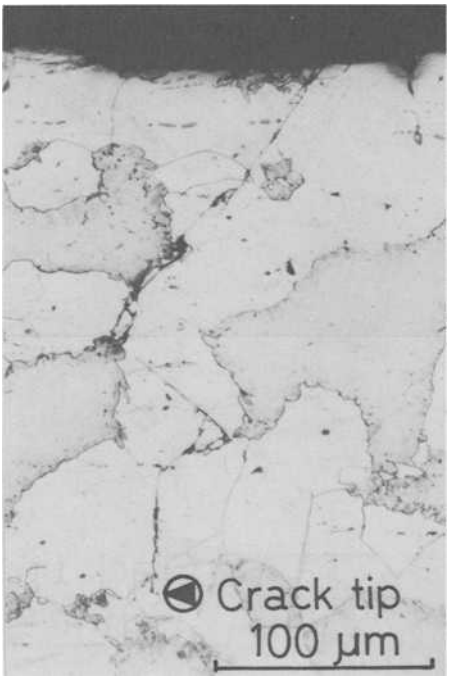

FIG. 9*d*—*Cross-section at Point D (Fig. 8) showing the crack path.*

FIG. 9e—*Cross-section at Point E (Fig. 8) showing the crack path.*

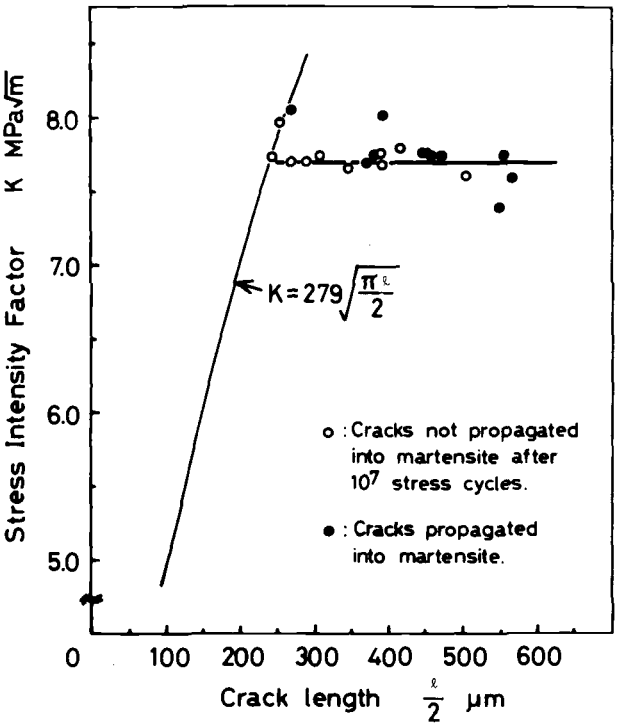

FIG. 10—*Relationship between the crack growth resistance of martensite and the stress intensity factor (SIF) of the nonpropagating cracks.*

length of about 500 μm. It appears from the foregoing evidence that the mean second-phase spacing would restrict the size of nonpropagating cracks to considerably shorter than the critical length.

Consequently, the role of the second-phase martensite on the endurance limit could be concluded as follows. First, the crack growth resistance of martensite plays a part in impeding the crack path. Second, a relatively narrow mean second-phase spacing gives geometrical restrictions to the possible site of crack nucleation and also to the length of a nonpropagating crack. This can be understood from the evidence shown in Fig. 4, namely, that the length of a nonpropagating crack has a peak value near the second-phase spacing. These nonpropagating cracks did not reach the critical size to propagate into the second-phase martensite, as mentioned previously. Thus, it is concluded that the threshold condition cannot be obtained by the condition of growth of a nonpropagating crack which does not reach the critical size at the endurance limit. Finally, in connection with the threshold condition of the crack, it is worthy of notice that the effective SIF range ΔK_{eff}, calculated by the elastoplastic analysis for a crack in the

model plate composed of two different materials with the same Young's modulus, decreases as the boundary of the higher yield stress material [*11*]. This can be applicable to the present case where the fatigue crack is nucleated in the soft matrix ferrite and impeded in its propagation by the second-phase martensite. In other words, the reduction of ΔK_{eff} would also contribute to the formation of nonpropagating cracks.

Conclusion

A threshold condition for nonpropagating microscopic cracks observed in two-phase microstructures of martensite and ferrite was studied from a mechanical-metallurgical viewpoint. Results obtained are summarized as follows.

1. It was found that the threshold condition of microscopic fatigue cracks in two-phase microstructures of martensite and ferrite can be evaluated from conventional linear fracture mechanics as $K = K_{thm}$, where K_{thm} is the crack growth resistance of the second-phase martensite and which represents a material characteristic. For smaller values of stress intensity factor K than the crack growth resistance of the martensite, K_{thm}, the fatigue cracks in matrix ferrite will remain as nonpropagating ones. The crack growth resistance of the martensite is 7.7 MPa$\sqrt{m}$ for the present material.

2. The mean second-phase spacing is not necessarily related to the critical length of the endurance limit stress.

Acknowledgments

The authors express their thanks to Prof. M. Shimizu for his valuable discussions and encouragement. The authors are indebted to Messrs. T. Naito and R. Ono for their assistance in conducting the experiments, and they also acknowledge financial support from the Takeda Science Foundation.

References

[*1*] Hempel, M. in *Proceedings*, International Conference on Fatigue of Metals, The Institution of Mechanical Engineers, 1956, p. 54.
[*2*] Wadsworth, N. J., *Philosophical Magazine*, Vol. 6, No. 63, 1961-63, p. 397.
[*3*] Watanabe, J. and Kumada, A., Preprint of the Annual Meeting, Japanese Society for Mechanical Engineers, No. 37, 1961, p. 67 (in Japanese).
[*4*] Forrest, P. G. and Tate, A. E. L., *Journal of the Institute of Metals*, Vol. 93, 1964-1965, p. 438.
[*5*] Kunio, T., Shimizu, M., and Yamada, K. in *Proceedings*, 2nd International Conference on Fracture, England, Chapman & Hall, 1969, p. 630.
[*6*] Awatani, J., Katagiri, K., Omura, A., and Shiraishi, T., *Metallurgical Transactions*, Vol. 6A, 1975, p. 1029.

[7] Kobayashi, H., Kawada, Y., and Nakazawa, H., *Journal of the Society of Materials Science,* Japan, Vol. 25, No. 276, 1976, p. 881 (in Japanese).
[8] Nishitani, H. in *Proceedings,* 22nd Japan National Symposium on Strength, Fracture and Fatigue, 1977, p. 29 (in Japanese).
[9] *Fracture Toughness and Its Applications, ASTM STP 381,* American Society for Testing and Materials, 1965.
[10] McClintock, F. A. and Argon, A. S., *Mechanical Behavior of Materials,* Addison-Wesley, Reading, Mass., 1966, p. 453.
[11] Ogura, K., Ohji, K., Honda, K., and Kawabata, Y., Preprint of the Annual Meeting, Japanese Society for Mechanical Engineers, No. 770-2, 1977, p. 48.

DISCUSSION

K. Miller[1] *(discussion)*—First let me say that I consider this paper has made a notable contribution to the literature. It has shown that in a two-phase structure the fatigue limit is not necessarily associated with the ability of a material to resist crack initiation but rather to resist the propagation of a small crack generated in one phase that is difficult to propagate across the second phase. The authors are to be congratulated on an extremely well-conducted series of experiments and the results published in Table 2 are recognized as being most valuable.

I will confine most of my discussion to the fracture mechanics approach to the problem and by asking the authors three questions.

Figure 3 shows that several short cracks have been initiated in the ferrite grains and these may have taken a considerable number of cycles to initiate in a surface grain. These become Stage I cracks growing by Mode II on 45-deg planes. Many shown in Fig. 3 are of Type IA,[2] that is, they are in the plane of the surface. This leads to the question of how early in the life of the nonpropagating crack specimens were cracks observed in the ferrite; and was there any evidence of Type IB shear cracks, that is, Stage I cracks, growing away from the surface into the interior á la Forsyth[3]?

The next issue for discussion concerns the applicability of linear elastic fracture mechanics (LEFM) analyses. It is my opinion that LEFM applies only to long cracks with correspondingly large-stress-intensity fields that dominate, and hence characterize, the relatively small plastic strain field. Further, and most important in any continuum mechanics approach to stable ductile fracture, the fracture process zone itself must be small

[1] Department of Mechanical Engineering, University of Sheffield, Sheffield, U.K.
[2] Brown, M. W. and Miller, K. J. in *Proceedings,* Institution of Mechanical Engineers, Vol. 187, No. 65/73, 1973, p. 745.
[3] Forsyth, P. J. E. in *Proceedings,* Symposium on Crack Propagation, Cranfield, U.K., 1961, p. 76.

in relation to the plastic zone size. It follows that if the plastic zone is equal to, or smaller than, important metallurgical features such as grain size, then the continuum mechanics elastic analysis approach may not apply. Our present authors indicate that the plastic zone size calculated from Eq 3 is considerably less than the grain size (4 μm versus 40 μm). Would the authors not expect that, in order to validate LEFM analyses, the plastic zone size minimum should be at least the grain size?

Admitting that the work here discussed is possibly on the boundary of LEFM applicability, it would be wise to consider the use of the authors' Eq 2. Now the first crack form, which could be assumed to be semicircular of radius a, has a Mode I stress intensity factor which is a function of

$$K_0 = 2\sigma \left[\frac{a}{\pi}\right]^{0.5} \tag{6}$$

(See Rooke and Cartwright[4] and Tada et al.[5]) This crack propagates along the entire front and may become any shape; Thus the data presented in Section 4.1.5 of the Rooke/Cartwright paper (footnote 4) are important. They show what stress intensity variations occur around the crack front as the crack front form changes. First they explain why the crack should grow along the surface more rapidly than into the interior. Furthermore, and most important to the present discussion, the data can be interpreted in the form given in Fig. 11 accompanying this discussion. This figure shows that for a crack of variable c/a ratio the maximum stress intensity factor at the root occurs when the crack front is semicircular. However, the crack front geometry changes as indicated in Fig. 7*b* of the paper; that is, the ratio c/a decreases, whereupon the stress intensity factor at the root decreases. This indicates that while the surface crack length measurement, l, is important, the crack form and depth are more important in determining threshold conditions.

Because of all the foregoing remarks, I have reinterpreted the data of Table 2 and Fig. 10 on the basis that, whatever parameter best characterizes the behavior of these short cracks, it can be safely assumed that an equation of the form

$$\sigma l^m = \text{constant} \tag{7}$$

should fit the data. Such an equation can be used in either linear elastic or elastic-plastic fracture mechanics analyses. Figure 12 herewith presents

[4] Rooke, D. P. and Cartwright, D. J., *Compendium of Stress Intensity Factors*, Her Majesty's Stationery Office, London, U.K., 1974.

[5] Tada, H., Paris, P. C., and Irwin, G. R., *The Stress Analysis of Cracks Handbook*, Del Research Corp., Hellertown, Pa. 1973.

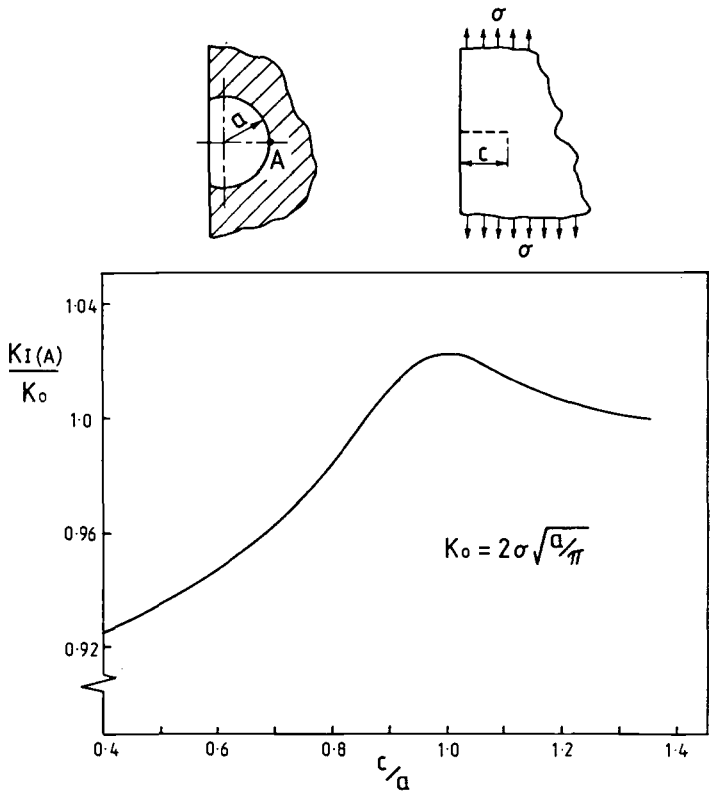

FIG. 11—*Variation of Stress-intensity factors of circular-front edge cracks of various radius-to-depth ratios.*

this interpretation and clearly illustrates the very careful experiments conducted by the authors; it shows also that the boundary between propagating and nonpropagating cracks is given by

$$\sigma l^{0.584} = 3.3865 \tag{8}$$

where σ is in MPa and l in metres. Furthermore Fig. 12 shows that, at the fatigue limit, l must be less than 524 μm for nonpropagating cracks to occur.

Finally it is worth noting that the crack development along the surface is easier than that into the interior because of less restraint on deformation [and crack-opening displacement (COD)] at the specimen surface. Surface conditions will also assist the crack to bypass the martensite. In the interior, however, not only does the stress intensity factor decrease relatively, but it becomes more difficult to bypass the martensite.

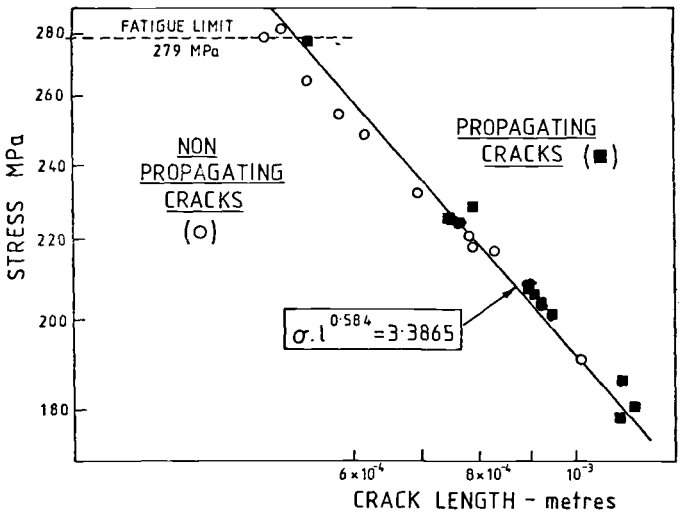

FIG. 12—*Derivation of the limiting conditions for nonpropagating cracks at and below the fatigue limit.*

From all previous statements, I would consider it useful to have some comparative histogram data in order to analyze the effect of

1. crack depth, and
2. maximum distance of crack length between martensite particles at the crack root,

on the behavior of nonpropagating cracks below the fatigue limit. Do the authors have such data?

In conclusion, would the authors please confirm that the experiments were conducted at room temperature in laboratory air. Also, I would be grateful to know the history and loading mode of the experiments mentioned in the fourth paragraph of the "Results and Discussion" section ("In a further experiment...").

R. Ritchie[6] *(discussion)*—The authors address the problem of nonpropagating fatigue cracks (NPFC) and the role of microstructure on the threshold conditions for such nonpropagation in a low-strength steel. They describe how, for a duplex ferritic-martensitic plain carbon steel, microcracks may initiate at the fatigue limit in the softer ferrite, yet become dormant through inability to propagate into the second-phase martensite. Their threshold condition for nonpropagation of microcracks is thus re-

[6] Department of Mechanical Engineering, Massachusetts Institute of Technology, Cambridge, Mass. 02139.

lated to the "obstruction effect" of a harder second phase. In aluminum alloys, however, this obstruction effect may be provided by grain boundaries, since NPFC's tend to be generally 1 to 2 grain diameters in length and terminated near boundaries.[7,8] Morris[7] has recently claimed that this transit of a microcrack through a boundary produces a high crack closure stress on the surfaces, resulting in a retardation. In this regard, the phenomenon of crack closure[9] may provide a more general mechanism of NPFC's. A further factor which may influence the retardation of microcrack growth is the interaction of neighboring microcracks (see Kung, footnote 8). Particularly in lower-strength materials, the process of initiation may involve the formation of many microcracks, and fatal macrocrack growth then results from the initial linkage of some of these cracks. Since coalesced cracks will propagate faster, neighboring microcracks will tend to stop growing.

Aside from the issue of the mechanism of NPFC's, however, there is the question of the threshold conditions for their formation. Above some critical microcrack length (~ 500 μm), the authors find that the threshold conditions for failure (that is, the fatal growth of a microcrack) are such that the *stress intensity* at the tip of the largest crack must exceed a critical value (in this case, the crack growth resistance of the martensite). Below this critical microcrack length, the condition for failure reverts to a constant threshold *stress*, the fatigue limit. A relationship between the transition crack length, which essentially defines the limiting crack size for analysis by continuum fracture mechanics, and some critical microstructural unit has not as yet been determined. As the authors point out, however, this provides a mechanism for NPFC since a microcrack may initiate at a *stress* just exceeding the fatigue limit (the threshold stress for short cracks), but subsequent microcrack growth, over a few grain diameters, may not raise the *stress intensity* above the threshold ΔK_0 for macro-crack growth (that is, the threshold stress intensity for long cracks).

In the light of this, it is probably time for a reevaluation of what we mean by threshold conditions for failure, and to decide the relevance of such parameters as the fatigue limit or endurance strength, the threshold stress intensity for (macro) crack propagation (ΔK_0), and, more recently, the threshold stress intensity for initiation (ΔK_0^i). Since fatigue failure involves several distinct processes—namely, (1) macrocrack initiation, (2) microcrack growth over first few grains, and (3) macrocrack growth—any one of these may provide the limiting conditions for failure. A disturbing aspect of these different thresholds, however, at least from an alloy design point of view, is that they do not respond in similar ways to micro-

[7] Morris, W. L., *Metallurgical Transactions, A*, Vol. 8A, 1977 p. 589.

[8] Kung, C. Y., Ph.D. Thesis, Northwestern University, Evanston, Ill., June 1978.

[9] Elber, W. in *Damage Tolerance in Aircraft Structures, ASTM STP 486*, American Society for Testing and Materials, 1971, p. 230.

structural changes.[10] This can be appreciated by examining the effect of increasing yield strength on fatigue threshold conditions in steels. As strength is raised, the fatigue limit or initiation threshold ($\Delta K_0{}^i/\sqrt{p}$) will generally be increased, whereas the (macrocrack) propagation threshold (ΔK_0) will be decreased. (Thus, for example, in a 4140 or 4340 steel tempered to a range of strength levels, the spheroidized structure, tempered at around 650°C, will show the least resistance to microcrack initiation and growth[11] and yet the greatest resistance to macrocrack propagation (Ritchie, footnote 10) compared with structures tempered at lower temperatures.) Clearly if we are to design and utilize materials for applications where maximum resistance to the early stages of fatigue failure is required, it is essential to decide which of these processes is critical, particularly in the light of the presence of preexisting defects and the applied stresses involved.

S. Weissman[12] *(discussion)*—If one considers a two-phase alloy with Phases A and B such that we may think of Phase A as being an obstacle to B, then there are two geometric properties which can be measured in a statistical sense, namely, the mean distance of the obstacles, and the distribution of the spatial separation of those obstacles. In the paper, the martensite may be considered as the obstacles. If I may take the viewpoint that, in precipitation hardening, the most effective blocking mechanism may be attributed to a homogeneous distribution of the obstacles, then my question is: Would you consider the distribution of the obstacles to be more important than the mean distance or spacing between obstacles?

K. Yamada (reply to S. Weissman)—The second-phase martensite has the following two effects on the fatigue behavior of the present alloy. One is the blocking effect for crack propagation. The other is the effect of limiting the possible site for crack initiation in the microstructure. When the crack starts in the ferrite and propagates up to the martensite-ferrite boundary, and when the crack is short (mean second-phase spacing is short), then the crack stays as a nonpropagating one. Some of the cracks which initiated in the preferred sites for crack propagation, or which already have propagated to the boundary of the ferrite and martensite, may reach a critical size. Those cracks may still stay as nonpropagating if the stress intensities of the cracks are below the crack growth resistance of the martensite. In this case, the critical size of the crack does not depend on the mean second-phase spacing, but is related to the crack growth re-

[10] Ritchie, R. O., *Journal of Engineering Materials and Technology, Transactions,* American Society of Mechanical Engineers, Series H., Vol. 99, 1977, p. 195.

[11] Kim, Y. H., Mura, T., and Fine, M. E., *Metallurgical Transactions, A,* in press.

[12] Department of Mechanics and Materials Sciences, Rutgers University, Piscataway, N.J. 08854.

sistance of the martensite. We cannot mention which factors, the distribution of the obstacles or the spacing between the obstacles, is more important from this experiment.

A. McEvily[13] (*discussion*)—I have a brief comment.

Dr. Suzuki, a former student of Professor Kunio's, spent last year in our laboratory and carried out some research on low-carbon steel which is relevant to Dr. Yamada's presentation.

In one heat-treated condition the alloy was similar to that described by Dr. Yamada. That is, there was a continuous martensitic network throughout the alloy. A second heat-treated condition was an inside-out version of the first. The ferritic phase was continuous, with islands of martensite encapsulated within the ferrite. The threshold level, when the ferrite phase was continuous, was of the order of 10 MPa$\sqrt{\text{m}}$. However, when the martensitic phase was continuous, the threshold level was of the order of 20 MPa$\sqrt{\text{m}}$.

From the metallurgist's point of view, this is quite an interesting result in that we have been able to control the threshold level through control of the microstructure.

K. Yamada (*reply to A. McEvily*)—Thank you very much for your comment.

In the present experiment we used the microstructure having the continuous ferrite network throughout the alloy as Prof. McEvily has pointed out. When we change the microstructure from the continuous-ferrite to continuous-martensite version, that is, when the ferrite is surrounded completely by the martensite, we may expect the increase of the threshold level from the result of the present experiment. However, our experiment in progress does not show an increase of the threshold level. This would be related to the preferential propagation of the crack along the prior austenite grain boundaries in the martensite. This could be an interesting problem. Therefore I think that at present it is not easy to control the microstructure for the purpose of increasing the threshold level, because the characteristics of the martensite for the growth of the crack are much too complicated.

M. Lamba[14] (*discussion*)—My question, related to fracture mechanics, concerns a crack in a homogeneous medium. If you have two systems, or two materials acting at an interface, with a crack in one of the systems and no crack in the other system, the stress intensity itself is affected by this condition. I want to question the basis for the treating of cracks in multi-

[13] Department of Metallurgy, Institute of Materials Science, University of Connecticut, Storrs, Conn. 06268.

[14] International Harvester, Hinsdale, Ill. 60521.

phase media under microstructural levels in the same way as one would treat a crack in, say, pure iron.

K. Yamada (reply to M. Lamba)—I will take it that the question is the applicability of linear fracture mechanics (LFM) to the microstructural phenomena having inhomogeneities. We simply applied the result of the LFM calculation to the present problem, satisfying the small-scale yielding condition. However, the effective stress intensity at the martensite-ferrite boundary might be different from the calculation, because the yield stress of the martensite is four times larger than the matrix ferrite, which is estimated from the micro-Vickers hardness. The effective stress intensity might be reduced at the crack which has reached the martensite boundary. In the paper we referred to this effective stress intensity, which might also be one of the reasons for the nonpropagating crack.

K. DeVries[15] *(discussion)*—I have a very short question on how universally applicable you feel your results might be. Do you feel that it is a general feature that all nonpropagating cracks are due to the presence of a second phase that arrests the crack growth? Is that a general observation?

K. Yamada (reply to K. DeVries)—In this material, yes.

K. Miller[16] *(discussion)*—The answer to Prof. DeVries's question is, in general, no. Cracks initiate due to plastic deformation that cannot be characterized by LEFM. If a crack cannot attain threshold length conditions, then it will become nonpropagating. Such cracks can therefore be due not only to second-phase particles, but to three-dimensional changes in crack front geometry, variation in stress levels and ratios, overloads, etc.

J. Beevers[17] *(discussion)*—I would just like to make a couple of comments. If you take something like ferrite, very low carbon, you can end up with thresholds, depending on R, (stress ratio), around the 7 to 10 region.

If you take a plain carbon martensite, you'll end up with thresholds around about the 3 to 5 region, maybe 6, depending on R (stress ratio) again.

So really we've got quite an interesting situation here that, although the authors have delightfully pointed out that the problem of the critical event is the propagation of the crack from the ferrite into the martensite, in actual fact the real base of the high threshold, which is about 7.8, would appear to be coming from the basic property of the ferrite.

[15] Department of Mechanical and Industrial Engineering, University of Utah, Salt Lake City, Utah 84112.

[16] Department of Mechanical Engineering, University of Sheffield, Sheffield, U.K.

[17] Department of Physical Metallurgy, University of Birmingham, Birmingham, U.K.

It really depends here upon what is the controlling feature within the natural microstructure. I mention this as a point of probable further discussion after the session, but I think we have to clarify what really is the controlling feature within this microstructure, and other two-phase microstructures, when we start to decide what is controlling the crack arrest conditions in these threshold regions.

Just one more point, when we talk about thresholds, they are quite distinct, and they are measured quite differently in many cases from the much shorter cracks that the present authors describe.

There is no reason at all why we should expect a correlation, for example, between grain size effects of fatigue limits and threshold levels vis-a-vis grain size effects.

T. Kunio and K. Yamada (authors' closure)—We appreciate the comments and discussions made by Professors Miller, Ritchie, Weissman, McEvily, DeVries, Beevers, and Dr. Lamba. Before we respond to each comment or discussion, however, we would like to give a brief explication on the background of this paper. It is quite an interesting problem to explore the behavior of microstructures due to cyclic stressing that involves the initiation and propagation of microcracks. Authors have been engaged in the study of the fatigue behavior of heat-treated low-carbon steel which has the martensite and ferrite duplex microstructure. In the present experiment, a special emphasis is placed on the effects of microstructure on the behavior of microcracks at the threshold level.

The role of the microstructure in the critical condition of the microcrack growth in this particular experiment is well characterized by application of the LFM. A straightforward application of this approach to any ductile material might be difficult. However, the concept that the threshold level of the material could be determined by the crack growth resistance of the microstructure might be generally accepted.

We will now respond to the several specific comments or questions of the discussers.

First, taking Professor Miller's questions in order:

1. ("How early in life of the nonpropagating crack specimen were the cracks observed in the ferrite?") The slipband crack was first observed by the $\times 400$ optical microscope at the stress reversal of about $N = 10^4$ at the threshold stress level. Details of the first appearance of the slipband crack were published by the authors in a previous paper.[18]

2. ("Was there any evidence of the Type IB crack?") All the cracks which are less than the ferrite grain size in the histogram of Fig. 4 would

[18] Kunio, T., Shimizu, M., and Yamada K. in *Proceedings*, 2nd International Conference on Fracture, Brighton, U.K., Chapman & Hall, 1969, p. 630.

be classified as Stage I cracks; however, we have not taken any pictures of the aforementioned cracks.

3. (" ... that in order to validate LEFM analyses the plastic zone size minimum should be at least the grain size?") This is quite a fundamental question, on whether the explanation of the effect of microstructure on microcrack growth can be attempted through LEFM. We cannot answer this question with the experimental data so far obtained. In this experiment, the microstructure ahead of the microcrack tip is not the ferrite grain, but martensite. The important metallurgical parameter could be the prior austenite grain or martensite packet in association with the plastic zone size. The size of the microstructural constituent would be comparable or less than the plastic zone size in this experiment.

4. ("Do the authors have such data?") No, we do not have such data.

5. ("Also, I would be grateful to know the history and loading mode of the experiments mentioned ... Further experiment. ...") All the specimens having nonpropagating cracks were fatigue-stressed to $N = 10^7$ at a stress level of 279 MPa under rotating bending. These specimens were then fatigued again at a stress level of 295-300 MPa in reversed bending in order to extend the aforementioned crack for stress cycles of $5\text{-}10 \times 10^5$.

Next, replying to Professor Ritchie's comment ("In this regard, the phenomenon of crack closure may provide a more general mechanism of NPFC's"), the microscopic crack at the endurance limit is generally associated with the Stage I crack growth. Thus it is difficult to apply the closure concept to the Mode II crack growth in order to explain the mechanism of NPFC's. Therefore, we consider that the closure phenomenon is not necessarily the general mechanism for NPFC's.

Next, we would like to respond to Professor Beever's comment on threshold (" ... which is about 7.8, would appear to be coming from the basic properties of the ferrite.") The threshold value $K_{thm} = 7.7$ MPa$\sqrt{m}$ gives the critical condition of the crack in the matrix ferrite to begin its growth into the martensite. So, the K_{thm} is the crack growth resistance of the martensite.

Finally, we would like to add one point about the properties of long and short cracks. The threshold value in the case of long cracks seems to give the average value of crack growth resistance at the entire crack front. On the other hand, the threshold value for the short crack in the present experiment means the crack growth resistance of the specific microstructure. This would be important to give an interpretation to the particular results due to long or short cracks.

We would like to thank all the discussers for their valuable comments and discussions.

P. Neumann,[1] *H. Fuhlrott,*[1] *and H. Vehoff*[1]

Experiments Concerning Brittle, Ductile, and Environmentally Controlled Fatigue Crack Growth

REFERENCE: Neumann, P., Fuhlrott, H., and Vehoff, H., **"Experiments Concerning Brittle, Ductile, and Environmentally Controlled Fatigue Crack Growth,"** *Fatigue Mechanisms,* Proceedings of an ASTM-NBS-NSF symposium, Kansas City, Mo., May 1978, J. T. Fong, Ed., *ASTM STP 675,* American Society for Testing and Materials, 1979, pp. 371-395.

ABSTRACT: Various experiments were carried out in copper and Fe-3Si under as simple as possible conditions in order to get unequivocal information about the mechanisms which are relevant for crack initiation and propagation. New results are reported about the conditions for Stage I crack growth. It is pointed out how extrusion-intrusion pairs can form as a consequence on Stage I cracks. Furthermore, the strain distribution around Stage II cracks is described in detail. Environmental effects on Stage I and Stage II crack propagation are reported and evidence is presented for rewelding during the compressive phases. Finally, a new experimental approach to study brittle crack initiation at plastified cracks is described.

KEY WORDS: brittle fracture, crack initiation, crack propagation, extrusion, fatigue, hold time, intrusion, mechanism, plastic zone, rewelding, single crystal, Stage I, Stage II

Fracture mechanical treatment of metal fatigue requires good knowledge of the mechanisms of crack initiation and propagation. The study of mechanisms is greatly facilitated if the processes of interest are studied in their simplest form under the most simple boundary conditions. Therefore single crystals of copper and Fe-3Si were chosen as representatives for face-centered-cubic (fcc) and body-centered-cubic (bcc) metals, respectively. With these materials a number of experiments were carried out in order to clarify some aspects of the mechanisms of crack initiation and propagation during fatigue.

[1]Department head and associate scientists, respectively Max-Planck-Institut für Eisenforschung GmbH, 4 Dusseldorf Max-Planck-Strasse 1, Germany. Coauthor Fuhlrott is now with TüV Essen, Essen, Germany.

Experimental Procedures

Instantaneous Plastic Strain Control

The mechanical testing was performed with a closed-loop testing system with a positional accuracy of 0.2 μm under plastic strain control. In this control mode the plastic elongation of the specimen can be prescribed at every instant of time by an external electrical signal. Therefore experiments with constant average plastic strain rate throughout the cycle can be performed. Within the elastic range the loading then occurs with the maximum speed of the hydraulic system (190 mm/s). Special care was taken to avoid repetitive elastic unloading during yielding.

Crack Length Measurements

For the plastic strain control, the elastic compliance, C, of the machine plus specimen had to be measured during every cycle. C was measured using a method similar to that described by Clarke et al [*1*].[2] The shearing of the hysteresis was, however, done on line by an analog computer such that the compliance signal can be used for on-line control of the hydraulic system [*2*]. C depends on the crack length, a, and thus can be used to determine the crack length as a function of cycle number, N, with a resolution of 5 μm. $C(a)$ was determined from rest lines on the fracture surfaces, which were produced by program loading. It was found that $C(a)$ depends on the crack advance rate. Therefore the compliance signal was used as a more convenient method only in tests for which a calibration of $C(a)$ was available under almost identical conditions.

Vacuum Chamber

For tests under vacuum (1 MPa $=$ 8 $\times$ 10^{-6} torr) a small vacuum chamber just enclosing the specimen was constructed [*3*]. With this chamber, only an area of 170 mm^2 is moved against the atmospheric pressure. This adds only 17 N to that load which is applied to the specimen. This load increment cannot be measured by the load cell outside the specimen chamber. For all vacuum experiments, 17 N is therefore subtracted from the load cell signal, since variations of this value due to atmospheric pressure changes are negligible.

Specimen

The experiments were carried out with single crystals of copper (99.98

[2]The italic numbers in brackets refer to the list of references appended to this paper.

percent) and Fe-3Si (carbon = 50 ppm, nitrogen = 6 ppm, oxygen = 10 ppm), both grown by the Bridgman technique. The final shape of the specimen with a diagonal notch is shown in Fig. 1 [*4*]. The specimens were notched in a spark erosion machine using a wire of 0.2-mm diameter. In order to guarantee crack initiation along a well-defined straight line, a razor blade was pressed manually into the root of the notch, producing a sharp cut of about 0.1-mm depth. In order to guarantee a homogeneous hardening (in copper single crystals the yield stress increases by a factor of 20) the specimens were cyclically hardened before notching.

Test Procedures

All tests were performed in stress control with $R = -1$ or in plastic strain control which resulted in an R-value between -1 and -0.95. Details are given in Ref *5*.

Results and Discussion

Stage I Crack Growth

Stage I crack growth is usually defined by a geometrical feature—the crack surface is parallel to the most highly stressed slip plane, which is inclined about 45 deg against the tensile stress axis [*6*]. However, Stage I crack propagation is usually observed near the specimen surfaces immediately following crack nucleation. Conflicting evidence is reported in the literature concerning the effect of environment on crack nucleation [*7*]. Therefore an attempt was made to separate experimentally Stage I from crack nucleation in the studies of the effect of environment on Stage I

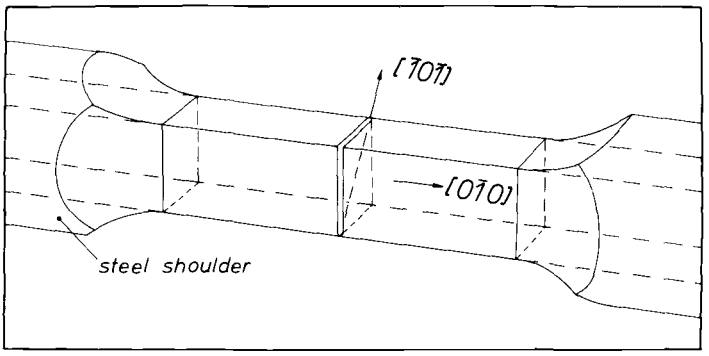

FIG. 1—*Specimen geometry. The orientation indicated is that of the copper crystals used. In the Fe-3Si crystals the crystal axis is [101] and the root of the notch is parallel to [111] if not otherwise noted. Cross section: 6 by 6 mm*^{2}.

crack propagation. With the specimen geometry described in the foregoing, plane Stage II cracks with straight crack fronts can be produced [*4*] such that Stage II crack propagation can be easily distinguished from Stage I crack growth. It was found that in air a Stage I crack can be induced at the tip of a growing Stage II crack by sufficiently reducing the load amplitude. By repetitively changing the load amplitude, Stage I and Stage II crack propagation can be alternatingly produced. Figure 2 shows a corresponding scanning electron microscope (SEM) fractograph. In the SEM the Stage I areas form a smaller angle with the incident electron beam and thus can easily be recognized by their bright appearance. Stage I crack growth in air was always found at growth rates lower than 10 nm/cycle and Stage II crack growth was always found at rates higher than 30 nm/cycle. Between 10 and 30 nm/cycle both fracture modes can be found.

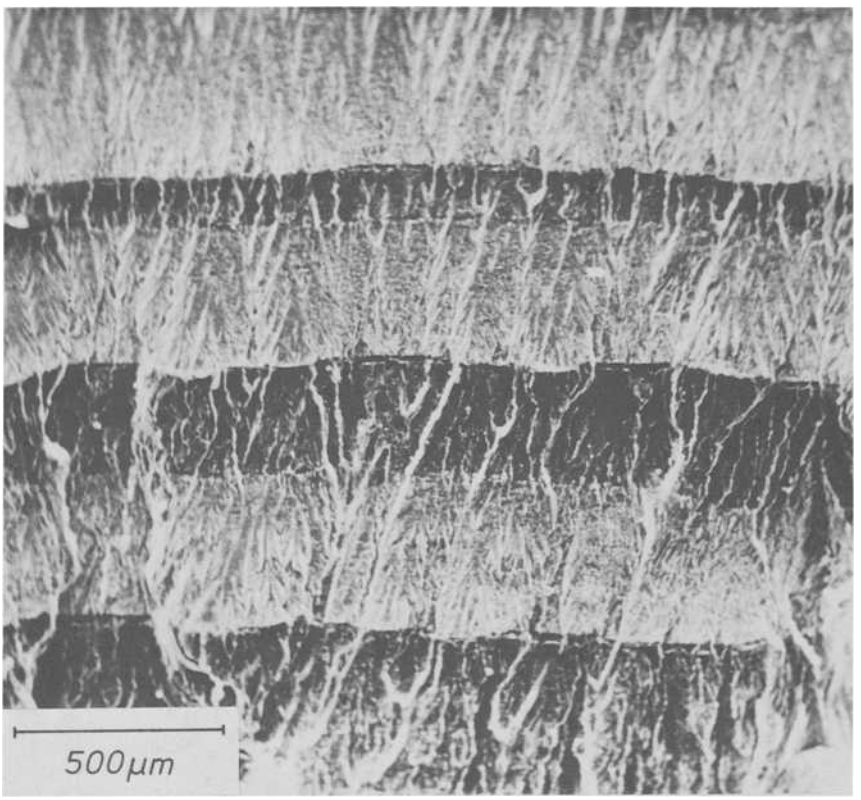

FIG. 2—*Fracture surface showing alternating Stage I (bright areas,* da/dN = *2 nm/cycle) and Stage II (dark areas,* da/dN = *20 nm/cycle) crack growth in copper. Mean load = 0; load amplitude was controlled as described in Ref* 5.

The same experiments were performed with copper in a vacuum of 1 MPa (8×10^{-6} torr) with negative results. No Stage I crack propagation was found, even when the crack advance per cycle was kept as low as 0.1 nm/cycle. This result indicates that a reacting environment is a necessary prerequisite for Stage I crack growth. This agrees well with the old ideas of explaining Stage I crack growth by adsorption or oxidation of the new surface which is produced at the slip steps [*8*].

Extrusions, Intrusions

In almost all materials extrusions have been observed and the accompanying intrusions are usually taken as the crack nuclei which grow and finally lead to failure. In the following, the general shape of extrusion-intrusion pairs is discussed in terms of slip processes. From this follows a mechanism of the formation of extrusion-intrusion pairs as the *consequence* of Stage I cracks, which may have formed *before,* according to Thompson's oxidation mechanism [*8*]. The line of the arguments is as follows. Since volume is conserved, it is difficult to envisage how isolated extrusions can form without forming a hole [*9*] or an intrusion nearby. Holes were not found [*10*]. There is, however, much evidence that the majority of the extrusions are formed as an integral part of extrusion-intrusion pairs of the form shown in Fig. 3*c* [*11,12*]. As pointed out earlier [*13*], this peculiar shape is obtained whenever coarse slipbands form, which are reversed, however, by more homogeneous slip. Figure 3 shows the details. There are two possible answers to the question: Which mechanisms can produce such a difference in the width of a slipband during formation and reversal?

1. The original slip occurs in a fatigue-hardened dislocation structure with only short-ranged internal stresses due to dislocation dipoles [*14*]. An avalanche of disintegrating dipoles produces a sharp slip line [*15*]. Slip stops since the large number of unpaired dislocations produces long-range stresses (local unidirectional work-hardening). The reversed slip takes place in this completely changed scenario in which avalanches are impossible and thus the reversed slip is more widely distributed.

2. The assumption is made that a Stage I microcrack without an extrusion-intrusion pair is present. It may have formed by the Thompson oxidation mechanism and is assumed to be a closed crack at a completely flat surface. On the specimen surface the development of the slip distribution in the vicinity of such a microcrack is considered in Fig. 4. In tension the crack is open and slip at the root of the crack tip will result in a displacement of the two crack faces (Fig. 4, T1). From the geometric point of view the displaced crack faces can be considered as a sharp tensile slip step. In other words, the open Stage I crack is parallel to the slip plane. In tension the crack can be considered as an area of a slip plane with zero yield stress, on which therefore all slip near the surface concentrates.

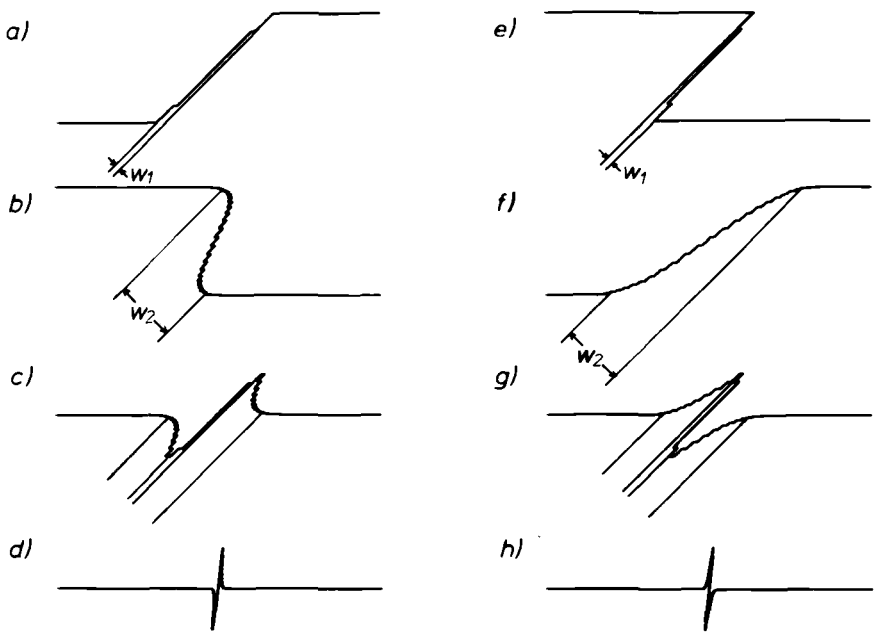

FIG. 3—*Computer plots of surface displacements (slip steps) for the analysis of extrusion and intrusion formation:* (a) *coarse slipband with half width* w_1; (b) *less coarse slip of opposite sign with half width* $w_2 = 10 \times w_1$; (c) *this picture was obtained by numerically adding the displacements shown in* (a) *and* (b); (d) *for easy comparison with taper sectioning micrographs* (c) *is recalculated at a tenth of its size but with the usual taper magnification of ten times along the* y-*direction;* (e) *to* (h) *the same as* (a) *to* (d), *but starting from a coarse compression slip step.*

Slip continues beyond the crack on slip planes which emanate from the crack tip. In compression, however, the crack is closed and the stress necessary to slide the crack faces past each other is not zero. This makes possible a spread of the slip onto slip planes parallel to the closed crack (Fig. 4, C1). In other words, since the crack closes during the compression phase of each cycle, there will be finite shear stresses applied to the material underneath the fracture surfaces only during compression. It follows that these shear stresses do not change sign during any cycle. Consequently the surface layers on the left-hand side of the crack (Fig. 4) will be pushed into the interior of the specimen, whereas the surface layers on the right-hand side of the crack will be pushed out of the specimen during every cycle (Fig. 4, T2 to C4). It is clear that in this case, only extrusion-intrusion pairs of one sign can be obtained (that of Fig. 4 or that on the left-hand side of Fig. 3). Some critical experiments are being carried out to test the ideas outlined in the foregoing.

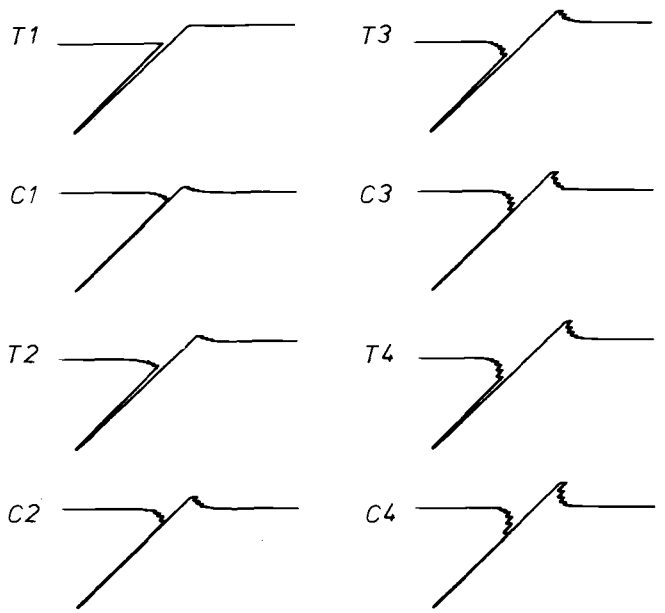

FIG. 4—*Development of an extrusion-intrusion pair at a Stage I crack due to crack closure. The profile of the specimen surface is shown after the tension* (T) *and compression* (C) *phases of four load cycles* (1, 2, 3, 4). *For details see text.*

Stage II Crack Propagation

There remains little doubt about the mechanism of Stage II crack growth. In straining experiments within a SEM, it can be observed directly how the alternating activation of two intersecting slip planes results in crack growth [*5*]. Figure 5 shows a characteristic sequence of the slip processes at the crack tip in an Fe-3Si crystal. These studies deal with the strains in the immediate neighborhood of the crack tip. More remote from the crack tip, the slipbands which emanate from the crack tip (A and A′ in Fig. 7) still dominate, because within these bands there is a geometrically necessary shear strain of about 100 percent [*16*]. Calculations of the stress field in the vicinity of a crack in an anisotropic crystal show [*17*] that the critical shear stress is exceeded also outside these bands. Experimentally, such additional slip can be observed with appropriate illumination under an optical microscope (Fig. 6). These secondary slip lines extend from within the main slipbands A and A′ (Fig. 7) to inner limitations which are remarkably well defined (Fig. 7, B and B′). It is clear from compatibility that at the boundaries B and B′ there must be a wall of dislocations, which is necessary to separate the strained from the unstrained material. Crystallographic analysis shows indeed that B and B′ coincide with the traces of tilt boundaries of those slip systems which

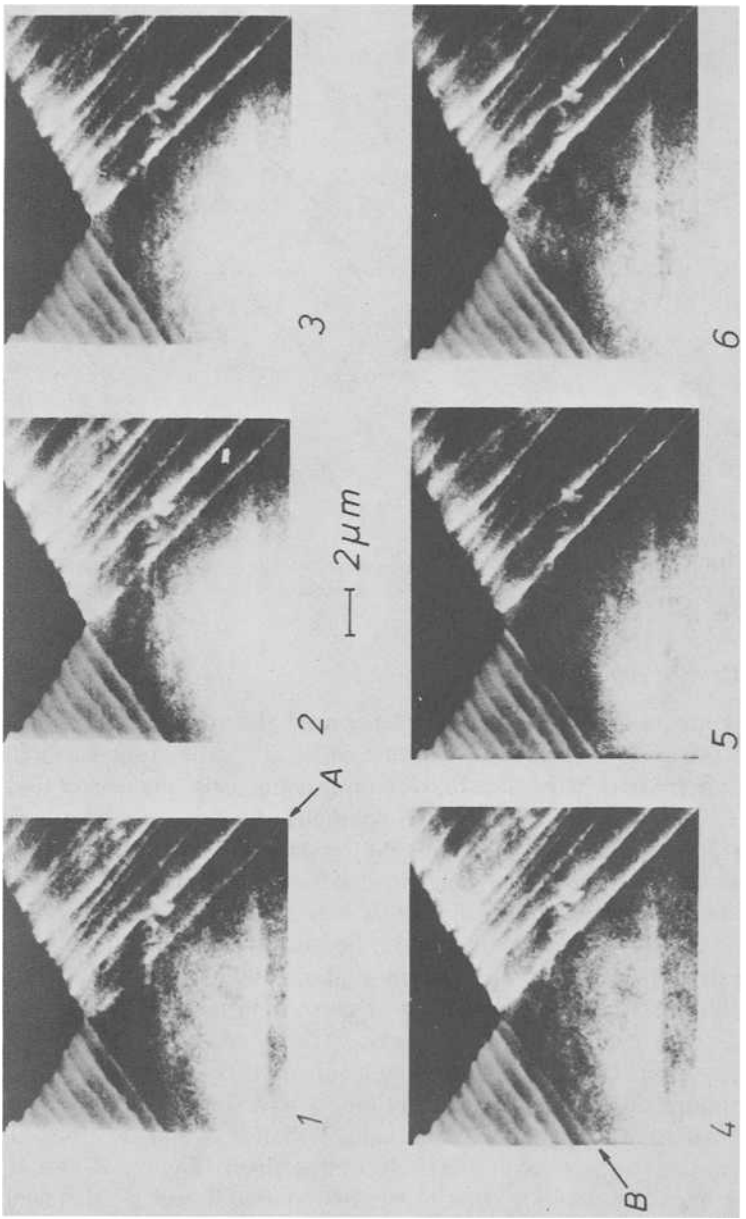

FIG. 5—*Crack growth due to alternating activation of two slip planes in Fe-3Si; from Ref* 5. *In* 1 *to* 3 *the slip line* A *is active and the right-hand side of the* V*-shaped crack tip moves to the lower right. In* 4 *to* 6 *the slip line* B *is active and the left-hand side moves to the lower left.*

are active in A′ and A, respectively. The complete geometry is described as follows. The undeformed specimen side face, S, on which the slip lines are observed is the (001) plane and the crack front, F, is the [101] direction (not perpendicular to S). The slip planes at A are $(\bar{1}11)$ planes ($(\bar{1}11)$ at A′). In A the two Burgers vectors $[\bar{1}10]$ and [011] are equally abundant and form a resultant Burgers vector $[\bar{1}21]$ which is perpendicular to F and is not contained in S. B′ is the trace of the tilt boundary belonging to the Burgers vector $[\bar{1}21]$. This tilt boundary is the bisecting plane between the $(\bar{1}21)$ planes in the deformed and in the undeformed material. Correspondingly in A′, the Burgers vectors $[\bar{1}\bar{1}0]$ and $[0\bar{1}1]$ form an effective Burgers vector $[\bar{1}\bar{2}1]$. The corresponding tilt boundary is found at B.

Due to the lattice rotation introduced by B, the slip lines between A and B are not exactly parallel to those in A′ although both are due to slip on the same slip system. The angle between these two sets of slip lines was measured in order to calculate the amount of slip between A and B. The same was done with various other angles [3]. Evaluation of these geometrical measurements as well as the direct orientation measurement by electron channelling patterns in the SEM yield a value of 23 percent shear strain in the area between A and B (and in the area between A′ and B′). With this value the pattern of slip lines can be explained with an accuracy of 2 deg.

A few things are worth mentioning in this context. The additional slip is not reversed during the compression phase of each cycle since the tilt boundaries are low-energy configurations which are not easily dissolved. The tilt boundaries do, however, move along continuously with the growing crack. The outer limitations of the additional slip are by far less well defined (in Fig. 6 somewhere in the main slipbands). This can be understood as well since there is no low-energy tilt boundary possible in the required orientation.

Rewelding

It was shown in an previous paper [16] that the crack growth per cycle for ideal ductile crack growth is given by

$$\Delta a = \delta \operatorname{ctg}(\alpha/2)/(1 + 1/c)$$

where

δ = crack tip opening displacement,
α = angle between the two slipbands emanating from the crack tip, and
c = material parameter (≥ 2) characterizing the coarseness of slip.

For the discussion of crack growth mechanisms it is therefore useful to

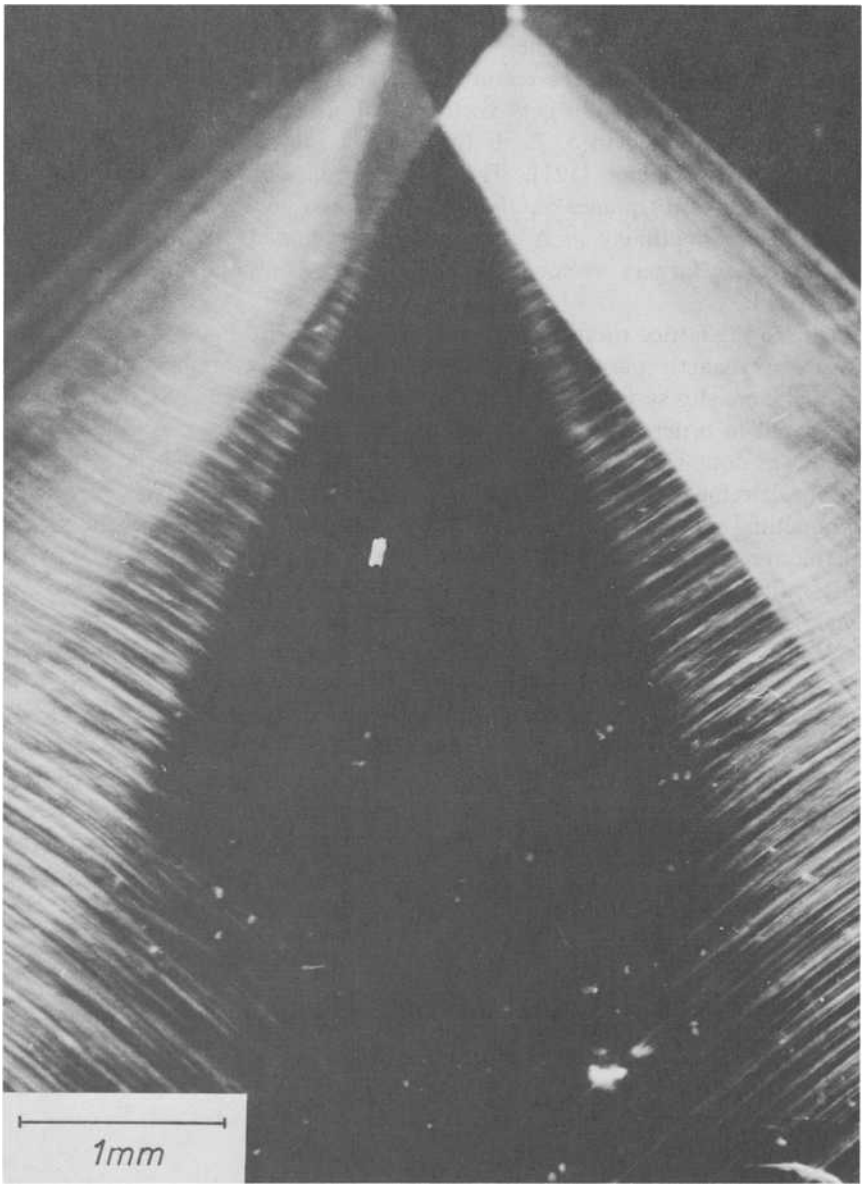

FIG. 6—*Plastic zone of ductile crack in copper. The illumination is selected to enhance the visibility of slip lines outside the main slipbands* A *and* A′ *(see Fig. 7).*

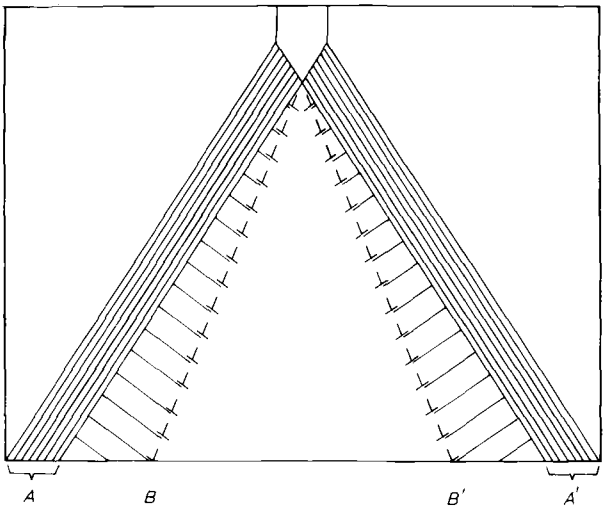

FIG. 7—*Schematic representation of the plastic zone shown in Fig. 6.* A *and* A' *are the main slipbands,* B *and* B' *are tilt boundaries.*

consider the normalized crack advance given by $a_n = \Delta a/\delta$. For ductile crack propagation with various values of c and α (the tilt boundaries can reduce α to 83 deg in copper!) we have $0.47 \leq a_n \leq 1.1$. Smaller values of a_n indicate special retarding factors (that is, rewelding), whereas larger values of a_n indicate partial cleavage or corrosion effects.

Studies of Stage II crack growth in copper single crystals show a surprisingly large effect of the environment [5]. Crack propagation is reduced in vacuum (1 MPa) by a factor of 10 at crack growth rates below 0.5 μm/cycle. At larger crack growth rates up to 25 μm/cycle, where normalized crack growth rates are measurable, the effect persists. Furthermore, it was shown [5] that the applied load at the beginning of a tension phase is larger than the applied load at the foregoing tension phase. This is a strong indication that rewelding at the crack tip has happened during the compression phase.

In this study it was tested whether hold times in tension and compression can influence the growth rate in air and vacuum. In order to separate the frequency effect from the effect of hold times, most experiments were carried out with hold times of fixed length (5 s) only. The results are shown in Fig. 8. There is a large scatter in the data and the lines shown are least-square fits. The error bars indicate the uncertainty in the position of these fitted lines. The results show that the normalized growth rate was not influenced by the hold times in air, whereas in vacuum the normalized crack growth rates are significantly lower with hold times in compression than with hold times in tension. It is felt that this result is an indication

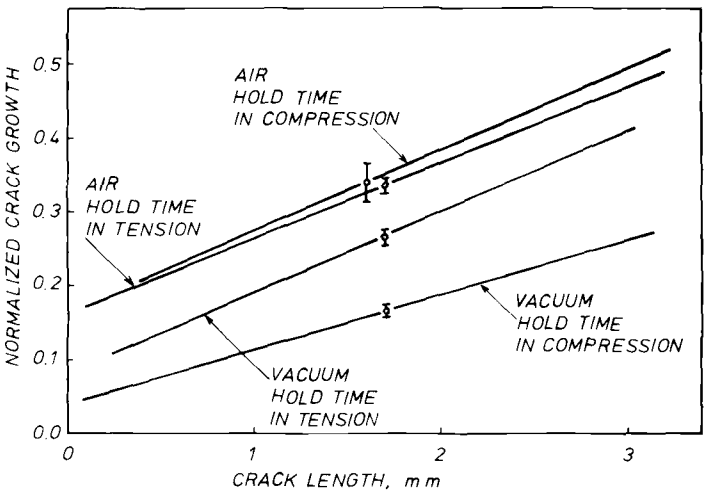

FIG. 8—*Normalized crack growth data* ($a_n = \Delta a/\delta$) *for tests with hold times in vacuum* (*1 MPa* = *8* × *10*$^{-6}$ *torr*) *and air. The straight lines are least-square fits and the error bars indicate the uncertainty in the position of these fitted lines. Constant plastic strain rate, plastic strain amplitude 25 μm, hold time 5 s, cycle time 7 s.*

of rewelding during the compression phases, although corrosive effects during the tension phase can not be excluded as an alternative explanation. In order to distinguish between these two possibilities, more data are required from tests without hold times. In addition, these experiments will be repeated under ultra-high-vacuum conditions.

Brittle Crack Growth

If Stage II crack propagation experiments are carried out in Fe-3Si, the mechanism of crack growth depends strongly on the rate of crack tip opening, $\dot{\delta}$. In our experiments, $\dot{\delta}$ can be controlled by means of the instantaneous plastic strain control facility, because δ is equal to the plastic elongation of the specimen. Figure 9 shows some normalized crack growth data versus temperature for two values of $\dot{\delta}$. The two lines mark the range of possible a_n-values for Stage II crack propagation [*16*]. It is obvious that above 40°C the fracture mode is of the ductile mechanism shown in Fig. 5. At lower temperatures, higher but finite a_n values were found. As discussed in the foregoing, the higher a_n values indicate a change in the fracture mechanism. Figure 10 shows the fracture surface after an experiment where the opening rate $\dot{\delta}$ was repetitively switched between 8 and 80 μm/s. The appearance of the fracture surface changes drastically whenever $\dot{\delta}$ is changed between these values. Stereo-evaluation shows that at $\dot{\delta}$ = 80 μm/s the fracture surface consists of (100)-facets which are not parallel to

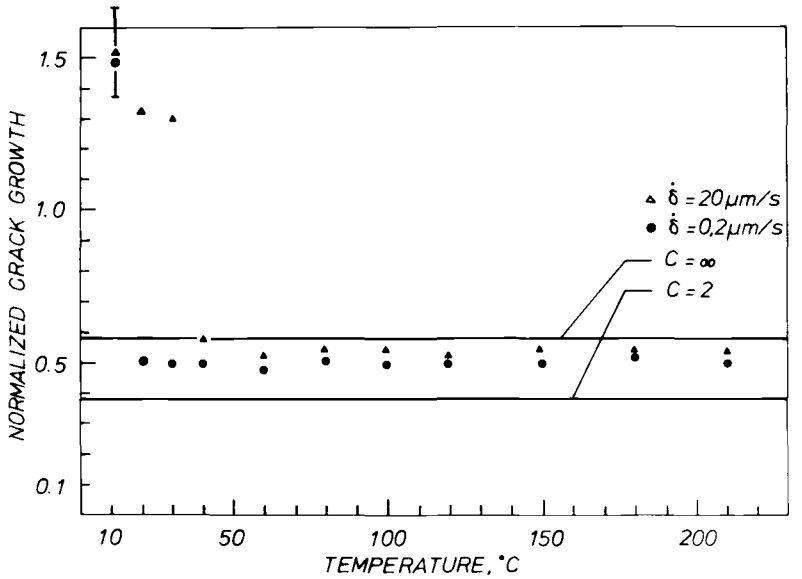

FIG. 9—*Normalized crack growth data as a function of temperature for two rates of crack tip opening, $\dot{\delta}$. The two lines mark the range of* a_n*-values for ductile crack growth in Fe-3Si with* $\alpha = 120$ *deg. Instantaneous plastic strain control, strain amplitude 50* μm. *The error bar indicates the scatter in the* a_n*-values in the (110) orientation in quasi-brittle crack growth.*

the cross section. In order to get a more simple geometry for this type of fracture, experiments were carried out with (100) single crystals. With this orientation a_n-values up to six were found. These values are approximately six times larger than the highest possible a_n-values for ductile Stage II propagation with this orientation. Because of these large but finite a_n values and the fact that the fracture surface is parallel to the cleavage planes (100), we will call this a quasi-brittle fracture. Such quasi-brittle crack growth with a_n-values below six has a remarkable property; there is no discontinuity on the load-elongation hysteresis, that is, there are no signs of unstable crack growth. Because of the finite a_n-values, the crack growth must be accompanied by plasticity. This agrees with the fact that program loading yields regular brittle striation patterns (Fig. 11) and that no electron channelling patterns (this means ϵ_{pl} must be larger than 10 percent [*18*]) can be observed on these brittle fracture facets.

Larger a_n-values than six are difficult to obtain because of pop-ins or unstable brittle failure. The fracture facets produced in such an unstable manner can easily be distinguished from the others, since electron channelling patterns can be observed on them. This indicates that the accompanying plasticity is less than 10 percent.

Since the initiation of brittle fracture depends on strain rate and tem-

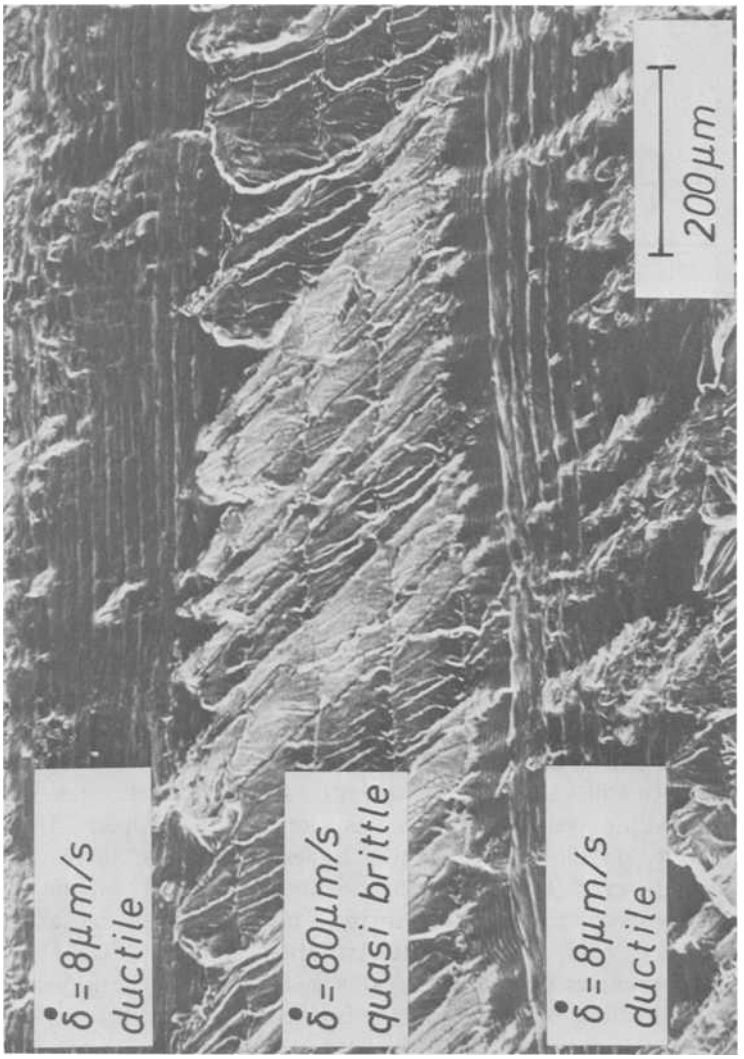

FIG. 10—*Fracture surface of an Fe-3Si single crystal showing ductile and quasi-brittle crack propagation due to different crack-tip opening rates (8 μm/s, 80 μm/s). Note the different* da/dN *values in spite of a constant crack-tip opening value of* $\delta = 50$ *μm. Crack propagation from top to bottom.*

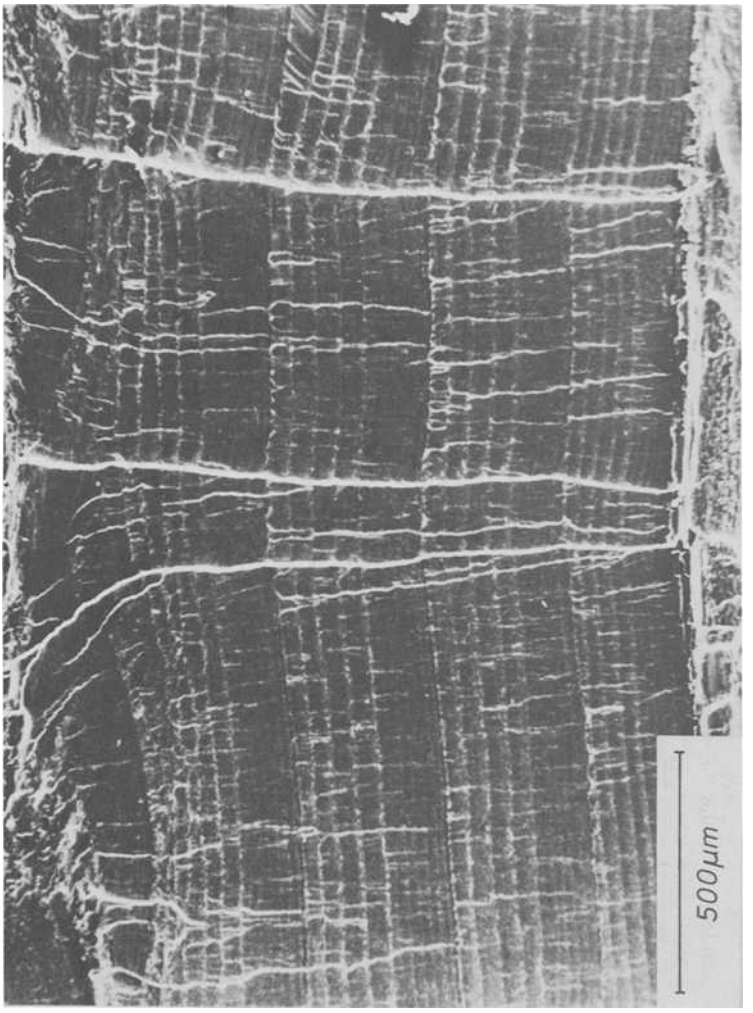

FIG. 11—*Fracture surface obtained by quasi-brittle crack propagation. Orientation: cross section parallel to (100), root of the notch parallel to [011]. Due to the stability of this crack propagation mode, program loading produces regular brittle striations. Plastic strain amplitude 10 and 15 μm, temperature 40°C, mean stress zero.*

perature, it must be intimately connected with some thermally activated process [*19*]. The activation energy of this process can be obtained in the usual way by logarithmically plotting $\dot{\delta}_c$, at which brittle crack growth starts, against $1/T$ (Fig. 12). From the slope of the resulting straight line, the activation energy $U = d \ln \dot{\delta}_c / d\,(1/kT)$ was determined to be approximately 0.5 eV. This value agrees with the activation energy for dislocation motion in Fe-3Si [*20*]. This leads to the following model for the initiation of brittle fracture in materials, in which ductile crack propagation is also possible: Whenever dislocation motion becomes so slow that the stresses near the crack tip cannot be kept close to the macroscopic yield point, but rise according to the elastic stress concentration until the decohesion stress is reached, brittle fracture is initiated. It is proposed, therefore, that criteria for brittle fracture at plastified cracks should take dislocation dynamics into account. To explain the effect of stable quasi-brittle crack growth with accompanying plasticity, further studies are required.

Conclusions

1. Stage I crack growth can be obtained in copper crystals at arbitrary crack lengths, if the growth rates are below 10 nm/cycle.
2. In crack propagation tests conducted in a vacuum of 1 MPa with

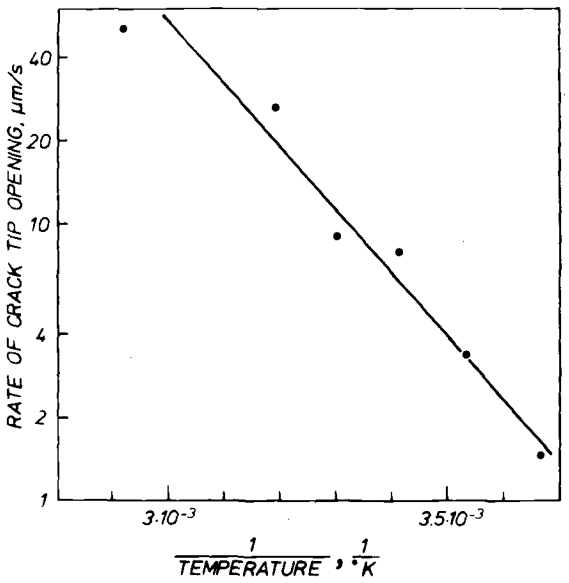

FIG. 12—*Rate of crack-tip opening, $\dot{\delta}$, which is necessary for brittle crack initiation, versus reciprocal temperature. The slope of the line gives an activation energy of 0.5 eV. For orientation see Fig. 11.*

growth rates down to 0.1 nm/cycle, Stage I (shear) crack growth could not be induced at the tip of existing Stage II cracks.

3. Extrusion-intrusion pairs are formed if coarse slip is reversed in a less coarse manner.

4. Slip around existing Stage I microcracks fulfills the requirements of Conclusion 3, and therefore extrusion-intrusion pairs may form as a consequence of stage I cracks.

5. Stage II cracks grow by the alternating activation of two slip planes. This was observed *in situ* in an SEM.

6. Stage II cracks in fcc crystals of proper orientation are accompanied by two characteristic tilt boundaries which introduce lattice rotations of up to 15 deg each.

7. Stage II crack growth depends on the environment and on hold times in compression. Rewelding is proposed as a possible explanation.

8. In Fe-3Si, a stable quasi-brittle fracture mode can be obtained by proper choice of the rate of crack-tip opening, $\dot{\delta}$.

9. With the help of quasi-brittle crack propagation in Fe-3Si, the activation energy for brittle crack initiation from plastified cracks was found to be equal to the activation energy of dislocation motion (0.5 eV).

Acknowledgment

This work was performed with financial support from the Deutsche Forschungsgemeinschaft.

References

[1] Clarke, G. A., Andrews, W. R., Paris, P. C., and Schmidt, D. W. in *Mechanics of Crack Growth, ASTM STP 590,* American Society for Testing and Materials, 1976, p. 27.
[2] Neumann, P. and Vehoff, H., to be published.
[3] Fuhlrott, H., Thesis, Technical University, Aachen, Germany, 1978.
[4] Neumann, P., *Acta Metallurgica,* Vol. 22, 1974, p. 1155.
[5] Neumann, P., Vehoff, H., and Fuhlrott, H., *Fracture 1977, Proceedings,* First International Conference on Fracture, University of Waterloo Press, Waterloo, Ont., Canada, Vol. 2, 1977, pp. 1313-1324.
[6] Laird, C. in *Fatigue Crack Propagation, ASTM STP 415,* American Society for Testing and Materials, 1967, p. 131.
[7] Laird, C. and Duquette, D. J., *Corrosion Fatigue,* National Association of Corrosion Engineers, Houston, Tex., 1972, p. 88.
[8] Thompson, N., Wadsworth, N. J., and Loaut, N., *Philosophical Magazine,* Vol. 1, 1956, p. 113.
[9] Mott, N. F., *Acta Metallurgica,* Vol. 6, 1955, p. 195.
[10] Forsyth, P. J. E., *Proceedings of the Royal Society,* Vol. A242, 1957, p. 198.
[11] Meleka, A. H., Barr, W., and Baker, A. A., British Iron and Steel Research Association Report P/16/60, 1960.
[12] Laufer, E. E. and Roberts, W. N., *Philosophical Magazine,* Vol. 14, 1966, p. 65.
[13] Neumann, P., *Acta Metallurgica* Vol. 17, 1969, p. 1219.

[14] Grosskreutz, J. C. and Mughrabi, H. in *Constitutive Equations in Plasticity*, A. S. Argon, Ed., M. I. T. Press, Cambridge, Mass., 1975, Chapter 7, pp. 251-326.
[15] Neumann, P., *Zeitschrift fuer Metallkunde*, Vol. 59, 1968, p. 927.
[16] Neumann, P., *Acta Metallurgica*, Vol. 22, 1974, p. 1167.
[17] Riedel, H., private communication.
[18] Stickler, R. and Booker, G. R. in *Proceedings*, 5th International Symposium on Materials, Berkeley, Calif., 1971, p. 301.
[19] St. John, C., *Philosophical Magazine*. Vol. 32, 1975, p. 1193.
[20] Zarubova, N. and Sestak, B., *Physica Status Solidi*, Vol. A30, 1975, p. 365.

DISCUSSION

J. Beevers[1] *(discussion)*—Peter Neumann and his co-workers have presented information which makes a valuable contribution toward our understanding of the microprocesses involved in the fatigue of metals and alloys.

The Stage II crack growth process in single crystals of copper is elegantly shown to occur as a consequence of alternating slip activity as revealed by direct SEM observations. In vacuum the crack growth rate is reduced in comparison with tests in laboratory air (Fig. 8). This reduction in crack growth rate as a result of hold times in compression is attributed to rewelding of the crack faces. The fatigue crack growth rate was also reduced in vacuum when hold times in tension were employed. In this instance the crack faces would not be expected to touch to any significant extent and therefore rewelding would not be a substantial occurrence. The reduction of fatigue crack growth rates in vacuum compared with air has been reported previously.[2-4] Fractographic evidence shows changes in growth rate with environment and the suggestion has been made that an air environment is sufficiently active to enhance crack extension; that is, the growth process in air has an environmentally aided component. Whether the environmental influence is a surface phenomenon or associated with the plastic flow process or a combination of both is not clear. Variations in levels of mean stress and extent of hold times in these types of experiments may facilitate further information.

In consideration of the formation of extrusion-intrusion pairs, the authors point out two possible mechanisms. The formation of coarse slip bands and a reverse slip process which is less coarse. Secondly, extrusions-intrusions may be associated with Stage I cracks. This second mechanism is associated with the differential deformation which takes place when the

[1] Department of Physical Metallurgy, University of Birmingham, Birmingham, U. K.
[2] Robinson, J. L. and Beevers, C. J., *Metal Science Journal*, Vol. 7, 1973, p. 153.
[3] Irving, P. E. and Beevers, C. J., *Metallurgical Transactions*, Vol. 5, 1974, p. 931.
[4] Irving, P. E. and Beevers, C. J., *Materials Science and Engineering*, Vol. 14, 1974, p. 229.

crack faces are open and fully closed. In situations where the crack faces remain open or closed, for example, high mean tensile or compressive stresses, this mechanism might not be as efficient as initially envisaged.

The quasi-brittle fracture reported in Fe-3Si single crystals has been observed in other polycrystalline iron-base alloys[5] when a critical K_{max} level was achieved. It is interesting that both the crack-tip opening displacement rate $\dot{\delta}$ and the stress intensity at the crack tip can be predictive in relation to the occurrence of brittle fracture in fatigue. The introduction of these static modes of fracture can be initiated by the presence of martensite in pearlitic steels and thus can lead to a severe curtailment of the expected fatigue life (see Beevers, footnote 5, and Fig. 13 herewith).

The definition of Stage I fatigue cracks, their origin, and their transition to Stage II are general points for further study and discussion. The authors of the present paper make the point that Stage I cracks did not form and propagate in the notched copper single crystals when tested in vacuum. Does a smooth-sided copper single crystal loaded in fatigue in vacuum ($<10^{-6}$ torr) fail by the formation and growth of Stage II cracks?

J. Beevers (separate question)—If you are in an entirely inert environment, would you not therefore have any Stage I cracks, and would any cracks formed be Stage II cracks?

P. Neumann—In an inert environment with material which does not cyclically soften as extremely as, for instance, the aluminum alloys, I would not expect a Stage I crack to develop. The results which you are quoting were obtained in copper single crystals under conditions that made it possible to switch at will from Stage I to Stage II crack growth in air. We then deliberately tried to make Stage I crack growth in vacuum and did not succeed.

J. Beevers—Therefore, does the crack always form or is it always formed as a Stage II crack?

P. Neumann—The experiments were done in the following way. First we tried to find whether Stage I propagation could also be produced at long cracks and not only during the initiation period in order to make sure that Stage I is a real mode of propagation and not just a characteristic of crack initiation.

The result was that in air any Stage II crack turns around into the typical 45 deg orientation when the loading amplitude is sufficiently lowered. This turning around did not happen in vacuum. The crack was growing perpendicular to the tensile axis even at the smallest rates.

[5] Beevers, C. J. et al, *Metal Science Journal*, Vol. 9, 1975, p. 119.

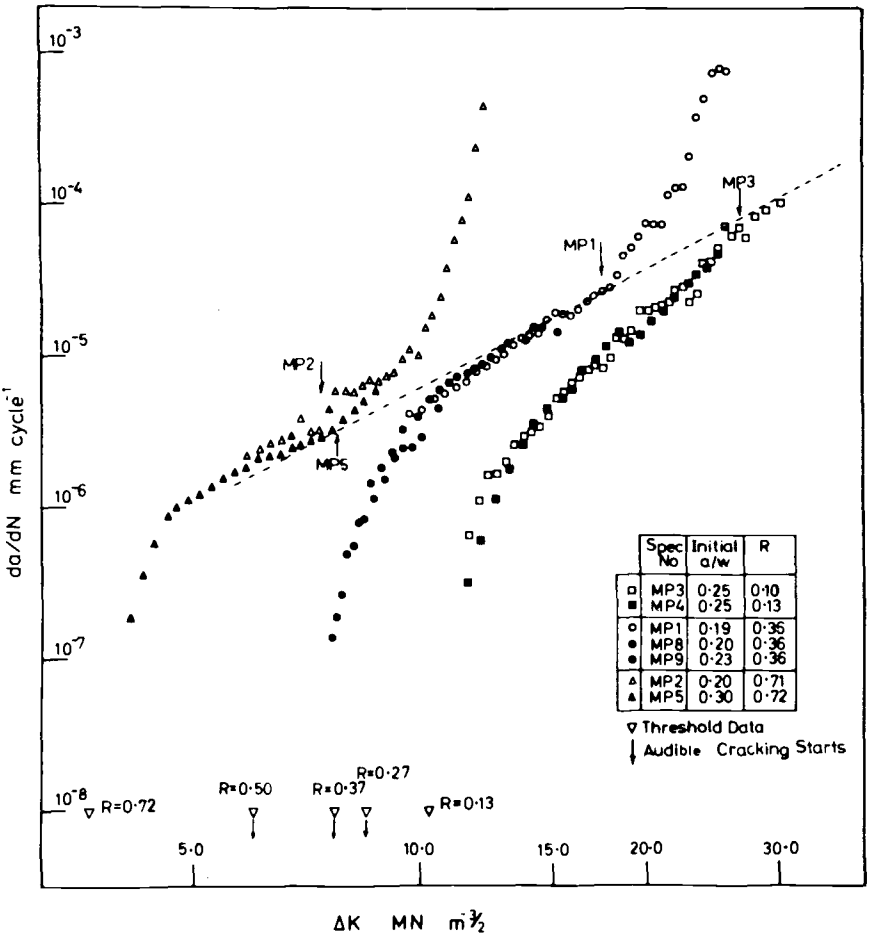

FIG. 13—*Fatigue crack growth curves of a carbon-manganese pearlitic steel containing banded martensite and tested in laboratory air (from footnote 5 of this discussion).*

J. Beevers—Does this mean then we should have a re-think about what we mean by Stage I and Stage II cracks?

P. Neumann—The definition which is commonly used is: 45 deg to the tensile axis. This is a distinct feature which can be easily used to distinguish between those two modes in single crystals.

J. Driver[6] *(discussion)*—I have two brief questions. The first is, what

[6]Ecole Nationale Superieure des Mines de Saint-Etienne, Department Metallurgie, Saint-Etienne, France.

does Dr. Neumann consider to be a proper orientation for the alternative slip mechanism to operate in bcc single crystals? I ask this question because we have done quite a few tests on single crystals of iron-based alloys and we observe that the preferential plane for crack propagation is the (110) plane in the [110] direction or the (110) plane in the [100] direction. I noticed that in his figure the example he uses is a crack plane that is the (110) which is induced to crack propagate in the [112] direction.

P. Neumann—In the bcc metals, we have comparatively large freedom for choosing the orientation, and you should not deduce from the examples given in the figures that this was the only possibility. We have the feeling that there is a large variety of orientations in bcc metals which do it simply because in bcc metals there are lots of slip planes, and the only requirement is that the intersecting line of two slip planes is lying in the crack front. We performed detailed experiments with two orientations. One is the (110) orientation you are also using. Brittle crack propagation, however, happens on (100) planes. Therefore, for the studies of brittle crack initiation, we used the (100) orientation which you are referring to in your last sentence.

J. Driver—Put it this way, we have never observed crack propagation by ductile mechanism for the orientation you use, but it is possible that this is because of slight differences in experimental technique.

P. Neumann—The (100) orientation is not as simple to use in ductile experiments as the (110) orientation. The point is that one has to be careful with the speed.

J. Driver—The second point I would like to make is that we have conducted low-cycle fatigue experiments on silicon iron, and strain control, and we find the same type of quasi-brittle propagation which you have discussed, and in fact our results are very close to what you have observed. We have also looked at the orientation dependence of this type of crack propagation and we find that, for example, for an orientation which is in the center of the stereographic triangle, roughly (149), about 80 percent of the crack surface is made up—takes place by this type of quasi-brittle propagation—whereas, for example, a (111) orientation does not exhibit this type of behavior. I would just like to ask if you have observed this orientation dependence?

P. Neumann—In the (110) orientation, which is good, and which is optimal for ductile and not for brittle crack growth simply because the cross-sectional plane is not a cleavage plane, one gets very distinct changes in the appearance of the brittle and ductile fracture surfaces (see Fig. 10).

This is the figure which we show if we want to make it really visible to the naked eye that we can switch between ductile and brittle fracture *at will.* Under constant conditions, there is no mixture of modes, however.

Finally, yes, the value of the plastic strain rate, which is necessary for the quasi-brittle fracture, does depend on the orientation.

J. Driver—I should like to make some brief remarks on the experiments on Stage I and II crack propagation, and comment mainly on the particularly interesting problem of quasi-brittle crack propagation in iron-silicon.

The demonstration, by load change experiments, that Stage I cracks can grow in copper single crystals at an arbitrary crack length in air but not in vacuum is clear proof that Stage I is related to the chemical reactivity of the environment. However, it should be noted that a change in the macroscopic appearance of single-crystal fracture surfaces on changing the load does not always imply a Stage I→Stage II transition. In experiments conducted on austenitic stainless steel single crystals[7] we have shown that the fracture surface can change from plane to nonplane as the growth rate increases. This transition, which is independent of the environment-related Stage I→Stage II transition observed by the authors, is apparently related, in the case of austenitic stainless steel, to the influence of the plastic zone size and the associated stress state.

The second remark concerns the alternating slip model of Stage II crack propagation in bcc metals. Single-crystal fatigue tests on several orientations of iron-26 at high frequencies (see Rieux et al, footnote 7) and iron-silicon at low frequencies[8] have shown that the preferential paths for ductile fatigue crack propagation in these alloys are along {100} ⟨011⟩ and {011} ⟨100⟩. These two orientations demonstrate the role of the ⟨111⟩ slip directions in the crack propagation of bcc materials. For both orientations, a pair of ⟨111⟩ slip directions are equally inclined to the crack plane and normal to the crack front; that is, they allow the formation of symmetrical shears irrespective of the slip "plane." We have not obtained plane fracture surfaces for the {110} ⟨112⟩ orientation as reported by the authors. This discrepancy may, of course, be due to slight differences in experimental technique.

Finally, I should like to report very good agreement with the present authors on the observations of quasi-brittle crack propagation in iron-silicon. In low-cycle strain-controlled fatigue tests of iron-silicon single crystals, Magnin et al (footnote 8) have observed extensive crack propagation by what appears to be repeated "cleavage" on {100} planes. At a total strain rate $\dot{\epsilon}_T = 2 \times 10^{-3}\ s^{-1}$, corresponding to a rate of elongation

[7] Rieux, P., Driver, J., and Rieu, J., to be published.

[8] Magnin, T., Driver, J., and Rieu, J., Paper presented at the Journées d'Automne de la Societe Francaise de Métallurgie, Sept. 1977; also, *Memoires Scientifiques de la Revue de Métallurgie,* May 1978.

$= 20\ \mu m\ s^{-1}$, and for applied strains of 0.2 percent, the sequence of events at room temperature is usually (1) crack initiation in slipbands, (2) propagation by repeated "cleavage" with spacings of 20 to 100 μm, and (3) final rupture by classical cleavage. These observations, on the ⟨149⟩, ⟨119⟩, and ⟨100⟩ axial orientations, are in good agreement with those of the authors. In addition, when the applied strain is increased above ~0.5 percent at the same strain rate, quasi-brittle propagation is largely eliminated and normal cleavage failure predominates. However, orientations close to ⟨111⟩ and ⟨110⟩ do not exhibit quasi-brittle failure when cycled at ±0.2 percent total strain. The necessary crystallographic conditions seem to be (1) promotion of "cleavage" by a relatively high normal tensile stress component on the (100) plane, and (2) simultaneous crack blunting by plastic deformation associated with shear band formation at the crack tip. The ⟨110⟩ orientation is less prone to this type of failure, presumably because it is a favorable orientation for propagation by ductile shear. The ⟨111⟩ orientation, on the other hand, is associated with relatively low normal stresses and limited shear band formation due to the threefold symmetry. Whatever the detailed mechanism, it is clear that this process, which depends upon strain rate, temperature, and orientation, will also be sensitive to interstitial content.

A. McEvily[9] *(discussion)*—This has to do with the matter of the intrusion-extrusion coupling. I think that idea got started with Forsyth, and in fact in Lou Coffin's opening remarks he had a slide shown of Forsyth's work with silver chloride in which one could see the extrusions and what were apparently intrusions. Peter Neumann in his presentation coupled these and indicated that it was a general phenomenon, but I would just like to point out that in my own experience, and perhaps that of others as well, in material such as silicon iron, there is a predominance of extrusions and a complete absence of intrusions, and that the crack forms when the extrusions of separate slip ends merge and create, I think, a stress raise at such a location. Silicon iron is not the only material that just shows a predominance of extrusions; copper does as well. What one sees in the taper sections is that an extrusion forms and within the extrusion there are apparent intrusions because of the serrated nature of the slipband. That's our observation, and if Peter has any comments on it, fine.

P. Neumann—I agree. Looking at the morphology of extrusions, one has to be careful. The ones which I was displaying on the slides were those configurations which I think show the usual appearance of intrusion-extrusion pairs *if they are separated from other pairs as far as possible.*

[9]Metallurgy Department, Institute of Materials Science, University of Connecticut, Storrs, Conn. 06268.

If there is a cluster of extrusion-intrusion pairs, they can of course overlap and make more complicated structures. But if you look for isolated extrusion-intrusion pairs, in my experience I think this is the most common configuration.

C. Laird[10] (*discussion*)—You reported that the angle of the crack tip can be related to the degree to which plastic or brittle fracture processes occur at the crack tip.

Could the observed angular variations be reinterpreted in terms of variations in the geometrical aspects of slip alone?

That is, can the bounds that you observed in that crack tip be explained by slip on various slip planes, oriented at various possible angles to the plane of the crack, and where the coarseness of slip is also a factor, or do they require introducing the extra variable of fracture mechanism at the tip?

P. Neumann—The bounds which I gave depend on the orientation, or let me put it this way—they depend simply on the angle between the slip planes which are active at the crack tip. If you once decided to take a specific orientation with uniquely determined slip planes, then you have an upper and a lower bound, and these two bounds come about like that: the largest a_n is obtained whenever there are sharp coarse slip lines, as was indicated on the slide of the sequence. If one considers also broad bands, which can be done, and this is the subject of a publication of mine (Ref *16* of the paper) which is quite involved in geometrical terms, you get the lower bound. Beyond these bounds, I think, there is no way of explaining the angle simply from plastic slip processes.

W. Gerberich[11] (*discussion*)—I was very interested in your observation of activation energy for crack velocity being similar to that for dislocation velocity in the iron silicon. In a series of studies on iron-nickel and iron-silicon alloys, we found about a 0.4 to 0.75-eV activation energy for slip over asymmetric barriers which allowed the modeling of deformation very nicely. The problem was that, when we tried to apply it to the fatigue crack propagation data, it was successful in predicting fatigue propagation exponents for the iron-nickel alloys but we were not successful in the iron-silicon alloys. The question is, are there other kinetic features besides dislocation of velocity that are controlling the fatigue crack propagation and kinetics in these kinds of materials?

P. Neumann—We have seen, and I cannot recall which talk it was, one

[10]Department of Metallurgy, University of Pennsylvania, Philadelphia, Pa. 19104.

[11]Department of Chemical Engineering, University of Minnesota, Minneapolis, Minn. 55455.

slide where the author was giving an activation energy for crack propagation and it was very much smaller than 0.5 eV, indicating a much smaller temperature dependence. You have to be very careful which process you are characterizing with your activation energy. We tried to make it unequivocal as we were measuring the rate of crack tip opening, which is necessary to induce brittle failure. If you simply look at crack rates and correlate crack propagation, for example, at constant ΔK, with temperature, then you might measure a different activation energy.

P. Neumann, H. Fuhlrott, and H. Vehoff (authors' closure)—There are only a few unanswered questions which we would like to cover in sequence:

1. J. Beevers ("Does a smooth-sided copper single crystal loaded in fatigue in vacuum ($<10^{-6}$ torr) fail by the formation and growth of Stage II cracks?") These experiments are not done yet, but will be carried out as a part of a more extended experimental program on fatigue crack initiation.

2. J. Driver ("... the macroscopic appearance of single crystal fracture surfaces on changing the load does not always imply a Stage I→Stage II transition.") We agree that the macroscopic appearance does indeed depend on the growth rate. In our experiments, however, the macroscopic appearance was not used to distinguish between Stage I and Stage II, but, more precisely, the angle between crack growth direction and the tensile axis.

3. J. Driver ("We have not obtained plane fracture surfaces on the {110} ⟨112⟩ orientation as reported by the authors.") Plane fracture surfaces with the {110} ⟨112⟩ orientation are obtained only at temperatures below 60°C, crack growth rates of 50 μm/cycle or more, and triangular ligament (see Fig. 1). If these conditions were not met, this may explain why Dr. Driver did not get the same results as we did.

In conclusion, we would like to thank all discussers for their valuable comments and vivid discussions.

R. B. Scarlin[1]

Some Effects of Microstructure and Environment on Fatigue Crack Propagation

REFERENCE: Scarlin, R. B., **"Some Effects of Microstructure and Environment on Fatigue Crack Propagation,"** *Fatigue Mechanisms,* Proceedings of an ASTM-NBS-NSF symposium, Kansas City, Mo., May 1978, J. T. Fong, Ed., *ASTM STP 675,* American Society for Testing and Materials, 1979, pp. 396-419.

ABSTRACT: Fatigue crack growth rates have been determined in nickel-base alloys both after a normal heat treatment and after heating for a further 10 000 h. The latter treatment causes coarsening of the γ'-particles so that they are no longer sheared by dislocations when the material is deformed. Differences in cracking rates at both ambient and elevated temperatures may be understood in terms of slip reversibility and oxide penetration when deformation occurs by shearing of precipitates.

A further result of the prolonged aging period is a considerable reduction in the cyclic fracture toughness of a cast alloy. This can be traced to a transition to intergranular cracking along regions of coarsened precipitation adjacent to the grain boundaries.

A comparison of cracking rates in air and vacuum shows that the presence of air can lead to an increase in growth rate and to a situation where no clear threshold is apparent. Crystallographic cracking (analogous to Stage I fatigue) is observed in both air and vacuum. One effect of oxygen in tests at high temperatures is to cause dissolution of the γ'-particles in the region of the crack tip. Under high-temperature corrosive conditions (air/SO_2/SO_3 atmosphere) an increase in scatter and in average propagation rate can be correlated with the formation of liquid sulphide films at the crack tip.

KEY WORDS: crack propagation, fatigue, fractography, fracture toughness, high-temperature properties, nickel alloys

Several publications have appeared in which the effect, if any, of microstructure on fatigue crack growth rates has been discussed. In general, it is now considered that at intermediate stress-intensity amplitudes the growth rate is primarily independent of microstructure and mean stress [*1*].[2] Rates of crack propagation can best be correlated with the elastic

[1]Department ZLM, BBC Brown, Boveri & Co., Ltd., CH-5041 Baden, Switzerland.

[2]The italic numbers in brackets refer to the list of references appended to this paper.

modulus; that is, growth rates in different materials are normalized by plotting against $\Delta K/E$ where ΔK is the stress-intensity amplitude and E the elastic modulus [2]. However, at lower propagation rates near the threshold stress-intensity amplitude, ΔK_o, and at higher stress-intensity amplitudes at which the cracking rate becomes immeasurably high, that is, near the cyclic fracture toughness, ΔK_c, a marked influence of the mean stress, R, and of microstructural parameters may be observed.

In the vicinity of the threshold value ΔK_o, higher propagation rates may accompany a change in fracture mode. For example, rapid cracking along prior austenite grain-boundary carbide particles has been noted in steels [3] and in the wrought nickel-base alloy, Nimonic 105 [2], when subjected to a three-stage heat treatment which develops almost continuous grain-boundary films of M_{23} C_6 carbides. When the presence of precipitates does not lead to a change in cracking mode, then cracking rates may be drastically reduced. For example, Santner and Fine [4] have shown that cracking rates in aged Al-4Cu alloys are over 100 times lower than in pure aluminium.

More recently, effects of crack branching and crystallographic orientation on fatigue crack propagation rates have been determined. Much higher values of the threshold stress-intensity amplitude are observed in cast rather than wrought alloys because crack branching, which occurs at primary γ/γ' eutectic modules, causes a reduction in the local value of ΔK [5]. In a directionally solidified cast nickel-base alloy, cracking may be accelerated if the loading is normal to a plane along which crystallographic (Stage 1) cracking can readily occur [6].

In summary, the following microstructural parameters have been investigated in some detail over a range of growth rates: crystal structure, homogeneous and grain boundary carbide precipitation, precipitate morphology, crystallographic orientation, and microstructure-enhanced crack multiplicity. In the present investigation tests have been carried out on nickel-base alloys both in the normally heat-treated condition and after a further 10 000 h heating which was intended to approximate service exposure. This treatment results in a coarsening of the γ'-precipitates and a change in the dislocation-particle interaction mechanism, the effect of which on fatigue crack propagation has been investigated.

An additional important influence on fatigue cracking, particularly in the threshold region, is exercised by the environment. It has been reported that the presence of oxygen at high temperatures assists crack growth [7] unless the oxide forming along a crack can reduce crack resharpening during compression [8] or the presence of oxygen encourages crack branching [9] when propagation rates may be actually reduced. Various studies have been undertaken to determine whether the frequency effect (higher growth rates per loading cycle at low frequencies), during tests at high temperature, is a result of creep or environmental processes. Experiments

on a wrought nickel-base alloy show a much-reduced rate of cracking in vacuum but still, at sufficiently low frequencies, the presence of a frequency effect [*9*] from which it appears that, in the absence of changes in cracking morphology at high temperatures, the environment can significantly accelerate the cracking process. Part of the present work has been carried out to investigate crack propagation mechanisms in a particularly aggressive environment designed to simulate gas turbine operating conditions.

Procedure

The chemical analyses and heat treatments of the alloys examined during this work are given in Table 1. The cast alloys, IN738LC and IN939, have grain sizes of approximately 3 mm and show coarse dendritic segregation, with large carbide particles and γ/γ' eutectic nodules, particularly in interdendritic regions. The wrought alloy Nimonic 105 shows a much finer grain size of approximately 80 to 100 μm and is, as for the cast alloys, strengthened by fine γ'-precipitation. The alloys Nimonic 105 and IN738LC were tested after receiving the heat treatments given in Table 1 and also after a further 10 000-h exposure at elevated temperature. The temperature of exposure and of subsequent elevated temperature testing was selected as 750°C for the wrought alloy and 850°C for the cast alloy.

Fatigue Testing in Air

Fatigue crack propagation measurements were made at ambient and elevated temperature for material in the normally heat-treated and in the thermally exposed conditions. Conventional double cantilever beam (DCB) specimens of 10-mm thickness were used for the wrought alloy whereas specimens with longitudinal face grooves were used for the alloy IN738LC in order to maintain the crack close to the center-line of the test specimen. Compliance calibrations had been previously performed for this modified specimen type [*5*]. Fatigue testing was carried out on a hydraulic closed-loop machine under load control at a frequency of 100 Hz and with a stress ratio, R (P_{min}/P_{max}) of 0.1. Crack growth rates were measured using the d-c potential-drop technique with an accuracy of better than 10 percent [*5*]. Metallographic examination of specimens was carried out optically and in the scanning electron microscope (SEM). Chemical analysis of small regions ($\sim$20 μm diameter) on polished specimens was performed in the electron microprobe whereas identification of small particles ($\sim$3 μm diameter) on fracture surfaces was accomplished using an energy-dispersive X-ray analysis attachment to an SEM.

TABLE 1—*Chemical compositions and heat treatments.*

Alloy	C	Cr	Co	Mo	W	Ta	Nb	Al	Ti	B	Zr	Heat Treatment
Nimonic 105	0.2	14.5	20.0	5.0	...	...	...	1.2	4.5	...	...	4 h/1150°C/AC + 16 h/1050°C/AC + 16 h/850°C/AC
IN 738 LC	0.17	16.0	8.5	1.7	2.6	1.7	0.9	3.4	3.4	0.01	0.10	2 h/1120°C/AC + 24 h/845°C/AC
IN 939	0.15	22.5	19.0	...	2.0	1.4	1.0	1.9	3.7	0.01	0.10	4 h/1160°C/AC + 6 h/1000°C/AC + 24 h/900°C/AC + 16 h/700°C/AC

AC = air-cooled.

Fatigue Testing in Vacuum

Fatigue crack growth rates were measured down to values in the region of ΔK_0 at room temperature, for the alloy IN738LC in the normally heat-treated condition only. The equipment used for these experiments was the same as that described in detail in Ref [*9*]. During the tests the vacuum was maintained below a value of 5×10^{-4} Pa.

Fatigue Testing Under Corrosive Conditions

In an attempt to simulate operating conditions in a gas turbine, specimens of normally heat-treated IN738LC were tested under highly corrosive conditions. A mixture of powdered oxides and sulphates (See Table 2), closely approximating those which have on occasion been analyzed in deposits on gas turbine blades after removal from service, was packed around the specimens, which were then tested at 850°C while air containing 0.015 volume percent each of SO_2 and SO_3 was circulated. The testing arrangement is shown schematically in Fig. 1.

Results

Effects of Microstructure

The results of heating the alloys for periods up to 10 000 h are a coarsening of the γ'-precipitates from a diameter of about 0.3 to 0.7 μm for IN738LC and from 0.05 to 0.15 μm for Nimonic 105, with a concomitant reduction in hardness of approximately 25 percent. In general, the particles adopt a more spherical form. The increase in precipitate size leads to a situation where the particles are no longer cut by dislocations during plastic deformation. In the normally aged condition at room temperature the precipitates in IN738LC are often sheared in long narrow continuous bands (Fig. 2) whereas, after exposure, deformation is more homogeneously distributed, probably on account of a change to a bowing of dislocations around precipitate particles (Orowan mechanism [*10*]).

TABLE 2—*Composition of oxide/sulphate mixture.*

Component	%
Fe_2O_3	22.3
SiO_2	10.4
Al_2O_3	6.5
MgO	2.8
$CaSO_4 \cdot 2H_2O$	22.7
$ZnSO_4 \cdot H_2O$	20.6
K_2SO_4	10.4
Na_2SO_4	4.3

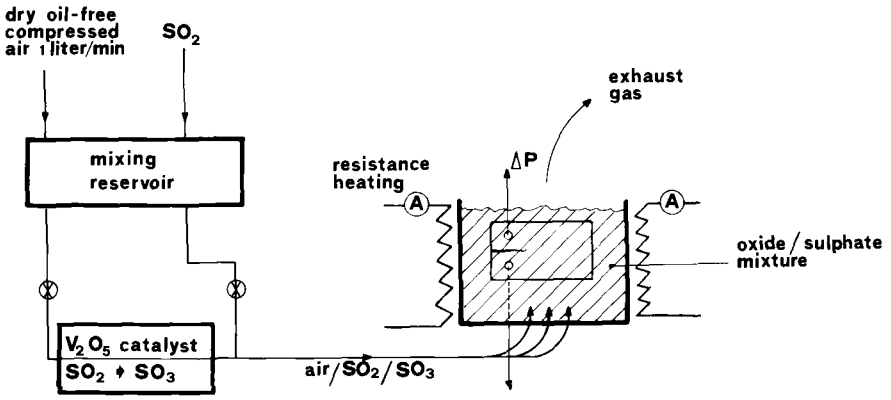

FIG. 1—*Schematic representation of the apparatus used for corrosion fatigue testing.*

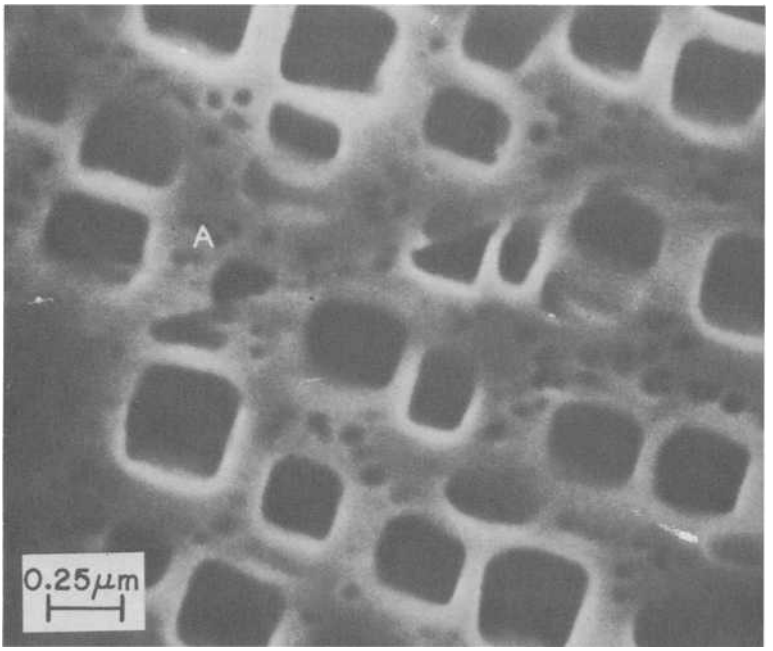

FIG. 2—*Scanning electron micrograph indicating precipitate cutting* (A) *at room temperature in normal-aged IN 738 LC.*

The extended heat treatment also results, for the cast alloy only in the formation of regions, 10 to 25 μm wide, of coarsened precipitates in interdendritic regions (Fig. 3). The γ'-particles in these regions are about twice as large as in the dendrite core regions. The coarsened regions possess a significantly reduced microhardness.

The rates of propagation of fatigue cracks are shown as a function of ΔK for IN738LC and Nimonic 105 at room temperature in Fig. 4 and 5 and at elevated temperature in Figs. 6 and 7.

Comparison of the diagrams shows that the value of ΔK_o is raised significantly through thermal exposure except in the case of IN738LC at room temperature, where no change is apparent. Values of the cyclic fracture toughness, ΔK_c, are unchanged for Nimonic 105 at room temperature and slightly increased for Nimonic 105 at high temperature, but drastically decreased for IN738LC at both temperatures. This large decrease in ΔK_c of the cast alloy is associated with a transition to intergranular cracking in the exposed material in the form of ductile tearing along the softened grain boundary zones of coarsened γ'-participates.

Electron microprobe analysis has shown local differences in chemical composition between the regions of coarse precipitation and the dendrite core of IN738LC, specifically with respect to titanium and tungsten. The

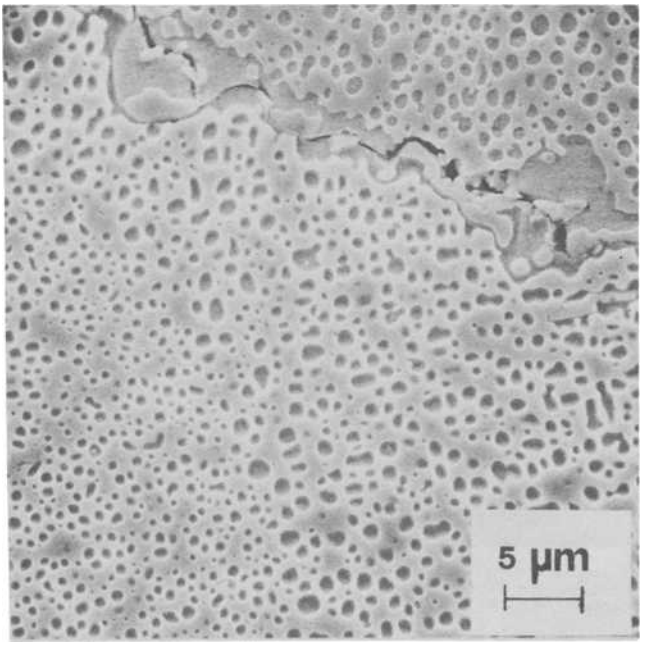

FIG. 3—*A region of coarsened precipitation in the vicinity of a grain boundary in exposed IN 738 LC.*

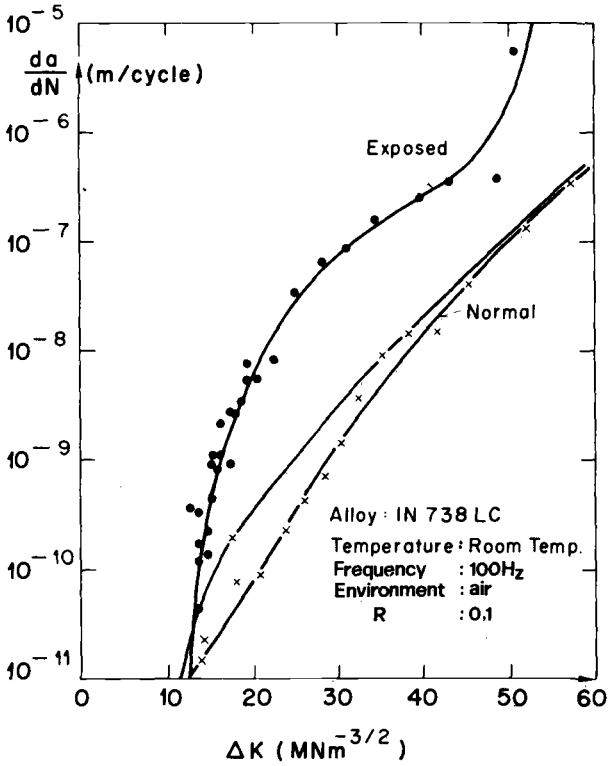

FIG. 4—*Room temperature fatigue crack propagation rates in IN 738 LC in the normal and thermally exposed conditions.*

respective concentrations are 1.5 percent tungsten with 3.4 percent titanium in the coarsened zone and 2.3 percent tungsten with 2.3 percent titanium in the core (fine precipitation). To determine whether such segregations and differences in precipitate distribution are present in all such cast nickel-base alloys, a specimen of IN939 (for composition and heat treatment, see Table 1) was examined after normal heat treatment and exposure for 3000 h at 850°C. Neither regions of different precipitate size (Fig. 8) nor variations in chemical composition for the major alloying elements, nor similar softened zones, could be detected. Similarly, no such heterogeneity in structure and properties could be determined for the wrought alloys.

Effect of Environment

The influence of the presence of air on fatigue crack propagation particularly in the threshold region is shown in Fig. 9 for IN738LC in the normally heat-treated condition. A rapid approach to a ΔK_o value in the

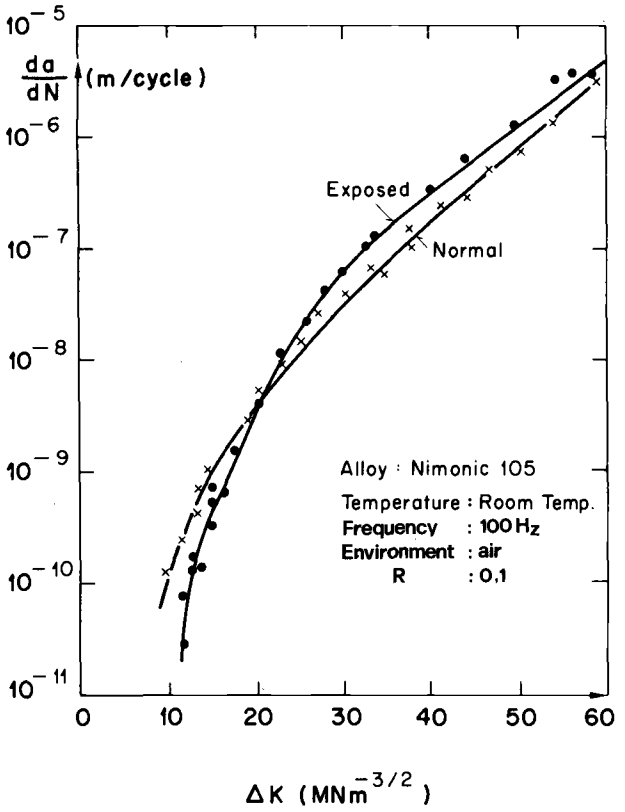

FIG. 5—*Room temperature fatigue crack propagation rates in Nimonic 105 in the normal and thermally exposed conditions.*

region of 10^{-11} m/cycle is observed only in vacuum. At propagation rates above 2×10^{-10} m/cycles, no significant difference is apparent between propagation in air and in vacuum. Vacuum experiments were not continued to higher growth rates. Crystallographic cracking, which is a type of propagation along preferred crystal planes and which has been previously reported in nickel-base [*11-14*] and other systems [*15,16*], is observed at low ΔK values in both air and vacuum tests. A region of multiple crystallographic cracking in a vacuum-tested specimen is shown in Fig. 10. Somewhat indistinct striations can occasionally be observed on the fracture surfaces of those cracks which had propagated rapidly in vacuum.

From a comparison of the growth behavior of fatigue cracks in normally aged IN738LC at ambient and elevated temperature in air (Figs. 4 and 6) it is apparent that a definite ΔK_o value is observed only at the higher temperature. Examination of metallographic sections in the SEM has

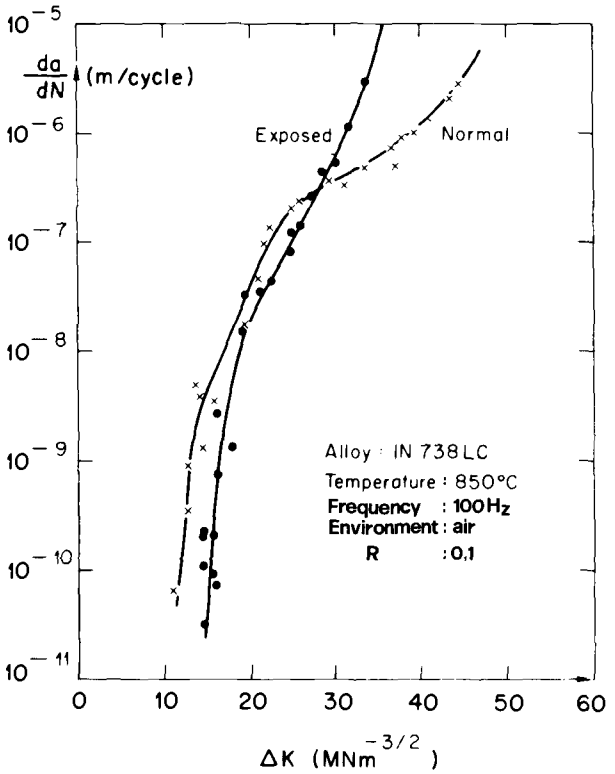

FIG. 6—*Elevated temperature fatigue crack propagation rates in IN 738 LC in the normal and thermally exposed conditions.*

shown that the crack surfaces are heavily oxidized and that the growth of the oxide layer leads to dissolution of the γ'-precipitates in the surrounding matrix (Fig. 11). This reduces the yield strength in the crack-tip region and causes rounding or blunting, thereby at sufficiently low growth rates, preventing further propagation, that is, showing a definite ΔK_0 value. This interpretation is supported by the observation that after interruption and unloading of a test for a period of several hours at elevated temperature the crack will no longer propagate until the loading amplitude is raised well above that at which the crack was originally propagating.

Results of the crack propagation measurements under corrosive conditions are shown, in comparison with those carried out in air, in Fig. 12. An increase in scatter of the data and a small decrease in ΔK_0 are apparent. Examination of tested specimens shows pitting corrosion at grain boundaries and a tendency to interdendritic cracking at higher ΔK values. Figure 13 shows balls of corrosion product which were distributed on the

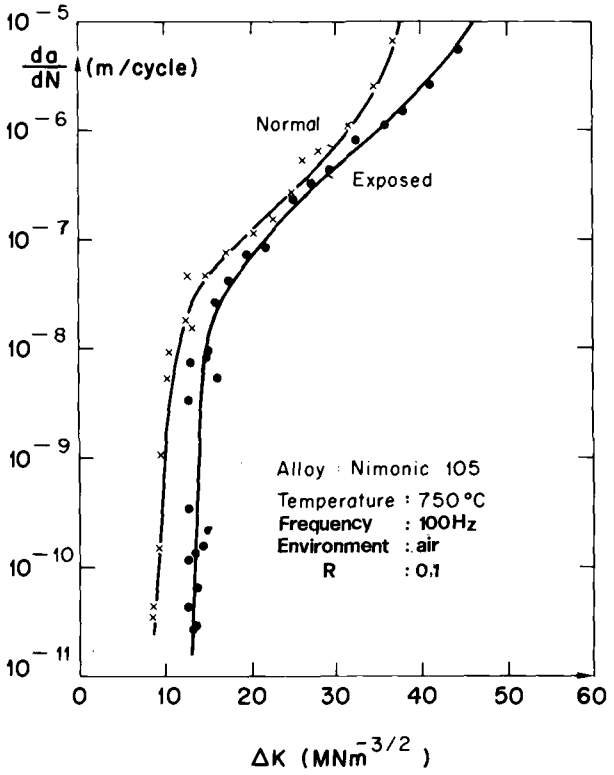

FIG. 7—*Elevated-temperature fatigue crack propagation rates in Nimonic 105 in the normal and thermally exposed conditions.*

fracture surface and which by energy-dispersive X-ray analysis in the SEM, were shown to contain nickel sulphide (the angular particles in the foreground of Fig. 13 are of the powder mixture intentionally added to simulate gas turbine operating conditions).

Discussion

Microstructure

The effects of overaging of stainless steels on fatigue crack propagation have been reviewed by James [*17*]. Aging, which causes coarsening of the heterogeneously nucleated carbide strengthening precipitates, decreases growth rates at high temperatures and increases those at room temperature. Rationalizations of this behavior involve interactions of the propagating crack directly with the carbide particles [*18,19*]. In the present case,

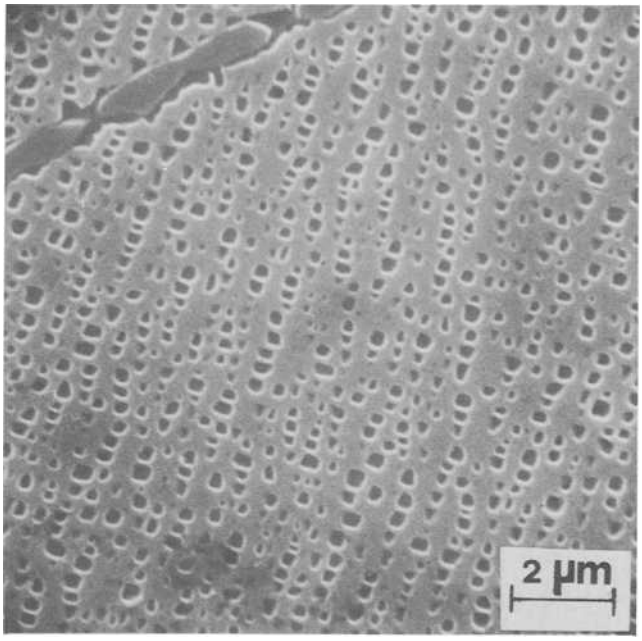

FIG. 8—*γ'-precipitate distribution in the vicinity of a grain boundary* (upper left) *of a specimen of IN 939 exposed for 3000 h at 850°C.*

strengthening is achieved by γ'-intermetallic precipitates which are cut by dislocations in the normally aged condition but around which dislocations bow in the thermally exposed condition. Crack propagation rates in an iron-nickel-aluminum alloy containing in one case cuttable and in another case noncuttable precipitates have been compared by Hornbogen and Zum Gahr [*20*]. The lower crack growth rate which is observed in the underaged condition is rationalized by the argument that in this condition deformation occurs in intense bands and dislocation movement can be reversed during unloading, thereby recovering the deformation. Such a mechanism is possible only when

1. dislocations remain on their original slip planes, that is, where precipitates are cut by dislocations,
2. stress intensities are low so that slip occurs predominantly on a single system, and
3. oxidation is minimized so that rewelding of the freshly exposed material at the crack tip is possible on unloading.

During high-temperature tests, rewelding is not possible so that no reduction in growth rate can occur during unloading. Moreover, when cuttable precipitates are present (planar slip material), higher propagation

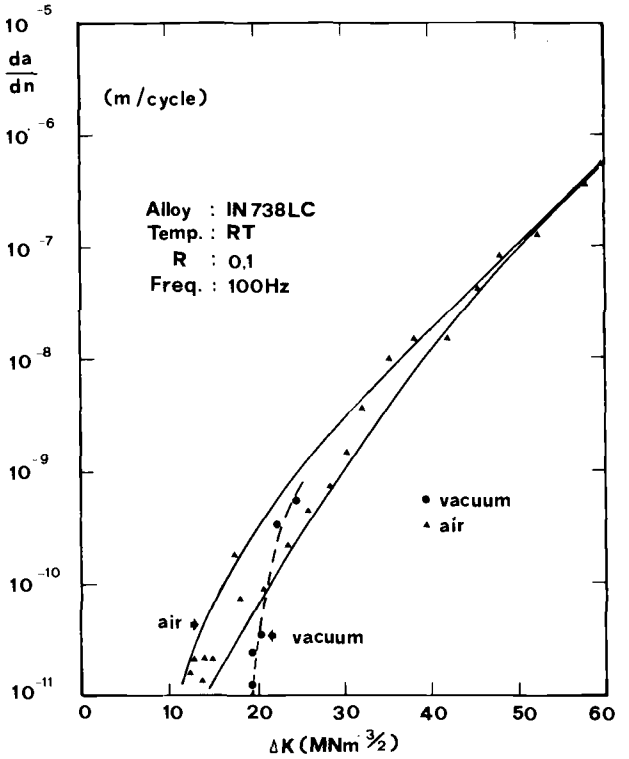

FIG. 9—*Room temperature fatigue crack growth rates in IN 738 LC in air and in vacuum.*

rates are caused by the increased ease with which embrittling species such as oxide ions diffuse down the intense slipbands.

Hence the presence of cuttable precipitates reduces cracking rates only where oxidation of the crack tip cannot occur, that is, at low temperatures and high propagation rates. The rate below which rewelding of the crack tip can occur on unloading can be estimated from the time required for a monolayer of oxide to form on the freshly exposed surface [*13*]. Such a calculation yields an estimate of approximately 3×10^{-9} m/cycle as the value below which cracking can occur more rapidly in the normally aged condition [*21*]. This is in good agreement with the results for the wrought nickel-base alloy but overestimates the crossover point for the cast alloy, which is more oxidation resistant and thereby exhibits environment-independent behavior to lower growth rates.

Crystallographic cracking has been observed only for normally aged material at room temperature and low ΔK values, supporting the suggestion [*20*] that planar slip is a necessary condition for this cracking mode.

The reduction in cyclic fracture toughness, ΔK_c, in the cast alloy IN738LC

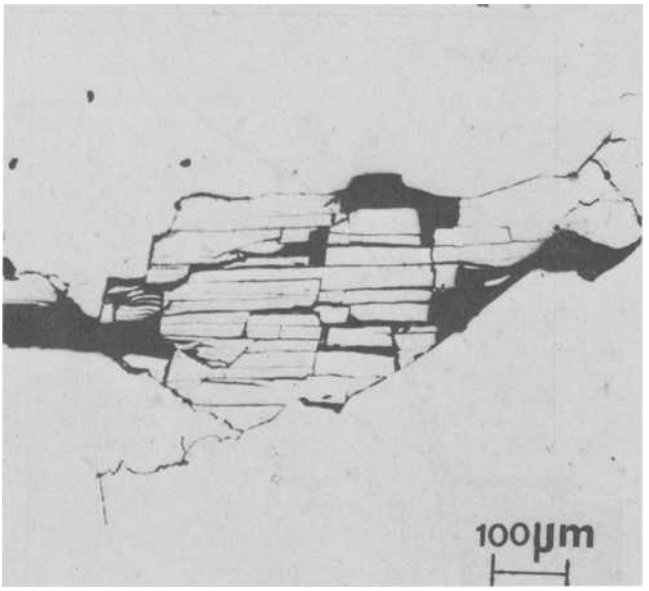

FIG. 10—*Region of multiple crystallographic cracking in a vacuum-tested specimen of IN 738 LC.*

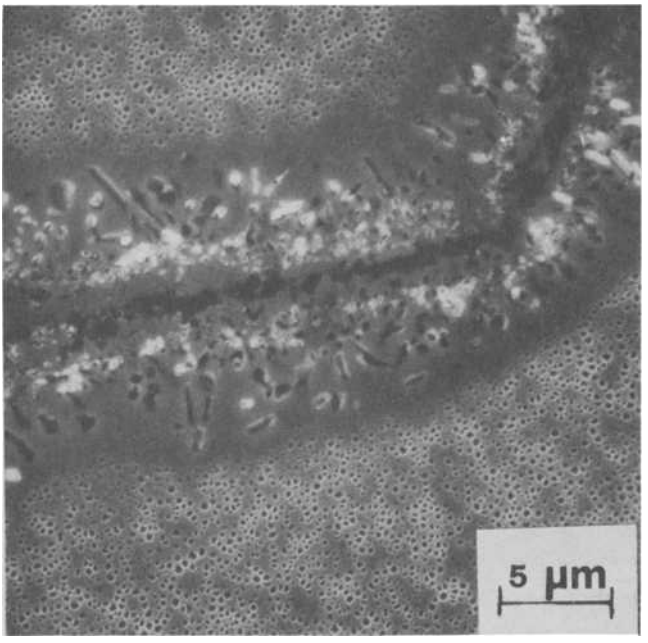

FIG. 11—*γ'-precipitate dissolution in the neighborhood of a slowly propagating crack in IN 738 LC at elevated temperature.*

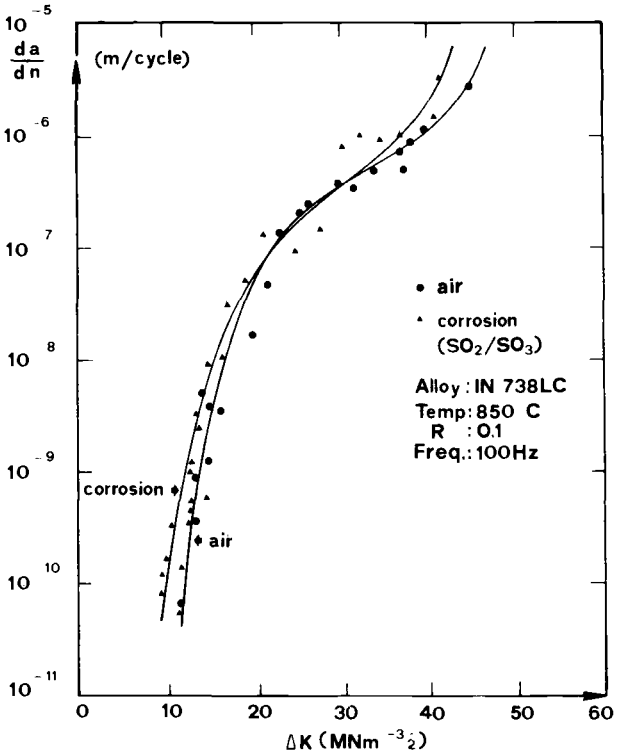

FIG. 12—*High-temperature fatigue crack growth rates in IN 738 LC in air and in the corrosive environment.*

dendritic regions of coarsened γ'-precipitates. This may be brought about by the higher W concentration in the dendrite cores, since this large substitutional atom associates strongly with vacancies, thereby reducing their mobility and the rate of γ'-precipitate coarsening.

The fact that a similar cast nickel-base alloy, IN939, shows no such inhomogeneity in precipitate size is probably determined by the longer time and higher temperature used in solution-treating this alloy. This treatment effectively removes the compositional gradients caused by segregation during casting. It is therefore likely that IN939 will not show a reduction in ΔK_c in the exposed condition and it is possible that the ΔK_c of IN738LC in the same condition would have been higher had the alloy been initially subjected to a more effective solution heat treatment.

Environment

Comparison of crack propagation rates in IN738LC at room temperature

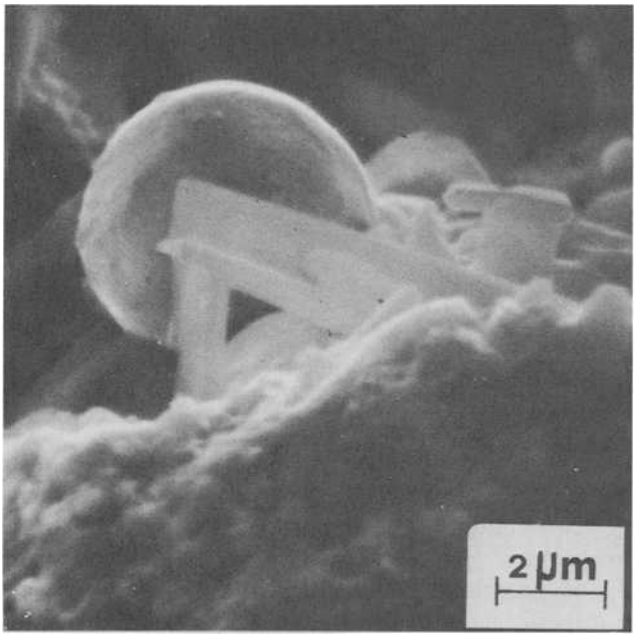

FIG. 13—*Spherical nickel sulphide-containing particle on the fracture surface of an IN 738 LC specimen tested in the corrosive environment.*

in air and vacuum shows a distinct difference, the vacuum data exhibiting a higher and more clearly defined value of ΔK_o. Bouchet et al [*22,23*] have also noted longer lives and much larger crack-tip plastic zones in vacuum-tested rather than air-tested aluminum-copper alloys, suggesting that dislocation mobility is reduced by the presence of air, possibly through pinning by oxide ions. Such diffusion of oxide ions would cause embrittlement in the crack-tip zone, leading to continued slow cracking even at very low ΔK values, thereby reducing ΔK_o. The presence of crystallographic cracking in vacuum, at least in the nickel-base alloy, indicates that this mode of cracking is not a form of environmentally enhanced cleavage [*16*].

The effect of more intensive oxidation during high-temperature crack growth on crack growth rate and appearance may be seen in Figs. 4 and 6. At low growth rates, oxidation leads to the formation of a precipitate-denuded zone which is of greater extent for the normally aged specimens (smaller precipitates). This zone is of lower yield strength than the matrix so that cracks can propagate through relatively easily. However, below a certain propagation rate, the crack tip may be mechanically blunted, leading to a rapid approach to a clearly defined ΔK_o value.

Under the highly corrosive conditions (air/SO_2/SO_3 at high temperature)

used in the present tests on the cast nickel-base alloy, it appears that nickel sulphides can be formed, as has also been observed under severe sulphidizing conditions in practice [*24*]. Moreover, this phase appears to have been in the liquid state (present as solidified droplets) at the test temperature of 850°C. This would be consistent with the formation of the nickel/Ni_3S_2 eutectic (melting point 637°C) which enhances corrosion rates, thereby leading to the observed reduction of ΔK_o. A further consequence of the presence of this phase is likely to be a reduction in the time required for crack initiation since intergranular pitting is observed under these conditions.

Summarizing the present results and some from elsewhere [*9*], it appears that the environment can react with the microstructure of a specimen in a variety of ways to influence the morphology and rate of cracking:

1. The simplest case is where the presence of air leads to crack acceleration without a change in cracking mechanism. Cracking rates may be enhanced by diffusion of oxide ions, the presence of oxide on the freshly exposed crack-tip metal surface preventing rewelding on unloading.
2. During low-frequency testing of a cast nickel-base alloy at high temperature, oxidation of interdendritic regions causes multiple cracking [*9*], thereby reducing growth rates. Such multiple cracking is not possible during vacuum tests so that, when this mechanism operates in the presence of air, the rate of propagation may be *reduced*. This cracking mechanism is not observed in wrought nickel-base alloys.
3. Oxidation of the crack tip may also lead to dissolution of adjacent γ'-precipitates which can (*a*) soften the crack tip, thereby increasing growth rates, or (*b*) at sufficiently low growth rates or during interruption of the test lead to crack tip blunting and the attainment of a clear ΔK_o value.
4. Interaction of an aggressive (for example, sulphidizing) atmosphere with the specimen can produce corrosive, possibly liquid, phases which accelerate the cracking rate and—because of local chemical segregation—tend to produce interdendritic propagation.

Conclusions

The effect of the type of dislocation/precipitate interaction (cutting or bowing) on fatigue crack propagation rate has been studied for wrought and cast nickel-base alloys. Under conditions where interaction with the environment is unimportant (relatively high growth rates at room temperature), fatigue crack propagation is reduced by reversal of slip when the precipitate particles can be cut, that is, in the normally aged condition. However, at low growth rates at room temperature and at all growth rates at elevated temperature, oxidation prevents slip reversal, so that propagation is more rapid when precipitates can be cut (heterogeneous slip) than when overaged precipitates are present (homogeneous slip deformation).

Extended aging (10 000 h) also leads to the formation of softened regions of coarsened precipitation in the interdendritic regions of insufficiently solution-treated cast alloys only. This inhomogeneous precipitate distribution is a result of chemical segregation during casting and causes a considerable reduction in cyclic fracture toughness.

Fatigue crack growth tests on the cast alloy IN738LC in air, vacuum, and in a corrosive environment have indicated a number of mechanisms by which the environment can affect cracking morphology and rate. These may be summarized as

1. Crack acceleration by oxidation of the crack tip preventing rewelding on unloading and diffusion of oxide ions ahead of the crack tip.
2. Interdendritic crack branching caused by oxide embrittlement leads to a reduction of propagation rate in air for cast alloys only.
3. Oxidation leads to γ'-precipitate dissolution at the crack tip, the resulting soft zone being easily deformed so that the crack tip is blunted and a clear threshold value is attained.
4. Interaction of an aggressive sulphidizing atmosphere can produce liquid sulphide films which accelerate cracking rates.

Acknowledgments

The author thanks Dr. M. O. Speidel for helpful discussions during the course of this work, Mr. C. Rey for his skilled technical assistance, and Dr. Hugi and Mrs. Posedel, who carried out the experiments in the electron microprobe and scanning electron microscope, respectively.

References

[1] Ritchie, R. O. in *Proceedings,* International Conference on Fatigue, University of Cambridge, Cambridge, U.K., 28 March 1977, p. 61.
[2] Speidel, M. O. and Scarlin, R. B. in *Proceedings,* International Conference "Gefüge und Bruch," Leoben, Austria, 25 Nov. 1976, P. 163.
[3] Richards, C. E. and Lindley, T. C., *Engineering Fracture Mechanics,* Vol. 4, 1972, p. 951.
[4] Santner, J. S. and Fine, M. E., *Metallurgical Transactions,* Vol. 7A, 1976, p. 583.
[5] Scarlin, R. B., *Materials Science and Engineering,* Vol. 21, 1975, p. 139.
[6] Scarlin, R. B., *Metallurgical Transactions,* Vol. 7A, 1976, p. 1535.
[7] Cook, R. H. and Skelton, R. P., *International Metallurgical Reviews,* Vol. 19, 1974, p. 199.
[8] Gell, M. and Leverant, G. R. in *Proceedings,* Second International Conference on Fracture, Brighton, U.K., 1969, p. 565.
[9] Scarlin, R. B. in *Fracture 1977, Proceedings,* Fourth International Conference on Fracture, Waterloo, Ont., Canada, June 1977, Vol. 2, p. 849-857.
[10] Gleiter, H. and Hornbogen, E., *Physica Status Solidi,* Vol. 12, 1965, pp. 235 and 251.
[11] Gell, M. and Leverant, G. R., *Acta Metallurgica,* Vol. 16, 1968, p. 553.
[12] Gell, M. and Leverant, G. R., *Transactions, TMS-AIME,* American Institute of Mining Engineers, Vol. 242, 1968, p. 1869.
[13] Tien, J. K. and Gamble, R. P., *Metallurgical Transactions,* Vol. 2, 1971, p. 1933.

[14] Duquette, D. J. and Gell, M., *Metallurgical Transactions,* Vol. 2, 1971, p. 1325.
[15] Thompson, K. R. L. and Craig, J. V., *Metallurgical Transactions,* Vol. 1, 1970, p. 1047.
[16] Garrett, G. G. and Knott, J. F., *Acta Metallurgica,* Vol. 23, 1975, p. 841.
[17] James, L. A., *Atomic Energy Review,* Vol. 14, 1976, p. 37.
[18] James, L. A., *Metallurgical Transactions,* Vol. 5, 1974, p. 831.
[19] Barnby, J. T. and Peace, F. M., "Effect of Second Phase Particles on the Mechanical Properties of Steel", The Iron and Steel Institute, London, U.K., 1971, p. 124.
[20] Hornbogen, E. and Zum Gahr, K. H., *Acta Metallurgica,* Vol. 24, 1976, p. 581.
[21] Scarlin, R. B., *Materials Science and Engineering,* Vol. 30, 1977, p. 55.
[22] Bouchet, B., de Fouquet, J., and Aguillon, M., *Acta Metallurgica,* Vol. 13, 1975, p. 1325.
[23] Bouchet, B. and de Fouquet, J. in *Proceedings.* Conference on Strength of Metals and Alloys, Nancy, France, Aug. 1976, p. 485.
[24] Stringer, J. and Whittle, D. P. in *Proceedings,* Conference on Deposition and Corrosion in Gas Turbines, Central Electricity Generating Board, London, U.K., Dec. 1972, p. 197.

DISCUSSION

L. Coffin, Jr.[1] *(discussion)*—This paper considers both microstructural and environmental aspects of fatigue crack growth of certain nickle-based superalloys. Microstructural variations are introduced by compositional variations, casts versus wrought structures, and by normal versus prolonged (10 000 h) high-temperature exposures. Environment is introduced by limited room-temperature vacuum testing and by testing in a service simulated environment. Emphasis is given to crack growth rate differences at the threshold and at the high-rate region. In the intermediate region the comparisons made were consistent with the commonly accepted view that growth in this region is independent of microstructure and mean stress.

Before commenting on these comparisons, it seems to this discusser that the single most significant effect shown in the crack growth results was not mentioned, that is, the effect of temperature. Comparing Fig. 4 and Fig. 6 for the cast alloy and Fig. 5 and Fig. 7 for the wrought alloy either in the normal state or exposed to 10 000 h, substantial differences in crack growth rates can be found particularly in the intermediate region of growth. What are the causes for these large differences? It would seem to this discusser that the use of high vacuum would be instructive in determining if the growth rate difference between room and high temperature is principally environmental or due to other causes.

Turning to the topics dealt with in the paper, one question which is basic to the arguments presented by the author on the effects of microstructure

[1]General Electric Company Corporate Research and Development Center, Schenectady, N. Y. 12301.

relates to whether lower crack rates arise as a consequence of deformation which occurs by intensive bands and reverse dislocation motion upon unloading. It would seem to me that deformation of this type would accelerate crack growth, since it is so highly localized and focussed on the crack tip. On the other hand, for the same loading conditions, if the mode of deformation were more diffuse, as a result of strain hardening and irreversibility of slip systems on unloading, crack advance could be blunted and slowed. This point needs to be clarified at least for this discusser.

Arguments presented in the paper in support of the differences in threshold conditions between air and vacuum for IN 738 LC at room temperature (Fig. 9) are interesting and require future study. Relative to the test performed under corrosive conditions (Fig. 12), the differences shown between this environment and air are not large and suggest that air at 850°C is equally agressive in crack growth. However, the frequency of testing is very high and this may obscure any important difference. Comparison at lower frequencies would be of interest.

No mention was made of film rupture, which is believed to be a principal reason for acceleration of oxidation and denudation on fracture surfaces in fatigue. In our own experience, denudation is always much more pronounced on active (deforming) surfaces than on passive (undeforming) surfaces. Has the author made similar observations?

Many points were brought out in this paper. There were so many different conditions discussed, including those involving temperature, materials, and environment, that it's a little bit difficult in a short time to bring them all together in any concise way. What the author was attempting to do is to emphasize the effects of these various conditions on Stage I crack growth. Now the thing that struck me about the various findings of this paper was not something Dr. Scarlin actually discussed in the paper. In examining the various crack growth results, the most striking effect was the role of temperature on Stage II crack growth in going from room temperature to 850°C. I would like to ask him first what his explanation is for these large temperature effects on crack growth, bearing in mind the work of Lee James, who was found that environment seems to be the most important factor in the temperature dependence of fatigue crack growth.

R. B. Scarlin (author's closure)—The large increase in crack propagation rate at high temperature results predominantly from a change in cracking mechanism. At ambient temperature, and particularly in the cast alloy, extensive crystallographic cracking is observed. This leads to multiple crack branching, which drastically lowers the propagation rate. Crystallographic cracking requires planar slip to occur. However, at elevated temperatures this is no longer the case, crystallographic cracking and crack branching are not observed, and propagation rates are correspondingly higher [5].

The experimental observations of changes in cracking rate with precipitate size are rationalized through the proposal that, when planar slip occurs and crack tip oxidation can be neglected, unloading leads to slip reversal and a reduction of effective damage per loading cycle. As is mentioned in the paper, this mechanism is consistent also with the work of Hornbogen and Zum Gahr. Dr. Coffin's suggestion of a mechanism involving strain-hardening under diffuse deformation could be appropriate in certain cases but is not consistent with the present experimental results.

I agree with the comments made in the fourth paragraph of Dr. Coffin's discussion. Tests at low frequency will certainly be of interest and may show a larger influence of the environmental conditions. However, the presence of sulphides at the crack tip shows that some interaction was also occurring at high testing frequencies.

No tests have been carried out specifically to investigate the effects of film rupture on precipitate dissolution, but this mechanism will certainly be operating in the crack-tip region and contributing to the formation of the observed denuded layer.

L. Coffin Jr.—A great amount of effort was undertaken in the study to look at the effects of aggressive environment at elevated temperature, but when I compared your crack growth data in that aggressive environment with those from the experiments done in air, within the region of scatter the two experiments gave precisely the same result. It seemed to me, from that, that air was just as aggressive an environment as this highly specialized environment that you were using. I wonder whether you feel the same way.

R. B. Scarlin—Basically I would agree with this. There was no very large difference in the threshold value, in view of the normal scatter you get in cast materials, anyway.

I think in your written discussion of the paper, which I read through, you also suggested that you would really only see any real difference at much lower testing frequencies, and as I showed on the last slide there, as you remove the environment, or you change the aggressive environment from an air test to this sulphidizing test, the difference is only clearly visible at the lowest testing frequencies.

That test we have not yet carried out, at low frequencies in sulphidizing conditions. It would be interesting.

T. Cruse[2] *(discussion)*—You mentioned on the one chart for the cast nickel-based alloy at 850°C that you got a transition from transgranular to intergranular that you attribute to aging. If it is aging, do you have other

[2]Pratt & Whitney Aircraft Co., Glastonbury, Conn. 06033.

reasons that I could use to explain the transition under other conditions and in wrought nickel-based alloys?

R. B. Scarlin—This transition is caused by the presence of softer zones at the grain boundaries. These arise from the segregation during casting, which results in a different aging response. After prolonged aging, the soft zone is well developed so that on deformation the strain capacity of this zone is exhausted and cracking is localized in this region. That would not apply to wrought material. In wrought alloys we do not see such intergranular failure.

J. Beevers[3] (*discussion*)—Could I ask about the faceting and crack branching that you observed? As I understood it, this was in the cast alloy in particular. What were the conditions that really optimized the occurrence of these facets and branching?

R. B. Scarlin—Basically the occurrence of facets requires planar slip, that is, cuttable precipitates, low stress intensities, and normal temperatures. At high temperature such crystallographic cracking does not occur. Crack branching reduces the stress intensity and reduces the crack propagation rate. At high temperatures crystallographic cracking and crack branching are not observed and crack propagation rates are much higher.

J. Beevers—So basically it's associated with the threshold region.

R. B. Scarlin—No, it extends to a ΔK of about 30 or 40 $MNm^{-3/2}$.

J. Beevers—Do you feel there's any compositional features which may lead to this type of failure?

R. B. Scarlin—Not to the crystallographic cracking itself, but to the crack branching. We find that the crack branching occurs at primary eutectic particles. It is not clear exactly why.

N. Stoloff[4] (*discussion*)—Tomorrow I'll be showing data for a nickel-base eutectic alloy whose composition isn't too different from that of your alloys. We get an enormous frequency effect at 825°C, in vacuum, our vacuum being about 10^{-6} torr, so I firmly believe that that last graph you showed, showing a frequency effect in vacuum, is a real effect. I would like to ask, though, just how good the vacuum was and also if you have any idea whether the aggressive nature of air is due to oxygen or perhaps water vapor.

[3]Department of Physical Metallurgy & Material Science, University of Birmingham, Birmingham, U. K.

[4]Department of Metallurgical Engineering, Rensselaer Polytechnic Institute, Troy, N.Y. 12181.

R. B. Scarlin—We have not determined which species is responsible for the frequency effect. The vacuum we used was of 2×10^{-6} torr. Calculations show that this is sufficiently low that no interaction would occur with oxygen in the testing environment. As to the effect of frequency in vacuum, I reported some work last year [9] whereby we looked at crack propagation rates in this cast nickel-based alloy at different frequencies. A frequency effect was still observed in vacuum. In fact, the presence of air is necessary for crack branching to occur. If the air is removed, no crack branching can take place and cracks grow more rapidly, which is the opposite of what might be expected.

B. Tomkins[5] (*discussion*)—You seem to be putting over quite strongly that you always saw air as an aggressive environment, even at room temperature as well as at high temperatures.

R. B. Scarlin—In principle, yes. This is simply a matter of defining in what way the environment is aggressive. An interaction with the crack tip whereby slip reversibility is prevented is also a form of aggressive attack.

B. Tomkins—You have expressed the view that air is an aggressive environment at both elevated and ambient temperature for the alloys tested. At elevated temperature, there is considerable evidence that this is true throughout the fatigue range. However, at lower temperatures the evidence from mechanistic studies presented earlier show that, particularly during Stage I growth, some reversibility can occur in an inert environment. Care should therefore be taken in interpreting data as indicating an aggressive environmental effect.

N. Dowling[6] (*discussion*)—Would you briefly describe your experimental technique for obtaining these very low growth rates, and particularly, how did you observe the crack under the environmental conditions? How did you unload? And again, how did you observe the crack?

R. B. Scarlin—The crack was observed by the potential drop system both during air tests and tests under corrosive conditions.

N. Dowling—What was your loading sequence during the test?

R. B. Scarlin—We would run the crack for, say, a millimetre at a certain stress amplitude and then we would step down the load by never more than

[5]Reactor Fuel Element Laboratories, U. K. Atomic Energy Authority, Springfields, Salwick, Preston, Lancs, U. K.

[6]Westinghouse Research and Development Center, Pittsburgh, Pa. 15235.

7 percent and take a series of measurements at this stress intensity to make sure we had a constant growth rate. This avoided any excessively rapid reduction of the load which would cause the crack to stop prematurely.

W. Plumbridge[7] (*discussion*)—You state that aging produces coarsening of the γ'-precipitates so that they are no longer sheared during deformation. Is this equivalent to their loss of coherency with the matrix?

R. B. Scarlin—In response to the question by Dr. Plumbridge, I wish to say that the coarsening of the γ'-precipitates during aging was not investigated during the present work, but one would expect Dr. Plumbridge's statement to be true if the full investigation is carried out.

[8]Department of Mechanical Engineering, University of Bristol, Bristol, U. K.

H. Kitagawa,[1] *S. Takahashi,*[1] *C. M. Suh,*[2] *and S. Miyashita*[3]

Quantitative Analysis of Fatigue Process—Microcracks and Slip Lines Under Cyclic Strains

REFERENCE: Kitagawa, H., Takahashi, S., Suh, C. M., and Miyashita, S., **"Quantitative Analysis of Fatigue Process—Microcracks and Slip Lines Under Cyclic Strains,"** *Fatigue Mechanisms,* Proceedings of an ASTM-NBS-NSF symposium, Kansas City, Mo., May 1978, J. T. Fong, Ed., *ASTM STP 675,* American Society for Testing and Materials, 1979, pp. 420-449.

ABSTRACT: Quantitative observations have been made on the microcracks or small surface cracks and slip lines on the surfaces of steels under cyclic strains, for the purpose of unifying two approaches to the study of fatigue, namely, that based on fracture by crack growth (fracture mechanics concept) and that of cyclic strain accumulation (low-cycle fatigue concept). Important results are: (1) initiation of cracks at the early stage of fatigue life even on unnotched smooth specimens; (2) growth of the small surface cracks below ΔK_{TH} level; (3) higher growth rate of small surface cracks than that of a large through crack; (4) dependence of ΔK versus da/dN relation on stress level for small surface cracks; and (5) a definite relation between λ, the ratio of the number of slipped grains to the number of total grains, and $\Delta\epsilon$, the cyclic strain range. From these results it is suggested that the growth rate of small surface fatigue cracks can be represented as either $da/dN = C\,(\Delta K_{\epsilon p})^m$ or $da/dN = C\,(\Delta K_{\epsilon t})^m$, where $\Delta K_{\epsilon p}$ is the plastic strain-intensity factor range given by $\Delta\epsilon_p\sqrt{\pi a}\cdot f(a)$, and $\Delta K_{\epsilon t}$ is the total strain-intensity factor range given by $\Delta\epsilon_t\sqrt{\pi a}\cdot f(a)$.

KEY WORDS: crack growth rate, crack initiation, crack measurement, cyclic strains, fatigue, fatigue life prediction, fatigue (materials), fracture mechanics, low-cycle fatigue, mechanisms of fatigue, slip line, steel, surface crack, threshold stress-intensity factor range

Two approaches have been successfully applied to practical fatigue problems: (1) accumulation of cyclic strains (low-cycle fatigue concept) and

[1] Professor, Institute of Industrial Science, and graduate student, Mechanical Engineering, respectively, University of Tokyo, 7-22-1, Roppongi, Minato-ku, Tokyo 106, Japan.

[2] Assistant professor, Mechanical Engineering, Gyungbuk National University, Taegu, Gyungbuk, Korea; presently, research fellow, University of Tokyo, Tokyo, Japan.

[3] Research engineer, Topy Industries Ltd., Tokyo, Japan; presently, research fellow, Institute of Industrial Science, University of Tokyo, Tokyo, Japan.

(2) fracture by crack growth (fracture mechanics concept). In general, these two have been applied independently (of each other). In some cases, the material with no flaw at the initial stage of fatigue is handled by Approach 1 and the material with a flaw or flaws by Approach 2. In other cases, the stage before crack initiation in fatigue life is treated by Approach 1 and the stage after crack initiation by Approach 2.

In addition to these two, the third approach given by combination or unification of the foregoing two, or an intermediate approach between the two, could be imagined to be available. This new additional approach, which is based on the previous approaches, seems to be useful for better understanding of a part of the whole process of fatigue fracture, and a useful tool for some of the following practical fatigue problems: (1) Analysis of fatigue processes or fatigue life prediction of unnotched parts, particularly in the low-cycle fatigue range. Most of the fatigue life in this case can be governed by the growth or successive initiation of small cracks, as stated later. (2) Detection, monitoring, and evaluation of small surface fatigue cracks or cracks in the early stage of fatigue life. (3) Prediction of behaviors of small cracks below the ΔK_{TH} level. (4) Application of data given by a simple sandglass-shaped specimen to complex structures.

A basic method for the analysis of the fracture process, which is governed by the initiation, interaction, connection, and coalescence of many closely spaced small cracks, was reported by one of the authors,[4] including an example of an application of the method to corrosion fatigue of unnotched specimens. For the next step, an analysis of a fracture process characterized mainly by growth of small- or micro-surface cracks seems to be important.

Some of the recent trials started from the foregoing considerations are presented in this paper. Based on the long-time developments of the techniques for monitoring or measuring the small- or micro-surface cracks and slip lines, quantitative analyses are made of the growth of small- or micro-fatigue cracks and related phenomena on the surfaces of steels, by combining the aforementioned two approaches.

Approaches and Experimental Procedures

Methodology

To combine the two approaches, that is, the cyclic strain accumulation concept (low-cycle fatigue concept) (LCF) and the fracture mechanics concept (FM), the following measurements were made.

1. Growth of surface cracks from a very small to larger size was measured over some area of the smooth surfaces of fatigue specimens under

[4]Kitagawa, H., Fujita, T., and Miyazawa, K. in *Corrosion-Fatigue Technology, ASTM STP 642*, American Society for Testing and Materials, 1978, p. 98.

the condition of cyclic strains, including low-cycle fatigue levels. Both types of cracks that start from a small surface flaw (notch) and that start on the smooth unnotched surfaces were included.

2. Histories of cyclic strains on the smooth surfaces were recorded intermittently throughout each fatigue life, and cyclic plastic and total strain ranges, $\Delta\epsilon_p$ and $\Delta\epsilon_t$, were compared with the surface crack growth data.

3. Slip lines on the surfaces from cyclic strains were measured, which are expected to bridge the two kinds of phenomenological behaviors obtained from Tasks 1 and 2 just given. The distribution pattern of slip lines usually looks irregular. For the quantitative determination of the number of such slip lines, the number of grains in which any slip-line area can be observed were counted. The ratio of the number of the slipped grains to the number of total grains was taken as a numerical measure of the degree of slip.

In formulating the relations of these data, the extension and combination of the two previous approaches (FM and LCF) seemed to be favorable for engineering use. If any limitation is found in this extension, a new trial will be required.

Experimental Procedures

Materials, specimens, and loading conditions for several series of tests are shown in Table 1 and Fig. 1. A slight curvature along the surface of the specimen in Fig. 1*b* is formed for preventing initiation of cracks at the corners of the specimen. The small notch on the surface of the specimen in Fig. 1*c* is formed by the arc strike. It is a round hole, 50 μm in diameter and 50 μm in depth.

Required data from the measurement of surface cracks are (1) fatigue crack growth rate, da/dN; (2) threshold conditions of fatigue crack growth, ΔK_{TH} and $\Delta\sigma_{TH}$; (3) density of cracks per unit area of the surface; and (4) statistical distribution of crack length.

Technology for the measurement of very small surface cracks has been developed by the authors[5] by the successive surface replica method. A temper coloring method, a natural oxidation method, and a beach mark method have also been successfully applied. Several thousand replicas and microphotographs have been made for the measurement.

Initiation Time, Sizes, and Density of the Surface Cracks Observed

The cycle ratios (N/N_f) for crack initiation, N_i/N_f, are shown on an S-N curve in Fig. 2 for the out-of-plane bending fatigue tests of Material

[5]Kitagawa, H. and Takahashi, S. in *Proceedings*, 53rd Meeting, Japan Society of Mechanical Engineers, No. 760-2, 1976, p. 213.

TABLE 1—*Series of tests and experimental conditions.*

Type of Loads	Rotating Bending		Out-of-Plane Bending		In-Plane Tension	
Initial Notch	Unnotched		Unnotched		A Round Hole Surface Notch (Diameter and Depth, 50 μm each)	
Frequency of load cycle, nearly, Hz	25	50	25		10	
Configuration of specimen	round bar Fig. 1*a*	Fig. 1*a'*	flat plate Fig. 1*b*		flat plate Fig. 1*c*	
Diameter or thickness, mm	8ϕ		3.5		8	
Material (standard or name)	A mild steel (SB22)	B mild steel (SB22)	C mild steel (SAPH38)	D mild steel (SAPH32)	E high strength steel (HT8O)	F weldable structural steel (SM50)
Heat treatment	1203°K (930°C) before machining	1203°K (930°C) after machining	873°K (600°C) in vacuum after machining		as received	893°K (620°C) in vacuum after machining
Yield strength σ_y, MN/m^2 (kg/mm^2)	280 (28.5)	226 (23)	265 (27)	206 (21)	726 (74)	373 (38)
Tensile strength σ_B, MN/m^2 (kg/mm^2)	441 (45)	422 (43)	432 (44)	333 (34)	785 (80)	500 (51)
Fatigue limit of unnotched specimen σ_{max}, MN/m^2 (kg/mm^2)	226 (23) ($R = -1$)	167 (17) ($R = -1$)	211 (21.5) ($R = -0.82$)	183 (18.7) ($R = -0.82$)	569 (58) ($R = 0.035$)	387 (39.5) ($R = 0.025$
Stress ratio in tests $R(= \sigma_{min}/\sigma_{max})$	-1	-1	-1 -0.82 -0.54 -0.33	-1 -0.82	0.03-0.06 minimum stress = 19.6 MN/m^2 (2 kg/mm^2)	0.04
Peak stress in tests, σ_{max} MN/m^2 (kg/mm^2)	226-353 (23-36)	147-216 (15-22)	196-373 (20-38) $\sigma_a = 18 \sim 38$kg/mm^2	181-294 (18.5-30) $\sigma_a = 17 \sim 27$kg/mm^2	314-706 (32-72)	384-432 (39-44)

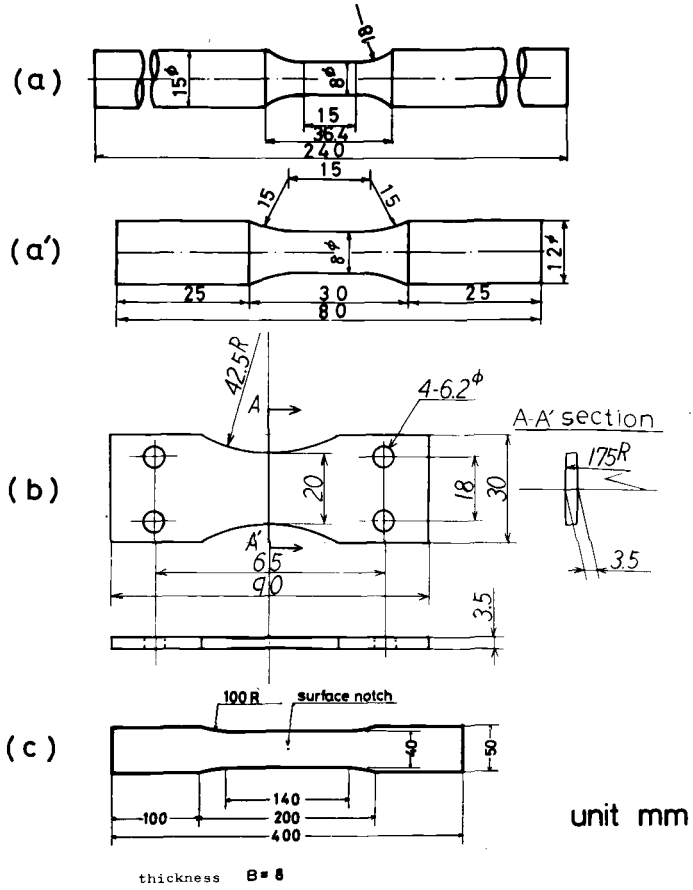

FIG. 1—*Configurations of specimens:* (a) *Specimens for rotating bending fatigue tests (for Material A, mild steel);* (a') *Specimens for rotating bending fatigue tests (for Material B, mild steel);* (b) *specimens for out-of-plane bending fatigue tests;* (c) *specimens for in-plane tension fatigue tests (with a small round hole surface notch).*

C, mild steel, as an example of the data on unnotched smooth specimens. The crack initiation time ($N = N_i$) in this figure is defined for 20 μm in surface length ($2a$). In rotating bending tests of unnotched specimens of Material B, cracks can be observed at $N/N_f = 0.1$. Consequently, even in the fatigue process of an unnotched smooth specimen, surface cracks initiate generally before 10 to 20 percent of its fatigue life.

After crack initiation, the number of cracks continues to increase up to fracture as shown in Fig. 2, by the curves of density of the number of cracks per unit area, 1 mm^2. At higher stress levels the number of cracks increases rapidly and can attain a very high density, more than several

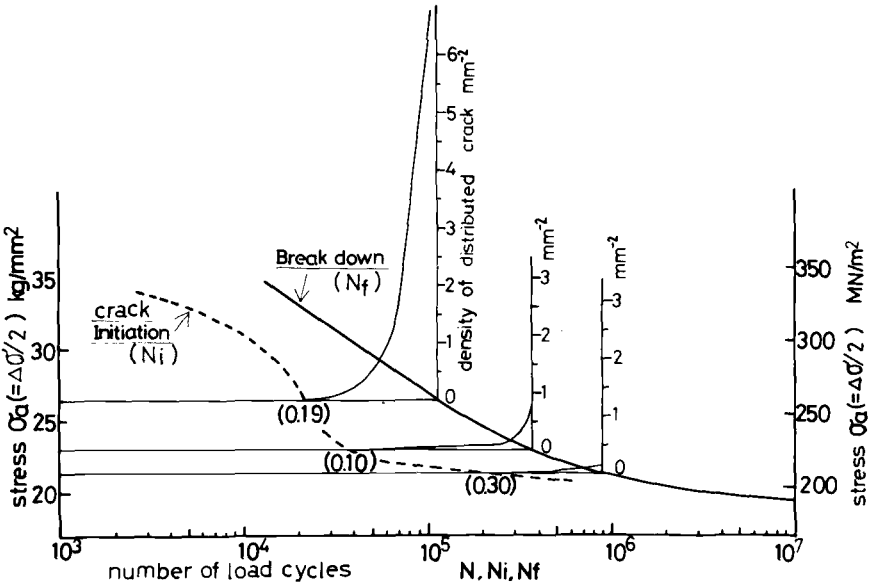

FIG. 2—*Initiation of cracks and increase of the number of cracks per unit area on a smooth surface at various stress levels in fatigue of Material C, mild steel* (R = −0.82). *The numbers in parentheses indicate cyclic ratio of loads,* N_i/N_f *or* N/N_f. N_i *is the number of cycles for the initiation of the crack (the load cycles when a 20-μm-length crack was found the first time);* N_f *is the number of cycles to fracture and* N *is another specified number of cycles.*

hundred cracks in an area of 1 cm^2, and often the cracks interact or coalesce with each other. At lower stress levels, the number of cracks increases very slowly, and several isolated cracks grow independently somewhat before fracture. An example of the distribution of the small cracks is shown in Fig. 3.

Variations of crack length at various cyclic ratios in specimen fatigue life are shown in Fig. 4, displayed by statistical logarithmic normal distribution graphs. This figure shows that the surface lengths, $2a$, of most cracks do not exceed 1 mm, even just before or at the breakdown of the specimen. The length of most cracks at $N/N_f = 0.5$ is less than 0.5 mm. This means that the crack lengths along the surface increase very slowly.

It is deduced from these figures that most of the fatigue life of a smooth unnotched specimen is occupied by the growth of very small surface cracks except at the fatigue limit stress level. Also, these figures suggest that small surface cracks can continue to grow even below the ΔK_{TH} level for a large through-thickness crack.

Similar behavior can be recognized for surface cracks which start from a very small notch on the surface of tension fatigue loaded specimens of

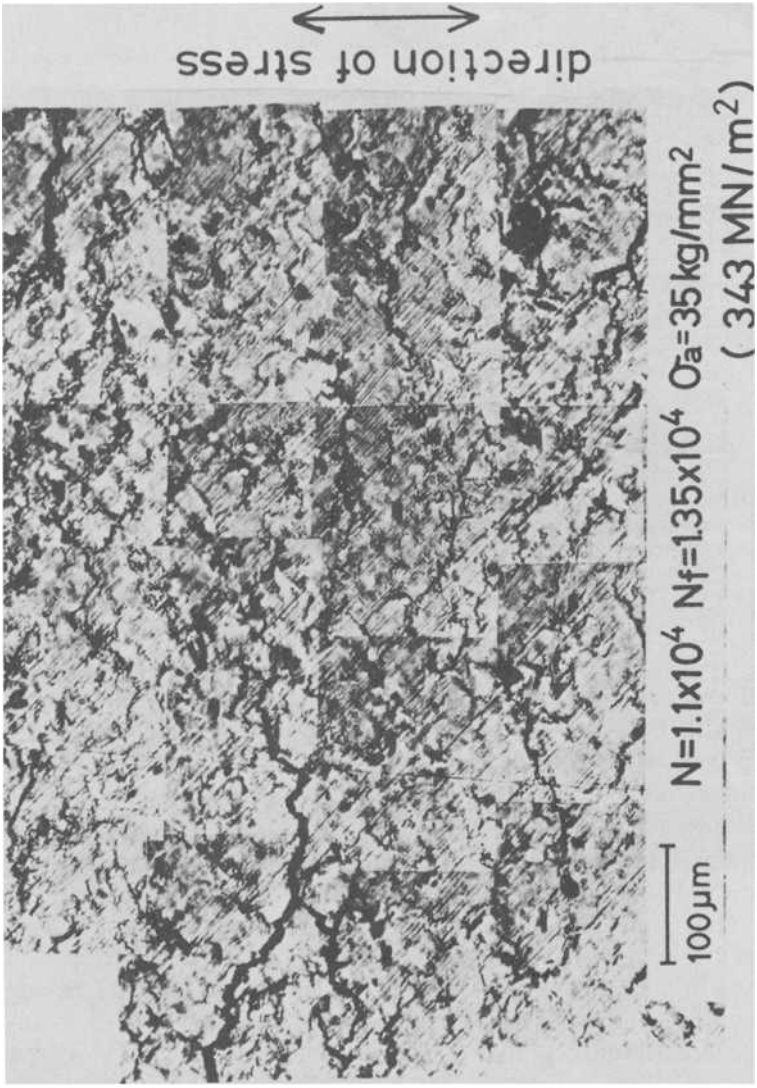

FIG. 3—*Many small fatigue cracks distributed on the smooth flat surface of Material C, mild steel; half stress range* $\Delta\sigma/2 = 343\ MN/m^2$ *(35 kg/mm*^{2}*), number of load cycles* $N = 1.1 \times 10^4$.

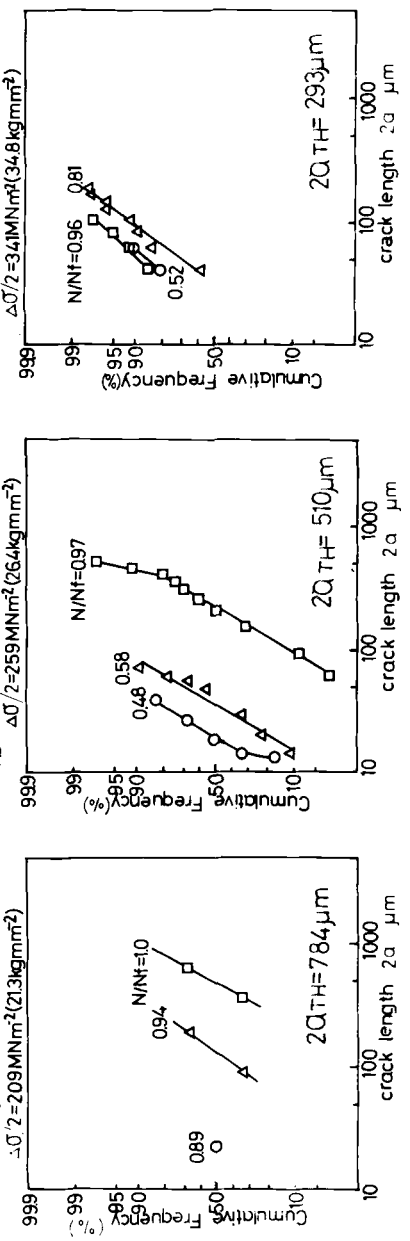

FIG. 4—*Statistical distributions of sizes (=2a) of fatigue cracks on the smooth surface of Material C, mild steel (on log-normal statistical diagrams). $2a_{TH}$ is the threshold crack length for fatigue crack growth given by the formula: $\Delta K_{TH} (=15.5\ kg \cdot mm^{-3/2}) = 1.03 \times (2/\pi) \times \sigma_a \sqrt{\pi a}$. σ_a is the stress amplitude tested.*

Materials E and F, as shown in Fig. 5. In this case, one crack initiates and grows.

Limitation of Dependence of Growth of Small Surface Cracks on Linear Fracture Mechanics

For the surface cracks which start from a small surface notch on the specimens of Materials E and F, the threshold conditions for fatigue crack growth were obtained by a very slow load-down method. The results are shown in Fig. 6. For a wide range of crack lengths, the values obtained for the ΔK_{TH} of surface cracks are constant and equal to the value for a large through-crack. The values of ΔK_{TH} for small surface cracks, however, do not follow the constant ΔK_{TH} rule anymore, and the threshold condition approaches gradually the constant stress condition, $\Delta\sigma_{TH}$ = constant. The values of $\Delta\sigma_{TH}$ were determined as the average stress of the whole cross section of the tension fatigue loaded specimen. The lower limit value of the surface crack length which follows the constant ΔK_{TH} rule decreases with increase of the fatigue limit for unnotched smooth specimens. The lower limit value mentioned is the crack length at which the $\Delta\sigma_{TH}$ value or ΔK_{TH} value does not follow the constant ΔK_{TH} rule and begins to approach gradually the constant $\Delta\sigma_{TH}$ line.

Nonpropagating small surface cracks were observed on the surface of the rotating bending fatigue specimens of Material A at the fatigue limit stress level. The data for these cracks are plotted in Fig. 6 with an assumed value of K.

Figure 6 as well as Figs. 2–4 show that small surface cracks can grow even below the ΔK_{TH} level.

Figure 7*a* is a ΔK - da/dN diagram for very small to normal-size surface cracks which started from a very small surface notch on the repeated tension loaded specimen ($R \approx 0$) of Material F. The peak value of the average stress in these specimens attained or exceeded the yield stress of the material tested. It is deduced from this figure that the crack growth rate of the surface crack which propagates in the yielded field is higher than the growth rate predicted from the ΔK - da/dN relation for a large through-crack.[6] Particularly for very small cracks, the value of da/dN is somewhat higher than the extension of the ΔK - da/dN relation.

A similar tendency appears more clearly in the growth of the small surface cracks which started on the smooth surfaces subjected to stresses at $R = -1.0 - -0.82$, as shown in Fig. 7*b* and *c*. Although the values of K for these surface cracks cannot be rigorously determined and a conventional alternative $[(1.03)(2/\pi)(\Delta\sigma)\cdot\sqrt{\pi a}\,]$ is used, the tendency that the da/dN of sufficiently small cracks is higher than that of larger cracks

[6]The crack which is growing in the elastic stress field.

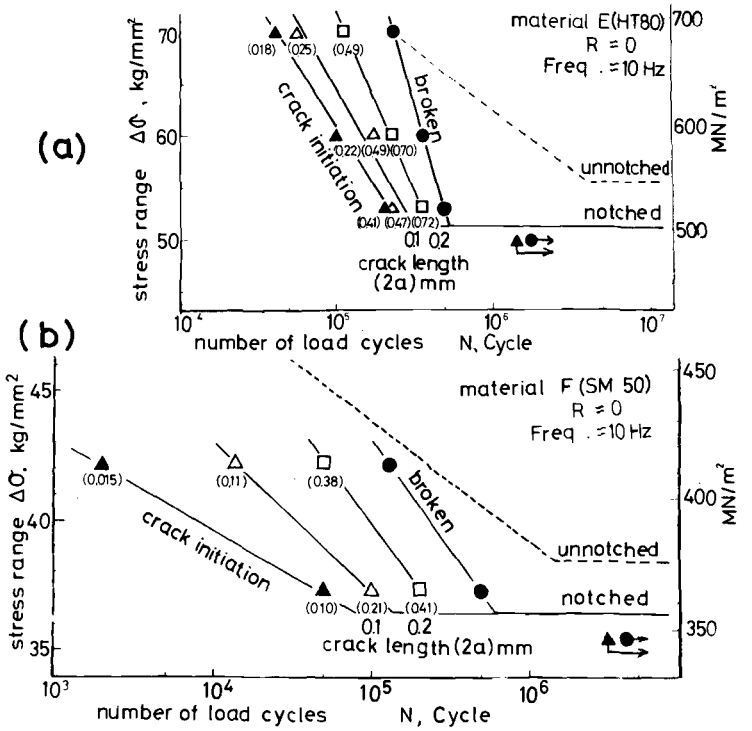

FIG. 5—*Initiation of a crack from a small round-hole surface notch and growth of the crack length along the surface at various stress levels.* (a) *Material E, high-strength steel (HT80);* (b) *Material F, weldable structural steel (SM50). The numbers in parentheses indicate* N_i/N_f *or* N/N_f. N_i *is the number of cycles for the initiation of the crack;* N_f *is the number of cycles to fracture and* N *is another specified number of cycles.*

Material	*E (HT80)*				*F (SM50)*		
Stress range tested $\Delta\sigma$ *(kg/mm²)*	*70*	*60*	*53*	*50*	*42.2*	*37.4*	*35.5*
Threshold crack length $2a_{TH}$ *(mm)*	*73*	*99*	*127*	*142*	*198*	*254*	*282*
Load cycle N *(cycles* $\times 10^4$*)*	*3.5*	*17.0*	*30*	...	*9.5*	*41*	...
N/N_f	*0.15*	*0.48*	*0.62*	...	*0.70*	*0.81*	...

$2a_{TH}$ *is the threshold crack length for fatigue crack growth given by the formula:* ΔK_{TH} $(=15.5\ kg \cdot mm^{-3/2}) = 1.03 \times (2/\pi) \times \Delta\sigma \sqrt{\pi a}$. $\Delta\sigma$ *is the stress range tested.*

seems to be recognized.

It also appears in Fig. 7*b* and *c* that separate ΔK - *da/dN* relations can be obtained for different materials and different (*average*) stress levels. In all of these cases, it seems that small surface cracks can grow below the estimated ΔK_{TH} level for a large through-crack.

From the results in this section, some special consideration or formulation might be required for the small surface crack which starts on the

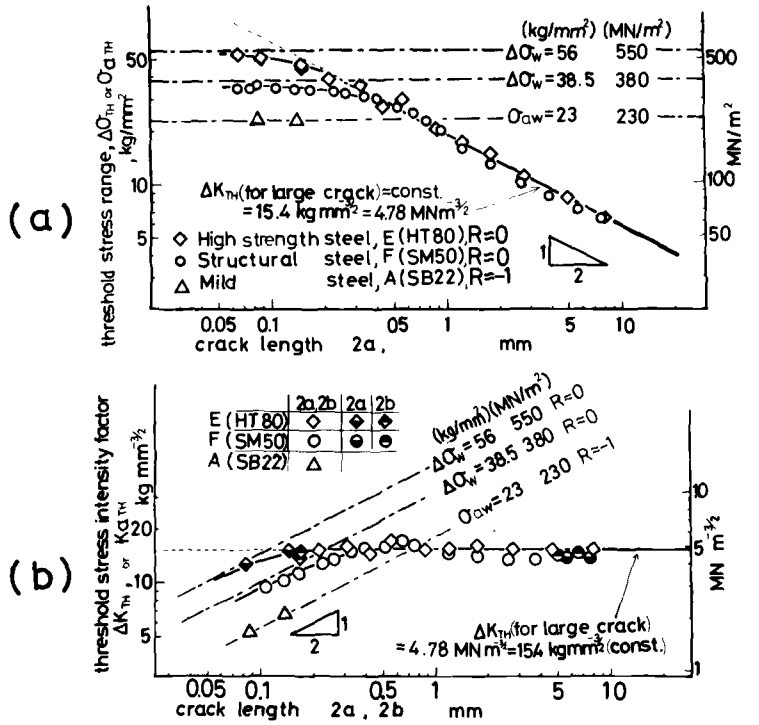

FIG. 6—*Dependence of threshold conditions for fatigue crack growth of a surface crack on stress-intensity factor range, and its limitation on small cracks. Suffix* w *means the fatigue limit of unnotched specimens.* 2a *represents the crack length at the specimen surface and* b *represents the crack depth of surface crack respectively.* (a) *Threshold conditions based on the stress range,* $\Delta\sigma_{TH}$ *or* σ_{aTH}. (b) *Threshold conditions based on stress-intensity factor range,* ΔK_{TH} *or* K_{aTH}. $K_{aTH} = \Delta K_{TH}/2$.

cyclically stressed surface, or the surface crack which is growing in the field subjected to cyclic plastic strains.

Relation of Cyclic Strains and Growth of a Small Surface Crack (Proposition of Cyclic Strain-Intensity Factor Range, ΔK_ϵ)

The cyclic stress-strain hysteresis was measured intermittently with strain gages (0.2 mm in gage length and 1.5 mm in width) throughout the fatigue tests. Both the total and plastic strain ranges, $\Delta\epsilon_t$ and $\Delta\epsilon_p$, obtained from the hysteresis curve, stabilized within the first 10 to 20 percent of fatigue life, as shown in Fig. 8. The $\Delta\epsilon_t$ or $\Delta\epsilon_p$ in the stabilized state shows an exponential relationship with the stress range, $\Delta\sigma$, as shown in Fig. 9.

ΔK for the small surface crack is given by

$$\Delta K = \Delta\sigma\sqrt{\pi a}\cdot f(a) \tag{1}$$

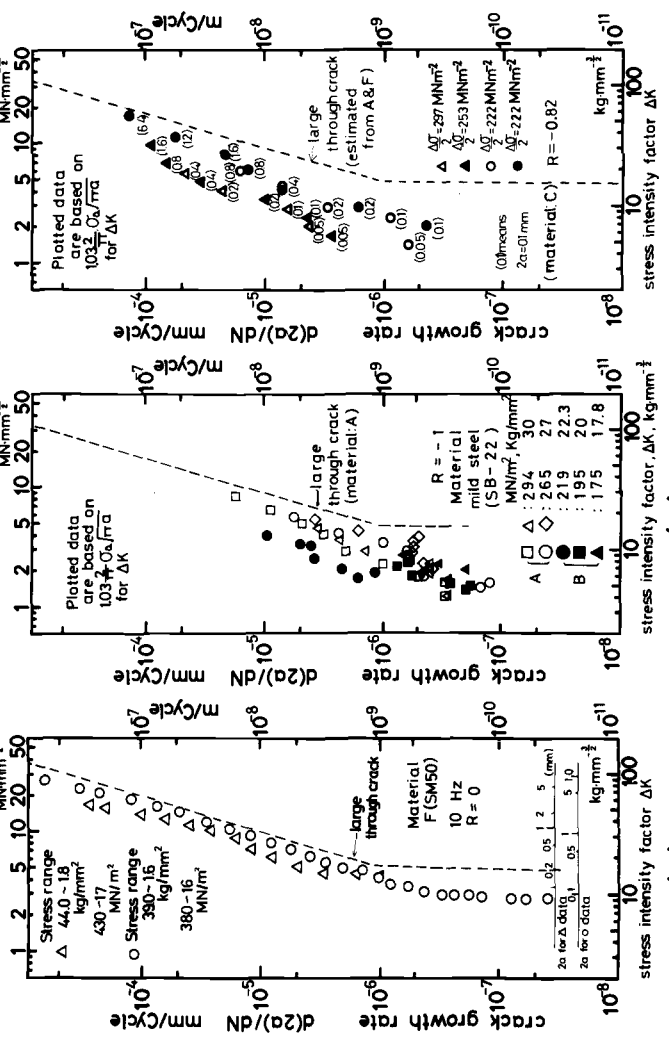

FIG. 7—*Dependence of the growth rate of small fatigue surface cracks upon the stress-intensity factor range,* ΔK, *above and below the* ΔK_{TH} *level (of a large through-crack), which varies with stress range for the material tested.* (a) *Material F, weldable structural steel, SM50.* (b) *Materials A and B, mild steel.* (*Crack lengths measured are 0.03–1.0 mm for* □ *data, 0.03–1.1 mm for* ○ *data, 0.10–0.51 mm for* ● *data, 0.09–0.40 mm for* ■ *data, 0.2–0.4 mm for* ▲ *data.*) (c) *Material C, mild steel.*

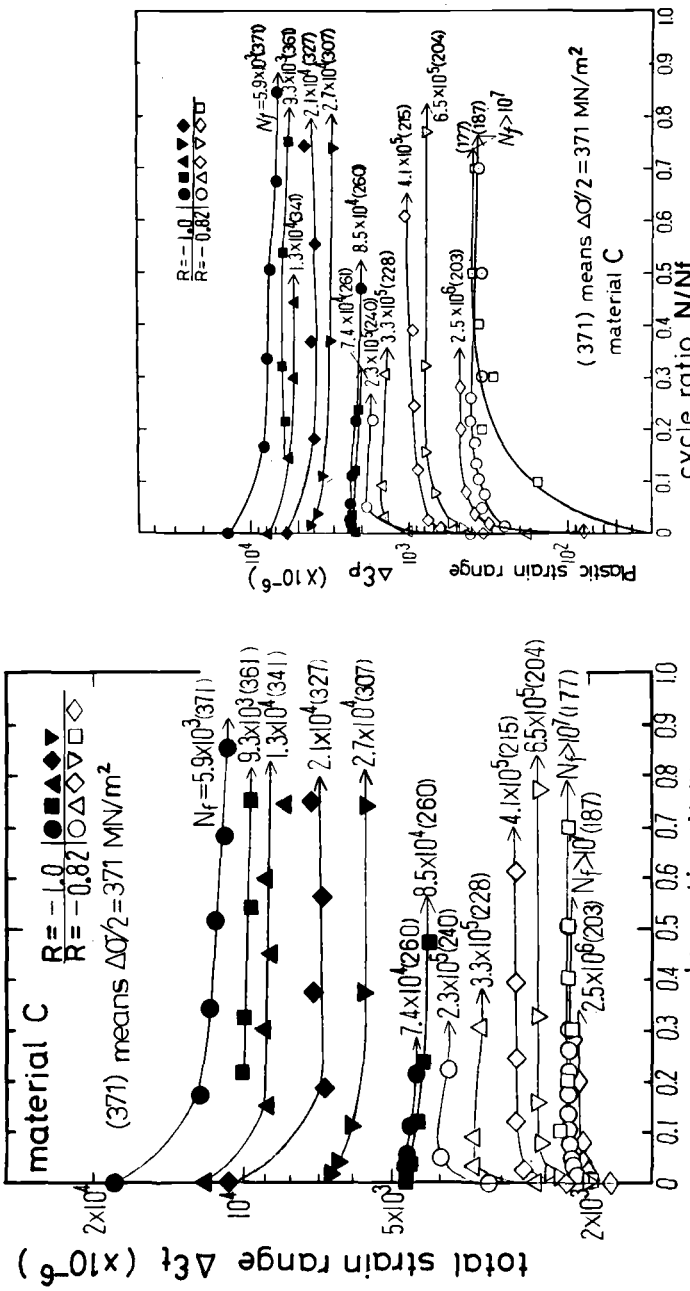

FIG. 8—*Stabilization of cyclic strain range Δε in the early stage of fatigue life.* N_f *(earlier than 20 percent of* N_f*).*

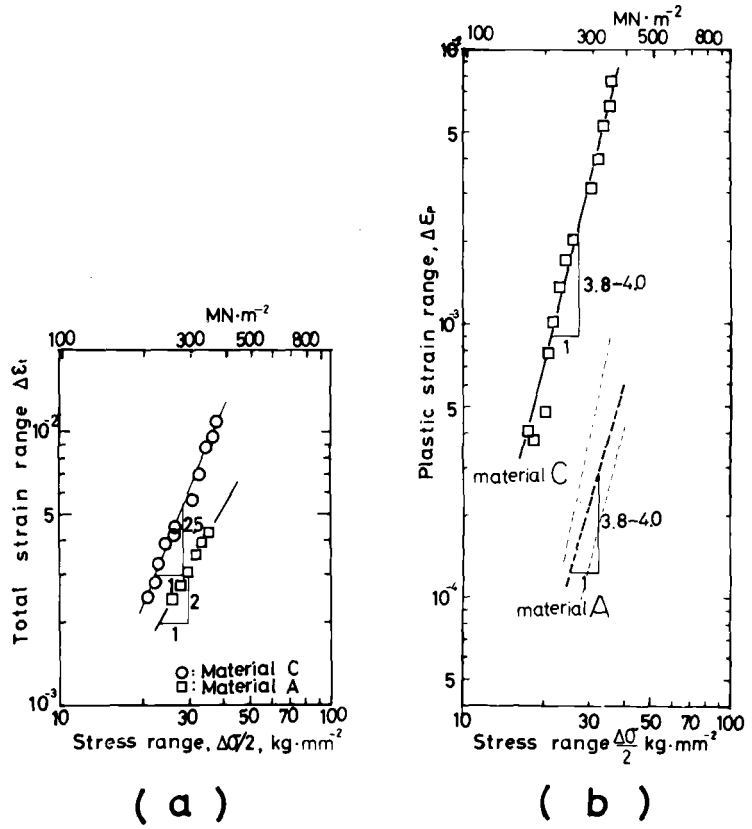

FIG. 9—*Relation between cyclic stress range, $\Delta\sigma$, and cyclic strain range, $\Delta\epsilon$. Along the lines of Material A in Fig. 8*b *a scatter band is indicated because their absolute values are very low and accuracy of measurement is not so high compared with Material C.*

Assuming the conventional linear relation between log (ΔK) and log (da/dN) for the surface crack, da/dN is expressed as

$$da/dN = C(\Delta K)^m = C(\Delta\sigma\sqrt{\pi a})^m [f(a)]^m \tag{2}$$

As the experimental data of log $(\Delta\sigma\sqrt{\pi a})$ and log (da/dN) for the small surface cracks fall on three straight lines for three different stress levels in the tests, respectively, as shown in Fig. 10*a* the function $f(a)$ is given as a constant. As the factor C in Eq 2 depends on the stress level, $\Delta\sigma$, as shown in Fig. 10*b*, Eq 3 is obtained

$$C = C_0 \cdot (\Delta\sigma)^p \text{ [putting } f(a) = 1] \tag{3}$$

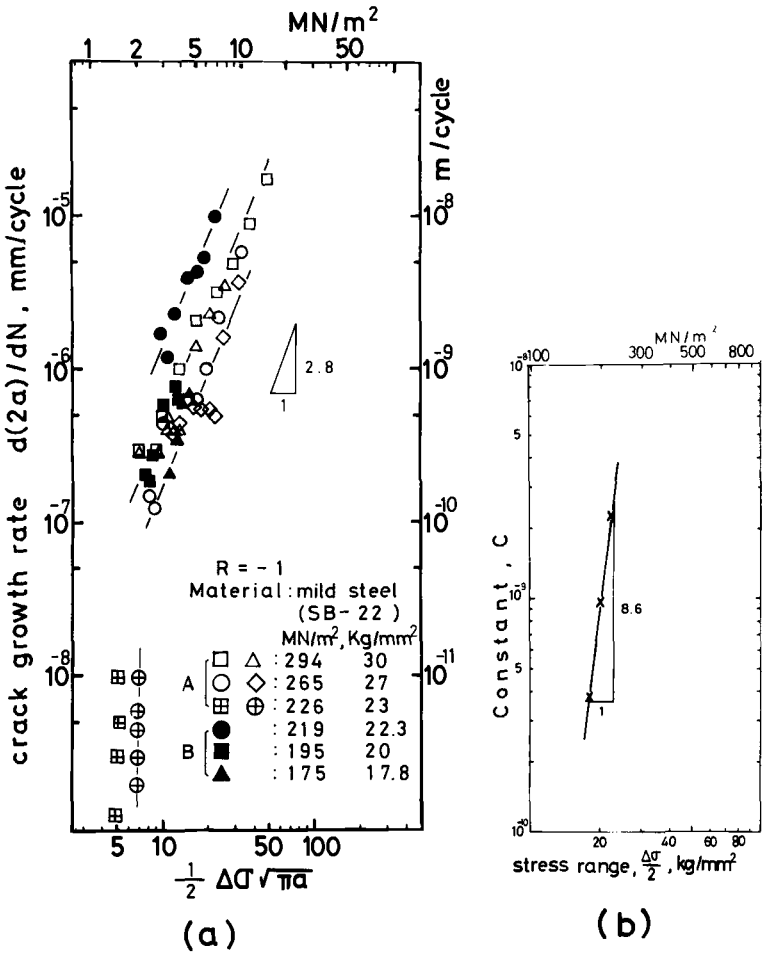

FIG. 10—*Determination of* f(a), m, *and* C *in the Eq 2;* $da/dN = C[\Delta\sigma\sqrt{\pi a}\, f(a)]^m$.

where C_0 and P are constants; da/dN is given by Eqs 2 and 3

$$da/dN = C_0 \cdot (\Delta\sigma)^p (\Delta\sigma\sqrt{\pi a})^m = C_0 \cdot (\Delta\sigma)^p (\Delta K)^m \tag{4}$$

These constants can be experimentally determined for each series of tests; for example, $m = 2.8$, $p = 8.6$, and $C_0 = 2.47 \times 10^{-21}$ (in kg/mm units).

Considering the relation between $\Delta\epsilon$ and $\Delta\sigma$ as shown in Fig. 9, the cyclic strain range $\Delta\epsilon$ can be generalized as follows

$$\Delta\epsilon = \eta \cdot (\Delta\sigma)^n \tag{5}$$

where η is a constant and n is the exponent in Fig. 9. Referring to the

experimental formula, Eq 4, with ΔK_ϵ which is proposed to be expressed as Eq 6, an expression for da/dN is proposed as follows

$$\Delta K_\epsilon = \Delta\epsilon\sqrt{\pi a} = \eta \cdot (\Delta\sigma)^n \sqrt{\pi a} \tag{6}$$

$$da/dN = C_1 (\Delta K_\epsilon)^{m_1} \tag{7}$$

$$= C_1 [\eta \cdot (\Delta\sigma)^n \sqrt{\pi a}]^{m_1}$$
$$= C_1 \cdot \eta^{m} \cdot (\Delta\sigma)^{(n-1)m_1} (\Delta\sigma\sqrt{\pi a})^{m_1}$$
$$= C_1 \cdot \eta^{m} \cdot (\Delta\sigma)^{(n-1)m_1} (\Delta K)^{m_1} \tag{8}$$

when $m_1 = m$ as shown in Figs. 10*a* and 11*c*, a good agreement can be obtained between the experimental formula, Eq 4, and the proposed formula, Eq 8, on case $n \cong 4$ as shown in Fig. 9*b*.

Figure 11*a* and *b* are the examples of the expressions of Eq 7 for $\Delta K_{\epsilon t}$ and $\Delta K_{\epsilon p}$, respectively, in which measured values for $\Delta\epsilon$ are used. Figure 11*c* is another example in which the measured values for $\Delta\sigma$ and n obtained from Fig. 9, for example, were used, and the values of $\Delta\epsilon$ were calculated by Eq 5; η was assumed to be 1.0. In these cases, where the effects of the difference of stress levels and sometimes the difference of materials or loading conditions (rotating bending and out-of-plane bending) can disappear, most data for the various tests fall on a fairly narrow straight band. The procedures for the arrangement used in Fig. 11*c* seem to be better for engineering use.

This ΔK_ϵ formula as shown in Eq 7 will be expected to be used as one of the formulas for predicting the crack growth rate of a small surface crack on a smooth surface subjected to cyclic strains. For general application, however, more data should be accumulated.

Cyclic Strains, Slip Lines, and Crack Growth

Growing small surface cracks are usually surrounded by the area composed of slipped and nonslipped areas, as shown in Fig. 12. The severely slipped microcrack area is considered to be highly strained locally, say, above yield stress.

For quantitative understanding of the phenomena stated in the previous sections, the number of the grains in which any slip-line area can be observed was counted. The ratio of the number of slipped grains to the number of total grains of λ is taken as a countable measure of the rate of slip.

Data of λ for mild steels (Materials A and B) are shown in Fig. 13 as functions of the stress range. The values of the gradient (the exponent is the relation $\Delta\sigma$ and λ) in Fig. 13 are 3.8 to 4.0. These values are nearly equal to some of the exponents in the relation of the cyclic strain range ($\Delta\epsilon_p$) and the stress range ($\Delta\sigma$ in Fig. 9*b*). Then, $\Delta\epsilon_p$ is proportional to λ. In such a case, macroscopically measured strain range seems to express the rate of local slips on the surface subjected to cyclic strain.

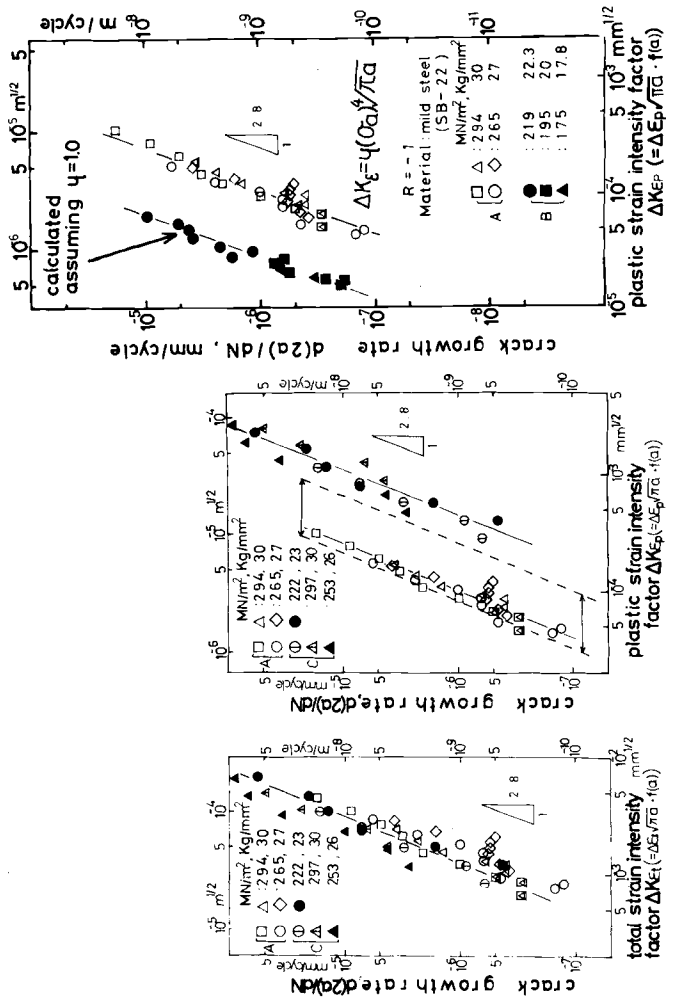

FIG. 11—*Dependence of fatigue crack growth rate of a small surface crack upon the strain intensity factor range. (a)* $\Delta K_{\epsilon t}$ - da/dN *relation obtained by the measured values of* $\Delta\epsilon_t$ *data for Materials A and C.* (b) $\Delta K_{\epsilon p}$ - da/dN *relation obtained by the measured values of* $\Delta\epsilon_p$ *data. Along the lines of Material A a scatter band is indicated, corresponding to the scatter band shown in Fig.* 8b. (c) $\Delta K_{\epsilon p}$ - da/dN *relation obtained by the measured values for* $\Delta\sigma$ *and* n *(obtained from Fig. 9, for example). For Material A,* $\Delta K_{\epsilon p}$ *values are calculated from* η *and* $\Delta\sigma$ *given by the central broken line in Fig.* 9b.

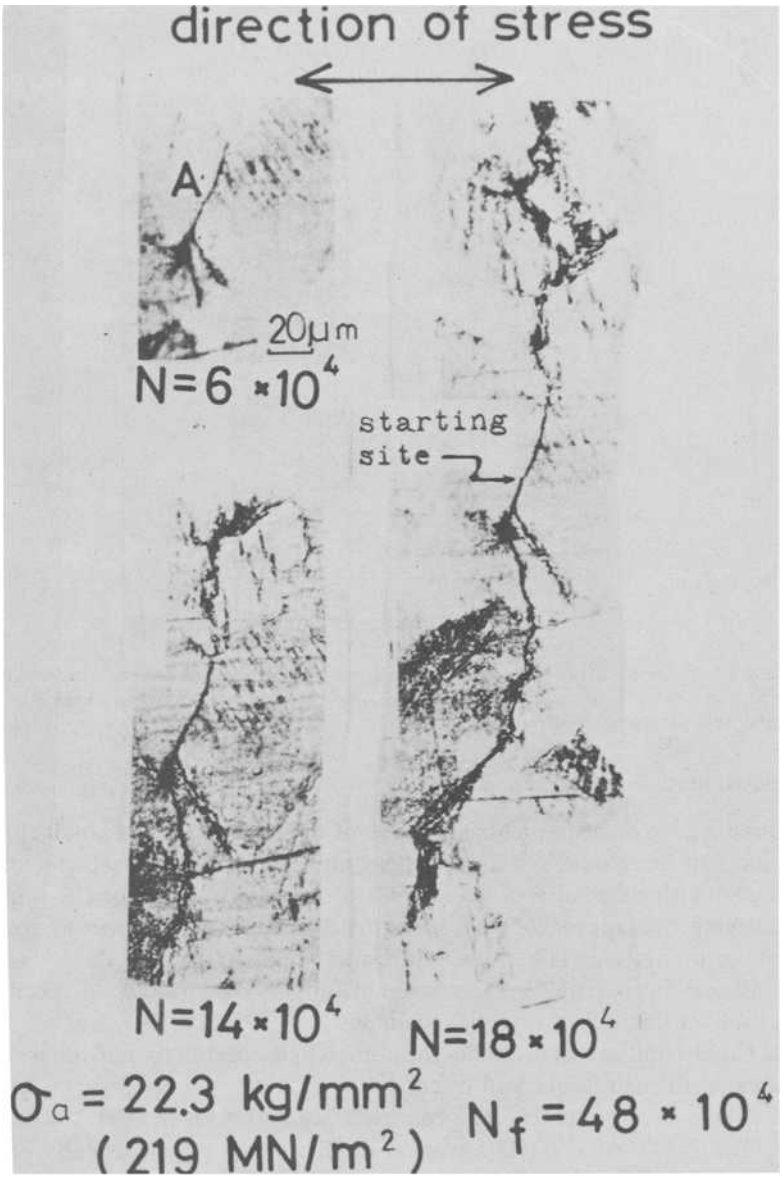

FIG. 12—*Growth of a small surface crack through the field enriched with slipped grains on Material B, mild steel; stress range* σ_a $(=\Delta\sigma/2)$ $=$ *219 MN/m*^{2} *(22.3 kg/mm*^{2}*), number of load cycles* N $= 6 \times 10^4$, 14×10^4, 18×10^4.

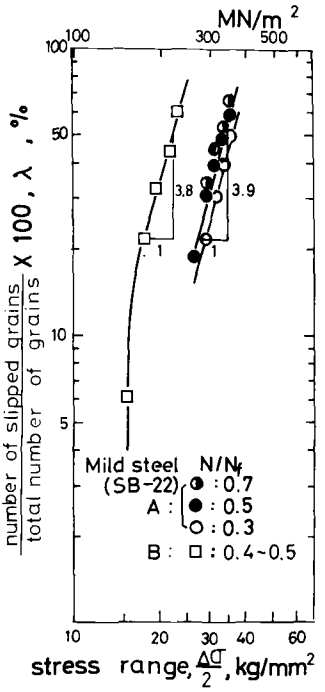

FIG. 13—*Relation between half cyclic stress range, $\Delta\sigma/2$ (=stress amplitude σ_a), and slipped grain ratio, λ, of mild steel, Materials A and B.* λ = [*number of slipped grains*]/[*number of total grains*] × *100.*

Conclusions

Quantitative measurements are made of the microcracks or small surface cracks, slip lines, and strain behaviors on the surface of steel specimens, with and without a micronotch subjected to cyclic strains, for the purpose of unifying two approaches based on fracture by crack growth and cyclic strain accumulation. The important results are as follows.

1. Cracks initiate at the early stage of fatigue life on notched specimens and even on unnotched smooth specimens.

2. Cracks initiate densely on the unnotched specimens and density increases up to coalescence and fracture.

3. A small surface crack can grow even below the ΔK_{TH} level.

4. The ΔK - da/dN relation of a small surface crack depends on the stress level for the test. The crack growth rate of a small surface crack is higher than the value predicted from the ΔK - da/dN relation for a large through-crack.

5. There is a simple relation between the ratio of the number of slipped grains to number of total grains, λ, and the stress range $\Delta\sigma$, and accordingly between λ and cyclic strain range $\Delta\epsilon$ ($\Delta\epsilon_t$ or $\Delta\epsilon_p$).

6. It is suggested that the crack growth rate of a small fatigue surface crack follows $da/dN = C\,(\Delta K_\epsilon)^m$, where ΔK_ϵ is the cyclic strain-intensity factor range, $\Delta\epsilon\sqrt{\pi a}\,f(a)$, and $\Delta\epsilon$ is the total or plastic strain range ($\Delta\epsilon_t$ or $\Delta\epsilon_p$).

7. The main differences between the crack which started from a small surface notch and the crack starting on the smooth surface are as follows: First, the crack initiates much earlier in the notched specimen particularly at lower stress levels. This conclusion is reached from the results that the cyclic ratios for initiation are almost the same and fatigue lines of notched specimens are much shorter. Second, at higher stress levels, only one crack contributes to fracture even in the specimen with the micronotch; in the unnotched specimen, however, many cracks initiate, grow, and coalesce to fracture.

Acknowledgment

The authors appreciate the cooperation of Prof. Chang-Soo Kang, Assistant Prof. R. Yuuki, Mr. K. Shigaki, and Mr. T. Ono, and also the suggestions and discussion by Prof. Emeritus H. Suzuki and Mr. M. Izumitani.

DISCUSSION

G. Sih[1] (*discussion*)—The metal fatigue process can be divided into two stages, namely, a stage of crack initiation and a stage of crack propagation. The delineation between these two stages, however, is not always clear in terms of specifying "a crack size." It can often be quite arbitrary, depending on the opinion of the investigator. Although the change from crack initiation to propagation has been discussed on a descriptive basis[2] with reference to crack growth behavior, only a few investigations have dealt with the quantitative aspects of relating the two fatigue stages. There are conceptual difficulties associated with determining the duration of crack initiation as this complicated physical process depends to a large extent on the combination of several factors such as specimen geometry, loading condition, and environment, and it is not always possible to sort out the influence of these individual factors.

The paper by Forsyth (see footnote 2) offers a quantitative analysis in an attempt to bridge the gap between crack initiation and propagation.

[1] Institute of Fracture and Solid Mechanics, Lehigh University, Bethlehem, Pa. 18015.

[2] Forsyth, P. J. E. in *Proceedings*, Crack Propagation Symposium, Cranfield, U. K., Vol. 1, 1961, pp. 76-94.

Suggested is an intermediate stage, during which period the growth of microcracks on the surface of the specimen is monitored in terms of the plastic stress-intensity factor range, $\Delta\epsilon_p$. Crack initiation is referred to a cumulative strain model while crack propagation is associated with the growth of a large through-crack as treated in the sense of conventional fracture mechanics. Experimental data for several grades of mild and structural steel are presented and tend to imply that the growth rate of small surface cracks and large through-cracks can be assessed quantitatively by da/dN as a function of the strain-intensity factor range ΔK_ϵ or the stress-intensity factor range ΔK.

As a general remark, the simple crack growth rate equation

$$\frac{da}{dN} = C(\Delta K)^m \tag{9}$$

is likely to be of limited use in quantifying crack initiation as connected with crack propagation. First of all, Eq 9, as it was originally proposed,[3] refers to the growth of a dominant crack at the macroscopic level where the constants C and m reflect the bulk mechanical behavior of the material. (Other crack growth rate relations similar to Eq 9 are also available and can be found in a paper by Kocanda.[4]) The range of stress intensity factor ΔK when expressed in the form

$$\Delta K = f(a)\,\Delta\sigma\sqrt{\pi a} \tag{10}$$

further implies the assumption of linear elasticity.[5] The authors adopt the da/dN versus ΔK relation to investigate the growth of surface microcracks. With regard to their analytical model, the following remarks are offered for discussion.

1. Since the authors assume C in Eq 3 of their paper to depend on the stress range $\Delta\sigma$, there is really no reason to introduce the stress-intensity factor range ΔK. Equation 4 when written as

$$\frac{da}{dN} = C_0\pi^{m/2}(\Delta\sigma)^{p+m}a^{m/2} \tag{11}$$

is basically of the form

$$\frac{da}{dN} = f(\Delta\sigma, a) = C_1(\Delta\sigma)^{m_1}a^{n_1} + \ldots \tag{12}$$

[3]Paris, P. C. and Erdogan, F., *Journal of Basic Engineering*, Vol. 88, 1963, pp. 528-535.

[4]Kocanda, S. in *Fatigue and Fracture*, Vol. 1, Sijthoff and Noordhoff International Publishers, Leyden, The Netherlands, 1978.

[5]The relation $K = \sigma\sqrt{\pi a}$ is a result based on the linear theory of elasticity.

2. The assumed form of the strain-intensity factor range

$$\Delta K_\epsilon = \Delta\epsilon\sqrt{\pi a} \tag{13}$$

tends to implicate linear elasticity[6] and is somewhat inconsistent with the assumption that the material undergoes cyclic plastic strain, $\Delta\epsilon = \eta\,(\Delta\sigma)^n$. Again, it may be more consistent simply to start with

$$\frac{da}{dN} = g(\Delta\epsilon, a) = C_2\,(\Delta\epsilon)^{m2}\,a^{n2} + \ldots \tag{14}$$

3. It appears that the proposed model considers only the exposed length of the surface crack with no consideration given to its depth of penetration into the material. The exposed length is not necessarily a true indication of the fractured surface or damage of the material. In this connection the conclusion stated in the paper and the results shown in Fig. 6 on the growth rate of microcracks being greater than or close to that of a large crack are subject to reexamination.

While it is informative to associate parameters such as λ, measuring the microscopic damage of the material, with the stress range $\Delta\sigma$ or strain range $\Delta\epsilon$, there is a lack of a consistent model which can quantify the complex processes involved in metal fatigue. The proposed form of *da/dN* does not appear to be suitable for defining crack initiation since there is a perceptional difficulty associated with specifying crack initiation in terms of a crack size.

K. Miller[7] (*discussion*)—In your small notches, Professor Kitagawa, have you monitored the decreasing crack propagating rate as the crack length increased? Have you got curves of the decreasing crack propagating rate as the crack length increased?

T. Yokobori[8] (*discussion*)—I am not quite sure whether the critical stress-intensity factor determined on smooth specimens by the usual method corresponds to actual ΔK_{TH} in the *da/dN* versus ΔK diagram. Concerning the threshold stress-intensity factor, I think the crack concerned should be the one which eventually leads to catastrophic final fracture. Since 1966 we have carried out a series of experimental works on the initiation and the initial growth of fatigue microcracks in smooth

[6]In the case of a power-hardening elastic-plastic material, the exponent on a in the plastic strain-intensity factor expression is different from one half.

[7]Professor, Department of Mechanical Engineering, University of Sheffield, Sheffield, U.K.

[8]Professor, Department of Mechanical Engineering, Tohoku University, Sendai, Japan.

specimens. For the case of high-strength eutectoid steel[9] and high-hardened heat-treated ball bearing steel (Fig. 14),[10] good data have been obtained. Especially, for the former, microcracks leading to final catastrophic fracture initiate mainly from the inclusion on or near the surface. The crack shape is fairly simple as shown in Fig. 15, and thus the value of C and n of the equation of da/dN can be determined, including the threshold region.

On the other hand, for the case of low-carbon, tempered, martensitic steel,[11] microcracks initiate not only from inclusions, but also from many other sites such as the prior austensite grain boundary, packet boundary, and precipitates along the packet boundary, and grow by joining mechanisms. We could trace the plastic replicas taken sequentially during testing back to the initiation stage of any site. In this case, however, the subsurface shape of the microcrack is not so well identified for steel of such a low-strength level. Nevertheless, as far as the power coefficient n is concerned, it could be obtained over the threshold region as shown in Fig. 16.

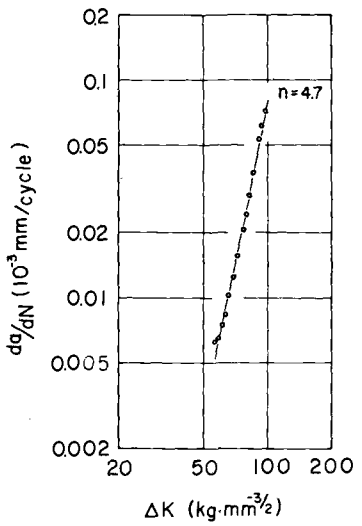

FIG. 14—*Relation between fatigue microcrack propagation rate* da/dN *and stress-intensity factor* ΔK *for heat-treated ball bearing steel HRC 62.*

[9]Yokobori, T., Sawaki, Y., Shono, S., and Kumagai, A., *Transactions,* Japan Institute of Metals, Vol. 17, No. 1, 1976, pp. 1-10; also, Report of the Research Institute, Tohoku University, Sendai, Japan, Vol. 12, No. 2, 1976, pp. 29-54.

[10]Yokobori, T. and Aizawa, T., Report of the Research Institute on Stress and Fracture, Tohoku University, Sendai, Japan, Vol. 13, No. 2, 1977, pp. 75-78.

[11]Yokobori, T., Kuribayashi, H., Kawagishi, M., and Takeuchi, N., Report of the Research Institute on Stress and Fracture, Tohoku University, Sendai, Japan, Vol. 7, No. 1, 1971, pp. 1-23.

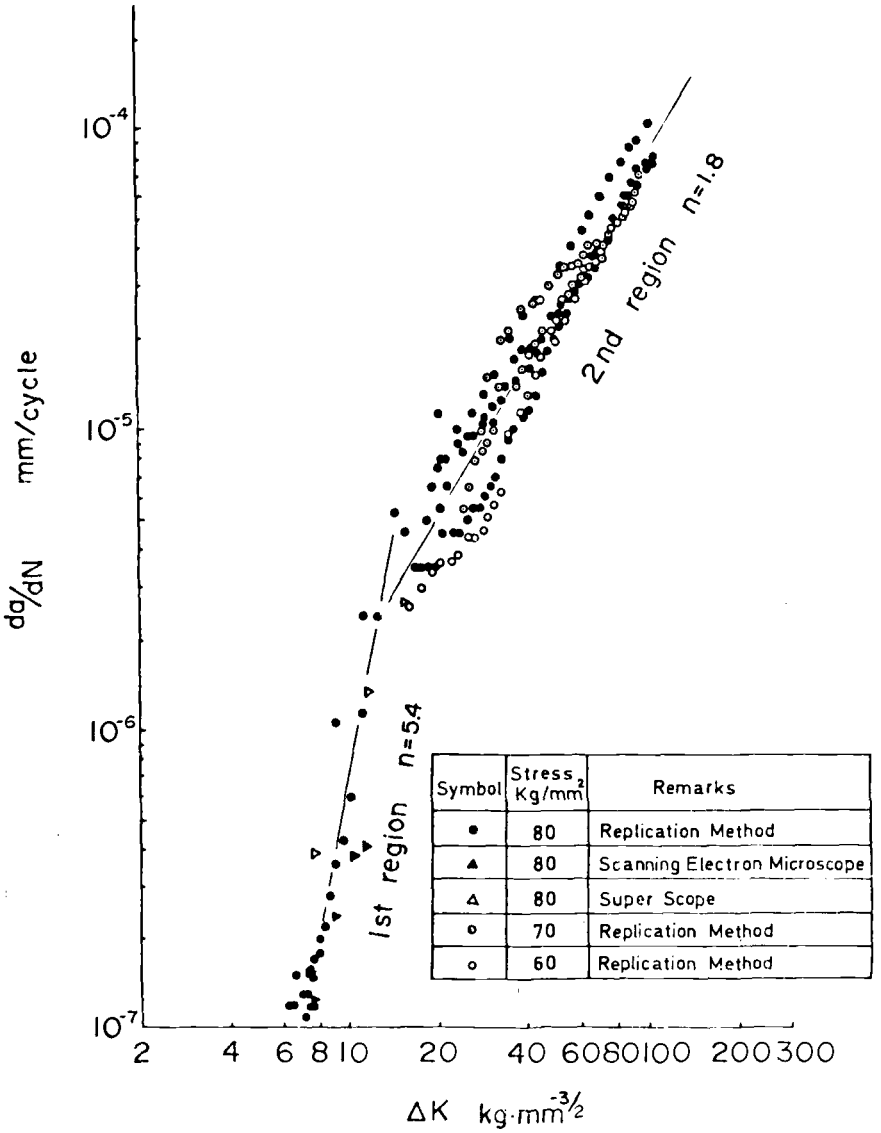

FIG. 15—*Fatigue microcrack propagation rate* da/dN *versus stress-intensity factor* ΔK *on smooth specimen (from Yokobori et al, footnote 9); high-strength euctectoid steel.*

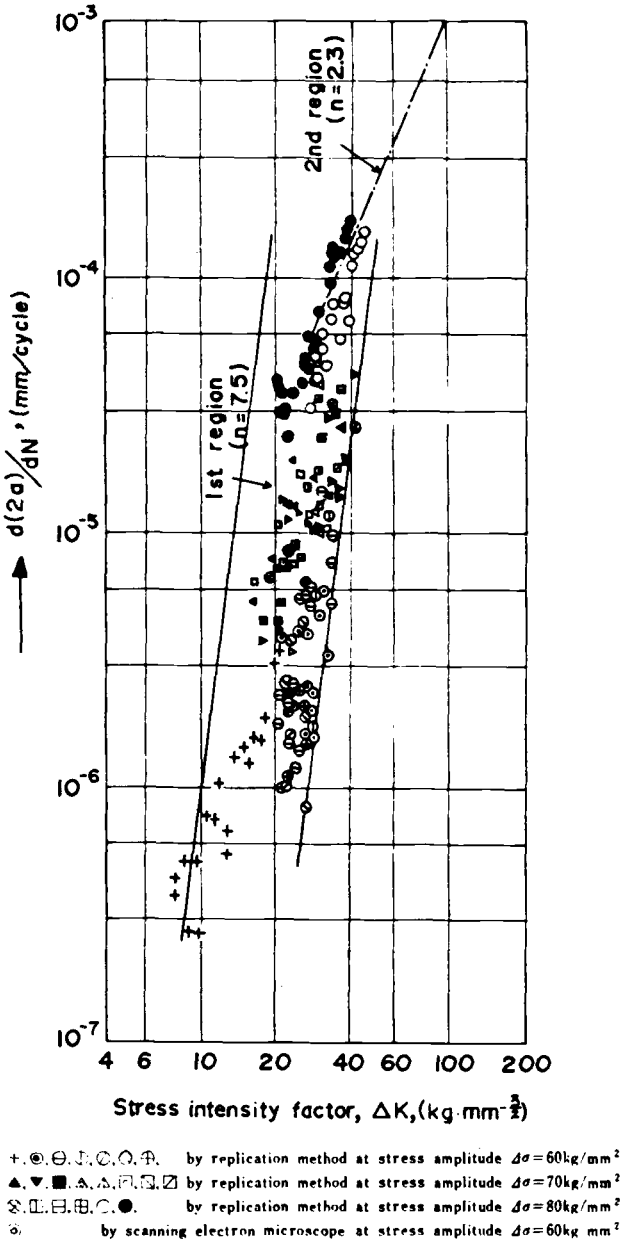

FIG. 16—*Fatigue microcrack propagation rate* da/dN *versus stress-intensity factor* ΔK *on smooth specimen (from Yokobori et al, footnote 11); low-carbon martensitic steel.*

For plain low-carbon steel of even lower strength level,[12] the initiation sites are mainly persitent slipbands and grain boundaries, and the number of initiation sites is smaller, but the situation is similar (Fig. 17) to the low-carbon tempered martensitic steel.

H. Kitagawa, S. Takahashi, C. M. Suh, and S. Miyashita (authors' closure)—Before we set out to answer each question or comment in detail, we wish to express our appreciation to Professors Sih, Miller, and Yokobori for their discussions.

Addressing first Prof. Sih's comments and questions (1 through 4): We believe he is theoretically right, but we also believe the following standpoint is useful, especially in the case of paying attention to the surface microcracks on the unnotched smooth surface.

1. We will not comment here on the accurate initiation period of microcracks, but we would like to emphasize the following most important considerations.

The stage of initiation of fatigue cracks (requiring more than half of fatigue life) used to be predicted by the "law of Manson-Coffins," and the prediction of crack propagation after initiation was carried out using the "power law of ΔK."

Actually, crack initiation being very early, we would like to emphasize that it is possible to neglect the stage of initiation of fatigue cracks, and to predict the whole part of fatigue life by use of propagation alone. This concept is also important from viewpoint of the estimation of the fatigue life by nondestructive inspection (NDI). On the "prediction" and "estimation" stated in the foregoing, the following point is important, as the growth of fine cracks is included in the object of the prediction and estimation. It is very dangerous to predict fatigue life by means of the conventional "power law of ΔK," because the greater part of the fatigue life is occupied by the propagation of microcracks, which are much faster than through-cracks (dotted line) as shown in Fig. 7.

At present, all over the world, the growth rate of fatigue cracks is measured by the use of ΔK. Accordingly, it is convenient for the application of fracture mechanics to this sort of fatigue problem (the micro-fatigue cracks), if the crack growth rate can be characterized by a parameter of the type similar to the stress intensity factor as our formula.

3. Even the propagation rate of the through-crack differs on the specimen surface from the inside. But generally we can use the length of the crack on the surface to calculate the growth rate of the fatigue crack. In the present study, we evaluated the values of ΔK by measurement of the

[12]Yokobori, T., Nanbu, M., and Takeuchi, N. in *Proceedings*, Third Conference on Dimensioning, Hungarian Academy of Sciences, 1968, p. 321; also, Report of the Research Institute on Stress and Fracture, Tohoku University, Sendai, Japan, Vol. 5, No. 1, 1969, pp. 1-17.

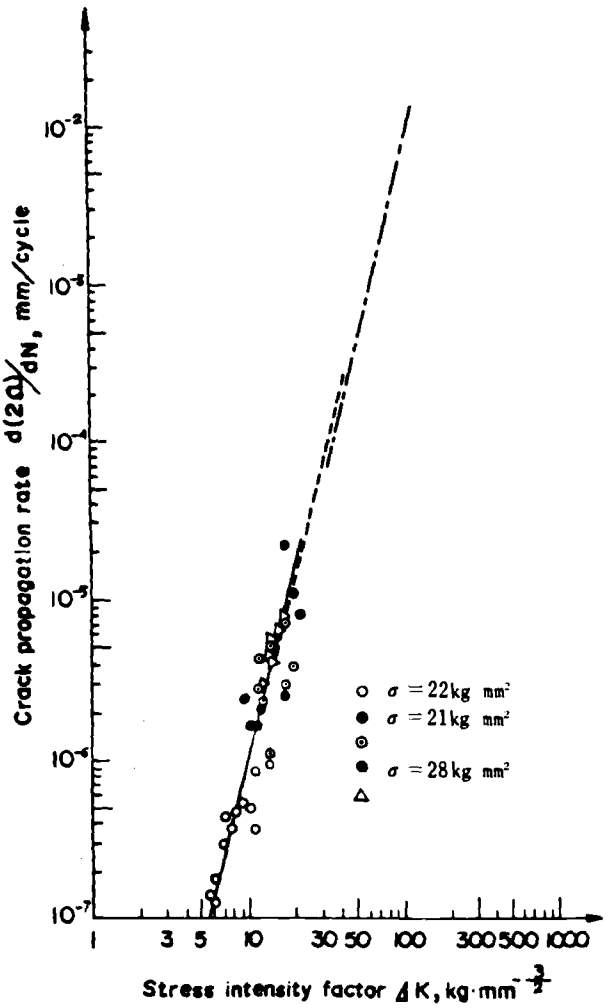

FIG. 17—*Fatigue microcrack propagation rate* da/dN *versus stress-intensity factor* ΔK *on smooth specimen (from Yokobori et al. footnote 12); plain low-carbon steel; dashed line is for the data on cracked specimen of the same material.*

aspect ratio of the crack[13] of the specimen shown in Fig. 1*c*. Of course, we are not satisfied with these results. The aspect ratio of the crack of the specimen of Fig. 1*a* was also measured partly.[14]

[13]Kitagawa, H. and Takahashi, S. in *Proceedings*, Second International Conference on the Mechanical Behavior of Materials, Boston, Mass., 1976, p. 627.

[14]Suh, C. M., Yuuki, R., and Kitagawa, H. in *Proceedings*, Second Pan Pacific Committee for Nondestructive Testing, Seoul, Korea, April 1978, p. 233.

If, from the results of Fig. 10*a*, we can put the modification factor $f(a)$ (of Prof. Sih's Eq 10) constant under a constant stress level, then Eq 10 can be applied to the growth rate of the crack length of surface microcracks. So we have used the surface length to formulate the growth rate. In NDI, moreover, only the exposed length could be evaluated with high accuracy and sometimes the exposed length was chosen for a true indication of fatigue cracks.

We do not understand correctly the meaning of "modeling" as you mention the word in your comments. Presently, at any rate, we do not think that it is reasonable to formulate generally to analyze the behaviors of surface microcracks on the smooth specimen. We would like to propose a general model when many other data are obtained under various test conditions.

In the present study we have arranged the data which obtained during the series of fatigue tests simply for the convenience of use. Anyway, the points mentioned in this report emphasize how important it is to accumulate many data for modeling of the surface microcracks on the unnotched specimen.

Prof. Miller's question is very important in the analysis of fatigue crack growth. The behavior of cracks initiated from small flaws or notches is no less important than the microcracks initiated on the unnotched smooth surface from the viewpoint of fracture mechanics.

In the present paper, we have monitored the behavior of a fatigue crack initiated from a small flaw formed by the arc-strike on the surface of only the specimen shown in Fig. 1*c*. The growth rate of the fatigue crack just after initiation from the artificial flaw sometimes decreases temporarily, and Fig. 18 herewith shows this phenomenon. We cannot conclude whether this phenomenon corresponds to the case (1) where there is a decrease in da/dN due to a decrease in ΔK, or (2) where there is an unusual decrease in da/dN without a decrease in ΔK, because it is difficult to analyze accurately the ΔK of the three-dimensional crack initiated from the notch-like pit.

We observed in another study[15] the sudden decrease and increase in da/dN just after initiation at a through-notch on the plate, when we plotted the da/dN versus ΔK, which is calculated by the crack length, including the initial notch size.

We would like to thank Prof. Yokobori for his valuable data and comments. On the micro-surface cracks or the cracks in the early stage of the fatigue life of a ductile material, very few data are available. Recently the importance of these problems of microcracks has been acknowledged in industrial application. So it is advisable to accumulate as many data

[15]Kitagawa, H. and Misumi, M. in *Proceedings*, International Conference on the Mechanical Behavior of Materials, Kyoto, Japan, Vol. 2, 1971, p. 225.

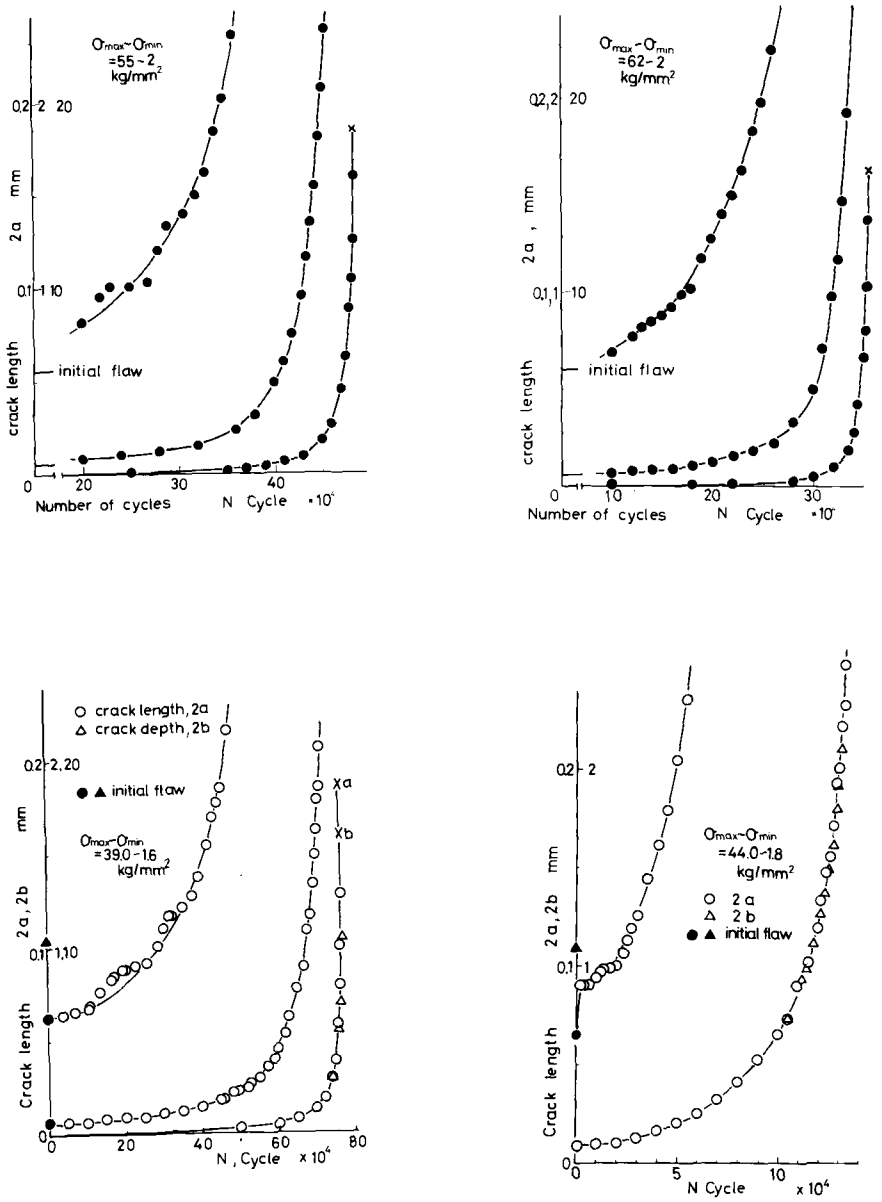

FIG. 18—*Crack growth behavior after initiation from the initial flaw* (a ~ n *relation*). *For the initial flaw, a pit-like small surface notch 50 μm deep and 50 μm in diameter is used. 2a; Crack length on specimen surface, b; crack depth.*

as possible. Our data of microcracks initiated on the surface of a smooth specimen of ductile material seem to have a tendency similar to those shown in Fig. 16 presented by Prof. Yokobori. His data seem to be composed of the curves nearly parallel to one another, having the values of the gradients $n = 3$-4.

In conclusion, we would like to thank the discussors for some extremely stimulating comments and questions, and we look forward to continuing collaboration with research workers on these subjects.

Chapter 5: Direct Observations of Microstructural Damage Due to Fatigue with Time Dependency

P. Beardmore[1]

Fatigue Behavior of Polymers

REFERENCE: Beardmore, P., **"Fatigue Behavior of Polymers,"** *Fatigue Mechanisms*, Proceedings of an ASTM-NBS-NSF symposium, Kansas City, Mo., May 1978, J. T. Fong, Ed., *ASTM STP 675*, American Society for Testing and Materials, 1979, pp. 453-470.

ABSTRACT: The overall cyclic response of ductile polymers is independent of the micromechanistic deformation phenomena and is always manifest as cyclic softening. Cyclic hardening does not occur irrespective of temperature and strain rate. Varying the deformation mechanisms by microstructural modification—amorphous versus crystalline versus composite—does not affect the response in kind, only in degree. In a similar manner, changing testing variables such as strain rate and temperature only results in a change in the magnitude of the softening. At sufficiently high strain rates, self-heating of the specimen can occur, resulting in failure due to thermal softening rather than true cyclic fatigue failure. The interaction of creep and fatigue in polymers is complex and although, in general, damage accumulation is accelerated, under certain conditions the combination is not deleterious.

KEY WORDS: fatigue polymers, cyclic softening, cyclic hardening, cyclic stress-strain curve, hysteresis, creep component, thermal effects

Fatigue failure in polymers can occur by either true mechanical failure or thermal softening or a combination of the two effects. Adiabatic thermal effects are easily induced in the cyclic testing of polymers and special precautions must be taken to minimize these effects if mechanical failure mechanisms are of paramount interest. Thermal effects are promoted by the use of high strain rates and large strains, whereas the use of very low strain rates promotes the contribution of time-dependent phenomena (for example, creep). Thus, the exact mechanisms of failure in a cyclic test are a sensitive function of the particular imposed test conditions. This paper reviews the cyclic failure mechanisms which are recognized in the fatigue of polymers. Examples are given to illustrate aspects of fatigue failure which are believed to be generally applicable.

[1] Engineering and research staff, Ford Motor Co., Dearborn, Mich. 48121.

Cyclic Effects—Mechanical

The typical first-cycle stress-strain response of a ductile polymer [*1,2*][2] at small strain limits is shown in Fig. 1. The unusual propeller-like shape of the hysteresis loop is in marked contrast to that of metals, in which roughly symmetric hysteresis loops are more characteristic. It is the viscoelastic/viscoplastic response of polymers which leads to the asymmetric hysteresis loop geometry. Qualitatively, it can be deduced that the deformation indicated by the hysteresis loop in Fig. 1 is predominantly elastic and anelastic with associated relaxation/recovery times approximately equal to the cycle time.

Another distinctive feature of the cyclic behavior of polymers is the strength differential; that is, the compressive stress is greater than the tensile stress for equal strains, Fig. 1. This strength differential is characteristic of the uniform nonelastic deformation in polymers and is related to the hydrostatic component of the applied stress [*3*]. The difference in stress

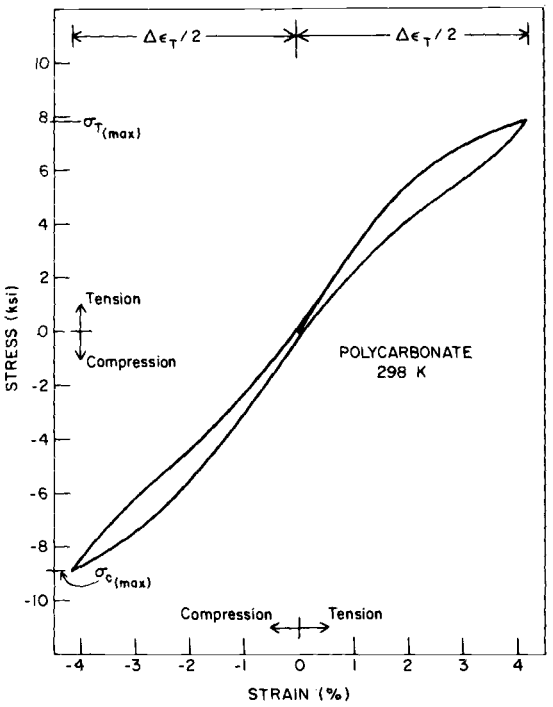

FIG. 1—*Typical initial low strain hysteresis loop for ductile polymers—material is polycarbonate.*

[2] The italic numbers in brackets refer to the list of references appended to this paper.

level is identical to that obtained in monotonic deformation. One important conclusion to be drawn from the strength differential effect is the nonequivalence of stress-controlled and strain-controlled fatigue in polymers even at small strain (stress) levels. Comparison of data using different control modes is difficult on an absolute basis unless allowance for any effects due to this nonequivalence is made.

The most important characteristic of the initial cyclic stress-strain response of ductile polymers is, however, the instability of this response to continued cycling. The resistance to nonelastic deformation and cyclic hysteresis undergoes significant change prior to fatigue crack propagation. Marked cyclic softening occurs in all ductile polymers [*1,2*] as illustrated in Fig. 2 for polycarbonate. Note the significant decrease in stress in both tension and compression to maintain the imposed strain levels. The amount of softening is obviously a function of the applied strain, and at very low strain levels no softening occurs.

The hysteresis loop symmetry is a function of both the strain level and the particular polymer. In Fig. 2, it can be seen that the cyclically softened state in polycarbonate generates hysteresis symmetry much closer to that of a metal. However, the hysteresis loop may not reflect total symmetry even in the softened state due to the complex deformation modes available in polymers. This is illustrated in Fig. 3, which show the hysteresis loops for nylon 6/6 and polyoxymethylene. The markedly different hysteresis loops reflect the different deformation accommodation mechanisms operative in the two polymers, and provides a direct contrast to the generally consistent hysteresis in metals.

The phenomena of cyclic softening, Figs. 2 and 3, can be taken to generally represent ductile polymers irrespective of the microstructure. Semicrystalline, amorphous, and composite polymers have all been shown to exhibit cyclic

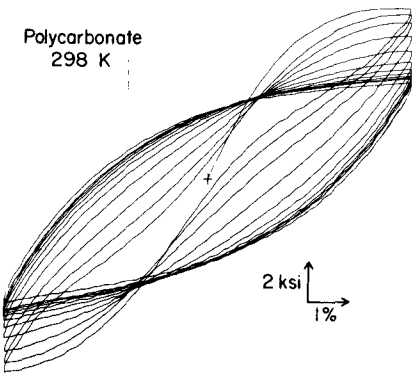

FIG. 2—*Typical nested hysteresis loops for cyclic softening in ductile polymers—material is polycarbonate.*

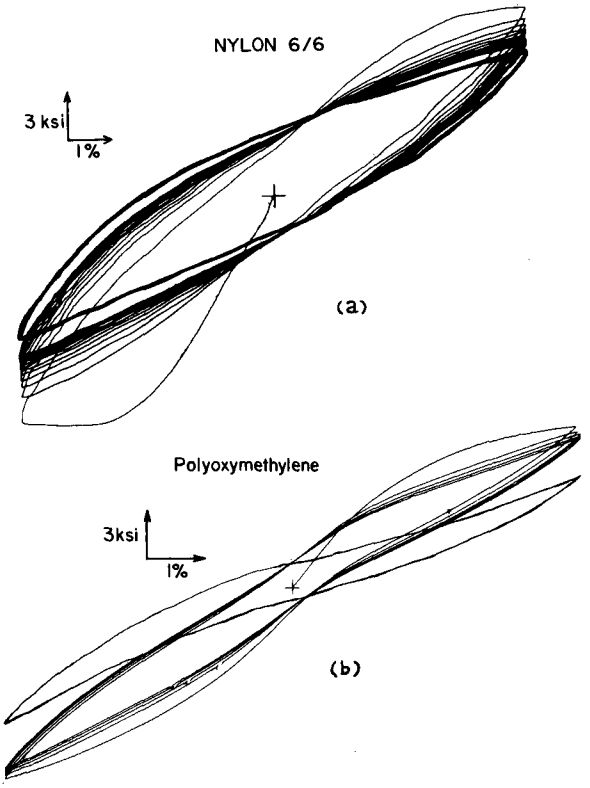

FIG. 3—*Continuous trace of hysteresis loops for* (a) *nylon 6/6, and* (b) *polyoxymethylene, showing the continuous cyclic softening to a new stable state.*

softening [*1,2*]. The only difference between the different types of polymer is one of degree, not kind. Amorphous polymers exhibit one slight variation in comparison with other polymers: at low cyclic strain levels, an incubation period occurs prior to macroscopic softening as illustrated in Fig. 4. The incubation period is a variable of imposed strain amplitude, and at high strain levels macroscopic softening occurs immediately.

The cyclic softening occurs during the first few cycles, Fig. 3, before a new cyclically stable state is attained. The amount of the fatigue life spent in the softening stage is very small and the greatest part of the fatigue process is in the new stable state. The softening is a true mechanical phenomenon, and the specimen retains the softened state irrespective of time (always provided the specimen is not heated to an elevated temperature to induce thermal recovery effects). Also, softening occurs in both tension and compression, indicating it is a homogeneous phenomenon unrelated to local effects such as crack propagation. The unique nature of the cyclic response

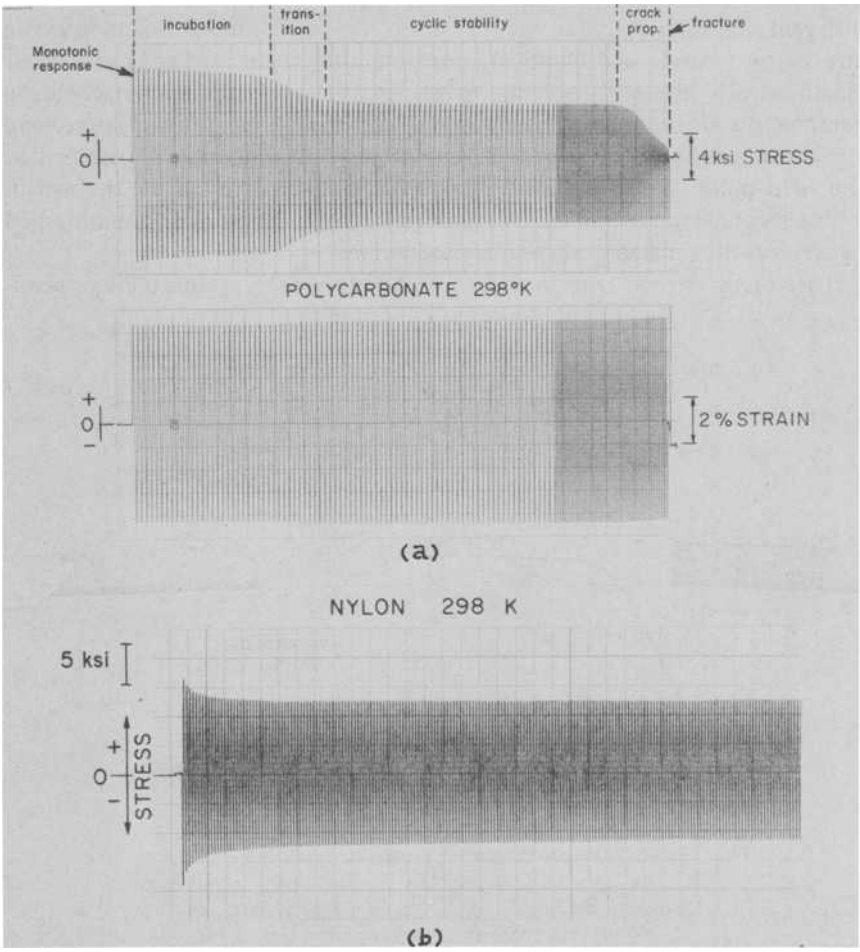

FIG. 4—*Experimental strip chart recordings of strain-controlled tests, showing* (a) *an incubation period prior to cyclic softening (typical of ductile amorphous polymers) and* (b) *immediate cyclic softening (typical of all other ductile polymers).*

in ductile polymers (that is, cyclic softening) is in direct contrast to metals, in which both cyclic softening and cyclic hardening are common.

The advent of macroscopic cyclic softening early in the fatigue life followed by a new stable cyclically softened state indicates that the monotonic stress-strain relation is not representative of the materials properties during the fatigue life. A cyclic stress-strain curve can be defined which gives a more meaningful definition of the mechanical behavior in the cyclic steady state [*1,2*]. By repeating the experiment illustrated in Fig. 4 at several different strain levels, the entire cyclic stress-strain curve can be

generated, and Figs. 5 and 6 illustrate typical examples for polymers of different microstructure. In the low strain region, the monotonic and cyclic stress-strain curves are identical, implying that cyclic softening is a non-elastic strain process involving primarily the anelastic and viscoplastic components of the strain. The amount of softening increases with increasing strain—a maximum of approximately 40 percent softening is attained at the yield point. A compressive cyclic stress-strain curve can be defined in a directly analogous manner [*1,2*] and the strength differential is maintained between cyclic tension and compression curves.

The cyclic stress-strain curves of homopolymers (amorphous, semi-

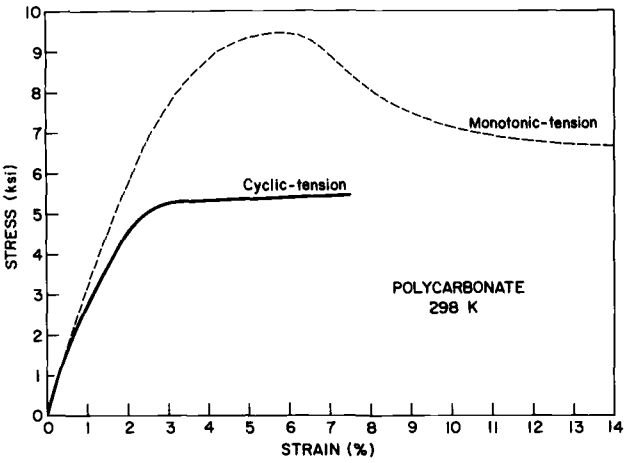

FIG. 5—*Cyclic stress-strain curve for polycarbonate at 298 K.*

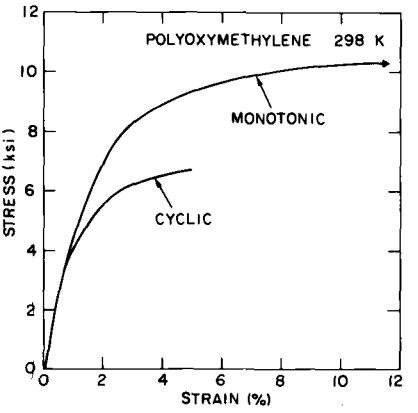

FIG. 6—*Cyclic stress-strain curve for polyoxymethylene at 298 K.*

crystalline) can be regarded as truly stable representatives of the mechanical properties. In more complex microstructure polymers, however, specifically composites containing a high volume fraction of the second phase [for example, acrilonytrile-butadiene-styrene (ABS), fiber-reinforced nylon], the softened state is not truly stable [*1,2*] and gradual softening occurs throughout the fatigue life after an initial macroscopic softening, Fig. 7. Thus, the cyclic stress-strain curve, Figure 8, is not truly stable and represents a relation between stress and strain at (say) 50 percent of the fatigue life.

The cyclic stress-strain relation just defined indicates the general mechanical behavior of the softened material. If a cyclically softened specimen is removed from the fatigue equipment and retested in monotonic tension, the stress-strain relation would trace the cyclic stress-strain curve. In addition, marked structural changes accompany cyclic softening [*1,2*]. One common manifestation of these changes is a measurable *increase* in density in the

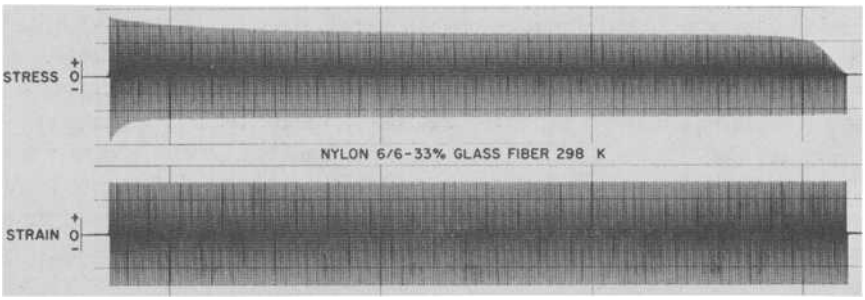

FIG. 7—*Experimental strip chart recording for 33 percent glass fiber reinforced nylon cycled under strain control at 298 K.*

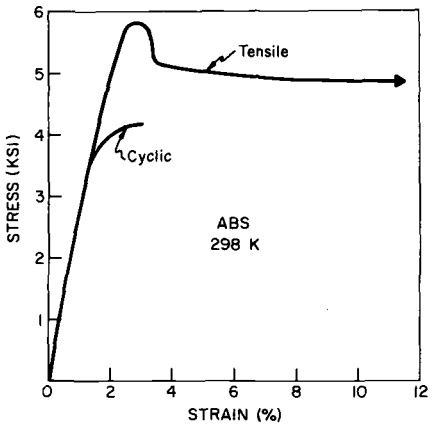

FIG. 8—*Cyclic stress-strain curve for ABS at 298 K.*

cyclically stable state—irrespective of the particular deformation mechanism operative in the polymer[*1,2*].

The strain-rate resistivity of polymers is fairly marked at ambient temperatures. Since room temperature is usually a fairly high fraction of the glass transition temperature, testing at room temperature in polymers is equivalent to testing metals at elevated temperatures. Thus, time- and temperature-dependent phenomena must always be allowed for in polymer testing. Tests combining the interactive effects of strain-rate sensitivity and creep [*4*] are illustrated in Figs. 9 and 10. Two specimens of polyoxymethylene (a semicrystalline polymer) were tested at 298 K in strain control to the same strain limits. One specimen was tested in sawtooth control (constant strain rate) and the other in sine-wave control (continuously varying strain rate with greater time at peak load). A comparison of the hysteresis loop width, Fig. 9, indicates that significantly greater damage accumulation occurs under the sine-wave control mode. In Fig. 10, similar specimens were subjected to stress control tests under sawtooth, sine-wave, and square-wave control modes with a constant cycle time for all three tests. A combination of cyclic creep and cyclic softening occurs, clearly a function of the control mode, Fig. 10. The sine-wave produces plastic strain accumulation faster than the sawtooth mode and consequently decreases the fatigue life. In direct contrast, however, in the square wave control mode, in which virtually all the cycle time is spent at the peak stress, the opposite effect occurred, Fig. 10. Although the maximum time at peak stress might be expected to accelerate the creep component, the plastic strain accumulation rate was considerably less than either of the other two cases, resulting in a longer fatigue life. This result clearly indicates that the creep component and the amount of time spent at the peak stress are not necessarily directly related. The creep strain which

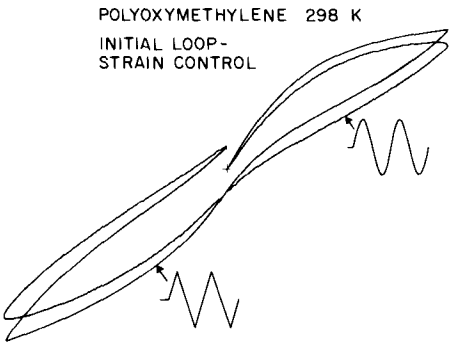

FIG. 9—*Initial hysteresis loop of two identical specimens of polyoxymethylene tested at the same strain level with different control modes—sine wave versus sawtooth wave.*

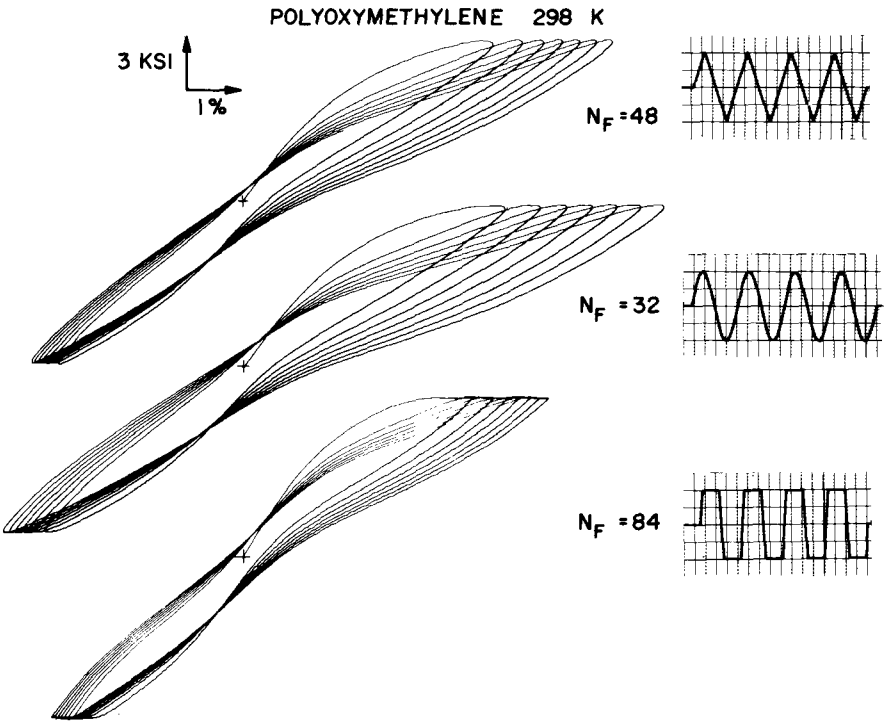

FIG. 10—*Effect of control wave form on the strain accumulation and fatigue life of polyoxymethylene tested in stress control.*

develops at the peak stress must be path dependent, that is, it must be a sensitive function of the rate at which the peak stress is attained.

Cyclic Effects—Thermal

Basically two types of thermal effects must be considered in the fatigue of polymers. Firstly, the self-heating of the specimens due to hysteresis, and secondly, thermal recovery effects due to testing in a temperature range where these recovery effects are of the order of the cycle time. The two effects are different in nature and it is clear that the second case is equivalent to continuous self-annealing. The present discussion will be limited to ambient temperatures where such self-annealing does not occur.

A direct result of hysteresis is energy dissipation in the form of heat. Adiabatic thermal effects are known to occur commonly in the cyclic testing of polymers [*5*] and are always likely to be a factor unless special precautions are taken to obviate the effect. The low damping capacity of polymers combines with the low heat capacity and low thermal conductivity

to promote heating effects. It is relatively easy to fail a polymer by the thermal softening induced by the appropriate combination of load and frequency. This type of thermal failure is a fatigue failure mechanism directly attributable to strength loss resulting from an increase in specimen temperature—the imposed stresses are too high to be sustained at this new elevated temperature. Some data on measured increases in temperature during fatigue are available (see, for example, Refs *6* and *7*) but the general trend can be described schematically by Fig. 11. The immediate temperature increase (Region I in Fig. 11) is followed by a region of decreased rate (Region II). The rate of temperature increase during Region II is totally a function of the imposed test conditions. Region II is followed by an abrupt increase in the rate of increase of temperature with number of cycles; this region is characteristic of the final fatigue/thermal failure.

Figure 11 presents the generalized temperature effects which can occur during cyclic testing of polymers. The amount of heat generated and the measured increase in temperature and rate of increase are directly dependent on the operative test conditions. The rate of increase in temperature in Region II can be made very low (that is, a plateau where the temperature increment above ambient remains constant) or very high (under high strains and high strain rates), and, obviously, any intermediate rate can also be induced. If Region II is flat (small constant temperature increment), the fatigue failure is isothermal and truly mechanical (the fatigue failure of polymers described in the previous section is of this type). If Region II has a positive slope, a thermal/fatigue failure will occur. Figure 11 can consequently be considered as representative of all fatigue tests, that is, both mechanical and thermal, with the essential difference lying in the level of temperature increase in Region II.

Under the appropriate test conditions, a fatigue failure combining both mechanical and thermal effects can occur in polymers. Usually, this combined failure mode occurs when test conditions necessary to maintain

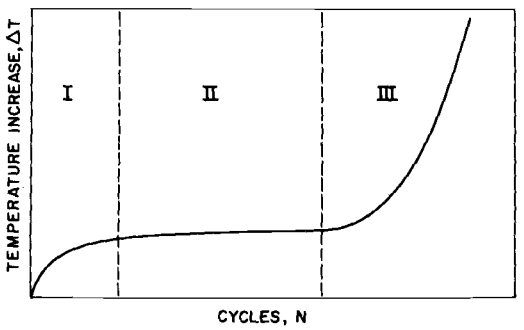

FIG. 11—*Schematic illustration of the temperature rise during cyclic testing of polymers.*

isothermal conditions are imposed on the specimen, and all the reversed deformation prior to crack initiation occurs with no increase in temperature. The onset of crack initiation and propagation produces a marked localization of high strain at the crack tip and significant heat generation occurs sufficient to raise the temperature of large volumes of the specimen [*4*]. In Fig. 12 the fracture faces of two polycarbonate specimens tested in fatigue are shown. Both specimens were tested such that all the cyclic straining prior to crack initiation took place isothermally. In Fig. 12*a*, crack propagation took place with an associated marked increase in temperature and the fracture markings are typical of a ductile crack blunting-resharpening mechanism through the entire cross section. In contrast, in Fig. 12*b* the fatigue crash has propagated incrementally across only about one third of the specimen prior to catastrophic failure, and is typical of isothermal failure throughout the test, including the crack propagation stage.

The amount of heat generated in the fatigue testing of polymers will vary with the particular polymer being tested. For a given strain level, the heat buildup will depend on the size of the nonelastic component of the total strain, and this varies from one polymer to another. The specific heat of the particular polymer is significant since this determines the temperature rise per unit of mechanical energy released. Thus, the response of a given polymer to a defined set of test conditions is a function of the physical and mechanical properties of that particular polymer, and the type of fatigue (mechanical versus thermal) will be a sensitive function of those properties.

Conclusions

There is ample evidence that all ductile polymers exhibit cyclic softening. The degree of softening is high and is accompanied by a measurable increase in density. The cyclic softening phenomenon is truly mechanical in nature and represents a new stable state of the material. The reverse phenomenon, cyclic hardening, never occurs in polymers. If testing conditions are imposed such that marked heat generation occurs during cycling, a failure can occur due to the thermal softening of the specimen and the associated inability to maintain the imposed loads. Combinations of the two mechanisms can occur, and the predominant mode can vary between the different stages of the fatigue life.

References

[*1*] Rabinowitz, S. and Beardmore, P., *Journal of Materials Science,* Vol. 9, 1974, p. 81.

[*2*] Beardmore, P. and Rabinowitz, S., *Treatise on Materials Science & Technology, Vol. VI: Plastic Deformation of Materials,* Academic Press, New York, 1975, pp. 267-331.

[*3*] Duckett, R. A., Rabinowitz, S. and Ward, I. M., *Journal of Materials Science,* Vol. 5, 1970, p. 909.

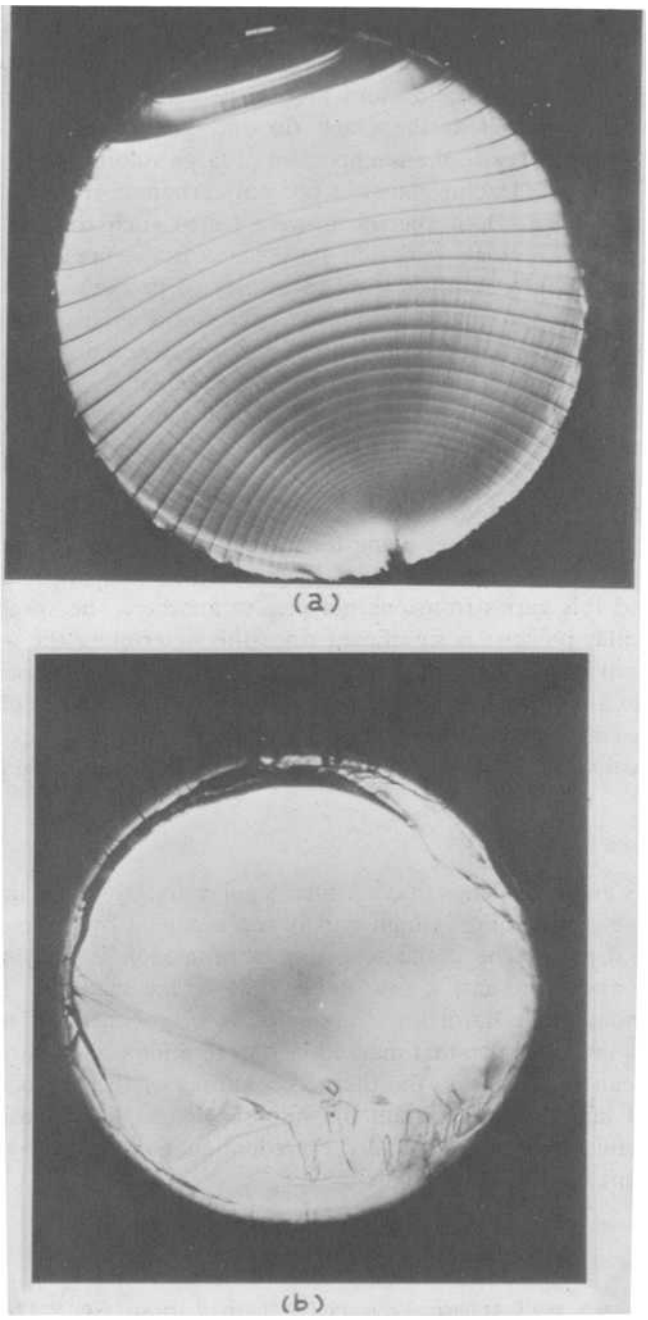

FIG. 12—*Fatigue fracture faces of polycarbonate under testing conditions such that* (a) *significant heating accompanied crack propagation, and* (b) *crack propagation occurred with no increase in temperature.*

[4] Beardmore, P. and Rabinowitz, S. in *Proceedings,* American Society for Metals Seminar on Polymer Material, Chicago, Ill., 1975, p. 551.
[5] Manson, J. A. and Hertzberg, R. W., Chemical Rubber Co. *Critical Reviews in Macrostructural Science,* Vol. 1, 1973, p. 433.
[6] Higuchi, M. and Imai, Y., *Journal of Applied Polymer Science,* Vol. 14, 1970, p. 2377.
[7] Cessna, L. C., Levens, J. A. and Thomson, J. B., *Polymer Engineering and Science,* Vol. 9, 1959, p. 339.

DISCUSSION

A. Peterlin[1] *(discussion)*—The paper treats cyclic straining $\epsilon = \epsilon_0 \sin \omega t$ at fixed maximum strain ϵ_0 so that the polymer specimen is alternately extended to a maximum elongational strain ϵ_0 and compressed to the same compression strain $-\epsilon_0$. The resulting assymmetry of the true strain, proportional to ϵ_0^2, and the dependence of the elastic modulus on the hydrostatic component of the strain make the maximum stress in compression higher than in extension. As a consequence of the prevailing true compression strain the polymeric material becomes denser (a graph would be highly welcome).

The dissipated mechanical energy, according to the hysteresis-type stress-strain curve, heats the specimen and thus accelerates the failure. This heating effect is proportional to the square of the stress or strain. Hence, it can be almost completely avoided by lowering the amplitude ϵ_0 of the cyclic loading (a curve showing this dependence would be welcome).

The time dependence of the stress-strain curve indicates the existence of an incubation period, of a transition period, and of the final new cyclic stability extending up to specimen failure. During the incubation period the specimen remains practically undamaged and the stress-strain curve is constant. During the transition period the specimen softens so that the same strain is obtained with steadily decreasing stress. Concurrently the density increases as a consequence of the prevailing effect of the compression.

The fatigue phenomenon strongly depends on the strain limits, ϵ_{max} and ϵ_{min}. The specimen behaves differently if both limits have the same sign (pure extension or pure compression) or the opposite sign (alternating extension and compression). In this paper, only the almost symmetrical straining of the second type was discussed. An understanding of the cyclic fatigue definitely requires an elucidation and systematic description of the whole spectrum of cyclic straining.

The dependence of the cyclic fatigue on the shape of the cyclus is only

[1] Center for Materials Science, National Measurement Laboratory, National Bureau of Standards, Washington, D. C. 20234.

marginally mentioned. No attempt is made for its interpretation in terms of the rate of deformation, relaxation, rest time, and amplitude. On a molecular scale, the simultaneous increase of the density and decrease of the resistance to stress are rather incompatible without a substantial structural change. Hence, one has to assume a change in the packing and spatial arrangement of the long chains in order to understand these two effects. The sliding motion of parallel chain sections and their shear displacement are the easiest deformation modes. Any increase of chain alignment also increases the density of the amorphous phase. Hence, one may think that the cyclic loading favors such a type of chain rearrangement. It could be detectable eventually as a change in infrared dichroism which separates the effect in the crystals from that in the amorphous phase. A critical survey of pertinent molecular models of the deformation modes would be highly appreciated.

A. Peterlin (separate discussion)—Your talk and the paper are mainly a shorter version of your talk at the American Society for Metals Seminar on Polymer Material in Detroit in September 1973 (Ref *4* of the paper). You omitted the asymmetric loading completely and concentrated uniquely on the case of regular alternating of almost equal positive and negative loading or straining of the specimen. My comments will be primarily concerned with the fatigue mechanism of plastic materials as presented in the paper. My first question is about the number of cycles a specimen can stand under a certain type of cyclic loading. The lifetime of a strained specimen is usually considered as the sum of two types of contribution. One is the nucleation time and the second one is the growth time of the nucleus to the critical size crack. I want to know what can be attributed to the first stage, that is, to the nucleation of the microcrack, and what to the next step, that is, to the growth of the microcrack.

P. Beardmore—I should first say that I should leave the growth of the microcrack to Dick Herzberg. That's a specific subject of his paper, so I don't want to encroach on that. In a general sense the development of the crack takes place in a manner analogous to that in metal. For example, if you take a transparent polymer and put polarized light through it and watch the strain, you can see initially that you get a strain distribution which is fairly uniform. What happens then is a function of the number of cycles and time as the strain starts to become localized. So, whatever the deformation mechanism is, it's a localization of the deformation mechanism, whether it be in crystalline or an amorphous polymer, which leads to localized strain displacements, and then you get the nucleus of a crack, whatever that is, and it varies with the specific mechanism. For example, in crystalline polymers, it may well be an interface between the amorphous and the crystalline region. In amorphous polymers, it may well

be—if people believe in it and I'm not sure I do—between the areas of so-called local high density. There are various theories about that, about how statistically you get a large number of chain ends in one particular center and that starts it. How you prove that is a different matter. It's a hypothesis, and there is no way, to my mind at this stage, of showing exactly where that thing nucleates.

A. Peterlin—If I make conclusion of what you have told me, most of what you have shown is related to the nucleation stage and very little to the crack growth stage.

P. Beardmore—All that I've said is related to the crack nucleation stage, yes.

A. Peterlin—The second question is about the type of cyclic loading. The damage to the specimen and the lifetime very much depend on whether during the cycle the specimen is all the time under tensile stress or compressive stress (asymmetric case) or whether the extension alternates with equally large compression (symmetric case). Your loading is not perfectly symmetric because the same value $|\Delta l/l_0|$ means a higher strain or load during compression than during extension. As a consequence of this slight asymmetry you observe a small density increase with progressive cycling. The situation is very much different if the maximum and minimum load are both compressive or both tensile. The specimen is either compressed or extended during the whole cycle. In your talk in Detroit you considered quite extensively the case of asymmetric straining or loading and pointed out the differences as compared with symmetric loading. Since you addressed only the quasi-symmetric loading, I would greatly appreciate some comments about this more general case. In particular I want to ask you how much of a difference in specimen behavior one may expect in such an asymmetric case as compared with what you have shown.

P. Beardmore—First of all, you are asking for 15 years of work in metals to be done on polymers, and we have hardly scratched the surface yet. The first thing to do is symmetric loading before we try to get nonsymmetric. I don't mean to be facetious, but that's literally true. There is an awful lot of work and everybody who is doing metals knows that. There is a great effect depending on the deformation mechanism of bias loading. Let me give you one example. Let us take crazing, whether you want to call it strain accommodation or brittling effect. You can condition polymers and then change, for example, the crazing stress.

Let us take polystyrene and go with the classic example of crazing. If you cycle in compression first and then go into fully reversed tension-compression, crazing occurs at a much lower stress than if you had gone straight

into fully reversed tension-compression. So if you precondition, or bias your loading, depending on the specific deformation mechanism, you're going to go from a large effect to a small in much the same way that you might in a variety of different conditions in metals. I can't give a general answer except to say there is a marked effect, but it's going to take a lot of work, particularly if you are throwing things like periods of arrest and stopping the test at a high stress. That's an awful lot of work for somebody to do, but I couldn't agree more that there will be the distinct effect and it will vary with the particular deformation mechanism that is involved.

A. Peterlin—My third question relates to the shape of the loading curve. A rough estimate of its influence on the lifetime of the specimen (t_b) can be derived from the Bailey criterion

$$\int_0^{t_b} d\tau/\tau_b(\sigma) = 1$$

where $\tau_b(\sigma)$ is the lifetime of the specimen under constant load σ. One must not expect an ideal description, although the general trend can be well derived from this criterion.

You have measured the damage resulting from sinusoidal, zigzag, and trapezoidal loading curves. The strain amplitude increases progressively with cycling in all three cases. The increase is fastest in the first case and slowest in the last case. Hence, one can anticipate the shortest lifetime for the sinusoidal and the longest lifetime for the trapezoidal loading curve. This is apparently in complete disagreement with the conventional Bailey criterion, which at constant stress amplitude predicts the shortest lifetime for the trapezoidal and the longest for the sinusoidal load shape.

The situation may be reversed if one takes into account the restitution of the specimen during the compression phase. The longer stay of the specimen at the compression amplitude in the case of the trapezoidal load shape may so much restitute the specimen that it overcompensates the large damage of the specimen during the longer stay at the extension amplitude. Such a compensation is not included in the conventional formulation of the Bailey criterion, which describes quite well the situation in the extreme asymmetric case where the tension and compression do not alternate at all. But it seems to fail completely in the case of alternating tensile and compressive load.

How general are these results and how well can the Bailey criterion be applied to specimens subjected to cyclic loading? The conventional formulation seems not to work in the three symmetric cases shown in your paper. But there may be other systems behaving in a different manner.

P. Beardmore—As I said before, I think the problem with doing these

types of tests—and we did only one to show that there was an effect—is that you have got to get into it and study specific deformation mechanisms.

For example, if you take a crazing polymer, you'll get exactly the opposite effect. You'll get a shorter life when you use the square wave, so the interpretation depends very much on what specific deformation method is involved, and those are all the data I have. I don't have anything more comprehensive, I'm sorry to say.

A. Peterlin—I am concerned only about what you have shown during your talk and said in the answers to my questions. You stated very clearly that you considered microcrack nucleation only and excluded completely microcrack growth. Hence, the consideration of crazing is not inherently connected with what we are discussing here. But the crazing may indeed reverse the sequence of the three loading curves. This sequence was based on the effects observed during the nucleation phase. As soon as the crazing during the growth of the microcrack to the critical size becomes the most time-consuming process in specimen failure, it dominates the lifetime. If the crazing is fastest with the trapezoidal loading curve, the corresponding lifetime will be shorter than in the case of a sinusoidal loading shape. In such a case the observed data would agree with the conventional Bailey criterion.

I would like to have a little more information about the molecular mechanism and background of the effects observed in the density increase and softening of the cycled specimen. You did not mention in your talk but stated very clearly in the paper that you have always observed a small increase in the density of the specimen as a consequence of the symmetric cyclic loading. As a rule, increased density leads to a higher elastic modulus, that is, to a smaller strain for the same stress amplitude. In contrast to that, you observe in all cases a progressive softening of the material. What could be the molecular mechanism for such an apparently controversial behavior?

P. Beardmore—I guess I forgot to mention that, but what happens after the initial cyclic softening, if you measure the density of the material (we did this, for example, on polycarbonate and on nylon), is that you actually get about a 1 percent increase in density. All polymers, of course, are not anywhere close to the theoretical packing density; in other words, the density is always lower than you might expect on theoretical grounds.

You actually get an increase in perfection of order to some extent, after cycling the packing density higher than it started. Now to deal with why it softens, and that question is asked a lot. For example, if I take a cyclically softened polycarbonate specimen and pull it the way you might a cyclically softened metal, what happens when you get to the work-hardening stage (which, as I said, might be out at 60 percent) is that it naturally

becomes stronger. This is akin to a mild steel, where you get cyclic softening at low strain simply because you free up nucleation centers for deformation, allowing dislocation multiplication, and then the stress-strain curves cross and in the work-hardening stage of the curve the steel becomes stronger. Exactly the same analogous type of thing is probably happening in polymers, except that everything is stretched out so far you rarely get out to the work-hardening stage because you're out at 60 percent. So to my mind what you are getting is the nucleation of all those things—deformation nuclei centers—in much the same way that cyclic stresses and strains free the dislocation locking mechanisms in mild steel types of nuclei.

R. W. Hertzberg,[1] *M. D. Skibo,*[2] *and J. A. Manson*[1]

Fatigue Fracture Micromechanisms in Engineering Plastics

REFERENCE: Hertzberg, R. W., Skibo, M. D., and Manson, J. A., **"Fatigue Fracture Micromechanisms in Engineering Plastics,"** *Fatigue Mechanisms*, Proceedings of an ASTM-NBS-NSF symposium, Kansas City, Mo., May 1978, J. T. Fong, Ed., *ASTM STP 675*, American Society for Testing and Materials, 1979, pp. 471-500.

ABSTRACT: This paper deals with an examination of fatigue micromechanisms present in polymers of various chemistry and microstructure. At low stress-intensity (ΔK) levels in several amorphous homopolymers, poly (methymethacrylate) (PMMA), polycarbonate (PC), poly (vinyl chloride) (PVC), polystyrene (PS), and polysulfone (PSF), each with viscosity-average molecular weight ($\overline{M}_V$) in the range $1 \times 10^5 < M_V < 4 \times 10^5$, the macroscopic and microscopic appearances of the fracture surface were observed. Observations were also made in both rubber-modified amorphous polymers such as an acrylonitrile-butadiene-styrene (ABS) copolymer and a rubber-toughened PS-poly (phenylene oxide) blend, and the crystalline polyacetal (PA). Regardless of the degree of surface roughness, the crack front in all these materials advanced discontinuously in increments equal to the bandwidth after remaining stationary for as many as 10^5 fatigue cycles (in PA). In single-phase amorphous polymers, the discontinuous growth process was identified with the failure of a single craze ahead of the crack tip. At high ΔK levels the fracture surfaces of most polymers were striated, with one striation representing the increment of crack advance during one load excursion. It is concluded that large errors can be made in estimating the overall fatigue life of engineering plastics if the significance of the microscopic bands observed at low ΔK and the striations observed at high ΔK as fatigue fracture markings is misinterpreted.

KEY WORDS: fatigue crack propagation, polymers, discontinuous crack growth, fatigue fracture mechanisms

It is well recognized that careful examination of fine-scale fracture surface details can provide significant information regarding various fracture processes in solids [*1,2*].[3] Often such studies have revealed some micro-

[1] New Jersey Zinc professor of metallurgy and professor of chemistry, respectively, Materials Research Center, Lehigh University, Bethlehem, Pa. 18015.

[2] Formerly, research associate, Materials Research Center, Lehigh University, Bethlehem, Pa. 18015. Present address: Sandia Laboratory, Livermore, Calif. 94550.

[3] The italic numbers in brackets refer to the list of references appended to this paper.

structural defect(s) that were responsible for the component's demise. On the basis of such enlightening observations, materials engineers are better able to improve overall component response through changes in composition or internal microstructure of the material, or both. In addition, fractographic investigations often provide useful quantitative information which can be used to analyze the continuum details of the fracture process. For these reasons, numerous failure analyses have been reported which make considerable use of fractographic information [*3,4*].

Perhaps the most useful fractographic features are the so-called fatigue striations. These markings correspond to the successive position of the advancing crack front as a result of individual load excursions; hence the spacing between each line represents the incremental crack advance during one load excursion. Therefore, the striations not only identify a cyclic loading condition, but also provide quantitative information regarding the kinetics of the fatigue cracking process. Such markings have been reported in a vast number of different metal alloy systems with their width being found to vary with the prevailing stress-intensity conditions at the crack tip. A useful empirical relationship [*5*] between the striation spacing and the stress-intensity factor is given by

$$\text{Striation spacing} \approx 6\left(\frac{\Delta K}{E}\right)^2 \tag{1}$$

where ΔK is the stress-intensity-factor range, $Y\Delta\sigma\sqrt{a}$, and E is the modulus of elasticity.

Since the stress-intensity factor is a function of the stress σ and defect size a, Eq 1 can be used to infer the prevailing stress level at any location on the fracture surface where a reliable striation width measurement can be made. In a sense then, fatigue striations serve as a permanent record of the fracture process.

It was appropriate, therefore, to determine whether polymeric solids generated similar fatigue markings on fracture surfaces produced under cyclic loading conditions. The earliest reported studies of polymer fatigue fracture surfaces, using optical microscopes, recorded the presence of fatigue striations in rubber and in such commercial engineering plastics as poly(methyl methacrylate) (PMMA) and polycarbonate (PC) [*6-13*]. Furthermore, striation width was found to increase with increasing crack length, consistent with the tendency for the striation spacing to increase with increasing stress-intensity factor (see Eq 1). More recently, it was shown that striation spacings in PMMA and PC increased with a power of ΔK greater than two [*14,15*].

Most surprisingly, a second type of fatigue arrest line was identified in poly(vinyl chloride) (PVC) but which did not correspond to the increment of crack growth resulting from a single load excursion [*16,17*]. Instead,

these bands reflected discrete crack advance increments which occurred after several hundred loading cycles of total crack arrest.

These preliminary findings pose a major challenge to the materials engineer/scientist. For one thing, how does one know whether a given set of fatigue fracture markings represents a record of crack advance from individual loading cycles rather than increments of hundreds of cycles? At least for cases involving laboratory specimens, the significance of the fracture bands could be determined by comparing their width with monitored macroscopic growth rates. As such, one can not emphasize too strongly the desirability of generating companion macroscopic fatigue crack growth rate data when careful fatigue fracture surface micromorphological studies are planned. Obviously such data are not available in actual service failures. Therefore, it becomes necessary to recognize clearly defined differences between the micromorphology of striations and the larger discontinuous crack growth bands. To this end, optical microscope fracture surface studies have yielded to electron microscopic fractographic inquiries. Coupling the much greater resolution capability of scanning and transmission electron microscopes (SEM and TEM) with their greater magnification capability, different fracture mechanisms have been identified and rationalized in the light of known polymer deformation characteristics.

The objectives of this paper, therefore, will be to describe the micromorphology of polymer fatigue fracture surfaces, to establish quantitative relationships between the various fracture bands and the prevailing crack-tip stress-intensity conditions, and to present a fracture model consistent with experimental findings.

Experimental Details

Fatigue fracture surfaces from commercially available polycarbonate (PC) (General Electric), poly(vinyl chloride) (PVC) (Cadillac), polysulfone (PSF) (Westlake), polystyrene (PS) (Cadillac), laboratory case poly(methyl methacrylate) (PMMA), acrylonitrile-butadiene-styrene copolymer (ABS) (Westlake), and polyacetal [(Delrin) (Du Pont) and (Celcon) (Allied Chemical)] were examined during this investigation.

Fractographic analysis was performed with an ETEC scanning electron microscope and an optical metallograph. Specimens prepared for use in the SEM were coated first with carbon and then with gold. The accelerating potential was set at 20 kV for all materials except PMMA and polyacetal, which were examined at 5 kV.

Wherever possible, attempts were made to not only describe the fracture micromorphology but also to determine the quantitative relationships that might exist between the fracture markings and the prevailing stress conditions. To this end, fracture surface studies were conducted from specimens that had been subjected to carefully controlled fatigue crack propagation

experiments. In this regard, the macroscopic crack growth rate for each specimen was monitored and related to the prevailing stress-intensity-factor condition. Fatigue tests were conducted in a 9-kN MTS electrohydraulic closed-loop testing machine at cyclic frequencies between 1 and 100 Hz [*18*]. The ratio of minimum to maximum loads was held constant at 0.1 for all tests. Crack advance was measured in increments of approximately 0.25 mm with an optical traveling microscope. All specimens were tested in a laboratory air environment at room temperature.

Experimental Findings

Striation Formation

It is helpful to examine polymer fatigue fracture surface markings within the context of the considerable literature for metals. For example, comparison of striations spacings in metals, with the details of variable block loadings, and comparison of their spacing with monitored macroscopic crack growth rates, established the very important fact that each striation represented the position of the advancing crack front at some instant in the life of the component. Futhermore, the striation width represented the increment of growth from one load excursion. Since the striation width proved to be dependent on the magnitude of the stress-intensity factor, a critical post-failure analysis diagnostic procedure was identified. For the case of metals, the striation spacing-ΔK relationship for all metals may be approximated by Eq 1. It has been suggested that this second power dependence of striation width on ΔK reflects the fact that the striation width represents a fraction of the crack opening displacement [*19*]. It is important to note that the macroscopic growth rate for metals varies with ΔK raised to the power 2.5 to 7 or more. Consequently, one finds ΔK regimes wherein the striation spacing may be either greater or less than the average value of the macroscopic crack growth increment per cycle. This reflects the fact that the macroscopic growth rate constitutes a summation of several fracture mechanisms which may be described by

$$\frac{da}{dn_{\text{macro}}} = \Sigma\, Af\,(K)_{\substack{\text{striation}\\ \text{mechanism}}} + Bf'\,(K)_{\substack{\text{void}\\ \text{coalescence}}} + Cf''\,(K)_{\text{cleavage}} + Df'''\,(K)_{\substack{\text{corrosion}\\ \text{component}}} + \ldots \qquad (2)$$

More extensive quantitative data are now available to determine whether a similar relationship exists in polymeric solids (that is, whether polymer striation spacings vary with ΔK^2 and whether other mechanisms in addition to striations are found at a given ΔK level). Figures 1 and 2 show the ex-

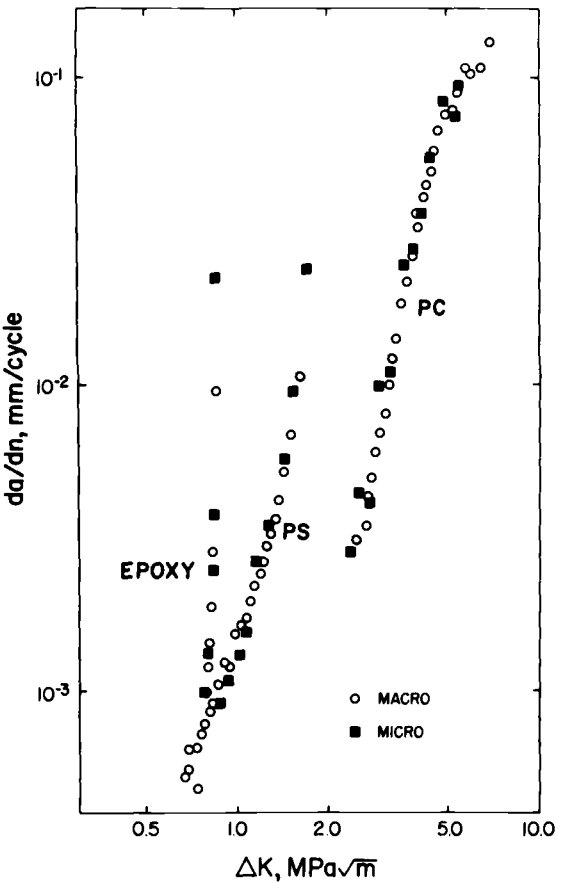

FIG. 1—*Comparison of macroscopic growth rates and striation measurements in epoxy, polystyrene, and polycarbonate.*

cellent one-to-one agreement between microscopic striation width and macroscopic crack growth increments per cycle for PMMA, polysulfone, polystyrene, polycarbonate, and an epoxy resin. This implies that in the ΔK regime where striations are found, they represent the only fatigue crack advance micromechanism and account for the entire crack growth increment during a given loading cycle. In agreement, no other fracture mechanism is found in these materials in the ΔK regime where striations are found. Also in sharp contrast with observations from metal fracture surfaces, it is obvious that the ΔK dependence of polymer striation width is not constant (and equal to two) but rather varies with the power of ΔK ranging from 4 to about 20! Obviously, striation width-crack opening displacement correlations are suspect for the case of polymer fatigue. Further-

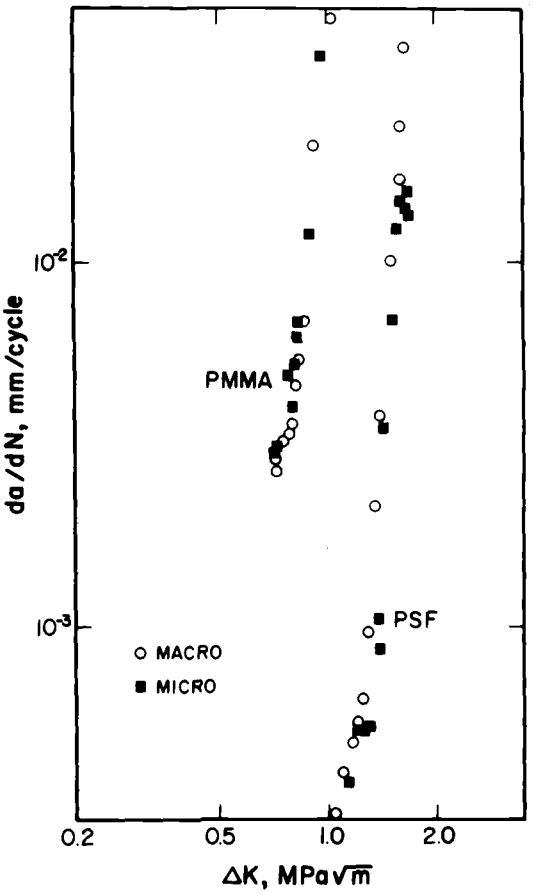

FIG. 2—*Comparison of macroscopic growth rates and striation measurements in polysulfone and poly(methyl methacrylate).*

more, post-failure analytical procedures aimed at using striation data to infer the prevailing ΔK conditions (for example, Eq 1 for the case of metals) are not possible at this time since a parallel unifying relationship for polymers has not been defined. Instead, investigators must have previous knowledge of a particular polymer's fatigue crack propagation (FCP) behavior (for example, da/dn versus ΔK data) before using striation spacing width measurements to infer ΔK conditions.

Representative fractographs showing fatigue striations in four polymers are shown in Fig. 3. These fracture surface markings are generally flat, especially at lower ΔK levels, and contain a fine linear structure which is oriented normal to the striation itself. Overall, there appears to be no change in morphology from one side of the striation to the other, in

marked contrast to the discontinuous growth bands to be discussed in the following. The slight striation curvature is similar to that found in metal specimens and belies the crack propagation direction.

In conclusion, it is emphasized again that with prior determination of the macroscopic fatigue crack growth, it is possible to clearly establish that the markings discussed in this section are striations. This point is reinforced in the following discussion.

Discontinuous Crack Growth

Reflecting the existence of considerable evidence of the one-load-cycle/one-fracture-band relationship in metals and plastics, it has become commonplace for investigators to instinctively conclude that a series of parallel fracture bands oriented normal to the crack direction represent individual striations. Often, this assumption cannot be proven since neither the macroscopic crack growth kinetics were monitored nor the micromorphology of the bands examined. As a result, investigators have been misled since, in some polymers under certain test conditions, fatigue cracks progress across the specimen in discontinuous increments associated with a large number of loading cycles [*15,20*].

As mentioned earlier, it was originally shown for the case of PVC [*16,17*] that fatigue fracture lines were formed but which corresponded to sudden crack advance increments resulting from several hundred loading cycles rather than one cycle (Fig. 4*a*). Of particular significance, Elinck, et al [*16*] performed calculations to show that the bandwidth varied with the square of the prevailing stress-intensity conditions and corresponded to the dimension of the crack-tip plastic zone as defined by the Dugdale-Muskelishvili formulation [*21*]. It was found that a craze zone grew continuously with load cycling, though characterized by a decreasing rate with increasing craze length, whereupon some critical condition was satisfied and the crack suddenly struck through the entire craze before arresting at the craze tip [*17*]. (This process has been verified more recently with the aid of television monitoring of the cracking process. In fact, many discontinuous cracking events generated an audible click.) For the case of commercial PVC, discontinuous crack growth constituted the only observed mode of crack advance prior to final specimen rupture. In this instance, striations were never observed on the smooth, mirror-like PVC fracture surfaces.

More recently, this discontinuous cracking process has been observed in at least seven other materials, thereby giving support to the generality of this cracking process in polymeric solids (Fig. 4*b-f*) [*22-24*]. In all the materials except polyacetal and ABS, the discontinuous growth bands (DGB's) were limited to the mirror-like regions of their respective fracture surfaces, which were generally confined to low ΔK values. At higher ΔK

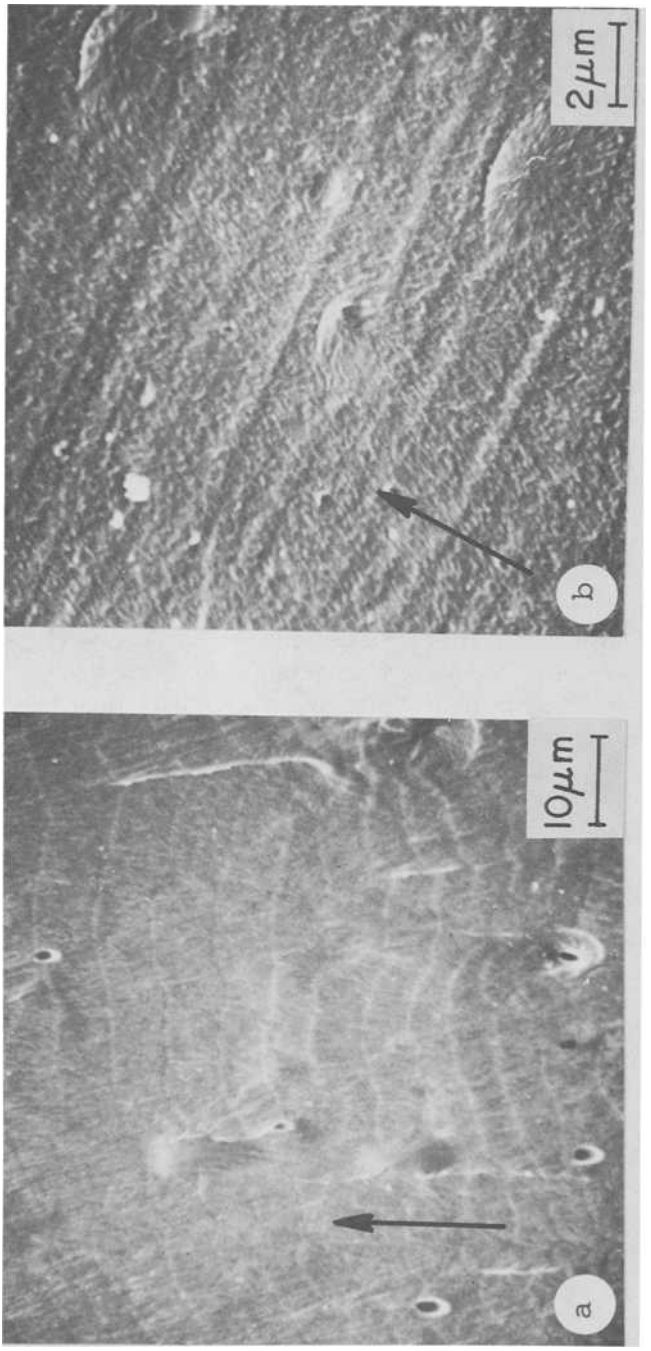
10μm
a
2μm
b

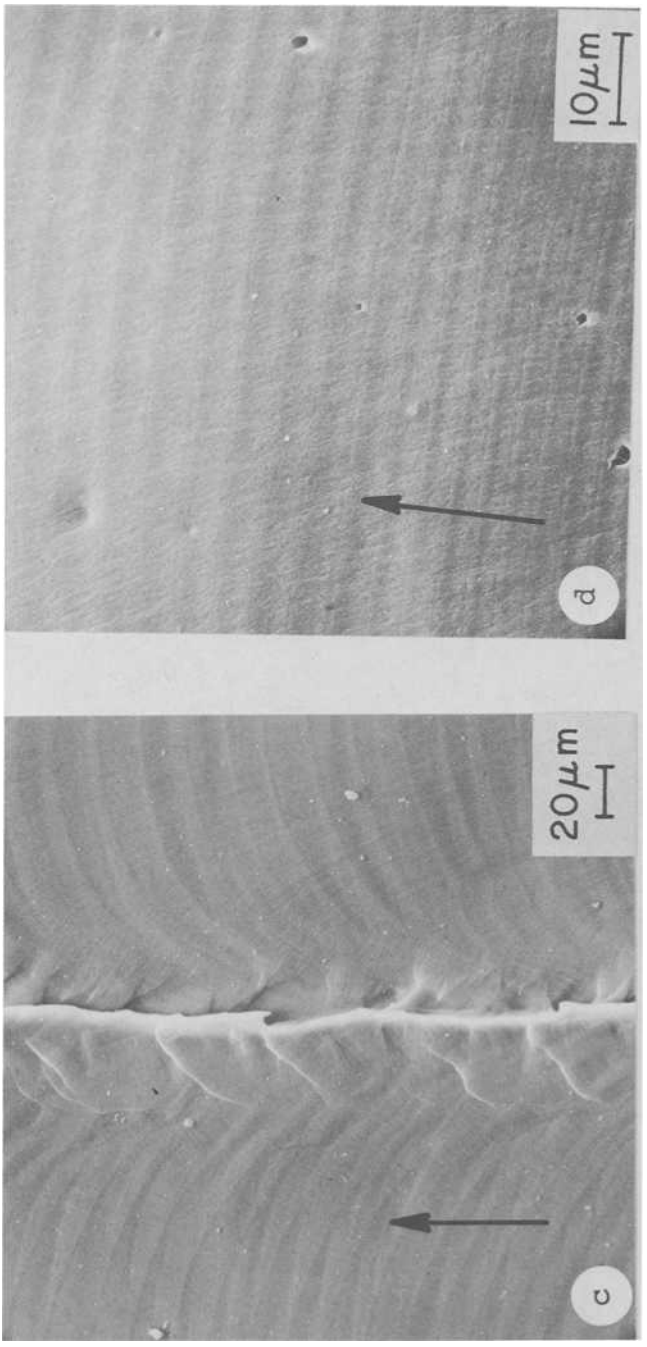

FIG. 3—*SEM micrographs of fatigue striations in PMMA, PS, PSF, and PC. Arrows indicate crack direction.*

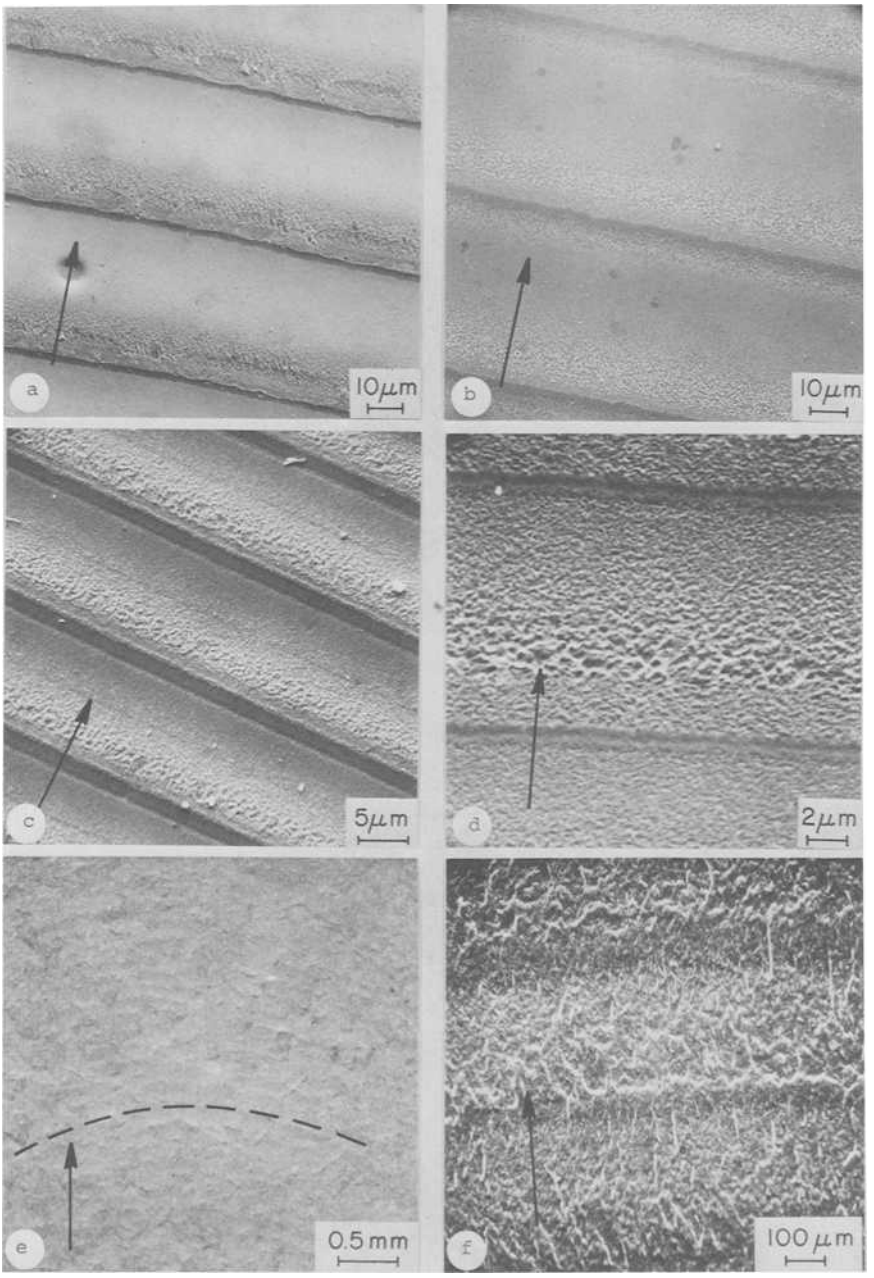

FIG. 4—*SEM fractographs of discontinuous growth bands in* (a) *PVC,* (b) *PS,* (c) *PSF,* (d) *PC,* (e) *PA, and* (f) *ABS. Arrows indicate crack direction.*

levels, the fracture surfaces were rougher in appearance due to multiple crazing; in this range of ΔK, actual fatigue striations were seen. In fact, some of the striation data shown in Figs. 1 and 2 were obtained from the very same specimens that displayed DG bands. By contrast, the entire fracture surfaces in polyacetal and ABS were generally rougher in appearance but did not also reveal individual striations at higher ΔK levels; however, Kitagawa has reported fatigue striations in ABS [*14*]. Figure 5 clearly shows the bandwidth to increase with the second power of the stress-intensity factor, consistent with the dependence of the crack-tip plastic zone size on K. (The deviation in band width in PC and PSF from a second-power dependency on the stress-intensity level is believed to result from an associated transition in the fracture surface appearance from a mirror-to-mist texture.) If one assumes that the bandwidth represents the extent of plastic zone development at specific crack length locations, one may infer an apparent yield strength at different K levels by computations based on the Dugdale plastic zone model. Furthermore, if we assume that crack-tip yielding occurs by crazing (at least in the amorphous polymers), the inferred yield strength computed from the Dugdale [*21*] formulation (Eq 3) would correspond to the tensile stress for craze yielding in the respective polymers

$$r_y \approx \frac{\pi}{8} \frac{K^2_{\max}}{\sigma_{ys}^2} \tag{3}$$

where

r_y = crack-tip plastic zone dimension,
$K_{\max}$ = maximum stress-intensity factor, and
σ_{ys} = material yield strength.

The computation involves setting the plastic zone dimension equal to the bandwidth at a given $K_{\max}$ level. The value of $K_{\max}$, in turn, is derived from the ΔK level after correction for the mean stress level. Hence $K_{\max} = [\Delta K/(1 - R)]$ where $R = K_{\min}/K_{\max}$. It was found in all cases that the computed yield strength was constant at all stress-intensity levels (for example, see Fig. 6). Furthermore, the respective yield strengths for each material corresponded to previously reported plane-strain yield strength or craze stress values (Table 1).

It is instructive at this point to examine the duration of the metastable arrest period associated with the discontinuous crack growth process. The number of loading cycles required for continuous craze development and discontinuous crack extension is estimated rather well by dividing the bandwidth dimension by the corresponding macroscopic crack growth rate. It is clear from Fig. 7 that the number of cycles per band decreases strongly with increasing stress-intensity level. This most likely reflects the greater

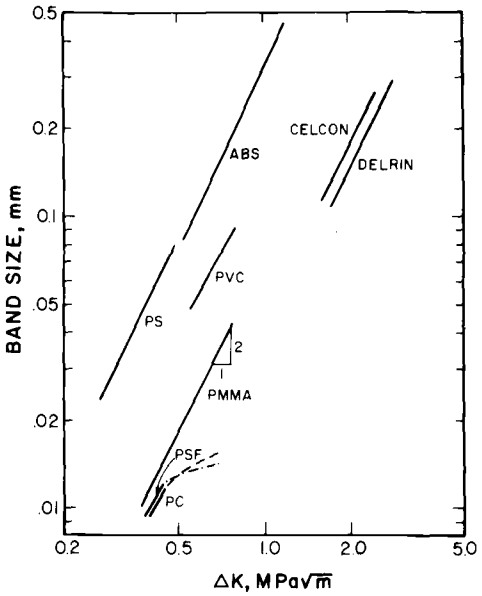

FIG. 5—*Dependence of band size on* ΔK *for six amorphous polymers and two grades of polyacetal (Celcon and Delrin).*

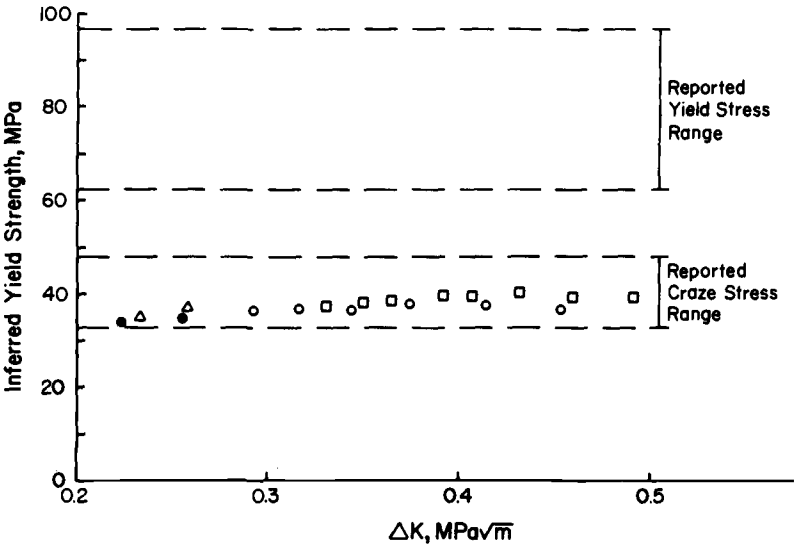

FIG. 6—*Relationship between inferred yield stress from discontinuous growth band measurements and stress range. Also shown are yield and craze stress values for polystyrene as reported in the literature.*

TABLE 1—*Yield strengths of polymers investigated.*

Polymer	Mean Inferred Yield Strength (Standard Deviation), MPa	Reported Plane Strain Yield Strength, MPa
PC	81 (3.6)	61 to 82[a]
PVC	51 (3.1)	47 to 65[b]
PSF	79 (1.5)	67 to 80[a]
PS	38 (1.84)	38[c,d]
PMMA	81 (0.95)	83[e]
PA		
Celcon	90 (3.7)	89[f]
Delrin	99 (3.2)	97[f]
ABS	38 (1.6)	28 to 60[f]

[a] Mills, N. J., *Engineering Fracture Mechanics*, Vol. 6, 1974, p. 537.

[b] Gales, R. D. R. and Mills, N. J., *Engineering Fracture Mechanics*, Vol. 6, 1974, p. 93.

[c] Rabinowitz, S., Krause, A. R., and Beardmore, P., *Journal of Materials Science*, Vol. 8, 1973, p. 11.

[d] Howard, R. N., Murphy, B. M. and White, E. F. T., *Journal of Polymer Science*, Vol. 9, No. A2, 1971, p. 801.

[e] Morgan, G. P. and Ward, I. M., *Polymer*, Vol. 18, 1977 p. 87.

[f] *Modern Plastics Encyclopedia*, McGraw-Hill, New York, Vol. 49, No. 10A, 1972, p. 143.

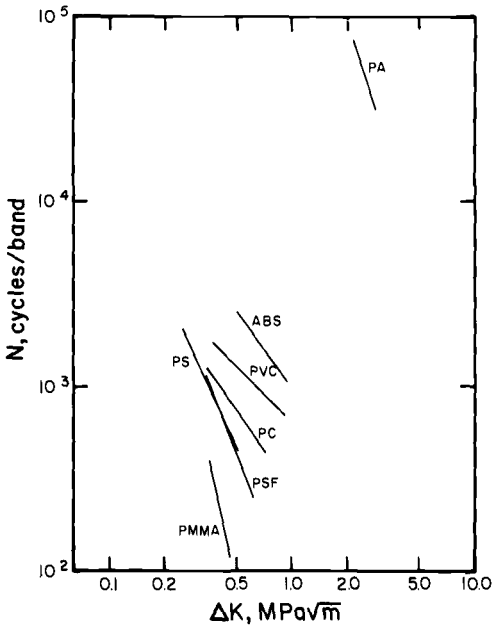

FIG. 7—*Effect of stress intensity level on the number of cycles required for growth through a discontinuous growth band in several polymers.*

extent of specimen damage of each load cycle at higher ΔK levels. From Fig. 7, the cyclic stability N^* is seen to vary with some inverse power of ΔK. Since the band size varies with K^2 and the crack growth rate with K^m, the cyclic life of the DG bands is found to vary inversely with ΔK^{m-2}. Alternatively, $N^*\Delta K^{m-2} = \text{constant}$, which takes on the appearance of the low-cycle fatigue relationship for metals proposed by Coffin and Manson [*25*]; that is, $\Delta\epsilon_P N^{*c} = \text{constant}$, where $\Delta\epsilon_P$ is the plastic strain range and c a relatively constant value.

It is tempting to extrapolate the experimental results in Fig. 8 to determine the ΔK level required to produce a discontinuous growth band in only one loading cycle. In turn, one might ask whether the corresponding bandwidth would be dimensionally consistent with the striation spacing at that extrapolated ΔK level (see Figs. 1 and 2). In fact, the two fracture bandwidths are far from equivalent and reflect the fact that two fundamentally different fracture mechanisms are operative at different stress intensity conditions. At the extrapolated ΔK levels, the hypothetical DGB widths and actual striation widths differ by two orders of magnitude or more.

From the foregoing, one must conclude that estimation of prevailing ΔK conditions based on service failure fracture bandwidth measurements is tenuous indeed, unless the investigator is able to make a clear distinction between DG bands and striations. Fortunately, this is made possible with the aid of electron fractographic observations. For the case of PVC, PC, PSF, PS, and PMMA, the discontinuous cracking process occurs within a single craze which developed at the crack tip from the cyclic loading conditions [*22*]. At some point (see the following), the crack jumps through the craze before arresting at the craze tip. A close examination of the DGB micromorphology reveals the presence of many microvoids which decrease in size in the direction of crack growth (see Fig. 4). This suggests that the cracking process occurs by a void coalescence mechanism with the void size distribution reflecting the internal structure of the craze just prior to crack extension. Note that the observed void size gradient is consistent with the presumed craze opening displacement distribution across the craze. The narrow dark bands (light for the case of PMMA) represent the surfaces of successive crack tips which repeatedly blunted and arrested

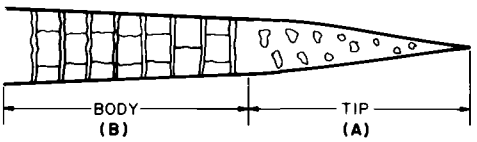

FIG. 8—*Schematic diagram of Verhaulpen-Heymans and Bauwens model of craze development.*

when the crack reached homogeneous uncrazed material. These narrow zones were delineated by narrow elongated tear dimples which pointed back to the crack origin. Therefore, by direct comparison of DGB and striation micromorphology (see Figs. 3 and 4), a clear distinction between these two micromechanisms is possible.

DGB Model

Previous studies have shown that, depending on the polymer, DGB formation may occur at all ΔK levels and frequencies, at only low ΔK values and high frequencies, or not at all. A model for craze fracture will now be proposed in order to rationalize these divergent material responses. Following the craze model of Verhaulpen-Heymans and Bauwens [*26*] we first assume that the craze consists of two regions as shown in Fig. 8. Within the craze tip region A, transformation of homogeneous polymer into craze matter is thought to take place. In contrast, the craze body B is considered as a region containing fully developed craze material, including some elongated fibrils; homogeneous craze matter transformation is thought not to take place in this region [*26,27*]. Following a DG event, a new craze is envisioned to grow, relatively fast at first. Based on recent cinematographic studies performed in our laboratory, we find the craze grows to about 80 percent of its final equilibrium length l_D—the Dugdale plastic zone width at that particular K_{max} value—within the *first* 10 percent of the band's cyclic life. The final 10 percent of craze length growth occurs during the *last* 10 percent of the band's cyclic life (Fig. 9). It was not possible to monitor changes in craze thickness t along with the cycle-dependent changes in craze length. However, we assume (see the

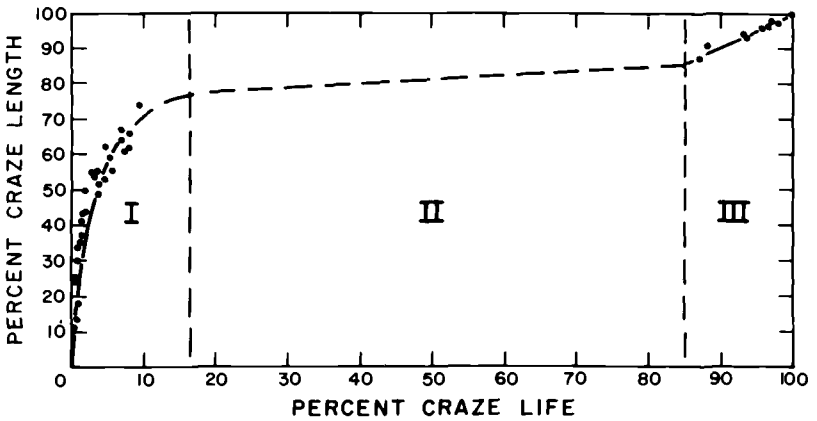

FIG. 9—*Relationship between band length and band life in PVC-6 percent dioctyl phthalate, under cyclic loading conditions.*

following) that the craze thickens slowly at first but reaches its limiting thickness t_{COD} (which probably corresponds to the critical crack opening displacement at the prevailing stress-intensity level) at a more rapid rate when the cyclic life approaches N^*, where N^* is the cyclic life of a given band. As a result, we believe that the somewhat accelerated craze length growth rate, dl/dn, during the final 10 percent of band life is related to an accelerated rate of craze thickening, dt/dn, just prior to craze breakdown. To this extent, we suggest that growth of the craze length to the Dugdale dimension l_D represents a necessary but not sufficient condition for fracture. Instead, craze breakdown is believed to be keyed to the craze thickening rate dt/dn (and to the associated limiting condition where $t \rightarrow \text{COD}_{max}$), which is obviously more sluggish than the craze length growth rate, dl/dn, during the final 10 percent of band life is related to increase at first but then to decrease with increasing craze length. The experimental findings of Bessonov and Kuvshinskii are consistent with this hypothesis (Fig. 10) [*28*].

To explain the craze instability condition and the effect of structural parameters such as molecular weight and molecular weight distribution (MWD) on FCP response, it is necessary to develop the craze model further. After material passes through Region A (Fig. 8), a craze structure is established, consisting of numerous microvoids and moderately aligned fibrils. These remaining craze fibrils are believed to contain many of the more highly entangled coils, comprising the longest molecules, from the original polymer bulk. Consequently, the remaining fibrils would be

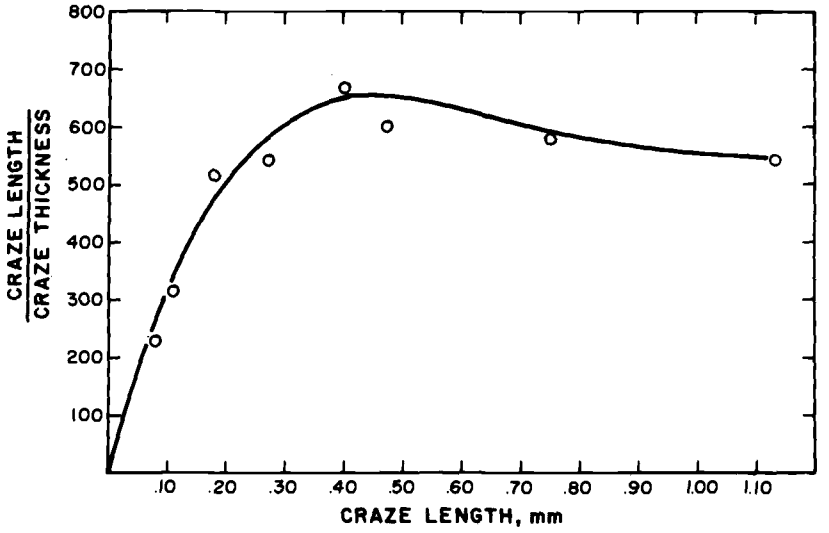

FIG. 10—*Change in craze aspect ratio (craze length/craze thickness) as a function of craze length (after Bessenov et al* [28].

expected to possess a much higher molecular weight (M) and narrower MWD than the bulk polymer.

Gradual thickening of the craze should occur under cyclic loading conditions as the most highly stressed fibrils disentangle and fracture. With the breakage of each additional fibril, the remaining unbroken ligaments are subjected to an ever-increasing load and associated strain; these fibrils then become stronger through a process of orientation hardening. The net effect is believed to be the establishment of a relatively constant stress across the craze zone based upon a constant product of fibril strength and remaining fibril volume fraction, $\sigma_f v_f$. Thus early in the cyclic life of a discontinuous growth band, a large volume fraction, v_f, of fibrils with moderate strength, σ_f, and limited alignment should exist. The failure of a fibril during this early stage of damage zone lifetime should result in minimal load transfer to the remaining fibrils. With continuing fibrillar fracture, the load to be transferred to the remaining fibrils should increase, with these fibrils undergoing further orientation hardening. Finally a critical condition is reached when the next fibril would break; the remaining fibrils would no longer be capable of absorbing the additional load and the entire craze zone would break down suddenly.[4]

The presumed relative constancy of $\sigma_f v_f$, therefore, reflects a metastable equilibrium condition between fibrillar orientation (strain hardening) and void growth (strain softening) which exists in Stage II of the craze length growth process (Fig. 9). Stage III would correspond to a condition of approaching instability with the final few fibrils to fracture redistributing an ever-increasing load to the remaining ligaments. By contrast, rapid longitudinal craze development in Stage I is believed to reflect an unbalanced condition wherein softening due to craze void formation overwhelms fibril orientation hardening. (Note the strong analogy with arguments set forth to rationalize the three stages of creep in engineering alloys [*4*].) Furthermore, the model, containing elements of strain-hardening exhaustion in the fibrils coupled with an increased fibrillar stress level, is analogous to the instability condition associated with the classic necking phenomenon in metals.

The craze fracture model is consistent with a number of additional experimental observations. In large measure, the incidence of DG bands

[4]Note that this sequence of fibrillar fracturing is consistent with the assumed trend in craze thickening rate discussed earlier. That is, during the initial stage of the DG band cyclic life, the fracture of some small number of fibrils will necessitate the redistribution of load among the large remaining number of unbroken craze ligaments. As a result, the additional load on each fibril should be small and the associated fibrillar stretching (resulting in craze thickening) should be small. Conversely, just prior to final craze breakdown, the fracture of some highly stressed fibrils will require a larger load to be assumed by the fewer remaining fibrils and result in a greater amount of fibrillar stretching (that is, craze thickening). As such, the rate of craze thickening dt/dn should be inversely proportional to the number of remaining unbroken ligaments, $(dt/dn) \propto [1/f(v_f)]$.

depends upon the existence of a single craze (or few crazes at most) at the crack tip. This ensures that cyclic damage will be focused within a narrow zone and is consistent with the observation that discontinuous crack extension is found primarily at high test frequencies and low ΔK levels. Low test frequencies and high ΔK conditions would provide the additional time and enlarged plastic zone sizes, respectively, for craze bundling to nucleate at the crack tip. The model also anticipates the large sensitivity of FCP to M and MWD previously reported for PS [*29*], PMMA [*30*], and PVC [*31*]. Recall that the model envisions craze formation to involve fibril formation from only the most highly entangled coils—presumably those containing the longest chains—within the polymer. Consequently, FCP resistance and craze breakdown are seen to be controlled by the long-chain fraction. For example, minor additions of a high-M component to a low-M matrix have resulted in substantial improvement in the FCP resistance of PMMA [*32*]. This is consistent with previous studies by others [*33,34*].

In related fashion, the model accounts for DGB formation only when M is below some critical level (roughly 2 to 4 $\times$ 10^5) [*22*]. When M is high, fibrillar disentanglement proceeds at a very sluggish rate and the polymer tends to form craze bundles which dissipate cyclic damage rather than focus it within a single craze. Consequently, the fatigue crack proceeds through the craze bundle in a continuous manner. Even when M is less than about 2 $\times$ 10^5, DGB formation may not occur. If the polymer possesses a bimodal MWD with some extra long chain molecules added to the matrix, resistance to cyclic-induced disentanglement may be great enough to suppress the discontinuous crack growth process. For example, Fig. 11 shows DGB formation in low-M PMMA but no DGB in a PMMA specimen containing a low M but with 2 weight percent of a high-M component. Note that the high M addition increased the average M only slightly.

Conclusions

It has been shown that fatigue fracture surfaces of numerous polymeric solids reveal at least two sets of fracture bands. At high ΔK levels, the bands were identified as fatigue striations and corresponded to the advance of the fatigue crack resulting from one load excursion. The other set of bands formed generally under low ΔK conditions and represented discontinuous crack growth bursts which occurred after the crack had remained dormant during hundreds or thousands of loading cycles. The fracture bandwidth corresponds to the Dugdale plastic strip dimension and the cyclic life of the band was seen to increase sharply with decreasing stress-intensity level. Fractographic studies have verified that the band corresponds to crack progression through a craze which formed ahead of

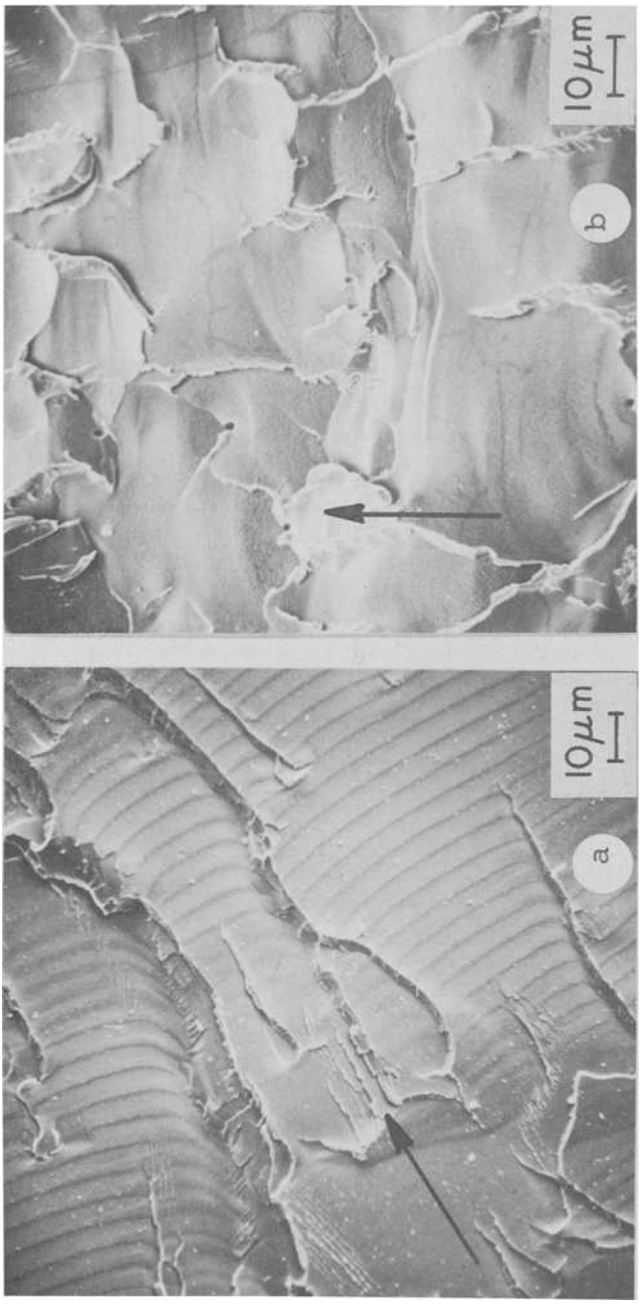

FIG. 11—*SEM fractographs of* (a) *low-M PMMA showing evidence of discontinuous crack growth and* (b) *low-M PMMA with 2 percent high M where no DGB are present. Stress-intensity levels are both about 0.33 MPa*$\sqrt{m}$. *Arrows indicate crack direction.*

the crack. A model for craze breakdown and discontinuous crack growth was proposed and found to be consistent with experimental findings.

Acknowledgments

The authors wish to express their appreciation to the Army Research Office-Durham, National Science Foundation-Polymer Division, and the Materials Research Center, Lehigh University, for their financial support of this effort.

References

[1] Phillips, A., Kerlins, V., and Whiteson, B. V., *Electron Fractography Handbook*, Air Force Materials Laboratory TDR-64-416, WPAFB, Wright-Patterson Air Force Base, Ohio, 1965.

[2] *Metals Handbook*, Vol. 9, American Society for Metals, 1974.

[3] *Case Studies in Fracture Mechanics*, T. P. Rich and D. J. Cartwright, Eds., Army Materials and Mechanics Research Center MS 77-5, Watertown, Mass., June 1977.

[4] Hertzberg, R. W., *Deformation and Fracture Mechanics of Engineering Materials*, Wiley, New York, 1976.

[5] Bates, R. C. and Clark, W. G., Jr., *Quarterly Transactions*, American Society for Metals, Vol. 62, No. 2, 1969, p. 380.

[6] Andrews, E. H., *Journal of Applied Physics*, Vol. 32, No. 3, 1961, p. 542.

[7] Feltner, C. E., *Journal of Applied Physics*, Vol. 38, 1967, p. 3576.

[8] Waters, N. E., *Journal of Materials Science*, Vol. 1, 1966, p. 354.

[9] Watts, N. H. and Burns, D. J., *Polymer Engineering and Science*, Vol. 7, 1967, p. 90.

[10] McEvily, A. J., Boettner, R. C., and Johnston, T. in *Fatigue, An Interdisciplinary Approach*, J. J. Burke, N. L. Reed, and V. Weiss, Eds., Syracuse University Press, Syracuse, N.Y., 1964.

[11] Jacoby, G. H. in *Electron Microfractography, ASTM STP 453*, American Society for Testing and Materials, 1969, p. 147.

[12] Broutman, L. J. and Gaggar, S. K., *International Journal of Polymeric Materials*, Vol. 1, 1972, p. 295.

[13] Jacoby, G. and Cramer, C. *Rheologica Acta*, Vol. 7, 1968, p. 23.

[14] Kitagawa, M., *Bulletin of the Japan Society of Mechanical Engineers*, Vol. 18, No. 117, 1975, p. 240.

[15] Zilvar, V., Havliček, V., and Bouška, P. in *Proceedings*, Fifth Conference on Dimensioning and Strengthening Calculations, Budapest, Hungary, 1974, p. II-471.

[16] Elinck, J. P., Bauwens, J. C., and Homès, G., *International Journal of Fracture Mechanics*, Vol. 7, No. 3, 1971, p. 227.

[17] Hertzberg, R. W. and Manson, J. A., *Journal of Materials Science*, Vol. 8, 1973, p. 1554.

[18] Skibo, M. D., Hertzberg, R. W., and Manson, J. A., *Journal of Materials Science*, Vol. 11, 1976, p. 479.

[19] McClintock, F. A. in *Fatigue Crack Propagation, ASTM STP 415*, American Society for Testing and Materials, 1967, p. 170.

[20] Havliček, V. and Zilvar, V., *Journal of Macromolecular Science*, Vol., B5, 1971, p. 317.

[21] Dugdale, D. S., *Journal of the Mechanics and Physics of Solids*, Vol., 8, 1960, p. 100.

[22] Skibo, M. D., Hertzberg, R. W., Manson, J. A., and Kim, S., *Journal of Materials Science*, Vol. 12, 1977, p. 531.

[23] Hertzberg, R. W., Skibo, M. D., and Manson, J. A., *Journal of Materials Science*, Vol. 13, 1978, p. 1038.

[24] Skibo, M., Janiszewski, J., Kim, S. L., Hertzberg, R. W., and Manson, J. A., *Proceedings, International Conference on Toughening of Plastics*, Plastics and Rubber Institute, London, July 1978, paper 25.

[25] Coffin, L. F. *Transactions*, American Society of Mechanical Engineers, Vol. 76. 1954, p. 931.
[26] Verhaulpen-Heymans, N. and Bauwens, J. C., *Journal of Materials Science*, Vol. 11, 1976, p. 7.
[27] Manson, J. A. and Hertzberg, R. W., *Fatigue of Engineering Plastics*, Academic Press, New York, in preparation.
[28] Bessonov, M. I. and Kuvshinskii, E. V., *Soviet Physics—Solid State*, Vol. 3, No. 5, 1961, p. 950.
[29] Sauer, J. A., Foden, E., and Morrow, D. R., *Society of Plastics Engineers Technical Papers*, Vol. 22, 1976, p. 107.
[30] Kim, S. L., Skibo, M. D., Manson, J. A., and Hertzberg, R. W., *Polymer Engineering and Science*, Vol. 17, No. 3, 1977.
[31] Skibo, M. D., Hertzberg, R. W., Manson, J. A., and Collins, E. A. in *Proceedings*, 2nd International Conference on PVC, Lyons, France, 1976, p. 233.
[32] Kim, S. L., Janiszewskii, J., Skibo, M. D., Manson, J. A., and Hertzberg, R. W. in *Proceedings*, Division of Organic Coatings and Plastics Chemistry, Vol. 38, No. 1, 1978, p. 317.
[33] Wellinghoff, S. and Baer, E., *Journal of Macromolecular Science*, Vol., B11, 1976, p. 367.
[34] Fellers, J. F. and Kee, B. F., *Journal of Applied Polymer Science*, Vol. 18, 1974, p. 2355.

DISCUSSION

K. DeVries[1] (*discussion*)—The studies described in this paper are very important and interesting and in an area of the utmost importance. If the use of polymers as structural elements in design is to continue to grow, an understanding of their fatigue behavior is essential. A phenomenological approach is, in my opinion, not sufficient nor are studies in which it is attempted to spell out analogies or differences in behavior or both with metal fatigue. In order to predict long-term service performance from short-term laboratory testing, it is essential that there be an understanding of the fundamental mechanisms involved. It is possible in macromolecules that several mechanisms might be active, depending on the temperature, time scales, environments, etc. involved. Such factors are probably more important in polymers than in any of the other generally used structural materials. I was pleased therefore to see these authors go into such detail as to the hypothesized mechanisms (microscopic and submicroscopic) involved in the fatigue crack growth process.

These investigators have applied the methods of fracture mechanics to alternating crack growth under loads. This is appropriate and informative for the type of study they have undertaken. The same basic approach is, in my opinion, of rather general applicability. Both the fracture mechanics approach and their description of possible occurrences at the crack tip

[1]Department of Mechanical and Industrial Engineering, University of Utah, Salt Lake City, Utah 84112.

are, phenomenologically at least, similar to that reported by others for different types of failure. As an illustration, Fig. 12 shows the crack growth rate during cyclic loading of adhesive joints according to Mostovy and Ripling.[2] It may be noted that the behavior represented by this figure is very similar to that of Fig. 1 and 2 in the paper discussed here. Likewise compare the authors' discussion in the "DGB Model" subsection of the craze and elongated fibrils at the tip of the crack with the photograph by R. A. Schapery, reproduced as Fig. 13[3] of this discussion, of a crack tip in a rubber-based solid propellant. Furthermore, the Dugdale model,[4] represented by their Eq 3 was first proposed for use in metals and has been used most extensively for the analysis of metallic fracture.

I find the authors' explanation of the discontinuous crack growth interesting, reasonable, and consistent with the observations they reported. It is consistent, for example (as the authors report) with their observation[5] and that of others[6,7] that molecular weight and molecular weight distribution drastically affect deformation mechanisms in polymers. For example, small amounts of very high molecular weight material added to a low molecular weight specimen may alter crack growth behavior from essential brittle growth to propagation involving appreciable crazing. An additional and perhaps more conclusive test would be to test the same polymers under temperatures or stress conditions or both that promote yielding rather than crazing (see Wellenghoff and Baer[7] and Sternstein and Myers[8]).

As important as the authors' study of crack propagation is, I cannot help wondering if it tells the whole story. Is crack propagation the most important part of the fatigue process? It is not clear, to me at least, that the total process of fatigue can be regarded simply as the incremental growth of preexistent flows. One might logically ask if the fatigue performance of a structural element might not be divided into two stages, crack nucleation and crack growth or propagation. The research described in this paper concentrates exclusively on the latter process. If we designate the number of cycles in these stages as N_i and N_g, respectively, the total number of cycles of failure N_T might be expressed as

$$N_T = N_i + N_g$$

[2] Mostovoy S. and Ripling, E. J., "Fracture Characteristics of Adhesive Joints," Final Report, Naval Air Systems Command Contract No. N0019-74-N0019-74-C-0274, 1975.

[3] Schapery, R. A., *International Journal of Fracture.* Vol. 11, 1975, p. 141.

[4] Dugdale, D. S., *Journal of the Mechanics and Physics of Solids.* Vol. 8, 1960, p. 100.

[5] Janiszewski, J., Skibo, M. D., Manson, J. A., and Herzberg, R. W., *Organic Coatings and Plastics Chemistry,* Vol. 38, 1978, p. 317.

[6] Sauer, J. A., Foden, E., and Morrow, D. R., *Society of Plastics Engineers Technical Papers.* Vol. 22, 1976, p. 107.

[7] Wellenghoff, S. and Baer, E., *Journal of Macromolecular Science—Physics.* Vol. B11, 1975, p. 367.

[8] Sternstein, S. S. and Myers, F. A. in *The Solid State of Polymers,* P. H. Geil, E. Baer, and Y. Wada, Eds., Marcel Dekker, New York, 1974.

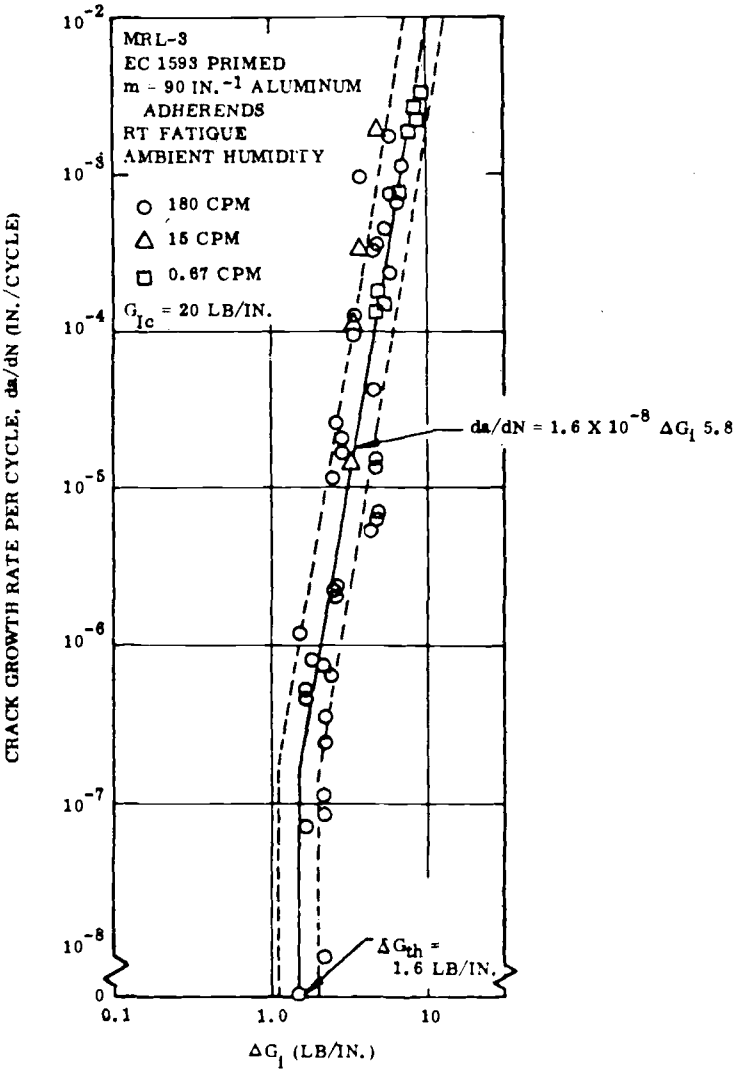

FIG. 12—*Crack growth rate per cycle,* da/dN, *versus* ΔG_i *for MRL-3 nitrile-phenolic commercial film adhesive (after Mostovy and Ripling). Note:* G_i *is proportional to* E *times* K *used by the authors.*

Fracture is at best a complex phenomenon that is not well understood. Fracture under repetitive loading is even less well understood. When one adds the complex morphology of plastics, our understanding is even less well developed. There are a number of important questions, the answer to which would be helpful in structural design, material design, and quality assurance. These include: (1) What portion of the total fatigue lifetime

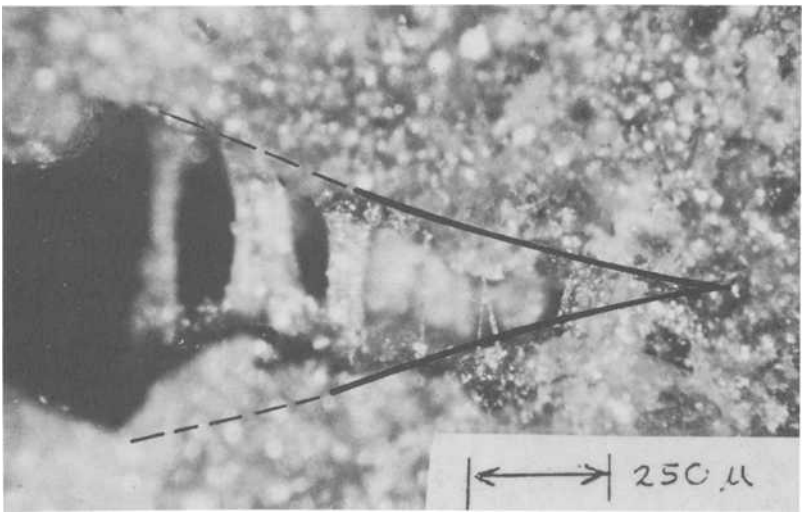

FIG. 13—*Crack growth in a rubber-based solid propellant (after Schapery* [2]).

might be attributed to the crack initiation and crack propagation stages? (2) Does one of these stages dominate the fatigue process? (3) Does the importance of these respective processes differ with material type, physical state, etc.? (4) For a given material, can the process dominate depending on temperature, time, and other service factors?

As far as I can ascertain, these questions have not been answered for polymers or even for metals. Metals have, of course, been much more thoroughly investigated in fatigue as well as under more simple loadings. In metals the fundamental mechanisms involved in plastic deformation are understood to be dislocation motion or twinning. This understanding has been helpful in model development of intrusion, extrusion, crack nucleation, crack propagation, and other factors involved in fatigue failure.[9] This, in turn, has been useful in behavior prediction, design, and material optimization. In polymers, there is not even complete agreement as to the mechanisms responsible for plastic deformation, let alone crack nucleation or growth. It is possible that these mechanisms differ for rubber, glassy, and semicrystalline polymers. Even polymers of a given type may not exhibit analogous behavior; for example, a glassy polymer of a given type may craze or slip or both, depending on molecular weight distribution, stress state, and temperature. I think this points out the very important, difficult, and challenging work that lies ahead for workers in

[9]Kennedy. A. J., *Processes of Creep and Fatigue in Metals*, Wiley, New York, 1968.

this area. The information from such studies should be useful in expanding the use of polymers in structural applications.

K. DeVries (additional discussion)—I enjoyed the paper very much. I would like to compliment the authors on what certainly is some very nice, careful work, characteristic of their laboratory and very good evidence of discontinuance crack growth. In leading into this topic, I do not want any of my comments to be taken as criticisms of the paper, because I think it is a significant paper.

Polymer science is a much newer field than metallurgy, and like myself and others, these authors have built essentially upon previous work in metals. To give you some idea, or perspective of just how new it is, we note that the study of metallurgy has been around a long time; on the other hand, polymer science really had its birth with the introduction of artificial polymers about the time that people were proving the existence of dislocations and characterizing them. We have a long way to go in building an adequate base for understanding fatigue in metals, and I am not sure that using only the approaches and models developed for metals tells us a lot about the basic mechanisms responsible for fatigue in polymers. We do not have an understanding of the basic mechanism for irreversible deformation in polymers. In metals it is known that dislocation motion, twinning, and so forth, give rise to plastic deformation but in polymers we're not even sure what fundamental mechanisms are responsible for deformation, let alone those responsible for the accumulations of damage.

The authors have applied the techniques of linear fracture mechanics to analyze their experimental observations of crack growth in polymers. Phenomenologically, at least, these seem to be applicable to a wide variety of systems. Referring again to Fig. 12 of my earlier discussion, an example is shown of the application of these techniques to adhesive failure. This is not my work. It's taken from a report by a group at the Materials Test Laboratory in Chicago. They used specimens in the form of double continuous beams to investigate adhesive failure. Both for the cases of failure of the polymer adhesive, as well as failure along the interface, they obtained da/dn curves that are very reminiscent of some shown today.

These similarities raise the question (in my mind at least) that if the same phenomenological approach is equally valid for all these different systems, can it reveal much about the fundamental mechanisms? Does the exponent of ΔG, for example, or the exponential coefficient provide any insight into the molecular mechanism responsible for damage in the materials being investigated?

R. W. Hertzberg—About 10 years ago, McClintock [*19*] commented on the fact that the striation spacing could be related to some fraction of the crack opening displacement.

As such, that would rationalize the second-power dependence of the striation spacing on ΔK, in which people find that the Bates and Clark relationship for striation spacing is based on the second-power dependence.

In Figs. 1 and 2 of the paper (the striation spacing was related to the macroscopic and microscopic behavior), where there is a one-to-one correlation, slopes of anywhere between 4 and 20 are shown.

McClintock's argument was that you should get a second-power crack growth rate relationship to ΔK, if striations are the only thing you have.

Well in these materials, that is the only thing we have in that regime. That is, the entire fracture surface is striated and the crack opening displacement relationship does really hold in that sense, because the striation spacings are 4th power to 20th power. I'm not sure what this slope means.

K. DeVries—I'm not certain either, and it seems to me that until we get to the point that these are more than simple curve-fitting parameters, our fracture mechanics approach will be largely phenomenological in nature.

Returning to Fig. 13 of my earlier discussion, this is somewhat reminiscent of the model described in the paper; I took this from Dick Shappery's work. It shows a tip of a crack in a rubber-based solid propellant. This crack is, again, phenomenologically very similiar to the model the authors describe but I would suspect very different in mechanism.

It seems to me that a key part of the model described in the paper is the assumed craze behavior of the material exhibiting the arrested crack-growth behavior. I wonder if you have any conclusive evidence for the fact that crazing must be present in order for the material to exhibit such behavior? It appears to me that this is something you could check not only by measurements of the effect of differences in molecular weight, as I've heard described in a previous paper you may want to briefly report here, but also by other means. You may, for example, also affect the amount of crazing that takes place by solvents or the testing atmosphere present, temperature, the stress state, etc., and it seems to me that this is also something that perhaps you or others might want to investigate. My final comment is similar to that of Dr. Peterlin. I am sure it is important to understand the propagation of fatigue cracks, but there is also the initiation stage and it appears that to date this stage had been relatively ignored. The initiation stage may be at least as important as (or perhaps more so than) the growth stage. One cannot have crack growth until cracks are present.

I am personally not aware of much work that has been done on the early stages of crack nucleation. There are some people, particularly in Russia and Europe, as well as Dr. Peterlin and myself in the United States, who have been attempting to use analytical tools to investigate the early stage of damage accumulation due to static and fatigue loadings, but we have only scratched the surface. Analytical techniques such as electron spin resonance

(ESR) and infrared have been used to detect damage accumulation as manifest by free radicals or new end groups as evidence of bond rupture. An example of this is manifested by the production of free radicals and the increase in incremental strain under cyclic loading.

R. W. Hertzberg—With regard to the question on the existence of the craze, we can report that we saw it both in examining the morphology of the fracture surface with voids indicating crazing, and in our videotapes where one can see the crack. What we did in these videotape studies was to take PVC and plasticize it.

K. DeVries—I believe you actually saw crazing. But how do you know whether there is no other kinds of deformation mechanisms dominating the flow process as well? If you take the same polymer and load it in a state of stress where it does not craze, would you still get discontinuous crack growth? I don't think you have conclusively proven that is not the case.

R. W. Hertzberg—No, we haven't, but what we have done is to take materials that are normally not considered as crazing materials, such as crystalline materials, and show that we can have discontinuous crack growth in those materials. We have shown this in polyacetel, for example. In fact, that was the material that had a cyclic life of 100 000 cycles.

K. DeVries—That seems to prove the opposite, but go ahead.

R. W. Hertzberg—The comment with regard to the relative life of the component, initiation versus propagation, is an age-old problem that I think is really at the heart of these discussions these three days. The answer is not an easy one. Regarding the results mentioned in your discussion, I might add that their specimens were unnotched and their initial conclusion that most of the life was initiation was a reasonable conclusion because people generally concluded that, when you have a smooth bar, most of the life is initiation.

However, when one goes back to look at those data and to reevaluate them and to reinterpret the fracture line data, one finds that most of the life was not initiation. So I think that the propagation stage is a very important one in these polymers.

We have taken the same polymer and loaded it to generate multiple crazing and it hasn't produced DG bands. On the other hand, we have taken materials that one does not think of as typical crazing materials, like crystalline polyacetal, and shown discontinuous crack growth. Obviously, more studies of this discontinuous cracking process are needed to clarify the points raised by Dr. DeVries.

P. Worthington[10] (*discussion*)—Peter Beadmore told us that carbon fiber reinforced epoxy resin was a material with some of the best fatigue properties in the world. In this paper, alarming crack growth curves for epoxy resin are presented, in terms of a very steep ΔK dependence at high growth rate and at very low ΔK values. I am also told that U-manufactured composites always contain numerous defects. As a design engineer, what am I supposed to make of this information?

R. W. Hertzberg—You must recognize that the addition of high-strength fibers to a polymeric matrix leads to a significant enhancement of fatigue life as compared with the polymer without reinforcement. Our results have focused on the relative fatigue response of only unreinforced polymers. The logical question then is: "Does the fatigue response of a filled polymer (fibrous or particulate additions or both) depend on the properties of the matrix or are the properties of the composite dominated by the additive constituent?" We can point to very few sets of experiments that can shed light on this question. However, a strong trend is noted wherein the fatigue life of the composite is enhanced when the fatigue properties of the matrix are improved.[11,12]

R. W. Hertzberg, M. D. Skibo, and J. A. Manson (*authors' closure*)—We thank the official reviewer, Dr. DeVries, Dr. Worthington, and the three referees for their considered evaluations of our manuscript. The various changes made in the text in response to suggestions made by these individuals have enhanced the paper's readability.

We will now respond to Dr. DeVries's discussion paragraph by paragraph.

1. We agree with the view that temperature, time scales, and environmental factors should exert a substantial influence on polymeric fatigue fracture micromechanisms. For example, changes in test cyclic frequency have affected the development of discontinuous crack growth bands [*18,22, 23*]. Similar effects of temperature and environment on the fatigue fracture process must still be identified. Regarding the role of internal structural variables on DGB formation, we have identified a major influence of molecular weight distribution [*22*]. See also Janiszewski.[13]

2. The authors are aware of the work of Mostovoy and Ripling (Fig. 12) and their finding that fatigue crack growth rates in numerous polymeric solids are dependent on the strain energy release rate range ΔG. In fact, these investigators have shown similar da/dn-ΔG plots with data derived from our previously published results showing the crack growth rate de-

[10] Research Division, Central Electricity Research Laboratories, Leatherhead, Surrey, U. K.

[11] Dally, J. W. and Carrillo, D. H., *Polymer Engineering Science*, Vol. 9, 1969, p. 434.

[12] Harris, B., *Composites*, Vol. 8, No. 4, 1977, p. 214.

[13] Janiszewski, J. A., "Molecular Weight Distribution Effects on Fatigue Crack Propagation in Poly(Methyl Methacrylate), M.S. Thesis, Lehigh University, Bethlehem, Pa., 1978.

pendence on ΔK [*14*]. We were most interested in the photomicrograph by Schapery (Fig. 13) which clearly reveals the void structure in the craze zone along with the highly elongated fibrils. Also note the craze opening distribution along the length of the craze which we proposed as accounting for the void size gradient observed on the fracture surfaces of the discontinuous growth bands. Though the Dugdale formulation was developed initially for the analysis of metallic fractures, it appears to be particularly well suited for modeling the fracture process in polymeric solids that contain long thin crack-tip plastic zones (that is, crazes).

3. Precious few tests have been conducted in our laboratory and elsewhere to evaluate the role of test temperature on active fracture mechanisms. We do note, however, that fatigue testing at high mean stress levels tends to suppress DGB formation [*15, 16*].

4-6. Dr. DeVries has touched upon a long-standing question in the fatigue fracture literature. At this time, the views of fatigue researchers are clearly polarized into two camps—one proposing that fatigue life is initiation-dominated and the other suggesting propagation-dominated behavior. The cyclic-strain experiments described by Dr. Beardmore in his paper are designed to establish a measurement of cyclic life needed for the development of a flaw of some nominal size in a component or specimem which is presumed not to be defective at the beginning of the test. The accuracy of this assumption depends heavily on the complexity of the engineering component or system and the level of quality control associated with component manufacture. When defects, either material, design, or manufacturing in nature, are unavoidable, the component fatigue life is found to be dominated by crack propagation; the latter is typically analyzed, as was the case in this paper, with the aid of fracture mechanics principles. On a number of occasions, researchers have attempted to determine the relative amounts of fatigue initiation and propagation through analysis of fracture surface markings. For example, by counting the number of fatigue striations on the fracture surface and equating that number to the number of loading cycles, the extent of the fatigue initiation stage could be determined directly by subtracting the number of observed fatigue striations from the total cyclic life. Havliček and Zilvar [*20*] employed this technique and concluded that more than 99.99 percent of the fatigue life of smooth polystyrene fatigue specimens was associated with fatigue crack initiation. However, a subsequent reexamination of these fracture surfaces showed the fatigue markings to be discontinuous growth bands rather than striations [*15*]. Consequently, the extent of the crack propagation stage was found to be several hundred to several thousand times greater than that originally

[14] Mostovoy, S. and Ripling, E. J., *Adhesion Science and Technology*, Vol. 9B, 1976, p. 513.
[15] Skibo, M. D. and Rimnac, C., private communication.
[16] Mills, N. J. and Walker, N., *Polymer*, Vol. 17, 1976, p. 335.

computed based on too hasty an interpretation of the fracture markings (see Fig. 7 of the manuscript). While this example may not resolve the problem of distinguishing between the initiation and propagation stages of fatigue damage, it does raise doubts about conclusions drawn from previous attempts to quantify the lengths of the respective initiation and propagation stages when those estimates were based on the assumption that all parallel fracture bands represented classical fatigue striations.

J. C. Runkle[1] *and R. M. Pelloux*[1]

Micromechanisms of Low-Cycle Fatigue in Nickel-Based Superalloys at Elevated Temperatures

REFERENCE: Runkle, J. C. and Pelloux, R. M., **"Micromechanisms of Low-Cycle Fatigue in Nickel-Based Superalloys at Elevated Temperatures,"** *Fatigue Mechanisms,* Proceedings of an ASTM-NBS-NSF symposium, Kansas City, Mo., May 1978, J. T. Fong, Ed., *ASTM STP 675,* American Society for Testing and Materials, 1979, pp. 501-527.

ABSTRACT: The micromechanisms of high-temperature fatigue crack initiation and crack propagation in solid-solution and precipitation-strengthened nickel-base superalloys are reviewed. The marked decrease in fatigue strength of a given superalloy with increasing temperature cannot be solely correlated with the temperature dependence of the short-time mechanical properties. The interactions between oxidation rates and fatigue strengths are very complex. The air environment plays a large role in accelerating the initiation and propagation of fatigue cracks at elevated temperatures. Increasing temperature and decreasing frequency lead to a transition from transgranular to intergranular fracture path.

The influence of different microstructural factors on the high-temperature low-cycle fatigue (LCF) behavior of a typical superalloy, Astroloy, was investigated in detail. A combination of fine 500 Å matrix γ' in conjunction with a wavy grain boundary produced by both coarse intergranular $M_{23}C_6$ carbides and primary γ' is found to offer the best LCF performance in the range of 0.2 to 0.7 T_M. The fine γ' retards Stage I cracking, and the wavy grain boundaries retard intergranular cracking. The observations made with Astroloy can be extrapolated to different γ/γ' nickel-base superalloys.

KEY WORDS: fatigue, low-cycle fatigue, elevated-temperature fatigue, superalloy, nickel-base superalloys

The flow stress of γ' precipitation-strengthened nickel-base superalloys remains approximately constant with increasing temperature up to about 0.6 T_M. By contrast, the fatigue strength of the same alloys decreases rapidly with increasing temperature, and the fatigue lifetime for a given stress range can be reduced by a factor of 20 from room temperature to

[1] Weizmann postdoctoral fellow and professor, respectively, Department of Materials Science and Engineering, Massachusetts Institute of Technology, Cambridge, Mass. 02139.

elevated temperature. It is thus important to develop a mechanistic understanding of the elevated-temperature fatigue of superalloys. The term superalloy refers to both solid-solution strengthened alloys of iron, cobalt, or nickel base and γ' precipitation-strengthened alloys of iron or nickel base. This paper will consider the fatigue behavior of both solid-solution and precipitation-strengthened nickel-base superalloys. For a more detailed discussion of the metallurgy of superalloys, the reader is referred to the text edited by Sims and Hagel [*1*].[2]

First, a short review of the present understanding of the mechanisms of elevated-temperature fatigue cracking will be given, and then the results of a recent program on the effects of different microstructures on the cyclic properties of low-carbon Astroloy will be presented.

Fatigue of Superalloys

All superalloys show a marked decrease in fatigue lifetime with increasing temperature, as shown in Fig. 1. The sharp drop in fatigue lifetime with increasing temperature is not accompanied by a corresponding decrease in short-time mechanical properties. On the contrary, as shown in Fig. 2, the flow stress of these alloys shows little decrease between 300 and 1000 K. In this temperature range the monotonic tensile ductility remains approximately constant [5], typically at 20 to 35 percent. Thus the pronounced decrease in fatigue lifetime with increasing temperature has been attributed to the important effect that the air environment plays in accelerating crack initiation and propagation. Solomon and Coffin [*6*] have clearly demonstrated this point by showing that the fatigue lifetimes at A286 at 866 K in vacuum are the same as those measured at 293 K in air. Therefore, any discussion of elevated-temperature fatigue mechanisms must consider the complex interactions between microstructure and oxidation.

Transgranular Crack Initiation and Propagation

The predominant mechanisms of crack initiation below 0.6 T_M in precipitation-strengthened nickel-base superalloys is extensive Stage I cracking along persistent slipbands. This is true for both wrought and cast alloys. A typical Stage I fracture surface in a cast Udimet 500 turbine blade is shown in Fig. 3 [*7*]. Similar Stage I cracking has been reported by Wells and Sullivan [*8*] and Moon and Sabel [*9*] in Udimet 700, by Merrick et al in Incoloy 901 [*10*], by Runkle in Waspaloy and low-carbon Astroloy [*2*], and by Leverant and Gell in single crystals of Mar-M200 [*11*]. Stage I crack initiation occurs in both fully plastic low-cycle fatigue and in high-cycle fatigue for lives greater than 10^6 cycles. Of course, during high-cycle

[2]The italic numbers in brackets refer to the list of references appended to this paper.

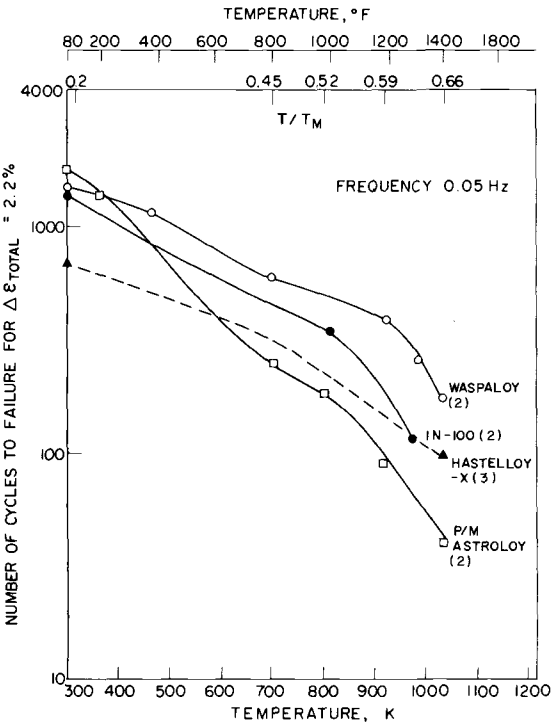

FIG. 1—*Variation in number of cycles to failure with temperature for several nickel-base superalloys tested at constant total strain range of 2.2 percent.*

fatigue, plastic deformation and crack initiation are concentrated around defects such as pores, inclusions, and carbides. Typical Stage I initiation adjacent to defects has been found by Gell and Leverant [*12*], during fatigue of single crystals of Mar-M200, and by Menon and Reiman [*13*] in Rene 95.

Solid-solution strengthened superalloys do not show extensive Stage I cracking. Jablonski [*3*] observed that between room temperature and 1033 K fatigue cracks initiated by Stage I cracking in Hastelloy-X, but the fracture path showed an almost immediate transition to Stage II cracking by ductile striation formation. Also, in contrast to nickel-base superalloys, Hastelloy-X showed no evidence of persistent slipbands on the specimen surface and thus little secondary Stage I cracking.

The susceptibility to strain localization and formation of Stage I cracks is dependent upon the type of planar slip, that is, homogeneous or heterogeneous. In solid-solution alloys, the planar slip is homogeneous, thus leading to limited Stage I cracking. On the other hand, in γ/γ' alloys the heterogeneous planar slip behavior accounts for the well-defined Stage I

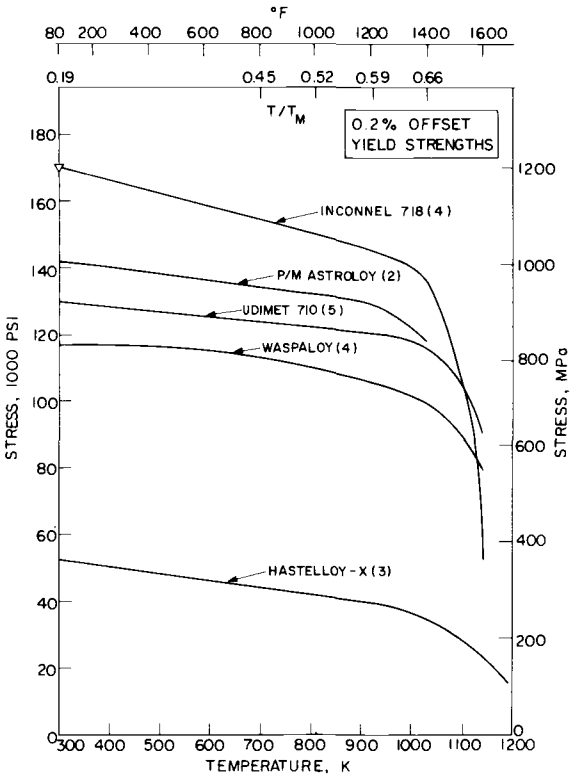

FIG. 2—*0.2 percent offset flow stress as a function of temperature for several nickel-base superalloys.*

crack initiation and propagation stages. When compared on the basis of ratio of room temperature fatigue strength at 10^7 cycles to 0.2 percent offset yield strength, γ/γ' alloys are markedly inferior to other alloy systems [*12*]. However, in room temperature low-cycle fatigue tests at a given plastic strain range, Waspaloy [*2*] and A286 [*14*] have equivalent lifetimes to failure to Hastelloy-X [*3*], a solid-solution alloy which exhibits homogeneous planar slip. Thus the relative fatigue performance of heterogeneous versus homogeneous slip materials depends on the method of comparison.

The air environment has a profound influence on Stage I cracking. Duquette and Gell [*14*] studied the effect of different environments on the mechanisms of Stage I cracking in single crystals of Mar-M200. Fatigue lives at room temperature were shorter in air than in vacuum and the fracture mode was Stage I cracking along persistent slipbands in both cases. However, Stage I fracture surfaces differed in appearance between air and vacuum. The Stage I fracture surfaces in vacuum were more ductile,

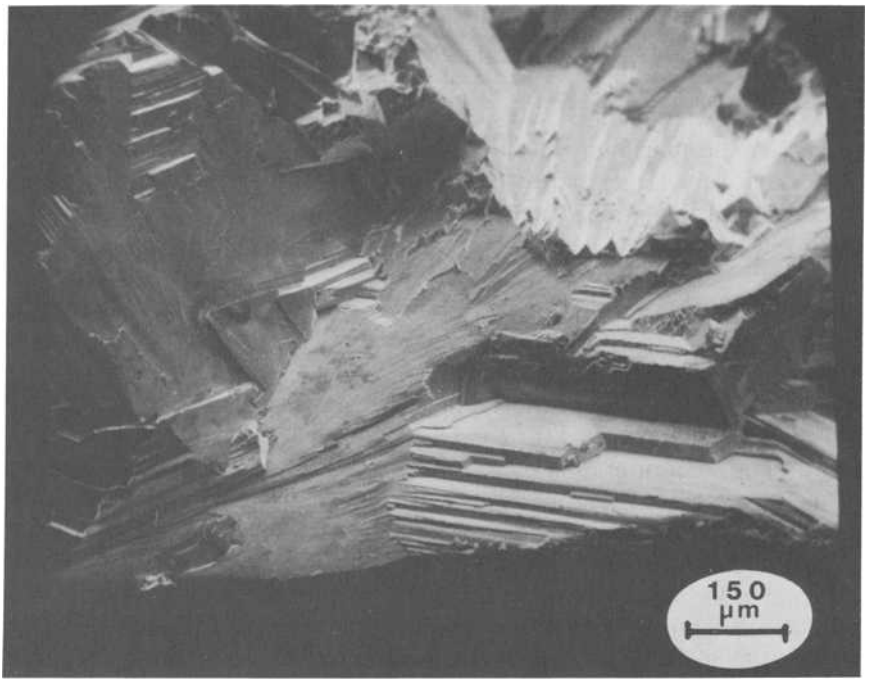

FIG. 3—*Extensive Stage I cracking in an LCF failure of a Udimet 700 compressor blade.*

with evidence of dimples indicating local ductility. In air the Stage I fracture paths were very planar, as if the air environment had lowered the fracture stress along the persistent slipbands. The effect of oxidation along the front of persistent slipbands appears to be very pronounced at elevated temperatures, thus explaining the rapid decrease in lifetime to failure with increasing temperature as shown in Fig. 1.

Following Stage I crack initiation the fracture path generally changes to a Stage II transgranular path. Leverant and Gell studied the transition from Stage I to Stage II cracking in single crystals of Mar-M200 [*11*]. At 923 K the Mar-M200 fatigue surface was 100 percent Stage I, while at 1223 K it was mostly by Stage II cracking. This fracture mode transition was found to be related to a transition in the micromechanism of deformation from planar slip to homogeneously dispersed slip.

A transition from Stage I to Stage II cracking is also observed in polycrystals but without a concomitant change in slip character. Superalloys show planar slip up to about 923 K (0.6 T_M) (depending on the γ' solvus temperature and strain rate) but a Stage I to Stage II transition occurs at high crack growth rates even at room temperature. The transition is governed in part by the ratio of reversed cyclic plastic zone size, R_c^p, at the crack tip

to the grain size. For small ratios of $R_c{}^p$ to grain size, the crack-tip opening is accommodated by Mode II displacement along Stage I cracks within individual grains. As $R_c{}^p$ becomes larger than the grain size, plastic deformation at the crack tip becomes more typical of continuous plasticity and the mode of cracking changes to a Stage II mode where the fracture plane is normal to the maximum tensile stress direction. This behavior explains the tendency for large-grained cast alloys, (Fig. 3), to show more Stage I cracking than fine-grained wrought alloys at equivalent temperatures and strain rates.

Intergranular Crack Initiation and Propagation

At temperatures greater than about 0.5 T_M, depending on strain rate and frequency, cracking during fatigue becomes intergranular. As shown in Fig. 4 from Jablonski [*3*], a fatigue crack may initiate intergranularly and propagate transgranularly. There is good reason to believe that two different mechanisms are involved in intergranular cracking. These mechanisms are oxidation and cavitation. Coffin has shown that in Udimet 500 and Rene 80 intergranular oxidation is the primary mechanism of fatigue crack initiation at 1144 K [*16,17*]. In Rene 80 he found that the fracture path changed to transgranular Stage II after one grain diameter but in Udimet 500 cracking remained intergranular.

The intergranular fracture surface features would be expected to differ depending on the relative contribution of oxidation and cavitation but, due to repeated crack closure, the microscopic evidence of cavitation is usually eliminated. Oxidation-enhanced intergranular cracking is most pronounced in the low-growth-rate regime where sufficient time exists for oxidation damage to take place along grain boundaries. Cavitation is enhanced by gross plastic deformation, for instance, in elevated-temperature tension tests. Thus intergranular cavitation is favored by large ratios of $R_c{}^p$ to grain size.

Intergranular cavitation has been modeled by Raj [*18*], who showed that grain boundary sliding near a crack tip leads to stress concentration at grain boundary precipitates and then to cavitation. At very low strain rates the stresses will be expected to relax by creep and slow down the cavitation process, but, at high strain rates, reversed sliding of the grain boundary will not allow stress relaxation and a strong "creep-fatigue interaction" effect will be observed. The model by Raj does not explain why precipitate-free grain boundaries are weaker than grain boundaries which contain precipitates. Experimental results suggest that there is an optimum size and volume fraction of grain boundary precipitates which will resist grain boundary sliding and cavitation independently of any oxidation effects [*2,10*].

FIG. 4—*Transgranular initiation of crack at surface and mixed-mode crack propagation in Hastelloy-X LCF specimen tested at 1033 K,* $\dot{\epsilon} = 8 \times 10^{-4}\ s^{-1}$, *and* $\Delta\epsilon = 0.00615$ (*1 = striations; 2 = intergranular fracture; 3 = river markings; 4 = secondary crack.*)

Contribution of the Air Environment

The air environment is clearly very important in accelerating fatigue failure of nickel-base superalloys at elevated temperature. Regardless of the mode of cracking, the air environment accelerates the crack initiation and crack propagation rates. The fatigue process is also known to enhance the environmental effects [*19*] due to transport of oxygen ahead of the crack tip. Evidence for oxygen transport ahead of the crack tip during fatigue of several alloys at room temperature was recently provided by Swanson and Marcus [*20*] in an Auger and scanning ion microscopy (SIM) study. In elevated-temperature fatigue of nickel-base superalloys, oxygen could penetrate along persistent slipbands to enhance Stage I cracking and along grain boundaries to enhance intergranular cracking as well as ahead of the crack tip to enhance Stage II type growth. The oxygen transport hypothesis also explains the recent reported sensitivity of crack growth rates to crack opening rate in square-wave versus sine-wave studies on Inconel 718 by Clavel and Pineau [*21*] and unbalanced-loop studies by Jablonski [*3*] on Hastelloy-X. In both cases the crack opening rate rather than the cycle frequency determined crack growth rates; as opening rate increased, growth rates decreased.

Fracture Path Mapping

Fracture path maps can be constructed from the fractographic results of elevated-temperature fatigue tests of superalloys. These maps are intended mostly as a conceptual framework, since not enough experimental data are available for accurate construction. Typical fracture path maps are shown in Figs. 5 and 6*a* and *b*.

Figure 5 is a fracture path map for Udimet 700 for crack initiation and for the low-growth-rate regime. In a T/T_M versus log frequency plot, this fracture map reports the regions of transgranular and intergranular fracture modes. This map is useful to study the effects of changes in grain boundary structure or changes in the fatigue test program wave shape. "Strong" or "wavy" grain boundaries, with optimally distributed grain boundary carbides and or γ'-precipitates, will show a transition to intergranular initiation at higher temperatures and lower frequencies than "weak" grain boundaries with an undesirable grain boundary microstructure such as a complete absence of carbides or a continuous carbide film. At constant frequency the wave shape will also influence the transgranular-intergranular transition. A slow-fast or a tensile hold will promote intergranular cavitation and oxidation and will shift the transgranular-intergranular transition downward. A fast-slow or compressive hold will promote healing of grain boundary voids, inhibiting intergranular cavitation to some extent and thus shifting the transition upward.

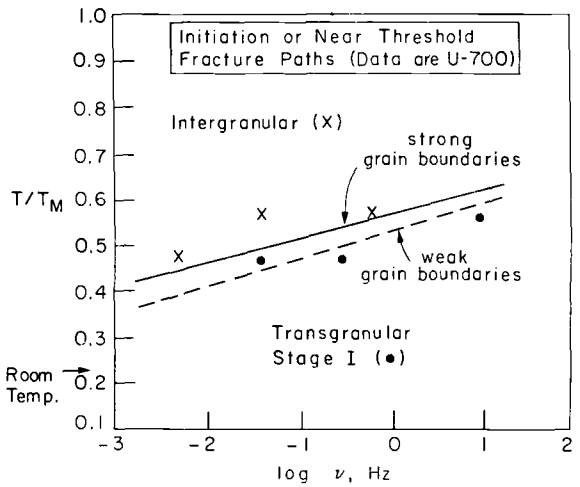

FIG. 5—*Fracture path map for crack initiation or near-threshold crack growth for Udimet 700.*

Another type of fracture path map is shown in Fig. 6. This map is constructed for elastic-plastic crack propagation at fixed frequency. In this case, the ratio of fully reversed cyclic plastic zone size, $R_c{}^p$, to grain size, d, is plotted on the abscissa. $R_c{}^p$ is estimated by the following equation

$$R_c{}^p = 0.05 \left(\frac{\Delta K}{Y_c}\right)^2$$

where ΔK is the variation of stress intensity and Y_c the cyclic flow stress.

The fracture path maps for air and vacuum in Fig. 6*a* and *b*, respectively, do not apply to any alloy in particular. They were constructed to show some experimentally observed transitions. Low growth rates and low temperatures are associated with Stage I cracking along persistent slipbands followed by a transition to a Stage II transgranular fracture path. Intergranular crack initiation is primarily caused by oxidation of grain boundaries, which is a time-dependent process. Thus, as the crack growth rate increases, a transition to Stage II transgranular propagation takes place. In the region of the fracture path map where the Stage I, Stage II, and intergranular oxidation regimes converge, it is conceivable as shown in Fig. 4 to have all three fracture paths active simultaneously.

In vacuum (see upper dotted line in Fig. 6*b*), the transition to intergranular cracking is controlled (at a given strain rate) by the ratio of plastic zone size to grain size and by the crack propagation rate. Thus, at low growth rates, cracks must propagate in Stage I or Stage II until the

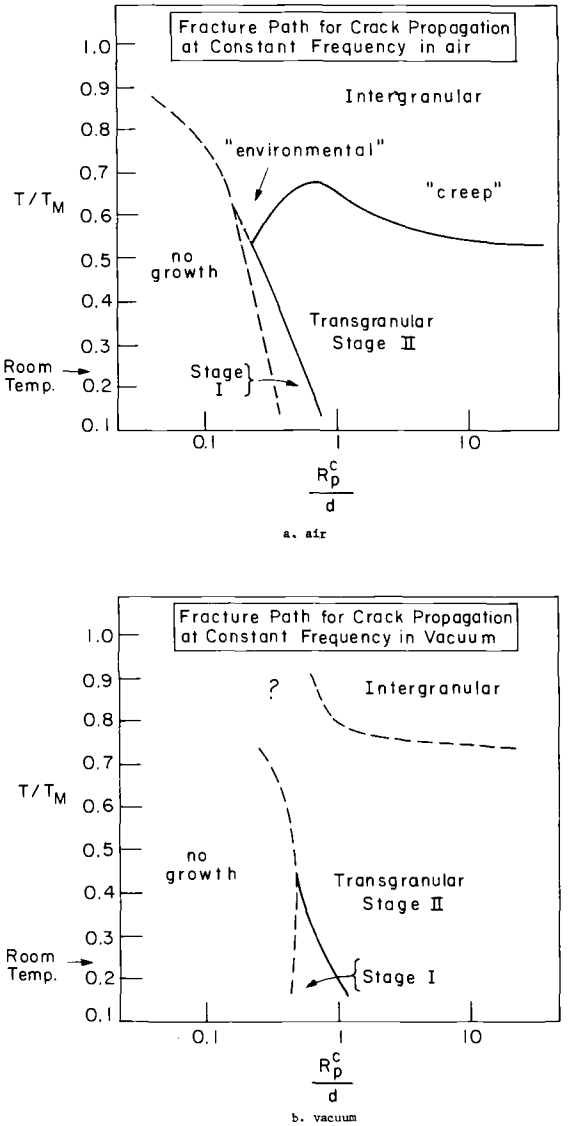

FIG. 6—*Fracture path maps in air and vacuum for a hypothetical superalloy.*

plastic zone size becomes large enough to produce appreciable grain boundary sliding. Since Stage I cracking is environmentally assisted by oxygen penetration along persistent slipbands, the Stage I regime is reduced in vacuum. Of course, the no-growth regime shifts to higher values of $R_p{}^c/d$ for tests in vacuum.

Experimental Low-Cycle Fatigue Program on Low-Carbon Astroloy

The effects of different microstructure variables on elevated-temperature low-cycle fatigue (LCF) behavior of a nickel-base superalloy were systematically investigated. Powder metallurgy low-carbon Astroloy was selected for this work on the basis of its relatively good combination of fatigue properties, homogeneity, and isotropy resulting from power processing, and because it can be heat treated to a wide variety of different microstructures.

Materials and Methods

Low-carbon Astroloy has a chemical composition similar to Udimet 700, but the carbon level is held to 0.02 to 0.03 weight percent to retard the formation of prior particle boundary carbides during consolidation of powder by hot isostatic pressing [*22,23*]. The low-carbon Astroloy used in this program was an argon-atomized prealloyed powder of composition given in Table 1 and consolidated above the γ' solvus by standard HIP powder metallurgy techniques at 1000 atm (103 MPa) and 1218 C for 3.0 h.

TABLE 1—*Composition of low-carbon Astroloy (% by weight).*

C	Mn	Si	Cr	Ni	Co	Fe	Mo	W	Ti	N	B	Zr	O
0.026	0.01	0.05	14.9	balance	16.9	0.06	4.9	0.03	3.6	4.0	0.024	0.031	94 ppm

Low-carbon Astroloy contains about 42 volume percent γ' which may be precipitated heterogeneously at grain boundaries and homogeneously in the matrix. The major carbide phases are MC and $M_{23}C_6$, both of which are normally found in the grain boundaries. The boride phases M(B,C) and M_3B_2 are also present [*19*]. By varying the heat treatment it is possible to produce a wide variety of microstructures with coarse or fine γ' and grain boundaries with and without γ' and or carbides.

The low-carbon Astroloy used in this LCF program was heat treated as follows to four very different microstructures

1. 1394 K/4 h/AC[3] + 1144 K/8 h/AC + 1255 K/4 h/AC + 922 K/24 h/AC + 1033 K/8 h/AC

2. 1423 K/4 h/AC + 1144 K/8 h/AC + 1255 K/4 h/AC + 922 K/24 h/AC + 1033 K/8 h/AC
3. 1380 K/4 h/OQ[4] + 1033 K/4 h/AC
4. 1394 K/4 h; cool at 0.5 deg C/min to 1033 K/AC

Resulting γ' size distributions, as determined by point counting on replica transmission electron microscope (TEM) photomicrographs, are plotted in Fig. 7, and grain boundary structures of all four microstructures are schematically sketched in Fig. 8. Replica TEM photomicrographs are included in Fig. 9*a-d*.

Microstructure I—This microstructure is utilized by the gas turbine industry for turbine disk application because it results in the best combination of tensile and stress rupture properties. It is characterized by "wavy" grain boundaries containing both primary γ' and $M_{23}C_6$ carbides. The matrix γ' varies in size with three modes in the distribution: 0.8, 0.2, and 0.05 μm.

Microstructure II—This microstructure contains no grain boundary γ' due to solution above the γ' solvus. $M_{23}C_6$ and MC carbides are present in the grain boundaries. The matrix γ' is one size, about 0.2 μm.

Microstructure III—In this case there are no carbides in the grain boundaries, but solution below the γ' solvus results in some 1-μm grain boundary and some 0.8-μm matrix γ'. Oil quenching and single-step aging produce fine matrix γ' of 0.05-μm.

Microstructure IV—A slow cool results in no grain boundary carbides and a very broad γ' size distribution. One half of the 42 percent γ' is 2-μm or larger.

Mechanical properties testing included tension tests at 298 and 811 K and low-cycle fatigue tests at 298, 700, 811, 922, and 1033 K. LCF tests were conducted on a servohydraulic machine using induction heating in derived longitudinal strain control on hourglass-shaped specimens 6.3 mm (0.25 in.) in diameter. A total strain range of 2.2 percent and a frequency of 0.05 Hz were chosen for all tests except those at 922 K, where strain ranges of 1.0 and 1.5 percent and frequencies of 0.5 and 0.005 Hz were also employed.

To study mechanisms of crack initiation, aluminum-shadowed plastic replicas were made of the polished specimen outer surface and examined by optical microscopy. Scanning electron microscopy (SEM) was conducted on the fatigue fracture surfaces of failed specimens.

Results

Results of 298 and 811 K tension tests are presented in Table 2. Tensile yield strengths are seen to be related to γ' size distribution. As expected,

[4]Oil quenched.

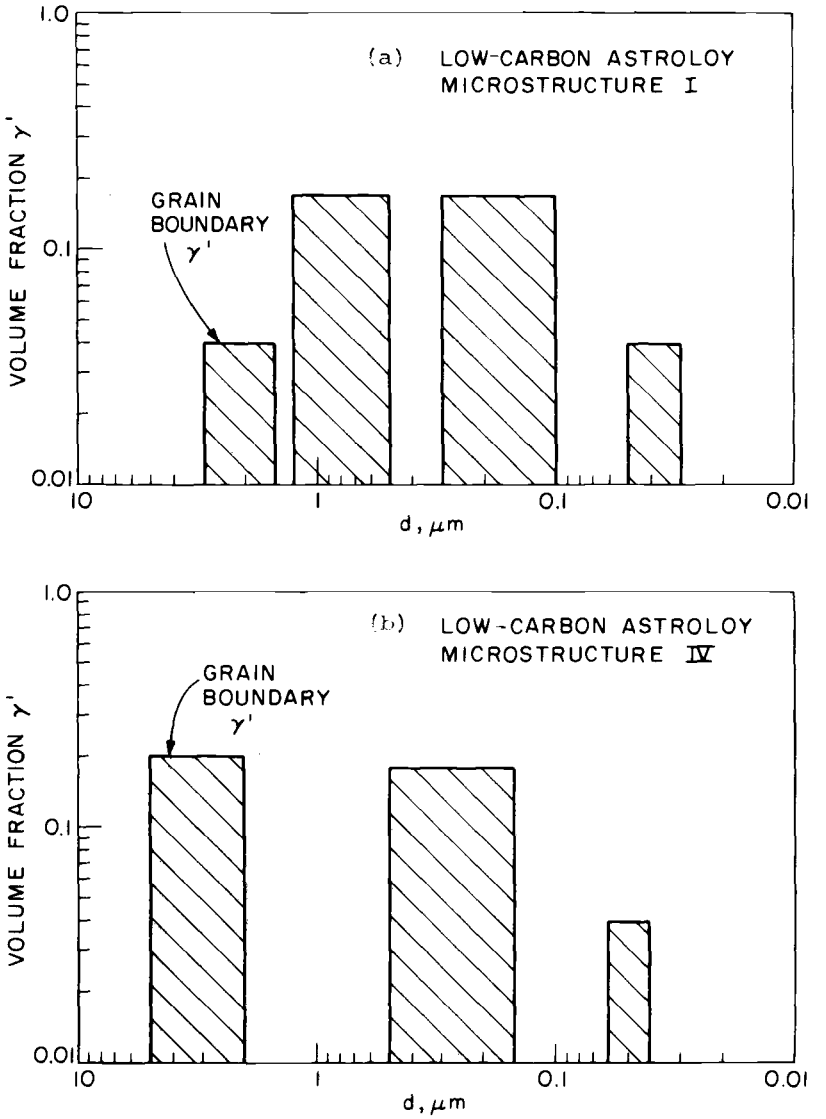

FIG. 7—γ' *size distributions of low-carbon Astroloy with Microstructure I in* (a) *and Microstructure IV in* (b).

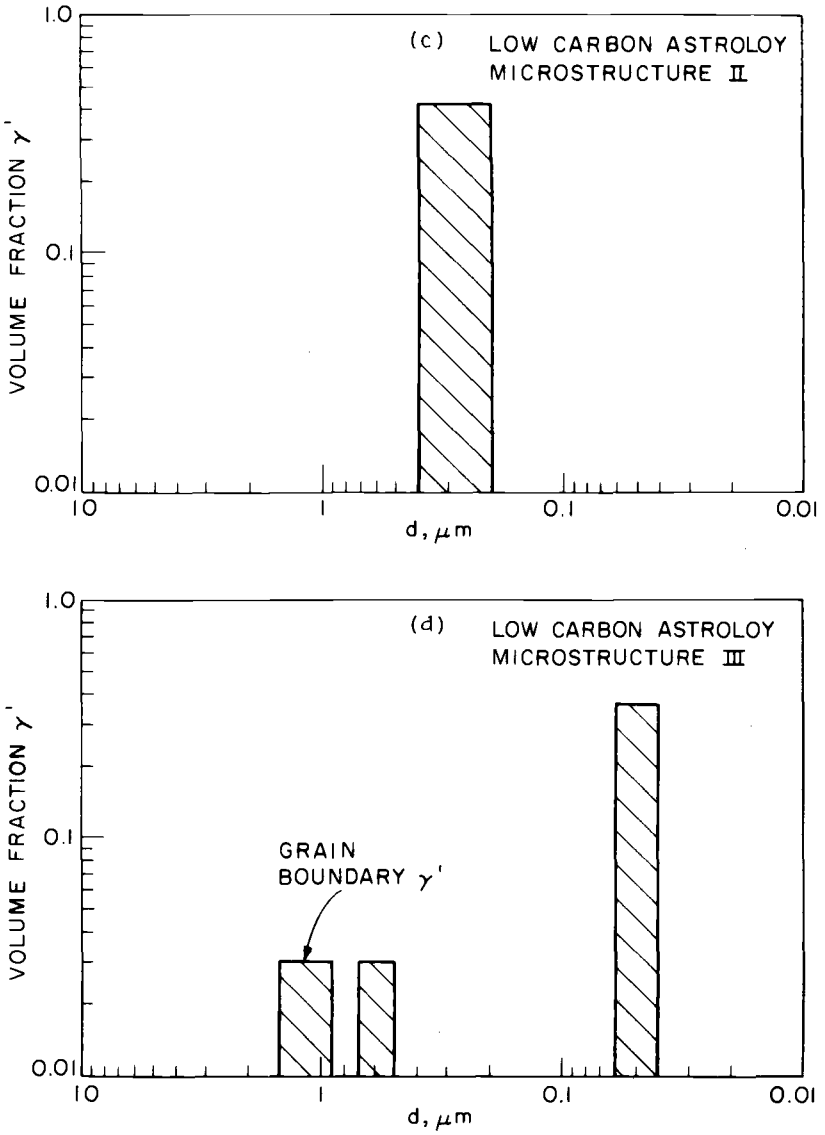

FIG. 7—*Continued.* γ' *size distributions of low-carbon Astroloy with Microstructures II in* (c) *and Microstructure III in* (d).

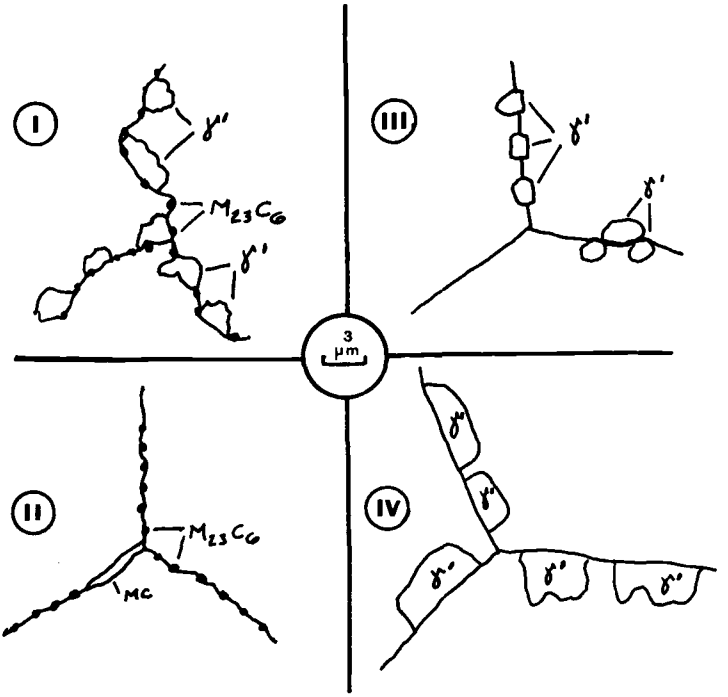

FIG. 8—*Sketches of low-carbon Astroloy grain boundaries.*

Microstructure III with nearly all fine 500 Å γ' is the strongest and Microstructure IV with mostly coarse γ' is the weakest. Ductilities and ultimate tensile strengths do not differ as markedly as yield strength.

In Fig. 10 the low-cycle fatigue performances for a total longitudinal strain range of 2.2 percent of all four microstructures of low-carbon Astroloy are compared as a function of temperature. Above 875 K, Microstructure III exhibits the worst behavior and Microstructure I the best. At 700 and 911 K, Microstructure II exhibits significantly lower fatigue lives than Microstructures I, III, or IV, which have approximately the same lifetimes to failure at these temperatures. At room temperature the ranking corresponds to initial cyclic flow stress with stronger microstructures showing longer lifetimes.

In order to determine modes of fatigue crack initiation and propagation, failed specimens were examined by two methods. First, plastic replicas were taken from the outer surface of the specimens in order to study mechanisms of initiation of secondary LCF cracks. Second, the fracture surfaces were examined by SEM. The results of these investigations plus those of similar investigations on Waspaloy [*2*] are summarized in Table 3 and reviewed in the following.

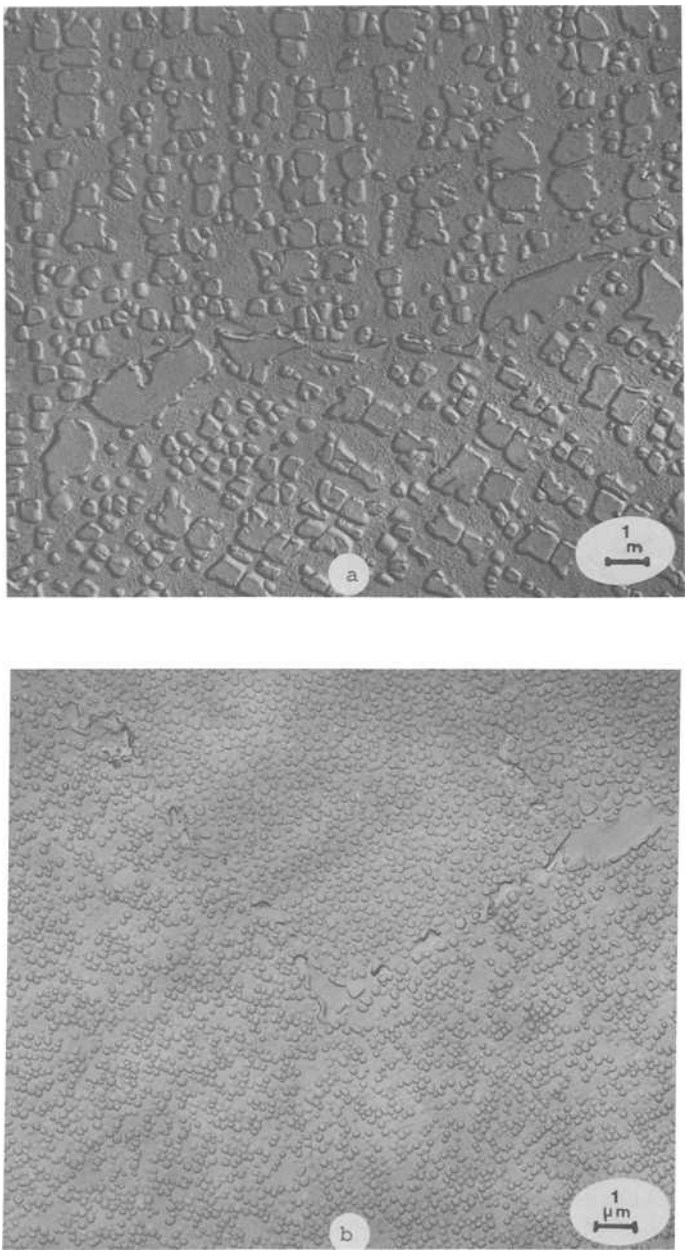

FIG. 9—*Low-carbon Astroloy microstructures.*

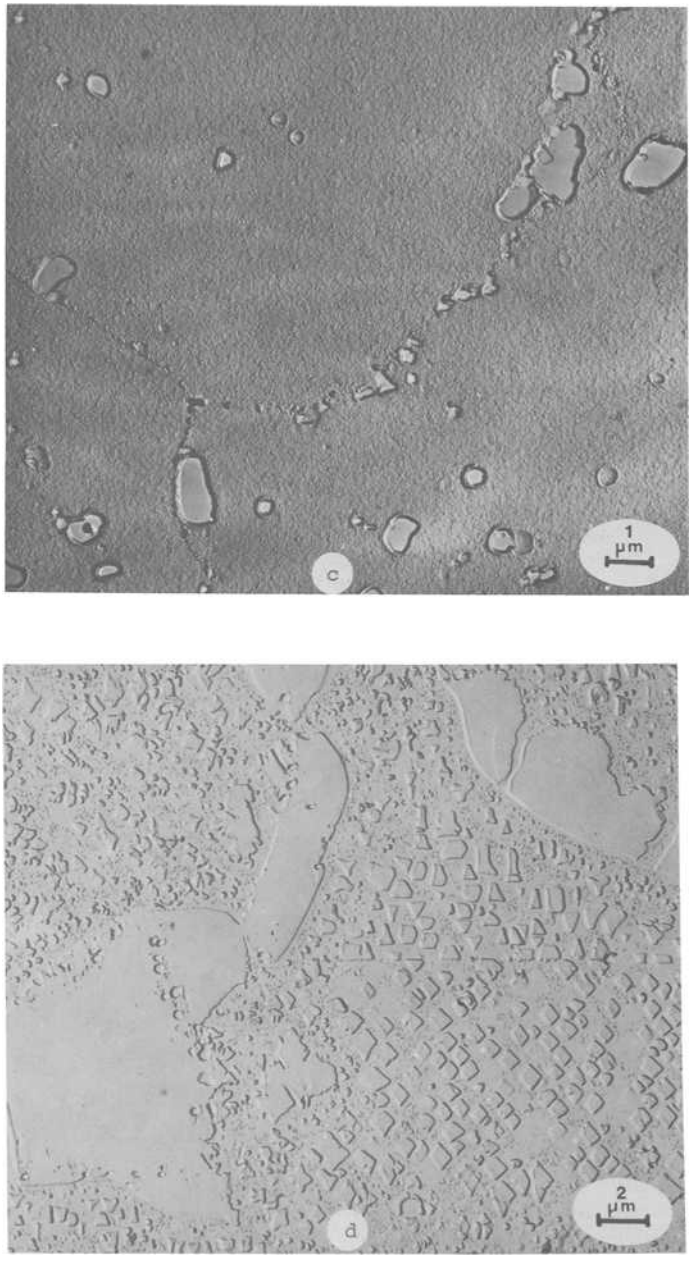

FIG. 9—*Continued.*

TABLE 2—*Tension test results.*

Alloy	Temperature	0.2% Yield MPa (ksi)	Ultimate Tensile Strength, MPa (ksi)	Elongation, %	Reduction in Area, %
Astroloy (I)	RT[a]	(126) (868)	1350 (196)	28	30
	811 K	(123) (847)	1212 (176)	22	22
Astroloy (II)	RT	(134) (923)	1357 (197)	24	24
	811 K	(132) (909)	1240 (180)	20	21
Astroloy (III)	RT	(147) (1013)	1371 (199)	18	19
	811 K	(140) (965)	1295 (188)	18	20
Astroloy (IV)	RT	(108) (744)	1326 (192)	30	32
	811 K	(105) (723)	1199 (174)	24	22

[a] Room temperature.

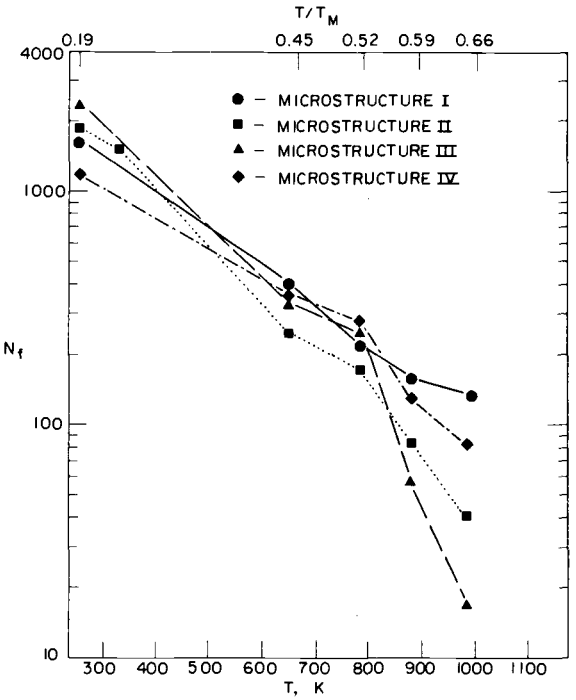

FIG. 10—*Variation of number of cycles to failure with temperature for the four microstructures of low-carbon Astroloy tested at a constant total strain range of 2.2 percent.*

TABLE 3—*Mode of LCF crack initiation and propagation.*

Temperature, K (°F)	Frequency, Hz	Alloy		Mode of Initiation	Initial Mode of Propagation[a]
RT[b]	0.04	Waspaloy		I	I
RT	0.05	L/C[c] Astroloy	(I)	I	I
			(II)	I	I
			(III)	I	I
			(IV)	I	I
700 (800)	0.05	Waspaloy		I	II
		L/C Astroloy	(I)	I	II
			(II)	I	I
			(III)	I	II
			(IV)	I	II
811 (1000)	0.05	L/C Astroloy	(I)	I	II
			(II)	I	I
			(III)	I	I + I
			(IV)	I	II
922 (1200)	0.05	Waspaloy		I	II
		L/C Astroloy	(I)	I	II
			(II)	I + IX	I + II
			(III)	IX	IX
			(IV)	I	II + I
	0.005	L/C Astroloy	(I)	IX	II + 50%IX
	0.5	L/C Astroloy	(I)	I	II
	0.5	L/C Astroloy	(II)	I	I
1033 (1400)	0.05	Waspaloy		I	II + 20%IX
		L/C Astroloy	(I)	IX	II (after less than 1 grain diameter
		L/C Astroloy	(II)	IX	IX
		L/C Astroloy	(III)	IX	IX
		L/C Astroloy	(IV)	IX	II

[a] KEY: I = Stage I; II = Stage II; IX = intergranular.
[b] Room temperature.
[c] Low carbon.

At room temperature, crack initiation was by Stage I transgranular fracture as shown by the surface replica micrograph in Fig. 11. Stage I initiation was followed by a transition to Stage II propagation after several grain diameters. At 702 and 811 K, crack initiation was still Stage I for all four microstructures but the extent of Stage I cracking varied considerably. Microstructures I, III, and IV with approximately the same fatigue lifetimes behaved as shown in Fig. 12, that is, Stage I initiation followed by immediate transition to Stage II propagation. Microstructure II with significantly shorter lifetimes exhibited extensive Stage I cracking as seen in Fig. 13. At 1033 K, intergranular crack initiation was noted in all four microstructures but intergranular propagation as in Fig. 14 was associated with the greatly reduced fatigue lifetimes of Microstructures II and III.

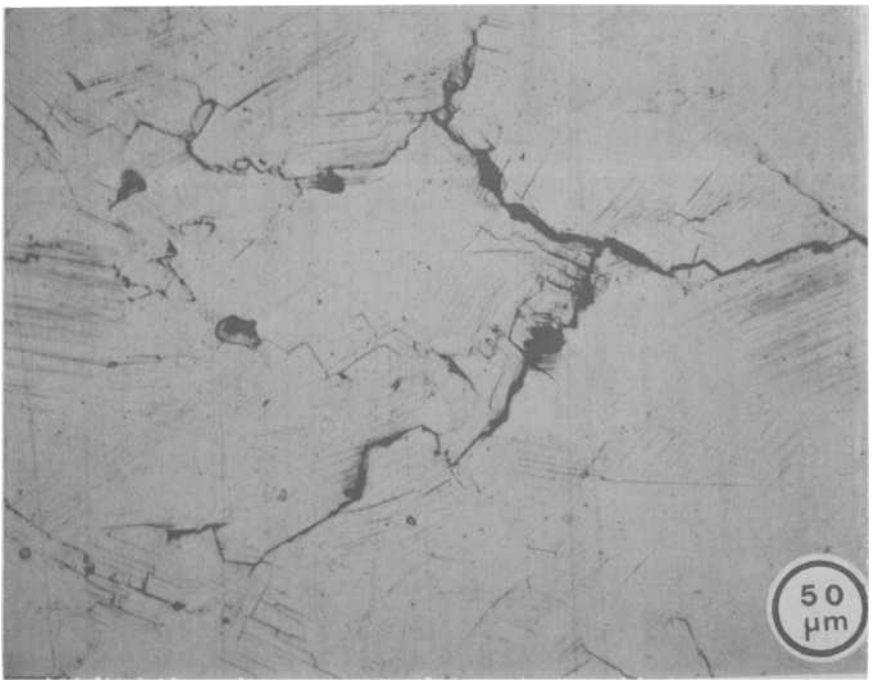

FIG. 11—*Photomicrograph of surface replica showing Stage I fatigue crack initiation at room temperature in low-carbon Astroloy with Microstructure III* ($\Delta\epsilon = 2.2$ *percent*).

Discussion

Near room temperature, differences in initial cyclic flow stress govern lifetimes to failure. Since the LCF tests were conducted under control of total strain range, Microstructure IV with coarse γ' had a larger cyclic plastic strain than Microstructure III with fine γ' and a correspondingly shorter fatigue lifetime. Thus, at low temperatures it is best to heat treat for fine γ' and optimum tensile strength.

At 700 and 811 K, low-carbon Astroloy with Microstructure II exhibited extensive Stage I cracking in conjunction with the shortest LCF lifetime. The air environment is the reason for this behavior. Extreme concentration of deformation in planar bands promotes rapid oxidation in these areas, reducing the normal fracture strain of the persistent slip-band. The reasons for more extensive Stage I cracking in Microstructure II are not yet known but are undoubtedly related to the γ' size distribution. All microstructures but Microstructure II had some fine 500 Å γ'; Microstructure II had only 2000 Å γ'. The best LCF strength in the room temperature to 825 K ($0.2 < T/T_M < 0.55$) is obtained with a fine γ' precipitation size distribution.

FIG. 12—*SEM photomicrograph showing Stage I fatigue crack initiation followed by Stage II crack propagation at 700 K and 9.95 Hz in low-carbon Astroloy with Microstructure IV* ($\Delta\epsilon = 2.2$ *percent*).

Above 875 K (0.55 T_M), a transition to intergranular cracking governs the LCF lifetime. The temperature and frequency of the transition and the rate of intergranular cracking are governed by the grain boundary microstructure. Both $M_{23}C_6$ carbides and primary γ' are important for the LCF crack-resistant grain boundaries. Microstructure I with wavy grain boundaries produced by $M_{23}C_6$ carbides and primary γ' was the best above 875 K (0.55 T_M) and Microstructure III with no grain boundary $M_{23}C_6$ carbides and little intergranular primary γ' was the worst.

For any superalloy it is necessary to experimentally determine the optimal heat treatment for the most LCF crack-resistant microstructure. It is reasonable to assume that a matrix-γ size distribution and a grain boundary microstructure which are resistant to LCF cracking would also be resistant to notched stress rupture failure and intergranular static crack growth. For a given superalloy the microstructure is a strong function of

1. solution temperature,
2. cooling rates, and
3. sequence of precipitation of carbides and γ' phases.

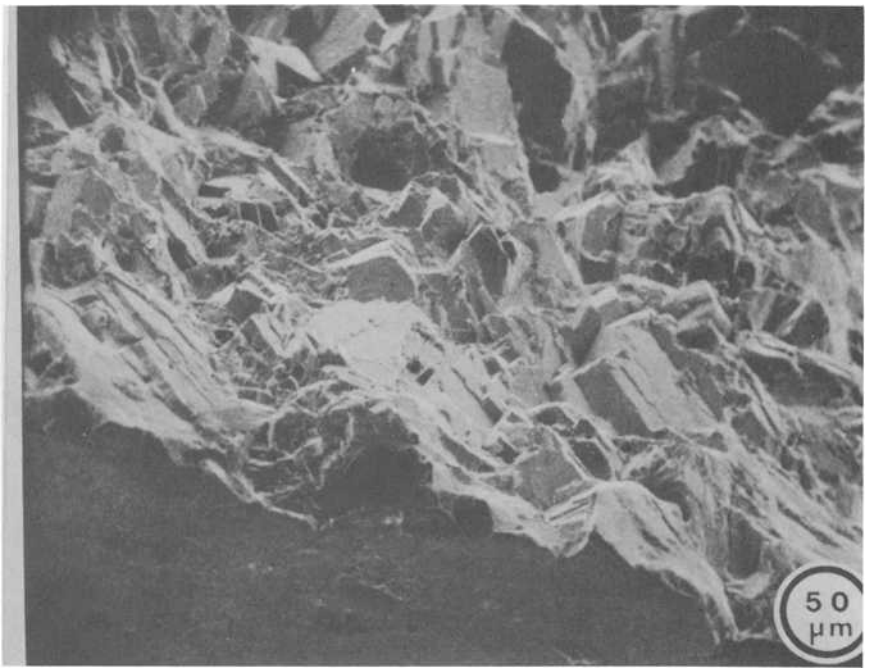

FIG. 13—*Stage I fatigue crack initiation and propagation at 700 K and 0.05 Hz in low-carbon Astroloy with Microstructure II* ($\Delta\epsilon = 2.2$ *percent*).

Although the microstructure is usually the result of complex empirically determined heat treatments, for optimum high-temperature LCF strength, we need

1. *Serrated grain boundaries* to minimize grain boundary sliding and to lower grain boundary cracking rates. The most effective serrated grain boundaries are produced by both coarse carbides and primary γ'.

2. *Fine* γ' *particles* to retard Stage I cracking. This refinement may be incompatible with Requirement 1 and, in general, there will be a range of optimum γ' precipitate sizes. It is important to have the largest possible V_f of fine γ' to increase the flow stress. However, at temperatures above 875 K (0.55 T_M) fine γ' may be detrimental because a high matrix strength will lead to grain boundary failure.

References

[1] Sims, C. T. and Hagel, W. C., *The Superalloys,* Wiley-Interscience, New York, 1972.
[2] Runkle, J. C., "The Elevated Temperature Fatigue of Nickel-Base Superalloys," Sc.D. Thesis, Massachusetts Institute of Technology, Cambridge, Mass., 1978.

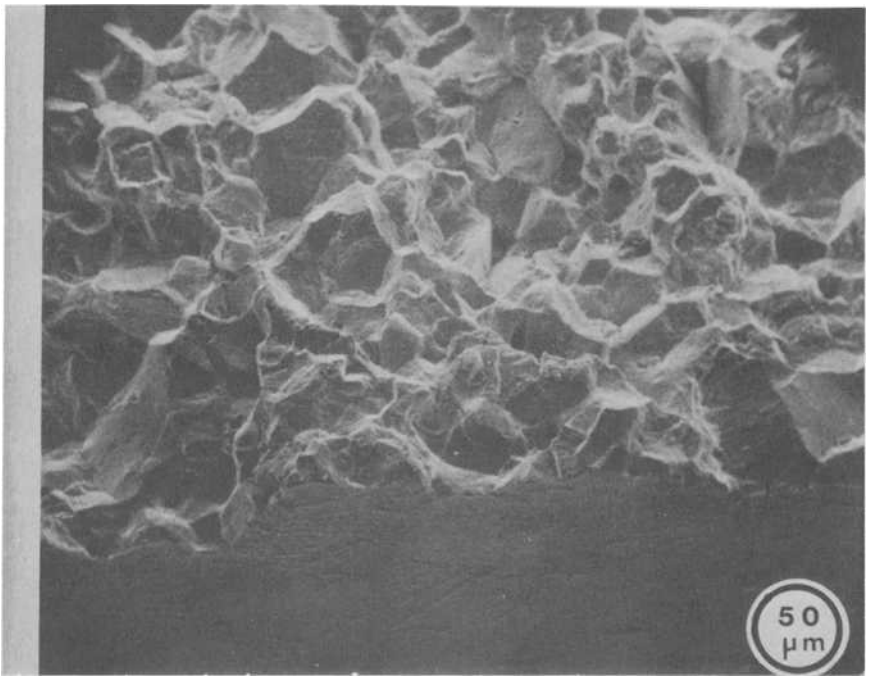

FIG. 14—*SEM photomicrograph showing intergranular fatigue crack initiation and propagation at 1033 K and 0.05 Hz in low-carbon Astroloy with Microstructure II* ($\Delta\epsilon = 2.2$ *percent*).

[3] Jablonski, D., "Fatigue Behavior of Hastelloy-X at Elevated Temperature in Air and Vacuum Environments," Ph.D. Thesis, Massachusetts Institute of Technology, Cambridge, Mass., 1978.
[4] "Description and Engineering Characteristics of Eleven New High-Temperature Alloys," Defense Materials Information Center, Memorandum 255, Battelle Memorial Institute, Columbus, Ohio, 1971 (document available from Defense Documentation Center, Alexandria, Va.).
[5] "High Temperature High Strength Nickel-Base Alloys," Product Bulletin, International Nickel Co.
[6] Solomon, H. and Coffin, L. F., Jr. in *Fatigue at Elevated Temperatures, ASTM STP 520,* American Society for Testing and Materials, 1972, p. 112.
[7] Pelloux, R. M., unpublished research, Massachusetts Institute of Technology, 1972.
[8] Wells, C. H. and Sullivan, C. P., *American Society for Metals Quarterly Transactions,* Vol. 60, 1967, p. 217.
[9] Moon, D. M. and Sabol, S. P. in *Fatigue at Elevated Temperatures, ASTM STP 520,* American Society for Testing and Materials, 1972, p. 438.
[10] Merrick, H. T. *Metallurgical Transactions,* Vol. 5, 1974, p. 891.
[11] Leverant, G. R. and Gell, M., *Metallurgical Transactions,* Vol. 6A, No. 2, 1975, p. 367.
[12] Gell, M. and Leverant, G. R. in *Ordered Alloys,* Claitors Publishing Division, 1970, p. 505.
[13] Menon, M. N. and Reiman, W. H., *Journal of Materials Science and Engineering,* Vol. 10, 1975, p. 1571.

[14] Duquette, D. J. and Gell, M., *Metallurgical Transactions*, Vol. 2, 1971, pp. 1325-1331.
[15] Coffin, L. F., Jr. in *Fatigue at Elevated Temperatures, ASTM STP 520*, American Society for Testing and Materials, 1972, p. 5.
[16] McMahon, C. J. and Coffin, L. F., Jr., *Metallurgical Transactions*, Vol. 1, 1970, p. 3443.
[17] Coffin, L. F., Jr., *Metallurgical Transactions*, Vol. 5, 1974, p. 1053.
[18] Pavinich, W. and Raj, R., *Metallurgical Transactions*, A, Vol. 8A, 1977, p. 1917.
[19] Sadananda, K. and Shahinian, P., "Crack Growth in Alloy 718 at 425°C," *Journal of Materials Science of Engineering Materials and Technology*, American Society of Mechanical Engineers, to be published.
[20] Swanson, J. W. and Marcus, H. L., *Metallurgical Transactions*, Vol. 9A, No. 2, 1978, pp. 291-293.
[21] Clavel, M. and Pineau, A., *Metallurgical Transactions*, 9A, No. 4, 1978, pp. 471-480.
[22] Price, P. E., Widmer, R., and Runkle, J. C. in *Proceedings*, International Powder/Metallurgy Conference, Vol. 11, 1976, p. 45.
[23] Podob, M. T. in *Proceedings*, International Powder/Metallurgy Conference, Chicago, Ill., Vol. 11, 1976, p. 25.

DISCUSSION

B. Tomkins[1] (*discussion*)—Although the paper contains only a limited amount of data on one superalloy, the authors have made a significant contribution in considering the effect of varying microstructures on endurance over a range of temperatures. Figure 10 summarizes the results and is worthy of more discussion.

Considering the region below 550°C, although the overall endurance drops by an order of magnitude between 25 and 550°C, at any one temperature endurances are within a factor of two. This indicates a relative lack of dependence on crack mode, the ratio of Stage I/Stage II crack growth varying considerably with microstructure, but a strong dependence on either oxidation rate or cyclic stress response. In their general initial statement, the authors seem to favor the former by comparison with data on the iron base alloy A-286, but if the ratio $\Delta\sigma/2T$ is considered, where T is the material flow stress close to the crack tip [$\approx$ ultimate tensile strength (UTS), which is relatively constant for this alloy], it increases considerably with increasing temperature and with resulting increase in crack-tip opening displacement (CTOD) and crack growth rate. Perhaps a more detailed analysis of data could isolate the mechanics contribution.

It is also worth noting that below 550°C, crack initiation features can have a considerable effect on endurance. For example, recent work on stainless steels by Wareing[2] has shown the following pattern for initiation. Below 550°C, electropolished surfaces give a few discrete initiation sites

[1] Reactor Fuel Element Laboratories, U.K. Atomic Energy Administration (Northern Division), Springfields, Salwick, Preston, Lancs, U.K.
[2] Wareing, J., to be published.

from which cracks develop with a constrained, approximately semicircular, geometry. On the other hand, as-machined surfaces produce multiple initiation sites which rapidly link to give a relatively unconstrained crack front extending around the specimen. The result is a factor of 2 to 4 on endurance as can be seen in Fig. 15 of this discussion, where Wareing's data for 2.2 percent strain is included from Fig. 1 of the text. Above 550°C, however, multiple initiation readily occurs at grain boundaries to give a relative independence of endurance on surface finish.

Above 550°C, the paper clearly shows the effect of grain boundary microstructure with endurance variations of almost an order of magnitude between Microstructures I and III at 760°C. At this temperature all four microstructures show intergranular initiation, but the two with lowest endurance also show intergranular propagation. It would be interesting to know whether these intergranular fracture paths involve cavity formation on grain boundaries ahead of the crack front which contributes to crack

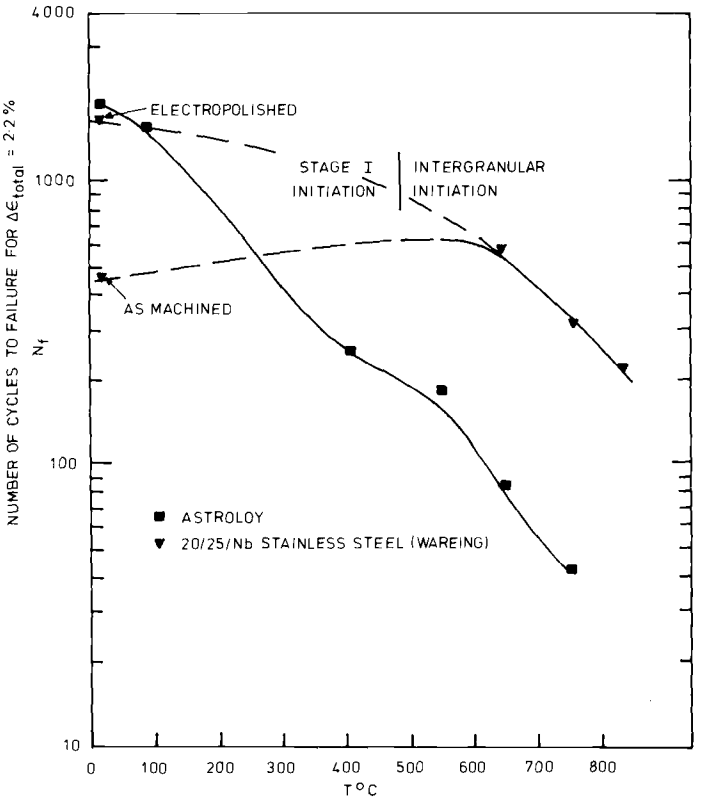

FIG. 15—*Stainless steel data compared with those of Fig. 1 of the text.*

advance. As a symmetrical cycle is used on fully plastic specimens, this is unlikely, in which case the effect could well be a simple lowering of the effective material flow stress along weak boundaries at the crack tip. Even so, the effective strain rate in this region would be considerably in excess of the applied strain rate of $\sim 2 \times 10^{-3}\,s^{-1}$.

Because the tests in the program are endurance tests, it is difficult to isolate and quantify the crack growth period although at such a high strain level one would expect crack initiation to be rapid for all situations. It would have been useful to know striation spacings from Stage II portions of the fractures for comparison between microstructures on a crack depth basis. Also, at the highest temperature some short crack growth studies would help to clarify the source of the large endurance changes.

In summary, the paper shows in a convincing way the strong effect of microstructure on high-temperature fatigue in the creep range. It does not, however, shed much light on the competing roles of oxidation, creep cavitation, and material constitutive relation changes.

D. Michel[3] (*discussion*)—This paper presents results from an interesting series of experiments concerning the influence of microstructure on fatigue in low-carbon Astroloy. The paper correctly notes the important effect of the persistent slipbands on the micromechanisms of the fatigue of the material at temperatures up to 0.6 T_M and points to the importance of oxidation to the intergranular failure mechanisms in the nickel-base superalloys. However, despite the short review of mechanisms of elevated-temperature fatigue cracking, the results do not develop evidence which would show the manner in which the related effects of grain boundary microstructure, oxidation, persistent slipband formation, and cavity formation influenced the micromechanisms of fatigue failure in the four microstructures investigated. Careful study of the failure surfaces of the test specimens would appear to be appropriate in an attempt to develop this additional information as an important corollary to the significant results presented in the paper.

J. C. Runkle and R. M. Pelloux (*author's closure*)—We appreciate the comments and questions of Dr. Tomkins and Dr. Michel. In agreement with the comment of Dr. Tomkins concerning the increase in CTOD with temperature due to the increase in cyclic flow stress, we acknowledge that this could account for some of the decrease in lifetime to failure. Regarding time to initiation versus time spent in propagation, in some other recent work on fully plastic crack propagation in Hastelloy-X, we have

[3]Thermostructural Materials Branch, Naval Research Laboratory, Washington, D.C. 20375.

found that as temperature increases, initiation time decreases, and time spent in propagation dominates fatigue lifetime.

With respect to the questions of both Dr. Michel and Dr. Tomkins, on fractography, we reiterate that fractography on elevated-temperature LCF specimens is difficult to interpret due to oxidation and repeated closure in the fully reversed cycle.

D. Sidey[1] *and L. F. Coffin, Jr.*[2]

Low-Cycle Fatigue Damage Mechanisms at High Temperature

REFERENCE: Sidey, D. and Coffin, L. F., Jr., **"Low-Cycle Fatigue Damage Mechanisms at High Temperature,"** *Fatigue Mechanisms.* Proceedings of an ASTM-NBS-NSF symposium, Kansas City, Mo., May 1978, J. T. Fong, Ed., *ASTM STP 675.* American Society for Testing and Materials, 1979, pp. 528–568.

ABSTRACT: Observed effects of wave shape on low-cycle fatigue resistance and on concomitant fracture appearance at elevated temperature are summarized. Additionally, previously unreported tests on oxygen-free high conductivity (OFHC) copper at 673 K, as well as available published results, are examined using unequal strain rates to produce the wave shape. For OFHC copper, the fatigue lifetimes decreased by an order of magnitude as the tensile-going strain rate was reduced from 1.7×10^{-3} s^{-1} to 1.7×10^{-5} s^{-1} with a constant cyclic period. Accompanying this reduction in lifetime, the fracture mode changed from a transgranular fracture for the fast-slow wave shape to an intergranular single-crack fracture for equal ramp rates to interior cavitation for the slow-fast test.

Based on these findings and related work of other investigators, a qualitative model is presented to predict the ranking in fatigue resistance and in fracture mode as a function of wave shape and environment, for a given temperature, strain range and overall frequency. Essential features of this model include the assumption of grain boundary cavity size variability depending on the magnitudes of the tensile-going and compressive-going strain rates of the hysteresis loop and recognition of the important role of environment in degrading life and affecting fracture mode, especially when tensile- and compressive-going strain rates are equal.

KEY WORDS: high-temperature fatigue, low-cycle fatigue, damage mechanisms

In keeping with the theme of the symposium, the present paper deals with the mechanisms of fatigue as they bear on fatigue damage at elevated temperature (defined as $T/T_m \geq 0.5$) where time and strain rate effects are important. This regime is often referred to as that of time-dependent

[1]Technical supervisor, Central Thermal Services, Ontario Hydro, 700 University Avenue, Toronto, Ont. M5G 1X6, Canada; formerly CEGB Fellow, Christ's College, Cambridge University, Cambridge, U.K.

[2]Mechanical engineer, General Electric Co. Corporate Research and Development, Schenectady, N.Y. 12301.

fatigue. The fatigue process is frequently treated in separate components of initiation and of crack growth. The present treatment considers the regime of crack initiation and early crack growth. Primarily, attention will be given to the observations and interpretations obtained from experiments on smooth specimens subjected to uniaxial loading in the low-cycle fatigue range. The interplay of important testing parameters will be considered as they relate to the micromechanisms believed to be responsible for the nature of the failures observed.

As indicated herein, the phenomenological information developed in time-dependent fatigue is voluminous. It is the purpose of the paper to review some of the significant experimental findings, including some new and unpublished information, to interpret these findings in terms of the microstructural response of the material to its testing conditions and to suggest a basis for a broader understanding of the phenomenon more generally. Much of the stimulus for this work began with an investigation undertaken while the authors were in residence at Cambridge University in 1976.

Damaging Processes from Cyclic Straining

As a consequence of the application of cyclic plastic strain at elevated temperature, a number of damaging processes can affect the microstructure and the resulting fatigue resistance. These damage processes can lead to premature failure by fatigue when compared with fatigue failure under conditions of time independency, that is, where frequency, strain rate and environmental effects are absent. In the latter, damage and failure arise from strain localizations on a microstructural level giving rise to crack initiation from instabilities such as intrusions and extrusions and to growth or coalescence of cracks from these initiation sites. The topic of elevated-temperature fagitue damage was reviewed in more detail in a recent paper [*1*][3] and brief mention will be made here only of the important damage categories. Included there were such topics as substructure, cyclic strain aging, grain boundaries, environment, wave shape, and plastic instability. Of particular interest to the present discussion are damage processes in grain boundaries, and from the environment. Wave shape effects will be treated later.

Grain boundary damage in time-dependent fatigue is viewed primarily as a process of cavity nucleation and growth and of triple-point cracking. These are processes which have been more generally studied in creep under static loading, but Veevers and Snowden [*2*] have recently reviewed the status of this topic in fatigue. Much of this work has been done with materials and conditions where grain-boundary migration can occur. Since this

[3]The italic numbers in brackets refer to the list of references appended to this paper.

paper is concerned with structural materials, migration is generally inhibited by grain boundary precipitates or compositional variations. This aspect will be discussed in more detail later. The grain boundary damage processes that are of importance here are those associated with cavitation and triple point cracks. Further discussion on this form of damage will be given later.

Damage from the environment is viewed as a synergistic effect when plastic deformation occurs at a free surface or an exposed crack tip. Brittle protective oxide films are ruptured, exposing fresh, nascent material, and chemical attack of this material proceeds until reformed protective films intervene. With fatigue, this process of straining, film rupture and attack occurs repeatedly, leading to localization of the cyclic strain and an abundance of the reaction products [*3*]. Grain boundaries are selectively attacked because of chemical segregation at the boundaries and because of ready oxidation of grain boundary species. At high frequencies, time is insufficient for local chemical reaction and cracking reverts to its normal transgranular mode [*4*]. At low frequencies or long hold times in tension, chemical processes lead to accelerations in micro- and macrocrack growth rates. It is important to note that, unlike grain boundary cavity formation, which is an interior damage process, environmental damage occurs mostly at the free surface where the environment is present. Some environmental effects can also be expected when diffusion from the surface occurs along the grain boundary by the environmental species.

Observations

In this section the rather extensive observations, obtained mostly from low-cycle fatigue tests, will be reviewed in the light of the aforementioned damage processes.

Strain Rate and Frequency

The effect of frequency and of strain rate on the low-cycle fatigue behavior of metals at high temperature has been extensively investigated using tests with balanced loading (equal ramp rates in tensile-going and compressive-going directions). The earliest work of interest was that by Eckel on lead [*5*], who correlated his results with frequency of cycle and failure time.

Berling and Slot [*6*] studied the effect of temperature (703, 923, and 1133 K) and strain rate (4×10^{-3}, 4×10^{-4} and 4×10^{-5} s^{-1}) on AISI 304, 316, and 348 stainless steel and found a progressive decrease in cyclic-strain fatigue resistance with increasing temperature and decreasing strain rate. Coffin and co-workers have reported on the frequency effect in nickel A [*7*], A286 [*8*], Udimet 500 [*9*], and René 80 [*10*] at elevated temperatures on smooth and notched [*4*] bars. From these results and those

of Berling and Slot [*6*], Coffin developed phenomenological representations for the frequency effect [*7*] by combining the Coffin-Manson equation with the results of Eckel [*1, 9, 10*].

Weeks et al [*11*] give results of extensive testing of AISI 304 and 316 over a wide range of strain rates and metallurgical conditions. The general conclusion from these test results, and many others not cited here, is that progressively decreasing frequency degrades the fatigue resistance of structural alloys at elevated temperatures under fully reversed cyclic strain conditions in air environments. Accompanying this decrease in life is a change in appearance of the fracture surface from that of transgranular fracture to intergranular as the frequency of cycling decreases [*4, 8*]. An important, but unanswered question, is whether eventual saturation in loss of life occurs at ever lower frequencies.

Environment

Recognition of the important role of environment on fatigue damage is evidenced by the early work of Achter et al [*12*] and of White [*13*]. McMahon and Coffin [*3*], in examining the fatigue results of Udimet 500 in air, found strong evidence that localized oxidation was critically important to the failure process and concluded that life degradation was more a result of "oxidation" fatigue (analogous to corrosion fatigue) than of creep damage processes. This work was followed by investigations of comparative effects [*6, 14*] in air and in vacuum [1.33 μPa (10^{-8} torr)] in which testing was conducted under fully reversed strains and equal ramp rates on a variety of materials. From these experiments it was concluded that the degradation processes were mostly environmental, since room temperature (time-independent) behavior could be produced by testing in vacuum, rather than in air, at elevated temperature. Evidence for this conclusion was seen by the occurrence of transgranular fracture, and by fatigue lives comparable with those found at room temperature (based on plastic strain considerations), and independent of frequency and temperature. Figure 1 is an example of this behavior in A286. Further work was done on the effect of low frequencies on AISI 304 stainless steel [*14*] to show that in high vacuum lives were unaffected by decreasing frequencies and fracture was still transgranular at 923 K at frequencies of 166 μHz (0.01 cpm). Other investigators have reported that inert environments significantly improve the fatigue life over that in air, as reported for example by Andrews and Kirschler on 2¼Cr-1Mo steel in sodium [*15*].

Wave Shapes

Laboratory tests can be carried out using a variety of wave shapes, and the findings from these experiments are extremely important to the present

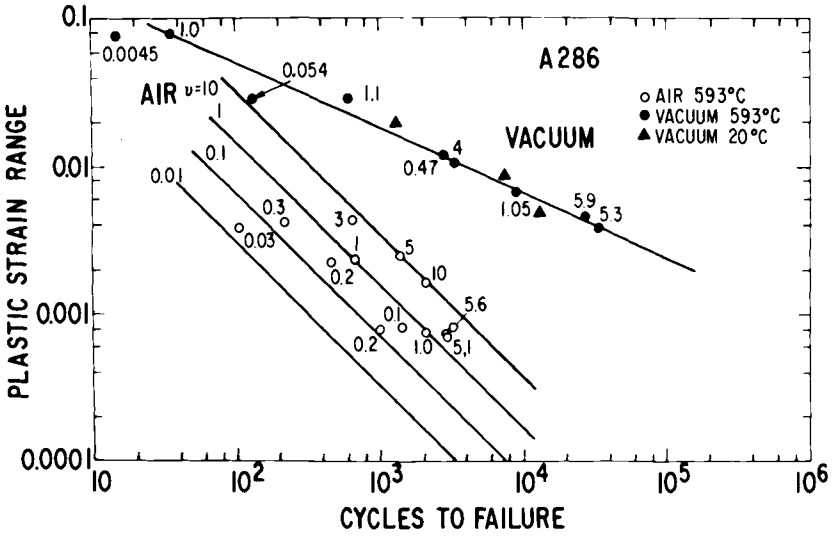

FIG. 1—*Plastic strain range versus fatigue life for A286 in air and vacuum at 866 K. Equal strain rates. Numbers adjacent to test points indicate frequency (cpm)* [8].

discussion. Some typical wave shapes are shown in Figs. 2 and 3 and include some tensile strain hold (Fig. 2*b*), stress-hold and strain limit, the so-called creep plastic (CP) cycle (Fig. 2*e*), and equal-equal, slow-fast, and fast-slow (Fig. 3). Over the years, a large amount of testing experience has shown that decreasing frequency of the cycle degraded the life [*16,17*], and that wave shape had an important influence on life. Strain hold-time studies on austenitic stainless steels [*18*] and materials of similar strength and ductility reveal that tensile strain holds are the most damaging mode for equivalent cycle periods. On the other hand, for the cast nickel-base superalloys, compressive strain hold tests are most damaging [*19,20*]. Tests on carbon and low-alloy steels show that frequency and wave shape generally have a smaller influence on life [*21*]. A discussion of these wave shape effects is given elsewhere [*1,22*].

In tensile strain hold time tests on AISI 304 stainless steel [*18,23*], a significant difference in fracture morphology and in life is found when compared with combined tensile and compressive holds. Fractures for the former were largely intergranular while additions of compression hold times of shorter duration cause largely transgranular fracture and increased life. Similar findings have been reported recently for AISI 304 stainless steel [*24*]. Internal cavities have also been noted in 20/25/Nb stainless steel at 1023 K [*25*] and in a 1 percent chromium-molybdenum-vanadium (1CrMoV) steel at 838 K [*26*].

Other types of unbalanced loop tests reveal similar degradations in life and changes in fracture morphology. These include fully reversed creep

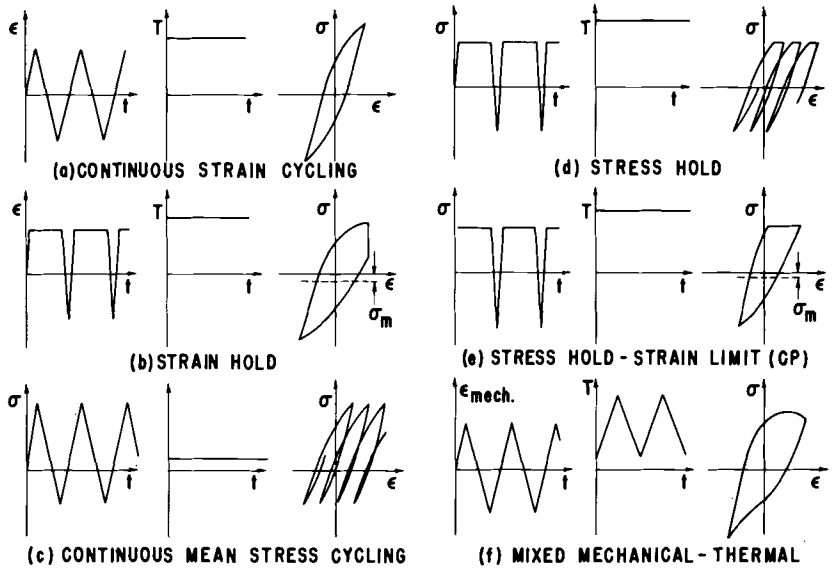

FIG. 2—*Wave shapes produced in closed-loop testing for life prediction.*

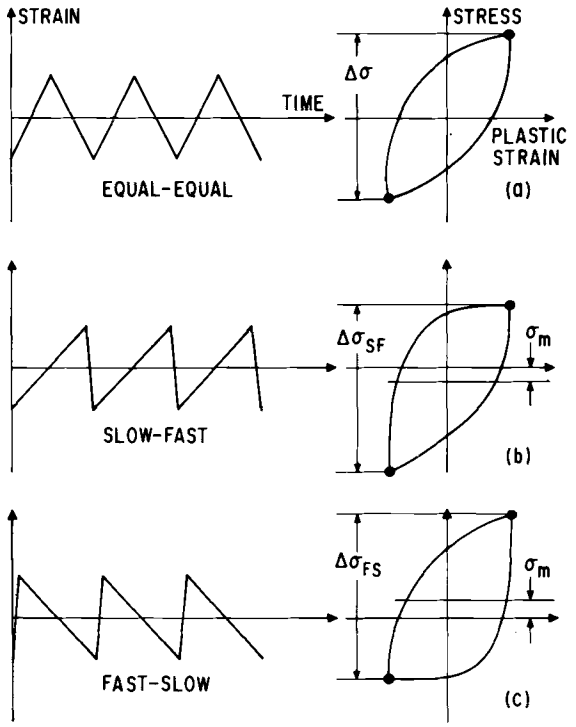

FIG. 3—*Wave shapes and resulting hysteresis loops for equal and unequal forward and reverse strain rates.*

at constant stress [*27,28*] of AISI 316 stainless steel at 977 K, strain range partitioning wave shapes such as CP loops [*22*], and thermal mechanical tests on A286 [*29*] at 868 K. The common feature of all of the foregoing tests was the significant decrease in life and the appearance of intergranular cracking and interior cracking and cavity formation when the time for which tensile stresses were applied exceeded the time spent under compressive stress in a given cycle. Recently consideration was given to unequal strain rate tests as an alternative form of testing which might better delineate these damaging effects. As discussed elsewhere [*22,30*], this particular wave shape has numerous advantages as a means for investigating the sensitivity of a given material to frequency and wave shape effects. Included are the following:

1. Ease of testing, including use of single control mode.
2. Control of strain rate rather than stress, so as to maintain fixed tensile-going and compressive-going times with each cycle.
3. Strain rate is considered to be the basic variable in deformation and fracture studies, and results can be more directly interpreted than results of constant stress or relaxation tests.
4. Greater proportion of time-dependent strain range to total strain range available for damage in each cycle than in strain hold tests.

In what follows, attention will be given principally to behavior resulting from this form of testing.

Observations from Unequal Strain Rate Testing

In conjunction with the preparation of an extensive survey on time-dependent fatigue [*22*], a series of experiments was performed on A286 at 868K and AISI 304 stainless steel at 923 and 1083 K in both air and high vacuum to determine the usefulness of unequal strain rate testing as a means of studying damage due to wave shape effects. The results are given in Table 1. Insofar as the air environment is concerned it will be noted that the slow-fast loops are more damaging than equal strain rates or fast-slow loops.

From the foregoing information, an uncertainty would appear to exist between the degrading effects found for unbalanced loop tests conducted in air and the insensitivity to time-dependent damage when balanced loop tests are conducted in high vacuum. For this reason, unequal strain rate tests were carried out both on A286 and on AISI 304 stainless steel in high vacuum. Results, shown in Table 1 and Fig. 4 for A286, reveal a pronounced wave shape effect on life in this environment. Sheffler [*29*] also noted this behavior, but his results were somewhat obscured by the thermo-mechanical nature of his tests. Looking particularly at the stainless steel results at 923 K in Table 1, note that the slow-fast test carried out in vacuum is nearly as damaging as the corresponding air test, while for

TABLE 1[a]—*Frequency-separation tests.*

A286 at 868 K				
$\Delta\epsilon_p$	ν_t, cpm	ν_c, cpm	N_f	Type
		Air		
0.01	10	0.101	500	fast-slow
0.01	0.2	0.2	280	equal
0.01	0.101	10	192	slow-fast
0.005	10	0.101	940	fast-slow
0.005	0.2	0.2	683	equal
0.005	0.101	10	320	slow-fast
		Vacuum		
0.01	10	0.1	1129	fast-slow
0.01	0.2	0.2	849	equal
0.01	0.1	10	296	slow-fast
0.01	0.1	10	284	slow-fast
AISI 304 Stainless Steel				
t_t (min)	t_c (min)		N_f	Type
	Air, $\Delta\epsilon_p = 0.02$, $T = 1093$ K, $\nu = 0.132$ cpm			
0.075	7.5		>374[b]	fast-slow
3.75	3.75		162	equal
7.5	0.075		52	slow-fast
	Air, $\Delta\epsilon_p = 0.02$, $T = 923$ K, $\nu = 0.1$ cpm			
0.1	9.9		198[b]	fast-slow
5.0	5.0		215	equal
9.9	0.1		106	slow-fast
	Vacuum, $\Delta\epsilon_p = 0.02$, $T = 923$ K			
10	10		1407	equal
10	0.1		148	slow-fast

[a] After Coffin [*22*].
[b] Failed off-center.

balanced loops (equal times in tensile and compressive going) the vacuum environment produces a nearly seven-fold increase in life over that in air. Fractography revealed that both the air and vacuum slow-fast tests failed by intergranular fracture, and, in addition, extensive interior grain boundary cracking was observed, as shown in Figs. 5 and 6. This indicates that interior damage processes are unaffected by the external environment, but appear to be strongly influenced by the wave shape. Support of this position is found in the results of the air versus vacuum equal strain rate tests where no interior damage was observed, Figs. 7 and 8. On the other hand, fatigue cracks originated at the surface and were transgranular in vacuum

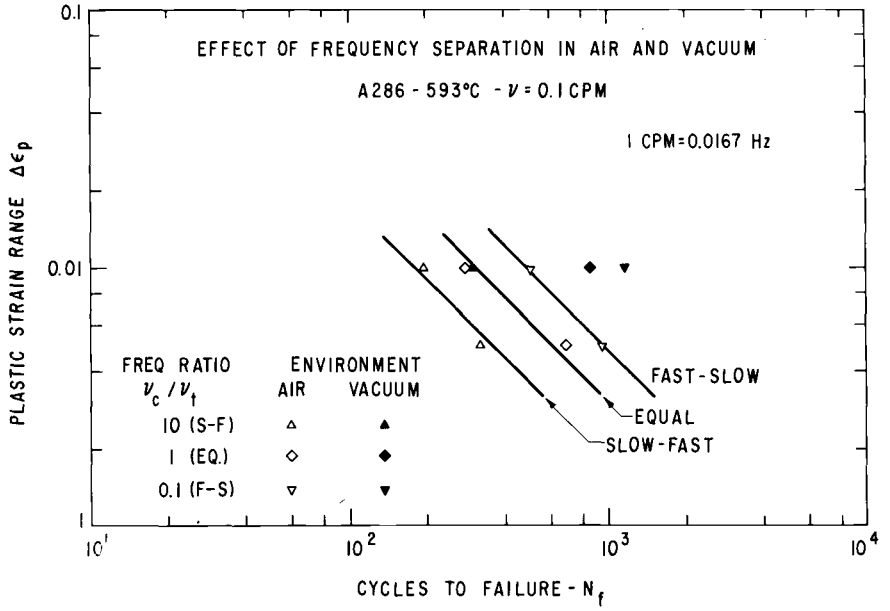

FIG. 4—*Effect of equal and unequal forward and reverse strain rates on A286 at 866 K in air and vacuum at constant frequency* [1].

but intergranular in air, showing environmental involvement. Of particular interest were the fast-slow test results on AISI 304 stainless steel at both 923 and 1083 K in which failures occurred away from the diametral control position from a ratchetting-instability process. Details of this behavior are discussed elsewhere [*31*].

Unequal strain rate testing has also been performed on two copper-based alloys at 811 K [*32*]. Alloys examined were identified as ½H AMZIRC and NARloy Z. Rates considered were $1 \times 10^{-2}/4 \times 10^{-4}$ s^{-1} (tension going/compression going), $4 \times 10^{-4}/1 \times 10^{-2}$ s^{-1} for the AMZIRC copper, and $1 \times 10^{-2}/4 \times 10^{-4}$ s^{-1}, $4 \times 10^{-4}/1 \times 10^{-2}$ s^{-1}, $4 \times 10^{-5}/1 \times 10^{-2}$, and $7 \times 10^{-6}/1 \times 10^{-2}$ s^{-1} for the NARloy Z alloy. Results obtained for this alloy are reproduced in Fig. 9 and reveal the striking degradation in fatigue life with increasing strain rate unbalance in slow-fast testing. Mean stresses were noted in the hysteresis loop, a behavior commonly found in unbalanced loop tests [*22,31*].

Majumdar and Maiya [*24*] have recently conducted experiments using both tension and compression strain hold tests and unequal strain rate tests in air on AISI 304 stainless steel at 866 K in support of a damage rate model they have developed. Significant in this work is the inclusion of damage from both crack growth and cavity growth or collapse, depending on the sign of the stress. A summary of their experimental findings is pre-

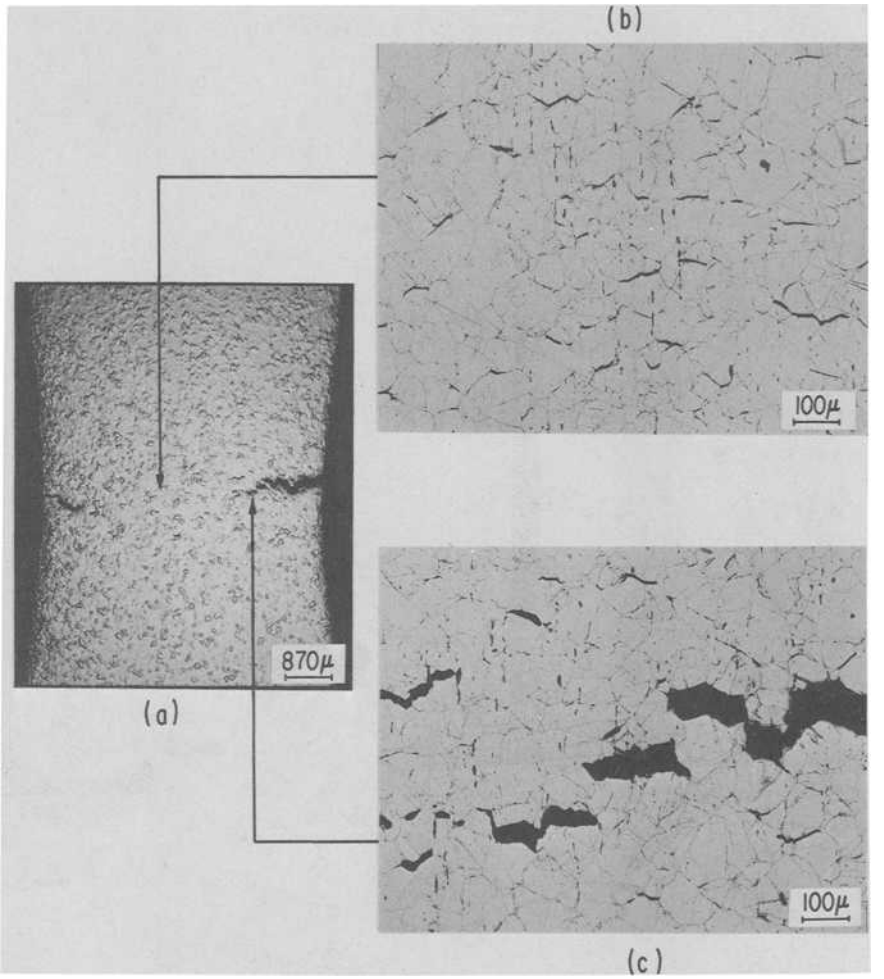

FIG. 5—*Microstructure of failed slow-fast strain rate test on AISI 304 stainless steel at 923 K in air. See Table 1 for details.*

sented in Table 2. Note that the greatest life occurs for the most rapid equally balanced (fast-fast) tests and the shortest life is for the most unbalanced slow-fast test. The tension hold test has a degrading effect on life, but not as severe as that of the slow-fast test. Metallographic and fractographic findings are similar to those described in the foregoing; the slow-fast tests developed intergranular cracks and grain-boundary cavities, while the fracture surfaces for the equal strain rate and fast-slow tests were transgranular.

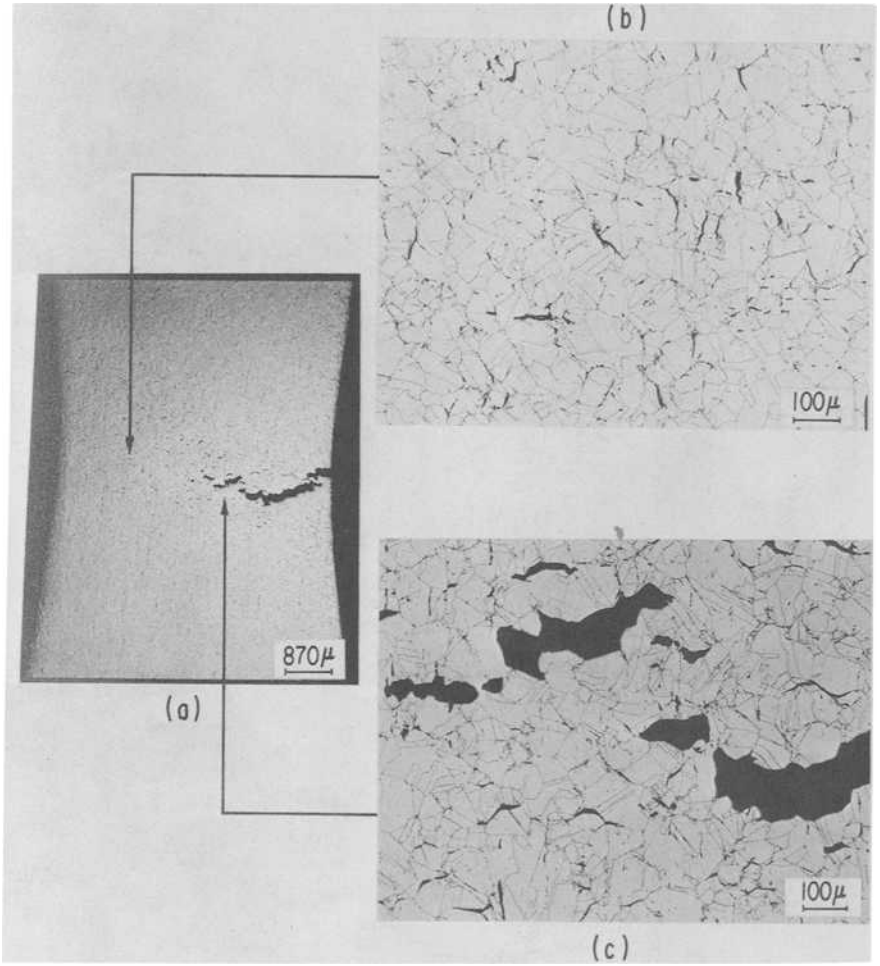

FIG. 6—*Microstructure of failed slow-fast strain rate test on AISI 304 stainless steel at 923 K in vacuum. See Table 1 for details.*

Effect of Wave Shape on the High-Temperature Low-Cycle Fatigue Behavior of OFHC Copper

Experimental Procedure

The material employed in the present study was OFHC copper which had been heat treated at 920 K in vacuum for 1½ h. This produced a grain size of about 60 μm and hardness of 38 DPN.

Specimens with a gage length of 12.7 mm and diameter of 6.35 mm were used (Fig. 10). Tests were carried out in a closed-loop servohydraulic

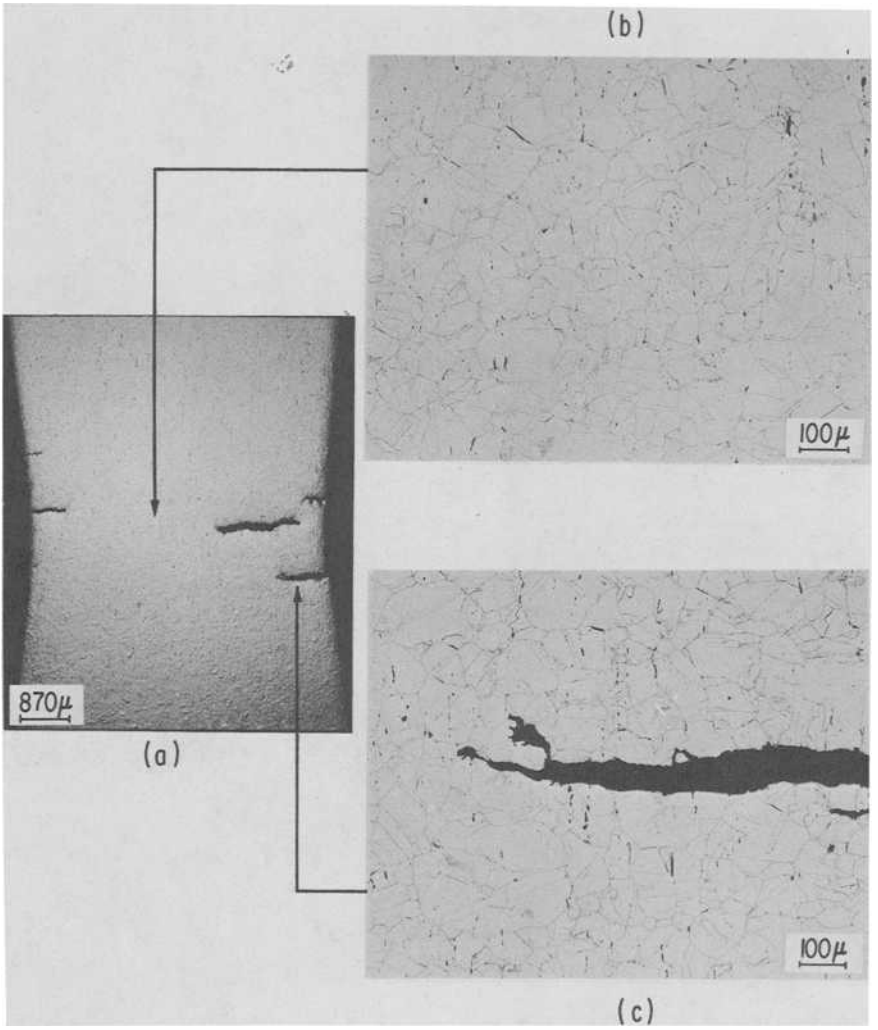

FIG. 7—*Microstructure of failed equal strain rate test on AISI 304 stainless steel at 923 K in air. See Table 1 for details.*

machine using a signal generator in which the positive and negative output ramp rates could be independently adjusted. The specimen was heated by an induction furnace and temperature was controlled via a Chromel/Alumel thermocouple by a Eurotherm three-phase controller.

Strain-controlled fatigue tests were carried out at 673 K (0.5 T_M) in air with a total strain range of 1.0 percent. The types of cycle employed are shown in Fig. 3. In each test the cycle time was kept constant at 600 s but the tensile and compressive strain rates were varied so that a study of wave-

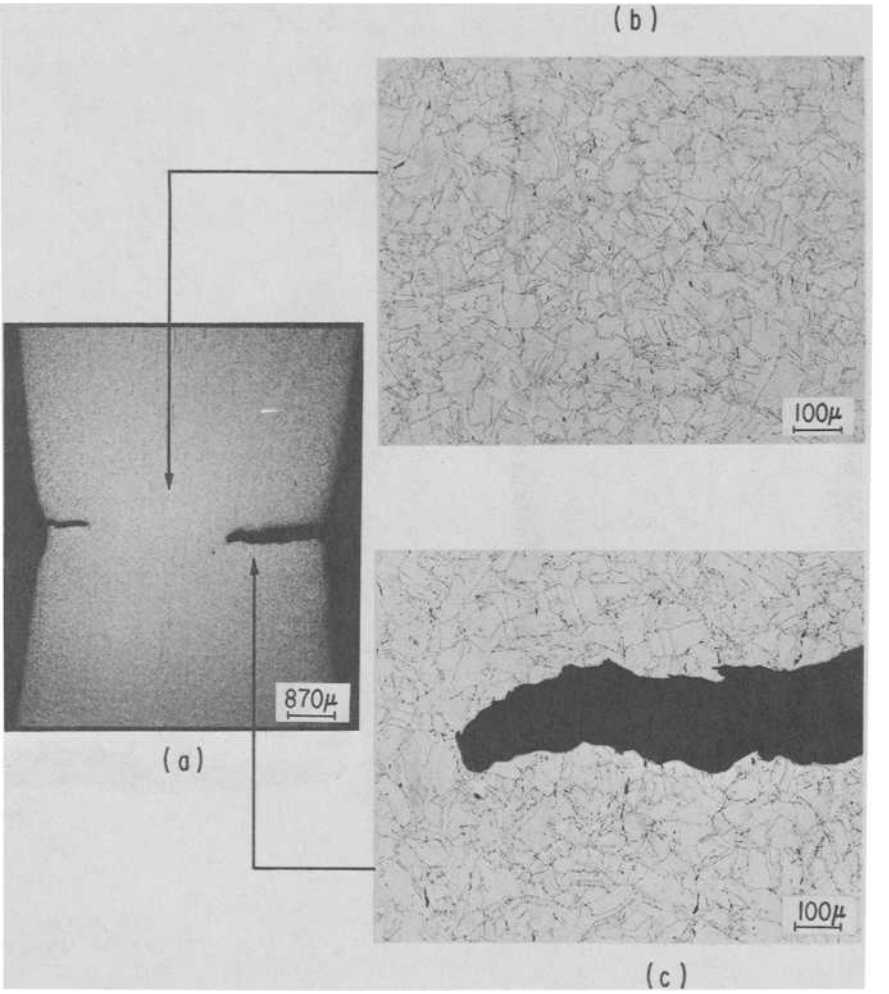

FIG. 8—*Microstructure of failed equal strain rate test on AISI 304 stainless steel at 923 K in vacuum. See Table 1 for details.*

shape effects could be made. In the case of the unbalanced loops, the ratio of fast to slow strain rates was fixed at 100 to 1 with the slow strain rate being 1.7×10^{-5} s^{-1}. A strain rate of 3.3×10^{-5} s^{-1} was used in equal ramp rate tests.

After failure, the gage-length was sectioned longitudinally for metallographic observations. The copper was etched in a solution consisting of 1-g potassium dichromate, 4-ml H_2SO_4, 1-ml HCl, and 50-ml H_2O.

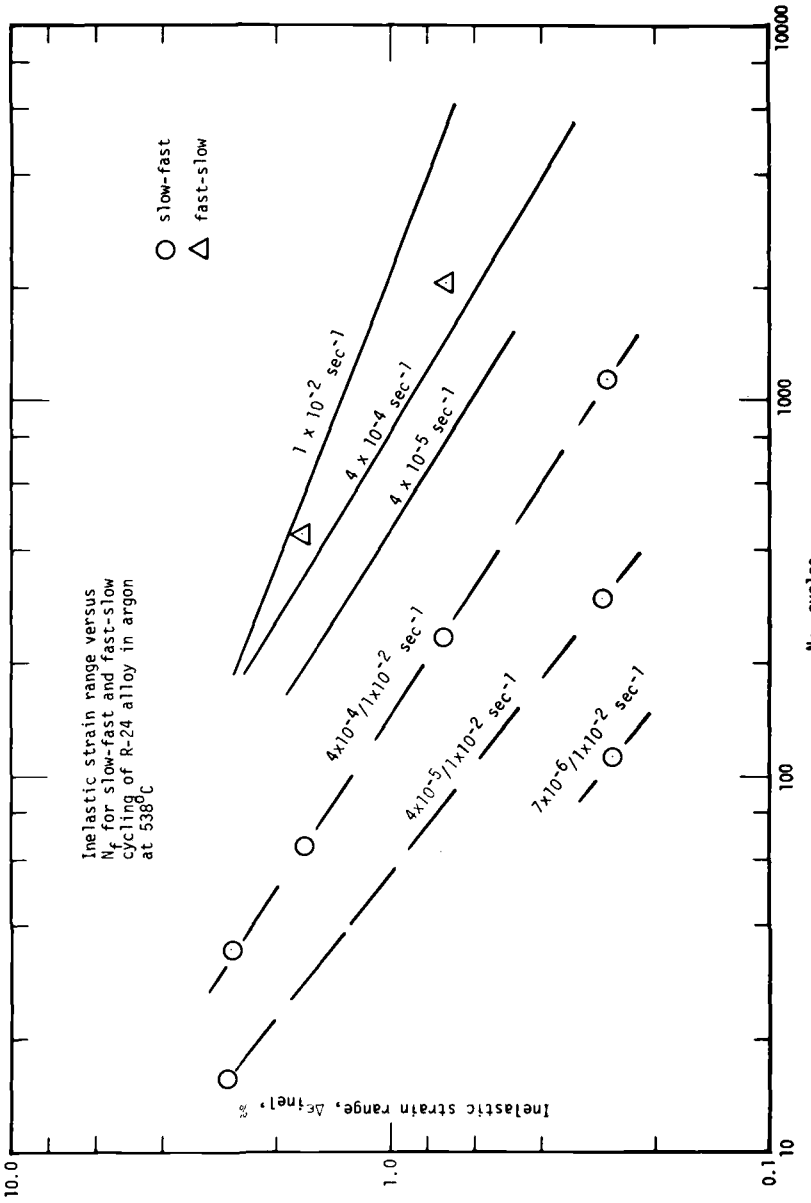

FIG. 9—*Slow-fast and fast-slow strain rate tests on copper alloy NARloy Z at 811 K; after Conway et al* [32].

TABLE 2[a]—*Effects of wave shape on the fatigue life of Type 304 stainless steel at 870 K.*

Specimen No.	$\Delta\epsilon_t$ (%)	$\Delta\epsilon_p$ (%)	$\Delta\sigma$ (MPa)	Tension $\dot{\epsilon}_t$ (s^{-1})	Compression $\dot{\epsilon}_t$ (s^{-1})	t_t (min)	t_c (min)	N_f (cycles)	Type of Test
T-389	1.00	0.67	494.0	1×10^{-4}	1×10^{-4}	0	0	1697	slow-slow
T-467	1.00	0.69	464.7	1×10^{-4}	1×10^{-2}	0	0	847	slow-fast
T-468	1.00	0.68	479.1	1×10^{-2}	1×10^{-4}	0	0	3025	fast-slow
T-320	1.01	0.70	473.0	4×10^{-2}	4×10^{-2}	0	0	5096	fast-fast
T-85	1.01	0.73	422.0	4×10^{-6}	4×10^{-6}	0	0	579	slow-slow
T-462	1.00	0.72	428.0	4×10^{-6}	4×10^{-3}	0	0	261	slow-fast
T-465	0.99	0.69	451.6	4×10^{-3}	4×10^{-6}	0	0	2421	fast-slow
T-35	1.00	0.66	518.0	4×10^{-3}	4×10^{-3}	0	0	3395	fast-fast
T-431	0.99	0.74	427.2	4×10^{-3}	4×10^{-3}	10	10	2507	symmetrical hold
T-472	1.01	0.77	417.6	4×10^{-3}	4×10^{-3}	15	5	1788	unsymmetrical hold
T-30	1.00	0.74	441.0	4×10^{-3}	4×10^{-3}	15	0	666	tensile hold
T-44	2.00	1.66	605.0	4×10^{-3}	4×10^{-3}	15	0	237	tensile hold
T-475	2.00	1.74	571.5	4×10^{-3}	4×10^{-3}	15	5	642	unsymmetrical hold

[a] After Majumdar and Maiya [*24*].

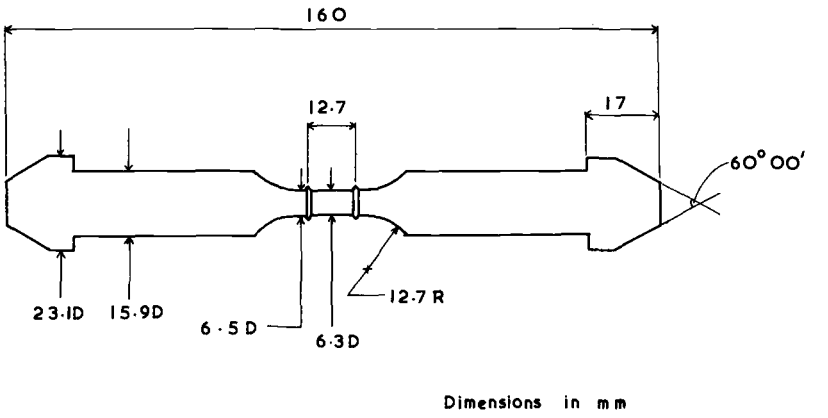

FIG. 10—*Specimen design for OFHC copper tests.*

Results

Fatigue Behavior—Table 3 shows the number of cycles to failure and the time to failure under the various testing conditions. It can be seen that when the total cycle time is kept constant the number of cycles to failure decreases as the tensile-going strain rate decreases.

A tension test at a strain rate equal to that of the slow ramp of the unbalanced loop gave a maximum stress of 88 MPa (12.8 ksi) and a failure elongation of 8 percent with negligible necking.

Metallography—Figure 11 shows the failure crack in the fast-slow test. The crack path is transgranular and has started from the surface. Many transgranular surface cracks had initiated and grown for depths up to ½ mm but presumably these had ceased growing when one crack became dominant. No internal intergranular cracks were observed.

In contrast, failure in the slow-fast test was intergranular (Fig. 12). Near the fracture edge, extensive intergranular cracks can be seen which have been opened out by the final failure. Many of these cracks were wedge type, but at higher magnifications linked cavities could be seen. Intergranular surface cracks of about one grain depth were also observed. It was noted that cavitation was present throughout the gage length (Fig. 13). Thus the

TABLE 3—*Effect of wave-shape on the number of cycles to failure of OFHC copper at 673 K.*

Cycle	Slow-Fast	Equal	Fast-Slow
N_f	104	380	1138
t_f (h)	17	63	190

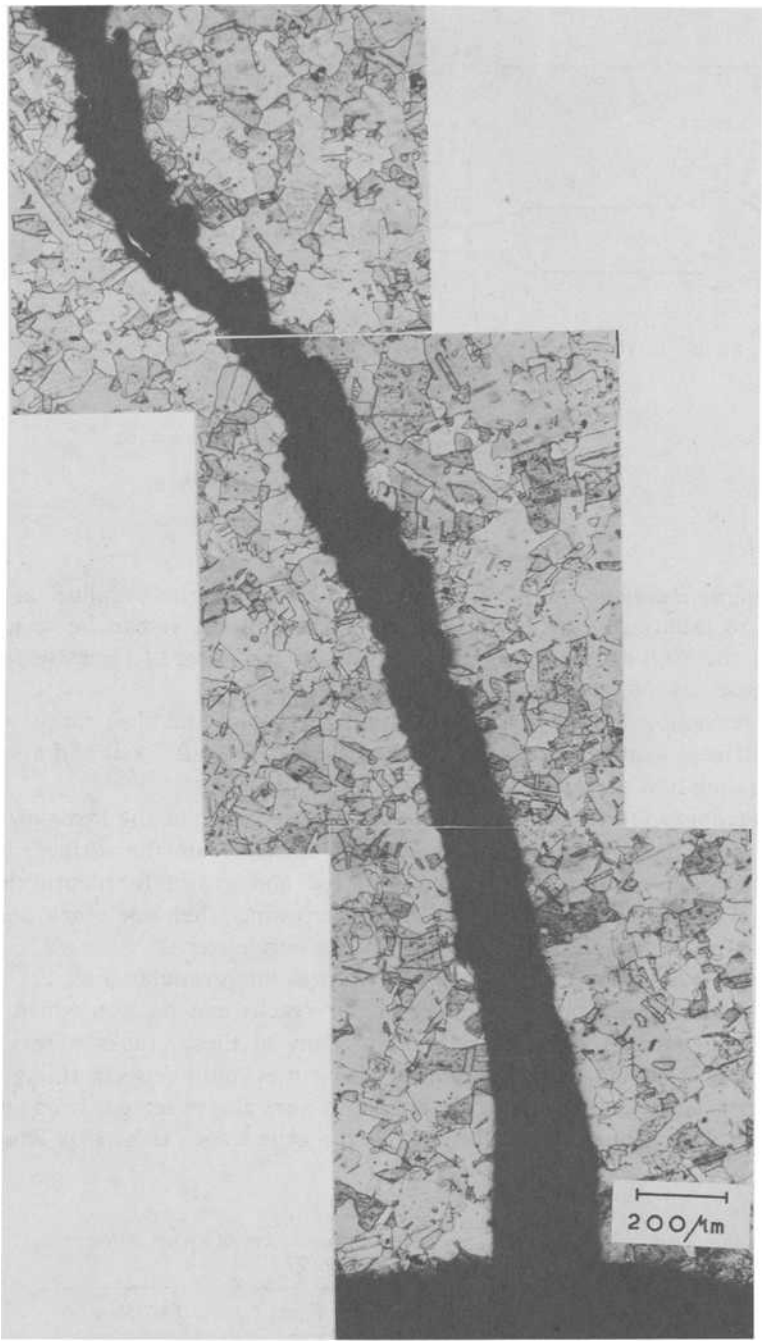

FIG. 11—*Main failure crack in OFHC copper after fast-slow cycling showing transgranular fracture mode.*

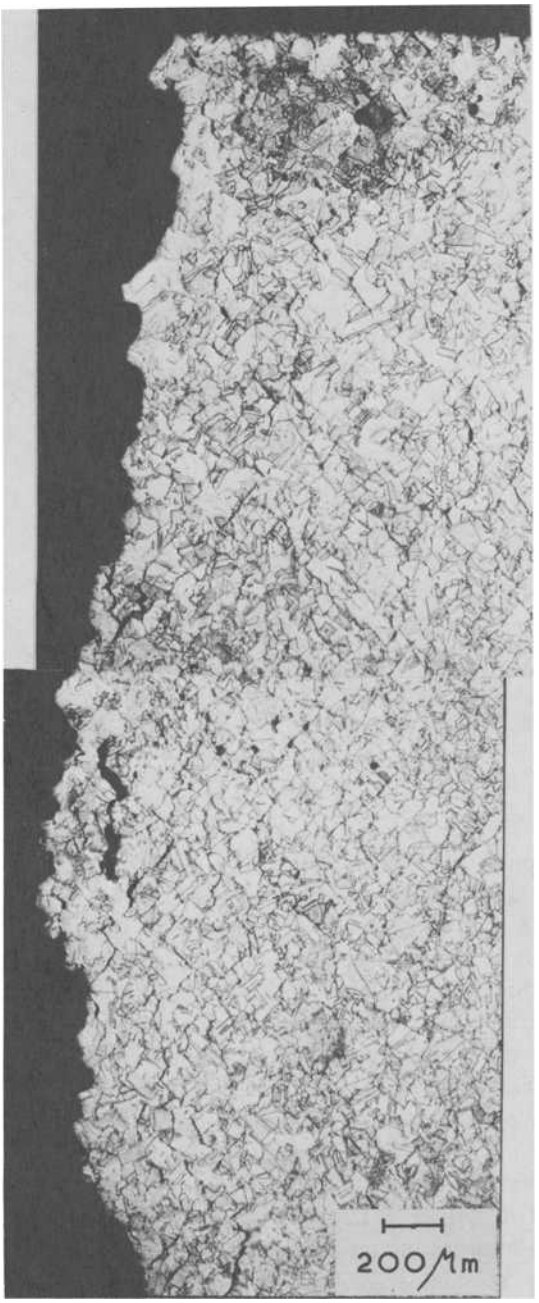

FIG. 12—*Fracture edge of slow-fast cycle specimen showing intergranular fracture path and surface and interior intergranular cracks.*

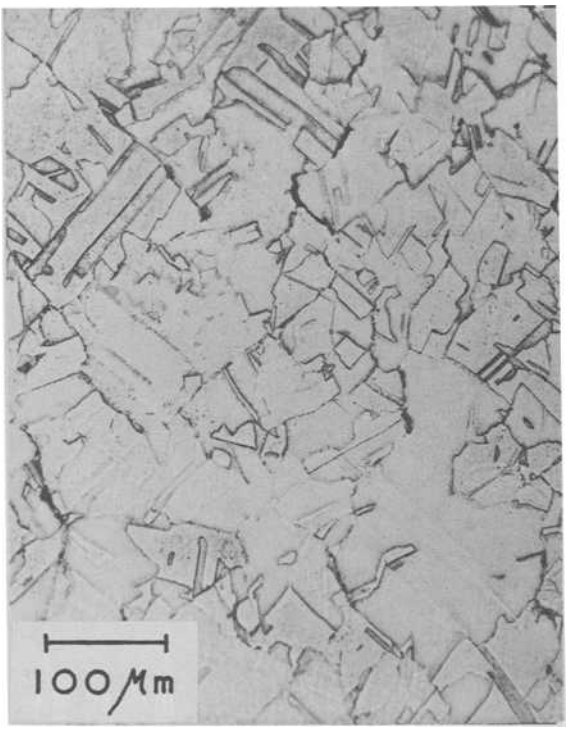

FIG. 13—*Grain boundary cavitation in bulk of gage length away from the fracture in slow-fast cycle specimen.*

failure was typical of that for creep fracture with most of the cracks being orientated at right angles to the applied stress direction.

The fracture path in the equal strain rate test was intergranular. Also, internal and short surface intergranular cracks were observed. The surface cracks were about one grain in depth and less numerous than in the slow-fast specimen. The internal cracks were concentrated within 2 mm of the main fracture and were wedge-shaped. Some of these had linked to form longer cracks as can be seen in the unetched condition in Figure 14. There was no evidence of cavities either near the fracture or in the bulk of the specimen.

The slow strain-rate tension test failed by the propagation of an intergranular crack. Microscopically the specimen was very similar to the equal ramp test with intergranular wedge cracks being situated near the fracture surface and no cracking in the bulk region.

Thus, metallography of the specimens indicated that the decrease in fatigue life was associated with a change in the fracture mode from transgranular to intergranular cracking. Cavity damage occurred only when the tensile-going strain rate was less than the compressive-going strain rate.

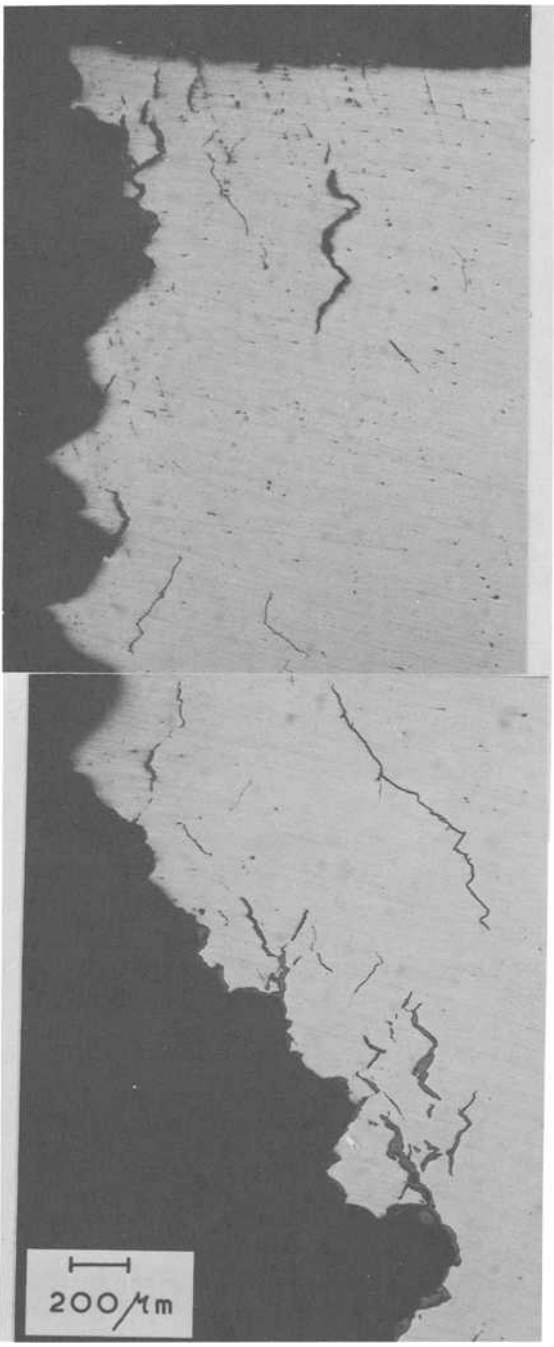

FIG. 14—*Equal ramp cycle specimen in unetched condition showing interlinkage of wedge cracks near the fracture edge.*

Discussion

Recent life prediction techniques have recognized the need to consider wave shape effects. The general approach has been to separate the hysteresis loop into components either of fully reversed strain elements of mixed rates, such as is done in the strain range partitioning approach [*22*] (PP, PC, CP, and CC), or into unidirectional strain elements of different rates such as tensile going or compressive going, as has been proposed by Coffin [*1,22,30*], Ostergren [*20*], and Majumdar and Maiya [*24*]. Tomkins and Wareing [*25*] have included the effect of creep damage in their crack propagation equations and suggest that such damage reduces lifetimes mainly through its effect in reducing the crack length to cause instability. The feature which these various approaches have in common is the recognition that multiple damage processes occur in a given cycle and that the predictive basis must involve, in some combination, damage from cyclic strain, environment, creep, and possibly other effects.

As indicated, intergranular cracking has often been observed in the high-temperature high-strain fatigue of metals. In many pure metals, however, such cracking occurs only after grain boundary migration has taken place. Wigmore and Smith [*33*] noted grain boundary migration in OFHC copper in high-strain fatigue tests at temperatures between 673 and 873 K and strain rates of approximately 10^{-3} s^{-1}. Failure occurred by the growth of triple-point cracks after migration of grain boundaries to 45 deg to the stress axis. Similar observations were reported by Abdel-Raouf et al [*34*] in OFHC copper at 923 K but migration was absent at 573 K. Westwood and Taplin [*35*] observed, in pure iron, extensive migration of grain boundaries at 45 deg to the stress axis. As a result of migration, grain boundaries become more favorably orientated to enhance grain boundary sliding and thus migration can increase the propensity for intergranular cracking. In the present OFHC copper tests as well as in the other experiments discussed earlier, no grain boundary migration occurred and the intergranular wedge cracks and cavities predominated on boundaries at right angles to the applied stress direction. Besides being dependent on temperature, the ability of boundaries to migrate is extremely sensitive to material purity. Even a small number of impurity particles on grain boundaries is capable of inhibiting migration. For instance, Wigmore and Smith [*33*] tested two batches of OFHC copper with slightly different purity levels and observed migration only in the higher-purity material. In the present case it is presumed that such particles are responsible for preventing migration.

The present results relate to the model proposed by Solomon and Coffin [*36*] and extended by Woodford and Coffin [*4*] to account for the role of frequency and environment in high-temperature fatigue (Fig. 15). The model assumes equal strain rate cycling so that frequency and strain rate are directly related. It also assumes that creep damage produced at low

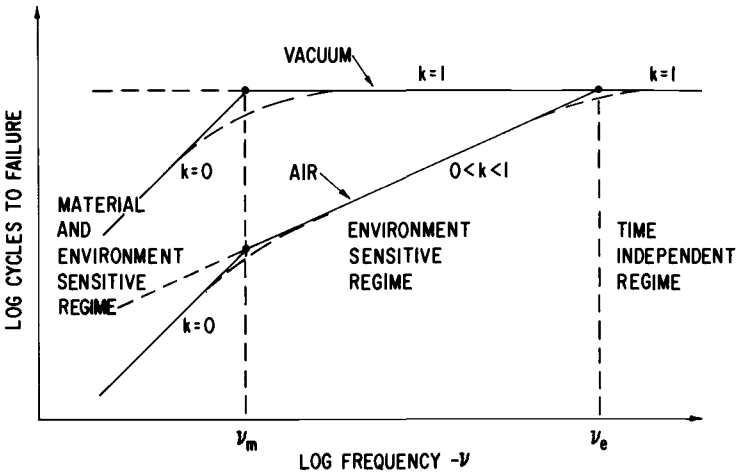

FIG. 15—*Model of the effect of frequency on fatigue life at constant plastic strain range at elevated temperature* [4].

strain rates in tension is balanced by equal recovery in compression. Hence the damage processes which occur are a result of environmental effects. Thus Woodford and Coffin [*4*] found a change in fracture mode from transgranular to intergranular in air in 304 stainless steel as the frequency of testing was decreased. In vacuum, however, failure was always transgranular even at a frequency of 1.6×10^{-4} Hz. Similar results were found for A286 [*36*]. In this model it is suggested that three frequency regimes exist in air which can be identified with different damage processes. At high frequencies ($\nu > \nu_e$) the damage process is independent of frequency and failure is by the normal transgranular fatigue mechanism. In the intermediate frequency range ($\nu_m < \nu < \nu_e$) the air environment is capable of interacting with the cracks and there is a change of fracture mode from transgranular to intergranular with decreasing frequency. At lower frequencies ($\nu < \nu_m$) microstructural instabilities may occur and intergranular fracture may result.

The purpose of the present paper is to modify this model to account for unbalanced hysteresis loops. Emphasis is given to the unequal strain rate results described in Fig. 3, under the assumption that this form of wave shape is a rational standard for damage evaluation. A qualitative damage picture is proposed, as shown in Table 4. Development of this table is presented in the following.

The OFHC copper tests were performed at constant frequency but the strain rates in the forward and reverse legs of the stress-strain loop were varied so that it is necessary to consider the damage processes associated with both legs of the loop. The unbalanced type of cycle may introduce

TABLE 4—*Wave shape damage summary.*

Assumes $T/T_m \geq 0.5$, Fixed Temperature, Strain Range, Overall Frequency				
		Wave Shape Type		
Environment	Damage Mode	Slow-Fast	Equal Rates	Fast-Slow
Air	fracture surface	Intergranular depending on $+ \dot{\epsilon}$	depends on $+ \dot{\epsilon}$	transgranular
	interior	grain boundary cracks	none	none
	environment	local to fracture, depends on $+ \dot{\epsilon}$	local to fracture, depends on $+ \dot{\epsilon}$	small, depends on $+ \dot{\epsilon}$
	damage-mode designation	C + E + F[a]	E + F	E + F
Vacuum	fracture surface	intergranular depends on $+ \dot{\epsilon}$	transgranular	transgranular
	interior	none	none	none
	environment	none	none	none
	damage-mode designation	C + F	F	F

[a] C = cavity damage; E = environmental damage; F = cyclic strain damage.

creep damage in addition to environmental damage. There is general agreement that intergranular cavitation and triple-point cracks in creep at high temperatures are produced by tensile and not compressive axial stresses [*37*] and that they are also enhanced by lowering the strain rate [*38*]. It might be expected that the reversal of stress in fatigue would tend to heal any creep damage caused by the tensile stress. Wigmore and Smith [*33*] presented some evidence which suggested that compressive healing of triple-point cracks could occur by rewelding of the crack surfaces. Healing could take place by reversed grain boundary sliding, but it was thought that sliding was more restricted in compression than in tension [*33*] so that complete healing would be unlikely. The strain rate in compression would be important and a fast compressive ramp would reduce the amount of healing. In addition, it must be remembered that cracks and cavities, once formed, may be difficult to eliminate due to gas stabilization [*39*].

Thus the picture that emerges in slow-fast testing is one of surface cracking and interior grain cavity growth under slow-fast loops, the growth rate depending on the temperature, strain range, the overall frequency, and the relative forward and reverse strain rates. This form of damage not only assists in the crack initiation and early growth processes by causing intergranular cracking, but also develops in the interior as clearly seen in Figs. 5, 6, and 12. Cavity damage is expected to be enhanced as the temperature is raised and to disappear at low temperatures. Similarly it should be more or less independent of external environment, except that diffusion of environmental species into cavities might impede collapse. Thus in slow-fast cycling in air, three contributing factors are operative as identified in Table 4: creep cavity damage, C, and environment, E, in addition to the cyclic strain damage, F. Effects of strain range, relative strain rates, and overall frequency are seen in Figs. 4 and 9 and Tables 1–3.

Also with reference to Table 4, when slow-fast tests are conducted in vacuum, the environmental damage contribution is removed. Intergranular cracking and grain boundary cavity damage persists as verified by Fig. 6, and the comparative air and vacuum fatigue results for this wave shape, given in Table 1 and Fig. 4, show only a small increase in life.

Considering the fast-slow loop, failure occurred in OFHC copper by the propagation of a single transgranular crack, Fig. 11. In this case the tensile-going strain rate is high so that the crack is only exposed to the environment for a short period of time. This is likely to lead to a normal transgranular fatigue crack. As far as creep processes are concerned, the compressive strain rate is low, so that if the tensile ramp introduces intergranular damage there is time during the reversal for such damage to be healed.

The factors important in fast-slow tests would thus differ considerably from those of slow-fast tests. No creep damage is expected, either in air or vacuum, environmental damage in air would depend on the forward strain

rate only, and lives in vacuum would be longer than in air tests, other conditions being equal. Initiation and early growth processes are expected to be transgranular. Unfortunately, the fast-slow test results are also influenced by shape instability effects [*22,31*]. However, with reference to Tables 1-3 and Fig. 9, lives are seen to be substantially longer than the corresponding slow-fast tests, and from Fig. 11 cracking is transgranular and no bulk damage is observed. The damage processes are so identified in Table 4.

In the OFHC copper tests the equal ramp cycle produced an intergranular main crack, intergranular surface cracks, and secondary intergranular interior cracks near the fracture. No bulk damage was produced. This is consistent with the environment-controlled fatigue regime. Oxidation promotes surface intergranular initiation and further growth takes place along the grain boundaries, which are the easiest diffusion paths for oxygen. Such diffusion would also lead to intergranular secondary cracks in the vicinity of the fracture. Since the process is controlled by the environment, the frequency at which the fracture path changes from transgranular to intergranular is material dependent. When the tensile and compressive strain rates are equal, any bulk cavitation damage produced in the tensile stroke may equal the damage recovered so that there would be little or no bulk damage accumulation, as discussed previously.

Thus in the model of Table 4 the damage processes in equal ramp rate regimes are identified as environmental and time-independent fatigue in air, while in vacuum damage is due only to time-independent fatigue. Fatigue cracks would be transgranular in vacuum at all frequencies, unless, according to Fig. 15, time-dependent metallurgical effects influence the behavior. In air, the degree to which the fracture is intergranular depends on the frequency or strain rate (assuming a given material and temperature), as indicated in Fig. 15. Frequency effects are seen in Figs. 1 and 9 and in Table 2.

With particular attention to the OFHC copper, this work indicates that the fatigue life is strongly dependent on the mode of damage. Although the cycle period was kept constant, the failure mechanism was dependent on the strain rates in each half of the cycle. An order-of-magnitude reduction in lifetime was recorded when a cycle producing grain boundary cavitation was employed compared with a cycle producing transgranular failure. Obviously the lifetime is controlled by the fastest fracture micromechanism which can operate under the test conditions. Similar conclusions can be drawn with regard to the other materials considered here.

Summary

High-temperature low-cycle fatigue resistance is wave shape dependent since the latter controls the micromechanism of failure.

Tests on OFHC copper at 673 K have been carried out using unequal

strain rates to produce the wave shape. The fatigue lifetime decreased by an order of magnitude as the tensile-going strain rate was reduced from 1.7×10^{-3} s^{-1} to 1.7×10^{-5} s^{-1} using a constant cyclic period. Accompanying this reduction in lifetime, the fracture mode changed from a transgranular fracture for the fast-slow wave shape to an intergranular single-crack fracture for equal ramp rates to internal cavitation for the slow-fast test.

A qualitative model is presented to explain these results and the observations of other investigators with respect to wave shape effects. Essential features of the model are the assumption of grain boundary cavity size variability depending on the magnitudes of the tensile-going and compressive-going strain rates of the hysteresis loop and recognition of the role of environment in degrading life and affecting fracture mode, especially when the tensile and compressive strain rates are equal.

Acknowledgments

A portion of the experimental work was carried out at Cambridge University Engineering Department by the kind permission of Professor W. A. Mair. One of the authors (DS) was supported by a Central Electricity Generating Board Senior Research Fellowship at Christ's College, Cambridge. Other experimental work reported here was performed at the General Electric Co., Research and Development Center. The authors acknowledge the able assistance of D. C. Lord in performing these tests.

References

[1] Coffin, L. F., Jr., in *Proceedings*, 4th International Conference on Fracture, Waterloo, Ont., Canada, June 1977, pp. 263-292.
[2] Veevers, K. and Snowden, K. V., *Journal of the Australian Institute of Metals*, Vol. 20, 1975, p. 201.
[3] McMahon, C. J. and Coffin, L. F., Jr., *Metallurgical Transactions*, Vol. 1, 1970, p. 3443.
[4] Woodford, D. A. and Coffin, L. F., Jr., in *Proceedings*, 4th Bolton Landing Conference, Claitors Publications Division, Baton Rouge, La., 1974.
[5] Eckel, J. F. in *Proceedings*, American Society for Testing and Materials, 1951, p. 745.
[6] Berling, J. T. and Slot, T. in *Fatigue at High Temperature, ASTM STP 465*, American Society for Testing and Materials, 1968, pp. 3-30.
[7] Coffin, L. F., Jr. in *Proceedings*, 2nd International Conference on Fracture, Brighton, U.K., April 1969, pp. 643-654.
[8] Coffin, L. F., Jr. in *Proceedings*, International Conference on Fatigue: Chemistry, Mechanics and Microstructure, NACE-2, National Association of Corrosion Engineers, Houston, Tex., 1972, pp. 590-600.
[9] Coffin, L. F., Jr., *Metallurgical Transactions*, Vol. 2, 1971, p. 3105.
[10] Coffin, L. F., Jr., *Metallurgical Transactions*, Vol. 5, 1974, p. 1053.
[11] Weeks, R. W., Diercks, D. R., and Cheng, C. F., "ANL Low Cycle Fatigue Studies—Program, Results and Analysis," ANL-8009, Argonne National Laboratory, Ill., Nov. 1973.
[12] Achter, M. R., Danek, G. J., Jr., and Smith, H. H., *Transactions of the Metallurgical Society of AIME*, Vol. 227, 1963, p. 1296.
[13] White, D. J. in *Proceedings*, Institution of Mechanical Engineers, Applied Mechanics Group, Vol. 184, 1969-1970, p. 223.

[14] Coffin, L. F., Jr., *Metallurgical Transactions*, Vol. 3, 1972, pp. 1777-1788.
[15] Andrews, R. C. and Kirschler, L. H., MSA Research Corp. Report MSAR-66-174, (1966).
[16] Coles, A. et al in *Proceedings*, International Conference on Thermal and High Strain Fatigue, Monograph and Report Series 32, The Metals and Metallurgy Trust, London, 1967, pp. 270-294.
[17] Coffin, L. F., Jr. in *Proceedings*, Air Force Conference on Fatigue and Fracture of Aircraft Structures and Materials, AFFDL-TR70-144, Air Force Flight Dynamics Laboratory, Wright-Patterson AFB, Ohio, 1969, pp. 301-309.
[18] Berling, J. T. and Conway, J. B., *Proceedings*, First International Conference on Pressure Vessel Technology, Delft, The Netherlands, 29 Sept-2 Oct., Part 2, 1969, pp. 1233-1246.
[19] Lord, D. C. and Coffin, L. F., Jr., *Metallurgical Transactions*, Vol. 4, 1973, p. 1657.
[20] Ostergren, W., *Journal of Testing and Evaluation*, Vol. 4, 1976, pp. 327-339.
[21] Leven, M. M., *Experimental Mechanics*, Vol. 13, 1973, p. 353.
[22] Coffin, L. F., Jr. in *Time-Dependent Fatigue of Structural Alloys*, ORNL 5073, Oak Ridge National Laboratory, Oak Ridge, Tenn., June 1977.
[23] Cheng, C. F. et al in *Fatigue at Elevated Temperatures, ASTM STP 520*, American Society for Testing and Materials, 1973, pp. 355-364.
[24] Majumdar, S. and Maiya, P. S. in *Proceedings*, American Society of Mechanical Engineers/Canadian Society of Mechanical Engineers Pressure Vessel and Piping Conf., Montreal, Que., Canada, June 1978.
[25] Tomkins, B. and Wareing, J., *Metal Science Journal*, Vol. 11, 1977, p. 414.
[26] Ellison, E. G. and Paterson, A. J. F. in *Proceedings*, Institution of Mechanical Engineers, Vol. 190, 1976, p. 333.
[27] Halford, G. R., "Cyclic Creep-Rupture Behavior of Three High Temperature Alloys," NASA-TN-D-6039, National Aeronautics and Space Administration, May 1971.
[28] Manson, S. S. in *Fatigue at Elevated Temperatures, ASTM STP 520*, American Society for Testing and Materials, pp. 744-782.
[29] Sheffler, K. D., "Vacuum Thermal-Mechanical Fatigue Testing of Two Iron Base High Temperature Alloys," NASA-CR-134524, National Aeronautics and Space Administration, 1974.
[30] Coffin, L. F., Jr. in *Proceedings*, ASME-MPC Symposium on Creep-Fatigue Interaction, MPC-3, American Society of Mechanical Engineers, Dec. 1976.
[31] Coffin, L. F., Jr., in *Thermal Fatigue of Materials and Components, ASTM STP 612*, American Society for Testing and Materials, 1976, p. 227.
[32] Conway, J. B. et al, "High Temperature Low-Cycle Fatigue of Copper-Base Alloys for Rocket Nozzles; Part II," NASA Report CR-135073, National Aeronautics and Space Administration, Aug. 1976.
[33] Wigmore, G. and Smith, G. C., *Metal Science Journal*, Vol. 5, 1971, p. 58.
[34] Abdel-Raouf, H., Plumtree, A., and Topper, T. H., *Metallurgical Transactions*, Vol. 5, 1974, p. 267.
[35] Westwood, H. J. and Taplin, D. M. R., *Metallurgical Transactions*, Vol. 3, 1972, p. 1959.
[36] Solomon, H. D. and Coffin, L. F., Jr. in *Fatigue at Elevated Temperatures, ASTM STP 520*, American Society for Testing and Materials, 1973, pp. 112-122.
[37] Dutton, R., *Materials Research and Standards*, Vol. 9, No. 4, 1969, p. 11.
[38] Perry, A. J., *Journal of Materials Science*, Vol. 9, 1974, p. 1016.
[39] Gittins, A., *Acta Metallurgica*, Vol. 16, 1968, p. 517.

DISCUSSION

E. Ellison[1] *(discussion)*—This paper is essentially a summary description of the cracking mechanism which occurs in materials subject to combina-

[1] Department of Mechanical Engineering, University of Bristol, Bristol, U.K.

tions of fatigue, creep, and environmental processes. It is based on what I term "intelligent observation," which I believe to be essential if we are to develop fundamentally sound constitutive equations to describe material behavior under complex service conditions of variable load/temperature over long periods of time. To this end, the authors have laudably attempted to simplify and generalize their conclusions, with which I broadly agree.

The authors commence with a straightforward description of the processes of cyclic plasticity at both room and elevated temperature, emphasizing the importance of grain boundaries at the higher temperatures. The synergistic effect of environment on fatigue in terms of the brittle oxide film being repeatedly fractured, exposing fresh material under cyclic stressing, especially at the tips of cracks, is also commented upon with reference to the obvious importance again of grain boundaries and time for the chemical processes to take place. In the summary of previous work it is shown that you cannot always generalize on the influence of wave shape; for example, for austenitic stainless steels a tensile hold is most damaging, whereas for cast nickel alloys it is the compressive hold which degrades the material most quickly. However, for carbon and low-alloy steels the authors state that, though frequency is important, wave shape is not. This does not agree with the Bristol work on a 1CrMoV steel with strain-controlled hold periods where the tensile hold can be very damaging, as for the austenitic steels.

The authors obviously favor the unequal strain rate type of test in which the rates are different in the tensile- and compressive-going parts of the cycle. Based on that reasonable representation, results are reviewed for A286 and Type AISI 304 steels, and for OFHC copper, in both air and vacuum at high temperature. Essentially, their conclusions are as follows (see Table 4 of the paper).

In slow-fast tests, both surface cracks and internal cavities and cracks can grow, the latter obviously being mainly dependent on the temperature and relative strain rates. Indeed, the internal defects caused by creep processes should be independent of environment; in fact, is there not an error in Table 4 where it indicates no interior cracks in vacuum? Surely there should be no difference between air and vacuum in this respect so that there would be little difference between lives in air and vacuum in a slow-fast test. Both cases are dominated by internal creep processes independent of environment.

For equal strain-rate tests it suggested in their model that the creep processes in tension and compression balance so that there are no interior cavities or cracks either in vacuum or air. However, there is an effect of environment as expected on the external cracks, being transgranular in vacuum and intergranular in air especially at the slower strain rates. In these circumstances lives would be expected to be very different in air and vacuum.

In a fast-slow test it is assumed that any cavities opened in tension will

be recovered by long-time processes in compression so that no internal cracks occur. External cracks would be transgranular. The results of Majumdar and Maiya follow this trend for Type 304 stainless steel, though the authors state that the slow-fast cycle is more degrading than one with a tensile hold. However, it should be noted that this latter statement may not be generally true, since the tension part of the slow-fast cycle took 42 min, while the tensile hold was only 15 min; we must compare like with like.

It is also interesting to compare the fast-slow and slow-fast results for the OFHC copper in Table 3. It seems that the ratio of lives (fast-slow)/(slow-fast) is 1138/104, which is approximately the same as the inverse ratio of time spent in tension in each of those cycles. Since cyclic and compressive creep processes must also be present, my observation is interesting though probably not useful.

In their model, the authors assume that intergranular cavitation and triple cracks are caused by tensile creep and not by compressive processes. In our work at Bristol[2] with strain-controlled compressive hold periods on 1CrMoV, we have observed extensive internal intergranular cracking near to failure; the crack shapes were blunter than those occurring in tensile hold tests. Interrupted tests showed that for tensile holds cavities initiated on grain boundaries perpendicular to the applied stress, while for compressive holds the cavities appeared to initiate more generally on grain boundaries at 45 deg or to the stress axis.

I believe that we have to more accurately define what we mean by damage. For example, the authors talk about "healing" when, say, compressive creep follows tensile creep. Certainly, this need not involve such processes as rewelding of cavities. In the Bristol model[3] we think in terms of grain boundary ratchetting, whereby microstrains can accumulate in the grain boundaries in an unbalanced cycle. For example, in a reversed strain cycle test with a tensile hold (for example, 30 min) and no compressive hold, there would be insufficient time in compression to reverse the tensile microstrain on grain boundary sliding occurring in each cycle. Hence, eventually this would accumulate over a number of cycles to form a microstrain concentration in the grain boundaries and hence a grain boundary defect. We have found that even a small amount of balancing compressive hold (for example, 30 min tension, plus 3 min compression) can effectively reduce the internal cracking and hence prolong the life. Indeed, associated with this latter point it has been observed with the 1CrMoV that at the beginning of the strain hold period the stress relaxes very rapidly. In fact, in a test with a 16-h tensile hold, approximately 0.4 of the relaxation strain was obtained in the first 12 s of the hold time. In the Bristol model we assume that this initial strain is not purely creep but is anelastic, what-

[2] Ellison, E. G. and Plumbridge, W. J., to be published.

[3] Ellison, E. G. and Paterson, A. J. F. in *Proceedings*. Institution of Mechanical Engineers, Vol. 190, 1976, p. 321.

ever that means. Possibly it does not matter what it is called as long as it plays its part in balancing the opposing damage. Have the authors noted this behavior and do they have any comments on it?

Finally, I agree with the authors conclusions when they state that fatigue lives may be reduced by up to an order of magnitude when cavities are formed; that is, lifetime is controlled by the fastest fracture mechanism which can operate. May I ask a question regarding interactions between the fatigue, creep, and environmental processes? First, I accept that interactions exist between environment and surface crack initiation and propagation, but is there much evidence for interaction between fatigue and creep processes? Certainly, in our strain-controlled hold period work on 1CrMoV the surface cyclic cracks and the internal creep crack systems are separate and do not appear to interfere with each other. Now the Tomkins/Wareing model implies accelerated fatigue crack propagation through creep-damaged material; this may be true for Type 316 stainless steel, but can the authors comment on the generality of this particular crack damage interaction? I know that deformation processes such as cyclic softening may have an effect on subsequent creep processes, but even here we must be careful. From the Bristol work[4,5] it appears that processes such as cyclic softening, which affect the grains, will also influence subsequent creep behavior if that creep process also occurs within the grains, but has far less effect if the creep process is intergranular. Hence, even in this case it may be said that there is no fatigue/creep interaction. Do the authors have comments?

I conclude by saying that I enjoyed the authors' sane, sound, sensible and simplifying paper and hope they will not mind me inserting my own thoughts and further questions as to possible mechanisms.

E. Krempl[6] *(discussion)*—The authors present a comprehensive overview of the interesting topic of wave shape effects in high-temperature low-cycle fatigue as it evolved from early hold-time testing using conventional testing machines to the present state where servocontrolled test systems are universally applied. Only this type of equipment together with dual-ramp function generators permits the now-favored unequal strain rate testing. Computer control offers further possibilities which have not yet been fully utilized. In the future, computerized testing will increase and we can look forward to further manifestations of the complex picture of high-temperature fatigue.

[4]Ellison, E. G. and Plumbridge, W. J. in *Proceedings*, 2nd International Conference on the Mechanical Behavior of Materials, Boston, Mass., Aug. 1976, p. 908.

[5]Bartlett, R. A., Plumbridge, W. J., Chung, T. E., and Ellison, E. G. in *Proceedings*, 4th International Conference on Fracture, Waterloo, Ont., Canada, June 1977.

[6]Department of Mechanical Engineering, Aeronautical Engineering and Mechanics, Rensselaer Polytechnic Institute, Troy, N.Y. 12181.

The present paper demonstrates the nonlinear time-dependence of fatigue, that is, the highly nonlinear dependence of fatigue life on strain rate and hold time. At a given strain amplitude and a given temperature, strain rate changes of two or three orders of magnitude are necessary to affect less than an order of magnitude change in fatigue life; see Tables 1-3 and Figs. 4 and 9. A similar argument applies for hold times.

The discusser feels that this nonlinear time dependence is present in any environment. An inert environment may increase the fatigue life at a given test condition without significantly affecting the nonlinear dependence on strain rate (hold time). The data in Figs. 4 and 9 as well as in Ref *13* support this view.

Because of this nonlinear dependence it is important that the same range of strain rates (or hold times) be investigated in every environment before comparisons are made. Excluding for the moment unequal strain ratio data, we see from the results cited in Table 1 and Fig. 1 that vacuum tests were performed only in a very limited range of frequencies. This fact, together with the coincidence of the room- and elevated-temperature data shown in Fig. 1, gave credence to the notions that "degradation is mostly environmental" and of "the insensitivity to time-dependent damage when balanced loop tests are conducted in high vacuum." These notions may be due to the limited range of frequencies investigated in vacuum, especially since the vacuum tests at frequencies of 0.0045 and 0.054 in Fig. 1 do not support the time independency of fatigue life.

In the unequal strain rate tests a strain rate range of up to three orders of magnitude is consistently covered both in vacuum and in air. The effect on the fatigue life in vacuum (similar to the results in air) is significant. The results of the unbalanced loop tests are a confirmation of the time-dependent nature of low-cycle fatigue in vacuum and in air.

There is, however, another significant aspect to the unequal strain rate tests, the strong influence on fatigue life by just altering the sequence from fast-slow to slow-fast without changing the strain rates. This effect is present in air and in vacuum and is therefore not caused by the environment. It cannot be a frequency or strain rate effect as these quantities are identical in both tests.

It appears that the fast-slow/slow-fast effect is a true *sequence effect*, that is, it is of the same character as the high-low versus low-high effect on cycles to failure found in block testing involving at least two blocks of cycles at different strain amplitudes. The presence of a slow-fast/fast-slow effect would, according to this view, also indicate the presence of a low/high versus high/low effect. This aspect, however, has not been explored.

This point of view was prompted by an observation of Ostergren that a

recently developed damage accumulation law as stated in his work [7,8] is unable to predict the fast-slow/slow-fast effect. This damage law was previously shown to be incapable of predicting sequence effects; see footnote 7.

To check on this observation, Eq 2 of Ostergren/Krempl (footnote 8) was integrated for the cycles of Fig. 3. We get

$$1 = N_f \left\{ \hat{C} \epsilon_0^{(m-1)p+1} \dot{\epsilon}_0^{p-1} (1 + (\alpha)^{p-1}) + \frac{\hat{D} \epsilon_0^{s+1}}{(s+1)\dot{\epsilon}_0} \left(1 + \frac{1}{\alpha}\right) + \frac{\hat{B} \epsilon_0^{r+1}}{(r+1)\dot{\epsilon}_0} \left(1 - \frac{1}{\alpha}\right) \right\} \quad (1)$$

where

$\hat{C}, \hat{B}, \hat{D}, p =$ } constants depending on environment, temperature, and material,
$m, s =$ even integer }
$r =$ odd integer,
$N_f =$ number of cycles to failure,
$\epsilon_0 =$ total strain amplitude,
$\dot{\epsilon}_0 =$ positive strain rate of first ramp,
$\alpha\dot{\epsilon}_0 =$ magnitude of strain rate of second ramp, where the positive parameter α describes the cycle type, for example

$$\alpha \begin{cases} < 1 \text{ fast-slow} \\ = 1 \text{ equal-equal} \\ > 1 \text{ slow-fast} \end{cases}$$

Using the constants developed by Ostergren and Krempl (footnote 8) for 304 stainless steel at 649°C (1200 F), the fatigue lives of the first four specimens of Table 2 were computed. A comparison of observed and computed lives is given in Table 5 of this discussion.

Although no direct comparison is possible due to the temperature difference, the following trends are worth noting:

1. The predicted lives of T-467 and T-468 are equal; Eq 1 is incapable of modeling the fast-slow/slow-fast effect. (This statement can also be obtained from Eq 1 directly for any value of the constants.)

2. The trend of the influence of frequency is predicted reasonably well.

[7]Ostergren, W. J. and Krempl, E., "A Uniaxial Damage Accumulation Law for Time-Varying Loading Including Creep-Fatigue Interaction," Report RPI CS 77-2, Rensselaer Polytechnic Institute, Troy, N.Y., Aug. 1977.

[8]Ostergren, W. J. and Krempl, E., "A Linear Uniaxial Damage Accumulation Law for Creep-Fatigue Interaction," ASME Paper 78-PVP-63, American Society of Mechanical Engineers, April 1978.

TABLE 5—*Comparison of observed and computed fatigue lives.*

Specimen No.	N_f Cycles Observed at 593°C (1100°F)	N_f Cycles Computed from Eq 1 [Constants Are for 649°C (1200°F)]
T-389	1697	746
T-467	847	1556
T-468	3025	1556
T-320	5096	2575

[Compare the actual fatigue life ratio at 593°C (1100 F), $N_{f\,T\text{-}389}$:$N_{f\,T\text{-}468}$:$N_{f\,T\text{-}320}$ = 1:1.78:3.00, to the predicted one, 1:2.09:345 at 649°C (1200°F).]

It appears, therefore, that the prediction of sequence effects requires damage laws that are not only based on the controlled quantity and the strain, but are also dependent on the stress evolving due to the strain control. Such laws, when consistently stated, were shown to be capable of predicting sequence effects.[9]

For this reason and also for constitutive equation development it would be extremely important to have hysteresis loops reported, in addition to the fatigue life information. It is unfortunate that such data are not included in the paper.

E. Krempl (additional discussion)—I will discuss this paper from a phenomenological point of view. I am not so much interested in the micromechanisms but rather in developing macroscopic predictive techniques.

I want to raise two points. One is with regard to the effect of environment and of wave shape and the second one is with regard to the classification of the wave shape effects in unbalanced tests.

The authors have summarized a considerable number of other results as well as their own results on the effect of wave shape on fatigue life at elevated temperature. When viewed from a phenomenological point of view, a characteristic of all of the data is that a change of several orders of magnitude in the strain rate is necessary to achieve a change of one order of magnitude in fatigue life. This effect seems to be the same in every environment. In vacuum, however, fatigue lives are much longer than in air if all the other parameters are constant.

Now, let me give you an example; see Fig. 16 taken from an early paper by White.[10] He was performing the same tests in vacuum and in air, respectively. I want to draw your attention to the 500°C continuous cycling

[9]Krempl, E. in *Proceedings*, Conference on the Environmental Degradation of Engineering Materials, Virginia Polytechnic Institute, Oct. 1977, pp. 587-598.

[10]White, D. J. in *Proceedings*, The Institution of Mechanical Engineers, Vol. 184, Part I, 1969/1970, pp. 223-240.

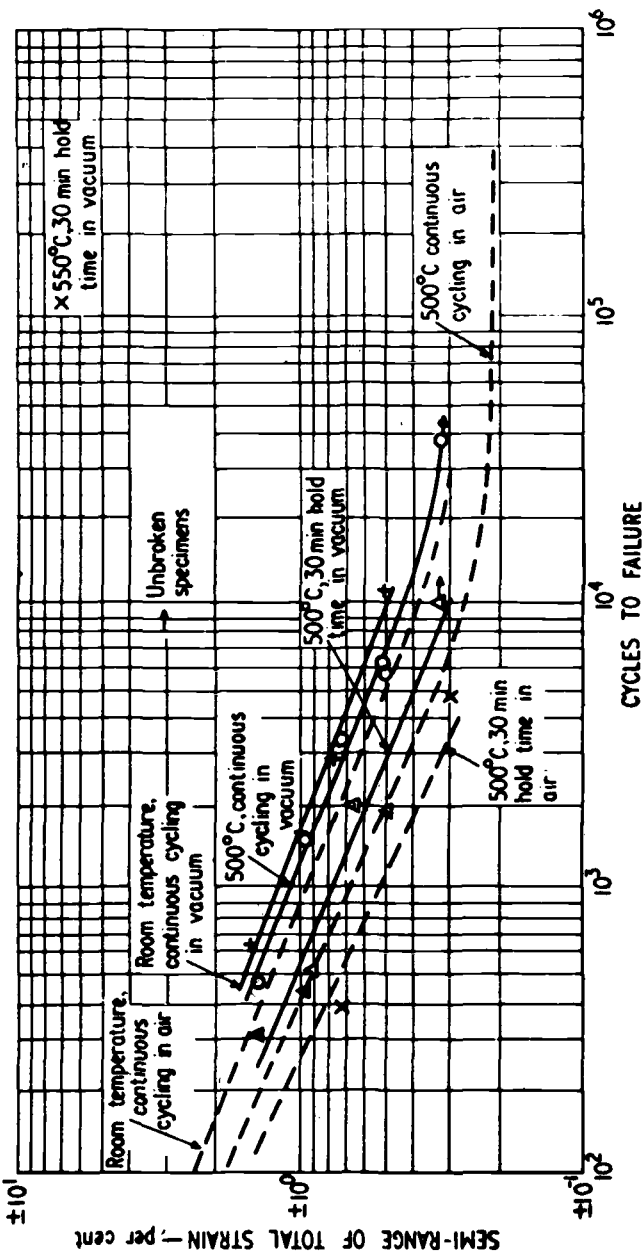

FIG. 16—*Tests in vacuum and in air [taken from a paper by White (see footnote 10)].*

tests in air and the 500°C 30-min hold-time tests in air. There is a life reduction. When this life reduction is compared with the corresponding vacuum tests, we see that they show roughly the same reduction in fatigue life. However, the lifetime in vacuum has increased, but there is still the life-reducing effect of hold time.

In the paper there is evidence presented that the unbalanced loop tests show such a reduction, that is, life reducing effects of wave shape. However, the authors assert that balanced loop tests would not experience such a reduction. I question this point and want to say that it appears the data presented do not support this conclusion as the range of test parameters (say strain rate) is much larger in the unbalanced loop tests than in the balanced loop tests.

In other words, I would expect, if the balanced loop tests were extended to a larger range of parameters of hold time or strain rate, that one would get a similar effect as presented for the unbalanced loop tests.

D. Sidey—Well, I think that is basically true. What must be remembered is that one can work only with the data one has obtained and great care has to be taken if extrapolation of the data beyond the region of direct observations is required.

There are conditions in which, for instance, in balanced loop testing, you could get a marked effect of what you might term the "creep effect." It just so happens that in the information we have obtained for quite a number of different materials, we never reach those conditions. I think the effect is going to occur at very low strain rates.

Of course, those low strain rates could be very important in practice. It is likely that under some conditions balanced loop tests will lead to cavitation failure and *a shorter life than predicted from tests at higher frequencies.*

E. Krempl—I have a second observation with regard to the fast-slow/slow-fast tests, which I found very intriguing. Again I want to present the phenomenological approach. Basically, in going from the fast-slow to the slow-fast tests we just reverse the order of the fast and the slow leg of the loop. We do not change the rates at all. We reverse only the order. In every case we find that the number of cycles for a slow-fast test is considerably less than those of the fast-slow test, typically resulting in a one-to-four life reduction.

It appears to me that this effect is a sequence rather than a rate effect, because I have changed only the sequence of the strain rates in the two tests. This sequence effect is similar to the high-low/low-high effect in two block loading and defined in Appendix I of the 1977 paper by Ostergren and this discusser.[11]

[11] Department of Mechanical Engineering, University of Sheffield, Sheffield, U.K.

D. Sidey—I don't think these two cases are equivalent. In the first instance we are talking about a rate and direction effect. The strain rates in the two parts of a cycle are critical, because the failure mechanism is dependent directly on the strain rates (and their ratio) in the tension and compression ramps. On the other hand, when we talk about the sequence effect, we are talking about the accumulation of damage from cycle to cycle. With a given sequence, we would be building-up a certain type of damage, for instance, by going fast for a while, and we could build up a lot of damage before going to the slow cycling. Similarly when you go slow first, followed by a fast sequence, you could build up a tremendous amount of damage which you are not going to eliminate at all later on by fast cycling. Thus I think the rate effect and the sequence effect are two separate phenomena.

K. Miller[11] (*discussion*)—It appears that the major variable of the experiments reported in the present paper is the strain rate in the tensile-going segment of the fatigue cycle. I would agree with this conclusion since this strain rate controls the time during which the fatigue crack is open. It follows that the strain rate in the compressive-going segment is of considerably less importance.

Thus in order to present a more coherent picture, I would strongly recommend that strain rate be kept constant throughout the full cycle and comparison be made between slow, intermediate, and fast strain rate test data. Certainly the present experimental results should be compared with the type of tests I suggest, and many more than three tests are required in order to separate environmental, cyclic, and time-dependent processes throughout the various parts of the fatigue lifetime.

To clarify some of these points an extensive series of high-temperature, cumulative damage, constant strain rate tests has been carried out[12] to assess the degree of interactions for Stage 1 crack growth since this phase represents the early part of the fatigue life. The work reported in the reference just quoted (footnote 12) and the work under discussion clearly indicate that strain rate control tests are more informative than constant-frequency tests although it is admitted that the latter type of tests is more traditional.

W. Plumbridge[13] (*discussion*)—Regarding your slow-fast cycle which produces intergranular cracking, have you studied the effect of changing the size of the difference in strain rates ($\dot{\epsilon}_{comp} - \dot{\epsilon}_{ten}$)? Is damage more pronounced, and life correspondingly shorter, as this term increases? Might there be a critical value below which voids are not produced?

[12] Miller, K. J. and Gardiner, T., *Journal of Strain Analysis*, Vol. 12, No. 4, 1977, pp. 253-261.

What, if any, is the justification for equating fast-slow tests etc. with strain-controlled tests which incorporate a hold or dwell period?

D. Sidey and L. F. Coffin, Jr. (authors' closure)—We shall answer the comments and questions in the order presented.

Referring first to Prof. Ellison's discussion:

1. The authors agree that wave shape has an effect on lifetime in low-alloy ferritic steels. The discusser's own work [*26*], as well as the results presented by earlier workers at the 1967 Thermal and High Strain Fatigue Conference,[14] indicate that tensile hold periods reduce lifetime. However, the magnitude of this effect seems to be smaller than in the case of austenitic stainless steels, particularly when, in addition, small compressive holds are introduced into the cycle [*26,21*].

2. The results of Majumdar and Maiya indicated that with their particular test conditions the slow-fast cycle was the most damaging, and sound arguments can be made that a slow-fast cycle will be more deleterious than a tensile-hold cycle. When comparing like with like, it must also be remembered that in the quoted case the hold period of 15 min was at maximum strain, while in the slow-fast test the 42 min was spent in straining the specimen from the maximum compressive strain to the maximum tensile strain. However, tests in an inert atmosphere would be necessary to eliminate the environment effects in this case.

The important point of this work, of course, is that unbalanced loops lead to reduced lives when compared with equal ramp cycles. For example, a slow-slow cycle with equal tensile and compressive-going strain rates of 10^{-6} s^{-1} gave a longer life than a slow-fast cycle with strain rates of 10^{-6} $s^{-1}/10^{-3}$ s^{-1}; the former was associated with a transgranular failure and the latter with intergranular fracture.

3. In the tests on the OFHC copper, there was a factor of 100 difference between the tensile-going times in the slow-fast and fast-slow tests, while the difference in lifetimes was a factor of 10. Thus I would not consider the ratio of lives in the two cases to be approximately equal to the inverse ratio of the times spent in tension in each cycle.

4. As stated in our paper, there are several ways in which grain boundary damage produced in tension can be healed or partially healed by compressive stresses. Further studies are required to determine the precise mechanism of healing, which presumably varies with material and test conditions. With our tests on copper, extensive cavitation was observed only in slow-fast tests and cavities were situated mainly on boundaries at right angles to the applied stress axis. In this context, the observations by Ellison and Plumbridge of cavities on 45-deg boundaries in compressive-

[14] *Proceedings*, International Conference on Thermal and High Strain Fatigue, Monograph and Report Series 32, The Metals and Metallurgy Trust, London, U.K., 1967.

hold tests on a low-alloy steel are very interesting. Similar observations have been made by Sidey et al[15] on a copper-chromium alloy at 673 K. In the case of creep tests in pure compression, cavities are not seen [*37*], but the reason for this is that cavities are difficult to nucleate in pure compression.[16] By cycling strain through tension and compression, it is likely that the difficulty of initiating cavities is overcome and that the maximum growth rate in a compression hold will occur on the boundaries experiencing the maximum shear stress. The general model of healing proposed by Prof. Ellison in his reference (see footnote 3) is interesting, but the micromechanisms of the process need to be indicated. Perhaps such a model should consider the effect of cycle shape on the mechanisms of cavity nucleation and cavity growth.

5. Creep damage is complex and can arise from many sources. Basically, however, creep results from deformation and fracture processes and thus it is extremely structure sensitive. Considering deformation processes only, it is to be expected that changes in substructure caused by cyclic softening or hardening will affect the subsequent creep behavior of a material. Acceleration of creep has been observed in a 1CrMoV steel as a result of cyclic softening processes[17] (see Fig. 17), while retardation in creep has been noted in an austenitic steel due to prior cyclic hardening of the material.[18] However, these effects do diminish as the fatigue strain range or the creep stress (or strain rate) or both are lowered. Therefore, in many practical situations which involve small strain ranges and long-time factors, negligible creep-fatigue interactions would be expected *to result from deformation processes.* The same is not true when fracture-damage processes are considered.

In recent studies on 1CrMoV steel at 838 K,[19] creep damage, which included internal intergranular cavitation and cracks, was found to reduce drastically the subsequent high-strain fatigue lifetime of the alloy. The reasons for this reduction in life were twofold. Cracks propagated from the interior so that the period required for surface initiation was eliminated. Secondly, cracks propagated along grain boundaries by interlinkage of the intergranular creep cracks, which was obviously faster than the propagation of a transgranular crack. This evidence supports the ideas of Tomkins and Wareing [*24*], who have suggested that the detrimental effects of inserting tensile-hold periods into the fatigue cycle in 316 stainless steel are due to enhanced crack propagation rates through creep-cavitated material. Such a process would be expected to occur in any material, but the extent of any

[15] Sidey, D., Collins, A. L. W., and Taplin, D. M. R., unpublished research.

[16] Davies, P. W. and Dutton, R., *Acta Metallurgica*, Vol. 14, 1966, pp. 1138-1140.

[17] Sidey, D. in *Proceedings*, 4th International Conference on Fracture, Waterloo, Ont., Canada, Vol. 2, 1977, pp. 813-819.

[18] Plumtree, A. and Persson, N. G. in *Proceedings*, 4th International Conference on Fracture, Waterloo, Ont., Canada, Vol. 2, 1977, pp. 821-830.

[19] Sidey, D., *Materials Science and Engineering*, Vol. 33, 1978, pp. 189-197.

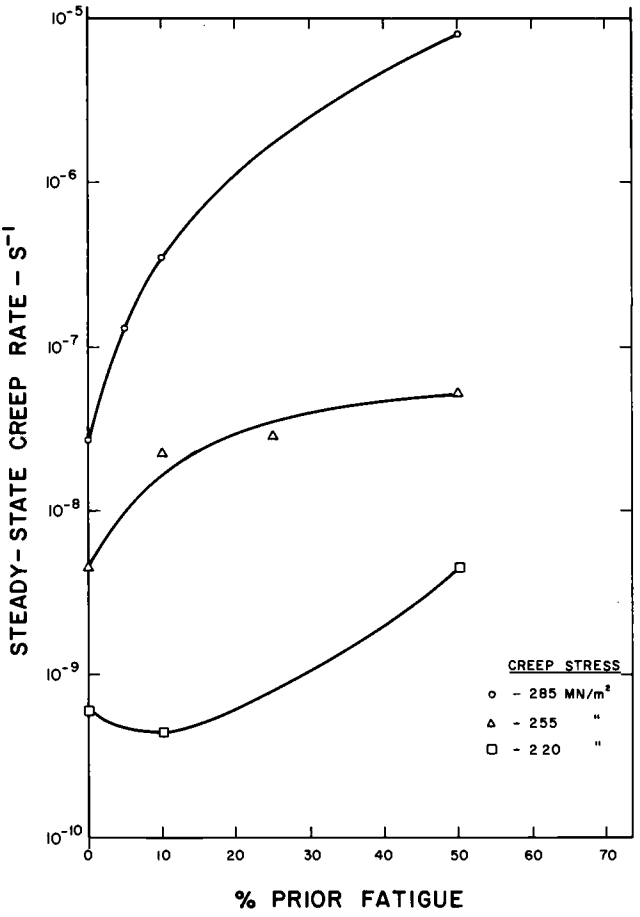

FIG. 17—*Effect of prior fatigue at 838 K in a 1CrMoV steel on the steady creep rate.*

interaction would depend on the cavitation characteristics of the particular material.

Turning next to Prof. Krempl's discussion:

1. The discusser states that we assert that balanced loop tests would not show life reductions in inert environments. This is not the case, as can be seen from an examination of the model presented in Fig. 15. This indicates that there is a frequency (ν_m) in balanced loop testing below which life degradation is expected even in vacuum. Below this frequency, creep effects become important. The value of ν_m is dependent on wave-shape and material.

2. With regard to the statement that the wave shape effect is a sequence effect rather than a rate effect, it is important to consider the micromechanisms which are involved. In the sense that all stress-strain responses of

metals at high temperatures are history dependent, the wave shape results are a sequence effect. The question which really has to be considered is, what causes this effect? Any effects result from differences in damage accumulation during the tension and compression parts of the cycle which in turn are dependent on the strain rates *in each part.* In the present tests, the micromechanism of failure in slow-fast tests was intergranular compared with transgranular in fast-slow tests. The differences in lifetimes are directly due to the different modes of fracture. It is necessary to know the conditions which produce intergranular fracture, and it is likely that conditions exist under which the fracture mechanism remains the same for fast-slow and slow-fast cycles, with resulting negligible differences in lifetime. In this case, the strain rates and differences in strain rates in the tensile-going and compressive-going parts of the cycle are controlling the fracture processes at the microscopic level. Thus contrary to Prof. Krempl's statement, a strain rate effect does exist.

Phenomenological models, such as the one mentioned by Prof. Krempl, are unsuccessful because they fail to consider the micromechanisms of failure. For instance, the particular model due to Ostergren assumes that the direction of straining is irrelevant with respect to the production of damage. While this may possess some validity in the case of deformation studies, where shear stresses are important, it is not the case for high-temperature fracture processes which are dependent on the maximum principal stress.

In reply to Prof. Miller's discussion:

The discusser implies that similar results would have been obtained from balanced loop tests covering the same range of strain rates. Table 2 shows that this is not the case for 304 stainless steel, where slow-slow tests have a longer lifetime than slow-fast tests. The important point is that the damage mechanisms are dependent on the unbalance in the loop. Not only does the tensile strain rate control the time during which any fatigue crack is open, but also it controls the propensity for internal cavitation. The compressive strain rate is important because it controls the amount of damage recovery in the cycle.

The authors agree that strain rate should be controlled in high-temperature fatigue tests but, in addition, consideration should be given to its importance in the tension and compression components of the fatigue cycle.

Finally, responding to Prof. Plumbridge:

1. The results of Majumdar and Maiya on 304 stainless steel presented in Table 2 show that when the ratio $\dot{\epsilon}_t{:}\dot{\epsilon}_c$ is changed from 100 to 1000, the number of cycles to failure is considerably reduced. It must be borne in mind that by changing the ratio of strain rates the cycle period is altered, so that the environmental factor cannot be ignored.

2. With respect to there being a critical value of the strain rate ratio below which cavitation is not produced, it must be remembered that this

ratio is not the only factor to be considered. Even in balanced loop tests, intergranular cavitation failure can be produced below a certain test frequency. The effect of tensile holds or slow-fast cycles is to encourage this type of failure compared with the equivalent balanced loop cycle. Therefore, it would be expected that such a critical value of the strain rate ratio would exist under certain conditions (for example, where the tensile strain rate is relatively high), but the critical value would decrease with increasing value of the cycle period.

3. It is generally observed that lifetimes are reduced and intergranular cracking appears when the tensile-going time exceeds the compressive-going time in a fatigue cycle. As the present results indicate, the unbalanced loop tests are very effective in indicating the damage processes which can accelerate failure. In particular, it is a method of determining the response of a given material to strain rate and wave shape. One cannot say that a slow-fast test can be equated exactly with a hold-time test, but a more general equivalence can be drawn if the micromechanisms of fracture are similar in both cases.

B. K. Min[1] *and R. Raj*[1]

A Mechanism of Intergranular Fracture During High-Temperature Fatigue

REFERENCE: Min, B. K. and Raj, R., "**A Mechanism of Intergranular Fracture During High-Temperature Fatigue,**" *Fatigue Mechanisms,* Proceedings of an ASTM-NBS-NSF Symposium, Kansas City, Mo., May 1978, J. T. Fong, Ed., *ASTM STP 675,* American Society for Testing and Materials, 1979, pp. 569-591.

ABSTRACT: We have studied the mechanism whereby grain boundary sliding in the crack-tip region causes a triple-junction fracture type of grain boundary damage. This results in an increase in the rate of fatigue crack propagation. It is argued that since grain boundary sliding is a strain rate sensitive process, sliding damage is possible only if the strain rate is below a critical value; an expression for the critical strain in terms of the microstructure and the yield strength is obtained. It is shown, by theory and experiment, that the maximum damage condition is achieved when the tensile-going strain rate is below the critical strain rate whereas the compressive-going strain rate is above the critical value. If both strain rates are below the critical value (enough if they are unequal), then damage due to sliding in one direction is removed by sliding in the reverse direction, and the increase in crack growth rate is not observed.

KEY WORDS: high-temperature fatigue, intergranular fracture, triple-junction cracking, grain boundary sliding, critical strain rate

A number of engineering alloys suffer a reduction in life when tested for low-cycle fatigue at elevated temperature. Often this reduction is caused by the initiation and propagation of a crack along the grain boundaries. In comparison, at room temperature the crack normally does not show a preference for an intergranular path. The switch to the intergranular fracture is influenced by the time and temperature parameters in the load history, and by the environment.

In this paper, we consider a micromechanism which can result in intergranular fracture. Starting from a micromechanical basis, we attempt to

[1] Research associate and assistant professor, respectively, Department of Materials Science, Bard Hall, Cornell University, Ithaca, N.Y. 14853.

explain the relationship between the microstructure and load history parameters, and the incidence of intergranular fracture. The results are supported by experimental measurements.

One mechanism by which creep and fatigue interact to produce intergranular fracture has been identified by us and reported in detail elsewhere [*1,2*].[2] This mechanism was concerned with the initiation of cavities in the grain boundaries when an unsymmetrical hold cycle (one which includes a longer hold period in tension than in compression) is applied to the specimen in axial loading. The initiation of the damage in itself, however, does not lead to an increase in the rate of fatigue crack growth. A second criterion is required for the interaction between the crack and the cavitation damage in the material ahead of the crack; this criterion is that sufficient displacement should be available at the crack tip so that the cavities are able to coalesce and produce a fracture. Measurements of low-cycle fatigue crack growth in 316 stainless steel showed that the second criterion could be satisfied only when the crack lengths were quite long, of the order of 1 mm, even when a large plastic strain range (of the order of 0.8 percent) was applied. Since the fatigue life is probably determined for the most part by the initiation and propagation of a crack much smaller than 1 mm, it is not expected that the aforementioned mechanism of interaction between the crack-tip displacement, and the cavitation damage ahead of the crack-tip, plays an important role in the determination of fatigue life.

In this paper we report on a second mechanism which can result in intergranular crack growth. The fundamental basis of this mechanism is that grain boundary sliding at the crack tip can severely localize the displacement at the grain boundary just ahead of the crack tip as shown in Fig. 1.[3] This can cause triple-junction fracture near the crack tip, which can accelerate fatigue crack propagation. Since grain boundary sliding is a time-dependent process, the strain rate applied to the specimen will determine the extent to which the boundaries can slide. That is, the rate at which the strain is applied to the specimen should be in harmony with the rate at which the boundaries can slide. If the applied strain rate is too fast, then the applied strain will be accommodated by grain matrix deformation rather than by grain boundary sliding. On the other hand, if the applied strain rate is too slow, then the stress concentrations produced at the triple point by grain boundary sliding will be relieved by creep processes and the triple-junction fracture will not be initiated.

The mechanism described in this paper is probably important in those

[2]The italic numbers in brackets refer to the list of references appended to this paper.

[3]There is a basic difference between this mechanism and the mechanism described in the preceding paragraph. In the first mechanism, grain boundary sliding does not contribute in the localization of displacement to the grain boundary plane. In the second mechanism the localization is almost entirely due to grain boundary sliding.

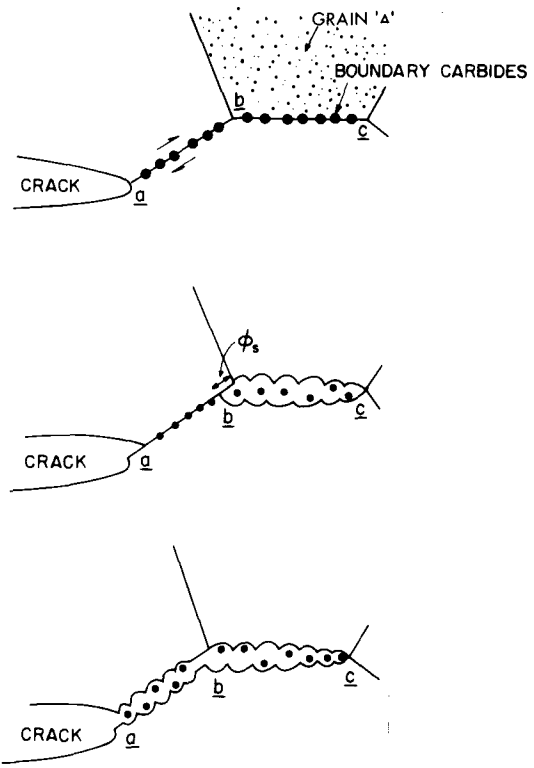

FIG. 1—*Mechanism of crack propagation by triple-junction fracture initiated at* b *as a result of sliding at* ab. *The rate-controlling step is expected to be the fracture of* bc.

instances where strain rate and frequency effects are known to influence low-cycle fatigue life. Two types of strain rate effects have been reported in the literature: one occurs under symmetrical strain rate cycling (frequency effect) and the other is observed only when an unsymmetrical strain rate cycle is applied (cycle shape effect). In symmetrical strain rate cycling the fatigue life increases with increasing frequency until a saturation value is reached; beyond it the fatigue endurance is largely frequency independent. It is often observed that below the transition frequency fracture tends to be intergranular while above it, it is transgranular. There is some evidence that at the lower end of the frequency spectrum fatigue life again approaches a saturation value [*3*]. The frequency effect is quite marked in Udimet 700 [*4*]; in 304 stainless steel [*5*] and chromium-molybdenum-vanadium steel [*6*] it is observed when the stress/strain amplitude is small. The effect of the application of unsymmetrical strain rates on the fatigue life of austenitic stainless steels is also quite striking. It has been shown that a slow tensile-going and fast compressive-going cycle (will be abbreviated

as slow-fast, etc.) results in a fatigue life which can be as much as a factor of 10 lower than if a fast-slow cycle is used [7]. Furthermore, the effect is observed whether the test is carried out in vacuum or in air [8], which suggests that at least in the case of the austenitic stainless steels the reduction in life is not caused by the environment. The implications of unsymmetrical strain in fatigue endurance are clearly important in the strain range partitioning approach for the rationalization of fatigue behavior as proposed by Manson [9].

In the following sections we discuss first the microscopic mechanism of triple-junction fracture (described in Appendix I), followed by a structural definition of grain boundary damage. By means of micromechanical modeling the damage parameter is correlated to the load history of the specimen with emphasis on the time- and temperature-dependent parameters and, finally, the results from fatigue experiments are interpreted in terms of the micromechanical model.

Mechanism and Definition of a Damage Parameter

The mechanism by which grain boundary sliding can cause the formation of grain boundary cracks in the region of the crack tip is illustrated in Fig. 1. The rate-controlling step in the advance of the crack is probably the opening up of segment *bc*. Once the secondary crack *bc* has formed, the segment *ab* can separate by the growth of cavities by diffusion, a process which has been shown to occur quite rapidly when bicrystals, such as *ab*, are loaded in tension [10]. We assume that the critical parameter in the formation of the crack *bc* is the net sliding displacement available at the triple junction *b* upon the completion of one full cycle. We call this ϕ_s. The magnitude of ϕ_s needed to form the crack will depend upon the distribution of the cavities in *bc*. It is estimated that the critical displacement, u_c, needed to separate a boundary is given by [11]

$$u_c = 0.23\lambda \exp[4/(n-1)] \tag{1}$$

where λ is the average spacing of the cavities and n the power-law stress exponent in the equation for steady-state strain rate

$$\dot{\epsilon}_{ss} = A \frac{D_V G b}{kT} \left(\frac{\sigma}{G}\right)^n \tag{2}$$

where

D_V = lattice self-diffusion coefficient,
G = shear modulus,

b = lattice parameter,
σ = equivalent shear stress and A is a numerical constant.[4]

Equation 1 is an empirical relation applicable to cases in which deformation is localized within a narrow band near the grain boundary, and where cavities grow by power-law creep. It is not necessary, of course, that u_c should be exceeded by ϕ_s in a single cycle; the damage can accumulate over several cycles until the segment bc becomes separated.

We consider now the manner in which the applied strain rate influences grain boundary sliding. Grain boundary sliding is a time-dependent process; for example, it occurs only at elevated temperatures when the boundaries lose their ability to sustain a shear stress, and respond by sliding when a shear stress is applied to them. The sliding resistance of a simple boundary, such as in a bicrystal, which is planar and does not contain second-phase particles, is quite low; boundaries in pure metals, for example, slide at a measurable rate at temperatures as low as 0.3 of the melting temperature (extrapolated from measurements in pure aluminum and pure copper; in stainless steels this corresponds to a temperature of about 505 K). Introduction of hard second-phase particles into the grain boundaries, such as the carbides in nickel-base alloys and austenitic stainless steels, can very significantly increase the sliding resistance of the grain boundaries [*12*]. The sliding properties of such boundaries can be determined by internal friction experiments [*13*].

Whereas the sliding behavior of grain boundaries is time and temperature dependent, the deformation of the grain matrix is either time independent, as is the case when metals are deformed at room temperature, or time and temperature dependent, which gives rise to the creep equation quoted in Eq 2. Going back now to the deformation in the crack tip region as shown in Fig. 1, the extent of sliding achieved across the segment ab will depend upon the competitive rates of grain boundary and grain matrix deformation. Low temperatures and high strain rates will favor grain matrix deformation, whereas high temperatures and intermediate strain rates will result in greater amounts of sliding.

The shear stress experienced by the boundary segment ab reverses when the applied strain rate changes from tensile-going strain rate, $\dot{\epsilon}_\alpha$, to compressive-going strain rate, $\dot{\epsilon}_\beta$. Since sliding can be reversed, the sliding offset produced at b during tensile-going half of the cycle may be fully or partly recovered during the compressive-going half of the cycle. The net sliding offset produced at the completion of one full cycle, ϕ_s, is then given by

$$\phi_s = \phi_t - \phi_c \tag{3}$$

[4]The numerical values of these parameters for 316 austenitic stainless steel are given in Appendix II.

where ϕ_t is the forward and ϕ_c the backward sliding displacement produced at b. Upon the completion of a cycle, net damage occurs only if $\phi_t > \phi_c$; the larger the difference between ϕ_t and ϕ_c, the greater will be the extent of grain boundary cracking. *The simplest way to accentuate this difference is to impose an unsymmetrical strain rate cycle.* It should be noted, however, that we are concerned with the local strain rates in the plastic zone around the crack tip. When the specimen is loaded to a condition of general yield, that is, when the plastic strain range is greater than the elastic strain range, it is likely that the local strain rates in the crack-tip region are approximately of the same order as the applied strain rates. Under these conditions, therefore, the applied strain rate to the specimen must be unsymmetrical in order to achieve greater sliding in the forward than in the reverse direction.

In those instances when the crack is loaded only to the extent of small-scale yielding near the crack tip [*20*], the local strain rates within the plastic zone would differ from the applied strain rates. It is known [*21*] that when a crack is unloaded, "reverse" yielding occurs at the crack tip. A physical explanation for this behavior is that the presence of the elastic-plastic boundary produces back stresses. Upon unloading, the back stresses remain and may cause reverse yielding. Extending the same arguments to the time-dependent deformation at the growing crack tip, we may assert that the local stress near the crack tip which drives the deformation would be generally lower during the tensile-going half of the cycle—when it will be equal to the elastic stress minus the back stress—than during the compressive-going cycle—when it will be the elastic plus the back stress. If this is so the local strain rates near the crack tip will be asymmetric even when the applied strain rates are symmetric. In these instances, triple-junction fracture can be expected near the crack tip under symmetrical strain rate cycling. This latter case is particularly important when testing at strain amplitudes which are less than the amplitude corresponding to the transition fatigue life.[5] For example, the frequency-dependent fatigue life, as a function of applied strain range, for chromium-molybdenum-vanadium steel is shown in Fig. 2 [*6*]. In all cases symmetrical strain rates were used. It is seen that the fatigue life becomes increasingly sensitive to the frequency as the total plastic strain range is decreased.

Application of Unsymmetrical Strain Rate During Cyclic Loading

In this section we consider fatigue crack propagation under conditions of general yield. In such a situation it is reasonable to assume that the applied strain rate will be equal, at least approximately, to the local strain

[5]The transition fatigue life is defined here as that condition in the fatigue endurance curve when the elastic and the plastic components of the applied strain range are equal.

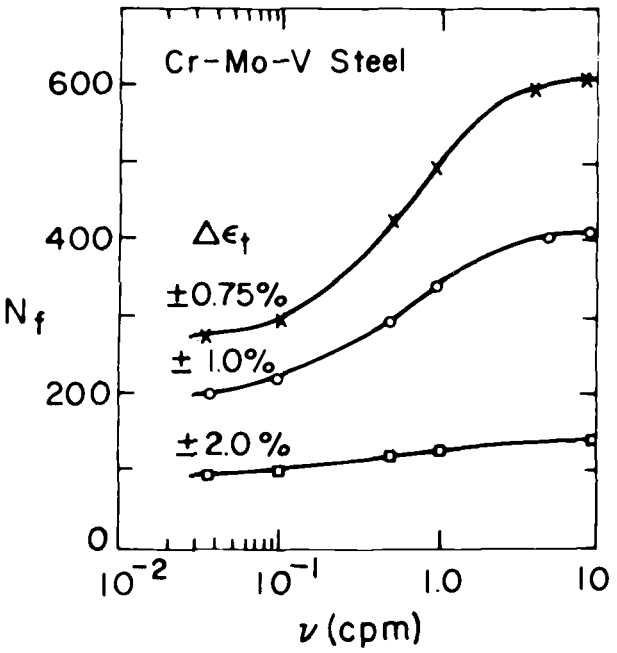

FIG. 2—*Effect of frequency on fatigue life becomes more marked as the strain amplitude is decreased* [6].

rate near the crack tip. We further assume that the rate of sliding of grain boundaries, such as *ab* in Fig. 1, is controlled by the presence of hard second-phase particles. A sustained rate of sliding in the presence of the particles is possible only if matter is transported around the particles. If the temperature is in the neighborhood of 0.5 T_M and the particles are smaller than about 1 μm, then it is expected that grain boundary diffusion will be the rate-controlling mechanism for sliding accommodation.[6] For this mechanism the rate of sliding of the boundary is given by [*12*]

$$\dot{u} = \frac{\sigma_s \Omega}{kT} \frac{8\delta D_B}{f_b p^2} \tag{4}$$

where

σ_s = shear stress applied to boundary,
δ = thickness of grain boundary,

[6]Sliding of the boundary segment *ab* (Fig. 1) leads to incompatible displacement at the triple junction *b* which must be accommodated by matrix deformation of the grain Δ, for example. Since the stresses in the grain exceed the yield stress, it is not expected that deformation of the grain Δ will offer significant resistance to sliding on *ab*.

D_B = grain boundary diffusion coefficient,
p = average particle size,
f_b = volume fraction of particles,
Ω = atomic volume,
K = Boltzmann's constant, and
T = temperature in Kelvin.[7]

Since most of the sliding is expected to occur during plastic deformation, it is reasonable to assume that $\sigma_s = \sigma_y$ where σ_y is the yield stress of the material. Recognizing that a sliding displacement u is equivalent to a strain of u/d, where d is the grain size, we obtain a condition on the strain rate for optimum sliding by extrapolation of Eq 4

$$\dot{\epsilon}_c = 8 \frac{\sigma_y \Omega}{kT} \frac{\delta D_B}{d f_b p^2} \tag{5}$$

Physically $\dot{\epsilon}_c$ represents the strain rate at which the boundaries can slide just fast enough to keep up with the rate of deformation. If the applied strain rate is faster, then the boundaries will essentially become "frozen" and the sliding component of the applied strain will decrease. Consequently the condition for triple-junction cracking becomes

$$\dot{\epsilon} \leq \dot{\epsilon}_c \tag{6}$$

Experimental Results

Description of Experimental Technique

We have measured the rate of fatigue crack propagation in 316 stainless steel under unsymmetrical strain rate cycling. Experiments were carried out at constant plastic strain range of about 0.8 percent in fully reversed loading. A significant shift in the mean stress was not observed. The details of each experiment are reported in Table 1.

The specimens had a uniform, square cross section of 6.4 by 6.4 mm and a gage length of 12.7 mm. A notch was spark-machined on one edge of the square cross section from which a fatigue crack was started at room temperature. The temperature was then raised to the desired value (range 773 to 898 K) and the fatigue crack growth rate measured. The temperature control across the gage length was better than ± 2 K. The testing fixture has been described elsewhere [*14*].

Two types of unsymmetrical strain rate cycles were used: a fast (tensile-going)-slow (compressive going) cycle and a slow-fast cycle. The slow strain

[7]For numerical values for 316 stainless steel, see Appendix II.

TABLE 1—*Summary of experimental data.*

Test Temperature, K	Cycle Shape	$\Delta\epsilon_t$ (%)		$\Delta\epsilon_p$ (%)		$\Delta\sigma$ (MPa)	
		Start[a]	Finish[b]	Start	Finish	Start	Finish
898	slow-fast	1.74	1.75	0.81	0.87	683	667
898	fast-slow	1.73	1.74	0.82	0.88	641	602
848	slow-fast	1.82	1.85	0.78	0.85	731	720
848	fast-slow	1.83	1.85	0.80	0.85	727	725
811	slow-fast	1.86	1.87	0.80	0.84	759	768
773	slow-fast	1.82	1.84	0.79	0.83	744	810
773	fast-slow	1.80	1.91	0.78	0.83	729	838
295	harmonic	1.98	1.98	0.82	0.85	866	892

[a] At the first cycle during crack growth measurement.
[b] At the last cycle during crack growth measurement.

rate in all experiments was 7×10^{-5} s^{-1} while the fast strain rate varied from 2×10^{-3} s^{-1} to 4×10^{-3} s^{-1}.

The specimens were annealed at 1073 K for 1 h to stabilize the carbide distribution in the grain boundaries. The distribution of the particles and their spacing in the boundaries was measured by a combination of optical and transmission electron microscopy as described in an earlier paper. In the present set of specimens the average particle size was 0.11 μm and the average spacing was 0.56 μm, which leads to a value of $f_b = 0.19$ for the area fraction of second-phase particles in the grain boundary.

In our experiments we determined the crack growth constant B in the empirical equation described in Eq 7. This equation was found to be valid in our experiments when the crack length was in the range 0.5 to 1.2 mm. The procedure for the determination of da/dN versus a[8] curves has been described in an earlier paper [2]. B was measured as a function of temperature and cycle shape

$$\frac{da}{dN} = Ba \tag{7}$$

Design of Test Variables

The experimental tests were designed in order to understand the importance of grain boundary sliding in fatigue crack propagation. The basic concept is that if the strain rate is less than $\dot{\epsilon}_c$ (Eq 5), then sliding would occur which, in turn, can lead to triple-junction fracture at the crack tip. Also, sliding is reversible and therefore a sliding offset in the forward direction can be recovered by sliding in the reverse direction provided that the

[8] a is the crack length and da/dN the crack growth per cycle.

reverse strain rate is also less than $\dot{\epsilon}_c$. Let us now consider that unsymmetrical strain rates are applied. Let the tensile-going strain rate be $\dot{\epsilon}_\alpha$ and the compressive-going strain rate $\dot{\epsilon}_\beta$. Various combinations of strain rates can now be used and, depending upon whether $\dot{\epsilon}_\alpha$ and $\dot{\epsilon}_\beta$ are less than or greater than $\dot{\epsilon}_c$, different results can be expected. These are described below in the following.

1. If both $\dot{\epsilon}_\alpha$ and $\dot{\epsilon}_\beta$ are less than $\dot{\epsilon}_c$, then sliding would take place in the forward as well as the reverse direction. As a result, $\phi_t \approx \phi_c$ and $\phi_s \approx 0$ (Eq 3); that is, the damage in the forward direction will be healed during reverse loading, and any significant amount of intergranular fracture should not be observed. Depending upon the temperature and the microstructure, this condition may be satisfied for any cycle shape.

2. If $\dot{\epsilon}_\alpha < \dot{\epsilon}_c$ but $\dot{\epsilon}_\beta > \dot{\epsilon}_c$, then sliding would occur in the forward direction and $\phi_s > 0$. *This is the condition of maximum damage. It can be achieved only in slow-fast cycling.*

3. If $\dot{\epsilon}_\alpha > \dot{\epsilon}_c$ while $\dot{\epsilon}_\beta < \dot{\epsilon}_c$, then damage will not occur since the triple junction can be expected to fracture only during the tensile-going half of the cycle. *This is the condition for minimum damage and can be achieved only during fast-slow cycling.*

Results

A plot of $\dot{\epsilon}_c$ as a function of T is given in Fig. 3. It applies to 316 stainless steel containing a grain size of 21.6 μm, particle size of 0.11 μm, and particle spacing of 0.56 μm. Curves for other mictrostructures can be plotted using Eq 5. The values of the other parameters are given in Appendix II. According to theory, sliding and hence triple-junction fracture should not occur in the region $\dot{\epsilon} > \dot{\epsilon}_c$. It follows that if $\dot{\epsilon}_\alpha$ and $\dot{\epsilon}_\beta$ *both* lie in Region I ($\dot{\epsilon} > \dot{\epsilon}_c$), then sliding will not occur at all; if both lie in Region II ($\dot{\epsilon} < \dot{\epsilon}_c$), then sliding would occur equally in the tensile-going *and* the compressive-going halves of the cycle and the net amount of sliding for each cycle would be nearly zero. The third "no damage" condition is that $\dot{\epsilon}_\alpha$ lies in Region I and $\dot{\epsilon}_\beta$ in Region II, since this will cause sliding in compression but not in tension, which should not cause triple junction failure.[9] The most damaging cycle clearly would be the one in which $\dot{\epsilon}_\alpha$ is in Region II but $\dot{\epsilon}_\beta$ is in Region I; that is, sliding occurs during tension but is suppressed during compression.

The "fast" and the "slow" strain rates used by us are also marked on Fig. 3 and the corresponding results for B for fast-slow and slow-fast

[9]This point needs some clarification since sliding, which is a shear stress controlled process, occurs in tension as well as in compression. There is a difference, however, for sliding at the crack tip since the presence of the free surface affords less resistance to sliding during tension than during compression.

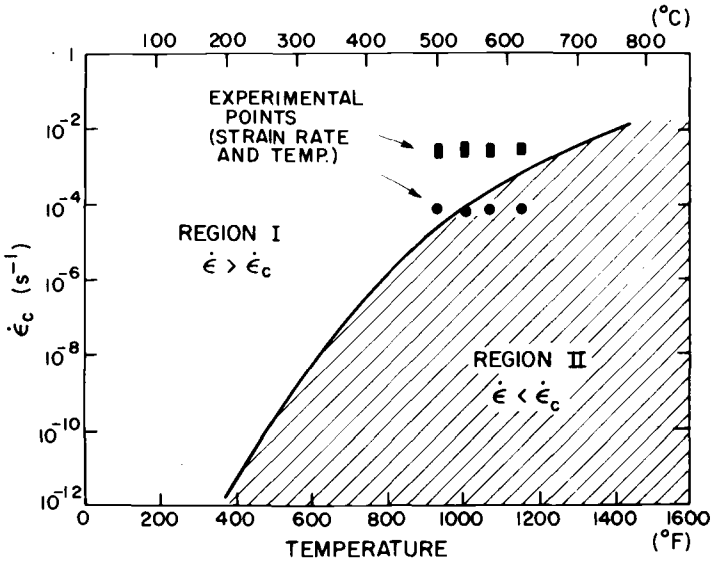

FIG. 3—*A plot of the critical strain rate for our 316 specimens as calculated by Eq 5. Unsymmetrical strain rate cycling can lead to increased crack growth rates only if the slow strain rate is below* $\dot{\epsilon}_c$ *but the fast strain rate is above* $\dot{\epsilon}_c$. *Our experimental strain rates are in agreement with theory.*

cycling are presented in Fig. 4. The agreement between theory and experiment is very good. The strain rates used agree nicely with the transition strain rate calculated from Eq 5. At 898 K fast-slow and slow-fast cycling gives similar values for B, and as seen in Fig. 3, except for a slight shift in the curve, both strain rates at this temperature fall in Region II. As the temperature is decreased, the separation of the two strain rates into Regions I and II becomes more pronounced and this is marked by an increasing difference between the B values for fast-slow and slow-fast cycling. Although we have not yet obtained points below 773 K, it is almost certainly expected that both curves in Fig. 4 will merge toward the room temperature value for B (as measured by us) since at room temperature fatigue behavior should be cycle shape independent.

Summary

A specific mechanism of grain boundary damage has been investigated in this paper. The mechanism involves the fracture of grain boundaries by triple-junction cracking in the crack tip region. Grain boundary sliding is the rate-limiting step in this fracture process. Since grain boundary sliding is a time- and temperature-dependent process, it is theorized that it will

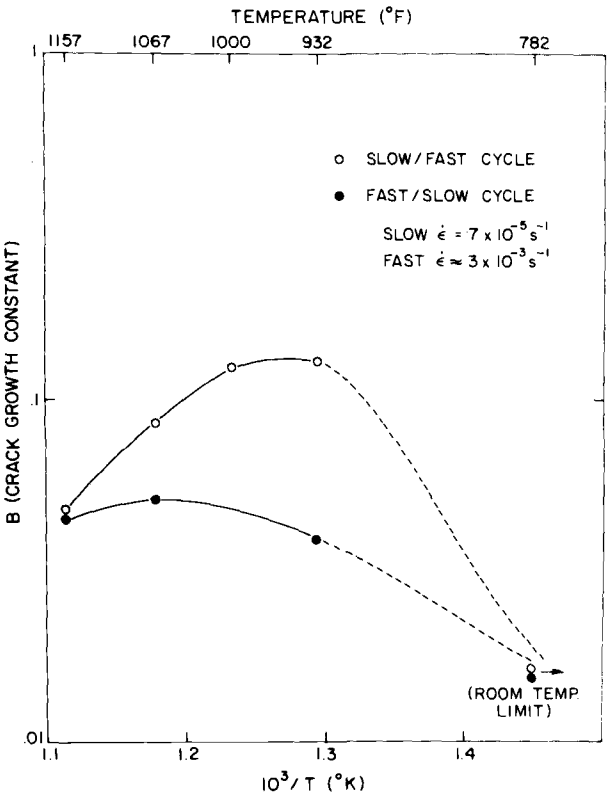

FIG. 4—*Variation of* B (*see Eq 7*) *with temperature* (*including the room temperature limit*) *for slow-fast and fast-slow cycling.*

not occur if the applied strain rate exceeds a critical value. An expression for the critical value of this strain rate (Eq 5) is derived in terms of the size and distribution of the second-phase particles (carbides) in the grain boundaries, the grain size, grain boundary self-diffusion coefficient, and the yield stress. Sliding, and hence damage, is expected when the applied strain rate is less than the critical strain rate.

Since grain boundary sliding is reversible, the damage produced by sliding in one direction can be removed by sliding in the opposite direction. Therefore, if the cycle shape is such that the tensile-going and the compressive-going strain rates are below the critical strain rate, then no net damage will be produced since sliding will occur equally in the forward and reverse directions. The condition for maximum damage is obtained when the tensile-going strain rate is less than but the compressive-going strain rate is greater than the critical strain rate (a slow-fast cycle); this leads to sliding in the forward direction but not in the reverse direction.

Low-cycle fatigue crack growth experiments were carried out in 316 stainless steel under constant plastic strain range (0.8 percent) but at various temperatures. Unsymmetrical strain rate cycling was employed and the crack growth constant B (see Fig. 4) was measured. At high temperature (898 K), B was equal for slow-fast and fast-slow cycling; this was because at this temperature both strain rates were below the critical value. At intermediate temperatures (775 to 866 K) B was greater for slow-fast than for fast-slow cycling, which was expected on the basis that in this temperature range the slow strain rate was less than but the fast strain rate was greater than the critical value. At room temperature, B was lower than either of the high-temperature values (see Fig. 3). The theoretical value of critical strain rate was within a factor of two of the measured values of the critical strain rate. Given the uncertainty in the diffusion coefficient, this agreement is quite good.

Acknowledgment

This work was supported by the Air Force Office of Scientific Research, AFOSR-76-2930, under the supervision of Dr. A. H. Rosenstein. Support was also received from the National Science Foundation through the Materials Science Center at Cornell University.

APPENDIX I

Triple Junction Fracture

There are at least two mechanisms of intergranular fracture in polycrystalline materials. The difference is illustrated by the optical micrographs shown in Fig. 5. In cavitation failure, cavities nucleate (usually at hard second-phase particles in the boundary) and grow in the entire cross section of the specimen. In triple junction fracture, localized cracks appear in the boundary produced by the unaccommodated component of grain boundary sliding (GBS) at the triple junction as illustrated in Fig. 5. Cavitation failure usually dominates at stresses much lower than the yield stress, while triple junction-fracture is observed more often at stresses which are close to the yield stress of the material. An illustration of the transition from cavitation to triple-junction failure is shown in Fig. 6. The data are taken from stress rupture experiments on copper containing a dispersion of silica particles. The transition is accompanied by a change in slope of the log t_f versus log σ curve. Since this material has poor strain-hardening properties, triple junction fracture (TJF) is soon overtaken by necking-type failure at slightly higher stresses. Most likely, the mechanism for triple junction fracture, as illustrated in Fig. 7, differs from cavitation failure only in the manner in which the cavities grow and coalesce. The formation of small cavities at second-phase particles (several such cavities form over the distance equal to one grain size) is common to both processes. But in cavitation failure the cavities link by deformation which is distributed rather uniformly in the entire specimen (Fig. 7*a*), whereas in TJF the displacement for

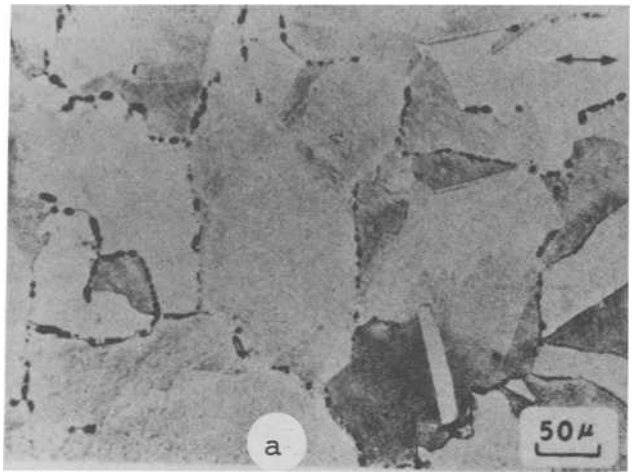

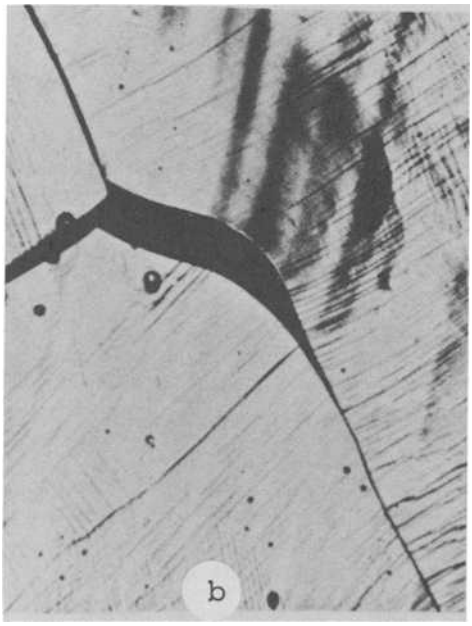

FIG. 5—(a) *Cavitation failure in copper at 673 K* [17]. (b) *Triple-junction failure in nickel* [18]. *Note the large-scale yielding associated with triple-junction fracture.*

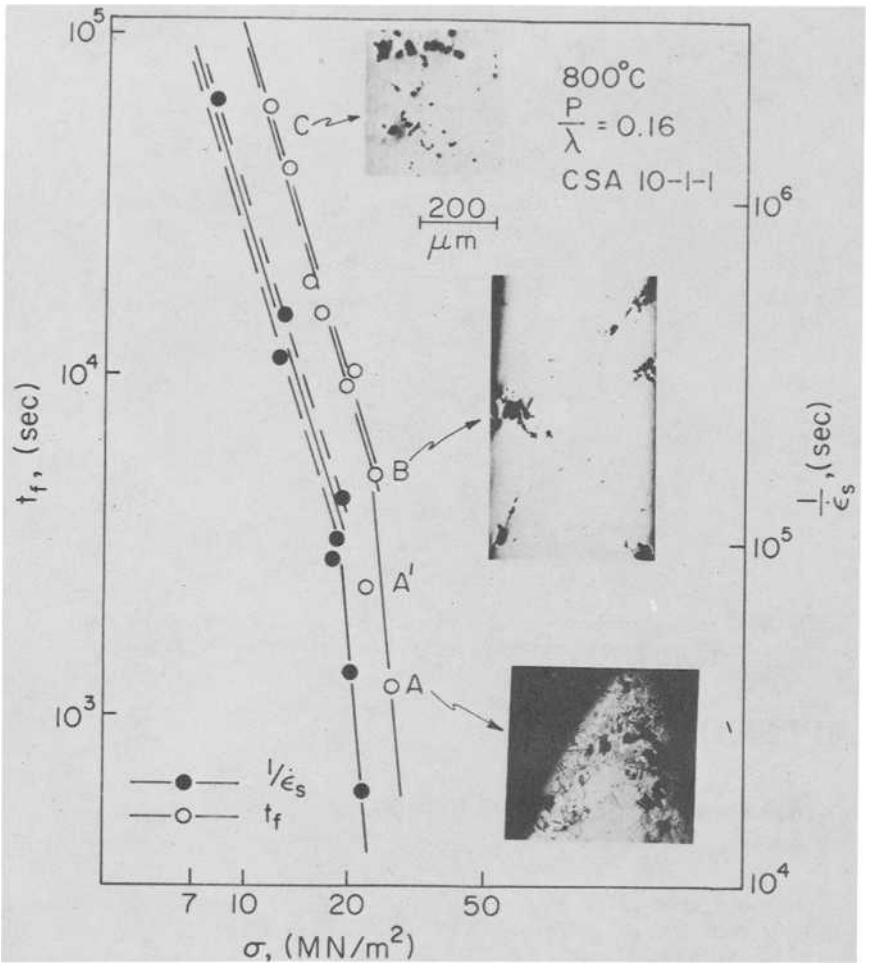

FIG. 6—*Transition from cavitation failure* (C) *to failure by initiation and propagation of a crack from the surface* (B), *to failure by necking* (A). *Triple-junction failure is believed to be important in the initiation of cracks in the crack propagation failure mode* [11].

cavity linkage is provided by the localized sliding displacement of the grain boundary (Fig. 7*b*). The latter process has three requirements. First, the large localized displacements at the grain boundary must be accommodated by yield elsewhere in the specimen (which, in practice, places the requirement that the average stresses in the region of TJF should be close to the yield stress of the material; in the case of fatigue crack propagation, this condition is nicely satisfied in the plastic zone surrounding the crack tip). Second, the TJF must be initiated so that further GBS can produce a localized displacement field in which cavities can grow. And third, the rate of strain rate in the surrounding material should be in harmony with the rate at which grain boundaries slide.

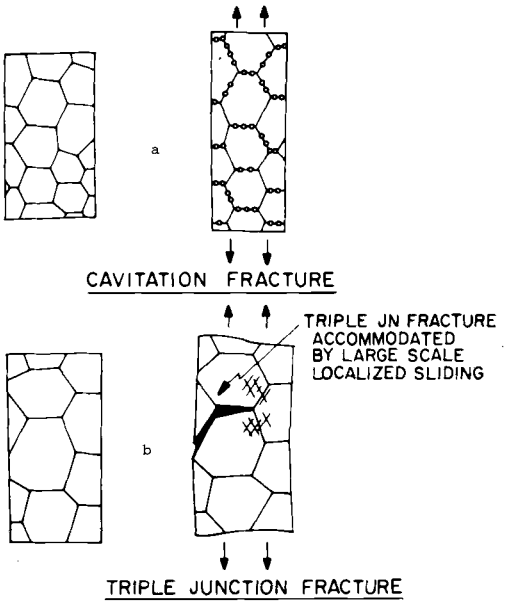

FIG. 7—*Cavitation fracture* (a) *is accompanied by macroscopically uniform strain, whereas triple-junction fracture* (b) *involves localized sliding which must be accommodated by inhomogeneous deformation* [19].

APPENDIX II

Creep and Diffusion Data for 316 Stainless Steel

Equation 2

$$A^{(15)} = 1.33 \times 10^{12}$$
$$D_V^{(16)} = 0.37 \times 10^{-4} \exp(-279.6 \text{ kJ mol}^{-1}/\text{RT}) \text{ m}^2 \text{ s}^{-1}$$
$$G = 81 \text{ GPa}$$
$$b = 0.258 \text{ nm}$$
$$n^{(15)} = 7.9.$$

Equation 4

$$\Omega = 1.21 \times 10^{-29} \text{ m}^3$$
$$\delta D_B^{(16)} = 2 \times 10^{-13} \exp(167.4 \text{ kJ mol}^{-1}/\text{RT}) \text{ m}^3 \text{ s}^{-1}$$

Yield stress data for 316 stainless steel:

Temperature (K)	σ_y (MPa)
477	179.3
700	137.9
811	126.2
923	117.2
1033	97.9

References

[1] Raj, R. and Min, B. K. *Mechanical Engineering*, Vol. 100, No. 11, 1978, p. 100; also Report #2957 issued by the Materials Science Center, Cornell University, Ithaca, N.Y.

[2] Min, B. K. and Raj, R., *Acta Metallurgica*, Vol. 26, 1978, pp. 1007-1022.

[3] Manson, S. S. "Time-Dependent Fatigue of Structural Alloys," ORNL Report 5073, Oak Ridge National Laboratory, Oak Ridge, Tenn., Jan. 1977, p. 157.

[4] Organ, F. E. and Gell, M., *Metallurgical Transactions*, A, Vol. 2A, 1971, p. 943.

[5] Harrod, D. L. and Manjoine, M. J. in *Proceedings*, Symposium on Creep Fatigue Interaction, ASME-MPC-3, American Society of Mechanical Engineers, 1976, p. 87.

[6] Coles, A., Hill, G. J., Dawson, R. A. T. and Watson, S. J. in *Proceedings*, Thermal and High Strain Fatigue Conference, Metals and Metallurgy Trust, London, U.K., 1967, p. 270.

[7] Majumdar, S. "Importance of Strain Rate in Elevated-Temperature Low Cycle Fatigue of Austenitic Stainless Steels," presented at the ASME/CSME Pressure Vessel and Piping Conference, Montreal, Que., Canada, 28-29 June 1978.

[8] Coffin, L. F., in *Proceedings*, Conference on Time-Dependent Fatigue of Structural Alloys, ORNL-Report 5073, Oak Ridge National Laboratory, Oak Ridge, Tenn., Jan. 1977, p. 128.

[9] Manson, S. S. in *Fatigue at Elevated Temperatures, ASTM STP 520*, American Society for Testing and Materials, 1973, pp. 744-782.

[10] Raj, R., *Acta Metallurgica*, Vol. 26, 1978, pp. 341-349.

[11] Pavinich, W. and Raj, R., *Metallurgical Transactions* A, Vol. 8A, 1977, pp. 1917-1933.

[12] Raj, R., *Journal of Engineering Materials and Technology*, Vol. 98, 1976, pp. 132-139.

[13] Mosher, D. R. and Raj, R., *Acta Metallurgica*, Vol. 22, 1974, p. 1469.

[14] Min, B. K. and Raj, R. *Journal of Testing and Evaluation*, American Society for Testing and Materials, Jan. 1979, pp. 24-28.

[15] Frost, H. J. and Ashby, M. F., University Engineering Department Report, Cambridge, England, July 1975.

[16] Perkins, R. A., Padgett, R. A., Jr., and Tunali, N. K., *Metallurgical Transactions*, Vol. 4A, 1974, p. 2535.

[17] Gell, M. and Leverant, G. R. in *Fatigue at Elevated Temperatures ASTM STP 520*, American Society for Testing and Materials, 1973, p. 37.

[18] Garofalo, S. in *Proceedings*, American Society for Metals Seminar, Metals Park Ohio, Oct. 1967, p. 101.

[19] Raj, R., "Mechanisms of Intergranular Fracture in High Temperature Fatigue," Materials Science Center Report 2873, Cornell University, Ithaca, N.Y., July 1977.

[20] Rice, J. R. and Johnson, M. A., *Inelastic Behavior of Solids*, M. F. Kanninen et al, Eds., McGraw-Hill, New York, 1970, p. 641.

[21] Rice, J. R. in *Fatigue Crack Propagation, ASTM STP 415*, American Society for Testing and Materials, 1967, p. 247.

DISCUSSION

J. Early[1] (*discussion*)—The phenomenological model described in this paper is a further step in the process of separating the macroscopic failure mode categories of transgranular failure and intergranular failure from the qualitative description of mechanical behavior, such as ductile failure and brittle failure. By focusing on local deformation conditions, the model extrapolates discrete microscopic behavior to average macroscopic behavior

[1] Fracture and Deformation Division, Center for Materials Science, National Bureau of Standards, Washington, D.C. 20234.

which can be tested in the laboratory. Several questions are raised, however, concerning not only the particular model proposed in this paper but also the relationship of this model to other elevated temperature fracture models.

In looking at the proposed mechanism for fatigue crack intergranular triple-junction crack (wedge crack) interaction, a question arises as to whether there is any relationship between this model and intergranular wedge cracks developed in monotonic testing. Can the condition for maximum damage, (slow-fast cycle) $\dot{\epsilon}$ (tension) $< \dot{\epsilon}_c$ but $\dot{\epsilon}$ (compression) $> \dot{\epsilon}_c$, be related to monotonic testing since the healing of damage during the backward or compression portion of the strain cycle is assumed to be zero or a minimum and thus damage occurs under a variable-tension strain rate? Further, it is indicated in the discussion of mechanisms of intergranular fracture that cavities form at second-phase particles in grain boundaries in both cavitation fracture and triple-junction fracture (wedge cracks) but the linking-up processes differ. Some recent studies of triple-junction fracture in creep-fractured specimens of iron have shown that wedge cracks formed as a result of fine cavitation. High-resolution microscopy revealed that the inner surfaces of the wedge cracks were made up of many cavities which had joined together either by coalesence or by sliding together. If triple junction cracks also develop by coalesence of cavities as well as by grain boundary sliding, would it be necessary for the model to account for this additional damage contribution, and if so, how might this be done?

In elevated-temperature situations where components could be subjected to static loading as well as cyclic loading, intergranular cracks could form independently of fatigue crack interactions. Would these independently formed cracks reduce the strong relationship of damage accumulation and local strain rate predicted by the proposed model since, in other recently reported work, increases and decreases of the fatigue crack propagation rate in 304 stainless steel due to previously introduced intergranular creep cracks at both room temperature and 371°C (700°F) are no larger than specimen-to-specimen scatter observable in fatigue studies?

Finally, there is one consideration not discussed specifically but which would be significant in applying the model in a predictive manner. This is the question as to whether the critical local strain rate, $\dot{\epsilon}_c$, possesses sufficient sensitivity to clearly delineate the two strain rate regions. The data supporting the proposed model is from one specimen per test parameter set and the effect of data scatter from multiple specimen tests should be addressed. Although the tests, carried out near the strain rate criterion boundary, appear to support the model, the large number of material and measurement variables which determine $\dot{\epsilon}_c$, such as yield strength (large variations from heat-to-heat), grain boundary diffusion coefficient (strongly affected by chemistry of the grain boundaries), and average particle size

and spacing, are really adjustable parameters and often are not known with any degree of accuracy. A limit analysis of the critical strain rate equation would be useful in determining the sensitivity required.

B. Min.—First I would like to discuss how the condition for damage accumulation can be related to the monotonic case. The strain rate conditions that we have proposed for triple-junction fracture damage are derived from the idea that grain boundaries must slide to produce stress concentration at triple junctions. Therefore the same condition for tensile-going strain rate of the cyclic loading must also be applied for the monotonic case to produce damage of the same type, namely

$$\dot{\epsilon} \text{ (tensile-going)} < \dot{\epsilon}_c$$

Of course, for the monotonic case, the condition for reverse loading strain rate [that is, $\dot{\epsilon}$ (compressive-going) $> \dot{\epsilon}_c$] is not necessary, whereas for the cyclic loading case, if this second condition is not met, damage may be healed during reverse loading.

The major difference between the two cases is the way they must meet conditions of cavity coalescence in order to separate a boundary. For the monotonic case, a larger amount of plastic strain may be necessary to produce the same degree of damge ϕ_s than for the cyclic loading case, in which it can be achieved by accumulation over a number of cycles by smaller plastic strain amplitude. Therefore, in order to meet the coalescence condition ($\phi_s \geq u_c$), the applied strain in the monotonic case must be much higher than the maximum strain of cyclic loading. This makes possible another fracture mechanism in the monotonic case. In monotonic loading, intergranular fracture is possible only if the applied strain necessary to produce the critical amount of ϕ_s is smaller than the strain necessary to produce ductile failure by shear deformation. Otherwise failure occurs by necking. Experimental observations actually show both of these fracture mechanisms under monotonic creep conditions. One such example is shown in Fig. 6 of the text.

The next question deals with the relations between cavitation damage and damage of a triple-junction fracture type. Our model implies that the latter occurs under two conditions. One is grain boundary sliding. The second condition is the presence of cavitation damage along the grain boundaries. The proposed mechanism is: In order to produce wedge cracking, grain boundary sliding must provide the displacement necessary for the cavities to grow and coalesce (by plastic deformation). The damage parameter ϕ_s is a measure of the available displacement. The cavity distribution along the grain boundaries determines the magnitude of the critical displacement (u_c) that has to be exceeded by ϕ_s, that is, the denser

the cavity distribution, the smaller the critical displacement (u_c) and vice versa. (See Eq 1 of the text.)

Our model is therefore consistent with the observation of fine cavities at the inner surfaces of wedge cracks, and accounts for the effect of their distribution.

On independently formed cracks: Independently formed intergranular cracks may have two effects on the proposed mechanism of creep-fatigue. One is to reduce the number of cycles during which damage accumulates until the critical displacement u_c is exceeded by the sliding offset ϕ_s. The other is to enhance the crack growth rate by direct interaction with the main crack. The 304 stainless steel results may indicate that the second effect is not important under the given conditions. The critical strain rate predicted by the present model is not expected to vary significantly with the introduction of independently formed intergranular cracks.

On the sensitivity of critical strain rate to control parameters: The scatter in the experimental values of crack growth rate in our multiple-specimen measurements comes from the variation of control parameters such as plastic strain range and temperature, and of the material parameters such as yield strength, grain boundary diffusion coefficient, and particle size and spacings along the grain boundaries. Our measurements clearly demonstrate that when specimens are carefully prepared—for example, all the specimens tested are from the same batch, from the same manufacturer, and heat treated in the same way—sufficient variation in the crack growth rate can be observed with temperature variations when other control parameters are kept constant, yielding valid experimental results. We believe that temperature is the parameter on which crack growth behavior is most sensitively dependent and experimentally well defined. However, we agree with Dr. Early that establishing limit values of critical strain rate will be useful to take into account the uncertainty of other parameters.

D. Michel[2] (*discussion*)—The authors have attempted to provide additional knowledge concerning the relationship between macroscopic failure and microscopic mechanisms during fatigue crack propagation. Their key point is the strain rate sensitivity of the grain boundary sliding process which they attempt to develop both theoretically and experimentally.

In their theoretical model, the authors make a distinction between cavity formation and growth resulting from "uniform" specimen deformation and that due to cavity linkage by grain boundary sliding. It is certainly conceivable, and monotonic experimental studies seem to show, that wedge crack development is directly related to cavity formation and linkage

[2] Thermophysical Materials Branch, Naval Research Laboratory, Code 6396, Washington, D.C. 20375.

during slow strain rate testing where "uniform" deformation and grain boundary sliding both occur. It is, therefore, questionable whether the "uniform" deformation approach to crack propagation and the triple-junction fracture due to grain boundary sliding approach are actually distinct mechanisms or whether they are really component parts of the same overall mechanism.

Experimentally, the authors have conducted crack propagation tests using various strain rates during the tension and compression portions of the fatigue cycle in an attempt to support the theoretical predictions. Their results seem to show that a slow-fast cycle produced a larger value of the crack growth constant, B, than a fast-slow cycle. This result, however, should not be considered as unambiguous proof that triple-junction fracture produced by grain boundary sliding rather than "uniform" cavity coalescence was responsible for the test results in the absence of definite microstructural evidence which would corroborate their findings. In fact, microstructural studies by this discusser on 316 stainless steel tested at 593°C suggest that cavity formation occurs rather uniformly at the grain boundary carbide particles and that the critical step may be the linkage of these cavities by both cavity growth and grain boundary sliding. Furthermore, the large variability in the material parameters for 316 stainless steel makes it questionable whether a clear distinction can be drawn between the two strain rate regions. It is therefore suggested that a broad-band region rather than a clear distinction should exist for 316 stainless steel wherein both types of cavity linkage process, if they are distinct, will operate.

B. K. Min and R. Raj (author's closure)—The authors deeply appreciate the comments and questions on their work by Drs. Early and Michel. Although one of the authors has replied separately to Dr. Early's comments, we would like to further emphasize the following points before we set out to answer the questions raised by both discussers.

The main proposal of the present model is that under conditions of fatigue during creep, crack growth rate may increase due to wedge cracking in the vicinity of the crack tip. The mechanism of wedge cracking itself, is suggested to be the linkage of cavities (which form at particles) by grain boundary sliding. Since sliding is strain rate sensitive, so is wedge cracking. These ideas have been cast into quantitative analysis to explain the strain rate effects in high-temperature fatigue crack propagation. Although measurements of the microstructural parameters which appear in these equations are usually not reported along with the fatigue data, our hope is that we have at least identified the correct parameters and that future studies will give attention to these parameters.

There are two requirements for the mechanism we have proposed. First is that to have triple-junction cracking, grain boundaries must slide and

produce high stress concentration at triple points. The second condition is that sliding should produce a large enough displacement so that the cavities just ahead of the triple junction coalesce and open up a wedge-shaped crack. The sliding displacement condition for cavity coalescence has been set from earlier work.[3] If the cavities are separated by average distance λ, and if they grow by power-law creep with stress exponent n, then

$$U_c = 0.23\,\lambda \exp\left(\frac{4}{n-1}\right)$$

If there are no cavities along the grain boundaries, $\lambda \sim d$ (d is the grain size) and $U_c \sim d$; that is, the grain boundary sliding offset must be of the order of grain size, which may be very difficult to achieve. On the other hand, if cavities are very densely distributed and if $\lambda \sim 0$, then $U_c \sim 0$, that is, a small amount of grain boundary sliding offset, may be sufficient to cause full separation of grain boundaries.

We are now ready to answer Dr. Michel's comment, "Monotonic experimental studies seem to show that wedge crack development is directly related to cavity formation and linkage ... " and Dr. Early's, "High resolution microscopy revealed that the inner surfaces of wedge cracks were made up of many cavities which had joined together ... ".

Our model totally agrees with these observations. Grain boundary sliding provides stress concentration at a triple point and initiates a triple-junction crack. Grain boundary sliding also provides necessary displacement for the cavities to grow and to coalesce with a triple-junction crack, yielding a large (or observable) wedge crack.

Responding to Dr. Michel's comment, "This result ... should not be considered unambiguous proof that triple-junction fracture rather than uniform cavity coalescence was responsible for the test results. ... ," let us ask this question. If our results were due to uniform cavity coalescence, how can the crack growth rate decrease at higher temperature (625°C) than at intermediate temperature (538°C)? Remember that the uniform cavity coalescence depends on matrix flow which occurs more readily at higher temperatures, and therefore cannot explain our experimental results.

In reply to another comment by Dr. Michel, "Microstructural studies by this discusser on SS 316 ... cavity formation occurs rather uniformly at the grain boundary carbide particles and the critical step may be the linkage of these cavities by both cavity growth and grain boundary sliding," we do not imply in our model that uniform cavity growth does not occur along the grain boundaries. Uniform cavity growth may occur during

[3] Pavinich, W. and Raj, R., *Metallurgical Transactions* A, Vol. 8A, 1977, pp. 1917-1933.

plastic deformation. Our model implies only that when grain boundary sliding occurs, the sliding offset locally provides the necessary displacement for these cavities to coalesce. When the applied strain rate is such that grain boundary sliding cannot occur, the only way of achieving cavity coalescence may be by large uniform plastic deformation, in which case failure may occur by uniform coalescence of cavities along the grain boundaries. This mechanism of intergranular failure was dealt with in an earlier paper.[4]

Therefore our model agrees well with Dr. Michel's suggestion except for our prediction that uniform cavity coalescence will occur without grain boundary sliding.

Finally, we would like to thank the discussers for their very stimulating comments on this work.

[4] Min, B. K. and Raj, R., *Acta Metallurgica,* Vol. 26, 1978, pp. 1007-1022.

S. P. Bhat[1] *and C. Laird*[1]

Cyclic Stress-Strain Response and Damage Mechanisms at High Temperature

REFERENCE: Bhat, S. P. and Laird, C., **"Cyclic Stress-Strain Response and Damage Mechanisms at High Temperature,"** *Fatigue Mechanisms,* Proceedings of an ASTM-NBS-NSF symposium, Kansas City, Mo., May 1978, J. T. Fong, Ed., *ASTM STP 675,* American Society for Testing and Materials, 1979, pp. 592-623.

ABSTRACT: The cyclic stress-strain response and damage of commercially pure nickel, thoria dispersed (TD) nickel, and Al-4Cu alloy aged to contain θ' and θ'' are investigated as a function of test temperature. Up to ⅔ melting point, the slipband morphology, and hence the crack nucleation mechanism, does not change in nickel and TD-nickel when tested under vacuum using a symmetrical sawtooth waveform. The microstructure containing θ', however, exhibits an increased tendency toward transgranular slip with increase in temperature. This is quite contrary to our intuition and is shown to be due to the plastic deformation of the θ' precipitate and subsequent dissolution at high temperatures. The θ'' microstructure exhibits intense slipband deformation and cracking at all tested temperatures; this is surprising in view of the metastability of the microstructure and the fact that cyclic disordering of the crystal structure could be reordered at high temperatures. Both of these factors would be expected to homogenize the slip, but this was not observed.

KEY WORDS: crack nucleation, cyclic stress-strain behavior, damage, dispersion hardening, hardening, intergranular, misorientation, planar slip, saturation, slip markings, softening, transgranular, wavy slip

The cyclic stress-strain behavior of commercial high-temperature materials is complex. For example, Inconel 718 work-hardens to a peak stress and then softens continuously at room temperature, but at temperatures above 723 K it softens from the first cycle [*1*].[2] Such softening behavior at high temperatures is by no means general; 2¼Cr-1Mo steel cyclically hardens to saturation even at 866 K [*2*]; AISI 304 and 316 steels show cyclic hardening followed by softening at 703 K but eventually reach a

[1] Post-doctoral fellow and professor and chairman, respectively, Department of Metallurgy and Materials Science, University of Pennsylvania, Philadelphia, Pa. 19104.

[2] The italic numbers in brackets refer to the list of references appended to this paper.

saturation value [3]. To understand such results, structural studies at high temperatures are required, but in the low-cycle fatigue region they are rare. Nahm et al [4] found that 304 steel produces band-like or planar dislocation arrangements at room temperature, but at 822 K they observed cell structures as in wavy slip materials. Fournier and Pineau [1] report that, in Inconel 718 at high temperatures, the deformation is carried almost exclusively by the propagation of twins. These and other microstructural complexities make the commercial high-temperature alloys difficult for detailed mechanistic studies of high-temperature cyclic stress-strain behavior. Abdel-Raouf et al [5] have investigated the high-temperature fatigue behavior of pure copper in the temperature range 202 to 923 K. The primary emphasis in their work was on elucidating the effects of temperature and strain rate on high-temperature cyclic deformation. We have undertaken a broader program in our laboratory, with the aim of elucidating the fundamental microstructural aspects of cyclic deformation at high temperatures [6]. The primary emphasis was placed on the role played by varying the microstructures at a chosen set of external test variables. Four model materials—commercial nickel, thoria dispersed (TD) nickel, and Al-4Cu alloy aged to contain θ' and θ''—were chosen for detailed investigation. Although these materials are relatively simple, much of the understanding obtained with them can be carried over to commercial materials, provided caution is used in assessing the differences in microstructure and the differences in external variables. The major emphasis in this work was on bulk cyclic deformation mechanisms inappropriate to the present symposium; the details will be published elsewhere. At low temperature it is well established that there is a close connection between cyclic deformation and damage mechanisms (see, for example, Refs 7 and 8). This has not been demonstrated explicitly for high temperatures and, in the following, some salient deformation observations and how they can give rise to different damage mechanisms at high temperatures are reported.

Experimental Details

For high-temperature testing, we employed a standard, tension-compression fatigue unit using Woods metal grips [6]. The specimen was enclosed in a glass chamber with provisions for measuring (1) the strain via a diametral strain gage, (2) the vacuum, and (3) the temperature. High temperatures were generated by direct induction heating. The specimens were machined in the form of an hourglass shape to avoid buckling problems and to simplify heating. Fully reversed, plastic strain controlled fatigue experiments were carried out using servohydraulic equipment combined with an analog computer (TR-20).

The temperature range investigated was from ambient up to a maximum of 1123 K (850°C). For nickel and TD-nickel, the temperatures chosen

were room temperature, 574 K (301°C), 862 K (589°C), and 1123 K (850°C). These temperatures correspond to ambient, $\frac{1}{3}T_M$, $\frac{1}{2}T_M$, and $\frac{2}{3}T_M$ where T_M is the homologous melting temperature. For a face-centered cubic (fcc) metal these temperatures are known to cover a range of recovery and recrystallization behavior in response to monotonic deformation [*9,10*] and, therefore, comparison with cyclic deformation could be made [*11,12*]. For the precipitation-hardened alloys the maximum test temperatures were limited to their respective aging temperatures. For the θ' microstructure the temperatures selected were room, 423 K (150°C), 473 K (200°C), and 523 K (250°C); the three temperatures selected for the microstructure containing θ'' were room, 373 K (100°C), and 433 K (160°C). The elevated-temperature fatigue tests were carried out in a vacuum of $\sim 10^{-5}$ mm Hg. All the tests were carried out at a constant strain rate ($\sim 6 \times 10^{-4}$), using a symmetrical sawtooth waveform, and for a range of plastic strain amplitudes from 0.001 to 0.01, although results only for 0.01 plastic strain amplitude are reported here.

Nickel-200 (supplied by Huntington Alloys Div.) and TD-nickel (supplied by Sherritt-Gordon Mines Ltd.) were cold swaged at room temperature, machined into fatigue specimens, and then annealed at ~1073 K for ~30 min under a vacuum of better than 10^{-5} mm Hg. The aluminum-copper alloy was vacuum melted and vacuum cast into ingots. These were then subjected to a series of cold-swaging and annealing treatments and then machined into fatigue specimens. They were then solutionized at 828 ± 1 K and immediately quenched into an ice-water bath. The θ' microstructure was obtained by aging at 523 K for 5 h and the θ'' precipitates were obtained by aging at 433 K for 5 h.

The TD-nickel used in this investigation contains a dispersion of about 2 percent (by volume) thoria distributed fairly uniformly within the grains. The details of the precipitation sequence in aluminum-copper alloys, the morphology of the precipitates, and other structural details are standard for the aging conditions used. It suffices to say here that, both θ' and θ'' are plate-like in shape and of diameters about 0.5 μm and 300 Å, respectively. θ' is coherent to the matrix for the aging time used but is rapidly rendered semicoherent by cyclic straining, whereas θ'' is fully coherent with the matrix.

Results and Discussion

The cyclic stress-strain (CSS) behavior and damage observed for the different microstructures are described in the following.

Nickel

At room temperature, a well-annealed fcc metal such as nickel exhibits a rapid hardening stage followed by a well-defined saturation [*13-15*]. The

same behavior was found to be true at elevated temperatures. This is shown for one strain amplitude in Fig. 1. The effects of increasing the test temperature are to decrease the rapid hardening period, decrease the hardening rate, and decrease the saturation stress. Detailed microscopic observations as a function of temperature and the relationship between the cyclic flow stress and temperature have also been carried out [*6*]. These are reported elsewhere [*11*]. It suffices to say here that, as might be predicted from previous room temperature works [*13-17*], and from the high-temperature work of Abdel-Raouf et al [*5*] on copper, the predominant dislocation structure observed at all temperatures under cyclic straining conditions is one of cells. Although the cell size increases at first gradually, it rises rather rapidly above 0.5 of the melting point. This upturn in cell size coincides with the precipitous drop in saturation flow stress (for details, see Ref *11*). With the aims of correlating the CSS behavior and the crack nucleation and growth mechanisms at play, the surfaces of specimens tested at various temperatures were observed by scanning electron microscopy (SEM). At the high strain amplitudes used in this investigation, grain boundary cracking confined to the surface was predominant at all temperatures; an example is presented in Fig. 2*a* corresponding to a test temperature of 862 K [½ melting point (mp)]. Fine slip markings within the grain and a good one-to-one correspondence of the slip lines across the twin may be seen in Fig. 2*b* and *c*. These slip-line observations are similar to those reported by Kim [*18*] for copper at room temperature. At 1123 K, surface rumpling was found to be coarse and often grain boundary cavities were seen (Fig. 2*d*), but these are confined to the near-surface region, and thus are considerably different morphologically from those generally observed in creep-fatigue experiments.

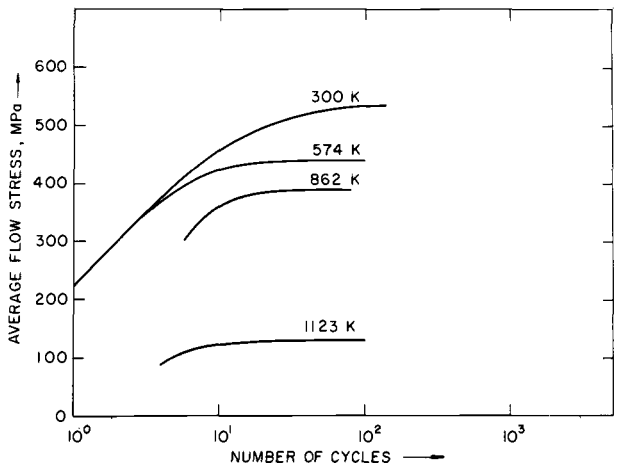

FIG. 1—*Effect of increasing the test temperature on cyclic hardening curves of nickel-200*

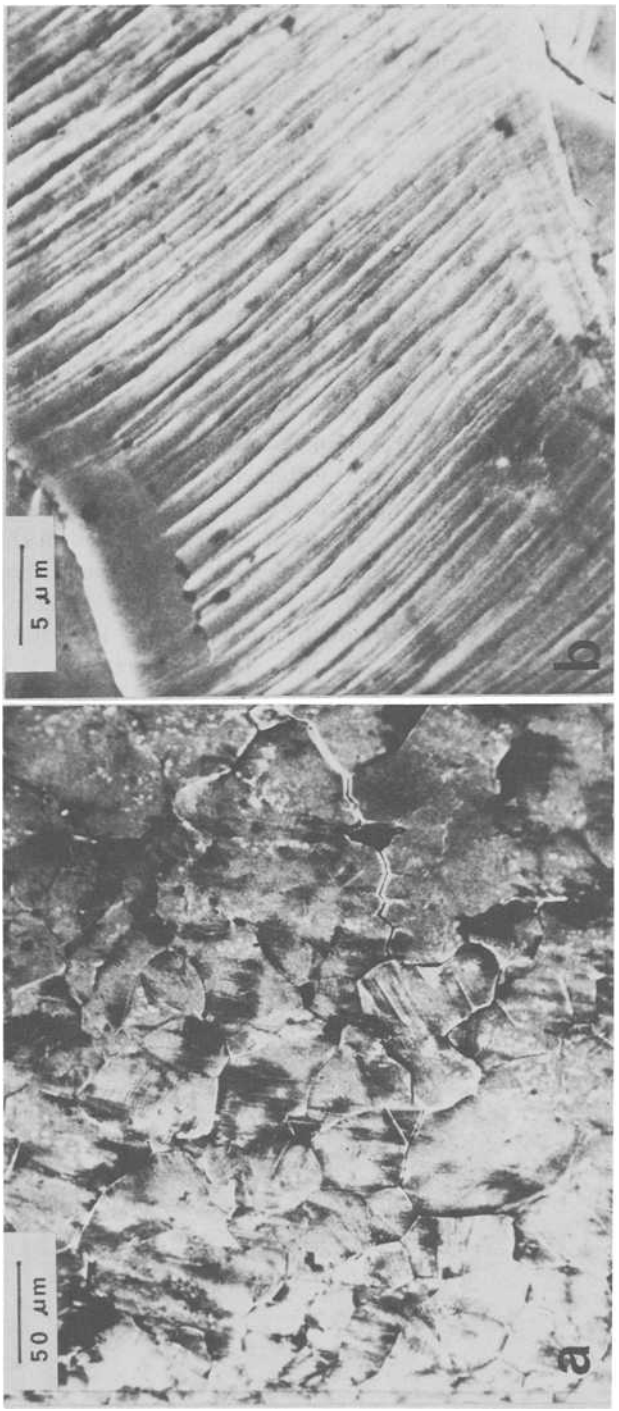
50 μm
a
5 μm
b

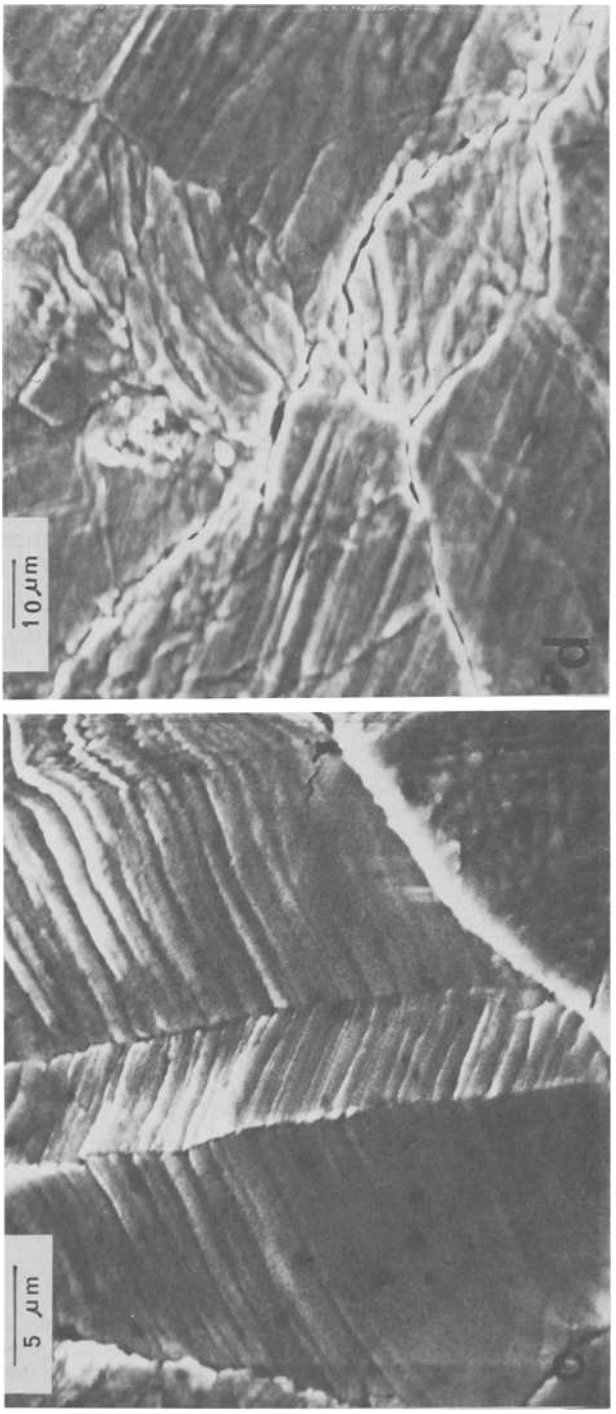

FIG. 2—(a) *Surface of nickel after fatigue at 862 K, intergranular cracks are seen.* (b) *and* (c) *Fine slip markings within the grain and across the twin may be noted.* (d) *Surface rumpling, grain boundary folding, and grain boundary cavities formed in a specimen fatigued at 1123 K. All specimens were strain cycled at an amplitude of 0.01.*

Numerous studies (for a review, see Laird and Duquette [*19*]) have shown that at high strain amplitudes, and room temperature, cracks nucleate primarily along the grain boundaries and they are accompanied by surface rumpling and grain boundary folding. From detailed microscopic observations of surfaces of copper specimens cycled at room temperature to different stages in life, Kim and Laird [*20,21*] have recently concluded that the primary requirements for crack nucleation in high-strain fatigue are rather geometric in nature. Specifically, two criteria must be satisfied: (1) the boundary has a high degree of misorientation, and (2) the active slip motions in the adjoining grains are directed at the intersection of the boundary with the specimen surface.

In the present investigation, it is shown that the general nature of the CSS behavior of nickel, to a first approximation, remains the same at elevated temperatures as at room temperature although the saturation stress is a strong function of temperature. Combined with this result, our surface observations suggest that the crack nucleation mechanism does not change either. Thus in wavy slip fcc metals, even at high temperatures, crack nucleation appears to be essentially a process of forming a small step with a sharp root radius as envisaged by Kim and Laird [*21*] and shown in Fig. 3. As may be appreciated from Fig. 2*d*, however, crack nucleation is aided by voids formed along the grain boundaries at very high temperatures. It is possible therefore, that as the test temperature is in-

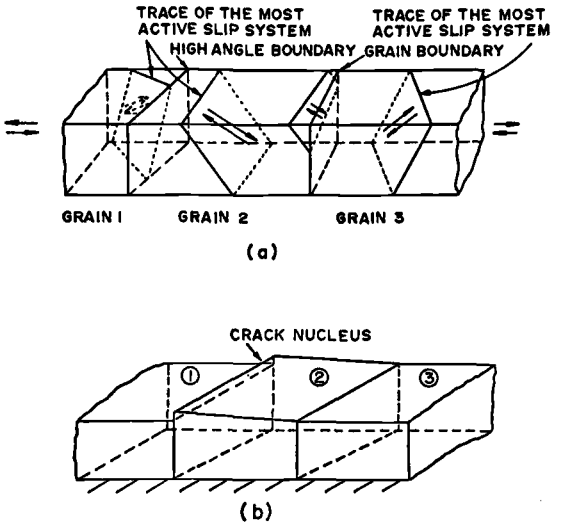

FIG. 3—*Schematic representation of the crack nucleation process in high-strain fatigue.* (a) *Active slip systems in either one of Grains 1 and 2 or in both of them are directed at the boundary between Grains 1 and 2 which is vulnerable to surface step formation and subsequent cracking while that between Grains 2 and 3 is not. After cycling,* (b) *a step is formed at the boundary of Grain 1/Grain 2.*

creased to $\frac{1}{2}T_M$ and higher, the minimum misorientation for grain boundary crack nucleation claimed by Kim and Laird [*21*] is reduced. Thus the grains with lesser degrees of misorientation might well become crack nucleation sites. It is worth noting that Laird and Feltner [*22*] observed grain boundary crack nucleation phenomena in copper even at 78 K, similar to that observed by Kim and Laird [*20,21*] at room temperature and that observed in this investigation. Thus is appears that in wavy slip fcc metals, the crack nucleation mechanism at short lives is essentially independent of temperature. It should be kept in mind, however, that all these observations were made for fully reversed, zero-mean-strain conditions and at one strain rate. Particularly at high temperatures the nucleation phenomena may well be varied considerably by the details of the testing method. For example, other effects due to grain boundary sliding might come into play, but such were not investigated here. Again, in the present investigation all the tests were carried out in a nominal vacuum of 10^{-5} mm Hg. An aggressive environment might be expected to modify the crack nucleation phenomena observed here in many details [*19*].

TD-Nickel

Since TD-nickel derives some of its strength from a dislocation substructure introduced during its complex thermomechanical processing, one might expect it to be susceptible to fatigue softening. However, in previous investigations, Leverant [*23*] and Leverant and Sullivan [*24*] showed that stress-relieved TD-nickel cyclically hardens to a constant saturation stress at room temperature just as pure nickel. From surface observations, they also showed that the presence of thoria particles in the nickel matrix helps to disperse the slip. At room temperature and high strains, cracks were usually formed at the grain boundaries, although occasionally the large stringers of particles were found as the crack nucleation sites. Interestingly, Leverant and Sullivan [*24*] found that in the low-cycle fatigue regime, nickel and TD-nickel showed virtually identical cyclic stress-strain response, although the dislocation cell sizes were observed to be different for the two materials after cycling at identical strain amplitudes. It was suggested that the distribution of the thoria particles in the TD-nickel effectively controlled the cell size and, therefore, unlike the fcc nickel, the cell size was independent of strain amplitude. Because thoria particles are known not to coarsen significantly even up to 1100°C [*25*], an interesting question is raised as to the effects of high temperatures on the CSS behavior, the dislocation structure of the TD-nickel, and consequently on its damage mechanisms. Leverant and Sullivan [*26*] also studied the low-cycle fatigue behavior of TD-nickel at 1255 K and found that the TD-nickel exhibits cyclic softening from the first cycle but the softening could be completely accounted for by the drop in load in the tension part of the cycle. As indicated, this

study was limited to just one temperature and we have extended the study to include four temperatures, and typical hardening curves obtained at one strain amplitude (± 0.01) are shown as a function of temperature in Fig. 4. It is seen that at all temperatures, TD-nickel exhibits a rapid hardening stage and then a well-defined saturation. Compared with nickel-200, the rapid hardening stage is very short and consequently the cyclic hardening achieved is rather small. However, it is significant to note that even at the highest temperature (1123 K) there is no cyclic softening; the form of the CSS curve is essentially the same as at room temperature. Typical electron micrographs of the cycled TD-nickel, shown in Fig. 5 for different temperatures, indicate that the dislocation structures do not significantly change with the test temperature. Therefore, the slip morphology is not expected to change either with temperature. In conjunction with the results on nickel just described, and Leverant and Sullivan's work at room temperature [*23*], we conclude that the dispersion of stable oxide particles does not alter the crack nucleation mechanism at high strains and high temperatures.

Al-4Cu Alloy Aged to Contain θ′ and θ″

Calabrese and Laird have reported the CSS response [*27,28*] and damage mechanisms [*8*] at room temperature in microstructures containing θ' and θ''. According to them, the microstructure containing θ' hardens in a few cycles to saturation. Failure occurs by intergranular cracking with no

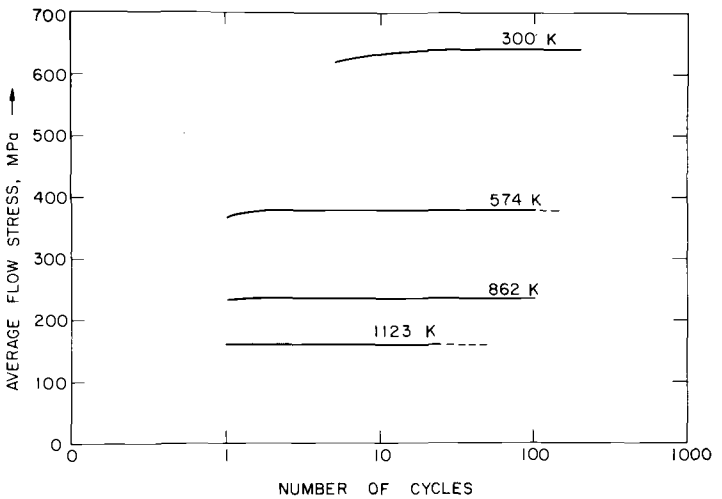

FIG. 4—*Effect of increasing the test temperature on cyclic hardening curves of TD-nickel at a plastic strain amplitude of 0.01.*

observable transgranular slip markings. On the other hand, the microstructure containing θ'' initially work-hardens to a peak stress and then continually softens until failure. The failure occurs in the intragranular surface slipbands.

Because θ' and θ'' are metastable phases, increasing the temperature during cycling certainly provides a driving force for transformation to more stabler phases. It was therefore considered that it would be interesting to investigate the CSS behavior and its effect on damage at higher temperatures than hitherto explored.

The CSS curves for the microstructure containing θ' at 300, 423, 473, and 523 K are shown in Fig. 6. While a pronounced saturation stage is evident at room temperature, it will be noted that, at high temperatures, gradual structural softening takes place. Detailed microscopic observations have revealed that under cyclic straining conditions, plate-like θ' particles become plastically deformed and, because of the surrounding matrix constraints, they exhibit bending and twisting to various degrees [*6*]. An example is shown in Fig. 7. The plastic deformation of θ' has important consequences both in its bulk and surface deformation behaviors. At elevated temperatures, it is found that the dissolution of θ' occurs along the twist axis as shown in Fig. 8 and schematically in Fig. 9. At still higher temperature (523 K) θ' transforms to θ. The details of the bulk microstructural changes are dealt with in a separate publication [*29*] and only their effects on the damage mechanisms are described herein.

Although θ' is effective in dispersing the slip at room temperature, at higher temperatures some tendency towards transgranular slip is observed. The surface observations of fatigued specimens are shown in Fig. 10. Although the primary cracking mode is still intergranular, evidence of slip passing through θ' is very clear in Fig. 10*b*. Such evidence of transgranular slip markings in this alloy at high temperatures is considered very significant and surprising because, intuitively, one would expect that increase in test temperature should aid dispersal of slip, thus enhancing grain boundary crack nucleation. The present observations are contrary to this expectation. As noted earlier, the θ' particles are plastically deformed under cyclic straining conditions, and then undergo partial dissolution. Thus with increase in temperature, glide dislocations pass through and between them rather easily and give rise to the observed transgranular slip. It is apparent that the gross plastic deformation in the grains controls the crack nucleation process as envisaged by Kim and Laird [*20,21*]. In long life fatigue, however, transgranular strain localization due to θ' twisting and dissolution may well dominate the cyclic deformation and can be expected to cause transgranular crack nucleation.

In microstructure containing θ'', the CSS curves, at all temperatures tested, exhibited peaks as shown in Fig. 11. θ'' is ordered and sufficiently small in size to be cut by dislocations. Therefore, they are easily scrambled

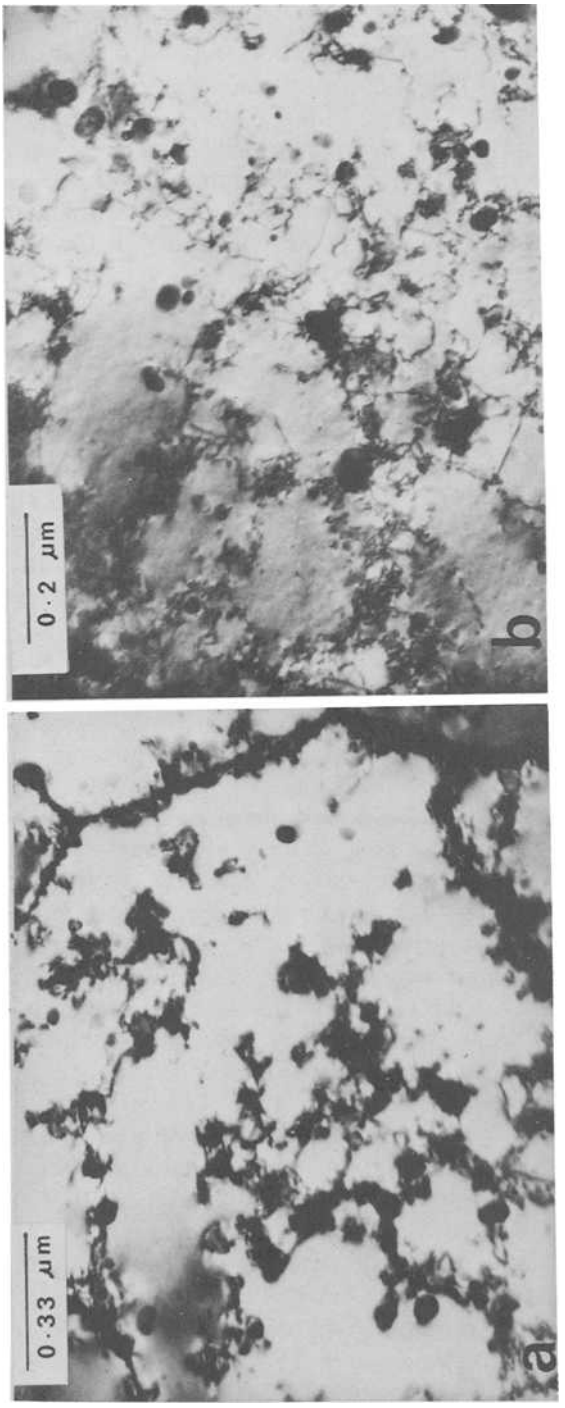
0·33 μm
a
0·2 μm
b

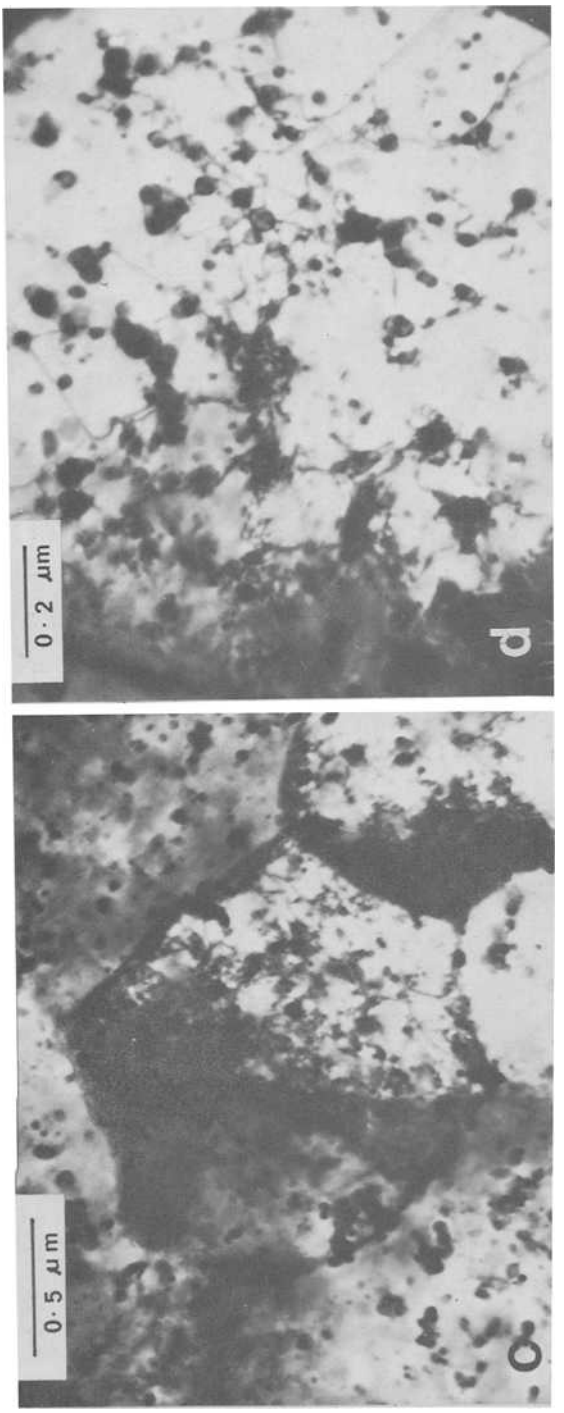

FIG. 5—*Microstructural changes in TD-nickel as a result of cycling at* (a) *300 K*, (b) *574 K*, (c) *862 K*, *and* (d) *1123 K*. *The plastic strain amplitude was 0.005*.

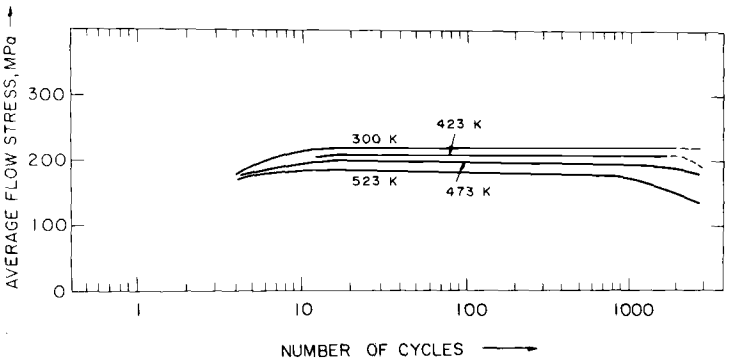

FIG. 6—*Effect of increasing the test temperature on the cyclic hardening curves of Al-4Cu alloy aged to contain θ'. The plastic strain amplitude was 0.01.*

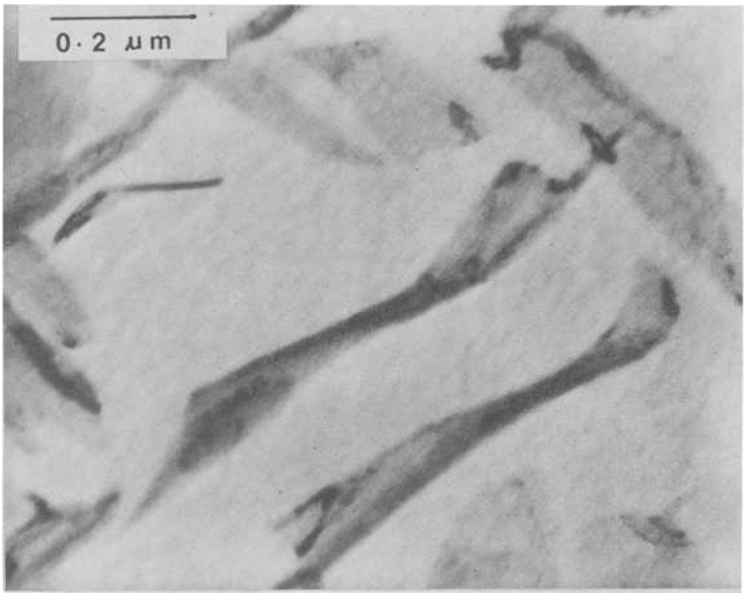

FIG. 7—*Cyclic deformation of the bulk alloy containing θ' leads to twisting of θ'*

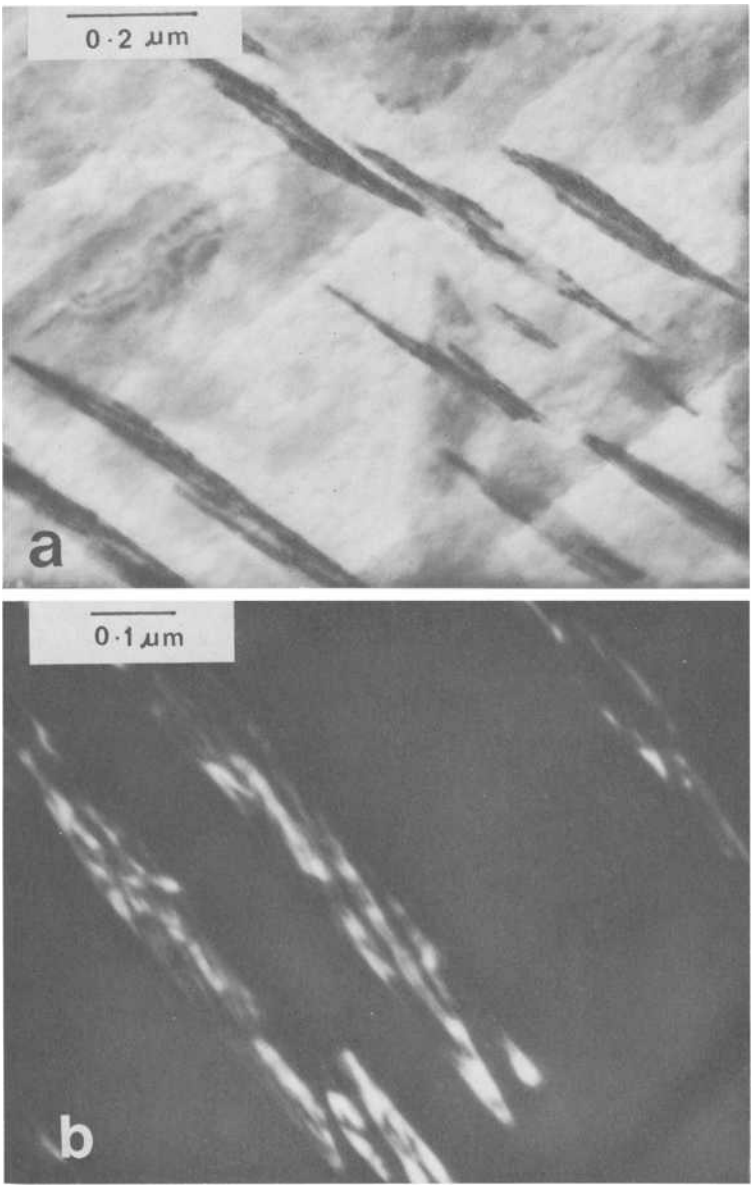

FIG. 8—*High-temperature cycling of the θ' microstructure leads to plate twisting and subsequent dissolution along the twist axis:* (a) *is a bright field picture and* (b) *dark field.*

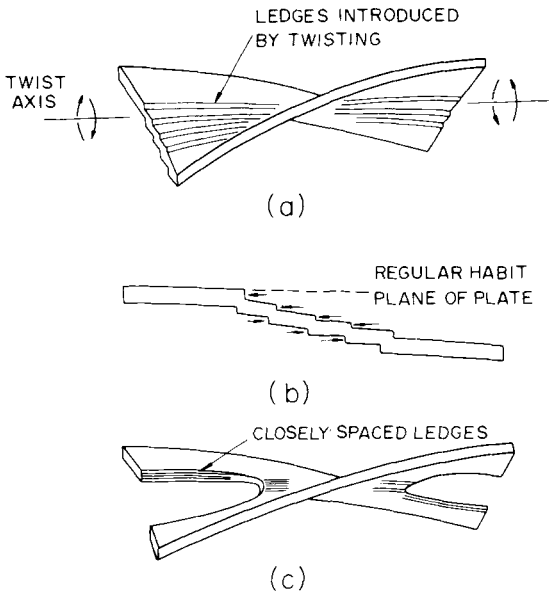

FIG. 9—(a) *Schematic representation of the distortion of θ' plates under reversed straining conditions and the ledges introduced due to twisting;* (b) *end view of a twisted plate showing, by arrows, the directions of ledge motion on the top and bottom surfaces of the plate. These opposite motions lead to ledge annihilation and precipitate dissolution of the kind shown in* (c).

by glide dislocations and this is considered to destroy their order [*28*]. With the loss of the ordering contribution to hardening, the plastic strain is localized into intense dislocation bands. An example is shown in Fig. 12. These bands are misoriented to the matrix, usually by about a degree. The observation that softening occurs at high temperatures just as at room temperature is surprising because Calabrese and Laird [*28*] and Abel and Ham [*30*] showed previously that the strength lost by softening at room temperature due to cycling can be regained by short periods of aging at high temperatures. One would then expect that simultaneous cycling and heating could maintain the ordered component of hardening. However, as shown, this expectation is not borne out.

As at room temperature, crack nucleation in this microstructure at elevated temperatures is found to occur in the transgranular surface slipbands. Figure 13*a* is an instructive example of this. Most grains are extensively marked with deep slipbands and the slip accommodation between grains occurs as shallow depressions at the boundaries (Fig. 13*b*). At a higher magnification these intense bands are seen to be the sites for extrusion-intrusion pairs. It appears that cracks nucleate in the most intense bands. At lower strain amplitudes (for example, 0.001) fewer slipbands are seen

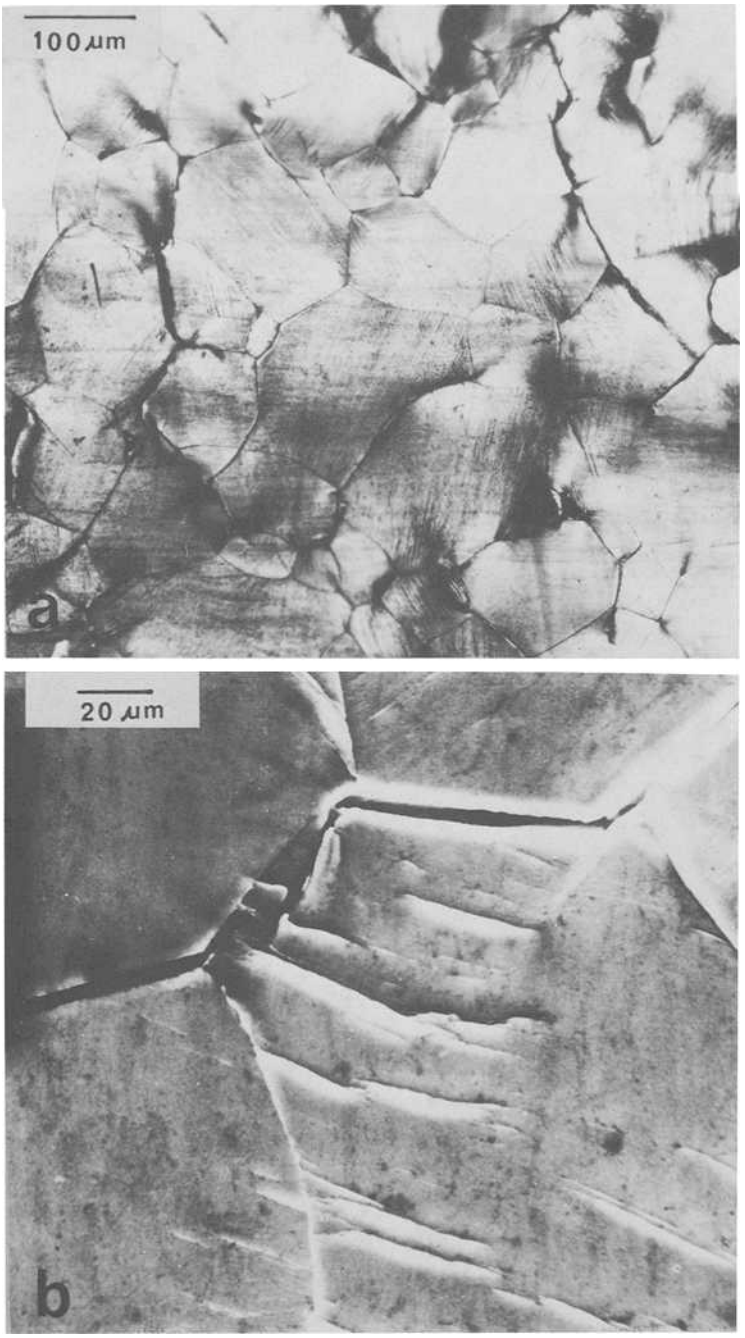

FIG. 10—*Surface observations of a specimen containing θ' and fatigued at 523 K and 0.01 plastic strain amplitude. The primary crack mode is intergranular. Evidence of transgranular slip is shown in* (b).

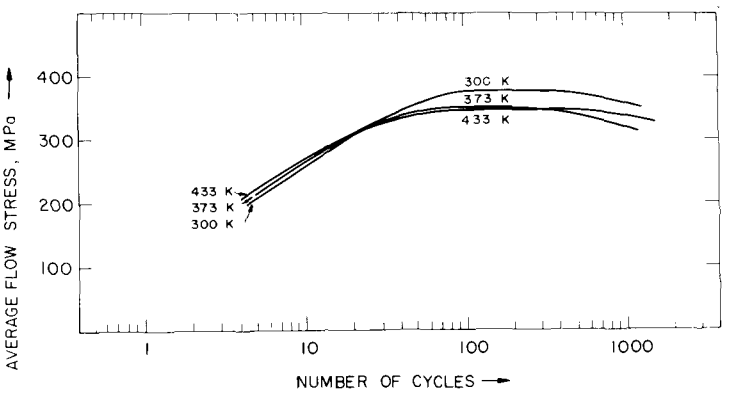

FIG. 11—*Effect of increasing the test temperature on the cyclic hardening curves of aluminum-copper alloy aged to contain θ". The plastic strain amplitude was 0.01.*

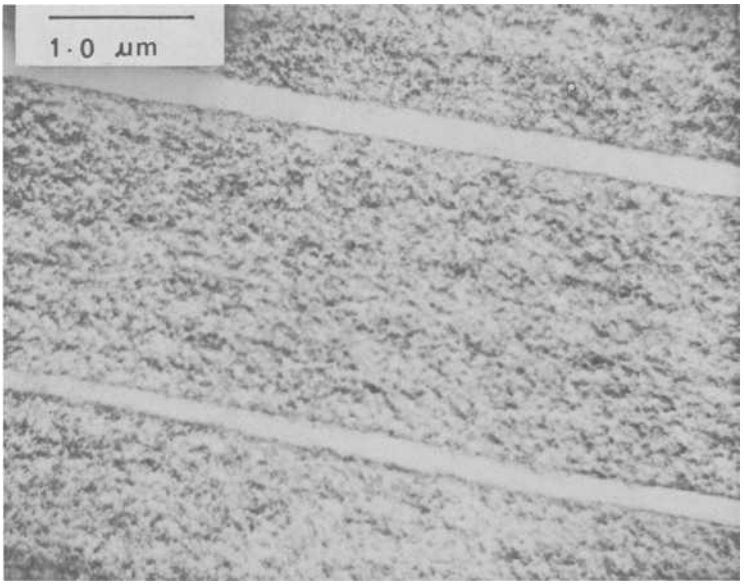

FIG. 12—*Deformation bands and the dense dislocation debris formed as a result of cycling θ" microstructure at room temperature.*

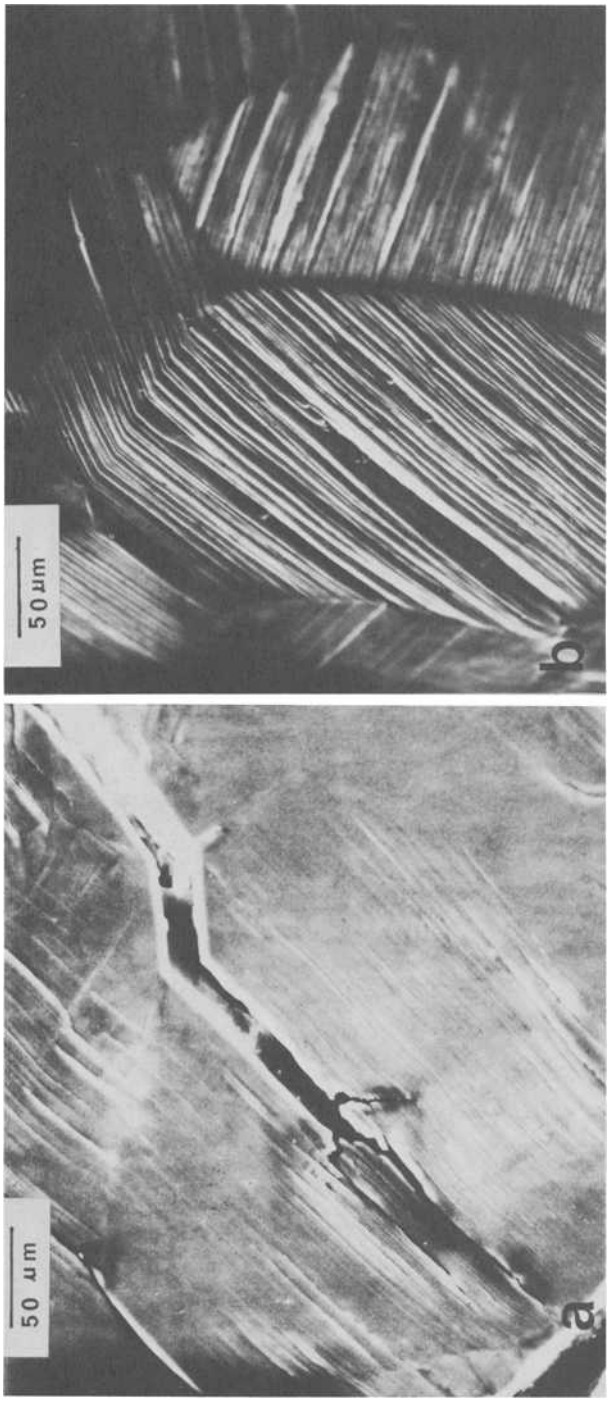

FIG. 13—(a)-(d) *Surface observations of specimen containing θ'' and fatigued at 373 K and 1 percent plastic strain amplitude. Slipband cracking, fine slip, and extrusion-intrusion pairs are seen.* (c) *and* (d) *are a stereo pair;* (e) *at lower strain amplitude (0.1 percent), the slipbands are fewer but more distinct.*

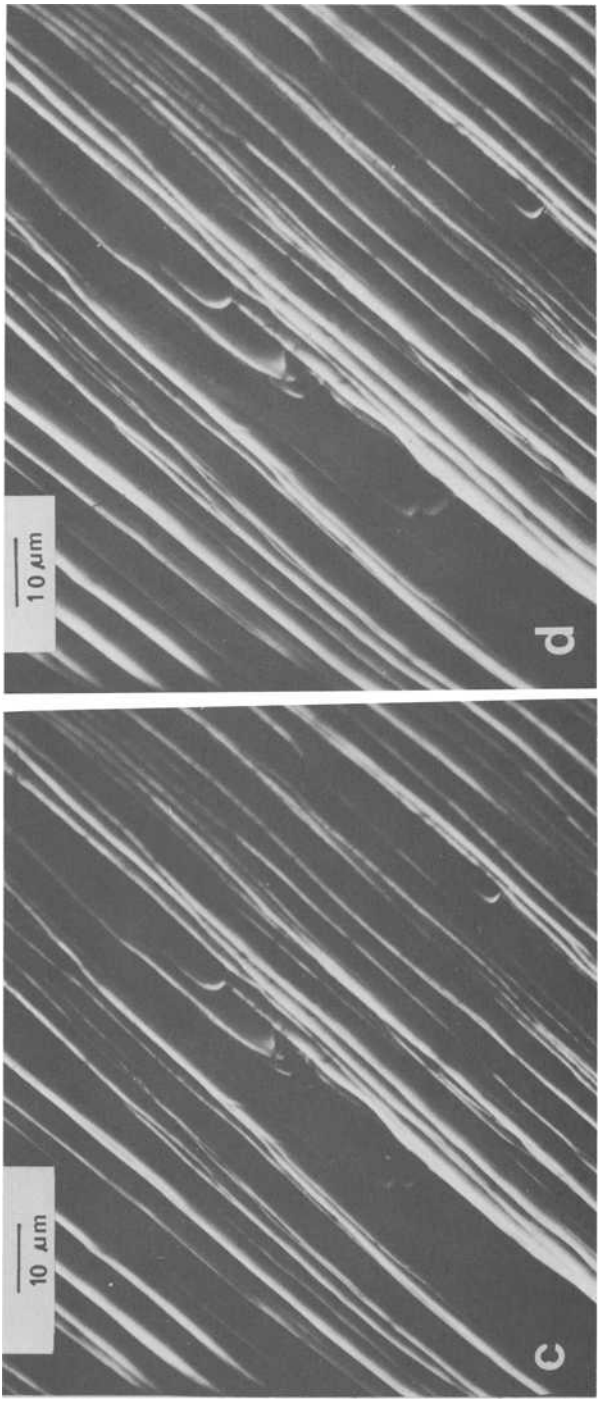

FIG. 13—*Continued.*

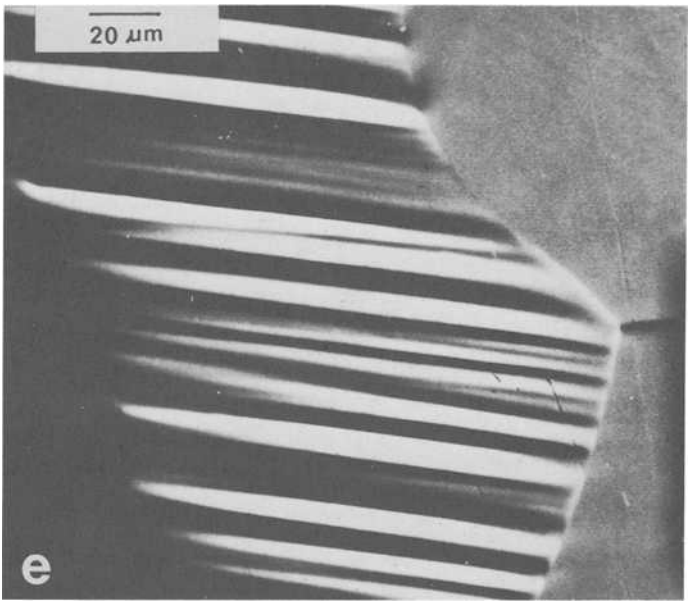

FIG. 13—*Continued.*

per grain (Fig. 13*e*) and they are less intense, but quite distinct compared with the bands at high amplitude.

Summary and Conclusions

It is demonstrated that there exists a close relationship between the changes in CSS behavior and damage mechanisms as a function of temperature.

1. In nickel and TD-nickel, the crack nucleation mechanisms remain unchanged when cycling is carried out at high temperatures in vacuum and using a symmetric waveform. Although the saturated flow stresses decrease with temperature, the dislocation structures and slip morphology do not change significantly with temperature. This explains why the crack nucleation mechanism does not change with increasing temperature. However, significant changes might be expected at high temperatures in an aggressive environment.

2. In Al-4Cu alloy containing large θ' plates, saturation is achieved rapidly but, at higher temperatures, softening gradually occurs due to twisting and subsequent dissolution of θ'. This allows transgranular slip to occur. Although intergranular cracking is still predominant at high temperatures and short lives, transgranular cracking may well be important in long-life fatigue.

3. In Al-4Cu alloy containing θ'' the CSS curves are essentially independent of temperature. Therefore, as at room temperature, slip remains localized and the crack nucleation mechanism remains transgranular even at high temperatures.

Acknowledgments

This work was supported by the National Science Foundation (Grant Nos. DMR 73-0754 and DMR 76-21926) and by a grant from the Alcoa Foundation. The research is related to that carried out in the Materials Failure Thrust area of the Laboratory for Research on the Structure of Matter, and it is a pleasure to acknowledge both the provision of testing facilities and the help of Mr. R. de la Veaux and Mrs. N. Y. C. Yang.

References

[1] Fournier, D. and Pineau, A., *Metallurgical Transactions,* Vol. 8A, 1977, pp. 1095-1105.
[2] Seeley, R. R. and Zeisloft, R. H. in *Fatigue at Elevated Temperatures, ASTM STP 520,* American Society for Testing and Materials 1973, pp. 332-344.
[3] Berling, J. T. and Slot, T. in *Fatigue at High Temperature, ASTM STP 459,* American Society for Testing and Materials 1969, pp. 3-30.
[4] Nahm, H., Moteff, J., and Diercks, D. R., *Acta Metallurgica,* Vol. 25, 1977, pp. 107-116.
[5] Abdel-Raouf, H., Plumtree, A., and Topper, T. H., *Metallurgical Transactions,* Vol. 5, 1974, pp. 267-277.
[6] Bhat, S. P., Ph.D. Thesis, University of Pennsylvania, Philadelphia, Pa., 1978.
[7] Laird, C. in *Cyclic Stress-Strain and Plastic Deformation Aspects of Fatigue Crack Growth, ASTM STP 637,* American Society for Testing and Materials 1977, pp. 3-25.
[8] Calabrese, C. and Laird, C., *Metallurgical Transactions,* Vol. 5, 1974, pp. 1785-1793.
[9] Mitchell, T. E., *Progress in Applied Materials Research,* Vol. 6, 1964, pp. 119-237.
[10] Sellars, C. M., and McG. Tegart, W. J., *International Metallurgical Reviews,* Vol. 17, 1972, pp. 1-24.
[11] Bhat, S. P. and Laird, C., *International Journal of Fatigue of Engineering Materials and Structures,* Vol. 1, 1979.
[12] Bhat, S. P. and Laird, C., *International Journal of Fatigue of Engineering Materials and Structures,* Vol. 1, 1979.
[13] Laird, C., Ph.D. Thesis, University of Cambridge, Cambridge, U. K., 1962.
[14] Coffin, L. F. and Tavernelli, J. F., *Transactions of the Metallurgical Society of AIME,* Vol. 215, 1959, pp. 794-807.
[15] Feltner, C. E. and Laird, C., *Acta Metallurgica,* Vol. 15, 1967, pp. 1621-1632.
[16] Feltner, C. E. and Laird, C., *Acta Metallurgica,* Vol. 15, 1967, pp. 1633-1653.
[17] Feltner, C. E. and Laird, C., *Transactions of the Metallurgical Society of AIME,* Vol. 242, 1968, pp. 1253-1257.
[18] Kim, W. H., Ph.D. Thesis, University of Pennsylvania, Philadelphia, Pa., 1976.
[19] Laird, C. and Duquette, D. J., *Corrosion Fatigue,* National Association of Corrosion Engineers, Houston, Tex., 1972, pp. 88-117.
[20] Kim, W. H. and Laird, C., *Acta Metallurgica,* Vol. 26, 1978, pp. 777-787.
[21] Kim, W. H. and Laird, C., *Acta Metallurgica,* Vol. 26, 1978, pp. 789-799.
[22] Laird, C. and Feltner, C. E., *Transactions of the Metallurgical Society of AIME,* Vol. 239, 1967, pp. 1074-1083.
[23] Leverant, G. R., *Transactions of the Metallurgical Society of AIME,* Vol. 239, 1967, pp. 1992-1993.
[24] Leverant, G. R. and Sullivan, C. P., *Transactions of the Metallurgical Society of AIME,* Vol. 242, 1968 pp. 2347-2353.

[25] Footner, P. K. and Alcock, C. B., *Metallurgical Transactions*, Vol. 3, 1972, pp. 2633-2637.
[26] Leverant, G. R. and Sullivan, C. P., *Transactions of the Metallurgical Society of AIME*, Vol. 245, 1969, pp. 2035-2039.
[27] Calabrese, C. and Laird, C., *Materials Science and Engineering*, Vol. 1, 1974, pp. 141-157.
[28] Calabrese, C. and Laird, C., *Materials Science and Engineering*, Vol. 1, 1974, pp. 159-174.
[29] Bhat, S. P. and Laird, C., submitted to *Acta Metallurgica*.
[30] Abel, A. and Ham, R. K., *Acta Metallurgica*, Vol. 14, 1969, pp. 1495-1503.

DISCUSSION

R. Thomson[1] *(discussion)*—Laird and his co-workers have brought a high degree of experimental sophistication to the study of fatigue in metals. This discussion relates to our fundamental understanding of the mechanisms of fatigue nucleation.

Fatigue must be reckoned one of the most difficult problems in material science. It combines the complexities of plastic deformation with those of fracture, and, because one works at macroscopic stresses well below the K_{Ic} point, the straightforward application of fracture mechanics is of little help. Likewise, from the standpoint of materials/microstructure, the problem of nucleation of a crack is conceptually difficult, because of the complexities of the dislocation configurations, and because it is difficult to know when one has a crack (that is, the stress concentrations around incipient cracks are difficult to estimate).

The authors have shown that the high-temperature nucleation mechanisms in pure nickel are the same as those at low temperature, and have referred to unpublished work on a specific mechanism proposed to be valid at the grain boundary external surface. It appears that this mechanism is similar to the one proposed by Neumann,[2] and it is hoped that these ideas will be described more fully at this conference.

Theoretical modeling in this field is almost as difficult as the careful experimentation carried out over the years by Laird. The modeling which exists begins from specific dislocation mechanisms, but is limited by making no prediction as to how often these configurations should appear, nor are the quantitative aspects of the early subcritical growth of an incipient nucleus addressed. It would appear that several general directions are available. The first would attempt to model a simple grain boundary deformation scenario by computer with distributions of slip sources and a realistic treatment of the stress distributions. The second might be to

[1] Center for Materials Science, National Measurement Laboratory, National Bureau of Standards, Washington, D.C. 20234.
[2] Neumann, P., *Acta Metallurgica*, Vol. 17, 1969, p. 1219.

address the problem from a statistical analytical view-point and attempt to estimate the frequency with which critical configurations might be achieved. Finally, theoretical work which attempts to characterize more precisely what an incipient nucleus is, and the conditions under which it can grow, would be most useful.

The discusser is under no allusion about the difficulty of carrying through such theoretical attempts.

S. P. Bhat—There are two points that Dr. Thomson has raised. Regarding comparison with the Neumann model, there are certain similarities and some differences in detail. I might point out that the Neumann model is applicable for single crystals, fatigued at low strain amplitudes, whereas here we are primarily considering high-strain fatigue in polycrystals where slip from two grains is directed towards the grain boundary. The details of the present model may be found in Ref *21*, p. 789.

As to the second question of developing quantitative and predictive modeling of crack nucleation, Dr. Thomson has given valuable suggestions and I would welcome more concrete suggestions from this conference.

E. Esztergar[3] (*discussion*)—First, I would like to summarize three issues which I presume the authors will answer in detail.

Point No. 1 is the claim in the paper that the crack nucleation mechanism in vacuum is unchanged with increasing temperature. A number of papers and discussions were presented at this symposium which show a number of time-dependent effects including frequency, hold time, strain rate, and slow-fast and fast-slow loading sequences. In general, the importance of these cycle-shape effects are demonstrably clear. The available information also shows these mechanisms are also dependent on the strain amplitude. The results presented in the paper correspond to a single cycle shape, a single frequency (and strain rate), and a single strain range of 1 percent. It is possible that this is sufficient for the practically pure nickel and the aluminum alloy investigated, but it is definitely not so for complex structural alloys and I will caution, as the authors themselves have, against interpreting these results as representative of the crack nucleation and propagation of structural materials in creep conditions.

The second point is the influence of environmental effects: Was the vacuum high enough to eliminate some of the time-dependent effects mentioned in the first point? There are indications of grain boundary cracking that has been observed in the surface regions at the higher temperatures. This would indicate that even though the environmental effects were supposedly eliminated by using a vacuum test setup, there may be a significant environmental component masking the temperature-dependent effects in all the results shown.

[3] Consultant, La Jolla, Calif. 92037.

The third point is that crack nucleation data are not sufficient to develop a viable model for fatigue damage mechanisms, notwithstanding the title of the paper. As we have discussed at this symposium and at many other conferences, there are essentially two schools of thought on the subject of crack appearance and fatigue damage. One maintains that fatigue damage is crack propagation and it is useless to investigate what seems to be nucleation because microcracks are always present from the beginning, that is, in virgin materials. Their detection is simply dependent on how powerful a microscope is used. The second group believes that the major part of the fatigue damage is incurred in the incubation of cracks by a multitude of time-dependent and environmental effects and that the crack propagation observed is only the last visible part of the damage process. In the first case the fatigue damage is equivalent to crack growth; in the second, the initiation mechanism is to be modeled for a viable damage measure. The paper opted for the second idea without considering what is really measured that is labeled as "damage."

These are my main comments on the paper, but I would like to add a few thoughts provoked by what I heard at these sessions, as related to the paper. The authors state, to quote verbatim, "At low temperatures, it is well established that there is a close correlation between cyclic deformation and damage mechanisms. This has not been demonstrated for high temperatures." I think this has not been demonstrated for low temperature either.

As discussed in the foregoing, we have to decide what is a measure of damage in elevated temperature as well as at low temperature, since we have at least the choice of either the crack length and propagation process or of some local deformation and microstructural changes needing to be systematically correlated with the developing gross failure, that is, the so-called fatigue endurance. The paper by Davidson[4] on electronchanneling methods for microstructural measurements showed that around the crack boundary there is a smudged area of a few angstrom width, unresolved at the electron energies used, which possibly could be related, if resolved, to some damage mechanism. However, Smith discussing the next paper[5] states: "A more complete characterization is essential until correlation between microstructural features and fatigue behavior is established and primary microstructural variables controlling fatigue have been identified." The present paper attempted to identify the damage by microstructural phenomena; however, there is yet no correlation with the fatigue data as influenced by the various observed effects. So for real damage correlation, rather than just producing a set, or rather subset, of microstructural measurements that have no calibration possibility with the known fatigue

[4] Davidson, D. L., this publication, pp. 254–275.
[5] Underwood, E. E. and Starke, E., this publication, pp. 633–682.

parameters, some new types of measurement are needed; for example, critical velocity or critical strain as discussed by Min and Raj.[6] Their results show that there is a critical strain rate for grain boundary sliding that is related to the thermally activated processes that may be correlated with crack propagation in creep environment. It seems to me that the authors of the present paper have overlooked these time and temperature effects for the simple reason that they have not tested in the regimes of the loading and time variables that would be in the critical range, which is the direct consequence of the cycle shape they choose to investigate.

To conclude, I suggest that instead of using the word "damage" in an unqualified way, we have to always answer two questions when making damage models: Is it initiation or is it propagation that we have measured or tested? If there is a microcrack incipient in the test specimen, then fracture mechanics methods can be applied to model "damage" propagation. If there is no macrocrack big enough to apply fracture mechanics as in the case of creep cavitation, the damage mechanism has to model the thermally activated diffusion rates as influenced by the local deformation mechanisms that are possibly one scale factor below the crack propagation mechanisms.

As a consequence, I think, it is important to remember, that the "damage front" shape may be drastically different from the crack front shape in creep environment, as the microstructural processes of diffusion and local deformation are producing microvoids by cavitation well ahead of the crack tip. These sites then become a dominant crack that can be usefully modeled by fracture mechanics methods. However, for such semi-micro-macro crack configurations the multiaxiality of the strain field in the vicinity of the crack tip cannot be disregarded if a viable model is sought that is applicable to design or safety evaluation.

The following paragraphs constitute the main body of my discussion.

Traditionally, evaluation of the behavior and integrity of structural components operating at elevated temperatures has relied on material properties that are related to the so-called "proof test" principles; tensile strength, yield strength, total elongation, creep, and creep rupture strength are the material data that the standard mill-specifications supplied. The testing methods generating this type of data use almost exclusively uniaxial bar specimens under monotonically increasing or sustained loads. The results are the values of stress and time at the terminal failure of the specimen. Fatigue data are generated in a conceptually similar way in "endurance" test cycling under sustained stress or strain amplitudes until complete separation of the specimen occurs.

This type of terminal failure state data provides little or no information on the nature of progressive deformation and damage accumulation under

[6] Min, B. K. and Raj, R., this publication, pp. 569-591.

various cyclic loading histories. Since operating conditions on most components include sequences of transient and partial load levels in the current design practice, the evaluation methods for the projected life are based on empirical relationships for the superposition of partial damage quantities defined as fractions of the terminal failure conditions. While the use of this kind of data base is a practical necessity at the present time, analytical solutions to the elevated-temperature fatigue design problems require a new type of data for the formulation of mechanical models for the cyclic deformation and incremental damage progression or retardation. Therefore the topic of the paper, "cyclic stress-strain response and damage mechanisms at high temperatures," is of great interest. The paper presents cyclic stress-strain response in the range of 100 to 1000 cycles and microstructural evaluation of the slip morphology and crack development of commercially pure nickel and TD-nickel and aluminum alloy in two aging states. The test temperature for the nickel is up to 850°C, for the aluminum alloy 250 and 150°C. The tests were conducted in vacuum (10^{-5} mm Hg) at a constant strain rate (6×10^{-4}) with triangular wave shape. These conditions are repeated here for easy references to the discussion since a number of conclusions have been presented that need qualification in view of the test conditions.

First, for nickel, the crack nucleation mechanism in a vacuum is stated to be unchanged with increasing temperature. In the literature on elevated-temperature fatigue a number of damage sources have been discussed, including frequency effects (for example, hold time), strain rate effects (for example, slow-fast fast-slow sequences or more generally the wave shape variation), grain boundary phenomena (for example, cavitation, sliding, triple-junction fracture), and the effects of environment. The available information shows that even in vacuum a number of different mechanisms are activated depending on the frequency,[7] cycle shape,[8] and strain amplitude.[9] The results presented in the paper, however, correspond to a single cycle shape, frequency, and strain range. Admittedly, the data in these references correspond to complex structural alloys and the relative importance of these processes may be different for nickel and TD-nickel as pointed out by the authors themselves calling for caution in carrying over the conclusion to commercial alloys. However, it is difficult to assess significance of the findings when data are not presented for the test variables known to be important in elevated-temperature applications.

[7] Harrod, D. L. and Manjoine, M. J. in *Proceedings,* Materials Properties Council Symposium on Creep Fatigue Interaction, ASME-MPC-3, American Society of Mechanical Engineers, New York, Dec. 1976.

[8] Coffin, L. F., Jr. in *Proceedings,* Conference on Time-Dependent Fatigue of Structural Alloys, ORNL Report 5073, Oak Ridge National Laboratory, Oak Ridge, Tenn., Jan. 1977, p. 157.

[9] Majumdar, S., "Importance of Strain Rate in Elevated Temperature Low Cycle Fatigue of Austenitic Stainless Steel," Argonne National Laboratory Report, Ill., Jan. 1978.

The second point is the sufficiency of the vacuum used in the test for eliminating the environmental effects. Boundary cracking is stated to be observed in the surface region at all temperatures with different morphology from those observed in creep fatigue experiments. This implies environmental effects of some importance in the evaluation of the conclusion that the crack nucleation mechanism is geometric in nature and remains the same at elevated temperature as at room temperature. Elsewhere in this volume Min and Raj (see footnote 6) discuss the critical strain rate for grain boundary sliding as related to the temperature and time-dependent diffusion and yield stress. This is at variance with the reported conclusion. Possible explanations for the reported temperature independence of the crack nucleation in the nickel alloy could be that the environmental effect and the strain-rate/frequency used in these tests are unique combinations that mask the true time dependency of the damage processes.

The third point to be raised is that data on crack nucleation alone may not be sufficient to develop a damage mechanism model in high-temperature fatigue. In fact, the nucleation phase is often regarded as insignificant in comparison with the propagation phase, particularly when the possibility of preexisting voids, grain boundary separation, and other microflaws cannot be discounted. Therefore, the rate of propagation of newly nucleated or preexisting cracks is also an important aspect of a damage model development. The authors may have data from their test that would greatly assist in the evaluation of their result.

S. P. Bhat—I am sympathetic to the views expressed by Dr. Esztergar as to the effects of the test variables on high-temperature fatigue behavior. There is ample literature covering the influences of external variables on high-temperature fatigue. As pointed out in the text, our primary emphasis in this work was to demonstrate the effects of microstructure of high-temperature fatigue under simplified experimental conditions, and one must exercise extreme caution in carrying over the conclusions to other commercial alloys or to different test conditions.

H. Mughrabi[10] (*discussion*)—Regarding the nickel data, namely, the question of what the dislocation mechanisms in saturation are, and assuming that one has a dynamic balance between dislocation multiplication leading to hardening and some recovery process leading to softening, then at room temperature dislocation annihilation could occur by cross slip and, as the temperature increases, one would have, in addition, due to enhanced diffusion, annihilation by climb. Could you indicate whether your work has been able to single out in which temperature ranges one or the other mechanism dominates?

[10] Max-Planck-Institut für Metallforschung, Institut für Physik, Stuttgart, Germany.

S. P. Bhat—Yes, we have attempted to identify the bulk cyclic deformation mechanism in nickel as a function of temperature. Just as at ambient temperature there are broad similarities between the cyclic and monotonic hardening of nickel at high temperatures, there are also significant differences in detail. For example, if one plots the dislocation cell size as a function of temperature, the cell size increases at first gradually and then rises rather rapidly above about 0.5 of the melting point. The details of the cyclic hardening and annihilation of dislocations at high temperatures are being published elsewhere (submitted to the *International Journal of Fatigue*).

S. Weissman[11] (*discussion*)—In your abstract and also in your talk you spoke about the surprising effect of θ'' being still disordered in spite of the presence of a high temperature for which one usually would expect an ordering.

Again, if the frequency changes, would you not expect also an ordering effect to occur? Of course, in fast cycling you will destroy the θ'', so if you were to change both the frequency and the temperature, a reordering or partial reordering may occur with the consequence of a change in properties. Unfortunately you only work with one frequency; is that correct?

S. P. Bhat—In room temperature cycling, the θ'' microstructure shows a peak in its CSS curve and the softening is attributed to disordering of the θ'' precipitates. After room temperature cycling, however, Calabrese and Laird showed that a short reaging treatment leads to reordering of the precipitate and the specimen behaves like a virgin specimen on recycling. One might therefore argue that a simultaneous application of temperature and cycling should keep the precipitates in their ordered states and therefore one should not see any softening in high-temperature cycling. However, our experiments show, to the contrary, peaks in the CSS curves. It is possible that the disordering kinetics are faster than the ordering kinetics for the combination of experimental conditions stated in the text and thus lead to the observed softening.

We might also point out that transformation to more stable θ' becomes a possibility with longer time and higher temperature.

A. Plumtree[12] (*discussion*)—The term "damage" is somewhat difficult to comprehend when on the one hand we tend to use it to describe plastic behavior, whereas, on the other, we use it to express some aspect of fracture. In the first case it suggests an operative strengthening mechanism and in the second, a weakening mechanism. My own view is that the latter is

[11] Department of Mechanics and Materials Sciences, Rutgers University, Piscataway, N. J. 08854.

[12] Department of Mechanical Engineering, University of Waterloo, Waterloo, Ont., Canada.

preferable since once cracks are present in a material its usefulness is permanently diminished (hence damaged).

Using this more rigorous definition, Lemaitre and Plumtree[13] have shown that the evolution of high-temperature cyclic damage (D) at constant strain range may be expressed by the constitutive equation

$$D = 1 - [1 - N/N_F]^{1/(p+1)} \quad (1)$$

where

N = any number of strain cycles,
N_F = number of cycles to failure, and
p = a material constant dependent upon the testing conditions (for example, temperature and strain range).

Douglas and Plumtree[14] investigated the fatigue behavior of smooth specimens of Alloy 800 at 600°C ($p = 28$ at $\Delta\epsilon_T = 1.4$ percent and $p = 18$ at $\Delta\epsilon_T = 2.0$ percent) cycled under strain control. They found that on measuring the size of the cracks and considering experimental damage as the area of the crack surface divided by twice the original cross-sectional area of the specimen, there was excellent agreement with the predicted damage given by Eq 1. This was found for both the cyclic strain ranges, as shown in Fig. 14 accompanying this discussion.

S. P. Bhat and C. Laird (authors' closure)—We appreciate the comments and discussion on our paper by Drs. Thomson, Esztergar, Mughrabi, Weissman, and Plumtree. Before answering some of the specific comments made, we feel that it is necessary to reemphasize the objective of our investigation. Traditionally, high-temperature fatigue research has taken the path of selecting a given alloy (of defined microstructural complexity) and investigating the effects of various test parameters (for example, temperature, strain rate, load history, wave shape). In these investigations microstructure itself is usually not treated as a variable. On the contrary, we have attempted to investigate how, for a chosen set of external test variables, the phenomena of high temperature fatigue damage mechanisms are influenced by the microstructure. While it is difficult to correlate the microstructure and fatigue damage processes quantitatively, we have chosen to correlate the cyclic deformation and damage mechanisms as a function of test temperature. (We implicitly assume that the cyclic deformation can be related to the microstructure as defined, for example,

[13] Lemaitre, J. and Plumtree, A. in *Proceedings*, Joint American Society of Mechanical Engineers/Canadian Society of Mechanical Engineers Pressure Vessels, and Piping Conference, Montreal, Que., Canada, 25–30 June 1978.

[14] Douglas, M. J. and Plumtree, A. in *Fracture Mechanics, ASTM STP 677*, American Society for Testing and Materials, 1979.

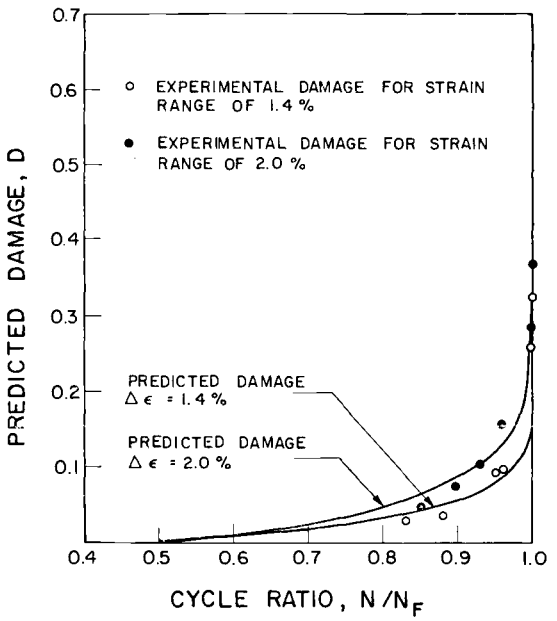

FIG. 14—*Plot of experimental and predicted damage at different life fractions for two strain levels.*

by stacking fault energy, size, shape and distribution of second-phase particles, and the stability of the alloy.) It was therefore necessary to hold constant the external test variables for all experiments. As emphasized in the text, and again brought out in the discussion, precaution has to be exercised in carrying over the conclusions to complex testing circumstances.

Our response to specific comments is as follows:

Dr. Thomson has called for theoretical modeling of fatigue crack nucleation to include grain boundary deformation. The effects of inhomogeneous deformation within polycrystalline grains, particularly near grain boundaries, even under simple tensile deformation, have only begun to emerge recently.[15] In principle, these concepts should be applicable to cyclic deformation and lead to better understanding of the behavior of polycrystals under reversed straining. Although the details are not as yet clear, the formation of a grain boundary step and its growth rate, discussed in the text, ought to be influenced by both the degree of misorientation of the two neighboring grains and by the details of the slip processes within the grains and at the grain boundary. Indeed, the inhomogeneous deformation at the grain boundary (via grain boundary dislocation sources)

[15] Thompson, A. W. in *Work Hardening in Tension and Fatigue*, A. W. Thompson, Ed., American Institute of Mining, Metallurgical and Petroleum Engineers, 1977, pp. 89-126.

might well be the source for grain boundary step formation. Careful comparative experiments in single crystals and perhaps in bicrystals at high strain amplitudes along with the modeling attempts suggested by Thomson would be helpful to our understanding of grain boundary crack nucleation. The relevance of the present high-temperature investigation to the understanding of these phenomena should be noted. It is shown that the crack nucleation mechanism in wavy-slip nickel under conditions of fatigue deformation (in the absence of any creep effects) is independent of temperature. Therefore, the conclusions from model experiments suggested in the foregoing, even if carried out at ambient temperature, should be applicable to high temperatures.

Dr. Esztergar has again emphasized the importance of test variables by drawing attention to the voluminous literature available on time-dependent effects on high-temperature fatigue of structural materials. We only reiterate our objectives and would like to point out that in high-temperature, high-strain fatigue, grain boundary folding and plastic deformation effects overshadow the time-dependent effects under the stated experimental conditions.

Dr. Mughrabi has asked about dominant recovery mechanisms in cyclic deformation as a function of temperature and some elaboration is required to the answer given at the meeting: The saturated cyclic flow stress for nickel-200 decreases linearly with increase of temperature to 0.5 T_M but then drops rather sharply. We attribute the initial linear portion to point-defect-enhanced softening mainly by cross-slip processes but partly by climb, and it appears that diffusion-enhanced climb becomes dominant only above 0.5 mp. Further details can be found in the paper to be published in the *International Journal of Fatigue in Engineering Materials and Structures.*

Both Dr. Esztergar and Dr. Plumtree have pondered upon the use of the term "fatigue damage." In fact, Dr. Plumtree has presented (1) a definition of damage in terms of crack growth; (2) an *empirical* equation for characterizing high-temperature fatigue damage, and (3) a test of this equation for alloy 800. We disagree with Dr. Plumtree on several grounds.

First of all, in our opinion, characterizing the damage only by crack growth is inadequate. The measurements presented by Plumtree et al (Fig. 14 of the discussion) apply only to the late stages of life ($N > 0.8\ N_f$) in which we know that Stage II crack propagation is occurring. Indeed, even in this range, it will be noticed that the data points are beginning to deviate significantly from the predicted curve at the lower end, and no data are presented for the early stages of life (for $N < 0.8\ N_f$). Thus "excellent agreement with the predicted damage" as claimed by Plumtree is, in fact, questionable. We cannot agree, therefore, that an empirical equation of the sort suggested is an adequate description of the damage. Perhaps failure to take proper account of the crack nucleation part is the source of

this discrepancy. In many important applications—for example, pressure vessels—the design life is determined by crack nucleation considerations.

Quite aside from the failure of this equation to characterize the damage precisely, we have a philosophical objection to such an approach because it fails to separate the nucleation and propagation parts of life. Nor does it provide any insight into the mechanisms involved in crack nucleation. While it happens that we understand the mechanism of Stage II crack growth covered by Plumtree et al's measurements, the total damage must reckon with crack nucleation and Stage I growth. Both of these phenomena are strongly influenced by the cyclic deformation, and hence the microstructure, which therefore should be studied as a function of temperature to elucidate their mechanisms.

Concluding Remarks on Session

B. Tomkins[1]—I would like to make a general comment on the role of mechanistic studies in the elevated-temperature area. In designing elevated-temperature plant and components, engineers encounter considerable difficulty in assessing time-dependent failure interactions. In some cases, what may turn out to be extremely conservative rules are used, while in others there is considerable uncertainty. A central feature to this problem lies in the use of end-state parameters (ductility, endurance, time to rupture) to characterize path-dependent failures which involve several time-dependent processes (crack development, creep cantation, aging, environmental attack). Increasingly, we must look at a differential approach based on the current rate of failure development, and here mechanistic studies, when quantified, play a central role. We may not be in a position to influence design for some time, but we can influence in-service assessment of plant and interpret situations revealed by monitoring. Elevated-temperature fatigue represents an area where mechanistic studies can play an important future role and our programs of work should be increasingly focused in this practical direction. On the design front, we are probably in a position to make the first attempts at mechanistically based life prediction rules, but much of the initiative would seem to rest with us.

S. Manson[2] *on Runkle/Pelloux and Tomkins*—I should like to address a remark made by Dr. Tomkins, in his discussion of the Runkle/Pelloux paper in this chapter, regarding the question of whether fundamental studies have a role in the development of materials. At the same time I would like to comment on the very interesting results presented by Runkle and Pelloux in their paper.

Runkle and Pelloux have made a very systematic study of the effect of microstructure on the fatigue life of a nickel-base alloy at elevated tempera-

[1]Reactor Fuel Element Laboratories, UKAEA (Northern Division), Springfields, Salwick, Preston, Lancs., U. K.

[2]Department of Mechanical and Aerospace Engineering, Case Western Reserve University, Cleveland, Ohio 44106.

ture. In particular their most interesting result to me is related to the comparison of alloys having the same matrix composition. Differences were achieved, however, in the shape and composition of the grain boundaries. Those alloys that had wavy boundaries containing particle precipitates had better fatigue life than the planar boundaries without precipitates. Although they did not analyze their results by the strain-range partitioning (SRP) framework, it is interesting to do so.

According to SRP, the relative fatigue damage of a given imposed strain range depends on whether the creep is absorbed in the slip planes or in the grain boundaries, and in particular whether slip plane sliding in one direction is reversed by grain boundary sliding in the reverse direction. In general, grain boundary sliding is more damaging than slip-plane sliding, and if both occur, one in tension the other in compression, a ratcheting of both types of strain develops, building up cycle by cycle. Eventually the material ductility is exhausted, causing fatigue in a low number of cycles. Runkle and Pelloux have found that it is desirable to have many boundaries or precipitate particles in these boundaries, as would be expected by SRP, since both have the effect of blocking grain boundary sliding.

It would be instructive to learn whether they interpret their results in a manner consistent with the SRP explanation, whether they have conducted some nonsymmetrical loading tests which would favor CP (tensile creep, compressive plasticity) or PC (tensile plasticity, compressive creep) straining. Have they measured the relative amounts of slip-plane and grain boundary strains for any of the microstructures obtained, and have they made any ductility measurements in tension or creep tests which can be reinterpreted in terms of the SRP framework?

My conclusion to Dr. Tomkin's question is that, indeed, understanding the fundamental mechanism does point to paths for tailoring materials to improve fatigue resistance. Understanding the mechanism also leads to logical procedures for treating technological problems. We believe that SRP is one such practical technological procedure based on some of the elements of the mechanistic process occurring during fatigue.

S. Manson on Sidey/Coffin and Min/Raj—It is important to emphasize in connection with the Sidey/Coffin paper of this chapter that the terminology "slow-fast" and "fast-slow" does not refer to the relative rates at which the tensile and compressive loadings are applied, but rather on absolute rates that may differ from temperature to temperature and from material to material. For example, in a test in which the tensile-going loading is 100 times faster than the compressive-going loading, the effect on life may be large or small depending on the absolute strain rates involved. If both are so small, and the temperature sufficiently high to favor creep in both the tensile and compressive halves of the cycle, the effect may in fact be small despite the large difference in absolute value of strain rate. Correspondingly, if both

rates are sufficiently high, or temperature sufficiently low, favoring plasticity in both directions, the effect may again be small. What is important is that the type of strain favored by the slow strain rate be different from that favored by the fast strain rate. For some materials creep in tension reversed by plasticity in compression is very detrimental; for others the reverse is true: tensile plasticity followed by compressive creep is the most damaging type of strain range.

Strain-range partitioning (SRP) explains these results on the basis of the generic type of strain induced: if both rates are low enough to favor creep (even if one is much faster than the other) $\Delta\epsilon_{CC}$ is induced; if both are fast enough to favor plastic flow, then $\Delta\epsilon_{PP}$ is induced (again, even if one rate is much faster than the other); but if one is slow enough to favor creep while the other is fast enough to favor plasticity, then either $\Delta\epsilon_{CP}$ or $\Delta\epsilon_{PC}$ is induced—depending on which direction produces the creep and which the plasticity. Thus the effect of fast-slow and slow-fast conditions depends on the relative lives associated with each of these types of strain range. Whether slow-fast or fast-slow is more damaging depends on whether the CP or PC lives are more damaging.

We have conducted such ramping tests on 316 stainless steel. Figure 1, based on a paper by Manson et al,[3] shows a sample result. In this case the "fast" part of the cycle was obtained in about 1 s while the "slow" ramping

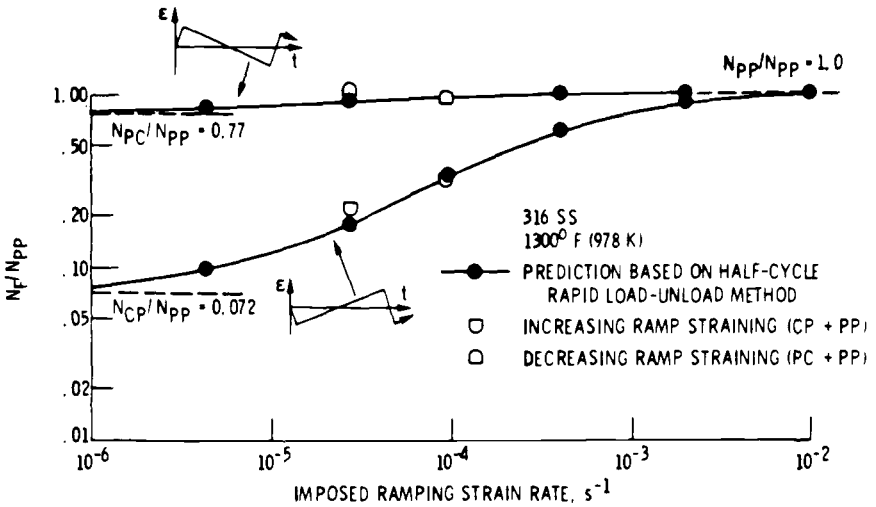

FIG. 1—*Comparison of predictions and experimental results for increasing and decreasing ramp straining. Predictions made by the half-cycle rapid load-unload method. Based on paper by Manson et al (see footnote 3).*

[3]Manson, S. S., Halford, G. R., and Nachtigall, A. C. in *Advances in Design for Elevated Temperature Environment*, American Society of Mechanical Engineers, 1975.

was accomplished at various rates as plotted along the horizontal axis. The vertical axis shows the cycle life achieved (normalized to the fast-fast life for the same strain range). It is seen that over the entire range of ramping rates, slow tensile ramping has a detrimental effect on life, reducing life by a factor of 10 at the slowest of the ramping rates tested, while slow compressive ramping has an almost negligible effect. For other materials, such as 2¼Cr-1Mo, the opposite effect can be expected according to SRP. This is so since PC loading is more detrimental than CP loading for this material.

The work of Min and Raj tends to verify the results shown in Fig. 1. They found that only when the slow ramping was below a critical value and the fast rate above the critical value did they get the detrimental effect. Looking at this conclusion from the SRP viewpoint, the interpretation would be that if both rates are below the critical value the major strain range induced is CC, while if both are above, the major strain range is PP, both of which are less detrimental than CP loading, which is achieved only when the slow rate is below the critical value and the fast rate above this value.

My question to both Sidey and Coffin and to Min and Raj is whether they have considered the SRP framework for interpreting their results, and what their opinion is regarding the relative merits of their approach compared with SRP. I should also appreciate Min and Raj's comments on the results we obtained during the fast-slow loading. Obviously these conditions also involve grain boundary sliding but the damaging effects are minimal. From the SRP viewpoint these results are so because PC loading for this material is much less damaging than CP loading. But how are these results to be explained mechanistically according to their theory? And how would we explain the opposite type of results for materials such as 2¼Cr-1Mo, for which PC loading is more damaging than CP?

D. Sidey[4] *on S. Manson*—It is well known that wave-shape influences high-temperature low-cycle fatigue lives, as evidenced, for instance, by the early experiments with hold times inserted in the fatigue cycle. The fatigue life is controlled by the damage mechanisms which operate at the microscopic level. The specific damage processes depend on the opening conditions, and the tests reported in our paper indicate that the micromechanisms of failure can depend on the strain rates associated with the positive and negative ramps of the cycle. Obviously, the type of damage will depend on many factors such as the absolute strain rate levels, the ratio of strain rates, the strain range, and the temperature. One of the objects of extrapolation techniques is to minimize the number of laboratory tests required to answer the problem at hand. However, experimental data can be extrapolated sensibly only if the failure mechanisms remain unchanged under the extrapolated conditions. Therefore, it is important to delineate the

[4]Ontario Hydro, Toronto, Ont., Canada.

boundaries between the various failure mechanisms in terms of the test parameters. This can be done by plotting fatigue maps which display the dependence of the failure mechanism on various fatigue parameters. For instance, in the case of a Cu-0.5Cr alloy at 673 K, metallographic evidence shows that three types of failure process can operate,[5] namely; single transgranular crack propagation, oxidation-enhanced failure, and bulk cavitation failure. Data in any one field can be extrapolated safely, provided the conditions remain within the field boundaries. The strain-range partitioning method, with its recognition of the importance of plasticity and creep, reflects the experimental observation of these changes in failure mechanisms, but the method cannot predict the boundaries between different failure processes, and without this knowledge extrapolation is unsafe.

Dr. Manson presents some results of unbalanced loop testing on 316 stainless steel (Fig. 1) which indicate, in effect, that slow-fast and fast-slow cycles produce similar damage to 'CP' and 'PC' type cycles. The advantages of using the strain-controlled unbalanced loop test have been discussed in our paper. It would have been interesting to see metallographs of the failures in conjunction with Fig. 1, as the latter suggests that various different failure processes are in operation. One of the difficulties in interpreting Dr. Manson's data is that the cycle period has been varied so that, unless the tests were performed in vacuum, the environmental and strain rate effects cannot be separated. Until strain-range partitioning takes into consideration the micromechanisms which lead to failure, its usefulness is restricted to 'predicting' the experimental data, and thus the analysis becomes tautological.

B. Min[6] *on S. Manson*—1. In your tests and predictions on 316 stainless steel (Fig. 1), it is shown that the slow ramp (slow-fast) loading is more detrimental than the fast ramp (fast-slow) loading, only when the tensile-going strain rate is lower than a critical value, approximately 10^{-3} s^{-1}. This agrees very closely with the value calculated from our model at the same temperature (Fig. 3 of our paper).

2. Our analysis is based on the assumption that damage is produced by grain boundary sliding during tensile-going half cycles only. Therefore the minimal damage effect of the fast-slow loading for stainless steel 316 (Fig. 1) is due to the absence of grain boundary sliding during tensile-going half cycles.

3. The results of 2¼Cr-1Mo reflect another aspect of our model. We believe that in addition to the critical strain rate that we have derived in this

[5]Collins, A. L. W., Sidey, D., and Taplin, D. M. R., *Canadian Metallurgical Quarterly*, June 1979.

[6]Department of Materials Science, Cornell University, Ithaca, N.Y.

paper (which we may call the upper-bound strain rate of wedge cracking), there is also a lower-bound strain rate condition.[7] The reason is that even when grain boundaries slide, if the sliding rate is too low, then the stress concentration at the triple junctions may not be high enough to initiate wedge cracks. Therefore if the strain rate during a tensile-going half cycle is too low, damage is reduced again, hence reversed effect.

In addition to this we think that the environmental effect must be better understood to fully account for the strain rate effect for this material.

[7] Min, B. K. and Raj, R., *Canadian Metallurgical Quarterly*, June 1979.

Chapter 6: Quantitative Microscopy and Mathematical Modeling for Basic Mechanisms of Fatigue

E. E. Underwood[1] *and E. A. Starke, Jr.*[1]

Quantitative Stereological Methods for Analyzing Important Microstructural Features in Fatigue of Metals and Alloys

REFERENCE: Underwood, E. E. and Starke, E. A., Jr., **"Quantitative Stereological Methods for Analyzing Important Microstructural Features in Fatigue of Metals and Alloys,"** *Fatigue Mechanisms*, Proceedings of an ASTM-NBS-NSF symposium, Kansas City, Mo., May 1978, J. T. Fong, Ed., *ASTM STP 675*, American Society for Testing and Materials, 1979, pp. 633-682.

ABSTRACT: This paper reviews the practical aspects of extracting quantitative microstructural data from microstructures of fatigued metals and alloys. In addition to the basic stereological information needed to characterize the essential geometrical elements of the structure, special methods are developed and described for quantifying more subtle effects. Thus, elongated structures, lamellar systems, gradients, and locational characteristics of particles are considered with respect to the fatigue process and its interactions with the microstructural features.

KEY WORDS: fatigue (materials), crack initiation, crack propagation, quantitative stereology, striations, quantitative analysis, microstructure, grain structure, inclusions, particle distribution

One of the primary goals of the materials scientist is to be able to design alloys for specific engineering applications using basic principles instead of trial-and-error methods. To reach this goal a thorough knowledge of the quantitative relationships between microstructure and engineering properties must be obtained. Considerable progress has been made in correlating microstructure with monotonic properties which involve gross yielding, such as yield strength and fracture toughness. However, our understanding of the quantitative effects of various microstructural features on both fatigue crack initiation and propagation is still lagging. The main difficulty can be attributed to the localized nature of the fatigue processes, and the fact that the

[1] Professor of metallurgy and professor of metallurgy and director, respectively, Fracture and Fatigue Research Laboratory, Georgia Institute of Technology, Atlanta, Ga. 30332.

important microstructural features are often heterogeneous. Thus they are more difficult to quantify than the generally uniform features that control the gross yielding process.

The routine stereological analysis [*1*][2] of the statistically uniform microstructural features is of definite value, not only for the sake of describing the type of alloy with which one is dealing, but also because any further quantification will require a quantitative base. First we describe methods for obtaining quantitatively the volume, surface area, line length, and number density of typical microstructural features important to fatigue. Both manual and automatic image analyses are employed. Next, we extract additional quantitative information that bears on the more intangible concepts, such as shape, orientation, and gradient effects. Also investigated are methods for improving the quantitative treatment of fracture surfaces, striation spacings, crack paths, particle randomness or segregation, and the projected images obtained from transmission electron microscopy (TEM). This is a difficult task, since sampling techniques, metallographic procedures, and stereological theory have not yet been fully worked out for these more specialized applications. However, much can be done at the present time to place the fatigue process on a closer quantitative basis with the alloy microstructure.

Basic Stereological Characterization of a Microstructure

Before it is possible to devise new techniques for the quantitative description of a particular microstructural feature, it is necessary to know quantitatively the basic characteristics of the microstructure. The measurements required for a basic characterization are fewer than generally realized. In the example chosen here for analysis, there are only three measurements to make, and they are all simple counting-type measurements. It should be emphasized that adequate sampling normally requires several fields of view and measurements on hundreds of particles or grains.[3] Here, however, we are only discussing methodology. The statistical confidence associated with the measurements is an important consideration, of course, and is dealt with in many publications [*2,3*].

Figure 1 shows a fairly equiaxed grain structure with largely spherical particles embedded in the matrix as well as the grain boundaries. Important basic quantities that can be obtained without assumptions concerning fea-

[2] The italic numbers in brackets refer to the list of references appended to this paper.

[3] An estimation of the number (N) of measurements (x) required to achieve a desired percent accuracy at a confidence level of 95 percent is given by

$$N = \left[\frac{200\, s(x)}{(\%\ \text{accuracy})\, m(x)}\right]^{1/2}$$

where x is the measurement P_P, P_L, N_A, etc. and $m(x)$ and $s(x)$ are the sample mean and sample standard deviation, respectively.

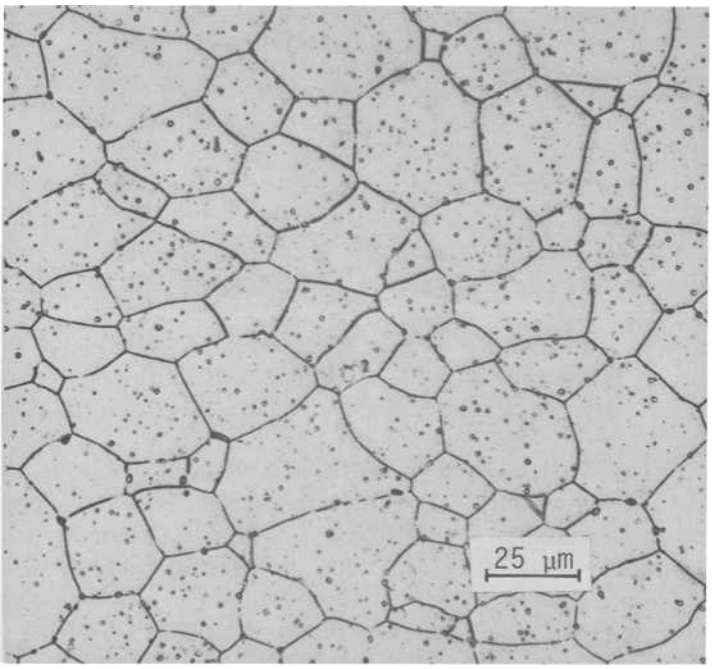

FIG. 1—*Light micrograph of an Al-5Mg-0.4Ag alloy illustrating equiaxed grain structure and spherical precipitates.*

ture size, shape, or location (other than the usual statistical requirements for sampling and measurements) are

- V_v volume fraction of particles,
- S_v grain boundary area per unit test volume,
- L_A length of grain boundary traces per unit test area,
- $\bar{L}$ mean grain (or particle) intercept length,
- N_A number of grains (or particles) per unit test area,
- $\bar{A}$ mean grain (or particle) intercept area, and
- λ mean free (straight-line) distance between particles.

Additional, more specialized information [*4*] may be desired about quantities such as:

- Q aspect ratio of nonequiaxed grains (or particles), equal to $\bar{L}_{\parallel}/\bar{L}_{\perp}$, the mean intercept lengths in the parallel and perpendicular directions, respectively,
- $(N_A)_{gb}$ number of grain boundary particles per unit test area
- N_l number of boundary particles per unit length of grain boundary traces

N_s number of boundary particles per unit area of the grain boundaries, and

N_v number of particles or grains per unit test volume [5].

Note that the subscript notation S_v, L_A, P_L, etc. represents fractions; for example, $S_v = S/V_T$, $L_A = L/A_T$, and $P_L = P/L_T$, where V_T, A_T, and L_T are the test volume, test area, and test line length, respectively.

The microstructure in Fig. 1 was subjected to three different types of point or number counting measurements [6]: a "point count," P_P; a point intersection count, P_L; and a grain or particle count, N_A.

The point count, P_P, was performed with a square net grid inscribed on a clear plastic sheet. The grid intersections (6 × 6) represent the test points, so $P_T = 36$. The grid is applied repeatedly to the microstructure at random locations and angles, and the number of points that hit the microstructural features of interest is counted. The ratio of hits to total number of test points gives P_P, or equivalently, V_v, the volume fraction.

The point intersection count, P_L, uses a linear test line or parallel array of test lines which is applied to the microstructure as described in the foregoing. The number of intersections of the test lines with grain boundary traces or particle boundaries is counted. Dividing by the total test line length gives P_L. Actually, the square net grid can be used for both the P_P and P_L counts, provided the length of the lines in the square grid is known. Here, for six horizontal and six vertical grid lines each of length 5 cm, $L_T = 2(6 \times 5$ cm$)/500 = 0.12$ cm, since the magnification is ×500.

The area density of grains and particles, N_A, is obtained by counting within a selected test area. (Normally this count would be repeated at several locations in several specimens.) In order to account for edge effects, the interior grains or particles N_{in} are counted as one each, while those cut by the edge of the test area N_e are counted as one-half each. Thus $N = N_{in} + \frac{1}{2}N_e$ and $N_A = N/A_T$. With a 5 × 5 cm test area and magnification of ×500, $A_T = 25/500^2 = 10^{-4}$ cm^2.

The results of the three counting measurements performed on Fig. 1 are summarized in Table 1. The basic quantities just listed are calculated first for the grains, using the applicable stereological equations [1]. The measurements for Q consist simply of P_L counts parallel and perpendicular to a chosen direction and show that the grains are somewhat elongated in the horizontal direction. The mean intercept length [7] $\bar{L}$ is still valid, however, regardless of grain shape or orientation. It has a single value for any single-phase structure, independent of grain boundary concavities or convexities, and is simply related to both S_v and L_A. Thus, it is an important quantity in its own right, in addition to being the "grain size" parameter of choice.

The particle calculations in Table 1 are similar to those for grains, except for the special counts of particles along the grain boundary traces [4]. Although both $(N_A)_{gb}$ and N_l are obtained experimentally, N_s requires some assumptions about particle size and shape. If we assume spherical particles

TABLE 1—*Procedure for determining basic microstructural data from Fig. 1.*

Grains

$S_v = 2P_L = 2(128/0.24) = 2(533.3) = 1066.7\ \text{cm}^{-1}$
$L_A = (\pi/2)P_L = 1.57(533.3) = 837.8\ \text{cm}^{-1}$
$\bar{L} = 1/N_L = 1/P_L = 1/533.3 = 1.87 \times 10^{-3}\ \text{cm}$
$N_A = (N_{\text{in}} + \frac{1}{2}N_e)/A_T = (13 + \frac{1}{2}\cdot 18)/10^{-4} = 22 \times 10^4\ \text{cm}^{-2}$
$\bar{A} = A_A/N_A = 1/N_A = 1/22 \times 10^4 = 4.55 \times 10^{-6}\ \text{cm}^2$
$Q = \bar{L}_{\parallel}/\bar{L}_{\perp} = (P_L)_{\perp}/(P_L)_{\parallel} = 600/466.7 = 1.29$

Particles

$V_v = P_p = 4/36 = 0.11$
$S_v = 2P_L = 2(1200) = 2400\ \text{cm}^{-1}$
$L_A = (\pi/2)P_L = 1.571(1200) = 1885\ \text{cm}^{-1}$
$\bar{L} = L_L/N_L = P_p/N_L = 0.11/600 = 1.8 \times 10^{-4}$
$N_A = (N_{\text{in}} + \frac{1}{2}N_e)/A_T = (610 + \frac{1}{2}\cdot 15)/10^{-4} = 6.2 \times 10^6\ \text{cm}^{-2}$
$\bar{A} = A_A/N_A = P_p/N_A = 0.11/6.2 \times 10^6 = 1.78 \times 10^{-8}\ \text{cm}^2$
$\lambda = (1 - V_v)/N_L = (1\text{-}0.11)/600 = 1.48 \times 10^{-3}\ \text{cm}$
$(N_A)_{\text{gb}} = N_{\text{gb}}/A_T = 64/10^{-4} = 64 \times 10^4\ \text{cm}^{-2}$
$N_l = (N_A)_{\text{gb}}/L_A = 64 \times 10^4/837.8 = 764\ \text{cm}^{-1}$

[*8*] of the same diameter D (which is not too bad an assumption in Fig. 1), then $\bar{A} = (2/3)A_{\max}$ and $A_{\max} = (\pi/4)D^2$ give us D, according to $D = [(6/\pi)\bar{A}]^{1/2} = [(6/\pi)(1.78 \times 10^{-8})]^{1/2} = 1.84 \times 10^{-4}$ cm. Since $N_s = (\pi/4)N_l/D$ for randomly positioned particles, we get $N_s = (\pi/4)764/1.84 \times 10^{-4} = 3.26 \times 10^6\ \text{cm}^{-2}$. The important spatial quantity N_v can also be estimated once D is known through the relationship [*9*] $N_v = N_A/D = 6.2 \times 10^6/1.84 \times 10^{-4} = 3.37 \times 10^{10}\ \text{cm}^{-3}$. Note that, more generally, D is the mean tangent diameter, and that the equation $N_v = N_A/\bar{D}$ is valid for any system of convex particles of the same shape.

A typical partially recrystallized microstructure is seen in Fig. 2. Because of the good contrast between recrystallized (light) and unrecrystallized regions (dark), the area fraction was determined both manually and automatically with the Bausch and Lomb Feature Analysis System (FAS). A comparison of results reveals that $P_P = 0.44\ (= A_A = V_v)$ was obtained with a 6×6 point grid, and the automatic measurements with the FAS gave an average value of 0.428. The areas selected for measurement were not the same, however, since the FAS sampled the entire metallographic specimen surface.

Spacings

Perhaps the most important, and general, spacing parameter is λ, the mean free distance [*10*]. This is the mean straight-line distance between particle perimeters, averaged over many directions of the test line. In a two-phase particulate alloy, λ is also the mean intercept length of the matrix, but because of its importance to particle strengthening and fatigue theories it is usually considered as a particle spacing instead.

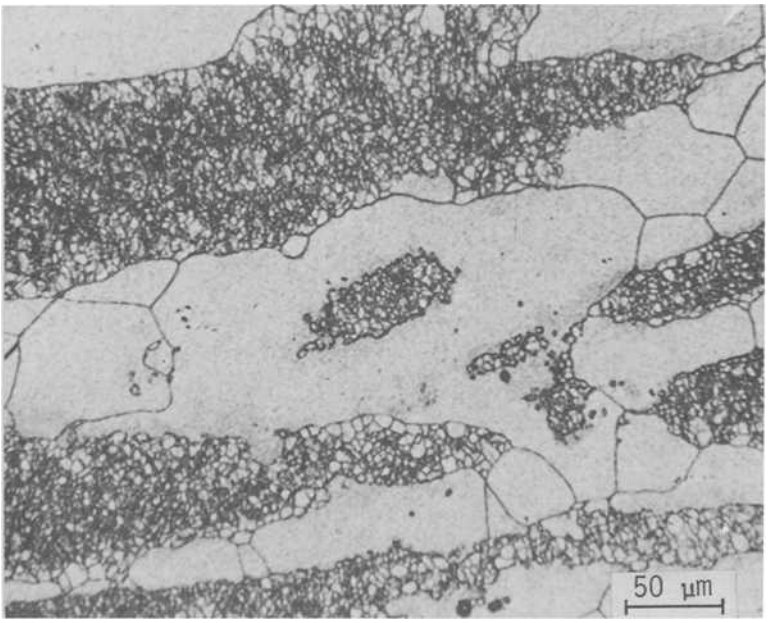

FIG. 2—*Light micrograph illustrating mixed recrystallized* (light) *and unrecrystallized* (dark) *structure of commercially processed 7050-T6X1 plate. Etched in 25 percent HNO_3 for 3 min at 70°C.*

Since $\lambda = (1 - V_v)/N_L$, where V_v and N_L refer to the particles, we see that λ is a completely general and assumption-free spacing parameter. When V_v is small with respect to unity, $\lambda \rightarrow 1/N_L$, which is the mean spacing between particle centers. In fact, for particles of any size, we define $\sigma = 1/N_L$ as the mean center-to-center particle spacing [*11*].

Another type of spacing that is used occasionally is the mean nearest neighbor spacing between particles or other features. Although many such spacings can be defined [*12*], there are only two rigorously correct expressions for point particles randomly located in a plane or in a volume [*13*], that is

$$\Delta_2 = \tfrac{1}{2} P_A^{-1/2} \tag{1}$$

and

$$\Delta_3 = 0.544 P_V^{-1/3} \tag{2}$$

where Δ_2 and Δ_3 are the mean two-dimensional and three-dimensional nearest neighbor spacings, respectively, and P_A and P_V are the number of

randomly located points in a plane, per unit area, and in space, per unit volume, respectively. From practical considerations, if the particles are small, we may substitute N_A for P_A and N_V for P_V without too much loss in accuracy. Because $\overline{D}$ can usually be estimated more readily than N_v, we use $N_v = N_A/\overline{D}$ and substitute in Eq 2, with $N_v \simeq P_v$, which results in

$$\Delta_3 = 0.544\overline{D}^{1/3} N_A^{-1/3} \tag{3}$$

Other relationships have been derived. For the planar distribution of inclusions in a fracture surface and in a section plane, Passoja and Hill [*14*] derive

$$\bar{r} = \frac{\sqrt{\pi}}{2} N_A^{-1/2} \tag{4}$$

where N_A is the number of particles per unit test area. In order to relate to dimple spacings, they use an expression due to Kocks [*15*]

$$\bar{\Delta}_{NN} = 1.18 N_A^{-1/2} \tag{5}$$

which takes into account the average distance $\bar{\Delta}_{NN}$ between a particle and the second or third nearest neighbors. This equation was used in an attempt to characterize particle spacings in a volume adjacent to the crack tip.

Characterization of Anisotropic Microstructures

A microstructure commonly encountered in fatigue studies is the partially or completely recrystallized structure [*16*]. In addition to the recrystallized regions, there may also be cold-worked regions, subgrain structure, particles, and anisotropic effects such as layering and grain elongation. The flattened, elongated grain structure is typical of metal-working operations, and is frequently encountered in alloys in which fatigue is important. There are several microstructural parameters that have proved useful for these elongated structures. One is a measure of the mean grain size L_3, that is, the mean intercept length for the three-dimensional grains; another is a shape parameter, the degree of orientation Ω_{23} for surfaces (2) in a volume (3); and a third is a directional spacing parameter, such as the mean distance $\overline{L(\theta, \psi)}$ between grain boundaries or other obstacles, in some specified direction.

The mean value of intercept length for a planar-linear system of surfaces [*17*] (which is the system seen in Fig. 3) can be determined according to

$$\bar{P}_L = 1/3\,[(P_L)_{\parallel} + (P_L)_{\mid} + (P_L)_{\perp}] = 1/\bar{L}_3 \tag{6}$$

where the directions of the P_L measurements parallel ($\parallel$ and $\mid$) and perpen-

dicular ($\perp$) to an orientation plane are specified graphically in Fig. 3. Also, an average grain volume can be calculated from the product of the three mean intercept lengths by the equation

$$\bar{V} = (\bar{L}_{\parallel\parallel})(\bar{L}_{\parallel})(\bar{L}_{\perp}) = \frac{1}{(P_L)_{\parallel\parallel}(P_L)_{\parallel}(P_L)_{\perp}} \tag{7}$$

This mean volume is equivalent to that of a rectangular parallelepiped, which is a good approximation to the actual grain shape. Or, if the diameter of an equivalent sphere of the same volume is required

$$D_{eq} = [(6/\pi)\bar{V}]^{1/3} \tag{8}$$

As before, the mean intercept length is still related to S_v through $2/\bar{L}_3$, and to L_A through $(\pi/2)/\bar{L}_3$.

For the particular system of oriented surfaces in our example—the planar-linear type—the degree of orientation is designated by $\Omega_{\text{pl-lin}}$ [*18*]. The value

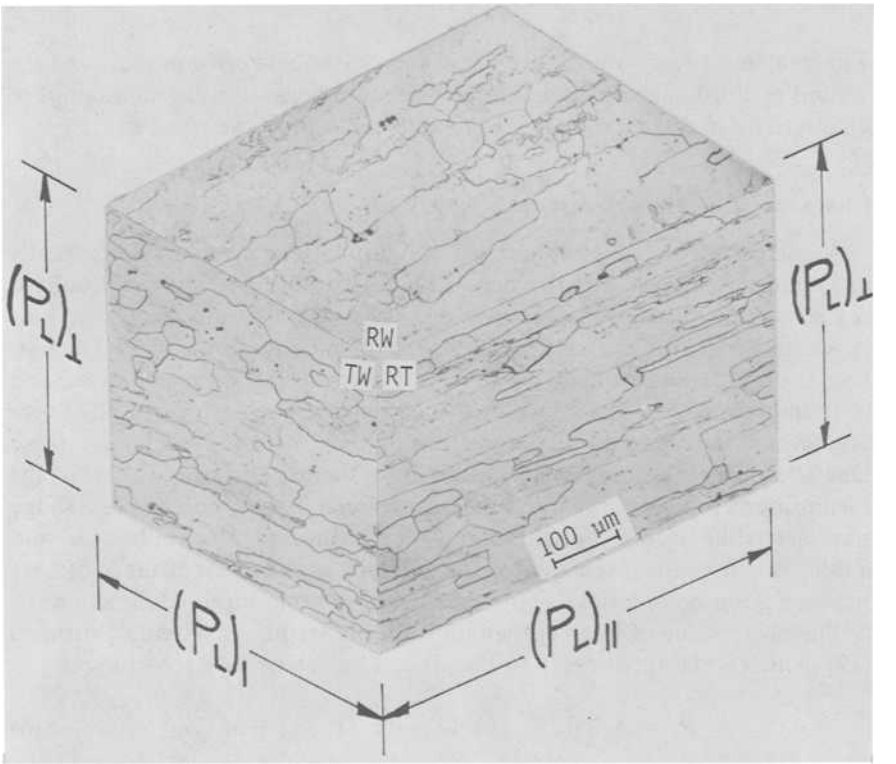

FIG. 3—*Microstructure of commercially processed 7050-T6X1 plate. Keller's etch.*

of this shape parameter varies between 0 and 1, representing, respectively, a complete lack of orientation and completely oriented surface elements of the system. In between, of course, we have the intermediate condition called a partially oriented system of surfaces. The defining equation is $\Omega_{\text{pl-lin}} = (S_v)_{\text{oriented}}/(S_v)_{\text{total}}$, where $(S_v)_{\text{oriented}} = (S_v)_{\text{planar}} + (S_v)_{\text{linear}}$. Since the derivation has been given elsewhere [*19*], the final expression for the total oriented surfaces is merely stated here

$$\Omega_{\text{pl-lin}} = \frac{(P_L)_\perp - 1.571\,(P_L)_{\parallel} + 0.571\,(P_L)_{|}}{(P_L)_\perp + 0.429\,(P_L)_{\parallel} + 0.571\,(P_L)_{|}} \tag{9}$$

The three orthogonal P_L measurements indicated by the isometric view were obtained in suitable directions from two photomicrographs of each plane. In order to indicate the amount of spread obtained, the individual values are given in Table 2. Substituting the three average values of $(P_L)_\perp$, $(P_L)_{\parallel}$, and $(P_L)_{|}$ from Table 2 into Eq 9 yields the answer, $\Omega_{\text{pl-lin}} = 69$ percent. This means that 69 percent of the total grain boundary surface area is oriented parallel to the orientation plane (the horizontal plane in Fig. 3). Successive changes in the microstructure as the result of further rolling, or annealing, can be followed by the new values of $\Omega_{\text{pl-lin}}$.

Another shape parameter that performs essentially the same function as $\Omega_{\text{pl-lin}}$ is the two-dimensional degree of orientation Ω_{12}, which measures the orientation of grain boundary traces, or lines (1) in a plane (2). Since the analysis requires only one plane, the amount of labor is considerably less. The applicable equations in this case [*20*] are

$$\Omega_{12} = \frac{(L_A)_{\text{oriented}}}{(L_A)_{\text{total}}} = \frac{(P_L)_\perp - (P_L)_{\parallel}}{(P_L)_\perp + 0.571\,(P_L)_{\parallel}} \tag{10}$$

By substituting appropriate values from Table 2, we find that $\Omega_{12} = 71$ percent. This is quite close to $\Omega_{\text{pl-lin}}$. In fact, a direct proportionality between $\Omega_{\text{pl-lin}}$ and Ω_{12} was observed experimentally in a study of foamed rubber cell

TABLE 2—*Basic microstructural data from Fig. 3 for calculation of* $\Omega_{pl\text{-}lin}$ *and* Ω_{12}.

	RT-Plane		TW-Plane	
	$(P_L)_{\parallel}$	$(P_L)_\perp$	$(P_L)_\perp$	$(P_L)_{|}$
Photo 1	54.4	204.2	216.7	111.1
Photo 2	48.9	277.1	289.6	118.9
Average	51.7 cm^{-1}	240.6	253.1	115.0 cm^{-1}
Avg $(P_L)_\perp$	..... 246.9 cm^{-1}			

structures in a number of specimens. If this finding proves valid for metallic specimens, then considerable saving in time and effort could be achieved. However, the planar-linear analysis does provide more information than the simpler two-dimensional treatment and may be required in some cases.

Directional Spacings

Directionality effects are frequently important, *per se*, and this is especially so in planar-linear structures. For example, in studies of crack growth in different directions, a linear parameter that reflects the mean spacing between barriers, in the same direction as the crack propagation direction (CPD), would have fundamental significance. The parameter of choice in many such cases would be the mean intercept length in the chosen direction. Thus, for crack growth studies in the short transverse direction in the transverse plane, we would need $\bar{L}_\perp$ (see Fig. 3). Provided grain boundaries were the only significant barrier, $\bar{L}_\perp$ can be calculated from $(P_L)_\perp = 246.9$ cm^{-1} (from Table 2), since $\bar{L}_\perp = 1/(P_L)_\perp = 4.05 \times 10^{-3}$ cm. For crack growth in other directions (θ, ψ) we could calculate the corresponding value of $\bar{L}(\theta, \psi)$, as required. If the important barriers proved to be layers of unrecrystallized material, or layers of fine recrystallized grains, their mean spacings could be calculated as readily as for the case of grain boundaries.

Another partially recrystallized microstructure selected for examination is shown in Fig. 4. This structure is considerably more complex than the first example, and several features are of interest. For example, the area fraction of recrystallized regions, their number, and their association with particles can influence the fatigue process. Because this is an anisotropic structure, the mean spacing perpendicular to the recrystallized lamellas is of interest, as is the mean spacing of grain boundaries normal to the crack growth direction. Other characteristics are also useful from time to time, such as the degree of orientation and the contiguity of particles and recrystallized regions. The results obtained from this microstructure are summarized in the following.

The mean spacings of the recrystallized lamellas, as well as the grain boundaries, were obtained in a direction normal to the orientation axis (horizontal direction). The applicable equation here for the lamellas is $(\bar{L})_\perp = 1/(N_L)_\perp$, where $(N_L)_\perp$ is the number of recrystallized layers intercepted per unit length of test lines normal to the orientation axis. For grain boundaries, we use $(\bar{L})_\perp = 1/(P_L)_\perp$ because the test lines are intersecting boundaries at a point. The results gave $(\bar{L}_\perp)_{lam} = 1/101.7$ $cm^{-1} = 98$ μm for the lamellas, and $(\bar{L}_\perp)_{gb} = 1/423.3$ $cm^{-1} = 24$ μm for the grain boundaries. A factor of over four times in spacing should help to reveal which barrier is the more important to crack growth.

Another outstanding attribute of this microstructure is its strong direc-

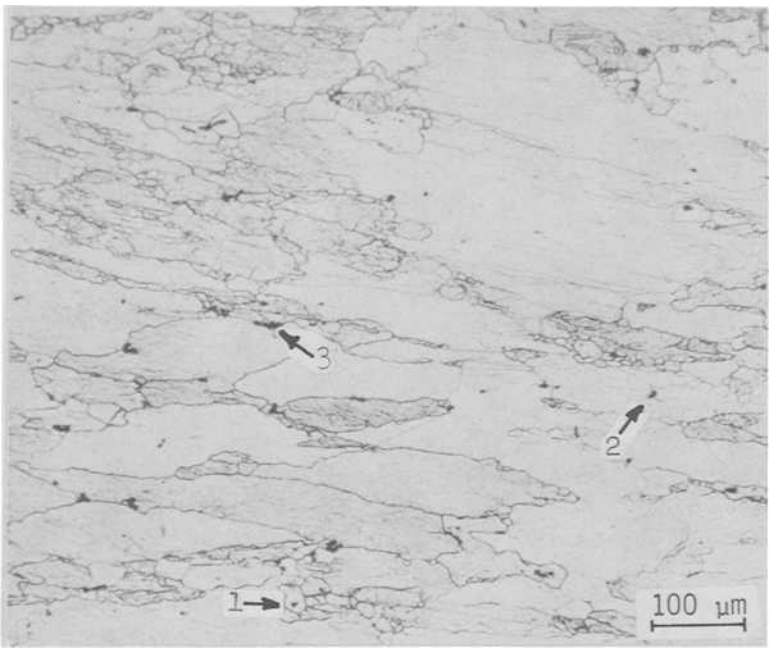

FIG. 4—*Microstructure of the TW section of a wrought Al-6Zn-1Cu-0.12Zr alloy. Keller's etch.*

tionality. Therefore, the degree of orientation Ω_{12} of boundary lines was calculated according to Eq 10 from values for $(P_L)_\perp = 258.3$ cm^{-1} and $(P_L)_{||} = 123.5$ cm^{-1}. The result, $\Omega_{12} = 41$ percent, demonstrates a strong directionality of boundaries in the rolling direction.

Contiguity [*21*]

One further facet of this structure was investigated. A strong correspondence was noted between particles (dark areas) and recrystallized regions in that particles were frequently observed embedded within or contiguous to recrystallized grains. A direct count of discrete, separated recrystallized regions totalled 90, while a count of associated particles yielded 64. Thus, 71 percent of the recrystallized clumps were associated with particles. Also of interest in this connection is the "contiguity" of particles and recrystallized grains [*22*]. This parameter can be expressed to give the ratio of interface area shared between particles (P) and recrystallized regions (R), compared with the total particle interface area ($PR + PM$), where M means

the "matrix" (or the balance of the microstructure). Thus we write the contiguity of particles as

$$C_{PR} = \frac{(S_v)_{PR}}{(S_v)_{\text{total}\,P}} = \frac{(S_v)_{PR}}{(S_v)_{PR} + (S_v)_{PM}} \tag{11}$$

or

$$C_{PR} = \frac{(P_L)_{PR}}{(P_L)_{PR} + (P_L)_{PM}} \tag{12}$$

In order to measure these quantities, a grid of parallel test lines is laid randomly over the microstructure, and the points of intersection with *PR* and *PM* interfaces are counted separately. The three arrows in Fig. 4 indicate the three possible types of particle interface combinations of interest here. One arrow points to a particle completely surrounded by a recrystallized grain (*PR* interface); another particle is completely surrounded by the matrix (*PM* interface); and the third particle is shared by recrystallized region and matrix (*PR* and *PM* interfaces). The contiguity parameter has demonstrated its usefulness in studies of crack propagation and fracture [*23*]; it should prove equally valuable in fatigue studies. (See later subsection, "Fatigue Cracks and Particles.")

Particle Positional Characteristics

A new procedure is discussed in this section for assessing the degree of randomness, or lack of randomness, of particle locations in a plane. The two photomicrographs shown in Fig. 5 are taken for examples. Pronounced "stringering" of particles is noted in the *RT*-plane with somewhat less layering effect in the *TW*-plane, which is a section normal to the *RT*-plane.

In order to obtain quantitative information on the degree of positional randomness, the particles locations are compared with those of a hypothetical statistically uniform distribution, and evaluated numerically by the χ^2 test for goodness of fit. The density of particles was determined within a 8 × 10 grid of 1-cm-square "cells" placed over the photomicrograph. For each of these 80 cells, the number of particles was counted separately and the cell densities recorded. Since the particles exhibited a preferential alignment, a modified cell was devised in which the basic square-cell data were amalgamated into eight horizontal strips each consisting of 10 of the original square cells. This new cell configuration, in which the cells are parallel to the stringers, can more easily reflect the physical realities of the microstructure.[4] Conversely, the data were also collected into 10 vertical strips in order to

[4] A similar procedure, based on point counts along parallel lines, has also been proposed [*24*].

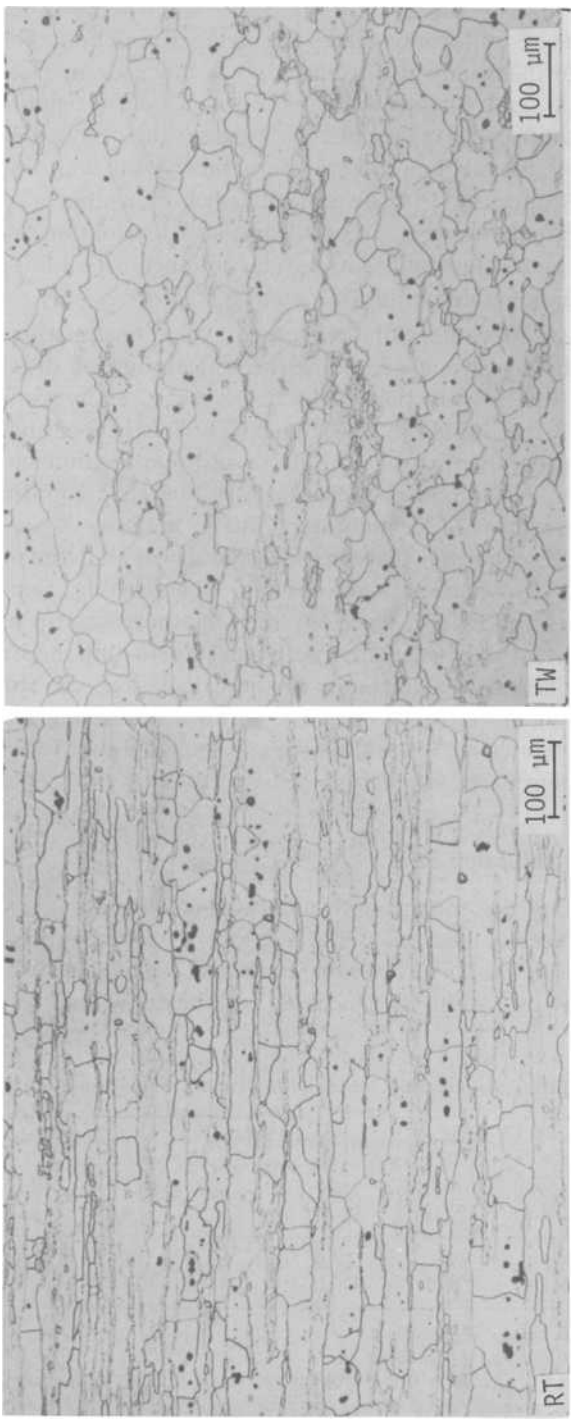

FIG. 5—*Microstructure of longitudinal (RT) and transverse (TW) sections of ITMT processed 7050-T6X1 plate. Keller's etch.*

check particle site uniformity across the stringer direction. The findings of this analysis for the two microstructures in Fig. 5 are summarized in Table 3.

The results are conveniently evaluated by means of the r-parameter, where $r = \chi_{meas}^2/\chi_{th}^2$. This parameter merely expresses the degree of divergency or fit of the experimental data referred to a theoretical uniform distribution with expected value E. The theoretical distribution appears to represent physically the attributes expected of a "random" distribution of particles in a plane, and compares favorably with results obtained with a Poisson distribution or from random number tables.

It can be seen in Table 3 that the particle locations measured with horizontal strips diverge strongly from the theoretical uniform distribution (r = 4.6 and 3.2). However, the particle locations measured by vertical strips are quite uniformly distributed (r = 0.7 and 1.1). This type of analysis appears to possess considerable practical utility in addition to simplicity of calculation. Moreover, with good particle contrast, the strip counting technique may be performed readily by automatic image analysis.

The same RT specimen which provided Fig. 5 was analyzed on the Bausch and Lomb FAS for particle heterogeneity. The variable frame control reduced the measured field on the TV screen to a narrow strip parallel to the particle stringers. Particle densities were measured within the strip at each of 12 successive locations. The results of the calculations are summarized as follows: $\chi_{meas}^2 = 59.71$; $\chi_{th}^2 = 18.31$; $r = 3.3$. Considering that a different field of view was analyzed here than the one shown in Fig. 5 (RT-plane), the agreement is considered excellent.

Fatigue Crack Initiation Sites

Microstructure control through modification of conventional processing methods has recently been examined as a way of upgrading the fatigue resistance of 7XXX alloys [*25*]. A commercially processed (CP) 7050-T6X1 alloy, with a partially recrystallized structure (~ 50 percent), and an intermediate

TABLE 3—*Analysis of locational randomness of particles in Fig. 5.*

Specimen	Total No. of Particles	Horizontal Rows (8)[a]			Vertical Columns (10)[b]		
		E	χ_{meas}^2	r	E	χ_{meas}^2	r
RT	195	24.4	57.9	4.6	19.5	11.2	0.7
TW	247	30.9	40.0	3.2	24.7	16.6	1.1

[a] $\nu = 6$, $p = 0.05$, $\chi_{th}^2 = 12.59$.
[b] $\nu = 8$, $p = 0.05$, $\chi_{th}^2 = 15.5$.
[ν is the degree of freedom, p the probability, and χ_{th}^2 the theoretical (tabular) value of χ-square. E is the expected value and r is the ratio $\chi_{meas}^2/\chi_{th}^2$.]

thermomechanically processed (ITMT) 7050-T6X1 alloy, with a fine, equiaxed, recrystallized grain structure, have been chosen for analysis. Micrographs were prepared from tension-compression low-cycle fatigue specimens, $\Delta\epsilon_T/2 = 1.2$ percent, at 100 cycles and at 300 cycles from the prepolished and unetched surfaces (see Figs. 6 and 7).

Several basic stereological measurements were performed on both alloys. With respect to the crack traces observed at the various sites, four quantities are of interest. They are L_A, the total length of crack traces per unit test area; N_A, the number of crack initiation sites per unit test area; $\bar{L}$, the mean crack length per site; and Ω_{12}, the degree of orientation of the crack traces with respect to the direction normal to the stress axis. These measurements are documented for the CP alloy at 100 cycles shown in Figure 6. The applicable equation for total crack length per unit area [*26*] is

$$L_A = \left(\frac{\pi}{2}\right) P_L \tag{13}$$

where P_L is the number of crack traces intersected by unit length of a test grid. In this case, a grid of 38 × 38 lines with ½-cm spacing was applied as described earlier to the micrograph, giving the number of intersections $P = 164$. The test length, L_T, when corrected for magnification, is equal to 7.16 cm. Thus $P_L(=P/L_T) = 164/7.16 = 22.91$ cm^{-1}, and $L_A = 35.99$ cm^{-1}. The next quantity, $N_A(=N/A_T)$, for the same alloy and condition, is obtained by a count of separate cracks, giving $N = 84$. The number of cracks per unit area, N_A, then equals $84/(19 \times 24/250^2)$ or 11.5×10^3 cm^{-2}, since the linear magnification is ×250. The mean crack length, L, is equal to L_A/N_A. In this case $\bar{L} = 35.99/11.5 \times 10^3$, giving a value of 31.3 μm. The fourth parameter calculated here is Ω_{12}, the degree of orientation for lines in a plane, which is defined in Eq 10. It has the value of 0 for crack traces with completely random orientations, and a value of unity when they are completely parallel to the orientation direction. Since the crack traces tend to lie normal to the stress axis, the horizontal direction is chosen for the orientation axis. Thus $\perp$ and $\parallel$ refer to measurement directions of the grid perpendicular and parallel, respectively, to the chosen orientation axis. In this case, we find that $(P_L)_\perp = 24.58$ cm^{-1} and $(P_L)_\parallel = 21.23$ cm^{-1}, giving a value for Ω_{12} of 9.13 percent. These four basic quantities are tabulated in Table 4 for each of the four alloy conditions shown in Figs. 6 and 7.

Note that the crack orientations in the CP alloy are almost random—only 9 percent of the linear elements are aligned parallel to the orientation axis. In the ITMT alloy, however, we see that about one fourth of the total crack trace length is oriented normal to the stress axis. It is also noteworthy that the degree of orientation for both alloys does not change significantly between 100 and 300 cycles, even though the total crack length increases by a factor greater than three.

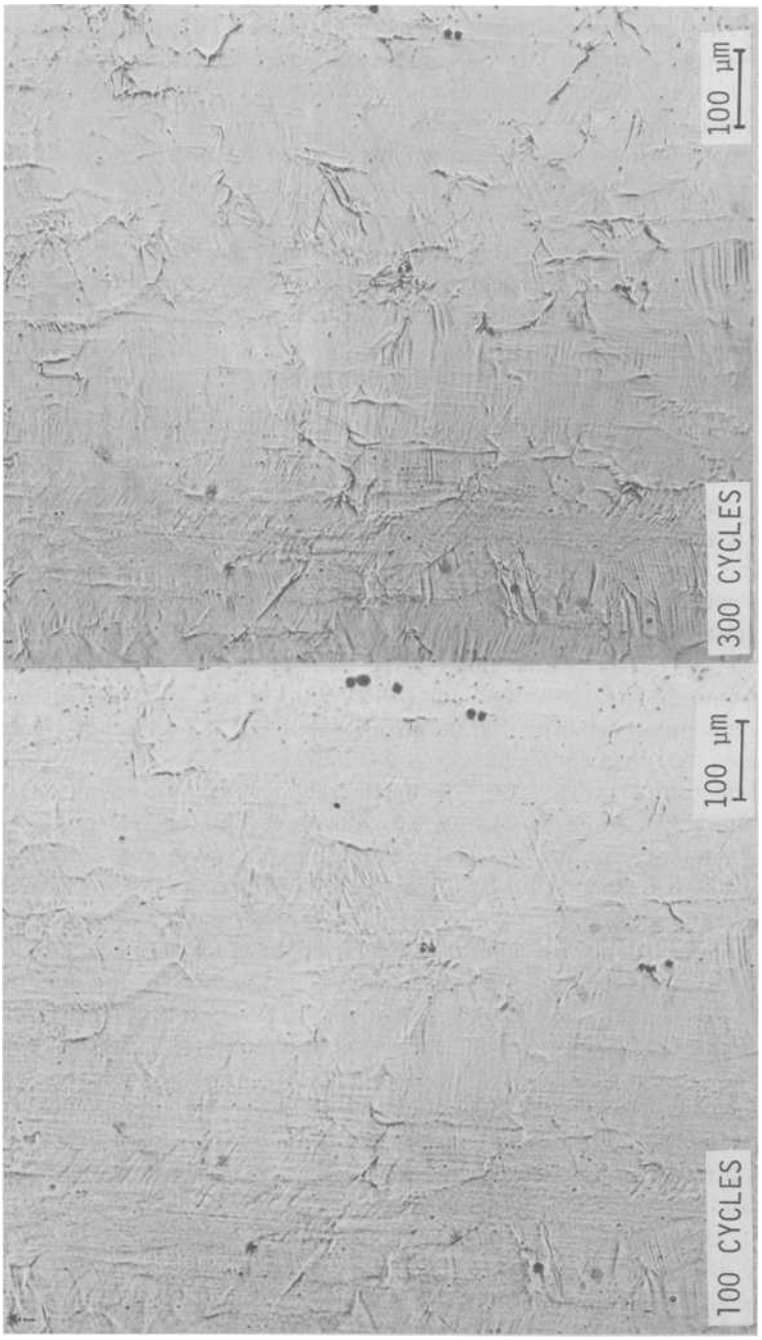

FIG. 6—*Light micrographs of a tension-compression low-cycle fatigue specimen of commercially processed 7050-T6X1. Stress axis vertical,* $\Delta\varepsilon_T/2 = 1.2$ *percent. Unetched.*

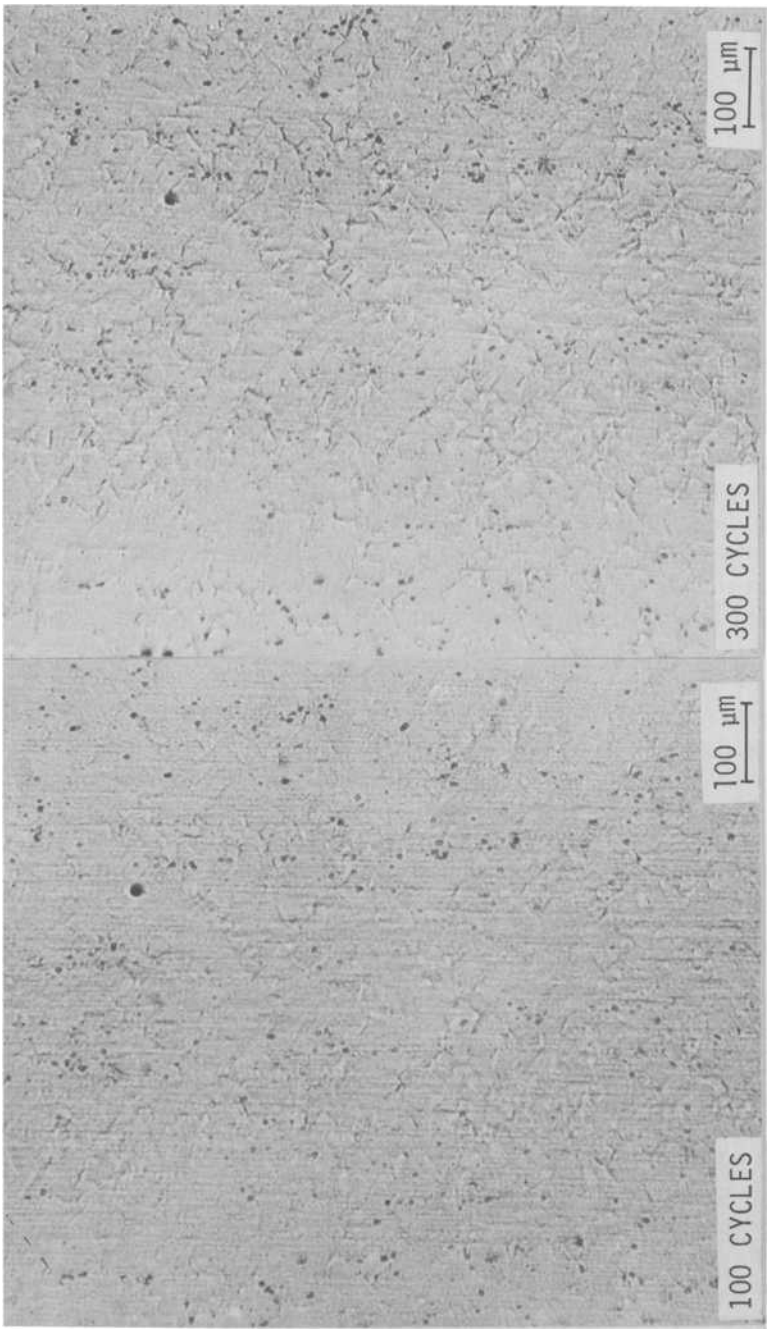

FIG. 7—*Light micrographs of a tension-compression low-cycle fatigue specimen of ITMT processed 7050-T6X1. Stress axis vertical,* $\Delta\epsilon_T/2 = 1.2$ *percent. Unetched.*

TABLE 4—*Basic microstructural crack parameters for CP and ITMT processed 7050 alloys after fatigue testing for 100 and 300 cycles.*

	CP-7050[a]		ITMT-7050[b]	
Parameter	100 Cycles	300 Cycles	100 Cycles	300 Cycles
L_A, cm^{-1}	35.99	108.82	19.45	63.34
N_A, cm^{-2}	11 513	32 740	9589	26 849
$\bar{L}$, μm	31.3	33.2	20.3	23.6
Ω_{12}, %	9.13	9.06	27.4	24.8

[a] See Fig. 6.
[b] See Fig. 7.

Etched specimens of the CP and ITMT alloys show that the grain size is much finer and more uniform in ITMT than CP, and that coarse slipbands appear only in the CP alloy. These factors may account for the 50 percent greater mean crack length in the CP alloy. Moreover, the stronger, finer grain size ITMT alloy also has fewer crack nuclei. The grain shape in ITMT is quite equiaxed and the alloy is completely recrystallized, while the CP alloy is only partially recrystallized and the grains are relatively large and elongated along the stress axis. Thus the ITMT grain boundaries are more randomly oriented, providing more boundaries at 90 deg to the stress axis for crack paths, as reflected in the higher values of Ω_{12}.

It may be significant that the number of crack initiation sites is greater in the CP alloy, even though there are fewer grains per unit area. Moreover, it appears that numerous crack nuclei have originated at slipband traces, which would account for the lower degree of orientation of crack traces in the CP alloy. It should be noted that grain size, grain shape, and length and orientation of the slipband traces can also be determined quantitatively, and the techniques for doing this have been described in the foregoing.

Additional information on the angular distribution of crack traces is provided by the rose-of-the-number-of-intersections (called the "rose," for short). This is a polar plot that portrays graphically the density of intersections $P_L(\theta)$ of crack traces with the test lines, as a function of angle θ, with respect to the orientation axis [*27*]. Figure 8 gives the rose plot for the ITMT alloy after 100 and 300 cycles. From the characteristics of these curves, it can be deduced that the angular distribution of crack traces belongs to the classification "partially oriented system of lines in a plane." It is also of interest that the degree of orientation (Ω_{12}) of both curves is essentially the same, even though P_L at 300 cycles is more than three times greater than at 100 cycles. The rose shows us that the value of $P_L(\theta)$ proceeds smoothly from a minimum value at $\theta = 0$ deg to a maximum value of $P_L(\theta)$ at $\theta = 90$ deg. This implies that the crack sites are preferentially located at the randomly oriented grain boundaries. The evidence in Fig. 7, as well as in etched photomicrographs, appears to confirm this suggestion qualitatively.

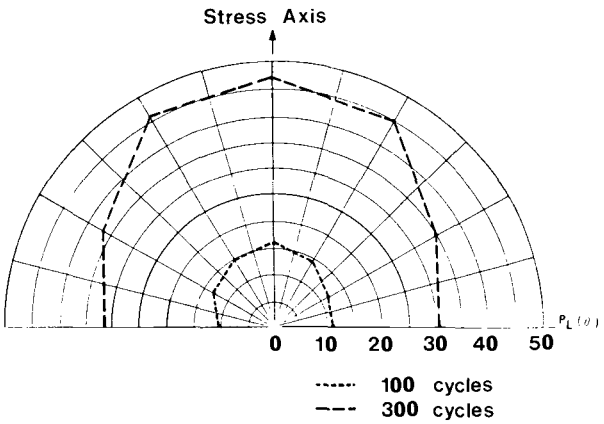

FIG. 8—*Distribution of crack traces represented as density of intersections* $P_L(\theta)$ *versus angle* θ *for the LCF specimen of ITMT-7050 shown in Fig. 7.*

Particle-Crack Site Interactions

The possible role of particles on the crack site initiation behavior can be investigated by a statistical technique. The relatively large particles in Fig. 7 are disposed more in vertical columns than randomly. Some particles are associated with crack sites, but many are not. In order to assess the degree of *positional* randomness, the particle locations are compared with those of a hypothetical uniform distribution, and evaluated numerically by the χ^2 test for goodness of fit as described earlier in "Particle Positional Characteristics." The experimental details are somewhat different. Here we use 9 vertical columns and 11 horizontal rows to analyze the particle locations. The results of this analysis for the ITMT alloy after 300 cycles are summarized in Table 5.

It can be seen immediately that the particle locations as measured with vertical strips diverge strongly from the theoretical uniform distribution, and

TABLE 5—*Particle and crack site uniformity of location analysis in ITMT 7050-T6X1 alloy after 300 cycles.*

Particle Distribution		Crack Site Distribution	
(Total No. Counted = 844)		(Total No. Counted = 182)	
Vertical Cells (9)	Horizontal Cells (11)	Vertical Cells (9)	Horizontal Cells (11)
$\chi_{vert}^2 = 55.67$ $\chi_{th}^2 = 14.067$	$\chi_{hor}^2 = 18.21$ $\chi_{th}^2 = 16.919$	$\chi_{vert}^2 = 13.00$ $\chi_{th}^2 = 14.067$	$\chi_{hor}^2 = 13.60$ $\chi_{th}^2 = 16.919$
$r = 3.96$	$r = 1.08$	$r = 0.92$	$r = 0.80$

this is reflected by a χ_{vert}^2 almost four times greater than χ_{th}^2. However, the particle locations measured by horizontal strips are quite uniformly distributed ($r = 1.08$). The same measurements were made for the crack site locations. In this case, the verticle and horizontal cell analyses both yield r-values less than unity ($r = 0.92$ and $r = 0.80$), which would indicate excellent uniformity of location of the crack sites. As a conclusion, we may state that the large, stringered particles in the ITMT alloy do not interact significantly with the randomly nucleated crack sites.

A less elaborate analysis of particle interactions with crack sites is afforded by the CP alloy microstructure. Figure 6 reveals that particle size and volume fraction are significantly less than in the ITMT alloy (Fig. 7). However, a close inspection of Fig. 6 shows that a large number of crack sites are associated with small particles. In fact, in the 100-cycles specimen, only 18 out of 84 crack sites do not appear to have particles present, and many of those without particles appear to originate at slipband traces. Thus there seems to be a critical particle size effect, such that below a certain size, particles at grain boundaries interact significantly with crack nucleation. At larger particle sizes, the effect appears to be lost.

Fatigue Crack Characteristics

Conventionally, crack lengths in fatigued specimens are monitored along the specimen surface by optical comparators or ultrasonic probes. Metallographic specimens usually show only the two-dimensional trace of the crack, edge-on and parallel to the CPD. The length measured actually corresponds to the *projected* length (from initial point to the crack tip) and not to the true length of the meandering crack. Moreover, for some purposes, it is the true crack surface area that is required, rather than the simple linear quantity.

Within these qualifications, there are still several important features of the crack—its own characteristics and the interactive aspects—that require quantification. Among these more important features are the extent of transgranular versus intergranular path length, the "true" crack length versus the projected crack length, the extent of branching, and the actual crack surface area. Interactions of cracks with grains and subgrains, with particles, recrystallized regions, and slipband traces are also important. The methods of quantification, both generally and for special cases, are discussed for several specific microstructures.

True Crack Lengths

Figure 9 represents a typical branched fatigue crack in an underaged (4 h at 120°C) aluminum-zinc-magnesium (zirconium) alloy, compact tension specimen, $\Delta K = 10$ MPa·m$^{-1/2}$. The first item of interest is the conventional crack length, or the length from initial point to the crack tip, mea-

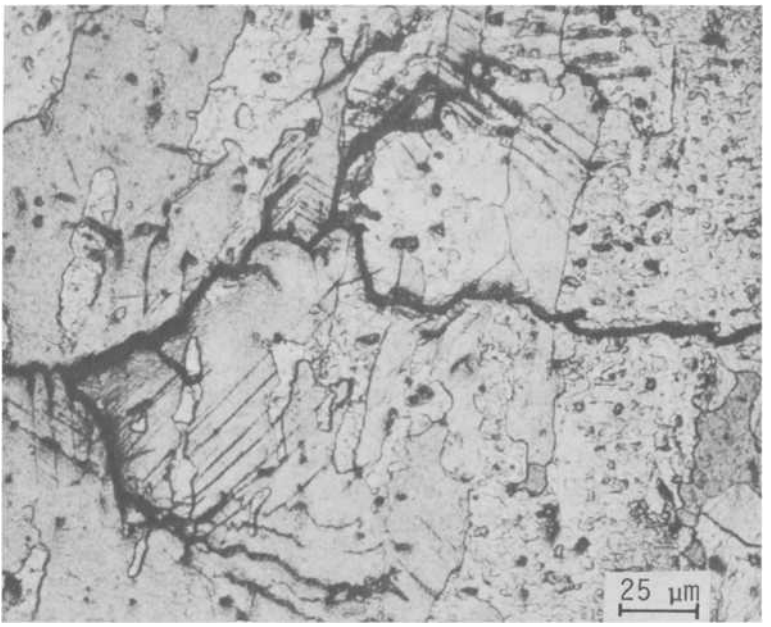

FIG. 9—*Light micrograph illustrating crack path of an underaged (4 h at 120°C) Al-6Zn-2Mg-0.11Zr alloy. Compact tension specimen, laboratory air, $\Delta K = 10$ MPa·m$^{-1/2}$. Keller's etch.*

measured in a direction parallel to the main crack growth direction. This distance, the projected length, is $L' = 0.025$ cm.[5] In contrast, the total true crack length L_t consists of all linear elements of the crack traces, whether belonging to the main branch, subbranches, or disconnected segments. The total true crack trace length per unit area is simply L_A or L_t/A_T, where A_T is the test area. Since $L_A = (\pi/2)P_L$, the absolute value of length is

$$L_t = \left(\frac{\pi}{2}\right) P_L A_T \tag{14}$$

and P_L is the number of points of intersection of crack traces with the test lines, applied at many angles, per unit length. In order to avoid some subtle problems, it is generally advisable to clearly define a convenient test area and then apply a test grid of parallel lines that covers the entire test area from all angles. The test line length in this case is considered to be the same regardless of angle of placement.

[5]The prime indicates a projected quantity; here, linear elements in a plane are projected to a projection line.

Based on the procedure just outlined, L_t for the total crack length is obtained from Eq 14 according to $L_t = (\pi/2)\ 70.6\ (9 \times 10^{-4}) = 0.0998$ cm. Intersection measurements on the main crack trace give a value of only $L_t = 0.0272$ cm. Thus, we have in summary

$$\begin{aligned} &\text{Total crack length:} \quad L_t = 0.0998 \text{ cm} \\ &\text{Main crack length:} \quad L_t = 0.0272 \text{ cm} \\ &\text{Projected length:} \quad L' = 0.025 \text{ cm} \end{aligned}$$

Some significant crack length ratios are:

$$\frac{(L_t)_{\text{total}}}{L'} = 3.99, \quad \frac{(L_t)_{\text{total}}}{(L_t)_{\text{main crack}}} = 3.67, \quad \text{and} \quad \frac{(L_t)_{\text{main crack}}}{L'} = 1.09$$

It is important that these typical characteristics of fatigue cracks be considered in the detailed analysis of the crack growth process.

In addition to crack length studies, the degree of orientation Ω_{12} for branched cracks is also pertinent to macroscopic crack growth measurements. Based on simple measurements of $(P_L)_\perp$ and $(P_L)_{||}$, Eq 10 yields a value of $\Omega_{12} = 17.5$ percent. This is a rather small percentage of total crack length to be oriented in the crack growth direction.

Crack Surface Area

A general problem is that of expressing the extent of cracking in terms of the actual crack surface area. When estimating the energy of forming a crack, for example, a parameter of interest is surely the true crack surface area. Two situations can be handled quantitatively from the usual crack trace on a polished specimen surface. For randomly oriented crack surface elements, we invoke the general equation

$$S_v = \left(\frac{4}{\pi}\right) L_A \tag{15}$$

between crack surface area per unit volume and crack trace length per unit area. Serial sectioning may be necessary to improve the accuracy of the results. On the other hand, when crack surface elements are all normal to the plane of the crack trace, then another equation [*28*] applies. It is

$$(S_v)_\perp = L_A \tag{16}$$

which states simply that the area per unit volume of crack surfaces perpendicular to the crack trace plane is equal numerically to the length of crack trace per unit area on that plane. The magnitude of the difference between these two cases is calculated for the main crack. For random crack surfaces

we would have $S_v = (4/\pi)L_A = 2P_L = 2(29.17) = 58.3\ \text{cm}^{-1}$; for oriented crack surfaces normal to the crack trace plane, we find $(S_v)_\perp = L_A = (\pi/2)P_L = 1.571\ (29.17) = 45.8\ \text{cm}^{-1}$. Thus there is a 27 percent difference in crack surface area between an oriented and a random crack surface for the same length of crack trace. As the crack surface tends more toward flatness, the coefficient between L_A and S_v will move closer to unity. Inspection of the fracture surface with SEM should serve to guide the estimate of the coefficient to be used.

Transgranular versus Intergranular Crack Paths

An analysis of the fatigue crack path through recrystallized grains of ITMT-7050-T6X1 alloy was also undertaken. Figure 10 shows a crack that

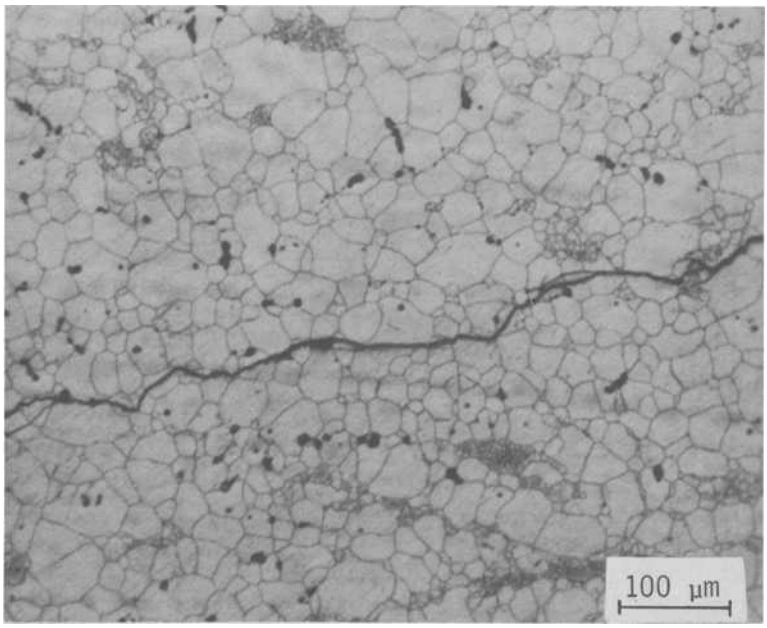

FIG. 10—*Light micrograph illustrating crack path of an ITMT-7050-T6X1 alloy. Compact tension specimen, dry* N_2, $\Delta K = 8\ MPa \cdot m^{-1/2}$. *Etched in 25 percent* HNO_3 *at 70°C.*

has progressed from left to right, across grains and through grain boundaries. In order to determine the extent of transgranular crack path versus the amount of intergranular fracture, a random P_L intersection count was performed. Intersections of a randomly applied linear test grid with transgranular crack elements gave $P_{trans} = 24$, and for intergranular crack

elements, $P_{inter} = 14$. Equation 14, $L_l = (\pi/2)P_L A_T$, gives the following results

$$L_{trans} = 1.571\ (14.0)\ 1.84 \times 10^{-3} = 40.5 \times 10^{-3}\ \text{cm}$$
$$L_{inter} = 1.571\ (8.17)\ 1.84 \times 10^{-3} = 23.6 \times 10^{-3}\ \text{cm}$$
$$L_{total} = 1.571\ (22.17)\ 1.84 \times 10^{-3} = 64.1 \times 10^{-3}\ \text{cm}$$

Ratios of these quantities show that

$$\frac{L_{trans}}{L_{inter}} = \frac{P_{trans}}{P_{inter}} = \frac{24}{14} = 1.7, \text{ and } \frac{L_{trans}}{L_{total}} = \frac{P_{trans}}{P_{total}} = \frac{24}{38} = 0.63 = (l_l)_{trans}$$

Thus it is seen that the crack definitely favors the transgranular path. The ratio $(l_l)_{trans} = 0.63$ is the lineal fraction of transgranular crack length *along the crack path*; as such it is not the same as the lineal fraction L_L obtained with straight test lines over the microstructure. Crack interaction with particles appears negligible, although particles on the fracture surface were noticeable.

A direct count was made of the grains in Fig. 10 that were cut transversely or intergranularly by the crack path. The numbers obtained, $N_{trans} = 20$ and $N_{inter} = 15$, yield a ratio $N_{trans}/N_{inter} = 1.33$, which compares roughly with $L_{trans}/L_{inter} = 1.7$. A simple count may suffice for some purposes when more elaborate procedures are not justified. The grain size was measured in a direction parallel to the crack path, giving the mean intercept length $\bar{L}_{||} = 20\ \mu\text{m}$. Cracking is also seen to occur through subgrains in an aluminum-zinc-magnesium-copper alloy, in Fig. 11. The crack path runs parallel to a layer of coarse recrystallized grains, and except for a few larger subgrains or grains, the crack follows a mostly intersubgranular path, that is, $L_{inter}/L_{total} = 0.61$. The ratio of $L_{inter}/L_{trans} = 1.55$ compares well with the grain count ratio $N_{inter}/N_{trans} = 1.62$ in these very fine subgrains ($\bar{L}_{||} = 2\ \mu\text{m}$). A TEM of the subgrains in the same alloy is shown in Fig. 12. The low-angle boundaries are heavily populated with η'-precipitates which are believed to be partially responsible for the crack preference for subgrain boundaries. A brief analysis is made later of precipitates at boundaries as measured from thin foil photomicrographs.

Fatigue Cracks and Particles

Cracking at particles is also a common occurrence in fatigued specimens. Figure 13 shows a cluster of particles in a fatigued ITMT-7475-T6 alloy. Several features of interest are observed, such as cracked particles, voids, debonding, and crack nuclei at the particle interface. Void volume fraction can be measured by a point count, $P_P = V_v$; particle crack length by an intersection count, $L_A = (\pi/2)P_L$; interfacial length where debonding occurs,

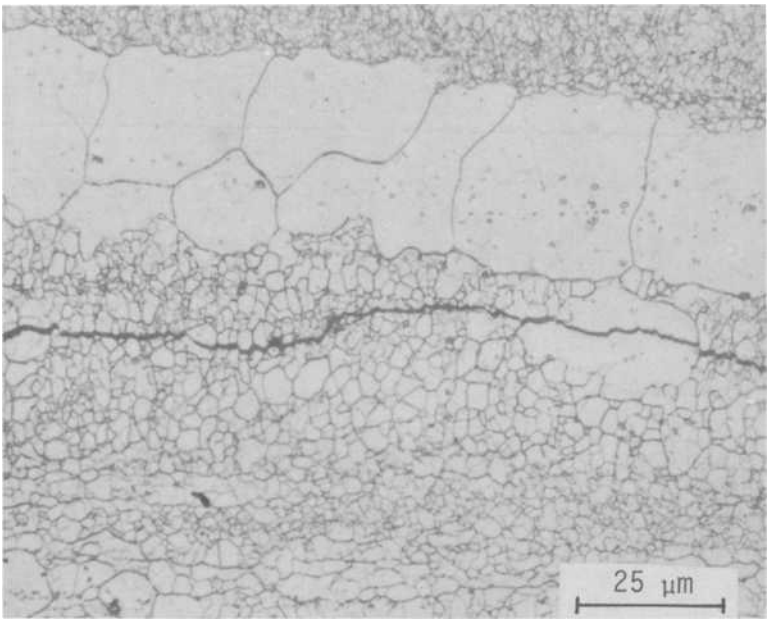

FIG. 11—*Light micrograph illustrating crack path in subgrains of unrecrystallized region of an Al-6Zn-2Mg-2Cu-0.12Zr alloy aged 24 h at 120°C. Compact tension specimen, distilled* H_2O, $\Delta K = 6\ MPa \cdot m^{-1/2}$. *Etched in 25 percent* HNO_3 *at 70°C.*

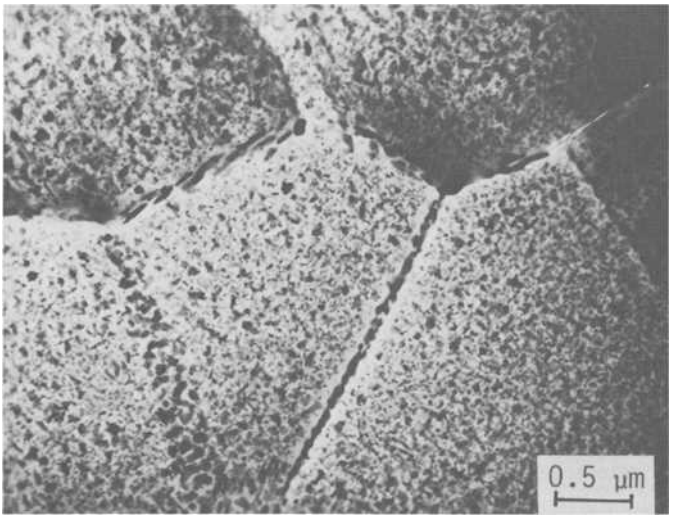

FIG. 12—*TEM of an undeformed section of the specimen shown in Fig. 11 illustrating precipitates along subgrain boundaries of unrecrystallized grains.*

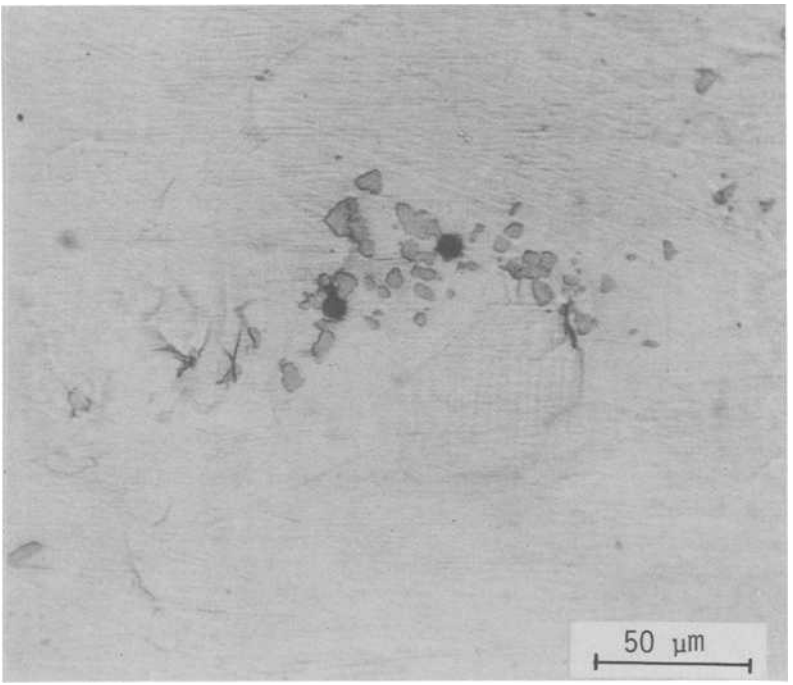

FIG. 13—*Light micrograph of an ITMT-7475-T6 LCF specimen showing cracked particles and small fatigue cracks. Stress axis horizontal. Unetched.*

also by L_A; and void-particle proximity can be evaluated by the contiguity parameter C (see Eqs 11 and 12).

The particle projected length with respect to a chosen projection line has been used in studies of fatigue-particle interactions [*29*]. The projected length L' can be obtained directly for each particle in the field of view by means of automatic image analysis. This would be extremely laborious if done manually. However, the *mean* projected length for a system of particles is not too difficult to measure. We use the equation

$$\bar{L}' = (N_L)_\perp / N_A \tag{17}$$

where $(N_L)_\perp$ is the number of particles intercepted by test lines perpendicular to the projection line, per unit length, and N_A is the number of particles per unit area.

To illustrate the procedure, we decide to measure the mean projected length of the particles in Fig. 13 with respect to a vertical projection line. A grid of parallel lines 1 cm apart was positioned perpendicular to the projection line at four different locations within the selected test area. Forty-eight

particles were hit, giving $(N_L)_\perp = (48 \times 4000)/(4 \times 80) = 600\ \text{cm}^{-1}$, since the magnification is $\times 4000$. The number of particles counted within the same test area was 37, and $N_A = (37 \times 4000^2)/80 = 7.4 \times 10^6\ \text{cm}^{-2}$. Therefore, the mean projected length is found to be $\bar{L}' = 600/7.4 \times 10^6 = 0.81\ \mu\text{m}$. Further details of the possibilities here can be found in the treatments of projections from a plane to a projection line [*30*].

Fatigue Striations

Microscopic features of the fracture surface have been correlated many times with macroscopically measured crack growth rates in mechanistic studies of fatigue crack propagation. One such feature, the fatigue striation spacing, is associated with local crack growths rates which may or may not be different from the macroscopically measured values. Theoretically, calculated crack growth rates should be correlatable with the striation spacing measured on the fracture plane in the local growth direction. This is only true, of course, when the striation mode of crack propagation controls the fatigue crack growth. For mixed-mode crack propagation, the amount of each mode must be assessed quantitatively for accurate theoretical analysis.

There are at least two general problems underlying the measurement of fatigue striation spacings (FSS). First, the normals to the striations do not always lie in the crack direction, and secondly, the striations usually occur on fracture surfaces that are decidedly nonplanar. These problems are illustrated in Fig. 14, which represents a typical fracture surface with striated facets oriented at many angles [*31*].

Measurement of "True" FSS in the Projection Plane

Most microscopic analysis is done on flat photomicrographs or images of the fracture surface, such as obtained from replicas by TEM or scanning electron microscopy (SEM). Thus we are dealing with projected images, and the stereological relationships applicable to this situation must be invoked in order to extract as much quantitative information from the projection plane as possible [*30,32*].

Four types of striated fracture surfaces are of interest to this study. Figure 15 illustrates their important characteristics as they would appear in a TEM photomicrograph. For example, the striations in Fig. 15*a* cover the specimen fracture surface completely. The FSS are quite uniform, and the striation directions (their normals) are all fairly close to the CPD. In Fig. 15*b*, the major difference is that the striation-facet directions are oriented differently with respect to the CPD. The striated facets in Fig. 15*c* are much the same as in Fig. 15*a* or *b*, but do not cover the fracture surface completely. This situation obscures the direct FSS relationships found in the literature [*33*] because of the mixed mode of fracture. In Fig. 15*d*, we see striations covering the

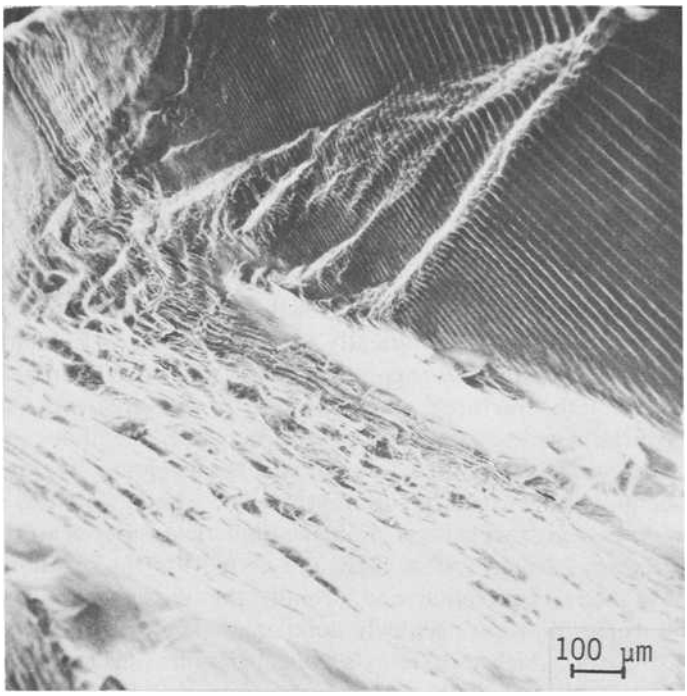

FIG. 14—*SEM of a disordered Cu_3Au single crystal LCF specimen.* $\Delta\epsilon_T/2 = 0.85$ *percent*, $N_f = 1800$ *cycles*.

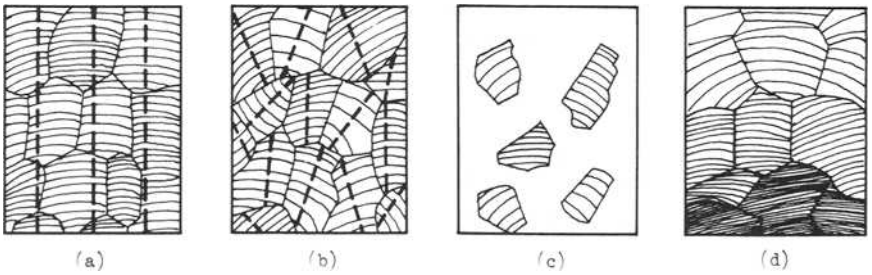

FIG. 15—*Typical types of striated fracture surfaces; crack growth direction vertical.* (a) *Uniformly-oriented striations*; (b) *randomly-oriented striations*; (c) *partial coverage by striations*; (d) *gradient of striation spacing.*

specimen completely, but there is a definite gradient of spacings along the CPD. In order to analyze these four prototype microstructures quantitatively, somewhat different measurements techniques should be employed. The details will be presented later, after discussing the advantages and disadvantages of different types of measurements.

Generally, the number (N) of striations intercepting a straight test line (of length L_T') is counted on a planar photomicrograph (the projection plane), giving the apparent mean center-to-center spacing (L_T'/N, or $1/N_L'$) between adjacent striations. In one measurement method [*34*], a straight test line (or better, a grid of parallel test lines) is laid down on the photomicrograph parallel to the CPD (see Fig. 15*a*). The interceptions are counted, regardless of striation orientation, and the total number of interceptions is divided by the total length of grid lines to give the average apparent striation spacing. This method is fairly fast.

In another method [*35*], the FSS in each striation facet is measured in a direction normal to the striation lines, regardless of the CPD (see Fig. 15*b*). The various values of FSS are then recalculated by projecting to a line parallel to the CPD. The corrected values are then averaged. This method is quite laborious and time-consuming if done manually, and considerable calculation is involved. However, some automatic image analysis systems can measure spacings within localized regions [*36*].

It should be noted, however, that the first method *overestimates* the "true" normal spacing, l_t', while the second method gives a value of FSS *smaller* than l_t'. The sketches in Figure 16 contain the essential geometrical relation-

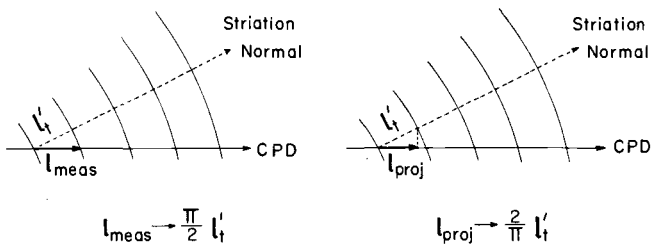

FIG. 16—*Geometry involved in two different techniques for striation spacing measurement.*

ships. In one case, the mean measured spacing ($\bar{l}_{meas}$) approaches a value $\pi/2$ greater than the value of l_t', while in the other the spacing employed ($\bar{l}_{proj}$) approaches a value of l_t' divided by $\pi/2$. These relationships are exact for parallel, equispaced striations, when all possible angles between striation normals and the CPD are present. It should also be remembered that these measurements are actually being made on projected images in a plane.

Correction of "True" FSS

In addition to the foregoing considerations, we must correct the measurements of FSS to allow for the nonplanar character of the fracture surface. In general, the striation spacings measured from the photomicrograph will be too small. Figure 17 sketches the elements of the structure as viewed in a vertical section through the fracture surface and parallel to the CPD. It can be seen that the measured spacing (L_T'/N) is not the true spacing (L_t/N), because L_T', the test line length in the projection plane, is less that L_t, the true length of line in the fracture surface.

Several techniques are available for estimating the true length of test line in the fracture surface, none of which are very satisfactory at the present time. A rather laborious procedure is to mount the specimen, make vertical sections through the fracture surface parallel to the overall CPD, and measure the true length L_t on each section. The appropriate relationship in this case is Eq 14, where A_T is the selected test area enclosing the fracture surface profile. Having obtained the value of L_t (or an average value), we apply the correction factor (L_t/L_T') as indicated by

$$l_t = \left(\frac{L_T'}{N}\right)\left(\frac{L_t}{L_T'}\right) \tag{18}$$

to get the true striation spacing in the fracture surface. Note that Eq 18 corrects only for lack of planarity of the fracture surface.

Some experimental data are available [*37*,*38*] on the magnitude of the ratio L_t/L_T', called the lineal roughness parameter R_L by Pickens and Gurland [*38*]. They measured this ratio from Charpy fracture surfaces in SAE 4620 steel and got values between 2.08 and 2.54, with the average equal to 2.32. The theoretical magnitude of this ratio is $\pi/2$ for a line in a plane randomly projected over all angles to a projection line. Thus, the coefficient $\pi/2$ is about 1.5 times smaller than the foregoing experimental value of 2.32. This discrepancy is understandable, however, provided the linear segments of L_t do not lie randomly at all possible angles to the projection line, but instead are biassed preferentially toward the smaller angles. Consequently, the observed coefficient is greater than the theoretical one, and a value of $(L_t/L_T') = 2.3$ does not appear unreasonable.

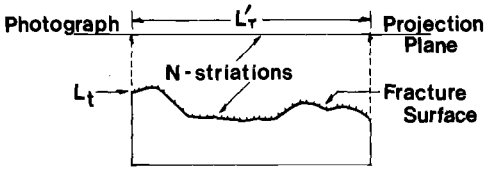

FIG. 17—*Schematic of vertical section through fracture surface and parallel to crack direction.*

Assessment of FSS Measurement Methods

Returning now to Fig. 15, we see that the measurement of striation spacings on the photomicrographs can be different in each case. The "best" method to use is probably that method which most satisfactorily fits the requirements of each job. For example, in Fig. 15*a* the "first method" discussed in the foregoing should prove adequate for most uniform, fairly well-oriented structures. In Fig. 15*b* however, where the striated regions are widely oriented with respect to the CPD, the "second method" mentioned may prove more useful. The availability of an automatic image analysis instrument may also influence the choice of method selected. The problems associated with the structure shown in Fig. 15*c* are not so much the measurement of striation spacings as the determination of the manner of their contribution to the controlling mechanism of crack growth. For example, if the area covered by striations represents the slower fracture mode, then the area fraction of striated regions may also enter into the required microstructural parameter. In Fig. 15*d*, where there is a local gradient of striation spacings, the simple average value may be satisfactory, or for more precise characterization, measurements of the spacings can be made at several locations along the gradient direction. On gradients that extend over the entire fracture surface, one technique is to measure the *average* local striation spacing at five or six locations, even though there may be a slight gradient within each specimen.

As a practical guide, it should be noted that even though the "first method" overestimates the "true" normal spacing, the measurement of striations on the projection plane (instead of the true fracture surface) tends to underestimate the spacings. Thus, the errors involved are compensated to some extent. The magnitude of the errors has not been thoroughly investigated, but could be estimated by careful quantitative experimental work and statistical analysis.

Gradient Structures

Although many microstructural features can be considered "random" in one way or another, there are other important classes of microstructures. We have dealt previously with oriented structures, including layering of unrecrystallized lamellas, elongated grains, particle stringers, and striations—all as part of anisotropic structures. Another familiar type of microstructure belongs to the "gradient" classification, which may have point symmetry [*39*] or line symmetry [*40*] (in two- or three-dimensional space), planar symmetry, etc.

Two common types of gradient structures are discussed here. General treatments for representing a gradient quantitatively are unavailable, so methods must be devised for each particular case. Figure 18 shows the

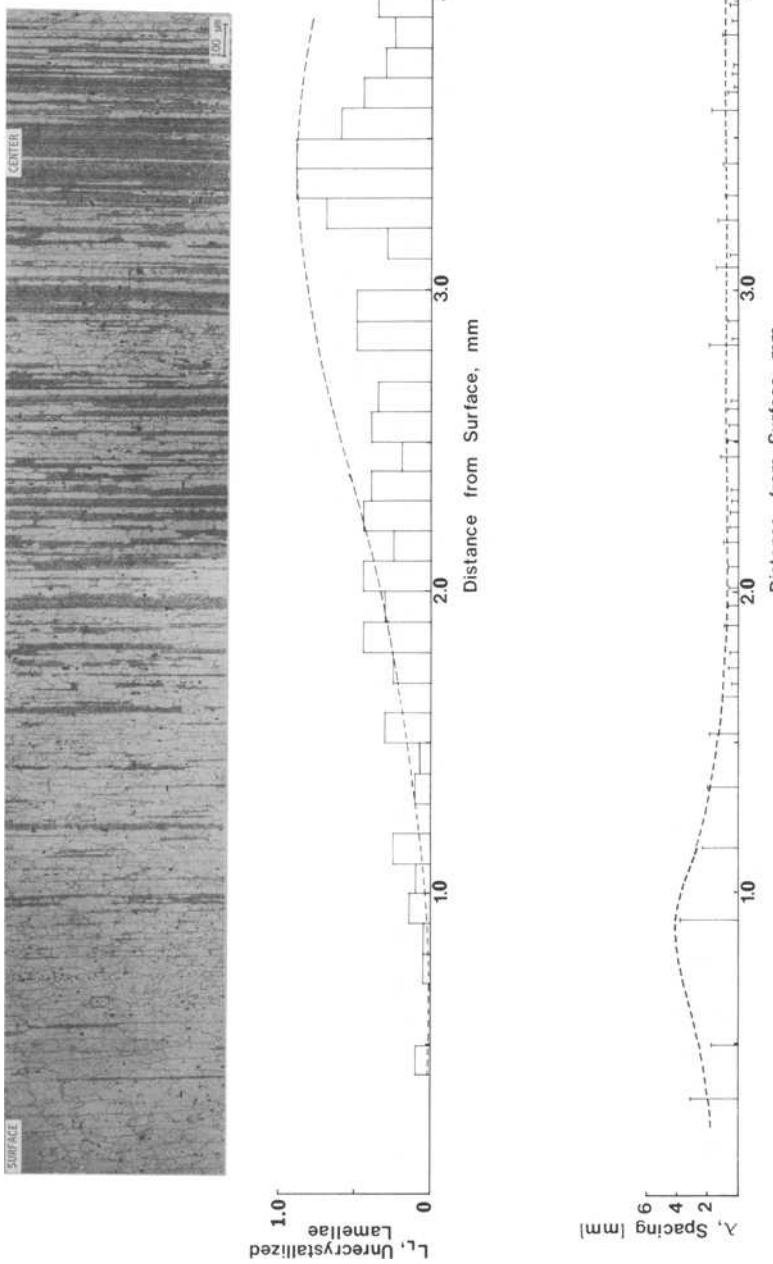

FIG. 18—*Gradient grain structure of an Al-6Zn-1Mg-2Cu-0.12Zr sheet. Etched in 25 percent* HNO_3 *at 70°C.*

surface-to-center microstructure of an Al-6Zn-2Mg-2Cu-0.12Zr alloy that has been rolled down from 3.8-cm plate to 0.6-cm sheet. The dark lamellas are unrecrystallized layers, alternating with lighter etching recrystallized grains. The gradient effect, of course, arises from the smaller and smaller spacings as the center is approached. We treat this structure as an example of gradient symmetry in a plane about a centerline, although it actually has planar symmetry in three dimensions.

A method was devised to extract some useful information for the case of fatigue cracks progressing inward from the surface. A grid of parallel lines (set parallel to the surface edge) was placed on the microstructure from surface to centerline. Within each strip various quantities were measured, such as spacings, volume fractions, and grain sizes. This technique has the property that fine detail can be smeared out, or overaccentuated, depending on the width of the strip with respect to the microstructural detail. For this microstructure, strips 0.1 mm wide were chosen which subdivided the field of view into 40 vertical strips.

To illustrate the type of data obtainable from a gradient structure, two plots are shown in Fig. 18. The first gives the volume fractions ($=L_L$) of unrecrystallized lamellas as a function of distance inward from the surface. A linear tranverse was run down the middle of the microstructure normal to the lamellas. The fraction of unrecrystallized material traversed across each strip was recorded as L_L and plotted as a function of distance from the surface. The bar graph portrays a gradual increase from zero lineal fraction at the surface to a maximum at the sheet center. A smoothed curve was faired in over the bar graph, based on the normal curve according to the equation $L_L = (2.25/\sqrt{2\pi}) \exp[-(x - 3.4)^2/2]$, with x equal to the inward distance in millimeters. This, or some other suitable curve, can then be used to represent the gradient analytically. Information of this type may be needed, for example, in order to predict crack growth rates as a function of position in the sheet. The second curve in Fig. 18 portrays the center-to-center lamellar spacing as a function of distance from the surface. The widest spacings occur about 1 mm under the surface, with a falloff to either side. This information may be useful in qualitative form, or else could be expressed analytically, as desired.

Another example of a gradient structure is seen in Fig. 19, which shows a single crystal of copper fatigued to fracture [*41*]. The fatigue striation spacings increase smoothly from the origin to the outer surface of the specimen. The data collected here are analyzed in three ways. First the overall average striation density N_L was found; that is, for 49 striations over a total diametral distance of 2.58 mm, $N_L = 18.99$ mm^{-1}. Then the mean striation spacing was determined for intervals of $D_{max}/16$ and then $D_{max}/8$ (that is, 0.161 and 0.323 mm; respectively). The plotted bar graphs show the smallest interval to best advantage—the striation density increases smoothly to a maximum density near the origin, reaching 72.2 mm^{-1}. For the $D_{max}/8$ interval, however,

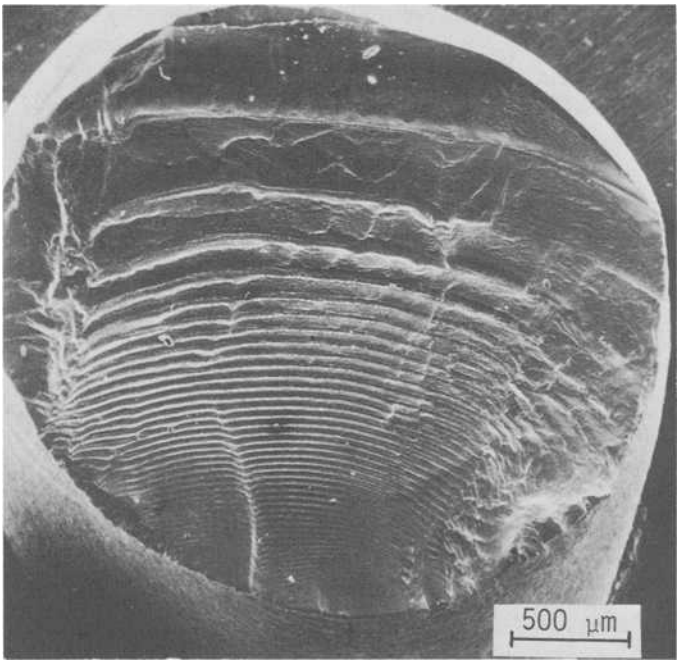

FIG. 19—*SEM of a copper single crystal LCF specimen.* $\Delta\epsilon_T/2 = 3.5$ *percent.*

the striation density is averaged out to a maximum density of only 46.5 mm^{-1} near the origin. Thus, this simple analysis shows how the gradient data can be altered by the choice of interval. This is an important consideration and must be optimized for each case.

Thin Foil Analysis

One of the most useful techniques available for revealing the fine structure of alloys is TEM from thin foils. Unfortunately, it is particularly difficult to get quantitative information from these projected images, primarily because of overlap and truncation problems. If foil thickness is small relative to particle diameter, however, overlap becomes less serious and useful estimates of volume fraction, particle size, and particle density can be obtained.

Figure 20 shows a thin foil micrograph of an Al-0.55Fe-0.5Co wire, taken transversely to the wire axis [*42*]. Several important quantities are calculated to illustrate the procedures involved. The number of Al_6 (Fe, Co) particles N' ($= 84$) in the projected test area A_T' ($= 9.92\ \mu m^2$) gives $N_A' = 8.47\ \mu m^{-2}$. A point count gave $P' = 31$ particles hit and $P_T' = 288$ total test points applied, with $P_P' = A_A' = 0.108$. The mean projected particle area $\bar{A}' = A_A'/N_A' = 0.0128\ \mu m^2$. The calculation of V_v and N_v without additional data

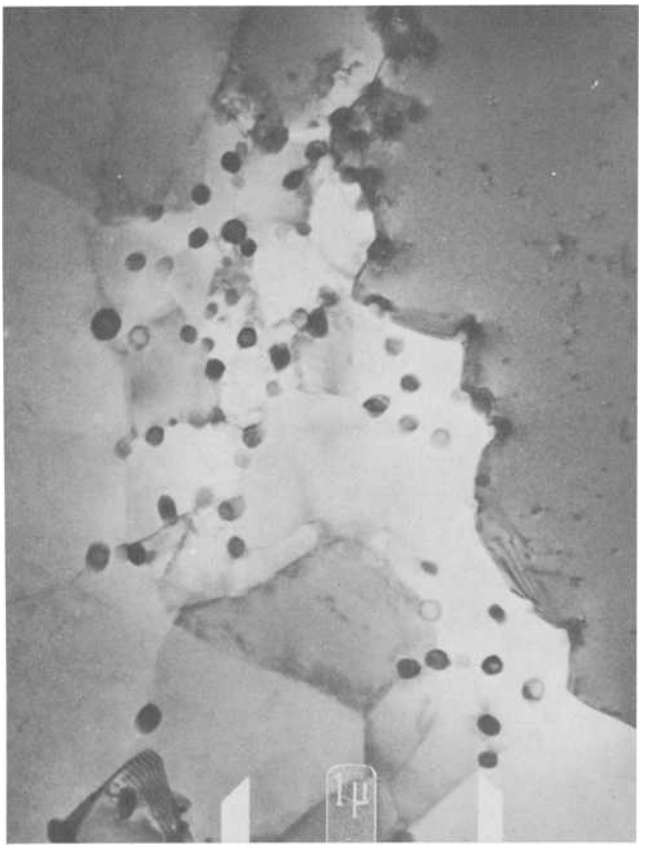

FIG. 20—*TEM of transverse section of Al-0.5Fe-0.5Co wire.*

requires some assumptions. We assume that the particles have a spherical shape, which gives a mean projected diameter $\bar{H}' = 0.1277\ \mu$m, and that the foil thickness $t \simeq 2000$ Å. The volume fraction [*43*] can now be calculated for three cases: (*a*) no correction for truncation or overlap; (*b*) a truncation correction only, and (*c*) both the truncation and overlap correction included. The applicable equations and results for spheres of diameter $D = \bar{H}'$ are, respectively

$$(a) \quad V_v = \frac{2}{3} A_A' D/t = \frac{2}{3} (0.108)\ (0.1277)/0.2 = 0.0461 \tag{19}$$

$$(b) \quad V_v = A_A' \left[\frac{2D}{2D + 3t}\right] = (0.108) \left[\frac{0.2554}{0.2554 + 0.6}\right] = 0.0322 \tag{20}$$

$$(c) \quad V_v = -\ln (1 - A_A') \left[\frac{2D}{2D + 3t}\right] = -\ln 0.892 \left[\frac{0.2554}{0.8554}\right] = 0.0341 \quad (21)$$

Note that the uncorrected volume fraction decreases with the truncation correction, and (*b*) increases slightly when the overlap correction is included.

The values of N_v[44] can also be calculated for the same three cases

$$(a) \quad N_v = N_A'/t = 8.47/0.2 = 42.3\ \mu\text{m}^{-3} \quad (22)$$

$$(b) \quad N_v = N_A'/(D + t) = 8.47/(0.1277 + 0.2) = 25.9\ \mu\text{m}^{-3} \quad (23)$$

$$(c) \quad N_v = (N_A' + M_A')/(D + t) = (8.47 + M_A')/0.3277 \quad (24)$$

Here M_A' is the number of particle images per unit area lost by overlap. M_A' is a function of the degree of particle overlap and the ability to resolve overlaps into the constituent particle images. It may be approximated by $M_A' = (3/2)/V_v(t/D)N_A' = 0.679\ \mu\text{m}^{-2}$, which, when introduced into Eq 24 for N_v, gives

$$N_v = (8.47 + 0.679)/0.3277 = 27.9\ \mu\text{m}^{-3} \quad (24a)$$

This value amounts to about a 7.8 percent increase in N_v due to overlap effects. As a rule of thumb, a correction for overlap should not be necessary if $V_v(t/D) < 0.04$. Here we find that this quantity equals 0.0534. It is obvious that the truncation correction can be appreciable, although sometimes its magnitude cannot be estimated. In any event, the value of A_A' should never be used for V_v, although this is seen occasionally in the literature.

A thin foil micrograph of ITMT-7050-T6X1 is shown in Fig. 21. The vertical grain boundary is heavily covered by η-precipitates. Of interest is the precipitate density in the actual grain boundary. If we assume that the boundary is vertical, we can use the simple equation $N_S = N_L'/t$. With experimental values of $N' = 21$, $L_T' = 0.7\ \mu\text{m}$, $N_l' = 30\ \mu\text{m}^{-1}$ (along the boundary edge), and $t \simeq 1000$ Å, $N_S = 30/0.1 = 300\ \mu\text{m}^{-2}$.

In cases where the boundary is inclined to the foil surface (as in Fig. 12), the calculation of N_S requires an estimate of the slant width from a knowledge of the foil thickness and the apparent boundary width, w'. Here we find that $N' = 155$ for the wide boundary at the lower left of the micrograph, and that $N_A' = 262.7\ \mu\text{m}^{-2}$. Correcting to true surface area using $t \simeq 0.4\ \mu\text{m}$ and $w' = 0.3\ \mu\text{m}$, we get $S_{\text{true}} = 0.98\ \mu\text{m}^2$ and $N_S = 158.2\ \mu\text{m}^{-2}$. These are simple examples that do not reveal the complexities that arise in other thin foil structures. However, when simplifying assumptions are justified, fairly reasonable estimates can be obtained.

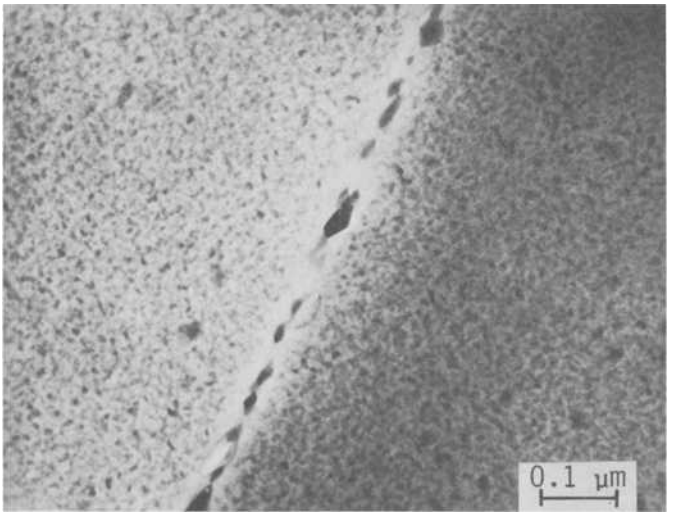

FIG. 21—*TEM of ITMT-7050-T6X1.*

Synopsis

Several typical microstructural features which are important in fatigue studies have been selected to demonstrate the quantitative procedures of stereology. Both manual methods and automatic measurements (using the Bausch and Lomb Feature Analysis System) are employed, yielding excellent agreement in suitable structures. In a general treatment of microstructures with uniform grains and particles, we show how three simple counting measurements can yield most of the basic microstructural parameters. Next we deal with anisotropic materials and demonstrate the use of special methods suitable for this type of structure, such as the degree of orientation of surfaces and grain traces, average grain size, and directional spacings. The contiguity of particle interfaces is analyzed for a particular application in a three-constituent alloy.

Some localized microstructural features, especially particles, are very important to a process such as fatigue. A new statistical procedure has been developed for assessing the degree of positional randomness, or deviations therefrom, of particles in an alloy. A similar treatment is applied to the location of crack initiation sites in order to assess the interaction of particles and crack initiation sites. Prominent features of typical fatigue cracks are analyzed and include true crack length, true crack surface area, and the quantitative evaluation of inter- and transgranular crack path lengths. A reevaluation of methods for measuring striation spacings reveals possible

sources of error, including errors arising from nonplanar fracture surfaces. An approach to the quantification of gradient structures is pointed out. Finally, we treat the difficult case of TEM of thin foils, showing how simple measurements in the projection plane can yield usable estimates of such quantities as the number per unit volume, volume fraction, and the particle density per unit area on vertical or inclined boundaries.

Acknowledgments

The authors would like to acknowledge the contributions of graduate students E. Y. Chen, E. H. Chia, K. H. Chien, E. J. Coyne, Jr., Fu-Shiong Lin, R. E. Sanders, Jr., and B. Sarkar for supplying the micrographs. Financial support by the U.S. Air Force Office of Scientific Research under Grant No. AFOSR-78-3471 and the Office of Naval Research under Contract NOOO14-75-C-0349 during the writing of the manuscript is greatly appreciated.

References

[*1*] Underwood, E. E., *Quantitative Stereology*, Addison-Wesley, Reading, Mass., 1970, Chapter 2, p. 23.
[*2*] Ref *1*, p. 18.
[*3*] *Quantitative Microscopy*, R. T. DeHoff and F. N. Rhines, Eds., McGraw-Hill, New York, 1968, pp. 29, 73.
[*4*] Ref *1*, p. 97.
[*5*] Ref *1*, p. 96.
[*6*] Ref *1*, p. 5.
[*7*] Ref *1*, p. 81.
[*8*] Ref *1*, pp. 90–91.
[*9*] Hilliard, J. E. in *Proceedings*, Second International Congress for Stereology, H. Elias, Ed., Springer-Verlag, New York, 1967, p. 211.
[*10*] Ref *1*, p. 82.
[*11*] Ref *1*, pp. 74, 82.
[*12*] Corti, C. W., Cotterill, P., and Fitzpatrick, G. A., *International Metallurgical Reviews* Vol. 19, 1974, p. 77.
[*13*] Ref *1*, p. 84.
[*14*] Passoja, D. E. and Hill, D. C., *Fractography-Microscopic Cracking Processes, ASTM STP 600*, American Society for Testing and Materials, 1976, pp. 30–46.
[*15*] Kocks, U. F., *Philosophical Magazine*, Vol. 13, 1966, p. 541.
[*16*] Sanders, R. E., Jr., and Starke, E. A., Jr., *Materials Science and Engineering*, Vol. 28, 1977, pp. 53–68.
[*17*] Underwood, E. E., *Practical Metallography*, Special Vol. No. 5, H. E. Exner, Ed., Dr. Riederer-Verlag GmbH, Stuttgart, Germany, 1975, p. 223.
[*18*] Ref *1*, p. 66.
[*19*] Saltykov, S. A., *Stereometrische Metallographie*, VEB Deutscher Verlag für Grundstoffindustrie, Leipzig, Germany, 1974, p. 174.
[*20*] Ref *1*, p. 58.
[*21*] Gurland, J., *Proceedings*, Second International Congress for Stereology, H. Elias, Ed., Springer-Verlag, New York, 1967, p. 250.
[*22*] Ref *1*, p. 100.
[*23*] Gurland, J., *Transactions*, American Institute of Mining, Metallurgical, and Petroleum Engineers, Vol. 227, 1963, p. 1146.

[24] Moore, G. A., *Practical Metallography*, Vol. 9, No. 2, 1972, p. 76.
[25] Sanders, R. E., Jr. and Starke, E. A., Jr., *Metallurgical Transactions*, Vol. 9A, 1978, p. 1087.
[26] Ref *1*, p. 38.
[27] Ref *1*, p. 57.
[28] Ref *1*, p. 64.
[29] Fine, M. E., Annual Technical Report, "Relation of Structure to Fatigue Properties in Aluminum-Base Alloys," Grant No. AFOSR-76-2892A, Air Force Office of Scientific Research, 10 Nov. 1977.
[30] Underwood, E. E., *Journal of Microscopy*, Vol. 95, Parts 1 and 2, 1972, p. 25.
[31] Chien, K. H. and Starke, E. A., Jr., *Acta Metallurgica*, Vol. 23, 1975.
[32] Ref *1*, Chapter 6, p. 148.
[33] Uchimoto, T., Sakamoto, A., and Nagata, S., *Transactions*, Iron and Steel Institute of Japan, Vol. 17, No. 3, 1977, p. 1.
[34] Bathias, C. and Pelloux, R. M., *Metallurgical Transactions*, Vol. 4, 1973, p. 1265.
[35] Bates, R. C. and Clark, W. G., Jr., *Transactions*, American Society for Metals, Vol. 62, 1969, p. 386.
[36] Camard, P., Chermant, J. L., and Coster, M. in *Quantitative Analysis of Microstructures in Materials Science, Biology and Medicine*, J. L. Chermant, Ed., Dr. Riederer-Verlag GmbH, Stuttgart, Germany, 1978, p. 126.
[37] Coster, M. and Deschanvres, A. in *Quantitative Analysis of Microstructures in Materials Science, Biology and Medicine*, J. L. Chermant, Ed., Dr. Riederer-Verlag GmbH, Stuttgart, Germany, 1978, p. 61.
[38] Pickens, J. R. and Gurland, J. in *Proceedings*, Fourth International Congress for Stereology, National Bureau of Standards, Special Publication 431, E. E. Underwood, R. deWit, and G. A. Moore, Eds., 1976, p. 269.
[39] Underwood, E. E. and Coons, W. C., *Deformation Twinning*, R. E. Reed-Hill, J. P. Hirth, and H. C. Rogers, Eds., Gordon and Breach, New York, 1964, p. 405.
[40] Flinn, J. E. and Philofsky, E. M., *Transactions*, American Society for Metals, Vol. 61, 1968, p. 37.
[41] Chen, E. Y. and Starke, E. A., Jr., *Materials Science and Engineering*, Vol. 24, 1976, pp. 209-221.
[42] Chia, E. Henry, and Starke, E. A., Jr., *Metallurgical Transactions*, Vol. 8A 1977, pp. 825-832.
[43] Underwood, E. E. in *Stereology and Quantitative Metallography, ASTM STP 504*, American Society for Testing and Materials, 1972, p. 35.
[44] Ref *1*, p. 186.

DISCUSSION

J. H. Smith[1] (*discussion*)—The authors describe several procedures for quantitatively characterizing the microstructures of materials for which fatigue may be important. They make a quite convincing case that considerable quantitative metallography of this type must be done if the results of fatigue tests can be correlated with microstructural features and permit the efficient design of more fatigue-resistant alloys. However, few results from actual fatigue tests are presented to demonstrate either that such correlations exist or that fine details of the microstructure are primary variables in determining fatigue behavior.

[1] Fracture and Deformation Division, Center for Materials Science, National Bureau of Standards, Washington, D. C. 20234.

The authors have presented an adequate description of each of the several quantitative microstructure procedures suggested for the analysis of materials susceptible to fatigue and have given a quite detailed analysis of the advantages, disadvantages, and particularly the potential sources of errors with each procedure. However, each of the procedures has specific applicability to only certain aspects of evaluation of the fatigue process in materials and it would be most useful if this were made more clear. For example, for basic research in the mechanisms of the fatigue process, all procedures have some value; however, only measurements of striations, gradient structures, and TEM foils would appear to offer any advantages. For alloy design and process development investigations, characterization of the crack features and characterization of particle distribution and crack initiation-particle distribution and correlation with measured fatigue crack initiation all are essential and have been almost totally neglected in alloy design and process development work to date. More complete characterization of the microstructure at the level obtained by these procedures seems essential until correlations between microstructural features and fatigue behavior have been obtained and at least the first-order (primary) microstructural variables controlling fatigue have been identified.

For material selection and design based on the use of fracture control plans, only the crack propagation rate da/dn as a function of stress intensity ratio, ΔK, is currently used for characterizing the fatigue behavior of the material. For all common structural materials the da/dn versus ΔK curves seem to be nearly independent of the alloy composition and dependent in a minor way on the grossest microstructural features, such as ferrite, austenite, or martensite phases. It seems that additional microstructural analysis would serve little if any additional purpose in this case, because the use of the "generic" da/dn versus ΔK curves for a given class of materials has proven satisfactory for materials selection and the development of a fracture control plan.

Features of crack initiation do not appear to be significant enough at this point to be of use in fracture control. The only exception may be in corrosion fatigue, where fine details of the microstructure may have a much greater influence on the behavior than in fatigue in benign atmospheres. Little information is currently available to demonstrate if da/dn versus ΔK curves for various microstructures are significantly different from one another under corrosive environments.

Although little discussion was made of the use of these procedures for the diagnosis of components that have failed by fatigue, it appears that the most significant use of these quantitative metallographic techniques would be in the interpretation and analysis of components during failure analysis to establish the mode of failure. Certainly the basic measurements and the analysis of anisotropy as well as the crack characterization should be done on any failed component and carefully related to the known or assumed stress

patterns and operating conditions. For certain specific components that have failed by fatigue and which have clear fatigue striations on the fracture surface, the striation analysis and gradient structure analysis will be useful to clearly define the origin/cause of the failure.

This paper describes quantitative metallographic procedures that could be used and may aid in explaining or reducing the scatter and statistical variability in data for fatigue crack initiation. Results of such complete characterization of the microstructure may assist in developing more reliable models of the mechanism of fatigue and in better alloy design and materials process development. For fatigue crack propagation, however, current experimental results demonstrate that crack propagation rates in common structural materials are quite insensitive to any but the most gross microstructural features. Therefore, little additional more quantitative analysis of the structure seems warranted because the current crack growth rate data have proven satisfactory for materials selection and design. However, some limited quantitative metallography analysis should be done, particularly to characterize the anisotropy of the materials, to ensure that the crack propagation rate data used in the calculation of the life of structural components are "worse case" or "lower bound" data.

E. A. Starke, Jr.—You are quite correct in your assessment that crack propagation rates, *in inert environments*, are not strongly sensitive to minor microstructural variations.

Unfortunately, most real-life systems are not inert, and there is an *environmental* effect. But the *environmental* effect is dependent on microstructure, and there is an interrelation between the microstructure of the alloy, the environment, and crack propagation processes. In order to separate and to elucidate these interactions and combinations, it is necessary to characterize the microstructure quantitatively, even for the Paris or intermediate ΔK region of the da/dN versus ΔK curve.

One must quantify the significant microstructural features in order to determine which ones control the environmental effects. As an example, in a high-strength aluminum alloy, shearable Guinier-Preston (GP) zones lead to strain localization which makes the material much more sensitive to environment than when incoherent precipitates and resulting homogeneous deformation are present.

These factors are interrelated, thus I think we must quantify the microstructure to really understand mechanisms and environmental fatigue and microstructural interactions.

A. Wilson[2] *(discussion)*—The quantification of the effects of microstructural features on fatigue behavior has been a very slowly developing

[2]Lukens Steel Co., Coatesville, Pa. 19320.

discipline. The authors indicate that "the main difficulty can be attributed to the localized nature of the fatigue processes, and the fact that the important microstructural features are often heterogeneous." The authors have reported a number of quantitative stereological methods that can be applied in fatigue research. However, they did not address the concern of how much specimen area must be examined in a quantitative analysis, whether it be by manual or automatic means, to be assured of the reliability of the microstructural data that one measures. For instance, how many specimens, micrographs, fractographs, thin foils, or fields on these items should the researcher examine? This is of a particular concern for studies of heterogeneous microstructural features. To workers in the field this appears to be a rather subjective concern, where one researcher feels one or two metallographic fields of examination are sufficient, while another claims even 1000 fields are not enough. In commenting on this particular aspect of the analysis I will pose a number of questions that may assist in their response.

1. Can one develop a rule-of-thumb by quantitatively analyzing an area equal to or greater than the cross section of the fatigue specimen?

2. Since most automated quantitative image analysis instruments can do a more *thorough* analysis of a particular field than might be done by manual counting means, can fewer fields be examined in determining a particular microstructural parameter?

My own feeling is that there are cases where the answer to each of these questions is in the affirmative; however, this is still subjectively based. What are the authors' thoughts in this area and can they suggest any objective guidelines that we might use?

The authors devoted a significant portion of their paper to the analysis of anisotropic structures. An anisotropic structure that has been of great interest to us is the nonmetallic inclusions in plate steels, and in particular the manganese sulfides and alumina inclusions in conventionally produced aluminum-killed steels. These types of inclusions are associated as groups in the steel and appear to have a more significant effect on fatigue crack propagation (FCP) and toughness properties than if they were present as evenly dispersed inclusions of the same size. For example, Fig. 22 shows the morphology of the manganese sulfide inclusions in the three major metallographic cross sections. Their group nature can be discerned to some extent in this figure. However, fractographic analysis shows this much more dramatically, as indicated in Fig. 23 for the manganese sulfide inclusions on a through-thickness, FCP test specimen fracture. These inclusions have a significant effect on the FCP properties of steel, particularly in the through-thickness testing direction at higher ΔK levels, as shown in Fig. 24 for A533B steel.[3] When these inclusions types are removed by various advanced

[3] Wilson, A. D., *Transactions*, American Society of Mechanical Engineers, *Journal of Pressure Vessel Technology*, Vol. 99, Series J, No. 3, Aug. 1977, pp. 459-469.

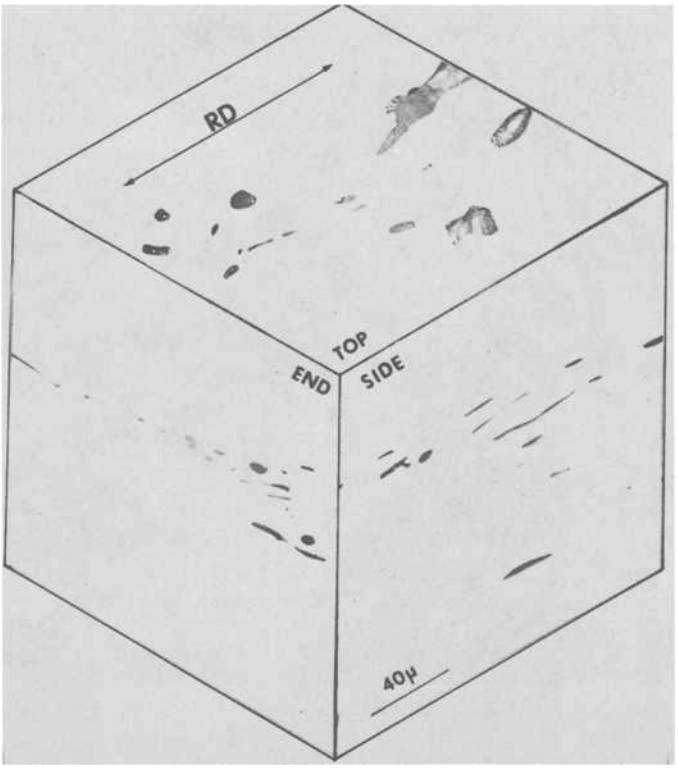

FIG. 22—*Composite of light photomicrographs showing manganese sulfide inclusions in a conventional A533B steel.*

steelmaking techniques, such as calcium treatment (CaT) or electroslag remelting (ESR), there is an improvement in the through-thickness FCP properties, as indicated in Fig. 25 in the ST orientation (footnote 3).

We have had some success in quantifying these detrimental inclusion structures using parameters similar to the authors. In particular the average area of an inclusion on the metallographic cross section corresponding to the plane of fracture has been found to correlate well with the FCP equation constants.[4] However, a way of demonstrating the additional detrimental nature of the group effect of these two types of inclusions has eluded us, particularly as could be measured in a Quantimet 720 instrument. We suspect that this would allow even better correlations to be developed. Do the authors have any suggestions for approaches that might be used?

[4]Wilson, A. D., *Transactions*, American Society of Mechanical Engineers, *Journal of Pressure Vessel Technology*, to be published.

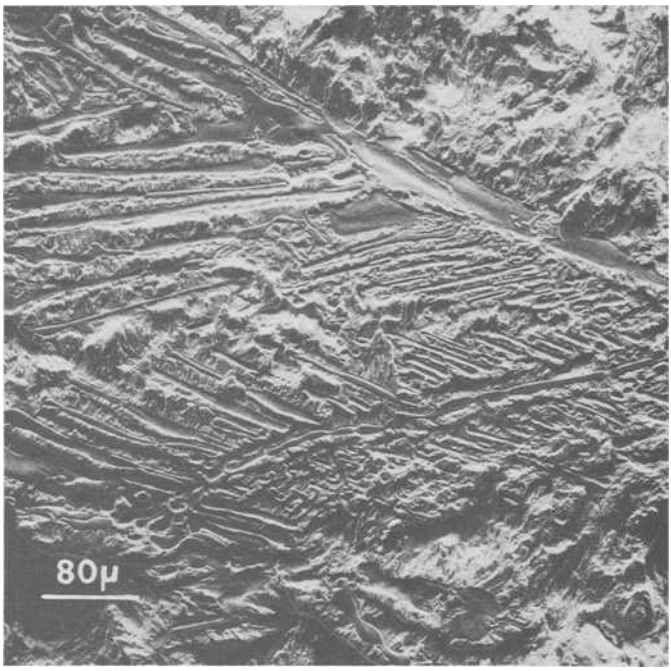

FIG. 23—*SEM fractographs of A533B FCP specimen in ST orientation at* ΔK *level of 25* $MPa \cdot m^{1/2}$ $(23\ ksi/in^{1/2})$.

The authors are to be commended for their contribution and suggestions in this difficult area of quantifying of microstructural features that influence fatigue behavior.

E. E. Underwood—Some important points are raised by Dr. Wilson concerning the sampling statistics in quantitative metallography, and the characterization of nonmetallic inclusions (NMI) in steels. I shall respond to these questions separately.

The statistical procedures required to evaluate the total sampling problem are quite complex. Involved are questions of (1) the number of samples required; (2) the number of specimens needed from each sample; (3) the number of fields of view necessary on each specimen; and (4) the number of measurements to make on each field of view.

I don't know of anyone who has tackled the total problem, but well-known workers on some aspects of this problem are Halle Abrams (Bethlehem Steel) and George Moore (formerly National Bureau of Standards), for example. In general, it appears that the scatter from sample to sample is usually much greater than that within one specimen; thus it behooves us to spend more time on more samples, and less time on each specimen.

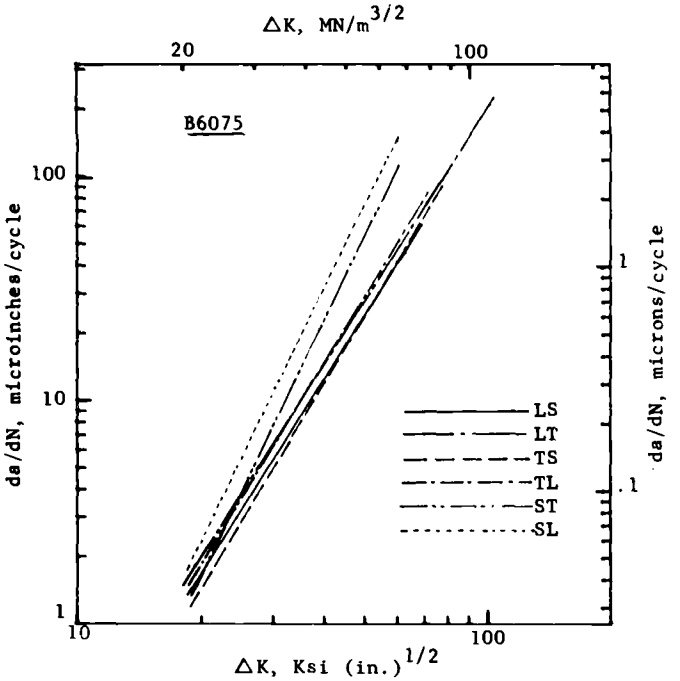

FIG. 24—*Plot of fatigue crack growth rate versus range of stress-intensity factor displaying anisotropy in a conventional A533B steel.*

From a stereological point of view, John Hilliard has published a number of papers on the general subject of measurements, variances, and efficiency.[5-12]

A. Wilson—My second question is motivated by a case study of my own. In the steel industry we are very concerned about the nature of inclusions in steels, and particularly in alumina-killed steels where you have a number of

[5]Hilliard, J. E. and Cahn, J. W., General Electric Research Laboratory Report No. 59-RL-2294M, Oct. 1959.

[6]Hilliard, J. E. and Cahn, J. W., *Transactions*, American Institute of Mining Engineers, Vol. 221, 1961, p. 344.

[7]Hilliard, J. E., General Electric Research Laboratory Report No. 61-RL-2652M, March 1961.

[8]Hilliard, J. E., General Electric Research Laboratory Report No. 62-RL-3133M, Dec. 1962.

[9]Hilliard, J. E. in *Recrystallization, Grain Growth and Textures*, American Society for Metals, Metals Park, Ohio, 1966, p. 267.

[10]Hilliard, J. E. in *Quantitative Microscopy*, R. T. DeHoff and F. N. Rhines, Eds., McGraw-Hill, New York, 1968, p. 45.

[11]Hilliard, J. E. in *Ceramic Microstructures*, R. M. Fulrath and J. A. Pask, Eds., Wiley, New York, 1968, p. 53.

[12]Hilliard, J. E., Cohen, J. B., and Paulson, W. M. in *Ultrafine Grain Ceramics*, J. J. Burke, N. L. Reid, and V. Weiss, Eds., Syracuse University Press, Syracuse, N. Y., 1970, p. 73.

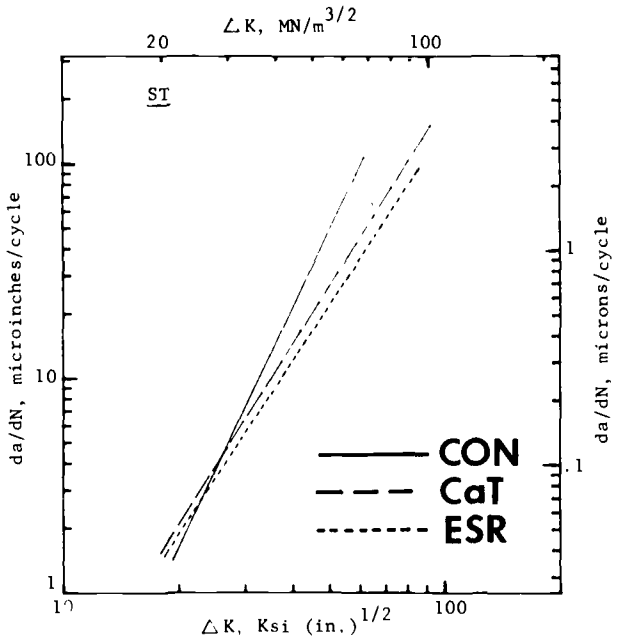

FIG. 25—*Plot of fatigue crack growth rate versus range of stress-intensity factor comparing conventional (CON), calcium-treated (CaT), and electroslag remelted (ESR) A533B steels in ST through-thickness orientation.*

nonmetallic inclusions. In the conventional quality steels, you also get manganese sulfides and alumina as inclusions. But we have steel-making methods to eliminate the inclusions selectively but not completely. My question to you is: Is there a way a researcher can quantify the group nature of these inclusions?

E. E. Underwood—You raise another difficult point when inquiring about the ways to express quantitatively the detrimental nature of the "group effect" of NMI. I have been aware of the general problem of NMI in steels, but have little specific research to report on at this time.

Let me consider the inclusions in two categories: (1) clusters, in which the inclusions are associated in small groups relatively far from each other, and which are more or less randomly located over the microstructure, and (2) stringers, in which the inclusions are aligned in a linear fashion, along parallel lines that are oriented in a preferred direction.

In general, as a metallurgist, I would first want a fairly simple, yet complete quantitative description of the basic microstructural properties of the inclusions. By this I mean the quantitative determination of such things as V_V (volume fraction), N_A (number of inclusions per unit test area), and $\bar{A}$

(the mean intercept area). Spacings are also of interest, but the conventional λ (mean free distance) is rather meaningless, physically, when the inclusions occur in separated, densely concentrated groups. Perhaps the mean spacing between *groups* of inclusions could be the import parameter here.

As for some measure of the clustering tendency, what appeals to me is an experimental area count of inclusion density within an array of square cells, normalized with respect to a hypothetical, statistically uniform distribution of inclusions. Thus, for a fairly uniform experimental distribution of inclusions in the field of view, the ratio would be near unity. As clustering becomes more pronounced, however, the ratio would get larger and larger. This type of measurement is readily adapted to automatic image analysis, provided the inclusion size and contrast are satisfactory.

With regard to the stringers, we can also measure V_V, N_A, and $\bar{A}$, plus any other basic quantities that are of particular interest to the producer or user of the steel. In addition, I would suggest a spacing parameter in the direction of FCP, which may be perpendicular to the stringer orientation direction. If so, this requires only a simple intersection count, $(N_L)_\perp$, which is the number of stringer lines intersected per unit length of test line perpendicular to the orientation direction. The reciprocal of $(N_L)_\perp$ is, of course, the mean perpendicular spacing between stringer lines.

The extent of segregation of inclusions along stringer lines can be measured and expressed quantitatively as indicated in the paper (see page 644) for the case of particle stringers. There, we describe a particle area count in strip-shaped cells which are aligned parallel to the stringer direction. The data are compared with a statistically uniform distribution of particles, giving a ratio as described in the foregoing for the inclusion clusters.

Other quantities may be of interest, depending on the applications of the alloy. For example, the shape of the inclusion is an important consideration. It can be handled simply (for example, as the mean aspect ratio), or in a more complicated manner (for example, in terms of a shape parameter).

In summary then, I have indicated procedures to quantify the "group nature" of inclusions in terms of three types of microstructural categories:

1. basic microstructural quantities,
2. spacing parameters, and
3. distributional (location) parameters.

These data can be used independently, or to supplement standard charts, or in combined form as a parameter composed of significant microstructural quantities.

J. A. Simmons[13] (*discussion*)—The problem that was just alluded to has

[13]Metal Science and Standards Division, Center for Materials Science, National Bureau of Standards, Washington, D. C. 20234.

been studied in astronomy for a long time. It is an old problem dealing with the clustering of galaxies and the technology is very advanced. There is one thing I would like to ask Dr. Underwood about: He is talking about very simple measurements, essentially geometric measurements. What about conditional probability measurements and correlation techniques? What is the state of the art in these kinds of areas?

E. E. Underwood—Interestingly enough, stereology is akin to astronomy in that three-dimensional (sample) space is studied on two-dimensional projections. In addition, stereology utilizes two-dimensional sections through sample space in order to calculate the true numbers, volumes, areas, etc. in the sample. Some of the astronomical work that you are referring to was done by Chandrasekhar[14] in 1943 and led to some very neat relationships for the mean nearest neighbor spacings of random point particles, either in a plane or in space. I am not aware, however, of how the astronomers handle the mathematical description of star clustering. Their results should prove interesting to metallurgists studying the behavior of nonmetallic inclusions in steel, for example.

Some of the other mathematical devices you mention, such as conditional probabilities and correlation techniques, are also of interest in devising new stereological procedures. The first has possible application in studies of random particle spacings, in which there is a cutoff at low values of the frequency distribution curve due to a forbidden volume effect arising from overlapping particles. (See, for example, Moran.[15])

As for correlation techniques, events are moving swiftly, especially in France at Fontainebleau, where Jean Serra and the Centre de Morphologie Mathématique are developing new applications of the covariance function to many microstructural problems.[16] Also of interest is the correlation work (called "radial distribution analysis") being done at the U.S. Bureau of Mines at Rolla, Missouri, as described by R. M. Doerr.[17] Also, the 2- and 3-dimensional correlation analysis of ores is being used at the Pennsylvania State University to characterize the spatial distribution of minerals.

G. A. Moore[18] (*written discussion*)—The authors do themselves an in-

[14] Chandrasekhar, S., *Reviews of Modern Physics*, Vol. 15, No. 1, Jan. 1943, p. 86.

[15] Moran, P. A. P. in *Proceedings*, Symposium on Statistical and Probabilistic Problems in Metallurgy, Seattle, Wash.; *Special Supplement on Advances in Applied Probability*, Dec. 1972, pp. 69-91.

[16] *Quantitative Analysis of Microstructures in Materials Science, Biology and Medicine*, J.-L. Chermant, Ed., in Special Issue No. 8 of *Practical Metallography*, Dr. Riederer-Verlag GmbH, Stuttgart, Germany, 1978.

[17] Doerr, R. M. in *Proceedings*, Fourth International Congress for Stereology, E. E. Underwood, R. deWit, and G. A. Moore, Eds., National Bureau of Standards Special Publication No. 431, 1976, p. 305.

[18] Metallurgist (ret.), National Bureau of Standards, Washington, D. C. 20234.

justice by using the word "reviews" in the first sentence of their abstract. The paper does in fact develop substantial new methodology which should prove useful in dealing with localized mechanical behavior, as contrasted with average mechanical properties.

Three extensions of method are particularly worth reemphasis. The first two are concerned with "texture," itself a rational expression of the combinations of the inaccessible parameters of individual particles (or grains).

1. The fact that anisotropy can be measured by making intercept counts in the three principal strain directions has long been known and is included in Section 10.6 of ASTM Estimating the Average Grain Size of Metals (E 112-77). The specified statement of intercept aspect ratios is not, however, particularly useful in predicting behavior. The ratios of oriented surface to total surface given in Eqs 9 and 10 are directly applicable to modeling either crack initiation or crack propagation. The authors note that the 2-dimensional ratio (Eq 10), which is a ratio of *projected* surfaces as well as boundary lengths, was "quite close" to the 3-dimensional ratio. For uniform deformation without fragmentation or recrystallization, the changes of mean intercept distance must exactly parallel the external dimensional changes. With volume constant, $(P_L)_1$ is determinable from the other two P_L measurements. This value is added in both the numerator and denominator of the 3-D ratio; thus its effect is minor. Recomputing the illustration in the paper, but using only the data from the "RT-plane" for the 2-D ratio, I obtained 69.1 and 69.9 percent for the 3-D surface and 2-D line ratios. The agreement apparently is *not* a coincidence!

2. "Degree of departure from random" is an important quantification for modeling any behavior which occurs at extrema. Extreme structure may be at a very small scale for crack initiation, or at a large scale for crack propagation, hence departure from a "uniform random structure" must be evaluated at various size scales. It has been known for some time [*24*] (See also Moore[19]) that, when a structure is repetitively measured through a window (or cell) of a size and shape corresponding to the suspected departure from uniformity, there will be a moiré effect if this nonuniformity is present. This appears as a high second moment in the data distribution, and can be expressed as the ratio of either the standard deviation or the rms average to the value which would be obtained for a Poisson particle distribution. Unfortunately, the correct average number of particles per window is often difficult to determine and the Poisson-uniform base difficult to establish. Introduction in this paper of the ratio from the x-squared test appears to be a major forward step since it permits evaluating nonrandomness of concentration or surface area without a necessity of ambiguous particle counting. Detection of a pattern of association even in an intrinsically non-Gaussian distribution ap-

[19]Moore, G. A. in *Ceramic Microstructures*, R. M. Fulrath and J. A. Pask, Eds., Wiley, New York, 1968, p. 94.

parently would be feasible, since the x-squared method can compare any two curves. Movable variable frames have been recently provided in at least two of the automatic scanners in order to produce the required data on the subfield basis. Larger scale texture is easily detected by analyzing field data in *sets* of fields, as in the "combined cells" in the paper.

3. Stereologists have usually avoided making computations based on measurements on nonflat surfaces. It is well known that such measurements are always biased, and the data to correct this bias are usually unavailable. In the section on striations, the authors show that one may, if necessary, measure the same quantity, spacing, by two methods, and further that one method is always low and the other always high, both within known limits. Thus by considering limiting values, and by using compensating measuring methods, it is possible to obtain probable true values within a precision quite sufficient for correlation with crack propagation data. Such serendipitous bracketing is certainly a great improvement over no measurements at all.

E. E. Underwood—Dr. Moore's kind remarks are deeply appreciated, especially coming from one who has innovated in so many areas himself during a long scientific career. His comments on anisotropy, positional deviations from randomness, and fatigue striation spacings provide a valuable background and additional insight into our discussion of these topics.

I should emphasize, perhaps, with regard to the FSS analysis, that the $\pi/2$-factor relating $\bar{l}_t'$ to the experimental spacings $\bar{l}_{meas}$ and $\bar{l}_{proj}$ is only a limiting value under the conditions specified. The actual value of the coefficient is, in general, unknown. However, when $\bar{l}_t'$ is expressed as the geometric mean of the two spacings, it may be that the coefficients cancel out regardless of their actual value.

E. E. Underwood and E. A. Starke, Jr. (authors' closure)—It is apparent from the discussions to this paper, as well as from conversations with others, that there is a wide and growing interest in quantitative microstructural methods. We have tried to illustrate applications of the basic stereological procedures to the special problems of fatigue. Our intent, of course, is to encourage interested researchers to use and extend these methods in order to more effectively advance our knowledge of fatigue.

> In this regard, we would like to quote from a statement by Grosskreutz[20]: The microstructural approach to achieving fatigue strength is undoubtedly the most rational approach .... However, the potential is far greater than (any) limited successes would indicate. There simply has not been enough work accomplished as yet which relates microstructure and fatigue resistance. The present state of the art does not allow accurate prediction of optimum microstructures for crack growth resistance. Until this type of knowledge is available, progress ... will be slow.

[20] Grosskreutz, J. C., *Metallurgical Transactions*, Vol. 3, 1972, pp. 1259-1260.

T. Yokobori[1]

A Critical Evaluation of Mathematical Equations for Fatigue Crack Growth with Special Reference to Ferrite Grain Size and Monotonic Yield Strength Dependence

REFERENCE: Yokobori, T., **"A Critical Evaluation of Mathematical Equations for Fatigue Crack Growth with Special Reference to Ferrite Grain Size and Monotonic Yield Strength Dependence,"** *Fatigue Mechanisms.* Proceedings of an ASTM-NBS-NSF symposium, Kansas City, Mo., May 1978, J. T. Fong, Ed., *ASTM STP 675,* American Society for Testing and Materials, 1979, pp. 683–706.

ABSTRACT: In order to select the correct mathematical equation among many, for fatigue crack growth or to develop a new criterion, some critical assessments are carried out by compiling the experimental data on the effect of ferrite grain diameter on fatigue crack growth rate for two low-carbon steels and a 3 weight percent silicon iron. The effect of monotonic yield strength is also studied. Emphasis is on fatigue crack growth in the second region of fatigue crack growth rate versus ΔK curve. Results suggest that, if fatigue crack growth rate is expressed as

$$da/dN = B\left(\frac{\Delta K}{\sqrt{s}\,\sigma_c}\right)^n$$

where σ_c is some constant with the dimension of stress and s is an appropriate measure of length, then σ_c and B are practically independent of monotonic yield strength, but n has the trend of a slowly increasing function of the ferrite grain diameter and, thus, indirectly a decreasing function of the monotonic yield strength. Moreover, it is suggested that n is also affected with some other microstructural factor.

KEY WORDS: fatigue crack growth, ferrite grain size, monotonic or static yield strength, initial cyclic yield strength, fatigue crack growth constants, plain low-carbon steel, silicon iron, tempered-martensitic steel, eutectoid steel, heat-treated bearing steel

[1] Professor, Mechanical Engineering Department II, and director, Research Institute for Strength and Fracture Materials, Tohoku University, Sendai, Japan.

Nomenclature

a Crack length (half length of crack for central crack)
B, b Constant
C, n Fatigue crack growth constants
d Averaged ferrite grain diameter
E Young's modulus
ΔK Stress range intensity factor
K_{max} Maximum stress intensity factor
K_{1c} Plane-strain fracture toughness
K_{fc} Fatigue fracture toughness
K_{TH} Threshold stress intensity factor
K_{eff} Effective stress intensity factor
k Bolzman constant
l_i An appropriate measure of length
m Dislocation velocity power exponent
N Repeated cycles
R $\sigma_{min}/\sigma_{max}$ = stress ratio
s An appropriate measure of length
T Absolute temperature
U_0, V_0 Constants
α_i Numerical factor
β Strain-hardening exponent in cyclic stress-strain relation
γ Specific surface energy
γ_p Effective surface energy for fatigue crack growth
ξ Material constant
λ Strain hardening exponent in monotonic stress-strain relation
μ Shear modulus
σ_{sy} Monotonic or static yield strength
σ_{max} Maximum stress in cycle (applied gross stress)
σ_{min} Minimum stress in cycle (applied gross stress)
$\Delta\epsilon_p$ Cyclic plastic strain range
$\Delta\sigma$ Cyclic stress range
σ_{cy} Initial yield stress for cyclic stress-strain relation, that is, $\Delta\sigma = \sigma_{cy}(\Delta\epsilon_p/\epsilon_{cy})^{\beta}$
ϵ_{cy} Strain at σ_{cy} in cyclic stress-strain relation $\sigma_{cy} = E\epsilon_{cy}$
σ_c Some constant with the dimension of stress
σ_a An appropriate measure of the strength of the alloy

There are many theories, models, criteria, and mathematical equations [*1–19*][2] for fatigue crack growth; however, there exist discrepancies therein. Most predict some experimental characteristics, but do not explain others.

[2]The italic numbers in brackets refer to the list of references appended to this paper.

Thus it is necessary to examine which is more correct or to develop a new criterion.

In regard to this complex problem, the following recognition may be fruitful.

1. The ln da/dN versus ΔK curve assumes S-type or sigmoidal behavior (Fig. 1), that is, the first region, the second region, and the third region, including final catastrophic fracture. Different factors may be predominant corresponding to each region, the mechanism of which still remains unsolved. Thus if we attempt now to describe behavior covering all three regions in terms of a single equation, it may be necessary to include very many parameters which may not be correlated with micromechanism. Also, it may even be awkward, and thus may not be so useful from the mechanisms point of view.

It is unrealistic to assume that, in the first region, however small ΔK may be, the crack will still grow. Thus, as a matter of course, the effective stress intensity factor ΔK_{eff}, smaller than ΔK, for instance, $\Delta K - \Delta K_{\text{TH}}$ should be used instead of ΔK only, where ΔK_{TH} is threshold stress intensity factor.

In the third region, it is also needless to say that da/dN will accelerate, and the factor controlling final catastrophic fracture should be included in the equations. Nevertheless, the maximum stress intensity factor $K_{\max}$ is, in general, different from K_{Ic} (so-called static fracture toughness) and, instead, fatigue fracture toughness K_{fc} is proposed [*20,21*].

2. If the mean stress is significant, then this effect should be included. As described in the foregoing, however, the first step is to approach the

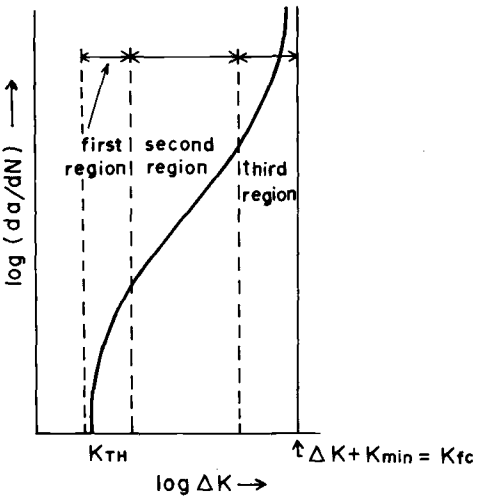

FIG. 1—*Schematic illustration of fatigue crack growth rate versus* ΔK.

case with a small or zero stress, and then to modify the equations to include it.

This paper focuses, from the foregoing point of view, on fatigue crack growth in the second region.

Assessment of Models by Experimental Data

The following equation proposed by Paris and Erdogan [*1*] is very well known

$$\frac{da}{dN} = C(\Delta K)^n \tag{1}$$

It was assumed applicable over all regions of crack growth. Before and after the proposal, there have been many theories, models, criteria, and mathematical equations for fatigue crack growth. I believe that the theory or model should be distinguished from the criterion, that is, from the rate-determining requisite, to avoid confusion. For instance, based on a similar dislocation model, different criteria may be obtained according to the rate-determining requisite. These criteria are illustrated in Table 1.

As can be seen in Table 1, most of the equations except Eqs I, L, M, N, and O, show that proportional constant C in Eq 1 is a function of monotonic yield strength, σ_{sy}. On the other hand, it has been shown by Hahn et al [*22*] that fatigue crack growth rate is relatively insensitive to monotonic yield strength.

In the present paper a critical assessment has been made by compiling the experimental data on the effect of ferrite grain diameter on the fatigue crack growth rate of two low-carbon steels [*23,24*], and of 3 weight percent silicon iron [*25*]. The effect of monotonic yield stress is also studied in this way. An additional assessment of the effect of monotonic yield strength has been attempted by compiling our data on tempered-martensitic steel [*24,26*], eutectoid steel [*27,28*] and heat-treated ball bearing steel [*29,30*].

Low-carbon steel of two kinds, 0.05 and 0.08 weight percent carbon content, were used.

An 0.05 weight percent carbon steel was supplied in the form of hot-rolled plates 3.2 mm thick, a killed type [*23*] (Table 2). Blanks with length of 200 mm and width of 73 mm were cut from the material so that their longitudinal direction coincided with the direction of rolling. A range of grain sizes for this study was produced by heat treatments at various temperatures for various times followed by cooling at several rates. After the heat treatments the fatigue specimens were ground to give a thickness of 2.7 mm. A central slit was made by first drilling a central hole 2 mm in diameter and then cutting diametrically opposite slits, about 0.5 mm long, perpendicular to the longitudinal direction of the specimen, by means of a

fine steel fretsaw blade. All of fatigue and tension specimens were stress-relief annealed in vacuum at 650°C for 2 h after the machining. The ferrite grain sizes after these final treatments are given in Table 3.

An 0.08 weight percent carbon steel was supplied in the form of plate 3.2 mm thick, hot-rolled from an electric-arc furnace ingot and normalized at 950°C for 1 h [*24*] (Table 2). The specimens were cut so that the longitudinal direction coincided with the direction of rolling, and ground to a thickness of 1.5 mm. A central slit was made by first drilling a 2-mm-diameter central hole and then cutting diametrically opposite slits 0.5 mm long. The slit thus formed is about 0.5 mm wide. After machining, the specimens were heated in vacuum at different temperatures and for different times to obtain different grain sizes (Table 3).

Next, all specimen surfaces were polished with 0/6 Emery paper and then buffed. Axial fatigue testing was carried out in a 10-ton Vibrophor (resonance type) fatigue machine at a frequency of 140 Hz. The grips were carefully aligned to ensure that no bending stresses were introduced into the specimen.

Fatigue tests were carried out at stress ratios $R = \sigma_{min}/\sigma_{max} = 0.24$-$0.40$ and 0.21-0.40 for 0.05 and 0.08 weight percent carbon steel, respectively. For such variations of R, there was no practical difference in the da/dN versus ΔK relation for the specified ferrite grain diameters in 0.05 and 0.08 weight percent carbon steel [*23,24*]. For the specimen series batch F, R was chosen as 0.03 so as to make σ_{max} smaller than the static yield strength. A microscope was used for measuring the crack length while the machine was running. All crack length measurements were made from the center of the sheet.

The effects of ferrite grain size on da/dN versus ΔK are shown in Figs. 2 and 3 for each material. In Fig. 4, the n obtained is plotted against $d^{-1/2}$ (d = averaged ferrite grain diameter) and static yield strength σ_{sy}. It should be noted that n decreases with increase of $d^{-1/2}$ or decrease of d (or increase of static yield stress σ_{sy}). Recently Ando et al [*25*] conducted similar experiments on 3 weight percent silicon iron and obtained similar results as shown in Fig. 5. In this case, in the range of considerably coarse grain diameter only, n becomes smaller with decrease of R. The rather low value of n in the specimen batch F for low-carbon steel was probably caused by the much lower (underestimated) value of R as compared with the other specimen batches.

Another important point is that if we plot the value of $\log_{10}C$ against n as shown in Fig. 6, $\log_{10}C$ is expressed as follows in a linearily decreasing equation with respect to n

$$\log_{10}C = \log_{10}U_0 - n\log_{10}V_0 \tag{2}$$

where $\log_{10}U$ and $\log_{10}V$ are really independent of static yield stress σ_{sy}. In Fig. 6 also, for 3 weight percent silicon iron, $\log_{10}C$ was plotted against n

TABLE 1—*Reviews of various mathematical equations for* da/dN *in literatures.*

Theory or Model	Criterion or Rate Determining Requisite	Mathematical Equation for da/dN		Author and Reference
Energy approach	energy balance	$\alpha_1 \left(\frac{\Delta K}{\sigma_{sy}}\right)^2$	A	Liu [2]
Energy approach	energy balance	$\frac{\alpha_2}{l_2}\left(\frac{\Delta K}{\sigma_{sy}}\right)^4$	B	Paris [3]
Energy approach	energy balance	$\alpha_3 \frac{\Delta K^4}{\sigma_{sy}^2(K_{Ic}^2 - K_{max}^2)}$; $K_{max} \ll K_1$, $\alpha_3 \frac{\Delta K^4}{\sigma_{sy}^2 K_{Ic}^2}$	C	Raju [4]
Energy approach	energy balance	$\alpha_4 \frac{\Delta K^4 E}{\sigma_{sy}^3 K_{Ic}^2}$	D	Cherepanov [5]
Crack opening displacement (COD)	critical value of cumulative displacement at crack tip	$\frac{\alpha_5}{l_5}\left(\frac{\Delta K}{\sigma_{sy}}\right)^4$	E	Rice [6]
Continuous dislocation formalism (not crystal dislocation theory)	critical value of cumulative displacement at crack tip	$\alpha_6 \frac{\Delta K^4}{\gamma E \sigma_{sy}^2}$	F	Weertman [7]
Continuous dislocation formalism (not crystal dislocation theory)	critical value of cumulative displacement at crack tip critical value of plastic work	$\alpha_7 \frac{\Delta K^4}{\gamma_p \mu \sigma_a^2}$	F′	Weertman [8] Mura and Lin [9]
COD	critical value of COD	$\alpha_8 \frac{\Delta K^2}{E\sigma_{sy}}$	G	Lardner [10]
COD	critical value of COD	$\alpha_9 \frac{\Delta K^2}{E\sigma_{sy}}$	H	Schwalbe [11]

COD	critical value of COD	$\alpha_{10}\left(\frac{\Delta K}{E}\right)^2$	I	Pook and Frost [12]
Slipband decohesion	critical value of COD	$\frac{\pi}{8}\left(\frac{\Delta K}{\sigma_{sy}}\right)^2\left(\frac{\Delta\sigma}{\sigma_0}\right)^{1/\beta}$	J	Tomkins [13]
Semi-experimental approach with COD	...	$\frac{(\Delta K-\Delta K_{TH})^2}{\sigma_{sy}E}f(\Delta K, K_{Ic}, K_{max})$	K	McEvily [14]
COD	critical value of COD	$\alpha_{11}\frac{\Delta K^2}{\mu\sigma_a}$	K′	Donahue et al [15]
Nucleation rate process approach (kinetic theory)	microcrack initiation at the crack tip	elastic approximation $\alpha_{12}\left(\frac{\Delta K}{\gamma E}\right)^{1/2\xi kT}$	L	T. Yokobori [16]
		elastic-plastic $\alpha_{13}\left(\frac{\Delta K}{\sqrt{s}\sigma_{cy}}\right)^{2\beta/(1+\beta)}\left(\frac{b\sigma_{cy}{}^2}{\gamma E}\right)^{1/2\xi kT}$	M	T. Yokobori et al [17]
Dislocations approach (kinetic theory)	dynamical emission of dislocation groups from crack tip	elastic approximation $\alpha_{14}\left(\frac{\Delta K}{\sqrt{s}E}\right)^{\frac{(m+1)^2}{m+2}}$	N	T. Yokobori et al [18]
		elastic-plastic $\alpha_{15}\left(\frac{\Delta K}{\sqrt{s}\sigma_{cy}}\right)^{\frac{2\beta}{1+\beta}\frac{(m+1)^2}{(m+2)}+\frac{1}{1+\beta}}\left(\frac{\sigma_{cy}}{E}\right)^{\frac{(m+1)^2}{m+2}}$	O	T. Yokobori et al [19]

TABLE 2—*Chemical composition of material concerned (percent).*

Material	C	Si	Mn	P	S	Cu	Al	Cr	Ni	Mo	B
Low-carbon steel [*23*]	0.05	0.01	0.33	0.006	0.022	0.03	0.046	...	...	...	...
Low-carbon steel [*24*]	0.08	0.21	0.37	0.015	0.011	...	...	0.05	0.12	...	...
Tempered-martensitic steel [*24, 26*]	0.16	0.24	0.92	0.018	0.006	0.3	...	1.06	...	0.51	0.001
High-strength eutectoid steel [*27, 28*]	0.82	0.34	0.83	0.017	0.009	0.04	...	...	...	...	...
Heat-treated ball bearing steel [*29, 30*]	0.98	0.26	0.33	0.024	0.009	0.10	...	1.44	0.14	...	...
3Si-Fe [*25*]	0.024	3.10	0.15	0.008	0.004	...	...	...	...	...	...

TABLE 3—*Value of* n *and* $\log_{10}$C.

Material	Batch (Specimen Series)	Mean Diameter of Ferrite, mm	ASTM GSNO	Upper Yield Strength, kg/mm^2	Lower Yield Strength, kg/mm^2	Ultimate Tensile Strength, kg/mm^2	Elongation, %	n	$\log_{10}C$	Remarks
Low-carbon steel [*23*]	M	0.012	9.6	27.9	25.9	36.1	45.1	2.99	−9.628	
	A	0.016	9.0	26.0	21.6	30.9	57.8	3.56	−10.703	R = 0.24–0.40
	B	0.025	7.6	22.7	20.6	30.2	55.5	3.47	−10.495	
	G	0.028	7.3	20.6	19.6	29.3	56.4	4.03	−11.404	$R \simeq 0.03$
	F	0.206	1.6	11.5	10.4	27.1	51.3	3.63	−10.681	
Low-carbon steel [*24*]	A[a]	0.031	7.0	...	21.7	...	...	3.18	−10.084	
	B[a]	0.062	5.0	...	15.2	...	...	4.32	−11.805	R = 0.21–0.40
	C[a]	0.103	3.6	...	12.8	...	...	4.26	−11.784	
Tempered-martensitic steel [*24,26*]	...	...	...	76.2	76.2	84.5	40	2.5	−8.905	$R \simeq 0$
High-strength eutectoid steel [*27,28*]	...	...	...		173[a]	191.9	5.9	1.8	−8.07	$R \simeq 0$
Heat-treated ball bearing steel [*29,30*]	...	...	...	...	...	152>	0.54	4.7	−14.76	$R \simeq 0$
3Si-Fe [*35*]	A	0.040	...	...	...	...	...	7.8	−16.4	R = 0.5
								6.4	−14.45	R = 0.27
	B	0.090	...	...	...	...	...	6.4	−14.31	R = 0.5
								5.97	−14.17	R = 0.27
	C	0.250	...	...	...	...	...	5.69	−13.48	R = 0.5
								5.55	−13.48	R = 0.27
	D	1.000	...	...	...	...	...	5.42	−13.20	R = 0.5
								5.28	−13.20	R = 0.27

[a] 0.2% proof stress.

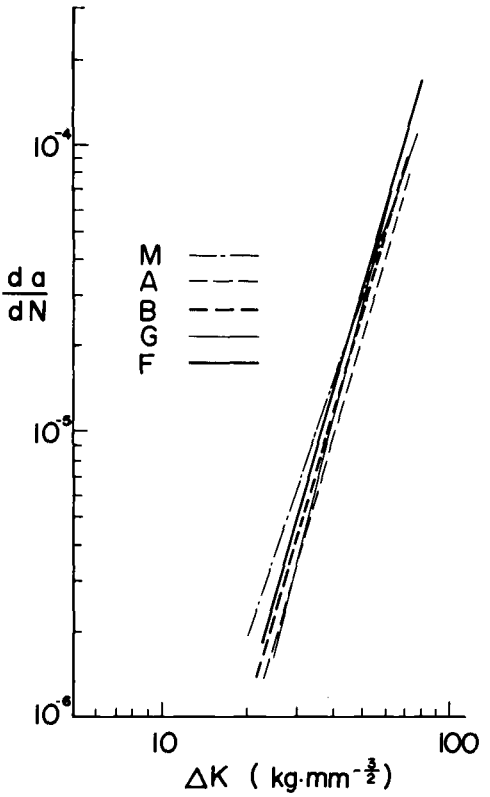

FIG. 2—*Experimental data on* da/dN *versus* ΔK *for 0.05 weight percent plain low-carbon steel as affected by ferrite grain size* [23].

from the data of Ref *25*, and it should be noted that for this material also Eq 2 holds, except that $\log_{10}U_0$ and $\log_{10}V_0$ are slightly different from those for low-carbon steel.

Additional Data for High-Strength Steels

The following presents an additional assessment of the effect of the monotonic yield strength on n for high-strength and highly hardened steels.

1. A tempered-martensitic high-strength steel was supplied in the form of plates 7 mm thick, hot-rolled and quenched and tempered [*24,26*] (Tables 2 and 3). The machining into specimens was similar to the 0.08 weight percent carbon steel described in the foregoing. The n obtained is about 2.5 and is plotted against $\log_{10}C$ in Fig. 6.

2. High-strength eutectoid steel was supplied in the form of 5.1-mm-diameter drawn wire, which was subjected to lead patenting, drawn, and

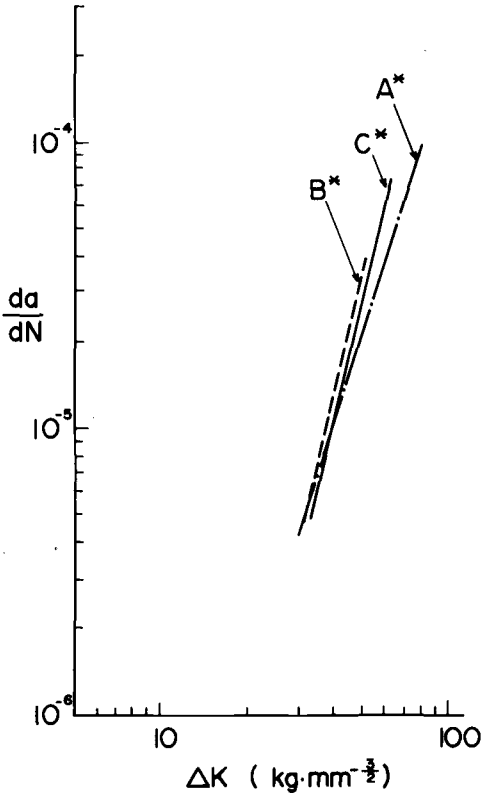

FIG. 3—*Experimental data on* da/dN *versus* ΔK *for 0.08 weight percent carbon steel as affected by ferrite grain size* [24].

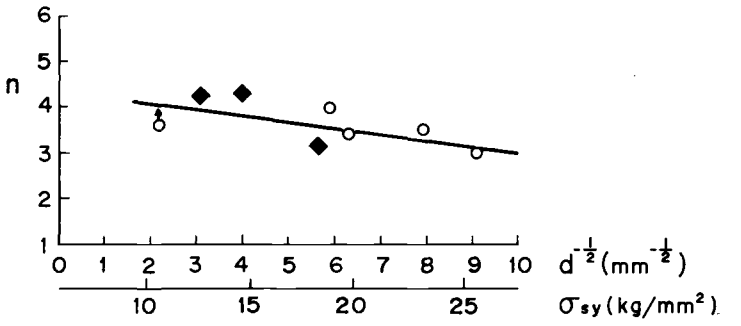

FIG. 4—*Value of* n *against ferrite grain diameter and static yield stress for low-carbon steels.* o *: 0.05 weight percent carbon steel* [23]; ◆ *: 0.08 weight percent carbon steel* [24].

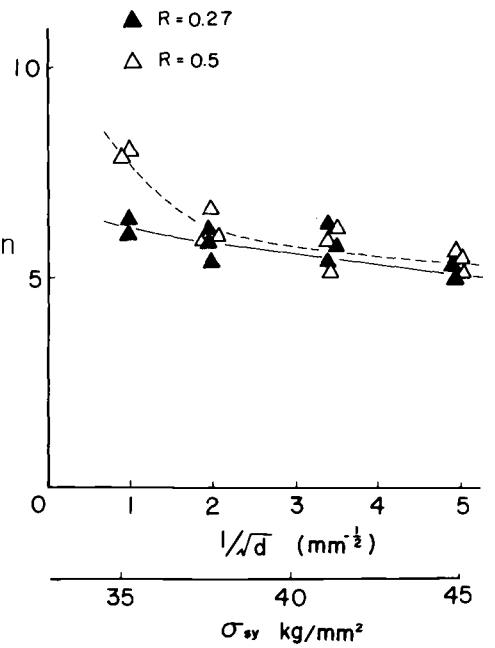

FIG. 5—*Value of* n *against ferrite grain diameter and static yield strength for 3 Si-Fe* [25].

blued at 350°C in a salt bath [*27,28*] (Tables 2 and 3). The gage length of the specimen is a smoothed plate 3 mm wide and 2.5 mm thick. After machining, the specimen surface was polished with 0/6 Emery paper and finally finished by buffing. Although the specimen was without artificial notch or crack, the measurement of the fatigue crack growth rate was possible by the plastic replication method, scanning electron microscope (SEM), and electron microscope because the crack initiates from a single inclusion and propagates in approximately circular form in such high hardened material. Observation of the specimen at suitable stages of propagation was attempted also by heat tinting decoration. The n thus obtained is about 1.8 and is plotted against $\log_{10}C$ in Fig. 6.

3. Heat-treated ball bearing steel was supplied in the form of 65-mm-diameter hot-rolled rods. After machining, the specimens were held for 25 min at 835°C, oil-quenched (60 to 80°C), and then tempered for 4 h at 160°C. The hardness obtained was HRC C-62 [*29,30*] (Tables 2 and 3). The specimen was smoothed plate 5 mm width and 2 mm thickness with a blank radius of 2.5 mm; it was ground and the final surface finishing was carried out with 0000 Emery paper. Fatigue crack growth rate was measured in the same way as for the eutectoid steel. The n obtained is about 4.7 and is plotted against $\log_{10}C$ in Fig. 6.

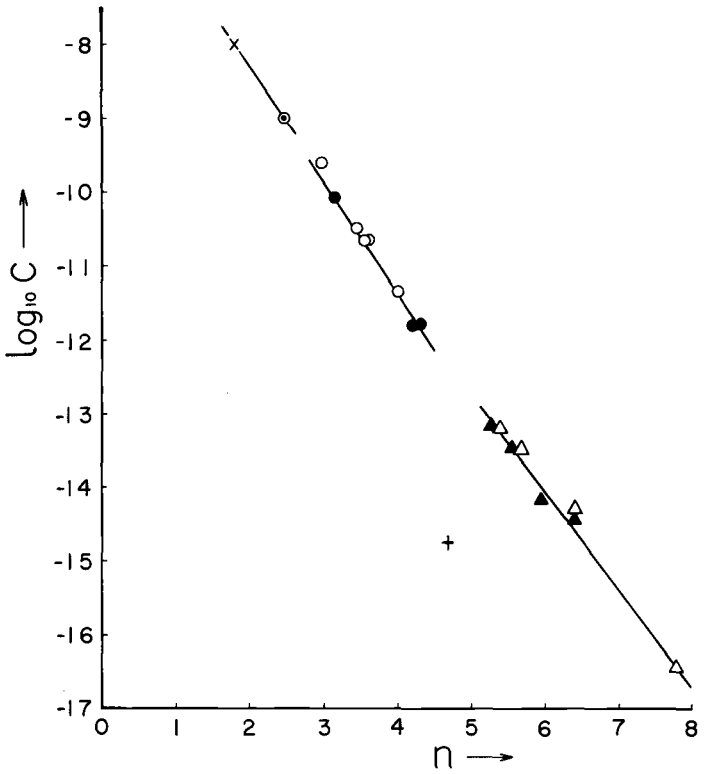

FIG. 6—*Plot of* $\log_{10} C$ *versus* n *for low-carbon steels and 3Si-Fe with various ferrite grain diameters, respectively.* ○*: 0.05 weight percent plain carbon steel* [23]; ●*: 0.08 weight percent plain carbon steel* [24]; ▲*: 3Si-Fe* (R = *0.27*) [25]; ×*: high-strength eutectoid steel* [27,28]; ⊙*: high-strength tempered martensitic steel* [24,26]; +*: high hardeness bearing steel* [29,30]. *Data on high strength and high hardened steels also are plotted.*

Discussion and Analysis

From dimensional analysis and comparison of Eqs A-0 in Table 1, Eq 1 may be written as

$$\frac{da}{dN} = B\left(\frac{\Delta K}{\sqrt{s}\sigma_c}\right)^n \tag{3}$$

or

$$\ln \frac{da}{dN} = \ln B + n\,(\ln \Delta K - \ln \sqrt{s}\sigma_c) \tag{4}$$

where σ_c is some constant with the dimension of stress. That is, C in Eq 1 is written as

$$C = B/(\sqrt{s}\sigma_c)^n \tag{5}$$

or

$$\log_{10}C = \log_{10}B - n \log_{10}\sqrt{s}\sigma_c \tag{6}$$

Now Fig. 6 shows that $\log_{10}B$ and $\log_{10}\sqrt{s}\sigma_c$ in Eq 6 are practically independent of static yield strength σ_{sy}, but n has the trend of slowly increasing function of the ferrite grain diameter, and thus, indirectly decreasing function of static yield strength for low-carbon steel and 3 weight percent silicon iron, respectively.

Equation 4 can be shown as in Fig. 7. If n assumes various values instead of a fixed value, say, 4 or 2, all the lines predicted by Eq 3 cross one point corresponding to $\ln \Delta K = \ln\sqrt{s}\sigma_c$ or $\ln (\Delta K/\sqrt{s}\sigma_c) = 1$. The data for the case of low-carbon steel as affected by ferrite grain size show that n increases with increase of d or the decrease of $d^{-1/2}$, and this trend is manifested in Figs. 1 and 2, as predicted in Fig. 7. It is interesting to note that in the region of the smaller da/dN (or ΔK), say, near the first region including threshold, da/dN is higher for smaller grain size at the

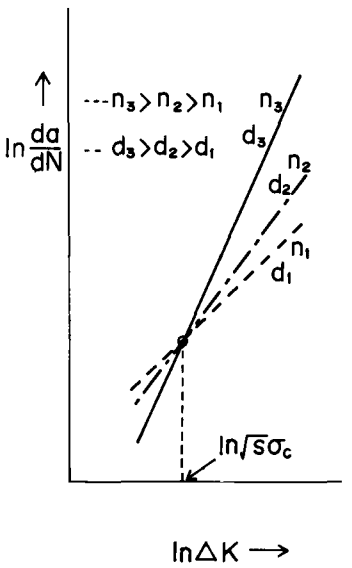

FIG. 7—*Schematic illustration of the proposed relation of* da/dN *versus* ΔK *as affected by ferrite grain size in the second region.*

same value of ΔK, as shown by Figs. 1, 2 and 7. The trend may correspond to the observations on titanium alloys by Pineau [*31*] and on the effect of grain size on K_{TH} of low-carbon steel [*32*].

In Fig. 8, n is plotted against static yield strength σ_{sy} for both low-carbon steels [*23,24*] and 3 weight percent silicon iron [*25*]. It should be noted that n is not uniquely determined by ferrite grain size or indirectly by static yield strength, but is also affected by some other microstructural factor. This feature may also be reflected in the data for $\log_{10}C$ and n for high-strength tempered-martensitic steel, eutectoid steel, and high hardened bearing steel plotted as in Fig. 6. It is shown in Fig. 6 that, for the two former steels, the higher the static yield strength, the smaller the value of n, and that, on the other hand, for the more hardened bearing steel, the value of n is rather larger than those of the two former steels. All these features probably show that n may be a function of the strain hardening exponent, especially of the cyclic strain hardening exponent, and this measure may be related to ferrite grain diameter (indirectly related to the monotonic yield strength).

If s is assumed to be the length over which the high value of ΔK is averaged, $\Delta K/\sqrt{s}$ in Eq 3 will mean a measure of high localized stress, and in this case local stress may be a criterion-determining factor. If σ_c is assumed to be the same as σ_{sy}, then s in Eq 3 should be proportional to the inverse of σ_{sy}^2, so that $\sqrt{s}\sigma_c$ is independent of σ_{sy} as seen from Fig. 6. In this case, however, s should not necessarily be the same as the total length of plastic zone, and therefore is not proportional to the inverse of σ_{sy}^2. Also it is

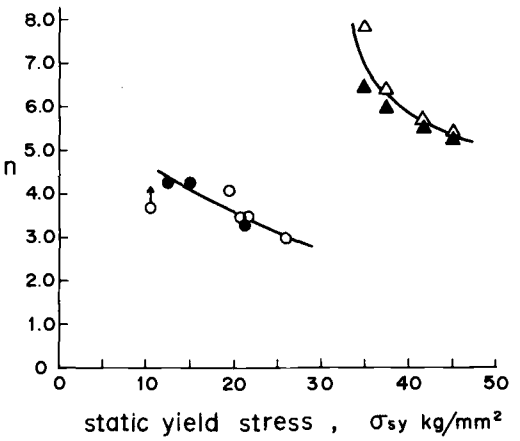

FIG. 8—*Comparison of* n *for low-carbon steel and 3Si-Fe as a function of static yield strength changed by ferrite grain size. Arrow shows this value will be higher for* R = *0.24-0.40. Legend is the same as shown in Fig. 6.*

concluded that $\sqrt{s}\sigma_{sy}$ is not proportional to ΔK, because, if this were the case, then Eq 3 would show no dependence on ΔK.

Further, even if we assume that a criterion-determining factor is energy, it is still not *a priori* that s should be proportional to the inverse of σ_{sy}^2.

From the foregoing argument, the existing equations of the type such as Eqs A-H, J, and K in Table 1 may not be adequate, at least for low-carbon steel and 3 weight percent silicon iron. In Eqs F′ and K′ the meaning of σ_a and γ_p is not specified with respect to the monotonic yield stress σ_{sy} dependence. In addition, the value of n inevitably is one definite value of 4 or 2, respectively, and this point is not in accord with these critical experiments. As far as n value is concerned, the situation is similar in Eqs A, B, or I in Table 1.

It is well known [*33*] that the static strain hardening exponent λ against static yield stress σ_{sy} is as shown in Fig. 9, which shows that λ is also a function of some microstructural parameter such as the percentage of carbon in steels. It has been proposed [*16,19,34*] that strain hardening characteristics, especially cyclic strain hardening characteristics, play a role in fatigue crack growth. Furthermore, the cyclic strain hardening exponent β has a similar dependence [*35*] on ferrite grain size or indirectly on static yield strength as λ, and thus shows similar characteristics as shown in Fig. 10.

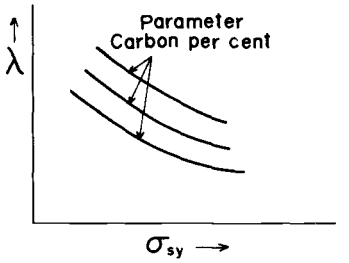

FIG. 9—*Schematic illustration of monotonic strain hardening exponent* λ *and monotonic yield strength* σ_{sy}.

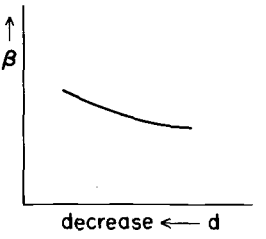

FIG. 10—*Schematic illustration of cyclic strain hardening exponent* β *and ferrite grain diameter* d.

On the other hand, da/dN based on elastic-plastic treatment in the criteria [*16,19,34*] is expressed as proportional to ΔK^n, where n is an increasing function of β. From this and Fig. 10 it may be inferred that the power coefficient n will show a decreasing function with decrease of ferrite grain size (or indirectly with increase of σ_{sy}) with some other microstructural parameter as shown in Fig. 8. Concerning the other microstructural parameter, the difference of the configuration of dislocation cell structures between low-carbon steel and 3 weight percent silicon iron may be mentioned.

Furthermore, σ_{cy} is not necessarily equal to or proportional to static yield strength σ_{sy}. Instead, σ_{cy} is considered as practically not nearly affected [*35*] by ferrite grain size, or indirectly by σ_{sy}.

For the foregoing reasons, equations of the type such as Eqs L-O in Table 1 may be more plausible.

Conclusions

From dimensional analysis and comparison of mathematical equations for fatigue crack growth in the literature, fatigue crack growth rate in the second region is expressed with sufficient generality for the case without significant mean stress as

$$\frac{da}{dN} = B\left(\frac{\Delta K}{\sqrt{s}\sigma_c}\right)^n$$

where σ_c and s are constants with dimensions of stress and length, respectively. By compiling the experimental data and using the foregoing equation, the following conclusions are obtained.

1. B and $\sqrt{s}\sigma_c$ in the foregoing equation are practically independent of monotonic yield strength, but n has the trend of a slowly increasing function of the ferrite grain diameter, and thus, indirectly a decreasing function of the monotonic yield strength for low-carbon steel and 3 weight percent silicon iron, respectively.
2. The latter features mean that n is an increasing function of the cyclic strain hardening exponent.
3. n may also be affected by some other microstructural factor.
4. From this point of view, most of the existing equations for fatigue crack growth should be subject to some criticism at least for low-carbon steel and 3 weight percent silicon iron.
5. In the region of smaller da/dN (or ΔK), say, near the first region including threshold, da/dN may be higher for smaller grain size at the same value of ΔK.

Acknowledgment

This work is part of a research program financially supported by the Mitsubishi Research Foundation, and the author expresses his sincere thanks for the grant.

References

[1] Paris, P. and Erdogan, F., *Transaction,* American Society of Mechanical Engineers, *Journal of Basic Engineering,* Vol. 85, 1963, p. 528.
[2] Liu, H. W., *Transactions,* American Society of Mechanical Engineers, *Journal of Basic Engineering,* Vol. 83, 1961, p. 23.
[3] Paris, P., *Fatigue—An Interdisciplinary Approach,* Syracuse University Press, Syracuse, N.Y., 1964, p. 107.
[4] Raju, K. N., *International Journal of Fracture Mechanics,* Vol. 8, 1972, p. 1.
[5] Cherepanov, G. P. and Halmanov, H., *Engineering Fracture Mechanics,* Vol. 4, 1972, p. 219.
[6] Rice, J. R. in *Fatigue Crack Propagation ASTM STP 415,* 1967, p. 247.
[7] Weertman, J. in *Proceedings,* First International Conference on Fracture, Sendai, Japan, Vol. 1, 1965, p. 153.
[8] Weertman, J., *International Journal of Fracture Mechanics,* Vol. 8, 1973, p. 125.
[9] Mura, T. and Lin, C. T., *International Journal of Fracture Mechanics,* Vol. 10, 1974, p. 284.
[10] Lardner, R. W., *Philosophical Magazine,* Vol. 17, 1971, p. 71.
[11] Schwalbe, K., *International Journal of Fracture,* Vol. 9, 1973, p. 381.
[12] Pook, L. P. and Frost, N. E., *International Journal of Fracture,* p. 53.
[13] Tomkins, B., *Philosophical Magazine,* Vol. 18, 1968, p. 1041.
[14] McEvily, A. J., *The Microstructure and Design of Alloys,* The Metals Society, London, 1974, p. 204.
[15] Donahue, R. J., Clark, H. M., Atanmo, P., Kumble, R., and McEvily, A. J., *International Journal of Fracture Mechanics,* Vol. 8, 1972, p. 209.
[16] Yokobori, T., *Physics of Strength and Plasticity,* A. S. Argon, Ed., Massachusetts Institute of Technology Press, Cambridge, Mass., 1969, pp. 327-338.
[17] Yokobori, T. and Ichikawa, M. in *Reports of Research Institute for Strength and Fracture of Materials,* Tohoku University, Sendai, Japan, Vol. 4, 1968, pp. 45-53.
[18] Yokobori, T., Yokobori, A. T., Jr., and Kamei, A., *International Journal of Fracture,* Vol. 11, Oct. 1975, pp. 781-788; also, Corrigenda, Vol. 12, Aug. 1976, pp. 519-520.
[19] Yokobori, T., Konosu, S., and Yokobori, A. T., Jr. in *Proceedings,* Fourth International Conference on Fracture, University of Waterloo, Waterloo, Ont., Canada, Vol. 1, pp. 665-682.
[20] Yokobori, T. and Aizawa, T. in *Reports of Research Institute for Strength and Fracture of Materials,* Tohoku University, Sendai, Japan, Vol. 6, No. 1, 1970, pp. 19-23.
[21] Kawasaki, T., Nakanishi, S., Sawaki, Y., Hatanaka, K., and Yokobori, T., *Engineering Fracture Mechanics,* Vol. 7, 1975, pp. 465-472.
[22] Hahn, G. T., Sarrate, M., and Rosenfield, A. R. in *Proceedings,* Conference on Fatigue and Fracture of Aircraft Structures and Materials, AFFDL TR 70-144(II), Air Force Flight Dynamics Laboratory, Ohio, 1970, pp. 425-449.
[23] Yokobori, T., Kawada, I., and Hata, H., *Reports of Research Institute for Strength and Fracture of Materials,* Tohoku University, Sendai, Japan, Vol. 9, No. 2, 1973, pp. 35-64.
[24] Yokobori, T., Tanaka, M., Hayakawa, H., Yoshimura, T., and Sasahira, S. in *Reports of Research Institute for Strength and Fracture of Materials,* Vol. 3, No. 2, 1967, pp. 39-71.
[25] Ando, K., Ogura, N., and Nishioka, T., Preprint, Japan Society of Mechanical Engineers, No. 760-2, 1976, p. 153 (in Japanese).
[26] Yokobori, T., Kuribayashi, H., Kawagishi, M., and Takeuchi, N. in *Reports of*

Research Institute for Strength and Fracture of Materials, Tohoku University, Sendai, Japan, Vol. 7, No. 1, 1971, pp. 1-23.
[27] Yokobori, T., Sawaki, Y., Shono, S., and Kumagai, A., *Transactions*, Japan Institute of Metals, Vol. 17, No. 1, 1976, pp. 1-10.
[28] Yokobori, T., Sawaki, Y., Shono, S., and Kumagai, A., *Reports of Research Institute for Strength and Fracture of Materials*, Tohoku University, Sendai, Japan, Vol. 12, No. 2, 1976, pp. 29-54.
[29] Yokobori, T. and Nanbu, M. in *Reports of Research Institute for Strength and Fracture of Materials*, Vol. 2, No. 2, 1976, pp. 29-44.
[30] Yokobori, T. and Aizawa, T. in *Reports of Research Institute for Strength and Fracture of Materials*, Vol. 13, No. 2, 1977, pp. 75-78.
[31] Pineau, A. G., private communication.
[32] Masounave, J. and Baflon, J. P., *Scripta Metallurgica*, Vol. 10, 1976, p. 165.
[33] Hollomon, J. H., American Institute of Mining Engineers Technical Publication No. 1879, 1945, p. 1.
[34] Yokobori, T. in *Reports of Research Institute for Strength and Fracture of Materials*, Tohoku University, Sendai, Japan, Vol. 5, 1969, p. 19.
[35] Yokobori, T., S. Koyama and H. Ishii, *Scripta Metallurgica*, June 1979 (in press).

DISCUSSION

V. Ivanova[1] *discussion*)—Professor Yokobori has shown that n in the ln $da/dN - K$ dependence is a function of ferrite grain size and other microstructural factors. That is the reason why dependence $da/dN - K$ is more complex, as has been suggested previously.[2] From this, Yokobori's conclusion follows that most of the exiting formulas for fatigue crack growth should be subjected to some criticism.

There are two types of kinetic diagrams of fatigue crack growth: the S-type (Fig. 11*a*) and the sigmoidal one (Fig. 11*b*). Kinetic diagram type depends on heat treatment, and finally it has been noted that, for different cyclic loading, critical states (either plastic instability or fracture instability controlled either by K_{IIc} or K_{Ic}) correspond to the same parameter K_{fc} (fatigue fracture toughness).

Fatigue fracture is a unique example of the realization of different limiting states controlled either by K_{Ic}, K_{IIc}, K_{IIIc}, or K_c.

The type of limiting state realized depends on specimen size, the initial structural state of the material, and loading conditions. Then the fatigue fracture toughness concept suggested by Yokobori and Alizawa[3] is more general than the static fracture toughness concept; fatigue fracture with the realization of K_{Ic} is a special case. On the basis of experimental data, the

[1] A. A. Baikov Institute of Metallurgy, U.S.S.R. Academy of Sciences, Leninsky Prospect, Moscow, U.S.S.R.

[2] Paris, P. and Erdogan, F., *Transactions*, American Society of Mechanical Engineers, *Journal of Basic Engineering*, Vol. 85, 1963, p. 528.

[3] Yokobori, T. and Aizawa, T. in *Reports of Research Institute for Strength and Fracture of Materials*, Tohoku University, Sendai, Japan, Vol. 6, 1970, p. 19.

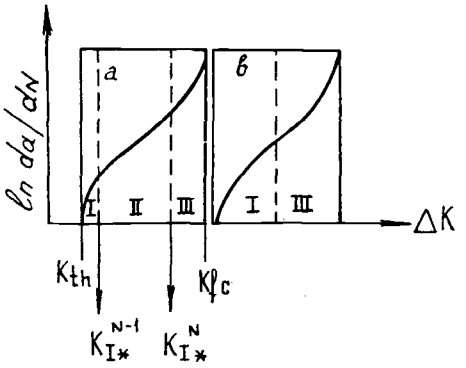

FIG. 11—*Types of kinetic diagrams of fatigue crack growth*: (a) *S type*; (b) *sigmoidal type*. I—*microshear fracture mode stage is controlled by* K_{II}; II—*microtension fracture mode stage is controlled by* K_I; III—*mixed fracture mode*.

sigmoidal type of kinetic diagram is observed when limiting states are controlled by K_{IIc}. In this case, Region II is absent (Fig. 11*b*) because the microshear fracture mechanism is realized during the stage of stable crack growth (Region I), and intergranalural fracture is observed in State III.[4,5] Here, the critical state is controlled by K_{IIc}. The S-type of kinetic diagram is observed when microtensile fracture mechanism are realized during Stage II under plane-strain conditions controlled by K_I.

Therefore, from this point of view, Yokobori's conclusion that n is not only a ferrite grain size (or static yield stress) function but also depends on some other microstructural factors is true. It means that it is necessary to take into account the crack growth mechanism at Region II for estimation of real $da/dN - K$ dependence.

Yokobori et al[6] have analyzed the brittle fracture process on the basis of the kinetic theory of fracture[7] with the use of physics and fracture macromechanics concepts. This analysis leads to the conclusion that fracture toughness represented by the parameters K_c or K_{Ic} can be expressed as

$$K_{I*} = \sqrt{2E\delta_p{}^*} \tag{7}$$

Here, $\delta_p{}^*$ is effective energy per unit length of the crack, depending on

[4]Otsuka, A., Mori, K., and Miyata, T., *Engineering Fracture Mechanics*, Vol. 7, 1975, p. 429.

[5]Romaniv, O. N., Deev, N. A., Gladkiy, Ja. M., and Student, A. G., *Phisiko-chimicheskaya Mechanika Materialov*, No. 5, 1975, p. 23.

[6]Yokobori, T., Konusu, S., and Yokobori, A. T., Plenary Paper in *Proceedings*, Fourth International Conference on Fracture, Vol. 1, 19-24 June 1977, p. 1.

[7]Yokobori, T. in *Reports of Research Institute for Strength and Fracture of Materials*, Tohoku University, Sendai, Japan, Vol. 5, 1969, p. 19.

the structure of material, the plain-strain mechanism controlling the crack development, and other factors. So, when passing from one mechanism of subcritical crack growth (for example, origin of voids in front of the crack) to another (for example, origin of dislocation crack in front of the main crack), the value δ_p* changes. It follows from the relationship (Eq 7) that, depending on the mechanism controlling the crack development, various limiting states can be realized.

According to Cherepanov's approach,[8] the subcritical crack growth controlled by K_I can be realized when $K_I < K_{Ic}$. Therefore, during subcritical crack growth under the cyclic loading conditions, the values K_{Ic} can fail to be achieved, and the limiting state is realized as a result of plastic instability at $K_I < K_{Ic}$ or as a result of transverse microshear mechanism at $K < K_{Ic}$ too, since $K_{IIc} < K_{Ic}$. This means that, to estimate the durability of a material under cyclic loading, it is insufficient to know only one parameter, K_{Ic}, for choosing the best materials to work under the fatigue conditions, but it is also necessary to know the spectrum of values, K, responsible for different limiting states. At the same time, it is essential to select the range of K or $4K$ variation within the limits of which the same mechanism of local fracture, controlling the subcritical crack growth, is preserved. It makes possible comparison of the durability of materials and alloys under similar conditions of local fracture.[9]

As shown earlier,[9,10] the following similarity criterion of subcritical crack growth may be used

$$\mu_\Delta = K_{I*}{}^{N-1}/K_{I*}{}^{N}$$

Here $K_{I*}{}^{N-1}$ is threshold K_I that defines the lower boundary, and $K_I{}^N$ is threshold K_I that defines upper boundary of possible stress intensity factor K_I variation when the crack length increases from l_{sII} to l_s. l_{sII} is the initial fatigue crack length at which the subcritical crack growth begins to be controlled by only one parameter, K_I or (K_I), and microtension fracture mode are realized.[11] l_s is the critical fatigue crack length when macroplastic instability arises near crack tip (footnote 9). Thus the value $l_s - l_{sII}$ is equal to the crack part length at which crack growth velocity is controlled only by the microtension fracture mode. The existence of the threshold values K_{I*} responsible for fracture mechanism change have been previously shown experimentally.[12]

[8] Cherepanov, G. P., *Brittle Fracture Mechanics*, Nauka, Moscow, U.S.S.R., 1974.

[9] Ivanova, V. S. and Terentjev, V. F., *The Nature of Metal Fatigue*, Moscow, Metallurgia, 1975.

[10] Ivanova, V. S. and Maslov, L. I. in *Proceedings*, Second International Conference on Mechanical Behavior of Materials, ICMII, Boston, Mass., 16-20 Aug. 1976, p. 1212.

[11] Botvina, L. R. and Saprikin, Joo, *Journal Metalli*, No. 1, 1977, p. 161.

[12] Gurevich, S. E. and Edidovich, L. D. in *Proceedings*, Conference on Fatigue and Fracture Toughness of Metals, Nauka, Moscow, U.S.S.R., 1974, p. 76.

In all cases, complete $da/dN - K$ curves are described by the following relationship[13]

$$da/dN = v_0 \left[\frac{K - K_{TH}}{K_{fc} - K} \right]^q \tag{8}$$

Here q is a constant and v_0 is a constant having the dimension of velocity. It makes it possible, as has been shown previously,[14] to represent Eq 8 as a function of the dimensionless variables $v/v_0 - K/K_{TH} \cdot K_{fv}$. The experimental data show the complex which remains constant for different alloys[14]

$$A_v = q \frac{p + 1}{p - 1} egP = \text{const} \tag{9}$$

Here $P = K_{fc}/K_{TH}$. There are only two values for A_v. For example, for iron alloys, $A = 1.61$ and $A = 1.76$ (footnotes 13 and 14). Our analysis shows that $A = 1{:}61 =$ constant for the S-type diagram (Fig. 11*a*) and $A = 1.76 =$ constant for sigmoidal-type diagram (Fig. 11*b*). Also, for the S-type of diagram the threshold value K_{v_0} corresponds to $da/dN = v_0$

$$KV_0 = \frac{K_{fc} - K_{TH}}{2} \tag{10}$$

as it follows from Eq 9. Under $K_I < K_{v_0}$, the tensile fracture, Mode I, is realized; under $K > K_{v_0}$ the mixed fracture mechanism (microshear plus tensile microtensile fracture) is realized during subcritical crack growth, as a result of the attained static yield stress at the crack front (if the limit state is controlled by K_{IIIc} or K_c).

There is good agreement between Professor Yokobori's analysis and our data. Probably there is the trend of the slowly decreasing function of the ferrite grain diameter (and, thus, indirectly the static yield stress) only if the limit state (K_{fc}) is controlled by K_{IIIc} or K_c. It is possible that for another type of limit state (controlled by K_{IIc} or K_{Ic}), n is a constant independent of heat treatment.

M. Kanninen[15] (*discussion*)—From the viewpoint of the mathematical analyst, improvements in fracture mechanics predictions can be expected when the assumption of linear elastic behavior at the crack tip is removed in favor of an explicit treatment of plastic behavior. In fatigue—where

[13] Yarema, S. Ya. and Mikitishin, S. I., *Physiko-chimicheskaya Mechanika Materialov*, No. 6, 1975, p. 47.

[14] Yarema, S. Ya., *Physiko-chimicheskaya Mechanika Materialov*, No. 4, 1977, p. 3.

[15] Battelle Columbus Laboratories, Columbus, Ohio 43201.

deformation created in previous load cycles surely has a significant effect on the crack growth process—this must be even more true. A mathematical model treating crack-tip plasticity will necessarily involve the yield stress of the material. Thus, it is perplexing that observed constant-amplitude fatigue crack growth rates are found to be rather insensitive to yield stress.

Definitive studies which may help to resolve this paradox are needed. Accordingly, this paper, which purports to provide a critical assessment of the yield stress dependence in fatigue crack growth predictions, could be of great value. It is therefore disappointing to find that Professor Yokobori has focused his efforts quite narrowly. Specifically, he has adopted a power-law relation involving a number of empirical constants, evaluated the constants for materials with a range of grain sizes, and then simply explored their dependence on the yield stress.

No connection between the values of the empirical parameters and any basic fatigue mechanics is revealed in the paper. Nor is any indication given of how well alternative relations could represent the results. In particular, since some investigators believe that K_{Ic} also reflects a yield stress dependence, there can be a tradeoff that masks the effect of yield stress variations. Such a possibility has certainly not been ruled out by this work. It can be concluded that, while the work may be of definite value for engineering assessments, it does not offer much help in understanding the fatigue crack growth process itself.

T. Yokobori (author's closure)—Needless to say, it can be seen very simply, as I indicated early in the paper, that da/dN should include in general ΔK_{TH}, K_m, and K_c or K_{fc}. Nevertheless, I would like to emphasize that the primary aim of this paper is to make some critical review of the existing mathematical formula on fatigue crack growth concerning the paradox effect of static yield stress, and to show the effect of ferrite grain size on fatigue crack growth, for which studies have not yet been clearly carried out. Thus the focus was on the second region and the simple case in this paper as a first step; the next step will be how to include ΔK_{TH}, K_m, and K_c or K_{fc}. We should remember that fatigue crack growth mechanisms still remain unsolved, although many mathematical formulas for them have been proposed. It may be seen from this situation that fatigue crack growth mechanisms cannot be elucidated by only one paper. In elucidating such difficult problems in any scientific and technical field, I think it may be fruitful to proceed to a more precise or detailed model or formula by starting from a simple one.

The discusser appears to think that in the author's conclusion the static yield stress σ_{sy} is not included in da/dN. This is not correct, and I believe it may be a misunderstanding. As was clearly described in the text, it is concluded that σ_{sy} is included indirectly in terms of ferrite grain size in n where $da/dN = C\Delta K^n$.

Furthermore, I would like the following to be noted: With respect to the rate-determining plasticity in fatigue crack growth, the idea limited only to the static yield stress may not be right *a priori.* In fatigue crack growth, I believe that plasticity connected with cyclic strain will play a role also. In Eqs M and O in Table 1, the plastic stress intensity factor in terms of this cyclic strain hardening was used.

Finally, concerning a connection between the values of empirical parameters and any basic fatigue mechanisms, and an indication of how well the relation, if any, could represent the results, only a mention was made in the text. For instance, as a possible or not inconsistent formula, I mentioned the formula based on the nucleation theory of microcrack initiation at the crack tip and also the dynamical emission theory of dislocation group from the crack tip. Equations L and N using a linear elastic approximation in Table 1 are in good agreement with the results so far as Eq 4 is concerned. On the other hand, Eqs M and O using the plastic stress intensity factor in Table 1 are in accord with all the results, if we assume that cyclic strain hardening has similar characteristics to static strain hardening and that the initial yield in cyclic strain may be considered not so much affected by ferrite grain size, at least within the second region. Say that the exponent of Eq O is an increasing function of cyclic strain hardening exponent β, and, on the other hand, the static strain hardening exponent λ in steel is a decreasing function of both static yield stress σ_{sy} and microstructure as shown in Fig. 13 of footnote 16. The trend of Fig. 8 in the text might be correlated if we use this assumption and Eq O.

[16] Hollomon, J. H., American Institute of Mining Engineers Technical Publication No. 1879, 1945.

T. H. Lin[1] *and S. R. Lin*[2]

Micromechanics Theory of Fatigue Crack Initiation Applied to Time-Dependent Fatigue*

REFERENCE: Lin, T. H. and Lin, S. R., **"Micromechanics Theory of Fatigue Crack Initiation Applied to Time-Dependent Fatigue,"** *Fatigue Mechanisms*, Proceedings of an ASTM-NBS-NSF symposium, Kansas City, Mo., May 1978, J. T. Fong, Ed., *ASTM STP 675*, American Society for Testing and Materials, 1979, pp. 707-728.

ABSTRACT: Different theories of fatigue crack initiation for time-independent fatigue are briefly reviewed. The micromechanics theory for time-independent fatigue proposed by Lin and Ito is shown to be applicable also for time-dependent fatigue. Three closely located parallel thin slices in a most favorably oriented crystal located at a free surface of a polycrystal are assumed to have small initial resolved shear stresses of opposite signs. From the slip rate versus resolved shear stress data of aluminum single crystals, the increases of local creep strains in the slices with cycles of stress loading were calculated by using the analogy between creep strain gradient and body force. This calculation was made for loading frequencies of 0.1 to 1000 cpm. It was found that the creep shear strain in the slices depends on the time of loading for frequencies greater than 10 cpm and becomes more dependent on cycles of loading at lower frequencies. The method is applicable also to loadings with given alternate strains instead of stresses.

KEY WORDS: crack initiation, creep, elevated temperature, extrusion, fatigue, intrusion, resolved shear stress, slipbands, slip lines

During 1953-1955, Forsyth [*1,2*][3] made a very important discovery in fatigue research. He found that during fatigue thin sheets of metal are sometimes extruded from slipbands. These sheets were found to reach a height of 10 μ and to have widths ranging from 1 μ to a substantial frac-

[1] Professor, Mechanics and Structures Department, School of Engineering and Applied Science, University of California, Los Angeles, Calif. 90024.

[2] Manager, Thermostructural Analysis Section, Structures Department, The Aerospace Corp., El Sequndo, Calif. 90245; formerly, postdoctoral scholar, University of California, Los Angeles, Calif.

* This work was supported by the National Science Foundation under Grant ENG74-93809 and was performed at the University of California at Los Angeles.

[3] The italic numbers in brackets refer to the list of references appended to this paper.

tion of the grain diameter. These sheets are less than 0.1 μ thick. The reverse of slipband extrusion, that is, slipband intrusion, also occurs as shown by Hull [*3–5*]. Hull showed that extrusions formed in copper subject to cyclic loadings even at temperatures as low as 4.2 K. Forsyth [*6*] has also found that, in silver chloride, extrusions form but they apparently leave no voids below the surface in the material. This shows that surface corrosion, gas adsorption, gas diffusion into a metal, or vacancy diffusion to form voids are not necessary to the formation of extrusion and intrusion [*7*]. The formation of an intrusion is considered as a crack initiation.

Single-crystal (aluminum) tests at room temperature [*8–10*] have shown that, under stress, slip occurs along certain crystallographic directions on certain crystal planes. The sliding direction and sliding plane generally are those of maximum atomic density. A slip direction on a sliding plane is called a slip system. The shear stress along the slip direction on the sliding plane is referred to as the resolved shear stress. Slip has been found to depend on the resolved shear stress and to be independent of the normal pressure on the slip plane [*11*]. This slip has been shown to be the main mechanism of plastic deformation of face-centered-cubic (fcc) metals at low and intermediate temperatures [*12*].

Single aluminum crystal tests also show that deformation at elevated temperatures [*13,14*] occurs by slip in primarily the same slip systems that are operative at room temperature. At elevated temperatures, the slip rate in a slip system was found to depend on the resolved shear stress and the amount of the resolved creep shear strain in the crystal. Both plastic strain and creep strain are caused by slip which is the result of the displacement of dislocations. The stress fields caused by plastic shear strain and that by creep shear strain are the same. Hence, the mechanics aspects of the fatigue crack initiation of metals loaded at room temperature and at elevated temperatures (below one-half the melting temperature) are essentially the same.

Gilman [*15*] has shown data on the variation of dislocation velocity with applied resolved shear stress of some materials at different temperatures. For some material, the velocity is negligible until certain resolved shear stress is reached. After this shear stress is reached, a small increase of this stress causes a large increase of the dislocation velocity. Then the rate of the increase of the velocity with further increase of the shear stress decreases. This resolved shear stress is very similar to the critical shear stress in plasticity and will be here referred to as the critical creep shear stress.

Previous Theories of Fatigue Crack Initiation

Several theories of fatigue crack initiation, based on the formation of extrusions and intrusions, have been proposed by different distinguished

investigators. Cottrell and Hull [*4*] suggested that Frank-Read sources exist on two intersecting slip planes. A complete cycle of forward and reversed loading results in an extrusion and an intrusion. Such a model would predict a close association of an extrusion and intrusion, and they would be inclined to each other at a rather large angle (angle between two slip planes of an fcc crystal) and would appear in neighboring slipbands. But they have often been observed to be parallel to each other and to occur together in the same slipband. Mott [*16*] proposed a mechanism based on the idea that a screw dislocation can repeat its path through cross slip. He considered an elementary crystal block containing a single screw dislocation intersecting a free surface. This screw dislocation travels a complete circuit in the metal. The volume contained by the circuit is translated parallel to the dislocation by an amount equal to its Burger's vector. This causes the material to extrude out of the free surface. As pointed out by Kennedy [*17*], this mechanism cannot be easily extended to explain intrusions and it is also hard to see why the dislocation under cyclic loading does not simply oscillate back and forth along the same path rather than traversing a closed circuit. Some *gating mechanism* is clearly needed to convert the back-and-forth oscillations of the screw dislocations into unidirectional circuits. Kennedy [*17*] proposed Lomer-Cottrell barriers as one such gating mechanism. But why these barriers would move synchronously with the dislocations is not explained.

Mott's mechanism is adopted by May [*18*] as the basic one, but he assumes the return path of a dislocation under an alternating stress to be shifted with respect to the original path by an amount which varies in a random fashion. Slip in each half-cycle is distributed randomly among the available slip planes. The distribution of slip in each half-cycle is taken to be independent of the distribution of slip in the previous cycles. As the surface roughens by this process, May assumes that the stress concentrations in the valleys increase the probability of slip in such regions and thus these valleys deepen locally to initiate fatigue cracks. As remarked by Kennedy [*17*], this model requires more detailed physical terms as this random switching from one slip plane to another is not a process which can be readily accepted. Besides, the slip in the previous cycles will render a residual stress field which will undoubtedly influence the subsequent slip.

Thompson [*19*] proposed an edge-screw interaction model for the initiation of extrusion. This model assumes a change of spacing of a pair of parallel screw dislocations after being cut by an edge dislocation. This cut causes jogs in the edge and screw dislocations. This will inhibit the change of the spacing of the two screw dislocations. It is hard to see why the same edge dislocation does not move back along the same path and causes no extrusion. It is also difficult to see how intrusions can be formed by such a model.

McEvily and Machlin [*20*] proposed a model with two screw dislocations

terminating in a free surface and intersecting a node where three dislocations meet. Under an alternating shear stress, each of the two screw dislocations is assumed to shift around a circuit. This causes an extrusion and an intrusion formed in the same slipband. However, it is not explained why these two dislocations travel around circuits instead of back and forth.

Wood [*21*] proposed a simple model of a single operative slip system. In unidirectional stressing, layers of metal slide in the same direction and no intrusion or extrusion can form. But forward and reverse stressing results in different amounts of net slip on different planes and yields peaks and valleys. This model [*17*] does not explain why, under an alternating loading, the slip continues to monotonically deepen the valleys and raise the peaks as observed in experiments.

Slip is caused by the movement of dislocations. Dislocations generally move along certain crystal directions on certain crystal planes. The velocity of this movement depends on the resolved shear stress. The models of fatigue crack initiation previously discussed consider mainly the paths of dislocation movement without calculating the resolved shear stress fields causing this movement. In the following, we analyze the effect of this resolved shear stress, which does supply a natural gating mechanism for the monotonic raising of the peaks and deepening of the valleys [*22*].

Stress Field Caused by Creep Strain

When the resolved shear stress is small, the shear strain rate is negligible. When the shear stress exceeds a certain value, the shear strain rate becomes appreciable and causes an incremental creep strain in a given time interval. This incremental strain combines with the previously existing strain to give a total creep strain. This creep strain causes a stress field in the metal. To find this stress field, the analogy between inelastic strain (plastic, creep, and thermal strains) and applied force is used. Referring to a set of rectangular coordinates, the strain components are considered to be composed of the elastic part e_{ij}^E and the creep part e_{ij}^C

$$e_{ij} = e_{ij}^E + e_{ij}^C \tag{1}$$

The elastic constants of crystals are generally anisotropic. This anisotropy varies from one metal to another and is small for aluminum. In the present study, this anisotropy is neglected. The stress is related to the elastic strain as

$$\tau_{ij} = \delta_{ij}\lambda e_{kk}^E + 2Ge_{ij}^E \tag{2}$$

where δ_{ij} is the Kronecker delta, λ and G are Lame's constants, and the repetition of subscript denotes summation from 1 to 3. Creep in the

temperature range considered produces no volume change; hence e_{kk}^{c} is taken to be zero

$$\tau_{ij} = \delta_{ij}\lambda e_{kk} + 2G(e_{ij} - e_{ij}^{c}) \tag{3}$$

The condition of static equilibrium gives

$$\tau_{ij,j} + F_i = 0; \qquad \tau_{ij}\nu_j = T_i^{\nu} \tag{4}$$

where

j (after the comma) = differentiation with respect to the j-axis,
F_i = ith component of the body force, and
T_i^{ν} = ith component of the surface force on the surface with outward unit normal ν.

Substitution of Eq 3 in Eq 4 yields

$$\lambda e_{kk,i} + 2Ge_{ij,j} + F_i - 2Ge_{ij,j}^{C} = 0 \tag{5}$$

$$\lambda e_{kk}\nu_i + 2Ge_{ij}\nu_j = T_i^{\nu} + 2Ge_{ij}^{C}\nu_j \tag{6}$$

It is seen that the term $-2Ge_{ij,j}^{C}$ has an equivalent effect as F_i, and $2Ge_{ij}^{C}\nu_j$ has an equivalent effect as T_i^{ν}, in causing the strain field e_{ij}. Hence, the strain distribution in a body with creep strain under external load is the same as that in a purely elastic body (no creep strain) with the additional equivalent forces

$$\overline{F_i} = -2Ge_{ij,j}^{C}; \qquad \overline{T_i^{\nu}} = 2Ge_{ij}^{C}\nu_j \tag{7}$$

This is similar to the well-known Duhamel analogy for thermal-elastic problems.

Charsley and Thompson [*23*] have shown that in single-crystal tests under cyclic tension and compression, a reversal of stress after a prior forward deformation yields new parallel slip lines in the early stage of fatigue cycles. Forsyth [*24*] found fresh slip lines produced during the reversed loading on an aluminum crystal lying very close to, but not coincident with, slip lines formed in the initial forward loading. Buckley and Entwistle [*25*] found compressive slip lines formed between the slip lines resulting from the prior tensile deformation. All these show that slip lines found in the reversed loading have been observed to lie very close to but distinct from those formed in the forward loading. Let positive shear strain occur in the slip line formed in tensile loading, and negative shear strain occur in the slip line formed in compressive loading. The layer between these slip lines would tend to extrude out of the surface [*22*]. Interchange

of the location of the slip lines tends to cause an intrusion to form. More slip lines may occur to cause an extrusion and an intrusion side by side to form in a slipband.

Wood and Bendler [*26*] tested copper circular rod specimens in torsion. The specimens were electropolished in phosphoric acid and then scratched as markers with a pad carrying 0.5-μ diamond dust. Some specimens were subject to alternate torsion and some to single twist through large angles. The deformation in a typical slipband AB on a specimen subject to single twist is shown in Fig. 1. Here, *a*, *b*, and *c* are typical scratches which were initially straight and continuous. The single twist caused the scratches above AB to displace relatively to those below. The deformation under cyclic torsion with Scratches *d*, *e*, *f* and a typical fatigue band CD is shown in Fig. 2. It is seen that cyclic torsion has caused no relative displacement of the scratches above and below the band CD, but, within the band, the scratches have displaced equally to the right and the left, producing a zigzag. A severely slid slip line with positive shear is sandwiched by two less

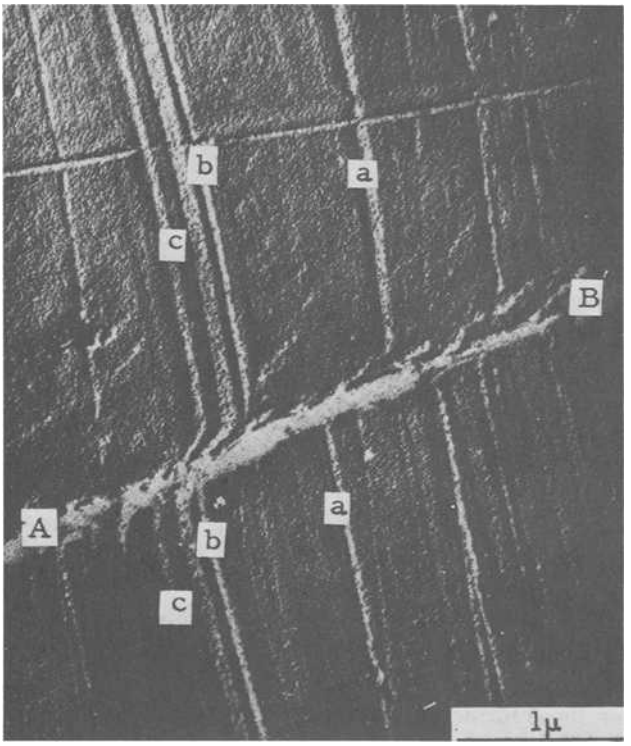

FIG. 1—*Initially straight scratches* a, b, *and* c *are displaced unidirectionally by static slip band* AB. *Reproduced from* Transactions, *Metallurgical Society of AIME. Courtesy of AIME.*

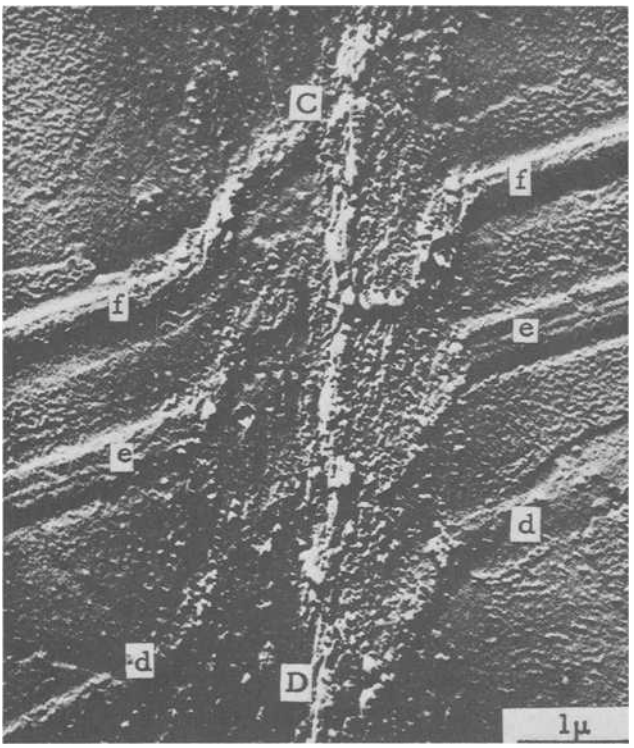

FIG. 2—*Cyclic slipband* CD *produces no overall displacement of Scratches* d, e, *or* f. *Within the slipband, the scratches are displaced equally backward and forward. Reproduced from* Transactions, *Metallurgical Society of AIME. Courtesy of AIME.*

severely slid lines with negative shear. When the slip direction is inclined to the free surface, these slip lines will cause one extrusion and one intrusion formed side by side in one slipband. This deformation yields severe strain in slipbands and little deformation in the remaining bulk of the material. This explains why the X-ray diffraction patterns of cyclically deformed metals retain their discrete spots like those of annealed metals and why X-ray patterns of monotonically loaded metals do not retain these spots [*21*].

Lattice imperfections exist in all metals and cause an initial heterogeneous stress field. The initial stress field favorable for the sequence of slip (as observed by Wood and Bendler) is one having positive resolved shear stress in the center slice P' and a negative one in the other two outer ones Q' as shown in Fig. 3. Assume such positive initial resolved shear stress τ^I to exist in P' and Q'', a negative one in slices Q' and P'', and zero resolved shear stress elsewhere in a favorably oriented crystal at the free surface. A tensile loading causes a positive resolved shear stress τ^A in the whole crystal.

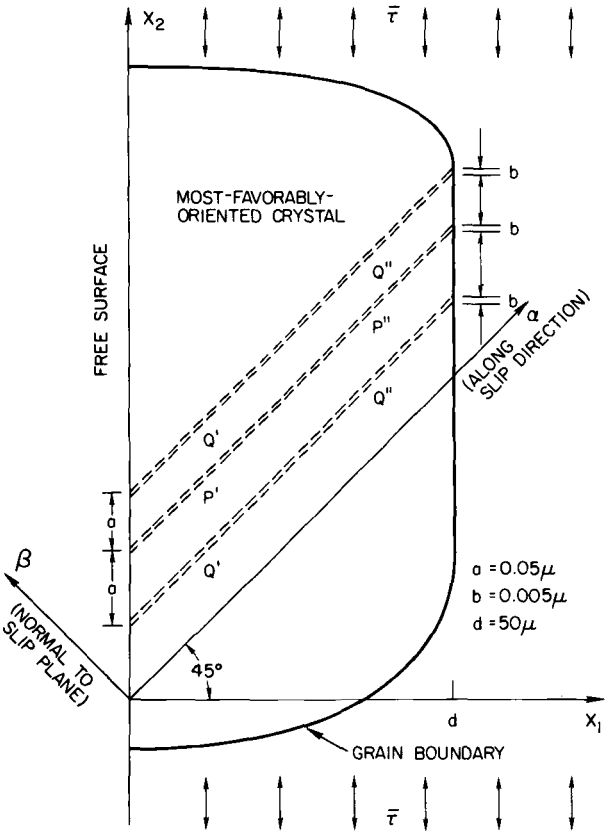

FIG. 3—*Three sliding thin slices* P *and* Q *of a most favorably oriented crystal at the free surface of a polycrystal slide alternately in cyclic loading.*

In P', the resolved shear stress will be the sum of τ^I and τ^A. This stress will be the first to reach the critical creep shear stress τ_c to cause slip. Due to the continuity of the stress field, slip in P' relieves not only the positive shear stress in P' but also in the neighboring region, including slices Q'. This keeps the positive resolved shear stress in the neighboring region from reaching that in P'. Hence, only P' slides in the forward loading. The relief of positive resolved shear stress gives the increase of negative resolved shear stress in Q'. During the reversed loading, Q' has the highest negative resolved shear stress and hence slides. This slip causes relief of negative resolved shear stress not only in Q' but also in the neighboring region including P'. This relief of negative resolved shear stress has the same effect as increasing the positive resolved shear stress in P', thus causing P' to be more ready to slide in the next forward loading. During the next forward loading, P' has the highest positive shear stress

and hence slides. This slip again relieves the positive shear stress and increases the negative shear stress in Q', thus causing Q' to be more ready to slide in the next reversed loading. This gives a natural gating mechanism to cause alternate sliding in P' and Q'. This process is repeated. Hence, the positive slip in P' and negative slip in Q' increase monotonically with cycles of loading. The reversed situation occurs in P'' and Q''. This explains the monotonic raising of the extrusions and deepening of the intrusions [*22,27*].

Recent tests by Woods [*28*] and Winter [*29*] of copper single crystals have shown that from the very early stages of fatigue tests the specimens develop into a state which contains two phases: a soft phase with persistent slipbands (PSB's) into which the deformation tends to concentrate [*27*] and a hard phase with almost inactive matrix which is comparatively dislocation-free. The regions in P and Q slices of the present model correspond to the observed soft-phase regions of high dislocation density, and the hard phase regions are outside P and Q. The present model also shows [*30,31*] that the microstructure due to fatigue is not confined to a surface layer but exists throughout the volume of the specimen as observed by Woods [*27*], and that the initial deformation has very little effect on the fatigue properties of specimens under alternating stress as observed by Winter [*32*].

Numerical Calculation of the Creep Initiation of Extrusions and Intrusions

The material considered is pure aluminum polycrystal subject to alternate tension and compression. The single-crystal creep properties are taken from the tests at 400 F performed by Johnson et al [*13*]. The single-crystal creep rates taken from Figs. 16-18 of Ref *13* at 50 min after the start of tests are

$$\dot{\gamma} = 21 \times 10^{-6}/\text{min} \; @ \; \tau = 1.3788 \times 10^6 \text{ N/m}^2 \; (200 \text{ lb/in.}^2)$$

$$\dot{\gamma} = 240 \times 10^{-6}/\text{min} \; @ \; \tau = 2.0682 \times 10^6 \text{ N/m}^2 \; (300 \text{ lb/in.}^2)$$

$$\dot{\gamma} = 470 \times 10^{-6}/\text{min} \; @ \; \tau = 2.7576 \times 10^6 \text{ N/m}^2 \; (400 \text{ lb/in.}^2)$$

This creep rate is the average macroscopic creep rate in the whole crystal. The creep rate in the slipband is much higher. For numerical calculations the creep rate is assumed to be a thousand times the foregoing. It is also found that the foregoing can be represented approximately by a linear relation

$$\dot{\gamma} = 3.26 \times 10^{-7}[\tau - 1.3167 \times 10^6 \text{ N/m}^2 \; (191 \text{ lb/in.}^2)] \tag{8}$$

The polycrystal considered is a fine-grain aggregate. The equivalent

force caused by slip in the crystal at the surface of the metal may be considered as an external force applied to a semi-infinite elastic medium. The thickness of the slices is much less than the length of the slip lines on the surface. The creep strain and the equivalent force are taken to be constant along the slip lines. Hence, this semi-infinite medium may be considered to be under plane deformation. The stress distribution caused by a point force in a semi-infinite plate for plane stress was shown by Melan [*33*]. Melan's solution was modified for plane strain by Tung and Lin [*34*]. This plane solution is used in the present analysis.

The creep strain $e_{ij}{}^{C}$ varies from point to point in the slices. For numerical calculation these three thin slices are divided along their lengths into thin rectangular regions R_n, where $n = 1, 2 \cdots 3N$ (see Fig. 4). The plane surfaces bounding R_n are denoted by S_n. To simplify calculations, creep strain $e_{\alpha\beta_n}$ in each region R_n is assumed to be constant; hence there is no equivalent body force in each region. In terms of x_1 and x_2 coordinates, the creep strain components are

$$e_{11_n}{}^{C} = -e_{\alpha\beta_n}{}^{C}, \qquad e_{22_n}{}^{C} = e_{\alpha\beta_n}{}^{C}, \text{ and } e_{12_n}{}^{C} = 0$$

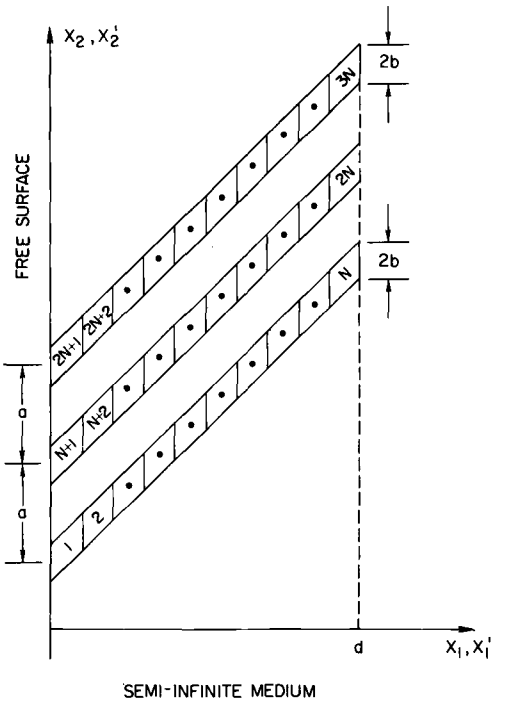

FIG. 4—*Grids of three sliding slices.*

The equivalent surface forces on S_n are

$$\overline{T}_{1_n}{}^{\nu} = -2Ge_{\alpha\beta_n}{}^{C}\nu_1; \qquad \overline{T}_{2_n}{}^{\nu} = 2Ge_{\alpha\beta_n}{}^{C}\nu_2 \tag{9}$$

From the plane-strain solution for a semi-infinite medium, the residual resolved shear stress field caused by a given distribution of creep strain $e_{\alpha\beta_n}{}^{C}$ in the regions R_n of the thin slices was given by Lin and Ito [*30*] as

$$\begin{aligned}\tau_{\alpha\beta_R}(x_1, x_2) &= -\sum_{n=1}^{2N} \oint_{S_n} \{K_1(x_1', x_2'; x_1, x_2)\overline{T}_{1_n}{}^{\nu} \\ &\quad - K_2(x_1', x_2'; x_1, x_2)\overline{T}_{2_n}{}^{\nu}\}dS - 2Ge_{\alpha\beta}{}^{C}(x_1, x_2) \\ &= 2G\sum_{n=1}^{2N} e_{\alpha\beta_n}{}^{C} \oint_{S_n} K_i(x_i', x_2'; x_1, x_2)\nu_i dS - 2Ge_{\alpha\beta}{}^{C}(x_1, x_2)\end{aligned} \tag{10}$$

where (x_1, x_2) denotes the field point and (x_1', x_2') denotes the force point. The functions K_i are given as

$$\begin{aligned}K_1(x_1', x_2'; x_1, x_2) &= -k\Bigg\{\frac{(x_1 - x_1')[(x_1 - x_1')^2 - (x_2 - x_2')^2]}{\rho^4} \\ &\quad + \frac{(x_1 - x_1')[(x_1 + x_1')^2 - (x_2 - x_2')^2] + 4x_1x_1'(x_1 + x_1')}{r^4} \\ &\quad - \frac{16x_1x_1'(x_1 + x_1')(x_2 - x_2')^2}{r^6} \\ &\quad + (1 - 2\sigma)\left[\frac{x_1 - x_1'}{\rho^2} + \frac{x_1 - x_1'}{r^2} - \frac{4x_1(x_2 - x_2')^2}{r^4}\right]\Bigg\}\end{aligned} \tag{11}$$

$$\begin{aligned}K_2(x_1', x_2'; x_1, x_2) &= k(x_2 - x_2')\Bigg\{\frac{(x_1 - x_1')^2 - (x_2 - x_2')^2}{\rho^4} \\ &\quad + \frac{(x_1 - x_1')^2 - (x_2 - x_2')^2}{r^4} - \frac{8x_1x_1'[(x_1 + x_1')^2 - (x_2 - x_2')^2]}{r^6} \\ &\quad - (1 - 2\sigma)\left[\frac{1}{\rho^2} + \frac{1}{r^2} - \frac{4x_1(x_1 + x_1')}{r^4}\right]\Bigg\}\end{aligned} \tag{12}$$

where

σ = Poisson's ratio,

$$k = \frac{1}{4\pi(1 - \sigma)},$$

$$\rho^2 = (x_1 - x_1')^2 + (x_2 - x_2')^2, \text{ and}$$

$$r^2 = (x_1 + x_1')^2 + (x_2 - x_2')^2.$$

The initial resolved shear stress field is expressed as follows

$$\tau_{\alpha\beta}{}^I(x_1, x_2) = 5\left(1 - \frac{2x_1}{d}\right) \text{lb/in.}^2 \text{ in } P$$

$$\tau_{\alpha\beta}{}^I(x_1, x_2) = -5\left(1 - \frac{2x_1}{d}\right) \text{lb/in.}^2 \text{ in } Q \tag{13}$$

$$\tau_{\alpha\beta}{}^I(x_1, x_2) = 0 \text{ elsewhere}$$

The resolved shear stress due to the applied cyclic stress $\bar{\tau}$ is

$$\tau_{\alpha\beta}{}^A(x_1, x_2) = \frac{1}{2}\bar{\tau} \tag{14}$$

After slip occurs, there is a residual resolved shear stress as given by Eq 10.

The total resolved shear stress is the sum of the applied, initial, and residual resolved shear stresses, that is,

$$\tau_{\alpha\beta}(x_1, x_2) = \frac{1}{2}\bar{\tau} + \tau_{\alpha\beta}{}^I(x_1, x_2)$$

$$+ 2G \sum_{n=1}^{2N} e_{\alpha\beta_n}{}^C \oint_{S_n} K_i(x_1', x_2'; x_1, x_2)\nu_1 dS - 2Ge_{\alpha\beta}{}^C(x_1, x_2) \tag{15}$$

In the following, the resolved shear stress and slip strain are referred to the $\alpha\beta$-slip system. Hence the subscript $\alpha\beta$ of τ and e^C are hereafter deleted. The resolved shear stress of grid R_q is given as

$$\tau_q = \frac{1}{2}\bar{\tau} + \tau_q{}^I$$

$$+ 2G \sum_{n=1}^{2N} e_n{}^C \oint_{S_n} K_i(x_1', x_2'; x_{1_q}, x_{2_q})\nu_i dS - 2Ge_q{}^C \tag{16}$$

where

$$q = 1, 2, \ldots, 3N$$

$$\tau_q \equiv \tau_{\alpha\beta}(x_{1_q}, x_{2_q}),$$
$$\tau_q{}^I \equiv \tau_{\alpha\beta}{}^I(x_{1_q}, x_{2_q}),$$
$$e_q{}^C \equiv e_{\alpha\beta}{}^C(x_{1_q}, x_{2_q}), \text{ and}$$
$$(x_{1_q}, x_{2_q}) = \text{center point of } R_q.$$

The initial stress field does not change with loading, so that $\Delta\tau_q{}^I = 0$. The incremental resolved shear stress of the grid R_q during loading is then

$$\Delta\tau_q = \frac{1}{2}\Delta\bar{\tau} + 2G\sum_{n=1}^{2N}\Delta e_n{}^C \oint_{S_n} K_i(x_1', x_2'; x_{1_q}, x_{2_q})\nu_i dS - 2G\Delta e_q{}^C \quad (17)$$

The loading is taken to be rectangular; that is, tension and compression are applied instantaneously and remain constant during each half cycle. The magnitude of the loading is taken to be 1.3099×10^6 N/m^2 (190 lb/in.^{2}). Each half-cycle is divided into 10 time increments. In each time increment, the resolved shear stresses are assumed to be constant and the incremental creep strain is evaluated at that stress. In the numerical example, the critical creep shear stress is taken from Eq 18 as 1.3167×10^6 N/m^2 (191 lb/in.^{2}). Calculations of the creep strain in the slices were made for different frequencies of cyclic loading. The frequency f varies from 0.1 to 1000 cpm. Let N be the total cycles of loading such that N/f gives the loading time. When the frequency exceeds 10 cpm the distribution of creep strain in the slices depends only on N/f. This shear strain distributions versus N/f for frequencies greater than 10 cpm is shown in Fig. 5 and that for 0.1 cpm in Fig. 6. The maximum surface shear strain versus

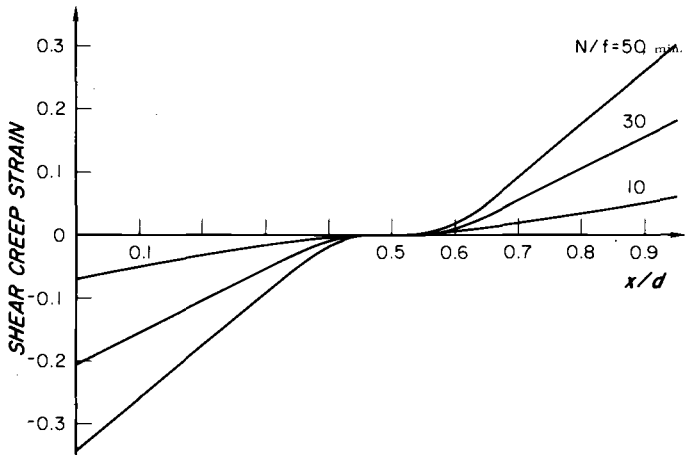

FIG. 5—*Creep shear strain distribution in Slice* P *for loading frequencies* f = *10 to 1000 cpm.*

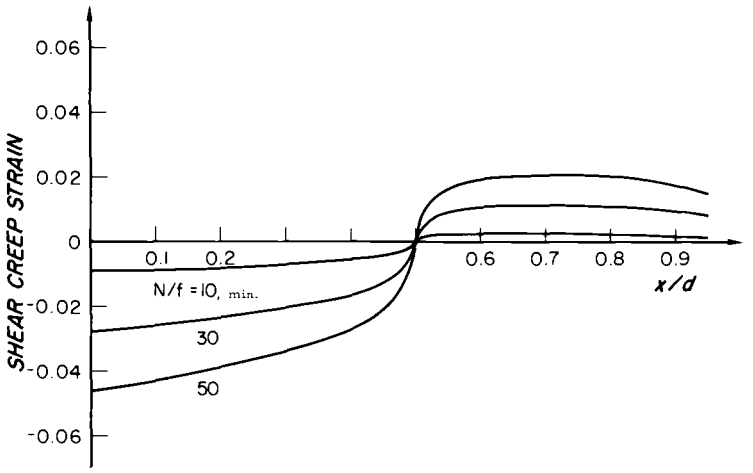

FIG. 6—*Creep shear strain distribution in Slice* P *at loading frequency* f = *0.1 cpm.*

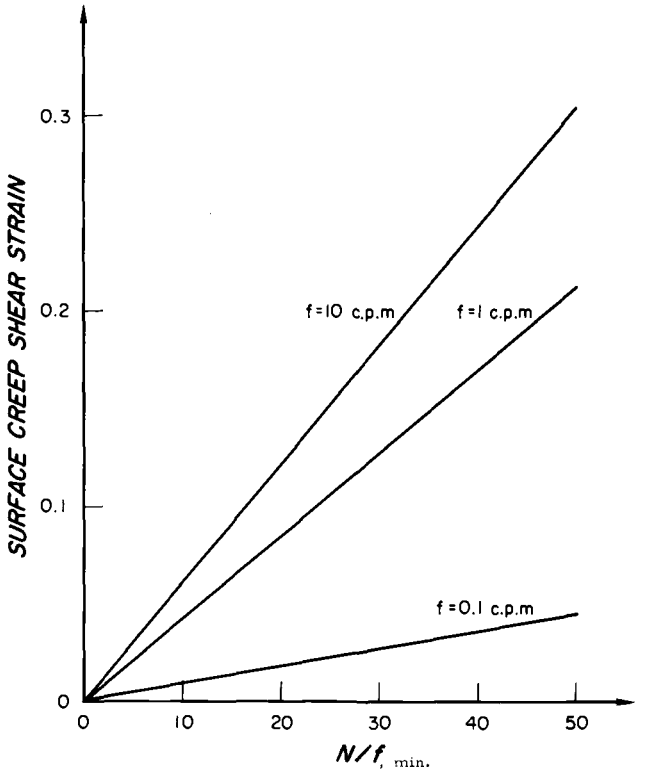

FIG. 7—*Variation of surface creep strain with time of loading* N/f *at different frequencies.*

N/f for different frequencies is shown in Fig. 7. This maximum shear strain at the surface is considered to be a measure of the progress of the crack initiation.

Conclusion and Discussions

The amount of creep shear strain at the surface is a measure of the extent of extrusion and intrusion and hence is taken as a measure of the crack initiation. In the high-frequency range, $f > 10$ cpm, creep strain is proportional to the total loading time, that is, N/f. While in the low-frequency range $f = 0.1$ to 1 cpm, creep shear strain depends on both the number of cycles N and the time of loading N/f. It is expected that further decrease in frequency will cause this surface to be more dependent on N and less on N/f as in time-independent fatigue.

At low frequency ($f = 0.1$ cpm), the shear strain at the surface is much larger than that in the interior, while at high frequencies, $f > 10$ cpm, the shear strains at the surface and in the interior are about the same.

In high-frequency loadings the two exterior slices Q have small residual stresses, while in low-frequency loadings these two slices have large residual stress at the surface and small at the interior. The differences in resolved shear stresses between P and Q are about the same in loadings of all frequencies.

This micromechanic model of fatigue crack initiation seems to be applicable to time-dependent fatigue as well as to time-independent fatigue. The present calculations were made for constant alternate stresses. The same method may be applied to calculate the creep shear strain for constant alternate strains.

References

[1] Forsyth, P. J. E., *Nature*, Vol. 171, 1953, p. 172.
[2] Forsyth, P. J. E. and Stubbington, C. A., *Journal of the Institute of Metals*, Vol. 83, 1954-1955, p. 395.
[3] Hull, D., *Journal of the Institute of Metals*, Vol. 85, 1955-1956, p. 527.
[4] Cottrell, A. H. and Hull, D. in *Proceedings of the Royal Society*, London, Series A, Vol. 242, 1957, p. 211.
[5] Hull, D., *Journal of the Institute of Metals*, Vol. 86, 1957-1958, p. 425.
[6] Forsyth, P. J. E. in *Proceedings of the Royal Society*, London, Series A, Vol. 242, 1957, p. 198.
[7] Grosskreutz, J. C. in *Fatigue, An Interdisciplinary Approach*, J. J. Burke, N. L. Reed, and V. Weiss, Eds., Syracuse University Press, Syracuse, N.Y., 1964, p. 27.
[8] Taylor, G. I. and Elam, C. F., in *Proceedings of the Royal Society*, Series A, Vol. 102, 1923, pp. 643-667.
[9] Taylor, G. I. and Elam, C. F. in *Proceedings of the Royal Society*, Series A, Vol. 108, 1925, pp. 28-51.
[10] Taylor, G. I. and Farren, W. S. in *Proceedings of the Royal Society*, Series A, Vol. 11, 1926, pp. 529-551.
[11] Taylor, G. I., *Journal of the Institute of Metals*, Vol. 62, 1938, p. 307.
[12] Dorn, J. F. and Mote, J. D., *Materials Science Research*, Vol. 1, 1962, pp. 11-56.

[13] Johnson, R. E., Shober, R. R., and Schope, A. D., National Advisory Committee for Aeronautics, Technical Note 2945, 1953.
[14] Johnson, R. D., Young, A. P., and Shope, A. D., National Advisory Committee for Aeronautics Technical Note 3351, 1955.
[15] Gilman, J. J., *Micromechanics of Flow in Solids*, McGraw-Hill, New York, 1969, pp. 176-179.
[16] Mott, N. F., *Acta Metallurgica*, Vol. 6, 1958, p. 195.
[17] Kennedy, A. J., *Processes of Creep and Fatigue in Metals*, Wiley, New York, 1963, pp. 331-341.
[18] May, A. N., *Nature*, Vol. 185, 1960, p. 303.
[19] Thompson, N. in *Proceedings*, International Conference on the Atomic Mechanisms of Fracture, Technology Press MIT and Wiley, New York, 1959.
[20] McEvily, A. J., Jr. and Machlin, E. S. in *Proceedings*, International Conference on the Atomic Mechanisms of Fracture, Technology Press MIT and Wiley, New York, 1959.
[21] Wood, W. A. in *Fatigue in Aircraft Structures*, A. M. Freundenthal, Ed., Academic Press, New York, 1956, pp. 1-19.
[22] Lin, T. H. and Ito, Y. M., *Journal of the Mechanics and Physics of Solids*, Vol. 17, 1969, pp. 511-523.
[23] Charsley, P. and Thompson, N., *Philosophical Magazine*, Vol. 8, 1963, p. 77.
[24] Forsyth, P. J. E., *Journal of the Institute of Metals*, Vol. 82, May 1954, pp. 449-454.
[25] Bendler, S. N. and Entwistle, K. M., *Acta Metallurgica*, Vol. 4, 1956, p. 352.
[26] Wood, W. A. and Bendler, A. M., *Transactions*, Metallurgical Society of AIME, American Society of Mining Engineers, Vol. 224, Feb. 1962, pp. 180-186.
[27] Finney, J. M. and Laird, C., *The Philosophical Magazine*, Vol. 31, 1975, pp. 339-366.
[28] Woods, P. J., *The Philosophical Magazine*, Vol. 28, 1973, pp. 155-191.
[29] Winter, A. T., *The Philosophical Magazine*, Vol. 30, 1974, pp. 719-738.
[30] Lin, T. H. and Ito, Y. M., *Journal of the Mechanics and Physics of Solids*, Vol. 17, 1969, pp. 511-523.
[31] Lin, T. H. in *Reviews on the Deformation Behavior of Materials, International Quarterly Scientific Reviews Journal*, P. Feltham, Ed., Vol. 2, No. 4, 1977.
[32] Winter, A. T., *The Philosophical Magazine*, Vol. 31, 1975, pp. 411-417.
[33] Melan, E., *Zeitschrift für Angewandte Mathematik und Mechanik*, Vol. 12, 1932, pp. 343-346; correction in Vol. 20, 1940, p. 368.
[34] Tung, T. K. and Lin, T. H., *Journal of Applied Mechanics*, Vol. 29, 1966, pp. 363-370.

DISCUSSION

C. Atkinson[1] *(discussion)*—This paper begins with an account of experimental observations of slipband extrusions and intrusions which lead to fatigue crack initiation. The authors then go on to discuss various theoretical attempts to explain these observations, and give reasons why they (and others) think each theory is inadequate, before presenting their own theory.

Briefly, one may say that with the exception of this work most theories are qualitative and are concerned with the geometry of the dislocation paths. An attempt is made to calculate the resolved shear stress responsible for dislocation movement, and in the model a particular initial stress field is *assumed.*

[1]Department of Mathematics, Imperial College, London, U.K.

Motivated by observation [*26*], they assume that three thin parallel slices within a grain intersect the free surface and that the slices lie parallel to the slip direction in the most favorably oriented crystal. A further assumption is that an initial heterogeneous stress field exists due to lattice imperfections etc., and is such that it gives rise to a resolved shear stress which is zero everywhere except in these thin slices and is positive at the outer slices. Stresses with opposite signs occur at the grain boundary so that the initial resolved shear stress changes sign in each slice. A detailed calculation is then made as to how cycles of loading give rise to a monotonic raising of the extrusions and deepening of the intrusions. Clearly at the beginning, when the tensile stress gives rise to a positive resolved shear stress, this plus the initial stress distribution will first cause slip in those regions where the initial shear stress distribution is positive. The reverse happens when the resolved applied shear stress is negative, but subsequent events require detailed calculation as presented in the paper.

The success of this theory rests of course on whether the foregoing assumptions are acceptable. One might ask how did, or could, such an initial stress distribution come about; did the authors motivate this via Ref *26*, or do other experimentalists substantiate it? Our worry is the initial resolved shear stress field given in the paper as

$$\tau_{\alpha\beta}{}^{I}(x_1, x_2) = 5\left(1 - \frac{2x_1}{d}\right) \text{ lb/in.}^2 \text{ in one slice}$$

$$\tau_{\alpha\beta}{}^{I}(x_1, x_2) = -5\left(1 - \frac{2x_1}{d}\right) \text{ lb/in.}^2 \text{ in the other slices}$$

$$\tau_{\alpha\beta}{}^{I}(x_1, x_2) = 0 \text{ elsewhere}$$

This stress field does not obviously satisfy the equation of equilibrium, $\tau_{ij,j} = 0$. However, any initial configuration of dislocations or point defects would lead to a stress field which did satisfy the equation $\tau_{ij,j} = 0$. The authors may argue that their initial stress distribution arises from some distribution of body forces F_i given from $F_i = \tau_{ij,j}{}^{I}$ or perhaps that the consequences of their model might not change much with a different $\tau_{\alpha\beta}{}^{I}$ that satisfied $\tau_{ij,j}{}^{I} = 0$. Such arguments, however, are not very satisfactory. Perhaps they can clarify this point?

To facilitate the discussion, I hope, an abbreviated version of theories of fatigue crack initiation via slipband extrusions and intrusions is given in Table 1. Most of this is abstracted from the very clear account given in the paper. The numbered references in Table 1 refer to their references, but we have added one or two that they may like to comment on. Perhaps more can be added by other discussers. A review has been given by Grosskreutz.[2]

[2] Grosskreutz, J. C., *Physica Status Solidi*, (b), Vol. 47, 1971, p. 359.

TABLE 1—*Theories of fatigue crack initiation via slipband extrusions and intrusions.*

Authors	Mechanism	Criticism
Wood [*21*]	single operative slip system	*Kennedy*—Does not explain monotonic raising of peaks and deepening of valleys
Partridge[a] and Watt[b]	dipoles swept to the surface by edge dislocations	*Atkinson*—Qualitative
Lin & Lin (this paper)	initial resolved shear stress distribution in neighboring thin slices intersecting surface. Then numerical calculation	*Atkinson*—Initial stress distribution does not obviously satisfy equilibrium equation. If not, why not?
Feltner[c]	dipole flip-flop mechanism (relevant to fcc metals?)	*Winter*—Does not believe it. See Winter's discussion of the paper by Mughrabi et al in this publication
Neumann et al[d]	extrusion-intrusion pairs can form as a consequence of Stage I cracks.	*Atkinson*—Qualitative
Cottrell and Hull [*4*]	Frank-Read sources on two intersecting slip planes	*L&L* (*Lin and Lin*)—Sources imply an association of extrusion and intrusion not borne out by experiment
Mott [*16*]	screw dislocation repeating its path by cross slip	*Kennedy* (*also in L&L*)—Mechanism does not explain intrusion
Kennedy [*17*]	Lomer-Cottrell barriers as a gating mechanism to make screw dislocations complete unidirectional circuit	*L&L*—Barriers need to move with dislocations
May [*18*]	Mott's mechanism but return path of dislocation shifted in random fashion under alternating stress	*Kennedy*—Random switching not easy to accept
Thompson [*19*]	edge-screw interaction model for initiation of extrusion.	*L&L*—Not clear how intrusions are formed or why edge dislocations move as in the theory
McEvily and Machlin [*20*]	two screws terminate in a free surface and intersect a node where three dislocations meet	*L&L*—Not explained why screws travel around circuits instead of back and forth

[a] Partridge, P. G., *Acta Metallurgica*, Vol. 13, 1968, p. 517.
[b] Watt, D. F., *Philosophical Magazine*, Vol. 14, 1966, p. 89.
[c] Feltner, C. E., *Philosophical Magazine*, Vol. 12, 1965, p. 1229.
[d] Neumann, P. et al, this publication, pp. 371-395.

There are two things particularly I liked about this paper. First is that it is probably the only genuinely quantitative paper from a theoretical point of view presented so far at this conference. The second thing is that in the beginning of this paper the authors discussed all of the various mechanisms for fatigue crack initiation and criticized them one by one as summarized earlier in my discussion. I would like the authors to clarify one point raised in my discussion; that is, does the initial stress distribution satisfy the equilibrium equation?

S. Lin—No. Mathematically the initial resolved shear stress distribution alone does not satisfy the equilibrium equation. But we could have balanced it arbitrarily by applying a set of direct stress in and between thin slices P and Q. However, these stresses would have very small impact on the outcome of our results.

C. Atkinson—So it does not satisfy the equilibrium equation. Your model is therefore an approximation.

S. Lin—Yes, it is an approximation. It is more difficult to explain physically how we can apply certain distributions of forces to balance our initial stress field and still maintain the assumed shear stress distribution along the slip direction. Inserting an initially variably compressed thin slice into a slot cut between P and Q and welding this slice back to the surrounding material may produce an initial shear stress field similar to that shown in this paper. This is Eshelby's inclusion problem. Positive shear and negative shear will be produced on the opposite sides of the thin slice. This system will satisfy the equilibrium condition. Of course it will produce other stress components which we neglect because they won't affect our results.

C. Atkinson—I think your answer is that it is not right. Does anyone know of a quantitatively correct model? I mean Neumann's model (presented earlier at this conference) was not really quantitative. Does anyone know of a quantitative model of fatigue crack nucleation using dislocation fields? As far as I am concerned, this paper has the virtue that it is quantitative though approximate. As a comparison, all of these models using Dugdale's formulation that we have heard a lot about at this conference are not in the same class as this paper.

S. Lin—I would like to make some further comment on the initial stress field. Some time ago we tried to consider an inclusion with known plastic strains imbedded in a crystal and to compute the initial stress field based on dislocation movement theory. But it reached a point where we had to make a decision whether we wanted to complicate our numerical calculation in this early stage of the development of a theory, or else. Finally, we decided to simplify the computation by assuming this very simple initial stress field.

J. Morrow[3] (*discussion*)—One of the motivations of this symposium was to bring together people from the micromechanics level, the metallurgy level, and the engineering level, and this paper represents an effort to do

[3]Department of Theoretical and Applied Mechanics, University of Illinois, Urbana, Ill.

that. It is worth recalling that the origins of the dislocation theory were developed primarily by mechanics people. All the equations for stresses around dislocations and so on are solutions to mechanics problems. Yet for the complicated problem of material damage, and particularly fatigue damage, little work out of the micromechanics field has been done such as that presented here.

P. Neumann[4] (*discussion*)—Dr. Atkinson made the comment that it is very desirable to have a quantitative theory and I agree with this. But first, one has to have the right qualitative ideas to point out the directions along which one has to go, and the best ideas seem to come from our experiments. As I said during my presentation, I would have wished to complete certain types of experiments concerning the qualitative ideas I was displaying. These experiments can be done by anybody. I only want to point out that very simple predictions can be derived from qualitative ideas, which should be tested experimentally first, and, if they are not correct, you forget the whole thing before you start calculating to 5 percent accuracy.

S. Lin—Even though we tried to quantify the initiation of fatigue cracks, we still cannot quote any values, such as the actual number of cycles to failure. We can only describe a trend. As in the last part of the paper, we mentioned that at lower frequencies the number of cycles to failure would be less than those at higher frequencies. We quantify it in this way instead of actually giving the number of cycles to failure. Again, this theory is only to show the initiation process of fatigue cracks, and we have made no attempt to discuss anything like crack propagation or final failure of the specimen.

T. Mura[5] (*discussion*)—This is not a question but a comment. I think I can support the authors' theory. It is a very interesting one. They simplified the status of initial stress in the way they assumed. I think their assumption on the initial stress state is a reasonable simplification.

Suppose there is a small crack under an applied load. Then there are two slip lines which can be expressed by dislocation distributions. When we unload, the stress distribution is changed to compression near the tip of the crack and to tension far away from the crack tip. A simplified description of the real stress state might be the one assumed by the authors of this paper.

D. Hoeppner[6] (*discussion*)—Aside from Dr. Atkinson's question regarding the equilibrium conditions, I have been following your work for some

[4] Max-Planck-Institut fur Eisenforschung Gmbh, Dusseldorf, Germany.
[5] Department of Civil Engineering, Northwestern University, Evanston, Ill.
[6] Cockburn Professor of Engineering Design, University of Toronto, Toronto, Ont., Canada.

time and have always found it very enlightening. But I often have difficulty in understanding what you mean by initiation of a fatigue crack and the kinetics or energetics thereof. Could you explain "crack initiation" in some quantitative sense regarding both on its kinetics and its energetics?

S. Lin—Let me try to do it with the help of a diagram. In Fig. 8 we have a free surface labeled as such. Let us assume a slip line here with positive initial shear stress, and another one there with negative initial shear stress. We calculate the buildup or accumulation of shear stresses in these two thin slices. We will have built up some positive shear strain here and some negative shear strain there. This thin slice will deform this way with positive shear, and the other will deform that way with negative shear. As a result, an extrusion is formed as the shear strain increases. If we change the signs in the initial stress field, we will have intrusion produced instead.

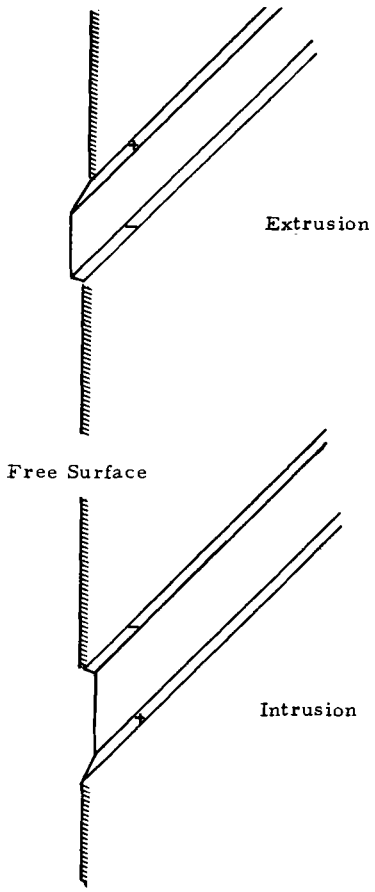

FIG. 8—*Formation of extrusion or intrusion near a free surface.*

From this basic engineering shear displacement diagram, we can see the formation of extrusion and intrusion. This is what we mean by the initiation of fatigue cracks when intrusion is formed due to the buildup of local shear strains to a certain value. Does this answer your question?

D. Hoeppner—No, it does not. I believe what you said is a pseudophysical concept. I have no problem with that personally. It is what follows that concept that bothers me. Apparently you have some formalized mathematical statement—displacement vectors, stress trajectories around this extrusion—to define the surface discontinuity, the crack, and the elasticity conditions around this crack as explained in your paper. My question is: How do you define these displacement discontinuities or stress trajectories in the vicinity of this surface discontinuity?

My second question is on "initiation," which means the beginning of a journey. The journey presumably starts the fatigue failure process. That gets us into the kinetics of the problem. Do you have a statement on some energy threshold in your model that defines the precise initiation of the journey, which in this case means the process of fatigue?

S. Lin—In our model, there is no displacement or surface discontinuity. To answer your second question, again, by "initiation" we mean the forming of valleys on the free surface known as intrusions when the local inelastic shear strains reach a certain reference value.

T. H. Lin and S. R. Lin (authors' closure)—We appreciate the several discussers' interest and comments on our work of micromechanics fatigue mechanism. The question on the assumption of an initial stress field is certainly a valid one, because it is the initial stress field which led us to our fatigue model.

The assumed initial resolved shear stress field given in the paper is not the total initial stress field. The actual initial stress field must satisfy equilibrium conditions. In order to satisfy the equilibrium condition, the assumed linear variation of the shear stress $\tau_{\alpha\beta}{}^{I}$ along β-direction in the thin slices implies a constant $\tau_{\alpha\alpha,\alpha}{}^{I}$ in the slices. In addition, the change of sign of the resolved shear stress from slice P to slice Q and the drop of a finite resolved shear stress in P to zero in the region exterior to P imply a direct stress field in the region between P and Q, and also in layers bounding P. These direct stresses do not affect the creep shear strain buildups in P and Q. Hence, they are not defined in the paper.

Jeffrey T. Fong[1]

Statistical Aspects of Fatigue at Microscopic, Specimen, and Component Levels

REFERENCE: Fong, J. T., **"Statistical Aspects of Fatigue at Microscopic, Specimen, and Component Levels,"** *Fatigue Mechanisms,* Proceedings of an ASTM-NBS-NSF symposium, Kansas City, Mo., May 1978, J. T. Fong, Ed., *ASTM STP 675,* American Society for Testing and Materials, 1979, pp. 729-758.

ABSTRACT: The study of fatigue mechanisms at the microscopic level is examined. The complexity of the microstructure and the availability of quantitative microscopy concepts created a need to introduce statistical tools to the fundamental aspects of fatigue research. Examples of the corrosion fatigue of high-strength steel, the bending fatigue of currency paper, and the swelling of nuclear fuel elements are used to illustrate this new viewpoint. The statistical concept of stress in a medium with distributed voids or other geometric imperfections is introduced to permit the use of models different from the conventional continuum viewpoint. The concept of a nested model and the incorporation of a size effect in the study of fatigue at three microscopic levels and three macroscopic (specimen, component, structure) levels are discussed.

KEY WORDS: fatigue, fracture, mathematical modeling, micromechanics, microstructure, nuclear fuel element, paper, quantitative microscopy, size effect, solid mechanics, statistical methods, steel

Statistical methods and concepts have been known to and applied by workers in fatigue for at least 30 to 40 years. A recent review of the literature on the specialized topic of the size effect on material strength alone [*1*],[2] for example, listed approximately 1000 papers. It is *not* the purpose of this paper to review the statistical aspects of fatigue and of fatigue mechanisms, as may well be expected. Rather, it is to point out new opportunities in the application of statistical methods to key areas of fatigue research which seem "ripe" for significant advances or possible breakthroughs in the next

[1] Physicist and project leader, Center for Applied Mathematics, National Engineering Laboratory, National Bureau of Standards, Washington, D.C. 20234.

[2] The italic numbers in brackets refer to the list of references appended to this paper.

five to ten years. To illustrate my arguments, I use freely results in the literature as well as some of my unpublished work, but the main intent of this paper is more on presenting a new way of thinking than on an exposition of those new results.

To begin with, there is probably unanimous agreement within the fatigue research and testing community that fatigue is, indeed, an interdisciplinary subject. In some sense, that view has hampered the development of the subject by providing a scapegoat whenever a fatigue failure is diagnosed to have occurred in spite of the best attention given by a team of fatigue engineers and scientists. In preparing this paper, I was struck by the similarity of the tone of *two* evaluations of the progress of fatigue research 20 years apart:

1952 ... a completely satisfactory general failure law for fatigue does not exist at present....

... some interesting results of fundamentals of fatigue have been contributed, ...

... much more work is needed in this general area.

—by Peterson [*2*]

1972 ... the synergistic interaction of elevated temperature and environment in high temperature fatigue is quite plausible and even obvious. Yet, this interaction and its characterization has been almost completely neglected in fatigue mechanisms research....

... In any event, these two important parameters (i.e., temperature and environment) have been subjected to an artificial separation in the analysis of experimental data so that their interaction has gone unappreciated....

... it is important that the mechanisms of elevated temperature fatigue be investigated far more thoroughly than they have in the past.

—from *ASTM STP 520* [*3.* p. 191]

Two questions need to be answered before we hide behind that word "interdisciplinary" whenever we have to explain a fatigue failure to the public:

Question No. 1—What is it in the nature of the problem of fatigue that after almost four decades of intensive research and testing with advances in methodology and instrumentation at a cost of, perhaps, a billion dollars a year,[3] engineers are still working with a scatter factor of 2 to 7.5 for

[3] In the absence of an official estimate of the worldwide expenditure on fatigue of man-made products, I made two attempts to arrive at the figure of a billion dollars a year as follows. There are at least 5000 fatigue testing machines in the United States with an average expenditure of $100 000 per machine by my own estimate. Multiplying the U.S. expenditure ($500 000 000) by two, a worldwide estimate of one billion is arrived at. My second attempt is based on an ASTM subcommittee report [*4*] which listed a total of 1570 copies of *ASTM STP*

civil aircraft fatigue life design in Australia, Japan, the United Kingdom, and the United States [5], and with a shockingly high factor of 20 in the fatigue design of pressure vessels [6]?

Question No. 2—What tools have we underutilized in our study of fatigue, even while assuring the public that we are doing as "thorough" a job as we possibly can?

To pave the way for answering both questions, I show first that the problem of fatigue involves not only a characteristic length as small as 10^{-10} m for the Burgers vector of a dislocation and as large as 100 m for the length of an aircraft wing, but also a dynamic microstructure which changes slowly but irreversibly in response to the repeated application of loading and unloading. Next I show that this changing microstructure creates a new opportunity for the application of statistical concepts, namely, the representation of a physical state. Then the concept of stress in a statistically characterized microstructure is introduced as a necessary ingredient in micromechanical modeling. Also, the concept of a nested model of a fatigue specimen and the notion of a size effect are discussed. Finally, the two questions posed in this section are answered with a brief discussion on the qualitative difference between the statistical aspect of fatigue at the microscopic level on the one hand, and the same at the specimen or component level on the other.

Characteristic Length and a Changing Microstructure

From elementary physics textbooks, for example, Feynman [7], we learn that there is a large "gap" in physical sizes between the typical atomic dimension of about 10^{-10} m and the nuclear dimension 10^{-15} m, that is, 10^{-5} times smaller. Since failure mechanisms at the atomic level are now essentially understood,[4] and a quantitative study of the physical situation from the atomic level up depends largely on the resolution of a modern electron microscope (about 2×10^{-10} m), it is reasonable to consider 10^{-10} m as the lower limit of the characteristic length of the problem of fatigue.

For the time being, let us consider the microstructure of a metal crystal with a lattice spacing of, say 2.5×10^{-10} m or 2.5 Å. According to Eshelby

---

566 (*Handbook of Fatigue Testing*. 1974) sold as of May 1977. Assuming a third of the active workers in fatigue purchased that book and assuming further that each worker in fatigue is entrusted an expenditure of about $100 000 per year including labor, material, equipment and overhead support, the U.S. expenditure on fatigue is again in the neighborhood of $500 000 000. Both estimates, are, of course, *ad hoc* and need further verification before they can be taken seriously.

[4] See, for example, Cottrell [8], who characterized the three basic types of failure at the atomic level as (1) crystallographic slip of a unit dislocation with a constant vector, (2) tensile cracking as a result of bond breaking, and (3) shear faulting with the creation of debris between the slipping surfaces.

[9], typically about one lattice site in 10^4 may be vacant in a metal just below the melting point. This means that in a cube with the length of each side equal to 10^{-8} m or 100 Å there are typically about six or seven vacancies whose relative locations within the cube may affect its response to an external loading in a variety of ways. Conceptually, it makes physical sense to examine a block of materials with inhomogeneities for a block size not exceeding 100 times its characteristic length along any dimension. Consequently, we can subdivide the microstructure from the lowest limit of 10^{-10} m to the upper limit of 10^{-4} m into three structural levels, each with its own geometric complexities and constitutive laws:

Microscopic Levels (Characteristic Length)	Range of Dimensions[5]	Sources of Imperfections
1.1 Dislocation level (10^{-10} m)	10^{-10} to 10^{-8} m	vacancies, interstitials, dislocation loops
1.2 Subgrain level (10^{-8} m)	10^{-8} to 10^{-6} m	slipbands, microvoids at grain boundary
1.3 Grain-size level (10^{-6} m)	10^{-6} to 10^{-4} m	microcracks, voids

As early as 1936 it was recognized by Gough and Wood [*10*] that failure by fatigue and failure under static stresses were characterized by changes in crystalline structure such as (1) a grain dislocation with tilt up to about 2 deg from the orientation of the parent grain; (2) the formation of crystallites, approximately 10^{-6} to 10^{-7} m in size, exhibiting a much wider divergence in orientation than the parts of a dislocated grain; and (3) the presence of lattice distortion in the crystallites. Using X-ray diffraction techniques, Gough and Wood [*10*] established conclusively that the fatigue of a mild steel specimen of dimensions in the neighborhood of 10^{-2} to 10^{-1} m involved a slow but irreversible change of its microstructure from the initial state of perfect grains (10^{-4} m) to the final degraded states of crystallites (10^{-6} to 10^{-7} m). In Fig. 1 the qualitative difference between the responses of the microstructure of two levels of cyclic stresses (± 139 MPa for Specimen 2A42 and ± 150 MPa for Specimen 2A45) in the neighborhood of the estimated endurance limit (± 143 MPa) is dramatically demonstrated in a plot of the amount of large grains remaining versus the number of stress cycles.

To complete the statement of the problem of fatigue, one may go to the other extreme of the problem by considering the information given in Fig. 2. As shown by Butler [*11*], it is possible to monitor the real-time structural fatigue performance of many large and different transport-type U.S.

[5] In reality, these dimensions will serve as guidelines for microscopic data analysis and modeling rather than precise limits for fundamental studies of fatigue at various levels. In fact, many studies will be interlevel rather than intralevel.

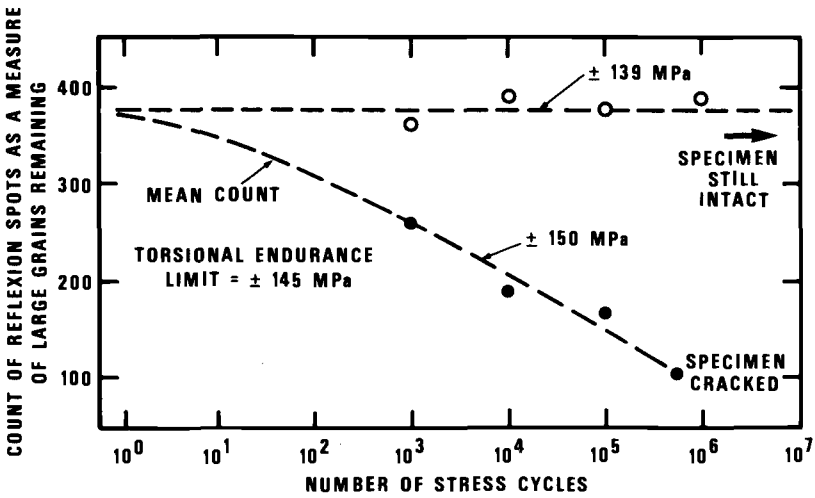

FIG. 1—*Estimate of large grains remaining for fatigue specimens of mild steel in torsion near endurance limit (after Gough and Wood* [10]).

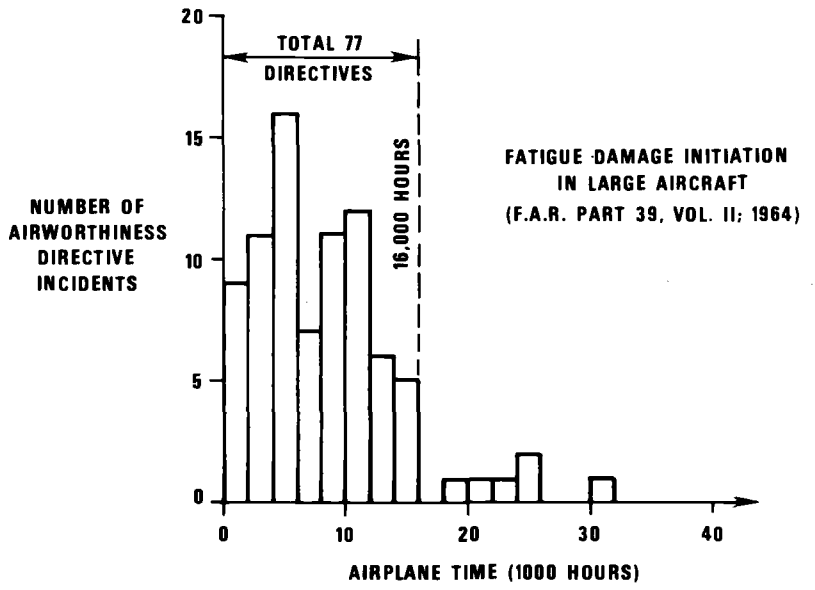

FIG. 2—*Real-time structural fatigue performance reliability of aircraft structures (after Butler* [11]).

aircraft by plotting the number of structural fatigue incidents described in the Airworthiness Directive Notes published by the Federal Aviation Agency and summarized in Ref *12*. The data in Fig. 2 indicated a total of 77

directives issued as of 1964 for the block of airplane time from 0 to 16 000 h, a far cry from the often-claimed design goals of 50 000 to 60 000 h of service for long-range transport-type aircrafts. Since each such directive named fatigue as the culprit, a proper study of the problem of fatigue must include not only the three sublevels of microscopic dimensions described earlier, but also three additional levels of macroscopic dimensions as follows:

Macroscopic Levels (Characteristic Length)	Range of Dimensions[6]	Sources of Imperfections
2. Specimen level (10^{-4} m)	10^{-4} to 10^{-2} m	cracks, pits, notches
3. Component level (10^{-2} m)	10^{-2} to 1 m	cracks, misalignments
4. Structural level (10^{-2} m)	10^{-2} to 10^{2} m	welds, joints, cracks

In short, fatigue is a unique problem in the physical world where the behavior of a component (Level 3) or a structure (Level 4) cannot be fully understood and predicted without first obtaining information at the specimen level (Level 2) and three microscopic levels, 1.1, 1.2, and 1.3. The interrelationship of observations at different levels can be quite complicated, but the difficulty is compounded by the enormous variety of internal rearrangements of atoms, molecules, grains, geometric imperfections, etc. so that a complete understanding of the mechanisms of fatigue would hardly be possible unless we recognize (1) the distributional and (2) the time-varying character of the microstructure. In the next section, I shall show how this recognition leads to some new opportunities in statistical applications.

Statistical Representation of Time-Varying Microstructural States

Having described the problem of fatigue in terms of six levels of measurement, with emphasis on quantifying the distributional character of the microstructure, I wish to draw your attention to the Rhines paper [*13*], presented earlier in this publication, on the relationship between fatigue research and quantitative microscopy.[7] Professor Rhines advises us to "measure every global parameter that is reasonably accessible, plot each one against any physical property that can be measured, and look for simple relationships." I would agree with that advice to some extent, but the effort may generate so much data that we may soon drown in a sea of

[6] Dimensions are again approximate to delimit various levels for conceptual convenience.

[7] For a good understanding of this subject, the reader may wish to consult Rhines [*14*], Underwood, deWit, and Moore [*15*], etc.

computer-aided microstructural observations. A natural tool to manage and interpret these new measurements, particularly at the three microscopic levels, is the method of statistical representation.

Let me use three examples to illustrate my point. Kitagawa and Suzuki [*16*] studied corrosion fatigue by applying repeated tensile loads to unnotched wide-plate specimens (70 by 440 by 2.3 mm) of a high-tensile-strength steel (HT 50,50-kg mm^{-2} or 490-MPa grade) in the well water of their laboratory. In Fig. 3 the histograms of observed microcracks at 48, 60, and 100 percent of life (1.85×10^6 cycles to failure) for stresses varying from 0 to 24 kg mm^{-2} (235 MPa) are shown. It was noted by Kitagawa and Suzuki [*16*] that "the distribution pattern of the crack size did not change with the number of stress cycles, and all of the data fell upon one log-normal distribution line. ... " The goal of their study was to suggest that the coalescence of many fine cracks is more fundamental than the determination of the crack growth law as a function of the stress-intensity-factor range. Instead of measuring da/dN, where a is the crack length and N the number of cycles, the Kitagawa/Suzuki data can easily yield two quantities, $d\zeta/dN$ and $d\sigma/dN$, where ζ and σ are the two parameters in a standard log-normal distribution as defined by

1. $U = (\log X - \zeta)/\sigma$, where X is the crack length, and
2. U is normally distributed; that is, the probability density function of U is

$$P_U(u) = (\sqrt{2\pi})^{-1} \exp(-u^2/2) \tag{1}$$

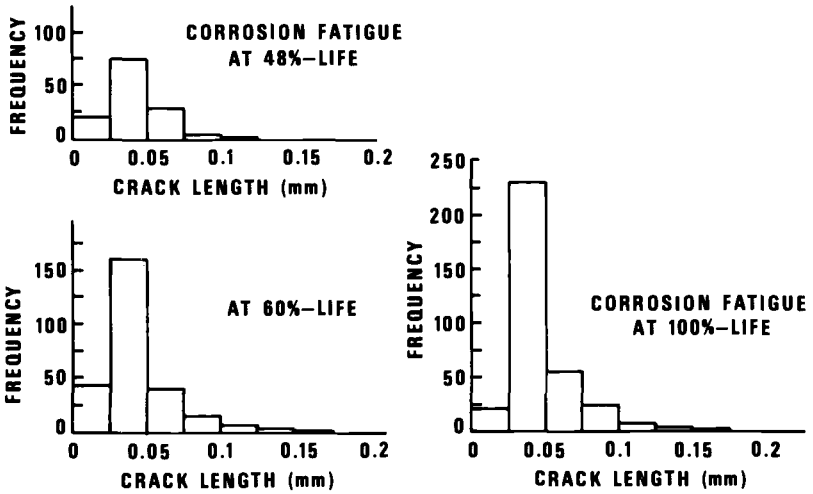

FIG. 3—*Histograms of microcrack lengths of HT 50 high-tensile-strength steel in tap water at selected stages of corrosion fatigue for a cyclic stress of 12 ± 12 kg/mm² (after Kitagawa and Suzuki* [16]).

The choice of a particular distribution depends largely on the taste of the investigator because there is usually more than one distribution to represent the microstructural data. One of my favorite distributions is the beta distribution defined over the finite range [0, 1] by the following simple equation

$$f(x) = \frac{(a + b + 1)!}{a!\, b!}\, x^a (1 - x)^b \tag{2}$$

where a and b are two parameters such that most unimodal shapes such as uniform, triangular, left-skewed, symmetrical, right-skewed, J-shaped, reverse J-shaped, or even a U-shaped curve, can all be approximated by this two-parameter distribution (see Fig. 4).

The second example of the representation of a changing microstructure came from a study reported by Fong, Rehm, and Graminski [*17*] on the folding fatigue of currency paper. We built a flexing machine to simulate the folding of the currency paper and, sure enough, after about 80 000 cycles or flexes on the machine, a high-grade rag paper specimen would degrade in terms of its fiber length distribution as shown in Fig. 5. The "before" and "after" histograms show that the number of fibers in the neighborhood of 2 to 3 mm in length decreases and the number of those around 1 mm in length increases after 80 000 flexes. Instead of choosing the log-normal distribution as the function to represent the data before and after the fatigue test, we tried a distribution originally due to Weibull [*18*] because its three parameters, m, x_0, and x_u, may have interesting

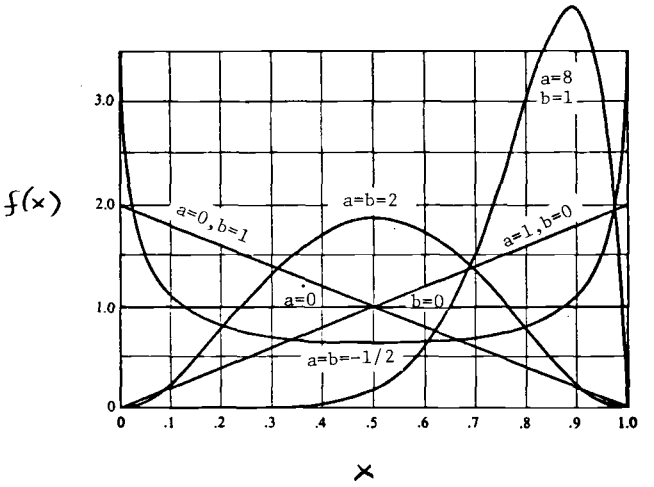

FIG. 4—*Beta density functions.*

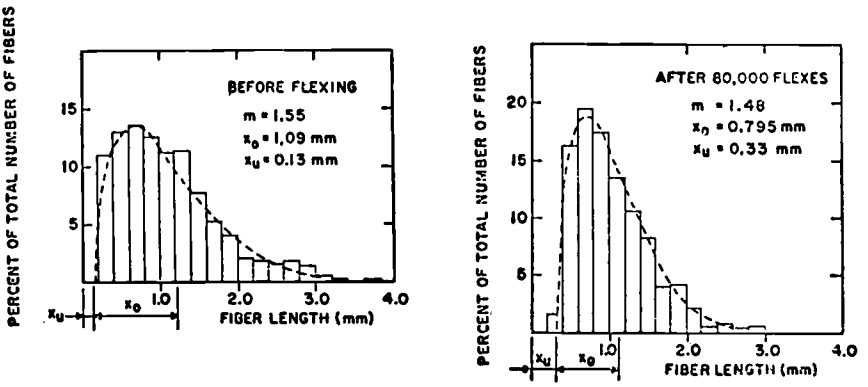

FIG. 5—*Frequency distribution of fiber length for high-grade rag paper before and after flexes (after Fong, et al* [17]).

physical meaning. The following is the probability density function of a three-parameter Weibull distribution

$$f(x) = \frac{m}{x_0}\left(\frac{x - x_u}{x_0}\right)^{m-1} \exp\left[-\left(\frac{x - x_u}{x_0}\right)^m\right] \tag{3}$$

where

x_u = location parameter,
x_0 = scale parameter, and
m = shape parameter.

In Fig. 6 we show the influence of the shape parameter as m varies from 1.5 (skewed to the right) to 5.5 (skewed to the left). As a matter of fact, for values of m in the neighborhood of 3.6, the Weibull distribution is almost indistinguishable from the normal (Gaussian) distribution [*19*, p. 253]. This makes the Weibull distribution an excellent choice for representing varying states of a microstructure, particularly if one state is known to be an equilibrium state with a shape factor of $m = 3.6$.[8] In the second diagram of Fig. 6, we also exhibit the influence of the scale parameter x_0, which was found to be important for our investigation of the currency paper fatigue problem (see Fig. 5).

So far, we have seen two examples of microstructures which suggest the usefulness of a statistical representation. The third example, taken from a paper by Merckx [*21*], and based on some rigorous mathematical results due to Nicholson [*22*], illustrates how the problem ought to be approached

[8]This fact was taken advantage of in a representation of the end-to-end distance of the classical Gaussian network of a vulcanized rubber specimen undergoing chemorheological degradation due to heating [*20*].

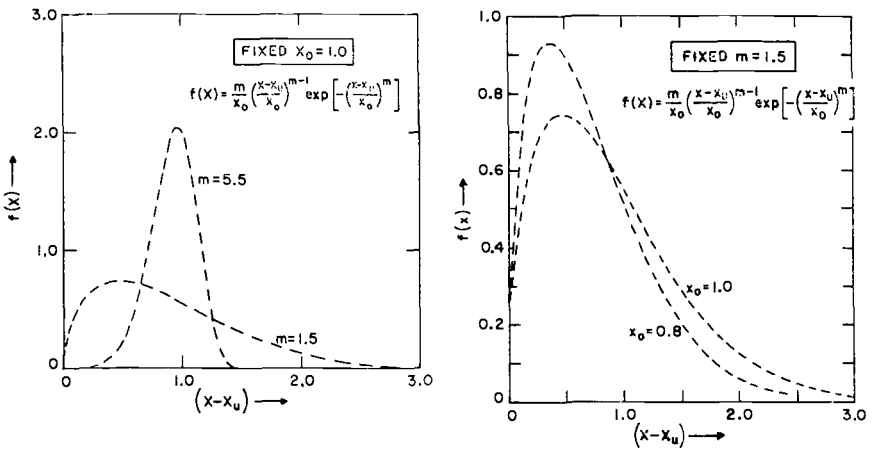

FIG. 6—*Weibull density functions.*

under the assumption that some microgeometric objects are uniformly distributed throughout the material. In Fig. 7 we reproduce Merckx's representation of the void density estimates for different void sizes in irradiated uranium specimens of reactor fuel elements annealed at 750°C for 10 min. About 1000 bubble counts and five pictures were used to obtain the input data used in Fig. 7. The mean and two-sigma limits of the void density given in number per cubic centimetre per micrometre of the histogram spacing are given for void sizes ranging from 0.9×10^{-6} to 5.0×10^{-6} m. Mathematical modeling of the phenomenon of annealing based on a change of the bubble size distribution has been reported by Baroody [*23*], and it is hoped that similar work on a statistical characterization of the microstructural state of a material may soon be developed to study the mechanisms of fatigue.

Statistical Representation of the Concept of Stress

To motivate this discussion, let us examine Fig. 7 again by estimating the average void density of, say, 1.0 ± 0.05-μm-diameter bubbles in an irradiated uranium specimen. The estimate is obtained by multiplying the reading of 5.1×10^{11} from the graph with the width of the histogram, namely, 0.1 μm. In other words, Merckx [*21*] estimated that there were about 5.1×10^{10} bubbles of diameter 1.0 ± 0.05 μm in a unit volume of 1 cm.^{3} Ignoring the fact that bubbles are spherical, we can first estimate that there are 10^{12} sites of size 1 μm^3 in a unit volume of 1 cm^3, and Merckx's measurement indicated that there is a chance of one in twenty that any particular lattice site is occupied by a bubble. A further examination of Fig. 7 shows that one can make similar statements for about 10

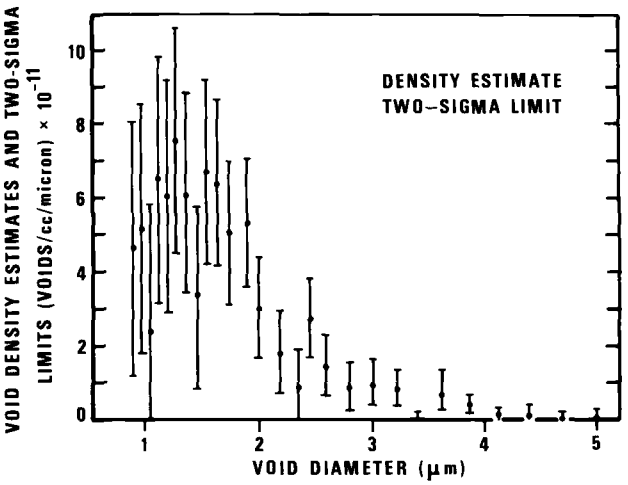

FIG. 7—*Void density estimates and their two-sigma variations versus void size for irradiated uranium specimens annealed at 750°C for 10 min (after Merckx* [21]).

sizes of bubbles between 1.0 and 2.0 μm, so that it is not unreasonable to assert that there is a fifty-fifty chance (or one in two) that any particular lattice site is occupied by a bubble. If the bubbles are considered to have a statistical distribution, then the mechanical response of the material medium, that is, the stress, should also have a statistical representation. This approach has been adopted in our laboratory [*17,20,24*] to examine the fatigue of a variety of materials ranging from high-grade rag paper, rubber, and polymer, to metal alloys. The porosity of a paper specimen, typically between 50 to 70 percent, provides a gross measure for all the microvoids (Fig. 8) that exist around the fibers and act as stress raisers. The concept of continuous stress field in classical continuum mechanics can no longer apply to a statistically represented microstructure.

An excellent exposition of a statistical concept of stress was given recently by Harr [*25*]. The concept arose naturally in estimating stresses in soils and particulate media [*25*, pp. 247–248] where the microvoids are measurable only in a statistical sense. In this paper, I would like to show that Harr's concept can be applied also to other materials as long as they possess a statistically measurable microstructure. To fix the basic ideas of the concept, let us work with one-dimensional quantities of stress at two levels, namely, a macrostress $\bar{s}$ corresponding to the stress of the classical continuum, and a microstress s which depends on the microstructure of the continuum and may equal zero if there is a void. In Fig. 9, we consider a block of material with width B such that at any section across the width of the block it is possible to identify subdivisions of the width as either continuous (for example, intervals [0,1], [2,3], etc.) or empty (for example,

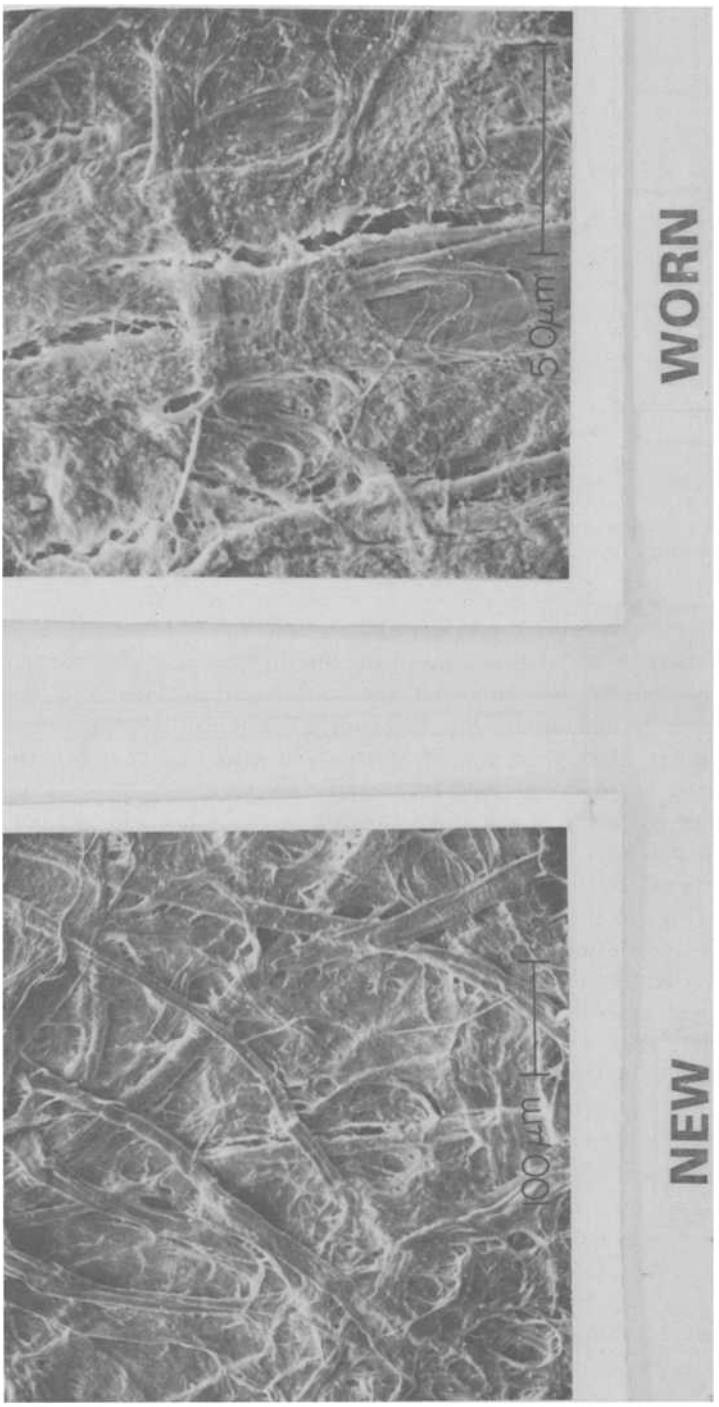

FIG. 8—*Dollar bill degradation: microstructures of high-grade rag paper before and after flexes to simulate fatigue of currency paper (after Graminski [24]).*

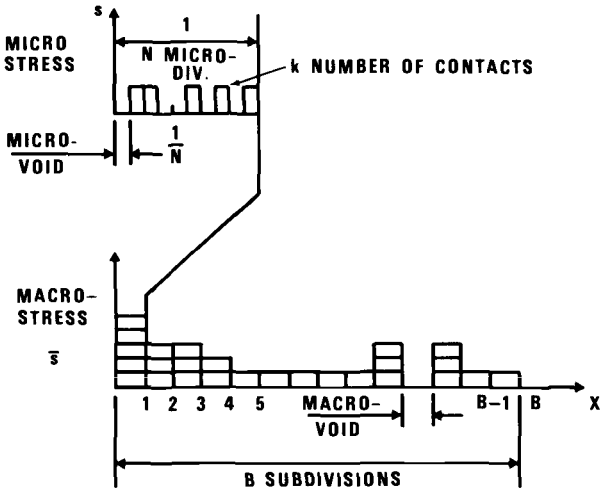

FIG. 9—*Schematic representation of microstress in a medium with voids.*

intervals [1,2], [3,4], etc.). In principle, these macrostresses as plotted in Fig. 9 can be computed if we assume an elastic medium and a known location of each macrovoid. If the macrostress $\bar{s}$ is nonzero, there is no *a priori* guarantee that the microstresses within the continuous interval are also nonzero. For instance, consider a further decomposition of the subdivision [0,1] into N microdivisions with k microdivisions making contacts such that they contribute k microstresses of equal magnitude. This is an important assumption of Harr's concept; that is, for each microdivision of contact or noncontact, a two-state probability statement can be made regarding the physical transmission of forces at the microstructural level. Furthermore, Harr assumes that the microstress s is defined by the number of contacts up to a normalizing constant equal to $\bar{s}$, the continuum stress. In short, Harr assumes that $s = k\,\bar{s}$. Let p be the probability that a microdivision is not empty. Using Harr's notation [*25*, pp. 213–222], the probability of registering a nonzero stress within the unit width, k times in N independent trials, is

$$b\,(k;\,N,\,p) = \binom{N}{k} p^k\,(1 - p)^{N-k} \tag{4}$$

Clearly, the average stress $\bar{s}$ is a fictitious quantity which should correspond to the expected value of the binomial distribution given in Eq 4, that is, $\bar{s} = Np$. Rewriting Eq 4 by substituting $p = \bar{s}/N$, and letting $N \to \infty$ while keeping $\bar{s}$ finite, we obtain a new expression for the probability b

$$b\,(k;\,\bar{s}) = \frac{\bar{s}^k}{k!}\,e^{-\bar{s}} \tag{5}$$

Equation 5 for the unit width [0,1] is now applicable to the entire specimen of width B. For the stress ratio k equal to zero, the probability measure $b(0;\,\bar{s})$ corresponds to the conventional definition of the porosity n of the given medium. Hence, we have, by definition

$$n = b\,(0;\,\bar{s}) = e^{-\bar{s}} \tag{6}$$

In this model the stres ratio k is confined to integral values of 0, 1, 2, . . . , and one can easily calculate the probability function given by Eq 5 for typical porosities such as $n = 0.6$ for paper, $n = 0.3$ for sand, and $n = 0.01$ for some densely compacted material. In Fig. 10 we show the probability plots for these three porosities with the connecting lines drawn purely to clarify the plots rather than to indicate the extension of the concept to a continuous k.

A close examination of Fig. 10 shows that the statistical concept of stress as given by Eq 5 appears reasonable for porosities 0.3 and 0.6, but not for $n = 0.01$, for which we would expect the distribution to be concentrated around $k = 1$. As shown by Harr [*25*] and Smoltczyk [*26*], this concept can be coupled with a random walk model of the average stress $\bar{s}$ to give a useful description of the state of stress in a soil medium subjected to foundation-type loadings ($n \sim 0.3$). For $n \sim 0.6$, as in the case of high-grade rag paper tested in our laboratory, the discrete distribution of the stress ratios can be coupled with the single fiber breaking strength data of the paper fiber to formulate a probabilistic model of fatigue [*17*]. But the

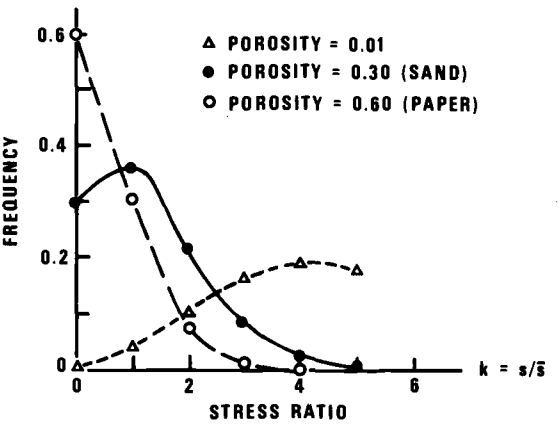

FIG. 10—*Microstress distribution for porosities, 0.01, 0.30, and 0.60.*

plot in Fig. 10 for the low porosity of 0.01 needs further clarification in the sense that the most probable microstress occurs at $s = 4\bar{s}$ rather than at $s = \bar{s}$, as would be expected of an almost perfect solid continuum.

Since stress is such a fundamental quantity in mechanics and material science, the appearance of a physically plausible and mathematically elegant alternative to the classical definition of stress is worth reporting. The need for a statistical concept of stress and the availability of such a concept as treated by Harr [25] have been demonstrated in this section.

Nested Model and Size Effect

As shown earlier, the complexity of a time-varying microstructure dictates a subdivision of microscopic modeling into at least three distinct levels, namely, the dislocation level, the subgrain level, and the grain-size level. With our current development in electron microscopy, there appears to be less a problem of quantifying the observations than that of mathematical modeling. Let us assume that for a specific material undergoing fatigue we had the good fortune of obtaining the best statistical characterization of all conceivable geometric and material imperfections at all three levels of observations. The question before us is: What can we do with the time-dependent distributional data of the specimen at all three levels?

The answer is, surprisingly, straightforward, but is contrary to the current practice of almost every research worker in fatigue mechanism, or in any other subject of material science. The concept I wish to propose for interpreting the three-level microstructural data may be conveniently called the nested model. Simply stated, a dislocation-level model takes the time-varying distributional data at that level as necessary ingredients of a constitutive equation. The dependent variables of the constitutive equation shall include the state variables of the higher level, that is, the subgrain level. Similarly, a subgrain-level model would take the time-varying distributional data at that level as ingredients for another constitutive equation having as dependent variables those state quantities of the next higher level, that is, the grain-size level, and so on. The net result is that it takes more than one constitutive equation to link the distributional data at the dislocation level to the fatigue-life data at the specimen level, and the composite relation through the three microscopic levels with a large amount of statistical linkage can be tested to verify the nested model.

How is that any different from what is being done today by some of our best material scientists? Let me make two points here to highlight the differences without going into specific details or mentioning names. In the first place, a nested model recognizes the limitations of the mathematical representation of any physically inhomogeneous problem by a systematic and controlled concept of scaling, whereas a conventional model attempts to deal with the multilevel problem with a single mathematical formulation

which inevitably has to be watered down with dubious assumptions in order to achieve some useful result. Secondly, a nested model has a built-in requirement to inject experimental observations into the process of modeling both as fundamental building blocks and as motivations for choosing an appropriate modeling strategy. The conventional practice is to consider modeling an activity for the theorists, whose contact with the limitations of an experiment is sometimes so weak that the predictions of the models may never be checked experimentally.

Why is nested modeling seldom practiced? For one thing, it lacks the experimental data to initiate even the simplest model at the dislocation level. It is hoped that this symposium will greatly enlarge the existing data base on fatigue mechanisms. A more important reason may be found in the implicit demand on each investigator to collaborate closely with someone outside his or her specific area of competence. For instance, the modeler must work very closely with a statistician, a collection of experimentalists with measurement expertise at different microscopic levels, and with any other specialists whose knowledge bears upon the degradation of materials under cyclic loadings. In short, it is not enough for us to recognize that the problem of fatigue is interdisciplinary, as I mentioned early in the introduction. My contention is that the problem will not be solved unless we also act as interdisciplinarians by working on nested models.

One further advantage of the concept of a nested model should be mentioned. As reviewed by Harter [*1*, p. 364], who attributed the following remark to Weibull, "it is safe to conclude that the size effect in fatigue exists, but is not easy to establish its magnitude, because many irrelevant factors mask the result and, even more significantly, the laws of size effect are quite different for the pre-crack and the post-crack stages of the fatigue process." By restricting the modeling aspect of the fatigue problem to a specific level and making sure that the linkages of models at neighboring levels are rigorous, the phenomenon of size effect is automatically incorporated in a nested model.

Fatigue Mechanisms and Fatigue Life Prediction

We are now ready to answer the two questions posed in the introductory section of this paper. In responding to the question on the nature of the problem of fatigue, we could point to the six levels of observations, time-varying statistical representation of three levels of microstructural data, the associated statistical concept of microstress, the need to discover a sequence of constitutive equations with statistical linkages, and a host of other attributes not discussed in this paper, as a partial catalog of the challenges that still face us today. Two developments during the past 20 years have greatly

expanded our ability to study fatigue—electron microscopes and computers. As far as fatigue mechanism study is concerned, the advances in statistical methods and concepts such as those given by Mann et al [*27*] on parameter estimation, Nicholson [*22*] on the estimation of properties of the particulate phase, and Harr [*25*] on the probabilistic theory of a particulate continuum have largely been ignored. Thus the answer to the question on neglecting the use of any specific tool must be related to the subject of this paper, namely, the statistical aspects of fatigue.

So far, all my comments have been directed to the application of statistical methods and concepts to fatigue mechanism research. I would be remiss if I did not mention the existence of an extensive literature on the statistical aspects of fatigue at the specimen and component levels.[9] At the risk of overstating my case, I wish to point out a qualitative difference between the use of statistical tools for mechanism research and that for fatigue life testing and prediction. In the former case, statistical concepts and methods are used to discover fundamental laws of nature, much like those in statistical physics, whereas in the case of life testing and prediction the tool is used to obtain statistical inference from incomplete information. Failure to recognize this qualitative difference may sometimes turn a material scientist against the use of the statistical tool on the grounds that the presence of a statistical argument in a theory dilutes its validity. The main thrust of this paper has been to show that the opposite is true.

Conclusion

The sophisticated use of electron microscopes and computers in fatigue mechanism research has created new opportunities in applying statistical concepts and methods. All three areas of opportunities are physically motivated: (1) the need to characterize the microstructural state variables as time-varying statistical quantities; (2) the associated need to introduce a statistical concept of microstress; and (3) the use of statistical inference techniques in formulating nested models for interpreting microstructural data at three levels of observations, namely, the dislocation level, the subgrain level, and the grain-size level. There is a qualitative difference between the use of statistical tools in mechanism research and that in fatigue specimen and component life testing. Much progress has been made in the latter application, but only a modest beginning on the former has taken place during the past 10 years. The problem of fatigue, if approached in a truly interdisciplinary manner, is amenable to a scientific as well as an engineering solution if the appropriate statistical concepts and methods are incorporated.

[9] See, for example, Ref. *28*, Heller [*29*], Little and Jebe [*30*], and Fong [*31*].

Acknowledgment

I wish to thank Dr. George Moore, who recently retired from the National Bureau of Standards, for stimulating discussions during the course of preparing this manuscript. Thanks are also due to Dr. Ed Graminski of the National Bureau of Standards for the use of two of his unpublished photographs on the microstructure of high-grade rag paper. I am indebted to the late Professor A. M. Freudenthal, whose pioneering paper [*32*] and inspiring lectures at Columbia University when I was a graduate student there motivated my long-term interest in applied statistics. Finally, I would like to thank Professor F. A. McClintock of Massachusetts Institute of Technology, whose papers on statistical theory of mechanical strength are too numerous to be cited here except one, Ref. *33*, which stimulated my recent work.

References

[*1*] Harter, H. L., "A Survey of the Literature on the Size Effect on Material Strength," Report AFFDL-TR-77-11, Air Force Flight Dynamics Laboratory, Wright-Patterson AFB, Ohio, 1977.

[*2*] Peterson, R. E., *Applied Mechanics Reviews*, Vol. 5, 1952, p. 1.

[*3*] *Fatigue at Elevated Temperatures, ASTM STP 520*, A. E. Carten, A. J. McEvily, and C. H. Wells, Eds., American Society for Testing and Materials, 1973, p. 191.

[*4*] Palmer, J. J., ASTM Committee E-9 on Fatigue, Executive Subcommittee Report, American Society for Testing and Materials, 1977.

[*5*] Kamiyama, T. in *Reliability Approach in Structural Engineering*, A. M. Freudenthal et al, Eds., Maruzen, Tokyo, Japan, 1975, pp. 175–189.

[*6*] Jaske, C. E. and O'Donnell, W. J., *Journal of Pressure Vessel Technology, Transactions*, American Society of Mechanical Engineers, Vol. 99J, 1977, p. 584.

[*7*] Feynman, R. P., Leighton, R. B., and Sands, M. in *The Feyman Lectures on Physics*, Addison-Wesley, Reading, Mass., Vol. 1, 1963, pp. 5–9.

[*8*] Cottrell, A. H. in *The Physics of Metals, Vol. 2, Defects*, P. B. Hirsch, Ed., Cambridge University Press, 1975, pp. 247–280.

[*9*] Eshelby, J. D. in *The Physics of Metals, Vol. 2, Defects*, P. B. Hirsch, Ed., Cambridge University Press, 1975, pp. 1–42.

[*10*] Gough, H. J. and Wood, W. A. in *Proceedings of the Royal Society of London*, Series A, Vol. 154, 1936, p. 510.

[*11*] Butler, J. P. in *Proceedings*, International Conference on Structural Safety and Reliability, A. M. Freudenthal, Ed., Washington, D.C., April 1969, Pergamon Press, New York, 1972, pp. 181–211.

[*12*] *Federal Aviation Regulations*, Part 39, Vol. II, *Summary of Airworthiness*, Directives for Large Aircraft. Superintendent of Documents, U.S. Government Printing Office, Washington, D.C., 1964.

[*13*] Rhines, F. N., this publication, pp. 23–46.

[*14*] Rhines, F. N., *Metal Progress*, Vol. 112, Aug. 1977, pp. 60–65, and Sept. 1977, pp. 47–51.

[*15*] *Proceedings*, 4th International Congress for Stereology, E. E. Underwood, R. deWit, and G. A. Moore, Eds., Gaithersburg, Md., Sept. 1975, National Bureau of Standards Special Publication 431, Superintendent of Documents, U.S. Government Printing Office, Washington, D.C., 1976.

[*16*] Kitagawa, H. and Suzuki, I in *Reliability Approach in Structural Engineering*, A. M. Freudenthal et al, Eds., Maruzen, Tokyo, Japan, 1975, pp. 217–233.

[*17*] Fong, J. T., Rehm, R. G., and Graminski, E. L., *Journal of the Technical Association of the Pulp and Paper Industry*, Vol. 60, 1977, p. 156.

[18] Weibull, W., *A Statistical Theory of the Strength of Materials*, published in English as *Handbook No. 151* by the Royal Swedish Institute for Engineering Research, Stockholm, Sweden, 1939.
[19] Johnson, N. L. and Kotz, S., *Continuous Univariate Distributions*, Houghton-Mifflin, Boston, Mass., Vol. 1, 1970.
[20] Fong, J. T. in *Proceedings*, 7th International Congress on Rheology, C. Klason and J. Kubat, Eds., Gothenburg, Sweden, Aug. 1976, pp. 200-201.
[21] Mereckx, K. R., *Nuclear Engineering and Design*, Vol. 9, 1969, p. 15.
[22] Nicholson, W. L., *Biometrika*, Vol. 57, 1970, p. 273.
[23] Baroody, E. M., *Journal of Applied Physics*, Vol. 38, 1967, p. 489.
[24] Graminski, E. L., unpublished data.
[25] Harr, M. E., *Mechanics of Particulate Media, A Probabilistic Approach*, McGraw-Hill, New York, 1977.
[26] Smoltczyk, H. U., *Journal of Soil Mechanics and Foundations Division, Transactions*, American Society of Civil Engineers, Vol. 93, No. SM2, 1967, p. 101.
[27] Mann, N. R., Schafer, R. E., and Singpurwalla, N. D., *Methods for Statistical Analysis of Reliability and Life Data*, Wiley, New York, 1974.
[28] *Proceedings*, Aerospace Reliability and Maintainability Conference, Washington, D.C., Society of Automotive Engineers, 1964.
[29] *Probabilistic Aspects of Fatigue, ASTM STP 511*, R. A. Heller, Ed., American Society for Testing and Materials, 1972.
[30] Little, R. E. and Jebe, E. H., *Manual on Statistical Planning and Analysis for Fatigue Experiments, ASTM STP 588*, American Society for Testing and Materials, 1975.
[31] Fong, J. T., *Nuclear Engineering and Design*, Vol. 51, 1978, p. 45.
[32] Freudenthal, A. M. in *Proceedings of the Royal Society of London*, Series A, Vol. 187, 1946, p. 416.
[33] McClintock, F. A. in *Fracture Mechanics of Ceramics*, R. C. Bradt et al, Eds., Plenum Press, New York, Vol. 1, 1974, pp. 93-114.

DISCUSSION

K. Heckel[1] *(discussion)*—The aim of the present paper is the treatment of the statistical aspect of fatigue behavior of a material subjected to time-varying loads and the proposal of a nested model which should be able to describe the mechanism of fatigue from the dislocation level up to the final crack. It is a fascinating idea to formulate such a nested model to link the distribution data at the dislocation level to the fatigue data at the specimen level.

It is not the task of a discusser to repeat the presentation of the author. But some remarks from the engineering viewpoint may be added.

The great advantage given by the nested model is evident. But the large amount of experimental data and the considerable scientific effort required to construct such a model can hardly be justified in many engineering applications. If we consider a structural part and if we neglect environmental and random loading effects, the fatigue behavior is usually determined by a technological, a geometrical, and a statistical size effect.[2]

[1] Hochschule der Bundeswehr München, Fachbereich Luft- u. Raumfahrttechnik, Munich, Germany.

[2] Heckel K. and Köhler, J. in *Proceedings*, Second International Conference on the Mechanical Behavior of Materials, 16-20 Aug. 1976, pp. 652-656.

The technological size effect is defined to be the volume-dependent structure of the material caused by manufacturing (heat treatment, forging, rolling, etc.).

The geometrical size effect is caused by the influence of the configuration of a part on the stress distribution. Specimens of different sizes, therefore, show different fatigue crack growth, different critical crack length, and accordingly different lifetimes to fracture. As the geometrical size effect is a macroscopic one, we can assume that we are able to consider this effect by the methods of continuum mechanics.

The statistical size effect is caused by the microdiscontinuities (crystal defects, flaws, grain boundaries, inclusions, slipbands, etc.) of the material that are present and their random distribution over the volume, although the material can be considered as a macroscopically homogeneous one. This effect has the greatest chance to be described by a nested model.

Great difficulties will arise in taking into consideration technological effects by a nested model as the material constants vary over the volume of the material. Therefore, the nucleation of a fatigue crack may occur within the volume as well as at the surface. In the latter case the microroughness of the surface has a greater influence on the fatigue crack nucleation than the random distribution of structural defects.

My second remark concerns the choice of the distribution function. In fatigue problems we can proceed on the assumption that the final crack is initiated by the "weakest link" of the structure. On this assumption the mathematical theory on extreme-value statistics[3] allows only three probability functions, namely

$$F(x) = 1 - \exp\{-\exp[b(x - a)]\} \tag{7}$$

$$F(x) = 1 - \exp\left\{-\left(\frac{a - x}{b}\right)^{-m}\right\} \tag{8}$$

$$F(x) = 1 - \exp\left\{-\left(\frac{x - a}{b}\right)^{m}\right\} \tag{9}$$

The great popularity of the latter (Weibull distribution) is justified for mathematical as well as for physical reasons. In applying this function to fatigue problems a great number of data are necessary to answer the question of whether a vanishes or not. If we are interested only in the 50 percent probability, it does not matter, and a can be regarded as zero. The value of a becomes of great interest in the region where $F(x) \to 0$.

My last comment deals with the statistical representation of the concept of stress. The following concept was applied to fatigue problems with great

[3]Gumbel, E. J., *Statistics of Extremes*, Columbia University Press, New York, 1958.

success.[4] It is assumed that each defect in the material is equivalent to a crack length a. For fatigue fracture, only the size a_0 of the largest defect in the specimen is important. For this largest flaw the following distribution function was derived by Frechet[5]

$$F(a_0) = \exp\left\{-c_1\left(\frac{1}{a_0}\right)^{c_2}\right\} \tag{10}$$

where c_1 and c_2 are constants, depending on the material. When an unnotched specimen is loaded with stress σ, the largest flaw causes a stress-intensity factor K_0 of

$$K_0 = \sigma\sqrt{a_0} \tag{11}$$

Substituting Eq 5 into Eq 4 gives the distribution of the largest stress-intensity factors

$$F(K_0) = \exp\left\{-c_1\left(\frac{\sigma}{K_0}\right)^{2c_2}\right\} \tag{12}$$

Assuming that flaw extension takes place only when K_0 exceeds a threshold value K_{th}, the probability P of the value of K_0 being greater than K_{th} is

$$P(K_0 > K_{th}) = 1 - \exp\left\{-c_1\left(\frac{\sigma}{K_{th}}\right)^{2c_2}\right\} \tag{13}$$

This is equal to the probability that fracture will occur after a finite number of cycles at a stress level σ. The distribution function of stress σ which leads to fracture is then given by

$$F(\sigma) = 1 - \exp\left\{-\left(\frac{\sigma}{b}\right)^{m}\right\} \tag{14}$$

This expression is equivalent to Eq 3 with $a = 0$. (For treatment of inhomogeneous macroscopic stress fields, see Heckel and Ziebart (footnote 4). It could be a task of great merit for material scientists to give a physical interpretation of the concept of the fictitious crack length a.

P. Perzyna[6] *(discussion)*—The objective of the paper, as stated by the author in the introduction, is twofold. The first aim is "to point out new

[4]Heckel, K. and Ziebart, W. in *Proceedings*, Fourth International Conference on Fracture, Waterloo, Ont., Canada, Vol. 2, 19-24 June 1977.

[5]Frechet, M., *Ann. Soc. Pol. Mat.*, Cracow, Poland, Vol. 6, No. 93, 1923.

[6]Polish Academy of Sciences, Institute of Fundamental Technological Research, Warsaw, Poland.

opportunities in the application of statistical methods to key areas of fatigue research ...." The second goal is to include some new results from the author's unpublished work to argue for "a new way of thinking ...."

The question arises to what extent the author achieved those two goals.

In my opinion, the author wrote an advocacy paper concerning the importance of the application of statistical methods to different problems of fatigue phenomena. He has given good physical motivations and has shown examples of problems for which statistical methods have to be applied. It is pointed out that in the consideration of fatigue mechanisms we should take into account the interaction between different effects. These effects are influenced by inelastic response of a material, temperature change, defects in a material, inhomogeneities, imperfections, etc. Thus, to develop a reasonable theory of fatigue we have to investigate the situation and to show clearly the most important effects which can influence fatigue mechanisms.

Based on consideration of three different levels, that is, dislocation, subgrain, and grain-size levels, the author has proved that investigation of the change of microstructure creates a new opportunity for the application of statistical concepts, namely, the representation of a physical state.

This statement is of great importance to the modern theory of inelastic materials. The author has posed an important question. If for a specific material undergoing fatigue we can obtain the best statistical characterization of all conceivable geometrical and material observations, what can we do with the time-dependent distributional data of the specimen at all three levels?

To have a good interpretation of the three-level microstructural data, the author has introduced a concept of the nested model. In my opinion, the same features have been included in a model recently developed to describe the elastic-viscoplastic response of a material.[7] This model has been constructed within the framework of a material structure with internal state variables. It has been shown that this model can be used for analysis of fracture and fatigue phenomena.[8] To describe different fracture modes and fatigue failure, two groups of internal state variables have been introduced. Both groups have been interpreted based on physical analysis of dissipative mechanisms and available experimental results. So, the three-level microstructural data are introduced in this model by the internal state variables. The internal state variables are motivated by the microscopic level but all of them are well-defined macroscopic quantities. A discussion of the coupling of dissipative effects is based on a statistical procedure.[9]

It seems that one of the possible realizations of the nested model is through the use of the internal state variable framework.

[7]Perzyna, P., *Archives of Mechanics* (Warsaw), Vol. 29, 1977, pp. 607-624.

[8]Perzyna, P., "Internal State Variable Approach to Flow and Fracture Phenomena in Inelastic Materials" (in press); also, "Fracture and Fatigue Phenomena of Inelastic Materials at Elevated Temperature and Large Strain Rates" (manuscript in preparation).

[9]Haken, H., *Reviews of Modern Physics*, Vol. 47, 1975, pp. 67-121.

E. Kroner[10] *(discussion)*—The contribution of Dr. Fong finds my support above all in the following four proposals made:

1. Fatigue is basically a field for interdisciplinary research.
2. A successful study of fatigue has to be based on the notion of a physical state which changes during the cyclic deformation.
3. Due to the lack of information and the complexity of the elementary processes, a statistical description of the physical state seems to be most appropriate.
4. Depending on the scale of observation, the physical state will have quite different appearances. This suggests the nested model described, which implies a description of the various scales with a suitable statistical linking between them.

Although the ideas behind the foregoing proposals, especially Nos. 1-3, have occurred in the literature, it is, in my opinion, an essential merit of Dr. Fong to have them represented in a closed and detailed form and to have given impressive examples in which they seem to work rather well. Nevertheless, there remain open a number of fundamental questions which, together with some remarks, I shall now try to formulate. Some of these questions are posed also in order to check my understanding of the author's presentation.

1. Will the proposed research lead to a *predictive* theory or will it rather produce an intelligent way of describing, in mathematical terms, what happens during the cyclic deformation? Although the second possibility possesses great interest in itself and adds to the physical insight, it seems to me that the final understanding of the fatigue phenomenon will be coupled intimately to a predictive theory.

2. Dr. Fong has discussed three special cases in which the internal structure of the fatigued specimen could be described by rather simple statistical distributions: the log-normal distribution for the crack lengths in corrosion fatigue, the Weibull distribution for the fiber lengths in paper fatigue, and the uniform distribution of the void sizes in irradiation fatigue. Besides their analytic form, these distributions are specified by only a few parameters which are the quantities which change during cyclic deformation, thus representing the change of the physical state. This result is conceptually simple. The physical part of the problem consists in explaining the *types* of distribution, predicting the change of the parameters during fatigue, and in investigating whether critical values of these parameters exist which correspond to a fatigue failure. The task of solving these problems is certainly not a simple undertaking.

3. It seems to me that the simple form of the foregoing statistics can be attributed to the fact that the structural defects of these examples develop rather independently from each other. In metal fatigue we expect the

[10]Institut fur Theoretische und Angewandte Physik der Universitat Stuttgart und Max-Planck-Institut fur Metallforschung, Stuttgart, Germany.

opposite, at least in certain stages. Not only is the glide process of a dislocation in cooperative motion of many atoms, but also of many dislocations which move often in a cooperative manner. It seems to me that none of the aforementioned defects, which were accessible to a description by a simple distribution function, have any similarity with the dislocation. A lot of work is still needed to find a good statistical description of dislocation structures. Perhaps this will not be possible without concepts as difficult as those of dislocation correlation functions. The situation might be better at that stage and level of observation where the dislocations form cells.

4. The concept of stress is certainly basic in the description of the physical state. Dr. Fong discusses the special case of porous media. Whereas the local stress is zero in the pores, it becomes very large in the dislocations. Thus Harr's concept of statistical stress has to be modified for *metal* fatigue. Is that an easy problem? Incidentally, the Harr's concept appeals to me because stress can be understood as a density of elastic dipoles; that is, it has the transformation property of a tensor *density* (rather than that of a tensor) in the sense of Weyl. Therefore it makes sense to add up microstresses in different microdivisions. This point deserves perhaps further consideration.

5. Harr's concept of scaling reminds me of the scaling procedures developed in the theory of critical phenomena. If the pores of some medium develop in such a way that the same picture appears at arbitrary magnification, then one could perhaps apply renormalization group techniques. In any case, an investigation in this direction could perhaps add to our understanding. For a further motivation I recall that similar investigations were quite successful in the theory of polymer solutions, which, as has been shown recently by de Gennes, des Cloiseaux, and others, are found to be in the neighborhood of a critical point.

6. If I understand it correctly, the nested model means that the equations for the phenomena on the largest scale depend on those of the second largest scale. The equations for these again depend on the phenomena of the third largest scale, etc. In some manner this is analogous to the situation in other physical theories, for instance, in the theory of turbulence, where the equations for the mean motion depend on the 2-point correlation function, the equations for this function depend on the 3-point correlation function, etc. Keeping this analogy in mind might also be useful.

The main aim of my comments is to show that Dr. Fong's paper has confronted us with many interesting and mostly difficult problems, the solution of which would certainly imply a big step toward a better understanding of fatigue.

H. Reemsnyder[11] (*discussion*)—In future years, Dr. Fong's paper is

[11] Fatigue and Fracture Division, Homer Research Laboratories, Bethlehem Steel Corp., Bethlehem, Pa.

likely to be recognized as one of the more prophetic presentations of this symposium. The probabilistic approach to discrete stresses at the microscopic level has a much greater potential than application of continuum mechanics at this level.

Dr. Fong calls for an interdisciplinary approach to nested modeling of microscopic flaws up to macroscopic discontinuities for life prediction. To be successful, this interdisciplinary approach must include a formally trained statistician. Background furnished by the reading of a book or a few papers on basic probability and statistics is simply inadequate.

I support Dr. Fong's implication that probability distributions selected to model phenomena are nothing more than curve-fitting functions to describe observed behavior of a specimen. One parameter of a probability distribution describes the variability of the material phenomenon or property being modeled and is generally estimated by the variability of the observations. However, the latter estimate includes other components of variability that often exceed the variability intrinsic to the property of the material. These sources reflect the sampling techniques and test methods required to develop the observations, and they include accuracy and precision of the measurements, material selection and specimen preparation, interaction of the test system with the phenomenon being studied, laboratory environment, and methods of data analysis. Design of the experiment and modeling of phenomena from observations in that experiment require input from the statistician mentioned earlier.

G. Moore[12] *(discussion)*—I wish to comment on Dr. Fong's paper with respect to certain implications regarding the question of extrema of structure emphasized by Dr. Rhines in an earlier paper in this symposium. Practically every paper considering crack initiation has stated or implied that this starts at some point where the microstructure is not average. There is considerable implication that crack propagation also favors non-average parts of the structure.

As indicated in my discussion of Dr. Rhines's paper, it is theoretically possible to observe about 2 million different standard (0.5 mm^2) microstructural fields per cubic centimetre of metal. Alternatively, it appears consistent with experiments described at this symposium to presume that crack initiation can occur within a cube about 100 μm on a side. Thus we should be concerned with extrema which may occur once in 1 to 2 million times per cubic centimetre, or possibly once in 100 million times in a real component. If the distribution were in fact Gaussian, we would expect to see a 4-σ deviation about once in a feasible survey of 10 000 fields. The odds against a 6-σ deviation in a normal distribution are 500 million to 1, so this would be *thought* a safe maximum in a component.

[12] Metallurgist (retired), National Bureau of Standards, Washington, D.C.

If, however, the real distribution is nonGaussian and positively skewed, both the magnitude and frequency of extrema may be greatly increased. The presumption of a 6-σ maximum then becomes totally unsafe. Dr. Fong shows numerous distribution curves in his paper. Not one of these resembles a Gaussian shape. I take this to indicate that he does not expect real distributions to be normal very often. Is there a fundamental reason for expecting abnormality?

I would have liked to see Dr. Fong emphasize the impact of his "nested models" concept on this question. We are all familiar with the one-dimensional theory of errors concept that when several not-quite-Gaussian measurement sets are added, the summation will become more nearly Gaussian. Nested models imply independent distribution—generating processes proceeding at different times or at different size scales. Treatment in two or more dimensions is now required. Each large-scale cell now yields a different new distribution at the smaller scale, with the overall final distribution being a combination of numerous unlike partial distributions. The result of multiple processes can never be Gaussian even if its components were individually normal. Combining many imperfect distributions may be expected to yield rather wild curves with most unexpected extrema.

It appears that the inclusion concentration distribution which I showed as Fig. 2 of my discussion of Dr. Rhines's paper does logically result from a nested model involving first a distribution of sizable slag globules at the ingot stage, followed by fragmentation and reshaping during working, then sampling at a smaller size scale. The result in that cases was 9- to 10-σ extrema at a frequency expected for 4-σ.

I believe, therefore, that the implications of nested effects should be promptly considered, even with very crude models, without waiting for data for a detailed treatment. The moral apparently is that we should pay a lot more attention to the occasional oddball data and considerably less attention to averages and their highly questionable confidence limits!

J. T. Fong (author's closure)—I would like to thank all the discussers for their valuable critical discussions. I am particularly gratified by the apparent existence of a consensus among the five discussers and numerous others who commented on my paper that the time has come for us to use statistical methods in a more fundamental way to explain the scatter of fatigue data. Since there are essentially two major points I raise in the paper, my response to the five discussers may also be conveniently classified as follows:

Statistical representation of morphological and stress parameters

K. Heckel—"... each defect in the material is equivalent to a crack length a. ... It could be a task of great merit for material scientists to give a physical interpretation of the concept of the fictitious crack length a."

J. T. Fong—Prof. Heckel's approach avoids the hard problem of characterizing the large variety of defects at different microscopic levels. While the approach is certainly interesting to see how successful it may be, it differs from mine in the sense that I wish to deal with direct observations which may not fit neatly into some standard statistical distributions. In particular, the question of a vanishing location parameter of the Weibull distribution cannot be settled simply because it is more convenient to work with a two-parameter Weibull function. Prof. Heckel's approach, therefore, invites a modeler to introduce simplifying assumptions which may have grave physical consequences.

P. Perzyna—"What can we do with the time-dependent distributional data of the specimen at all three levels?"

J. T. Fong—If we assume the three-parameter Weibull distribution with $x_0(t)$, $x_u(t)$, and $m(t)$ all depending on the time t, then a first approximation will rank the three parameters according to how strong each varies with t. For instance, in our studies on the fatigue of paper, we found that (see Fig. 5 of the text) x_u varied the most, x_0 varied a little less, and m did not vary at all. This type of information, while not definitive, provides a guide for us to select the most relevant parameter for the next stage of modeling. If we use this technique for data at different levels, we may end up with a choice of parameters for constructing a nested model.

E. Kroner—(1) "Will the proposed research lead to a *predictive* theory ...?"

J. T. Fong—Yes. A lot of sophisticated techniques such as computer simulation, sampling theory, symmetry groups, and renormalization group techniques may be used to "crack" the problem, but the problem is not solvable unless we ask the experimentalists to furnish us with a minimal amount of microscopic data. It is preferred that the data be uninterpreted and not reported to prove a specific hypothesis or theory. Such data on fatigue are today almost nonexistent.

E. Kroner—(3) "A lot of work is still needed to find a good statistical description of dislocation structures."

J. T. Fong—At the dislocation level, experimental data for guiding statistical representation are extremely hard to come by. I agree with Prof. Kroner that a lot of work is still needed, but I am optimistic because there are a lot of competent theoreticians and experimentalists in this area of investigation.

E. Kroner—(4) "Whereas the local stress is zero in the pores, it becomes very large in the dislocations. Thus Harr's concept ... has to be modified for *metal* fatigue. Is that an easy problem?"

J. T. Fong—Yes, it is an easy problem. No, Harr's concept need not be revised for metal fatigue just to deal with the large stress in the dislocations. What Harr's concept boils down to is to ask the question: Given a block of material, how often do we have zero stress, how often do we have stress equal to the continuum stress, how often twice the continuum stress? And so on. It is conceivable to have a block of material with N dislocations such that the probability expressed as a certain percentage of the volume is almost zero for very large stresses because the cores of those dislocations are volumetrically very, very small.

H. Reemsnyder—"... this interdisciplinary approach must include a formally trained statistician."

J. T. Fong—While agreeing with Dr. Reemsnyder that we need to have the assistance of a statistician, I might add that the responsibility of modeling fatigue should largely be in the hands of the physical scientist or engineer who is trained to interpret the data and to make judgmental decisions based on experience which the statisticians lack. In short, the statistician advises; he does not dictate.

G. Moore—"Practically every paper considering crack initiation has stated or implied that this starts at some point where the microstructure is not average. ... Is there a fundamental reason for expecting abnormality?"

J. T. Fong—At this point, I do not have a fundamental reason for expecting abnormality except that intuitively I believe that a nonaverage microstructure can lead to unfavorable stress distributions which in time will distort the microstructure even more. If the concept of an endurance limit is still valid, then it is conceivable that, at stresses below the endurance limit, the microstructure will remain "average" forever. We hope some experimentalists will furnish some data to prove that statement.

Concept of Nested Modeling

K. Heckel—"... the large amount of experimental data and the considerable scientific effort required to construct such a model can hardly be justified in many engineering applications."

J. T. Fong—I disagree. The use of statistical tools is natural for dealing

with a large amount of experimental data provided we couple the application with sound control of sampling procedure and experimental design. If we believe that fatigue is a problem that spans a huge spectrum ranging from engineering and material science to fundamental solid-state physics, then any progress in fatigue mechanism modeling is bound to lead to a better prediction in the fatigue life of engineering components and structures.

P. Perzyna—"... the author has introduced a concept of the nested model. In my opinion, the same features have been included in a model recently developed to describe the elastic-viscoplastic response of a material. This model has been constructed within the framework of a material structure with internal state variables."

J. T. Fong—I am afraid Prof. Perzyna misinterpreted my concept of a nested model. In Prof. Kroner's discussion, under Item 6, he came closer to what I intended to say. I wish to state that the theory of internal state variables is different from the concept of a nested model because the former allows each internal state variable an equal status in the initial formulation of the model and is almost impossible to check experimentally when data are sorted according to their characteristic lengths. In the theory of a nested model, experimentally measurable quantities are admitted as state variables and a selection process is defined to explain experimental data at different levels of observations.

E. Kroner—(2) "The physical part of the problem consists of explaining the *types* of distribution, predicting the change of the parameters during fatigue, and in investigating whether critical values of these parameters exist which correspond to a fatigue failure. The task of solving these problems is certainly not a simple undertaking."

J. T. Fong—The task is actually easier than one might think. I believe today we have the physical instruments and analytical tools (including simulation via computer) to solve the problem if we can first convince ourselves that we must band together rather than each trying to come up with a piecemeal model. I believe we need to involve experimentalists to contribute the data, applied mathematicians to contribute the modeling expertise and analysis, engineers to contribute the product performance data to check a predictive model, and the managers to support the work in order to provide the public with a safer and more durable product.

E. Kroner—(5) "Harr's concept of scaling reminds me of the scaling procedures developed in the theory of critical phenomena."

J. T. Fong—There are similarities, but there are also differences. I hope to contribute a more detailed discussion of this topic in future publications.

E. Kroner—(6) See original text of discussion by Kroner.

J. T. Fong—I agree with your observation.

G. Moore—"... the implications of nested effects should be promptly considered ... without waiting for data ..."

J. T. Fong—I appreciate Dr. Moore's remarks on the concept of nested modeling. I would caution that the concept is highly physical in the sense that its application is closely tied to the availability of a large amount of raw and carefully "sorted" data (by levels).

Chapter 7: Fatigue of Composite Materials and Environment-Assisted Fatigue

Jeffrey T. Fong[1]

Opening Remarks by Session Chairman

This, the sixth and last session of our symposium, examines some recent progress in fatigue mechanisms of composite materials and certain classes of environment-assisted degradation phenomena. During the previous five sessions, we examined the basic mechanisms of fatigue, both experimentally and theoretically, for some relatively simple material systems. This is necessarily so, because progress in basic understanding usually involves a long march from simple concepts to a systematic combination of those concepts.

It is the purpose of this session to see if the time has come for us to try our wings, so to speak, and tackle some real and technologically important problems of fatigue by applying the concepts we learned in dealing with simple problems. The four authors of this sesssion were invited on the basis of their willingness to contribute not only definitive results but also new concepts or ideas that could be controversial. It is clear that in the area of composite materials and corrosion fatigue, we have a long way to go to settle some of the puzzling phenomena of degradation. I hope during this session many of you will share your ideas with the speakers whenever you feel a "controversial" point has been brought up. As the eminent physicist R. P. Feynman once said, "We do not know where we are 'stupid' until we 'stick our neck out,' and so the whole idea is to put our neck out."[2] The spirit of this session is to encourage all of us, including the four speakers, to put our neck out. Professor Feynman[2] then said, "And the only way to find out that we are wrong is to find out *what* our predictions are. It is absolutely necessary to make constructs."

Let us now see what "constructs" our four speakers have in store for us.

[1]Physicist and project leader, Center for Applied Mathematics, National Engineering Laboratory, National Bureau of Standards, Washington, D.C.

[2]Feynman, R. P. et al, *The Feynman Lectures on Physics*, Addison-Wesley, Reading, Mass., Vol. 1, 1963, pp. 38-39.

W. W. Stinchcomb[1] *and K. L. Reifsnider*[1]

Fatigue Damage Mechanisms in Composite Materials: A Review

REFERENCE: Stinchomb, W. W. and Reifsnider, K. L., **"Fatigue Damage Mechanisms in Composite Materials: A Review,"** *Fatigue Mechanisms,* Proceedings of an ASTM-NBS-NSF symposium, Kansas City, Mo., May 1978, J. T. Fong, Ed., *ASTM STP 675,* American Society for Testing and Materials, 1979, pp. 762-787.

ABSTRACT: Some of the earliest investigations concluded that the basic mechanisms of fatigue in composites and fatigue in homogeneous materials differ greatly. Instead of the initiation and propagation of a fatigue crack traditionally identified with homogeneous materials, fatigue in composites consists of various combinations of matrix, fiber, and interfacial cracks and debonds to form a very complex damage state. Furthermore, fatigue mechanisms are dependent upon a number of parameters, including the material system, stacking sequence of plies, geometry, stress state, and environment.

The variety of damage modes, the complexity of their interactions, and the subsequent effect on engineering properties make it difficult to interpret fatigue damage in order to define and predict fatigue failure or lifetime for composite materials. A brief synopsis of the current knowledge of fatigue damage mechanism in fiber-reinforced composite materials is presented along with some suggestions to help advance the level of understanding of the fatigue response of composite materials.

KEY WORDS: composite materials, damage, fatigue, mechanisms

The subject of fatigue has been of interest to engineers and materials scientists for more than 125 years; however, most of the present-day knowledge and understanding of fatigue has been obtained from work performed during the past 50 years. If the number of technical papers written on a subject can be used as an indicator of interest in that subject, it must be said that there was only minimal activity in the area of composite materials at the time the last ASTM symposium on basic mechanisms of fatigue was held in 1958. Since that time, advanced fiber-reinforced composites have emerged as a new class of engineering materials and have been gaining increasing acceptance in engineering design. The desirable properties of high strength-to-weight and stiffness-to-weight ratios and good fatigue resistance coupled with an

[1] Associate professor and professor, respectively, Department of Engineering Science and Mechanics, Virginia Polytechnic Institute and State University, Blacksburg, Va. 24061.

increasing emphasis on energy conservation have made composites strong candidate materials for many structural applications, including aircraft, spacecraft, seacraft, and automobiles. The resulting demand for new manufacturing and quality-control technologies, design methodology, and an understanding of material response has given impetus to an interest in composite materials which has increased greatly during the past 10 years.

Because composite materials are frequently used in structures subjected to dynamic loads, it is important that their response to cyclic loads be well known and understood. Fatigue and fracture of composite materials are primary areas of research in many government, industrial, and university laboratories in the United States and other countries. Working committees within technical and professional societies have been established to further study and write standards relating to fatigue of composites. Several symposia and many sessions of meetings and conferences have been devoted specifically to the subject. One result of the interest and activity is an immense volume of literature consisting of papers, reports, and proceedings all dealing with some aspect of fatigue of composite materials. Several review articles, including Refs *1–5*, have been written on fatigue of composite materials and present a discussion of much of the work through the early 1970's. Compared with the vast number of publications on fatigue of composite materials, the number of articles contributing to the understanding of basic fatigue mechanisms in these materials is relatively small.

Fatigue damage in composite materials consists of various combinations of matrix cracking, fiber-matrix debonding, delamination, void growth, and local fiber breakage. The mechanism, type, and distribution of damage depend upon the material system (combination of fiber and matrix materials), stacking sequence of plies, fabrication techniques, geometry of the component, stress state, and the loading history. Furthermore, the mechanisms are sensitive to a number of other parameters, including hole size, type of loading, frequency of cyclic loading, temperature, and moisture.

A review of the literature on fatigue of composites reveals that most of the work to date has been in axial tension-tension fatigue. From a mechanistic viewpoint, however, there is a natural division of the subject into two major categories—the behavior of notched materials and the behavior of unnotched materials. Within each category, the influences of parameters such as material system, stacking sequence, and type of loading will be discussed.

Unnotched Behavior

Studies have shown that fatigue damage initiation is associated with interactions of the fibers and matrix at the fiber-matrix interface [*2–4*].[2] The respective roles which the fibers, matrix, and the fiber-matrix interface play

[2] The italic numbers in brackets refer to the list of references appended to this paper.

in the fatigue damage initiation process depend upon the material system, loading mode, and the amplitude of the cyclic stress. In glass and graphite fiber reinforced plastics, Owen [*2,3*] has observed damage initiation due to debonding between fibers and matrix. The subsequent development of the damage state is progressive and is determined by the properties of the fibers and matrix as well as the load history. In metal matrix composites, Hancock [*4*] has also observed crack initiation at fiber-matrix interfaces; however, broken fibers on as-machined surfaces can act as crack initiation sites.

Under conditions of high cyclic stress, crack initiation can occur on the first cycle and new cracks develop as loading continues. Dharan [*6*] noted three regions in the *S-N* curve for unidirectional glass fiber composites. When the applied cyclic stress is large enough to be within the strength distribution of the fibers, local fiber failures occur on the first cycle. As additional cycles are applied, the local failures join together until fracture of the specimen occurs within a few cycles. If the applied stress is not sufficiently large to cause a large number of fiber fractures, matrix microcracks initiate and propagate during cycling until delamination of the ply interfaces begins. Although some fiber breaks may occur early in the life of the material, they do not appear to have a major influence on fatigue response. If the applied stress level is below that required to initiate matrix microcracks, fatigue lives greater than 10^6 cycles can be obtained, although some microcracks do develop in the matrix during cyclic loading.

In metal matrix-brittle fiber composites, such as boron-aluminum, some fiber fractures can be expected to occur on the first loading cycle due to wide distribution of fiber strengths, and the number of broken fibers increases with the number of cycles. The local fiber fractures are possible sites for the initiation of fatigue cracks in the metal matrix due to locally high shear stresses in the matrix. Although microcracks may initiate and grow, it is possible to avoid fatigue failures. Using a two-parameter model to determine shakedown limits, Dvorak and Tarn [*7*] have made theoretical predictions of fatigue limits which are in agreement with experimental results for several metal matrix composites. The fatigue limit can be determined from the requirement that the stresses acting in the constituent materials during cyclic loading do not exceed the respective fatigue limits of either the fiber or the matrix.

The modes and rate of crack growth depend on the relative moduli, yield strength, and ductility of the constituent materials as well as on the strength of the fiber-matrix interface. Hancock [*8*] suggests that the fatigue properties of metal matrix composites are improved by having a low-yield-strength ductile matrix, a high-strength brittle fiber, and weak interfacial bonds, allowing local failures to occur at the interface instead of in the matrix. This behavior is shown in Fig. 1 (from Ref *4*), where crack branching is evident in the low-yield-strength 1235 aluminum matrix but not in the higher-strength 6061-MT6 aluminum. Subsequent work by Dvorak and Tarn [*7*], however,

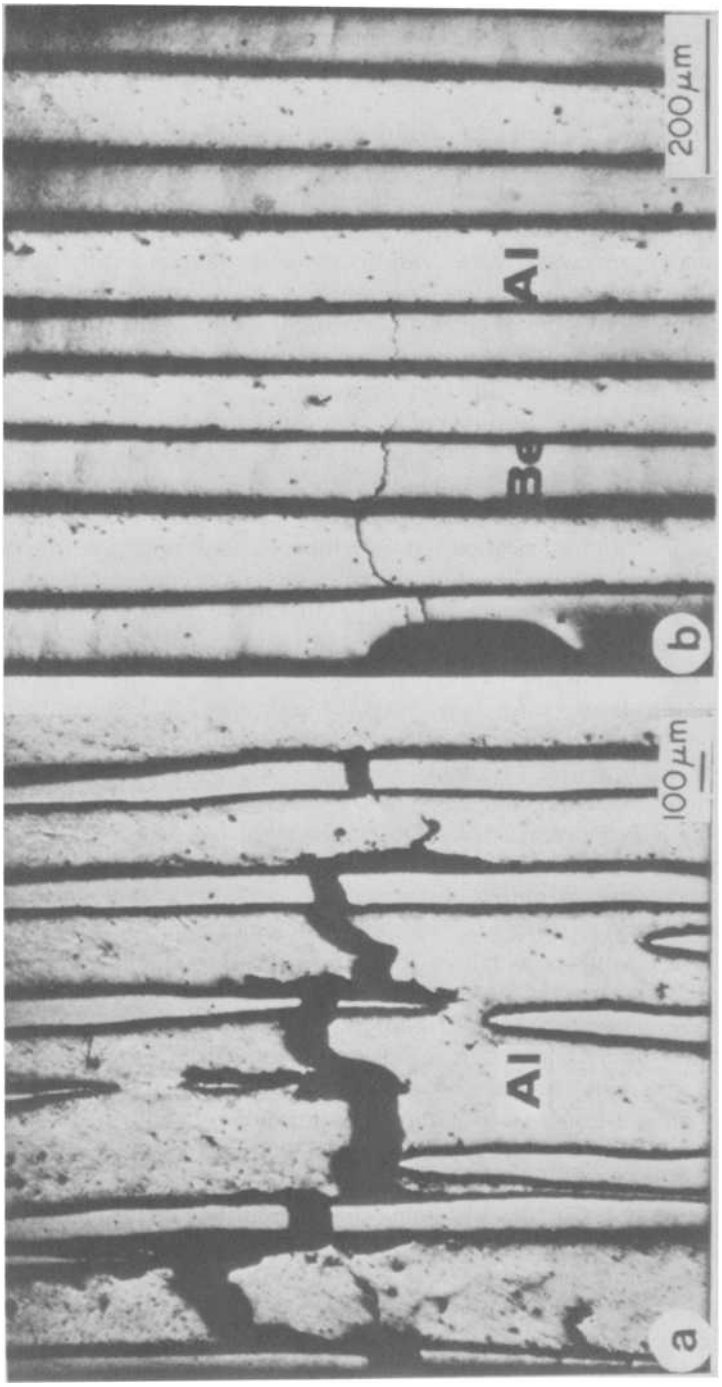

FIG. 1—*Growth of fatigue cracks in beryllium-filament composites with different matrix materials:* (a) *1235 aluminum-beryllium for* $\Delta\epsilon = 0.007$; (b) *6061-MT6 aluminum-beryllium for* $\Delta\epsilon = 0.005$ *(after Ref* 4).

shows that the requirement of low matrix yield strength alone does not improve the fatigue strength of the composite. High matrix yield strength is allowable as long as it does not exceed the fatigue strength of the metal matrix.

The macroscopic behavior of unidirectional composites closely follows from the microscopic observations. Awerbuck and Hahn [*9*] report that unidirectional graphite-epoxy specimens, cyclically loaded parallel to the fibers, failed abruptly, without early warning, and in a mode typical of static failures at maximum cyclic stresses within the scatter band of tensile strength data. At cyclic stresses slightly less than this level, fatigue damage was in the form of longitudinal matrix cracks between fibers near the edge of the specimens; however, most of these specimens survived between 10^5 and 10^6 cycles with no measureable reduction in strength.

The fatigue strength of unidirectional composites suffers when the loading direction is not parallel to the fiber direction. At large deviations from the loading directions, the fibers become less effective in carrying the load and the fatigue behavior is much more sensitive to local inherent defects such as resin-rich regions and fabrication irregularities. Fatigue tests performed by the authors [*10*] on 90-deg graphite-epoxy specimens produced fatigue and residual strength test failures which were parallel to the fibers with no visible evidence of fatigue damage on the surface of the specimen.

Because the properties of a composite lamina are highly anisotropic, most structural applications require that several laminae be stacked together to form a laminate with the fibers in individual plies having a specified orientation. Figure 2 (from Ref *11*) shows the effect of fiber orientation on the fatigue strength of unidirectional, angle-ply, and cross-ply laminates. Some strengthening may be realized if the angle between the load direction and fiber direction is small. In general, reducing the degree of anisotropy improves the transverse strength and stiffness of a laminate while reducing the overall strength and creating a very complex and challenging class of fatigue problems. For example, a simple cross-ply 0/90 deg stacking sequence laminate is in a state of biaxial in-plane stress in interior regions. Near the unloaded (free) edges, the presence of interlaminar shear and normal stresses creates a three-dimensional state of stress. When the external loading is cyclic, the cyclic multiaxial stresses cause a variety of damage modes which interact to form a complex state of damage. Variations of the 0/90 deg stacking or other stacking sequences, such as quasi-isotropic (combinations of 0, +45, −45, 90-deg plies), produce different stress states and therefore different damage states. One additional and important point concerning laminates should be made. The anisotropy of thermal expansion coefficients creates a state of thermal residual stresses (curing stresses) in laminates as a result of fabrication. In some cases, these stresses are large enough to create initial cracks in weaker plies.

Tension-tension fatigue in cross-ply and quasi-isotropic laminates begins

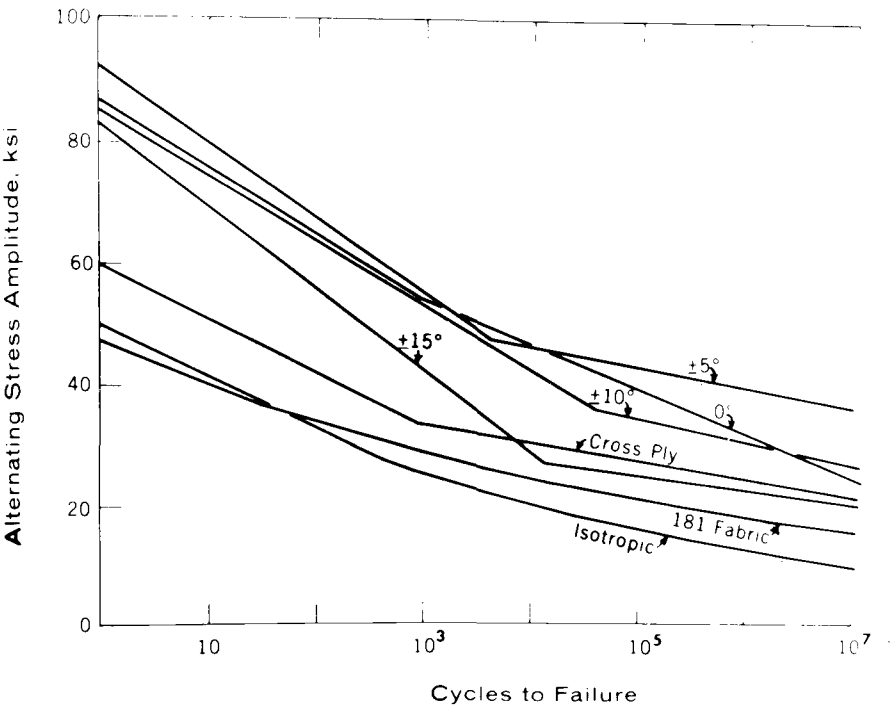

FIG. 2—*Effect of fiber orientation on fatigue strength of composite materials (after Ref* 11).

with transverse cracks in the 90-deg plies. In many engineering situations, these cracks may initiate on the first loading cycle and increase in density and extent in a fashion dependent on the loading history, stacking sequence, and material system as observed by Tanimoto and Amijima [*12*] and Stalnaker and Stinchcomb [*13*]. These authors report that the density of transverse cracks increases with stress or cycles until a stable density for a particular laminate configuration is reached (Fig. 3, from Ref *12*). For several different graphite-epoxy laminates, the observed stable crack spacings are in good agreement with the analytical predictions of Reifsnider [*14*]. It also appears that achieving a stable or saturation density of cracks in the 90-deg plies corresponds to the proportional limit in the static stress-strain curve. Grimes [*15*] has found the proportional limit stress to be the endurance limit for cross-ply graphite-epoxy laminates.

Additional fatigue damage develops by delamination between plies and crack growth into adjacent plies (Fig. 4, from Ref *13*). Under cyclic tensile loads, laminates with tensile interlaminar normal stresses at the free edges, such as those with basic $[0/90]_s$ and $[0/\pm 45/90]_s$ stacking sequences, develop delaminations which interact with the transverse cracks in the 90-deg

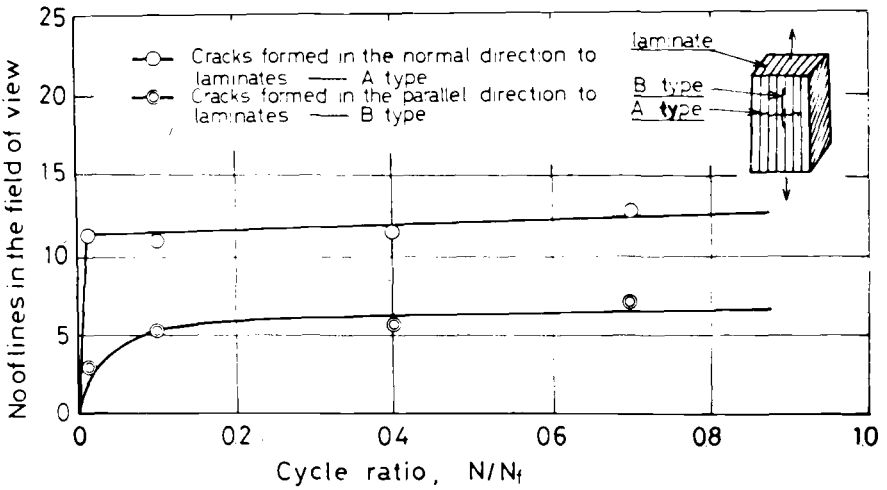

FIG. 3—*Density of fatigue cracks in woven glass cloth reinforced polyester resin (after Ref* 12 *published by Technomic Publishing Co., Inc.).*

plies. The delaminations then progressively grow along the length and through the width of the specimen. Sendeckyj and Stalnaker [*16*] have noted that delaminations are an important fatigue failure mode; however, they may not significantly influence residual strength or the site of residual strength test failures [*13*]. The tendency for a composite material to delaminate is strongly dependent on the stacking sequence and mode of loading. For example, the two basic laminates mentioned previously would develop compressive interlaminar normal stresses upon compression loading and would not be expected to delaminate.

Sendeckyj and Stalnaker [*16*] have also studied the effect of frequency on the fatigue behavior of unnotched composites. Using two zero-to-tension-to-zero trapezoidal waveforms differing only in the length of time at load, they have found that the longer hold time reduced the fatigue life.

While fatigue strength and fatigue life are important properties of composite materials, stiffness is also an important property, and in some engineering designs, such as those in which stability is important, it may be a critical design factor. Broutman and Sahu [*17*] have presented data showing the correlation between the amount of fatigue damage, modulus change, and strength reduction, Fig. 5. Salkind [*1*] suggests that the change in stiffness could be used as one definition of fatigue failure in composite materials. O'Brien and Reifsnider [*18*] have used experimental debonding and fiber breakage data along with a reduced stiffness analysis to predict stiffness changes in boron-epoxy laminates. The amount of matrix damage correlates well with stiffness change and fiber breakage correlates with strength reduction.

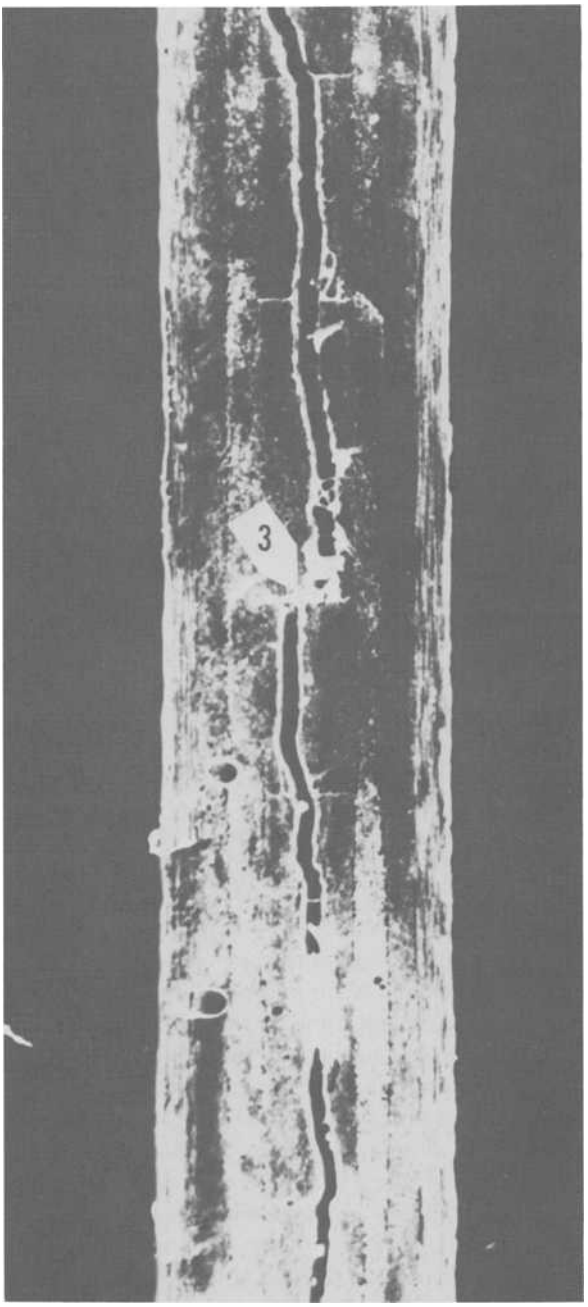

FIG. 4—*Transverse cracks (such as No. 3) and delamination on the edge of a* $[0/\pm 45/90]_s$ *graphite-epoxy specimen after* 10^4 *cycles at a maximum stress of 234 MPa (after Ref* 13).

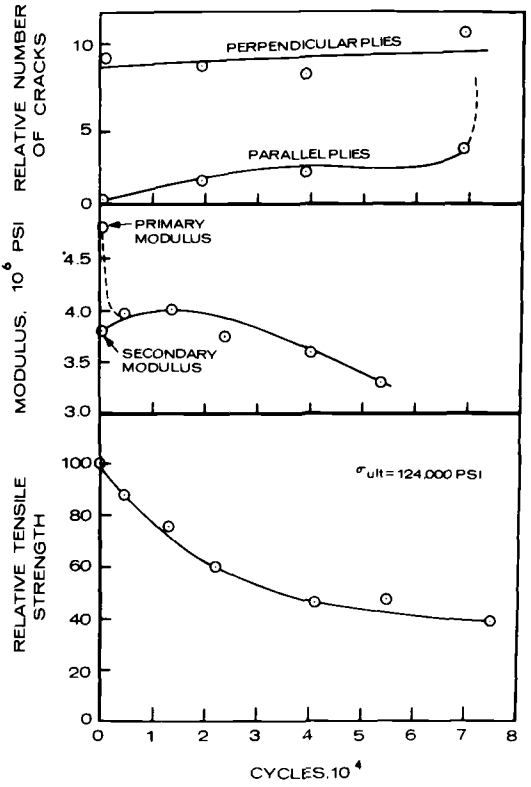

FIG. 5—*Correlation between fatigue damage, change in modulus, and strength reduction in a 0/90 glass-reinforced epoxy (after Ref* 17) *(1 psi = 6.895 kPa).*

The response of composite materials when loaded in modes other than tension-tension fatigue has been studied much less extensively, although currently there is widespread interest in tension-compression and compression-compression fatigue behavior. It appears that cyclic compression loading is more detrimental than cyclic tension at the same stress level. Dharan [*6*] noted that graphite polyester specimens cycled in one-way four-point bending always failed on the compression side. Damage was observed to initiate at a zone of fiber buckling and develop by local delamination, crack propagation into the specimen, and large-scale delamination. Berg and Salma [*19*] observed similar microbuckling mechanisms at the tip of a notch on the compression side of graphite-epoxy specimens under cyclic bending. The cracks grew perpendicular to the fibers when the notch was on the compression side and parallel to the fibers when the notch was on the tension side. In cyclic bend tests, Pipes [*20*] found interlaminar shear damage to be important in the fatigue behavior of boron-epoxy and graphite-epoxy.

A major damage mode in compression fatigue is delamination followed by out-of-plane buckling. Although delaminations can develop in tension-tension loading of quasi-isotropic laminates, as noted previously, they are more critical when the cyclic loading contains compression excursions as pointed out by Ryder and Walker [*21*]. Specimens tested in tension-compression loading usually failed soon after delaminations formed. These specimens failed on a compressive portion of the load cycle due to fracture of the plies which were buckled out-of-plane. A second laminate, containing 67 percent 0-deg fibers, also failed due to delaminations and local out-of-plane buckling under tension-compression loading. Unlike the first laminate, however, failure in tension-tension cyclic loading occurred soon after delamination.

Fatigue of composite materials under biaxial loading is a new area of investigation. Francis and co-workers [*22*] have found the fatigue life of graphite-epoxy tubes loaded in combinations of tension, torsion, and internal pressure biaxial fatigue to be reduced when the cyclic stress range spans across the first-ply failure envelope as compared to situations where the same stress range was entirely within the envelope. Although higher peak stresses contribute to the reduced life when crossing the failure envelope, changes in state of micromechanical damage also contribute to the decrease in fatigue life.

The effects of environmental parameters, such as moisture and temperature, on fatigue mechanisms is another area which is just starting to receive needed attention. Hofer et al [*23*] have examined the effects of moisture on fatigue and residual properties of an S-glass/graphite-epoxy hybrid composite and found no basic alteration in response due to moisture. From tests at cryogenic temperatures, Kasen et al [*24*] have found fatigue response of boron-aluminum and boron-epoxy to be similar to that at room temperature, and Tobler and Read [*25*] report the fatigue life of glass-epoxy at 4 K to be an order of magnitude greater than that at room temperature. Much of the work at this point has been concerned with the effect of environment on fatigue properties and has not addressed the specific topic of mechanisms.

Notched Behavior

General Characteristics

We will consider the term notch to include holes, slits, slots, and cracks. Many of the peculiarities associated with the fatigue response of composite materials with cutouts are common to those notch types. The load situation caused by a notch is extremely complex, even for unidirectionally reinforced materials. Whereas a macroscopic (anisotropic) stress analysis will frequently suffice for unnotched material response determination, damage

development near a notch is sensitive to microscopic (sometimes inhomogeneous) stress analysis considerations. A simple consequence of this complexity of local stresses is the complexity of damage that develops near a notch. Only in very special cases (which are generally of little interest to engineering applications) does a notch extend in a planar, self-similar manner. Rather, a wide variety of damage types and mechanisms is observed. We will review them in this section by first indicating general damage characteristics and their condition (and sometimes the method) of observation. Then specific details and associations will be discussed.

Matrix damage is a universal component of notch-related fatigue damage. Polymer-matrix materials are subject to crazing, cracking, and debonding. In semitransparent materials such as glass-epoxy, crazing can be observed with the naked eye [*26*]. In other materials evidence of crazing can be seen on the surface as regions generally lighter in color or brighter under reflected light [*27,28*]. It is sometimes difficult to distinguish matrix cracking from crazing. It would appear that they frequently occur together. Of course, cracking will create regions which can be invaded by foreign substances, so that it is possible to delineate cracks by introducing a liquid opaque dye (such as tetrabromoethane) prior to examination by X-ray radiographic methods [*29,30*]. Debonding, especially of reinforcing fibers from the matrix, is also common. This is particularly true for large fiber materials such as boron and glass. Matrix crazing, cracking, and debonding between reinforcing fibers (or fiber bundles) frequently combine to produce "splitting" along the fiber directions near the tip of a notch [*26–31*]. Perhaps the most common type of fatigue-related matrix damage, at least for polymeric matrix materials, is delamination. Perhaps because tensile through-the-thickness normal stress and very large shear stresses are nearly always present in some region at a notch, delamination frequently plays a major part in the development of notch-related fatigue damage [*26,29,32–38*]. Ultrasonic C-scan techniques appear to be best suited to the detection of delamination [*33*]. X-ray radiography aided by opaque penetrants has also proven to be very successful in detecting delamination [*29,32,33,35*].

Damage in metal matrix material is somewhat less complex: crazing does not occur and debonding of the matrix from the reinforcing fibers is much less common [*38*]. However, plastic flow and cracking of the matrix do occur and delamination is observed [*31,38*].

Fiber (or fiber bundle) breakage usually occurs near a notch if sufficient load levels are reached. In large fiber materials such as glass and boron, individual fiber breakage events can be identified [*36,39*]. Materials which are more nearly homogeneous, such as graphite-epoxy (GEp), show less evidence of distinct fiber (or fiber bundle) damage events, and more tendency to form cracks through the thickness of a ply (lamina) or plies. While both shear and normal stress components cause matrix damage, fibers usually fail due to the action of normal stresses along their length or due to bending (or kinking) [*36,39,40*].

Damage growth in unidirectional materials is dominated by the fiber direction. Damage will generally spread along the fibers, even when they are parallel to the load axis, under fatigue loading [*10*]. Since notched unidirectional materials are of little practical use, most of the available data describe notched laminate behavior. We will consider tensile loading of notched laminates first.

Lamination has the effect of constraining damage and creating different internal stress states (including out-of-plane stresses) which significantly influence damage development. For example, Kendall has found that the life of a $[90/0]_s$ laminate with a single-edge notch (SEN) was significantly less than that of a $[0/90]_s$ laminate. A more specific effect involves vertical splitting in laminates with 0-deg plies (relative to the axis of load application). Several investigators have observed damage growth from a notch in discontinuous increments (or ligaments) [*26,28,29,41*]. The mechanism of growth is controlled by the 0-deg plies, and consists of alternate events. First, damage develops along the fibers in a slow, rather disperse way (usually by matrix damage or debonding) and then an increment of crack extension occurs perpendicular to the fibers, breaking several fibers or fiber bundles. Then the process repeats itself. The exact nature of this mechanism is greatly influenced by laminate constraints, and by the damage development in the constraining plies. When the 0-deg plies are constrained by 90-deg plies, longitudinal splitting is reduced, but generally present. This effect may reduce the static toughness since this growth in directions transverse to the notch direction has a blunting or arresting effect [*26,28*]. The constraint may increase the effective life in the [90/0] laminate by arresting the spread of damage, however. The degree to which the constraint due to lamination affects the damage mechanism also depends on the constituent materials. In polymeric matrix materials, matrix damage is generally more extensive and splitting along fibers is a more dominant mechanism than for a metal matrix laminate under otherwise identical conditions. A $[0/\pm 45/0]_s$ boron-epoxy (BEp) laminate with a center hole may develop predominantly longitudinal damage along the 0-deg ply directions as shown in Fig. 6*a*, or if the matrix is changed to aluminum the damage will develop perpendicular to the load axis (and fiber direction of the 0-deg plies) as shown in Fig. 6*b* [*27*]. The same kind of mode change can be induced by constraint, however. Roderick et al have shown that a $[0/\pm 45]_s$ laminate with a center hole sustains damage predominantly along the 0-deg directions on either side of the hole. When 90-deg plies are added to make it a $[0/\pm 45/90]_s$ BEp laminate, the principal damage regions are in 90-deg directions, as determined by fiber break counts [*36*]. As mentioned earlier, the damage in the constraining ply may also be a significant part of the mechanism. Roderick et al found that more 45-deg ply fibers were broken than 0-deg fibers in the predominantly longitudinal failure mode observed in $[0/\pm 45]_s$ BEp laminates [*36*]. For the $[0/\pm 45/90]_s$ laminate with the transverse mode, he found more 45-deg fiber breaks than 0-deg fiber breaks, but about the same percentage of fibers of both types

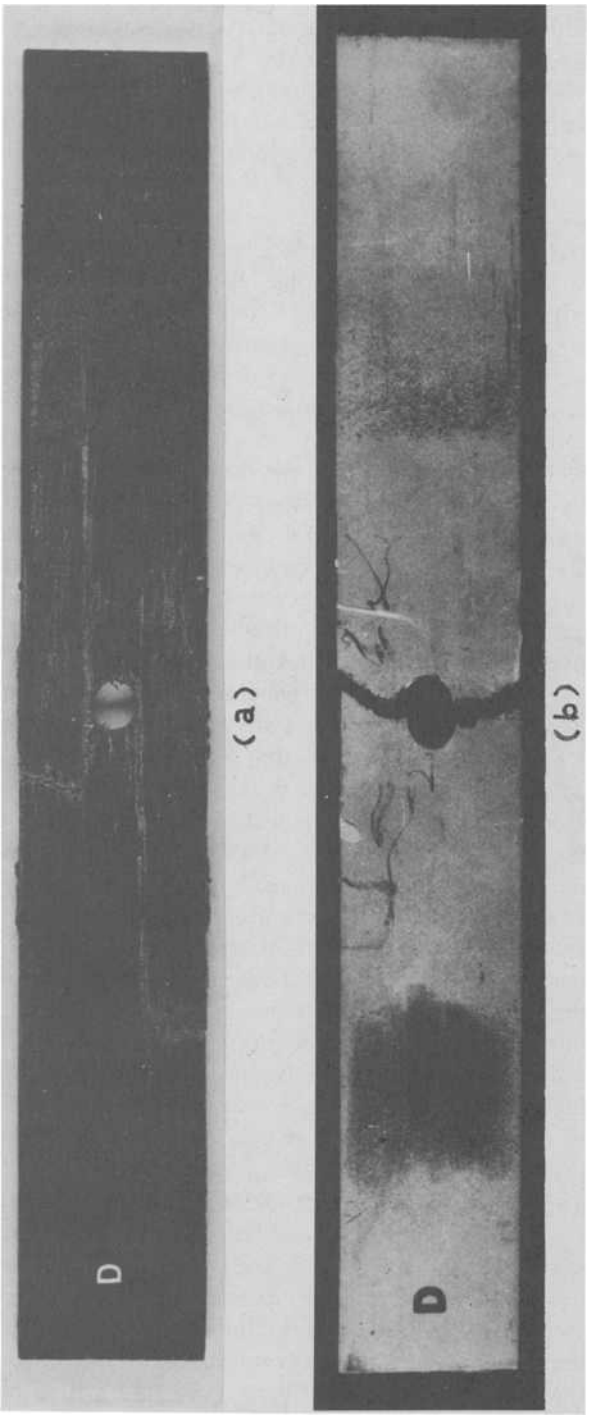

FIG. 6—*Fatigue damage in notched* $[0/\pm 45/0]_s$ *boron-reinforced laminates:* (a) *epoxy matrix,* (b) *aluminum matrix* (*after Ref* 27 *copyrighted by the American Institute of Mining, Metallurgical and Petroleum Engineers*).

broke [*36*]. Matrix damage in the constraining plies can also be important. Underwood et al noted that a glass-epoxy (GFRP) laminate with an SEN having a stacking sequence of $[0/90]_s$ developed significant longitudinal splitting while a $[0/\pm 60]_s$ laminate, otherwise identical, developed damage predominantly between angles of ± 30 deg to the notch axis, that is, along constraint-ply directions [*26*]. From the standpoint of resistance to notch growth (in the notch direction), damage which is constrained or restricted to local regions around the notch, especially if those regions are predominantly along the notch axis, reduces the material resistance to notch propagation, reducing strength and life [*26*]. Further evidence of the effect of lamination constraint on notched cyclic response is provided by investigations of the effect of grouping 0-deg plies together in a laminate as opposed to interspersing the off-axis (constraint) plies. As one might expect, fiber-direction splitting is enhanced when 0-deg plies are grouped, although the static strength is increased by such grouping [*30,42*].

The nature of the mechanism of damage also affects residual properties. Several investigators report an increase in notched strength following cyclic loading [*29,32,43,44*]. When the mechanism of damage involves growth of damage parallel to the load axis and perpendicular (or nearly so) to the notch axis, an effective blunting of the notch is realized with an attendant increase in residual strength, sometimes referred to as "wear-in." In some cases, if the cyclic load level is not too high, the growth of the notch may be arrested by such a process [*26,27,32*]. By stepping up the load amplitude it may be possible to cycle a given component for many cycles at amplitudes which exceed the ultimate strength. Chang reports one case when a $[0/\pm 45]_s$ GEp laminate with a center slit sustained without failure 0.2 million cycles at a stress amplitude which was 130 percent of the static ultimate strength [*29*]. While similar behavior is observed in both polymer and metal matrix materials, the tendency for matrix damage along fiber directions is substantially less for metal matrix than for polymer matrix materials, so that, generally, less wear-in due to the "blunting" effect of matrix damage along fiber directions is observed, and the damage is more commonly in the notch direction than along the fibers [*27,31*].

Delamination of lamina in a laminate is nearly always observed near a notch under cyclic loading. It is generally thought that delamination is most often caused by tensile normal stresses [*37*]. In any case, interlaminar stresses of all types are usually present at or near the edge of an angle-ply laminate, especially in the region of a notch where the in-plane stresses are complex and nonuniform. When internal damage forms, especially when cracks form in one lamina and terminate at its interface with other surrounding lamina in a laminate, severe interlaminar shear and normal stresses may also appear in that region. Hence, delamination may occur because of undamaged laminate stresses, or it may be induced by damage. In both cases delamination usually occurs after some other cracking has occurred and can

act as a mechanism for connecting microcracks. Delamination is not naturally arrested during cycling as other cracks sometimes are. It continues to cause separation, sometimes separating the specimen into two pieces along the load axis [*34,37*]. Delamination may become extensive for materials with a significant percentage of off-angle plies [*29*]. It is much more extensive under cyclic loading than during static loading [*32*]. It would appear that delamination is controlled by matrix properties and increases greatly with increasing temperature for polymer matrix materials, for example [*33*]. One of the most interesting, but least understood, aspects of delamination is the relationship of delamination to other damage in the neighborhood of a notch. Commonly, delamination follows matrix cracking and crazing along fibers (for large fibers) or along fiber directions in GEp, and precedes the bulk of fiber breakages that occur when it is present [*29,34,36,39,45*]. The rate of delamination has been observed to increase as fracture is approached [*29*]. Sendeckyj has pointed out that delamination along a lamina or interlaminar position may separate the laminate into two pieces which are not symmetric; that is, these pieces may have nonzero bend-extension moduli so that they develop internal moments and resultant curvature [*34*]. Delamination also reduces in-plane stiffness which may lead to buckling (or microbuckling) in the presence of compressive stress [*10*]. In general, the effect of delamination is not clear. It would appear that it causes or enhances damage development, but its effect on notch growth (in the notch direction) is not clear [*28*]. It is obvious that the internal stress state is changed by delamination and, in particular, that the constraint of one lamina on another is relaxed by delamination of the two.

Fatigue damage mechanisms in notched composite laminates also appear to be influenced by the frequency of cyclic loading, that is, by the number of cycles of loading per unit time. At moderate frequencies between about 1 and 40 Hz these effects can result in variations in failure mode, changes in residual life and strength, and differences in the amount of stiffness change [*43*]. In general, damage appears to be more widely dispersed at higher frequencies and more localized at lower ones. At these frequencies no direct effects of specimen heating have been established, but there is reason to believe that time-at-load effects in the matrix phase do play a major role in this phenomenon. At higher frequencies specimen heating can cause degradation which appears to have a direct effect on the strength and life of polymeric matrix composites [*46*]; however, no such effects have been reported in metal matrix materials [*47*]. Since all materials commonly used in composite laminates demonstrate some hysteresis at various frequencies, specimen heating is always a potential problem.

Compressive loading of notched laminates produces most of the damage mechanisms just mentioned, with appropriate changes in the selection of damage types corresponding to the change in the sign of the stresses. The growth of damage from a notch has been observed to be discontinuous with

slow growth in the fiber direction alternating with rapid fracture of fibers (or fiber bundles) [*40*]. Kunz and Beaumont report that there is less crack deceleration by longitudinal splitting, more delamination, and more localized through-specimen failures for $[0/90]_s$ GEp laminates than for $[0]_n$ laminates under four-point bending [*40*]. Several investigators have reported that more damage is produced by compressive loading than by tensile loading [*35,36,42*]. However, it would appear that microbuckling is the only substantially new damage mechanism produced by compressive loading [*40*].

Biaxial loading of composite tubes produces fatigue results which are dependent on the ratio of loading mode stresses and the corresponding stress concentration factors. Data developed by Francis et al [*48*] on notched $[\pm 45]_s$ tubes show that as the ratio of tension-to-torsion stresses increases from 1:2 to 2:1, and the stress concentration factor decreases, the fatigue strength increases.

Another unsettled question is, What effect do local variations in properties due to material irregularities or manufacturing difficulties have on the mechanisms of failure? During the manufacture of laminates the boundaries of each lamina seek equilibrium positions with their neighbors, and become crooked in the process. Generally this is not a large effect but variations of 40 percent in individual ply thicknesses have been reported [*49*]. In thin laminates, surface irregularities caused during manufacture may become involved in the fracture process [*10*]. Sendeckyj has studied the effect of surface notches by introducing machined notches of various types into angle-ply laminates [*33*]. Among other things, he found that delamination appeared to be a principal mode of failure; local buckling in the delaminated region was also observed.

Generalizations are difficult to make, especially since the available information is incomplete. It is quite unfortunate that a systematic investigation of the precise nature of damage development in a representative number of notched situations has not been undertaken. Lacking that, the following sequence of events is suggested by existing data. The first few cycles of loading, or the first few cycles of loading at a specific level in a variable-amplitude test, introduce transverse cracks in off-axis plies (relative to the load axis). The level of load determines the type of cracks that form and the layers in which they will form depending upon the local stress fields, a reasonably deterministic situation if the stress fields can be calculated accurately. These cracks will generally extend through only one ply or adjacent like-plies and will frequently lie in a plane which includes the fiber direction and a line (through the ply thickness) which is perpendicular to the axis of load axis. While the type of transverse cracks is determined by the load level, the number of such cracks is a function of the number of cycles of loading. The most continuous mechanism of damage as cyclic loading continues is matrix damage. Matrix crazing and cracking, usually along fiber directions, create a damage zone around the notch, and delamination, which may have been

initiated during the first few cycles, begins to spread. To a large degree, delamination becomes the damage development control mechanism in the "third quarter" of life. As it separates plies of the laminate, constraint is relaxed and further damage (including transverse cracking and fiber-direction matrix cracking) may occur. As the end of the life draws near, all damage components begin to accelerate [*29*]. Fiber breakage develops in the damage zone and the crack or notch advances. Depending upon toughness considerations, the material may fracture or the damage may arrest and repeat the mechanistic cycle.

It is not the purpose of this paper to discuss analytical models. There are many, and they reflect the incomplete nature of our understanding of these mechanisms. As a starting point for the interested reader, Refs *50–53* are listed. The complexity of modeling these mechanisms is demonstrated by the investigation of compressive behavior discussed by Kulkarni et al [*54*]. However, this is a rapidly developing area and contact with current authors is suggested before any substantive use of the models is attempted.

Concluding Remarks

Fatigue damage mechanisms in composite materials are quite complex and difficult to describe in a general way. The damage state is formed by various combinations of fiber, matrix, and interfacial damage; however, the ways in which these damage components interact and combine govern the fatigue response of composites. The investigations carried out to date show that the state of damage in a composite material is strongly dependent on material, laminate configuration, geometry, stress state, load history, and environment. From an applications viewpoint, one of the most important and, yet, incompletely answered questions concerns the fatigue response of notched composite materials.

It is difficult to find statements which summarize the mechanisms observed for notched response. Instead, it may be more useful at this point to attempt three tentative conclusions to be drawn from our review of the observed mechanisms. It would appear that mechanisms that cause the development of dispersed damage, especially transverse to the axis of the notch, result in more notch growth resistance, while more restricted, localized damage, especially in the notch-axis direction, results in shorter life and lower residual strength. It would also appear that laminates that have higher static strength also have more notch growth resistance (in constrast to common behavior in metals). Finally, compression can cause local buckling which can lead to delamination and further damage, resulting in a progression which may result in a larger degradation than a tensile stress of equal magnitude. Indeed, the mechanisms of fatigue damage of notched components are an area of special ignorance, but of considerable importance in some cases if existing data are representative.

One of the major factors controlling the means by which fatigue damage progresses in composite laminates is the constraint imposed by adjacent plies. The manner in which damage spreads from a notch depends on the orientation of the major strength and stiffness directions in neighboring plies relative to the local stress state. The through-the-thickness rate of growth and extension of cracks from 90-deg plies, for example, is highly dependent on the orientation of the fibers in surrounding plies. Cracks are much more likely to extend into a 45-deg ply than into a 0-deg ply, all other factors being equal. By carefully designing and conducting a systematic series of studies on the development of fatigue damage for basic constraint situations, much can be learned about fatigue mechanisms and how the damage state controls strength, stiffness, and lifetime. Perhaps only then can proper choices of material, stacking sequence, and geometry be made for specific engineering applications.

Finally, there is an immediate need for the development of reliable and quantitative nondestructive investigation methods which are capable of detecting and measuring the types of damage found in composite materials. These methods would be used in the quality control of manufactured components, periodic in-service inspections, and in the laboratory to assist in our understanding of fatigue mechanisms in composite materials.

Acknowledgments

The authors extend their appreciation to the National Bureau of Standards and to the National Science Foundation for their interest in and support of the ASTM Symposium on Fatigue Mechanisms. They also express their thanks to Mrs. Phyllis Schmidt for typing the manuscript.

References

[1] Salkind, M. S. in *Composite Materials: Testing and Design (Second Conference), ASTM STP 497,* American Society for Testing and Materials, 1972, pp. 143-169.

[2] Owen, M. J. in *Composite Materials, Vol. 5, Fracture and Fatigue,* L. J. Broutman, Ed., Academic Press, N. Y., 1974, pp. 313-340.

[3] Owen, M. J. in *Composite Materials, Vol. 5, Fracture and Fatigue,* L. J. Broutman, Ed., 1974, pp. 341-369.

[4] Hancock, J. R. in *Composite Materials, Vol. 5, Fracture and Fatigue,* L. J. Broutman, Ed., 1974, pp. 371-414.

[5] Reifsnider, K. L., "Fatigue in Composite Materials," Advisory Group for Aeronautical Research and Development, Report No. 638, 1976.

[6] Dharan, C. K. H., *Journal of Materials Science,* Vol. 10, 1975, pp. 1665-1670.

[7] Dvorak, G. J. and Tarn, J. Q. in *Fatigue of Composite Materials, ASTM STP 569,* American Society of Testing and Materials, 1975, pp. 145-168.

[8] Hancock, J. R. in *Composite Materials: Testing and Design (Second Conference), ASTM STP 497,* American Society for Testing and Materials, 1972, pp. 483-502.

[9] Awerbuck, J. and Hahn, H. T. in *Fatigue of Filamentary Composite Materials, ASTM STP 636,* K. L. Reifsnider and K. N. Lauraitis, Eds., American Society for Testing and Materials, 1977, pp. 248-266.

[10] Stinchcomb, W. W., Reifsnider, K. L., Yeung, P., and O'Brien, T. K., "Investigation and Characterization of Constraint Effects on Flaw Growth During Fatigue Loading of Composite Materials," Second Semi-Annual Status Report, NASA Grant NSG-1364, Virginia Polytechnic Institute and State University, Blacksburg, Va., Nov. 1977.

[11] Boller, K. H. in *Composite Materials: Testing and Design, ASTM STP 460,* American Society for Testing and Materials, 1969, pp. 217-235.

[12] Tanimoto, T. and Amijima, S., *Journal of Composite Materials,* Vol. 9, Oct. 1975, pp. 380-390.

[13] Stalnaker, D. O. and Stinchcomb, W. W. in *Composite Materials: Testing and Design (Fifth Conference), ASTM STP 674* American Society for Testing and Materials, March 1978, pp. 620-641.

[14] Reifsnider, K. L. in *Proceedings,* 14th Annual Meeting of Society of Engineering Science, Lehigh University, Bethlehem, Pa., 14-16 Nov. 1977, pp. 373-384.

[15] Grimes, G. C. in *Composite Materials: Testing and Design (Fourth Conference), ASTM STP 617,* American Society for Testing and Materials, 1977, pp. 106-119.

[16] Sendeckyj, G. P. and Stalnaker, H. D. in *Composite Materials: Testing and Design (Fourth Conference), ASTM STP 617,* American Society for Testing and Materials, 1977, pp. 39-52.

[17] Broutman, L. and Sahu, S. in *Proceedings,* 24th Society of the Plastics Industry Conference, Feb. 1969, pp. 1-12.

[18] O'Brien, T. K. and Reifsnider, K. L., *Journal of Testing and Evaluation,* Vol. 5, No. 5, 1977.

[19] Berg, C. A. and Salma, M., *Journal of Materials,* Vol. 7, No. 2, June 1972, pp. 216-230.

[20] Pipes, R. B. in *Composite Materials: Testing and Design (Third Conference), ASTM STP 546,* American Society for Testing and Materials, 1974, pp. 419-432.

[21] Ryder, J. T. and Walker, E. K., "Ascertainment of the Effect of Compressive Loading on the Fatigue Lifetime of Graphite Epoxy Laminates for Structural Applications," AFML-TR-76-241, Air Force Materials Laboratory, Wright-Patterson Air Force Base, Ohio, 1976.

[22] Francis, P. H., Walrath, D. E., and Weed, D. N., "Investigation of First Ply Failure in Graphite/Epoxy Laminates Subjected to Biaxial Static and Fatigue Loadings," AFML-TR-77-62, Air Force Materials Laboratory, Wright-Patterson Air Force Base, Ohio, 1977.

[23] Hofer, K. E., Jr., Bennett, L. C., and Stander, M. in *Filamentary Composite Materials, ASTM STP 636,* K. L. Reifsnider and K. N. Lauraitis, Eds., American Society for Testing and Materials, 1977, pp. 103-122.

[24] Kasen, M. B., Schramm, R. E., and Read, D. T. in *Filamentary Composite Materials, ASTM STP 636,* K. L. Reifsnider and K. N. Lauraitis, Eds., American Society for Testing and Materials, 1977, pp. 141-151.

[25] Tobler, R. L. and Read, D. T., *Journal of Composite Materials,* Vol. 10, Jan. 1976, pp. 32-43.

[26] Underwood, J. H. and Kendall, D. P. in *Proceedings,* 1975 International Conference on Composite Materials, Metallurgical Society of the American Institute of Mining Engineers, Vol. 2, 1976, pp. 1122-1147.

[27] Stinchcomb, W. W., Reifsnider, K. L., Williams, R. S., and Marcus, L. A. in *Failure Modes in Composites II,* J. Fleck and R. Mehan, Eds., Metallurgical Society of the American Institute of Mining Engineers, 1975, pp. 3-15.

[28] Mandell, J. F. and Meier, U. R. S. in *Fatigue of Composite Materials ASTM STP 569,* American Society for Testing and Materials, 1975, pp. 28-44.

[29] Chang, F. H., Gordon, D. E., Rodini, B. T., and McDaniel, R. H., *Journal of Composite Materials,* Vol. 10, July 1976, pp. 182-192.

[30] Porter, T. R. in *Fatigue of Filamentary Composite Materials, ASTM STP 636,* K. L. Reifsnider and K. N. Lauraitis, Eds., American Society for Testing and Materials, 1977, pp. 152-170.

[31] Kendall, D. P. in *Fatigue of Filamentary Composite Materials, ASTM STP 636,* K. L. Reifsnider and K. N. Lauraitis, Eds., American Society for Testing and Materials, 1977, pp. 47-56.

[32] Chang, F. H., Gordon, D. E., and Gardner, A. H. in *Fatigue of Filamentary Composite Materials, ASTM STP 636,* K. L. Reifsnider and K. N. Lauraitis, Eds., American Society for Testing and Materials, 1977, pp. 57-72.

[33] Sendeckyj, G. P., Stalnaker, H. D., and Kleismit, R. A. in *Fatigue of Filamentary Composite Materials, ASTM STP 636,* K. L. Reifsnider and K. N. Lauraitis, Eds., American Society for Testing and Materials, 1977, pp. 123-140.

[34] Sendeckyj, G. P. in *Failure Modes in Composites III,* T. T. Chiao and D. M. Shuster, Eds., Metallurgical Society of the American Society of Mining Engineers, 1976, pp. 100-114.

[35] Ramani, S. V. and Williams, D. P. in *Fatigue of Filamentary Composite Materials, ASTM STP 636,* K. L. Reifsnider and K. N. Lauraitis, Eds., American Society for Testing and Materials, 1977, pp. 27-46.

[36] Roderick, G. L. and Whitcomb, J. D. in *Fatigue of Filamentary Composite Materials, ASTM STP 636,* K. L. Reifsnider and K. N. Lauraitis, Eds., American Society for Testing and Materials, 1977, pp. 73-88.

[37] Reifsnider, K. L., Henneke, E. G., and Stinchcomb, W. W. in *Composite Materials: Testing and Design (Fourth Conference), ASTM STP 617,* American Society for Testing and Materials, 1977, pp. 93-105.

[38] Williams, R. S. and Reifsnider, K. L., "Fracture Analysis of Fatigue Damaged Mechanisms in Fiber Reinforced Composite Materials Using Scanning Electron Microscopy," College of Engineering Report, AFOSR-TR-75-0041 Virginia Polytechnic Institute and State University, Blacksburg, Va., 1975.

[39] Roderick, G. L. and Whitcomb, J. D., *Journal of Composite Materials,* Vol. 9, Oct. 1975, pp. 391-393.

[40] Kunz, S. C., Beaumont, W. R. in *Fatigue of Composite Materials, ASTM STP 569,* American Society for Testing and Materials, 1975, pp. 71-94.

[41] Olster, E. F. and Jones, R. C. in *Composite Materials: Testing and Design (Second Conference), ASTM STP 497,* American Society for Testing and Materials, 1972, pp. 189-205.

[42] Walter, R. W., Johnson, R. W., June, R. R., and McCarty, J. E. in *Fatigue of Filamentary Composite Materials, ASTM STP 636,* K. L. Reifsnider and K. N. Lauraitis, Eds., American Society for Testing and Materials, 1977, pp. 228-247.

[43] Reifsnider, K. L., Stinchcomb, W. W., and O'Brien, T. K. in *Fatigue of Filamentary Composite Materials, ASTM STP 636,* K. L. Reifsnider and K. N. Lauraitis, Eds., American Society for Testing and Materials, 1977, pp. 171-184.

[44] Waddoups, M. E., Eisenmann, J. R., and Kaminski, B. E., *Journal of Composite Materials,* Vol. 5, Oct. 1971, pp. 446-454.

[45] Kulkarni, S. V., McLaughlin, P. V., Jr., Pipes, R. B., and Rosen, B. W. in *Composite Materials: Testing and Design (Fourth Conference), ASTM STP 617,* American Society for Testing and Materials, 1977, pp. 70-92.

[46] Williams, R. S., Reifsnider, K. L., Stinchcomb, W. W., and Turgay, H., "The Effect of Frequency and Strain Amplitude on the Fatigue Damage of Boron-Epoxy Fiber Reinforced Composite Materials," AFOSR-TR-75-1387, Air Force Office of Scientific Research, Bolling Air Force Base, Washington, D.C., Oct. 1974.

[47] Williams, R. S., Reifsnider, K. L., Stinchcomb, W. W., and Turgay, H., AFOSR-TR-75-1394, Air Force Office of Scientific Research, Bolling Air Force Base, Washington, D.C., Oct. 1974.

[48] Francis, P. H., Walrath, D. E., Sims, D. F., and Weed, D. N., "Biaxial Fatigue Loading of Notched Composites," NASA CR-145198, Southwest Research Institute, San Antonio, Tex., June 1977.

[49] Papirno, R., *Journal of Composite Materials,* Vol. 11, Jan. 1977, pp. 41-50.

[50] Kulkarni, S. V., McLaughlin, P. V., Jr., and Pipes, R. B., NASA CR-145039, Materials Sciences Corp., Blue Bell, Pa. 1977.

[51] Whitney, J. M. and Nuismer, R. J., *Journal of Composite Materials,* Vol. 8, July 1974, pp. 253-265.

[52] Zweben, C., *Journal of the Mechanics and Physics of Solids,* Vol. 19, 1971, pp. 103-116.

[53] Kanninen, M. F., Rybicki, E. F., Griffith, W. I., and Broek, D., "Fundamental Analysis of the Failure of Polymer-Based Fiber Reinforced Composites," Final Report, Battelle Memorial Laboratories, Columbus, Ohio, Sept. 30, 1975.

[54] Kulkarni, S. V., Rice, J. S., and Rosen, B. W., *Composites,* Vol. 5, Sept. 1975, pp. 217-225.

DISCUSSION

G. Dvorak[1] *(discussion)*—The authors should be commended for their admirable review of fatigue damage mechanisms. It is clear that much of our present understanding of the fatigue processes in composites is based on qualitative descriptions of experimental observations. Analytical models for interpretation of test data and for prediction of fatigue life of structural parts are not well developed. I would like to make some remarks about my own work on the relation between shakedown and fatigue in metal matrix composites which provides certain qualitative insights into the fatigue damage mechanisms.[2,3]

As the authors pointed out in their review, the mechanisms of fatigue damage in composites are very different from those observed in homogeneous materials. Instead of few major fatigue cracks, there is a complex state of microstructural damage distributed in a large volume of the composite material. In metal matrix composites reinforced with brittle fibers, such as boron-aluminum, the initial source of fatigue damage is fiber cracks at random locations due to the variation of fiber strength. These microcracks appear during the first cycle of loading and their density increases with the number of cycles. Under favorable conditions the fiber microcracks can initiate new cracks in the matrix and along fiber-matrix interfaces. Another source of fatigue cracking in the metal-matrix composites is associated with cyclic plastic straining of the matrix which invariably results in low-cycle fatigue of the material. These two damage sources may interact and cause the formation of the complex damage state.

The important distinction between fiber and matrix cracking is that the former is unavoidable, whereas the latter can be prevented by limiting the amplitude of the overall applied stresses to a level which does not cause continuous cyclic plastic straining of the matrix. A quantitative method for evaluation of cyclic loading ranges within which the matrix will be strained elastically is based on shakedown theory in plasticity. The shakedown state, that is, a new state of elastic straining, is reached after a limited number of plastic loading cycles if there is a possibility of development of a residual stress state in the composite lamina or laminate which, in combination with the elastic stress state caused by the overall cyclic loading, will not violate the matrix yield condition. In general, shakedown states may develop for any given cyclic loading program, or a sequence of such programs, provided that the load amplitudes do not exceed certain limits in each of these programs.

[1]Department of Civil Engineering, Duke University, Durham, N. C.

[2]Dvorak, G. J. and Tarn, J. Q. in *Fatigue of Composite Materials, ASTM STP 569,* American Society for Testing and Materials, 1975, pp. 145-168.

[3]Tarn, J. Q., Dvorak, G. J., and Rao, M. S. M., *International Journal of Solids and Structures,* Vol. 11, 1975, pp. 751-764.

The shakedown condition in fibrous composites and laminates limits only the amplitude, not the mean value of the overall applied stress, although, as a general rule, different amplitude limits may be required at different levels of mean stress. This possible effect of the mean stress has not been encountered so far in our shakedown studies of laminated plates. In fact, successive shakedown states may develop if the mean stress changes from one to another stationary value. If such changes do not cause an excessive number of plastic straining cycles, their effect on fatigue life should be negligible.

If a shakedown state is to develop at a given value of the mean stress, the range of amplitudes of the variable cyclic load must be contained within a shakedown envelope. The size of the envelope is directly proportional to the magnitude of the *in situ* matrix yield stress. Since the matrix may experience cyclic strain hardening during the plastic deformation which precedes shakedown, the actual yield stress magnitude which determines the size of the shakedown envelope may be significantly higher than that of the undeformed matrix material. In any event, the *in situ* matrix properties are difficult to measure; their best estimate can be obtained by calculation from an experimentally established section of the shakedown envelope. For example, in unidirectional composites one can follow the procedure discussed in connection with Fig. 4 of Ref *1*, evaluate the shakedown limit from an *S-N* curve, calculate the corresponding matrix yield stress, and use this value in predicting the shakedown conditions for other loading states. Since matrix strains will be generally higher at larger mean stress values, one may expect proportionally larger cyclic strain hardening, higher yield stresses, and magnified shakedown envelopes.

The coincidence of calculated shakedown limits and fatigue strengths (at 10^6 to 10^7 cycles) of unidirectional 6061 A1-B composites was demonstrated in Ref *1*. This relationship probably can be attributed to the remarkable property of certain aluminum alloys that their fatigue and cyclic yield strengths are equal up to the stress level of about 142 MPa (20 000 psi).[4] Thus, the matrix can become insensitive to fatigue (up to 10^6 to 10^7 cycles) in the shakedown state, and apparently can have the ability to contain the fiber cracks. If the matrix yield stress becomes much larger than the fatigue strength, as in 6061-T6 aluminum, the shakedown state offers no protection against fatigue, and fatigue strength of tempered composites can be significantly reduced.

In conclusion, the shakedown effect offers a promising possibility for predicting the fatigue strength of certain metal matrix composites and their laminates, and deserves further investigation.

W. W. Stinchcomb—I agree with your remarks on the fatigue mechanisms of metal matrix composites.

[4]*Aluminum*, K. R. Van Horn, Ed., American Society for Metals, Metals Park, Ohio, 1967.

G. Sendeckyj[5] *(discussion)*—I would like to supplement what Coauthor Stinchcomb said and possibly to respond to his very last figure where he indicated that we need to have a quantitative nondestructive inspection method for composites that can characterize the shape of the damage.

What I would like to offer are three pieces of information on a hybrid specimen. The specimen was loaded statically with a notch machined into it. It was instrumented with a clip gage and when the clip gage showed unusual displacement changes, indicating the presence of damage, the test was stopped and upon unloading the damage was examined by three different techniques, namely

(1) the through-transmission ultrasonic (C-scan) inspection method to document the damage accumulation process,
(2) the TBE or tetrabromoethane-enhanced X-ray radiography method to supplement the C-scan data, and
(3) the holographic method also to supplement the C-scan data.

I might add that the holographic method is a nice technique to use because it not only can give you strain information on the solid but it can show you the damage. With this technique, one could obtain the in-plane displacements and perform the stress analysis or strain analysis on that type of specimen. Another technique which is quite powerful is to take two X-ray pictures and make them into a stereo pair. One can then locate all the damages as well as the planes on which they occur. In other words, we could tell where the cracks really are.

To conclude, I would like to comment on a statement made earlier at this symposium where people seem to have trouble getting spatial information on defects, precipitate particles, and other signs of damage in the microstructure of metals. I would like to suggest that by using either a stereo pair in neutron radiography or the X-ray technique, one may obtain a three-dimensional image of the particles under examination and actually be able to count the particles through the thickness.

W. W. Stinchcomb—I agree with your remarks.

H. Lamba[6] *(discussion)*—Let us assume that we know the failure modes of polymers and the failure modes for fibers by themselves. Can we from mechanisms of polymers and from fibers quantify what effect the mechanisms will have when you put them together in the laminated composite?

W. W. Stinchcomb—We can get some idea of how the laminate is going to

[5]Structural and Mechanics Division, Air Force Flight Dynamics Laboratory, Wright-Patterson Air Force Base, Ohio.
[6]International Harvester, Hinsdale, Ill.

behave; however, when you have just properties of fibers or failure mechanisms of fibers and properties or failure mechanisms of matrix material, you have neither the fiber-matrix interface nor the properties of that interface. The way the interface interacts with the matrix and with the fibers is quite important in determining fatigue damage initiation in composite materials.

H. Lamba—How can the delamination in the area between laminates be quantified for a particular situation, analytically, let us say? How could one predict or analyze delamination failures occurring in a particular notch situation?

W. W. Stinchcomb—One of the primary features that controls delamination is the sign of the out-of-plane normal stress in composite laminates. In some laminates, such as a quasi-isotropic laminate with a $[0/90/\pm 45]_s$ stacking sequence, major delamination will not occur under static tensile loading. In other quasi-isotropic laminates, such as a $[0/\pm 45/90]_s$ laminate, delamination will occur under static tensile loading.

The reason for the different behavior is the change in the sign of the out-of-plane normal stress. In the $[0/90/\pm 45]_s$ laminate, the maximum out-of-plane normal stress is compressive for tensile loading and major delaminations do not develop.

On the other hand, tensile loading of the $[0/\pm 45/90]_s$ laminate produces tensile out-of-plane normal stress throughout the thickness of the laminate and delamination will occur. The strength of the interface is low and is comparable to the magnitude of those out-of-plane normal stresses that develop.

Now, when the loading is changed, that is, when the laminates are loaded in compression, the signs of the out-of-plane normal stresses will change also. The laminate that did not delaminate when loaded in tension will now delaminate under compressive loading. The damage mechanisms are very complex when you have loads which alternate between tension and compression.

D. Davidson[7] *(discussion)*—For a propagating fatigue crack, when do you get the crack propagation, on the compressive or unloading portion of the cycle, or is it on the loading portion of the cycle? Where is it that the failure occurs?

W. W. Stinchcomb—First of all, we have to decide whether or not there is a propagating fatigue crack in composite materials.

D. Davidson—Is it not possible to get a propagating fatigue crack in this composite material?

[7]Division of Engineering Sciences, Southwest Research Institute, San Antonio, Tex.

W. W. Stinchcomb—That depends, to some extent, on the particular composite material. A single self-similar crack, of the type normally formed in metals, usually does not develop in composites. In composite materials, there are a number of damage modes, such as fiber splitting, interactions between fiber and matrix, cracking of the matrix, or breaking of the fibers. They do not combine to form the single crack that we commonly think about when we talk about crack propagation in metals. It is not possible to say that cracks grow on the compressive portion or that cracks grow on the tensile portion of the cycle. There are different mechanisms acting in tension and there are different mechanisms acting in compression which combine to form a very complex damage state in the composite laminate.

W. W. Stinchcomb and K. L. Reifsnider (authors' closure)—Composites have emerged as one of the most promising and most challenging classes of materials to meet the present and future materials requirements of engineering. The response of composite materials to time-varying loads is a subject of particular importance and interest to many current and potential users. However, fatigue behavior is one of the least understood areas of response, due, in part, to our incomplete knowledge of basic fatigue mechanisms in composite materials.

The question of interaction between fiber and matrix material, addressed by Prof. Dvorak and Dr. Lamba, is one which needs further study. Certainly as new fiber and matrix materials are considered for composite and hybrid material systems of the future, it would be advantageous to be able to select constituent materials which act in concert to create materials with a high resistance to fatigue damage.

Although the subject of this paper is damage mechanisms, there are other important and related aspects of fatigue in composite materials. They include test methods, data interpretation (including statistics), predictive analytical models, and flaw criticality. Mr. Davidson's question draws attention to a topic of major importance at the present time—compression fatigue and fatigue test methods for cyclic compressive loads. Test methods range from full side supports to partial side supports to no side supports. The mechanisms of compression fatigue damage and, therefore, the fatigue data, are subject to the influences of the test method and extreme caution must be exercised in interpreting the results.

The need for reliable nondestructive investigation (NDI) methods which are applicable to composite materials has been pointed out in the paper and in Dr. Sendeckyj's discussion. NDI methods must not only be capable of detecting defects, such as fatigue damage, but must also determine type, size, shape, and location of defects. Without this information, it is not possible to assess the criticality of a flaw with respect to its effect on strength, life, stiffness, and other properties.

Analytical models were mentioned only briefly in the paper. Certainly, any attempt to develop a model of the fatigue response of composites must be

done with a clear understanding of fatigue damage mechanisms and their complex interactions. As our understanding of fatigue damage mechanisms increases, the predictive capability of the models should advance.

Finally, the work in this paper is not an exhaustive review and summary of the literature on fatigue damage mechanisms in composite materials. Many of the topics presented are those on which there is a general consensus of opinion; however, some topics are the subject of discussion and investigation at the present time. We hope that readers, especially those who are new to composite materials, will find this review helpful.

N. S. Stoloff[1] *and D. J. Duquette*[1]

Fatigue Mechanisms in Nickel and Cobalt-Base Eutectic Composites

REFERENCE: Stoloff, N. S. and Duquette, D. J., **"Fatigue Mechanisms in Nickel and Cobalt-Base Eutectic Composites,"** *Fatigue Mechanisms,* Proceedings of an ASTM-NBS-NSF symposium, Kansas City, Mo., May 1978, J. T. Fong, Ed., *ASTM STP 675,* American Society for Testing and Materials, 1979, pp. 788-815.

ABSTRACT: The high-cycle fatigue behavior of several nickel and cobalt-base eutectic composites is described. Major test variables include test temperature, frequency, alloy composition, and microstructural modifications induced by postsolidification heat-treatments. Lamellar γ/γ'-δ type eutectic alloys are shown to have superior fatigue resistance to the fibrous alloys, with regard to both total life and crack propagation rates, provided that the microstructures are perfectly aligned. Cracking at 25°C in all alloys tends to be along crystallographic planes (Stage I cracking), although striations associated with Stage II propagation were occasionally observed in solution-treated Nitac. At 825°C there is no evidence of Stage I crack growth or Cotac or Nitac. A pronounced frequency effect occurs in Nitac at 825°C (0.7 T_m) in vacuum, suggesting a creep-fatigue interaction.

KEY WORDS: composite materials, eutectics, mechanical properties, fatigue, nickel, cobalt, precipitation hardening

Nickel and cobalt-base eutectic composites have been under intensive development for possible applications in advanced aircraft gas turbines. It has been recognized for some time that these alloys, as well as other eutectics with lower melting temperatures, have excellent resistance to both low-cycle and high-cycle fatigue at room temperature. More recently it has been demonstrated that while resistance to fatigue failure deteriorates with increasing temperature, these alloys are still vastly superior to conventional alloys [*1,2*].[2]

This paper will discuss the high-cycle fatigue properties of several representative fibrous (Cotac, Nitac, nickel-aluminum-molybdenum) and lamellar (nickel-aluminum-chromium-niobium) eutectic composites, and will

[1] Professor of materials engineering and professor of metallurgical engineering, respectively, Department of Metallurgical Engineering, Rennselaer Polytechnic Institute, Troy, N.Y. 12181.

[2] The italic numbers in brackets refer to the list of references appended to this paper.

show how microstructure plays a major role in determining both overall life and resistance to both crack initiation and propagation. The most important microstructural features are perfection of aligned microstructure and the interphase spacing, the latter being controlled by the directional solidification (DS) rate of the alloy. In addition, postsolidification heat-treatment to induce fine precipitates can have a significant effect on fatigue life. Varying alloy composition is shown to have a significant effect on fatigue life and fracture morphology of several alloys.

Alloy Description

Both lamellar and fibrous eutectics are of interest for high-temperature applications. Nickel and cobalt-base alloys reinforced by tantalum-carbide fibers (Nitac and Cotac, respectively) are typical of fibrous alloys with a brittle reinforcing phase. Nickel-base alloys containing niobium and molybdenum also are fibrous, but the molybdenum fibers are ductile. Among lamellar alloys, nickel-chromium-aluminum-niobium type alloys (γ/γ'-δ) and nickel-niobium (γ-δ) alloys are representative. Compositions of the principal alloys reviewed in this paper are summarized in Table 1.

Ingots of each of these alloys are prepared by melting in an induction unit, followed by directional solidification in a steep temperature gradient. Microstructural control is achieved in several ways for each alloy system. For example, increasing chromium reduces the tendency for branched lamellar growth; at a growth speed of $R = 5$ cm/h in Co-5Cr-TaC, tantalum-carbide occurs as both 0.3-μm diameter fibers and tristar-shaped lammellae with branches at 120 deg and a fiber growth axis of $\langle 111 \rangle$.[3] Increasing the growth speed to 15.75 cm/h produces virtually all rods with a few blade-shaped lamellas [3]. At $\simeq$ 10 percent chromium, on the other hand, the fiber growth axis changes from $\langle 111 \rangle$ to $\langle 100 \rangle$, and the tristar lamellae are suppressed [3-5]. In a 15 percent chromium alloy, growth speeds of 0.4 to 2.36 cm/h produce irregular rods and increased growth speeds result in still finer structures, although no quantitative relationship between speed and spacing has been established. At 4.72 cm/h, structural breakdown to cells occurs [5]. Increasing solidification rate also reduces interphase spacing with concomitant reductions of strength, but can result in a breakdown of microstructure if a critical rate is exceeded. In some cases alloys can be heat-treated to resolutionize the matrix, rapidly cooled, and then reheated at an intermediate temperature, in order to control matrix precipitate distribution. In Nitac-type alloys containing aluminum, aging precipitates γ' (Ni_3Al) between the tantalum-carbide fibers. Similarly, γ/γ'-δ type alloys can be solution-treated and aged to control the distribution of γ'. Alternatively, tantalum-carbide

[3] R should not be confused with the ratio of minimum to maximum stress, which was held positive in all fatigue tests.

TABLE 1—*High-temperature eutectic alloy compositions.*

Alloy	Morphology	V_f	Ni	Co	Cr	Al	Nb	Mo	Ta	C
Nitac	F[a]	0.05	69	...	10	5	...	...	14.9	1.1
Cotac	F	0.10	10	65	10	...	...	...	14	1
Cotac (0%Cr)	F	0	10	75	...	...	...	...	14	1
γ/γ'-δ (6%Cr)	L[b]	0.37	71.5	...	6	2.5	20	...	...	...
γ/γ'-δ (0%Cr)	L	0.3	76.5	...	...	2.5	21	...	...	...
γ'/γ-Mo (AG-15)	F	0.26	65.5	...	...	8.1	...	26.4	...	...
γ'/γ-Mo (AG-34)	F	0.26	62.5	...	...	6.3	...	31.2	...	...

[a] F = fibrous.
[b] L = lamellar.

particles may be precipitated in the matrix for dispersion strengthening. To illustrate the influence of these various microstructural conditions on mechanical properties, Table 2 summarizes tensile data, both at room and elevated temperatures, for most of the alloys described in this paper. Note that there is little effect of heat-treatments on tensile properties of Nitac; however, significant effects on fatigue resistance will be described later. All alloys and conditions except for γ/γ'-δ with 6 percent chromium reveal substantial room-temperature ductility.

Experimental Details

The standard solidification rate for Nitac and Cotac alloys was 0.64 cm/h; for γ/γ'-δ, 3 cm/h; for AG-15 (Ni-26.4Mo-8.1A1), 1.9 cm/h and for AG-34 (Ni-31.2Mo-6.3Al), 0.76 cm/h. Occasionally, higher rates were employed, as will be described later.

Cylindrical fatigue specimens used in most of this investigation were ground to 0.31-cm gage diameter by 0.635-cm gage length. All specimens were mechanically polished with diamond paste and electropolished prior to testing. Single-edge cracked plate specimens of Cotac in longitudinal orientation with gage section widths of 1.27 cm were used for crack propagation studies. Transverse specimens were compact-tension type of 2.0-cm width. All crack propagation specimens were 0.25 cm thick. Load-controlled tension-tension fatigue tests in air at room temperature or in 10^{-5} torr vacuum at 825°C were conducted in a closed-loop electrohydraulic test frame. A constant minimum stress of 34.5 MN/m^2 (5000 psi) was utilized for all tests.

Fracture surfaces and longitudinal specimen surfaces were examined by light, scanning, and transmission (replica) electron microscopy.

Fatigue Behavior

Fibrous Alloys

Figure 1 summarizes the results of a series of fatigue tests on Nitac in several microstructural conditions [solution-treated, aged, and as directionally solidified (DS)]. Also shown, for comparison, are data for an alloy corresponding to the matrix composition (nickel-chromium-aluminum) and a group of specimens which exhibit a cellular microstructure. The latter two materials clearly show inferior properties. Postsolidification aging, on the other hand, provides the best fatigue resistance for aligned Nitac at stresses above $\Delta\sigma = 552$ MN/m^2 (80 ksi); water-quenching appears to produce a slightly deleterious effect relative to the as-DS condition at lower stress levels. The 10^7-cycle fatigue limit for aligned Nitac appears to be near $\Delta\sigma = 483$ MN/m^2 (70 ksi). At 825°C (0.7 T_m) in vacuum, aged Nitac clearly provides

TABLE 2—*Longitudinal tensile properties of as-grown aligned eutectics, 25°C.*

Alloy[a]	Type[b]	T_m, °C	ρ, g/cc	R, cm/h	σ_y		σ_{UTS}[c]		% Elongation
					MN/m^2	ksi	MN/m^2	ksi	
Nitac—as directionally solidified	D-B	1348	~8.8	0.6	796	115	1282	189	28
Nitac—solution-treated	D-B	1348	~8.8	0.6	771	112	1228	178	29
Nitac—aged	D-B	1348	~8.8	0.6	769	111	1216	176	23
Cotac (Co, Cr, Ni-TaC)	D-B	1402	9.0	0.6	787[d]	114[d]	963	139.5	30
Cotac (Co, Cr, Ni-TaC)	D-B	1402	9.0	2.5	842[d]	122[d]	1042	151	33
γ/γ'-δ (0%Cr)	D-SB	1272 to 1274	...	3	814	118	1193	173	~30
γ/γ'-δ (6%Cr)	D-SB	1244 to 1257	8.6	3	649	94	1187	172	3.0
γ'/γ-Mo (AG-15)	D-D	1306	8.2	1.9	621	90	1346	195	21.9
γ'/γ-Mo (AG-34)	D-D	...	...	0.76	580	84	1446	209.6	19.2

[a] Matrix phase listed first.
[b] D = ductile.
B = brittle.
SB = semibrittle.
[c] UTS = ultimate tensile strength.
[d] Fiber fracture stress (upper yield stress).

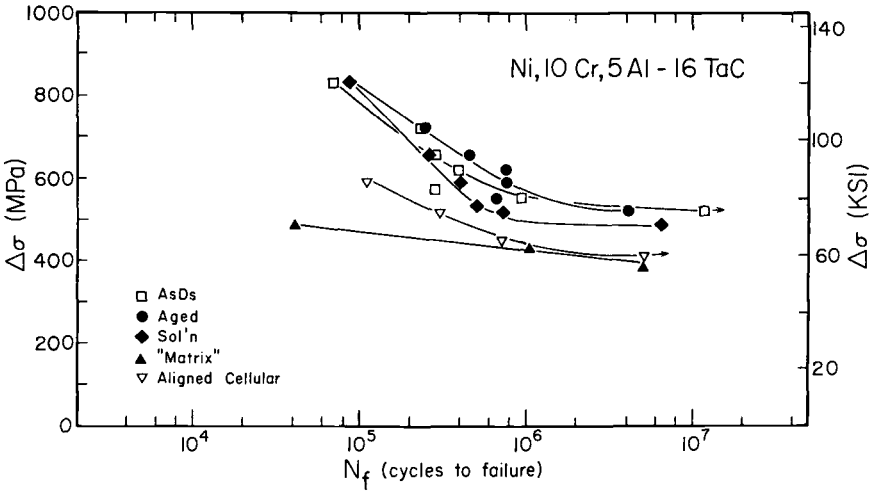

FIG. 1—*Microstructural effects on fatigue lives of Nitac at 25°C* [12].

the best fatigue resistance, with the high-cycle results very comparable to room temperature air data for as-DS material (Fig. 2). A pronounced frequency effect is noted at 825 °C (Fig. 3), with a decrease in frequency from 20 to 0.2 Hz producing approximately an ×500 decrease in fatigue life. Recently, an almost identical influence of frequency on fatigue life of Cotac at 825 °C in vacuum has been recorded [*13*]. Data for both Cotac and Nitac at 825 °C are compared in Fig. 4. The positive slopes of graphs of specimen life (cycles) versus frequency for both alloys indicate a creep shortening of fatigue life. (In a purely fatigue process the lines would be horizontal.) Also, the increasing specimen life (time) at high frequencies is contrary to what would be expected from a pure creep process. Consequently, a creep-fatigue interaction clearly exists for these alloys. A similar effect has previously been noted also for the Al-Al_3Ni eutectic [*6*], tested in air at 0.75 T_m, where T_m is the melting point.

Growth speed (R) effects in Nitac have not been studied, primarily because of the difficulty in obtaining a well-aligned microstructure as R increases from 0.6. However, it has been possible to perform such tests on Cotac, with the results shown in Fig. 5. There is a marked improvement in room temperature fatigue life upon increasing R from 0.6 to 2.5 cm/h [*7*]. However, at 825 °C, in vacuum, the growth speed effect virtually disappears. The importance of chromium in maintaining high-temperature fatigue resistance of Cotac is shown in Fig. 6. Removal of chromium results in a large decrease in fatigue resistance at all stress levels. A smaller but still significant effect of chromium is noted at 25 °C.

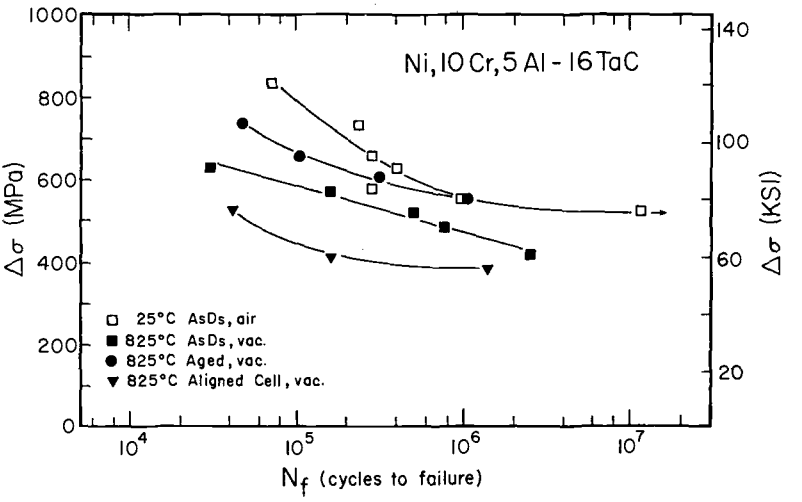

FIG. 2—*Effects of microstructure, test temperature, and environment on fatigue lives of Nitac* [12].

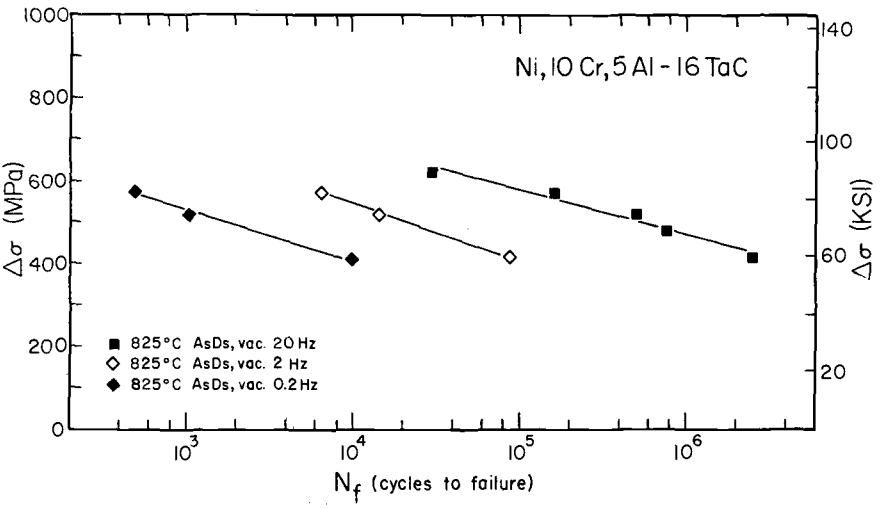

FIG. 3—*Frequency effects of fatigue lives of as-directionally solidified Nitac* [12].

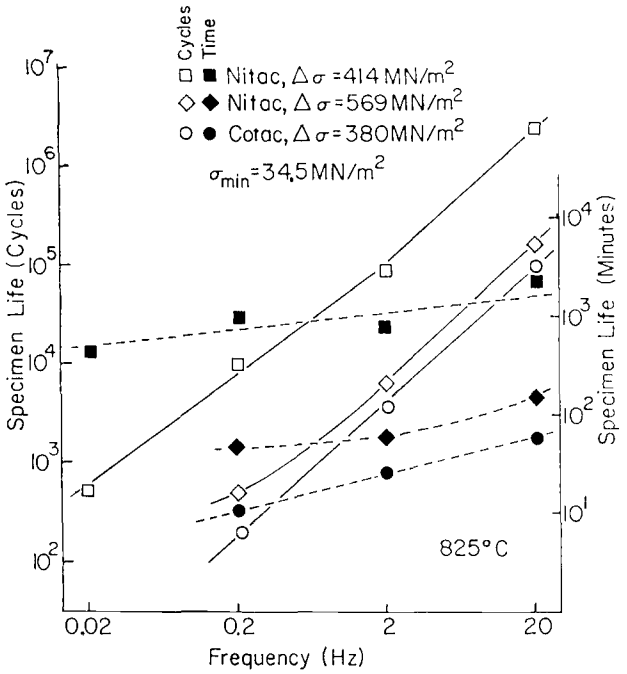

FIG. 4—*Effect of frequency on fatigue lives of as-directionally solidified Nitac and Cotac expressed as* N_f *and as time-to-failure at constant cyclic stresses* [12].

The nickel-aluminum-molybdenum alloys, in spite of their ductile molybdenum fibers, do not demonstrate particularly good fatigue resistance when compared with Nitac and Cotac. Figure 7 reveals that, on the basis of ratio of applied stress to ultimate tensile strength, AG-15 and AG-34 fall between the fatigue responses of Nitac and Cotac. The best fatigue resistance of all of the alloys studied, however, is exhibited by γ/γ'-δ (0 percent chromium) solidified at 3 cm/h. A detailed evaluation of γ/γ'-δ alloys follows.

Lamellar Alloys

Ni-21Nb-2.5Al (γ/γ'-δ) reveals excellent resistance to high-cycle fatigue, as is shown in Fig. 7. Figure 8 reveals further details of the factors leading to such properties. The 10^7-cycle fatigue limit is near $\Delta\sigma = 966$ MN/m^2 (140 ksi) for solidification rates of both 3 and 5.7 cm/h. At higher stress levels, however, there is a distinctly beneficial effect of increasing R. For example, at $\Delta\sigma = 1021$ MN/m^2 (148 ksi) the life is increased fourfold, from approximately 1.5×10^5 to 6×10^5 cycles.

In contrast to the superior fatigue properties of the percent chromium

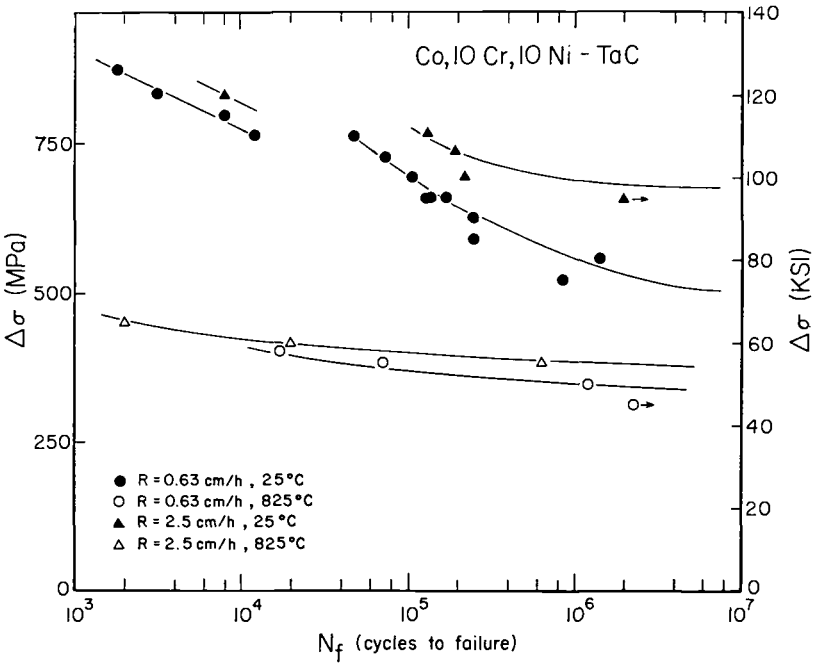

FIG. 5—*Effects of test temperature and solidification rate on the fatigue behavior of Cotac* [13].

alloy, the presence of 6 percent chromium in γ/γ'-δ leads to a marked deterioration in fatigue life, also shown in Fig. 8. The 10^7-cycle fatigue limit of the 6 percent chromium alloy is near $\Delta\sigma = 675$ MN/m^2 (95 ksi), or about 65 percent of the level for the 0 percent chromium alloy. Also shown in Fig. 8 are the results of several experiments on a single specimen of the 6 percent chromium alloy; stress was increased successively in each test. All tests were terminated with no fracture after at least 2×10^6 cycles.

Crack Propagation

Fatigue crack propagation (FCP) data for Cotac cycled at room temperature obey a power relation

$$\frac{da}{dN} = C\Delta K^m$$

See Fig. 9. Also shown are crack propagation data from the literature for γ/γ'-δ, γ-δ, 304 stainless steel, and maraging steel. Note that crack growth rates in Cotac are higher than in the lamellar eutectics, no doubt indicative of the superior fatigue response of γ/γ'-δ illustrated in Fig. 7. Transverse

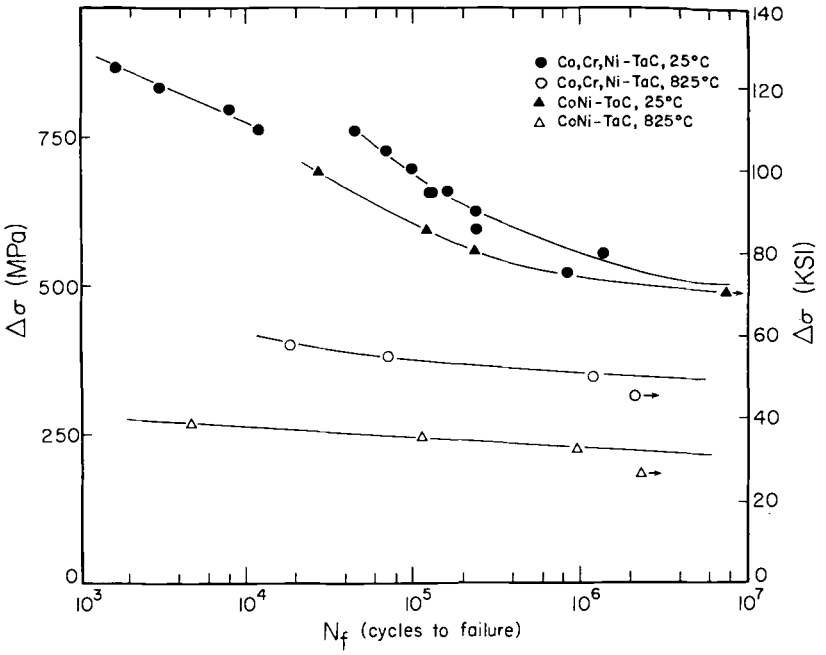

FIG. 6—*Influence of chromium on fatigue behavior of Cotac* [13].

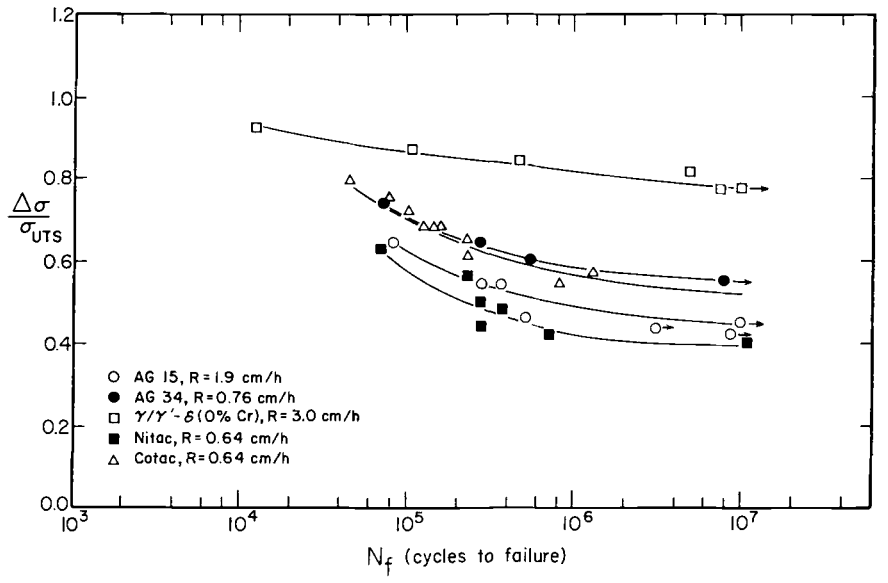

FIG. 7—*Comparison of fatigue behavior of several nickel and cobalt-base aligned eutectics; data normalized by tensile strengths.*

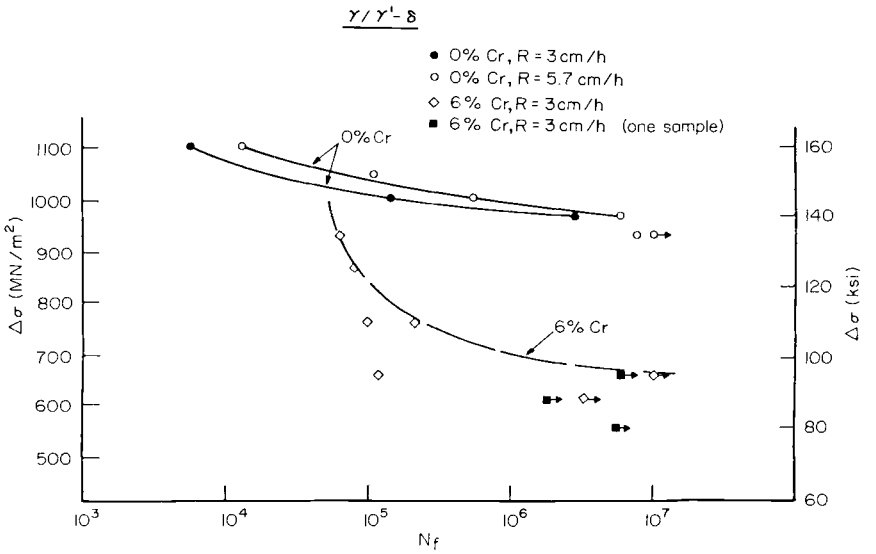

FIG. 8—S-N *curves of* γ/γ'-δ *as-directionally solidified* [14].

loading of Cotac produces still higher FCP rates, particularly at high stress intensities [*8*].

Preliminary data indicate significant effects of environment (at 20°C) and frequency (at 750°C) on crack growth rates. Figure 10 shows that crack growth in vacuum at 20°C is reduced by at least an order magnitude at low stress intensities, but the effect disappears completely for $\Delta K \geq 35$ MNm$^{-3/2}$ [*8*]. Also shown in Fig. 10 is a pronounced increase in crack growth rate at lower frequency at 750°C, but again the effect is dependent upon ΔK; for $\Delta K \leq 14$ MNm$^{-3/2}$, the results at 2 and 20 Hz are identical.

Metallographic and Fractographic Observations

Previous work on Nitac and Cotac has established that fibers may be cracked on the first quarter cycle, provided that the applied stress is sufficiently high. The source of these cracks is the intense planar slip in the nickel-rich and cobalt-rich matrix, respectively. In the current program, a major effort has been devoted to studying the influence of growth speed and postsolidification heat-treatments on crack paths in the matrix.

Figure 11 reveals clearly the crystallographic nature of cracking in the matrix for as-DS Nitac and Cotac. Figure 11*a* is a general scanning electron microscope (SEM) view of secondary microcracks in a specimen tested at $\Delta\sigma = 828$ MN/m^2 (120 ksi). At this stress level, fibers were undoubtedly broken on the first cycle, since $\sigma_y = 814$ MN/m^2 (118 ksi) (Table 2) and the peak tensile stress in this test was 863 MN/m^2 (125 ksi). Crystallographic

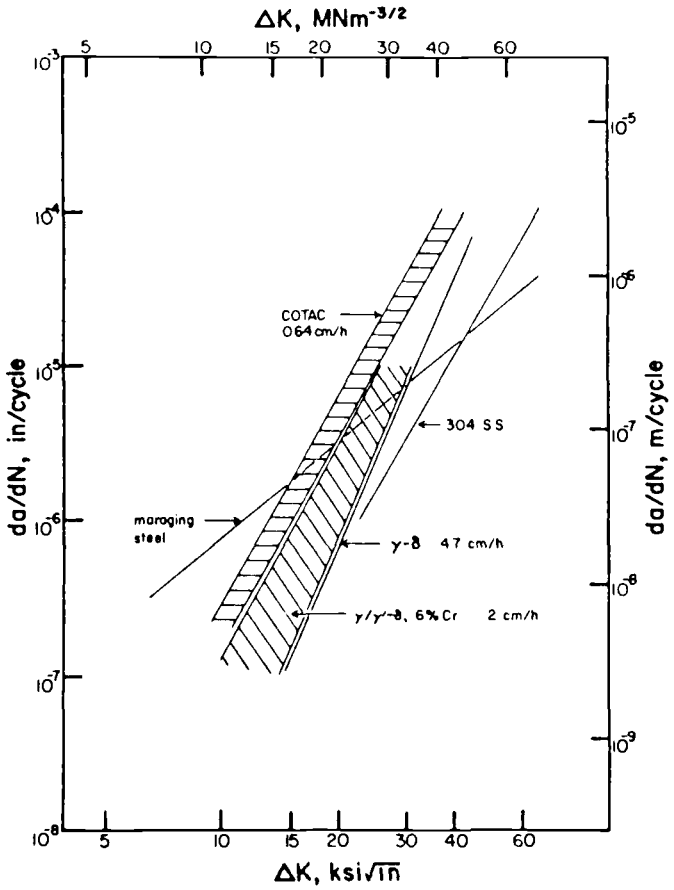

FIG. 9—da/dN *versus* ΔK *for Cotac, and comparisons with other materials* [10].

cracking along a longitudinal surface of Cotac is shown in Fig. 11*b* and a fractograph of Stage I cracking is included in Fig. 11*c* for heat-treated Cotac.

Fatigue cracking in γ/γ'-δ tends to be considerably less coplanar in the 0 percent chromium alloy, as shown in Fig. 12*a* and 12*b*. Interface cracking and splitting of the σ-phase are clearly visible in Fig. 12*a*. However, cracking in the 6 percent chromium alloy is along coplanar slipbands, Fig. 13*a*. A general view of the crack path in the 6 percent chromium alloy is shown in Fig. 13*b*; again some cracking parallel to the lamellar (growth) axis is visible.

The tendency for crystallographic Stage I type cracking in Nitac, γ'/γ-Mo, Cotac, and γ/γ'-δ at room temperature was confirmed in fractographic examination of fatigued specimens, as is shown in Fig. 11*c* for Cotac. Striations have been noted infrequently only in Nitac in the solution-treated condition tested at 25°C. as shown in Fig. 14.

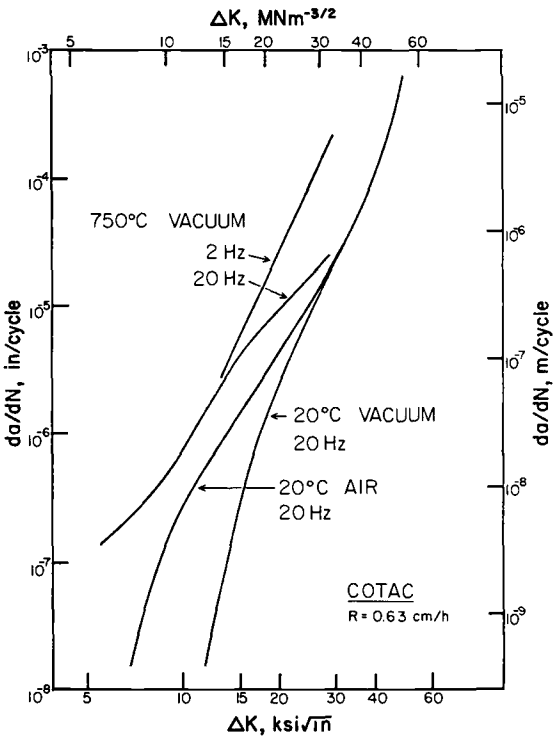

FIG. 10—*Comparison of fatigue crack propagation rates of Cotac in air and vacuum, and at 750°C* [8].

Fracture surfaces for Cotac reveal no striations under any test conditions. Tests at 825°C in vacuum revealed no faceted fractures in either Nitac or Cotac. Rather, a diffuse dimpled structure is noted.

The nature of fatigue crack in γ/γ'-δ (0 percent chromium) is shown in Fig. 15. Secondary cracking along colony boundaries is common (Fig. 15*a*). Cracking generally occurs in a brittle manner in the δ Ni_3Nb phase, and in a more ductile manner in the matrix (Fig. 15*b*). An interphase boundary crack also is clearly visible in Fig. 15*b*. Taken together with Fig. 12, it appears that cracking occurs along twin planes in the δ-phase, but often tends to occur at nearly 90 deg to the lamellar (tensile) axis in the γ-phase; slip-plane cracking in γ has not been unambiguously identified.

In the 6 percent chromium alloy, cracking occurs both parallel and perpendicular to the stress axis (on a macroscopic scale), the parallel cracks tending to follow colony boundaries, Fig. 16*a*. The faceted nature of interphase cracking in this alloy is clearly visible in Fig. 16*b*. A strong tendency for cracks to follow colony boundaries was noted also in AG-15 and AG-34, tested at 25°C.

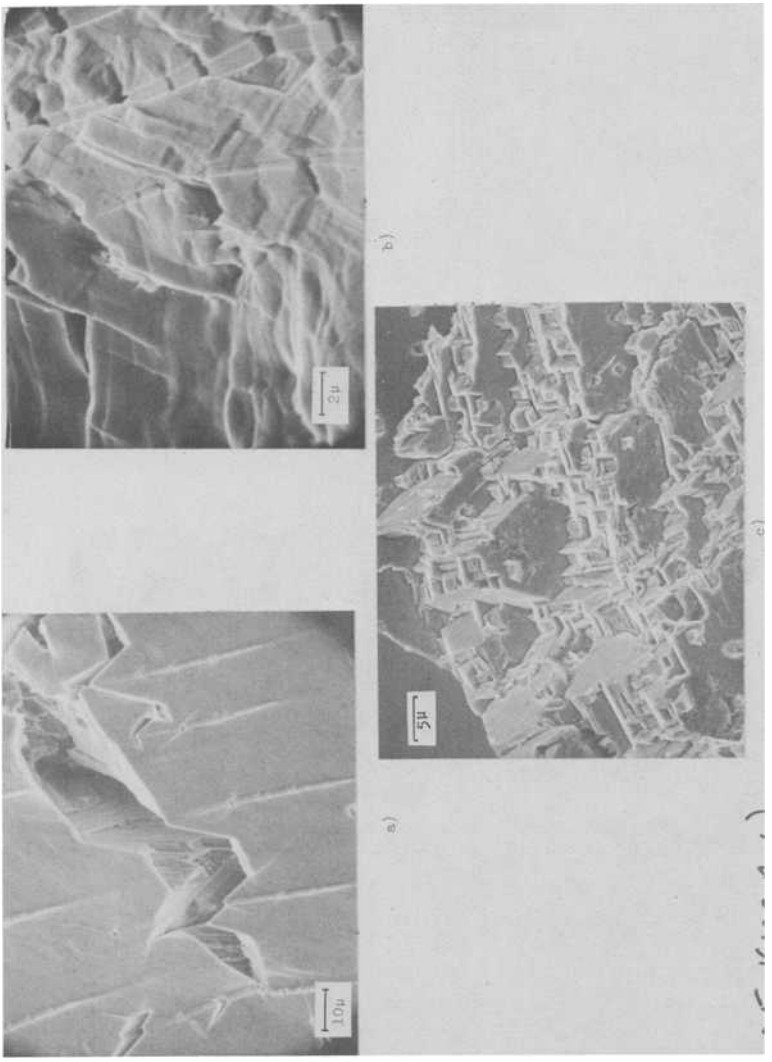

FIG. 11—*SEM micrographs of Stage I (crystallographic) cracking, 25°C:* (a) *longitudinal surface, Nitac,* $R = 0.6$ *cm/h,* $\Delta\sigma = 828$ *MN/m*^{2}; (b) *longitudinal surface, Cotac,* $R = 0.6$ *cm/h,* $\Delta\sigma = 830$ *MN/m*^{2}; (c) *initiation site, Cotac, heat-treated, 25°C,* $R = 0.6$ *cm/h;* $N_f = 9.4 \times 10^4$.

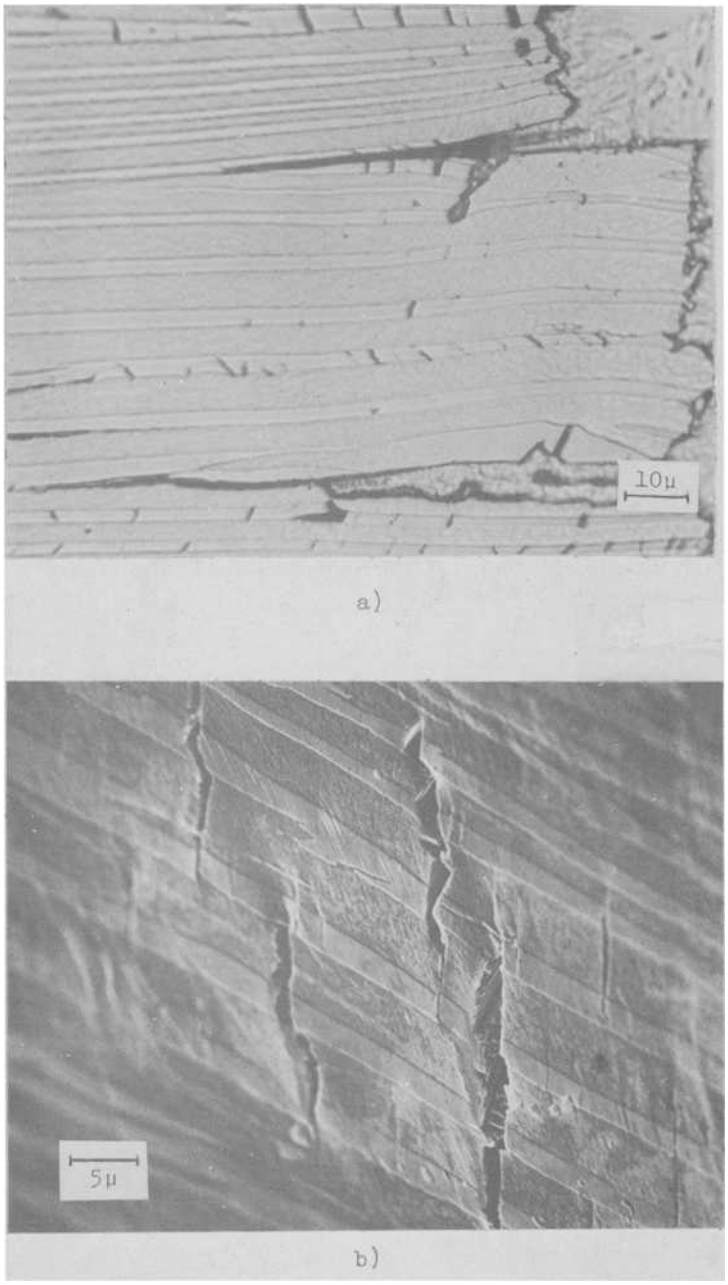

FIG. 12—*Secondary crack paths in* γ/γ'-δ *(0 percent chromium), 25°C,* R = *3 cm/h,* $\Delta\sigma$ = *1103 MN/m*^{2} *(160 ksi),* $N_f = 5.7 \times 10^3$. (a) *Optical micrograph showing interfacial and transverse cracking;* (b) *SEM micrograph* [14].

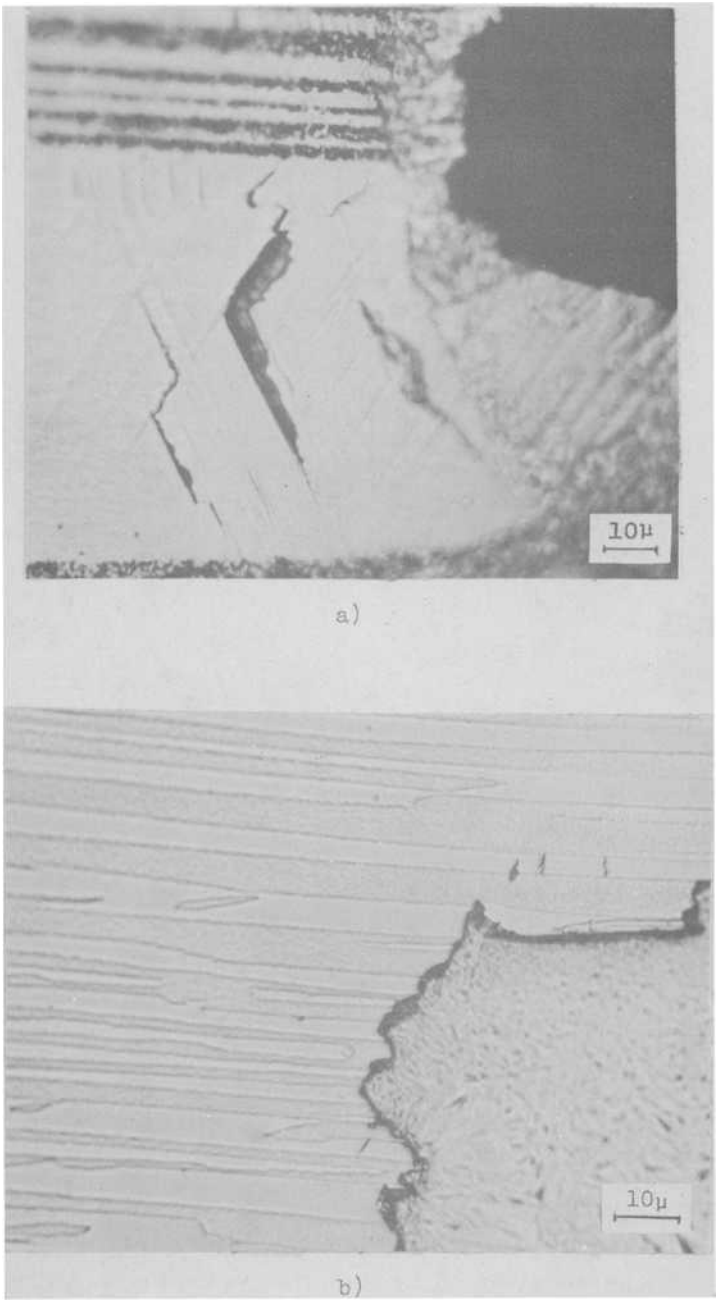

FIG. 13—*Secondary crack paths in* γ/γ'-δ *(6 percent chromium), 25°C,* R = *3 cm/h.* (a) *Stage I cracking in large* δ *lamellae,* $\Delta\sigma$ = *759 MN/m*^{2} *(120 ksi),* $N_f = 10^5$; (b) $\Delta\sigma$ = *656 MN/m*^{2} *(95 ksi),* $N_f = 1.2 \times 10^5$ [14].

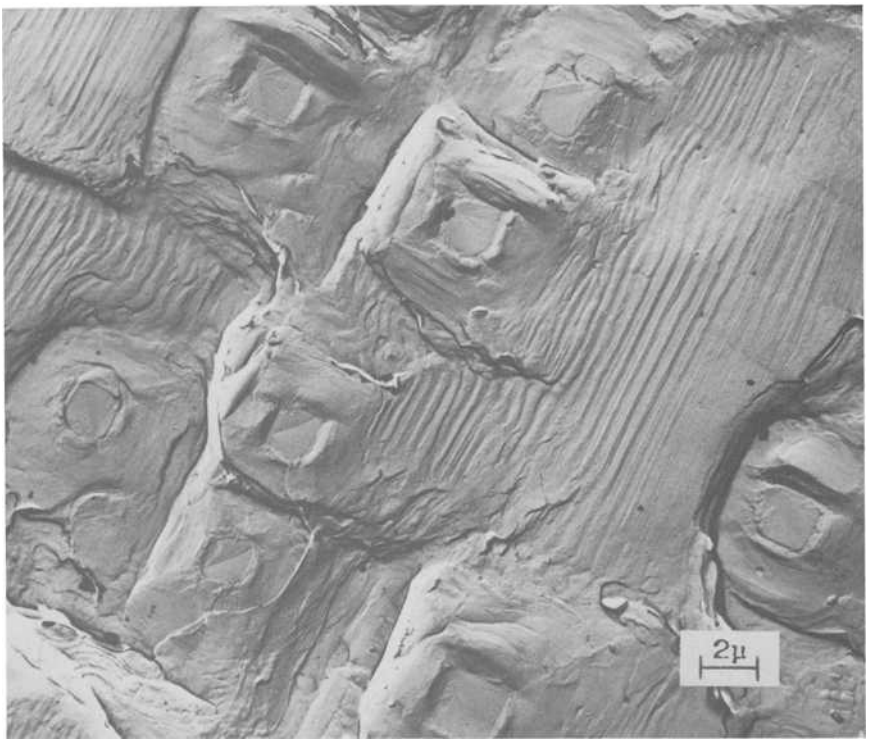

FIG. 14—*Fatigue striations in Nitac, solution-treated, tested at 25°C, 20 Hz,* $\Delta\sigma = 828$ *MN/m*^{2} [12].

Discussion

The results of our studies to date indicate that there are significant differences between the resistance to high-cycle fatigue of the various nickel and cobalt-base aligned eutectics. Table 3 is a summary of fatigue limit data. The fatigue limit of Nitac, when expressed as a function of the ultimate tensile strength (UTS), is the lowest of the alloys tested.[4] Similar results showing inferior fatigue properties for a Nitac alloy of somewhat different composition, tested in rotating bending [*1*], are thereby confirmed. The prospects for improving the room-temperature fatigue resistance of Nitac at low stress levels (near the 10^7-cycle limit) do not seem promising, since it is difficult to produce aligned structure at a growth rate faster than 0.6 cm/h without resorting to extremely high-temperature gradients, and since postsolidification heat-treatments have not produced significant improvements. Nevertheless, at

[4]Note that mean stress effects can be significant. Therefore, these comparisons should be made strictly with the aid of a Goodman diagram.

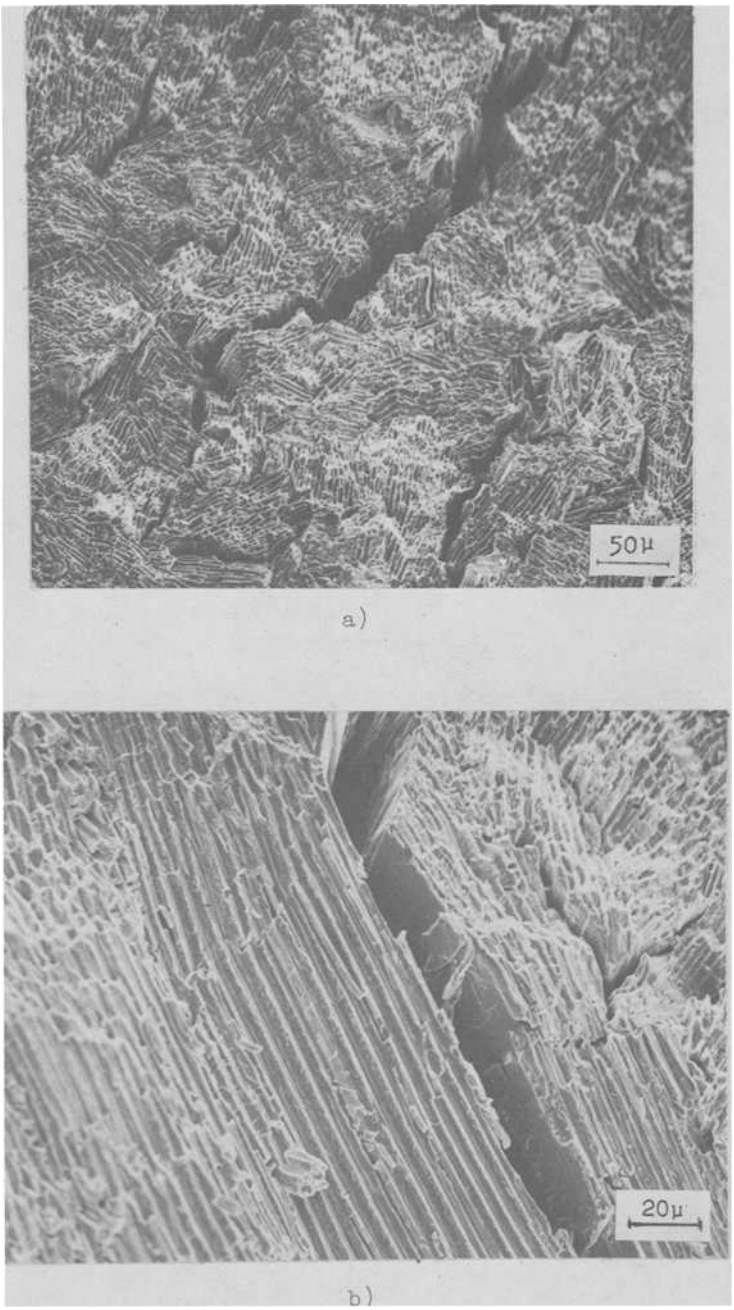

FIG. 15—*SEM micrographs of* γ/γ'-δ *(0 percent chromium), 25°C,* $R = 3$ *cm/h,* $\Delta\sigma = 966$ *MN/m*^{2} *(140 ksi),* $N_f = 2.97 \times 10^6$. (a) *General view showing colony boundary cracking;* (b) *interface crack and view of transverse fracture surface.*

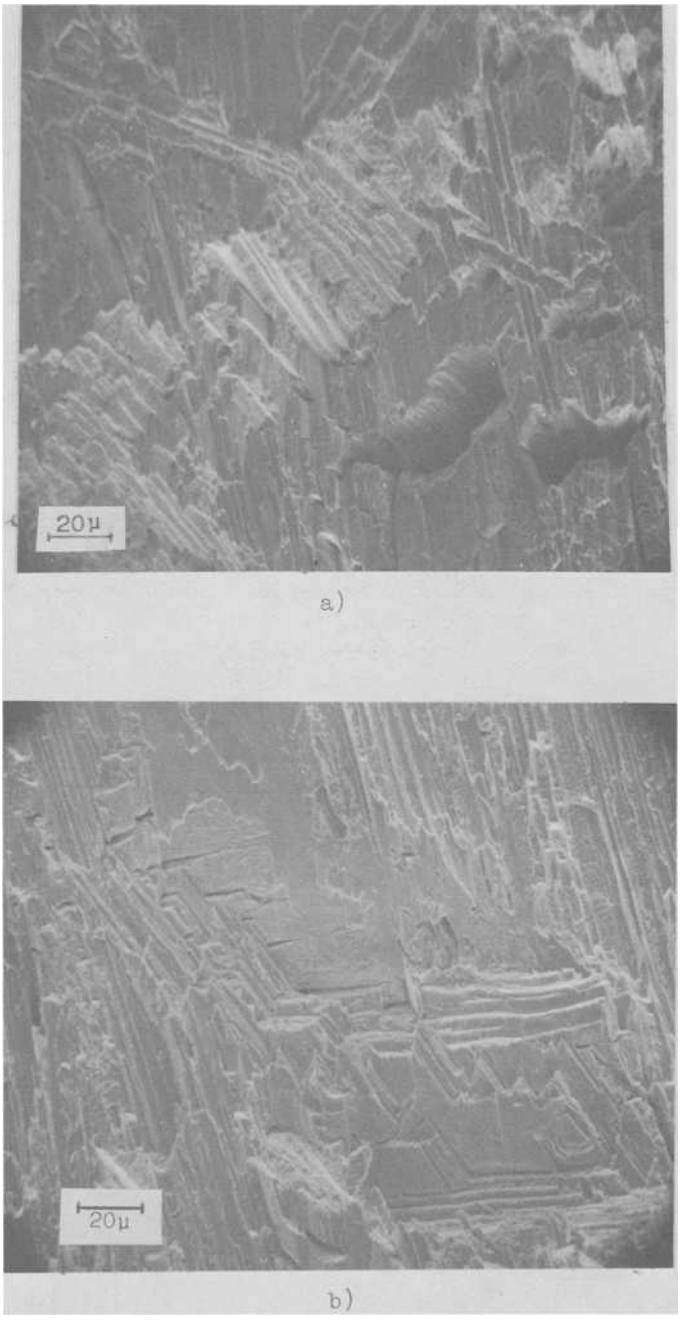

FIG. 16—*SEM micrographs of* γ/γ'-δ *(6 percent chromium), 25°C,* R = *3 cm/h.* (a) *General view showing secondary cracks,* $\Delta\sigma = 792\ MN/m^2$ *(115 ksi),* $N_f = 9.1 \times 10^4$; (b) *Stage I facets along interfaces,* $\Delta\sigma = 793\ MN/m^2$ *(115 ksi),* $N_f = 9.1 \times 10^4$.

TABLE 3—*Comparison of fatigue limits of aligned eutectics. 25°C.*

	R, cm/h	Condition[b]	σ_{UTS}[a], MN/m^2	$\Delta\sigma_{10^7}$, MN/m^2	$\frac{\sigma_{10^7}}{\sigma_{UTS}}$	Reference
Nitac	0.6	as-DS	1304	518	0.42	[12]
Nitac	0.6	solution treated	1249	483	0.41	[12]
Nitac	0.6	aged	1228	...	...	[12]
Cotac (10% Cr)	0.6	as-DS	963	518	0.57	[7, 19]
Cotac (10% Cr)	2.5	as-DS	1042	690	0.7	[7]
Cotac (10% Cr)	0.6	aged	994	587	0.59	[7]
Cotac (0% Cr)	0.6	as-DS	987	483	0.49	[d]
γ/γ'-δ (0% Cr)	3	as-DS	1193	966	0.84	[14]
γ/γ'-δ (0% Cr)	5.7	as-DS	...	966	...	[14]
γ/γ'-δ (6% Cr)	3	as-DS	1187	656	0.58	[14]
Ni-Cr	...	as-DS	~828	587	0.71	[15]
γ-δ	4.7	as-DS	745	414[c]	0.56[c]	[16]
γ'-δ	...	as-DS	1173	690	0.59	[17]
Ni-W	3.0	as-quenched	920	350	0.38	[18]

[a]UTS = ultimate tensile strength.
[b]DS = directionally solidified.
[c]Notched.
[d]Present work.

higher stress levels, that is, $\Delta\sigma \geq 552$ MN/m^2 (80 ksi), there appears to be a significant increase in life with aging (Fig. 1), and there is an even greater improvement in high-temperature properties (Fig. 2).

Cotac, which exhibits a $\sigma_{10}{}^7/\sigma_{UTS}$ ratio of 0.57 for $R = 0.6$, can be improved still further by utilizing $R = 2.5$ cm/h, for which the ratio rises to 0.7. Unfortunately, the beneficial effect of the high solidification rate is not maintained at 825°C in vacuum (Fig. 5). This result is surprising, since previous work on Al-Al_3Ni showed that rapid solidification rates became more beneficial at high test temperatures [*6*]. This discrepancy may be related to the deformation substructure since the matrix of Al-Al_3Ni characteristically shows wavy slip behavior (dislocation cell substructure) at all temperatures. Cotac, on the other hand, appears to change its deformation substructure from planar at room temperature to wavy at elevated temperatures. Further improvements in fatigue resistance of Cotac have, however, been accomplished by heat-treatment to produce fine carbide particles between the as-grown carbide fibers [*7*]. This heat-treatment has also been shown to improve tensile and creep properties of Cotac [*9*].

The relative room-temperature fatigue resistance of γ/γ'-δ (0 percent chromium) is the highest ($\sigma_{10}{}^7/\sigma_{UTS} = 0.84$) of any alloy or condition shown in Table 3. Increasing growth speed appears to have little effect on the fatigue limit, but has a beneficial effect at high stress levels.

There is some potential for improving fatigue resistance of γ/γ'-δ alloys still further by postsolidification aging.

One of the most significant aspects of the present work is the striking drop in fatigue resistance of γ/γ'-δ when 6 percent chromium is added (Fig. 8 and Table 3). The fatigue/UTS ratio drops from 0.84 to 0.58 at the same growth speed when chromium is added. The 6 percent chromium alloy is comparable in its fatigue resistance to Cotac grown at a slower rate, but is significantly less resistant than Cotac grown at nearly the same rate. This is surprising, since crack propagation rates measured in tension-tension on flat tension specimens reveal substantially higher rates of propagation for Cotac [*10*] relative to γ/γ'-δ with 6 percent chromium [*11*]. In Cotac, on the other hand, chromium has a mildly beneficial effect at 25°C, and contributes significantly to fatigue resistance at 825°C in vacuum (Fig. 6). In the case of Cotac, however, chromium significantly improves tensile strength without severely degrading the microstructure. Therefore, evaluation of the effect of any alloying element on fatigue resistance requires knowledge of effects on both tensile properties and microstructure.

The metallographic and fractographic observations confirm that Stage I (crystallographic) cracking predominates in Cotac, Nitac, γ/γ'-δ, and γ/γ'-δ (0 percent chromium). The high fatigue resistance of the latter, therefore, cannot be attributed to Stage I cracking alone, which is often regarded as a slower mode of growth than Stage II cracking. The extensive colony bound-

ary cracking and interface splitting noted in Figs. 15 and 16 may be the most important factor in slowing crack growth. No evidence of cracking parallel to fibers was noted in the fibrous eutectics. In addition, differences in crack initiation resistance of the lamellar γ/γ'-δ and the fibrous alloys may be involved. This factor remains to be investigated.

Opportunities for improving room-temperature fatigue resistance of nickel and cobalt-base eutectic alloys through control of microstructure have been demonstrated. However, even greater opportunities for enhanced fatigue resistance may occur at elevated temperatures where creep can contribute to the fatigue process. At high frequencies creep is suppressed and fatigue resistance is excellent. For Cotac, crack growth at high ΔK is slowed at higher frequencies, but at low ΔK growth rate is unaffected (Fig. 9). Similar data have not yet been obtained for Nitac, but it appears from Figs. 3 and 10 that both crack initiation and propagation may be influenced by test frequency and environment. In the case of Al-Al_3Ni, significant effects of growth speed on fatigue life were noted only when the test temperature reached 0.5 T_m [6]; in Cotac no such beneficial effect was noted.

Summary and Conclusions

The high-cycle fatigue resistance of γ/γ'-δ (0 percent chromium) has been shown to be the greatest of all nickel and cobalt-base eutectics tested to date. Nitac, on the other hand, demonstrates inferior fatigue resistance. Postsolidification heat-treatments for Nitac and increasing growth rates for Cotac and γ/γ'-δ have been shown to increase fatigue lives at stresses above the respective fatigue limits. Opportunities for further improvements in the latter two alloys by postsolidification heat-treatments are indicated. At 825°C, fatigue resistance of Nitac and Cotac in vacuum is shown to be very sensitive to test frequency. Cracking is crystallographic at room temperature in the fibrous eutectics; less so in γ/γ'-δ, particularly with 0 percent chromium. At 825°C, no evidence of crystallographic cracking was noted. Measurements of crack initiation times, crack propagation rates, and further evaluation of properties at test temperatures above 0.5 T_m are clearly indicated in order to maximize the beneficial aspects of microstructure control.

Acknowledgment

This work was supported by the Office of Naval Research under Contract N00014-75-C-0503, NR031-745 and by the National Science Foundation under Grants No. GH-42520 and DMR76-09405. The authors are grateful to W. Johnson, C. Austin, J. Tartaglia, and C. Koburger for their contributions to these programs.

References

[1] Henry, M. F. and Stoloff, N. S. in *Fatigue of Composite Materials ASTM STP 569*, American Society for Testing and Materials, 1975, pp. 189-209.
[2] Bibring, H. in *Proceedings* Conference on *In-Situ* Composites, NMAB 308, National Research Council, Washington, D.C., Vol. 2, 1973, pp. 1-69.
[3] Bibring, H. and Seibel, G., *Comptes Rendus*, Vol. 268C, 1969, pp. 144-147.
[4] Walter, J. L. and Cline, H. E. in *Proceedings* Conference on *In-Situ* Composites, NMAB 308, National Research Council, Washington, D.C., Vol. 1, 1973, pp. 61-74.
[5] Bibring, H., Rabinovitch, M., and Seibel, G., *Comptes Rendus*, Vol. 268C, 1969, pp. 1666-1669.
[6] Maurer, G. E., Duquette, D. J., and Stoloff, N. S., *Metallurgical Transactions*, Series A, Vol. 7A, 1976, pp. 703-709.
[7] Koburger, C. W., Duquette, D. J., and Stoloff, N. S., *Acta Metallurgica*, Vol. 26, 1978, pp. 81-91.
[8] Austin, C. M., Stoloff, N. S., and Duquette, D. J., Rensselaer Polytechnic Institute, Troy, N.Y., unpublished research.
[9] Trottier, J. P., Khan, T., Stohr, J. F., Rabinovitch, M., and Bibring, H., *Cobalt*, 1974, No. 3, p. 54.
[10] Austin, C. M., Duquette, D. J., and Stoloff, N. S., *Metallurgical Transactions*, Series A, Vol. 8A, 1977, pp. 1621-1627.
[11] Yuen, A. and Leverant, G. R., *Metallurgical Transactions*, Series A, Vol. 7A, 1976, pp. 1443-1450.
[12] Johnson, W. A., Ph.D. Thesis, Rensselaer Polytechnic Institute, Troy, N.Y., 1978.
[13] Koburger, C. W., Ph.D. Thesis, Rensselaer Polytechnic Institute, Troy, N.Y., 1978.
[14] Grossman, J. E. and Stoloff, N. S., *Metallurgical Transactions*, Series A, Vol. 9A, 1978, pp. 117-125.
[15] Sadananda, K., DiPrimio, J. C., and Salkovitz, E. J., Technical Report Advanced Research Projects Agency Contract No. DAHC-15-67-C-0176, Pittsburgh, Pa., 1969.
[16] Hoover, W. R. and Hertzberg, R. W., *Metallurgical Transactions*, Vol. 2, 1971, pp. 1289-1292.
[17] Thompson, E. R., George, F. D., and Kraft, E. H., Final Report, United Technologies Research Laboratories, E. Hartford, Conn., to Office of Naval Research, Contract No. N00019-70-C-0052, July 1970.
[18] Garmong, G. and Williams, J. C., *Metallurgical Transactions*, Series A, Vol. 6A, 1975, pp. 1711-1719.
[19] Koburger, C. W., Stoloff, N. S. and Duquette, D. J. in *Proceedings*, Second Conference on *In-Situ* Composites, Xerox Inc., Lexington, Mass., 1976, pp. 587-596.

DISCUSSION

R. Stephens[1] (*discussion*)—The first sentence in the Introduction of this paper indicates that these nickel and cobalt-base eutectic composites have been under intensive development for possible applications in advanced aircraft gas turbines. This implies to me that elevated-temperature fatigue, creep, and microstructure interactions would be the major emphasis of research efforts. The major emphasis of this paper from the standpoint of both phenomenalogical fatigue behavior and microstructural alterations and mechanisms, however, appears to be at room temperature. Elevated-

[1]Materials Engineering Division, University of Iowa, Iowa City, Iowa.

temperature fatigue results and mechanisms are included, but to a much lesser extent. All scanning and optical microscopy figures deal only with room-temperature mechanisms. It is stated, however, that "tests at 825°C in vacuum revealed no faceted fractures in either Nitac or Cotac." I assume the authors have significant reasons why so much emphasis was placed on room-temperature behavior and mechanisms even though the goal was or is to develop alloys for elevated temperatures. Perhaps some correlation exists between room-temperature and elevated-temperature fatigue behavior and mechanisms? I invite the authors to comment on this philosophy and possible extrapolation.

Concerning the phenomenological conclusions in the paper, I would like to raise a question of concern about scatter, variability, and number of tests for a given test condition. I personally do not see much so-called "coaxing" effect which could be just scatter or variability effects. Some coaxing may be there, however, but it is hidden in the unknown scatter effects. The three top curves in Fig. 1 appear to be very similar in view of the limited data and undetermined scatter.

Perhaps the most striking influence on the fatigue results was the effect of frequency at 825°C. Is this very large influence similar for other alloys at elevated temperatures? What is the significance of this large frequency effect?

All tests were performed in load control with tension-tension conditions. Is this the most significant spectrum for gas turbine engines? Fatigue behavior can be substantially different in load control or strain control. The influence of compression can also have a substantial effect on total fatigue life. What are the best constant-amplitude or variable spectra to aid in alloy development for gas turbine engines at elevated temperatures?

N. S. Stoloff—The first question may be rephrased: Are things pretty much similar at high temperatures as at low temperatures? If anything, the data that we have so far indicate that the alloys are at least as good at elevated temperatures as at low temperatures, based not only on the high-cycle fatigue data presented here but also on low-cycle fatigue data that Henry and co-workers have produced at General Electric Co.

These alloys are outstanding when compared with conventional nickel and cobalt-based superalloys.

R. Stephens—Thank you. I think I will jump to my last question and that deals with the spectrum that you used in comparing your materials, which was essentially a constant-amplitude condition, load control, R equals zero or greater. Again, you are seeking to compare materials for elevated-temperature conditions. ASTM has been very active in spectrum loading lately. We have another symposium coming up in a year and I am just wondering if your comparison of these materials under this spectrum could

be used in choosing materials, or do you feel that different spectra would be necessary in order to make a proper rational decision as to which are the best materials for the conditions you are seeking, and if so, what would those spectra be?

N. S. Stoloff—The impetus to do this work was to understand the metallurgical factors underlying fatigue resistance, not to design gas turbine alloys, even though they are meant to be gas turbine alloys. However, we clearly have chosen the type of loading that has been prevalent in the literature for this class of materials, namely, tension-tension loading. All of the comparisons in my final table were made in the same way, from data in the literature as well as our own data. Therefore, we are not trying to compare different R ratios. We have, in our own crack propagation data, shown very clearly—and Hertzberg has in a γ-δ alloy—that these alloys are sensitive to R ratio. As R goes up, the crack growth rate goes up. As far as fully reversed loading is concerned, there are very few strain-controlled experiments that have been conducted and those that have have been in fully reversed tension and compression. As I said before, these alloys seem to be as outstanding in reversed loading as in tension-tension cycling, when compared with conventional nickel-base alloys which they are meant to replace.

R. Stephens—I have an additional question. I notice that in your constant-amplitude and high-temperature da/dN work you are using K, the stress-intensity parameter. I do not recall what your yield strengths were, but I am just kind of guessing that you have a lot of plasticity at the tip of the cracks. So I wonder if at this high elevated temperature it is a good thing to be using the elastic parameter, the stress intensity, for this condition, and if it is not a good condition in your opinion, what would you recommend?

N. S. Stoloff—The only figure shown of da/dN was for room-temperature data.

S. Kulkarni[2] (*discussion*)—The high-cycle fatigue behavior of several fibrous (Cotac, Nitac, nickel-aluminum-molybdenum) and lamellar (nickel-aluminum-chromium-niobium) directionally solidified eutectics (DSE's) has been investigated in the paper. Major test variables include alloy composition, growth speed, microstructural modifications induced by postsolidification heat-treatments, test temperature, and frequency. The significant conclusions of this investigation are interpreted in light of the present understanding of the fatigue behavior of fiber-reinforced epoxy and metal matrix composites.

[2]Lawrence Livermore Laboratory, Livermore, Calif.

Due to the fact that DSE's are *in situ* composites, the matrix-reinforcement interface is chemical rather than mechanical in nature. Thus, in order to develop an understanding of the unique nature of the chemical interface, properties which are influenced by it (such as the longitudinal compression, and transverse and shear moduli and strengths) should be determined. Knowledge of these properties will be beneficial in interpreting the fatigue behavior, failure modes, crack propagation rates, fracture toughness, and postsolidification heat-treatment effects. In this context, it should be noted that in graphite-aluminum composites there exists a chemical interface which has a rather deleterious effect on the transverse and shear strengths of the composite and, possibly, on its fatigue behavior also.

It has been pointed out in the paper that lamellar DSE's (particularly those with percent chromium alloy) have superior fatigue resistance to the fibrous DSE's, both with regard to total life and crack propagation rates. This may be attributed to the fact that there is no evidence of cracking parallel to the fibers in the fibrous DSE's while considerable interfacial splitting (resulting in crack blunting) occurs in the lamellar DSE's.

Little effect of heat-treatment on the tensile properties of Nitac has been noted; however, the effect on fatigue resistance was significant. Similar, but limited, studies of boron-epoxy composites have indicated the same trends. A possible explanation for this may be the presence of residual stresses due to heat-treatment.

An interesting observation in the paper is that the nickel-aluminum-molybdenum fibrous DSE's, in spite of the ductile nature of molybdenum fibers, do not demonstrate particularly good fatigue resistance when compared with Nitac and Cotac, which have brittle tantalum-carbide fibers. This aspect needs further investigation.

A pronounced frequency effect is noted at 825 °C for Nitac, with a decrease in the frequency from 20 to 0.2 Hz producing a 500-fold decrease in fatigue life. At high frequencies creep is suppressed, while at lower frequencies the possibility of creep-fatigue interaction increases. Frequency effects for fiber-reinforced composites are now being studied and the observation should prove to be of considerable interest.

In contrast to the superior fatigue properties of 0 percent chromium alloy, the presence of 6 percent chromium in γ/γ'-δ leads to a marked deterioration in fatigue life. The significant measured change in the mechanical properties with 6 percent chromium is the reduction in the ductility (percent elongation). For the 0 percent chromium DSE, cracks occur in the twin planes of the δ-phase and at 90 deg to the tensile axis in the γ-phase. In addition, cracking is of a brittle nature in the δ-phase and ductile in the matrix. For the 6 percent chromium DSE, cracking occurs along and at 90 deg to the stress axis on a macroscopic scale. Perhaps a detailed study of the transverse and shear properties and testing of notched specimens will provide additional insight into the behavior of these DSE's.

R. Scarlin[3] (*written discussion*)—We also have been involved in looking at these eutectic materials and as far as we can see the main possible application is for high-temperature turbine blades, which are subjected to complex loading, comprising bending and tension. The transverse properties of the material are therefore very important. We believe that the transverse properties are particularly poor. Do you believe, in view of this, that there is a real application for these materials?

N. S. Stoloff—Well, there are two parts to that question. The transverse fatigue properties of Cotac, as far as crack propagation goes, are not tremendously inferior to the longitudinal properties. Furthermore, there are indications from work on γ/γ'-δ at Pratt and Whitney Aircraft that heat-treatment can control transverse strength, and, as far as I know, the question of the use of heat treatment to control microstructure and thereby control properties is just being touched now by a few investigators, including our own group.

Certainly, in the absence of any definitive widespread information on this subject, I think that these materials are still candidates for blades and, furthermore, have undergone successful engine testing in at least three locations. So the answer is, I believe there is a potential application.

W. Stinchcomb[4] (*discussion*)—You mentioned that there was a pronounced frequency effect in the Nitac at high temperature. I was wondering if you had any data at room temperature at different frequencies and if the effect was still there or as pronounced.

N. S. Stoloff—We have performed most of our frequency work at high temperatures. For Cotac at room temperature the crack growth rate was nearly the same for tests at 2 Hz and 20 Hz. I will point out that we have found a distinct frequency effect at elevated temperature in at least one other eutectic alloy in air, but that datum was open to the question of whether it was an environmental effect. I believe that here we have at least minimized if not eliminated the environmental contribution.

D. Hoeppner[5] (*discussion*)—Would the ranking and the significance of your results change if I were to look at some other fatigue-crack growth response behavior, such as strain cycling data or fatigue-crack growth data?

N. S. Stoloff—Yes. In terms of fatigue-crack growth data, the relative rankings are roughly the same, and Cotac is poor in stress-number of cycles to failure rankings and in crack propagation on prenotched bars. Generally there is a crude correlation between the two.

[3]BBC Brown, Boveri & Co., Baden, Switzerland.

[4]Department of Engineering Science and Mechanics, Virginia Polytechnic Institute and State University, Blacksburg, Va.

[5]Department of Mechanical Engineering, University of Toronto, Toronto, Ont., Canada.

C. J. Beevers[6] (*discussion*)—In materials with a very high ratio of fatigue limit to ultimate tensile strength, do you believe that there is an inhibition of initiation or a restriction of crack propagation?

N. S. Stoloff—We think that the properties of these materials are decidedly propagation-controlled. We have had no difficulty at all in initiating cracks in individual fibers by intentionally precracking or running our tests at relatively high loads. We have actually watched fiber cracks that are stable for 90 percent of the fatigue life and then ultimately take off. Therefore, we believe it is the crack propagation properties of these materials that will control their fatigue behavior.

N. S. Stoloff and D. J. Duquette (*authors' closure*)—We appreciate the detailed comments of Drs. Stephens and Kulkarni as well as the questions of Drs. Scarlin, Stinchcomb, Hoeppner, and Beevers. Although the original draft of this paper did indeed contain a preponderance of room-temperature data, the published paper contains considerable information on fatigue tests at 825°C for both Nitac and Cotac. These data, which were obtained only in the past few months, demonstrate that elevated-temperature fatigue properties of fibrous eutectics remain superior to those of conventional superalloys by a wide margin. With regard to specific comments of Dr. Stephens:

The three curves in Fig. 1 for aligned Nitac tested in various microstructural conditions at 20°C do indeed seem to fall within one scatter band. However, at 825°C, Fig. 2, there is a decided difference in the fatigue resistance of three alloy conditions, aged material exhibiting fatigue lives at least 10 times those of as-DS material at all stress levels.

Frequency effects in vacuum at 825°C were similar for Nitac and Cotac, as shown in Fig. 4 of the paper, and in both cases can be attributed to a creep-fatigue interaction.

We agree with Dr. Kulkarni that studies of transverse and shear properties of eutectic composites are needed. Some recent data reported by Pratt and Whitney Aircraft indicate that shear properties will, in fact, be life-limiting for $\gamma/\gamma'\delta$.[7]

[6]Department of Physical Metallurgy, University of Birmingham, Birmingham, U.K.

[7]Sheffler, K. D. and Jackson, J. J., NASA CR-135005 (Pratt and Whitney No. 5472), National Aeronautics and Space Administration, Dec. 1976.

R. P. Wei[1]

On Understanding Environment-Enhanced Fatigue Crack Growth—A Fundamental Approach

REFERENCE: Wei, R. P., **"On Understanding Environment-Enhanced Fatigue Crack Growth—A Fundamental Approach,"** *Fatigue Mechanisms,* Proceedings of an ASTM-NBS-NSF symposium, Kansas City, Mo., May 1978, J. T. Fong, Ed., *ASTM STP 675,* American Society for Testing and Materials, 1979, pp. 816-840.

ABSTRACT: Corrosion fatigue is a generic term that is used to describe the phenomenon of cracking (including environment-enhanced fatigue crack growth) in materials under the combined actions of an applied cyclic stress and a corrosive (aggressive) environment. Quantitative characterization and understanding have been hampered by the complexity of the problem, difficulties in separating the effects associated with crack initiation and crack growth, and by the absence of a truly interdisciplinary attack of the problem. With the development of fracture mechanics technology and sophisticated techniques such as Auger electron spectroscopy and low-energy electron diffraction analysis, quantification of environment-enhanced fatigue crack growth has now been placed on a reasonably firm basis in terms of both steady-state and transient responses. Understanding of the chemical processes that control environment-enhanced fatigue crack growth is beginning to emerge from coordinated mechanical, metallurgical, and chemical studies. A fundamental approach that underlies these studies and recent progress using this approach are described. Areas and directions for future research are discussed.

KEY WORDS: corrosion fatigue, fatigue crack growth, fracture mechanics, metals, surface chemistry

Metal fatigue as an engineering problem has been well recognized. It is one of the major causes, if not the major cause, for failure of engineering structures in service. Considerable engineering and scientific efforts have been devoted, especially during the past two decades, to the characterization of fatigue response and to the understanding of the mechanisms for fatigue. Such characterization and understanding are essential to service life prediction, fracture control, and the development of fatigue-resistant alloys. Quan-

[1]Professor of mechanics, Department of Mechanical Engineering and Mechanics, Lehigh University, Bethlehem, Pa. 18015.

titative characterization and understanding, however, have been hampered by the complexity of the problem, by difficulties in separating the effects associated with crack initiation from those associated with crack growth, and by the influences of external chemical environments on both the initiation and growth processes.

With the development of fracture mechanics technology since the mid-1950's and the increased concern with fatigue crack growth in many applications, it was more or less natural to consider separately the processes associated with fatigue crack growth. This separation narrowed the problem scope considerably and by and large has been beneficial. By restricting attention to the growth of a dominant crack,[2] one essentially circumvents nearly all of the issues associated with crack initiation. Characterization of crack growth response can be and has been carried out in a straightforward manner, and the data utilized directly for estimating service performance. In terms of understanding fatigue crack growth, the problem can be further divided into two areas as follows:

1. Mechanisms for fatigue crack growth and
2. Environment enhancement of fatigue crack growth.

The first of these two areas is concerned with understanding the purely mechanical processes for fatigue, that is, fatigue in the absence of environmental influences. The second area deals with understanding fatigue crack growth response under the conjoint actions of mechanical fatigue and chemical attack. Progress has been made in both of these areas during the past 20 years and has been documented in a number of review articles and in the proceedings of several symposia [*1–6*].[3] In this paper, a brief review is given of the progress during the past 10 years toward understanding environment-enhanced fatigue crack growth (particularly in high-strength alloys) and establishing the need for an interdisciplinary approach to the problem. The development of a fundamental approach involving fracture mechanics, materials science, and surface chemistry is described. The usefulness of this approach is discussed in terms of recent experimental results. Areas and directions for future research are considered.

Fracture Mechanics Basis for Fatigue Crack Growth Studies

One of the principal obstacles in the development of understanding of the various aspects of fatigue had been the difficulty in relating material response to the appropriate driving forces in a consistent and quantitative manner. By isolating the problems of fatigue crack growth for study, some simplification has been made possible. The material response then becomes

[2]Delineation between initiation and growth is neither well defined nor definable. A dominant crack here implies that the planar dimensions of the crack are large with respect to the microstructural (for example, grain) sizes.

[3]The italic numbers in brackets refer to the list of references appended to this paper.

simply the rate of fatigue crack growth and can be readily measured. The appropriate driving force has been defined through the development of linear fracture mechanics and the application of this technology to fatigue crack growth problems [*7–10*]. Because crack growth is most likely to proceed from the highly stressed region at the crack tip, it is most appropriate to characterize the mechanical crack driving force in terms of the crack-tip stress-intensity factor, K, or stress-intensity factor range, ΔK [*7–10*]. The assumptions, utility, and restrictions of this approach have been discussed in detail elsewhere [*7–10*]. Two of the following three related loading variables are commonly used for characterizing fatigue crack growth: maximum stress intensity factor, K_{max}; cyclic stress-intensity factor range, ΔK, ($\Delta K = K_{max} - K_{min}$); and stress ratio, or load ratio, R, ($R = K_{min}/K_{max}$).[4] (K_{min} is the minimum stress-intensity factor in a load cycle.) These variables have their counterparts in conventional fatigue analysis. They are the maximum stress, σ_{max}, stress range, $\Delta\sigma$, and stress ratio, R, ($R = \sigma_{min}/\sigma_{max}$), respectively.

Some Significant Variables Affecting Fatigue

Many variables can influence fatigue crack growth. Some of the significant variables are listed in the following, along with the aforementioned loading variables [*11*].

Mechanical Variables

Maximum stress or stress-intensity factor, σ_{max} or K_{max} (see footnote 4),
Cyclic stress or stress-intensity factor range, $\Delta\sigma$ or ΔK (see footnote 4),
Stress ratio, or load ratio, R (see footnote 4), that is, ratio of minimum to maximum stress (load) or stress-intensity factor in one cycle,
Cyclic load frequency, f,
Cyclic load waveform (for constant-amplitude loading),
Load interactions in variable-amplitude loading,
State of stress, and
Residual stress.

Geometrical Variables

Crack size and relation to component dimensions,
Crack geometry,
Component geometry adjoining crack, and
Stress concentrations associated with design.

[4]These three parameters are interrelated. Only two of the three need to be specified. For loading into compression, stress-intensity factor is not defined and the effective K_{min} is either zero or nearly zero. An operational definition of $\Delta K = K_{max}$, with stress or load ratio (R) specified in terms of the applied stress or load, is being adopted for $R \leq 0$ [*12*]. The reader should examine published fatigue crack growth data to determine how ΔK was defined.

Metallurgical Variables

Alloy composition,
Distribution of alloying elements and impurities,
Microstructure and crystal structure,
Heat-treatment,
Mechanical working,
Preferred orientation of grains and grain boundaries—(texture), and
Mechanical properties (strength, fracture toughness, etc.).

Environmental Variables

Temperature, T,
Pressure,
Types of environments—gaseous, liquid, liquid metal, etc.,
Partial pressure of damaging species in gaseous environments, P_i,
Concentration of damaging (or beneficial) species in aqueous or other liquid environments, C_i,
Electrochemical potential, ϕ,
pH,
Viscosity of environment, η,
Velocity of the environment, and
Coatings, inhibitors, etc.

Many of these variables have been examined, and the results are summarized in a number of review papers [*5,10,13–16*].

Phenomenological Observations

Serious studies of the influence of environment on fatigue crack growth (vis-á-vis fatigue, per se) began in the mid-1960's and continued through the past decade [*5,10,13,14*]. Work during this period was concerned mainly with characterizing fatigue crack growth response and with examining the influences of the different variables on environment-enhanced fatigue crack growth. Development of mechanistic understanding was by and large by inference and was often incidental to the studies. The results from the various investigations have been reviewed in detail previously [*5,10,13,14*] and will not be repeated here.

It is important to note that crack growth is influenced by a broad range of loading variables, some of which can interact with the environment. Many of the observed effects of loading variables can be traced directly to environmental interactions [*5,10,13,14*]. On the basis of data gathered over the past 15 years, the steady-state response of fatigue crack growth to environments may be grouped into three basic types and may be discussed in relation to

K_{Iscc},[5] Fig. 1 [*10*]. Type A behavior is typified by the aluminum-water system. Environmental effects result from the interaction of fatigue and environmental attack [*5,10*]. Type B behavior is represented by the hydrogen-steel system [*18*]. Environmental crack growth is directly relatable to sustained-load crack growth, with no interaction effects [*5,10,18*]. Type C represents the behavior of most alloy-environment systems. Above K_{Iscc} the behavior approaches that of Type B, whereas below K_{Iscc} the behavior tends toward Type A, with the associated interaction effects. The transition between the two types of behavior is not always sharply defined.

Extensive work on the aluminum alloys (Type A behavior) indicates that practically all aluminum alloys are susceptible to environment-enhanced fatigue crack growth [*5,19,20*]. The environmental effect is a function of thickness or state of stress. There is no effect of frequency for crack growth in an inert environment and a small effect in fully saturated and aqueous environments. The effect of frequency can be very large in partially saturated environments and is related to the partial pressure of water vapor [*5,21,22*]. The influence of temperature can be quite strong and depends on the mechanical crack driving force, ΔK [*5,23*].

Work on Type B systems [*5,14,24–26*] indicates that fatigue crack growth in an aggressive environment depends on frequency, stress or stress-intensity

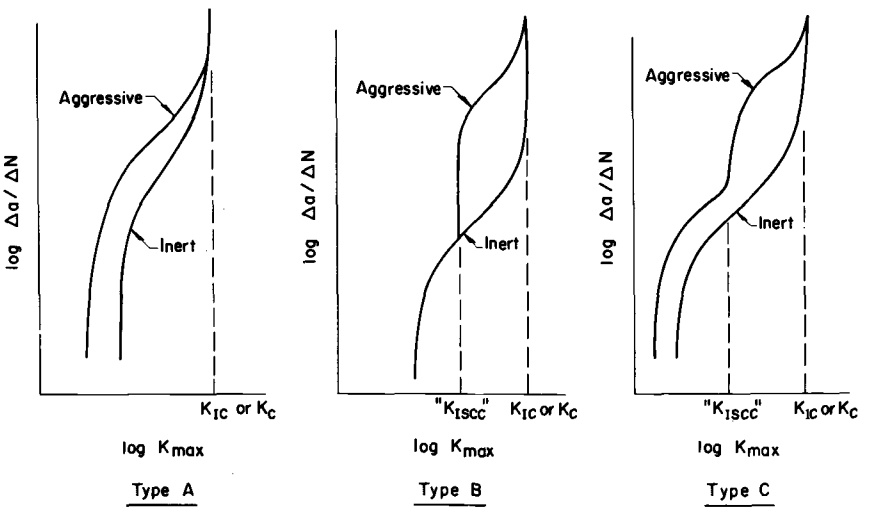

FIG. 1—*Types of fatigue crack growth behavior* [10].

[5] K_{Iscc} is the apparent threshold K level for stress-corrosion cracking and is defined as the asymptotic value of K as the rate of crack growth under sustained load approaches zero [*17*]. Environment-enhanced crack growth can and does occur below K_{Iscc} in fatigue, and K_{Iscc} serves only as a convenient line of demarcation.

level, stress ratio, and waveform. The influences of all of these loading variables may be accounted for, to a fair degree of approximation, by the simple superposition model proposed by Wei and Landes [*18*] which relates fatigue and sustained-load crack growth.

In studies by Barsom [*27*] and Gallagher [*28*], it was found that environment-enhanced fatigue crack growth below K_{Iscc} in certain steels (exhibiting Types A or C response) is a function of both frequency and waveform. Environmental effect was found to be nearly zero at high frequencies, reached a maximum at an intermediate frequency, and then showed a slight apparent decrease, or no decrease, with further reduction in frequency [*27,28*]. Environmental effect was observed only for certain waveforms (such as sine and triangle) and not for others (such as square waves) [*27*]. These waveform effects were not observed on an aluminum alloy tested in distilled water [*29*] or on a high-strength steel tested in water vapor [*30,31*].

In addition to the steady-state response, a number of nonsteady-state crack growth behaviors have been reported. Nonsteady-state behavior refers to cases in which the rate of crack growth differs from the steady-state rate for the prevailing K or ΔK, and is transitory in nature [*17*]. Nonsteady-state fatigue crack growth has been observed at the start of fatigue loading and following "prolonged" load interruption [*24*], and with changes in cyclic-load frequency [*31*] in high-strength steels. These nonsteady-state phenomena have been shown to be associated principally with fatigue crack growth in aggressive (corrosive) environments [*24,30,31*].

Although one had hoped to infer mechanistic understanding from these various studies, it became quite obvious by 1970 that the key issues were not being addressed and that the parallel though separate studies by researchers in chemistry, materials science, and mechanics were not adequate. A search for an integrated interdisciplinary approach was begun in earnest.

An Interdisciplinary Approach to Fatigue Studies

The search for an integrated interdisciplinary approach followed similar development in the area of sustained-load crack growth (or stress-corrosion cracking) and is based on the following premises gleaned from the available experimental data.

1. Environmental influences are superimposed on the basic process of fatigue and can be studied without the need for understanding the underlying mechanism for fatigue crack growth. (Note that the converse is not true in that verification of proposed mechanisms for fatigue cannot be made without properly accounting for environmental effects.)

2. The controlling processes (for example, surface reaction, diffusion) for crack growth under sustained load and in fatigue are expected to be essentially the same for a given material-environment combination.

3. The observed influences of loading variables, in the absence of creep,

are principally environmental effects. These effects relate to both steady-state and nonsteady-state responses.

4. Quantitative understanding of environment-enhanced fatigue crack growth requires a "link" between the kinetics of crack growth and the kinetics of the relevant controlling processes.

5. Quantitative understanding, in all likelihood, would require all relevant (chemical, mechanical, and metallurgical) experiments to be carried out on the same material under essentially identical environmental conditions to permit direct comparison.

The need to involve corrosion and surface chemists, material scientists, and fracture mechanicians becomes immediately obvious. By the same token, the key issues concerning the nature and kinetics of the controlling processes, and their influences on steady-state and nonsteady-state crack growth, can be readily identified. The difficulty now lies in establishing a "link" between the kinetics of crack growth and those of the relevant controlling process. This crucial link, however, became available through investigations on the kinetics of sustained-load crack growth [*17*]. These investigations showed that there is a stage of crack growth in which the rate is essentially independent of the mechanical driving force. This independence indicates that the rate of sustained-load crack growth is limited by the underlying controlling process, and provides an avenue for identifying the rate-controlling process by direct comparisons between the rates and activation energies for crack growth and for the various probable controlling processes.

As an illustration of this integrated interdisciplinary approach, results from recent studies of sustained-load and fatigue crack growth in an AISI 4340 steel in water/water vapor are described briefly [*31,32*].

An Illustration of the Interdisciplinary Approach

One of the key issues for crack growth in high-strength steels exposed to water/water vapor relates to the identity of the rate-controlling process for crack growth [*32*]; see Fig. 2. To address this issue, sustained-load crack growth experiments were carried out on an AISI 4340 steel in hydrogen and in water, to determine the kinetics of crack growth as a function of temperature. Using Auger electron spectroscopy (AES), companion experiments were carried out on the same steel to determine the kinetics of water-metal surface reaction. These studies were supplemented by detailed fundamental studies of reactions of water vapor with iron single crystal of known orientation by AES and low-energy electron diffraction (LEED) [*33*], and by AES analysis of the elemental composition of fracture surfaces produced by environment-assisted crack growth [*34*]. Through these coordinated interdisciplinary studies and comparisons of activation energies for crack growth and for surface reaction (see Fig. 3), the rate-limiting process for crack growth was identified as a slow step in the reaction of water/water vapor with iron

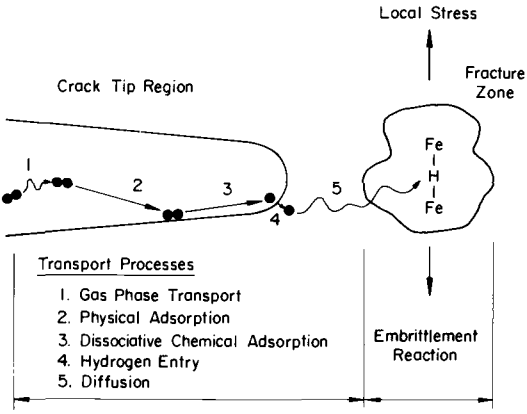

FIG. 2—*Schematic illustrations of various sequential processes involved in embrittlement by external gaseous environments. (Embrittlement reaction is depicted schematically by the iron-hydrogen-iron bond.)*

and possibly iron carbide (vis-á-vis hydrogen diffusion) [*32–34*]. This reaction step is associated with the nucleation and growth of oxide on the surface, and the presumed concomitant production of hydrogen [*32*].

After the rate-limiting process for crack growth was identified, its implication in terms of fatigue crack growth response was examined [*31*]. The effect of cyclic-load frequency on fatigue crack growth in water vapor at 585 Pa (4.4 torr) at room temperature is illustrated in Fig. 4, and the influence of changing frequency on crack growth response under constant-load-amplitude fatigue is illustrated in Fig. 5. These results confirm the existence of a significant effect of frequency at K_{max} levels well below that required for producing significant crack growth under sustained loads (that is, below K_{Iscc}) [*27,28*]. The extent of crack growth, following a change in frequency, that is required to reestablish steady state appeared to depend on the magnitude of the frequency change (for example, from 1 to 0.1 Hz versus 10 to 0.1 Hz) and on crack length or ΔK. Since frequency effect was absent in an inert environment [*5,30*], the observed transient phenomenon was attributed to interactions with the environment [*31*]. Fractographic examinations of fracture surfaces produced at the different loading frequencies showed that at high frequency (namely, 10 Hz) the morphology was akin to that for "pure" (mechanical) fatigue. At the lower frequencies (that is, below 1 Hz) the morphology exhibited increasing amounts of intergranular separation along prior-austenite grain boundaries that is typical for sustained-load crack growth in water/water vapor [*31,32*].

These observations, taken *in toto* and in conjunction with the earlier study on sustained-load crack growth [*32*], provided a rational basis for explaining environment-enhanced fatigue crack growth response in this case. Fatigue

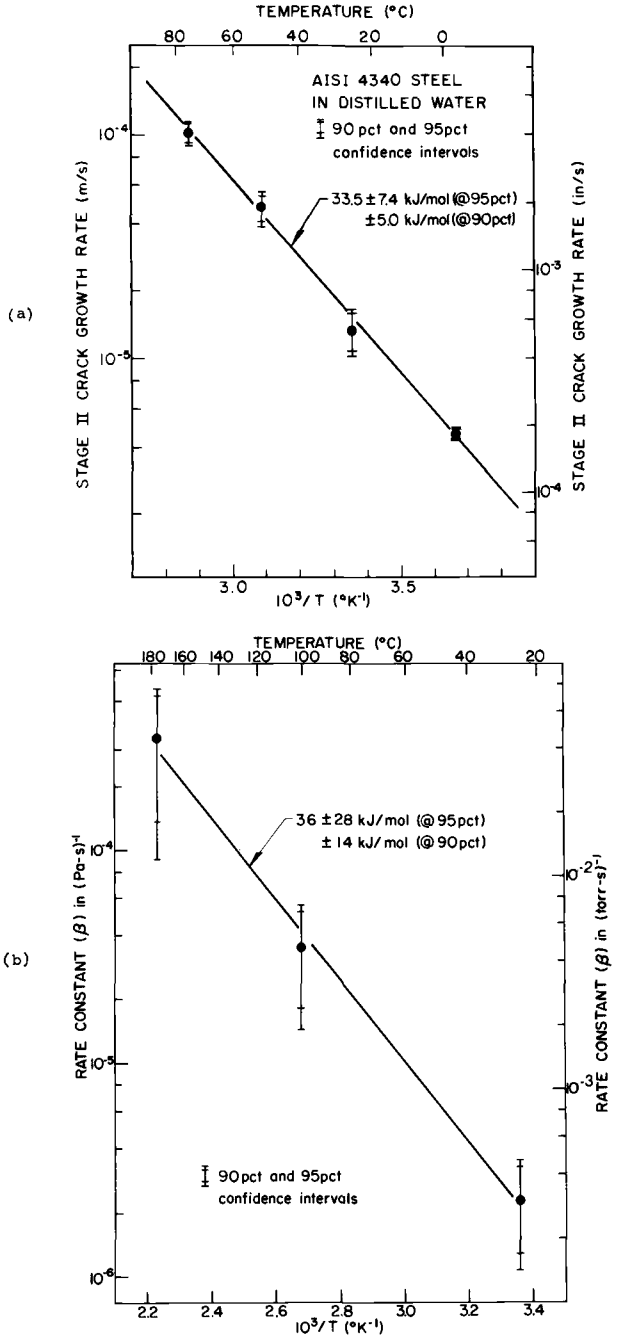

FIG. 3—*Correlation between* (a) *the kinetics of Stage II (rate-limited) crack growth under sustained load and* (b) *the rate of water vapor/metal (carbide) surface reaction for an AISI steel* [22]

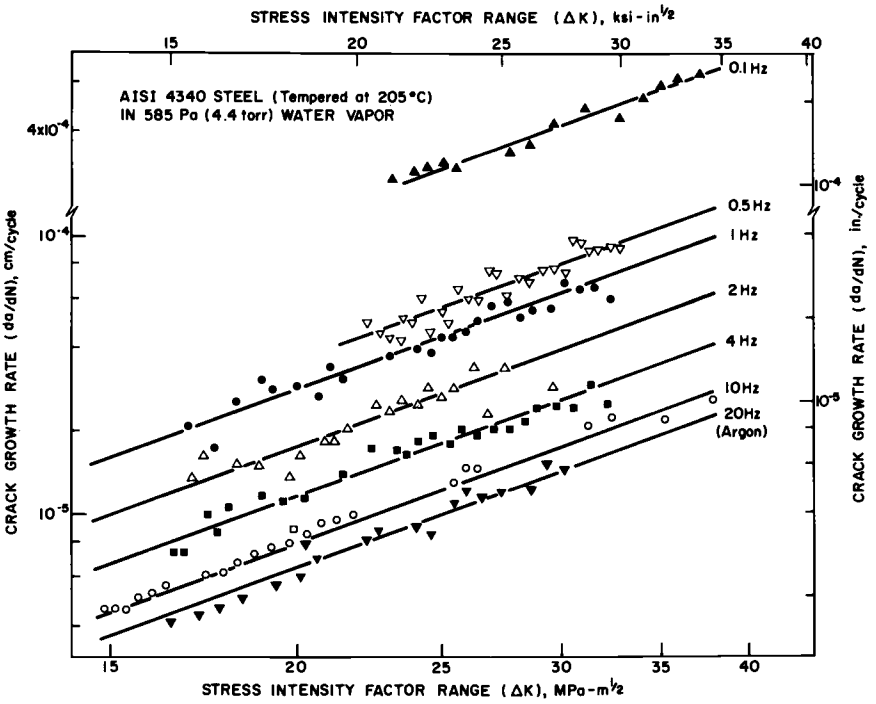

FIG. 4—*Room-temperature fatigue crack growth kinetics on AISI 4340 steel tested in dehumidified argon and in water vapor (below* K_{Iscc}*) at* R = *0.1* [31].

crack growth rate in an aggressive environment, $(da/dN)_e$, is considered to be the sum of two components—one for "pure" fatigue, $(da/dN)_r$, and one for the environmental contribution, $(da/dN)_{cf}$

$$(da/dN)_e = (da/dN)_r + (da/dN)_{cf}$$

More generally

$$(da/dN)_e = (da/dN)_r + (da/dN)_{cf} + (da/dN)_{scc}$$

$$= (da/dN)_r + (da/dN)_{cf} + \int_0^{\tau} [da/dt(K)]dt$$

where $(da/dN)_{scc}$ is the contribution by sustained-load crack growth at K levels above K_{Iscc} [*18*]. Environmental contribution is expected to involve a region of "embrittled" or "damaged" material ahead of the crack tip (that is, "volume embrittlement" vis-á-vis "surface embrittlement").[6] Because the

[6]Hydrogen embrittlement is considered to be the responsible mechanism, although the details of this mechanism are not understood [*31,32*].

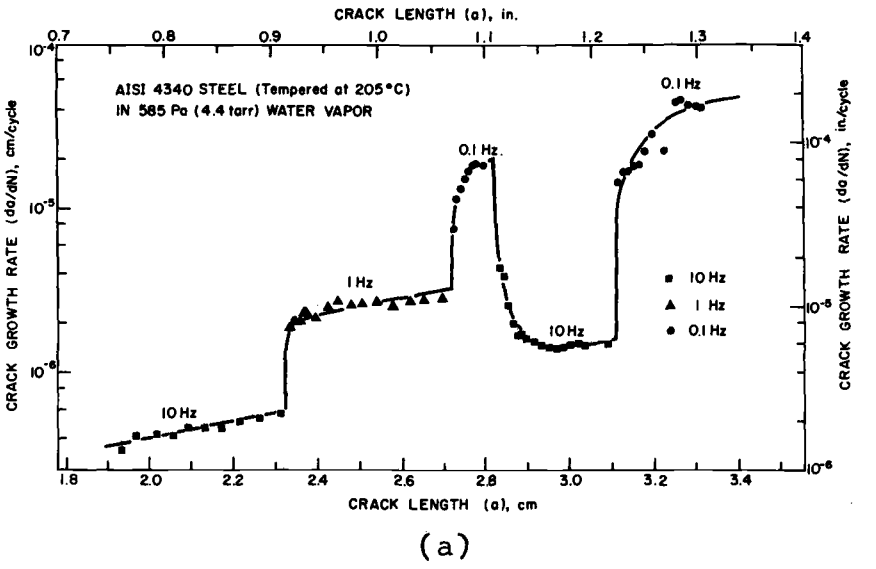

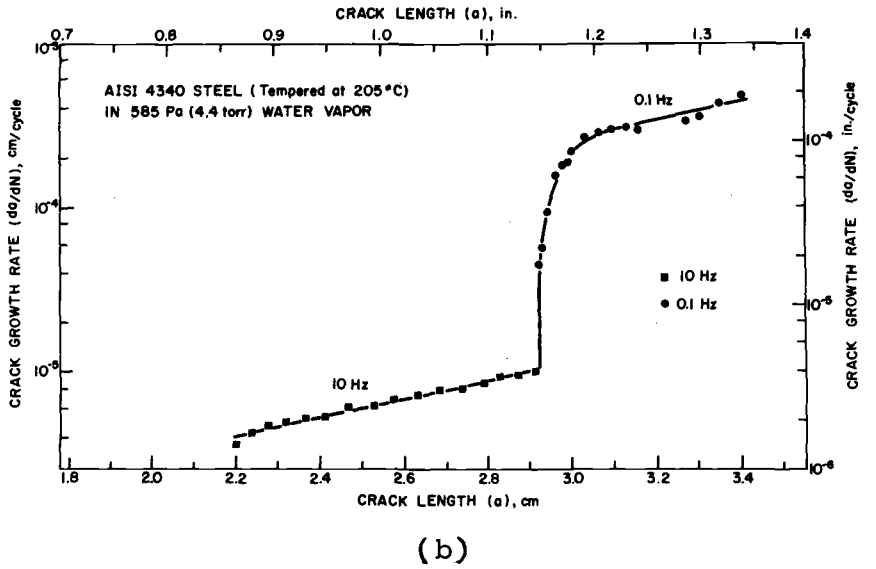

FIG. 5—*Room-temperature fatigue crack growth response resulting from changes in cyclic load frequency* [31]

rate-controlling process is that of surface reaction, the size of this region would depend on the time available for reaction (namely, cyclic load period) and on the reaction kinetics.

A conceptual model was suggested in which a steady-state zone of "embrittled" material existed ahead of the crack tip under steady-state conditions (that is, for prescribed ΔK, cyclic load frequency, and environment). This model is illustrated schematically in Fig. 6 [*31*]. The damaged or embrittled zone is depicted as circles, representing some appropriate hydrogen concentration contours ahead of the crack tip. Because more hydrogen is produced at the lower frequencies (longer exposure time), the size of the damaged zone or the hydrogen concentration within the zone is expected to be larger at these frequencies (Fig. 6). On each cycle of loading, the crack

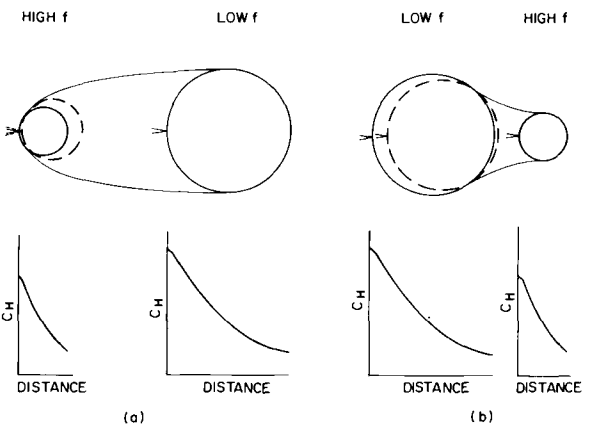

FIG. 6—*Schematic illustration of conceptual model for environment-enhanced fatigue crack growth below* K_{Iscc} [31].

would extend, in one step, through a fraction of this zone. Following this increment of growth, a steady-state zone is reestablished ahead of the new crack tip through reactions of the environment with the freshly created crack surface, and hydrogen diffusion and redistribution. The existence of environmental effects at K_{max} levels below K_{Iscc} in fatigue is not inconsistent with the definition of K_{Iscc} (defined for sustained loading), since fatigue is a more proficient process for producing fresh surfaces to react with the environment to produce the subsequent embrittlement.

The model appeared to be consistent with the experimental data on crack growth kinetics and with the kinetics of surface reactions (see Fig. 7) [*31,32*]. For the range of frequencies used in the fatigue experiments, at a water vapor pressure of 585 Pa, the surface reaction data suggested that the environmen-

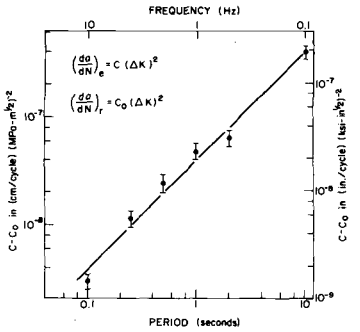

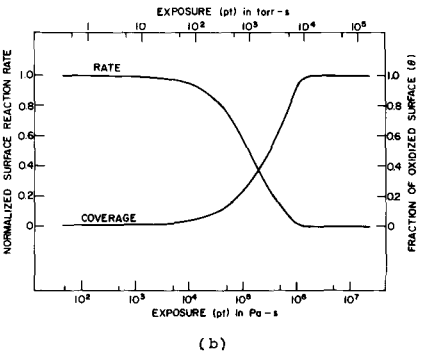

FIG. 7—*Comparison between* (a) *the environment-dependent component of fatigue crack growth as a function of cyclic load period and* (b) *the extent and normalized rate of reaction with water vapor as a function of exposure for an AISI 4340 steel at room temperature* [31,32].

tal contribution[7] should vary almost linearly with the cyclic load period or inversely with frequency (see Fig. 7*a*). At high frequencies, environmental effect should be essentially negligible; and at low frequencies, it should reach a maximum (or a saturation value). The general trend suggested by the model is consistent with data reported by Gallagher [*28*] for fatigue crack growth in HY-80 steel in 3.5 percent sodium chloride (NaCl) solution, by Vosikovsky [*35*] on an X-65 pipeline steel in sour (H_2S-containing) crude oil, and by Bradshaw and Wheeler [*21*] on an aluminum alloy in water vapor. In the latter two material-environment combinations, the surface reaction rates are expected to be 6 to 8 orders of magnitude faster than that of the water-iron reactions [*31–34*]. The model also provided a reasonable explanation for the

[7]The environmental contribution is represented by the difference between two empirical constants, C-C_o, determined by least-squares fit to the data in Fig. 4 using $da/dN = C\Delta K^2$ [*3*]. This empirical relationship provided a useful basis for representing these data, but does not have general validity.

observed nonsteady-state response associated with changes in cyclic load frequency (see Fig. 5) [*31*]. The nonsteady-state response was attributed to the process for establishing a new steady-state zone size following a change in loading frequency.

Summary

Work during the past decade has contributed significantly to the phenomenological understanding of environment-enhanced fatigue crack growth (or corrosion fatigue) and has brought greater recognition of the importance of this problem. As a result, corrosion fatigue is being considered explicitly in a diverse range of applications; for example, in aircraft structures, offshore structures, highway bridges, transmission linepipes, and coal conversion systems. It has also brought a recognition that quantitative understanding of this important phenomenon would require well-coordinated interdisciplinary approaches that can address the relevant chemical, mechanical, and metallurgical issues in concert. One such approach, incorporating fracture mechanics technology and modern surface analysis and metallurgical techniques, has shown considerable promise in developing understanding of environment-enhanced crack growth in gaseous environments [*31,32*]. Considerably more studies are needed to develop understanding in other material-environment systems, particularly for aqueous environments. Similar approaches need to be developed for understanding the processes of environment-assisted fatigue crack initiation.

The significant influence that environments (even those normally thought to be innocuous, such as moist air) can have on fatigue crack growth needs to be taken more seriously than before by those working on the mechanisms for fatigue crack growth. Since almost all of the proposed mechanisms do not explicitly include the influences of environment, one must be careful in selecting available data for use in model verification. By the same token, one should be extremely wary of generalizations concerning fatigue crack growth mechanisms that are formulated on the indiscriminate use of existing data.

Acknowledgment

Support of this work by the Office of Naval Research under Contract N00014-75-C-0543, NR 036-097, is gratefully acknowledged.

References

[*1*] *Mechanisms of Fatigue in Crystalline Solids, (Proceedings,* of International Conference, Orlando, Fla., 15-17 Nov. 1962), *Acta Metallurgica*, Vol. 11, 1963, pp. 639-828.

[*2*] *Fatigue—An Interdisciplinary Approach,* Syracuse University Press, Syracuse, N.Y., 1964.

[*3*] *Fatigue Crack Propagation, ASTM STP 415,* American Society for Testing and Materials, 1967.

[4] *Corrosion Fatigue: Chemistry, Mechanics and Microstructure,* NACE-2, National Association of Corrosion Engineers, 1972.
[5] Wei, R. P., *Journal of Engineering Fracture Mechanics,* Vol. 1, 1970, pp. 633–651.
[6] Hoeppner, D. W. and Krupp, W. E., "Prediction of Component Life by Application of Fatigue Crack Growth Knowledge," Report LR-25123, Lockheed-California Co., Burbank, Calif., 1972.
[7] Paris, P. C., *Fatigue—An Interdisciplinary Approach,* Syracuse University Press, Syracuse, N.Y., 1964, pp. 107–132.
[8] Johnson, H. H. and Paris, P. C., *Journal of Engineering Fracture Mechanics,* Vol. 1, No. 3, 1968, p. 3.
[9] Wei, R. P. in *Proceedings,* Conference on the Fundamental Aspects of Stress Corrosion Cracking, NACE-1, National Association of Corrosion Engineers, 1969, pp. 104–112.
[10] McEvily, A. J. and Wei, R. P. in *Corrosion Fatigue: Chemistry, Mechanics and Microstructure,* NACE-2 National Association of Corrosion Engineers, 1972, pp. 381–395.
[11] Wei, R. P. and Speidel, M. O. in *Corrosion Fatigue: Chemistry, Mechanics and Microstructure,* NACE-2 National Association of Corrosion Engineers, 1972, pp. 379–380.
[12] "Tentative Method of Test for Constant-Load-Amplitude Fatigue Crack Growth Rates Above 10^{-8} m/cycle," (ASTM E647-78T) American Society for Testing and Materials, 1977 (in the final stage of approval process).
[13] Achter, M. R. in *Fatigue Crack Propagation, ASTM STP 415.* American Society for Testing and Materials, 1967, pp. 181–204.
[14] Gallagher, J. P. and Wei, R. P. in *Corrosion Fatigue: Chemistry, Mechanics and Microstructure,* NACE-2, National Association of Corrosion Engineers, 1972, pp. 409–423.
[15] Hudson, C. M. and Raju, K. N., NASA TN D-5702, National Aeronautics and Space Administration, 1970.
[16] Schijve, J., "Fatigue Crack Propagation in Light Alloy Sheet Material and Structures," Report MP 195, National Aerospace Laboratory NLR, Amsterdam, The Netherlands, Aug. 1960.
[17] Wei, R. P., Novak, S. R., and Williams, D. P. in *Proceedings,* AGARD Conference No. 98, Specialists Meeting on Stress Corrosion Testing Methods 1971, and *Materials Research and Standards,* American Society for Testing and Materials, Vol. 12, 1972, p. 25.
[18] Wei, R. P. and Landes, J. D., *Materials Research and Standards,* American Society for Testing and Materials Vol. 9, No. 7, July 1969, p. 9.
[19] Feeney, J. A., McMillan, J. C., and Wei, R. P., *Metallurgical Transactions,* Vol. 1, 1970, p. 1741.
[20] Hartman, A. and Schijve, J., National Aerospace Laboratory NLR Technical Note MP 68001 U, Amsterdam, The Netherlands, 1968.
[21] Bradshaw, F. J. and Wheeler, C., *Applied Materials Research,* Vol. 5, 1966, p. 112.
[22] Hartman, A., *International Journal of Fracture Mechanics,* Vol. 1, 1965, p. 167.
[23] Wei, R. P., *International Journal of Fracture Mechanics,* Vol. 4, 1968, p. 159.
[24] Miller, G. A., Hudak, S. J., and Wei, R. P., *Journal of Testing and Evaluation,* American Society for Testing and Materials, Vol. 1, 1973, p. 524.
[25] Bucci, R., "Environment Enhanced Fatigue and Stress Corrosion Cracking of a Titanium Alloy Plus a Simple Model for Assessment of Environmental Influence of Fatigue Behavior," Ph.D. Dissertation, Lehigh University, Bethlehem, Pa., 1970.
[26] Landes, J. D., and Wei, R. P., *Journal of Engineering Materials and Technology, Transactions,* American Society of Mechanical Engineers, Series H, Vol. 95, 1973, p. 2.
[27] Barsom, J. M. in *Corrosion Fatigue: Chemistry, Mechanics and Microstructure,* NACE-2, National Association of Corrosion Engineers, 1972, pp. 424–436.
[28] Gallagher, J. P., "Corrosion Fatigue Crack Growth Behavior Above and Below K_{Iscc}," NRL Report 7064, Naval Research Laboratory, Washington, D.C., May 1970.
[29] Hudak, S. J., Jr. and Wei, R. P. in *Corrosion Fatigue: Chemistry, Mechanics and Microstructure,* NACE-2, National Association of Corrosion Engineers, 1972, p. 433.
[30] Hutin, J. P., "Sub-Critical Crack Growth in AISI 4340 Steel in Water and Water Vapor," M.S. Thesis, Lehigh University, Bethlehem, Pa., 1975.
[31] Pao, P. S., Wei, W., and Wei, R. P., "Effect of Frequency on Fatigue Crack Growth Response of AISI 4340 Steel in Water Vapor," *Proceedings,* Symposium on Environment

Sensitive Fracture of Engineering Materials, Chicago, Ill., 24-26 Oct. 1977, American Institute of Mining, Metallurgical and Petroleum Engineers, (to be published).
[32] Simmons, G. W., Pao, P. S., and Wei, R. P., "Fracture Mechanics and Surface Chemistry Studies of Subcritical Crack Growth in AISI 4340 Steel," *Metallurgical Transactions A*, Vol. 9A, 1978, p. 1147.
[33] Dwyer, D. J., Simmons, G. W., and Wei, R. P., *Surface Science*, Vol. 64, 1977, p. 617.
[34] Wei, R. P. and Simmons, G. W., *Scripta Metallurgica*, Vol. 10, 1976, p. 153.
[35] Vosikovsky, O., *Corrosion*, Vol. 32, 1976, p. 472.

DISCUSSION

R. Ebara[1] *(discussion)*—The author is to be congratulated for an excellent paper. I am very specially impressed that the author has been successfully developing an approach, incorporating fracture mechanics technology, modern surface analysis (AES, LEED), and metallurgical techniques, for a fundamental understanding of the corrosion fatigue mechanism. It has been proved in the author's recent works that such an approach is readily available for understanding environment-enhanced crack growth in gaseous environments. I believe that such an approach also holds the key for clarification of corrosion fatigue mechanisms in an aqueous corrosive environment.

In this discussion I would like to summarize surface and fracture surface appearances due to corrosion fatigue by surveying recently published papers, including the results of my own observations. These microscopic features are the results of the process of crack propagation, and its full understanding would seem to be helpful in applying an integrated interdisciplinary approach to the clarification of the corrosion fatigue mechanism.

It was clarified by scanning electron microscopy (SEM) observations that deformation in dry nitrogen is heavier at the crack tip of mild steel than deformation in air (Fig. 8).[2] It was also revealed by an optical microscopic observation of steels surfaces that the number of slip lines around the crack tip in air is fewer than in dry nitrogen (footnote 2). It is inferred from these results that crack propagation is associated with more plastic deformation in an atmosphere without oxygen or moisture or both than in air.

A couple of papers[3,4] describing the difference of plastic zone size at the crack tip due to the difference of environments can be found. The measured plastic zone size around the crack tip of pure iron (footnote 3) and 5083 aluminum alloy (footnote 4) in vacuum is larger than in dry air or moist air.

[1] Hiroshima Technical Institute, Mitsubishi Heavy Industries, Ltd., Hiroshima, Japan.
[2] Masumoto, I. and Ebara, R., *Journal of the Japan Welding Society*, Vol. 40, 1971, pp. 152-160.
[3] Ohta, A. and Sasaki, E., *Acta Metallurgica*, Vol. 20, 1972, pp. 657-660.
[4] Endo, K. and Komai, K., *Journal of the Japan Materials Science Society*, Vol. 26, 1977, pp. 143-148.

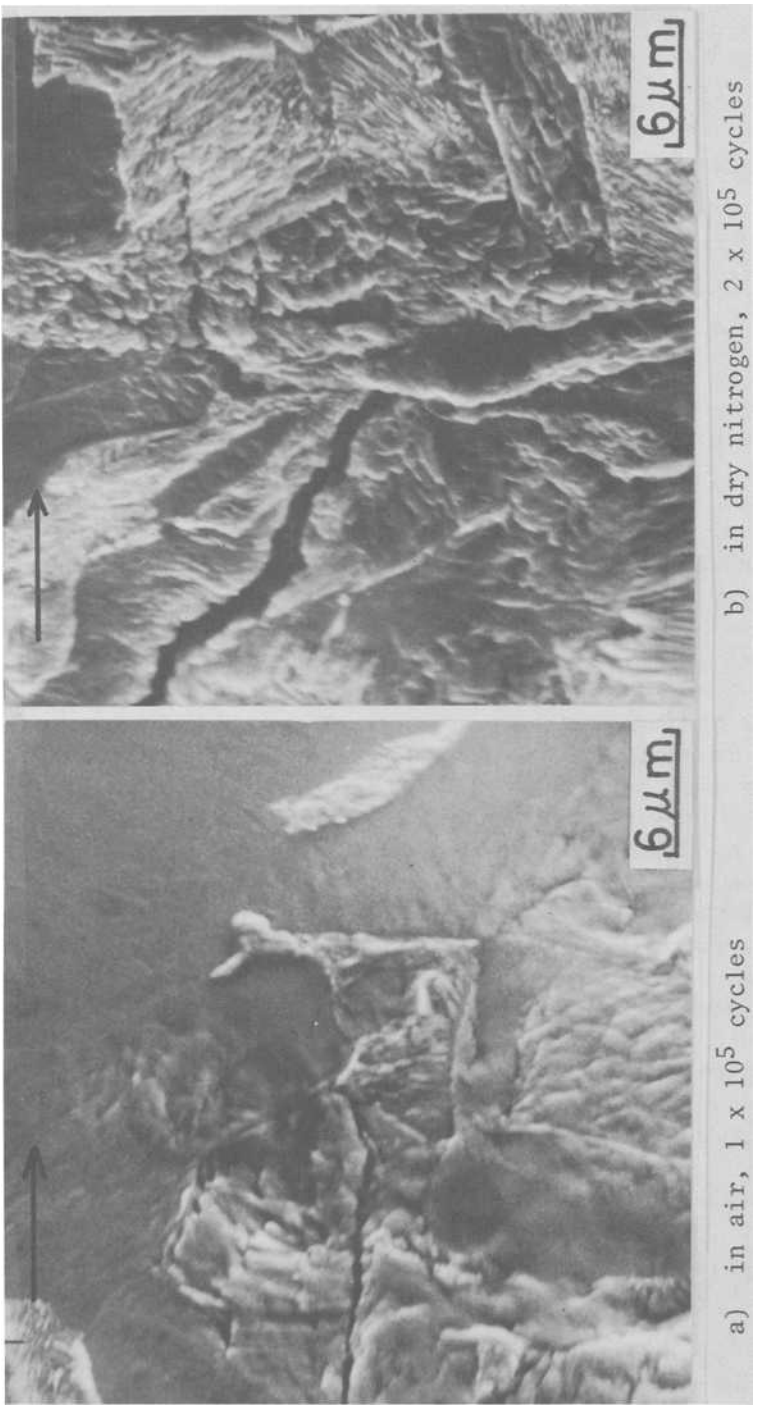

FIG. 8—*Electron micrographs in the vicinity of the fatigue crack tip of mild steel in air and dry nitrogen: alternating bending stress = 240 MPa; crack length = 1500 μm; arrow shows crack propagation direction (footnote 2).*

The plastic zone size decreases with decreasing stress or stress-intensity factor range (ΔK) in the same atmosphere. Its difference due to the environmental difference at same stress or ΔK decreases with decreasing stress or ΔK.

This phenomenon seems to imply that the influence of oxygen or humidity or both on fatigue life or crack propagation rate decreases with the decrease of stress or ΔK. To date it has not been clarified how embrittlement reaction influences the extent of plastic deformation at the fatigue crack tip. Quantitative determination of embrittlement size at the crack tip seems to be necessary for an evaluation of fatigue life or fatigue crack propagation rate in a corrosive environment.

As one of a number of noticeable surface phenomena, it has been recognized that the crack propagates along a transcrystalline path and winds near the pearlite in dry nitrogen, while the crack in air propagates almost straight along a transcrystalline path and occasionally through the pearlites.[5] The reason for this phenomenon has not been clarified yet; however, an explanation of the mechanism of the interaction between environment and microstructure is being sought.

There have been numerous observations by SEM of well-defined striations in air, while no striations, even ill-defined, have been observed in an atmosphere without oxygen or moisture or both.[6-9]

It has been shown also that in high-strength steels fractographical patterns change completely with the change of atmosphere. In 250G maraging steel, ductile striations were observed in dehumidified argon, while in dry and humidified hydrogen cleavage fracture appeared predominantly.[10]

Recent fractographic results on AISI 4140 steel by Shaw and Le May indicate that there is a strong interdependence between relative humidity, stress-intensity factor, and tempering temperature. The mechanism and mode of crack propagation is determined by all these factors.[11]

Frandsen and Marcus reasonably concluded from their experimental results on HP-9-4-20 steel that a transition from intergranular to transgranular fracture occurred when the reverse-yield plastic zone diameter was equal to the prior austenite grain size, since the extensive deformation surrounding the grain boundary and multiple slip required for grain boundary contiguity reduce the probability of hydrogen-assisted intergranular fracture.[12]

[5] Masumoto, I., Ebara, R., and Ueda, K., *Metal Construction and British Welding Journal*, Vol. 2, 1970, pp. 423-426.

[6] Bradshaw, F. J. and Wheeler, C., *International Journal of Fracture Mechanics*, Vol. 5, 1969, pp. 255-268.

[7] Pelloux, R. M. N., *Fracture*, Chapman and Hall, New York, 1969, pp. 731-744.

[8] Wahnhill, R. J. H., *Corrosion*, Vol. 30, 1974, pp. 28-35.

[9] Ebara, R. and McEvily, A. J., Jr, unpublished work.

[10] Spitzig, W. A., Talda, P. M., and Wei, R. P., *Engineering Fracture Mechanics*, Vol. 1, 1968, pp. 155-166.

[11] Shaw, W. J. D. and Le May, I., "The Influence of Environment on Fatigue," The Institution of Mechanical Engineers, 1977, pp. 93-100.

[12] Frandsen, J. D. and Marcus, H. L., *Scripta Metallurgica*, Vol. 9, 1975, pp. 1089-1094.

There is a paucity of fractographic data on engineering materials in an aqueous corrosive environment because of the heavy scale on the fracture surface. Recently, however, much attention has been focused on fractography on corrosion fatigue fracture surfaces. Misawa et al showed for 0.5Cr-0.5Mo-0.25V low-alloy steel that the percentage of intergranular facets is a function of stress-intensity factor (K); a percentage of intergranular facets increases with decreasing K.[13]

The same relationship between applied stress and fraction of intergranular fracture has been recognized in our recent results on 13Cr stainless steel in a sodium chloride aqueous solution.[14] It can also be seen in Fig. 9 that the fraction of intergranular fractures close to the initiation site is very small compared with that in the propagation region (footnote 14). This phenomenon in an agressive environment like sodium-chloride aqueous solution might be explained by the aforementioned (footnote 12) relationship between plastic

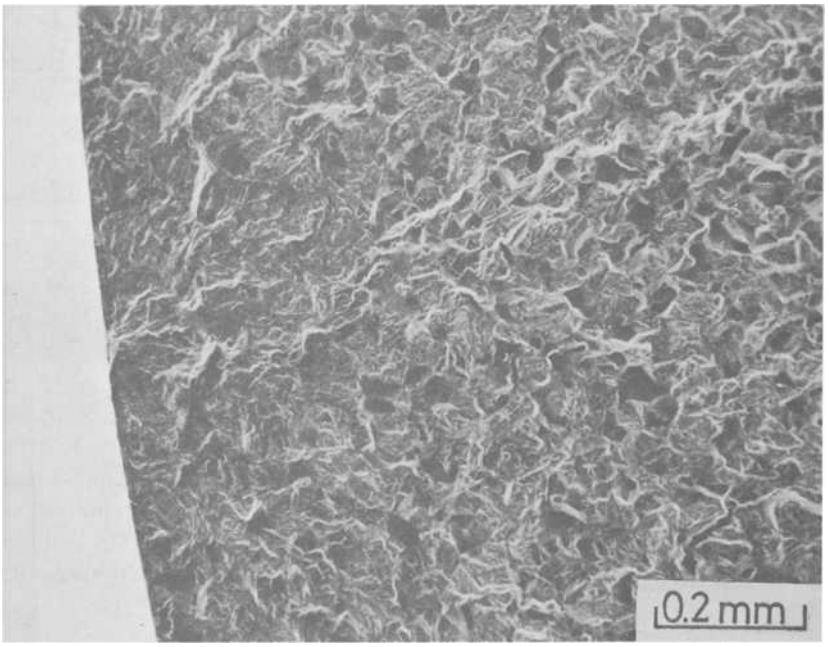

FIG. 9—*Intercrystalline fracture near the initiation area of 13Cr stainless steel in 0.03NaCl aqueous solution (footnote 14): rotating bending stress = 345 MPa; number of cycles = 9.5 × 10^5.*

[13] Misawa, T., Ringshall, N., and Knott, J. F., *Corrosion Science*, Vol. 16, 1976, pp. 805–818.

[14] Ebara, R., Kai, T., and Inoue, K., *Journal of the Japan Materials Science Society*, Vol. 27, 1978, pp. 64–68; also in *Proceedings*, 21st Japan Congress on Materials Research, 1978, pp. 89–92.

zone size at the crack tip and the prior austenite grain size. Considerable study will be needed to accumulate fractographical data at the low stress-intensity range.

There seem to be very few surface and fracture surface observation results of environmental effects on crack initiation. One of the characteristic features of corrosion fatigue is a corrosion pit at initiation. In our experiments, even in a very dilute environment of 3×10^{-4} percent sodium chloride aqueous solution, a subcrack associated with very small corrosion pits of approximately 1 μm was found on the surface of 13Cr stainless steel (Fig. 10).[15] A corrosion pit was found at the initiation site on the fracture surface and its depth was 10 to 20 μm notwithstanding the sodium chloride contents and stress amplitude (footnote 14). (See Fig. 11.) Not only the mechanism of pit formation but also the critical size of the pit dominating corrosion fatigue crack propagation should be clarified in detail.

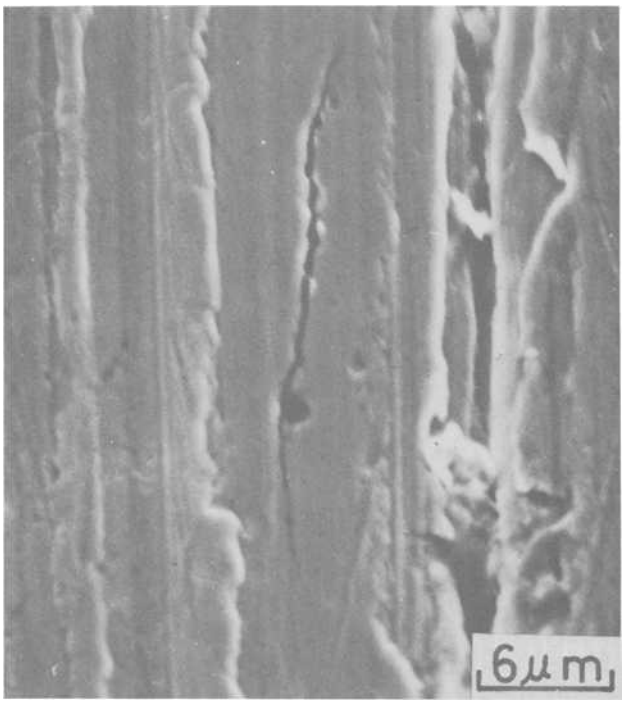

FIG. 10—*Subcrack associated with corrosion pits found on 13Cr stainless steel in* 3×10^{-4} *percent sodium chloride aqueous solution (footnote 15): rotating bending stress = 342 MPa; number of cycles* $= 6.3 \times 10^7$.

[15]Ebara, R., Kai, T., and Inoue, K. in *Corrosion Fatigue Technology, ASTM STP 642,* American Society for Testing and Materials, 1978, pp. 155–168.

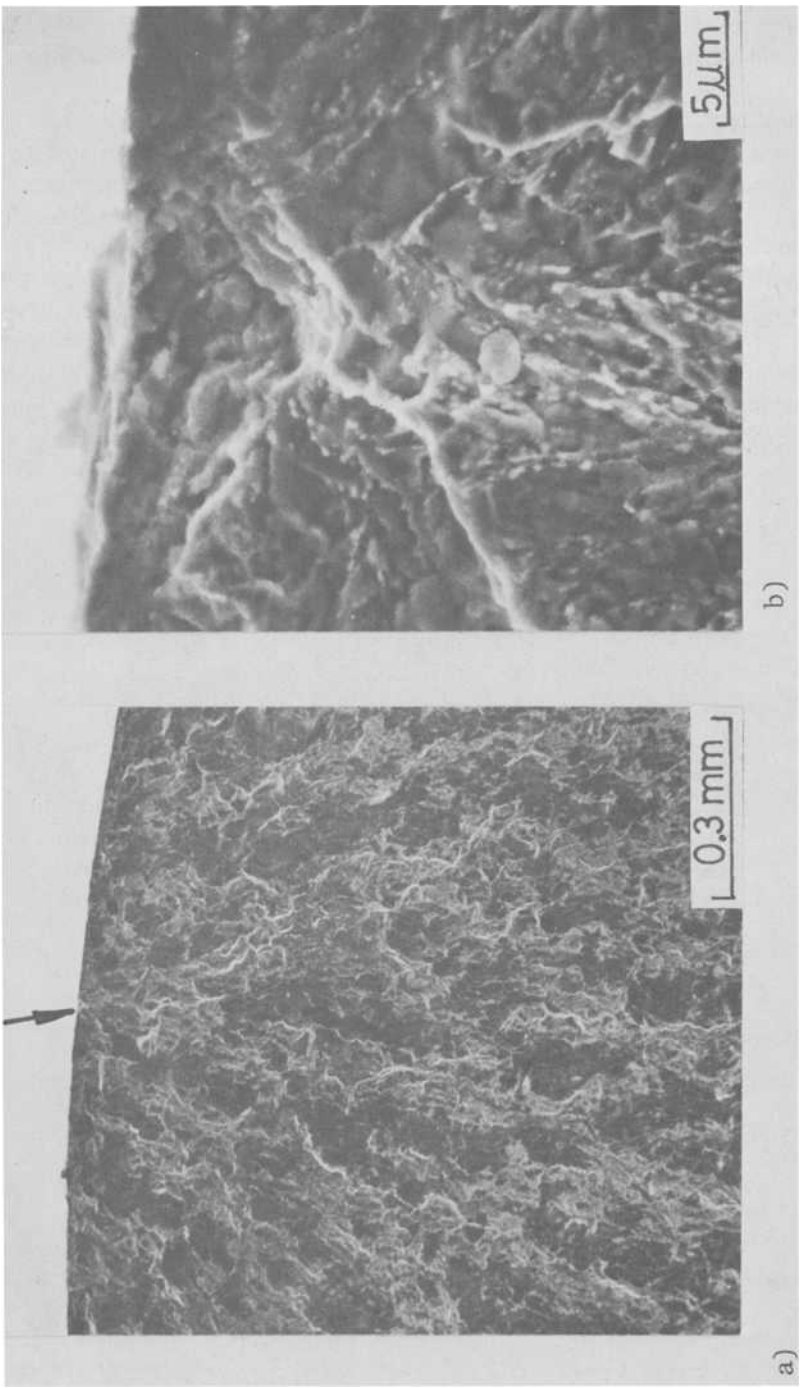

FIG. 11—*An example of corrosion pit found at the initiation area of 13Cr stainless steel in 0.03NaCl aqueous solution (footnote 14): rotating bending stress = 255 MPa; number of cycles = 1.4 × 10⁶.*

From an engineering standpoint, determination of long-life design stresses and improvement of corrosion fatigue strength are most important. Extensive integrated interdisciplinary research should be conducted to clarify corrosion fatigue mechanisms of engineering materials.

J. Kruger[16] (*discussion*)—Professor Wei has provided us with a very perceptive view on how environment-enhanced fatigue should be approached. There is no doubt in my mind or, indeed, in the opinion of most broad-thinking modern workers in the field that an appreciation of the interplay of chemistry, metallurgy, and fracture mechanics is absolutely essential in gaining an understanding of the mechanisms (note plural) of fatigue. Professor Wei and his colleagues have provided us with very important examples of how one goes about bringing these disciplines together in a significant way. My few comments are directed toward a few issues that would probably have been included in the paper were there more time and space available. These issues are crack initiation, passive film ductility, and electrochemical considerations.

Crack Initiation

Although this paper is concerned only with crack growth, and most fracture mechanics techniques eliminate the initiation stage, it would have been useful in terms of providing a perspective to discuss the initiation stage in terms of our understanding, or gaps in our understanding, of fatigue. For example, Brown[17] pointed out a number of years ago that a special environment develops in a growing crack. How does a special environment develop, or is it necessary for a special environment to develop, on a metal surface prior to crack initiation? Parenthetically, the development of special environments in the crack should have been discussed or mentioned in this paper.

Passive Film Ductility

This is an issue that Vermilyea[18] called attention to for stress corrosion cracking (SCC). Since passive film rupture is as involved in fatigue as in SCC film ductility affects the possibility for film rupture. A cyclic stress on a ductile film may produce different effects than a sustained stress. It would be interesting to look at the fatigue of tantalum, a metal which forms a ductile film and one that does not suffer SCC readily.

[16] Chemical Stability and Corrosion Division, Center for Materials Science, National Bureau of Standards, Washington, D.C. 20234.

[17] Brown, B. F. in *Theory of Stress Corrosion Cracking of Alloys*, J. C. Scully, Ed., North Atlantic Treaty Organization, Brussels, Belgium, 1971, p. 197.

[18] Vermilyea, D. A. in *Proceedings*, International Conference on Stress Corrosion Cracking and Hydrogen Embrittlement of Iron Base Alloys, Association of Corrosion Engineers, Houston, Tex., 1978.

Electrochemical Considerations

The system chosen for study by Prof. Wei, high-strength steel in water vapor is not very suitable for examining electrochemical considerations. For more conductive environments these considerations become very important regardless of whether the mechanism of crack growth depends on metal dissolution or hydrogen embrittlement. A more complete understanding of fatigue requires consideration of the role of electrochemical potential, exchange current densities, the relation of the kinetics of anodic film growth during repassivation to the kinetics of dissolution or hydrogen production (see Ambrose and Kruger[19]), and other electrochemical issues.

P. Neumann[20] (*discussion*)—You very carefully looked at the frequency effect and, because of experiments that we were running, I would like to know whether you also tried to find out in which part of the cycle the time is really needed to make the effect. In other words, did you try to find whether hold times in tension or in compression make a significant difference? This might tell you something about the mechanism.

N. Dowling[21] (*discussion*)—I would like to have the question answered that the first discusser (Dr. Ebara) asked about the relationship between the plastic zone size and the distance involved in the chemical reaction.

I. Le May[22] (*discussion*)—My comment is on the role of relative humidity instead of partial pressure as an important parameter in the study of environment-enhanced fatigue crack growth. I have some data on 4140 steel where I show crack propagation rate versus (1) relative humidity and (2) moisture content at a constant relative humidity so that at 10 and 40 percent relative humidity you have in fact the critical phenomenon defined by relative humidity and not necessarily the partial pressure. Would you like to comment?

R. Stephens[23] (*discussion*)—My question has to go back to interaction influences again. I know you have done research on this and it just seems to me that under variable-amplitude spectra the results in a corrosive environment may be even more drastically different than air results. Would you have some comments on that?

R. P. Wei (*author's closure*)—I appreciate the thoughtful comments and

[19] Ambrose, J. R. and Kruger, J., *Journal of the Electrochemical Society*, Vol. 121, 1974, p. 599.

[20] Max-Planck-Institut fur Eisenforschung Gmbh, Dusseldorf, Germany.

[21] Westinghouse Research and Development Center, Pittsburgh, Pa. 15235.

[22] Department of Mechanical Engineering, University of Saskatchewan, Saskatoon, Canada.

[23] Materials Engineering Division, University of Iowa, Iowa City, Iowa.

questions of Drs. Ebara, Kruger, Neumann, Dowling, Le May, and Stephens on my paper. The main purpose of the paper is to reemphasize the need for multidisciplinary approaches to the understanding of environment-enhanced fatigue crack growth (corrosion fatigue) in a quantitative way, and to describe and illustrate one such approach. As such, it is incomplete, inasmuch as our understanding of the problem is incomplete. Nevertheless, I believe that encouraging results have been derived by using this approach, and hope that others will also be encouraged to adopt similar approaches to address this highly complex, but important, engineering and scientific problem. Within this context, let me now try to respond to the specific issues and questions raised by the discussers.

Dr. Ebara has pointed out the role of metallographic and fractographic techniques in understanding corrosion fatigue, and has given a summary of some of the important recent findings. This aspect was not emphasized in my paper and I appreciate this addition by Dr. Ebara. Two specific points are raised by Dr. Ebara. The first one deals with the influence of environment on plastic deformation, and the second relates to the interaction of environment with microstructure. On the first question (seconded by Dr. Dowling), our results on AISI 4340 steel tested in water vapor suggest the presence of a "hydrogen damaged" zone ahead of the crack tip. The size of this zone is estimated to be of the order of 0.1 to 1 mm, which is substantially larger than the formally calculated cyclic plastic zone size and the relevant microstructural dimensions. One can indeed rationalize the influence of environment on plastic deformation that takes place within this "damaged" region. The interaction of environment with microstructure is also expected to take place within this region and can be similarly rationalized. This second point, however, would require understanding at a different level and would require contribution from researchers other than those already involved (for example, solid-state physicists). The interpretation of fracture path or morphology, I suspect, is not as straightforward as one likes to believe; and one should do so with considerable caution and with support from other independent physical measurements. I agree with Dr. Ebara that the mechanistic questions have not been answered satisfactorily up to now and that considerably more work needs to be done. Metallographic and fractographic methods undoubtedly should be included as a part of the investigative tools.

Dr. Kruger raised three important points which, I agree, would require additional attention. We have chosen to study crack growth in gaseous environments, initially, to simplify experimental problems and interpretation. We recognize that corrosion fatigue (more generally, environment-enhanced cracking) in aqueous environments is of great practical significance, for which electrochemical considerations become important. We believe an approach similar to that outlined in the paper is needed and plan to pursue the electrochemical questions in the next phase of our research. I cannot really do justice to the other two points, and would simply offer a few observations.

Initiation is a very difficult topic, particularly when few people can agree on its definition (that is, the problem of "crack" size at initiation). No doubt special environmental conditions are associated with steady-state crack growth in aqueous environments. Such conditions may also be associated with or be required for initiation. Special conditions, however, are not essential for all environments, since cracking in water vapor and other gaseous environments does not appear to involve any special conditions. The importance of passive film ductility has been considered principally when "thick" films are presumed to be involved, such as, in the case of stress corrosion cracking of brass, in ammonia. Our results indicate that passive film associated with corrosion fatigue in water/water vapor is only 1 to 2 atomic layers in thickness. When such thin films are involved, the concept of film ductility (a macroscopic concept) may not be applicable and needs to be reexamined.

To answer Dr. Neumann's question, we really cannot tell precisely when environment-enhanced crack growth takes place during a given loading cycle, since growth per cycle is typically of the order 10^{-7} to 10^{-4} cm and is well below the resolution limits of most, if not all, crack length measurement techniques. The experiments that we do, of necessity, are done only in tension-tension fatigue. Our belief is that the enhancement is due to a buildup of hydrogen ahead of the crack tip during the prior cycle so that the environment effect is a manifestation of a crack "jump" during the loading portion of the cycle, and hold time, if you are below the stress corrosion threshold, will have no effect.

Dr. Le May raised an interesting point. Without benefit of his illustrations, I can comment only generally. Our fatigue experiments were carried out in pure water vapor, and we had been able to correlate our crack growth data with surface reaction kinetics. Dr. Le May and his co-worker suggest that crack growth rate may depend on relative humidity rather than partial pressure of water vapor. If their experiments were carried out in moist air, the data may well reflect the combined influence of oxygen and water vapor, since we know that the presence of oxygen can alter the kinetics of reaction with water vapor.

Dr. Stephens's question does not have a simple and universal answer. The environment influence can be either negative or apparently positive under spectrum loading (that is, can either degrade or apparently improve fatigue life) depending on the material-environment system.

Let me express my appreciation to the discussers for their thoughtful and stimulating comments and questions, and I look forward to a continuing collaboration with research workers on this subject for many years to come.

D. W. Hoeppner[1]

Model for Prediction of Fatigue Lives Based Upon a Pitting Corrosion Fatigue Process

REFERENCE: Hoeppner, D. W., **"Model for Prediction of Fatigue Lives Based Upon a Pitting Corrosion Fatigue Process,"** *Fatigue Mechanisms.* Proceedings of an ASTM-NBS-NSF symposium, Kansas City, Mo., May 1978, J. T. Fong, Ed., *ASTM STP 675,* American Society for Testing and Materials, 1979, pp. 841-870.

ABSTRACT: The pitting corrosion fatigue process is postulated to be a possible environment/deformation synergism that might explain the initiation of Mode I cracking in materials subjected to the combined action of environment and alternating strain. A conceptual model for such a process is presented that involves utilization of an empirical pitting rate curve and a Weibull fit of the appropriate crack growth data. An experimental technique for observing the growth of pits under cyclic loading is described. Some shortcomings of the conceptual model and needs for additional research are discussed.

KEY WORDS: corrosion fatigue, crack energy, fatigue, fracture mechanics, initiation, kinetics, modeling, pitting, threshold

A large number of studies have been conducted and reported in the literature related to mechanism(s) of fatigue "initiation" or "propagation" or to both. It is now clear that many processes of physical deformation can be involved in the fatigue behavior of materials. This paper deals with one such process, namely, pitting corrosion fatigue. A conceptual physical model to explain the process of this insidious failure mode is presented in terms of physical events that subsequently can be mathematically described in order to calculate the time (cycles) to fatigue failure, or alternately to calculate the time (cycles) to a defined physical event in the development of fatigue failure. Predictions of the model compare favorably with some corrosion fatigue data for 7075-T6 aluminum.

The utility of the model is its potential usefulness in estimating total

[1]Cockburn professor of engineering design, Department of Mechanical Engineering, University of Toronto, Toronto, Canada.

fatigue life for pre-Mode I cracking and Mode I crack growth. The basic features of the model are as follows:

1. Use pitting rate theory to predict the number of cycles required to generate a pit that is large enough for a Mode I fatigue crack to develop at the pit.
2. The size of pit, at a given stress condition, at which a Mode I crack will form is determined from the Mode I fatigue crack growth threshold.
3. The Mode I fatigue crack growth threshold is determined from numerically fitting fatigue crack growth data for specific boundary conditions.
4. Determine the number of cycles to propagate from a Mode I crack to fracture using fatigue crack growth prediction methodology.
5. Sum the cycles to failure for the total fatigue life.

Aside from its use for fatigue life prediction, this model also is a means whereby quantitative comparisons of materials operating under corrosion fatigue can be made based upon the quantitative assessment of differences in either pitting behavior or fatigue crack growth behavior or both. Thus, quantitative studies of pitting corrosion fatigue mechanisms will be possible.

The following sections present the model and an experimental procedure for observing the growth of pits under cyclic loadings.

Background

During the past 30 years the development of linear elastic fracture mechanics (LEFM) has been very rapid. The application of LEFM and other areas of fracture mechanics to fatigue offers the attractive feature of dealing quantitatively with the "cumulative damage" (that is, crack extension) during the fatigue process. The principal quantities of interest in applying fracture mechanics to fatigue are the initial flaw size, applied load, location of the flaw with respect to the stress field, environment, load spectrum and frequency, and the properties of the material of interest. In this case, the properties of interest are the fatigue crack growth threshold (K_{th} or K_o), the crack instability parameter, K_{1b}, and the fatigue crack growth *curve* for the material(s) of interest for the conditions of interest. The apparent relative simplicity of fracture mechanics as a useful tool for dealing with the physical aspects of fatigue has, however, a concomitant difficulty. This difficulty is associated with the initial flaw.

Many investigators have classified the fatigue process as comprising three stages, namely, initiation, propagation, and final fracture. On numerous occasions, an attempt has been made to ascertain the quantitative meaning of researchers when they refer to fatigue crack initiation [*1-5*].[2] Some papers have been published related to either the

[2]The italic numbers in brackets refer to the list of references appended to this paper.

concept of fatigue crack initiation or a model for fatigue crack initiation. Very few authors, if any, have attempted to characterize "fatigue crack initiation" in terms of a flaw size for a given physical process. It has frequently been discussed in the literature that subsequent to the attainment of a given flaw size (fatigue crack initiation) one need simply apply fatigue crack growth concepts based on LEFM to "predict life."

It is now generally recognized that fatigue of a member (specimen or structure) occurs as the result of either microplastic flow or constraint to flow or both. The physical flow or fracture processes that may lead to the development of a Mode I (Forsyth—Stage II; see Ref *6*) fatigue crack are slip, twinning, cleavage, grain boundary flow or fracture, phase boundary flow or fracture, and particle boundary flow or fracture [*4,6*]. Aside from time-dependent synergisms that occur with cyclic loading, one of which is the subject of this paper, these physical deformation processes occur at either an inherent continuum discontinuity (notch, scratch, blowhole, pore, etc.) to create fatigue crack extension or they are the processes that may lead to the development of a Mode I crack to which the principles of LEFM or generalized fracture mechanics may be applied. Thus, it is generally recognized that even though a continuum flow may not be favorably located and of sufficient size for fatigue crack extension from the flaw, a fatigue crack can initiate at another point from pure deformation or localized fracture from point or line defect motion or interaction [*7*]. Since fatigue cracks may therefore be developed without the presence of a continuum flaw, the many methods of potential nucleation must be dealt with in order to formulate fatigue-resistant materials and structural/environmental systems.

Many synergisms for accelerating, or generating, the fatigue process are possible [*8,9*]. In this brief paper, only one will be dealt with as it relates to fatigue. Pitting *corrosion fatigue* is one of the most insidious of the synergisms that can occur [*1,5-7*]. However, very little is understood relative to the kinetics of corrosion fatigue. More understanding is required to develop materials, to formulate prospective and retrospective corrosion fatigue resistant design methodology, and to understand the *mechanisms* of fatigue in a universal sense.

There are, of course, many types of corrosion that can interact with cyclic loading to produce the corrosion fatigue synergism. One of the corrosion mechanisms is pitting corrosion [*1,10*], for which there is very little information in the literature. At a recent ASTM Symposium on Corrosion Fatigue Technology (*ASTM STP 642*) two papers were presented that considered the development of corrosion fatigue from a corrosion/mechanical load synergism. A paper by Van der Horst [*11*] dealt with corrosion fatigue initiated by stress corrosion cracking and thus is not directly relevant to this work except that conceptually it has similarities. The other paper, by Kitagawa et al, dealt more specifically with the nucleation of fatigue cracks at corrosion fatigue-induced pits [*12*]. They showed that probabilistic

concepts could be employed to predict the corrosion fatigue process. This latter reference is the only one in the literature of corrosion fatigue that relates to formulating a prediction of corrosion fatigue life based upon the observation of physical crack size. As with the present paper, Kitagawa et al had to employ the rationale of fracture mechanics in formulating the analysis methodology. This effort was indeed noteworthy, since following the dictates of the physical fatigue process these authors attempted to formulate a method of prediction of corrosion fatigue lives by coupling reliability concepts with fracture mechanics to yield a graphical display. The present paper provides a slightly different approach to the problem.

Herein, therefore, we shall review a conceptual model of corrosion fatigue and apply the knowledge of pitting corrosion to predict when a crack depth, a_o, will be achieved that will yield a value of stress intensity such that the threshold for fatigue crack growth (K_{th}) will be achieved. Subsequent to the presentation of the model, results of experiments that have been completed will be presented. Concepts similar to these have been developed related to fretting fatigue [*12-14*] and pure fatigue [*4*] and this paper is intended to illustrate the versatility of the concept.

Review of Model

In Ref *1* a conceptual model for the corrosion fatigue process was presented and its essential elements are as follows:

1. Corrosive attack under cyclic loading,
2. Generation of Mode I fatigue crack of observable size,
3. Environmentally enhanced Mode I fatigue crack growth (the opposite is possible),
4. Stress-intensity-dominated fatigue crack growth (Modes I, II, or III), and
5. Unstable fracture.

Pitting corrosion fatigue was initially selected for verification of the model of corrosion fatigue since it physically has all five of the foregoing components. Component 1 can be the *initiation* of pitting corrosion due to the material/environment/cyclic loading combination. Thus, by applying the knowledge of pitting theory it should be possible to ascertain the amount of time (number of cycles) to propagate a corrosion fatigue pit to become a Mode I crack for the crack-type/loading combination. In order to accomplish this prediction, the fatigue crack growth threshold of a Mode I fatigue crack in the material must be known. Thus, the cycles to propagate a pit to a dimension adequate to initiate a Mode I fatigue crack at a pit can be determined. In a practical case, the Mode I crack then can grow to become an observable (inspectable) crack. It is a known fact that fatigue cracks usually initiate well before they are "observable." Subsequently, if

the load is known, it is possible to predict the fatigue crack growth life if a prediction methodology exists and the crack growth parameters are known. Fortunately, these methods are well established [*2*]. The exact fitting of the fatigue crack growth data remains a subject of study. However, it appears that utilization of the Weibull survivorship function [*15-18*] is an effective way to describe fatigue data since the data appear to be distributed on a Weibull basis [*15-19*]. The foregoing point is attained when the fracture toughness, K_{Ic}, or other suitable measure of crack instability is attained (da/dN approaches infinity in the limit). Thus, *initiation* of final fracture (crack instability) occurs when the crack reaches sufficient size at a given load level.

The fitting power of Weibull's relation lies in part in the fact that it fits the physical processes and relates to the physical boundary conditions. A power of the Weibull function also lies in its discriminating power of an effect of a variable on fatigue life. A brief review of fatigue crack growth curve fitting is given since it is an essential part of the model.

Fatigue Crack Growth Curve-Fitting Relations

It is usual to plot fatigue crack propagation test results in the form

$$Da/DN = f(\Delta K) \tag{1}$$

where Da/DN is the crack propagation rate and ΔK the stress-intensity range. A suitable curve-fitting relation for this type of application is one with a mathematical fit to the total physical behavior of fatigue crack growth. This relation must have the following properties [*12,15*]:

1. The relation should lend itself to distinction between slow and fast crack growth rate segments.

2. As K approaches an upper limit, K_b, the crack growth rate should increase indefinitely

$$\lim_{\Delta K/K_b \to 1} \left\{ \frac{Da}{DN} \right\} = \infty \tag{2}$$

3. As K approaches a lower threshold limit, K_{th}, the crack growth rate should diminish to zero

$$\lim_{\Delta K \to K_{th}} \left\{ \frac{Da}{DN} \right\} = 0 \tag{3}$$

A new class of exponential curve-fitting relations with mathematical

form in the fatigue data reduction Weibull distribution function has been explored recently. Three members of the class are

Type	Relations	
(A)	$1 - F = \exp\left[-\left(\frac{H - e}{v - e}\right)\right]^k$, or $H = e + (V - e)\lvert(-\log_e(1 - F))\rvert^{1/k}$	(4)
(B)	$1 - F = \exp\left[-\left(\frac{\log_e(H + 1) - e}{v - e}\right)^k\right]$, or $H = -1 + \exp(e + (v - e)[(-\log_e(1 - F))]^{1/k})$	(5)
(C)	$1 - F = \exp\left[-\left(\frac{\log_e \log_e [H + \exp(1)] - e}{v - e}\right)^k\right]$, or $H = -\exp(1) + \text{expexp}(e + (v - e)[-\log_e(1 - F)]^{1/k})$	(6)

These relations meet the three criteria of acceptability previously stated. The fitting routine contains logic for estimating the curve-fitting parameters k, e, and v by a combination of linear regression and correlation coefficient optimization. In practice, Da/DN and ΔK values of a data set are stored as one-dimensional arrays. The regression analysis is performed on variables X and Y, in terms of the equation of regression

$$(-\log_e Y)^w = bX + a \tag{7}$$

which has alternative form

$$Y = \exp\left(-\left[\frac{X - e}{v - e}\right]^k\right) \tag{8}$$

where

$k = 1/w$,
$e = -a/b$, and
$v = (1 + be)/b$.

The following operations are performed, for example, when applying candidate Type B curve fitting

DO $i = 1$ TO N
$X = \log_e [DaDN(i) + 1]$

$$Y = [- \log_e (1 - dK(i) / K_b))^w$$

. .

. .

Regression and Correlation Coefficient Logic

. .

END

In this case, the routine yields the Type B relation

$$1 - \Delta K / K_b = \exp \left[- \left(\frac{\log_e (Da/DN + 1) - e}{v - e} \right)^k \right] \tag{9}$$

where

$\Delta K / K_b = F$, and
$Da/DN = H$.

Parameter K_b is the stress-intensity range where Da/DN is indefinitely large. Estimation of K_b requires exercise of judgment in addition to interactive computing effort. At the outset of data set analysis, all three types of exponential curve-fitting relations are tested, with $F = \Delta K / K_b$ and $H = Da/DN$ for each type. Relative "goodness of fit," based on an evaluation of the correlation coefficients, is used in deciding which type, if any, is suitable. For all three types, the particular stress-intensity range where $Da/DN = 0$ is called the threshold stress intensity, K_{th}, where

$$K_{th} = K_b \left(1 - \exp \left(- \left(\frac{-e}{v - e} \right) \right)^k \right) \tag{10}$$

Physical significance is attached to threshold K_{th} for cases where threshold parameter $e \leq 0$.

1. For $e = 0$, $K_{th} = 0$.
2. For $e < 0$, $K_{th} > 0$.
3. For $e > 0$, the suggestion is that crack growth begins at some $Da/DN > 0$ for arbitrarily small $\Delta K > 0$.

In Ref *19* we discuss some further results on the formulation of measures of "goodness of fit" for Weibull distributions. Some of these results have also been discussed in Refs *16-18*. We have also developed procedures for distinguishing between fast and slow crack growth. These procedures are not discussed here since they are rather lengthy numerical statements.

In noting Eq 9, it certainly is somewhat more complex than the typical Paris relation $da/dN = D (\Delta K)^n$ utilized in a great deal of crack growth correlation. However, since it is desirable to formulate an accurate fatigue life prediction methodology herein, it is worth noting that Eq 9 fits the physical data over the entire range of fatigue crack growth whereas Eq 1

does not. Thus it would be difficult if not impossible to apply the Paris relation to pitting corrosion fatigue situations since a change in C or n would not necessarily yield a change in K_{th} or K_b (K_{Ic}). Thus, a life calculation could be in serious error. Also if procedures for optimizing the fit of Eq 9 were available, and if a generalized integration routine could be established, a physically rational and reliable fatigue life prediction methodology would be available for pitting corrosion fatigue. This is the subject of other efforts, but the Weibull technique has been developed adequately to test it on the pitting corrosion fatigue model.

The four Weibull parameters of interest here are

K_b, crack instability parameter,

e, threshold parameter,

v, characteristic value, and

K, shape parameter.

Equation 10 gives the threshold value of stress intensity required to establish when a pit becomes of sufficient physical size to become a Mode I crack, for a defined load/environment/frequency to propagate in the regime where Eq 9 can be applied.

In order to apply the model, an analytical and experimental method must be available to establish the size of pit and time (or cycles) to develop a pit of given size. This is available from pitting theory as it now stands [*15,20*]. However, it is noted after a review of pitting literature that it has not been established if dynamic loading accelerates pitting or not. This was not a subject of the present study but it needs to be established in order to fully understand the mechanisms of corrosion pitting fatigue. Current research is being directed at this crucial question. In addition, the specific mechanism(s) of corrosion pitting are not dealt with herein. This is not to say they are not important, but the postulated model does not require knowledge of the mechanism, only knowledge of the pitting rate and pitting geometry.

Pitting

Corrosion pitting has been found to be related to area of exposure, time of exposure, and the material/environment under consideration. At this time the equations that are used to determine pit depth are those due to Rowe [*21*], Godard [*22*] and others. They are, respectively

$$d = bA^2 \tag{11}$$

and

$$d = C(t)^{1/3} \tag{12}$$

where

d = maximum pit depth,
A = area of exposure,
t = time, and
C = a parameter related to the material/environment combination.

Although extreme-value statistics also can be used to represent pitting data [*16*], they will not be used in this paper. Conceptually, it is now clear that to determine the pit depth as a function of time it is necessary to conduct experiments to get the value of C in Eq 12. This procedure was employed to obtain the pit depth at which, for a defined load/environment combination, the fatigue crack growth threshold will be attained.

It must be emphasized that very limited information on pitting rates is available. The author has numerous studies of this nature underway at present and this will allow confirmation of Eq 12 or further development of the model.

Summary of Prediction Model

The model can now be summarized as follows:

1. Calculate the time (cycles) for a pit to develop to sufficient depth, a_{th}, to attain the fatigue crack growth threshold at the stress level of interest. The environment and alloy must be known. Pitting data must be available. A flaw geometry must be assumed. If a surface flaw[3] is assumed, an $a/2c$ ratio must be assumed for the pit growth

$$1a) \qquad K_{sf} = 1.1\, s\sqrt{\pi\,(a/Q)}$$

where

K_{sf} = stress-intensity factor corresponding to a surface flaw,
S = applied stress,
a = size of the flaw, and
$Q = f\,[(a/2c), S_{ty}]$ (where S_{ty} is the tensile yield stress).

1*b*) ΔK_{th} (fatigue crack growth threshold for Mode I crack) must be known from experiments for the environment/material/frequency/spectrum/waveform combination.

2. Calculate the cycles (time) required to grow the Mode I crack that initiated from the pit to final fracture. Fatigue crack growth data must be

[3]A surface flaw is assumed as an idealization of the pitting process. It is recognized that other pit geometries can occur.

available for the alloy and environment determined at the proper test condition. Fracture toughness data should be available if applicable.

It should be noted that for those conditions where LEFM does not apply, plane stress or "large" strain, some modification of the model will be necessary.

Thus, this model must be verified and tested. In order to test the model based upon the pitting/corrosion fatigue mechanism, experiments on pitting corrosion fatigue and fatigue crack growth must be conducted. The verification experiments are reported in the remainder of the paper.

It is worth noting that several initiation and propagation events are involved in this mechanism of fatigue failure. They are

1. Initiation of corrosion pits

(1*p*) *Propagation* of pits

2. *Initiation* of a Mode I crack at a corrosion pit site

(2*p*) *Propagation* of the *Mode I* crack

3. *Initiation* of fracture instability

(3*p*) Unstable crack *propagation*

Thus, to attempt to simply characterize the corrosion fatigue mechanism by terms such as initiation and propagation is a conceptual misunderstanding of the physical process. With this mechanism of fatigue it is possible to mathematically determine, for a given material in a given loading condition, the point at which Processes 2 and 3 occur. In a relativistic sense, however, it does not today appear possible to be able to mathematically determine the precise nucleus size which leads to the initiation of corrosion pits. We can determine, however, on a statistical basis, the factors that control the growth of pits.

Experimental Verification of the Model

In order to verify the proposed model, it was decided to use 7075-T6 aluminum alloy tested in air and salt water. This material was selected since LEFM can be used to describe its behavior and also because it is known to undergo pitting in salt water. Although some steels yield greater pitting rates in some environments, aluminum was selected for the initial verification studies in order to avoid oxidation contamination which would make production of the movies difficult. The unnotched specimen used for the studies is shown in Fig. 1.

The experimental apparatus used for the observation of crack develop-

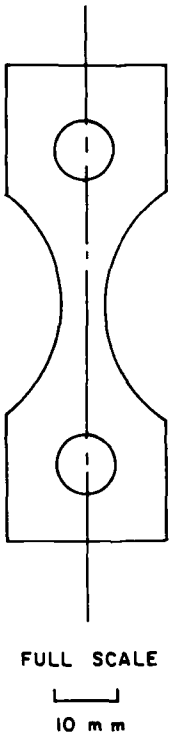

FIG. 1—*Fatigue specimen used for pitting studies.*

ment is shown in Fig. 2 with the specimen position indicated in the upper left-hand portion of the figure. A viewing eyepiece was positioned to allow the observer to view the specimen and select the area for detailed studies with recording on the film as shown. The movie system was quite elaborate and my colleague Vance Danford and I some years ago named the overall observation scheme a Sync-Strobe System for *In Situ* Study of Fatigue. The system was designed to allow synchronization of the movies with the fatigue cycle or to allow the synchronization to be slipped over numerous cycles if desired. In this manner the motion can be stopped for easier viewing.

The unnotched fatigue tests were conducted under constant-deflection axial loading with a sine wave at a frequency of 30 Hz. An R ratio ($R = S_{min}/S_{max}$) of + 0.1 was utilized for the initial verification studies. A small transparent container was constructed to contain the environment around the central section of the unnotched specimen. The environment always was introduced within minutes of starting the test. Tests were conducted on a continuous basis from start to fracture. Fatigue crack growth data for these verification studies were taken from a previous effort [*23*] and other unpublished work of the author.

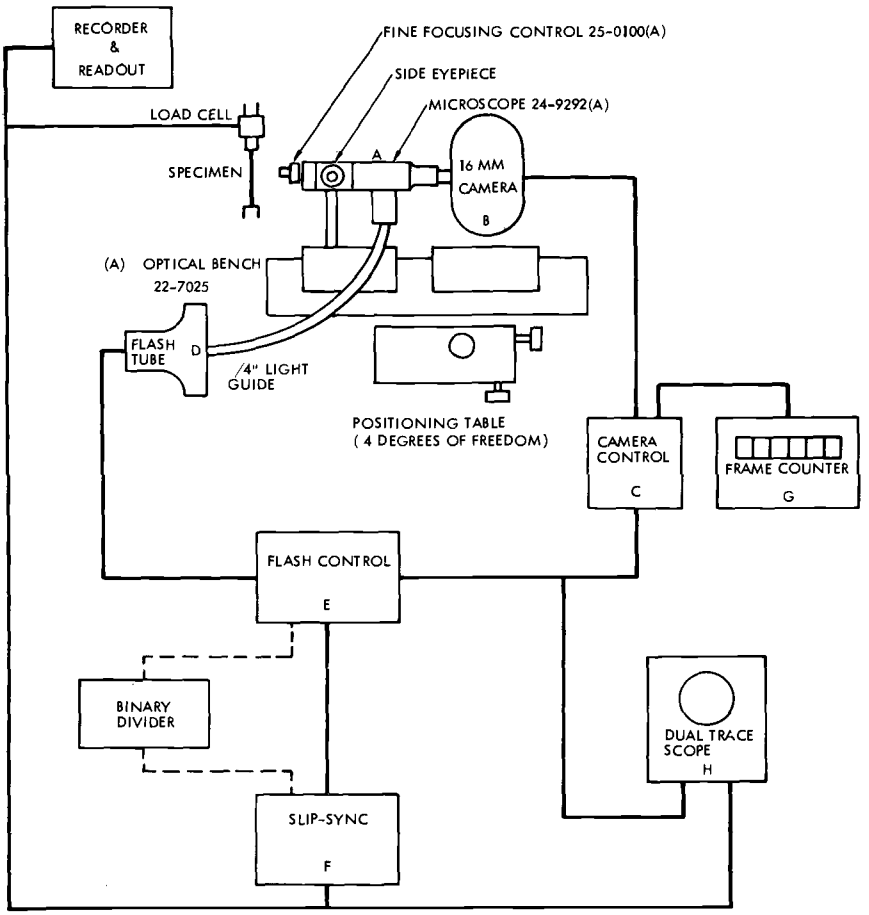

UNIT	MODEL	MANUFACTURER
A MICROSCOPE & BENCH	SEE ABOVE	EALING
B CAMERA	370	CHADWICK-HELMUTH
C CAMERA CONTROL	352A	CHADWICK-HELMUTH
D FLASH TUBE	71	CHADWICK-HELMUTH
E FLASH CONTROL	136	CHADWICK-HELMUTH
F SLIP-SYNC	109	CHADWICK-HELMUTH
G COUNTER	5221B	HEWLETT-PACKARD
H SCOPE	561A	TECTRONIX

FIG. 2—*Instrumentation for observation of fatigue specimens during cyclic loading. Specimen is located at upper left.*

Results

The results for the unnotched specimens tested in laboratory air, distilled water, and 3.5NaCl are shown in Fig. 3. As expected, salt water reduces the fatigue life a considerable amount. The initiation points indicated in Fig. 3 are for development of a 0.127-mm crack. The lines drawn through

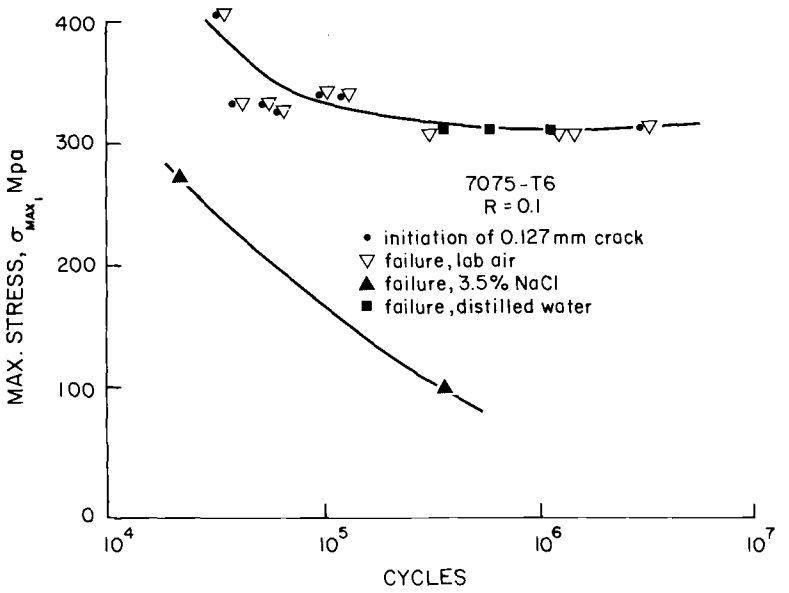

FIG. 3—*Fatigue results for unnotched fatigue specimens tested in air, distilled water, and salt water. "Initiation" is to a crack 0.127 mm long.*

the data are in no way numerical fits of the data and should not be construed as such. Figures 4 and 5 present the fatigue crack growth curves utilized for model verification for the air and saltwater fatigue crack growth tests. Tests were conducted on 15.24-cm-wide center-cracked panels tested in closed-loop load control with a sine wave at 10 Hz. It was determined from previous work [*23*] that no effect of frequency would occur between 10 and 30 Hz. The Weibull parameters are shown in the upper left portion of the figures.

Figures 6 and 7 present several photographs that were selected for reproduction from the movies that were made during the tests. The specimen that was tested at 103.4 MPa (N_f = 357 810 cycles) yielded most of the photographs shown. Figure 6*a* is a typical pit from the specimen tested at 275.8 MPa (N_f = 21 822 cycles). From pitting data on 7075 in salt water, a prediction of time to develop a Mode I crack will be made for the specimen tested at 103.4 MPa. Figures 6*b* through 7*d* will be used in conjunction with the prediction. From Fig. 4 the Weibull parameters are used to calculate the threshold from Eq 10.[4] Using the values indicated in

[4]The computer programs currently are written for dealing with data acquired in English units; thus, the parameters listed in Figs. 4 and 5 are for English units except for K_8 and K_b.

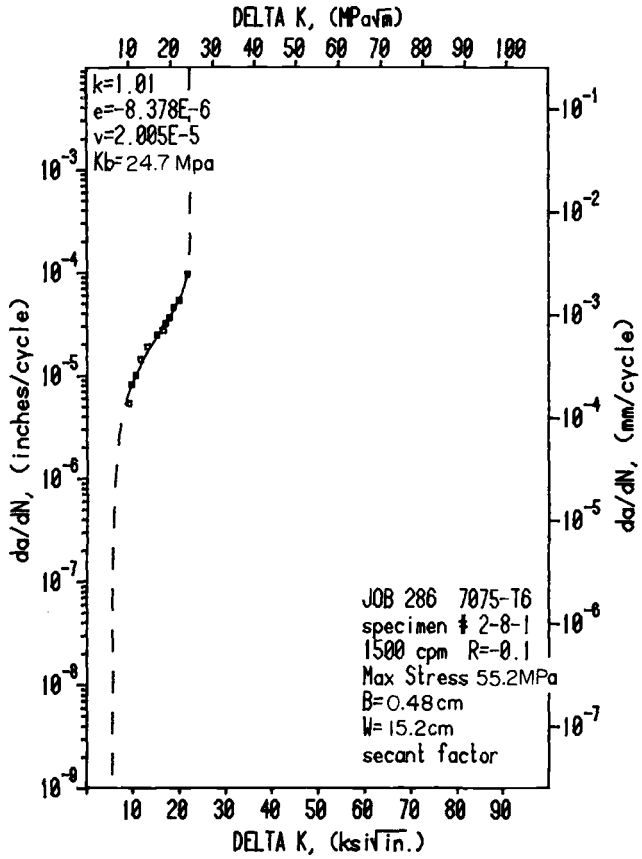

FIG. 4—*Typical fit to fatigue crack growth data for 7075-T6 15.24-cm-wide panel fatigue-tested in air.*

the figure, a threshold value of 57.74 MPa $\sqrt{\text{cm}}$ results. For an edge crack, through the edge in this case, a pit depth of

$$a_{th} = \frac{1}{\pi}\left(\frac{57.74}{1.1S}\right)^2 = \frac{1}{\pi}\left(\frac{57.74}{1.1 \times 103.4}\right)^2 = 0.08 \text{ cm}$$

results. The actual pit (through edge crack) that resulted in a size sufficient to generate a Mode I crack is 0.00635 cm. This is reasonable agreement. Further refinement can occur dependent on the number of specimens used to obtain the Weibull parameters and the care with which the pit depth is determined.

Use of Eq 12 in conjunction with the C-value and time yields a number of cycles to a crack depth of

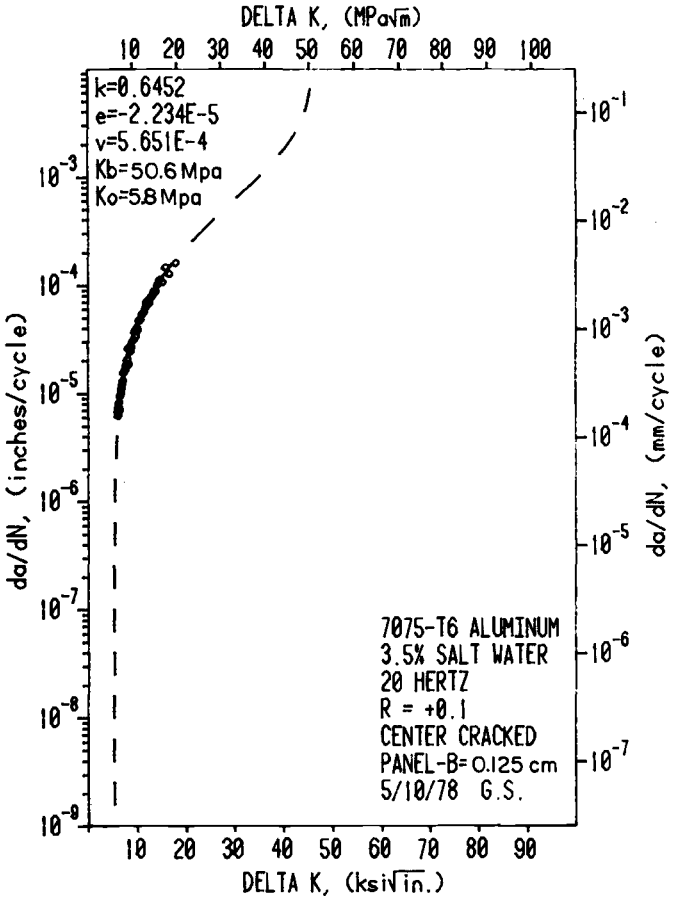

FIG. 5—*Typical fit to fatigue crack growth data for 7075-T6 15.24-cm-wide panel fatigue-tested in 3.5NaCl solution.*

$$d = C(t)^{1/3}$$

$$t = \left(\frac{d}{C}\right)^3$$

substitute the actual a_{th} for d

$$t = \left(\frac{a_{th}}{C}\right) = \left[\frac{0.00635 \text{ cm}}{0.000305 \text{ cm/s}^{1/3}}\right]^3$$

$$\simeq 9050 \text{ s}$$

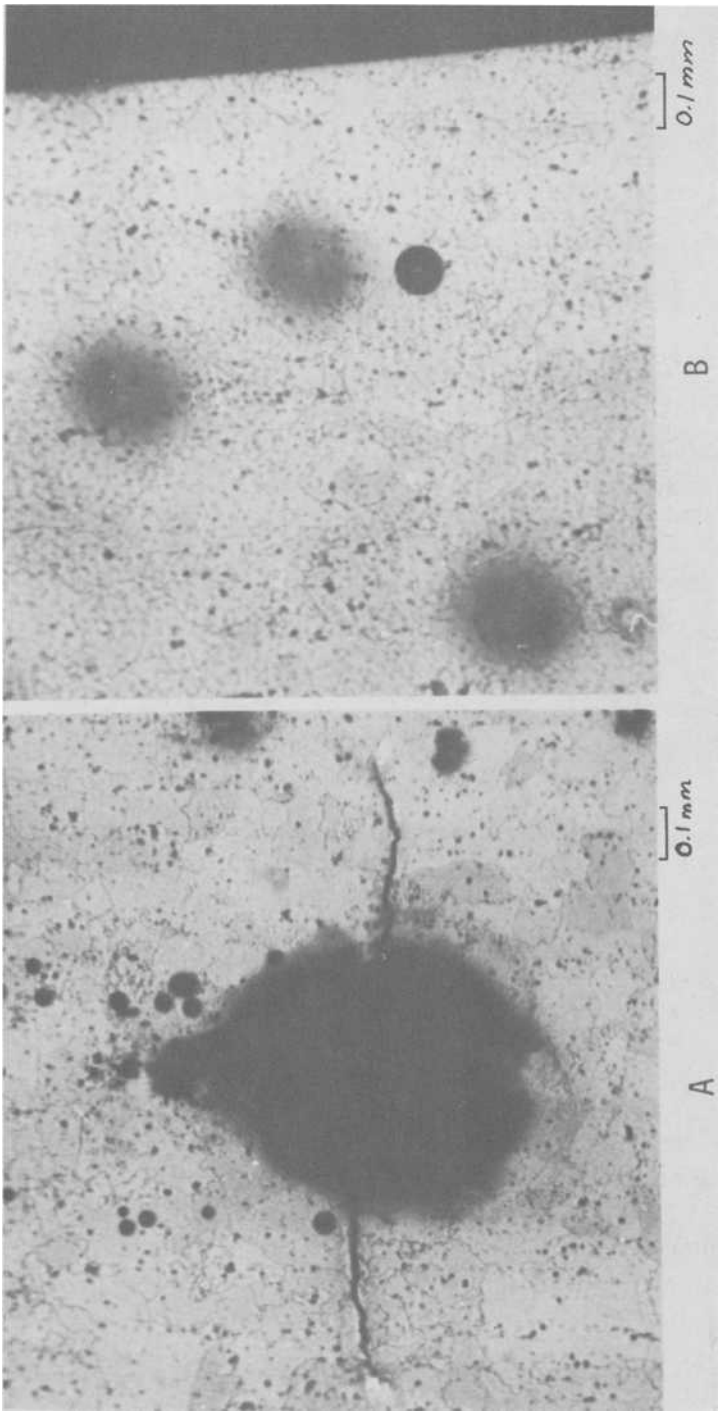
0.1 mm
B
0.1 mm
A

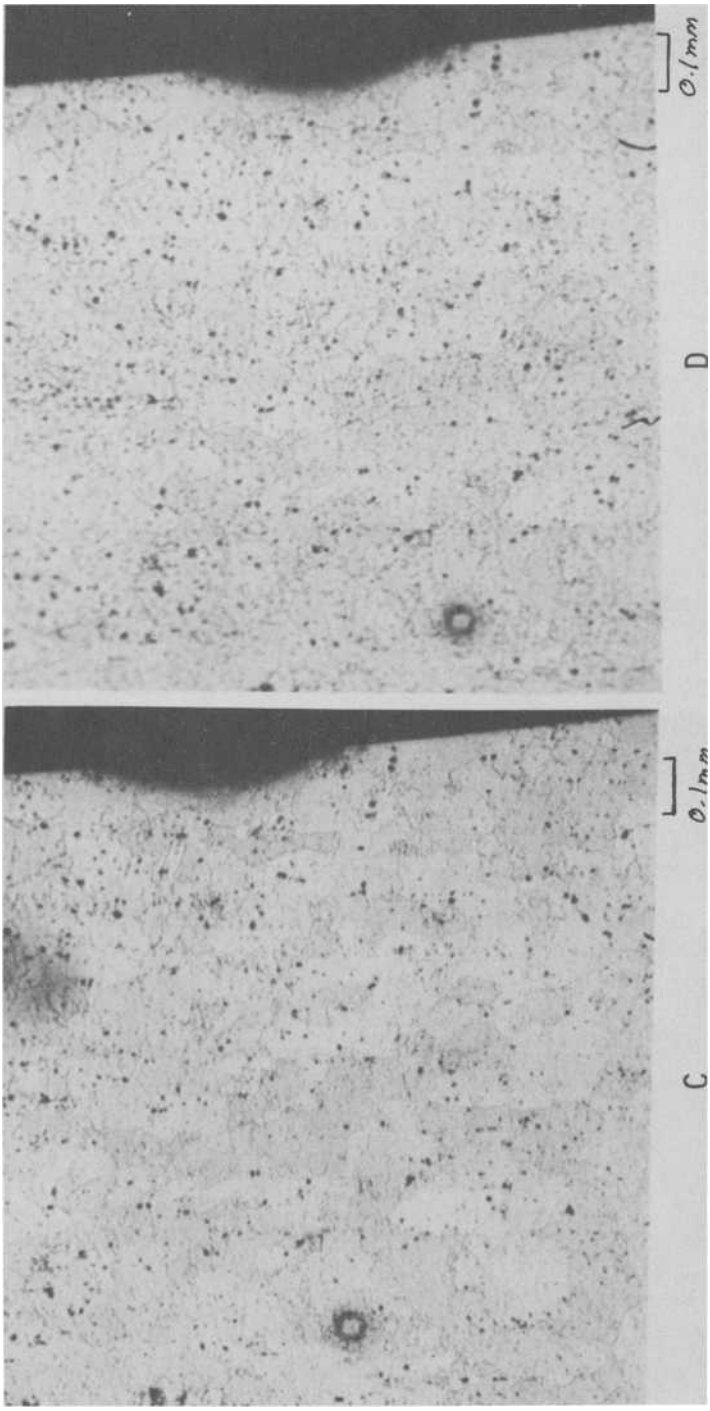

FIG. 6—*Photomicrographs taken from movies for specimens tested at* (a) *275.8 MPa and* (b–d) *103.4 MPa.* (a) *Typical pit with Mode I fatigue crack;* (b) *edge of specimen showing area where corrosion pit initiated that developed a Mode I crack;* (c) *pit area after 146 000 cycles; and* (d) *pit area after 204 000 cycles.*

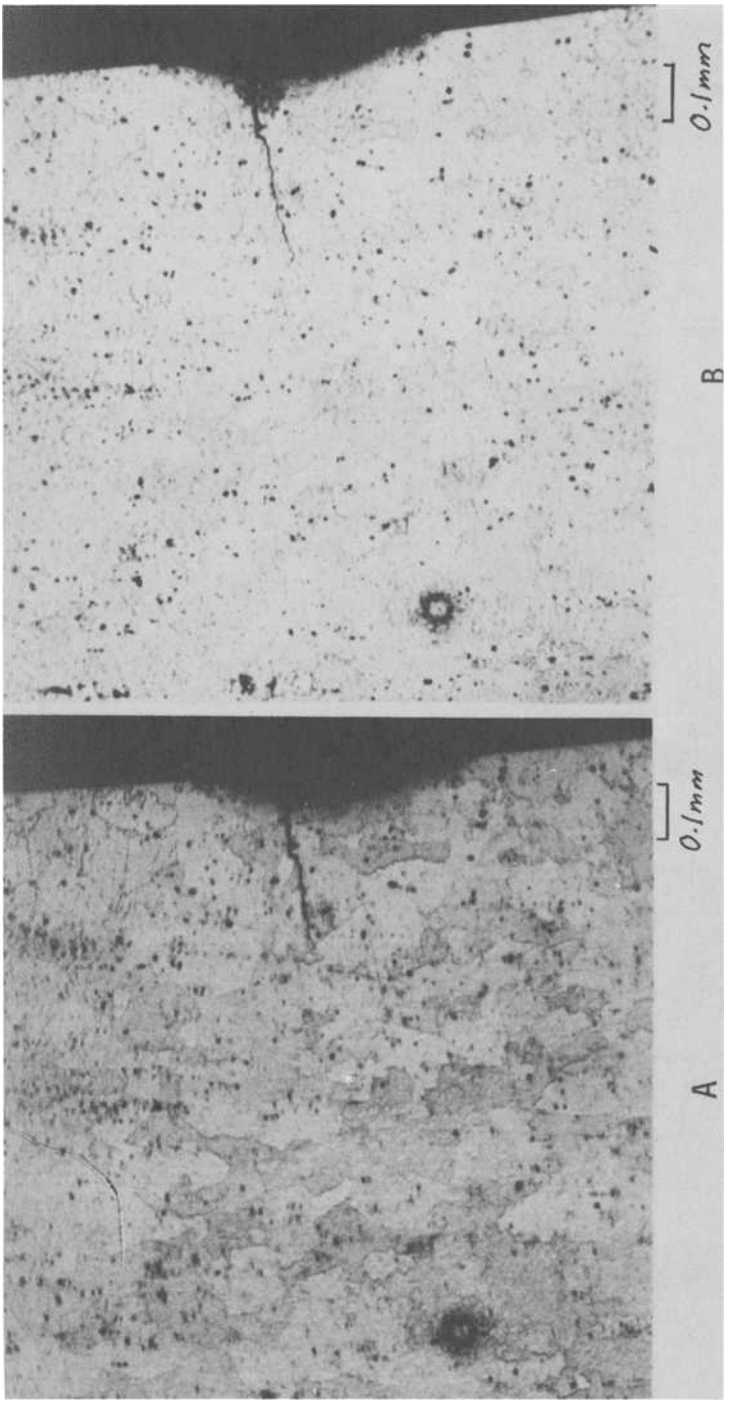
0.1mm
B
0.1mm
A

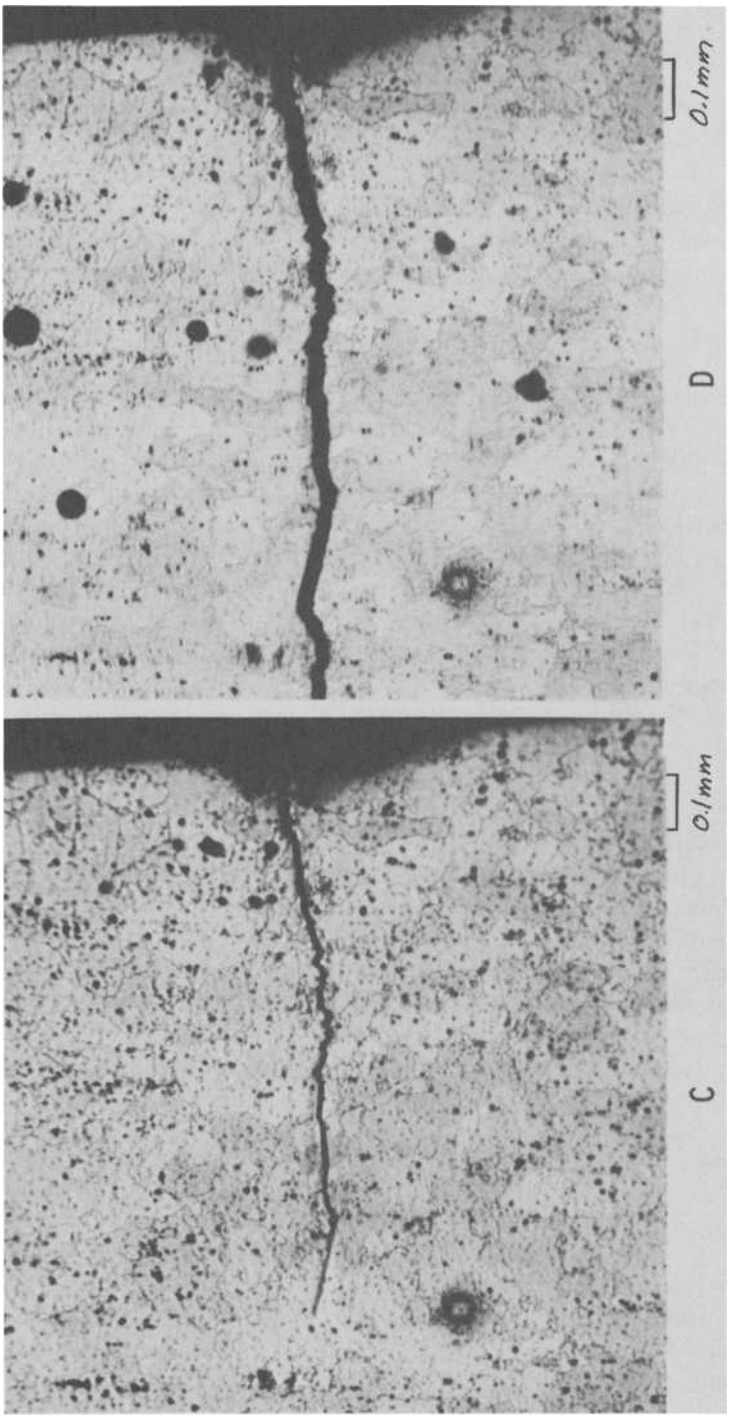

FIG. 7—*Photomicrograph taken from movie for specimen tested at 103.4 MPa.* (a) *Pit area after 321 292 cycles;* (b) *pit area after 330 592 cycles;* (c) *pit area after 346 700 cycles;* (d) *final fracture 354 700 cycles.*

In 9050 s at 30 Hz, approximately 300 000 cycles was required to initiate the Mode I crack. It is noted from Figs. 6*d* and 7*a* that the Mode I crack developed somewhere between 204 000 (Fig. 6*d*) and 324 412 cycles. A value of 300 000 cycles appears reasonable when an extrapolation on the one-third power of time is taken. Unfortunately, the exact $t(N)$ at initiation of the Mode I crack was not obtained. Nonetheless, very good agreement is obtained and the conceptual model has been verified for this material and environment.

Discussion

From the limited success of this model and the experimental technique developed to support the data base, it is believed that other forms of the corrosion fatigue process may be modeled along a similar line. Among the candidates for further modeling are stress corrosion-induced cracks, erosion, cavitation, and crevice corrosion. Some work on modeling fretting-initiated fatigue has already been mentioned in the text. Much more data are needed, however.

Additional questions on corrosion pitting fatigue are, does dynamic loading change the kinetics of pitting and what are the fundamental mechanisms of pitting corrosion under either static or dynamic loadings? A great deal of additional statistically based pitting data also are needed.

Summary and Conclusion

It is clear from the photos shown in Figs. 6 and 7 that corrosion pits produce a local discontinuity that acts as the site of initiation of a Mode I fatigue crack. The fatigue process, represented as the total number of cycles, comprises the cycles needed to produce the pit and the cycles needed to propagate to failure the Mode I crack that initiates at the pit. This is depicted in the simple a-N plot shown in Fig. 8 and in Fig. 9, a representation of the stress-cycles-to-failure curve.

The four-parameter Weibull fits to the fatigue crack growth data that resulted for the 7075-T6 tested in salt water yield the fatigue crack growth threshold, K_o. This value is then used to determine the size pit that will produce a stress intensity of sufficient magnitude to initiate a Mode I fatigue crack. The verification of the model worked well for the tests that were conducted. Further refinements appear probable as discussed earlier.

Figure 10 shows transmission electron fractographs taken from the vicinity of the origin for the air tests (Fig. 10*a* and 10*b*) and the saltwater tests (Fig. 10*c* and 10*d*). A pronounced difference in the fracture appearance is noted in the origin areas. The air results show well-defined fatigue striations whereas the saltwater results show the more typical "brittle striations" [*6*]. Additional effort will be needed to clarify the detailed

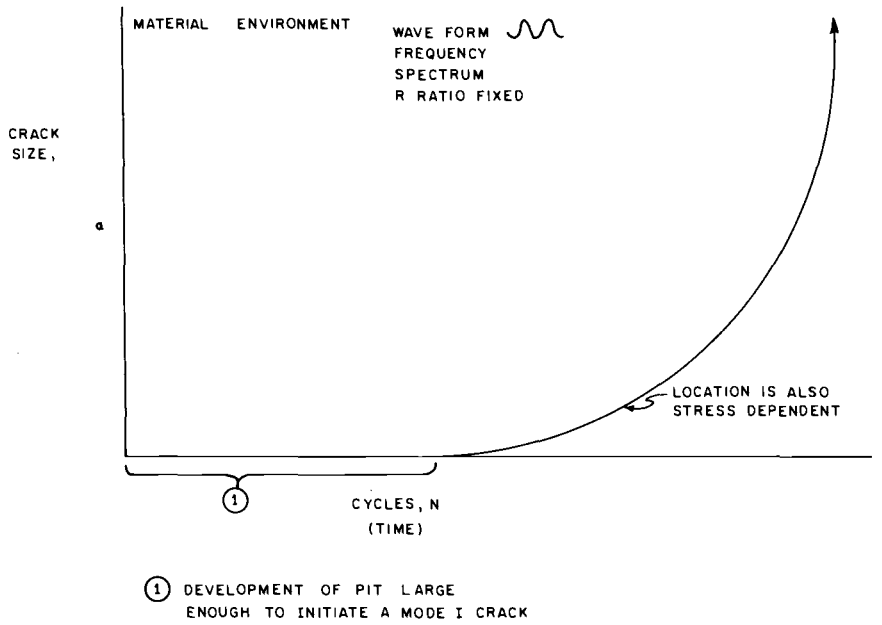

FIG. 8—*A conceptual crack length* (a) *versus cycles* (N) *plot for the corrosion pitting fatigue model.*

deformation mechanisms that produce the difference in fracture surface detail.

The following conclusions are offered:

1. Corrosion pits may act as initiation sites for Mode I fatigue cracks in 7075-T6 cyclically loaded in salt water.

2. Pitting theory can be used to predict the rate of growth of pits and their size at various times.

3. The four-parameter Weibull fit to fatigue crack growth data can be used to obtain the fatigue crack growth threshold.

4. Using the combined knowledge on pitting rates and the fatigue crack growth threshold, it is possible to predict either the size pit that will produce a Mode I fatigue crack or the cycles to do so or both.

5. The total number of cycles to failure can be predicted from a combined knowledge of the kinetics of pitting corrosion and fatigue crack growth.

6. Continued emphasis must be placed on the kinetics of all potential fatigue mechanisms in order to formulate fatigue-resistent materials and fatigue design concepts.

7. The concepts elucidated herein may be applied in failure analysis as well as in understanding the mechanism of the fatigue process.

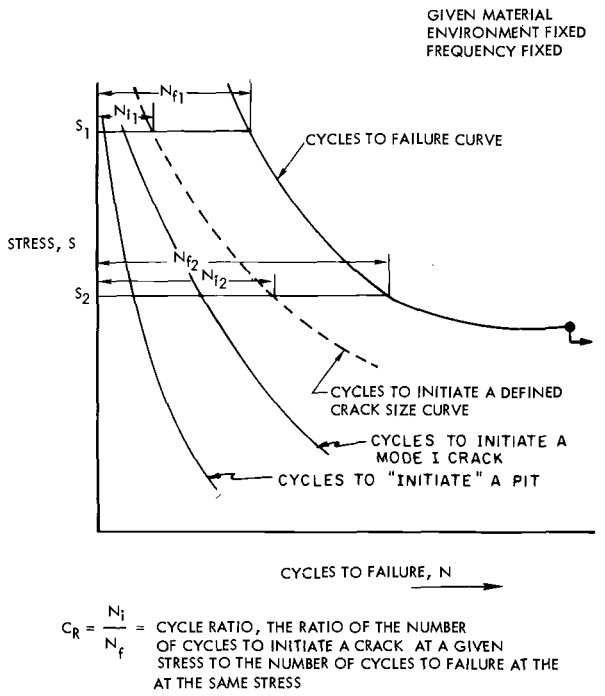

FIG. 9—*Various critical event curves on the stress-cycles-to-event plot.*

Acknowledgment and Dedication

I want to thank my colleagues (W. Krupp, D. Pettit, E. K. Walker, J. C. Ekvall, G. Goss, J. C. Ryder, G. Bowie, J. Fritzen, V. Danford, P. Sandifer, J. Van Orden, S. Bocarsly, and K. E. Weber, all with Lockheed California Co.) for their many stimulating discussions over the years when this work was in progress. I am also indebted to Mr. David Mauney of Alcoa and Mr. R. Jeal of Rolls Royce-Derby for many discussions on this subject. Mrs. Geraldine Hoch provided many stimulating thoughts on the corrosion aspect of this work and her untimely death during its progress was, in a sense, a serious loss. I dedicate this paper to the living memory of Mrs. Geraldine Hoch.

In recent years the Office of Naval Research and the Air Force Office of Scientific Research have provided support to my researchers on corrosion fatigue under Contracts N 00014-75-C-0670 and AFOSR 77 3178, respectively, with Dr. Phillip Clarkin and Dr. William Walker the respective technical monitors.

References

[1] Hoeppner, D. W., *Corrosion Fatigue: Chemistry, Mechanics and Microstructure*, NACE-2, National Association of Corrosion Engineers, 1972, pp. 3-11.

[2] Hoeppner, D. W. and Krupp, W. E., *Engineering Fracture Mechanics*, Vol. 6, 1974, pp. 47-70.

[3] Freudenthal, A. M., *Engineering Fracture Mechanics*, Vol. 5, 1973, pp. 403-414.

[4] Hoeppner, D. W., "Fatigue Crack Initiation Concepts in Solids," *Journal of Mechanics and Physics of Solids*, for publication, 1978.

[5] Coffin, L. F., Jr., *Metal Science*, Feb. 1977, pp. 68-71.

[6] Forsyth, P. J. E., *Acta Metallurgica*, Vol. 11, No. 7, July 1963, pp. 703-717.

[7] Grosskreutz, J. C., *Physica Status Solidi*, (b), Vol. 47, 1971, pp. 359-396.

[8] Laird, C. and Duquette, D. J., *Corrosion Fatigue: Chemistry, Mechanics, and Microstructure*, NACE-2, National Association of Corrosion Engineers, 1972, pp. 88-117.

[9] "Fatigue-1977," *Metal Science*, The Metals Society, Aug./Sept. 1977, Entire proceedings.

[10] *Galvanic and Pitting Corrosion—Field and Laboratory Studies, ASTM STP 576*, American Sociey for Testing and Materials, 1976, pp. 117-295.

[11] Van der Horst, J. M. A., "Corrosion Fatigue Initiated by Stress Corrosion Cracking," personal communication.

[12] Kitagawa, H., Fugita, T., and Miyazawa, K. in *Corrosion-Fatigue Technology, ASTM STP 642*, American Society for Testing and Materials, 1978, pp. 98-117.

[13] Hoeppner, D. W. and Goss, G. L., *Wear*, Vol. 27, 1974, pp. 61-70.

[14] Edwards, P. R., Ryman, R. J., and Cook, R., "Fracture Mechanics Prediction of Fretting Fatigue," Royal Aircraft Establishment Publication presented at the International Conference on Aeronautical Fatigue-1977, to be published.

[15] Endo, K. and Goto, H., *Wear*, Vol. 38, 1976, pp. 311-324.

[16] Bowie, G. and Hoeppner, D. in *Proceedings*, International Conference on Computer Simulation for Material Applications, *Nuclear Metallurgy*, Vol. 20, Part 2, 1976.

[17] Kondas, K. R., "Influence of Microstructural and Load Wave Form Control on Fatigue Crack Growth Behavior of Precipitation Hardening Stainless Steels," Ph.D. Dissertation, University of Missouri-Columbia, July 1976.

[18] Reeves, R. K., "Microstructural and Environmental Effects on Fretting Fatigue," Ph.D. Dissertation, University of Missouri-Columbia, May 1977.

[19] Reeves, R. K. and Hoeppner, D. W., "A Weibull Analysis of Center Cracked Panel Crack Growth Data of a .40/.50 Carbon Steel," *Engineering Fracture Mechanics*, Vol. 10, 1978, pp. 571-581.

[20] Mueller, L., "The Optimization of the Weibull Survivorship Function in Fitting Fatigue Crack Growth Data," M.S. Thesis, University of Missouri-Columbia, May 1978.

[21] Rowe, L. C. in *Galvanic and Pitting Corrosion—Field and Laboratory Studies, ASTM STP 576*, American Society for Testing and Materials, 1976, pp. 203-216.

[22] Godard, H. P., *Canadian Journal of Chemical Engineering*, Vol. 38, Oct. 1960, p. 167.

[23] Krupp, W. E., Hoeppner, D. W., and Walker, E. K., *Corrosion Fatigue: Chemistry, Mechanics and Microstructure*, NACE-2, National Association of Corrosion Engineers, 1972, pp. 468-483.

DISCUSSION

R. Pelloux[1] *(discussion)*—We have not seen too many engineers in here. I am assuming that most of us are scientists and call ourselves scientists.

[1] Department of Metallurgy, Massachusetts Institute of Technology, Cambridge, Mass.

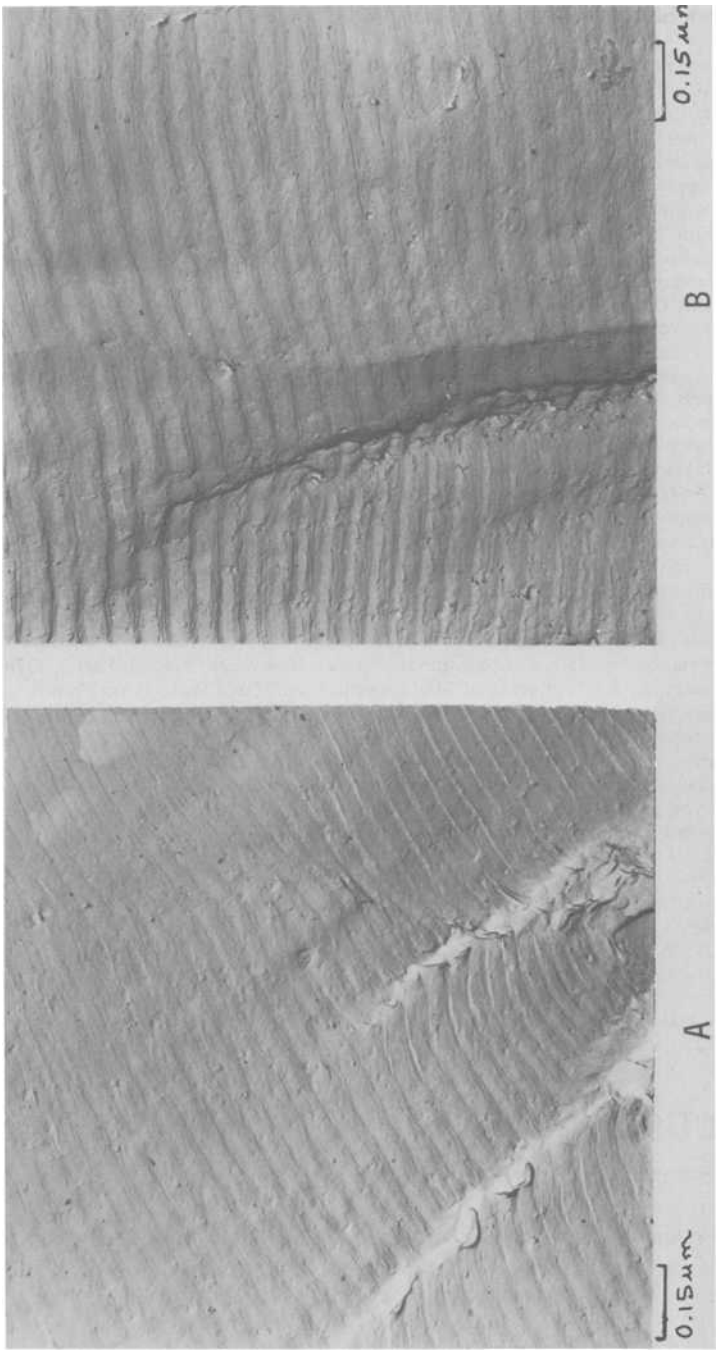
0.15μm
A
B
0.15μm

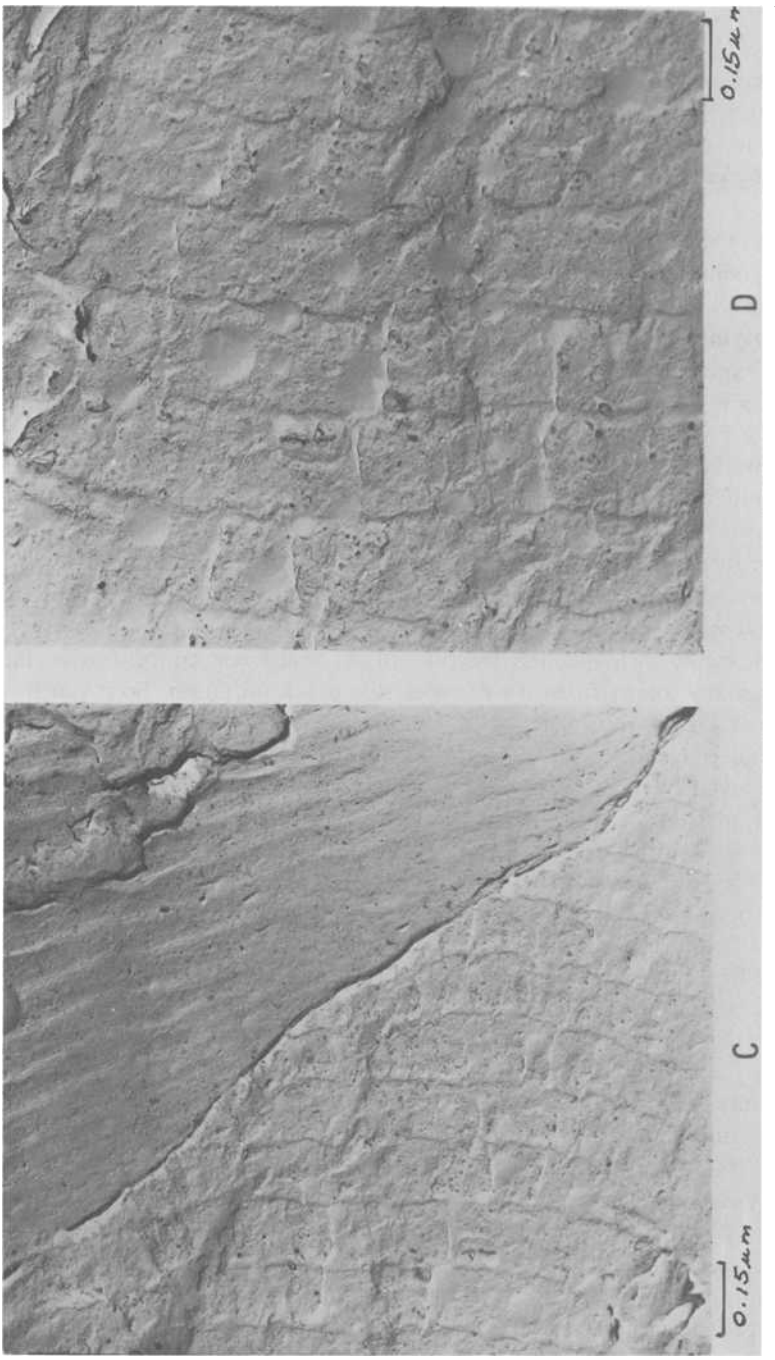

FIG. 10—*Electron fractographs in origin areas for fatigue test in air* (a, b) *and in salt water* (c, d).

J. T. Fong—No, I think we are mostly engineers here.

R. Pelloux—Good. I am pleased to hear that, because someone made a statement that corrosion fatigue is an engineer's nightmare but a scientist's meal ticket.

In my case a paper by our friend Dave Hoeppner is a discusser's nightmare.

I don't want to exaggerate that, but I guess the text of the paper did not follow completely on the broad scope of crack initiation and corrosion fatigue, which is a very tough problem. Dave limited himself to the problem of crack initiation from the pits.

My experience is with 7075 aluminum alloys. You get a lot of Stage I, not Mode I, but Stage I, crack initiation in the corrosive environment. Those are shear cracks. If anything, you get a tremendous enhancement of crack initiation by a process which we can call enhancement of the slipband extrusion/intrusion and of the persistent slipbands. I don't know why this is so.

I agree with you that there are some pits, but I made many sections and in many sections I saw Stage I cracks without any pit. So that is one problem that we have to face.

I also agree with you that the pit will act as a stress concentration factor and in many, many cases it will accelerate crack initiation. So if you have a pit now, I find your fracture mechanics analysis rather simplistic. I am sure that you make it fit the test data. I find that it needs some refinement because you have a threshold extrapolated from a high crack growth rate and, if anything, the threshold for corrosion fatigue in aluminum alloys for long cracks is down to 10.3 or 13.8 MPa (1.5 or 2 ksi $\sqrt{\text{in.}}$), and not 34.4 MPa (5 ksi $\sqrt{\text{in.}}$).

Furthermore, if you are going to use a threshold ΔK that you obtained from a large or long crack, you have to make sure that you can apply LEFM for very short cracks, cracks as short as 10 or 50 mils.

Now, if you check all that, you may find out that the prediction you get from integrating a crack growth rate from the bottom of your pit and predicting the S–N life is purely accidental. But I would like to see you handle more data and do it with you, and it would be a worthwhile exercise.

If anything, if it works, it will show that you can apply LEFM crack growth data to a very short crack.

My view is that corrosion fatigue cracks in many materials do not initiate at pits. What you see is an enhanced activity of slipbands. If you have an inert environment, it will take 10^6 cycles to get nice persistent slipbands; with an active environment like distilled water or seawater, it might take 10^4 to get the same density of slipband.

This is where the problem is, I think.

D. W. Hoeppner—I think Professor Pelloux's points are well taken. If I confused anyone in terms of not trying to cover those, I didn't mean to do that. There are many material environment area synergisms which, in the space-time continuum, would involve the generation of cracks by mechanisms other than corrosion pitting and I would certainly agree with that.

I think I will have to get together with Reggie to go over in more detail the fact that we used pitting rate theory to predict the growth of the pit and that we had to get the fatigue crack growth threshold, which is not a single-valued function. The threshold is a function of frequency, material, environment, waveform, and R ratio. Aside from trying to apply LEFM to "short cracks," I have also had trouble with the shape of the pit. As to Dr. Pelloux's concern about the threshold determination from extrapolation, the procedure I am using is one of the better ones available. There is adequate information in the literature on this method, and if Dr. Pelloux has experimental evidence coupled with numerical analysis that provides a better estimate of the threshold I'm sure it will appear in the literature in the future.

P. Worthington[2] (*discussion*)—The paper highlights the problem of initiation and focuses attention away from Stage II onto the initiation and early growth stages. This is important because a large fraction of a component's fatigue life may be spent in this region.

Moreover, a move is made away from a rigid three-stage classification of fatigue crack growth, which is represented by a single equation, thus avoiding possible large errors in fatigue life calculations.

An equation is also defined for the threshold stress-intensity, K_{th}. However, the defined threshold stress intensity is presumably associated with the situation where a growing crack stops propagating, which may not be the same as that required for a pit to become a growing crack. Thus, I am surprised that such good agreement has been obtained in these experiments since I would not expect a pit to become a crack at a size determined from sharp fatigue crack growth results, and it would be useful to know the errors on the predicted threshold stress intensity. I believe much more attention needs to be given to the region up to the threshold stress intensity in terms of the barriers to defect growth and the mechanisms of crack formation. The importance of the environment in this region is clearly demonstrated in this paper.

Care must be taken in applying this model generally because in some systems the pit depth/time relationship changes with pit depth and time, and essentially no pit growth occurs for very many cycles. Thus, we must ask, how does a pit become a growing crack, for this will determine when

[2] Research Division, Central Electricity Research Laboratories, Letterhead, Surrey, U.K.

it occurs? In power plant components, one often sees very small oxide-filled pits and occasionally there is a crack associated with one of these pits. It may be that instead of a large number of cycles being required to grow a pit to some critical size, these fatigue cycles are required to turn a blunt pit into a sharp crack in the presence of an environment at submacroscopic threshold levels. Clearly, further work is required to determine any effect of frequency, waveshape, and R ratio on pit growth kinetics, and whether dynamic loading accelerates pitting or not.

Residual stresses and surface finish can markedly affect pitting behavior and so it may be difficult to apply results of this type to practical components. And indeed, as a design engineer, I wonder how much of the information presented at this symposium can be applied to real situations.

One last general comment. Take the grain size dichotomy. Big deal. What is a design engineer supposed to do with this information? Too many people are stopping just when they should be starting. As a scientific community, I believe we haven't even begun to answer some of the questions that design engineers are asking.

D. W. Hoeppner—I would like to thank Peter Worthington for his careful reading of my final completed manuscript; he has made excellent comments on several areas that need further attention, some of which I know others are looking after and we are also pursuing. I think if you examine his comments you will find they were all well-formulated, and I really have nothing more to add.

R. Ebara[3] *(discussion)*—I could see a very small corrosion pit from the data given in the paper. I would like to draw your attention to some of my work on this subject. In a paper I co-authored in 1978,[4] I showed a figure on the subcrack associated with a corrosion pit found in 13Cr stainless steel in 3×10^{-4} percent sodium chloride aqueous solution and subjected to a rotating bending stress of 342 MPa with a life of 6.3×10^{7} cycles. That corrosion pit had a diameter equal to almost 1 μm. In a recent paper[5] we reported an example of a corrosion pit found at the initiation area of 13Cr stainless steel in 0.03 NaCl aqueous solution and subjected to a rotating bending stress of 255 MPa at 1.4×10^{6} cycles. We observed that the crack propagation did occur from this corrosion pit. The depth of the pit was almost 10 to 20 μm, but was constant for various concentrations of sodium chloride.

[3]Hiroshima Technical Institute, Mitsubishi Heavy Industries, Ltd., Hiroshima, Japan.

[4]Ebara, R., Kai, T., and Inoue, K. in *Corrosion Fatigue Technology, ASTM STP 642*, American Society for Testing and Materials, 1978, p. 162.

[5]Ebara, R., Kai, T., and Inoue, K. in *Proceedings*, 21st Japan Congress on Materials Research, 1978, p. 90.

My question to Professor Hoeppner is, what is the critical size of the corrosion pit and what do you think about the growth of the corrosion pit?

D. W. Hoeppner—The critical size of the pit is related to the fatigue crack growth threshold. If a Mode I crack results from that pit, we have to know the Mode I fatigue crack growth threshold and some knowledge of the distributional properties of that quantity. With that, we should be able to determine the depth at which the pit becomes a Mode I crack for some given stress or strain field. We should, of course, be aware that there is a statistical distribution of the growth properties of the pits, so we have to approach this from a probabilistic rather than from a deterministic point of view. Within that framework, we should be able to apply the conceptual model to your observation.

K. Miller[6] (*discussion*)—I want to make a comment on one of your statements which concerned the very early growth of the pit in question and I would like to relate it to the point made by Reggie Pelloux. We think that the growth of the pit can also be from considerations of the mechanics of slip in the extension of the slipbands due to the environment, and the growth of the pit, in fact, can be a pure matter of shape, and this we see under various multiaxial stresses and strains.

It does not matter whether it is uniaxial or torsion or whether it is mixed modes, but these pits in fact are generated due to 45-deg planes, shear planes, such that the pit must be developed first before it goes into a Stage II crack. And sometimes a Stage II crack can very soon go into a Stage I crack. So we have a reverse procedure.

But you are quite right, I believe, in pointing out that the very early, early growth regime, is the one that has to be studied, and I don't think we have focused attention on that problem yet. It is the problem that Reggie mentioned. It is the problem that you mentioned. But I think that we have got to do a lot more work in that area.

H. Kitagawa[7] (*discussion*)—I would like to address my short comment to both Professors Hoeppner and Pelloux.

From our recent experiments, we have obtained many data on the statistical distribution function of corrosion pits. Some of them were reported in 1978 at the 7th International Congress on Metallic Corrosion,[8] and others will be delivered at the 3rd International Conference on the Mechanical Behavior of Materials in August 1979.[9]

[6]Department of Mechanical Engineering, University of Sheffield, Sheffield, U.K.

[7]Institute of Industrial Science, University of Tokyo, Tokyo, Japan.

[8]Tsuji, K., Nakasone, Y., and Kitagawa, H. in *Proceedings*, 7th International Congress on Metallic Corrosion, Rio de Janeiro, Brazil, 1978.

[9]Nakasone, Y., Tsuji, K., and Kitagawa, H. in *Proceedings*, 3rd International Conference on the Mechanical Behavior of Materials, Cambridge, U.K., Aug. 1979.

The statistical distributions of sizes of pits and the density of pits are influenced considerably by the cyclic stress. We are now trying to correlate the distribution of pits and microcracks initiated on the smooth surface. We've already found good correlations between the locations of pits and cracks; however, we could not find good correlations between the crack lengths and the diameters of pits in corrosion fatigue of a structural steel in distilled water.

D. W. Hoeppner (author's closure)—Professor Miller's point about the possibility of a pit forming at a slipband is very well taken. However, even though one would expect this as a highly probable pitting site, I have not seen evidence for this postulated mechanism of pitting in slipbands induced by cyclic loading. If there have been publications related to the actual observation of pits in slipbands in engineering materials (not model materials like single crystals), I am not familiar with them. As Professor Miller points out, the mechanism of pitting deserves much more extensive study.

My colleagues and I have also been having difficulty correlating pit diameter and crack depth as Dr. Kitagawa reports. We plan to continue studying this in more detail to attempt to define the pitting crack site correlations.

In concluding, I wish to indicate that a great deal more research is required to unravel this fascinating synergism of corrosion-pitting fatigue. Whenever one tries to model a process conceptually and then tries to apply some mathematics to the model, one runs a great many risks until extensive experimental data are developed. Thus, I have run a high risk in presenting this model in such a simplistic way. More work, however, is underway by many colleagues and will shed much needed light on the subject. I wish to thank all of those persons who chose to provide some discussion on these thoughts.

Chapter 8: Summary and Concluding Remarks

I. LeMay[1]

Symposium Summary and an Assessment of Research Progress in Fatigue Mechanisms

In his introduction to the 1958 Symposium on Basic Mechanisms of Fatigue, Professor Dolan noted that a great deal was known about fatigue failure and the basic mechanisms of fatigue, but that it was impossible to evolve an exact design on a quantitative basis largely because of the statistical nature of the phenomenon. A review of the papers of that symposium [*1*][2] shows clearly that a great deal was indeed known at that time concerning basic fatigue mechanisms without the benefit of thin-foil transmission electron microscopy (TEM) and other sophisticated techniques which we regard today as being essential tools in such studies, but there is no question whatsoever that we are today in a position of having an understanding in detail which may be considered to be several orders of magnitude greater than that obtaining in 1958. This has come about through the many specialized studies made over the past 20 years and through the use of much more sophisticated techniques such as thin-foil TEM, scanning electron microscopy (SEM), electron channeling, and Auger spectroscopy, as have been discussed and illustrated in the papers of the present symposium. However, despite all this progress in detail we are still faced with considerable uncertainties when attempting to design a component or structure to avoid the occurrence of fatigue failure or in predicting its fatigue life. This was well brought out by Fong [*2*] and it certainly appears shocking (at first sight, at least) to be considering a scatter factor of 20 in the fatigue life or of 2 in the mean strain range for fatigue failure of pressure vessels [*3*].

Several major advances in our understanding are, however, apparent when one reviews the papers presented here and in comparing their emphasis with those of 20 years ago. Specifically, there is now a clear understanding

[1]Professor of Mechanical Engineering, University of Saskatchewan, Saskatoon, Canada.
[2]The italic numbers in brackets refer to the list of references appended to this paper.

that the effects of gaseous, aqueous, or other environments can greatly affect the fatigue life and, indeed, the very mechanisms of fatigue.[3] The science of fracture mechanics has been developed and is widely applied to predict crack propagation rates and, hence, fatigue life. The initiation of cracks from persistent slipbands (PSB's) has been examined in great detail and the changes in dislocation arrangement in PSB's and in general under cyclic deformation are now well known and understood. What then is the reason for our lack of precision in predicting fatigue life when we *appear* to have all the background facts to hand?

The answer seems to lie still in the words of Professor Dolan, namely, that we have not yet been able to appreciate and apply the statistical aspects of the various components of the fatigue phenomenon, nor are we yet able to separate and then integrate the individual aspects of the process.

Rhines [*4*] and Underwood and Starke [*5*] have described the basic principles whereby we may quantify microstructure and fatigue damage and fracture phenomena, and it appears certain that many of us will, in future, be attempting to quantify the microstructures of alloys when we conduct fatigue studies on them. This should certainly allow us to better define and predict fatigue properties for service materials and components. However, we must also be much more careful in measuring the intrinsic scatter in material properties which should be related directly to variations in microstructure. All too often the scatter in fatigue data is confused because of environmental factors which have not been controlled, and such factors can be properly determined only when base data have been evaluated for a particular material. This point may be illustrated by showing crack propagation data for 4140 steel tested in fatigue at the same temperature and frequency but at different times of the year when the laboratory relative humidity (RH) varied considerably (Fig. 1) [*6*]. Careful control of relative humidity allowed determination of the variation in crack propagation rate with RH (Fig. 2) [*7*] and determination of the intrinsic scatter inherent in the material (Fig. 3) [*8*].

Another major uncertainty in life prediction, and one which, by design, has not received attention in this symposium as the latter is concerned with mechanisms, is specification of operating conditions. Components and structures contain defects and local stress raisers, and the local stresses can vary considerably from those which nominally apply. In addition, in order to make an accurate prediction of life, we need to know what the environmental (indeed, the *local* environmental) conditions will be, and this is by no means always possible to predict in advance. The spectrum and sequence of loads to which the component will be subjected is also required, although we are certainly in a much improved position today

[3]A distinction is made between such environmental effects on fatigue and corrosion fatigue in its classical sense, which has been recognized and studied for many years.

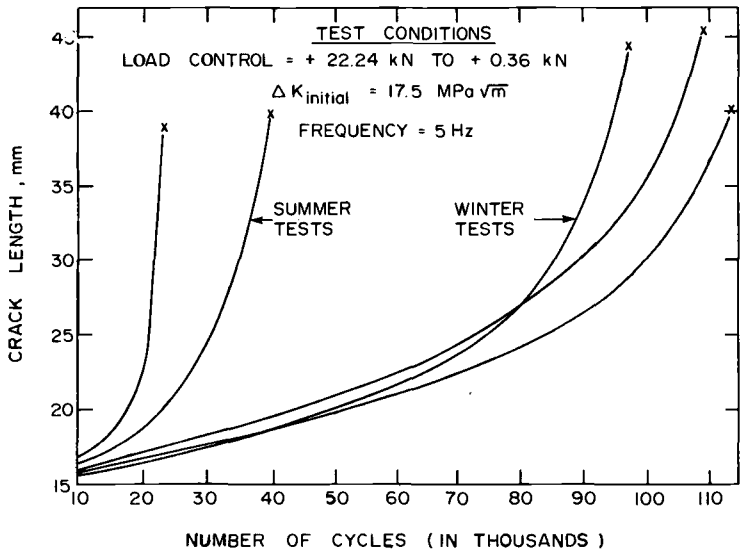

FIG. 1—*Fatigue crack propagation in 4140 steel in summer and winter conditions under identical loading and room temperature conditions. The laboratory humidity level was considerably different. After Ref.* [6].

in terms of knowledge in this area from detailed records which have been made in many practical cases of interest (for example, aircraft flight records). Thus, in theory we should be able to model the process of fatigue in a continuous manner from crack initiation under the projected loading spectrum, through crack propagation to the critical condition for failure, taking into account the environmental effects at each stage and with a knowledge of the statistical scatter inherent in each stage, and arrive at least at a much more precise estimate of life than could be done only a few years ago. Essential to such predictions is the use of computers, proper statistical data, detailed knowledge of crack initiation and propagation mechanisms and of crack growth laws, and an understanding and *quantitative* knowledge of environmental effects.

In the following, I propose to point out some of the distinct advances in our knowledge of fatigue mechanisms as reported at this symposium and at the same time attempt to indicate what seem to me to be gaps in our knowledge.

Fatigue Damage and Crack Initiation

In the recent past, it was considered that fatigue cracks initiated at a free surface or else at a subsurface inclusion or defect in particular circumstances, although it has been known for some time that titanium

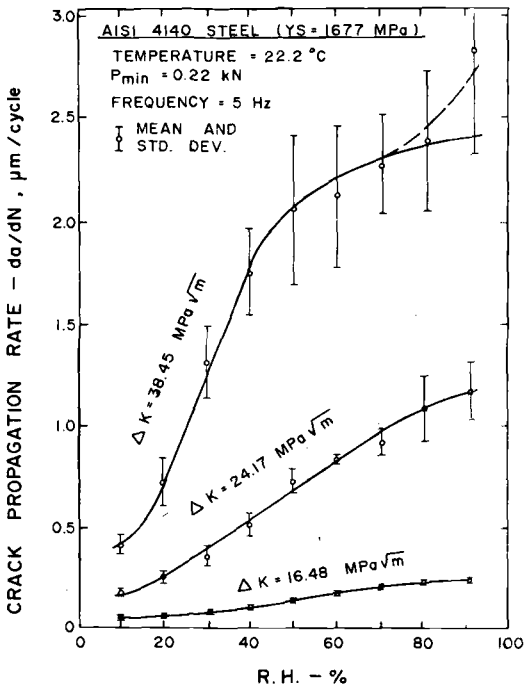

FIG. 2—*Variation in crack propagation rate as a function of relative humidity for 4140 steel at different* ΔK *ranges. After Ref* [7].

alloys provided an exception to this rule, with frequent subsurface crack initiation taking place. McEvily and his co-workers [*9*] have now identified the mechanisms thought to be responsible and have tied them in with the microstructural features of such alloys. Persistent slipbands have been recognized as an important feature in the initiation of Stage I[4] fatigue cracks for many years in face-centered cubic (FCC) metals: however, Mughrabi et al [*11*] have demonstrated how they can arise in body-centered cubic (BCC) metals under specific conditions, and have discussed the relevant mechanisms. The use of high-voltage electron microscopy (HVEM) has allowed the dislocation arrangements around crack tips to be identified with much greater precision than heretofore and certainly this area of activity needs to be extended to consider the cases where environmental effects are of importance in modifying the deformation processes and plastic zone size, and this point will be considered further herein. Thus, much remains to be done to extend HVEM studies of the type made by Katagiri et al [*12*]. Because of the limited availability of such instruments,

[4]The nomenclature of Forsyth [*10*] for initial/Stage I (slant mode) and Stage II (tensile mode) fracture is followed.

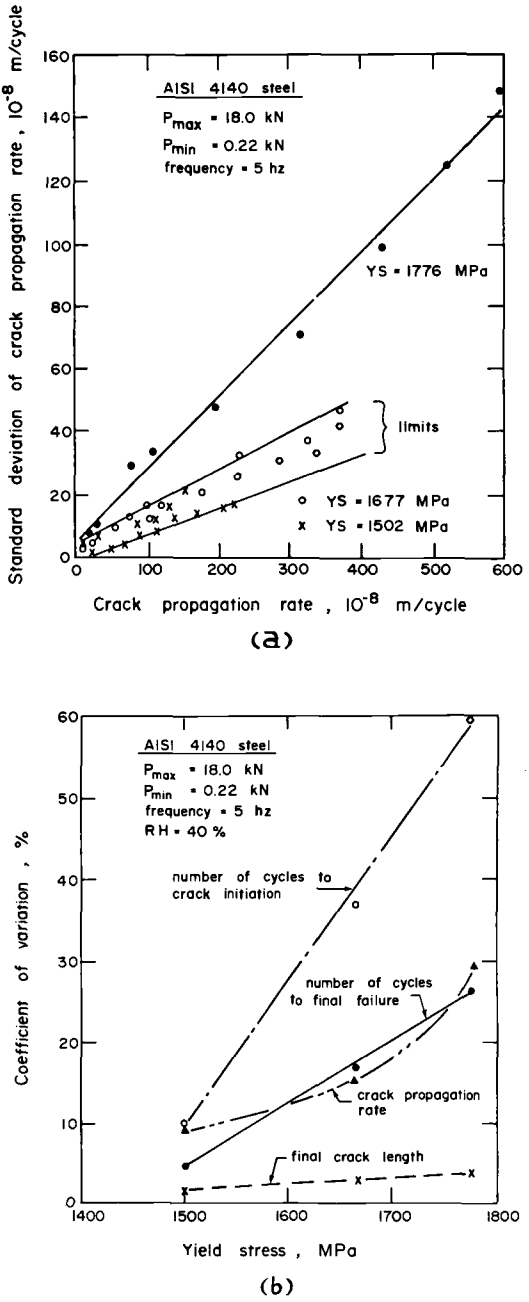

FIG. 3—(a) *Standard deviation of fatigue crack growth rate in 4140 steel as related to crack propagation rate.* (b) *Intrinsic standard deviation of 4140 as dependent on tempering temperature. After Ref* [8]

one must also hope for cooperative projects between the various groups involved.

Missing from the symposium was much consideration of the nature of fatigue damage on other than these specific aspects, and the author considers this to be one of the key gaps in our knowledge. Currently, we seem to be unable to model the accumulation of damage up to crack initiation on a mechanistic and statistical basis, and we do require an adequate understanding of the mechanisms involved in "damage" and the potential for reversing such a process. It is hoped that we may be able then to model crack initiation on a probabilistic basis [*13*] in a quantitative rather than a qualitative manner.

Turning from mechanisms of damage to crack nucleation, Taira et al [*14*] have made an important contribution in applying linear elastic fracture mechanics (LEFM) methods to study the growth of surface microcracks, finding that the same da/dN versus ΔK relationship applies as for through-cracks. They have been able to explain the grain size dependence of the near-threshold crack growth rate and fatigue limit in low-carbon steel, and have provided needed information on cycles for crack initiation as a function of cyclic stress. This study should provide a stimulus for further related work, and the application of quantitative metallographic techniques to measurements of microcrack density and distribution is certainly called for. Similarly, Kunio and Yamada [*15*] have applied LEFM to determine the threshold condition for crack propagation in a two-phase, ferritic-martensitic structure; in this latter study some consideration to the distribution of cracks was also given. Additionally, Kitagawa et al [*16*] have applied LEFM and quantitative metallography to the study of small surface cracks, and have also attempted to relate this approach to the concepts of cyclic strain accumulation or low-cycle fatigue.

Environmental Aspects of Crack Growth

Roughly half the papers presented at this symposium include consideration of environmental effects specifically, and recognition of the importance of such effects is surely one of the greatest advances in our approach to fatigue studies over the past 20 years. Indeed, it would be foolish today to attempt to discuss fatigue mechanisms or fatigue life prediction without including such considerations, or else excluding them *by design* in considering base material behavior, and it may be noted that a conference devoted entirely to environmental effects on fatigue was held in 1977 [*17*].

It has become clear that the basic mechanisms of deformation can be affected by environment and that the crack opening displacement and the size and shape of the plastic zone at the tip of a crack are dependent on environment. Davidson and Lankford [*18*] previously illustrated some of these features in a low-carbon steel exposed to dry nitrogen and water

vapor, and the important technique of electron channeling, using the SEM which they employed, has been described in some detail by Davidson [*19*] at this symposium. It is clear that, with the widespread availability of SEM's, this technique will become one of our more important tools in the future. Detailed examinations of slip processes at the tips of cracks propagating in Stage II fatigue have been described by Lynch [*20*] for a variety of environments. It was shown that there are similarities between crack growth in aqueous, moist air, and liquid metal environments with promotion of dislocation nucleation at crack tips being indicated *via* the mechanism of chemisorption. In an inert environment slip was seen to be more widespread on crack opening with greater crack blunting; on load reversal, slip took place behind the crack tip to provide crack resharpening. Lynch [*20*] has also examined the effect of microstructure using pure aluminum and aluminum-zinc-magnesium heat-treated in several ways; he discussed the formation of "ductile" and "brittle" striations and correlated these with environment and material condition. In addition, Lynch has reviewed some earlier studies relating to Stage I crack growth and striation formation during this process [*21*].

Work reported by Wilhelm et al [*22*], which appears to be a more complete reporting of previously reported data [*23*], indicates the effects of both microstructure and environment in sustaining crack growth in Stage I or initiating Stage II growth. The conclusion reached, namely, that hydrogen, produced by dissociation of water vapor at the crack tip, is adsorbed on the freshly exposed surface and diffuses into the plastic zone, so producing embrittlement, is in contrast to the mechanism proposed by Lynch [*19*], although the material used was approximately the same. Further work to clarify these opposing theories is certainly required.

The work of Kikukawa et al [*24*], involving observation of crack growth in an iron-silicon alloy in an SEM, has produced direct evidence of rewelding of the crack tip in compression, as has been suggested previously [*25*]. The mechanism of crack propagation corresponded to that proposed by Neumann [*26*] with alternate slip occurring at the sharp crack tip. Another paper concerned with crack-tip rewelding was that of Neumann et al [*27*]; in this work, copper single crystals were observed to undergo rewelding at the crack tip during compressive loading in vacuum. The alternating slip mechanism of crack growth from the crack tip during tensile loading [*26*] was also observed directly. An interesting observation reported is that Stage I crack growth did not occur in vacuum even at very low strain rates, whereas it took place in air provided the strain rate was not too high. This indicates the importance of a reacting environment for the promotion of Stage I growth, and the idea of such an environment being required for localization of deformation is in agreement with the observations of Lynch [*20*] for localization of deformation in Stage II growth.

Wei [*28*] has provided an overview of environmental enhancement of

fatigue crack growth with emphasis on the fracture mechanics approach, treating the particular case of high-strength steel in moist air in which the mechanism of environmental influence is considered to be hydrogen embrittlement ahead of the crack tip, and the rate limiting process is identified as the nucleation and growth of oxide on the surface with evolution of hydrogen. While Wei emphasizes the importance of the *partial pressure* of water vapor, it should be noted that Shaw and Le May [*7*] have demonstrated that it is the *relative humidity* which is of prime importance, and this is illustrated in Fig. 4.

Some apparent contradiction appears to be present between some of the foregoing observations concerning slip localization in *aggressive* atmospheres and the observations of Schijve [*29*] and Shaw and Le May [*7*], who have reported that slant mode fracture is promoted by inert or dry atmospheres. It was reported that a crack starting at an internal defect (and, hence, in vacuum) may propagate right through a specimen in slant mode as opposed to a crack starting at the outside (in air), which propagates in tensile mode [*29*]; also cracks propagating in tensile mode transform more readily to slant mode when tested in low-humidity atmospheres [*7*]. The observations perhaps relate to the differences in detailed mechanisms of deformation which are operative, and to the differences in plastic zone size and shape occurring as a result of environment, although it may be noted that to date Stage I deformation has not been investigated as fully as one might wish. Rewelding, with reverse slip taking place, may favor continuation of Stage I growth, whereas slip on unloading in an oxidizing or aggressive atmosphere, and production of a Stage I striation, may be expected to trigger Stage II growth more readily on reloading, this growth taking place from a Stage I striation formed as described by Lynch [*20*]. Certainly, localization of slip to such a region would appear to favor a transition to Stage II growth. The transition from tensile to shear-mode fracture under inert conditions may likewise be considered in terms of the larger plastic zone with more widespread slip which occurs under such conditions, rather than localization of strain on planes emanating from the crack tip and alternate slipping on these, as takes place in aggressive surroundings. Widespread and dispersed slip would tend to favor shear-mode fracture, whereas the localized alternate slipping would promote flat fracture.

It has become clear from these and other studies of environmental influences on fatigue that so-called frequency effects on crack propagation rate and fatigue life are, in fact, environmentally induced and that frequency enters into the picture only for high-frequency conditions where adiabatic heating becomes important.

In concluding this brief discussion of environmental effects, one is struck by the need to undertake a comprehensive program of study in order to correlate the many different results reported in the literature, using tests

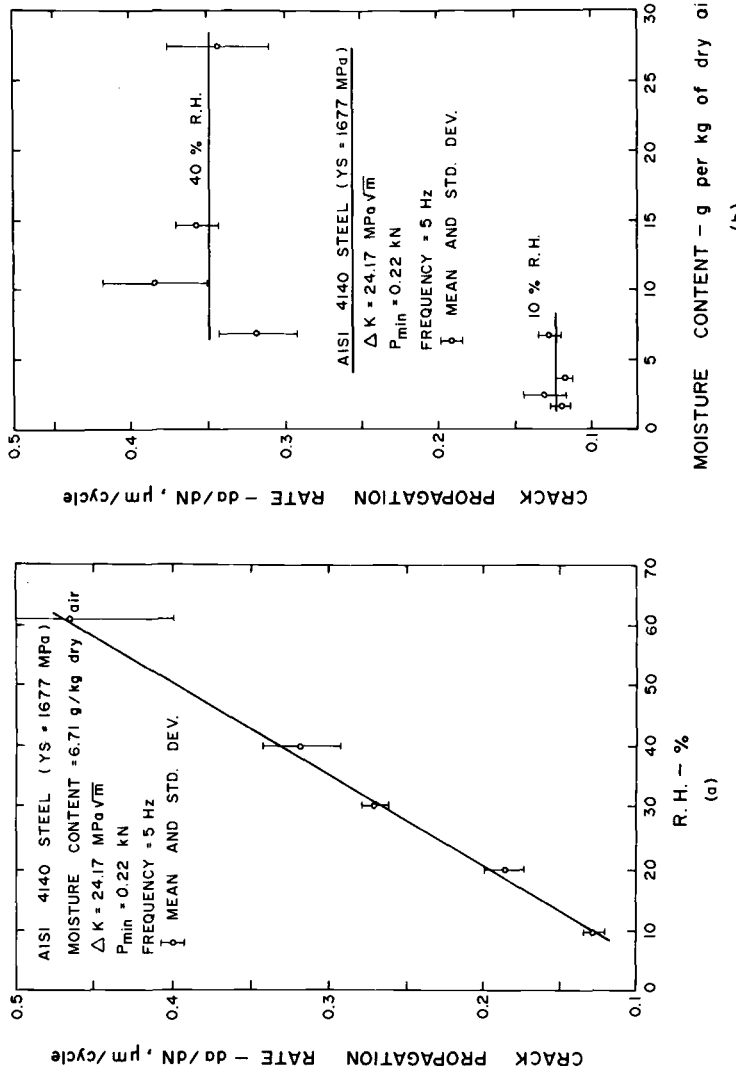

FIG. 4—(a) *Effect of relative humidity on fatigue crack propagation in 4140 steel with* ΔK *and moisture content (and, thus, partial pressure) maintained constant.* (b) *Effect of moisture content on crack propagation rate for 4140 steel at constant values of* ΔK *and relative humidity. After Ref* [7].

involving a wide range of environments and a range of materials, together with full utilization of all available observational methods. Perhaps we should be looking to the planning of a further symposium in two or three years' time which will deal primarily with *fatigue mechanisms and environment,* rather than engineering or life prediction aspects involving environmental effects. The time appears ripe for preliminary planning along these lines to commence.

Fracture Topology and Crack Propagation Laws

Fatigue fracture surface topology is affected sensitively by microstructure as well as by environment and loading conditions, and Gerberich and Moody [*30*] have discussed the various topological effects to be seen. Apart from its relevance in elucidating fundamental crack propagation mechanisms, such information is important in identifying fracture mechanisms on failed components, and the laws governing fatigue crack growth may be modified considerably. Gerberich and Moody comment on the formation of intergranular ductile fatigue striations and suggest that they have not been reported previously: however, such features have been reported previously [*31,32*] in a high-strength steel. In discussing the effect of low temperatures on fatigue crack propagation, the paucity of data is commented upon, and with this point the present author agrees fully. There is a need to provide substantially more information in this area, particularly for situations where the ambient temperature conditions fall below the ductile-brittle transition temperature. Some data by Le May and Lui [*33*] for a high-strength low-alloy (HSLA) steel indicate that the crack propagation law exponent, n, in the Paris-Erdogan equation [*34*], $da/dN = C\Delta K^n$, may be sensitive to temperature in a more complex manner than is indicated in the Gerberich and Moody paper, although the significance of such plots showing variations in n is not altogether clear.

Yokobori [*35*] has reexamined a large number of the fatigue crack growth laws over the intermediate region of a logarithmic plot of da/dN versus ΔK to determine how they are affected by ferrite grain size and static yield stress. While a slight dependence on these of the exponent, n, was found, the effect appears to be a minor one when compared with the effect of grain size on the threshold for crack propagation and in the initial growth rate close to the threshold [*14,30*]. Further effects of microstructure on crack propagation rate were examined by Scarlin [*36*] for nickel-base alloys; this work has emphasized the importance of precipitate distribution and morphology in that ductile tearing was reported to occur along softened grain boundaries containing coarse γ'-particles.

There has been little material presented in this symposium concerning the overall micromechanical modeling of fatigue crack growth from theshold to fracture, Yokobori's paper [*35*], for example, dealing primarily with the

intermediate or straight-line region of the da/dN versus ΔK plot, as just noted. The process of modeling is not a simple one and it is to be hoped that the discussions on threshold effects, in particular, will assist in the modeling process.

There is also need for more unequivocal definition of the stress-intensity factor at crack closure (or crack opening), which is required for accurate prediction of crack propagation rates using the effective range of stress-intensity factor, ΔK_{eff}, rather than ΔK. This is likely to be altered by environment in terms of modification of the plastic zone configuration and resulting residual stress distribution, although the author is unaware of any systematic work in this area.

McEvily [*37*] has recently proposed a modification of a semi-empirical equation proposed earlier [*38*], and which appears to fit experimental data over the complete range of ΔK, while Irving and McCartney [*39*] have proposed a new relation based on an energy balance criterion and containing the concept of a crack-tip process zone. They have shown that this relation fits closely to experimental data derived in *inert* environments from theshold to fracture. Certainly, additional work is urgently needed in this area of micromechanical modeling, but two points must be made. First, environmental effects must be recognized and basic laws should first be formulated for inert environments before being modified to account for active environments; second, a major problem in examining and correlating da/dN versus ΔK data relates to the unreliability or scatter in such data, and further evaluation of computational methods to derive such curves from original plots of a versus N is required.

Fatigue Mechanisms at High Temperatures

In this symposium, high-temperature fatigue mechanisms have been discussed by Scarlin [*36*], Runkle and Pelloux [*40*], Sidey and Coffin [*41*], Min and Raj [*42*], and Bhat and Laird [*43*], while Lin and Lin [*44*] have discussed the application of a micromechanical theory of fatigue crack initiation to time-dependent fatigue, that is, where creep effects become important. In addition, two papers concerning fatigue in polymeric materials [*45,46*] were placed deliberately with the high-temperature metal fatigue papers in an attempt to allow unifying concepts to be brought out, at least in discussion.

Although much work has been carried out on fatigue at high temperature since the publication of the 1972 symposium [*47*], it appears that we still do not have good quantitative predictive methods developed except on a largely empirical basis. The effects of wave shape have been investigated and reported on in some detail by Sidey and Coffin [*41*], and they emphasize the critically important role of environment in high-temperature fatigue. Earlier work indicated that time-dependent or creep effects, as evidenced

by the effect of frequency, may be relatively unimportant as compared with environmental effects [*48*]; however, it is now recognized that wave shape can be of considerable importance also. The authors have utilized test procedures involving unequal strain rates in tension and compression as discussed previously be Coffin [*49*], and have presented a *qualitative* model for fatigue damage which can account for wave shape, environmental, strain range, and frequency effects. However, it is essential that such a model be quantified for the purposes of design in the absence of a large quantity of test data. Currently, one appears to come back to the purely empirical strain-range-partitioning method for quantitative life predictions [*50*], but this method depends on the availability of test data for the particular material of interest at the temperature of concern. Rather than depend on such an empirical approach, in the longer term we need better modeling of elevated-temperature fatigue behavior from a sound micromechanical basis, and the work of Coffin and his associates does recognize and emphasize the importance of mechanisms and of microstructure.

Min and Raj [*42*] have taken an important step in the direction of micromechanical modeling for the process of grain boundary sliding at the crack tip leading to triple-junction grain boundary fracture. This and a related model [*51*] provide an approach for elevated-temperature conditions where intergranular creep-fatigue fracture occurs, as under low strain rates.

Both Scarlin [*36*] and Runkle and Pelloux [*40*] have provided information concerning the role of microstructure and, in particular, second-phase particles and grain boundary shape on fracture mode at high temperature. The importance of environment is well brought out in their work, although quantitative modeling is not possible at present. It is relevant to note, however, in the context of this symposium and its concern with quantitative aspects, that detailed size distributions of second-phase particles have been obtained by Runkle and Pelloux as part of their study. Bhat and Laird [*43*] have, in their paper, described cyclic stress-strain behavior and fatigue damage for precipitation- and dispersion-hardened alloys at elevated temperature, and have found a close relationship to exist between these. While this is to be expected, it is important that such studies be conducted in order to bridge the gap between high-strain, low-cycle fatigue studies of a phenomenological nature and the detailed mechanisms of fatigue with which this symposium is primarily concerned.

The two papers presented concerning polymeric materials [*45,46*] indicate the differences in mechanisms from those occurring in metals as well as some similarities. Beardmore [*45*] has emphasized the cyclic softening phenomenon which occurs independent of microstructure, while Hertzberg et al [*46*] have elucidated the crack propagation mechanisms during Stage II crack growth. Because of the differences in behavior and in crack growth mechanisms, it seems doubtful if unifying micromechanical models for high-temperature or time-dependent behavior can be developed for both

metals and polymers, and this author's impression is that an enormous amount of work is both possible and called for to allow fatigue design of polymeric materials to be undertaken on a rational and sound basis. This is important to materials engineers because of the increasing use of such materials in critical components which are subject to cyclic load, these ranging from aircraft parts to replacement heart valves. Perhaps we may see funding for such studies more easily forthcoming by concentrating on topics such as the latter, where support often seems to be greater!

Composite Materials

As with polymeric materials, there has been a large increase in interest in the fatigue behavior of composites as their use has expanded. In their review of damage mechanisms in fiber-reinforced composites, Stinchcomb and Reifsnider [*52*] discuss the phenomenology of the damage processes and stress the complex and anisotropic nature of the material. While the structure is not simple, it is in many ways much simpler than that of polycrystalline metal having a wide and uneven distribution of second-phase particles, inclusions, etc. Thus, it would appear to the author that considerable opportunities exist to quantify both the microstructure and the fatigue damage which occurs in this in composite materials. While no specific suggestions are made, casting the net wide, as suggested by Professor Rhines [*4*], may be particularly profitable in dealing with fatigue in composites.

Stoloff and Duquette [*53*] examined fatigue mechanisms in *in situ* eutectic composites, and the area covered spans the gap between fiber composites and alloys with a distribution of second-phase particles. The appropriateness of postsolidification heat-treatment to produce a distribution of second-phase particles in the matrix was shown, and once again the important influence of environment on high-temperature fatigue behavior has been demonstrated.

Closing Remarks

Obviously the emphasis and coverage given in this survey of the symposium are personal ones, as the material presented has covered a wide range of topics under the general heading of fatigue mechanisms. For example, while environmental effects have been recognized as being of great importance both in this survey and in the course of the symposium, little has been said in either concerning the effects of severely corrosive environments, with the exception of the paper by Hoeppner [*54*] concerning the initiation of a fatigue crack from a corrosion pit. The importance of corrosion fatigue is recognized, but it is, in the author's view,

such a major topic in itself as to justify separate treatment as has, indeed, been done in the past few years [*55,56*]; however, it is appropriate that we are reminded of such factors at this time.

It would appear to the author that this symposium has provided a much needed review of the current state of knowledge concerning fatigue mechanisms and has, at the same time, identified several topics and areas in which our knowledge is lacking and where further study is needed. We may confidently expect that quantitative determination of microstructure and the utilization of such information in analyzing fatigue behavior will be much more widespread in future. Similarly, integration of effort between different individuals and groups in order to formulate more valid micromechanical models appears probable. The widespread availability of computers is likely to aid in the obtaining of more reliable data concerning intrinsic material scatter, while it is hoped that in future few workers will ignore the influence or potential influence of environment on fatigue behavior.

A number of specific comments and observations concerning needed research have been made during the course of this survey, but the real test of the usefulness of this and subsequent symposia will be the realization of the possibility of predicting service fatigue life and designating the stress to cause failure in a statistically specified time for the purpose of design, with a good precision and on the basis of microstructure and mechanical properties. It is hoped that it will not require another symposium in 20 years' time to point out how far we still have to go in that direction.

Acknowledgments

The author wishes to acknowledge the support of the National Science Foundation in assisting him to present this symposium review. Thanks are also expressed to the National Research Council of Canada for support of his work in the area of metal fatigue.

References

[*1*] *Symposium on Basic Mechanisms of Fatigue, ASTM STP 237,* American Society for Testing and Materials, 1959.

[*2*] Fong, J. T., this publication, pp. 729-758.

[*3*] Jaske, C. E. and O'Donnell, W. J., *Journal of Pressure Vessel Technology, Transactions* American Society of Mechanical Engineers, Vol. 99, 1977, pp. 584-592.

[*4*] Rhines, F. N., this publication, pp. 23-46.

[*5*] Underwood, E. E. and Starke, E. A., Jr., this publication, pp. 633-682.

[*6*] Le May I., Whelan, J. M., and Shaw, W. J. D., "Design for Fatigue in Notched High-Strength Steel," ASME Paper 75-DE-31, American Society of Mechanical Engineers, 1975.

[*7*] Shaw, W. J. D. and LeMay, I. in *Fatigue Testing and Design,* R. G. Bathgate, Ed., Society of Environmental Engineers, London, U.K., Vol. 2, 1976, pp. 31.1-31.24.

[8] Shaw, W. J. D. and LeMay, I. in *Proceedings,* Conference on the Influence of Environment on Fatigue, Institution of Mechanical Engineers, London, U.K., 1977, pp. 93-100.
[9] Ruppen, J., Bhowal, P. B., and McEvily, A. J., this publication, pp. 47-68.
[10] Forsyth, P. J. E. in *Proceedings,* Crack Propagation Symposium, The College of Aeronautics, Cranfield, U.K., 1961, pp. 76-94.
[11] Mughrabi, H., Ackerman, F., and Herz, K., this publication, pp. 69-105.
[12] Katagiri, K., Awatani, J., Omura, A., Koyanagi, K., and Shiraishi, T., this publication, pp. 106-128.
[13] Provan, J. W. in *Proceedings,* Fracture 1977, Vol. 2, D. M. R. Taplin, Ed., University of Waterloo Press, Waterloo, Ont., Canada, 1977, pp. 1169-1176.
[14] Taira, S., Tanaka, K., and Hoshina, M., this publication, pp. 135-173.
[15] Kunio, T. and Yamada, K., this publication, pp. 342-370.
[16] Kitagawa, H., Takahashi, S., Suh, C. M., and Miyashita, S., this publication, pp. 420-449.
[17] *Proceedings.* Conference on the Influence of Environment on Fatigue, Institution of Mechanical Engineers, London, U.K., May 1977.
[18] Davidson, D. L., and Lankford, J. in *Proceedings,* Fracture. 1977, Vol. 2, D. M. R. Taplin, Ed., University of Waterloo Press, Waterloo, Ont., Canada, 1977, pp. 897-904.
[19] Davidson, D. L., this publication, pp. 254-275.
[20] Lynch, S. P., this publication, pp. 174-213.
[21] Lynch, S. P., *Metal Science,* Vol. 9, 1975, pp. 401-410.
[22] Wilhelm, M., Nageswarao, M., and Meyer, R., this publication, pp. 214-233.
[23] Nageswarao, M. and Wilhelm, M. in *Proceedings,* Fracture, 1977, Vol. 2, D. M. R. Taplin, Ed., University of Waterloo Press, Waterloo, Ont., Canada, 1977, pp. 703-709.
[24] Kikukawa, M., Jono, M., and Adachi, M., this publication, pp. 234-253.
[25] Pelloux, R. M. N., *Transactions,* American Society for Metals, Vol. 62, 1969, pp. 281-285.
[26] Neumann, P., *Acta Metallurgica,* Vol. 22, 1974, pp. 1167-1178.
[27] Neumann, P., Fuhlrott, H., and Vehoff, H., this publication, pp. 371-395.
[28] Wei, R. P., this publication, pp. 816-840.
[29] Schijve, J. in *Proceedings,* Institution of Mechanical Engineers, London, U.K., Vol. 191, 1977, pp. 107-114.
[30] Gerberich, W. W. and Moody, N. R., this publication, pp. 292-341.
[31] Lui, M.-W. and LeMay, I. in *Grain Boundaries in Engineering Materials,* J. L. Walter, J. H. Westbrook, and D. A. Woodford, Eds., Claitor's Publishing Division, Baton Rouge, La., 1975, pp. 397-407.
[32] LeMay, I. and Lui, M.-W., *Metallography,* Vol. 8, 1975, pp. 249-252.
[33] LeMay, I., and Lui, M.-W. in *Proceedings,* Conference on the Influence of Environment on Fatigue, Institution of Mechanical Engineers, London, U.K., 1977, pp. 117-122.
[34] Paris, P. C. and Erdogan, F., *Journal of Basic Engineering, Transactions,* American Society of Mechanical Engineers, Vol. 85, 1963, pp. 528-539.
[35] Yokobori, T., this publication, pp. 683-706.
[36] Scarlin, R. B., this publication, pp. 396-419.
[37] McEvily, A. J., *Metal Science,* Vol. 11, 1977, pp. 274-284.
[38] McEvily, A. J. in *The Microstructure and Design of Alloys,* Vol. 2, Metals Society, London, U.K., 1974, pp. 204-225.
[39] Irving, P. E. and McCartney, L. N., *Metal Science,* Vol. 11, 1977, pp. 351-361.
[40] Runkle, J. C. and Pelloux, R. M., this publication, pp. 501-527.
[41] Sidey, D. and Coffin, L. F., Jr., this publication, pp. 528-568.
[42] Min, B. K. and Raj, R., this publication, pp. 569-591.
[43] Bhat, S. P. and Laird, C., this publication, pp. 592-623.
[44] Lin, T. H. and Lin, S. R., this publication, pp. 707-728.
[45] Beardmore, P., this publication, pp. 453-470.
[46] Hertzberg, R. W., Skibo, M. D., and Manson, J. A., this publication, pp. 471-500.
[47] *Fatigue at Elevated Temperatures, ASTM STP 520,* A. E. Carden, A. J. McEvily, and C. H. Wells, Eds., American Society for Testing and Materials, 1973.

[48] Henry, M. F., Solomon, H. D., and Coffin, L. F., Jr. in *Creep and Fatigue in Elevated Temperature Applications,* Vol. 1., Institution of Mechanical Engineers, London, U.K., 1975, pp. 182.1–182.7.

[49] Coffin, L. F., Jr. in *Proceedings,* ASME-MPC Symposium on Creep-Fatigue Interaction, MPC-3, American Society of Mechanical Engineers, New York, 1976, pp. 349–363.

[50] Manson, S. S., Halford, G. R., and Hirschberg, M. H., *Design for Elevated Temperature Environment,* American Society of Mechanical Engineers, New York, 1971, pp. 12–24.

[51] Raj, R., and Min, B. K., "The Effect of Cycle Shape on Creep-Fatigue Interaction in Austenitic Stainless Steel," ASME Paper No. 78-PVP-89, American Society of Mechanical Engineers/Canadian Society for Mechanical Engineers, Pressure Vessel and Piping Conference, Montreal, Que., Canada, 28–29 June 1978.

[52] Stinchcomb, W. W. and Reifsnider, K. L., this publication, pp. 762–787.

[53] Stoloff, N. S. and Duquette, D. J., this publication, pp. 788–815.

[54] Hoeppner, D. W., this publication, pp. 841–870.

[55] *Corrosion Fatigue: Chemistry, Mechanics and Microstructure,* NACE-2, National Association of Corrosion Engineers, Houston, Tex., 1972.

[56] *Corrosion-Fatigue Technology, ASTM STP 642,* H. L. Craig, Jr., T. W. Crooker, and D. W. Hoeppner, Eds., American Society for Testing and Materials, 1978.

General Discussion and Concluding Remarks

S. Manson[1]—My hope when I first registered at this conference was that most of the answers regarding fatigue mechanisms would be found here, answers that would put many conflicting claims and counterclaims into proper perspective, answers from the many participating countries that would clarify numerous mysteries of the subject. Although the R factor for the conference is high (R = ratio of realization to expectation), it must in some ways be regarded as disappointing. Not so because the investigators in the field have not worked hard enough, nor that they have not been creative enough, but rather because there is not enough support for this type of research to insure a constant flow of new understanding that will guarantee eventual success in the completely rational treatment of this subject. So my first conclusion is that we must gain this support from sponsors who can appreciate the value of its significance. As Jeffrey Fong pointed out in his introductory comments, financial support of this effort will more than pay for itself in the long run.

Despite this minor tone of disappointment, I think it is fair to say that on the whole this conference has been very successful in at least three respects:

1. The organization and arrangements have been superb, and for this we have Jeffrey Fong to thank, as well as the many participants who marched to his drum.

2. It provided a marvelous opportunity for workers in the field to get together, particularly those from other countries. The personal exchange of amenities and technical discussion is bound to have long-lasting value in inspiring mutual respect and affection, and will no doubt likewise be reflected in future scientific discovery and development.

3. The technical content has been good, if not complete, and much value will emerge, particularly when the *Proceedings* are published and it is possible to study the whole conference in perspective.

As for future study, it is my hope that the incompleteness of this conference will inspire the financial support required to elucidate some of the questions yet unanswered. I would hope, for example, a better rationale

[1] Department of Mechanical and Aerospace Engineering, Case Western Reserve University, Cleveland, Ohio.

for the power-law relationship between plastic strain-range fatigue life proposed over 25 years ago by Coffin and myself, the Universal Slopes equation proposed nearly 15 years ago, the extension of the plastic-power relation into the high-temperature region (using strain-range partitioning) by introducing four such relations instead of one, the various crack propagation laws initiating with the work of Paris and studied by investigators too numerous to mention, and the extension of these laws into the high-temperature range. A thorough understanding of the mechanistic basis for the relationships that govern the fatigue process could be of tremendous help not only in the treatment of current technological problems but in the design of new material capable of fulfilling the rigorous requirements of tomorrow's technology.

R. Stephens[2]—I would like to make a comment on Professor Le May's summary where he talked about the environmental influence on fatigue as if that were a major item of mechanism research. I started looking back through history and trying to put my eyes through P. G. Forrest's book of 1963. That book had a lot of McAdam's work on corrosion fatigue first reported way back in the 1920's. If we go farther back to McAdam, Gough, Moore, Kommers, etc., we find that these people were well aware of the environmental aspects of fatigue and have included them in their work. By emphasizing the environmental influence today, I am wondering if we are just bringing out this earlier work again, or if we are reinventing the wheel and not taking full advantage of the results of our forefathers. So I guess I wasn't quite as strong about environmental aspects as Ian Le May because I know they have been around at least 50 years and nowhere have they been emphasized as at this conference.

J. Fong[3]—Ralph, if I may add a little perspective in this, I am sure you will agree that the earlier investigators were handicapped for not having the sophisticated instrumentation such as the electron microscope and Auger spectroscopy that we have today. Perhaps when we increase our observational power, we tend to tackle a problem that appeared to be hopeless in the earlier days and hence was never emphasized in the literature.

Professor Taira, would you like to share your thoughts with us on anything related to this conference on the subject of fatigue in general?

S. Taira[4]—I am very much interested in the symposium and I think it has been very successful. I would like to thank you and Professor JoDean Morrow for all the efforts that went into this conference.

[2]Materials Engineering Division, University of Iowa, Iowa City, Iowa.

[3]Physicist and project leader, Center for Applied Mathematics, National Engineering Laboratory, National Bureau of Standards, Washington, D.C.

[4]Department of Engineering Science, Kyoto University, Kyoto, Japan.

L. Coffin[5]—I think that Dr. Le May and I agree relative to our general advance of understanding on fatigue mechanisms. Nevertheless, I don't feel that the fact we still know so little is necessarily bad. In many respects, the conference itself has been quite a successful enterprise. I think we have all learned something and maybe we have learned a lot more about what we don't know than what we do know, and that is half the struggle. Having been involved in the formation of this symposium from the very beginning and knowing pretty much who has done what to make this thing go, I want to make it quite clear that the success of this venture is due almost entirely to one man and his enthusiasm in rallying the necessary forces to get this thing going and make it successful, and that man is Dr. Jeffrey Fong.

J. Fong—Thank you, Lou, for your kind words. Before we turn the podium over to Professor JoDean Morrow, who chairs Subcommittee E9:01 on Fatigue Research which initiated this conference, I would like to thank my colleague, Dr. Richard Fields, whom I had the good fortune of meeting about two years ago at Cambridge and who has been extremely helpful in getting this meeting well coordinated. Thanks, Richard.

J. Morrow[6]—I have one complete page of notes that I collected during the week to use in these closing remarks. One by one every item on this list has been mentioned by somebody else this afternoon. Please let me make one or two remarks and then we will adjourn. Somebody compared the fatigue process to a horse race. All I've seen this week are snapshots of horses. Nobody mentioned or showed evidence of the dynamic process responsible for fatigue damage which I feel is very important.

A number of us have tried to eliminate the concept of an endurance limit from our thinking and from the thinking of people who have to design parts to last under service conditions. I am disappointed, frankly, that some of you backslide to thinking of a safe stress below which fatigue will never be a problem, and a threshold stress below which cracks will not propagate. I think that is a mistake and certainly has no place in the design philosophy of engineers who try to make parts that last a safe period of time.

Finally, I am somewhat disappointed that I don't have any better idea of what fatigue damage is than I did at the beginning of this symposium. It hasn't been defined. Nobody knows how to reverse the process, which would seem to me to be the optimistic approach to the problem of fatigue.

[5]Mechanical engineer, General Electric Co. Schenectady, N.Y.; also, chairman of ASTM Committee E9 on Fatigue.

[6]Department of Theoretical and Applied Mechanics, University of Illinois-Urbana, Urbana, Ill.

Why can't we reverse the process of damage? Shouldn't some of us be approaching the fatigue problem from such a viewpoint? Certainly we would understand about damage if we could learn to reverse the process. With that, I would like to adjourn this meeting and wish you all bon voyage, auf wiedersehen, and sayonara.

Appendix: List of Symposium Participants and Correspondents

SYMPOSIUM ON FATIGUE MECHANISMS

May 22-24, 1978
Kansas City, Missouri, U.S.A.

AUSTRALIA

Finney, J. M.
Aeronautical Research Laboratory
Melbourne, Australia 3001

Lynch, S. P.
Aeronautical Research Laboratory
Melbourne, Australia 3001

CANADA

Ericsson, Torsten
University of Waterloo
Waterloo, Ontario

Hornaday, J. R.
Deutz Diesel Ltd.
Montreal, Quebec

LeMay, I.*
University of Saskatchewan
Saskatchewan, Saskatoon

Plumtree, Alan
University of Waterloo
Waterloo, Ontario

Provan, James W.
McGill University
Montreal, Quebec

Sidey, Duncan
421 Chartwell Rd.
Oakville, Ontario L6J 4A4

FRANCE

Bhandari, M. Surender
NOVATOME
Paris, France

Driver, J. H.
Department of Metallurgie
Saint-Etienne, France

GERMANY

Heckel, Klaus
Hochschule der Bundeswehr
Munchen, Germany

Kroner, E.
Universitat Stuttgart
Stuttgart, Germany

Mughrabi, H.
Max-Planck-Institut fur
Metallforschung
7000 Stuttgart-80, W. Germany

Neumann, Peter
Max-Planck-Institut fur
Eisenforschung
4000 Dusseldorf, W. Germany

Sturm, Dietmark
MPA Stuttgart
Stuttgart, W. Germany

*Symposium Organizing Committee.
Symposium Advisory Board.

Wilhelm, M.
Max-Planck-Institut fur Metallforschung
7000 Stuttgart-80, W. Germany

Wilhelm, Manfred
Max-Planck-Institut
Stuttgart, Germany

JAPAN

Ebara, R.
Hiroshima Technical Inst.
Hiroshima, Japan

Jono, Masahiro
Osaka University
Osaka, Japan

Katagiri, Kazumune
Osaka University
Osaka, Japan

Kikukawa, Makoto
Osaka University
Osaka, Japan

Kitagawa, Hideo
University of Tokyo
Tokyo, Japan

Koibuchi, Koji
Hitachi, Ltd.
Tsuchiura, Japan

Koyanagi, Kazuo
Osaka University
Osaka, Japan

Kunio, T.
Keio University
Yokohama, Japan

Nisitani, H.
Kyushu University
Fukuoka 812, Japan

Taira, Shuji
Kyoto University
Kyoto, Japan

Takao, Ken-ichi
Saga University
Honjo-machi, Japan

Tanaka, Keisuke
Kyoto University
Kyoto, Japan

Yamada, K.
Keio University
Yokohama, Japan

Yokobori, Takeo
Tohoku University
Sendai, Japan

POLAND

Perzyna, Piotr
Polish Academy of Sciences
Warsaw, Poland

SOUTH AFRICA

Pelser, J. Gus
University of Pretoria
Pretoria, South Africa

SWEDEN

Johansoon, E. Rune
Sandrik, A. B.
Sandriken, Sweden

SWITZERLAND

Scarlin, Richard B.
Brown Boveri & Co.
Baden, Switzerland

UNITED KINGDOM

Atkinson, Colin
Imperial College
London, England

Beevers, C. J.
University of Birmingham
Birmingham, England

Brett, S. J.
British Aluminum Co., Ltd.
Buckinghamshire SL9 0QB, England

Dabell, Brian
GKN Group Technological Ctr.
Wolverhampton, England

Ellison, E. G.
University of Bristol
Bristol, England

Hollox, Graham E.
Ransome Hoffman Pollard Ltd.
Chelmsford, Essex, England

Miller, K. J.
University of Sheffield
Sheffield, England

Plumbridge, W. J.
University of Bristol
Bristol, England

Tomkins, Brian
U.K. Atomic Energy Authority
Preston, England

Worthington, Peter J.
Central Electricity Research
Leatherhead, England

UNITED STATES

Abelkis, P. R.
McDonnell Douglas Corp.
Long Beach, Calif. 90846

Adams, J. H.
Pittsburgh DesMoines Steel
Pittsburgh, Pa. 15225

Albertin, Leopold
Westinghouse Electric Corp.
Pittsburgh, Pa. 15235

Alic, J. A.
Wichita State University
Wichita, Kans. 67208

Allbeyer, Earl R.
The Marley Company
Mission, Kans. 66202

Alstetter, Carl J.
University of Illinois
Urbana, Ill. 61801

Amin, Kamal E.
Bendix Research Laboratory
Southfield, Mich. 48076

Argon, A. S.
MIT-Department of Mechanical Engineering
Cambridge, Mass. 02139

Armstrong, E. L.
Mobil R&D Corp.
Paulsboro, N.J. 08066

Asphahani, A. I.
CABOT
Kokomo, Ind. 46901

Astill, C. J.
NSF-Engineering Division
Washington, D.C. 20550

Baik, Sunggi
Cornell University
Ithaca, N.Y. 14853

Baxter, W. J.
General Motors Research Laboratory
Warren, Mich. 48090

Beardmore, P.
Ford Motor Co.
Dearborn, Mich. 48121

Bench, Dennis M.
ARMCO Steel Corp.
Middletown, Ohio 45043

Bennett, John A.
Bethesda, Md. 20014

Bhat, S. P.
University of Pennsylvania
Philadelphia, Pa. 19104

Bicicchi, Richard
Sun Ship
Chester, Pa. 19015

Boardman, Bruce
Deere & Co.
Moline, Ill. 61265

Bogan, W. W.
General Electric Co.
Cincinnati, Ohio 45215

Bogucki, Gregg R.
Hampton Technical Center
Hampton, Va. 23665

Braun, Arthur A.
University of Missouri
Columbia, Mo. 65201

Brinkman, C. R.
Oak Ridge National Laboratory
Oak Ridge, Tenn. 37830

Brinson, H.
Virginia Polytech Institute
Blacksburg, Va. 24061

Brown, S. A.
Dartmouth Medical School
Hanover, N.H. 03755

Bucci, R. J.
ALCOA Laboratories
ALCOA Center, Pa. 15069

Burck, Larry H.
University of Wisconsin
Milwaukee, Wis. 53209

Burk, J. D.
McDonnell Douglas Astronautics
St. Louis, Mo. 63166

Byrne, J. G.
University of Utah
Salt Lake City, Utah 84112

Carey, R.
Beckman Institute, Inc.
Palo Alto, Calif. 94304

Chait, R.
Army Materials and Mechanical Research
Watertown, Mass. 02172

Chen, Wen-Ching
University of Illinois
Urbana, Ill. 61801

Chesnutt, James C.
Rockwell Science Center
Thousand Oaks, Calif. 91360

Chien, Kuang-Ho
Cameron Iron Works, Inc.
Houston, Tex. 77001

Chisholm, Matthew
Reynolds Metals Company
Richmond, Va. 23261

Chung, Jin-Ho
University of Iowa
Iowa City, Iowa 52242

Coburn, S. K.
U.S. Steel
Pittsburgh, Pa. 15230

Coffin, L. F., Jr.*
General Electric Co.
Schenectady, N.Y. 12301

Collins, J. A.
Ohio State University
Columbus, Ohio 43210

Cooper, Robert A.
Rockwell International
Canoga Park, Calif. 91304

Cowles, Brad
Pratt & Whitney Aircraft
West Palm Beach, Fla. 33402

Cruse, Thomas A.
Pratt & Whitney Aircraft
East Harford, Conn. 06108

Cutler, Verne C.
University of Wisconsin
Milwaukee, Wis. 53201

Davidson, David L.
Southwest Research Institute
San Antonio, Tex. 78284

deHoff, R. T.
University of Florida
Gainsville, Fla. 32611

DeVries, K. L.
University of Utah
Salt Lake City, Utah 84112

DeWit, Roland
National Bureau of Standards
Washington, D.C. 20234

Diercks, Dwight R.
Argonne National Laboratory
Argonne, Ill. 60439

Ditchek, Brian
National Bureau of Standards
Washington, D.C. 20234

Donaldson, Kelly
MTS Systems Corp.
Eden Prairie, Minn. 55343

Dorsey, Jim
Micro-Measurements Division
Romulus, Mich. 48174

Dowling, Norman E.
Westinghouse Research
Pittsburgh, Pa. 15235

Dvorak, G. J.
Duke University
Durham, N.C. 27706

Early, J.
National Bureau of Standards
Washington, D.C. 20234

Eaton, Lyle
WABCO
Peoria, Ill. 61639

Eiffler, E.
Westinghouse Electro-Mechanical Division
Cheswick, Pa. 15024

Eisenstadt, R. E.
Union College
Schenectady, N.Y. 12308

Ekvall, J. C.
Lockheed California Co.
Burbank, Calif. 91520

Esztergar, E. P.
6308 Avenida Cresta
LaJolla, Calif. 92037

Faix, Charles R.
Westinghouse Electric Co.
Lester, Pa. 19113

Fields, R. J.
National Bureau of Standards
Washington, D.C. 20234

Fong, J. T.*
National Bureau of Standards
Washington, D.C. 20234

Forte, Thomas P.
Battelle Columbus Laboratories
Columbus, Ohio 43229

Fox, A.
Bell Laboratories
Murray Hill, N.J. 07094

Gerberich, W.
University of Minnesota
Minneapolis, Minn. 55455

Gilbertson, Leslie N.
Zimmer—USA
Warsaw, Ind. 46580

Goleniewski, Stanley
Lord Kinematics Corp.
Erie, Pa. 16512

Grandt, A. F.
Wright-Patterson AFB, Ohio 45433

Green, R. E.
Johns Hopkins University
Baltimore, Md. 21218

Greenfield, I.
University of Delaware
Newark, Del. 19711

Greenstreet, William L.
Oak Ridge National Lab.
Oak Ridge, Tenn. 37830

Gregory, Glinka
University of Iowa
Iowa City, Iowa 52242

Grosskreutz, J. C.
Solar Energy Research Institute
Golden, Colo. 80401

Gruen, Richard G.
Wisconsin Steel Co.
Chicago, Ill. 60617

Hanlin, Robert
Allis-Chalmers Corp.
Independence, Mo. 64051

Hartt, Wm. H.
Florida Atlantic University
Boca Raton, Fla. 33431

Hebel, A. G.
Benal Corp.
Detroit, Mich. 48216

Hellebrand, Heinz S.
FAA
Washington, D.C. 20590

Helmer, Jerry
Medical Engineering
Racine, Wis. 53404

Hertzberg, R. W.
Lehigh University
Bethlehem, Pa. 18015

Hillberry, B. M.
Purdue University
West Lafayette, Ind. 47907

Ho, New-Jin
University of Illinois
Urbana, Ill. 61801

Hoeppner, D. W.*
University of Missouri
Columbia, Mo. 65201

Hrusovsky, Louis
Rockwell International
Troy, Mich. 48084

Huang, T. C.
University of Wisconsin
Madison, Wis. 53796

Huddleston, Roy L.
Union Carbide Corp.
Concord, Tenn. 37720

Hyatt, Barry Z.
Westinghouse Atomic Lower Laboratory
Bethel Park, Pa. 15102

Jerina, K. L.
MTS Systems Corp.
Minneapolis, Minn. 55424

Jones, David R.
TRW Value Division
Cleveland, Ohio 44110

Jones, Wendell B.
Sandia Laboratories
Albuquerque, N. Mex. 87185

Jordan, R. E.
Allied Chemical Corp.
Moundsville, W. Va. 26041

Kaisand, Leonard
General Electric Company
Schenectady, N.Y. 12345

Kanninen, M. F.
Battelle Memorial Institute
Columbus, Ohio 43201

Kapadia, Behram M.
U.S. Steel Research
Monroeville, Pa. 15146

Kaufman, J. G.
ALCOA
Pittsburgh, Pa. 15219

Ke, Jeng Shyong
Sundstrand Corp.
Rockford, Ill. 61101

Kilpatrick, N. L.
Westinghouse Electric Corp.
East Pittsburgh, Pa. 15112

Krafft, J. M.
U.S. Naval Research Laboratory
Washington, D.C. 20375

Kramer, Irvin R.
David W. Taylor Naval Ship Research and Development Center
Annapolis, Md. 21402

Krempl, E.
Rensselaer Polytechnic Institute
Troy, N.Y. 12181

Kruger, Jerome
National Bureau of Standards
Washington, D.C. 20234

Kulkarni, Satish
Lawrence Livermore Laboratories
Livermore, Calif. 94550

Kurath, Peter
University of Illinois
Champaign, Ill. 61820

Laird, Campbell
University of Pennsylvania
Philadelphia, Pa. 19104

Lamba, Hari
International Harvester
Hinsdale, Ill. 60521

Landgraf, Ronald W.
Ford Motor Co.
Dearborn, Mich. 48121

Langenbeck, Sharon
University of Missouri
Columbia, Mo. 65211

Lankford, James
Southwest Research Institute
San Antonio, Tex. 78284

Lawrence, F. V.
University of Illinois
Urbana, Ill. 61801

Lawton, Carl W.
Combustion Engineering
Windsor, Conn. 06095

Lazaridis, Nassos
Inland Steel Research
East Chicago, Ill. 46312

Leax, Thomas R.
Westinghouse Electric Corp.
East Pittsburgh, Pa. 15112

Leis, Brian
Battelle Columbus Laboratories
Columbus, Ohio 43201

Lewis, Frank M.
Wright Manufacturing Co.
Memphis, Tenn. 38002

Liang, S. J.
Xerox Corp.
Rochester, N.Y. 14623

Lillybeck, Norman P.
Deere & Company
Moline, Ill. 61265

Lin, S. R.
The Aerospace Corporation
El Segundo, Calif. 90245

Lin, T. H.
University of California
Pacific Palisades, Calif. 90272

Little, Robert E.
University of Michigan
Dearborn, Mich. 48128

Liu, H. W.
Syracuse University
Syracuse, N.Y. 13210

Lou, Alex Y.
Firestone Tire & Rubber Co.
Akron, Ohio 44317

Mahmoodi, Parviz
3 M Company
St. Paul, Minn. 55133

Majumdar, S.
Argonne National Laboratory
Argonne, Ill. 60439

Maiya, P. S.
Argonne National Laboratory
Argonne, Ill. 60439

Manson, S. Stanford
Case Western Reserve University
Cleveland, Ohio 44106

Marcus, Harris L.
University of Texas
Austin, Tex. 78759

Mauney, David A.
ALCOA Laboratories
ALCOA Center, Pa. 15069

Mayor, Michael B.
Dartmouth Hitchcock Medical Center
Hanover, N.H. 03755

McEvily, A. J.
University of Connecticut
Storrs, Conn. 06268

Michel, M.
Naval Research Laboratory
Washington, D.C. 20375

Miller, Alan K.
Stanford University
Stanford, Calif. 94305

Min, B. K.
Cornell University
Ithaca, N.Y. 14853

Mitchell, M. R.
Rockwell International
Thousand Oaks, Calif. 91360

Moore, George A.
Rockville, Md. 20851

Moran, George
PSE&G Research Corp.
Maplewood, N.J. 07040

Mordfin, Leonard
National Bureau of Standards
Washington, D.C. 20234

Morrow, J.*
University of Illinois
Urbana, Ill. 61801

Mowbray, Donald F.
General Electric Co.
Schenectady, N.Y. 12345

Mueller, Larry
University of Missouri
Columbia, Mo. 65201

Mura, T.
Northwestern University
Evanston, Ill. 60201

Nemerguth, B. F.
Deere & Co. Technical Center
Moline, Ill. 61265

Nichols, Fred A.
Argonne National Laboratory
Western Springs, Ill. 60558

Novak, Stephen R.
U.S. Steel Corp.
Monroeville, Pa. 15146

Ostergren, Warren J.
General Electric Co.
Schenectady, N.Y. 12345

Palmer, J.
American Society for Testing and Materials
1916 Race St.
Philadelphia, Pa. 19103

Patten, David T.
Bendix Research Laboratory
Southfield, Mich. 48076

Paquin, William P.
Pratt & Whitney Aircraft
Bristol, Conn. 06010

Pelloux, R.
M.I.T.
Cambridge, Mass. 02139

Penn, Robert A.
National Bureau of Standards
Washington, D.C. 20234

Peterlin, A.
National Bureau of Standards
Washington, D.C. 20234

Phippen, Charles G.
Pratt & Whitney Aircraft
Middletown, Conn. 06457

Piotrowski, George
University of Florida
Gainsville, Fla. 32611

Poon, Cheung
University of Missouri
Columbia, Mo. 65201

Preston, John L.
Instron Corp.
Canton, Mass. 02021

Raj, Rishi
Cornell University
Ithaca, N.Y. 14853

Raske, D. T.
Argonne National Laboratory
Argonne, Ill. 60439

Reemsnyder, H.
Bethlehem Steel Corp.
Bethlehem, Pa. 18016

Reeves, Roger
Shell Development Co.
Houston, Tex. 77001

Reifsnider, K.*
Virginia Polytechnic Institute
Blacksburg, Va. 24061

Rhines, F. N.
University of Florida
Gainsville, Fla. 32611

Ridd, Walter J.
General Motors Corp.
Dayton, Ohio 45401

Ritchie, R. O.
M.I.T.
Cambridge, Mass. 02139

Ruff, A. W., Jr.
National Bureau of Standards
Washington, D.C. 20234

Rungta, Ravindra
Ohio State University
Columbus, Ohio 43210

Runkle, J. C.
M.I.T.
Cambridge, Mass. 02139

Ruppen, J.
University of Connecticut
Storrs, Conn. 06268

Salivar, Gary C.
University of Missouri
Columbia, Missouri 65201

Salmella, L. J.
Hexcel Corp.
San Francisco, Calif. 94108

Sandoz, George
Office of Naval Research
Chicago, Ill. 60605

Santangelo, Richard D.
Naval Air Station
Jacksonville, Fla. 32212

Sarver, L. W.
Babcock & Wilcox Co.
Alliance, Ohio 44601

Seeley, R. Rodger
Babcock & Wilcox Co.
Alliance, Ohio 44601

Sendeckyj, G. P.
Wright Patterson Air Force Base, Ohio 45433

Sharma, V. K.
International Harvester Co.
Hinsdale, Ill. 60016

Sih, George C.
Lehigh University
Bethlehem, Pa. 18015

Simmons, John A.
National Bureau of Standards
Washington, D.C. 20234

Skibo, M. D.
Lehigh University
Bethlehem, Pa. 18015

Smith, J. H.
National Bureau of Standards
Washington, D.C. 20234

Socie, Darrell
University of Illinois
Urbana, Ill. 61801

Stafford, Robert
McDonnell Douglas
St. Louis, Mo. 63145

Starke, E. A., Jr.
George Institute of Technology
Atlanta, Georgia 30332

Stentz, Ray
Mar-Test Inc.
Cincinnati, Ohio 45215

Stephens, R. I.*
University of Iowa
Iowa City, Iowa 52242

Stinchcomb, W. W.
Virginia Polytechnic Institute
Blacksburg, Va. 24061

Stoloff, N. S.
Rensselaer Polytech Institute
Troy, N.Y. 12181

Swearengla, Jack C.
Sandia Laboratory
Livermore, Calif. 94550

Sweigart, John
University of Missouri
Columbia, Mo. 65211

Swindeman, R. W.
Oak Ridge National Laboratory
Oak Ridge, Tenn. 37830

Tapay, Harold
University of Santa Clara
Santa Clara, Calif. 95053

Taylor, William H.
#5 Grimal Court
Randolph, N.J. 07801

Thomson, Robb
National Bureau of Standards
Washington, D.C. 20234

Throop, Joseph F.
Benet Weapons Laboratory
Watervliet, N.Y. 12189

Tomita, Nobuya
U.S. Industrial Chemical Co.
Cincinnati, Ohio 45046

Torcolini, Robert J.
Carpenter Technology Corp.
Reading, Pa. 19601

Torrey, Charles
Pratt & Whitney Aircraft
West Palm Beach, Fla. 33402

Underwood, Ervin E.
Georgia Institute of Technology
Atlanta, Ga. 30332

Van Den Avyle, James A.
Sandia Laboratories
Albuquerque, N. Mex. 87185

Vander Sande, J. B.
M.I.T.
Cambridge, Mass. 02139

VanderVelde, Gordon
Dana Corp.
Richmond, Ind. 47374

Van Orden, Jerold M.
Lockheed-California Co.
Burbank, Calif. 91520

Vitale, David
Turbodyne
Wellsville, N.Y. 14895

Waldon, L. E.
Richards Manufacturing Co.
Memphis, Tenn. 38116

Walker, Ken
Lockheed-California Co.
Burbank, Calif. 91520

Walson, Robert P.
Deere & Co. Technical Center
Moline, Ill. 61265

Wang, Tzuu Po
University of Iowa
Iowa City, Iowa 52240

Wei, R. P.
Lehigh University
Bethlehem, Pa. 18015

Weissmann, Sigmund
Rutgers University
Piscataway, N.J. 08854

Wells, C.
Southwest Research Institute
San Antonio, Tex. 78284

Wheeler, J.
ASTM
Philadelphia, Pa. 19103

Wildey, Jim
National Transportation Safety Board
Washington, D.C. 20594

Wilkins, Dick J.
General Dynamics
Fort Worth, Tex. 76101

Williams, Wendall
NSF-Materials Division
Washington, D.C. 20550

Wilson, Dale A.
University of Missouri
Columbia, Mo. 65201

Wilson, Alexander D.
Lukens Steel Co.
Coatsville, Pa. 19320

Wilson, William
A. Finkl
Chicago, Ill. 60614

Winter, Alan
Brookhaven National Laboratory
Upton, L.I., N.Y. 11973

Wnuk, Michael P.
South Dakota State University
Brookings, S. Dak. 57006

Wolf, Stanley M.
Department of Energy
Rockville, Md. 20850

Wright, B. E.
Buick Motor Division
Flint, Mich. 48550

Zinkham, R. E.
Reynolds Metals Co.
Richmond, Va. 23218

Zuk, Irena M.
Interdevelopment, Inc.
Arlington, Va. 22202

USSR

Ivanova, V. S.
Baikove Institute of Technology
Moscow, USSR

Pisarenko, G. S.
Academy of Sciences
Kiev, USSR

Zhurkov, S. N.
Ioffe Physics and Technical Institute
Leningrad, USSR

Subject/Keyword Index

A

Acoustic fatigue, 10, 13
Age-hardening, 215
α-iron, 71
Aluminum alloys, 177, 182, 215, 257, 278
Analytical models, 293
Area fraction, 31, 33
Average geometric properties, 29

B

Benjamin Rush, 288
Bloodletting, 288
Brittle fracture, 382

C

Chemisorption, 194, 196
Cobalt, 789
Composite materials, 763, 789
Connectedness, 26, 27, 31, 34
Copper, 71
Copper alloys, 215
Corrosion fatigue, 816, 841, 843
Cost-benefit, 7, 8
Crack energy, 842
Crack growth, 135, 146
Crack growth rate, 435
Crack growth resistance, 345
Crack initiation, 175, 373, 422, 646, 708
Crack measurement, 422
Crack nucleation, 11, 136, 139, 145, 598, 601, 606
Crack propagation, 20, 116, 180, 183, 215, 255, 278, 377, 396, 651
Crack propagation mechanism, 237
Crack tip angle, 237
Crack-tip opening displacement, 237
Creep, 710
Creep component, 460
Critical strain rate, 579
Cross slip, 76, 80
Curvature, 26, 28, 31, 33
Cyclic deformation, 216
Cyclic hardening, 463
Cyclic softening, 455
Cyclic strains, 430, 435
Cyclic stress-strain behavior, 594
Cyclic stress-strain curve, 458
Cyclic stress-strain response, 72

D

Damage, 601, 763
Damage mechanisms, 529
Direct observation, 234, 287
Discontinuous crack growth, 477
Dislocation arrangements, 107
Dislocation microstructure, 72, 76
Dislocation motion, 11
Dislocations, 26, 47, 177

Dispersion hardening, 594
Dynamic strain aging, 93

E

Electron channeling, 254
Electron diffraction contrast, 255
Electron microscopy (*see also* Quantitative electron microscopy and Scanning electron microscopy), 48
Elevated temperature, 708
Elevated temperature fatigue, 502, 520
Endurance limit, 342
Engineering, 4
Environmental effects, 183
Eutectics, 789
Eutectoid steel, 686
Extrusion, 375, 715

F

Fatigue, 5, 10, 31, 47, 69, 215, 234, 287, 292, 371, 396, 420, 501, 707, 729, 762, 788, 841
Fatigue (materials), 106, 135, 175, 646
Fatigue (mechanics), 420
Fatigue crack growth, 683, 817
Fatigue crack growth constants, 684, 686
Fatigue crack propagation, 292, 474, 477
Fatigue failure, 93
Fatigue fracture, 277
Fatigue fracture (materials), 256
Fatigue fracture mechanisms, 471
Fatigue life prediction, 421
Fatigue mechanism, 6, 10, 23, 287, 345
Fatigue polymers, 453
Fatigue threshold, 303
Feasibility, 5
Ferrite grain size, 687
Fractography, 174, 292, 397
Fracture, 729
Fracture mechanics, 6, 135, 421, 428, 817, 841
Fracture toughness, 397

G

Global parameters, 25
Grain boundary sliding, 570, 572
Grain size, 30, 136
Grain structure, 634

H

Hardening (*see also* Cyclic hardening and Dispersion hardening), 215, 216, 223, 594, 599
Heat-treated bearing steel, 686
High-temperature fatigue (*see also* Elevated temperature fatigue), 531, 538, 569
High-temperature properties, 398, 402, 404, 411
Hold time, 381
Hydrogen embrittlement, 227
Hysteresis, 454

I

Inclusions, 633
Influence of frequency, 216, 222, 227
Influence of water vapor, 222, 227
Initial cyclic yield strength, 683
Initiation, 844
Intergranular, 600
Intergranular fracture, 569
Internal friction, 13
Interstitial impurities, 71, 87
Intrusion, 375, 715
Iron (polycrystalline), 107, 293, 295

K

Kinetics, 841

L

Linear fracture mechanics, 348
Liquid-metal environments, 183, 193
Long-range internal stresses, 76, 80
Low-carbon steel, 136
Low-cycle fatigue, 13, 420, 511, 530, 538
Low temperature, 306, 314

M

Martensite-ferrite microstructure, 343
Mathematical modeling, 6, 743
Mechanical properties, 295, 791
Mechanism (*see also* Fatigue mechanism), 174, 373, 377, 422, 763
Metallography, 174
Metals, 816
Micromechanics, 136, 731
Microscopic fatigue crack, 345
Microstructure, 24, 28, 136, 139, 177, 182, 295, 305, 634, 731
Misorientation, 598
Modeling, 844, 849
Monotonic or static yield strength, 686

N

Nickel, 70, 789
Nickel-base alloys, 279, 398
Nickel-base superalloys, 502
Niobium, 70, 71
Nonpropagating crack, 345, 353
Nuclear fuel element, 738
Nucleation (of persistent slipbands), 77

P

Paper, 736
Particle distribution, 634
Persistent slipbands, 69, 70, 218
Pierre Louis, 289
Pitting, 848
Plain low-carbon steel, 686
Planar slip, 595
Plastic properties, 256, 259
Plastic strain, 13
Plastic zone, 372
Polymers, 473
Precipitation hardening, 789

Q

Quantitative medicine, 289
Quantitative microscopy, 6, 26, 33, 290, 734
Quantitative stereology, 634

R

Resolved shear stress, 710
Rewelding, 379

S

Saturation, 594, 598
Scanning electron microscopy, 277
Second phase spacing, 345, 353
Silicon iron, 686
Silver, 70, 71
Single crystals, 70, 215, 372
Size effect, 731, 743
Slip line, 435, 708
Slip markings, 595, 601
Slip mechanism, 11
Slipbands, 707
Softening (*see also* Cyclic softening), 216, 223, 594, 599
Solid mechanics, 729
Stage I, 373

Stage II, 377
Statistical analysis, 6
Statistical aspects of fatigue, 290
Statistical methods, 734, 738
Steel, 422, 735
Stereology, 6
Strain, 259
Strain rate, 72, 83, 87
Stress relaxation, 10, 13
Structure-property relationship, 28
Superalloy, 502
Surface chemistry, 821
Surface crack, 422

T

Tempered-martensite steel, 686
Thermal effects, 461
Threshold, 845
Threshold condition, 150, 153, 345
Threshold stress-intensity factor range, 428, 430
Titanium alloys, 48, 293, 298
Transgranular, 601, 606
Triple-junction cracking, 581

U

Ultrasonics, 10, 13

W

Wavy slip, 598

Author/Discussor Index

A

Ackermann, F., 69
Awatani, J., 107
Adachi, M., 234
Atkinson, C., 340, 722

B

Beardmore, P., 453, 466
Beevers, J., 368, 388, 417, 815
Bhat, S. P., 592, 620
Bhowal, P., 47
Brett, S., 231

C

Coffin, L. F., Jr., 9, 129, 414, 528, 891
Cruse, T., 416

D

Davidson, D., 248, 254, 271, 277, 785
De Vries, K., 337, 368, 491
deWit, R., 97
Ditchek, B., 101, 269
Dowling, N., 418, 838
Driver, J., 390
Duquette, D. J., 788
Dvorak, G., 782

E

Early, J., 585
Ebara, 831, 868
Ellison, E., 554
Esztergar, E., 614
Eylon, D., 47

F

Fong, J. T., 3, 287, 340, 729, 754, 761, 890, 891
Fuhlrott, H., 371

G

Gerberich, W. W., 292, 336, 394
Grosskreutz, J. C., 133, 276

H

Heckel, K., 747
Hertzberg, R., 336, 471, 498
Herz, R. K., 69
Hoeppner, D., 726, 814, 841, 870
Hoshina, M., 135

I

Ivanova, V., 701

J

Jono, M., 234

K

Kanninen, M., 704
Katagiri, K., 107, 127
Kikukawa, M., 234, 251
Kitagawa, H., 420, 445, 869
Koyanagi, K., 107
Krempl, E., 338, 557
Kroner, E., 751
Kruger, J., 837
Kulkarni, S., 812
Kunio, T., 342, 369

L

Laird, C., 101, 203, 394, 592, 620
Lamba, H., 367, 784
Langford, J., 277, 335
Le May, I., 208, 339, 838, 873
Lin, S. R., 707, 728
Lin, T. H., 707, 728
Liu, H., 251
Lynch, S. P., 174, 208

M

Manson, J. A., 471
Manson, S. S., 624, 889
Mayr, P., 249
McEvily, A. J., 47, 162, 367, 393
Meyer, R., 214
Michel, D., 526, 588
Miller, A., 337
Miller, K., 361, 441, 563, 869
Min, B. K., 569, 589, 628
Miyashita, S., 420
Moody, N. R., 292
Moore, G. A., 35, 680, 753
Morrow, J., 725, 891
Mughrabi, H., 69, 102, 126, 338, 618
Mura, T., 65, 726

N

Nageswararao, M., 214
Neumann, P., 68, 207, 338, 371, 395, 726, 838

O

Omura, A., 107

P

Patten, D. T., 43
Pelloux, R. M., 501, 526, 863
Perzyna, P., 749
Peterlin, A., 465
Plumbridge, W., 97, 208, 419, 563
Plumtree, A., 123, 619

R

Raj, R., 569, 589
Reemsnyder, H., 752
Reifsnider, K. L., 762, 786
Rhines, F. N., 23, 44
Ritchie, R., 364
Ruff, A. W., 269
Runkle, J. C., 501, 526
Ruppen, J., 47, 67

S

Scarlin, R. B., 396, 415, 814
Sendeckyj, G., 784
Shiraishi, T., 107
Sidey, D., 528, 564, 627
Sih, G., 439
Simmons, J., 125, 251, 679
Skibo, M. D., 471
Smith, J. H., 671
Starke, E., Jr., 230, 633, 682
Stephens, R., 101, 340, 810, 838, 890
Stinchcomb, W. W., 762, 786, 814

Stoloff, N., 417, 788, 815
Suh, C. M., 420

T

Taira, S., 135, 170, 890
Takahashi, S., 420
Takao, K., 206
Tanaka, K., 135, 169
Thomson, R., 613
Tomkins, B., 208, 418, 524, 624

U

Underwood, E. E., 40, 633, 682

V

Vander Sande, J. B., 42
Vehoff, H., 371

W

Wei, R. P., 207, 816, 838
Wells, C., 334
Weissman, S., 163, 366, 619
Wilhelm, M., 214, 232
Wilson, A., 673
Winter, A., 101
Worthington, P., 498, 867

Y

Yamada, K., 342, 369
Yokobori, T., 167, 441, 683, 705